

# Handbook of Optical Constants of Solids II

edited by

Edward D. Palik

Copyrighted material

# Handbook of Optical Constants of Solids II

This book is printed on acid-free paper. ♾

Copyright © 1998, 1991, Elsevier Science (USA).

All Rights Reserved.
No part of this publication may be reproduced or transmitted in any form or by any means, electronic or mechanical, including photocopy, recording, or any information storage and retrieval system, without permission in writing from the publisher.

Permissions may be sought directly from Elsevier's Science & Technology Rights Department in Oxford, UK: phone: (+44) 1865 843830, fax: (+44) 1865 853333, e-mail: permissions@elsevier.com.uk. You may also complete your request on-line via the Elsevier Science homepage (http://elsevier.com), by selecting "Customer Support" and then "Obtaining Permissions."

Academic Press
*An imprint of Elsevier Science*
525 B Street, Suite 1900, San Diego, California 92101-4495, USA
http://www.academicpress.com

Academic Press
84 Theobald's Road, London WC1X 8RR, UK
http://www.academicpress.com

**Library of Congress Cataloging-in-Publication Data**

Handbook of optical constants of solids II / edited by Edward D. Palik.
p. cm.
Includes bibliolographical references.
International Standard Book Number: 0-12-544422-2
1. Solids. 2. Optical properties. 3. Handbooks, manuals, etc.
I. Palik, Edward D.
QC176.8.06H63 1991 90-826
530.4'12 CIP

PRINTED IN THE UNITED STATES OF AMERICA
03 04 05 06 07 9 8 7 6 5 4 3

# Contents

List of Contributors xv

**Part I DETERMINATION OF OPTICAL CONSTANTS**

Chapter 1 **Introductory Remarks** 3
EDWARD D. PALIK

I. Introduction 3
II. The Chapters 3
III. The Critiques 5
IV. The Tables 6
V. The Figures of the Tables 7
VI. General Remarks 7
VII. Errata 8
References 11

Chapter 2 **Convention Confusions** 21
R. T. HOLM

I. Introduction 21
II. Units 22
III. Wave Equation 22
IV. Polarization 26
V. Fresnel's Amplitude Reflection Coefficients 37
VI. Nomenclature 50
VII. Concluding Remarks 51
Acknowledgments 52
References 52

Chapter 3 **Methods for Determining Optical Parameters of Thin Films** 57
E. PELLETIER

I. Introduction 57
II. An Example of Comparison between the Different Techniques of Index Determination 58
III. Principle Methods of Index Determination 60
IV. Sensitivity and Accuracy of the Determination Methods 64
V. Overlapping and Tests of Validity of the Model 67
VI. Results and Conclusion 71
References 71

Chapter 4 **The Attenuated Total Reflection Method** 75
G. J. SPROKEL AND J. D. SWALEN

I. Introduction 75
II. Surface-Plasmon Oscillations 77
III. Optical Analysis of ATR Structures 81
IV. Guided Modes 84
V. Applications of ATR 87
VI. Conclusion 94
References 94

Chapter 5 **Optical Properties of Superlattices** 97
P. APELL AND O. HUNDERI

I. Introduction 97
II. The Classical Optical Response of a Multilayer System 98
III. Semiconductor Superlattices 101
IV. Amorphous Superlattices 109
V. Collective Excitations 112
VI. Lattice Disorder 118
VII. The Effect of Nonlocal Dielectric Functions 120
VIII. Concluding Remarks 122
References 122

Chapter 6 **Calculation of the Refractive Index of Compound Semiconductors below the Band Gap** 125
B. JENSEN

I. Introduction 125
II. The Quantum-Density-Matrix Formulation of the Complex Dielectric Constant 128
III. Comparison with Experimental Results 138
IV. Summary 147
References 148

Chapter 7 **Calculation of Optical Constants, *n* and *k*, in the Interband Region** 151
A. R. FOROUHI AND I. BLOOMER

I. Introduction 151
II. The Extinction Coefficient, $k(E)$, and the Refractive Index, $n(E)$ 154
III. Discussion 163
IV. Examples 166
V. Summary 174
References 175

Chapter 8 **Temperature Dependence of the Complex Index of Refraction** 177
MICHAEL E. THOMAS

I. Introduction 177
II. Temperature Dependence of $n$ and $k$ 179

III. Conclusions 199
References 199

Chapter 9 **Measurement of *n* and *k* in the XUV by the Angle-of-Incidence Total-External-Reflectance Method** 203

MARION L. SCOTT

I. Introduction 203
II. General Considerations 204
III. Aluminum Reflectance versus Angle in UHV 206
IV. Determination of *n* and *k* 207
V. Comparison with Other Results 210
References 212

Chapter 10 **Spectroscopic Ellipsometry in the 6–35 eV Region** 213

J. BARTH, R. L. JOHNSON, AND M. CARDONA

I. Introduction 213
II. The Bessy VUV Ellipsometer 217
III. Theory 226
IV. Results and Comparison with Reflectance Spectra 237
V. Summary 244
Acknowledgment 245
References 245

Chapter 11 **Methods Based on Multiple-Slit Fourier Transform Interferometry for Determining Thin-Film Optical Constants in the VUV/Soft X-Ray Range** 247

ROMAN TATCHYN

I. Introduction to MSFTI 247
II. Fundamental Dimensional Constraints and Inequalities 253
III. Relationship of MSFTI to Alternative Metrological Techniques 254
IV. General Experimental Equations and Sensitivity Analysis 258
V. A Characterization of the Optical Constants of Au Using MSFTI in the 280–640 eV Range 265
VI. Problems and Prospects in Sample Preparation 270
VII. Prospects for MSFTI in Other Spectral Regimes 272
VIII. Summary 273
Acknowledgments 274
References 274

Chapter 12 **Determination of Optical Constants from Angular-Dependent, Photoelectric-Yield Measurements** 279

H.-G. BIRKEN, C. BLESSING, AND C. KUNZ

I. Introduction 279
II. Theoretical Background 280
III. Experimental Details 285

IV. Examples 286
V. Conclusions and Future Prospects 289
References 292

Chapter 13 **Determination of Optical Constants by High-Energy, Electron-Energy-Loss Spectroscopy (EELS)** 293
J. PFLÜGER AND J. FINK

I. Introduction 293
II. Description of an EELS Experiment 295
III. Scattering Cross-Section 297
IV. Exact Determination of the Loss Function 298
V. Kramers–Kronig Analysis 299
VI. Brief Summary of the Evaluation Procedure 300
VII. Comparison with Reflectivity Measurements 300
VIII. Optical Properties of TiC, VC, TiN, and VN 303
References 310

Chapter 14 **Optical Parameters for the Materials in *HOC I* and *HOC II*** 313
EDWARD D. PALIK

I. Introduction 313
II. The Parameters 313
References 334

**Part II CRITIQUES**

**Subpart 1 Metals**

**An Introduction to the Data for Several Metals** 341
DAVID W. LYNCH AND W. R. HUNTER

I. Introduction 341
References 341
II. Alkali Metals 342
References 344
III. Lithium (Li) 345
References 347
IV. Sodium (Na) 354
References 357
V. Potassium (K) 364
References 367
VI. Chromium (Cr) 374
References 376
VII. Iron (Fe) 385
References 387
VIII. Niobium (Nb) 396
References 397
IX. Tantalum (Ta) 408
References 409

**Beryllium (Be)**
E. T. ARAKAWA, T. A. CALLCOTT, AND YUN-CHING CHANG 421
References 425

**Cobalt (Co)** 435
L. WARD
References 440

**Graphite (C)** 449
A. BORGHESI AND G. GUIZZETTI
References 453

**Liquid Mercury (Hg)** 461
E. T. ARAKAWA AND T. INAGAKI
References 465

**Palladium (Pd)** 469
A. BORGHESI AND A. PIAGGI
References 472

**Vanadium (V)** 477
G. GUIZZETTI AND A. PIAGGI
References 480

**Subpart 2 Semiconductors**

**Aluminum Arsenide (AlAs)** 489
EDWARD D. PALIK, O. J. GLEMBOCKI, AND KENICHI TAKARABE
Acknowledgments 492
References 492

**Aluminum Antimonide (AlSb)** 501
DAVID F. EDWARDS AND RICHARD H. WHITE
References 505

**Aluminum Gallium Arsenide ($Al_xGa_{1-x}As$)** 513
O. J. GLEMBOCKI AND K. TAKARABE
Acknowledgments 515
References 515

**Cadmium Selenide (CdSe)** 559
H. PILLER

References 563

**Cadmium Sulphide (CdS)** 579
L. WARD

References 586

**Gallium Antimonide (GaSb)** 597
DAVID F. EDWARDS AND RICHARD H. WHITE

References 601

**Silicon–Germanium Alloys ($Si_xGe_{1-x}$)** 607
J. HUMLÍČEK, F. LUKEŠ, AND E. SCHMIDT

References 611

**Lead Tin Telluride (PbSnTe)** 637
H. PILLER

References 639

**Mercury Cadmium Telluride ($Hg_{1-x}Cd_xTe$)** 655
P. M. AMIRTHARAJ

Acknowledgments 666
References 667

**Selenium (Se)** 691
EDWARD D. PALIK

Acknowledgments 693
References 694

**Cubic Silicon Carbide ($\beta$-SiC)** 705
SAMUEL A. ALTEROVITZ AND JOHN A. WOOLLAM

References 706

**Tellurium (Te)** 709
EDWARD D. PALIK

Acknowledgments 713
References 713

**Tin Telluride (SnTe)** 725
H. PILLER

References 727

**Zinc Selenide (ZnSe)**
**Zinc Telluride (ZnTe)** 737
L. WARD
References 747

**Subpart 3 Insulators**

**Aluminum Oxide ($Al_2O_3$)** 761
FRANÇOIS GERVAIS
References 764

**Aluminum Oxynitride (ALON) Spinel** 777
WILLIAM J. TROPF AND MICHAEL E. THOMAS
References 780
Notes Added in Proof 781

**Barium Titanate ($BaTiO_3$)** 789
CHUEN WONG, YE YUNG TENG, J. ASHOK, AND P. L. H. VARAPRASAD
Acknowledgments 793
References 793

**Beryllium Oxide (BeO)** 805
DAVID F. EDWARDS AND RICHARD H. WHITE
References 807

**Calcium Fluoride ($CaF_2$)** 815
D. F. BEZUIDENHOUT
References 825

**Amorphous Hydrogenated "Diamondlike" Carbon Films and Arc-Evaporated Carbon Films** 837
SAMUEL A. ALTEROVITZ, N. SAVVIDES, F. W. SMITH, AND JOHN A. WOOLLAM
References 840

**Cesium Iodide (CsI)** 853
JOHN E. ELDRIDGE
References 857

**Copper Oxides ($Cu_2O$, CuO)** 875
CARL G. RIBBING AND ARNE ROOS
References 878

**Magnesium Aluminium Spinel ($MgAl_2O_4$)** 883
WILLIAM J. TROPF AND MICHAEL E. THOMAS

References 887

**Magnesium Fluoride ($MgF_2$)** 899
THOMAS M. COTTER, MICHAEL E. THOMAS, AND WILLIAM J. TROPF

References 903

**Magnesium Oxide (MgO)** 919
DAVID M. ROESSLER AND DONALD R. HUFFMAN

Acknowledgments 939
References 939

**Polyethylene $(C_2H_4)_n$** 957
J. ASHOK, P. L. H. VARAPRASAD, AND J. R. BIRCH

References 968

**Potassium Bromide (KBr)** 989
EDWARD D. PALIK

References 992

**Potassium Dihydrogen Phosphate ($KH_2PO_4$, KDP) and Three of Its Isomorphs** 1005
DAVID F. EDWARDS AND RICHARD H. WHITE

References 1008

**Sodium Fluoride (NaF)** 1021
I. OHLÍDAL AND K. NAVRÁTIL

References 1024

**Strontium Titanate ($SrTiO_3$)** 1035
FRANÇOIS GERVAIS

References 1037

**Thorium Fluoride ($ThF_4$)** 1049
I. OHLÍDAL AND K. NAVRÁTIL

References 1054

**Water ($H_2O$)** 1059

MARTIN R. QUERRY, DAVID M. WIELICZKA, AND DAVID J. SEGELSTEIN

References 1063

**Yttrium Oxide ($Y_2O_3$)** 1079

WILLIAM J. TROPF AND MICHAEL E. THOMAS

References 1084
Notes Added in Proof 1086

# List of Contributors

Numbers in parentheses indicate the pages on which the authors' contributions begin.

SAMUEL A. ALTEROVITZ (705, 837), Space Electronics Division, NASA Lewis Research Center, Cleveland, Ohio 44135
P. M. AMIRTHARAJ (655), U.S. Army Center for Night Vision and Electro-Optics, Mail Code AMSEL-NV-IT, Ft. Belvoir, Ft. Belvoir, Virginia 22060
P. APELL (97), Institute of Theoretical Physics, Chalmers University of Technology, S-412 96 Göteborg, Sweden
E. T. ARAKAWA (421, 461), P.O. Box 2008, Oak Ridge National Laboratory, Oak Ridge, Tennessee 37831
J. ASHOK (789, 957), Department of Applied Physics, Andhra University, Visakhapatnam 530 003, India
J. BARTH (213), Elktro-Optik GmbH, Fördestr. 35, D-2392 Glücksburg, Federal Republic of Germany
D. F. BEZUIDENHOUT (815), Division of Production Technology, P.O. Box 395, Council for Scientific and Industrial Research, Pretoria, South Africa
J. R. BIRCH (957), Division of Electrical Science, National Physical Laboratory, Teddington, Middlesex TW11 0LW, United Kingdom
H.-G. BIRKEN (279), Institute für Experimentalphysik, Universität Hamburg, Luruper Chausee 149, D-2000 Hamburg 50, Federal Republic of Germany
C. BLESSING (279), Institut für Experimentalphysik, Universität Hamburg, Luruper Chausee 149, D-2000 Hamburg 50, Federal Republic of Germany
I. BLOOMER (151), Department of Physics, San José University, One Washington Square, San José, California 95192
A. BORGHESI (449, 469), Dipartimento di Fisica "A. Volta," Università di Pavia, Via A. Bassi, 6, 27100 Pavia, Italy
T. A. CALLCOTT (421), Physics Department, The University of Tennessee, Knoxville, Tennessee 37933
M. CARDONA (213), Max-Planck Institut für Festkörperforschung, Heisenbergstrasse 1, D-7000 Stüttgart 80, Federal Republic of Germany
YUN-CHING CHANG (421), Physics Department, The University of Tennessee, Knoxville, Tennessee 37933

T. M. COTTER (899), Applied Physics Laboratory, The Johns Hopkins University, Johns Hopkins Road, Laurel, Maryland 20707
DAVID F. EDWARDS (501, 597, 805, 1005), University of California, Lawrence Livermore National Laboratory, P.O. Box 808, Livermore, California 94550
J. E. ELDRIDGE (853), Department of Physics, 6224 Agriculture Road, The University of British Columbia, Vancouver, British Columbia V6T 2A6, Canada
J. FINK (293), Kernforschungszentrum Karlsruhe, Institute für Nukleare Festkörperphysik, P.O. Box 3640, D-7500 Karlsruhe, Federal Republic of Germany
A. R. FOROUHI (151), Loral Fairchild Imaging Sensors, 1801 McCarthy Boulevard, Milpitas, California 95035
FRANÇOIS GERVAIS (761, 1035), Centre de Recherches sur la Physique des Hautes Températures, 1D Avenue de la Recherche Scientifique, 45071 Orléans Cedex, France
O. J. GLEMBOCKI (489, 513), Code 6833, Naval Research Laboratory, Washington, D.C. 20375
G. GUIZZETTI (449, 477), Dipartimento di Fisica "A. Volta," Università di Pavia, Via A. Bassi, 6, 27100 Pavia, Italy
R. T. HOLM (21), Code 6833, Naval Research Laboratory, Washington, D.C. 20375
DONALD R. HUFFMAN (921), Physics Department, University of Arizona, Tucson, Arizona 85721
J. HUMLÍČEK (607), Department of Solid State Physics, Masaryk University, Kotlářská 2, 611 37 Brno, Czechoslovakia
O. HUNDERI (97), Division of Physics, NTH, N 7034 Trondheim, Norway
W. R. HUNTER (341), S.F.A., Inc., 1401 McCormick Dr., Landover, Maryland 20785
T. INAGAKI (341, 461), P.O. Box 2008, Oak Ridge National Laboratory, Oak Ridge, Tennessee 37831
B. JENSEN (125), Department of Physics and Applied Physics, College of Pure and Applied Science, University of Lowell, Lowell, Massachusetts 01854
R. L. JOHNSON (213), Institut für Experimentalphysik, Universität Hamburg, Luruper Chausee 149, D-2000 Hamburg 50, Federal Republic of Germany
C. KUNZ (279), Institut für Experimentalphysik, Universität Hamburg, Luruper Chausee 149, D-2000 Hamburg 50, Federal Republic of Germany
F. LUKEŠ (607), Department of Solid State Physics, Masaryk University, Kotlářská 2, 611 37 Brno, Czechoslovakia
DAVID W. LYNCH (341), Department of Physics, 12 Physics Building, Iowa State University, Ames, Iowa 50011

K. NAVRÁTIL (1021, 1049), Department of Solid State Physics, Masaryk University, Kotlářská 2, 611 37 Brno, Czechoslovakia
L. OHLÍDAL (1021, 1049), Department of Solid State Physics, Masaryk University, Kotlářská 2, 611 37 Brno, Czechoslovakia
EDWARD D. PALIK (3, 313, 489, 691, 709, 989), Institute of Physical Sciences and Technology, University of Maryland, College Park, Maryland 20742
E. PELLETIER (57), Laboratoire d'Optique des Surfaces et des Couches Minces, Unité Associée au CNRS, Ecole Nationale Supérieure de Physique de Marseille, Domaine Universitaire de St. Jérôme, 13397 Marseille Cedex 13, France
J. PFLÜGER (293), Synchrotronstrahlungslabor, HASYLAB at DESY, Notkestrasse 85, D-2000 Hamburg 52, Federal Republic of Germany
A. PIAGGI (469, 477), Dipartimento di Fisica "A. Volta," Università di Pavia, Via A. Bassi, 6, 27100 Pavia, Italy
H. PILLER (559, 637, 725), Department of Physics and Astronomy, Louisiana State University, Baton Rouge, Louisiana 70803
MARVIN R. QUERRY (1059), Department of Physics, University of Missouri-Kansas City, Kansas City, Missouri 64110
CARL G. RIBBING (875), School of Engineering, Department of Technology, Uppsala University, Box 534, S-751 21 Uppsala, Sweden
DAVID M. ROESSLER (921), Physics Department, General Motors Research Laboratories, 30500 Mound Road, Warren, Michigan 48089
ARNE ROOS (875), School of Engineering, Department of Technology, Uppsala University, Box 534, S-751 21 Uppsala, Sweden
N. SAVVIDES (837), CSIRO Division of Applied Physics, National Measurements Laboratory, Sydney, Australia 2070
E. SCHMIDT (607), Department of Solid State Physics, Masaryk University, Kotlářská 2, 611 37 Brno, Czechoslovakia
MARION L. SCOTT (203), E 549, Los Alamos National Laboratory, Los Alamos, New Mexico 87545
DAVID J. SEGELSTEIN (1059), Bell Communications Research, Red Bank, New Jersey 07701
F. W. SMITH (837), Department of Physics, City College of CUNY, New York, New York 10031
G. J. SPROKEL (75), IBM Almaden Research Center, Department K33, 650 Harry Road, San Jose, California 95120
J. D. SWALEN (75), IBM Almaden Research Center, Department K33, 650 Harry Road, San Jose, California 95120
KENICHI TAKARABE (489, 513), Department of Natural Science, Faculty of Science, Okayama University of Science, 1-1 Ridai-cho, Okayama City, Okayama 700, Japan
ROMAN TATCHYN (247), Stanford Electronics Laboratory, Stanford University, Stanford, California 94305

YE YUNG TENG (789), Department of Physics and Applied Physics, University of Lowell, 1 University Avenue, Lowell, Massachusetts 01854
MICHAEL E. THOMAS (177, 777, 883, 899, 1079), The Johns Hopkins University, Applied Physics Laboratory, Johns Hopkins Road, Laurel, Maryland 20707
WILLIAM J. TROPF (777, 883, 899, 1079), The Johns Hopkins University, Applied Physics Laboratory, Johns Hopkins Road, Laurel, Maryland 20707
P. L. H. VARAPRASAD (789), Department of Applied Physics, Andhra University, Visakhapatnam 530 003, India
L. WARD (435, 579, 737), Department of Applied Physical Science, Coventry (Lanchester) Polytechnic, Coventry CV1 5FB, United Kingdom
RICHARD H. WHITE (501, 597, 805, 1005), University of California, Lawrence Livermore National Laboratory, P.O. Box 808, Livermore, California 94550
DAVID M. WIELICZKA (1059), Department of Physics, University of Missouri-Kansas City, Kansas City, Missouri 64110
JOHN A. WOOLLAM (705, 837), Center for Microelectronic and Optical Materials Research and Department of Electrical Engineering, University of Nebraska, Lincoln, Nebraska 68588
CHUEN WONG (789), Department of Physics and Applied Physics, University of Lowell, 1 University Avenue, Lowell, Massachusetts 01854

# Chapter 1
# Introductory Remarks

EDWARD D. PALIK
Institute for Physical Science and Technology
University of Maryland
College Park, Maryland

I. Introduction 3
II. The Chapters 3
III. The Critiques 5
IV. The Tables 6
V. The Figures of the Tables 7
VI. General Remarks 7
VII. Errata 8
References 11

## INTRODUCTION I

The original list of materials prepared for the *Handbook of Optical Constants of Solids (HOC I)* [1] contained about 60 materials, but because of a lack of critiquers, the published handbook contained only 37 materials, more or less evenly divided among metals, semiconductors, and insulators. Useful, important materials had to be omitted. More than three years after the publication of *HOC I*, I approached Academic Press about a second volume to cover these additional materials. Having now added another 48 materials to the list, I can see another 30 materials that might be of interest also.

## THE CHAPTERS II

As with *HOC I* the first part of the *Handbook of Optical Constants of Solids II (HOC II)* consists of short topics dealing with the determination of optical constants.

In Chapter 2, R. T. Holm discusses sign and polarization conventions


Copyright © 1991 by Academic Press.
All rights of reproduction in any form reserved.
ISBN 0-12-544422-2

starting with the form of the electromagnetic wave used to solve Maxwell's equations. It seems that in many optics books and papers I read, the authors have not stated this wave form and used it consistently; they sometimes change wave forms. Although this does not affect the final calculated answers, it surely confuses the student with + and − signs and sines and cosines.

In Chapter 3, E. Pelletier discusses the problems involved in determining the optical constants of a film on a substrate (a common sample in this day and age of epitaxial layers, and reflection and antireflection coatings). Also, the improvement in deposition processes is now providing thin-film samples, which look more and more like bulk material (except for strain, perhaps).

In Chapter 4, G. J. Sprokel and J. D. Swalen discuss the determination of $n$ and $k$ by the technique of attenuated total reflection. This is a powerful technique of examining deposited, single or multiple thin films; oxide layers on substrates; bulk material; and surface properties such as surface plasmons and phonons.

In Chapter 5, P. Apell and O. Hunderi extend thin-film structures to superlattice structures, discussing how fundamental optical properties are changed and how we can treat a superlattice as a new material with new, effective $n$ and $k$ values different from the parent materials. This should be very important as multiple-quantum wells, and so forth, become routine optical samples in the future, and as the field of textured surfaces and textured bulk becomes optically more interesting in the context of photonic band structure.

In Chapter 6, Barbara Jensen calculates the index of refraction at and below the fundamental band gap of semiconductors from quantum mechanics principles, stressing the ternary and quaternary materials of widespread interest. This gives a calculational way of determining $n$ for $Al_xGa_{1-x}As$ for any value of $x$, for example.

In Chapter 7, A. R. Forouhi and I. Bloomer develop a model for electronic transitions across the band gaps, which accounts for $n$ and $k$ in the interband region. They assign the several peaks in $k$ to transitions with strengths and widths, fitting the experimental $k$ spectrum and then Kramers–Kronig analyzing it to get the $n$ spectrum. Thus, one has an analytical form for $n$ and $k$ in the interband region.

In Chapter 8, Michael E. Thomas develops a model to account for multiphonon absorption as a function of temperature in the region straddling the fundamental transverse optical phonon resonance. This is useful in determining the intrinsic (versus extrinsic) absorption coefficient, especially in studies of laser-window materials in the IR.

The next three chapters concentrate on the determination of $n$ and $k$ in the UV–X-Ray regions. Because of the advent of synchrotron radiation sources, this is a very active spectral region.

In Chapter 9, Marion L. Scott discusses the use of total external reflection to determine $n$ and $k$ in the UV–X-Ray region. All materials eventually have $n<1$ above the interband region where this technique applies, and variable-angle-of-incidence measurements can yield $n$ and $k$.

In Chapter 10, J. Barth, R. L. Johnson, and M. Cardona describe spectroscopic ellipsometry, extending it beyond the usual region of 1.5–6 eV to as high as 35 eV. Linear polarization is not so good at these higher photon energies, and the data must be analyzed in terms of partially linearly polarized radiation.

In Chapter 11 Roman Tatchyn describes the interference effects of a microfabricated Au transmission grating in the soft x-ray region and how the complex index of refraction can be extracted from such interference patterns by comparing relative intensities of interference orders.

There now follow two chapters describing "nonoptical" techniques for determining $n$ and $k$ in the interband region. Although in the critiques we do not often use the numbers obtained from such techniques, they are still of interest.

In Chapter 12, H.-G. Birken, C. Blessing, and C. Kunz describe the angular-resolved photoemission process as a probe of optical constants in the interband region. Although light is used to produce the electrons, it is the electron currents emitted by a crystalline sample (proportional to $k$) that are of interest.

In Chapter 13, J. Pflüger and J. Fink describe how $n$ and $k$ are obtained from a truly nonoptical experiment, electron-energy-loss spectroscopy. This technique has been used for many years as a way of determining $\mathrm{Im}(-1/\varepsilon)$ for unsupported thin films.

Finally, in Chapter 14, I have attempted to collect many optical parameters for the 86 materials in *HOC I* and *II* and display them in a gigantic table. Again, these are parameters that I have often needed but could not find in one place, things like crystal symmetry, lattice constant, irreducible representation, TO and LO resonant frequencies, plasma frequency $\omega_p$, fundamental band gap $E_g$, d.c. dielectric constant $\varepsilon_0$, and so on.

In regards to Chapter 2, which discusses conventions, it is interesting to note that in three of the chapters $n-ik$ is used, whereas in four others $n+ik$ is used. The other chapter writers have avoided making the choice. In the critiques both conventions are also used.

## THE CRITIQUES III

The critiques are meant to be the critiquer's own judgment of the best values of $n$ and $k$ over the widest spectral range. Some spectral-region

values can overlap slightly to indicate typical differences among laboratories and methods. When possible, estimates of uncertainties are stated, but a rule of thumb is that $n$ is good to two figures and $k$ is good to a factor of two. Beyond this, one has to examine the experimental methods; $n$ can be good to five figures for minimum-deviation techniques, and $k$ can be good to two figures if one measures transmittance carefully.

In a few cases, data such as reflectance $R$ and transmittance $T$ are found in the literature, but no determination of $n$ and $k$ has been made; in such cases we can only cite the work. This happens most often in the UV interband region and in the IR reststrahlen region.

A good review and source of references for properties of many materials (including optical) is "Landolt–Börnstein Numerical Data and Functional Relationships in Science and Technology," (K.-H. Hellwege, ed.), Springer-Verlag, Berlin, 1983. This series consists of 23 volumes, which cover quite a few of the materials discussed in *HOC I* and *II*.

## IV THE TABLES

The biggest change from *HOC I* is in the use of camera-ready tables of $n$ and $k$. Although uniformity could not be achieved in every case, the tables should be more free of typographical errors. We have given the various critiquers more leeway in the format. The eV, $cm^{-1}$, and $\mu m$ units may not run continously from X-ray to mm-wave regions, but may "back up" for another author's values to overlap, and then continue on. The exponential form of $k$ varies; sometimes $\times 10^{-5}$ runs down to $\times 10^{-4}$ line by line. (This is because it is easier for the critiquers than the typesetter to include every single $\times 10^{-5}$. Other critiquers leave the intermediate lines blank and $\times 10^{-5}$ is understood until a change takes place at $\times 10^{-4}$. Although we try to continue exponents down to $\times 10^{-2}$, then switch to decimals for $\times 10^{-1}$, $\times 10^{0}$, $\times 10^{1}$, this is not done consistently. Sometimes 4.6 E − 03 is used, and sometimes a star indicates the multiplication sign ($4.6 * 10^{-2}$). Some authors have carried $cm^{-1}$ up into the millions; we usually stop mentioning it above 50,000 $cm^{-1}$. Always keep in mind the conversion factor 8065.48 $cm^{-1}$/eV. Although we have used this conversion factor to move among the units in most cases, some critiquers have used values differing by one digit in the fourth significant figure. This should cause no problems in an experiment until the fourth figure is reached in the eV, $cm^{-1}$ or $\mu m$ units, which is not frequently. Values of $n$ and $k$ are identified by a reference number in brackets, which is understood to apply in that particular column until a new reference appears.

Several alloy semiconductors have been included, such as $Al_xGa_{1-x}As$,

$Pb_{1-x}Sn_xTe$, $Hg_{1-x}Cd_xTe$, $Si_xGe_{1-x}$. Although it would be nice to list $x$ in tenths from zero to one, these are not necessarily available from UV to IR, so in most instances we have taken what the literature supplies for a few representative values of $x$. Hopefully, the dependence of band gap and optical-phonon frequencies on $x$ can be obtained from the cited literature.

Values of $n$ and $k$ have been read from expanded graphs, from tables in the original papers, original reports, and data kindly supplied by the investigators in private communications, and in at least one or two cases, the critiquers have made additional measurements for their particular critiques.

## THE FIGURES OF THE TABLES V

Log–log plots of $n$, $k$ versus $\mu$m have been prepared in a uniform format. The details are often lost in the thickness of the pen line, but the reader can always return to the tables to interpolate values. The figures give an instant bird's-eye view of $n$ and $k$.

We also cannot plot all the data for every $x$ tabulated for an alloy semiconductor, for example, so we have chosen only a few examples, where hopefully there is a wide spectrum of data for one or two values of $x$.

## GENERAL REMARKS VI

In *HOC I*, we had concentrated on room-temperature (often not stated in the original papers) values of $n$ and $k$. Some critiquers have included temperature dependence of $n$ at various wavelengths and commented on what raising or lowering the temperature does to $k$. Of special interest is the fact that lowering the temperature significantly widens the spectral windows in the optic-phonon regions, and materials that are optical windows on dewars at room temperature invariably become much better windows when used as low-temperature windows inside the dewar (sapphire is a good example).

We cannot hope to tabulate every useful optical parameter for these materials, although in Chapter 14 there is a table listing some of the parameters for each material.

Of some interest is the effort that has gone into a material like $BaTiO_3$ (for physics and technology), but its UV properties have not been

measured to 30 eV. Also, a material like $Cu_2O$ is very prominent in solar research and is used as an example in a book on IR and Raman selection rules for optic phonons, but again no UV data are available. Even a material of great interest for quantum-well studies and superlattices in general, like $Al_xGa_{1-x}As$, has not been studied from UV to far IR for $x = 0, 0.1, 0.2, \ldots, 1.0$ in detail. Only bits and pieces seem to be done with existing or readily grown materials for a few values of $x$. The uncertainty in $x$ is also a problem, often being $\pm 0.01$.

Our knowledge of deposited films improves steadily. Ion-beam-assisted layer growth is producing samples that look more and more like bulk materials (either single crystal or polycrystal). Variations in $n$ from the substrate to outer surface, related to the columnar growth process, are now seen; the strain effects in films on substrates are not yet optically clear.

I proposed the title of this volume to be *Handbook of Optical Functions of Solids* because $n$ and $k$ are not constant, and physicists use the term often. However, to relate to *HOC I* better, we retain the use of optical constants in the title and in most of the critiques and chapters.

We have stretched the truth a little in the title, in that two liquids are discussed: Hg (as a classic liquid metal) and water (because $H_2O$ surrounds us). Also, we have included polyethylene because it is a prototype plastic and has been widely used in IR spectroscopy. In addition, it shows scattering in the visible because of its structure and therefore provides a tricky task for the experimentalist to characterize it. Also, a-C:H (amorphous hydrogenated carbon) is of considerable interest (as is a-Si:H), so we touch upon this material.

Among the materials offered but not claimed by critiquers are AgCl, CsBr, NaBr, KI, BaO, NiO, $PbF_2$, HgS, HgSe, GaN, Mg, Cd, Pb, Mn, Ti, Teflon, Plexiglas, mica, and liquid nitrogen (the only material not at room temperature). The high-temperature superconductors were considered for inclusion, but at this date, the optical properties have not "stabilized."

## VII ERRATA

In using *HOC I*, I have found mistakes and typographical errors; a few readers have also pointed out mistakes.

**p. 6,** line 18: insulators

**p. 7,** line 5: for the choice $n + ik$ the wave form is $\exp[i(-\omega t \pm \mathbf{q} \cdot \mathbf{r})]$; for $n - ik$ the wave form is $\exp[i(\omega t \pm \mathbf{q} \cdot \mathbf{r})]$. The $\pm$ on the term $\mathbf{q} \cdot \mathbf{r}$ pertains to propagation in the $\pm r$ direction for $n + ik$, and to propagation in the $\mp r$ direction for $n - ik$. The variations used in the chapters and critiques testify

to the fact that we will never agree on one convention, and it behooves us to learn how to switch back and forth between them. See Chapter 2, Table 1 in this volume to sort out the ± signs.

**p. 15,** line 7: $f = \ln(\hat{m}) = \ln(\hat{\xi}\hat{\gamma})$
$g = \ln(\hat{m}/\hat{\gamma}^2) = \ln(\hat{\xi}/\hat{\gamma})$

**p. 19,** in denominator in two lines after Eq. (22):

$1 + \hat{r}_{0f}\hat{r}^*_{0f} + 2\,\mathrm{Re}(\hat{r}_{0f})$

$1 + \hat{R}_{0f} + 2\,\mathrm{Re}\,(\hat{r}_{0f})$

**p. 21,** numerator in last line: $\hat{t}'_f\hat{t}'^*_f\,\mathrm{Re}(1/\zeta_{fo})$

**p. 23,** denominator of Eq. (36):

$1 - \{R_{01}R_{12}(1-W^2) + 2(1-W)\,\mathrm{Re}(\hat{r}_{01}\hat{r}_{12})$

$+ 4W\sin\delta[\sin\delta\,\mathrm{Re}(\hat{r}_{01}\hat{r}_{12}) - \cos\delta\,\mathrm{Im}(\hat{r}_{01}\hat{r}_{12})\}/D$

with

$D = 1 + R_{01}R_{12} + 2\,\mathrm{Re}(\hat{r}_{01}\hat{r}_{12}),$

**p. 24,** denominator of Eq. (38):

$1 - 4\{\beta d[R_{01}R_{12} + \mathrm{Re}(\hat{r}_{01}\hat{r}_{12})] - \delta\,\mathrm{Im}(\hat{r}_{01}\hat{r}_{12})\}/D$

**p. 25,** denominator of Eq. (31): $1 - R'_fR_bE^2$

**p. 27,** line 9 up from bottom:

$g_{jk} = [(P_j^2P_k^2 - S^4)(P_k^2 - P_j^2) - 4S^2(\alpha_j^2\beta_k^2 - \alpha_k^2\beta_j^2)]/D_{jk}$

$h_{jk} = 2[(\varepsilon'_j\varepsilon'_k + \varepsilon''_j\varepsilon''_k)(\alpha_j\beta_k - \alpha_k\beta_j) + \cdots$

**p. 28,** line 2 below Fig. 1: $T_f = (1 + R_{02} + 2g_{02})\dfrac{W}{D_f}\,\mathrm{Re}\left(\dfrac{\zeta_0}{\zeta_2}\right),$

**p. 28,** line 3: $T'_f = (1 + R_{02} - 2g_{02})\dfrac{W}{D_f}\,\mathrm{Re}^{-1}\left(\dfrac{\zeta_0}{\zeta_2}\right);$

**p. 28,** line 4: $\dfrac{T_b(1-R_{02})}{1+R_{02}-2g_{02}}\,\mathrm{Re}\left(\dfrac{\zeta_0}{\zeta_2}\right) = T_{02}$

**p. 28,** line 7: $T_f = (1-R_{02}),\ T'_f = (1-R_{02})\left(1 + \left(\dfrac{2\,h_{02}}{1-R_{02}}\right)^2\right)$

**p. 28,** line 10:

$$T_f=(1+R_{02}+2g_{02})\frac{W}{D_f}\mathrm{Re}\left(\frac{\zeta_0}{\zeta_2}\right),\ T_f'=(1+R_{02}-2g_{02})\frac{W}{D_f}\mathrm{Re}^{-1}\left(\frac{\zeta_0}{\zeta_2}\right)$$

**p. 28,** line 11: $T_fT_f'=T_fT_b$

**p. 31,** line 6: $2(S^2-n_1^2)^{1/2}d_1=2\beta_1 d_1$

**p. 31,** denominator in line 7: $h_{01}^2+(S^2-n_1^2)d_1^2$

**p. 38,** line 14: advantage

**p. 62,** line 7: arithmetic

**p. 70,** lines 20, 21: the term $(n^2-k^2-\sin^2\phi)$ in brackets [ ] should be squared

**p. 310,** $16.8\,\mathrm{eV}-0.07380\,\mu\mathrm{m}$

**p. 429,** last line: is given by Bennett

**p. 466,** line 9: $D\lambda^2/(\lambda^2-E)$

**p. 470,** Fig. 4: $k$ curve should be dashed between $3\times10^{-3}$ and $6\times10^{-3}\,\mu\mathrm{m}$

**p. 480,** line 13: subtracted

**p. 480,** line 21: footnote b

**p. 623,** $ReAs_2Se_3$: Room-temperature data for $\alpha$ and $\varepsilon_2$ in the 2–12 eV region can be obtained from R. E. Drews, R. L. Emerald, M. L. Slade, and R. Zallen, *Solid State Commun.* **10**, 293 (1972).

**p. 704,** Eq. (2): dn/dT is in units of $10^{-5}\,\mathrm{K}^{-1}$

**p. 704,** line 15 up from bottom: Tomiki

**p. 704,** line 8 up from bottom: Tomiki

**p. 706,** Refs. 9, 10, 11: Tomiki

**p. 719,** line 9 up from bottom: The wavelength $\lambda$, index

**p. 731,** on $0.1579\,\mathrm{eV}-1{,}274\,\mathrm{cm}^{-1}$ line: $k_0=6.949$

**p. 778,** line 15 up from bottom: Miyata

**p. 798,** Ref. 9: (1974)

In the critiques for ZnS (cubic), LiF, and $SiO_2$ (glass) in *HOC I*, the Henke model was used to calculate $n$ and $k$ in the X-ray region. The densities used in this calculation are: ZnS (cubic), 4.1; LiF, 2.635; $SiO_2$ (glass), 2.648. In the critiques for AlAs and $Al_xGa_{1-x}As$ in *HOC II*, the densities used were calculated from the density equation $g=5.36-1.6x$

given in the $Al_xGa_{1-x}As$ critique: AlAs, 3.76; $Al_{0.3}Ga_{0.7}As$, 4.88. Since slightly different densities can be found in various handbooks for the same material, it is important to know the value used.

Regarding the LiF, ZnS, and $SiO_2$ critiques in *HOC I*:

Since the publication of *HOC I*, it has been brought to our attention that the $k$ values for LiF calculated using the scattering factors reported by Henke *et al.* [2] do not agree with experiment and appear to be too small by approximately a factor of two. This discrepancy was discovered by Powell and Tanuma [3] during an investigation of mean free paths of photoelectrons in LiF. On closer scrutiny of our calculations, and in consultation with Mark Thomas of Lawrence Berkeley Laboratory, we found that indeed the formulas converting scattering factors to $n$, $k$ had been misinterpreted. The consequence is that the calculated $n$, $k$ values for LiF, ZnS, and $SiO_2$ reported in *HOC I* are too small. Using the corrected formulas the difference in $n$ is small, but the new $k$ is larger by about a factor of two for the binary compounds and about 30% larger for the ternary compound. Calculations for the elements are not changed. We take this opportunity to present the newly calculated values for these three materials in Table I at the end of this chapter. These values are calculated from a new set of scattering factors disseminated by Henke *et al.* [4] and cover a wider range of wavelengths, 1.24–240 Å. We regret any inconvenience that may have been caused through use of the older values.

## REFERENCES

1. Edward D. Palik, ed., "Handbook of Optical Constants of Solids," Academic Press, Orlando (1985).
2. B. L. Henke, P. Lee, T. J. Tanaka, R. L. Shimabukuro, and B. K. Fujikawa, "Low Energy X-ray Diagnostics—1981" (D. T. Attwood and B. L. Henke, eds.), p. 340, *AIP Conf. Proc.* No. 75, American Institute of Physics, New York, 1981.
3. C. J. Powell, National Institutes of Science and Technology, Gaithersburg, MD 20899, USA, and S. Tanuma, Central Research Laboratories, Nippon Mining Company, Ltd., 3-17-35 Niizo-Minami, Toda, Saitama 335, Japan, private communication.
4. B. L. Henke, J. C. Davis, E. M. Gullikson, and R. C. C. Perera, "A preliminary report on x-ray photoabsorption coefficients and atomic scattering factors for 92 elements in the 10–10000 eV region," Lawrence Berkeley Laboratory Report 26259, Nov. 1988, Berkeley, CA.

**TABLE 1**

**Optical Constants of LiF, ZnS, and $SiO_2$ Obtained from Reference [3]**

| | | LiF | | ZnS | | $SiO_2$ | |
|---|---|---|---|---|---|---|---|
| eV | Å | *n* | *k* | *n* | *k* | *n* | *k* |
| 10000.0 | 1.240 | 0.9999949 | 1.48E-08 | 0.9999928 | 7.09E-07 | 0.9999945 | 4.68E-08 |
| 9772.4 | 1.269 | 0.9999947 | 1.63E-08 | 0.9999925 | 7.69E-07 | 0.9999942 | 5.13E-08 |
| 9549.9 | 1.298 | 0.9999944 | 1.79E-08 | 0.9999919 | 1.75E-07 | 0.9999939 | 5.62E-08 |
| 9332.5 | 1.329 | 0.9999942 | 1.97E-08 | 0.9999913 | 1.91E-07 | 0.9999936 | 6.16E-08 |
| 9120.1 | 1.359 | 0.9999939 | 2.16E-08 | 0.9999908 | 2.09E-07 | 0.9999933 | 6.75E-08 |
| 8912.5 | 1.391 | 0.9999936 | 2.38E-08 | 0.9999903 | 2.28E-07 | 0.9999930 | 7.40E-08 |
| 8709.6 | 1.424 | 0.9999933 | 2.61E-08 | 0.9999897 | 2.50E-07 | 0.9999927 | 8.10E-08 |
| 8511.4 | 1.457 | 0.9999930 | 2.87E-08 | 0.9999893 | 2.73E-07 | 0.9999923 | 8.88E-08 |
| 8317.6 | 1.491 | 0.9999926 | 3.16E-08 | 0.9999887 | 2.98E-07 | 0.9999920 | 9.73E-08 |
| 8128.3 | 1.525 | 0.9999923 | 3.47E-08 | 0.9999881 | 3.26E-07 | 0.9999916 | 1.07E-07 |
| 7943.3 | 1.561 | 0.9999919 | 3.81E-08 | 0.9999875 | 3.56E-07 | 0.9999912 | 1.17E-07 |
| 7762.5 | 1.597 | 0.9999915 | 4.19E-08 | 0.9999869 | 3.88E-07 | 0.9999908 | 1.28E-07 |
| 7585.8 | 1.634 | 0.9999911 | 4.60E-08 | 0.9999863 | 4.24E-07 | 0.9999903 | 1.40E-07 |
| 7413.1 | 1.673 | 0.9999907 | 5.05E-08 | 0.9999856 | 4.63E-07 | 0.9999899 | 1.53E-07 |
| 7244.4 | 1.711 | 0.9999903 | 5.55E-08 | 0.9999849 | 5.06E-07 | 0.9999894 | 1.68E-07 |
| 7079.5 | 1.751 | 0.9999898 | 6.09E-08 | 0.9999842 | 5.52E-07 | 0.9999889 | 1.84E-07 |
| 6918.3 | 1.792 | 0.9999893 | 6.69E-08 | 0.9999834 | 6.03E-07 | 0.9999884 | 2.01E-07 |
| 6760.8 | 1.834 | 0.9999889 | 7.35E-08 | 0.9999826 | 6.58E-07 | 0.9999878 | 2.20E-07 |
| 6606.9 | 1.877 | 0.9999883 | 8.06E-08 | 0.9999818 | 7.18E-07 | 0.9999872 | 2.41E-07 |
| 6456.5 | 1.920 | 0.9999877 | 8.85E-08 | 0.9999809 | 7.83E-07 | 0.9999866 | 2.64E-07 |
| 6309.6 | 1.965 | 0.9999872 | 9.71E-08 | 0.9999800 | 8.55E-07 | 0.9999860 | 2.89E-07 |
| 6166.0 | 2.011 | 0.9999865 | 1.07E-07 | 0.9999790 | 9.32E-07 | 0.9999853 | 3.16E-07 |
| 6025.6 | 2.058 | 0.9999859 | 1.17E-07 | 0.9999780 | 1.02E-06 | 0.9999846 | 3.46E-07 |
| 5888.4 | 2.106 | 0.9999852 | 1.28E-07 | 0.9999769 | 1.11E-06 | 0.9999839 | 3.79E-07 |
| 5754.4 | 2.155 | 0.9999846 | 1.41E-07 | 0.9999758 | 1.21E-06 | 0.9999831 | 4.14E-07 |
| 5623.4 | 2.205 | 0.9999838 | 1.54E-07 | 0.9999747 | 1.32E-06 | 0.9999823 | 4.53E-07 |
| 5495.4 | 2.256 | 0.9999831 | 1.69E-07 | 0.9999735 | 1.44E-06 | 0.9999815 | 4.96E-07 |
| 5370.3 | 2.309 | 0.9999822 | 1.86E-07 | 0.9999722 | 1.57E-06 | 0.9999806 | 5.42E-07 |

| | | | | | | | |
|---|---|---|---|---|---|---|---|
| 5248.1 | 2.362 | 0.9999814 | 2.04E-07 | 0.9999709 | 1.71E-06 | 0.9999797 | 5.93E-07 |
| 5128.6 | 2.418 | 0.9999805 | 2.24E-07 | 0.9999694 | 1.87E-06 | 0.9999787 | 6.48E-07 |
| 5011.9 | 2.474 | 0.9999796 | 2.45E-07 | 0.9999680 | 2.03E-06 | 0.9999777 | 7.09E-07 |
| 4897.8 | 2.531 | 0.9999786 | 2.69E-07 | 0.9999664 | 2.22E-06 | 0.9999766 | 7.75E-07 |
| 4786.3 | 2.590 | 0.9999776 | 2.95E-07 | 0.9999648 | 2.42E-06 | 0.9999755 | 8.47E-07 |
| 4677.4 | 2.651 | 0.9999765 | 3.23E-07 | 0.9999632 | 2.63E-06 | 0.9999744 | 9.26E-07 |
| 4570.9 | 2.712 | 0.9999754 | 3.54E-07 | 0.9999614 | 2.87E-06 | 0.9999731 | 1.01E-06 |
| 4466.8 | 2.776 | 0.9999743 | 3.88E-07 | 0.9999596 | 3.12E-06 | 0.9999719 | 1.11E-06 |
| 4365.2 | 2.840 | 0.9999730 | 4.25E-07 | 0.9999577 | 3.40E-06 | 0.9999705 | 1.21E-06 |
| 4265.8 | 2.906 | 0.9999717 | 4.66E-07 | 0.9999557 | 3.71E-06 | 0.9999691 | 1.32E-06 |
| 4168.7 | 2.974 | 0.9999704 | 5.10E-07 | 0.9999536 | 4.04E-06 | 0.9999676 | 1.44E-06 |
| 4073.8 | 3.043 | 0.9999689 | 5.59E-07 | 0.9999514 | 4.40E-06 | 0.9999661 | 1.58E-06 |
| 3981.1 | 3.114 | 0.9999675 | 6.12E-07 | 0.9999491 | 4.79E-06 | 0.9999645 | 1.72E-06 |
| 3890.5 | 3.187 | 0.9999660 | 6.70E-07 | 0.9999467 | 5.21E-06 | 0.9999629 | 1.88E-06 |
| 3801.9 | 3.261 | 0.9999643 | 7.34E-07 | 0.9999442 | 5.68E-06 | 0.9999611 | 2.05E-06 |
| 3715.4 | 3.337 | 0.9999626 | 8.03E-07 | 0.9999416 | 6.18E-06 | 0.9999592 | 2.24E-06 |
| 3630.8 | 3.415 | 0.9999608 | 8.79E-07 | 0.9999389 | 6.72E-06 | 0.9999573 | 2.44E-06 |
| 3548.1 | 3.494 | 0.9999590 | 9.62E-07 | 0.9999360 | 7.32E-06 | 0.9999554 | 2.67E-06 |
| 3467.4 | 3.576 | 0.9999570 | 1.05E-06 | 0.9999331 | 7.96E-06 | 0.9999532 | 2.91E-06 |
| 3388.4 | 3.659 | 0.9999550 | 1.15E-06 | 0.9999300 | 8.66E-06 | 0.9999510 | 3.17E-06 |
| 3311.3 | 3.744 | 0.9999529 | 1.26E-06 | 0.9999268 | 9.42E-06 | 0.9999487 | 3.46E-06 |
| 3235.9 | 3.832 | 0.9999506 | 1.38E-06 | 0.9999235 | 1.02E-05 | 0.9999464 | 3.77E-06 |
| 3162.3 | 3.921 | 0.9999482 | 1.50E-06 | 0.9999201 | 1.11E-05 | 0.9999439 | 4.11E-06 |
| 3090.3 | 4.012 | 0.9999458 | 1.65E-06 | 0.9999165 | 1.21E-05 | 0.9999412 | 4.48E-06 |
| 3020.0 | 4.105 | 0.9999431 | 1.80E-06 | 0.9999128 | 1.32E-05 | 0.9999385 | 4.89E-06 |
| 2951.2 | 4.201 | 0.9999405 | 1.97E-06 | 0.9999090 | 1.43E-05 | 0.9999356 | 5.32E-06 |
| 2884.0 | 4.299 | 0.9999376 | 2.15E-06 | 0.9999050 | 1.55E-05 | 0.9999326 | 5.80E-06 |
| 2818.4 | 4.399 | 0.9999346 | 2.35E-06 | 0.9999011 | 1.69E-05 | 0.9999296 | 6.32E-06 |
| 2754.2 | 4.502 | 0.9999315 | 2.56E-06 | 0.999897 | 1.83E-05 | 0.9999263 | 6.88E-06 |
| 2691.5 | 4.607 | 0.9999282 | 2.80E-06 | 0.999893 | 1.99E-05 | 0.9999230 | 7.49E-06 |
| 2630.3 | 4.714 | 0.9999248 | 3.06E-06 | 0.999889 | 2.16E-05 | 0.9999195 | 8.15E-06 |
| 2570.4 | 4.824 | 0.9999213 | 3.34E-06 | 0.999885 | 2.35E-05 | 0.9999159 | 8.86E-06 |
| 2511.9 | 4.936 | 0.9999175 | 3.65E-06 | 0.999883 | 2.55E-05 | 0.9999121 | 9.64E-06 |
| 2454.7 | 5.051 | 0.9999136 | 3.98E-06 | 0.999890 | 1.68E-05 | 0.9999082 | 1.05E-05 |

(*continued*)

**TABLE 1 (*Continued*)**

| | | LiF | | ZnS | | $SiO_2$ | |
|---|---|---|---|---|---|---|---|
| eV | Å | *n* | *k* | *n* | *k* | *n* | *k* |
| 2398.8 | 5.169 | 0.9999095 | 4.35E-06 | 0.999871 | 1.82E-05 | 0.9999042 | 1.14E-05 |
| 2344.2 | 5.289 | 0.9999051 | 4.74E-06 | 0.999863 | 1.98E-05 | 0.9999000 | 1.24E-05 |
| 2290.9 | 5.412 | 0.9999006 | 5.18E-06 | 0.999855 | 2.15E-05 | 0.999896 | 1.35E-05 |
| 2238.7 | 5.538 | 0.999896 | 5.65E-06 | 0.999848 | 2.34E-05 | 0.999891 | 1.46E-05 |
| 2187.8 | 5.667 | 0.999891 | 6.17E-06 | 0.999840 | 2.55E-05 | 0.999887 | 1.59E-05 |
| 2138.0 | 5.799 | 0.999886 | 6.73E-06 | 0.999832 | 2.77E-05 | 0.999882 | 1.72E-05 |
| 2089.3 | 5.934 | 0.999880 | 7.34E-06 | 0.999824 | 3.00E-05 | 0.999878 | 1.87E-05 |
| 2041.7 | 6.073 | 0.999875 | 8.01E-06 | 0.999816 | 3.26E-05 | 0.999873 | 2.03E-05 |
| 1995.3 | 6.214 | 0.999869 | 8.73E-06 | 0.999807 | 3.54E-05 | 0.999869 | 2.20E-05 |
| 1949.8 | 6.359 | 0.999862 | 9.52E-06 | 0.999798 | 3.84E-05 | 0.999865 | 2.38E-05 |
| 1905.5 | 6.507 | 0.999856 | 1.04E-05 | 0.999789 | 4.17E-05 | 0.999861 | 2.58E-05 |
| 1862.1 | 6.658 | 0.999849 | 1.13E-05 | 0.999779 | 4.52E-05 | 0.999863 | 2.80E-05 |
| 1819.7 | 6.813 | 0.999842 | 1.23E-05 | 0.999769 | 4.91E-05 | 0.999858 | 9.04E-06 |
| 1778.3 | 6.972 | 0.999834 | 1.35E-05 | 0.999758 | 5.33E-05 | 0.999843 | 9.87E-06 |
| 1737.8 | 7.135 | 0.999827 | 1.47E-05 | 0.999748 | 5.78E-05 | 0.999833 | 1.08E-05 |
| 1698.2 | 7.301 | 0.999819 | 1.60E-05 | 0.999736 | 6.26E-05 | 0.999823 | 1.18E-05 |
| 1659.6 | 7.471 | 0.999810 | 1.74E-05 | 0.999725 | 6.78E-05 | 0.999813 | 1.28E-05 |
| 1621.8 | 7.645 | 0.999801 | 1.90E-05 | 0.999713 | 7.35E-05 | 0.999802 | 1.40E-05 |
| 1584.9 | 7.823 | 0.999792 | 2.07E-05 | 0.999701 | 7.96E-05 | 0.999792 | 1.53E-05 |
| 1548.8 | 8.005 | 0.999782 | 2.25E-05 | 0.999688 | 8.62E-05 | 0.999781 | 1.66E-05 |
| 1513.6 | 8.191 | 0.999772 | 2.46E-05 | 0.999676 | 9.34E-05 | 0.999770 | 1.81E-05 |
| 1479.1 | 8.382 | 0.999762 | 2.67E-05 | 0.999663 | 1.01E-04 | 0.999758 | 1.98E-05 |
| 1445.4 | 8.578 | 0.999750 | 2.91E-05 | 0.999649 | 1.10E-04 | 0.999746 | 2.15E-05 |
| 1412.5 | 8.778 | 0.999739 | 3.17E-05 | 0.999636 | 1.19E-04 | 0.999734 | 2.35E-05 |
| 1380.4 | 8.982 | 0.999727 | 3.45E-05 | 0.999622 | 1.28E-04 | 0.999721 | 2.55E-05 |
| 1349.0 | 9.191 | 0.999714 | 3.75E-05 | 0.999609 | 1.39E-04 | 0.999707 | 2.78E-05 |
| 1318.3 | 9.405 | 0.999701 | 4.08E-05 | 0.999596 | 1.51E-04 | 0.999693 | 3.03E-05 |
| 1288.2 | 9.625 | 0.999688 | 4.43E-05 | 0.999583 | 1.63E-04 | 0.999678 | 3.30E-05 |

| | | | | | | | |
|---|---|---|---|---|---|---|---|
| 1258.9 | 9.849 | 0.999674 | 4.82E-05 | 0.999572 | 1.76E-04 | 0.999662 | 3.59E-05 |
| 1230.3 | 10.08 | 0.999659 | 5.23E-05 | 0.999561 | 1.89E-04 | 0.999646 | 3.91E-05 |
| 1202.3 | 10.31 | 0.999644 | 5.69E-05 | 0.999552 | 2.02E-04 | 0.999629 | 4.25E-05 |
| 1174.9 | 10.55 | 0.999628 | 6.17E-05 | 0.999542 | 2.15E-04 | 0.999611 | 4.62E-05 |
| 1148.2 | 10.80 | 0.999612 | 6.70E-05 | 0.999535 | 2.30E-04 | 0.999593 | 5.03E-05 |
| 1122.0 | 11.05 | 0.999595 | 7.28E-05 | 0.999530 | 2.45E-04 | 0.999573 | 5.47E-05 |
| 1096.5 | 11.31 | 0.999578 | 7.90E-05 | 0.999531 | 2.62E-04 | 0.999553 | 5.95E-05 |
| 1071.5 | 11.57 | 0.999560 | 8.57E-05 | 0.999540 | 2.79E-04 | 0.999532 | 6.48E-05 |
| 1047.1 | 11.84 | 0.999541 | 9.30E-05 | 0.999570 | 2.98E-04 | 0.999510 | 7.05E-05 |
| 1023.3 | 12.12 | 0.999522 | 1.01E-04 | 0.999644 | 3.18E-04 | 0.999487 | 7.66E-05 |
| 1000.0 | 12.40 | 0.999502 | 1.10E-04 | 0.999572 | 7.60E-05 | 0.999464 | 8.29E-05 |
| 977.2 | 12.69 | 0.999483 | 1.19E-04 | 0.999485 | 8.21E-05 | 0.999439 | 9.00E-05 |
| 955.0 | 12.98 | 0.999462 | 1.29E-04 | 0.999427 | 8.87E-05 | 0.999413 | 9.80E-05 |
| 933.3 | 13.28 | 0.999442 | 1.40E-04 | 0.999376 | 9.59E-05 | 0.999386 | 1.07E-04 |
| 912.0 | 13.59 | 0.999421 | 1.51E-04 | 0.999327 | 1.04E-04 | 0.999358 | 1.16E-04 |
| 891.3 | 13.91 | 0.999400 | 1.64E-04 | 0.999281 | 1.13E-04 | 0.999329 | 1.25E-04 |
| 871.0 | 14.23 | 0.999380 | 1.77E-04 | 0.999234 | 1.22E-04 | 0.999299 | 1.36E-04 |
| 851.1 | 14.57 | 0.999359 | 1.91E-04 | 0.999187 | 1.32E-04 | 0.999268 | 1.47E-04 |
| 831.8 | 14.91 | 0.999340 | 2.07E-04 | 0.999138 | 1.43E-04 | 0.999235 | 1.60E-04 |
| 812.8 | 15.25 | 0.999322 | 2.24E-04 | 0.999089 | 1.55E-04 | 0.999202 | 1.74E-04 |
| 794.3 | 15.61 | 0.999306 | 2.42E-04 | 0.999038 | 1.68E-04 | 0.999167 | 1.89E-04 |
| 776.3 | 15.97 | 0.999294 | 2.61E-04 | 0.99899 | 1.82E-04 | 0.999132 | 2.06E-04 |
| 758.6 | 16.34 | 0.999286 | 2.83E-04 | 0.99893 | 1.97E-04 | 0.999096 | 2.23E-04 |
| 741.3 | 16.73 | 0.999288 | 3.06E-04 | 0.99888 | 2.13E-04 | 0.999059 | 2.42E-04 |
| 724.4 | 17.12 | 0.999310 | 3.30E-04 | 0.99882 | 2.30E-04 | 0.999021 | 2.63E-04 |
| 708.0 | 17.51 | 0.999394 | 3.57E-04 | 0.99876 | 2.49E-04 | 0.99898 | 2.85E-04 |
| 691.8 | 17.92 | 0.999465 | 2.56E-05 | 0.99869 | 2.68E-04 | 0.99895 | 3.08E-04 |
| 676.1 | 18.34 | 0.999278 | 2.82E-05 | 0.99863 | 2.88E-04 | 0.99891 | 3.33E-04 |
| 660.7 | 18.77 | 0.999180 | 3.11E-05 | 0.99856 | 3.12E-04 | 0.99887 | 3.62E-04 |
| 645.7 | 19.20 | 0.999102 | 3.43E-05 | 0.99849 | 3.38E-04 | 0.99883 | 3.93E-04 |
| 631.0 | 19.65 | 0.999031 | 3.78E-05 | 0.99841 | 3.65E-04 | 0.99879 | 4.26E-04 |
| 616.6 | 20.11 | 0.99896 | 4.16E-05 | 0.99834 | 3.94E-04 | 0.99876 | 4.61E-04 |
| 602.6 | 20.57 | 0.99889 | 4.56E-05 | 0.99826 | 4.25E-04 | 0.99874 | 4.99E-04 |
| 588.8 | 21.06 | 0.99883 | 4.99E-05 | 0.99817 | 4.58E-04 | 0.99872 | 5.40E-04 |

(*continued*)

**TABLE 1 (*Continued*)**

| | | LiF | | ZnS | | $SiO_2$ | |
|---|---|---|---|---|---|---|---|
| eV | Å | *n* | *k* | *n* | *k* | *n* | *k* |
| 575.4 | 21.55 | 0.99876 | 5.47E-05 | 0.99808 | 4.95E-04 | 0.99871 | 5.85E-04 |
| 562.3 | 22.05 | 0.99868 | 5.99E-05 | 0.99799 | 5.34E-04 | 0.99874 | 6.33E-04 |
| 549.5 | 22.56 | 0.99861 | 6.55E-05 | 0.99790 | 5.77E-04 | 0.99890 | 6.86E-04 |
| 537.0 | 23.09 | 0.99853 | 7.16E-05 | 0.99780 | 6.24E-04 | 0.99887 | 2.04E-04 |
| 524.8 | 23.63 | 0.99845 | 7.83E-05 | 0.99769 | 6.74E-04 | 0.99862 | 2.21E-04 |
| 512.9 | 24.17 | 0.99837 | 8.56E-05 | 0.99759 | 7.29E-04 | 0.99848 | 2.39E-04 |
| 501.2 | 24.74 | 0.99828 | 9.35E-05 | 0.99748 | 7.88E-04 | 0.99835 | 2.58E-04 |
| 489.8 | 25.31 | 0.99819 | 1.02E-04 | 0.99736 | 8.52E-04 | 0.99824 | 2.79E-04 |
| 478.6 | 25.91 | 0.99810 | 1.12E-04 | 0.99724 | 9.22E-04 | 0.99812 | 3.02E-04 |
| 467.7 | 26.51 | 0.99800 | 1.22E-04 | 0.99712 | 9.97E-04 | 0.99801 | 3.26E-04 |
| 457.1 | 27.12 | 0.99790 | 1.34E-04 | 0.99700 | 1.08E-03 | 0.99789 | 3.52E-04 |
| 446.7 | 27.76 | 0.99779 | 1.46E-04 | 0.99688 | 1.16E-03 | 0.99778 | 3.80E-04 |
| 436.5 | 28.40 | 0.99768 | 1.60E-04 | 0.99674 | 1.25E-03 | 0.99765 | 4.11E-04 |
| 426.6 | 29.06 | 0.99756 | 1.75E-04 | 0.99661 | 1.34E-03 | 0.99753 | 4.44E-04 |
| 416.9 | 29.74 | 0.99743 | 1.91E-04 | 0.99647 | 1.44E-03 | 0.99740 | 4.80E-04 |
| 407.4 | 30.43 | 0.99731 | 2.09E-04 | 0.99633 | 1.55E-03 | 0.99727 | 5.18E-04 |
| 398.1 | 31.14 | 0.99717 | 2.29E-04 | 0.99618 | 1.67E-03 | 0.99713 | 5.60E-04 |
| 389.0 | 31.87 | 0.99703 | 2.50E-04 | 0.99603 | 1.80E-03 | 0.99698 | 6.05E-04 |
| 380.2 | 32.61 | 0.99688 | 2.73E-04 | 0.99589 | 1.93E-03 | 0.99683 | 6.53E-04 |
| 371.5 | 33.37 | 0.99673 | 2.96E-04 | 0.99574 | 2.06E-03 | 0.99667 | 7.06E-04 |
| 363.1 | 34.15 | 0.99657 | 3.22E-04 | 0.99558 | 2.20E-03 | 0.99651 | 7.64E-04 |
| 354.8 | 34.94 | 0.99640 | 3.51E-04 | 0.99541 | 2.35E-03 | 0.99634 | 8.26E-04 |
| 346.7 | 35.76 | 0.99622 | 3.81E-04 | 0.99524 | 2.51E-03 | 0.99616 | 8.93E-04 |
| 338.8 | 36.60 | 0.99603 | 4.15E-04 | 0.99507 | 2.68E-03 | 0.99598 | 9.65E-04 |
| 331.1 | 37.45 | 0.99584 | 4.51E-04 | 0.99489 | 2.86E-03 | 0.99579 | 1.04E-03 |
| 323.6 | 38.31 | 0.99563 | 4.91E-04 | 0.99471 | 3.05E-03 | 0.99559 | 1.13E-03 |
| 316.2 | 39.21 | 0.99542 | 5.34E-04 | 0.99453 | 3.26E-03 | 0.99539 | 1.22E-03 |
| 309.0 | 40.12 | 0.99520 | 5.81E-04 | 0.99435 | 3.48E-03 | 0.99518 | 1.32E-03 |
| 302.0 | 41.05 | 0.99496 | 6.32E-04 | 0.99417 | 3.71E-03 | 0.99496 | 1.43E-03 |

| | | | | | | | |
|---|---|---|---|---|---|---|---|
| 295.1 | 42.01 | 0.99472 | 6.86E-04 | 0.99399 | 3.96E-03 | 0.99473 | 1.54E-03 |
| 288.4 | 42.99 | 0.99446 | 7.45E-04 | 0.99381 | 4.22E-03 | 0.99450 | 1.66E-03 |
| 281.8 | 44.00 | 0.99419 | 8.09E-04 | 0.99364 | 4.50E-03 | 0.99426 | 1.79E-03 |
| 275.4 | 45.02 | 0.99391 | 8.78E-04 | 0.99349 | 4.78E-03 | 0.99401 | 1.92E-03 |
| 269.1 | 46.07 | 0.99362 | 9.52E-04 | 0.99334 | 5.04E-03 | 0.99375 | 2.07E-03 |
| 263.0 | 47.14 | 0.99331 | 1.03E-03 | 0.99317 | 5.32E-03 | 0.99348 | 2.22E-03 |
| 257.0 | 48.24 | 0.99299 | 1.12E-03 | 0.99299 | 5.61E-03 | 0.99320 | 2.39E-03 |
| 251.2 | 49.36 | 0.99265 | 1.21E-03 | 0.99281 | 5.92E-03 | 0.99291 | 2.57E-03 |
| 245.5 | 50.50 | 0.99229 | 1.32E-03 | 0.99263 | 6.24E-03 | 0.99260 | 2.77E-03 |
| 239.9 | 51.68 | 0.99192 | 1.43E-03 | 0.99245 | 6.59E-03 | 0.99229 | 2.98E-03 |
| 234.4 | 52.89 | 0.99154 | 1.55E-03 | 0.99226 | 6.95E-03 | 0.99197 | 3.21E-03 |
| 229.1 | 54.12 | 0.99113 | 1.68E-03 | 0.99208 | 7.34E-03 | 0.99165 | 3.46E-03 |
| 223.9 | 55.37 | 0.99071 | 1.82E-03 | 0.99190 | 7.76E-03 | 0.99131 | 3.72E-03 |
| 218.8 | 56.67 | 0.99027 | 1.97E-03 | 0.99174 | 8.21E-03 | 0.99097 | 4.01E-03 |
| 213.8 | 57.99 | 0.9898 | 2.13E-03 | 0.99161 | 8.69E-03 | 0.99063 | 4.32E-03 |
| 208.9 | 59.35 | 0.9893 | 2.31E-03 | 0.99152 | 9.17E-03 | 0.99028 | 4.66E-03 |
| 204.2 | 60.72 | 0.9888 | 2.50E-03 | 0.99143 | 9.67E-03 | 0.9899 | 5.02E-03 |
| 199.5 | 62.15 | 0.9883 | 2.71E-03 | 0.99137 | 1.02E-02 | 0.9896 | 5.41E-03 |
| 195.0 | 63.58 | 0.9878 | 2.93E-03 | 0.99134 | 1.08E-02 | 0.9892 | 5.83E-03 |
| 190.6 | 65.05 | 0.9872 | 3.17E-03 | 0.99136 | 1.13E-02 | 0.9889 | 6.28E-03 |
| 186.2 | 66.59 | 0.9866 | 3.43E-03 | 0.99146 | 1.19E-02 | 0.9886 | 6.78E-03 |
| 182.0 | 68.12 | 0.9860 | 3.71E-03 | 0.99164 | 1.26E-02 | 0.9884 | 7.30E-03 |
| 177.8 | 69.73 | 0.9853 | 4.01E-03 | 0.99194 | 1.32E-02 | 0.9882 | 7.76E-03 |
| 173.8 | 71.34 | 0.9847 | 4.33E-03 | 0.99237 | 1.38E-02 | 0.9881 | 8.21E-03 |
| 169.8 | 73.02 | 0.9840 | 4.68E-03 | 0.99310 | 1.44E-02 | 0.9879 | 8.61E-03 |
| 166.0 | 74.69 | 0.9832 | 5.06E-03 | 0.99454 | 1.51E-02 | 0.9878 | 8.92E-03 |
| 162.2 | 76.44 | 0.9825 | 5.46E-03 | 0.99827 | 9.47E-03 | 0.9875 | 9.18E-03 |
| 158.5 | 78.22 | 0.9817 | 5.90E-03 | 0.99434 | 9.90E-03 | 0.9872 | 9.48E-03 |
| 154.9 | 80.04 | 0.9809 | 6.37E-03 | 0.99289 | 1.04E-02 | 0.9868 | 9.79E-03 |
| 151.4 | 81.89 | 0.9800 | 6.87E-03 | 0.99203 | 1.08E-02 | 0.9863 | 1.02E-02 |
| 147.9 | 83.83 | 0.9791 | 7.41E-03 | 0.99142 | 1.13E-02 | 0.9859 | 1.08E-02 |
| 144.5 | 85.80 | 0.9782 | 8.00E-03 | 0.99103 | 1.18E-02 | 0.9855 | 1.15E-02 |
| 141.3 | 87.75 | 0.9772 | 8.63E-03 | 0.99059 | 1.19E-02 | 0.9853 | 1.23E-02 |
| 138.0 | 89.84 | 0.9763 | 9.32E-03 | 0.9899 | 1.20E-02 | 0.9853 | 1.29E-02 |

(*continued*)

**TABLE 1 (*Continued*)**

| | | LiF | | ZnS | | $SiO_2$ | |
|---|---|---|---|---|---|---|---|
| eV | Å | *n* | *k* | *n* | *k* | *n* | *k* |
| 134.9 | 91.91 | 0.9752 | 1.01E-02 | 0.9890 | 1.25E-02 | 0.9853 | 1.34E-02 |
| 131.8 | 94.07 | 0.9742 | 1.09E-02 | 0.9883 | 1.31E-02 | 0.9854 | 1.38E-02 |
| 128.8 | 96.26 | 0.9731 | 1.17E-02 | 0.9878 | 1.38E-02 | 0.9854 | 1.41E-02 |
| 125.9 | 98.48 | 0.9720 | 1.26E-02 | 0.9873 | 1.45E-02 | 0.9854 | 1.43E-02 |
| 123.0 | 100.8 | 0.9709 | 1.36E-02 | 0.9869 | 1.51E-02 | 0.9855 | 1.44E-02 |
| 120.2 | 103.1 | 0.9697 | 1.46E-02 | 0.9864 | 1.57E-02 | 0.9853 | 1.41E-02 |
| 117.5 | 105.5 | 0.9685 | 1.57E-02 | 0.9860 | 1.63E-02 | 0.9849 | 1.39E-02 |
| 114.8 | 108.0 | 0.9672 | 1.69E-02 | 0.9855 | 1.69E-02 | 0.9843 | 1.37E-02 |
| 112.2 | 110.5 | 0.9659 | 1.82E-02 | 0.9850 | 1.76E-02 | 0.9834 | 1.38E-02 |
| 109.7 | 113.0 | 0.9646 | 1.95E-02 | 0.9844 | 1.82E-02 | 0.9827 | 1.39E-02 |
| 107.2 | 115.7 | 0.9631 | 2.10E-02 | 0.9840 | 1.89E-02 | 0.9819 | 1.42E-02 |
| 104.7 | 118.4 | 0.9616 | 2.27E-02 | 0.9835 | 1.96E-02 | 0.9813 | 1.45E-02 |
| 102.3 | 121.2 | 0.9601 | 2.45E-02 | 0.9830 | 2.03E-02 | 0.9809 | 1.48E-02 |
| 100.0 | 124.0 | 0.9588 | 2.67E-02 | 0.9824 | 2.10E-02 | 0.9821 | 1.52E-02 |
| 97.7 | 126.9 | 0.9575 | 2.88E-02 | 0.9818 | 2.17E-02 | 0.9792 | 1.09E-02 |
| 95.5 | 129.8 | 0.9562 | 3.12E-02 | 0.9812 | 2.24E-02 | 0.9762 | 1.16E-02 |
| 93.3 | 132.9 | 0.9550 | 3.37E-02 | 0.9806 | 2.32E-02 | 0.9740 | 1.24E-02 |
| 91.2 | 135.9 | 0.9542 | 3.65E-02 | 0.9800 | 2.40E-02 | 0.9721 | 1.32E-02 |
| 89.1 | 139.2 | 0.9536 | 3.92E-02 | 0.9793 | 2.48E-02 | 0.9702 | 1.40E-02 |
| 87.1 | 142.3 | 0.9531 | 4.16E-02 | 0.9786 | 2.56E-02 | 0.9683 | 1.49E-02 |
| 85.1 | 145.7 | 0.9526 | 4.39E-02 | 0.9779 | 2.65E-02 | 0.9665 | 1.59E-02 |
| 83.2 | 149.0 | 0.9518 | 4.63E-02 | 0.9771 | 2.75E-02 | 0.9646 | 1.69E-02 |
| 81.3 | 152.5 | 0.9511 | 4.88E-02 | 0.9763 | 2.85E-02 | 0.9627 | 1.80E-02 |
| 79.4 | 156.2 | 0.9503 | 5.12E-02 | 0.9755 | 2.96E-02 | 0.9608 | 1.92E-02 |
| 77.6 | 159.8 | 0.9492 | 5.38E-02 | 0.9747 | 3.06E-02 | 0.9588 | 2.04E-02 |
| 75.9 | 163.4 | 0.9479 | 5.67E-02 | 0.9740 | 3.18E-02 | 0.9568 | 2.18E-02 |
| 74.1 | 167.3 | 0.9466 | 6.00E-02 | 0.9732 | 3.29E-02 | 0.9547 | 2.32E-02 |
| 72.4 | 171.2 | 0.9453 | 6.39E-02 | 0.9724 | 3.41E-02 | 0.9525 | 2.46E-02 |
| 70.8 | 175.1 | 0.9444 | 6.84E-02 | 0.9716 | 3.53E-02 | 0.9503 | 2.62E-02 |

| | | | | | | | |
|---|---|---|---|---|---|---|---|
| 69.2 | 179.2 | 0.9438 | 7.35E-02 | 0.9708 | 3.65E-02 | 0.9481 | 2.79E-02 |
| 67.6 | 183.4 | 0.9444 | 7.96E-02 | 0.9700 | 3.77E-02 | 0.9457 | 2.97E-02 |
| 66.1 | 187.6 | 0.9464 | 8.48E-02 | 0.9691 | 3.90E-02 | 0.9434 | 3.16E-02 |
| 64.6 | 191.9 | 0.9492 | 8.97E-02 | 0.9682 | 4.03E-02 | 0.9409 | 3.37E-02 |
| 63.1 | 196.5 | 0.9525 | 9.35E-02 | 0.9673 | 4.16E-02 | 0.9384 | 3.59E-02 |
| 61.7 | 200.9 | 0.9558 | 9.65E-02 | 0.9664 | 4.29E-02 | 0.9359 | 3.82E-02 |
| 60.3 | 205.6 | 0.9593 | 9.94E-02 | 0.9654 | 4.43E-02 | 0.9333 | 4.07E-02 |
| 58.9 | 210.5 | 0.9632 | 0.102 | 0.9646 | 4.58E-02 | 0.9307 | 4.33E-02 |
| 57.5 | 215.6 | 0.9680 | 0.103 | 0.9637 | 4.70E-02 | 0.9279 | 4.61E-02 |
| 56.2 | 220.6 | 0.9738 | 0.104 | 0.9626 | 4.82E-02 | 0.9252 | 4.91E-02 |
| 55.0 | 225.4 | 0.9891 | 0.104 | 0.9614 | 4.95E-02 | 0.9224 | 5.23E-02 |
| 53.7 | 230.9 | 0.9741 | 8.02E-02 | 0.9602 | 5.08E-02 | 0.9196 | 5.56E-02 |
| 52.5 | 236.2 | 0.9650 | 8.37E-02 | 0.9589 | 5.21E-02 | 0.9168 | 5.92E-02 |
| 51.3 | 241.7 | 0.9600 | 8.74E-02 | 0.9576 | 5.35E-02 | 0.9140 | 6.31E-02 |

# Chapter 2

# Convention Confusions

R. T. HOLM
Naval Research Laboratory
Washington, D.C.

I. Introduction 21
II. Units 22
III. Wave Equation 22
IV. Polarization 26
A. Linear Polarization 28
B. Circular Polarization 30
V. Fresnel's Amplitude Reflection Coefficients 37
A. *s* Polarization 38
B. *p* Polarization 40
C. Phase Change 41
VI. Nomenclature 50
VII. Concluding Remarks 51
Acknowledgments 52
References 52

## INTRODUCTION I

As with other scientific fields, optics has its own genre of conventions. The general subject of conventions includes units, symbols, definitions, nomenclature, and sign choices. One of the criticisms of *HOC I* was a lack of a consistent set of conventions by the contributing authors. This criticism can also be voiced about optics literature in general. Almost everyone, even "old hands," has experienced that frustrating feeling of trying to reconcile differences caused by conventions. However, most authors (for whatever reasons) sidestep the convention issue completely.

We do not intend to advocate any particular set of conventions. Instead, we present different conventions that are in general use and discuss conflicts that result because of their differences. We also include reasons that are put forward to justify a particular convention. Here and there, we weave in some history. For a detailed account of the beginnings of the wave theory of light, see the book by Buchwald [1].


Copyright © 1991 by Academic Press.
All rights of reproduction in any form reserved.
ISBN 0-12-544422-2

In this chapter we discuss the plane-wave solutions to the electromagnetic wave equation. The solution of choice dictates which of the two forms of the complex refractive index ($n + ik$ or $n - ik$) is used. We point out that opposite terms are used to label the same polarization state. The different sign conventions used in Fresnel's reflection equations and the subsequent misunderstandings that this leads to are discussed. The various definitions for the expressions *phase change, in phase,* and *out of phase*, and the resulting ambiguities, are presented. Finally, the meanings of *reflection*, *reflectance*, and *reflectivity* are given. We assume the reader has some familiarity with optic and electromagnetic theory.

The actual set of conventions that one uses is completely arbitrary—the physics, after all, has to be independent of convention. As far as we know, Muller has provided the most extensive discussion of different conventions that are used in optics [2]. At the Second International Conference on Ellipsometry, held at the University of Nebraska in 1968, he proposed a standard set of conventions, which have become known as the Nebraska conventions. Bennett and Bennett have also commented on the convention issue [3]. Although the comments and recommendations by Muller and by Bennett and Bennett are addressed primarily to the ellipsometric community, they are relevant to anyone working with electromagnetic waves.

## II UNITS

Since 1960, the single convention in optics that should be standard is electromagnetic units. The *International System of Units*, abbreviated SI units, has been adopted nearly worldwide [4–6]. The SI system is based on the rationalized MKSA (meter, kilogram, second, ampere) system of units. Although most journals request that SI units be used, many authors continue to use one of the other systems (Gaussian, practical [7], and so on). Jackson [8] and Frankl [9] provide enlightening comparisons of the common systems of units and conversion tables between systems. We use SI units in this chapter.

## III WAVE EQUATION

The wave equations for the electric and magnetic fields, as developed in any electromagnetic textbook, are

$$\nabla^2 \mathbf{E} = \varepsilon\varepsilon_0\mu_0 \frac{\partial^2 \mathbf{E}}{\partial t^2} + \sigma\mu_0 \frac{\partial \mathbf{E}}{\partial t} \tag{1a}$$

$$\nabla^2\mathbf{H} = \varepsilon\varepsilon_0\mu_0\frac{\partial^2\mathbf{H}}{\partial t^2} + \sigma\mu_0\frac{\partial\mathbf{H}}{\partial t}, \tag{1b}$$

where **E** is the electric field strength in volt/meter (V/m), **H** is the magnetic field strength in ampere/meter (A/m), $\varepsilon_0$ is the permittivity of free space in coulomb$^2$/newton meter$^2$ (C$^2$/N m$^2$), $\mu_0$ is the permeability of free space in weber/ampere meter (Wb/A m), $\varepsilon$ is the dielectric constant (relative permittivity), and $\sigma$ is the conductivity in siemens/meter (S/m). The wave equations shown above are applicable to media that are homogeneous, isotropic, linear, and nonmagnetic. For simplicity, one usually establishes a right-handed Cartesian coordinate system in which the wave propagates along one axis, say the $z$ axis. For layered media, the $z$ axis is chosen to be perpendicular to the interfaces.

Whether the wave equation is for an electromagnetic wave, a stretched string, or a sound wave, the same four well-known plane-wave solutions apply [10, 11]. These four solutions for the electric field of an electromagnetic wave may be formally expressed in complex form as

$$\mathbf{E} = \mathbf{E}_0 e^{c_1 i(c_2 qz - \omega t)}, \tag{2}$$

where $c_1$ and $c_2$ are sign coefficients and can take the values of $\pm 1$; $q(=2\pi/\lambda)$ is the wave number [12] and is the magnitude of the wave or propagation vector, **q**; $\lambda$ is the vacuum wavelength; $\omega(=2\pi f)$ is the angular frequency; $f$ is the frequency; and $\mathbf{E}_0$ is a vector representing the direction and maximum amplitude of **E**.

In Eq. 2 the coefficient $c_2$ determines the direction of propagation. Time, $t$, is inherently positive and always increasing. When $c_2 = +1$, $z$ must increase so that the phase term $qz - \omega t$ remains constant. Thus, the wave propagates toward increasing $z(+z$ direction). When $c_2 = -1$, the phase term $-qz - \omega t$ remains constant for decreasing $z$, that is, propagation toward decreasing $z(-z$ direction).

As will be discussed shortly, the choice of $c_1$ determines the form in which complex numbers have to be expressed. If $c_1 = +1$, complex numbers take the form $a' + ia''$, whereas if $c_1 = -1$, complex numbers take the form $a' - ia''$, where prime and double prime denote the real and imaginary parts of a complex quantity, respectively. The effects of the values of $c_1$ and $c_2$ are summarized in Table I.

We have now reached the point at which the first arbitrary choice must be made. One has to decide to use either $c_1 = +1$ or $c_1 = -1$, that is, to use either a minus sign or a plus sign in front of $\omega t$. However, whichever choice is made for $c_1$, both values of $c_2$ are admissible. A general solution consists of a linear superposition of two waves propagating in opposite directions.

In the early days of electromagnetic theory, the $\exp[i(\omega t \pm qz)]$ solution was commonly used. Today, most opticists still prefer that solution. However, physicists (at least since the advent of quantum mechanics)

**TABLE I**

**Possible Forms of Solution to Wave Equation, with Corresponding Propagation Direction and Form for Complex Numbers**

| $c_1$ | $c_2$ | $e^{c_1 i(c_2 qz - \omega t)}$ | Propagation direction | Complex numbers |
|---|---|---|---|---|
| 1 | 1 | $e^{i(qz-\omega t)}$ | $+z$ | $a'+ia''$ |
| 1 | −1 | $e^{i(-qz-\omega t)}$ | $-z$ | $a'+ia''$ |
| −1 | 1 | $e^{i(\omega t-qz)}$ | $+z$ | $a'-ia''$ |
| −1 | −1 | $e^{i(\omega t+qz)}$ | $-z$ | $a'-ia''$ |

$$(n+ik)^2=\tilde{\varepsilon}=\varepsilon_\infty\left(1-\frac{\omega_p^2}{\omega(\omega+i\gamma)}+\frac{\omega_L^2-\omega_T^2}{\omega_T^2-\omega^2-i\Gamma\omega}\right)$$

$$(n-ik)^2=\tilde{\varepsilon}=\varepsilon_\infty\left(1-\frac{\omega_p^2}{\omega(\omega-i\gamma)}+\frac{\omega_L^2-\omega_T^2}{\omega_T^2-\omega^2+i\Gamma\omega}\right)$$

Included is the infrared dielectric function for polar semiconductors expressed in the two complex-number forms.

prefer to use the $\exp[i(\pm qz-\omega t)]$ solution. The one-dimensional form of the Schrödinger wave equation for a free particle of mass $m$ is [13]

$$i\hbar\frac{\partial\psi}{\partial t}=-\frac{\hbar^2}{2m}\frac{\partial^2\psi}{\partial z^2}. \tag{3}$$

Note that the Schrödinger equation contains a first derivative with respect to time rather than a second derivative as the electromagnetic wave equation does. As a result, the kinetic energy of the particle is positive [13] only if the $\exp[i(\pm qz-\omega t)]$ solution is used. Being comfortable with this form, physicists carry this solution from quantum mechanics to other fields, such as optics.

Other reasons have been proffered for picking one choice of $c_1$ over the other. One consideration is whether one is dealing with temporal or spatial phenomena. For temporal effects, it is the damping in time at a fixed point in space that is important. In this situation, the angular frequency, $\omega$, is taken as complex [14], so that the imaginary term accounts for damping in time. Hence, it is convenient to choose $\exp(i\omega t)$ and discard the spatial terms.

Circuit theory primarily deals with temporal phenomena, so electrical engineers are usually reared on $\exp(\mathrm{i}\omega t)$. Then, when they study wave propagation, they continue to use the $\exp(i\omega t)$ formalism because that is what they are comfortable with.

Spatial phenomena are primarily concerned with steady-state effects.

For a wave propagating in the $z$ direction, for example, it is the spatial damping that is important. Thus, $q$ is complex, and it is convenient to use $\exp(iqz)$ and to discard the temporal terms. In either case, a positive exponent is chosen, so that one does not continually have to carry a minus sign along when writing equations (laziness).

Many textbooks simply state a solution to the wave equation without discussing reasons for their choice or even mentioning that another possibility exists. Several textbooks first give an abstract solution of the form $f(qz-\omega t)+g(qz+\omega t)$. Then without any explanation, however, they say that it is "convenient" to use the $\exp[i(\omega t \pm qz)]$ solution. An otherwise excellent optics book actually uses both conventions throughout the book. Although each section is consistent within itself, it becomes confusing when comparing sections.

Before leaving this section, let us have that talk about complex numbers. In a lossy material the wave number is complex and given by

$$\tilde{q}=\frac{\omega}{c}\tilde{n}, \tag{4}$$

where $\tilde{n}$ is the complex refractive index and a tilde ($\tilde{}$) signifies complex numbers. All complex quantities must be expressed in the form

$$\tilde{a}=a'+ic_1a'', \tag{5}$$

so that

$$\tilde{q}=q'+ic_1q'', \tag{6a}$$

and

$$\tilde{n}=n+ic_1k, \tag{6b}$$

where $n$ is the refractive index, $k$ is the extinction coefficient [15], and $c_1$ takes the value chosen in Eq. 2. Note that $q'$, $q''$, $n$, and $k$ are all positive. The factor $c_1$ in Eq. 5 assures that a wave decays (rather than grows) exponentially as it propagates; see Table I. To reiterate, if one uses the $\exp[i(\pm qz-\omega t)]$ solution, the complex refractive index must be written $\tilde{n}=n+ik$. For the $\exp[i(\omega t \pm qz)]$ solution, the $\tilde{n}=n-ik$ form is required.

An equation expressed in one form of complex number can be converted to the other form by taking its complex conjugate [16]. As an example, we

have included in Table I the equation for the classical dielectric function, $\tilde{\varepsilon}$, which describes the optical properties of a polar semiconductor in the infrared [17]. Free carriers (second term) and phonons (third term) are formulated in terms of the Drude and Lorentz models, respectively. In the dielectric function $\varepsilon_\infty$ is the high-frequency dielectric constant; $\omega_p$ is the bulk plasma frequency; $\gamma$ is the free-carrier damping constant; $\omega_L$ and $\omega_T$ are the longitudinal and transverse optic-phonon frequencies, respectively; and $\Gamma$ is the phonon damping constant.

One must exercise caution when programming reflectance (and other) formulas that contain complex variables [18]. When taking the square root of a complex number, whether it be in the $(a'+ia'')$ or the $(a'-ia'')$ form, most (all?) compilers will return the answer in the correct form. However, when taking the square root of a negative real number, compilers return a positive imaginary number; for example, $(-4)^{1/2}=+2i$. This is the correct answer for the $(a'+ia'')$ form, but for the $(a'-ia'')$ form, the correct answer is $-2i$.

If one writes one's own programs and uses formulas that require the $(a'-ia'')$ form, it is easy to test complex variables before taking a square root. Just insert a line of code that sets (square root) $=-$(square root) if a complex number has only a negative real part. Such situations arise when calculating internal reflection spectra (IRS) [19], in which terms like $[1-(n_i\sin\theta_i)^2/n_t^2]^{1/2}$, with $n_i\sin\theta_i > n_t$, are encountered. As Spiller [18] points out, commercial computer programs may not offer any provision for setting the form of complex numbers. To obtain the correct answer, either assign negative values to the thicknesses of those films whose extinction coefficients are zero, or set $k$ to some small value that does not significantly affect the results.

Before those who use the $(n-ik)$ form panic, we point out that reflectance programs that do not test complex numbers yield the correct results most of the time. We had used an IRS program successfully for over a year before it gave reflectances greater than unity for a particular IRS configuration. It takes a long time to find such a "bug." To be on the safe side, put in a test.

Finally, let us give a gentle reminder. The form for $\tilde{n}$ (and other complex variables) has nothing to do with the direction of propagation. The form is determined solely by the sign of $\omega t$ in Eq. 2.

## IV POLARIZATION

In addition to its amplitude, frequency, and direction of propagation, an electromagnetic wave is characterized by the orientation of its field vectors,

**E** and **H**. Since, in an isotropic medium, an electromagnetic wave is transverse rather than longitudinal, its field vectors are normal to its wave vector. The temporal behavior of the orientation of the electric field, **E**, as observed at a fixed location along the propagation direction, determines the *polarization state* of the wave [20–22]. The polarization state is represented by the curve traced out by the tip of the instantaneous **E** vector. The electric field is chosen as the descriptor of the polarization state because it exerts a much stronger force on electrons than the magnetic field [23].

Polarization terminology and even the word *polarization* itself [24–26] are perplexing, if not downright contradictory. The first reported observation of an effect arising directly from polarization was by Erasmus Bartholinus [27, 28]. In 1670 he described double refraction, in which two images are seen, in calcite (Iceland spar) [29]. It was not until 1808 that Etienne Louis Malus discovered polarization by reflection. While looking through a calcite crystal at the reflection of the setting sun from a window of a nearby building, he saw only one image, rather than two, for certain orientations of the crystal [30, 31]. Malus introduced the term *polarization* to distinguish the two light beams that emerge from a calcite crystal. We shall now present the various ways that polarization terms are defined and used.

When a phase term $\delta$ is included, four different forms can be found in the literature to express the electric-field strength of a monochromatic wave propagating in the $+z$ direction [2]:

$$\mathbf{E} = \mathbf{E}_0 e^{i(\omega t - qz + \delta)} \tag{7a}$$

$$\mathbf{E} = \mathbf{E}_0 e^{i(\omega t - qz - \delta)} \tag{7b}$$

$$\mathbf{E} = \mathbf{E}_0 e^{i(qz - \omega t + \delta)} \tag{7c}$$

$$\mathbf{E} = \mathbf{E}_0 e^{i(qz - \omega t - \delta)}. \tag{7d}$$

Most authors, when describing polarization, revert to the real form. The real parts of Eq. 7 are

$$\mathbf{E} = \mathbf{E}_0 \cos(\omega t - qz + \delta) \tag{8a}$$

$$\mathbf{E} = \mathbf{E}_0 \cos(\omega t - qz - \delta) \tag{8b}$$

$$\mathbf{E} = \mathbf{E}_0 \cos(qz - \omega t + \delta) = \mathbf{E}_0 \cos(\omega t - qz - \delta) \tag{8c}$$

$$\mathbf{E} = \mathbf{E}_0 \cos(qz - \omega t - \delta) = \mathbf{E}_0 \cos(\omega t - qz + \delta). \tag{8d}$$

Thus, we see that Eqs. 8a and 8d are mathematically equivalent, as are Eqs. 8b and 8c. We shall refer to Eqs. 8a and 8d as the $(\omega t + \delta)$ form, and to Eqs. 8b and 8c as the $(\omega t - \delta)$ form. What is important is the relative sign of the time and phase terms [2, 22, 32]. If the phase term has the same sign as $\omega t$ (that is, $\delta > 0$ with the $(\omega t + \delta)$ form and $\delta < 0$ with the $(\omega t - \delta)$ form), then $\delta$ represents an increase in time, or a phase advance (leading). Likewise, if the sign of the phase term is opposite that of $\omega t$ (that is, $\delta < 0$ with the $(\omega t + \delta)$ form and $\delta > 0$ with the $(\omega t - \delta)$ form), then $\delta$ represents a phase retardation (lagging).

An arbitrary wave, **E**, propagating in the $+z$ direction can be treated as a superposition of two orthogonal waves, $E_x$ and $E_y$, expressed in the $(\omega t - \delta)$ form by

$$\begin{aligned} E_x &= E_{x0} \cos(\omega t - qz - \delta_x) \\ E_y &= E_{y0} \cos(\omega t - qz - \delta_y), \end{aligned} \tag{9a}$$

and in the $(\omega t + \delta)$ form by

$$\begin{aligned} E_x &= E_{x0} \cos(\omega t - qz + \delta_x) \\ E_y &= E_{y0} \cos(\omega t - qz + \delta_y), \end{aligned} \tag{9b}$$

such that

$$\mathbf{E} = \hat{\imath} E_x + \hat{\jmath} E_y, \tag{10}$$

where $\hat{\imath}$ and $\hat{\jmath}$ are unit vectors in the $+x$ and $+y$ directions, respectively, of an (again arbitrary) right-handed Cartesian coordinate system. However, practical considerations based on the experimental system ultimately dictate the selection of a coordinate system. The actual polarization state of the wave depends on the relative values of $E_{x0}$ and $E_{y0}$ and of $\delta_x$ and $\delta_y$. For arbitrary values of $E_{x0}$, $E_{y0}$, $\delta_x$, and $\delta_y$, the wave is *elliptically polarized*. Two special cases result: (A) when $\delta \equiv \delta_y - \delta_x = 0$ or $\pm\pi$; and (B) when $E_{x0} = E_{y0}$ and in addition $\delta = \pm\pi/2$. (Almost every author defines $\delta$ as $\delta_y - \delta_x$, rather than as $\delta_x - \delta_y$.)

## A Linear Polarization

Even though polarization is referenced to the temporal variation of the orientation of **E**, many authors provide a spatial visualization of the

component ($E_x$ and $E_y$) and resultant (**E**) waves at an instant of time. Such a snapshot [22, 33] is shown in Fig. 1 for $\delta = 0$. A sinusoidal curve is an expedient representation of a monochromatic light wave. If we fixed our attention at some point on the $z$ axis, we would see that **E** oscillates, with time, along a fixed line that is normal to the $z$ axis. **E** would change direction every half cycle, having maximum extensions of $\pm E_0$ $[= (E_{x0}^2 + E_{y0}^2)^{1/2}]$. The curve is drawn by connecting the tips of the instantaneous **E** vectors along the $z$ axis at an instant of time. The resultant wave lies in a plane inclined at an angle $\alpha[= \tan^{-1}(E_{y0}/E_{x0})]$ to the $x$ axis. Such a wave is said to be *linearly polarized*. Sometimes a linearly polarized wave is referred to as being *plane polarized* because the wave lies in a plane, as in Fig. 1; however, many authors discourage the use of this term [24, 26].

Three points are worth noting. First, both $E_x$ and $E_y$ in Fig. 1 are also linearly polarized. Second, if $\delta = \pm\pi$, then $E_y$ inverts, which means that **E** lies on the other side of the $x$ axis. Third, both the $(\omega t - \delta)$ and $(\omega t + \delta)$ forms (Eq. 9) give the same description of linear polarization.

Another expression that has long been in disfavor [24, 26] is *plane of polarization*. The plane of polarization, as originally defined by Malus [27], is the plane that is normal to the crystal surface and contains the light ray polarized by reflection. That plane is nothing more than the plane of incidence. Malus' definition was more closely tied to the procedure of producing polarized light than to the physical nature of light. About forty years later, people discovered the vector (**E** and **H**) nature of light, and they figured out that it is actually the **H** field, rather than the **E** field, that lies in Malus' plane of polarization. As a result, some authors have tried to redefine the plane of polarization to be the plane containing **E** and the wave vector **q**; such are the ways that ambiguity raises its evil head.

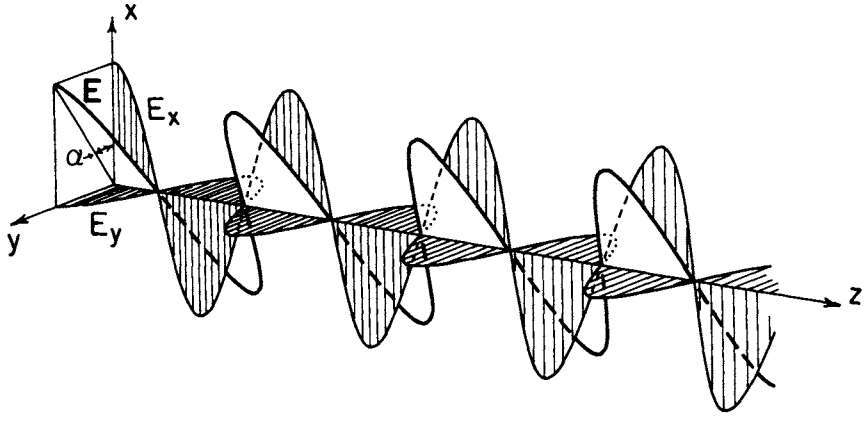


**Fig. 1.** Snapshot of a linearly polarized wave propagating in the $+z$ direction. $E_x$ and $E_y$ are the component fields; **E** is the resultant field inclined at an angle $\alpha$ to the $x$ axis.

To make matters worse, the IEEE has defined the plane of polarization [34] to be the plane containing **E** and **H**. Thus, the IEEE plane of polarization is perpendicular to that of opticists.

Several authors [24, 25] have pointed out that a plane of polarization does not define a unique wave (although a particular wave does have a unique plane of polarization). As an alternative, many authors prefer to prescribe a linearly polarized wave by the direction of its wave vector and the direction of vibration of the **E** field. Clark [26] suggests that azimuth (rather than direction) of vibration is a better term to describe the orientation of the **E** field.

## B Circular Polarization

When $E_{x0} = E_{y0}$ and $\delta = \pm \pi/2$, electromagnetic waves are *circularly polarized*. The sense of rotation depends on the sign of $\delta$ and which form of Eq. 9 is used. Since it is the *difference* between the phases of $E_x$ and $E_y$ that is important, we let $\delta_x = 0$ so that $\delta = \delta_y$. Initially, circular polarization will be described from a strictly mathematical point of view. Then the contradictory ways in which various disciplines label circular polarization will be presented.

### 1 *($\omega t - \delta$) Form*

First, consider the $(\omega t - \delta)$ form with $E_{x0} = E_{y0} = E_0$. The component field equations from Eq. 9a for $\delta = -\pi/2$ are

$$\begin{aligned} E_x &= E_0 \cos(\omega t - qz) \\ E_y &= -E_0 \sin(\omega t - qz), \end{aligned} \tag{11a}$$

and the equations for $\delta = +\pi/2$ are

$$\begin{aligned} E_x &= E_0 \cos(\omega t - qz) \\ E_y &= E_0 \sin(\omega t - qz). \end{aligned} \tag{11b}$$

Figure 2a shows a plot of the $E_x$ and $E_y$ components as a function of $\omega t$ for $\delta = -\pi/2$, and Fig. 2b shows a similar plot for $\delta = +\pi/2$. It can be seen that when $\delta = -\pi/2$, $E_y$ leads $E_x$ by $\pi/2$ (Fig. 2a), whereas when $\delta = +\pi/2$, $E_y$ lags $E_x$ by $\pi/2$ (Fig. 2b).

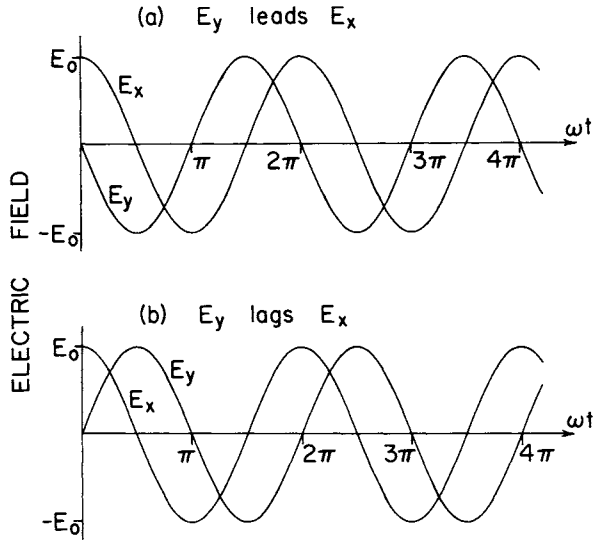


**Fig. 2.** The orthogonal components of circularly polarized waves as a function of time. In (a) $E_y$ leads $E_x$, and in (b) $E_y$ lags $E_x$.

Recall that the resultant field, **E**, is the vectorial sum (Eq. 10) of $E_x$ and $E_y$ and that polarization is related to the time variation of **E** at a fixed location along $z$. Figures 3a and 3b show the position (orientation) of **E** in the $x$–$y$ plane located at $z=0$, at several values of $\omega t$, for $\delta=-\pi/2$ and $\delta=+\pi/2$, respectively. In Fig. 3a, **E** rotates, with constant amplitude and angular frequency $\omega$, from the positive $x$ axis toward the negative $y$ axis. In

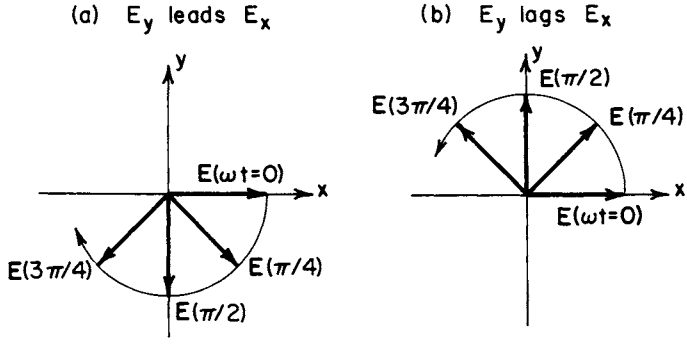


**Fig. 3.** Orientation of the field vector, **E**, of circularly polarized waves at several values of $\omega t$, with the sense of rotation indicated. In (a) $E_y$ leads $E_x$ (right-handed, traditional optics), and in (b) $E_y$ lags $E_x$ (left-handed).

contrast, **E** rotates from the positive $x$ axis toward the positive $y$ axis in Fig. 3b.

## 2 $(\omega t+\delta)$ Form

Let us now repeat the above procedure for the $(\omega t+\delta)$ form. The component field equations from Eq. 9b for $\delta=-\pi/2$ are

$$\begin{aligned} E_x &= E_0\cos(\omega t-qz) \\ E_y &= E_0\sin(\omega t-qz), \end{aligned} \tag{12a}$$

and the equations for $\delta=+\pi/2$ are

$$\begin{aligned} E_x &= E_0\cos(\omega t-qz) \\ E_y &= -E_0\sin(\omega t-qz). \end{aligned} \tag{12b}$$

We see that Eq. 12a is identical to Eq. 11b and that Eq. 12b is identical to Eq. 11a. Thus, it is apparent that Fig. 2b ($E_y$ lags $E_x$) and Fig. 3b are applicable to the $(\omega t+\delta)$ form when $\delta=-\pi/2$. Likewise, Fig. 2a ($E_y$ leads $E_x$) and Fig. 3a are applicable to the $(\omega t+\delta)$ form when $\delta=+\pi/2$.

We suspect that the reader feels befuddled by now. The crux of the analysis can be summarized in two statements.

(1) If the phase term has the same (opposite) sign as $\omega t$, then $E_y$ leads (lags) $E_x$ (see the discussion between Eqs. 8 and 9).

(2) If $E_y$ leads (lags) $E_x$, then the sense of rotation of **E** is from the positive $x$ axis toward the negative (positive) $y$ axis [35].

## 3 Spatial Visualization

In addition to the temporal pictures given in Figs. 2 and 3, many authors also present a spatial visualization. Let us do so at $\omega t=0$. Rather than depicting in detail the four combinations obtained from the $(\omega t\pm\delta)$ forms with $\delta=\pm\pi/2$, it will suffice to consider only one combination, let us say the $(\omega t-\delta)$ form with $\delta=-\pi/2$.

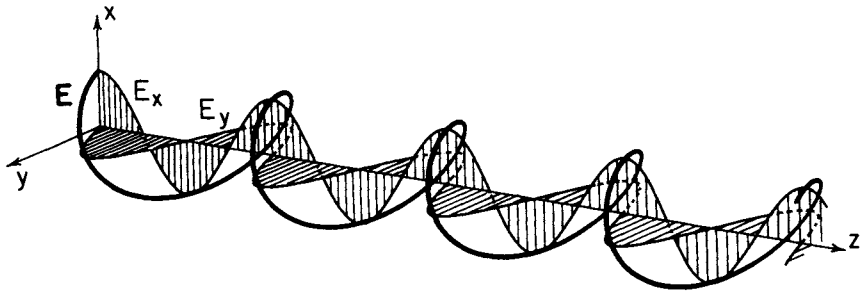


**Fig. 4.** Spatial representation (snapshot) of a circularly polarized wave propagating in the $+z$ direction. $E_x$ and $E_y$ are the component fields; **E** is the resultant field, in the form of a right-handed helix.

The component fields are

$$E_x = E_0 \cos(qz)$$
$$E_y = E_0 \sin(qz). \tag{13}$$

The tip of the vector representing the resultant field, **E**, traces out a helix whose axis coincides with the $z$ axis. The helix, along with the component fields, is shown in Fig. 4. The helix has the same pitch direction as a right-handed screw. The $(\omega t - \delta)$ form with $\delta = +\pi/2$ gives a left-handed helix. As one would expect (by now, we hope), the $(\omega t + \delta)$ form with $\delta = +\pi/2$ and $\delta = -\pi/2$ results in right-handed and left-handed helices, respectively. Note that the handedness of a helix is independent of an observer's viewpoint—a right-handed screw looks like a right-handed screw, no matter from what direction you look at it.

The temporal behavior of the helix has been the subject of some confusion. Several authors [36–38] have stated that the helix rotates as time increases, whereas others [39–41] point out that the helix moves forward without rotating. Since both scenarios cannot be correct, which one is?

Figure 5 shows six snapshots of a right-handed helix at $\omega t = \pi$ for the first snapshot and incrementing by $\pi/4$ for each succeeding snapshot. The spatial patterns of the component and resultant waves are shown between $z = 0$ and $z = 2\lambda$. In addition, the resultant **E** vector lying in the $x$–$y$ plane at $z = (9/8)\lambda$ is shown. If the helix were to rotate as it moved forward, then the resultant **E** vector at a fixed point (say, at $z = (9/8)\lambda$) would remain fixed in space. Any ***E*** vector in front of the $x$–$y$ plane at $z = (9/8)\lambda$ would rotate into the position shown in the top picture in Fig. 5 as it passed through that plane. The helix would appear to be passing through a hole, located at the tip of the **E** vector, in the $x$–$y$ plane. Therefore, in order for

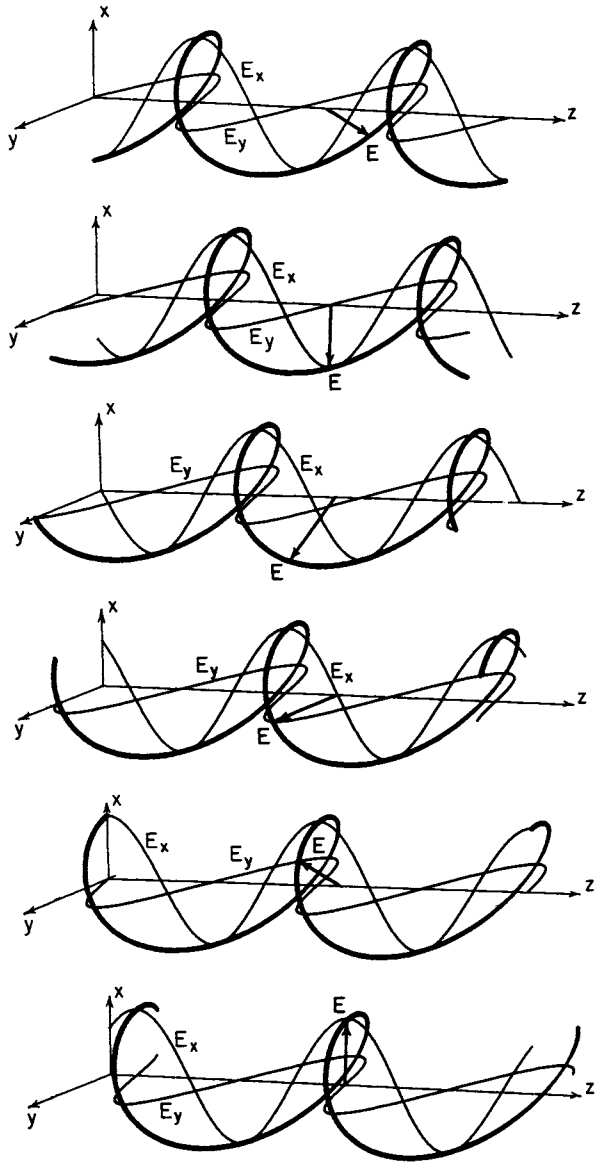


**Fig. 5.** Snapshots of a propagating circularly polarized wave and its components. The snapshots, taken every $\pi/4\omega$ of a second, show the wave between $z=0$ and $z=2\lambda$. The field vector, **E**, at $z=9\lambda/8$ rotates clockwise, as viewed by looking toward the source ($-z$ direction).

the resultant **E** vector to rotate in a plane, the helix must move forward without rotating, as demonstrated in Fig. 5. As the helix moves forward a distance of $\lambda$, it scribes out a complete circle in any $x$–$y$ plane.

## Terminology 4

The terminology used to classify circular polarization varies with country and field of science and has changed with time [42]. To begin with, there are two ways to view a circularly polarized wave: opticists and physicists prefer to look into the oncoming wave (that is, toward the source); and radio and microwave engineers usually look at the receding wave (that is, in the direction of propagation). Thus, opticists and physicists say that **E** is rotating clockwise in Fig. 3a and counterclockwise in Fig. 3b, whereas engineers say just the opposite. As the reader looks at Fig. 3, the $+z$ axis is normal to the page and pointing toward the reader. Therefore, the view corresponds to the optics convention of looking toward the source. Engineers would be behind the figure looking out at the reader.

When explaining the convention you use to define clockwise and counterclockwise, it is important to be specific and to avoid ambiguous phrases, such as "as seen looking down the beam." Which direction is down?

The traditional optics convention refers to the clockwise (counterclockwise) rotating field **E** as being right (left) circularly polarized. One reason for this is that the spatial pattern for a right-handed (left-handed) wave would then be a right-handed (left-handed) helix, even though polarization is supposed to be referenced to the temporal variation. Of course, the helix serves as a good mnemonic, since its sense of inclination is invariant to the point of observation.

Engineers usually reverse the definitions for the handedness of circularly polarized waves [34, 43–45]. For them, the **E** vector of a right-handed wave rotates clockwise (as seen looking in the direction of propagation), but has a left-handed helix. This definition is appropriate for a right-handed, helical-beam antenna, which receives right circular (left-handed helix) polarization [45].

As everyone knows, a light wave has a linear momentum **p**. In addition, a circularly polarized wave also carries an angular momentum **L** [46–51]. The direction of angular momentum is obtained from the right-hand rule. When the right hand curls around the direction of propagation with the fingers pointing in the direction that **E** is rotating (see Fig. 3), the thumb points in the direction of the angular momentum. Thus, the linear and angular momenta of a left circularly polarized wave (traditional optics definition) point in the same direction, whereas they point in opposite directions for a right circularly polarized wave. The direction that the angular momentum of the wave points determines whether electron or

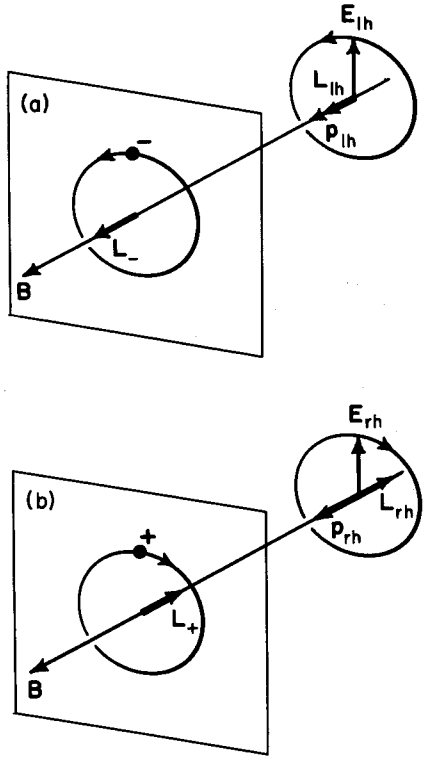


**Fig. 6.** Schematic representation of (a) electron and (b) hole cyclotron resonance. The charge carriers revolve in a plane normal to the applied dc magnetic induction, **B**. The election and hole angular momenta are $\mathbf{L}_-$ and $\mathbf{L}_+$, respectively. The angular momenta of the left and right circularly polarized waves are $\mathbf{L}_{lh}$ and $\mathbf{L}_{rh}$, respectively, and the linear momenta are $\mathbf{p}_{lh}$ and $\mathbf{p}_{rh}$.

hole cyclotron resonance is excited in a semiconductor [52]. As depicted schematically in Fig. 6, left and right circularly polarized waves are propagating in the direction of the applied dc magnetic induction, **B**. In Fig. 6a, electrons revolve counterclockwise around **B** (looking against **B**), and in Fig. 6b, holes revolve clockwise around **B**. Electron and hole angular momenta are parallel and antiparallel to **B**, respectively. In order to satisfy selection rules [52], the angular momentum of a circularly polarized wave must point in the same direction as that of the charge carrier. Therefore, electrons absorb left circular polarization, and holes absorb right circular polarization.

Modern physics has also seen fit to reverse the meaning of right-handed from that of traditional optics. The convention of particle physics is that both the linear momentum and the angular momentum of a right-handed

wave point in the same direction. Thus, the wave represented in Fig. 3b is right-handed in modern physics.

## FRESNEL'S AMPLITUDE REFLECTION COEFFICIENTS V

Augustin Fresnel's derivation in 1823 of the amplitude reflection coefficients of light waves is a classic case of knowing the answer and working backwards [53]. Working nearly fifty years before Maxwell published his electromagnetic theory, Fresnel was fettered by a bogus concept known as the *luminiferous ether (aether)*. Making an analogy between sound and light, early scientists had postulated the existence of the ether. Since sound could not propagate in vacuum, it seemed logical that light could not either, that it needed some medium which filled all space out to the farthermost star [54]. Even though common sense (at that time) dictated the existence of the ether, common sense was noticeably absent when the ether was endowed with some rather remarkable properties [55]: it must be millions of times more rigid than steel to transmit waves having the frequency and velocity of light; it offers no resistance to the passage of the earth and planets around the sun; and it is composed of extremely minute particles, far smaller than atoms.

Working within the *elastic-solid theory*, Fresnel adjusted his concept of the ether until he was able to derive reflection formulas that agreed with experiment [56]. Fresnel knew that something was vibrating, and whatever it was, the vibration was transverse to the direction of propagation. He also assumed that the vibration was normal to the plane of polarization (the $\mathbf{q} - \mathbf{H}$ plane). He finally based his concept of the elastic-solid theory on the following three tenets [57]:

(1) Conservation of energy—the energy of the incident wave is equal to the sum of the energies of the reflected and transmitted waves.

(2) Uniform elasticity—the densities of the ether in each medium could be different, but not the elasticity (the ether is incompressible).

(3) Continuity of displacement—there is no tangential slipping of the ether across the interface.

Using these principles and without any knowledge of the electromagnetic character of light waves, Fresnel was able to derive the correct formulas.

Since Maxwell's time, however, Fresnel's reflection coefficients have been derived in the more familiar way of using the **E** and **H** fields and their associated boundary conditions. In 1890, Otto Wiener demonstrated that a node in the electric field exists at the surface of a mirror, indicating that the electric field reverses phase upon reflection at normal incidence [58, 59].

Thus, the reflection coefficients are usually derived in terms of the electric field. The standard procedure is to resolve the electric field of the incident wave into two orthogonal, linearly polarized components, one normal to the plane of incidence ($E_s$), and the other parallel ($E_p$). These two components are then treated as independent cases.

For both the normal case and the parallel case, three waves are involved—incident, reflected, and transmitted—and each of the three waves can be represented by an **E** vector that can point in one of two opposite directions. The first step is to pick the direction for the **E** vector of the incident wave. This choice may depend on many factors, including type of experiment, personal preference, academic heritage, and so on. The second step is to select the direction for the reflected (and transmitted) **E** vector. Hindsight usually influences this choice. We do not know a priori in which direction the **E** field of the reflected wave will point; indeed, its direction depends on the relative refractive indices of the two contiguous media at the interface. It does not matter which direction we choose because the reflection coefficient will ultimately provide the correct direction for the reflected **E** field relative to that of the incident wave. Since each field can point in one of two opposite directions, there are eight possible arbitrary ways to arrange the three electric fields at the interface for both the normal and parallel cases. Fortunately, all eight configurations of each case have not been used; but those used have been enough to cause confusion. Luckily, some are redundant in that they give the same expressions for the reflection coefficients [60].

In general, reflection must be treated as a three-dimensional problem. Thus, an orthographiclike drawing aids the reader in visualizing the field vectors in relation to the plane of incidence and the reflecting surface. Over the past forty years or so, several excellent variations [61–68] have been presented. Figure 7 is typical of the type presented to depict the relative orientations of the field vectors of the incident, reflected, and transmitted waves. The coordinate system has been chosen so that the reflecting surface is in the $x$–$y$ plane and the plane of incidence is in the $y$–$z$ plane. The angles of incidence and transmission, related by Snell's law, are $\theta_i$ and $\theta_t$, respectively.

## A *s* Polarization

In Fig. 7a, the electric fields are normal to the plane of incidence. Such waves are usually denoted as $s$-polarized, transverse electric (TE), or $\perp$ waves. Almost every author has chosen $E_{is}$, $E_{rs}$(FC), and $E_{ts}$ to point in the same direction [69, 70], which is usually the $+x$ direction. The subscripts, is, rs, and ts, designate the incident, reflected, and transmitted waves,

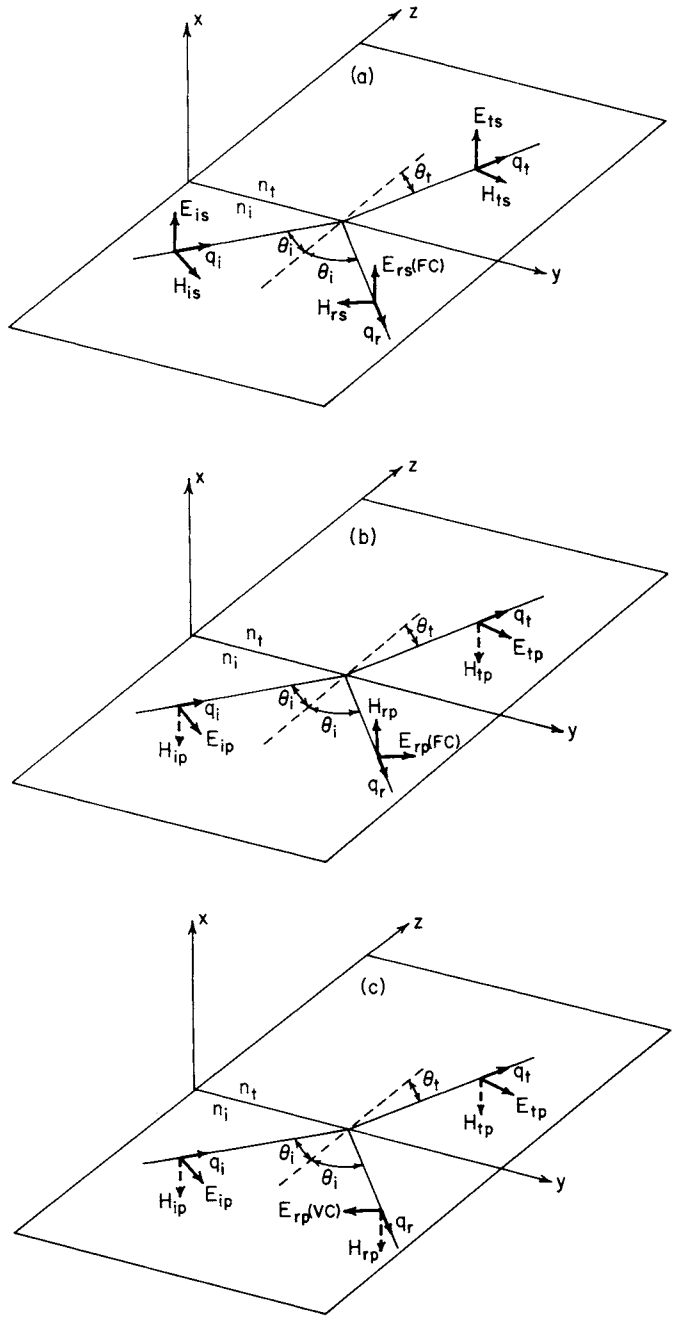


**Fig. 7.** The conventions used to derive the Fresnel reflection coefficients. The field (**E** and **H**) and wave (**q**) vectors of the incident (i), reflected (r), and transmitted (t) waves are shown for (a) *s* polarization, (b) *p* polarization, Fresnel convention, and (c) *p* polarization, Verdet convention.

respectively, for *s* polarization. The FC label attached to the reflected wave in Fig. 7a signifies the Fresnel convention. We use this label to emphasize that $E_{rs}(FC)$ is an arbitrarily selected vector from which one derives the Fresnel reflection coefficient. The actual reflected field may point in the same direction as the convention vector in Fig. 7a or in the opposite direction. Once the direction of **E** is chosen, the direction of **H** is determined by $\mathbf{q} \times \mathbf{E} = \omega\mu_0 \mathbf{H}$.

It must be pointed out that Fig. 7 is just a schematic representation of the actual situation. Although it is the field vectors located at the interface that satisfy the boundary conditions, the field vectors are drawn some distance from the interface for clarity [71]. In addition, the vectors represent peak values, rather than instantaneous values, and the direction each vector points is defined as the positive direction for that vector [72]. The Fresnel amplitude reflection coefficient for *s* polarization is [73]

$$\tilde{r}_s \equiv \frac{E_{rs}(FC)}{E_{is}} = \frac{\tilde{n}_i \cos\theta_i - \tilde{n}_t \cos\theta_t}{\tilde{n}_i \cos\theta_i + \tilde{n}_t \cos\theta_t} = -\frac{\sin(\theta_i - \theta_t)}{\sin(\theta_i + \theta_t)}, \tag{14}$$

where $\tilde{n}_i$ and $\tilde{n}_t$ are the complex refractive indices of the incident and transmission media, respectively.

## B *p* Polarization

For the other case in which the electric field is parallel to the plane of incidence, a wave is denoted as a *p*-polarized, transverse magnetic (TH), or ∥ wave. One of the oldest (and continuing) controversies in optics is associated with the sign of the reflection coefficient for *p* polarization. Fresnel felt that the tangential component of the displacement associated with the reflected wave should point in the same direction as that of the incident wave [74]. This means, in electromagnetic terms, that the tangential components of $E_{ip}$ and $E_{rp}(FC)$ point in the same direction, as shown in Fig. 7b. For this situation, the Fresnel amplitude reflection coefficient for *p* polarization is [75]

$$\tilde{r}_p(F) \equiv \frac{E_{rp}(FC)}{E_{ip}} = \frac{\tilde{n}_i \cos\theta_t - \tilde{n}_t \cos\theta_i}{\tilde{n}_i \cos\theta_t + \tilde{n}_t \cos\theta_i} = -\frac{\tan(\theta_i - \theta_t)}{\tan(\theta_i + \theta_t)}. \tag{15}$$

Fresnel argued for this form because at normal incidence ($\theta_i = 0°$), $r_s = r_p(F)$. It was intuitively consistent because at normal incidence there

is no distinction between *s* and *p* polarizations. However, and herein lies the root of the controversy, at glancing incidence ($\theta_i \to 90°$), $r_s = -r_p(F)$.

When Verdet published Fresnel's work, he changed the sign of $r_p$ because he felt that $r_s$ should equal $r_p$ at glancing incidence rather than at normal incidence [76]. This is equivalent to reversing the direction of the **E** vector of the reflected wave, as shown by $E_{rp}(VC)$ in Fig. 7c, where the VC label signifies the Verdet convention. Thus, in this case, the form of the reflection coefficient for *p* polarization is [73]

$$\tilde{r}_p(V) \equiv \frac{E_{rp}(VC)}{E_{ip}} = \frac{\tilde{n}_t \cos\theta_i - \tilde{n}_i \cos\theta_t}{\tilde{n}_t \cos\theta_i + \tilde{n}_i \cos\theta_t} = \frac{\tan(\theta_i - \theta_t)}{\tan(\theta_i + \theta_t)}. \tag{16}$$

There is nothing wrong with $r_s = -r_p(V)$ at normal incidence. Figures 7a and 7c do not correspond to the same convention at $\theta_i = 0°$, so why should $r_s$ necessarily equal $r_p$?

The reasons for choosing either Fig. 7b or 7c have changed over time. Now they are related to whether one relates the field vectors to a coordinate system tied to the sample surface or to a coordinate system localized with the field vectors themselves [77].

Fresnel's reflection formula for *p* polarization was not universally accepted in the beginning because it did not completely agree with experiment. (Presumably, the data were in error.)

## Phase Change C

Everyone knows that an electromagnetic wave "suffers a phase change" upon reflection. As expected, the various conventions discussed so far result in different phase changes. However, as we shall show, they all yield the same reflected $\mathbf{E}_r$ field in the final analysis. There is, in addition, no consensus on the meanings of the expressions *in phase* and *out of phase*. We shall first give the pertinent mathematical expressions for reflection phase change. Next, we shall summarize some of the ideas about phase change that are encountered in the literature. Finally, we shall discuss the physical significance of phase change.

The Fresnel reflection coefficients may be formally expressed in the form

$$\tilde{r}_s \equiv r'_s + ir''_s = |r_s| e^{i\delta_s} \tag{17a}$$

$$\tilde{r}_p \equiv r'_p + ir''_p = |r_p| e^{i\delta_p}, \tag{17b}$$

where

$$|r_{s,p}| = [(r'_{s,p})^2 + (r''_{s,p})^2]^{1/2} \tag{18a}$$

$$\delta_{s,p} = \tan^{-1}\left(\frac{r''_{s,p}}{r'_{s,p}}\right). \tag{18b}$$

The corresponding electric fields for the reflected waves are given by

$$E_{rs}(F) = |r_s| e^{i\delta_s(F)} E_{is} \tag{19a}$$

$$E_{rp}(F, V) = |r_p| e^{i\delta_p(F,V)} E_{ip}, \tag{19b}$$

where $E_{is}$ and $E_{ip}$ point as shown in Fig. 7. $E_{rs}(F)$ and $E_{rp}(F,V)$ are the actual reflected fields for $s$ and $p$ polarization, respectively, and are distinguished from the fields $E_{rs}(FC)$ and $E_{rp}(FC,VC)$ used to establish the reflection conventions in Fig. 7.

The reflection phase changes (shifts), $\delta_s$ and $\delta_p$, are usually thought of as the difference between the phases of the incident and reflected waves. However, this thought is somewhat misleading. Electric field, being a vector, has a magnitude and a direction. Equations like Eq. 19 account for the magnitude. The direction is implicit through the conventions expressed in Fig. 7. Therefore, it is more apropos to think of $\delta_p$ as the difference between the phases of $E_{rp}(F,V)$ and $E_{rp}(FC,VC)$, with $E_{rp}(FC,VC)$ related to $E_{ip}$ through Fig. 7. $E_{rp}(FC,VC)$ acts as an intermediary between $E_{rp}(F,V)$ and $E_{ip}$. In other words, $E_{rp}(F,V)$ is what $E_{rp}(FC,VC)$ looks like after $r_p(F,V)$ is taken into account. Similar points of view hold for $\delta_s$. Since the phase change also depends on whether one uses $(n+ik)$ or $(n-ik)$, there are two expressions for $\delta_s$ and four expressions for $\delta_p$. From Eqs. 14–18, one finds

$$\begin{array}{lll} & \underline{n+ik \text{ form}} & \underline{n-ik \text{ form}} \\ \delta_s = & \tan^{-1}\left(\dfrac{-s_{num}}{s_{den}}\right) & \tan^{-1}\left(\dfrac{s_{num}}{s_{den}}\right) \\ \delta_p(V) = & \tan^{-1}\left(\dfrac{p_{num}}{p_{den}}\right) & \tan^{-1}\left(\dfrac{-p_{num}}{p_{den}}\right) \\ \delta_p(F) = & \tan^{-1}\left(\dfrac{-p_{num}}{-p_{den}}\right) & \tan^{-1}\left(\dfrac{p_{num}}{-p_{den}}\right), \end{array} \tag{20}$$

where

$$s_{\text{num}} = 2\beta \cos \theta_i \tag{21a}$$

$$s_{\text{den}} = \cos^2 \theta_i - \alpha^2 - \beta^2 \tag{21b}$$

$$p_{\text{num}} = 2 \cos \theta_i [2n_t k_t \alpha - (n_t^2 - k_t^2)\beta] \tag{21c}$$

$$p_{\text{den}} = (n_t^2 + k_t^2)^2 \cos^2 \theta_i - \alpha^2 - \beta^2 \tag{21d}$$

$$\alpha^2 = \tfrac{1}{2}\{[(n_t^2 - k_t^2 - \sin^2 \theta_i)^2 + (2n_t k_t)^2]^{1/2} + n_t^2 - k_t^2 - \sin^2 \theta_i\} \tag{21e}$$

$$\beta^2 = \tfrac{1}{2}\{[(n_t^2 - k_t^2 - \sin^2 \theta_i)^2 + (2n_t k_t)^2]^{1/2} - n_t^2 + k_t^2 + \sin^2 \theta_i\}, \tag{21f}$$

where num and den refer to numerator and denominator, respectively [78], and assuming $n_i = 1$. Note that the equation for $\delta_p(\text{F}, n + ik)$ has a minus sign in both the numerator and the denominator. As we shall show, one must not inadvertently cancel out these minus signs.

There is another, equivalent expression for the numerator of the reflection phase shift for $p$ polarization; this alternative form was derived by Abelès and is used by some authors [79–81]. Abelès expressed the reflection coefficients in terms of effective refractive indices. For $p$ polarization these are $n_i^{\text{eff}} = 1/\cos \theta_i$ and $\tilde{n}_t^{\text{eff}} = \tilde{n}_t/\cos \theta_t$, with $n_i = 1$. In the Abelès method, $p_{\text{num}}$ (Abelès), which is equivalent to $p_{\text{num}}$ in Eq. 21c, is given by

$$p_{\text{num}}(\text{Abelès}) = 2 \cos \theta_i \beta(\alpha^2 + \beta^2 - \sin^2 \theta_i). \tag{22}$$

Figure 8 presents the phase changes as a function of the angle of incidence, $\theta_i$, calculated from Eq. 20 for steel ($\lambda = 589.3$ nm, $n_t = 2.485$, $k_t = 3.432$) [82, 83]. The $(n + ik)$ forms are in Fig. 8a and the $(n - ik)$ forms in Fig. 8b. Note that the four $\delta_p$ curves are different, as are the two $\delta_s$ curves. Figures 8a and 8b are mirror images of each other, and the $\delta_p$ curves in Fig. 8a differ by 180°, as do those in Fig. 8b.

Care must be exercised to place $\delta_s$ and $\delta_p$ in the correct quadrant of the complex $r_s$ and $r_p$ planes, especially when calculating phase changes with a computer. By convention, angles are measured positive in a counterclockwise direction starting from the positive real axis [84]. One must test separately the signs of the numerator and denominator to determine proper placement. If both $r'$ and $r''$ are positive (negative), $\delta$ lies in quadrant I (III). If $r'$ is positive (negative) and $r''$ is negative (positive), $\delta$ lies in quadrant IV (II). Thus, $\tan^{-1}(a/b)$ and $\tan^{-1}(-a/-b)$ differ by

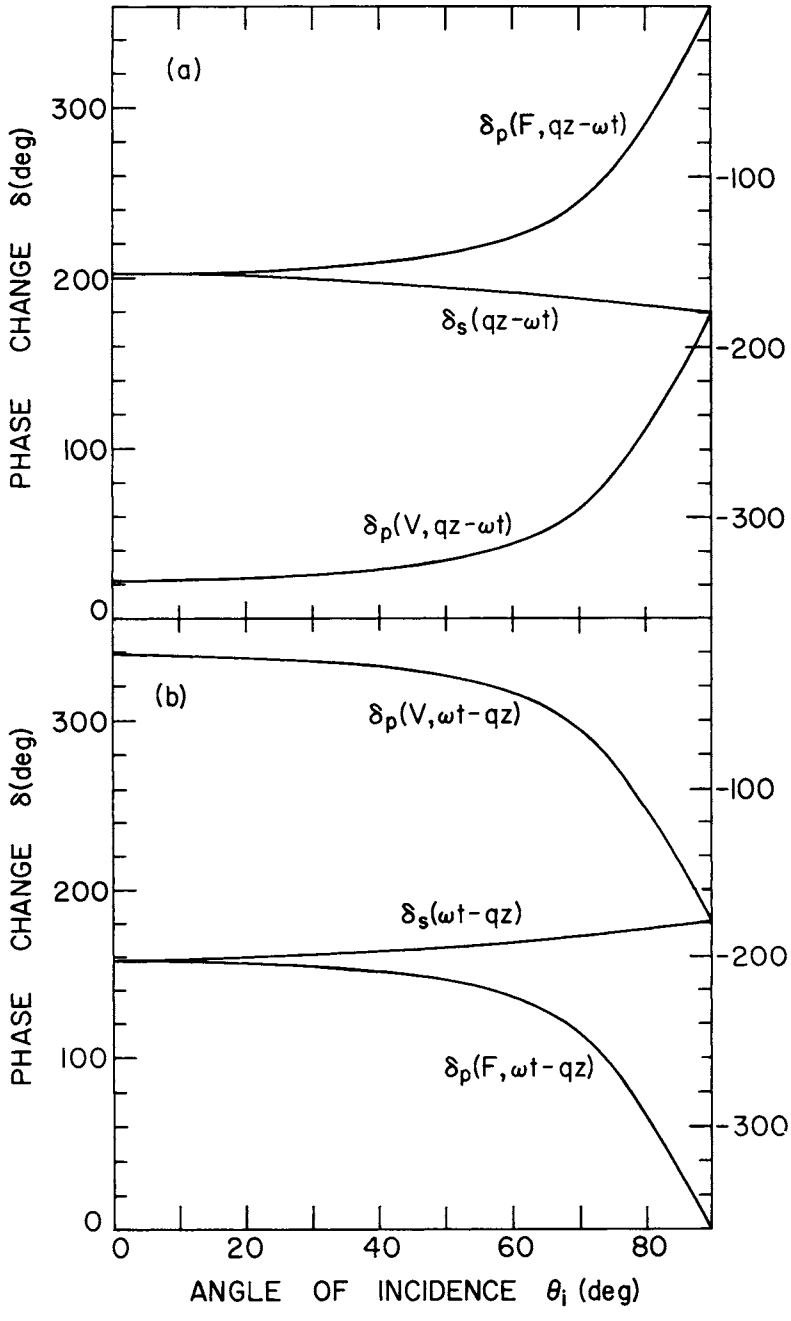


**Fig. 8.** Reflection phase change for steel as a function of the angle of incidence for (a) the $(n+ik)$ form and (b) the $(n-ik)$ form.

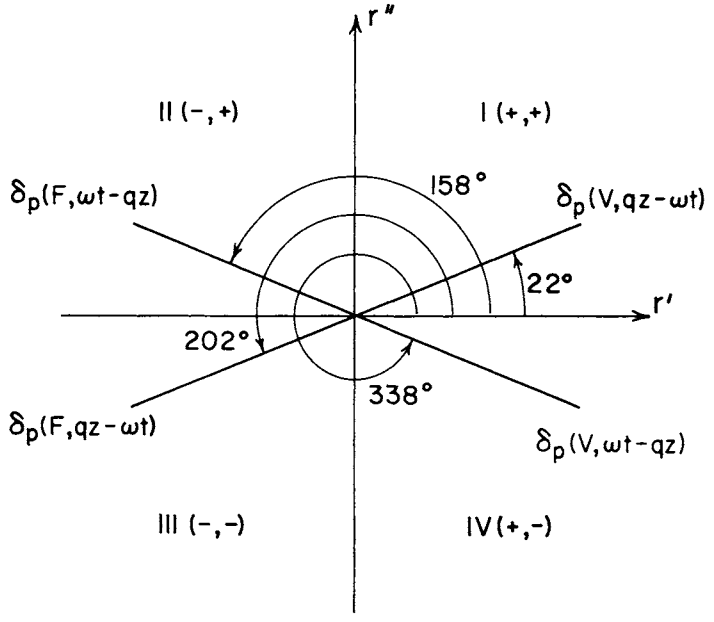


**Fig. 9.** The four values of $\delta_p$ at $\theta_i = 0°$ from Fig. 7, located in the complex $\tilde{r}$ plane.

180°. As an example, Fig. 9 shows the four $\delta_p$ phase changes from Fig. 8 for $\theta_i = 0°$.

Even though the four values of $\delta_p$ in Fig. 9 are different, each is correct within its own convention. It is easy to show that they all yield the identical reflected field, $E_r$ (as they must!). For example, from Eq. 19b,

$$\begin{aligned} E_{rp}(F, n+ik) &= |r_p| e^{i202°} E_{ip0} e^{-i\omega t} \\ &= |r_p| E_{ip0} e^{i(360° - 158° - \omega t)} \\ &= |r_p| E_{ip0} e^{-i(158° + \omega t)} \\ &= E_{rp}(F, n-ik), \end{aligned} \tag{23}$$

remembering to take the real parts [85]. Likewise, $E_{rp}(V, n-ik) = E_{rp}(F, n-ik)$ when one takes into account the fact that the $p$-polarized reflected $E$ fields in Fig. 7 point in opposite directions for the Fresnel and Verdet conventions.

There is a nitpicking point (which we have never seen discussed) that a purist might raise concerning Eq. 17 when $\tilde{n} = n - ik$ is used. Since complex quantities must then be expressed in an $(a' - ia'')$ form, why is Eq. 17 not

written as

$$\tilde{r}_s \equiv r'_s - ir''_s = |r_s| e^{-i\delta_s} \tag{24a}$$

$$\tilde{r}_p \equiv r'_p - ir''_p = |r_p| e^{-i\delta_p}, \tag{24b}$$

where again

$$\delta_{s,p} = \tan^{-1}\left(\frac{r''_{s,p}}{r'_{s,p}}\right)? \tag{25}$$

Equation 24 is the complex conjugate of Eq. 17. If one rederives the expressions for the $(n-ik)$ form of $\delta_{s,p}$ from Fresnel's reflection coefficients using Eqs. 24 and 25, one finds that they are the same as those in Eq. 20 for the $(n+ik)$ form. In other words, the same numeric values are obtained for $\delta_{s,p}$ whether $\tilde{n} = n + ik$ or $\tilde{n} = n - ik$ is used.

The expressions *phase change, in phase*, and *out of phase* convey a sense of comparison or relation. The meanings of these expressions are a matter of definition and, of course, different people prescribe different definitions. Essentially, there are two approaches in defining *in phase* and *out of phase*. In one approach, positive phase is associated with some particular direction [86]. The other approach is concerned with the superposition of the incident and reflected waves. The relevant points can be made by considering reflection from a dielectric ($k_t = 0$).

Figure 10 shows incident and reflected electric-field vectors, $\mathbf{E}_i$ and $\mathbf{E}_r$, respectively, for reflection from a more dense optical medium (that is, $n_i < n_t$). The angle of incidence, $\theta_i$, is less than Brewster's angle in Fig. 10a and greater in Fig. 10b. The incident and reflected waves are resolved into their *s* and *p* polarized components, with $E_{rs}$ and $E_{rp}$ pointing in the correct directions after reflection [87]. As is commonly done [88–90], separate coordinate systems are attached to the incident and reflected waves. The coordinate systems are oriented so that they are right-handed as the viewer looks into the oncoming wave [91, 92], with $E_{ip}$ and $E_{is}$ pointing in the positive *x* and *y* directions, respectively. (Note that in Fig. 7 the coordinate system is attached to the sample). The coordinate system for the reflected wave has the same relative orientation as that of the incident wave [93]. For *s* polarization, everything is fairly straightforward. Incident and reflected fields are colinear. In Fig. 10, $E_{rs}$ points in the opposite direction as $E_{is}$ and is $\pi$ out of phase with respect to $E_{is}$. If $r_s$ is positive (reflection from a less optically dense medium), $E_{rs}$ and $E_{is}$ point in the same direction and are in phase. The above two statements are true for all angles of incidence (except above the critical angle for the latter statement [94]).

The situation is not as clear-cut for *p* polarization, in which electric-field

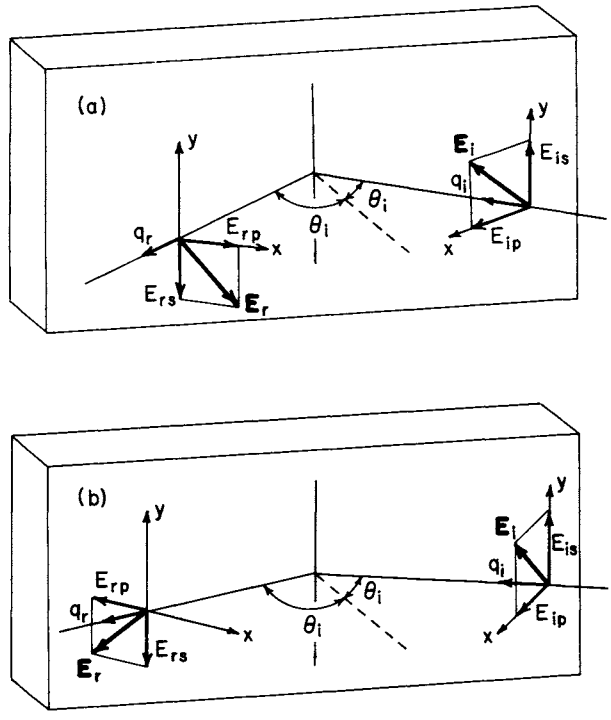


**Fig. 10.** Reflection of a linearly polarized wave (a) above and (b) below Brewster's angle for $n_i < n_t$. The rs and rp components point in their true directions.

vectors for incident and reflected waves are coplanar but not colinear (except at $\theta_i = 0$ and 90°). In Fig. 10a, the components of $E_{ip}$ and $E_{rp}$ that are parallel to the surface point in opposite directions, whereas the components that are normal to the surface point in the same direction. Are $E_{ip}$ and $E_{rp}$ in phase or out of phase? According to the first approach, if $E_{ip}$ and $E_{rp}$ point in the same direction relative to their individual coordinate systems, they are in phase. In Fig. 10a, they both point in the $+x$ direction, so they are in phase by definition. In Fig. 10b, $E_{rp}$ points in the $-x$ direction, so it is $\pi$ out of phase with respect to $E_{ip}$. According to this definition, $E_{rp}$ is in phase with $E_{ip}$ at near-normal incidence ($\theta_i \approx 0°$), but $\pi$ out of phase at glancing incidence ($\theta_i \approx 90°$), even though $E_{ip}$ and $E_{rp}$ are antiparallel in both limits. This apparent incongruity is not as bad as it seems because one is usually more concerned with the phase of $\mathbf{E}_r$ relative to the experimental setup rather than to $\mathbf{E}_i$.

The above definitions of *in phase* and *out of phase* for *p* polarization are incompatible with the concept of superposition [95]. As we have mentioned, there is a node in the electric field at the surface of a mirror at

normal incidence. In the Lloyd's mirror experiment [96], a node (dark fringe) also occurs at the point of contact of the mirror and screen for grazing incidence. Thus, from this point of view, $E_{rp}$ is $\pi$ out of phase with respect to $E_{ip}$ for all angles of incidence as long as $n_i < n_t$.

In the general case, the $s$ and $p$ reflection coefficients and phase changes vary with the angle of incidence. In addition, the reflection coefficients are not equal, nor are the phase changes. Thus, if the incident wave is linearly polarized and inclined 45° to the $x$ axis (that is, $E_{x0} = E_{y0}$), the reflected wave is elliptically polarized. (This is the working principle of ellipsometry [89]). To be consistent, one should use the Verdet convention for the $p$-polarized component when analyzing the polarization state of the reflected wave. In Fig. 7, the three vectors $\mathbf{E}_{is}$, $\mathbf{E}_{ip}$, and $\mathbf{q}_i$ (in that order) form a right-handed triad for the incident wave. For the reflected wave, $\mathbf{E}_{rs}$(FC), $\mathbf{E}_{rp}$(VC), and $\mathbf{q}_r$ form a commensurate right-handed triad. Some authors (for example, [65]) use a different layout for the $s$ and $p$ components and the wave vector from that presented in Fig. 7. In those cases, right-handed triads are formed by $\mathbf{E}_{ip}$, $\mathbf{E}_{is}$, $\mathbf{q}_i$ and by $\mathbf{E}_{rp}$(VC), $\mathbf{E}_{rs}$(FC), $\mathbf{q}_r$. Balanis derives $r_p$ in the Fresnel convention. Then, when he discusses polarization changes upon reflection, he draws the incident and reflected field vectors for $p$ polarization in the Verdet convention. To account for this, he introduces a minus sign into the equation for $\mathbf{E}_{rp}$ [97].

When an elliptically polarized wave reflects from a metallic surface, the handedness of the wave reverses, independent of the angle of incidence [98–101]. When the reflection surface is a dielectric, the handedness reverses if the angle of incidence is less than Brewster's angle and remains the same for angles of incidence greater than Brewster's angle.

To grasp the physical significance of phase change, consider a fictitious surface for which $|r| = 1$ at normal incidence. The incident and reflected waves form a standing wave in front of the surface [102–105]. The nodal positions in front of the surface depend on the phase change. If we assume the Fresnel convention and the $(n - ik)$ form, the incident and reflected waves can be expressed as

$$\begin{aligned} E_i &= E_0 \cos(\omega t - qz) \\ E_r &= E_0 \cos(\omega t + qz + \delta). \end{aligned} \tag{26}$$

The superposition of these two waves yields

$$E = E_i + E_r = 2E_0 \cos(\omega t + \delta/2) \cos(qz + \delta/2). \tag{27}$$

The envelope (maximum curve) of the standing wave obtains when

$\cos(\omega t + \delta/2) = \pm 1$. Then

$$E_{\max} = \pm 2E_0 \cos(qz + \delta/2). \tag{28}$$

Thus, it is clear that nodes occur when

$$qz = (2m+1)\pi/2 - \delta/2, \tag{29}$$

for those integral values of $m$ that place $qz$ in front of the reflecting surface.

Figure 11 shows several periods of a standing wave envelope. As can be seen, when $\delta$ equals 0° and 180°, an antinode and a node, respectively, occur at the surface. If $\delta$ is less than 180°, it is as if the node appears behind

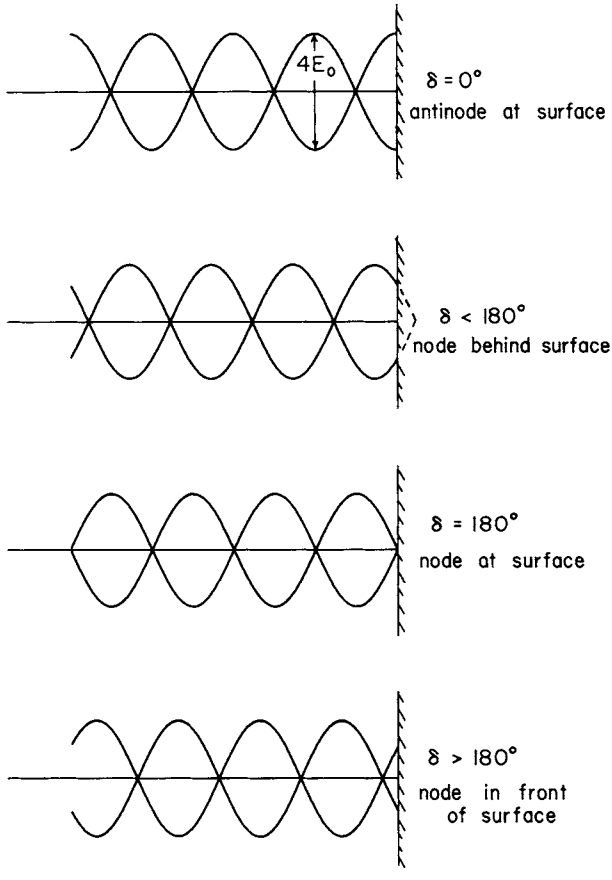


**Fig. 11.** Standing wave pattern in front of a surface with $|r| = 1$. The dependence of the nodal position on $\delta$ is shown. The values of $\delta$ are for the Fresnel convention with the $(n - ik)$ form.

the surface, whereas if $\delta$ were greater than 180°, the node would occur in front of the surface. Once again, we point out that Eqs. 26–29 are applicable only for the Fresnel convention and the $(n-ik)$ form. For the other cases in Fig. 8, Eqs. 26–29 have to be adjusted accordingly. However, all conventions result in the same standing wave pattern.

The preceding discussion is mathematically rigorous, but does not completely comply with physical reality. First of all, $|r|$ never equals unity so that the nodes are minima in the standing wave pattern, rather than zeros. Second, phase shift does not vary over the entire range from 0 to $2\pi$. Thus, in Fig. 10, an antinode occurs at the surface when reflection is from a less optically dense dielectric ($k=0$); a node occurs when reflection is from a more optically dense dielectric. When the incident medium is transparent and the transmission medium is lossy ($k\neq 0$), the phase shift will lie between 0 and $\pi$ (Fresnel convention, $(n-ik)$ form, normal incidence). Therefore, the node would appear to be behind the surface. Since phase shift cannot exceed $\pi$, a node will not occur in front of the surface (within a distance of $\lambda/4$).

Before proceeding to the next section, four points are worth making. First, reflection coefficients are characterized by two parameters: a magnitude and a phase. It is difficult to express meaningfully the values of both these parameters in an orthographic figure of the type shown in Fig. 7. A drawing such as in Fig. 9, in which $E_i$ is drawn along the positive real axis and $E_r$ has the appropriate magnitude and phase angle, is more informative [106].

The second point is that some authors express phase changes as negative values. In other words, they measure phase change clockwise from the positive real axis. Thus, if everything is done correctly, $\delta$(clockwise) = $\delta$(counterclockwise) − 360°. The right-hand ordinate in Fig. 8 measures the phase changes as negative quantities. The final $E_r$ field is the same—just the intermediate steps are different.

The third point concerns phase change when $k_t=0$. As might be surmised from Fig. 8, when the angle of incidence is less than the Brewster angle (and for $n_i<n_t$) [83, 107], $\delta_p(\mathrm{V}, n-ik)=360°$, not 0° as most books state. Likewise, above the Brewster angle, $\delta_p(\mathrm{F}, n+ik)=360°$.

Finally, an interesting optical morsel. Abelès [108–110] showed that at $\theta_i=45°$, $|r_p|=|r_s|^2$. In addition, for the Verdet form of $r_p$, $\delta_p=2\delta_s$. This is true in general for reflection from any semi-infinite medium.

## VI NOMENCLATURE

Nomenclature is not a burning issue, but is worthy of mention. The distinctions between *reflection*, *reflectance*, and *reflectivity* are subtle [111–

115] but are favored by many authors. Reflection is the act or process by which the incident wave is redirected back into the incident medium. Reflectance is a measured value. It is the fractional amount of the incident energy or intensity that is reflected from the surface. Reflectivity refers to a fundamental or characteristic property of a material. It is the theoretical reflectance that a semi-infinite medium would have. Applying the *-ion, -ance,* and *-ity* suffixes to the words *transmit* and *absorb* yields *transmission*, *transmittance*, and *transmissivity*, and *absorption, absorptance*, and *absorptivity*. These words have the same usage as the corresponding words derived from *reflect.*

## CONCLUDING REMARKS VII

Although we did not cover such specific topics as Jones matrices, Poincaré sphere, $\psi$ and $\Delta$ in ellipsometry, and so forth [2], we have presented the fundamental conventions dealing with electromagnetic wave propagation. It is important to recognize that conventions are a matter of definition or convenience. One must be able to separate physics from conventions and one convention from another. An amusing example of the misunderstandings that can arise is presented by a series of papers (and counter-papers), which discusses the "proper way" to account for reflection phase changes in interferometric measurements [116–122]. Since the various authors involved were using different conventions, they did not agree on the proper way and made scathing comments about each other. Finally, in an effort to end the controversy, the editors of *Optics and Spectroscopy* stated that they ". . . consider the discussion of phase shifts during reflection of light to be closed [117]." Of course, the controversy continues.

Even though we do not advocate a particular set of conventions, we do have one recommendation. Textbook authors should devote more time to the convention issue. They should point out the various conventions that a student is likely to encounter.

How can you determine which conventions an author uses if he fails to mention them? Look for obvious clues. Try to find equations, figures, tables, and so on, in which either $\exp(i\omega t)$ or $\exp(-i\omega t)$ is used. Are optical constants listed as $n-ik$ or $n+ik$? Is $r_p$ given in the Fresnel or Verdet convention? Review papers may by their very nature contain mixed conventions, especially when they quote from the original papers. For example, Weinberg [123] states that a metal is characterized by $\tilde{n}=n-ik$ but then presents phase changes in an $(n+ik)$ form. Also, he presents dielectric constants in the $(a'+ia'')$ form.

The two watchwords are convention and consistency. When you write a paper, either state your conventions explicitly or refer to a paper that does. Regardless of which set of conventions you choose, use them consistently throughout [3].

**ACKNOWLEDGMENTS**

The author wishes to express his thanks and appreciation to J. M. Bennett, D. M. Roessler, E. D. Palik, A. S. Glass, W. R. Hunter, and P. J. McMarr for valuable comments and suggestions. It is a pleasure to acknowledge the effort by M. E. Dixon in typing the manuscript.

**REFERENCES**

1. J. Z. Buchwald, "The Rise of the Wave Theory of Light," University of Chicago Press, Chicago (1989).
2. R. H. Muller, *Surf. Sci.* **16**, 14 (1969); P. S. Hauge, R. H. Muller, and C. G. Smith, *Surf. Sci.* **96**, 81 (1980).
3. J. M. Bennett and H. E. Bennett in "Handbook of Optics," (W. G. Driscoll, ed.), McGraw-Hill, New York, 10-1 (1978).
4. "The International System of Units (SI)," NBS Special Publication 330 (1986).
5. "Units of Measure," ISO Standards Handbook 2, 1st ed., International Organization for Standardization, Switzerland (1979).
6. R. A. Nelson, "SI: The International System of Units," American Association of Physics Teachers, Stony Brook, New York (1981).
7. M. Abraham, "The Classical Theory of Electricity and Magnetism," 2nd ed., Blackie & Son, London, 158 (1950).
8. J. D. Jackson, "Classical Electrodynamics," 2nd ed., John Wiley and Sons, New York, 811 (1975).
9. D. R. Frankl, "Electromagnetic Theory," Prentice-Hall, Englewood Cliffs, N.J., 147 (1986).
10. J. B. Marion and S. T. Thornton, "Classical Dynamics of Particles and Systems," 3rd ed., Harcourt Brace Jovanovich, New York, 476 (1988).
11. See Ref. 9, p. 260.
12. Many books use $k$ for both the wave number and the imaginary part of the refractive index. Be careful.
13. L. I. Schiff, "Quantum Mechanics," 3rd ed., McGraw-Hill, New York, 20 (1968).
14. A. V. Sokolov, "Optical Properties of Metals," English ed., Elsevier, New York, 20 (1967).
15. Some authors define the refractive index as $\tilde{n}=n(1+i\kappa)$ or $n(1-i\kappa)$, where $\kappa$ is the index of absorption (not to be confused with the absorption coefficient, $\alpha=2\omega k/c$). Also, $n$ and $k$ are referred to as the optical constants, even though neither is constant.
16. H. C. Chen, "Theory of Electromagnetic Waves," McGraw-Hill, New York, xiii (1983).
17. S. S. Mitra in "Handbook of Optical Constants of Solids," (E. D. Palik, ed.), Academic Press, New York, 213 (1985).
18. E. Spiller, *Appl. Opt.* **23**, 3036 (1984).
19. N. J. Harrick, "Internal Reflection Spectroscopy," John Wiley and Sons, New York, (1967); F. M. Mirabella and N. J. Harrick, "Internal Reflection Spectroscopy: Review and Supplement," Harrick Scientific Corp., Ossining, N.Y. (1985).
20. See Ref. 16, p. 93.
21. P. Yeh, "Optical Waves in Layered Media," John Wiley and Sons, New York, 14 (1988).

22. E. Hecht, "Optics," 2nd ed., Addison-Wesley, Reading, Mass., 270 (1987).
23. M. Born and E. Wolf, "Principles of Optics," 6th ed., Pergamon Press, London, 28 (1980).
24. W. A. Shurcliff, "Polarized Light: Production and Use," Harvard University Press, Cambridge, Mass., 6 (1962).
25. D. Clark and J. F. Grainger, "Polarized Light and Optical Measurement," Pergamon, Oxford, 173 (1971).
26. D. Clark, *Appl. Opt.* **13**, 3 (1974); ibid. **13**, 222 (1974).
27. E. Mach, "The Principles of Physical Optics," republication of 1926 English translation, Dover Publications, 186 (1953).
28. T. Preston, "The Theory of Light," 4th ed., Macmillan and Co., London, 25 (1944).
29. See Fig. 8.21 in Ref. 22.
30. See Ref. 27, p. 190.
31. See Ref. 1, p. 41.
32. F. L. Pedrotti and L. S. Pedrotti, "Introduction to Optics," Prentice-Hall, Englewood Cliffs, N.J., 341 (1987).
33. For an algorithm to generate perspective drawings, see R. E. Myers, "Microcomputer Graphics," Addison-Wesley, Reading, Mass., Chapter 6 (1982).
34. "IEEE Standard 145-1983, IEEE Standard Definitions of Terms for Antennas," *IEEE Trans. Antenna Propagat.* **AP-31**, Part II, 1 (1983).
35. The sense of rotation is determined by rotating the phase-leading component toward the phase-lagging component. See C. A. Balanis, "Advanced Engineering Electromagnetics," John Wiley and Sons, New York, 163 (1989).
36. M. V. Klein, "Optics," John Wiley and Sons, New York, 487 (1970).
37. R. F. Harrington, "Time-Harmonic Electromagnetic Fields," McGraw-Hill, New York, 46 (1961).
38. J. Strong, "Concepts of Classical Optics," W. H. Freeman and Company, San Francisco, 28 (1958).
39. See Ref. 24, p. 5.
40. See Ref. 25, p. 19.
41. J. A. Kong, "Electromagnetic Wave Theory," John Wiley and Sons, New York, 37 (1986).
42. S. Shibuya, "A Basic Atlas of Radio-Wave Propagation," John Wiley and Sons, New York, 14 (1987).
43. J. D. Kraus, "Electromagnetics," 3rd ed., McGraw-Hill, New York, 497 (1984).
44. P. A. Rizzi, "Microwave Engineering," Prentice-Hall, Englewood Cliffs, N.J., 36 (1988).
45. See Ref. 35, p. 158.
46. See Ref. 22, p. 275.
47. R. H. Webb, "Elementary Wave Optics," Academic Press, New York, 80 (1969).
48. R. W. Ditchburn, "Light," 3rd ed., Academic Press, New York, 638 (1976).
49. R. P. Feynman, R. B. Leighton, and M. Sands, "The Feynman Lectures on Physics," Vol. 1, Addison-Wesley, Reading, Mass., 33-10 (1963).
50. See Ref. 36, p. 488.
51. F. H. Read, "Electromagnetic Radiation," John Wiley and Sons, New York, 37 (1980).
52. B. D. McCombe and R. J. Wagner in "Advances in Electronics and Electron Physics," (L. Marton, ed.), Vol. 37, Academic Press, New York, 1 (1975).
53. E. Whittaker, "A History of the Theories of Aether and Electricity," Vol. 1, Philosophical Library, New York, 125 (1951).
54. See Ref. 28, p. 29.
55. R. W. Wood, "Physical Optics," 3rd ed., Macmillan, New York, 4 (1934).

56. A. Schuster, "An Introduction to the Theory of Optics," 3rd ed., Longmans, Green, and Co., New York, 241 (1924).
57. See Ref. 28, p. 360.
58. F. A. Jenkins and H. E. White, "Fundamentals of Optics," 4th ed., McGraw-Hill, New York, 244 (1976).
59. See Ref. 55, p. 211.
60. G. Friedmann and H. S. Sandhu, *Am. J. Phys.* **33**, 135 (1965).
61. F. W. Sears, "Optics," 3rd ed., Addison-Wesley, Reading, Mass., Fig. 7-3 (1958).
62. B. Rossi, "Optics," Addison-Wesley, Reading, Mass., Figs. 8-9, 8-10 (1957).
63. See Ref. 22, Figs. 4.20 and 4.21.
64. W. N. Hansen, *J. Opt. Soc. Am.* **58**, 380 (1968).
65. D. T. Paris and F. K. Hurd, "Basic Electromagnetic Theory," McGraw-Hill, New York, Fig. 8-5 (1969).
66. See Ref. 32, Figs. 23-1 and 23-2.
67. R. I. Sarbacher and W. A. Edson, "Hyper and Ultrahigh Frequency Engineering," 8th printing, John Wiley and Sons, New York, Figs. 4-4, 4-5 (1950).
68. D. R. Corson and P. Lorrain, "Introduction to Electromagnetic Fields and Waves," W. H. Freeman and Co., San Francisco, Figs. 11-4, 11-5 (1962).
69. Three books (Refs. 61, 67, 70) present figures in which $E_{rs}$ points in the opposite direction. However, the expression for the reflection coefficient given by Refs. 61 and 70 corresponds with the convention of Fig. 7a.
70. A. B. Winterbottom, "Optical Studies of Metal Surfaces," Kgl. Norske Vedenskab. Selskabs Skrifter, Trondheim, Norway, 15 (1955).
71. See how much easier it is to visualize Fig. 7-3 than Fig. 7-4 in Ref. 61.
72. See Ref. 61, p. 167.
73. See Ref. 22, p. 94.
74. See Ref. 28, p. 361.
75. See Ref. 68, p. 363.
76. See Ref. 25, p. 55.
77. See Ref. 14, p. 31.
78. L. Ward, "The Optical Constants of Bulk Materials and Films," Adam Hilger, Bristol, 10 (1988).
79. F. Abelès, in "Progress in Optics," (E. Wolf, ed.), Vol. 2, North-Holland, Amsterdam, 251 (1963).
80. See Ref. 3, p. 10-10.
81. P. H. Berning, in "Physics of Thin Films," (G. Hass and R. E. Thun, eds.), Vol. 1, Academic Press, New York, 69, (1963).
82. F. A. Jenkins and H. E. White, "Fundamentals of Physical Optics," 1st ed., McGraw-Hill, New York, 402 (1937). Note that Fig. 18O and Eqs. (18n) and (18o) do not appear in later editions.
83. See Ref. 3, p. 10-12.
84. Typically, $x$ is chosen to be the real axis and counterclockwise rotation is from the positive $x$ axis toward the positive $y$ axis.
85. In a calculation, phase angles must be expressed in radians, not degrees. See H. Anders, "Thin Films in Optics," English ed., The Focal Press, London, 24, footnote (1967).
86. R. S. Longhurst, "Geometrical and Physical Optics," 2nd ed., John Wiley and Sons, New York, 471 (1967).
87. Since we are showing the actual reflected field vectors, we have dropped the F and V labels.
88. See Ref. 48, p. 514.
89. R. M. A. Azzam and N. M. Bashara, "Ellipsometry and Polarized Light," North-Holland, Amsterdam, 67 (1977).

90. See Ref. 3, p. 10-20.
91. See Ref. 58, p. 528.
92. H. E. Bennett and J. M. Bennett, in "Physics of Thin Films," (G. Hass and R. E. Thun, eds.), Vol. 4, Academic Press, New York, 66 (1967).
93. A trivial but not necessarily inconsequential point is that no author (that we know of) tells the reader where to put his feet when looking into the oncoming wave. Left and right, as well as up and down, are relative to the body's orientation. Thus, the reader must be able to position (in his mind, at least) his body correctly to a sample surface, plane of incidence, optical element, or whatever. If the viewer stands on a plane parallel to the plane of incidence in Fig. 10 and looks into the wave, either incident or reflected, the $y$ axis points up and the $x$ axis points to the right.
94. See Ref. 22, p. 100.
95. See Ref. 25, p. 44.
96. See Ref. 58, p. 268.
97. See Ref. 35, Fig. 5-22 and Eq. (5-90a).
98. See Ref. 25, p. 48.
99. See Ref. 35, p. 236.
100. See Ref. 43, p. 519.
101. See Ref. 42, pp. 18 and 53.
102. G. W. DeBell, *SPIE Proc.* **140**, 2 (1978).
103. See Ref. 43, p. 439.
104. E. E. Wahlstrom, "Optical Crystallography," 5th ed., John Wiley and Sons, New York, 154 (1979).
105. See Ref. 58, p. 242.
106. J. M. Bennett, *J. Opt. Soc. Am.* **54**, 612 (1964).
107. R. H. Muller, in "Advances in Electrochemistry and Electrochemical Engineering," (R. H. Muller, ed.), Vol. 9, John Wiley and Sons, New York, 167 (1973).
108. F. Abelès, *C.R. Acad. Sci.* **230**, 1942 (1950).
109. R. M. A. Azzam, *Opt. Acta* **26**, 113 (1979); ibid. **26**, 301 (1979).
110. See Ref. 3, p. 10-86.
111. J. F. Snell, in "Handbook of Optics," (W. G. Driscoll, ed.), McGraw-Hill, New York, 1-1 (1978).
112. D. L. MacAdam, *J. Opt. Soc. Am.* **57**, 854 (1967).
113. G. Hass, J. B. Heaney, and W. R. Hunter, in "Physics of Thin Films," (G. Hass, M. H. Francombe, and J. L. Vossen, eds.), Vol. 12, Academic Press, New York, 1 (1982).
114. E. D. Palik and J. K. Furdyna, *Rept. Prog. Phys.* **33**, 1193 (1970).
115. J. D. Rancourt, "Optical Thin Films," Macmillan, New York, 12 (1987).
116. I. N. Shklyarevskii and N. A. Nosulenko, *Opt. Spec.* **14**, 127 (1963).
117. I. N. Shklyarevskii and V. K. Miloslavskii, *Opt. Spec.* **12**, 449 (1962).
118. L. Dunajsky, *Opt. Spec.* **12**, 448 (1962).
119. I. N. Shklyarevskii, N. A. Vlasenko, V. K. Miloslavskii, and N. A. Noculenko, *Opt. Spec.* **9**, 337 (1960).
120. N. Y. Gorban and I. A. Shaikevich, *Opt. Spec.* **11**, 404 (1961).
121. P. E. Ciddor, *Opt. Acta* **7**, 399 (1960).
122. I. N. Shklyarevskii, *Sov. Phys. Tech. Phys.* **1**, 327 (1956).
123. W. H. Weinberg, in "Solid State Physics: Surfaces," (R. L. Park and M. G. Lagally, eds.), Vol. 22, Academic Press, New York, 22, Fig. 26b (1985).

# Chapter 3

# Methods for Determining Optical Parameters of Thin Films

E. PELLETIER
Laboratoire d'Optique des Surfaces et des Couches Minces
Unité Associeé au CNRS
Ecole Nationale Supérieure de Physique de Marseille
Domaine Universitaire de St. Jérôme
Marseille, France

I. Introduction 57
II. An Example of Comparison between the Different Techniques of Index Determination 58
III. Principle Methods of Index Determination 60
IV. Sensitivity and Accuracy of the Determination Methods 64
V. Overlapping and Tests of Validity of the Model 67
VI. Results and Conclusion 71
References 71

## I INTRODUCTION

The aim of this chapter is to give an overview of the different methods used for determining the parameters that optically characterize a thin film. We limit ourselves to the case of a single layer deposited on a substrate, the properties of which are well known, and the materials involved are exclusively those generally used for optical multilayer coatings. Practically, these coatings can be used in the ultraviolet, visible, or infrared regions of the spectrum (100 nm to 100 $\mu$m). In a filter some wavelengths are transmitted, and others are completely reflected, according to the characteristics of the layers that constitute this optical filter.

In a general way, each layer is characterized by its refractive index $n$, its extinction coefficient $k$, and its thickness $d$ [1].

For the production of optical filters, we will deal more precisely with the materials in their transparent region, that is, the spectral range in which the extinction coefficient is very weak.


Copyright © 1991 by Academic Press.
All rights of reproduction in any form reserved.
ISBN 0-12-544422-2

Concerning the optical characterization of a single film, we can find in the literature numerous references with particularly exhaustive review articles. It is impossible to give an analysis of these works in a short chapter. However, it seems useful to display the evolution of the problems and the techniques used to solve them for some decades. In 1963, Abelès [2] gave a general review of the work done by different groups in the world. Some years later, with the introduction of computers, data processing greatly improved, and numerous ways were found to ease the acquisition of experimental results and the characterization of thin films. On this subject, we can refer to Liddell's book in which a complete chapter is devoted to the question of index determination [3]. At present, with the development of very high-performing optical filters, a more precise determination of the index values is of great importance.

What kinds of methods can meet these requirements? What progress has been made recently and how can we go further? We will try to give answers to these questions.

## II AN EXAMPLE OF COMPARISON BETWEEN THE DIFFERENT TECHNIQUES OF INDEX DETERMINATION

To have access to the values of refractive indices of thin layers, we will attempt to exploit directly the optical measurements made on these layers. Different techniques can be of potential use according to the transparency or nontransparency of the material. According to each case, measurements of transmission and reflection parameters or ellipsometric measurements of $\Delta$, $\Psi$ angles can be used [4].

Each author has his preferred method, and it is not possible to distinguish clearly the advantages and disadvantages of each without a detailed study, at least from the point of view of accuracy. We are indebted to the Optical Materials and Thin Films technical group of the Optical Society of America, with J. A. Dobrowolski as leader, for an attempt to address this question [5]. Seven laboratories were given films of different thicknesses of $ScO_2$ and Rh. The substrates used for the coatings were commercially polished fused silica (Dynasil). All the samples of each material were prepared in a single deposition run; the aim of the panelists (R. M. Azzam, J. M. Bennett, W. E. Case, C. K. Carniglia, J. A. Dobrowolski, U. J. Gibson, H. A. Macleod, and E. Pelletier) was to compare the optical constants obtained.

The results are meaningful: Table I gives the optical constants for scandium oxide. We give here only the values and variances of refractive index for different wavelengths in the 400–750 nm spectral range. Two

**TABLE I**

**From Results in Arndt *et al.* [5], Concerning Index Measurements on Two Scandium Oxide Layers $d_1$ and $d_2$ in the Spectral Range 400–750 nm (Substrate: Fused Silica)**

| Method | R, T and d | Reflection ellipsometry | Wide-band spectrophotometric | Modified Valeev turing point | Algebraic inversion | Inverse synthesis | Envelope | |
|---|---|---|---|---|---|---|---|---|
| $d_1$ (nm) | 224.5 | 228.2 | 217.6 | 219.0 | 225.0 | 221.2 | 219.4 | 222.2±3.9 |
| $d_2$ (nm) | 452.5 | 462.6 | 447.8 | 447.4 | 450.0 | 450.3 | 449.6 | 451.5±5.2 |
| | A | B | C | D | E | F | H | |
| $\lambda$ (nm) | | | | | | | | Mean values |
| 400 $d_1$ | — | 2.07 | 1.89 | 1.91 | — | 1.87 | 1.90 | 1.93 |
| $d_2$ | — | | 1.89 | 1.90 | — | | 1.89 | ±0.08 |
| 450 $d_1$ | 1.70 | 2.01 | 1.88 | 1.89 | 1.84 | 1.86 | 1.88 | 1.88 |
| $d_2$ | 1.86 | | 1.87 | 1.88 | 1.87 | | 1.89 | ±0.07 |
| 500 $d_1$ | 1.86 | 1.93 | 1.87 | 1.88 | — | 1.85 | 1.86 | 1.87 |
| $d_2$ | 1.85 | | 1.86 | 1.87 | 1.86 | | 1.87 | ±0.03 |
| 550 $d_1$ | 1.84 | 1.85 | 1.87 | 1.86 | 1.87 | 1.85 | 1.85 | 1.86 |
| $d_2$ | 1.87 | | 1.85 | 1.85 | — | | 1.86 | ±0.01 |
| 600 $d_1$ | 1.84 | 1.82 | 1.87 | 1.85 | 1.84 | 1.84 | 1.83 | 1.84 |
| $d_2$ | 1.86 | | 1.85 | 1.84 | 1.87 | | 1.85 | ±0.02 |
| 650 $d_1$ | 1.84 | 1.81 | 1.86 | 1.84 | 1.82 | 1.84 | 1.82 | 1.83 |
| $d_2$ | 1.82 | | 1.84 | 1.83 | 1.82 | | 1.84 | ±0.01 |
| 700 $d_1$ | 1.83 | — | 1.86 | 1.84 | 1.81 | 1.84 | 1.81 | 1.83 |
| $d_2$ | 1.84 | — | 1.84 | 1.83 | 1.83 | | 1.83 | ±0.01 |
| 750 $d_1$ | 1.82 | — | — | 1.83 | — | 1.84 | — | 1.83 |
| $d_2$ | 1.84 | — | — | 1.82 | — | | — | ±0.01 |

Seven measurement techniques (referenced from A to H in [5]) are compared.

layers of different thicknesses were studied, and here the problem is thickness measurement. The thicknesses determined by different methods were remarkably close to the average values 222.2±3.9 and 451.5±5.2 nm. The refractive index agreement is not bad—on the order of 0.01 for the 550–750 nm wavelength range. The extinction coefficient is very low; the methods were not able to determine significant values for it. Some panelists assumed that the $Sc_2O_3$ layers were nonabsorbing, and this assumption was not disturbing.

The results of determination of the optical constants of the Rh films are less satisfactory (Table II). The average variances in the determination of $n$ and $k$ in the 400–750 nm spectral region were 0.35 and 0.26, respectively, or 13% and 8%. The disparity of the thickness measurement results is of the same order. However, we must note Dobrowolski's important observation: compared with the optical properties of the bulk material, the values found for the optical constants of the material in thin-film form are sometimes disconcerting, but this may be the reason why the field of thin-film physics is so fascinating! And our attempt to compare the different techniques of index determination is not simplified, either.

At this stage, it is necessary to investigate the detail of the different methods compared; we will begin by examining the principles behind these methods, before approaching more technical aspects.

## III Principle Methods of Index Determination

For a first approach, we will consider two extreme cases as above.

In the first case, we will consider a transparent layer, and our problem is the determination of $n(\lambda)$, the refractive index for each of the wavelengths, together with the thickness $d$ of the layer, assuming that $k(\lambda) = 0$ is valid at all wavelengths.

In the second case, the layer is absorbing and the values $n(\lambda)$, $k(\lambda)$, and $d$ have to be determined.

We have to consider three steps.

- measuring of optical properties;
- choosing of a technique to calculate the optical properties with a model of the layer included in it; and
- the numerical treatment used for the compiling of data.

We must note that except for very particular cases, the value of the refractive index is not obtained by a rapid calculation. We must generally proceed with successive approximations to fit $n$ in order to obtain good agreement between the calculated and the measured optical properties.

**TABLE II**

**From results in Arndt *et al.* [5], Concerning Index and Thickness Measurements on Two Rhodium Thin Layers $d_1$ and $d_2$ in the Spectral Range 400–750 nm (Substrate: Fused Silica)**

| Method | R, T and d Method | | Reflection Ellipsometry | | Nestell and Christy | | Algebraic Inversion | | Inverse Synthesis | | Bennett and Booty | | | |
|---|---|---|---|---|---|---|---|---|---|---|---|---|---|---|
| $d_1$ (nm) | 14.2 | | 15.5 | | 17.2 | | 12.0 | | 16.9 | | 17.0 | | 15.5±2.1 | |
| $d_2$ (nm) | 27.1 | | 31.6 | | 30.1 | | 27.5 | | 31.7 | | — | | 29.6±2.2 | |
| | A | B | D | E | F | G | | | | | | | | |
| | *n* | *k* | *n* | *k* | *n* | *k* | *n* | *k* | *n* | *k* | *n* | *k* | *n* | *k* |
| $\lambda$ (nm) | | | | | | | | | | | | | Mean | values |
| 400 $d_1$ | — | — | 2.10 | 3.00 | 1.86 | 2.88 | 2.50 | 3.45 | 1.80 | 2.85 | 3.16 | 2.15 | 2.18 | 2.91 |
| $d_2$ | — | — | | | 1.86 | 2.97 | 2.40 | 3.00 | | | — | — | ±0.45 | ±0.34 |
| 450 $d_1$ | 2.40 | 3.29 | 2.35 | 3.12 | 2.04 | 3.02 | 2.75 | 3.55 | 2.11 | 3.00 | 3.19 | 2.34 | 2.38 | 3.08 |
| $d_2$ | 2.27 | 3.25 | | | 1.96 | 3.12 | 2.75 | 3.15 | | | — | — | ±0.38 | ±0.29 |
| 500 $d_1$ | 2.60 | 3.40 | 2.56 | 3.25 | 2.18 | 3.14 | 3.10 | 3.55 | 2.20 | 3.15 | 3.22 | 2.54 | 2.55 | 3.21 |
| $d_2$ | 2.39 | 3.42 | | | 2.04 | 3.27 | 3.00 | 3.15 | | | — | — | ±0.40 | ±0.26 |
| 550 $d_1$ | 2.78 | 3.53 | 2.74 | 3.41 | 2.32 | 3.28 | 3.20 | 3.75 | 2.40 | 3.25 | 3.19 | 2.79 | 2.68 | 3.36 |
| $d_2$ | 2.51 | 3.58 | | | 2.13 | 3.43 | 3.10 | 3.30 | | | — | — | ±0.37 | ±0.24 |
| 600 $d_1$ | 2.95 | 3.65 | 2.92 | 3.54 | 2.46 | 3.40 | 3.30 | 3.90 | 2.55 | 3.35 | 3.15 | 3.03 | 2.81 | 3.50 |
| $d_2$ | 2.62 | 3.75 | | | 2.23 | 3.59 | 3.30 | 3.40 | | | — | — | ±0.36 | ±0.23 |
| 650 $d_1$ | 3.11 | 3.77 | 3.08 | 3.68 | 2.61 | 3.52 | 3.35 | 4.15 | 2.75 | 3.50 | 3.13 | 3.26 | 2.94 | 3.65 |
| $d_2$ | 2.75 | 3.89 | | | 2.36 | 3.74 | 3.35 | 3.50 | | | — | — | ±0.32 | ±0.24 |
| 700 $d_1$ | 3.23 | 3.91 | — | — | 2.75 | 3.63 | 3.60 | 4.20 | 2.90 | 3.60 | 3.07 | 3.47 | 3.03 | 3.77 |
| $d_2$ | 2.87 | 4.04 | | | 2.47 | 3.88 | 3.50 | 3.60 | | | — | — | ±0.36 | ±0.25 |
| 750 $d_1$ | 3.35 | 4.03 | — | — | 2.88 | 3.74 | | | 3.00 | 3.75 | 3.07 | 3.61 | 2.99 | 3.86 |
| $d_2$ | 3.01 | 4.16 | | | 2.60 | 4.01 | | | | | — | — | ±0.22 | ±0.20 |

One of these steps cannot be solved without taking account of the other two, which can simultaneously affect the efficiency of the method of characterization.

Let us now consider the first point: What optical properties must be measured?

The answer is not the same for the different authors. Dobrowolski [5] is very explicit on this subject. In this paper we find

- measurement of normal incidence reflectance $R$ and transmittance $T$ for a single wavelength;
- measurement of polarization states of collimated monochromatic light before and after reflection from a surface to obtain the ratio $\rho = R_p/R_s = \tan \psi \exp(i\Delta)$ of the complex $p$ and $s$ reflection coefficients;
- measurement of normal-incidence reflectance and transmittance over a wide spectral range; and
- measurement of $R$ and $T$ for normal and oblique angles of incidence (45°; 60°) for the polarizations $T_E$ and $T_M$, over a wide spectral range.

The second point we consider is calculation of optical properties. Determination (with a computer) of the optical properties is easy only if we accept some hypotheses, mainly related to the model of the layer. In a classical way, it is assumed that the layer is optically homogeneous and isotropic with plane and parallel surfaces. With Maxwell equations, parameters $n$, $k$ and $d$ describe theoretically the optical properties of the layer. However, a comparison between theory and experiment requires some precautions.

(1) Illumination conditions: angle of incidence and wavelength must be specified. In monochromatic or wide-spectral-range methods, $R$ and $T$ must be measured for the same angle of incidence. In the calculations, we consider a monochromatic plane wave. What about the spectrophotometer set up, with respect to aperture, angle of incidence, and monochromaticity of the measurement beam?

(2) In the calculations, we assume that the layer is deposited on a substrate of well-determined index $n_s(\lambda)$ and of infinite thickness. In other words, the layer is inserted between two semi-infinite media of index $n_0$ and $n_s$. Very often, the experimental conditions are different, because the substrate has a finite thickness, relatively large with respect to the layer thickness, so that the interference effects in the substrate are not resolved; but—and this is an essential problem—the back face of the substrate does give rise to a reflected and a transmitted beam, which can perturb the reflectance and transmittance measurements. To this must be added the surface of the substrate itself, whose quality determines the quality of the two interfaces of the layer, which are never absolutely plane.

Different techniques have been proposed to minimize these undesirable

experimental conditions; the solutions are more or less successful, depending mainly on the experimental conditions used.

When comparing the results, we observed systematic differences between the authors, probably due to these problems of measurement. A more complete analysis of this subject can be found elsewhere [3, 5, 6].

Finally, we consider the numerical treatment used for compilation of the data. We compare the experimental results with the theory to determine the values of the optical constants. The mathematical solution is not obvious. However, knowing that the optical properties at wavelength $\lambda_i$ can be described with the three parameters $n_i$, $k_i$, and $d$, we can find a solution by simplifying the problem. For example, for an absorbing material, $d$ can be determined with a complementary method (interferometry or mechanical stylus [7]), thus reducing the problem to two unknown quantities, $n$ and $k$. In the case of a transparent material, the first approximation $k=0$ makes the work easier, especially if we note that transmittance and reflectance are functions of the variable $2\pi nd/\lambda$. So, if we consider two measurements, we can determine two unknowns. From 3, 4, or even $L$ measurements, we could determine the same number of unknowns, such as $n$ and $k$, for a series of different wavelengths. And if $L$ is large, we can verify the results by cross-checking. It is obvious that the problem of data compilation will require a powerful computer, if we want to exploit these data better.

We can give a quick presentation of the methods of index determination, the common base of which is as follows: we will consider the case of a layer of refractive index greater than the substrate index. First, we exploit the values of the extrema of $R(\lambda)$ (Fig. 1). Neglecting the effects of index dispersion for the values of $\lambda$ corresponding to these extrema, the layer has an optical thickness, which is an odd multiple of $\lambda/4$, and we can find that the reflectance is maximum and given by

$$R=\left(\frac{n^2-n_0n_s}{n^2+n_0n_s}\right)^2.$$

With low-index layers, the minima of $R(\lambda)$ are used because for the same optical thickness, the reflection is minimum, and the reflectance is given by the same formula. We can find many papers in the literature that exploit the turning-point method [8].

To determine $n$ for other wavelengths, two methods can be followed. The first consists of plotting the two curves enveloping the extrema of the profile of $R(\lambda)$ and analyzing these envelopes [9]. The second directly uses the profile of $R(\lambda)$ and synthesizes the spectrum to determine the parameters that account for the effective optical properties of the layer. The more sophisticated synthesis methods, such as Dobrowolski's, are easily

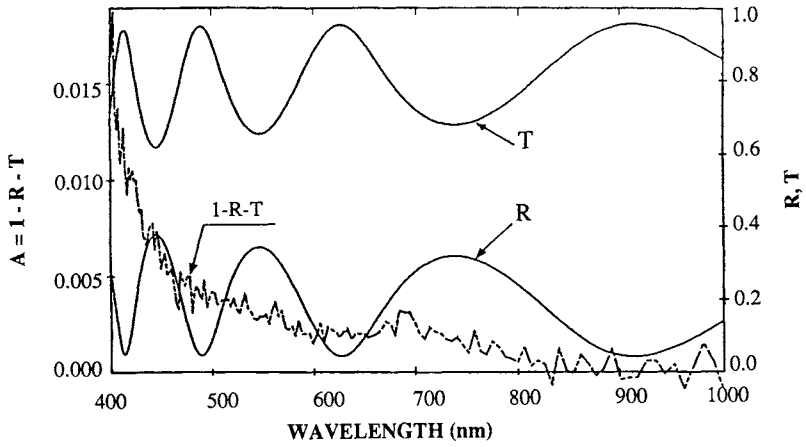


**Fig. 1.** $TiO_2$ layer, after J. P. Borgogno *et al.* [6]. From the measurement of reflection, $R(\lambda)$, and transmission, $T(\lambda)$, coefficients, we have plotted the variations of the absorption $A(\lambda) = 1 - R(\lambda) - T(\lambda)$ versus wavelength $\lambda$. Maximums of $R(\lambda)$ lead to a rapid determination of $d$ and $n(\lambda)$.

applied here, since they involve a single layer and not a multilayer [10].

Either process, by successive approximations, results in a determination of the parameters' values, giving better interpretation of the measured values of the optical properties. A figure of merit is used, and a convergence process drives the cycle of approximations. The difficulties of this technique are well-known: the solution is not necessarily unique, and the efficiency of the convergence process essentially depends on the values assigned at the beginning of the iteration process.

The completely automatic programs of index determination must avoid these difficulties [11], and great precautions must be taken at the beginning of the synthesis calculation, in particular for determining initial $d$ and $k$ values, even before $n$ values [12]. For highly absorbing materials, the efficiency of these programs is not so obvious.

## IV SENSITIVITY AND ACCURACY OF THE DETERMINATION METHODS

We get a preliminary idea of the accuracy of the methods of index determination by examining the results of data processing. As an illustration, we present in Fig. 2 the amplitude of errors on $n$, when measurements of $R$ and $T$ are affected by an error $\Delta R = \Delta T = \pm 0.003$. We note the well-known result [13]: the precision of $\Delta n$ is strongly dependent on the particular wavelength. To continue in our investigation, it is interesting to compare systematically the agreement obtained between the optical

properties measured and those calculated from the determined values of parameters $n$, $k$, and $d$. The result is very often surprising, particularly if we consider a sampling of wavelengths different from that used for the measurements. On this subject, it is interesting to recall the technique of representing the law of index dispersion by a limited equation such as Cauchy's [14]:

$$n = A + \frac{B}{\lambda^2} + \frac{C}{\lambda^4}$$

under the express condition that its validity is well verified.

There appears a systematic disagreement between calculation and experiment, at least for particular spectral ranges (Fig. 3). Discontinuities can also be seen on the graph (Fig. 2) of the curve $n(\lambda)$, for particular regions of the spectrum. It can be shown that it is not sufficient just to blame the measurement techniques and the numerical techniques of convergence. We have here a more fundamental difficulty in the problem of index determination, which concerns the validity of the model used to account for the effective properties of the layers. We have assumed in the simple model that the layer was homogeneous and isotropic with plane and parallel surfaces. At a given degree of perfection, it is no longer possible to assume these three hypotheses. The problems of inhomogeneity and anisotropy will prevent us from using these methods to their maximum

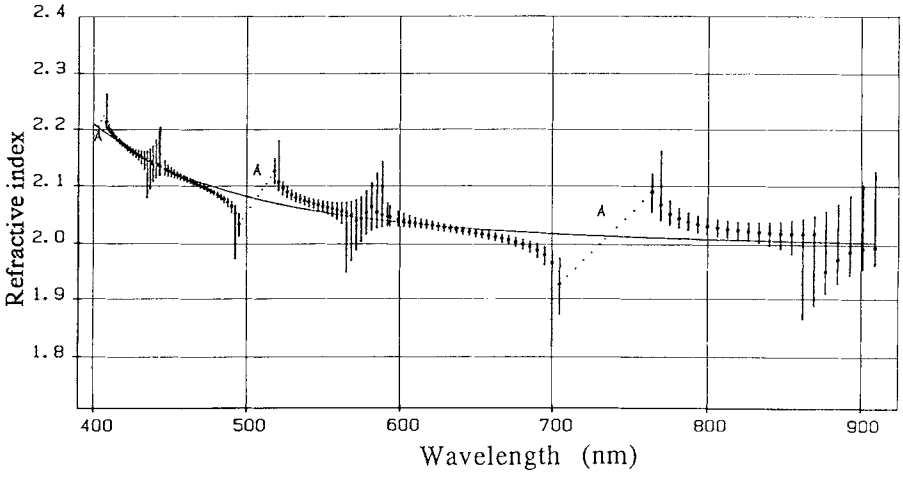


**Fig. 2.** Refractive index of a titanium oxide layer using the classical model of homogeneous layer. Note the parts of the graph deviating from the mean-value curve and the two ranges ($A$) where index determination is impossible.

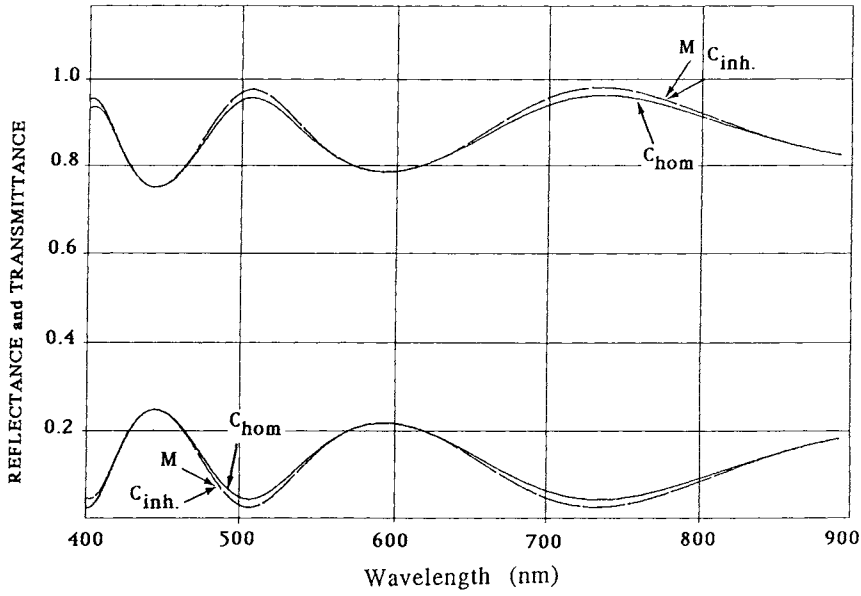


**Fig. 3.** For the $TiO_2$ layer of Fig. 2, disagreement between calculation and experiment. $M$ indicates measurements of reflectance and transmittance for normal incidence. $C_{hom}$ is the calculated result using a nonclassical homogeneous model. A better agreement, $C_{inh}$, can be obtained by introducing inhomogeneity in the model (after Borgogno *et al.* [11]).

potential. Planarity and roughness of the surfaces, from which light scattering originates, are hopefully negligible for substrates of good optical quality [15].

Numerous authors agree to the obvious presence of inhomogeneity in transparent layers [11, 16]. We can take advantage of the fact that a layer with optical thickness of $\lambda/2$ or a multiple of $\lambda/2$ is *absent*, that is, it does not modify, for this wavelength, the reflectance of the substrate. From the experimental results concerning the values of $R$ for these wavelengths, we can deduce information about the global variation of refractive index in the volume of the layer. So we often give the value $\Delta n/n$ with $\Delta n = n_0 - n_i$, where $n_0$ and $n_i$ represent the refractive index at the interfaces on the air or on the substrate side, respectively. The form of the gradation of $n$ inside the layer is not of great importance, and a linear variation seems a reasonably good approximation (Fig. 4). Other forms of gradation can be used, depending essentially on the layers considered, since the structure of the coatings depends in great part on the deposition technique [17].

Some results of $n(\lambda)$ with measurements of inhomogeneity $(\Delta n/n)(\lambda)$ have been published [18] (see Fig. 5). We can consider that the introduction of the parameter $\Delta n/n$ has a decisive role here in the improvement of accuracy of the method of index determination.

We can understand the differences observed among the results of the different authors, such as those presented in Section II. Three difficulties are simultaneously involved: accuracy of the measurements, efficiency of calculations, and validity of the layer model. For a well-characterized yttrium oxide layer, Daugy *et al.* [19] have shown how divergences can appear as soon as we neglect absorption and inhomogeneity in the analysis techniques already mentioned [8, 9, 11]. Figure 6 displays the results, including the result of ellipsometric measurements. In addition, the values of bulk yttrium oxide from Nigara [20] are reported, but the comparison between the optical constants of the material in the bulk and thin-film form cannot be of much help in corroborating the results for the methods of index determination of the layers. Only a systematic cross-checking of the different techniques applied to a thin film can give us a clue for obtaining better accuracy. We will now give a short overview of this subject.

## V OVERLAPPING AND TESTS OF VALIDITY OF THE MODEL

The optical measurements are, unfortunately, never perfect, and this sometimes prevents the calculations from converging toward a good

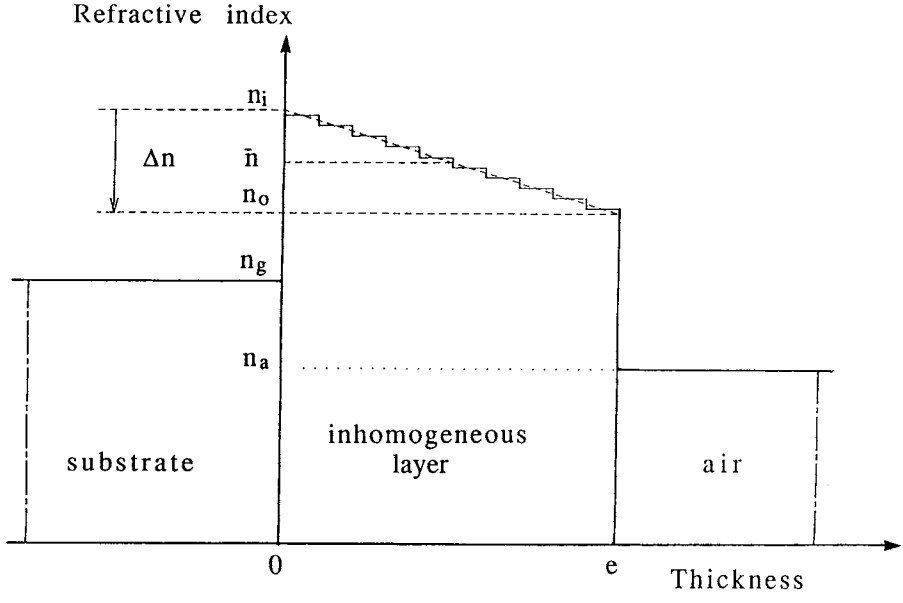


**Fig. 4.** Model of inhomogeneous layer used in the calculation: $\Delta n = n_0 - n_i$. The value $\Delta n$ is negative for index decreasing from the substrate (after Borgogno *et al.* [11]).

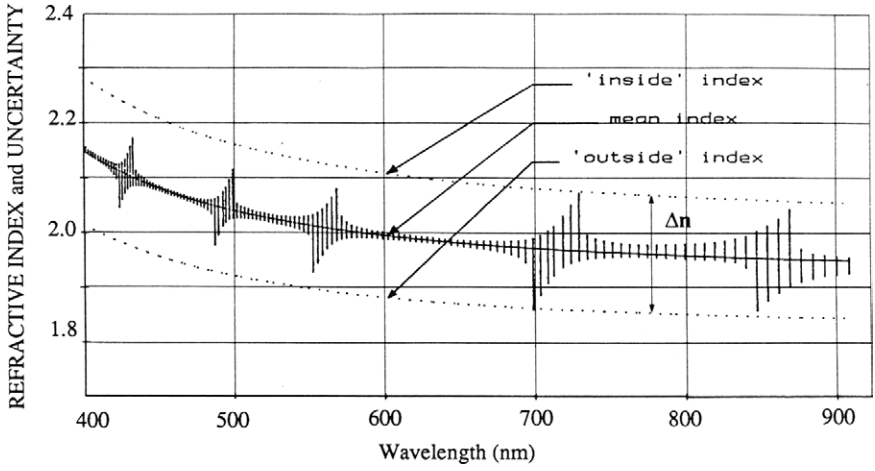


**Fig. 5.** Determination of $n(\lambda)$ and $\Delta n(\lambda)$ for a $TiO_2$ layer with the model of Fig. 4. The results can be easily described by a Cauchy equation.

solution. A priori, under these conditions, it is always interesting to add some complementary measurements to help in searching for the solution, and especially to remove any ambiguity.

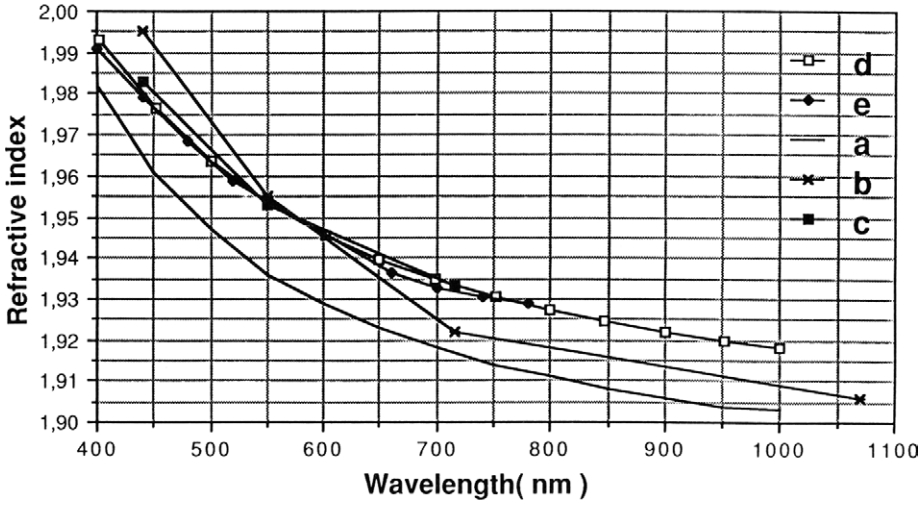


**Fig. 6.** Study of a $Y_2O_3$ layer. Refractive-index values given by different techniques: (a) bulk material, after Nigara [20]; (b) from $T$ measurements, after Daugy *et al.* [19]; (c) from $T$ and $R$, after Daugy *et al.* [19]; (d) after $T$ and $R$ measurements, from Borgogno *et al.* [11, 12]; (e) ellipsometric measurements of Sté SOPRA, France (see Daugy *et al.* [19]).

In this way, the use of oblique incidence can be of great assistance, mainly for absorbing materials [10, 21]. The same principle leads authors to measure both the values of $R$ measured "on the air side" and $R'$ measured "on the substrate side," either for dielectrics [22] or for metals on substrates [23]. In fact, this technique allows the quality of the spectrophotometric measurements to be tested and eventually reveals structure defects in the layer. If we want to go further in this analysis, we must consider that, far from being competitive, spectrophotometric and ellipsometric methods are rather complementary [24].

Until now, we have limited ourselves to the classical methods of index determination, but we must note that in the last few years, complementary characterization methods have been proposed for very particular applications. Improving the accuracy of $n$ and especially of $k$ is of great interest for transparent layers. And for absorbing materials, an unambiguous determination of $k$ is essential.

For studying highly transparent materials, guided-wave techniques are particularly interesting. Following Ulrich and Torge [25], one can exploit the idea of using the layer as a light guide, by coupling light with a prism of known refractive index.

Basically, parameters $n$ and $d$ of the layer are the unknowns: it is sufficient to study the propagating conditions of two different modes to determine these two values. Given the accuracy obtained for angular measurements, the refractive index value can be measured to within almost the third decimal place.

With three modes, the overlapping can be exploited to test the validity of the layer model used in the calculation. This technique has been used to show an optical anisotropy induced by the particular microstructure of dielectric materials evaporated under vacuum. We know that they condense in a columnar form, the orientation of which depends on the incidence angle of the flux emitted by the crucible and arriving on the surface being coated.

From ellipsometric and absorption measurements, Hodgkinson *et al.* and Horowitz have developed a layer model to account for the optical anisotropy induced by this columnar structure [26] (Fig. 7). Measurements with guided waves [27] allow a complete validation of the model proposed. Table III is an illustration of the results obtained.

Coupling light into metallic layers gives rise to more difficult problems. Known as *surface-plasmon effect*, it can lead to index measurements in some particular cases. Macleod has shown how to exploit this phenomenon, well-known by the optical scientists [28].

Concerning the determination of extinction coefficients $k(\lambda)$ of dielectrics, we must note the measurements of propagation attenuation: they give access to the value of $k$, at least in the case where scattering losses can be neglected.

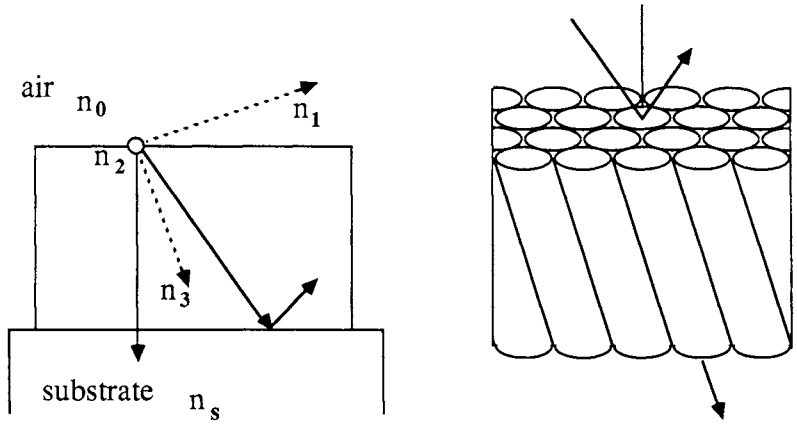


**Fig. 7.** Columnar structure model (after Horowitz [26]). For the calculation of anisotropy, the three principal indices of refraction are $n_1$, $n_2$, and $n_3$. With this model, in the columnar growth direction, the index value is $n_3$.

For some years, works on acousto-optical and mainly photothermal methods have also led to the measurement of absorption in thin layers. It is probable that the method of Boccara *et al.* [29] will be more widely utilized, under conditions of good calibration of the measurements, either for very low values of $k$ [30] or for specific absorptions [31].

**TABLE III**

**Measurement of Anisotropy: $TiO_2$, ZnS, $Ta_2O_5$ Layers Produced by Evaporation and $Ta_2O_5$ Layers Produced by Ion Assisted Deposition**

| | $TiO_2$ | ZnS | $Ta_2O_5$ | $Ta_2O_5$ |
|---|---|---|---|---|
| $n_1$ | 2.320 | 2.349 | 2.119 | 2.151 |
| $n_2$ | 2.321 | 2.351 | 2.115 | 2.151 |
| $n_3$ | 2.357 | 2.356 | 2.127 | 2.155 |

The angle between the normal to the substrate and the direction of the material flux is 19°. Macleod and Horowitz model (Fig. 7): measurements with guided waves of the values of the three principal indices $n_1$, $n_2$, and $n_3$ (which corresponds to the columnar growth direction) [27].

## RESULTS AND CONCLUSION VI

Some amount of humor is necessary to use the expression *optical constant* in referring to the complex refractive index of a thin layer. In this chapter, we have shown that an accurate measurement implies taking account of the dependence of $n$ and $k$ on a series of parameters, which are wavelength, layer thickness, angle of incidence, and so forth. It remains to introduce the dependence with time: the layers are in equilibrium with the surrounding medium, and the amount of absorbed water or contaminants is a function of the hydroscopic character of this medium, of the void-fraction of the deposited material, and of the temperature. A comparison of the results obtained in air and in vacuum gives significant differences [32], which can be explained as absorption–desorption phenomena.

For relatively thick transparent layers (several $\lambda/4$) deposited on transparent substrates, we can determine $n$ in a transparent region with a precision no better than 1%.

Concerning $k$ (except for photothermal measurements), the precision is very limited for values of $k < 1 \times 10^{-3}$. Outside the transparent region, the conclusions are still more pessimistic. All numerical extrapolation for wavelengths outside the measurement range can lead to nonreliable results.

Often, when we plot the graphs $n(\lambda)$ and $k(\lambda)$ on a wide spectral range (as is done in this handbook), we often observe discontinuities between two ranges where the techniques used were different.

So, should we give up determining the layer index to more than two decimals? Certainly not; the need for all the applications is much too important. But we must take account of the detail of the technique of fabrication of the layers; it determines the microstructure of the materials. It is interesting to note that with a classical evaporation, a repeatability better than 1% in the index cannot be guaranteed. It is the order of magnitude of the accuracy of the classical methods of index determination. Modern technologies of layer production, particularly those using ion bombardment, lead to coatings with a more compact structure, similar to that of bulk material, resulting in a clear improvement of the validity of the theoretical models; the methods of index determination are then more reliable.

### REFERENCES

1. H. A. Macleod, "Thin Film Optical Filters," Adam Hilger, Bristol, 1986.
2. F. Abelès, "Methods for determining optical parameters of thin films," in "Progress in Optics," (E. Wolf, ed.) vol. 2, North-Holland, Amsterdam, 250 (1963).
3. M. Liddell, "Computer Aided Techniques for Design of Multilayer Filters," Adam Hilger, Bristol, 1981.

4. R. M. A. Azzam and N. M. Bashara "Ellipsometry and Polarized Light," North-Holland, Amsterdam, 1977.
5. D. P. Arndt, R. M. A. Azzam, J. M. Bennett, J. P. Borgogno, C. K. Carniglia, W. E. Case, J. A. Dobrowolski, U. J. Gibson, T. Tuttlehart, F. C. Ho, V. A. Hodgkin, W. P. Klapp, H. A. Macleod, E. Pelletier, M. K. Purvis, D. M. Quinn, D. H. Strome, R. Swenson, P. A. Temple, and T. F. Thonn, Multiple determination of the optical constants of thin-film coating materials," *Appl. Opt.* **23**, 3571 (1984).
6. J. Lafait, "Goniospectrophotomètre à polarisation de 0,25 à 1 $\mu$m," *Optica Acta* **20**, 365 (1973); J. P. Borgogno and E. Pelletier, "Determination of the extinction coefficient of dielectric thin films from spectrophotometric measurements," *Appl. Opt.* **28**, 2895 (1989).
7. H. E. Bennett and J. M. Bennett, "Precision measurements in thin film optics," in "Physics of Thin Films," (G. Hass and R. E. Thun, eds.) vol. 4, Academic Press, New York, 1 (1967).
8. J. F. Hall and W. F. C. Fergusson, "Optical properties of cadmium sulphide and zinc sulphide from 0.6 micron to 14 microns," *J. Opt. Soc. Am.* **45**, 714 (1955); A. S. Valeev, "Constants of thin weakly absorbing layers," *Opt. Spectrosc. USSR* **18**, 498 (1965).
9. J. C. Manifacier, J. Gasiot, and J. D. Fillard, "A simple method for the determination of the optical constants $n$, $k$, and the thickness of a weakly absorbing thin film," *J. Phys. E.* **9**, 1002 (1976).
10. J. A. Dobrowolski, F. C. Ho, and A. Waldorf, "Determination of optical constants of thin film coating materials based on inverse synthesis," *Appl. Opt.* **22**, 3191 (1983).
11. J. P. Borgogno, B. Lazaridès, and E. Pelletier, "Automatic determination of the optical constants of inhomogeneous thin films," *Applied Optics* **21**, 4020 (1982).
12. J. P. Borgogno, B. Lazaridès, and P. Roche, "An improved method for the determination of the extinction coefficient of thin film materials," *Thin Solid Films* **102**, 209 (1983).
13. C. Bazin, "Influence des erreurs commises lors des mesures expérimentales sur la détermination de l'indice d'une couche mince absorbante," *Compt. Rend. Acad. Sc.* **260**, 83 (1965).
14. D. J. Schroeder, "Interference transmission filters for the far ultraviolet," *J. Opt. Soc. Am.* **52**, 1380 (1962).
15. P. Baumeister, "Reflectance and transmission measurements," *Proc. Soc. Photo-Opt. Instrum. Eng.* **50**, 37 (1974).
16. R. Jacobsson, "Inhomogeneous and coevaporated homogeneous films for optical applications," in "Physics of Thin Films," (G. Hass, ed.), vol. 8, Publisher, City, 51 (1975).
17. H. A. Macleod, "Microstructure of optical thin films," *Proc. Soc. Photo-Opt. Instrum. Eng.* **325**, 21 (1982).
18. J. P. Borgogno, F. Flory, P. Roche, B. Schmitt, G. Albrand, E. Pelletier, and H. A. Macleod, "Refractive index and inhomogeneity of thin films," *Appl. Opt.* **23**, 3567 (1984); J. M. Bennett, E. Pelletier, G. Albrand, J. P. Borgogno, B. Lazaridès, C. K. Carniglia, R. A. Schmell, T. H. Allen, T. Tuttle-Hart, K. H. Guenther, and A. Saxer, "Comparison of the properties of titanium dioxide films prepared by various techniques," *Appl. Opt.* **28**, 3303 (1989).
19. E. Daugy, B. Pointu, C. Audry, and C. Hervo, "Correlations entre les caractéristiques optiques et physico-chimiques de couches minces de $Y_2O_3$ et $ZrO_2$ obtenues par pulvérisation par canon à ions," paper presented at "Horizons de l'Optique," Jouy en Josas, August 1989. *J. of Optics* **21**, 99 (1990).
20. Y. Nigara, "Measurements of the Optical Constants of Yttrium Oxide," *Jap. J. Appl. Phys.* **7**, 404 (1967).
21. J. E. Nestell, Jr. and R. W. Christy, "Derivation of optical constants of metals from thin-film measurements at oblique incidence," *Appl. Opt.* **11**, 643 (1972).

22. E. Pelletier, P. Roche, and B. Vidal, "Détermination automatique des constantes optiques et de l'épaisseur de couches minces: application aux couches diélectriques," *Nouv. Rev. Optique* **7**, 353 (1976).
23. P. Rouard, "Etude des propriétés optiques des lames métalliques très minces," *Ann. Phys.* **7**, 291 (1937).
24. D. E. Aspnes, "The characterization of materials by spectroscopic ellipsometry," *Proc. Soc. Photo-Opt. Instrum. Eng.* **452**, 60 (1983).
25. R. Ulrich and R. Torge, "Measurement of thin film parameters with a prism coupler," *Appl. Opt.* **12**, 2901 (1973).
26. F. Horowitz, "Structure Induced Optical Anisotropy in Thin Film," Ph.D., diss. University of Arizona, Optical Sciences Center (1983); I. J. Hodgkinson, F. Horowitz, H. A. Macleod, M. Sikkens, and J. J. Wharton, "Measurement of the principal refractive indices of thin films deposited at oblique incidence," *J. Opt. Soc. Am. A* **2**, 1693 (1985).
27. E. Pelletier, F. Flory, and Y. Hu, "Optical characterization of thin films by guided waves. *Appl. Opt.* **28**, 2918 (1989).
28. H. A. Macleod, "Surface plasmon resonance effects and the admittance diagram," *Proc. Soc. Photo-Opt. Instrum. Eng.* **777**, 300 (1987); H. Raether, "Surface plasma oscillations and their applications," *Phys. Thin Films* **9**, 145 (1977).
29. A. C. Boccara, D. Fournier, W. Jackson, and N. M. Amer, "Sensitive photothermal deflection technique for measuring absorption in optically thin media," *Opt. Letters* **5**, 377 (1980).
30. M. Commandré, L. Bertrand, G. Albrand, and E. Pelletier, "Measurement of absorption losses of optical thin film components by Photothermal Deflection Spectroscopy," *Proc. Soc. Photo-Opt. Instrum. Eng.* **805**, 128 (1987).
31. N. M. Amer, W. Jackson, in "Semiconductors and Semimetals," (J. I. Pankore, ed.), vol. 21B, Academic Press, New York, 83 (1984).
32. B. Schmitt, J. P. Borgogno, G. Albrand, and E. Pelletier, "In situ and air index measurements: influence of the deposition parameters on the shift of $TiO_2/SiO_2$ Fabry-Perot filters," *Appl. Opt.* **25**, 3909 (1986).
33. P. J. Martin, "Ion-based methods for optical thin film deposition," *J. Mat. Sci.* **21**, 1 (1986).

# Chapter 4

# The Attenuated Total Reflection Method

G. J. SPROKEL and J. D. SWALEN
IBM Research Division
Almaden Research Center
San Jose, California

I. Introduction 75
II. Surface-Plasmon Oscillations 77
III. Optical Analysis of ATR Structures 81
IV. Guided Modes 84
V. Applications of ATR 87
A. Optical Constants of Metals 87
B. Molecular Films 87
C. Organic Dyes 89
D. Dielectric Films 90
E. Surface Tilt Angle of Nematic Liquid Crystals 90
F. Tutorial Demonstration of ATR 93
G. Guided Modes and ATR 93
H. Long-Range Surface-Plasmon Waves 93
VI. Conclusion 94
References 94

## INTRODUCTION I

Attenuated total reflection (ATR) is a technique for determining the optical constants of thin-film samples, that is, the refractive index and the absorption coefficient. It differs from other, perhaps better-known procedures, such as ellipsometry and reflectometry, in that ATR probes the sample with an evanescent wave rather than a collimated beam of light. As is well-known, evanescent waves near an interface decay away exponentially over a distance comparable to the wavelength. There is no energy transport across the interface, and thus the reflectivity is unity. However, for very specific conditions, an evanescent wave can be made to interact


Copyright © 1991 by Academic Press.
All rights of reproduction in any form reserved.
ISBN 0-12-544422-2

with material in its field and energy can be transported. Then the reflectivity will be less than unity and hence the term *attenuated total reflectivity*. In practice, a light beam is directed through a prism or rhomb such that the angle of incidence at the base exceeds the critical angle, and the sample is placed within the evanescent field either in contact with the prism or separated by a narrow gap, which must be smaller than one wavelength. Evanescent waves can also be generated by gratings, and historically the use of gratings preceded that of prisms; however, the prism technique is simpler by far. The prism geometry has been employed in internal reflection spectroscopy (IRS) for many years. The light enters a prism, and the sample is pressed to its base. It is well detailed by Harrick [1].

Here ATR is taken to encompass such widely differing phenomena as plasmon waves on metal surfaces and certain organic dyes, guided modes in dielectric films, and surface waves on diffraction gratings. In ATR experiments, the probe is an evanescent wave rather than the incident beam itself, and resonance is observed by measuring reflectivity as a function of the angle of incidence or the wavelength. It is more common to scan the angle of incidence. In IRS, as in all spectroscopy, the wavelength is scanned.

ATR evolved as a technique in 1968 mostly through the work of Otto in Munich [2–5] and Raether and Kretschmann in Hamburg [6–10]. Although surface-plasmon waves were known since the work of Sommerfeld [2] in radio-wave propagation (1909), they received little attention in optics until the work of Fano in 1941 [11]. Fano's paper dealt with anomalies in the diffraction spectra of metal gratings known as Wood's anomalies. He recognized that surface electromagnetic (EM) waves are evanescent waves with wave vectors larger than that of the incident beam, and that the grating increased the incident wave vector. Much later (1967–1968) this was again taken up by Teng and Stern [12] and by Ritchie *et al.* [13], who used coupling by gratings to excite surface-plasmon waves.

Otto [4, 5], Raether [9], and Burstein *et al.* [14] all published review papers between 1974 and 1977 discussing the physical optics of ATR. Palik and Holm [15] reviewed IRS in 1978. Later papers have dealt more with specific topics. Swalen [16] reviewed the optics of Langmuir–Blodgett films (1986). Rabolt and Swalen [17] discussed integrated optics and its application to Raman scattering (1988). Debe [18] made an extensive review on the optics of organic thin films (1987). The following is a brief discussion of physical optics applied to ATR and outlines the calculation of the dielectric function of the sample. Surface-plasmon oscillations (SPO) and guided modes are discussed. Gratings could not be included because of space limitations. Next, some recent papers are reviewed, selected to exemplify both the versatility and limitations of ATR.

## SURFACE-PLASMON OSCILLATIONS II

Surface-plasmon waves are EM waves propagating along the interface of a metal and a dielectric (or air). The conditions for their existence can be derived from Maxwell equations. Take a coordinate system such that the interface is the xy plane, the x axis is the propagation direction and z is the normal. Let the index 0 refer to the dielectric and 1 to the metal. Superscript + indicates the direction into the metal ($0 \rightarrow 1$).

First consider $p$-polarization ($E_z$, $E_x$, $H_y$, $k_x$, and $k_z$). The continuity equations for $E$, $D$, and $H$ are

$$E_{0x}^{+} = E_{1x}^{+} \tag{1}$$

$$H_{0y}^{+} = H_{1y}^{+} \tag{2}$$

$$D_{0z}^{+} = D_{1z}^{+}. \tag{3}$$

The Maxwell relation for harmonic waves is

$$\mathbf{k} \times \mathbf{H} = \left(\frac{\omega}{c}\right)\mathbf{D}. \tag{4}$$

Substitution of Eqs. 1, 2, and 3 into Eq. 4 yields the following relations between the **k** vectors:

$$\frac{k_{0z}}{\varepsilon_0} + \frac{k_{1z}}{\varepsilon_1} = 0 \tag{5}$$

$$k_{0x} = k_{1x}. \tag{6}$$

By inserting this into the dispersion equation, the result is

$$k_{0x}^2 = k_{1x}^2 = \left(\frac{\omega}{c}\right)^2 \frac{\varepsilon_0 \varepsilon_1}{\varepsilon_0 + \varepsilon_1}. \tag{7}$$

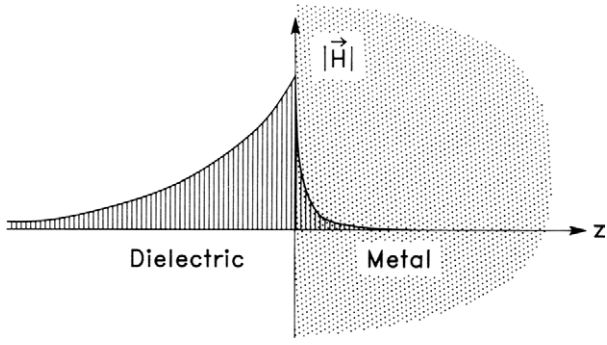


**Fig. 1.** Schematic showing the optical field at an interface that supports surface plasmons. $\mathbf{E}_z$, $\mathbf{E}_x$, $\mathbf{H}_y$, $\mathbf{k}_x$, and $\mathbf{k}_z$ define a surface plasmon propagating down the $x$ axis (into the page); see the discussion of Eqs. 1–7.

Following the same sequence for $s$-polarization ($E_y$, $H_x$, $H_z$), the relation for the $k$ vectors is

$$k_{0z} + k_{1z} = 0 \tag{8}$$

$$k_{0x} = k_{1x}. \tag{9}$$

Inserting this in the dispersion equation leads to

$$k_0^2 = \left(\frac{\omega}{c}\right)^2 \varepsilon_0 = k_1^2 = \left(\frac{\omega}{c}\right)^2 \varepsilon_1, \tag{10}$$

but this is an inconsistency, which means that the boundary conditions have solutions only for $p$-polarized waves; $s$-polarized surface-plasmon waves do not exist.

Inside the metal, the amplitude of the normal component of the plasmon wave decreases, as shown schematically in Fig. 1 and according to the expression

$$\exp(-2ik_{1z}z) \approx \exp\left(-4\pi \operatorname{Im}\sqrt{\varepsilon_1}\frac{z}{\lambda}\right) \tag{11}$$

for small $k_{0x}$. The wave penetrates much less than one wavelength. The tangential component, $k_{0x}$, is also complex; however, the imaginary part is

small compared with the real part, and the wave can be regarded as a damped oscillation propagating some distance along the surface.

In the visible spectrum, the propagation distance is small compared with the width of the incident beam, whereas in the infrared (IR), propagation attains macroscopic dimensions, although it is still a damped wave. Thus, the plasmon wave is limited to the surface region and is said to be *nonradiative*. Radiative surface plasmons do exist, but they are beyond the scope of this discussion. Nonradiative plasmon waves cannot be excited by light incident on a metal surface in vacuum or air because the vacuum wave vector is always smaller than that of the plasmon. There are two ways to excite plasmon waves on smooth surfaces.

Historically, Otto [2, 3] was the first to show that if a prism is used in total reflection, the wave vector of the evanescent wave outside the reflecting surface can match that of the plasmon.

The tangential component of the evanescent wave is

$$k_{\parallel}=\frac{\omega}{c}\sqrt{\varepsilon_p}\sin\phi_i \tag{12}$$

where $\varepsilon_p$ is the permittivity of the prism and $\phi_i$ is the incidence angle inside the prism. At the critical incidence angle, $\sqrt{\varepsilon_p}\sin\phi_i=1$ and $k_{\parallel}=\omega/c$. At normal incidence, $k_{\parallel}=\omega/c\sqrt{\varepsilon_p}$. Thus, $k_{\parallel}$ increases from $\omega/c$ to $\omega/c\sqrt{\varepsilon_p}$ as $\phi_i$ is increased beyond total reflection.

If a metal surface is brought close to the prism, a surface-plasmon wave is generated when $k_{\parallel}$ equals the plasmon wave vector $k_{0x}$. The plasmon dissipates energy, and the reflected intensity decreases. The normal component of the evanescent wave in the gap is

$$k_{\perp}=\frac{\omega}{c}\sqrt{1-\varepsilon_p\sin^2\phi_i}, \tag{13}$$

and the intensity decreases as

$$\exp\left(-4\pi\,\mathrm{Im}\sqrt{1-\varepsilon_p\sin^2\phi_i}\,\frac{z}{\lambda}\right). \tag{14}$$

Thus, the gap between the prism and the metal surface must be of the order of the wavelength, which requires care in the visible region, but which is easier in the IR.

A second method was suggested in a paper submitted about four months later. Kretschmann and Raether [7] showed that a thin metal film evaporated directly onto the prism can serve to excite plasmon waves at the *metal/dielectric* (air) interface, provided the index of refraction of the prism is larger than the index of the dielectric (air). In addition, there are some restrictions on the dielectric function of the metal. Optically, the system now has two interfaces: prism/metal and metal/dielectric (air) and there are four boundary equations:

$$E_{0x}^{-} = E_{1x}^{+} + E_{1x}^{-} \tag{15}$$

$$H_{0y}^{-} = H_{1y}^{+} + H_{1y}^{-} \tag{16}$$

$$E_{1x}^{+}\exp(-ik_{1z}d) + E_{1x}^{-}\exp(+ik_{1z}d) = E_{2x}^{+}\exp(-ik_{2z}d) \tag{17}$$

$$H_{1y}^{+}\exp(-ik_{1z}d) + H_{1y}^{-}\exp(+ik_{1z}d) = H_{2y}^{+}\exp(-ik_{2z}d), \tag{18}$$

where index 0 refers to the prism, 1 to the metal, and 2 to the dielectric (air). The 0/1 interface is at $z_0$, the 1/2 surface at $z_1$ and $d = z_1 - z_0$. Superscript + indicates the direction prism→metal→dielectric.

On eliminating $H$, the relation for the incident and reflected $E$ vectors is

$$\begin{bmatrix} \dfrac{k_{1z}}{\varepsilon_1} + \dfrac{k_{0z}}{\varepsilon_0} & \dfrac{k_{1z}}{\varepsilon_1} - \dfrac{k_{0z}}{\varepsilon_0} \\ \left(\dfrac{k_{1z}}{\varepsilon_1} - \dfrac{k_{2z}}{\varepsilon_2}\right)\exp(-ik_{1z}d) & \left(\dfrac{k_{1z}}{\varepsilon_1} + \dfrac{k_{2z}}{\varepsilon_2}\right)\exp(ik_{1z}d) \end{bmatrix} \begin{pmatrix} E_{0x}^{+} \\ E_{0x}^{-} \end{pmatrix} = 0. \tag{19}$$

Solutions exist only if the determinant is zero:

$$\left(\frac{k_{0z}}{\varepsilon_0} + \frac{k_{1z}}{\varepsilon_1}\right)\left(\frac{k_{1z}}{\varepsilon_1} + \frac{k_{2z}}{\varepsilon_2}\right)\exp(ik_{1z}d)$$

$$+ \left(\frac{k_{0z}}{\varepsilon_0} - \frac{k_{1z}}{\varepsilon_1}\right)\left(\frac{k_{1z}}{\varepsilon_1} - \frac{k_{2z}}{\varepsilon_2}\right)\exp(-ik_{1z}d) = 0, \tag{20}$$

which then is the condition for the existence of a plasmon wave in the metal

film. Equation 20 is the form used by Raether [9]. It can be condensed by introducing the Fresnel coefficients for $p$-polarization:

$$r_{01} = \left(\frac{k_{0z}}{\varepsilon_0} - \frac{k_{1z}}{\varepsilon_1}\right) \Big/ \left(\frac{k_{0z}}{\varepsilon_0} + \frac{k_{1z}}{\varepsilon_1}\right) \tag{21}$$

$$r_{12} = \left(\frac{k_{1z}}{\varepsilon_1} - \frac{k_{2z}}{\varepsilon_2}\right) \Big/ \left(\frac{k_{1z}}{\varepsilon_1} + \frac{k_{2z}}{\varepsilon_2}\right) \tag{22}$$

$$r_{01} r_{12} \exp(-2ik_{1z}d) + 1 = 0. \tag{23}$$

Although the analysis is more complicated, the Kretschmann configuration relies on the same principle as the Otto scheme. The wave vector of the light in the prism has increased to $\omega/c\sqrt{\varepsilon_p}$ and at some angle of incidence can equal $k_{0x}$ for the plasmon. Since this experimental arrangement is more manageable, it is now widely used. The metal film on the prism is usually about 50 nm of Ag or Au, these metals having optimum permittivities in the visible spectrum; Al has been used at short wavelengths. The film to be examined is deposited on the metal film. Analysis of this structure is discussed below. It is of interest here that nine years before the Kretschmann paper, Turbadar [19, 20] reported that thin Al films deposited on a prism have near-zero reflectivity for an incident angle slightly above total reflection and for $p$-polarization. He showed this to be in agreement with thin-film theory. However, surface-plasmon oscillations were not mentioned, and seemingly, the work did not receive further attention.

## OPTICAL ANALYSIS OF ATR STRUCTURES III

Samples are prepared and measured in steps. First, a 50 nm Ag or Au film is evaporated onto a prism or half-cylinder of high-index glass. The reflectivity is measured for $p$-polarized light as a function of the angle of incidence starting near the angle of total reflection. The reflectivity versus angle curve will show a sharp minimum at a certain angle depending on the index of the prism. Typically, the minimum will be at about 0.05, the width at half-height about 1°. From the angle, the minimum, and the width, one obtains the exact thickness and the permittivity of the layer. Next, the layer to be analyzed is deposited. This can take many forms, from evaporated

films of a dielectric or a metal, to molecular layers deposited by the Langmuir–Blodgett technique, and even operating liquid-crystal cells and metal electrodes in an electrolytic cell. Examples are discussed in the next section. However, the analysis is applicable to all cases. The new layer will change the critical angle and thus the position of the minimum. It may also impose more damping, and thus the curve will be wider. More than one layer can be applied but for each layer one must obtain the ATR curve. The total thickness of all layers should not be larger than the wavelength of the evanescent wave in the sample, typically a fraction of a micron in the visible.

An ATR sample, then, is a stratified multilayer structure. The optical analysis of such structures has been well documented in textbooks [21, 22] and papers [23, 24]. It is based on the continuity of the tangential components of the $E$ and $H$ fields and the normal components of $D$ at each interface as was exemplified in Eqs. 1–3. Also in each layer there are the Maxwell relations between the tangential components of $E$ and $H$. Thus, the entire structure is described by a set of linear equations, which can become rather large, because there are 12 equations for each interface. Only the external values of $E$ are observable quantities (reflectance and transmittance); all others can be eliminated algebraically. Eliminating $H$ for each layer results in a relation for the $E$ vectors on the two sides of each interface, which is conveniently written as a Jones $2 \times 2$ matrix. Next, the two matrices for each layer are combined, and one obtains a new matrix, called the *characteristic matrix*, which relates the $E$ vectors on the two sides of each layer. The structure is then described by the product of these matrices taken in succession.

Take—as before—all interfaces in consecutive xy planes at $z_0, z_1 \ldots z_n$ and the plane of incidence xz so that the plasmon propagates in the x direction. The result of this vectorization is

$$\begin{pmatrix} E_{0x}^{+} \\ E_{0x}^{-} \end{pmatrix} = [M_0][M_1] \ldots [M_{n-1}] \begin{pmatrix} E_{nx}^{+} \exp(-ik_{nz}z_n) \\ 0 \end{pmatrix} \tag{24}$$

$$[M_i] = \frac{\dfrac{k_{iz}}{\varepsilon_i} + \dfrac{k_{i+1,z}}{\varepsilon_{i+1}}}{2\dfrac{k_{i+1,z}}{\varepsilon_{i+1}}} \exp(ik_{iz}d_i) \begin{bmatrix} 1 & r_{\mathrm{pi}} \\ r_{\mathrm{pi}}Ex & Ex \end{bmatrix}, \tag{25}$$

where $E_{0x}^{+}$ is the $x$-component of the incident wave; $E_{0x}^{-}$ is the $x$-component of the reflected wave; $r_{\mathrm{pi}}$ is the Fresnel coefficient at interface $i$; $Ex = \exp(-2ik_{iz}d_i)$; $d_i = z_{i+1} - z_i$ is the thickness of layer $i$.

The product of the matrices $M_i$ is again a $2 \times 2$ matrix. If $c_{ij}$ denotes the matrix terms, then the Fresnel reflectance is the ratio of $c_{21}$ and $c_{11}$:

$$\begin{pmatrix} E_{0x}^{+} \\ E_{0x}^{-} \end{pmatrix} = \begin{bmatrix} c_{11} & c_{12} \\ c_{21} & c_{22} \end{bmatrix} \begin{pmatrix} E_{nx}^{+} \exp(-ik_{nz}z_n) \\ 0 \end{pmatrix} \tag{26}$$

$$r \equiv \frac{E_{0x}^{-}}{E_{0x}^{+}} = \frac{c_{21}}{c_{11}} \tag{27}$$

and the calculated reflectance is

$$R = rr^{*}. \tag{28}$$

To obtain the observed values, this has to be corrected by the reflections at the two prism surfaces.

The phase difference between the reflected and incident beam is

$$E_{0x}^{-} = E_{0x}^{+} r = E_{0x}^{+}(r' + ir'') = E_{0x}^{+} \sqrt{R} \exp i\phi \tag{29}$$

$$\phi = \tan^{-1} \frac{r''}{r'}. \tag{30}$$

Note that only ratios of matrix terms are involved. The factors outside the matrix brackets need not be evaluated. This saves computer time, but much more important, it avoids accumulation of round-off errors. Retaining the exponential terms in the matrices can lead to instabilities [25].

It will now be clear why it is necessary to obtain an ATR curve for each layer. Then all previous parameters are known, and there is only one set of $d$ and $\varepsilon$ values to be determined. The procedure is entirely iterative, but programming details will not be discussed here.

For a two-interface system, for example, prism/Ag/air, the $[c_{ij}]$ matrix is readily evaluated:

$$\begin{bmatrix} 1 & r_{01} \\ r_{01} & 1 \end{bmatrix} \begin{bmatrix} 1 & r_{12} \\ r_{12}E_x & E_x \end{bmatrix} = \begin{bmatrix} 1 + r_{01}r_{12}E_x & r_{12} + r_{01}E_x \\ r_{01} + r_{12}E_x & r_{01}r_{12} + E_x \end{bmatrix}, \tag{31}$$

and one obtains the well-known expression,

$$r=\frac{r_{01}+r_{12}\exp(-2ik_{1z}d)}{1+r_{01}r_{12}\exp(-2ik_{1z}d)}. \tag{32}$$

Kretschmann [8] analyzed Eq. 32 analytically and compared the theory and his experimental results. The paper presents graphs of the reflectivity versus wavelength for constant film thickness and for the reflectivity versus film thickness at constant wavelength for Ag films deposited on a prism. At longer wavelength the damping increases and the curves are wider. The optimum film thickness is about 50 nm for Ag. For thinner films the minimum decreases, and the curves flatten out.

Pockrand [26] studied damping by thin transparent and absorbing coatings. The coating changes the field at the interface. The net result is that for transparent coatings the ATR resonance minimum shifts to larger angles, and the half-width of the curve increases, but the minimum itself remains unaffected. For absorbing coatings the resonance minimum shifts, the curves become wider and asymmetric, and the reflectivity minimum is less pronounced. These results are reproduced in Fig. 2. Optimum thickness of the metal is that for which radiative losses equal the internal loss. Thus, if $|\varepsilon''|$ is larger, the film thickness must be decreased.

For a multilayer system the algebraic expressions for the matrix terms become unwieldy, but numerical techniques can be used to extend these results.

## IV GUIDED MODES

Thin-film waveguides were first discussed in a series of papers by Tien and Ulrich [27–29] in 1969 and 1970. Shortly thereafter, Marcuse [30] published a monograph on the theory of dielectric optical waveguides (1974). Tien [31] published a comprehensive tutorial paper in 1977. Swalen [32] reviewed optical-wave spectroscopy in 1979. Rabolt and Swalen [33] reviewed integrated optics for Raman spectroscopy in 1988.

Tien *et al.* [27, 28] showed that a thin dielectric film deposited on a substrate that has a lower index of refraction can form a perfect waveguide. A wave propagating through the film is then totally reflected at both interfaces; outside the film only evanescent waves exist. The light is coupled in by the evanescent wave of a prism in the Otto configuration. The essential difference with the Otto experiment lies in the permittivity of the film. Otto used a metal with $\varepsilon'<0$, $\varepsilon''\gg 0$. Tien and Ulrich used a dielectric with $\varepsilon'>0$, $\varepsilon''\approx 0$.

A wave can propagate in a light guide only if the phase difference after one cycle is a multiple of $2\pi$; otherwise, there will be destructive interference. In addition, the imaginary part of the permittivity must be very small.

By using the matrix method, the amplitude after one cycle is

$$E_{1x}^{+2} = E_{1x}^{+0} r_{10} r_{12} \exp(-2ik_{1z}d), \tag{33}$$

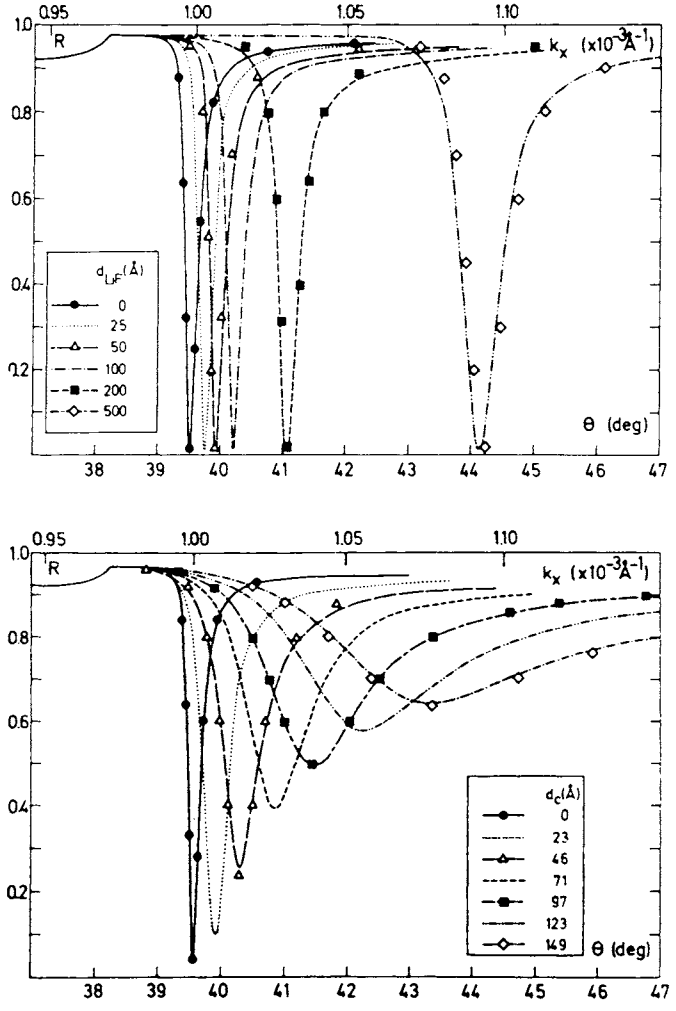


**Fig. 2.** Measured and calculated SPO resonance curves for Ag films with LiF coatings (top) of various thicknesses and carbon coatings (bottom) of various thicknesses. From I. Pockrand, *Surf. Sci.* **72**, 577 (1978). With permission from the publisher.

where $r_{12}$ is the Fresnel coefficient at the film-substrate interface and $r_{10}$ the coefficient at the film-air surface. The phase shift is obtained as in Eq. 30 from the ratio of the imaginary and real parts.

Thus, for a given film structure there exist only a discrete set of values for $k_{1z}$ for which the phase shift will be an integral value of $2\pi$. The tangential component of the wave vector in the prism equals $k_{1x}$ in the film, and thus, propagating waves are generated only if the angle of incidence is such that

$$k_{\parallel}^2 + k_{1z}^2 = \left(\frac{\omega}{c}\right)^2 \varepsilon_1. \tag{34}$$

Tien and Ulrich considered the special case $k_{1z}$ real, $k_{0z}$ and $k_{2z}$ purely imaginary. Then the Fresnel coefficients have the form

$$r_{10} = \exp iQ_{10} \rightarrow \tan Q_{10}/2 = \frac{k_{0z}}{\varepsilon_0}\frac{\varepsilon_1}{k_{1z}} \tag{35}$$

$$r_{12} = \exp iQ_{12} \rightarrow \tan Q_{12}/2 = \frac{k_{2z}}{\varepsilon_2}\frac{\varepsilon_1}{k_{1z}}, \tag{36}$$

and the mode equation can be written as

$$Q_{10} + Q_{12} - 2k_{1z}d = 2\pi m. \tag{37}$$

Notice that the mode equation is the Bragg equation with terms added to account for the phase shift caused by total reflection. Equations 34 and 37 impose no restrictions on the polarization of the incident beam. Of course, the Fresnel coefficients are different, as will be the positions of the guided modes. For $\varepsilon$ real and scalar, the film thickness $d$ and $\varepsilon$ can be obtained if at least two modes can be observed. Many films are not isotropic and $\varepsilon$ is a tensor. Then the film must be scanned in two mutually perpendicular directions. A four-sided pyramid can be used instead of a prism; examples of this are given in the next section. However, even if sufficient data are available, the problem is still undetermined: an *a priori* assumption must be made for the tilt angle of the optic axis.

ATR and guided modes are often combined by using an ATR prism, that is, by first evaporating about 50 nm of Ag. At a certain angle a plasmon wave is excited at the Ag surface. At other angles the evanescent wave at the Ag surface can excite guided waves in the waveguide. For *s*-polarization there is of course no ATR minimum.

From Eq. 34 or 37, tables or graphs for the function with the mode number as parameter can be made as a guide for the design of the waveguide (for examples, see [27, 53]).

## APPLICATIONS OF ATR V

We review here a number of papers selected to demonstrate the versatility and the limits of ATR and integrated optics.

### Optical Constants of Metals A

Gugger *et al.* [34, 35] determined the dielectric function for Ag from 441.6 nm to 676.4 nm using the Kretschmann configuration, prism/Ag/air. Data for two samples agreed to about 1%. If the air is replaced by hexane or carbon tetrachloride, slightly larger values for the dielectric function were obtained. This was attributed to a surface modification of the dielectric function of silver.

Bradberry *et al.* [36] measured $n$ and $k$ for W and Mo at 3.39 $\mu$m using the Otto configuration with gap spacings in the order of 10 $\mu$m. For all metals, $n$ and $k$ are larger in the IR than in the visible part of the spectrum. Thus, there is more damping. The minimum ATR reflectivity is larger, and the resonance is wider. For Ag, for example, at 0.6328 $\mu$m $n = 0.14$, $k = 4.4$, and the ATR minimum is typically 0.04. At 3.26 $\mu$m $n = 1.54$, $k = 19.8$, and the observed minimum is only 0.8. Recently [37] the work was extended to include Ni, Pd, and Pt. The gap was varied between 5 $\mu$m and 10 $\mu$m, and the results agree to about 2%.

### Molecular Films B

The Langmuir–Blodgett (LB) technique allows repetitive deposition of a single molecular layer of a fatty-acid salt (thickness 25Å–30Å, approxi-

mately equal to the chain length). An ATR curve can be made readily after each deposition, which makes it an elegant way to study ATR molecular layers. In 1986, Swalen [16] reviewed the extensive literature on optical properties of LB films. Here we summarize only the important ATR papers leading to the more recent work.

Gordon and Swalen [38] obtained ATR curves for the system Cd-arachidate on Au. Up to four monolayers were deposited. The peak shift is of the order of 0.5° per layer, much larger than the angular resolution 0.02°.

Pockrand *et al.* [40] extended the work, using Ag as the ATR metal, and calculated the index for Cd-arachidate for each monolayer deposited. The film is obviously anisotropic. However, one cannot determine the complete $\varepsilon$ tensor from a single SPO resonance curve. Assuming a constant difference, $n_0 - n_e = 0.043$, $n_0$ and $n_e$ were calculated. Later [41], the work was extended to include dyes having a strong absorption band in the visible region. The dyes chosen had C18 hydrocarbon chains, as in arachidic acid. As it turned out for one dye, the molecular alignment in the film is identical with that of Cd-arachidate. Thus, the film is anisotropic, and again the dielectric function is a tensor. It was assumed that the permittivity perpendicular to the film plane is the same as that of Cd-arachidate (real), whereas the parallel component is complex. The inplane permittivity was determined from surface-plasmon resonance curves at different wavelengths.

Swalen *et al.* [42, 43] determined the indices of Cd-arachidate films using the guided-mode techniques (1978). The films were deposited on glass or on PMMA, and mode patterns were obtained for both *s*- and *p*-polarization at three wavelenghts. The film thickness was obtained from the number of monolayers for each run (30–40), and the ordinary and extraordinary indices were calculated. These results are reproduced in Fig. 3.

Barnes and Sambles [44, 45] used much thicker LB films, about 1.1 microns. The light was coupled in by the evanescent wave from an Ag film deposited on the base of a four-sided pyramid. From the ATR curves combined with the guided-mode resonances in the xz and yz planes, there was enough information to determine the complete tensor if the tilt angle was known. As it turned out, the sample used, 22-tricosenoic acid, is best described as a biaxial birefringent film.

Loulergue *et al.* [46] used ATR to study the effect of a static electric field on an LB film of an azo dye. The dye (DPNA) has a C12 aliphatic chain and can be deposited on an Ag film on a slide using the technique. A second Ag-coated slide is mounted with spacers onto the first, so that a field can be applied across the film. Light is coupled in through a prism and an index-matching oil. Curves are shown for the ATR reflectivity and the differential reflectivity versus applied electric field.

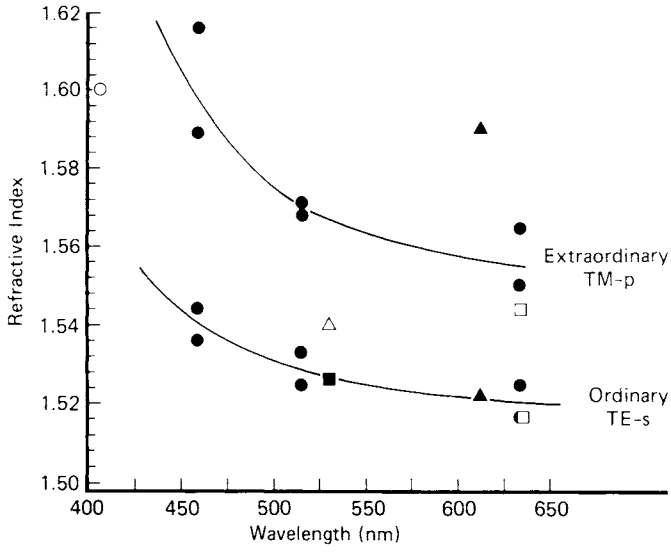


**Fig. 3.** Dispersion curves for the optical constants of Cd-arachidate. From J. D. Swalen, K. E. Rieckhoff, and M. Tacke, *Opt. Commun.* **24**, 146 (1978). With permission from the publisher.

## Organic Dyes C

Philpott *et al.* [47–48] obtained ATR curves for three organic dyes at wavelengths within the absorption bands. The dyes chosen all reflect light with a metallic luster although they are insulators. The reflection is, of course, quite different from metallic reflection, and a new name, *exciton surface polaritons*, was introduced to distinguish this effect from *plasmon surface polaritons* at metal surfaces. The dyes are anisotropic, and the permittivity is a tensor. The dielectric function is assumed to be given by a Lorentz–Lorenz expression, and practical formulas are given to calculate ATR spectra. Again, the criterion is that within the exciton band $|\varepsilon'| < -1$ (Otto configuration). The important difference from metals is that for exciton surface polaritons, the ATR minimum can occur at either side of the critical angle. One of the dyes (TCNQ) indeed has ATR minima below the critical angle.

The ratio of the imaginary and real parts of the permittivity for these dyes is much larger than it is for Ag or Au, and thus, the damping is much larger. Half-widths are typically 4°.

## D Dielectric Films

Levy *et al.* [49] were probably first in using a four-sided pyramid instead of a prism to analyze anisotropic films. The dielectric is a thick (570 nm) film of angularly deposited $SiO_x$. Angular deposition is used to produce liquid-crystal (LC) cells with large surface tilt angle. (For LC cells, much thinner layers (20 nm) are used, but thin films cannot be examined by SEM.)

For thin films only surface-plasmon oscillations are observed. For thick films both SPO and guided modes were observed, the $SiO_x$ film acting as the waveguide (see Fig. 4). The calculated indices for the $SiO_x$ film were $n_0 = 1.253$ and $n_e = 1.239$, well below the value for $SiO_x$ glass. Reflectivity curves obtained with the film immersed in hexane showed a large shift in the SPO minimum, and it was concluded that void areas surrounded the $SiO_2$ columns. By applying effective-media theory, it was shown that the columns have an index of about 1.47 but occupy only 0.54 of the film's volume.

## E Surface Tilt Angle of Nematic Liquid Crystals

Thin layers of nematic liquid crystals will align uniformly between two specially prepared glass surfaces. The liquid layer then is uniaxial birefringent. A thin $SiO_2$ film obtained by oxidizing silane in an Ar-$O_2$ plasma will produce parallel alignment; that is, the optic axis of the cell is parallel with the substrate surface, and its direction is determined by the deposition geometry. A polyfluorocarbon film produced from tetrafluoroethylene in an RF plasma will produce cells in which the optic axis is perpendicular to the surface [50]. Swalen and Sprokel [51] used ATR prisms of the Kretschmann configurations as one of the substrates of an aligned LC cell and determined $n_0$ and $n_e$ for the LC.

A gold film (approximately 50 nm) was evaporated onto a prism cut from glass having an index larger than $n_0$ of the liquid crystal. The ATR curve was obtained, and $d$ and $\varepsilon$ for the Au film were calculated. Next, the aligning layer was deposited and from the new ATR curve, $d$ and $\varepsilon$ for the aligning layer were obtained. Finally, the LC cell was assembled, and the index for the aligned LC was obtained. Thus, $n_0$ and $n_e$ are obtained independently and without *ad hoc* assumptions for the orientation of the optic axis. The results were in good agreement with the bulk data.

Since ATR probes about 100 nm into a 6 $\mu$m LC cell, it can be used to obtain the surface tilt angle of the LC molecules. This is an important parameter in the theory for the deformation of an LC in an electric field.

Sprokel *et al.* [52] obtained ATR curves for an operating LC cell initially aligned with the optic axis parallel to the surface and in the plane of incidence. The parameters were determined as described above, then ATR

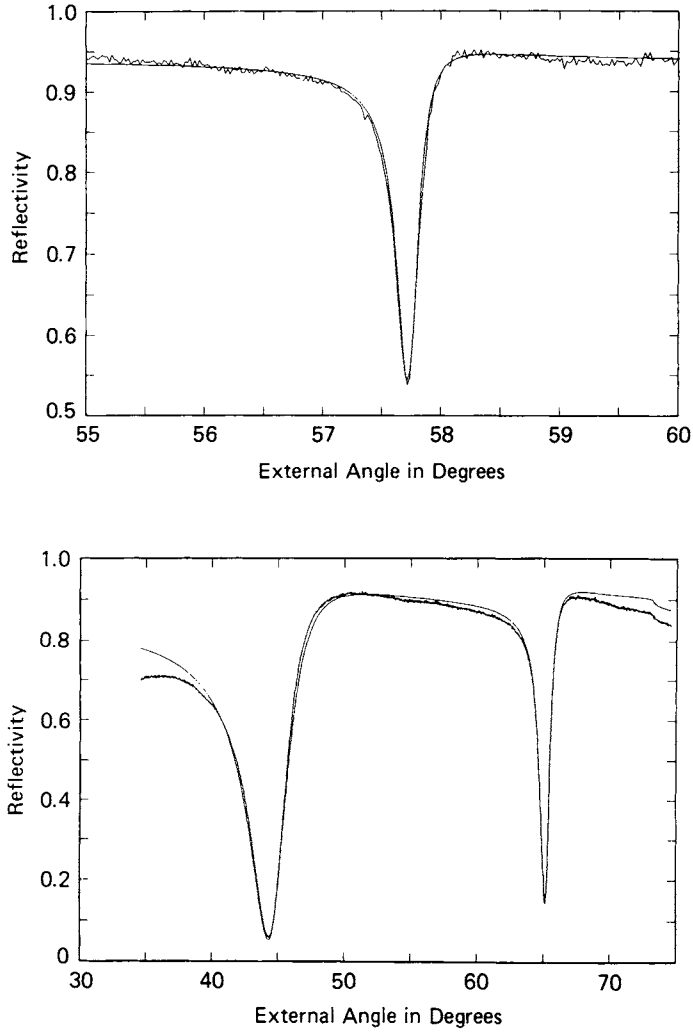


**Fig. 4.** Measured and calculated ATR reflectivity curves for thick $SiO_x$ films on Au. Top: *s*-polarized incident wave, guided-mode resonance at 57.7 nm. Bottom: *p*-polarized incident wave, guided-mode resonance at 44.32 nm, SPO resonance at 65.2 nm. From Y. Levy, M. Jurich, and J. D. Swalen, *J. Appl. Phys.* **57**, 2601 (1985). With permission from the publisher.

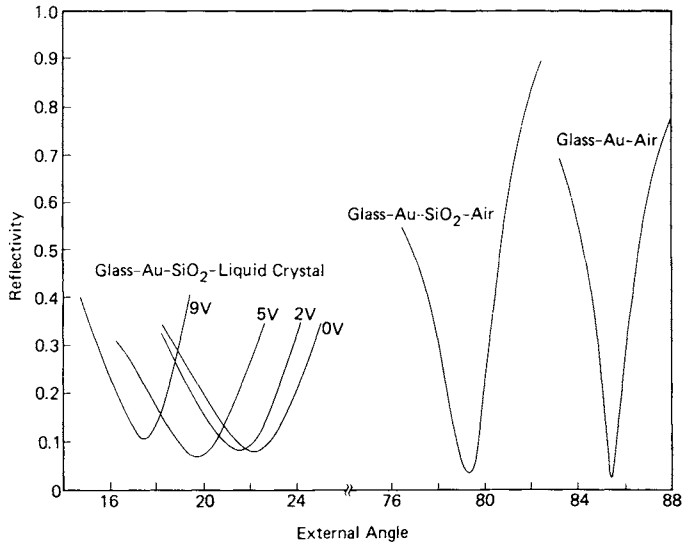


**Fig. 5.** ATR reflectivity curves on an operating liquid-crystal cell. Initially the optic axis is parallel with the surface and in the plane of incidence. The tilt angle at the surface can be calculated from the observed index. From G. J. Sprokel, R. Santo, and J. D. Swalen, *Mol. Cryst. Liq. Cryst.* **68**, 29 (1981). With permission from the publisher.

curves were obtained as a voltage was applied across the cell. Since the indices for parallel and perpendicular orientation are known, the tilt angle near the surface can be calculated from the ATR curves at each applied voltage without introducing new assumptions. It was found that liquid crystals bent away from the surface much faster than indicated by the Frank–Oseen theory and the standard boundary conditions. Figure 5 exemplifies the ATR resonance curves as a square-wave voltage is applied to the cell.

Starting in 1987, the group at Exeter University, U.K., has published extensively on ATR experiments with LC cells [53, 54]. Their method is identical: the cell has the Kretschmann configuration; parameters of the successive layers are determined one at a time as in the original work. Of interest is the fact that guided modes appear near the ATR minimum, which was not observed in the earlier work. An important difference is in the aligning layers used by the two groups. The IBM group used a smooth and dense $SiO_2$ film (it had the same index as $SiO_2$ glass, $n = 1.457$). The Exeter group used an $SiO_x$ film deposited by angle evaporation. Such films are rough and porous because of columnar growth and can couple to a surface plasmon as a grating as well as through the evanescent wave.

The aligning layers in both experiments are too thin to support guided modes. However, the alignment of the liquid crystal near the surface is quite different. The overall effect of a field on parallel and tilted aligned

cells was studied in some detail [54]. Information about the change in surface tilt for tilted aligned cells by an external field is not available.

### Tutorial Demonstration of ATR F

Swalen *et al.* [57] demonstrated ATR using a Kretschmann prism, a cylindrical lens, a prism, and a light source available in any optics lab. The prism produces a continuous spectrum that is focused by the lens onto the base of the Kretschmann prism. The projected light is in effect a display of wavelength versus incident angle, and it consists of the continuous spectrum except for the angles where surface-plasmon resonance occurs, reducing the reflectivity to almost zero. Similarly, using a stepped LB wedge, the effect of each step can be shown.

### Guided Modes and ATR G

If an Ag-coated prism is used to excite guided modes in a waveguide, the ATR resonance will probably occur at an angle different from those for the guided modes. However, by choosing the proper thickness of the waveguide, it should be possible to match the ATR resonance with one of the guided modes.

Nakagawa *et al.* [58] showed experimentally that this is feasible by using a waveguide of the correct thickness to excite a plasmon-surface-polariton wave in an Ag film deposited on the waveguide. The cavity was a $Ta_2O_5$ film on a quartz substrate. The light was coupled in and out by $TiO_2$ prisms. The Ag film is deposited on an $SiO_2$ film on the $Ta_2O_5$. The mode chosen to excite the plasmon resonance is sharply attenuated (10 dB), whereas other modes show very little attenuation.

### Long-Range Surface-Plasmon Waves H

In his review paper, Raether [9] discussed coupling of the modes at the two interfaces of a thin metal film as in the Kretschmann configuration. The topic was later taken up by Sarid *et al.* [59–61], Stegeman *et al.* [62], and others, and this led eventually to a proposal for electro-optic modulators [63].

If the metal film is bounded by identical dielectric layers, the surface-plasmon oscillations on both sides are also identical. If the film is thin enough, the evanescent waves extending into the metal overlap and split into symmetric and antisymmetric modes [9]. If the dielectric layers have slightly different indices, each of the two modes will split in two branches.

The metal film can be regarded as a waveguide, and the standard Eq. 37 can be used to obtain the propagation constants. The antisymmetric mode carries most of its intensity in the dielectric layers; hence, the damping is smaller and the propagation distance is longer. Craig *et al.* [60] obtained 0.25 mm on a 10 nm Ag film. Schildkraut replaced the lower dielectric with an electro-optic film. As a voltage is applied across the film, its index will change, and the coupling between the modes will change. Operated in the antisymmetric mode (*long-range surface-plasmon mode*), a potential of 100V changes the reflectivity from 0 to 0.84, whereas in the *normal surface-plasmon mode* the reflectivity changes from 0 to 0.12.

## VI CONCLUSION

The ATR method was described using classical physical optics. The technique is useful not only to obtain the optical constants of thin films, but more generally to study a variety of surface phenomena. Examples from recent literature were given to exemplify its versatility and its limitations.

### REFERENCES

1. N. J. Harrick, "Internal Reflection Spectroscopy," Wiley, New York, (1967).
2. A. Otto, *Z. Physik* **216**, 398 (1968).
3. A. Otto, *Z. Angew. Physik* **27**, 207 (1969).
4. A. Otto, *Festkörperprobleme*, **XIV**, 1 (1974).
5. A. Otto, in "Optical Properties of Solids," Elsevier, Amsterdam, chapter 13 (1976).
6. E. Kretschmann and H. Raether, *Z. Naturforschung*, **22a**, 1623 (1976).
7. E. Kretschmann and H. Raether, *Z. Naturforschung*, **23a**, 3135 (1968).
8. E. Kretschmann, *Z. Physik* **241**, 313 (1971).
9. H. Raether in *Physics of Thin Films*, Vol. 9, (G. Hass, M. H. Francombe, and R. W. Hoffman, eds.), Academic Press, New York, 145 (1977).
10. K. Holst and H. Raether, *Opt. Commun.* **2**, 313 (1970).
11. U. Fano, *J. Opt. Soc. Am.* **31**, 213 (1941).
12. Y. Y. Teng and E. A. Stern, *Phys. Rev. Lett.* **19**, 511 (1967).
13. R. H. Ritchie, E. T. Arakawa, J. J. Cowan, and R. N. Hamm, *Phys. Rev. Lett.* **21**, 1530 (1968).
14. E. Burstein, W. P, Chen, Y. J. Chen, and A. Hartstein, *J. Vac. Sci. Technol.* **11**, 1004 (1974).
15. E. D. Palik and R. T. Holm, *Opt. Eng.* **17**, 512 (1978).
16. J. D. Swalen, *J. Mol. Electronics* **2**, 155 (1986).
17. J. F. Rabolt and J. D. Swalen, in "Spectroscopy of Surfaces," (R. J. H. Clark and R. E. Hester, eds.), Wiley, New York, chapter 1 (1988).
18. M. K. Debe, *Prog. Surf. Sci.* **24**, 1 (1987).
19. T. Turbadar, *Proc. Phys. Soc. London* **73**, 41 (1959).
20. T. Turbadar, *Opt. Acta* **11**, 207 (1964).
21. H. Wolter, in "Handbuch der Physik," Vol. XXIV, (S. Flugge, ed.), Springer-Verlag, Berlin, 461 (1956).

22. O. S. Heavens, "Optical Properties of Thin Solid Films," Dover Publications, New York, 1965.
23. D. W. Berreman, *J. Opt. Soc. Am.* **62**, 502 (1972).
24. G. J. Sprokel, *Mol. Cryst. Liq. Cryst.* **68**, 39 (1981).
25. D. Y. K. Ko and J. R. Sambles, *J. Opt. Soc. Am. A* **5**, 1863 (1988).
26. I. Pockrand, *Surf. Sci.* **72**, 577 (1978).
27. P. K. Tien, R. Ulrich, and R. J. Martin, *Appl. Phys. Lett.* **14**, 291 (1969).
28. P. K. Tien and R. Ulrich, *J. Opt. Soc. Am.* **60**, 1325 (1970).
29. R. Ulrich, *J. Opt. Soc. Am.* **60**, 1337 (1970).
30. D. Marcuse, "Theory of Dielectric Optical Waveguides," Academic Press, New York, (1974).
31. P. K. Tien, *Rev. Mod. Phys.* **49**, 361 (1977).
32. J. D. Swalen, *J. Phys. Chem.* **83**, 1438 (1979).
33. J. F. Rabolt and J. D. Swalen, in "Spectroscopy of Surfaces," (R. J. H. Clark and R. E. Hester, eds.) Wiley, New York (1988).
34. H. Gugger, M. Jurich, J. D. Swalen, and A. J. Sievers, *Phys. Rev. B* **30**, 4189 (1984).
35. H. Gugger, M. Jurich, J. D. Swalen, and A. J. Sievers, *Phys. Rev. B* **34**, 1322 (1986).
36. G. W. Bradberry and J. R. Sambles, *Opt. Commun.* **67**, 404 (1988).
37. Y. Fuzi, G. W. Bradberry, and J. R. Sambles, *J. Mod. Opt.* **36**, 1405 (1989).
38. J. G. Gordon and J. D. Swalen, *Opt. Commun.* **22**, 374 (1977).
39. I. Pockrand, *Opt. Commun.* **13**, 311 (1975).
40. I. Pockrand, J. D. Swalen, J. G. Gordon, and M. R. Philpott, *Surf. Sci.* **74**, 237 (1977).
41. I. Pockrand, J. D. Swalen, R. Santo, A. Brillante, and M. R. Philpott, *J. Chem. Phys.* **69**, 4001 (1978).
42. J. D. Swalen, M. Tacke, R. Santo, and J. Fischer, *Opt. Commun.* **18**, 387 (1976).
43. J. D. Swalen, K. E. Rieckhoff, and M. Tacke, *Opt. Commun.* **24**, 146 (1978).
44. W. L. Barnes and J. R. Sambles, *Surf. Sci.* **177**, 399 (1986).
45. W. L. Barnes and J. R. Sambles, *Surf. Sci.* **187**, 144 (1987).
46. J. C. Loulergue, M. Dumont, Y. Levy, P. Robin, J. P. Pocholle and M. Papuchon, *Thin Solid Films* **160**, 399 (1988).
47. M. R. Philpott and J. D. Swalen, *J. Chem. Phys.* **69**, 2912 (1978).
48. M. R. Philpott, A. Brillante, I. R. Pockrand, and J. D. Swalen, *Mol. Cryst. Liq. Cryst.* **50**, 139 (1979).
49. Y. Levy, M. Jurich, and J. D. Swalen, *J. Appl. Phys.* **57**, 2601 (1985).
50. G. J. Sprokel and R. M. Gibson, *J. Electrochem. Soc.* **124**, 557 (1977).
51. J. D. Swalen and G. J. Sprokel, "The Physics and Chemistry of Liquid Crystal Devices," (G. J. Sprokel, ed.), Plenum, New York, (1979).
52. G. J. Sprokel, R. Santo, and J. D. Swalen, *Mol. Cryst. Liq. Cryst.* **68**, 29 (1981).
53. K. R. Welford and J. R. Sambles, *Appl. Phys. Lett.* **50**, 871 (1987).
54. K. R. Welford, J. R. Sambles, and M. G. Clark, *Liquid Crystals* **2**, 91 (1987).
55. R. A. Innes, K. R. Welford, and J. R. Sambles, *Liquid Crystals* **2**, 843 (1987).
56. G. J. Sprokel and N. Chou, *Liq. Cryst. Ordered Fluids*, Vol. 4, (A. G. Griffin and J. E. Johnson, eds.), Plenum, New York, 865 (1982).
57. J. D. Swalen, J. G. Gordon, M. R. Philpott, A. Brillante, I. Pockrand, and R. Santo, *Am. J. Phys.* **48**, 669 (1980).
58. Y. Nakagawa, M. Kaneko, and N. Terunuma, *Appl. Phys. Lett.* **53**, 2141 (1988).
59. D. Sarid, *Phys. Rev. Lett.* **47**, 1927 (1981).
60. A. E. Craig, G. A. Olson, and D. Sarid, *Opt. Lett.* **8**, 380 (1983).
61. D. Sarid, R. T. Deck, and J. J. Fasano, *J. Opt. Soc. Am. A* **72**, 1345 (1982).
62. G. I. Stegeman, J. J. Burke, and D. G. Hall, *Appl. Phys. Lett.* **41**, 906 (1982).
63. J. S. Schildkraut, *Appl. Opt.* **27**, 4587 (1988).

# Chapter 5

# Optical Properties of Superlattices

P. APELL
Institute of Theoretical Physics
Chalmers University of Technology
S-412 96 Göteborg, Sweden
and
O. HUNDERI
Division of Physics
Norwegian Institute of Technology
and
SINTEF, Applied Physics
N 7034 Trondheim, Norway

I. Introduction 97
II. The Classical Optical Response of a Multilayer System 98
III. Semiconductor Superlattices 101
A. Excitons and Single-Particle Excitations 102
B. Phonons 108
IV. Amorphous Superlattices 109
V. Collective Excitations 112
VI. Lattice Disorder 118
VII. The Effect of Nonlocal Dielectric Functions 120
VIII. Concluding Remarks 122
References 122

## INTRODUCTION I

The first GaAs/GaAlAs superlattice (SL), made by Chang *et al.* [1], realizing ideas put forward by Esaki and Tsu [2], represents a milestone in "material engineering" through the use of MBE technology. It consists of a periodic repetition of alternating layers of lattice-matched GaAs and $Ga_{1-x}Al_xAs$. The properties of the bulk materials are retained in the direction perpendicular to the stacking, whereas if the layer width is less than the Bohr radius ($a_0^*$) for the bulk material, novel quantum-mechanical confinement effects are obtained. These are to a certain extent


Copyright © 1991 by Academic Press.
All rights of reproduction in any form reserved.
ISBN 0-12-544422-2

controllable, leading to a wide range of applicabilities of such a material, especially in linear and nonlinear optical engineering. We refer the interested reader to the excellent textbook by M. Jaros [3]. In what follows we will discuss the new or modified optical characteristics that the SL shows, and that differ from the properties of the constituent materials. Our discussion will be in terms of the elementary excitations of such structures, especially their characteristics in the SL environment and most important, the new elementary excitations having origins in the SL construction, while being absent in the constituents. Our survey will basically cover single-particle excitations, excitons, phonons, and collective excitations such as plasmons and polaritons. Before starting, we notice that the original proposal by Esaki and Tsu was rejected for publication for being "too speculative" and invoking "no new physics" [4].

We will start this review by a discussion of the classical optical response of a superlattice in terms of the macroscopic dielectric functions of its constituents. This will be followed by a more detailed description of the elementary excitations in the SL, including collective excitations such as plasmons and polaritons. We conclude the review by a brief look at the effect of nonlocal dielectric functions.

## II THE CLASSICAL OPTICAL RESPONSE OF A MULTILAYER SYSTEM

When the layers in the superlattice are sufficiently thin, we can describe the optical properties of the SL on the average as those of a uniaxial material. Expressions for the effective dielectric constants can be derived for an ideal superlattice in the limit of infinitely thin, individual layers, and can be extended to finite layer thicknesses. If the lattice is aperiodic, if nonlocal effects are included, or if quantum-size effects are important, this effective-medium theory breaks down. However, we will illustrate by model calculations the effects of aperiodicity and nonlocality on the properties of metal-insulator superlattices. These show strong resonant excitation in the region above the bulk plasmon frequency. The existence of interfaces and potential steps at these lead to the creation of narrow quantum wells in such structures. This has a profound influence on band structure and band gaps even in the case of amorphous semiconductors.

The effective-medium response of a multilayer superlattice system of thin films may be derived in several ways; see [5, 6] and references therein. The most fruitful approach seems to be by way of transfer matrices. In this approach one considers a two- or multicomponent superlattice of materials a, b, c . . . , a, b, c, . . . with dielectric constants $\varepsilon_a$, $\varepsilon_b$, $\varepsilon_c$ . . . and thicknesses $d_a$, $d_b$, $d_c$ and total stack thickness $D$. The structure a, b, c . . .

represents the unit cell in a periodic structure. The transfer matrix of the total system is given by the product $M_aM_bM_c \ldots M_aM_bM_c \ldots$. Taking the limit $d_a$, $d_b$, $d_c \to 0$, $N \to \infty$, where $N$ is the total number of periods in the stack, in such a way that the total stack thickness is kept constant, leads to a transfer matrix, which is a function of four parameters only [5], namely $\langle\varepsilon\rangle$, $\langle 1/\varepsilon\rangle$, $D$, and the angle of incidence. Furthermore, this transfer matrix is identical in form to the transfer matrix of a single uniaxial film. This allows us to draw the following conclusion: a superlattice is optically equivalent to a uniaxial material with optic axis normal to the surface and with optical constants given by

$$\begin{aligned} \varepsilon_o &= \langle\varepsilon\rangle \\ 1/\varepsilon_e &= \langle 1/\varepsilon\rangle. \end{aligned} \tag{1}$$

Here $\varepsilon_o$ is the ordinary and $\varepsilon_e$ is the extraordinary dielectric constant, and the average is taken over one unit cell of the superlattice. These equations in the form given here are correct irrespective of the number of layers in the unit cell of the superlattice, as long as the total thickness of the unit cell is small compared to the wavelength of light in the material. These values for the effective constants are the same as the Wiener bounds. The superlattice thus exhibits the maximum optical anisotropy possible for a multicomponent mixture.

To illustrate the uniaxial nature of superlattices, we have calculated the effective dielectric constant for a hypothetical metal/insulator superlattice [5]. The metal was assumed to have a Drudelike, frequency-dependent dielectric constant; the insulator was assumed to have a frequency-independent dielectric constant, $\varepsilon_i$, equal to 2.25. Figure 1a shows the imaginary part of the calculated dielectric constants. The ordinary dielectric constant is that of a Drude metal with an electron density equal to the average electron density in the superlattice. The extraordinary spectrum is the same as that of a single bound oscillator shifted from $\omega_0 = 0$, characteristic of a metal, to

$$\omega_o = \omega_p / \sqrt{1 + \varepsilon_i f/(1-f)}, \tag{2}$$

where $\omega_p$ is the plasmon frequency, and $f$ is the filling factor of metal; $f = 1$ corresponds to only metal. The corresponding reflectivity at 60° for $\omega_p = 10$ eV and $f = 0.5$ is shown in Fig. 1b. At short wavelengths it behaves like a typical metal and it becomes transparent at roughly 5.5 eV. The high reflectivity around the plasmon frequency of the Drude metal is somewhat reminiscent of the reststrahlen band in insulators. In our case, the high

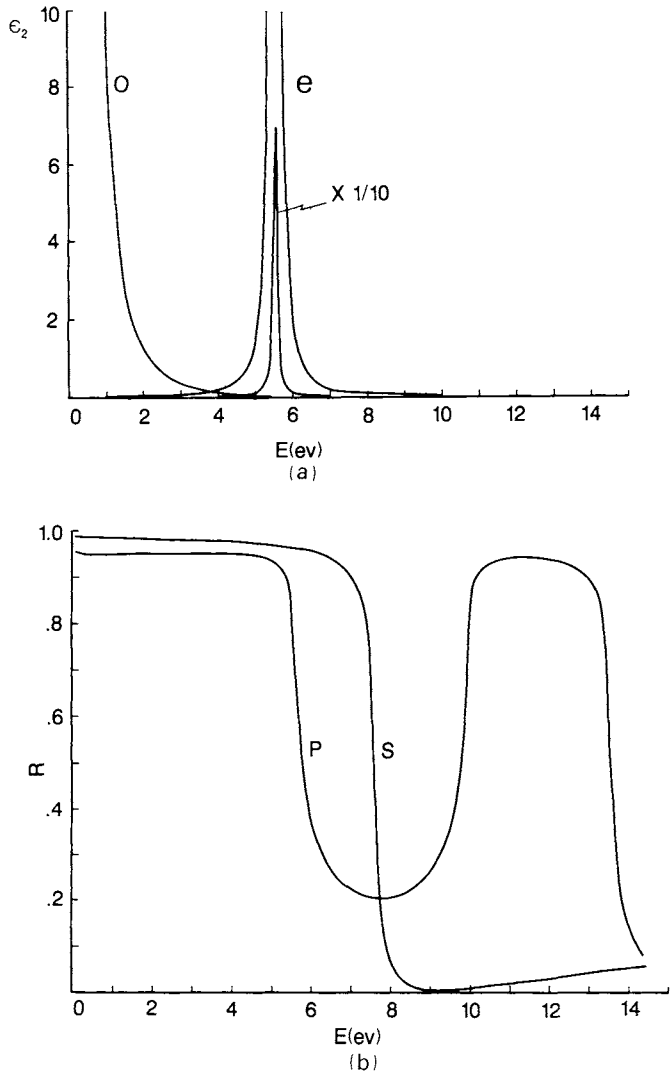


**Fig. 1.** (a) Imaginary parts of the ordinary (o) and extraordinary (e) dielectric constants, $\varepsilon_{o2}$ and $\varepsilon_{e2}$, versus energy, and (b) the corresponding reflectivity $R$ for both $s$- and $p$-polarized light at 60° angle of incidence. The parameters used in the calculation are $\hbar\omega_p = 10\,\text{eV}$, $\hbar/\tau = 0.1\,\text{eV}$ and filling factor $f = 0.5$.

reflectivity is caused by evanescent bulk-polariton excitation in the superlattice.

An effective-medium dielectric constant is meaningful and can be derived in the case of finite-layer-thickness superlattices if the unit cell is

symmetric. Consider, for example, the structure *b/2abababab . . . bab/2*. This notation represents a stack where the two outermost layers have half the thickness that they have in the rest of the stack. A symmetric unit cell can then be defined, leading to a total transfer matrix with $M_{11} = M_{22}$. This transfer matrix allows one to extract a unique set of effective dielectric constants, but these are, in principle, dependent on both thickness and angle of incidence. Further details are given elsewhere in [5].

When the layer thickness becomes comparable to the wavelength of the light in the medium, new effects arise. Bragg reflection gives rise to forbidden-frequency bands or stopgaps where optical propagation cannot occur, in much the same way as band gaps occur when electrons propagate in the periodic potential of a crystal. In the stopgaps the effective dielectric constant is purely imaginary, resulting in an electromagnetic wave that decays exponentially with distance into the medium; in a pass band it is real, and the wave is a propagating wave. The concept of photonic band structure has been introduced and concepts such as gaps, dispersion, density of states, and localization are as relevant for photons as they are for electrons, but the vector character adds a new component to the problem, which shows itself, for instance, in the importance of the polarization of the waves [7, 8]. We will return briefly to localization in a disordered superlattice below. The concept of stopgaps is an important part of optical-filter design, but will not be treated further here.

We have described the general optical features of a multilayer system in terms of macroscopic dielectric functions of the materials in the SL. We now turn a more detailed description of the elementary excitations, giving the structure of the dielectric function. Before doing so, we note that the simplest modification of the macroscopic response in a superlattice is caused by the scattering at the interfaces in the SL. If the scattering of electrons at the interfaces is diffuse, the mean free path of electrons will be reduced from the value in the bulk to something of the order of the layer thickness. In the case of metals, this effect can be incorporated through a modification of the Drude part of the dielectric constant, and may alter considerably the dielectric response in the layers.

## SEMICONDUCTOR SUPERLATTICES III

The GaAlAs SL is a so-called type I SL, where the band-gap energy difference between GaAs and $Ga_{1-x}Al_xAs$ is shared by potential steps in both the valence ($\Delta E_v$) and conduction ($\Delta E_c$) bands of the GaAs, which leads to holes and electrons being confined to the GaAs layers, thus making up quantum-mechanical wells. The $Ga_{1-x}Al_xAs$ layers in between

provide the barriers between these wells (see Fig. 2). We can approach the SL from two directions. One way is to start from one quantum well being characterized by a few discrete levels in accordance with the confining potential and having bulklike dispersion in the perpendicular direction. When many of those are assembled to a so-called multiple-quantum-well (MQW) material, they retain their discrete energy level character as long as they are separated by a reasonable distance. Bringing them closer leads to electronic well–well coupling, and the levels broaden into narrow bands: we have reached what one usually means by an SL. We can also reach this limit by going in the other direction from the bulk materials introducing a periodicity equal to the one for the SL, and we then expect, on general grounds from band-structure arguments, that the Brillouin zone opens up into mini-zones having subbands and subgaps. In what follows, we will see results pertaining both to SL and MQW materials. In Fig. 3a, we show a comparison between the absorption spectrum for a thick GaAs sample and a 77-period SL with 102 Å GaAs layers alternating with 207 Å AlGaAs layers at room temperature [9]; in Fig. 3b we show a similar comparison at 2 K, [10] (50 layers of 140 Å GaAs/ > 250 Å $Ga_{0.8}Al_{0.2}As$). An SL absorption spectrum is shown on a more expanded energy scale in Fig. 4 [11] with the characteristic plateaus of a material having two-dimensional character.

## A Excitons and Single-Particle Excitations

There are four major, more or less interrelated, differences between the SL absorption spectrum and the absorption spectrum for the corresponding bulk material (in practice, the low-gap material): (i) stronger excitonic features, (ii) split excitons due to the new symmetry in the SL, (iii)

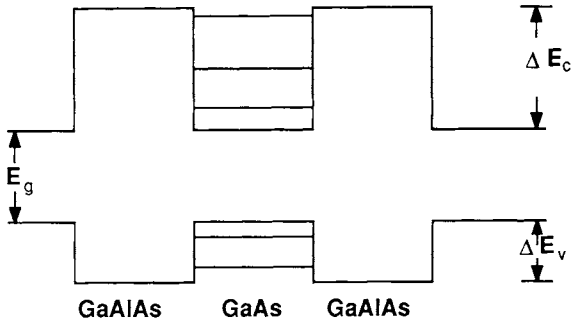


**Fig. 2.** Schematic band structure of GaAlAs superlattice. Electrons and holes are confined to the GaAs layers due to the different band gaps of the constituent materials.

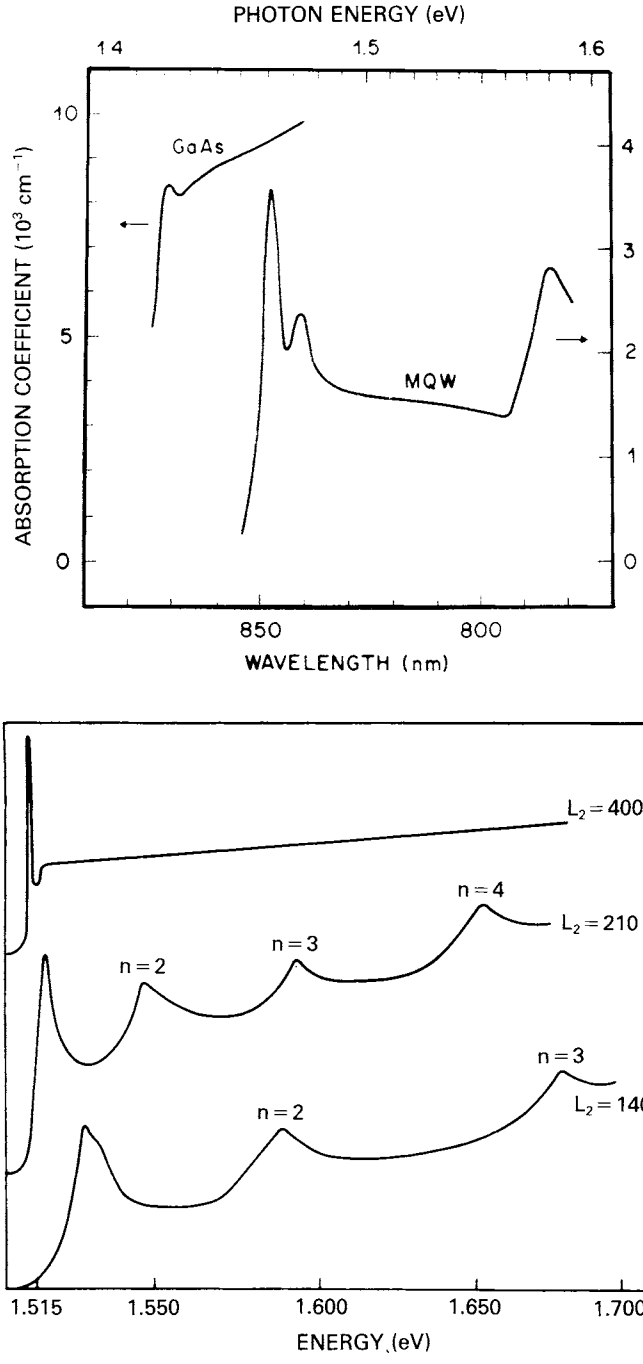


**Fig. 3.** (a) Comparison between absorption spectrum of bulk GaAs and SL GaAlAs at room temperature [9]. (b) Same comparison as in (a) but at 2 *K* [10].

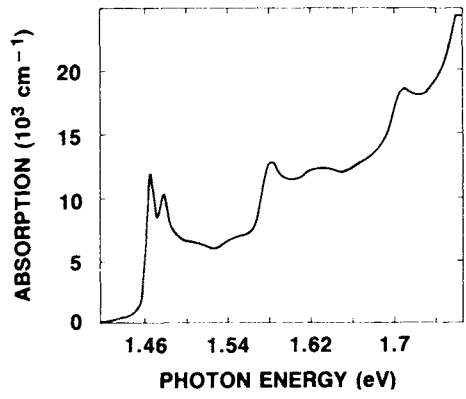


**Fig. 4.** Room-temperature absorption spectrum of GaAlAs showing excitonic resonances and two-dimensional plateaus [11].

different selection rules affecting possible peaks, and (iv) less than three-dimensional characteristics appearing as a result of the confinement. We now discuss these differences in turn:

### 1 *Stronger Excitonic Features*

As for the bulk semiconductors, the excitons play a major role in the absorption spectrum for an SL also. The exciton, which is created in the excitation process, should be distinguished from the single-particle excitation, which is a particle already present, but which of course will also be affected by the SL environment. The confinement effect present in an SL turns the three-dimensional excitons into quasi-two-dimensional ones, increasing the binding energy of the exciton and increasing the exciton absorption strength relative to the continuum absorption strength. Both effects lead to more visible excitons for an SL, as Figs. 3 and 4 show, where the SL exciton at room temperature (Fig. 3a) is as visible as the bulk exciton at 2 K (Fig. 3b). It is not only this visibility effect that is responsible for this. The new symmetry introduced by the confinement reduces the interaction with polar phonons, which are usually responsible for ionizing the excitons by the strong electric fields they produce. The major source of thermal broadening, the LO phonons, give an exciton linewidth of approximately 7 meV in bulk (3D) GaAs [12] and 5 meV in an SL ($\approx$2D) [13]. However, the excitonic transitions in SL are, in general, broader than the ones observed in their component materials. The reason for this is that the excitonic resonance is not only a function of temperature but also of the well width, the quality of the interfaces, structural disorder in the constit-

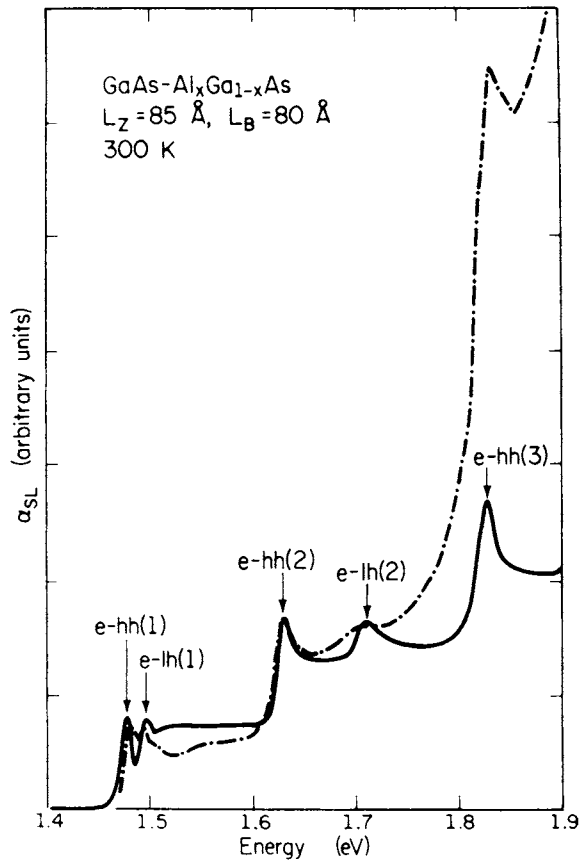


**Fig. 5.** Comparison between experimental (dashed) and theoretical (full) absorption in GaAs-$Al_{0.5}Ga_{0.5}As$ SL [17].

uents, and so on. This means that the low-temperature exciton features can be used as fairly reliable measures of the quality of the microstructure product [14, 15]. For a GaAs well with thickness $L > a_0^*$ ($\approx$300 Å; bulk exciton radius), the excitons are, in general, three-dimensional with bulk broadening, whereas if $L < 50$ Å the material-quality factors dominate the broadening. The best value of $L$ is therefore around 100 Å and gives sharp excitons with two dimensional character [16], provided the well–well distance is larger than on the order of 100 Å to minimize the well–well coupling. In Fig. 5 we show a theoretical calculation [17] for the experimental absorption spectrum of a GaAlAs SL, which shows the relatively good account one can achieve in the modeling of the essential features for the absorption process. It is specifically demonstrated in [17] that the anisotropy and structure-dependence of the dielectric function, and hence,

the index of refraction, come from the Γ region, while the $X$ and $L$ regions of the Brillouin zone give contributions very much like the compositional-alloy values. The reason for this is the difference in conduction-band effective masses.

## 2 Split Excitons

A comparison between the bulk and SL absorption curves in Fig. 3a shows clearly how the bulk exciton is split in the SL, which is demonstrated even more clearly in Fig. 6 [18]. The reason for the split exciton peak is that the degeneracy in bulk GaAs between the valence heavy- and light-hole bands is lifted by the perturbation introduced when constructing the SL, affecting the light- and heavy-hole energies differently.

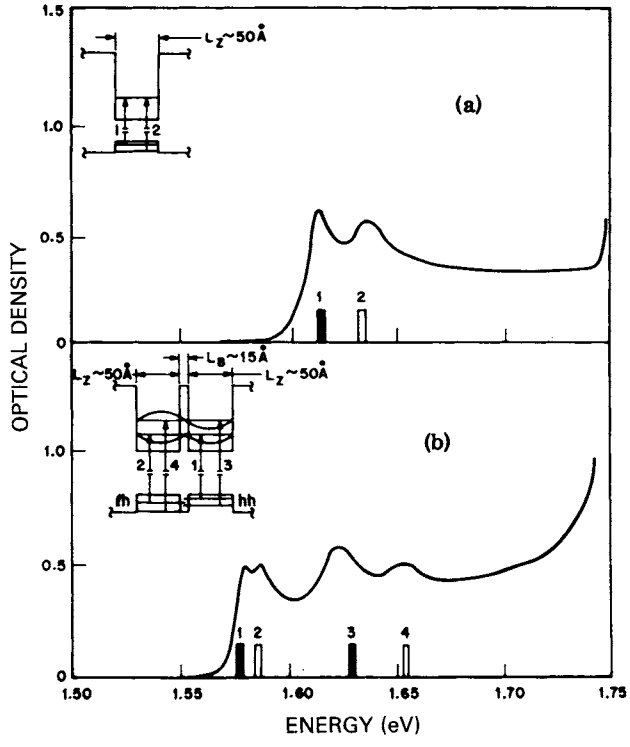


**Fig. 6.** Comparison between single-well and double-well SL, illustrating the effect of well–well coupling. Notice the lowest split exciton [18].

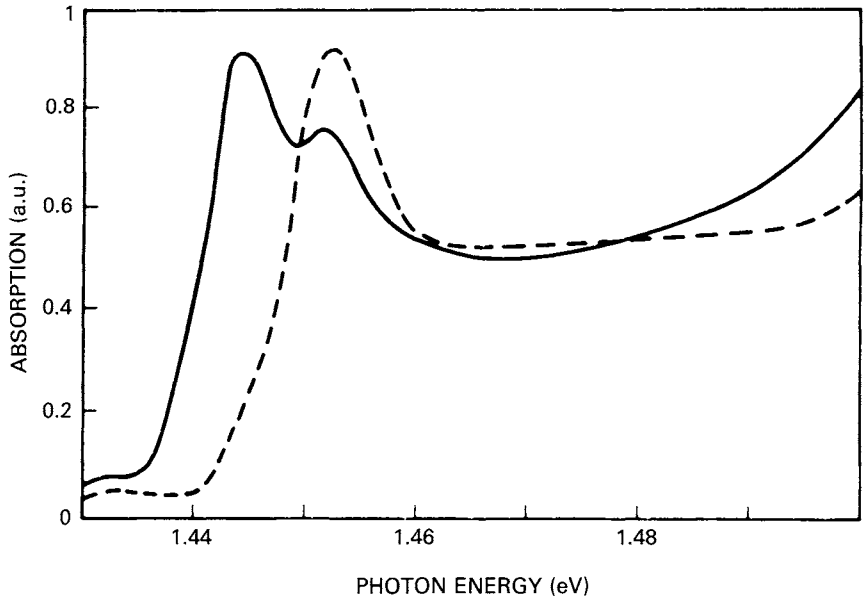


**Fig. 7.** Room-temperature absorption with light polarization parallel to the layers (solid) and perpendicular to them (dashed) [11].

### *Selection Rules* 3

As soon as we introduce a stacking, a high degree of anisotropy is introduced in a system, and this can be used to design novel optical properties, as already mentioned above. The main effect is to give an absorption that is depending very sensitively on whether the incident light is parallel or perpendicular to the barriers [19]. Let $M_{nm}$ $(k, q)$ denote the matrix element between two levels $n$ and $m$ in the valence and conduction bands, respectively (interband transition), and where $k$ is the SL wave vector along the stacking and $q$ is perpendicular to it. For type I SL, for light having its propagation vector along the stacking, one finds that $M_{nm}$ is almost independent of $k$ and $q$, and is parity-forbidden if $n-m$ is odd and parity-allowed if $n-m$ is even. The $n=m$ transition is by far the most intense. As a general illustration, we show in Fig. 7 the absorption spectrum close to threshold, when the electric field is parallel and perpendicular to the stacking, respectively. Light polarized parallel to the layers involves both light- and heavy-hole excitons, whereas the other polarization involves only one of them as a result of the specific selection rules for this configuration. The absorption for an optical field polarized normal to the layer is in general difficult to investigate for thin-film samples due to the strong refraction at the interface of the sample. A waveguide configuration, however, enabled polarizations both parallel and perpendicular to the layers to be studied. Further details are given elsewhere [11].

### 4 Two-Dimensional Density of States

As is seen in Figs. 4 and 5, the general absorption characteristic of the SL is that of a two-dimensional electron gas, whose constant density of states generates a staircase of absorption features with superimposed excitonic transitions. By properly designing well parameters, including the possibility of doping, one can tune the absorption features from less than 5 $\mu$m to more than 100 $\mu$m [20]. From measurements on such designed systems, one finds very large dipole matrix elements $\langle z \rangle \approx 21$ Å, corresponding to large spatial separations between the ground and first excited states, leading to large oscillator strength and, therefore, to potential technological applications. It should be stressed that the strength and energies of these transitions, and especially the *unconfined* ones, that is, those above the conduction band or below the valence band, are strong functions of the barrier widths. The reason is that the states penetrate far into the neighboring wells [21]. Effects of confinement and interlayer coupling on the optical interband transitions (1.5–5.5 eV) of $(GaAs)_m(AlAs)_m$ superlattices with $m$ ranging from 1 to 15 and with SL periods from 0.6–9 nm are summarized in the work by Garriga *et al.* [22].

Apart from absorption, there are many other optical probes that are useful when investigating SL systems. Here we shall mention only luminescence [23, 24]. The main finding when using this probe is that the SL luminescence spectrum is dominated by so-called intrinsic luminescence (free-exciton recombination processes) in contrast to the bulk GaAs, which is dominated by extrinsic luminescence (recombination with neutral acceptors, that is; impurities, such as carbon). Another often-used probe is Raman scattering, which we will discuss in the next section about phonons in SL.

## B Phonons

With the help of Raman scattering and especially resonant Raman scattering, one can utilize the relatively sharp excitonic transitions in the form of a derivative spectrum, and the signal of interest is then not swamped by a large background as with the absorption spectrum. In this way the phonon spectrum of SL can be studied. Of the different kinds of phonons in a material, one finds for a GaAlAs SL that the dominating phonon is the GaAs LO phonon (36.5 meV) [25], the TO phonons being absent because of the usual Raman selection rules. The phonons associated with the $Ga_{1-x}Al_xAs$ layers are not seen, since the electrons and holes involved are confined to the GaAs regions. Phonons are also affected by the periodicity in the SL construction leading to Brillouin-zone folding and

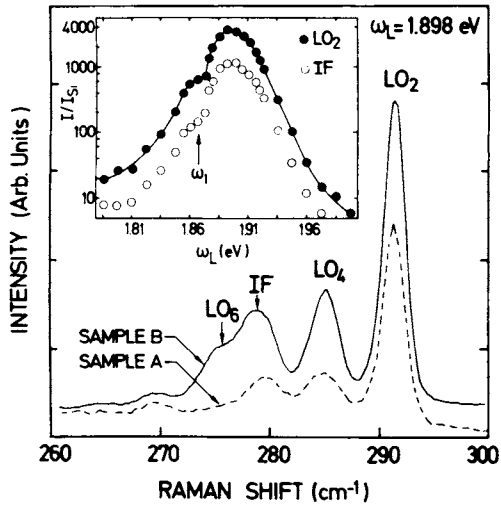


**Fig. 8.** Raman spectrum showing confined LO phonons and GaAs-like interface mode (IF). Insert shows resonant behavior of $LO_2$ and IF mode [28].

the appearance of gaps in the phonon spectrum for wave vectors satisfying the Bragg condition [26]. This is most important for LA phonons, since the acoustical branches in different materials overlap energetically, leading to propagation of vibrations and folding. The optical branches, however, are usually separated in energy, and they show confinement effects in the individual slabs [27]. On top of this, we have the possibility of interface vibrational modes [28], (see Fig. 8). These are in nature very similar in structure to the coupled plasmon modes that we will discuss in Section V, showing both band effects and folding. Using a photoelastic continuum model [29], one can give a good account for the observed features in the resonant Raman scattering spectra. Raman scattering spectroscopy also has the potential to provide structural information similar to that obtained by X-ray diffraction [29, 30]. The relative intensities of the folded-acoustic-phonon peaks give a measure of the interface sharpness and layer widths. In this context we shall discuss a related SL construction: the amorphous SL, which still shows sharp interfaces.

## AMORPHOUS SUPERLATTICES IV

Semiconductor superlattices and, in particular, crystalline semiconductor superlattices exhibit many interesting transport and optical properties that are associated with the periodic nature of the superlattices and with

the repeat distance in the structure, for example, quantum size effects. The production of crystalline superlattice structures requires lattice matching, and this considerably limits the choice of material and the number of systems that can be produced. Amorphous superlattices, on the other hand, do not require lattice matching and epitaxy. It has been demonstrated that uniform multilayers of amorphous semiconductors can be grown with interfaces that are sharp and essentially defect-free down to very small individual layer thickness [31–37]. This allows for a much larger variety in the systems to be studied. The amorphous superlattice will, therefore, offer an attractive alternative to crystalline superlattices, since amorphous superlattices will exhibit many of the effects seen in crystalline superlattices with the obvious exception of effects associated with the existence of a long mean free path of the carriers.

Quantum size effects on the band gap have been seen in the optical properties of amorphous semiconductors [31–37]. Optical studies will thus constitute an important base for the understanding of quantum size effects on the band structure and effective mass in these systems. We will illustrate this by the studies of Bittar *et al.* [36] on the $Si/SiO_x$ superlattices. This is an attractive system to study, since the band gaps in the two materials are quite different, and for such systems, theories based on an effective-medium approach are expected to be valid. The samples were made by evaporation onto room-temperature substrates. High-resolution transmission electron microscopy and small-angle electron diffraction indicated that the multilayers indeed constituted superlattices with sharp interfaces and well-defined periods.

The optical properties of the samples were studied by means of normal-incidence reflection and transmission measurements in the range 0.9–4 eV. At this stage it is appropriate to discuss the validity of an effective absorption coefficient for a multilayer sample. Can the optical properties of a superlattice be described in a way that allows the extraction of a value for the optical gap? We have outlined above an effective-medium theory for superlattices. This approach assumes a localized response in each layer, that is, electron wavefunctions, which are localized to one layer. This is the case for amorphous superlattices. Therefore, extracting effective constants from optical measurements gives information about the response in the individual layers. Also, normal-incidence reflectance and transmission are determined by the ordinary dielectric constant $\varepsilon_0$ only. Furthermore, in the region below the $SiO_x$ absorption edge, the absorption is, in the absence of long-range interactions and long mean free paths, determined by the Si layers only. For semiconductors the band shapes near the absorption edge are often parabolic. In these cases the optical gap can be determined from the equation

$$(\alpha\hbar\omega)^{1/2} = B(\hbar\omega - E_g), \tag{3}$$

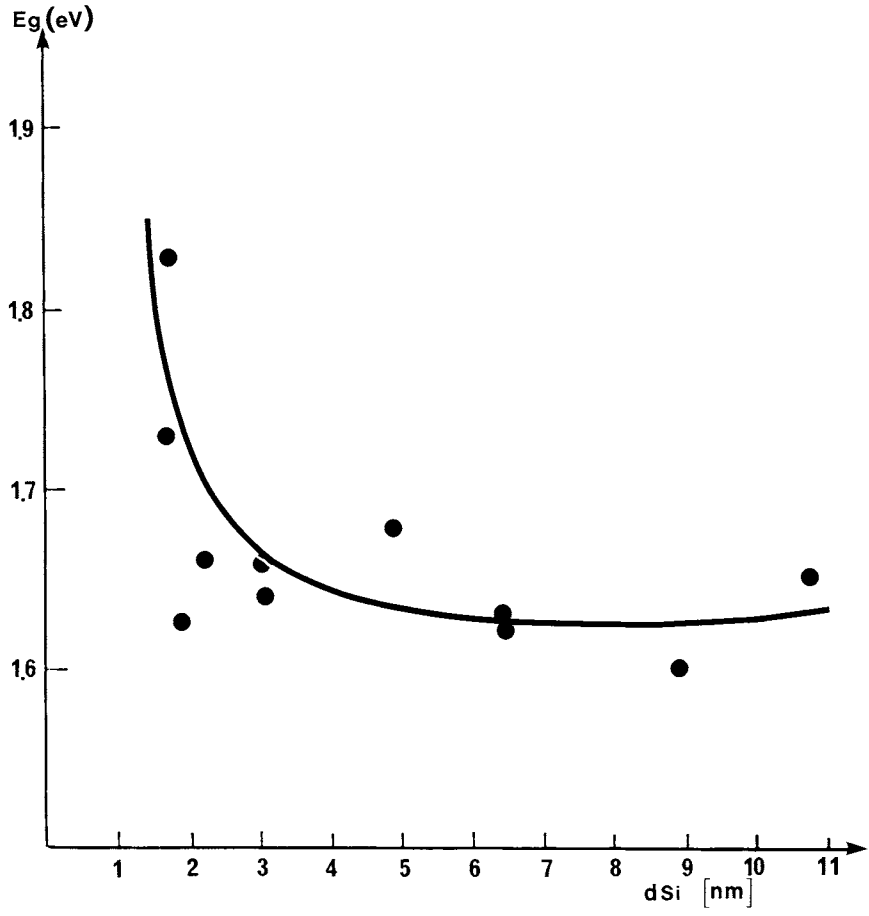


**Fig. 9.** Experimental band gap, $E_g$, as a function of silicon layer thickness, $d_{Si}$, for the $Si/SiO_x$ system [36].

in the region of photon energies above the gap $E_g$. Thus, by plotting the measured absorption coefficient $\alpha$ in a so-called Tauc plot given by Eq. 3, values for the band gap in the Si layers can be obtained.

The results of these studies are summarized in Fig. 9, where values of the band gap $E_g$ are plotted as a function of Si layer thickness. The figure shows band-gap values that are influenced by quantum-well confinement for layer thicknesses below 3 nm. The absence of any firm information about the modulation profiles of the valence- and conduction-band edges, or about electron and hole effective masses, prevents an exact comparison of the measured gap with calculations. Nonetheless, the magnitude of the

shift, and the layer-thickness value at which it sets in, can be modeled with a square-wave modulation of band edges [37]. This modeling demonstrates that the variation in bandgap with layer thickness is indeed a quantum size effect.

## V COLLECTIVE EXCITATIONS

So far we have said very little about the coherent motion of single-particle excitations in the form of collective excitations such as plasmons and polaritons. The very nature of the SL makes it possible to have or construct collective modes of almost any frequency and dispersion. Lately, this has been an intense field of research, where we would particularly like to mention the theoretical contributions by Bloss and Brody [38], Tselis and Quinn [39], Das Sarma and Quinn [40], and the very condensed presentation by Camley and Mills [41]. Experimentally the first confirmation of collective modes in layered structures, which were in-between those for two- and three-dimensional systems, came about at the same time by Olego and co-workers [42], using inelastic light scattering. In this section we will give a simple description of how to analyze the SL response with respect to collective modes as seen in elastic light scattering. The interested reader should consult Rytov [43] and Brekhovskikh [44] to get some flavor of the original work being done on the optical properties of SL. It should be mentioned, however, that during recent years there have appeared two very powerful methods for the optical-response description of SL; one is based on a continued fraction-approach by Lambin *et al.* [45] and the other is a very useful transfer-matrix formulation by Mocha'n *et al.* [46]. The latter actually goes back to a description of the optical properties of thin films by Jones *et al.* [47] in terms of the surface-impedance concept. The surface impedance is defined as the ratio between the parallel-field components of the electric and magnetic fields at an interface (the conserved quantities). It turns out that when relating the field components at the two sides of a layer in an SL through a transfer matrix, its elements can be expressed in terms of surface impedances for field components that are symmetric and antisymmetric with respect to the layer in question. We will return to this in a following section; right now we will outline the simplest way of analyzing the possibility of having collective modes in a two-component, semi-infinite SL using the surface-impedance construction.

The optically equivalent medium of the ideal superlattice is fully specified by giving the surface impedance of the uniaxial crystal found earlier:

$$Z_{ep} = p_e / q\varepsilon_o \tag{4}$$

for $p$-polarized light, where $p_e$ is the perpendicular wave-vector component of the bulk "extraordinary" polariton with

$$p_e^2 = (q^2 - k_\parallel^2/\varepsilon_e)\varepsilon_o, \qquad q = \omega/c, \tag{5}$$

and

$$Z_{es} = p_o/q, \tag{6}$$

with $p_o^2 = q^2\varepsilon_o - k_\parallel^2$ for $s$-polarized light. Notice how $s$-polarized light only involves $\varepsilon_o$. This is because $s$-polarized light does not have any field component perpendicular to the surface, as is also the case for $p$-polarized light at normal incidence ($k_\parallel = 0$ yields $p_e$, independent of $\varepsilon_e$, *cf.* Eq. 5).

With the surface impedance, a number of interesting physical quantities can be calculated [6]. For a semi-infinite medium with surface impedance $Z$ (which is calculated classically from bulk quantities) adjacent to vacuum, with $p$-polarized light $c$ incident at an angle $\theta$ with the surface normal, we have the following reflection coefficient:

$$r_p = \frac{\cos\theta - Z_p}{\cos\theta + Z_p}, \tag{7}$$

which yields our superlattice reflection coefficient $r_{ep}$ simply by replacing $Z_p$ with $Z_{ep}$, the surface impedance for the infinite medium being equivalent to our superlattice. The general behavior of $r_{ep}$ is easily found from an inspection of Eq. 5. Since whenever $p_e^2 < 0$, $Z_{ep}$ becomes imaginary, the reflectance $|r_{ep}|^2$ from this system approaches unity. This occurs provided the imaginary part from $p_e^2 < 0$ dominates the imaginary parts in the component dielectric constants $\varepsilon_a$ and $\varepsilon_b$ describing the Drude damping ($\tau$). In the optical regime this is a good approximation, since usually $1/\tau \sim (10^{-3} - 10^{-2})\omega_p << 1$ eV, for typical plasma frequencies on the order of 10 eV and where 1 eV is the typical energy for $|p_e|\, c$. Using this form for $p_e$ thus facilitates an easy inspection of the reflective properties of a superlattice.

When the denominator of Eq. 7 vanishes, we have a situation with a divergent reflection coefficient; we can have a reflected field without any incoming one. This is characteristic of an eigenmode of the coupled vacuum-superlattice system and corresponds to what is called a *surface polariton*. Whereas the dispersion relation of the bulk polariton is obtained from Eq. 5, yielding $\omega = \omega(k_\parallel, p_e)$, the surface-polariton dispersion relation, which is a solution to $\cos\theta + Z_{ep} = 0$, yields $\omega = \omega(k_\parallel)$ with $\cos\theta =$

$\sqrt{1-(k_\parallel c/\omega)^2}$. Using $Z_{ep}$ from Eq. 4 and a little algebra, we arrive at the following dispersion relation for the surface polariton in a superlattice with the "optical axis" perpendicular to the stacking:

$$k_\parallel^2 = q^2 \frac{\varepsilon_o - 1}{\varepsilon_o - 1/\varepsilon_e}, \tag{8}$$

which goes over to the appropriate limit $k_\parallel^2 = q^2\varepsilon_a/(1+\varepsilon_a)$ if medium $b$ is absent ($\varepsilon_o = \varepsilon_e = \varepsilon_a$). When solving Eq. 8, it should be complemented with the condition that only ($\omega$, $k_\parallel$) values that make $p_e^2 < 0$ are physical solutions, that is, that correspond to decaying (localized) solutions. This automatically ensures that we find no mode to the left of the light line in vacuum ($\omega = k_\parallel c$).

Letting $c \to \infty$, we reach the electrostatic regime ($p_e \to ik_\parallel$), where the dispersion relation in Eq. 8 goes over to its short-wavelength limit ($k_\parallel \gg \omega/c$):

$$\varepsilon_e \varepsilon_o = 1. \tag{9}$$

The surface mode is now called a *surface plasmon*, since it no longer has any photon character, and for a semi-infinite medium of material a only, Eq. 9 goes over to $\varepsilon_a + 1 = 0$. However, for the superlattice, which has a unit cell with two components, we will actually find two possible solutions (modes).

For a metal–metal superlattice described by Drude dielectric functions $\varepsilon_{a,b} = 1 - \omega^2_{a,b}/\omega^2$, with $\omega_a = 2\omega_b$ and $f = 1/2$, we show in Fig. 10 the possible surface-polariton modes. The lower mode follows the photon line for small $k (= k_\parallel c/\omega_a)$ and approaches $\omega_i^2 = \omega_a^2\omega_b^2/(\omega_a^2 + \omega_b^2)$ for large $k$ (a solution of Eq. 9). The other mode is unphysical; it stays outside the dotted area that corresponds to a solution which is confined to the surface ($p_e^2 < 0$), until it reaches the light line $\omega = k_\parallel c$ and then goes rapidly towards the interface plasmon frequency for a bimetallic junction: $\omega_s^2 = (\omega_a^2 + \omega_b^2)/2$. Notice that this mode measures the average electron density in the superlattice, since $\omega^2_{a,b} \propto n_{a,b}$, $n$ being the electron density. On the other hand, the lower mode is a measure of the sum of the inverse electron densities.

Our second example, shown in Fig. 11, is for a metal–insulator system with $\varepsilon_a = 1 - \omega_p^2/\omega^2$, $\varepsilon_b = \varepsilon_i = 9/4$, and $f = 1/2$. Again we have a lower mode starting out following the light line, and it approaches the surface plasmon for a metal in contact with an insulator having dielectric function $\varepsilon_i$, namely, $\omega_0^2 = \omega_p^2/(1+\varepsilon_i)$. The upper mode is very different compared to the metal–metal case, both in absolute frequency and dispersion. It starts out

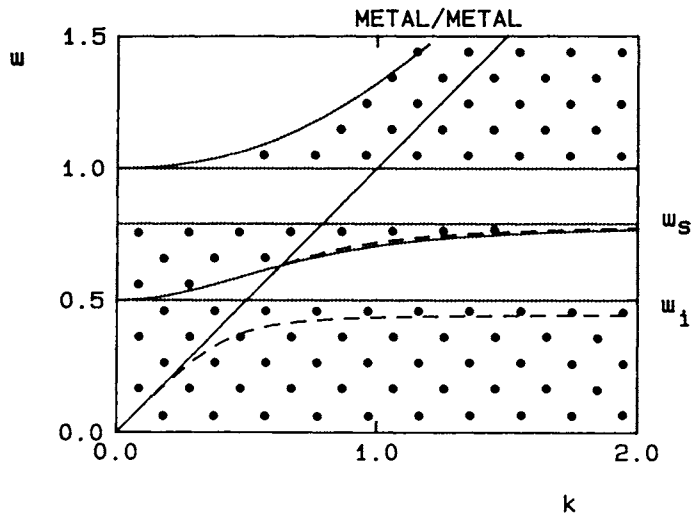


**Fig. 10.** Surface polariton dispersion relation for a metal–metal superlattice, with $\omega_a = 2\omega_b$ and $f = 1/2$, adjacent to vacuum. Only solutions within dotted areas satisfy the criterion for being surface localized ($p_c^2 < 0$) and are retained. The two physical modes are to the right of the light line (full curve) and soon approach $\omega_s^2 = (\omega_a^2 + \omega_b^2)/2$ and $\omega_i^2 = \omega_a^2\omega_b^2/(\omega_a^2 + \omega_b^2)$, respectively. $k$ is in units of $\omega_a/c$ and $\omega$ in units of $\omega_a$.

from the light line $\omega = k_\parallel c$ exactly at the point where the border line corresponding to a decaying solution (dotted area) cuts the light line (full curve). It stays within the allowed region and approaches $\omega_i^2 = \omega_p^2\varepsilon_i/(\varepsilon_i - 1)$ for large $k_\parallel c/\omega_p$.

As we have just seen, the presence of interfaces allows for the propagation of interface polaritons, and this can have a dominating influence on the optical response for a metal–metal or a metal–insulator superlattice. The most prominent aspect of the optical properties of an insulator is the reststrahlen band in the infrared. The reflectance of a semi-infinite medium increases sharply near the pole in $\varepsilon(\omega)$ caused by the resonance of the transverse-optical-phonon polariton and decreases again at the longitudinal-optical-phonon polariton. For a thin film the reflectance at normal incidence continues to exhibit a structure at the TO resonance, but no structure is seen at the LO resonance. At oblique incidence a structure is, however, seen for $p$-polarized light, but not for $s$-polarized light. This phenomenon was first discussed by Berreman [48]. In the case of free electrons discussed previously, the same effect occurs at the frequency of the bulk plasmon. The Berreman effect in the case of a single thin insulating film has been studied in detail by Harbecke *et al.* [49]. The effect can be very prominent, particularly for an insulating film on a metallic backing. This is illustrated in Fig. 12, which in a three-dimensional plot

shows how the reflectance varies with frequency and layer thickness [49]. The Berreman effect shows a maximum at a particular layer thickness given by

$$d_B = \frac{\lambda \cos\theta}{2\pi \sin^2\theta}[\mathrm{Im}\{-1/\varepsilon\}]^{-1}, \tag{10}$$

which is called the *Berreman thickness*.

In the case of superlattices, the effect may again be strongly enhanced due to the presence of many interfaces. This is the case for an insulator–insulator superlattice if one of the materials is transparent at the LO frequency of the other material. This is illustrated in Fig. 13, which shows the reflectance of such a system [50]. The model superlattice has been calculated for two values of the damping parameter $\Gamma = \omega_0\tau$. Here $\omega_0$ is the TO phonon frequency and $\tau$ is the corresponding lifetime. The parameters for the material showing the Berreman effect are typical for those of $SiO_2$ in curve 2, whereas curve 1 shows the same superlattice for a value of $\Gamma$, which is roughly three times larger.

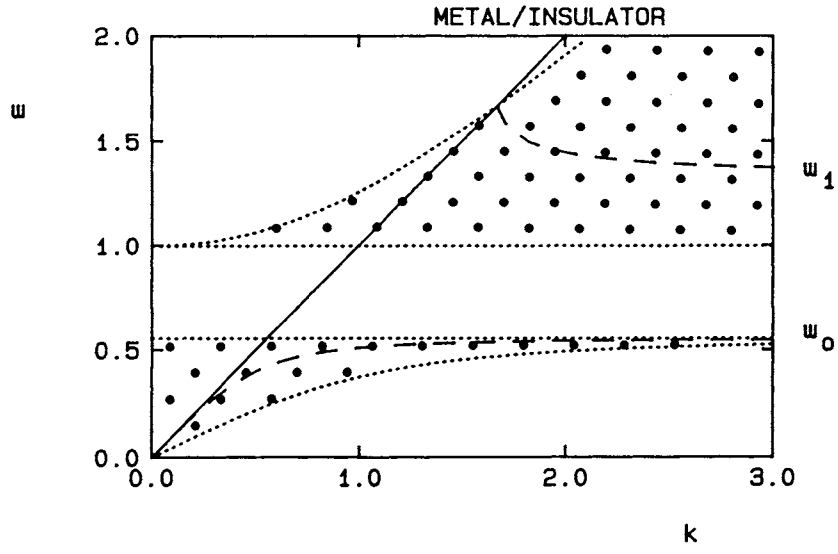


**Fig. 11.** Surface polariton dispersion relations for a metal–insulator superlattice, in contact with vacuum. $f = 1/2$, $\varepsilon_a = 1 - \omega_p^2/\omega^2$, and $\varepsilon_b = 9/4$. $\omega$ is in units of $\omega_p$ and $k_\parallel$ is in units of $\omega_p/c$. The lower mode starts out from the light line (full curve) and approaches the electrostatic result $\omega_0^2 = \omega_p^2/(1+\varepsilon_b)$. The upper mode starts out from the light line and is surface-confined immediately, since the dotted areas in the figure correspond to physical surface solutions. The upper mode approaches $\omega_1^2 = \omega_p^2\varepsilon_b/(\varepsilon_b - 1)$ for large $k$.

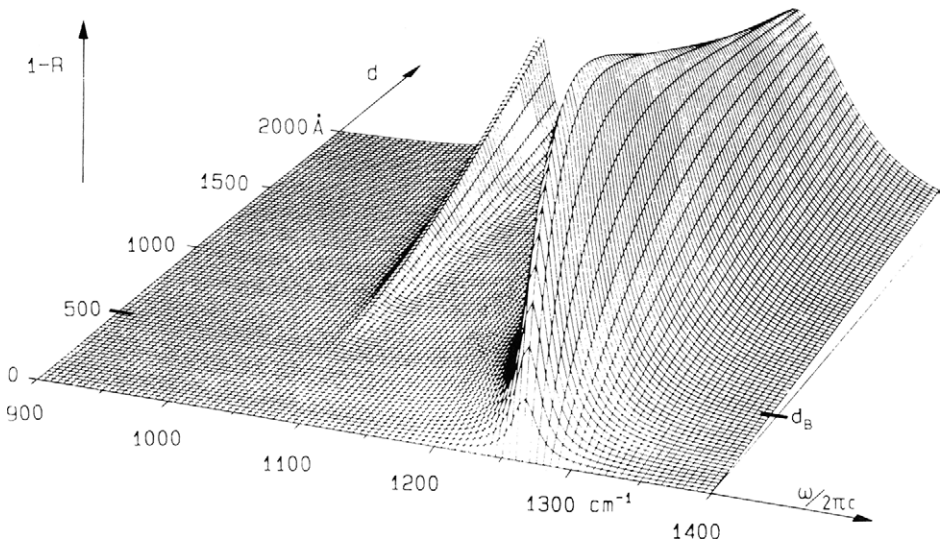


**Fig. 12.** Three-dimensional plot of the dependence of the absorptance 1-$R$ of an $SiO_2$ film on a metal substrate against frequency and thickness. The parameters used in the calculation are given elsewhere [49].

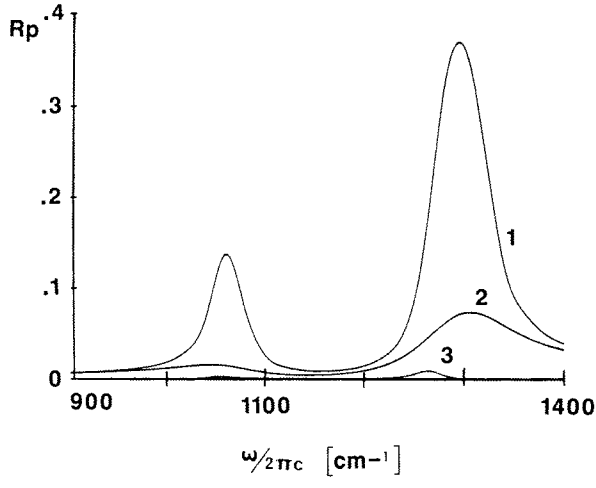


**Fig. 13.** Model calculation for the reflectance of a single $SiO_2$ film, (3); and two insulator–insulator superlattices, (1 and 2), versus frequency. The filling factor of $SiO_2$ in the superlattice is 0.5. Curves 2 and 3 have $\Gamma = 30$; curve 1 has $\Gamma = 100$. The angle of incidence was 70°. The other parameters used in the calculation are given elsewhere [50].

Grosse *et al.* [51] have studied the optical properties of GaAs heterostructures in the infrared (70–2500 $cm^{-1}$). The main structures in the spectra are due to phonon reststrahlen bands (TO), Fabry–Perot interferences, and Berreman modes. A fit to data allows one to extract carrier concentration and thickness of the epitaxial films as well as carrier concentration of the GaAs substrate. The films in this study were thick, and no quantum-well effects were expected, but they demonstrate that the reststrahlen region provides a powerful tool for nondestructive profiling of the heterostructure.

Maslin *et al.* [52] have studied a superlattice in the reststrahlen region. The superlattice consisted of 150 periods, each period composed of two monolayers of GaAs and two monolayers of AlAs with cladding layers of 0.1 $\mu$m of $Al_{0.7}Ga_{0.3}As$ on each side, and the complete structure was grown on a GaAs substrate. The effective-medium description, which the same authors found to be adequate for relatively long-period superlattices, cannot describe the structures observed in the reststrahlen region. Account must be taken of the contribution to the dielectric susceptibility of the zone-folded optic phonons and of the way in which long-range electrostatic interactions responsible for the LO–TO splitting are modified by the periodicity of the superlattice. The spectrum also shows a pronounced structure below about 250 $cm^{-1}$, which most probably arises from the free-carrier response.

In the case of a metal–insulator superlattice, the optical properties are very much dominated by those of the metal. For somewhat thicker films in the superlattice the response also depends strongly on whether the outer layer is metal or insulator. If the outer layer is metal the incoming light is damped through the metal layer, and the effect is weak. If the outer layer is an insulator, the effect is similar to an insulator on a metallic backing. The Berreman effect is still prominent in a metal insulator superlattice. We have a balance between the damping due to the metal layers and an enhancement due to the presence of many interfaces. This effect has been studied experimentally for a $Pt/Al_2O_3$ multilayer system [50]. The samples were made by sequentially sputtering Pt and Al in a reactive atmosphere. The experimental results were in reasonable agreement with model calculations based on macroscopic dielectric functions.

## VI LATTICE DISORDER

Up to now, all our discussion has been based on the assumption of a perfect superlattice. It is of interest to study the effect of deviations from

this assumption, that is, to study realistic superlattices. This can be done by introducing a statistical variation in the thickness of the individual layers. It is only in the limit of thin individual layers or a symmetric unit cell that the total transfer matrix will have equal diagonal elements, and thus allows the extraction of effective dielectric constants. Therefore, the effect of lattice disorder was studied by simulation, using the exact transfer matrix formalism [53]. A Drude metal–insulator superlattice was taken as a model system. The film consisted of 1000 layers. The layer thicknesses were generated by means of a Gaussian distributed random-number generator. The average layer thickness was 2 nm, and the standard deviation was 0.5 nm.

The resulting reflectance in the 5–8 eV range, where the absorption coefficient is small so that the light penetrates many layers in the superlattice, is shown in Fig. 14. The effect of finite layer thickness on the reflectance is small for 4 nm unit-cell size, for an ideal superlattice. If we let the layer thickness vary, however, the difference between the effective-medium theory and the exact theory may be large indeed (see Fig. 14). The strong variations seen in the reflectance are the result of the statistical variations in the phases of the waves reflected from the various interfaces.

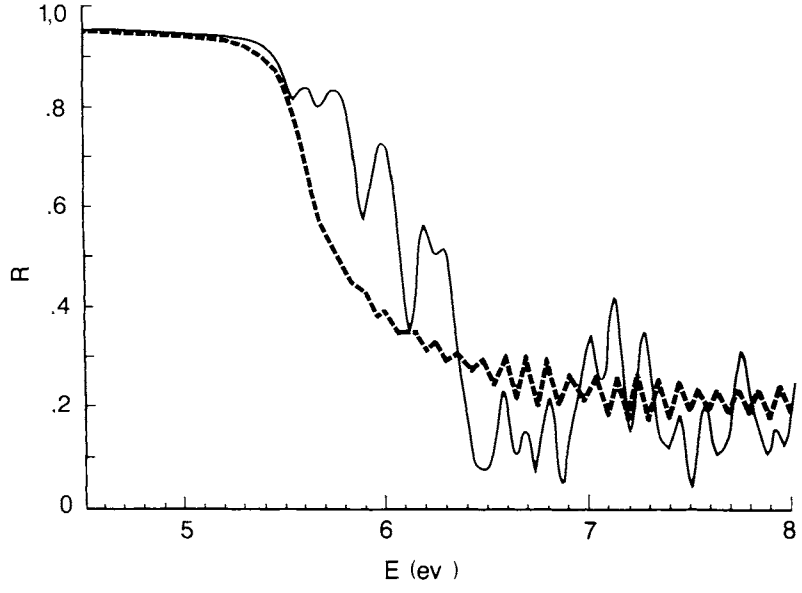


**Fig. 14.** Reflectance for *p*-polarized light at a 60-degree angle of incidence for an ideal superlattice (dashed) and with a statistical variation in the layer thicknesses (solid). The rms variation in layer thickness was 25%. The parameters are otherwise as in Fig. 1.

In the absence of absorption, these fluctuations would be reminiscent of the speckle pattern in the reflection from a rough object. There, the highest frequency is given by the size of the object; here, the highest frequency would be given by the total thickness of the sample. Another way of looking at these structures is to compare them to the Anderson localization in a random potential in solid-state physics. Here we have a localization of an electromagnetic wave in a random superlattice. Such localization, for example, has been observed experimentally by Genack [54] in a dense random packing of microspheres and is also predicted in quasiperiodic media [55].

For superlattices with finite thickness *and* where the unit cell is not symmetric, *or* if we include a statistical variation in the layer thickness, the total transfer matrix of the system will not have equal diagonal elements. In this case the system is not equal to a simple film, and we cannot extract effective dielectric constants. It has been stated in the literature that a transfer matrix with unequal diagonal elements is equivalent to a double film [56]. It takes a total of six parameters to characterize a double film, two complex dielectric constants and two thicknesses, and these could in principle be extracted from the transfer matrix.

## VII THE EFFECT OF NONLOCAL DIELECTRIC FUNCTIONS

For nonnormal incidence onto a metal surface, the electromagnetic wave propagating into the metal is no longer purely transverse; it also has a longitudinal component. A description of the interaction of the wave with the electrons will then involve both the transverse dielectric function, $\varepsilon_T$, and the longitudinal dielectric function, $\varepsilon_L$. Furthermore, the field varies very rapidly near the surface, and the usual dipole approximation is no longer valid. A common name for all these effects in optics is *nonlocal*. Several authors have studied the effect of nonlocal transverse and longitudinal dielectric functions on the optical properties of a single slab. A superlattice consists of a very large number of slabs, and the effect of nonlocality can be important. We therefore include a review of the effect of nonlocality. A fruitful approach is as follows: one uses the expansion of the surface impedance in terms of waves of even and odd parity, which was first derived by Jones *et al.* [47]. Then one expresses the transfer matrix of a single film in terms of the surface impedance $Z_0$ for odd waves and $Z_e$ for even waves. We have shown that this leads to the following transfer matrix [5]:

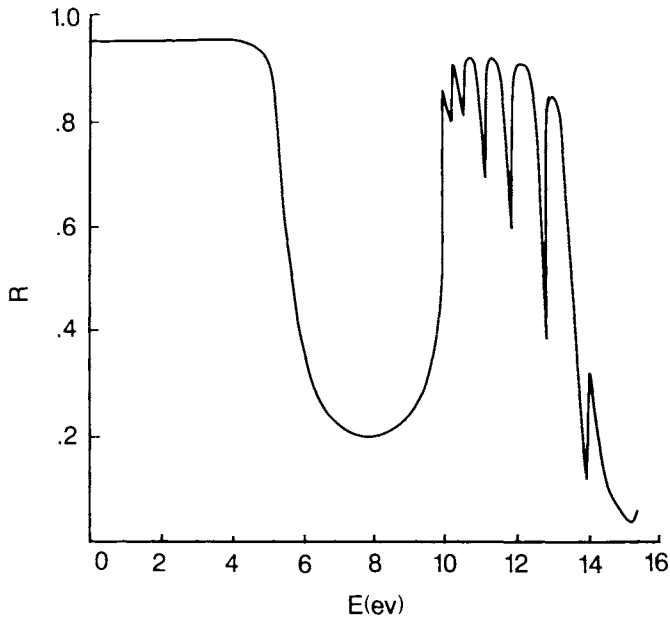


**Fig. 15.** Reflectance for $p$-polarized light at a 60 degree angle of incidence with nonlocal dielectric constants. The other parameters used in the calculation are given elsewhere [5].

$$M_u = \begin{vmatrix} \dfrac{Z_e + Z_o}{Z_e - Z_o} & \dfrac{2Z_eZ_o}{Z_e - Z_o} \\ \dfrac{2}{Z_e - Z_o} & \dfrac{Z_e + Z_o}{Z_e - Z_o} \end{vmatrix}. \tag{11}$$

Explicit expressions for $Z_o$ and $Z_e$ were given by Jones *et al.* Those expressions have been used to calculate the reflectance from a stack of the form $b/2ab \ldots ab/2$. Here $b$ represents thin layers of an insulating material; $a$ represents the metallic slabs. For the transfer matrix of the insulating slabs, we use the usual expressions for the transfer matrix. The layer thicknesses are sufficiently small for the effective-medium expressions to apply if a local dielectric constant is used for the metal. Figure 15 shows the reflectance for $p$-polarized light with nonlocal dielectric functions. These were obtained from the Boltzman equation for a free-electron gas. We used the Fermi velocity $v/c = 2.8 \times 10^{-3}$, and the metallic-layer thickness was chosen to be 2 nm. The parameters are otherwise the same as those in Fig. 1. The structure associated with the excitation of bulk plasmons is much more pronounced in the superlattice than in a single film [5]. These calculations indicate that nonlocal effects can play a role in the

optical properties of metal–metal and metal–insulator superlattices. The position and strength of the longitudinal-plasmon peaks are, however, exceedingly sensitive to the thickness of the metal layers. Sample quality is therefore important for the overall optical spectrum.

## VIII CONCLUDING REMARKS

The engineering of SL semiconducting materials with novel physical properties has been extensively studied over the last decade. Because of the important optoelectronic applications of these structures, large emphasis has been placed on determining their optical properties. These may, as we have seen in this review, be strongly modified by localization and quantum-confinement effects. Much less effort has been expended to produce and to study the properties of metallic superlattices, although such superlattices can be made [57, 58]. The emphasis there has been on magnetic properties, and no study of the optical properties of metallic superlattices has to our knowledge been carried out yet. It is clear that the band structure of a metallic SL will be very different from those of the constituents if the layer thickness is only one or a few atomic layers thick. Such a material would in many respects be an "ordinary" uniaxial material, and the optical properties would be an important tool to study the band structure of the material. There has again been little or no experimental effort to make and study the optical properties of metal–insulator or insulator–insulator superlattices. The superlattice phenomenon to be studied are in particular collective modes: plasmons and polaritons. These have been studied extensively theoretically; the lack of experimental data is, in part, related to difficulties in sample preparation, but it should also be recognized that the industrial emphasis has been on semiconductor superlattices due to their vast potential applications.

### REFERENCES

1. L. L. Chang, L. Esaki, W. E. Howard and R. Ludeke, *J. Vac. Sci. Technol.* **10**, 11 (1973).
2. L. Esaki and R. Tsu, IBM Research Note RC-2418 (1969).
3. M. Jaros, "Physics and Applications of Semiconductor Microstructures," Clarendon Press, Oxford (1989).
4. L. Esaki, "Science Citation Index," number 28, July (1987).
5. O. Hunderi, *J. Wave-Mat. Int.* **2**, 29 (1987).
6. P. Apell, R. Monreal, and O. Hunderi, *Physica Scripta* **34**, 348 (1986).
7. A. Yariv and P. Yeh, "Optical Waves in Crystals," Wiley, New York, (1984).
8. S. John, *Phys. Rev. Lett.* **58**, 2486 (1987).

9. D. S. Chemla, D. A. B. Miller, and P. W. Smith, *Opt. Eng.* **24**, 556 (1985).
10. R. Dingle, W. Wiegmann, and C. H. Henry, *Phys. Rev. Lett.* **33**, 827 (1974).
11. D. S. Chemla and D. A. B. Miller, *J. Opt. Soc.* **B2**, 1155 (1985).
12. V. I. Alperowich, V. M. Zal, A. F. Kranchinko and A. S. Terekhev, *Phys. Stat. Solidi* **b77**, 466 (1976).
13. D. S. Chemla, D. A. B. Miller, P. W. Smith, A. C. Gossard, and W. Wiegmann, *IEEE J. Quantum Electron.* **QE-20**, 265 (1984).
14. K. K. Bajaj and D. C. Reynolds, Proceedings of Advances in Semiconductors and Semiconductor Structures, *SPIE* **794**, 2 (1987).
15. D. C. Reynolds, K. K. Bajaj, C. W. Litton, Jasprit Singh, P. W. Yu, P. Pearah, J. Klem, and H. Morkoc, *Phys. Rev.* **B33**, 5931 (1986).
16. J. E. Zucker, A. Pinczuk, D. S. Chemla, A. Gossard, and W. Wiegmann, *Phys. Rev. Lett.* **51**, 1293 (1983).
17. K. B. Kahen and J. P. Leburton, *Phys. Rev.* **B33**, 5465 (1986).
18. R. Dingle, A. C. Gossard, and W. Wiegmann, *Phys. Rev. Lett.* **34**, 1327 (1975).
19. P. Voisin, *Surf. Sci.* **142**, 460 (1984).
20. B. F. Levine, R. J. Malik, J. Walker, K. K. Choi, and C. G. Bethea, Proceedings of Advances in Semiconductors and Semiconductor Structures, *SPIE* **792**, 157 (1987).
21. J. J. Song, Y. S. Yoon, P. S. Jung, A. Fedotowsky, and Y. B. Kim, Proceedings of Advances in Semiconductors and Semiconductor Structures, *SPIE* **794**, 55 (1987).
22. M. Garriga, M. Cardona, N. E. Christensen, P. Lautenschlager, T. Isu, and K. Ploog, *Phys. Rev.* **B36**, 3254 (1987).
23. R. C. Miller, A. C. Gossard, W. T. Tsang, and O. Munteanu, *Phys. Rev.* **B25**, 3871 (1982).
24. C. Weisbuch, R. C. Miller, R. Dingle, A. C. Gossard and W. Wiegmann, *Solid State Commun.* **37**, 219 (1981).
25. P. Manuel, G. A. Sai-Halasz, L. L. Chang, Chin-An Chang, and L. Esaki, *Phys. Rev. Lett.* **37**, 1701 (1976).
26. C. Colvard, R. Merlin, M. V. Klein, and A. C. Gossard, *Phys. Rev. Lett.* **45**, 298 (1980).
27. A. K. Sood, J. Menéndez, M. Cardona, and K. Ploog, *Phys. Rev. Lett.* **54**, 2111 (1985).
28. A. K. Sood, J. Menéndez, M. Cardona, and K. Ploog, *Phys. Rev. Lett.* **54**, 2115 (1985).
29. C. Colvard, T. A. Gant, M. V. Klein, R. Merlin, R. Fischer, H. Morkoc, and A. C. Gossard, *Phys. Rev.* **B31**, 2080 (1985).
30. C. Colvard, Proceedings of Advances in Semiconductors and Semiconductor Structures, *SPIE* **794**, 209 (1987).
31. B. Abeles and T. Tiedje, *Phys. Rev. Lett.* **51**, 2003 (1983).
32. N. Ibaraki and H. Fritsche, *Phys. Rev.* **B30**, 5791 (1984).
33. T. Tiedje, B. Abeles, P. D. Persans, B. G. Brooks, and G. D. Cody, *J. Non-Cryst. Solids* **66**, 339 (1984).
34. H. Munekata, M. Mizuta, and H. Kukimoto, *J. Non-Cryst. Solids* **59 & 60**, 1167 (1983).
35. H. J. Trodahl and M. W. Wright, *Solid State Commum.* **59**, 699 (1986).
36. A. Bittar, O. Hunderi, and H. J. Trodahl, Proceedings of Advances in Semiconductors and Semiconductor Structures, *SPIE* **792**, 249 (1987).
37. A. Bittar, G. V. M. Williams, and H. J. Trodahl, *Physica* **A157**, 411 (1989).
38. See, for example, W. L. Bloss and E. M. Brody, *Solid State Commun.* **43**, 523 (1982); ibid. **44**, 363 (1982) and ibid. **48**, 927 (1983).
39. See, for example, A. C. Tselis and J. J. Quinn, *Phys. Rev.* **B29**, 2021 (1984); ibid. 2318 (1984).
40. See, for example, S. Das Sarma and J. J. Quinn, *Phys. Rev.* **B25**, 7603 (1982).
41. R. E. Camley and D. L. Mills, *Phys. Rev.* **B29**, 1625 (1984).
42. D. Olego, A. Pinczuk, A. C. Gossard, and W. Wiegmann, *Phys. Rev.* **B25**, 7867 (1982).
43. S. M. Rytov, *Sov. Phys. JETP* **2**, 466 (1956).

44. L. M. Brekhovskikh, "Waves in Layered Media," 2nd edition, Academic Press, New York (1980).
45. Ph. Lambin, J. P. Vigneron, and A. A. Lucas, *Solid State Commun.* **54**, 257 (1985).
46. W. L. Mocha'n, M. del Castillo-Mussot, and R. G. Barrera, *Phys. Rev.* **B35**, 1088 (1987).
47. W. E. Jones, K. L. Kliewer, and R. Fuchs, *Phys. Rev.* **178**, 1201 (1969); R. Fuchs and K. L. Kliewer, *Phys. Rev.* **185**, 905 (1969).
48. D. W. Berreman, *Phys. Rev.* **130**, 2193 (1963).
49. B. Harbecke, B. Heinz, and P. Grosse, *Appl. Phys.* **A38**, 263 (1985).
50. O. Hunderi, *Physica* **A157**, 309 (1989).
51. P. Grosse, B. Harbecke, B. Heinz, W. Jantz, and M. Maier, *Appl. Phys.*, in press.
52. K. A. Maslin, T. J. Parker, N. Raj, D. R. Tilley, P. J. Dobson, D. Hilton, and C. T. B. Foxton, *Solid State Commun.* **60**, 461 (1986).
53. O. Hunderi and K. Johannessen, *Superlatt. and Microstruct.* **3**, 193 (1987).
54. A. Genack, *Phys. Rev. Lett.* **58**, 2043 (1987).
55. M. Kohmoto, B. Sutherland, and K. Iguchi, *Phys. Rev. Lett.* **58**, 2436 (1987).
56. A. Herpin, *Comptes Rendus des Sciences* **225**, 182 (1947).
57. I. K. Schuller, *Phys. Rev. Lett.* **24**, 1597 (1980).
58. C. M. Falco, *Journal de Physique, Coll C5*, **45**, 499 (1984).

# Chapter 6

# Calculation of the Refractive Index of Compound Semiconductors below the Band Gap

B. JENSEN
Department of Physics
University of Lowell
Lowell, Massachusetts

I. Introduction 125
II. The Quantum-Density-Matrix Formulation of the Complex Dielectric Constant 128
III. Comparison with Experimental Results 138
IV. Summary 147
References 148

## I INTRODUCTION

The interaction of the radiation field with the free carriers and bound electrons in a compound semiconductor can be described in terms of a complex dielectric constant

$$e = \varepsilon_1 - i\varepsilon_2 = N^2, \tag{1}$$

where the real and imaginary parts of the complex dielectric constant $\varepsilon_1$ and $\varepsilon_2$ are functions of the complex refractive index $N$ as follows:

$$N = n - ik \tag{2}$$

$$\varepsilon_1 = n^2 - k^2 \tag{3}$$

$$\varepsilon_2 = 2nk = 4\pi\sigma/\omega. \tag{4}$$


Copyright © 1991 by Academic Press.
All rights of reproduction in any form reserved.
ISBN 0-12-544422-2

In Eq. 2, $n$ is the real and $k$ the imaginary part of the complex refractive index, and $\sigma$ is the optical conductivity, which is proportional to $\varepsilon_2$ and to the absorption coefficient $\alpha$ with

$$n\alpha = 4\pi\sigma/c = (\omega/c)\varepsilon_2. \tag{5}$$

The classical Drude model may be used to extract the mobility and the free-carrier density $n_e$ from an analysis of the reflection and the transmission data in the far infrared. The Drude model gives the complex dielectric constant in terms of a high-frequency lattice dielectric constant $\varepsilon_\infty$, the plasma frequency $\bar{\omega}_p$, and the electron scattering time $\tau$ as

$$\varepsilon_1 = \varepsilon_\infty[1 - (\bar{\omega}_p^2/\omega^2\eta)] \tag{6}$$

$$\varepsilon_2 = (\omega_p^2/\omega^2\eta)(1/\omega\tau), \tag{7}$$

where

$$\eta = 1 + (1/\omega^2\tau^2) \rightarrow 1, \qquad \omega\tau \gg 1 \tag{8}$$

$$\omega_p^2 = 4\pi n_e e^2/m_n \tag{9}$$

$$\bar{\omega}_p^2 = \omega_p^2/\varepsilon_\infty. \tag{10}$$

The real and imaginary parts of the complex refractive index are obtained from $\varepsilon_1$ and $\varepsilon_2$ as follows:

$$\varepsilon = (\varepsilon_1^2 + \varepsilon_2^2)^{1/2} = n^2 + k^2 \tag{11}$$

$$n = [(\varepsilon + \varepsilon_1)/2]^{1/2} \tag{12}$$

$$k = \varepsilon_2/2n = [(\varepsilon - \varepsilon_1)/2]^{1/2}. \tag{13}$$

The experimental determination of $n$ and $k$ involves measuring the reflectivity of a bulk, opaque sample and the transmittance of a slab from which values of $n$ and $k$ can be obtained.

The absorption of radiation by free carriers is represented by $\varepsilon_2$ or $\alpha$, and is a function of the plasma frequency and the electron scattering rate $1/\tau$ for an $n$-type material. The high-frequency lattice dielectric constant arises from the interaction of the radiation field with the bound electrons. It is

assumed, in writing Eqs. 6 and 7, that the photon energy is small compared with the band gap energy, $G$, of the semiconductor. This is the condition for the validity of the quasi-classical Boltzmann transport equation, or Drude theory, in terms of the frequency-independent electron scattering rate $1/\tau$. It is expected that deviations from the quasi-classical Boltzmann equation should occur when photon energies become large compared with electron energies. The latter are of the order of $k_0T$ or $e_f$ for nondegenerate or degenerate materials, respectively, where $e_f$ is the electron Fermi energy measured relative to the conduction-band edge. In particular, quantum effects may be expected to occur when the photon energy is of the order of the band-gap energy in materials such as InP and GaAs. In this case, a generalized Boltzmann equation is obtained, which reduces to the quasi-classical Boltzmann transport equation when the wave vector of the driving field tends to zero and $\omega$ is small [1–4]. When $\omega$ is large, a solution of the Boltzmann equation in terms of a frequency-dependent relaxation time is obtained under certain conditions [1, 4]. This relaxation rate has been tabulated as a function of frequency and carrier concentration for various materials, [5–7], and can be used in the usual expressions of the classical Drude theory in Eq. 7 to obtain the quantum result for $k$ from Eq. 13 as

$$k = \varepsilon_2/2n = (1/2n)(\omega_p^2/\omega^2)(1/\omega\tau), \qquad \omega\tau \gg 1. \tag{14}$$

This problem has been discussed in some detail for the imaginary part of the complex dielectric constant, or the absorption coefficient, to which it is proportional. In the case of $k$ or $\varepsilon_2$, the quantum effects are notable. The low-frequency limit of the result for $\tau$ gives a good estimate for the dc electron mobility when used to calculate this quantity from the usual formula; at high frequencies, it predicts the change in wavelength dependence observed in $k$ or the absorption coefficient $\alpha$ when used in Eq. 14. The exact wavelength dependence of the observed high-frequency absorption coefficient depends on the dominant scattering mechanism, which is polar-optical-mode scattering at low carrier concentrations, or charged-impurity (ionic) scattering in highly doped materials [6, 8].

One also expects quantum effects to occur in the real part of the dielectric constant near the fundamental absorption edge. When the imaginary part of the complex refractive index, that is, the extinction coefficient $k$, is small, a change in $\varepsilon_1$ is essentially a change in $n^2$, and hence, a change in the real part of the refractive index. Although this change is small, and less dramatic than the change in $k$, it is of technological importance, and its study provides insight into how to effect variations in $n$ in this important spectral region, which is also the region of operation of a double-heterostructure, semiconductor diode laser. It is this subject to which this chapter is addressed. We will outline the calculation of $\varepsilon_1 \cong n^2$

for $\hbar\omega \leqslant G$ and identify the parameter $\varepsilon_\infty$ in the Drude theory with the value of $\varepsilon_1$ at $\hbar\omega = G$, when the carrier concentration and hence the plasma frequency are zero.*

The usual method of calculation of $\varepsilon_1$ near the band edge involves the calculation of $\varepsilon_2$ due to direct interband transitions and subsequent integration of this result to obtain $\varepsilon_1$ via the Kramers–Kronig relations [9]. Here, $\varepsilon_1$ is determined directly by calculating the interaction energy of the lattice polarization due to valence electrons and the radiation field. One obtains from this the real part of the susceptibility, which is then related to $\varepsilon_1$ and hence to $n$.

## II THE QUANTUM-DENSITY-MATRIX FORMULATION OF THE COMPLEX DIELECTRIC CONSTANT

We consider a system consisting of a number of dynamically independent electrons, a scattering system taken to be optical- or acoustical-mode phonons or charged impurities, and an equilibrium radiation field. A perturbing field is then applied. The system is described by a quantum density matrix $R$ with the equation of motion [4, 10]

$$\begin{aligned} i\hbar\dot{p} = i\hbar sp = [H, R] \\ R = R^o + p, \end{aligned} \tag{15}$$

where $R^o$ is the equilibrium density matrix, and $p$ is the deviation from equilibrium. The total Hamiltonian of the system, denoted by $H$, is given by

$$H = H^o + H^i \tag{16}$$

$$H^o = H^e(n) + H^s(\nu) + H^r(\gamma), \tag{17}$$

where $H^o$ is the sum of the Hamiltonians of the noninteracting subsystems consisting of electrons ($n$), phonons ($\nu$), and photons ($\gamma$). The interaction between subsystems is specified by

$$H^i = H' + H^{er}, \tag{18}$$

* The calculation of $n$ for $\hbar\omega \geqslant G$ is treated in a forthcoming publication; B. Jensen, W. D. Jensen, *IEEE J. Quant. Electron.*, in press.

where $H'$ is the scattering interaction of the electrons with the phonon field, and $H^{er}$ is the interaction of the electrons with the radiation field:

$$H^{er} = -(e/mc)\mathbf{A} \cdot \mathbf{P}. \tag{19}$$

The form of $H'$ depends on the scattering mechanism. Various cases are given in Refs. [4] and [8].

In the occupation-number representation, $H^o$ is diagonal and the eigenstate $|N\rangle$ of $H^o$ is the product of the eigenstates of $H^e$, $H^s$, and $H'$,

$$|N\rangle = |n\rangle|\nu\rangle|\gamma\rangle. \tag{20}$$

The coulomb gauge is used, which implies that the vector potential of the radiation field $\mathbf{A}$ and the electric field $\mathbf{E}$ are related as follows:

$$\mathbf{E} = -(1/c)\dot{\mathbf{A}}. \tag{21}$$

We let $q$ denote the wave vector of the applied radiation field.

In Eq. 19, $\mathbf{P}$ denotes the momentum operator for the electron system. In the occupation-number representation, $H_q^{er}$ has no diagonal elements,

$$H_{N'N}^{er} = \langle N'|H_q^{er}|N\rangle = \begin{cases} 0 & |N\rangle = |N'\rangle \\ H_{N'N}^{er} & |N\rangle \neq |N'\rangle. \end{cases} \tag{22}$$

The derivation of the perturbation energy $\langle \delta H_q \rangle$, arising from the interaction of the electron–photon system, is given in Ref. [10]. The perturbation energy is proportional to the real part of the susceptibility $\chi_1$ and is found on taking the trace of $p_N$ and $E_N^{(2)}$:

$$E_N^{(2)} = \sum_{N'} \frac{H_{NN'}^{er} H_{N'N}^{er}}{E_N - E_{N'}}, \qquad p_N = (N|p|N) = 2F_N \tag{23}$$

$$\langle \delta H_q \rangle = \sum_N p_N E_N^{(2)} = \chi_1 \langle E_q^2 \rangle, \tag{24}$$

where $p$ is found from the solution of Eq. 15. In the derivation, the Bloch

functions of the electrons in the crystal lattice are taken to be

$$|k\rangle = |n, k, s\rangle = e^{i\mathbf{k}\cdot\mathbf{r}} U_{nks}, \tag{25}$$

where $k$ denotes the electron wave vector, $s$ the spin index, and $n$ the band index. These wave functions and the corresponding electron energies are given by the Kane theory [11], and are useful in calculating a number of properties of electrons in compound semiconductors [12, 13, 8].

The real part of the susceptibility is the ratio of the perturbation energy $\langle \delta H_q \rangle$ to $\langle E_q^2 \rangle$, and the real part of the complex dielectric constant is obtained as $\varepsilon_1 = 1 + 4\pi\chi_1$ [10, 14]:

$$\varepsilon_1 = 1 + (4\pi e^2/\omega^2) \sum_{v_i, k} \hat{\mathbf{e}} \cdot \mathbf{V}_{v_i, k; c, k+q} \mathbf{V}_{c, k+q; v_i, k} \cdot \hat{\mathbf{e}} \frac{(f^0_{v_i, k} - f^0_{c, k+q})}{E_{c, k+q} - E_{v_i, k} - \hbar\omega}, \tag{26}$$

where $\hat{\mathbf{e}}$ is the photon polarization vector and

$$\mathbf{V}_{c, k+q; v_i k} = (1/m)\langle c, k+q, s' | \mathbf{p} | v_i, k, s \rangle \tag{27}$$

is the matrix element of the single-electron momentum operator $\mathbf{p}$ between states $|v_i, k, s\rangle$ in the $i$th valence band and $|c, k+q, s'\rangle$ in the conduction band, and is calculated using the band structure of the Kane theory. In Eq. 26, $q$ denotes the wave vector of the photon, which is negligible for vertical transitions in $k$ space, and hence is neglected. The energies $E_{c, k}$ and $E_{v_i, k}$ are the positive energy of an electron in the conduction band with wave vector $k$ and the negative energy of an electron in band $v_i$ with the same wave vector. The sum over valence bands $v_i$, $i = 1, 2, 3$ is taken over the heavy-hole band, the light-hole band, and the spin-orbit split-off valence band. The quantities $f^0_{c, k}$ and $f^0_{v_i, k}$ are the occupation probabilities for electrons in states $|c, k, s'\rangle$ and $|v_i, k, s\rangle$, respectively. We now consider unpolarized radiation and cubic crystals.

Using the results of Ref. [8], Table 1, one can show that the following result is obtained on summing over final and averaging over initial electron spins,

$$\frac{1}{2} \sum_{ss'} |\langle v_i, k, s | \mathbf{p} | c, k, s' \rangle|^2 \Big|_{k=0} = m^2 \mathcal{P}^2 / \hbar^2 \tag{28}$$

for $i = 1, 2, 3$, where $G$ is the direct-band-gap energy, $m_n$ is the effective

electron mass and

$$\frac{m^2\mathcal{P}^2}{\hbar^2} = (3/2)m^2(G/2m_n)\frac{(1+r)}{(\frac{3}{2}+r)}. \tag{29}$$

Defining

$$\bar{\eta} = \frac{1}{2}\frac{(1+r)}{(\frac{3}{2}+r)} \rightarrow \begin{cases} 1/3, & r \rightarrow 0 \\ 1/2, & r \rightarrow \infty, \end{cases} \tag{30}$$

where $r$ is the ratio of the spin-orbit-splitting energy to the direct-band-gap energy, one has for the angle average in a cubic crystal

$$(1/3m^2)\left[\frac{1}{2}\sum_{ss'}|\langle v_i, k, s'|\mathbf{p}|c, k, s\rangle|^2\right]\Bigg|_{k=0} = \bar{\eta}(G/2m_n). \tag{31}$$

We use the fact that the term

$$(f^0_{v_i,k} - f^0_{c,k})/(E_{c,k} - E_{v_i,k} - \hbar\omega) \tag{32}$$

falls off rapidly with $k$ to evaluate the coefficient of this term in Eq. 26 at $k=0$, as in Eq. 31, and remove it from the integration over $k$ space. We consider the case of arbitrary spin-orbit splitting and define

$$r = \Delta/G \tag{33}$$

$$X = \hbar\omega/G \tag{34}$$

$$1/m_{r_i} = (1/m_n) + (1/m_{p_i}), \qquad i = 1, 2, 3 \tag{35}$$

$$\lambda^2_{r_i} = \hbar^2/2m_{r_i}G. \tag{36}$$

Summing over photon polarizations, Eq. 26 may then be written

$$\varepsilon_1 = 1 + \frac{(4\pi e^2/m_n)}{\omega^2}\bar{\eta}\sum_{\substack{v_i,k \\ i=1,2,3}}\frac{(f^0_{v_i,k} - f^0_{c,k})}{(1 + r\delta_{i3} - X) + \lambda^2_{r_i}k^2}. \tag{37}$$

In Eq. 35, $m_n$ and $m_{p_i}$ are the effective electron mass in the conduction band and the effective hole mass at the band edge of the $i$th valence band, and $m_{r_i}$ is the corresponding reduced mass. The quantity $\delta_{i3}$ is the Kroneker delta. To recover the Drude theory from Eq. 37, neglect the term $\hat{\lambda}_{ri}^2 k^2$ in the denominator of the summation over $k$, the sum over $v_2$, and $v_3$, and set $r=0$, $X \ll 1$, and $\bar{\eta}=1$. On defining

$$\varepsilon_\infty = 1 + \frac{4\pi e^2/m_n}{\omega^2} \sum_k f^0_{v_1,k}$$

$$n_e = \sum_k f^0_{c,k},$$

one recovers Eq. 6 as

$$\varepsilon_1 = \varepsilon_\infty - [\omega_p^2/\omega^2] = \varepsilon_\infty[1 - (\bar{\omega}_p^2/\omega^2)], \qquad \frac{1}{\tau} \ll \omega \ll \frac{G}{\hbar},$$

which gives the Drude-theory result. We note that $\varepsilon_\infty$ is the value of $\varepsilon_1$ obtained when there are no electrons in the conduction band and $f^0_{c,k}=0$.

Returning to the evaluation of Eq. 37 and defining

$$\begin{aligned} z_i &= (1 + r\delta_{ik} - X)^{1/2} \\ z &= (1-X)^{1/2}, \end{aligned} \tag{38}$$

and converting from summation to integration in the usual fashion, one has

$$\varepsilon_1 = 1 + \frac{4\pi e^2}{m_n \omega^2} \bar{\eta} \frac{8\pi}{(2\pi)^3} \sum_{i=1}^{3} \int_0^{k_B} \frac{k^2\, dk}{z_i^2 + \hat{\lambda}_{r_i}^2 k^2} [f^0_{v_i,k} - f^0_{c,k}]. \tag{39}$$

We define the following quantities:

$$N_v^* = 1/3\pi^2 \hat{\lambda}_{r_1}^3 \tag{40}$$

$$e^*_{v_i,k} = \frac{\hbar^2 k^2}{2m_{p_i}} + rG\delta_{i3} \tag{41}$$

$$e_{c,k} \cong \hbar^2 k^2 / 2m_n \tag{42}$$

$$f^0_{c,k} = 1/[e^{\beta(e_{c,k}+G/2-E_F)}+1], \qquad \beta = 1/k_0T \tag{43}$$

$$f^0_{v_i,k} = 1/[e^{-\beta(e^*_{v_i,k}+G/2+E_F)}+1]. \tag{44}$$

In Eqs. 43 and 44, $E_F$ is the Fermi energy, measured relative to the center of the band gap, and $e_{c,k}$ and $e^*_{v_i,k}$ are the absolute values of the electron energy measured relative to the conduction-band edge, and the hole in the $i$th valence band measured relative to the edge of the valence band $v_1$, (that is, the heavy-hole band). The (negative) energy of the electron in the $i$th valence band, measured relative to the center of the band gap, is $E_{v_i,k}$ in Eq. 26.

Expanding $\omega$ to lowest order around $\omega_g = G/\hbar$ in the coefficient of the integral and defining a new variable of integration $y = \lambda_{r_i} k$, Eq. 39 can be written

$$\varepsilon_1 = 1 + \frac{[4\pi N^*_v e^2]}{m_n \omega_g^2}(3\bar{\eta}) \sum_{i=1}^{3} \frac{[1+(m_n/m_{p_1})]^{3/2}}{[1+(m_n/m_{p_i})]^{3/2}} \times \int_0^{y_B} \frac{y^2\,dy}{z_i^2+y^2}[f^0_{v_i,k} - f^0_{c,k}] \tag{45}$$

To proceed further, one must specify the type of material ($n$-type or $p$-type), which then specifies the $E_F$ in Eqs. 43 and 44. Treating a degenerate semiconductor as a poor metal, we consider several cases in the limit $T \to 0$. The lower limit of the integrand in Eq. 45 is then determined by $E_F$, and hence, by the type and carrier concentration of the material. For $n$-type materials, this dependence is due to the exclusion principle. The dielectric constant decreases from that of the pure material as free electrons are added and fewer conduction-band states are available for virtual transitions. The upper limit $y_B$ of the integrand is a function of the lattice constant, and its determination will be discussed.

Case 1: Degenerate $n$-Type Material

$$E_F = G/2 + e_F, \qquad e_F \gg k_o T \to 0,$$

$$f^0_{v_i,k} \cong 1$$

$$f^0_{c,k} \cong \begin{cases} 1, & e_{c,k} \le e_F, \quad y \le y_F \\ 0, & e_{c,k} > e_F, \quad y > y_F. \end{cases}$$

$$\varepsilon_1 = 1 + [4\pi N^*_v e^2/m_n\omega_g^2](3\bar{\eta}) \sum_{i=1}^{3} \left[\frac{(1+(m_n/m_{p_1})}{(1+(m_n/m_{p_i})}\right]^{3/2} \times [(y_B - y_F) - z_i(\tan^{-1}(y_B/z_i) - \tan^{-1}(y_F/z_i))]. \tag{46}$$

In the limit of small spin-orbit splitting, $r \ll 1$, $z_i = z$, and Eq. 46 assumes the simple form

$$\varepsilon_1 = 1 + 2C_o[(y_B - y_F) - z \tan^{-1}(y_B/z) - \tan^{-1}(y_F/z))], \tag{47}$$

where

$$C_o = (3/2)\eta(\omega_v^2/\omega_g^2) \tag{48}$$

$$\omega_v^2 = 4\pi N_v^* e^2/m_n \tag{49}$$

$$\eta = \bar{\eta} S \tag{50}$$

$$S = \sum_{i=1}^{3} [(1 + (m_n/m_{p_1}))/(1 + (m_n/m_{p_i}))]^{3/2}. \tag{51}$$

In practice, $m_{p_1} > m_{p_2}$, $m_{p_3}$ and hence, $S$ lies between the limits of one for $m_{p_2} \ll m_n \ll m_{p_1}$, $m_{p_3} \ll m_n \ll m_{p_1}$, and three for $m_{p_2} = m_{p_1}$, $m_{p_3} = m_{p_1}$.

The quantity $y_F$ is related to the Fermi level of the $n$-type material and hence to the carrier concentration $n_e$. Because $m_n \ll m_{p_1}$, $y_F$ is determined mainly by the electron Fermi level. For high carrier concentrations, we also note that the dispersion relation of the conduction band becomes hyperbolic at large values of $k$ [8]. We therefore define $y_F = \lambda\!\!\!^{-}_c k_F$, where $k_F$ is the electron wave vector at the Fermi surface and

$$\lambda\!\!\!^{-}_c = \hbar/m_n \alpha_o c \tag{52}$$

$$\alpha_o = (G/2m_n c^2)^{1/2} \tag{53}$$

$$N_v = (8/3\pi^2 \lambda\!\!\!^{-3}_c). \tag{54}$$

One then has, for the relation between $y_F$ and the carrier concentration $n_e$,

$$y_F = 2(n_e/N_v)^{1/3}, \quad \text{high carrier concentrations.} \tag{55}$$

At low carrier concentrations, a parabolic dispersion relation can be used to give the relation between $y_F$ and $n_e$ as $y_F = (1/2)(m_n/m_{r_1})^{1/2} \lambda\!\!\!^{-}_c k_F$, where $k_F = (3\pi^2 n_e)^{1/3}$.

Case 2: Degenerate $p$-Type Material:

$$E_F = -G/2 - e_F, \quad e_F \gg k_o T \to 0.$$

In this case, the second term in brackets in the integrand of Eq. 45 may be neglected, while the first term in brackets may be written

$$f^0_{v,k} = 1 - f^0_{v,k}(p) = 1 - [1/(e^{\beta(e^*_{v,k} - e_F)} + 1)], \tag{56}$$

where $f^0{}_{v,k}(p)$ is the hole occupation probability for a hole in the valence band $v$. We consider the case of $m_{p_1} \gg m_{p_2}$, $m_{p_3} \to 0$, so that only the heavy-hole valence band contributes in Eq. 45. Under the conditions of case 2, $f^0_{v,k}(p)$ is approximately unity for $e^*_{v,k} < e_F$ and negligible for $e^*_{v,k} > e_F$. Therefore, defining $y_F = \hat{\lambda}_{r_1} k_F$, where $k_F$ is the wave vector at the Fermi surface and the Fermi level lies inside the valence band, and where $p$ is the hole concentration in the heavy-hole valence band, one has

$$\begin{aligned} k_F &= (3\pi^2 p)^{1/3} \\ \hat{\lambda}^2_{r_1} &= \hbar^2/2m_{r_1} G \\ y_F &= \hat{\lambda}_{r_1} k_F. \end{aligned} \tag{57}$$

Hence, Eqs. 47–50 apply to $p$-type materials with $S$ replaced by 1 and with $y_F$ given by Eq. 57.

Case 3: Inversion

In the case of inversion, we express the electron- and hole-occupation probabilities in terms of the electron quasi-Fermi level $\mu_e$ and the hole quasi-Fermi level $\mu_h$. We again consider that $m_{p_1} \gg m_{p_2}$, $m_{p_3} \to 0$, so that only the heavy-hole band contributes. In the limit $T \to 0$, one has

$$f^0_{c,k} = \frac{1}{e^{\beta(e_{c,k} - \mu_e)} + 1} = \begin{cases} 1, & e_{c,k} \le \mu_e \\ 0, & e_{c,k} > \mu_e \end{cases} \tag{58}$$

$$f^0_{v_1,k} = 1 - \frac{1}{e^{\beta(e^*_{v_1,k} - \mu_h)} + 1} = \begin{cases} 0, & e^*_{v_1,k} \le \mu_h \\ 1, & e^*_{v_1,k} > \mu_h \end{cases}. \tag{59}$$

Using Eqs. 58 and 59 in Eq. 45, one obtains

$$\varepsilon_1 \cong n^2 = 1 + (\omega_v^2/\omega_g^2)(3\bar{\eta})[[y_B - y_F(p) - y_F(n_e)] - z[\tan^{-1}(y_B/z) - \tan^{-1}(y_F(p)/z) - \tan^{-1}(y_F(n_e)/z)]], \quad (60)$$

where $y_F(n_e)$ and $y_F(p)$ are the quantities defined for $n$-type and $p$-type materials, respectively. In the case of an undoped material, the requirement $n_e = p$ implies $y_F(n_e) = y_F(p)$ if the parabolic dispersion relation, Eq. 57, is used for both types of material. If Eq. 55 is used for $y_F(n)$ and Eq. 57 for $y_F(p)$, the requirement $n_e = p$ implies

$$y_F(p) = \tfrac{1}{2}(m_n/m_{r_1})^{1/2} y_F(n_e). \quad (61)$$

The quantity $y_B$ in Eq. 47 is a function of the lattice constant $a$, and can be expanded as a Taylor series in $a$ (for a cubic crystal) as

$$y_B(a) = y_B(a_0) + \left.\frac{dy_B}{da}\right|_{a=a_o} (a - a_o) + \frac{1}{2!}\left.\frac{d^2 y_B}{d^2 a}\right|_{a=a_o} (a - a_o)^2 + \ldots \quad (62)$$

Comparison with experimental results on a given series of compounds, such as III-V or II-IV materials, indicates that only the linear term is significant, and $y_B$ can be written to a good approximation as

$$y_B = M(a_o - a) \quad (63)$$

$$M = \begin{cases} 3.04 \pm 0.08\ \text{Å}^{-1}, & \text{III-V compounds} \\ 0.346 \pm 0.020\ \text{Å}^{-1}, & \text{II-VI compounds} \end{cases} \quad (64)$$

$$a_o = \begin{cases} 7.49 \pm 0.04\ \text{Å}, & \text{III-V compounds} \\ 17.37 \pm 0.88\ \text{Å}, & \text{II-VI compounds.} \end{cases} \quad (65)$$

We note that $y_B$ is related to the linear coefficient of thermal expansion as follows:

$$\frac{dy_B}{dT} = -M\frac{da}{dT} = -Ma\alpha_T \quad (66)$$

$\alpha_T = (1/a)\, da/dT =$ linear thermal coefficient of expansion.

The thermo-optic coefficient dn/dT, which can be obtained from Eq. 46 or 47 when $\varepsilon_1 \cong n^2$, is important in the design of optical components [14].

If higher conduction bands, which have not been considered here, make a contribution to $n$ at $\hbar\omega \cong G$, they may be shown to appear as a contribution to the constant term in Eq. 63. It is necessary to consider higher-conduction-band contributions explicitly in order to calculate $n$ for $\hbar\omega > G$, where the approximation $\varepsilon_1 = n^2$ no longer holds, because the imaginary part of the refractive index is not negligible.*

Two useful limiting cases of $n^2$ will now be obtained from Eq. 46 and used for comparison of theoretical and experimental results in the following section. In the limit that $m_{p_1} \gg m_{p_2}$, $m_{p_3} \to 0$, the contribution of the light-hole band and the split-off band are negligible, and one obtains from Eq. 46

$$n^2(z, y_F) = 1 + 2C_o[(y_B - y_F) - z \times (\tan^{-1}(y_B/z) - \tan^{-1}(y_F/z))] \tag{67}$$

$$C_o = (3/2)\bar{\eta}[\omega_v^2/\omega_g^2] \to (1/2)[\omega_v^2/\omega_g^2],$$

$r \to 0$ small spin-orbit-splitting limit.

If the spin-orbit splitting is small compared with $G$, so that $z_3 \cong z$, but $m_{p_2}$ and $m_{p_3}$ are not small enough so that the contributions of bands $v_2$ and $v_3$ can be neglected, one has, from Eq. 46,

$$n^2(z, y_F) = 1 + 2C_o[(y_B - y_F) - z(\tan^{-1}(y_B/z) - \tan^{-1}(y_F/z))] \tag{68}$$

$$C_o = (3/2)\bar{\eta}[\omega_v^2/\omega_g^2]S < (3^2/2)\bar{\eta}[\omega_v^2/\omega_g^2] = C_{o_{max}}.$$

An upper bound on $C_{0_{max}}$ is obtained by setting $\bar{\eta} = 1/2$. Hence, one can say

$$(1/2)[\omega_v^2/\omega_g^2] \leq C_o < (3/2)^2[\omega_v^2/\omega_g^2]. \tag{69}$$

The exact expression for $n^2$ may be obtained from Eq. 46 as

$$n^2(z, y_F) = 1 + (3\bar{\eta})[\omega_v^2/\omega_g^2] \sum_i S_i \left[ (y_B - y_F) - z_i \left[ \tan^{-1} \frac{y_B}{z_i} - \tan^{-1} \frac{y_F}{z_i} \right] \right], \tag{70}$$

* See footnote page 128. The refractive index is continuous at $\hbar\omega = G$, but changes its functional form for $\hbar\omega > G$.

where

$$S_i = [(1 + (m_n/m_{p_1}))/(1 + (m_n/m_{p_i}))]^{3/2}. \tag{71}$$

The refractive index is therefore a function of measurable material parameters only. These are the band-gap energy $G$, the effective electron mass $m_n$, the effective hole masses $m_{p_i}$, the lattice constant $a$ (Å), and the spin-orbit-splitting energy $\Delta$. In the limit that $m_{p_1} \gg m_{p_2}$, $m_{p_3} \to 0$, these reduce to five material parameters: $G$, $m_n$, $m_{p_1}$, $a$, and $\Delta$.

## III COMPARISON WITH EXPERIMENTAL RESULTS

The result calculated for $n$ in the previous section will now be applied to the ternary III-V compound $Al_xGa_{1-x}As$, the quaternary III-V compound $In_{1-x}Ga_xAs_yP_{1-y}$ lattice matched to InP (which requires that $x = 0.466\,y$), and the ternary II-VI compound $Hg_xCd_{1-x}Te$. Formulas specific to each compound and room-temperature values of band-structure parameters will be given, so that $n$ may be calculated for any value of $x$.

Case 1: $In_{1-x}Ga_xAs_yP_{1-y}$ (lattice matched, $x = 0.466\,y$) [15]

The calculation of $n$ for this compound requires an accurate expression relating the experimental parameters to the mole fraction $x$ of Ga and the mole fraction $y$ of As. The experimental parameters are the band-gap energy $G$, the electron and heavy-hole effective mass, the lattice constant $a$, and the spin-orbit splittir⁻, or equivalently $\eta$. In the limit that $m_{p_1} > m_{p_2}$, $m_{p_3}$ and $r \ll 1$, one has $z_i \cong z$, $i = 1, 2, 3$ and Eq. 46 becomes

$$n^2 = 1 + 2C_o[(y_B - y_F) - z(\tan^{-1}(y_B/z) - \tan^{-1}(y_F/z))] \tag{72}$$

$$2C_o = [\omega_v^2/\omega_g^2](3\eta), \qquad \eta = \bar{\eta}S \tag{73}$$

$$z = [1 - (\hbar\omega/G)]^{1/2}. \tag{74}$$

Table I lists the values of $y_B$, $G$, $C_o$, and lattice constant $a$ as a function of $y$, with $x = 0.466y$. The values of $C_o$ have been calculated using the following expressions for $G$, $m_n$, and $m_p$ (where $m_p = m_{p_1}$):

$$G(\text{eV}) = 1.35 - 0.72y + 0.12y^2 \quad \text{(Ref. [16])} \tag{75}$$

**TABLE I**

**The Numerical Values of $G$ (eV), $C_0$, $a$ (Å), and $y_B$ as a Function of $y$ for $In_{1-x}Ga_xAs_yP_{1-y}$ with $x = 0.466y$ (Lattice Matched to InP)**

| $y$ | $G$ (eV) | $a$ (Å) | $C_o$ | $y_B$ |
|---|---|---|---|---|
| 0.0 | 1.350 | 5.86960 | 1.113 | 4.9246 |
| 0.1 | 1.279 | 5.86910 | 1.143 | 4.9261 |
| 0.2 | 1.211 | 5.86872 | 1.171 | 4.9273 |
| 0.3 | 1.145 | 5.86847 | 1.199 | 4.9280 |
| 0.4 | 1.081 | 5.86834 | 1.224 | 4.9284 |
| 0.5 | 1.020 | 5.86832 | 1.247 | 4.9285 |
| 0.6 | 0.961 | 5.86843 | 1.270 | 4.9282 |
| 0.7 | 0.905 | 5.86866 | 1.289 | 4.9275 |
| 0.8 | 0.851 | 5.86901 | 1.306 | 4.9264 |
| 0.9 | 0.799 | 5.86949 | 1.320 | 4.9249 |
| 1.0 | 0.750 | 5.87008 | 1.330 | 4.9231 |

$$m_n = xym_n(\text{GaAs}) + x(1-y)m_n(\text{GaP}) + y(1-x)m_n(\text{InAs}) + (1-x)(1-y)m_n(\text{InP}) \tag{76}$$

$$m_p = xym_p(\text{GaAs}) + x(1-y)m_p(\text{GaP}) + y(1-x)m_p(\text{InAs}) + (1-x)(1-y)m_p(\text{InP}). \tag{77}$$

The values of $m_n$ and $m_p$ that have been used for GaAs, GaP, InP, and InAs are listed in Table II.

Figure 1 shows the refractive index of $In_{1-x}Ga_xAs_yP_{1-y}$ as a function of photon energy and mole fraction $y$, assuming that $x = 0.466y$. The numerical values of Table I have been used. The refractive index increases as $y$

**TABLE II**

**Values of $m_n/m$ and $m_p/m$**

| Material | $m_n/m$ | $m_p/m$ |
|---|---|---|
| GaAs | 0.07 | 0.5 |
| GaP | 0.13 | 0.8 |
| InP | 0.07 | 0.4 |
| InAs | 0.028 | 0.33 |

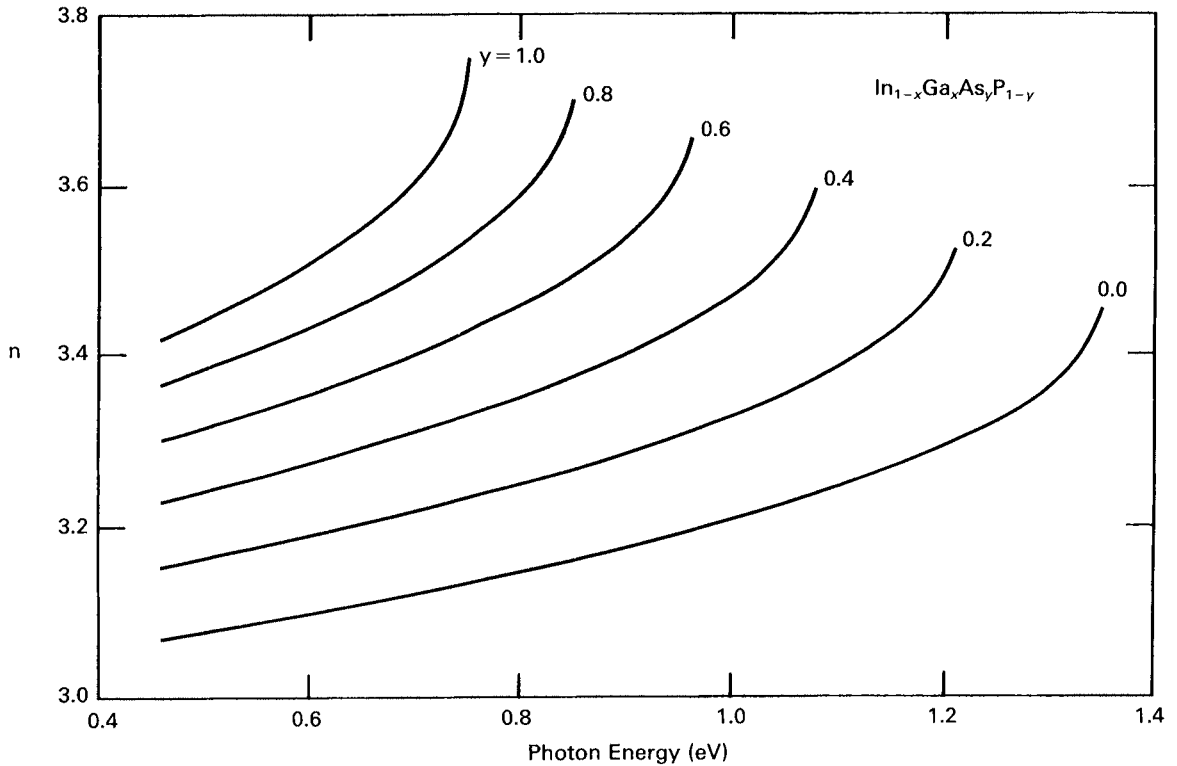


**Fig. 1.** Theoretical values of the refractive index $n$ for the quaternary compound $In_{1-x}Ga_xAs_yP_{1-y}$ as a function of photon energy (eV) and $y$ increments of 0.2. We assume the sample to be intrinsic with no carrier concentration. The requirement of lattice matching to InP implies $x = 0.466y$.

increases, due mainly to the dependence of $G$ on $y$ in Eq. 75. This behavior has been verified experimentally. Figure 2 compares theory and experiment [17].

Case 2: $Al_xGa_{1-x}As$ [18]

In the ternary III-V compound $Al_xGa_{1-x}As$, the AlAs concentration can be changed continuously, thus changing the refractive index without substantially altering the lattice constant. $Al_xGa_{1-x}As$ has a refractive index less than that of GaAs for $x$ greater than zero at all wavelengths [19]. Hence, it is possible to design waveguides on $Al_xGa_{1-x}As$ substrates by varying the parameter $x$.

Using the limit of $n^2$ in Eq. 67 or Eq. 68, one requires values of $G$, $m_n$, and $m_{p_l} = m_p$ as functions of $x$. Various expressions given in the literature are as follows.

$$\begin{aligned} G(\text{eV}) &= 1.424 + 1.247x \text{ [20]} \\ &\quad 1.435 + 1.209x + 0.386x^2 \text{ [21]} \\ &\quad 1.424 + 1.59x + x(1-x)(0.127 - 1.310x) \text{ [22]} \end{aligned} \tag{78}$$

$$\begin{aligned} m_p/m &= 0.48 + 0.81x \text{ [20]} \\ &\quad 0.45 + 0.302x \text{ [23]} \end{aligned} \tag{79}$$

$$\begin{aligned} m_n/m &= 0.067 + 0.083x \text{ [20]} \\ &\quad 0.0775 + 0.0830x \text{ [23]}. \end{aligned} \tag{80}$$

Values of $G$, $m_n/m$, and $m_p/m$ calculated from Eqs. 78–80 are used to calculate $C_0$, $y_B$, and the index of refraction of a pure material $n(0, 0)$ at $\hbar\omega = G$ in Table III, where

$$n(z, y_F)\Big|_{\substack{z=0 \\ y_F=0}} = n(0, 0) = [1 + 2C_o y_B]^{1/2}. \tag{81}$$

Since $y_B$, which depends on the lattice constant, and $C_o$ remain approximately constant as $x$ is varied, $n(0, 0)$ is also slowly varying. Theoretical and experimental values of $n$ versus $\hbar\omega$ are given in Fig. 3 for various values of $x$.

Case 3: $Hg_{1-x}Cd_xTe$ [24]

The ternary II-VI compound $Hg_{1-x}Cd_xTe$ is of importance as a detector

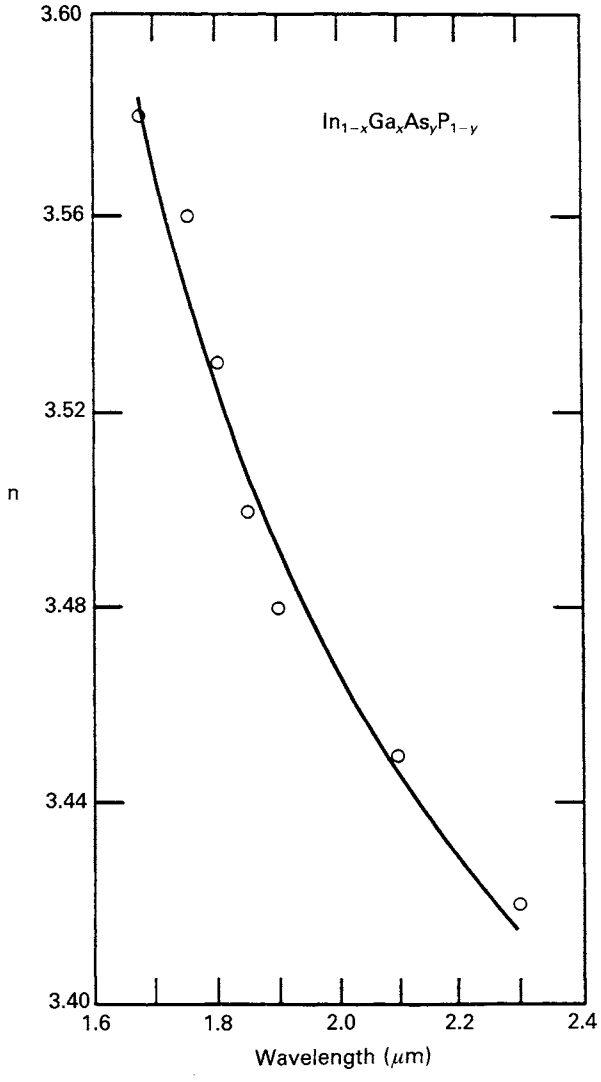


**Fig. 2.** Theoretical (solid lines) and experimental (open circles) values of the refractive index of $In_{1-x}Ga_xAs_yP_{1-y}$ versus wavelength ($\mu$m). The experimental results of Ref. [17] for the case of $y = 1.0$ and $x = 0.415$ have been used. The fit of data to the theoretical refractive index $n$ gives the carrier concentration as $n_e = (1.26 \pm 0.60) \times 10^{17}$ ($cm^{-3}$).

**TABLE III**

**Values of $G$ (eV) Calculated for Direct Gap $Al_xGa_{1-x}As$ from Expressions Given in Refs. [19–22] and Calculated Results for $C_o$ and $y_B$.**

| | $G$ (eV) | $C_o$ | $y_B$ | $n(0,0)$ |
|---|---|---|---|---|
| $x=0.07$ | 1.467 [19][a] | 1.13 | 5.48 | 3.66 |
| | 1.511 [20] | 1.11 | | 3.63 |
| | 1.522 [21] | 1.11 | | 3.62 |
| | 1.538 [22] | 1.10 | | 3.61 |
| $x=0.10$ | 1.533 | 1.12 | 5.54 | 3.66 |
| | 1.549 | 1.12 | | 3.66 |
| | 1.560 | 1.12 | | 3.66 |
| | 1.583 | 1.11 | | 3.64 |
| $x=0.15$ | 1.592 | 1.13 | 5.47 | 3.66 |
| | 1.611 | 1.12 | | 3.64 |
| | 1.625 | 1.12 | | 3.63 |
| | 1.654 | 1.11 | | 3.62 |
| $x=0.20$ | 1.650 | 1.13 | 5.44 | 3.65 |
| | 1.673 | 1.12 | | 3.65 |
| | 1.692 | 1.11 | | 3.62 |
| | 1.721 | 1.10 | | 3.61 |
| $x=0.24$ | 1.700 | 1.13 | 5.40 | 3.63 |
| | 1.723 | 1.12 | | 3.62 |
| | 1.747 | 1.11 | | 3.61 |
| | 1.772 | 1.10 | | 3.60 |
| $x=0.29$ | 1.788 | 1.13 | 5.41 | 3.64 |
| | 1.785 | 1.13 | | 3.64 |
| | 1.818 | 1.12 | | 3.62 |
| | 1.834 | 1.12 | | 3.61 |

[a] Estimated from Fig. 1 of Ref. [19].

The index of refraction for a pure material is given by $n(0,0)=(1+2C_oy_B)^{1/2}=(\varepsilon_\infty)^{1/2}$, and $\varepsilon_\infty$ is identified as the lattice dielectric constant in the Drude theory. Since $y_B$, which depends on the lattice constant, and $C_o$ remain approximately constant as $x$ is varied, $n$ (0,0) is also slowly varying.

in infrared technology, since its band gap can be continuously varied from 0–1.5 eV by variation of the mole fraction $x$ of cadmium. The calculation of the refractive index for II–VI compounds is discussed in Ref. [24]. One calculates the value for $y_B$ as specified for II-VI compounds in Eqs. 63–65. Values of the lattice constants $a$(Å) and $y_B$ as a function of $x$ are given in Table IV for $Hg_{1-x}Cd_xTe$. The calculation also requires an accurate expression relating the band-gap energy $G$, and the effective electron and heavy-hole masses $m_n$ and $m_p$ to the mole fraction $x$ of cadmium. The

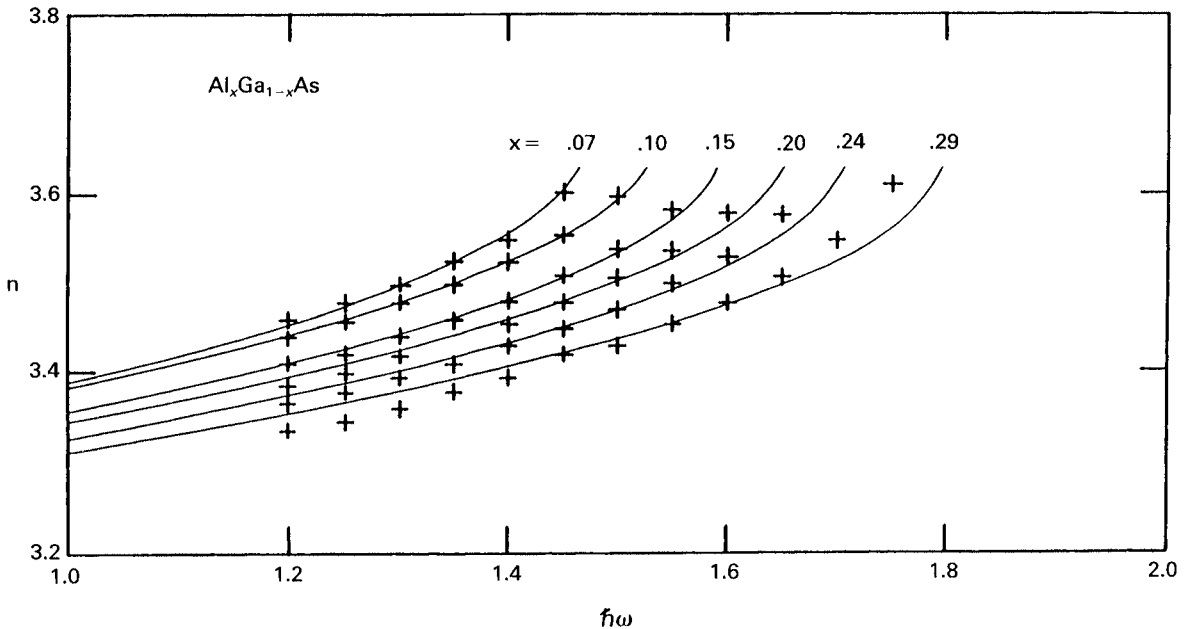


**Fig. 3.** Theoretical (————) and experimental (+ + + + + + +) values of the refractive index of $Al_xGa_{1-x}As$ versus photon energy. The band-gap energy of Ref. [21] given in Eq. 78 has been used, and a carrier concentration of $n_e = 10^{16}$ cm$^{-3}$ has been assumed. Experimental results of Ref. [19] have been used. Agreement is best at smaller $x$. There is an experimental uncertainty in $x$ of $\pm 0.02$, and the best fit at higher $x$ is obtained by choosing the smallest value for $x$ consistent with the uncertainty involved. For example, one obtains a better fit of the curve marked $x = 0.29$ to the experimental data by taking $x = 0.27$ instead, which is still within the limits of the uncertainty involved in $x$. Other difficulties in the comparison of theoretical and experimental results are that no exact information on the carrier concentration of the experimental samples is given, and it has been reported that at a constant doping level, the carrier concentration varies as $x$ is varied [36]. Also, the refractive index is a sensitive function of the dependence of $G$ on $x$, and a precise determination of this dependence needs to be made, so that one may better choose from the various expressions given in the literature.

values of $G$, $m_n$, $m_p$, and $C_o$ given in Table IV can be calculated as a function of $x$ using the following expressions [25, 26].

$$G\,(\text{eV}) = 6.006 \times 10^{-4} T(1 - 1.89x) + 1.948x - 0.337 \text{ [25]} \qquad (82)$$

$$G(x, T) = G(x, 0) + dG/dT|_x T$$

$$G(x, 0) = 1.948x - 0.337$$

$$dG/dT| = 6.006 \times 10^{-4}(1 - 1.89x)$$

**TABLE IV**

**Values of Lattice Constants a (Å) and $y_B$ as a Function of $x$ for $Hg_{1-x}Cd_xTe$**

| $x$ | $a$ (Å) | $y_B$ |
|---|---|---|
| 0.35 | 6.464 | 3.7765 |
| 0.50 | 6.469 | 3.7748 |
| 0.65 | 6.473 | 3.7734 |
| 0.75 | 6.475 | 3.7727 |
| 0.85 | 6.477 | 3.7720 |

**Values of $y_F$ and $C_o$ Using the Band Gap of Ref. [25] with $n_e = 1.0 \times 10^{17}$ cm$^{-3}$.**

| $x$ | $G$ (eV) | $y_F$ | $C_o$ |
|---|---|---|---|
| 0.35 | 0.3581 | 0.391 | 1.942 |
| 0.50 | 0.5645 | 0.283 | 1.634 |
| 0.65 | 0.7906 | 0.209 | 1.439 |
| 0.75 | 0.9606 | 0.191 | 1.336 |
| 0.85 | 1.1518 | 0.167 | 1.245 |

**Values of $y_F$ and $C_o$ Using the Band Gap Calculated from Eq. 82 with $n_e = 1.0 \times 10^{17}$ cm$^{-3}$.**

| $x$ | $G$ (eV) | $y_F$ | $C_o$ |
|---|---|---|---|
| 0.35 | 0.4057 | 0.368 | 1.825 |
| 0.50 | 0.6469 | 0.264 | 1.526 |
| 0.65 | 0.8880 | 0.208 | 1.358 |
| 0.75 | 1.0487 | 0.183 | 1.279 |
| 0.85 | 1.2095 | 0.163 | 1.215 |

$$m_n/m = 0.11x + 0.029(1-x) \tag{83}$$

$$m_p/m = 0.35x + 0.3(1-x). \tag{84}$$

In Eq. 82, $T$ is the temperature in degrees Kelvin. We assume the sample to be $n$-type with a carrier concentration of $n_e = 1.0 \times 10^{17}\,\mathrm{cm}^{-3}$. The quantities $C_0$ and $y_F$ calculated using these expressions are given in Table IV.

Figure 4 shows the refractive index of $Hg_{1-x}Cd_xTe$ as a function of photon energy and different mole fractions $x$. The numerical values of Table IV and Eq. 82 have been used. The reduction of refractive index as one increases $x$ is noticeable and is similar to that observed in the

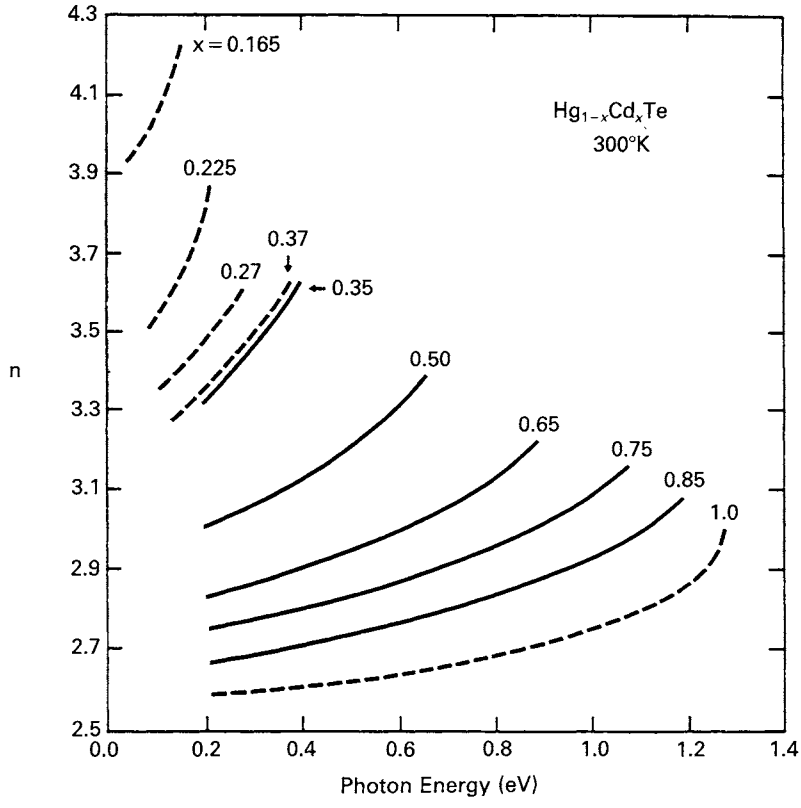


**Fig. 4.** Theoretical refractive index $n$ (solid lines) along with the experimental refractive index (dashed lines) for the compound $Hg_{1-x}Cd_xTe$ as a function of photon energy (eV) and mole fraction $x$. The sample is assumed to be $n$-type with a carrier concentration of $n_e = 1.0 \times 10^{17}\,\mathrm{cm}^{-3}$ in the theoretical calculation. Results are taken from Ref. [24].

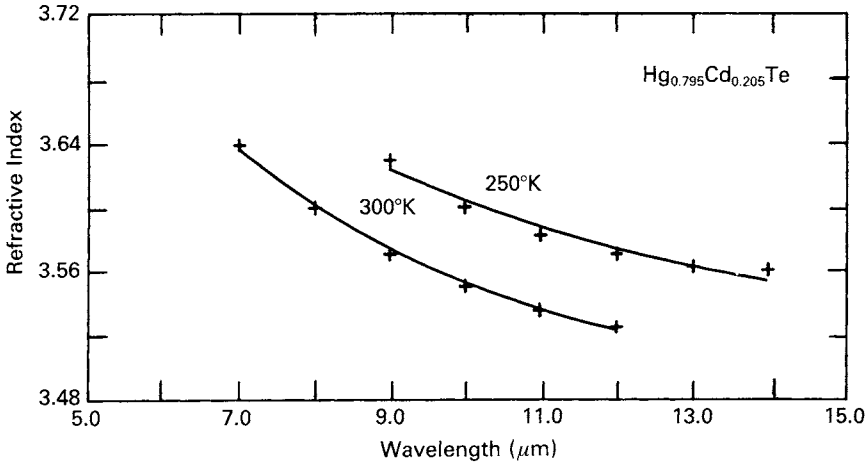


**Fig. 5.** Theoretical refractive index $n$ (solid lines) and experimental refractive index [37] (crosses) as functions of temperature for $Hg_{0.795}Cd_{0.205}Te$. Numerical results are given and discussed in Ref. [24].

compound $Al_xGa_{1-x}As$, as one increases the Al mole fraction at frequencies just below the fundamental absorption edge [18, 19]. Numerical results for theoretical and experimental values of $n$ are given in Ref. [24]. Theoretical and experimental values of $n$ are given in Fig. 5 for a specific material $Hg_{0.795}Cd_{0.205}Te$ at two temperatures.

## SUMMARY IV

The calculation of the real part of the complex refractive index from the quantum-density-matrix formulation of the complex dielectric constant has been outlined and the result given for the refractive index in terms of measurable material parameters only. These material parameters are the band-gap energy $G$, the effective electron mass $m_n$, the effective hole masses of the three valence bands $m_{p_i}$, $i=1, 2, 3$, the lattice constant $a$ (Å), and the spin-orbit-splitting energy $\Delta$. Under certain simplifying assumptions enumerated in the text, the number of material parameters can be reduced to $G$, $m_n$, $m_{p_1}=m_p$, $a$ (Å), and $\Delta$. The refractive index is also a function of frequency and of carrier concentration. The major contribution to the refractive index at $\hbar\omega=G$ arises from valence band electrons

making virtual transitions with intermediate states lying in the conduction band. When free carriers (electrons) are added, their role is considered as blocking possible intermediate states through the exclusion principle, and they would also block possible final states for direct transitions and hence shift the absorption edge (that is, the Burstein–Moss effect). The process of an electron *in* the conduction band absorbing and re-emitting a photon and the corresponding contribution to $\varepsilon_1$ is neglected for $\hbar\omega = G$, because it is a small contribution at these frequencies. The value of $n^2$ at $\hbar\omega = G$ for a pure material with no free carriers, denoted by $n^2(0, 0)$, is identified as the high-frequency lattice dielectric constant $\varepsilon_\infty$ appearing in the Drude theory.

The result obtained for $n$ has been applied to the III-V quaternary $In_{1-x}Ga_xAs_yP_{1-y}$ lattice matched to InP ($x = 0.466y$), the III-V ternary $Al_xGa_{1-x}As$, and the II-VI ternary compound $Hg_{1-x}Cd_xTe$. The necessary parameters for the calculation of the refractive index as a function of frequency, carrier concentration, and mole fraction $x$ are given. Results are given for $n$ in the literature for the II-VI compounds CdSe, CdS, and $CdSe_xS_{1-x}$ [27], ZnTe [28, 10], ZnSe [29, 10], CdTe [10], and $Cd_xZn_{1-x}Te$ [30]. Results are also given for the III-V compounds InP [28, 10], GaAs [10], and InSb [10]. The refractive index is calculated for the IV-VI binary compounds PbS, PbSe, and PbTe in Ref. [31], and for the IV-VI ternary compound $Pb_{1-x}Sn_xTe$ in Ref. [32]. The accuracy of the theoretical result calculated for $n$ is limited by the accuracy with which $G$, $m_n$, $m_p$, $a$ (Å), and $\Delta$ are known as functions of mole concentration $x$, by experimental uncertainty in the value of $x$ itself, and by the fact that carrier concentration is often unknown or unspecified. It is hoped that future experimental work will improve matters in this respect. An analytical model for $n$ for various materials in terms of experimental parameters is a useful result to have as an aid in the design of electro-optic devices and components, and in the fabrication of materials with desirable optical properties. In addition, one gains insight into the physical mechanism of how the variation of the carrier concentration affects the variation in the refractive index, which is a topic of considerable interest [33]. An extension of the above theory to two-dimensional, quantum-well structures, and a study of carrier concentration as a function of applied voltage and the resultant effect on the refractive index [34, 35] would be interesting areas for future investigation, as would be a study of $n$ at photon energies greater than $G$.

## REFERENCES

1. P. J. Price, *IBM J. Res. Dev.* **10**, 395 (1966).
2. W. Kohn and J. M. Luttinger, *Phys. Rev.* **108**, 590 (1957); W. Kohn and J. M. Luttinger, *Phys. Rev.* **109**, 1892 (1958).
3. P. N. Argyres, *J. Phys. Chem. Solids* **19**, 66 (1961).
4. B. Jensen, *Ann. Phys.* **95**, 229 (1975).

5. B. Jensen, in "Handbook of Optical Constants of Solids," (E. D. Palik, ed.), Vol. 1, Academic Press, Orlando, (1985).
6. B. Jensen, in "Infrared and Submillimeter Waves," (K. J. Button, ed.), Vol. 8, Academic Press, New York (1983).
7. B. Jensen, *Phys. Status Solidi* **86**, 291 (1978); *Solid State Commun.* **24**, 853 (1977); *J. Appl. Phys.* **50**, 5800 (1979).
8. B. Jensen, *Ann. Phys.* **80**, 284 (1973).
9. S. Adachi, *J. Appl. Phys.* **53**, 5863 (1982); *J. Appl. Phys.* **58**, R1 (1985).
10. B. Jensen, *IEEE J. Quant. Electron.* **QE-18**, 1361 (1982); B. Jensen, A. Torabi, *IEEE J. Quant. Electron.* **QE-19**, 448 (1983).
11. E. O. Kane, *J. Phys. Chem. Solids* **1**, 249 (1957).
12. H. Ehrenreich, *J. Phys. Chem. Solids* **2**, 131 (1957).
13. M. Asada, A. Kameyama, and Y. Suematsu, *IEEE J. Quant. Electron.* **QE-20**, 745 (1984).
14. B. Jensen and A. Torabi, *J. Opt. Soc. Am. B*, **2**, 1395 (1985).
15. B. Jensen and A. Torabi, *J. Appl. Phys.* **54**, 3623 (1983).
16. R. E. Nahory, N. A. Pollack, W. D. Johnson, Jr., and R. L. Barns, *Appl. Phys. Lett.* **33**, 659 (1978).
17. P. Chandra, L. A. Colden, and K. E. Strege, *Electron. Lett.* **17**, 6 (1981).
18. B. Jensen and A. Torabi, *IEEE J. Quant. Electron.* **QE-19**, 877 (1983).
19. H. C. Casey, D. D. Sell and M. B. Panish, *Appl. Phys. Lett.* **24**, 63 (1974).
20. H. C. Casey, *J. Appl. Phys.* **49**, 3684 (1978).
21. J. C. Dyment, Y. C. Cheng, and A. J. Springthorpe, *J. Appl. Phys.* **46**, 1739 (1975).
22. D. E. Aspnes, S. M. Kelso, R. A. Logan and R. Bhat, *J. Appl. Phys.* **60**, 754 (1986).
23. M. D. Camras, *Appl. Phys. Lett.* **41**, 317 (1982).
24. B. Jensen and A. Torabi, *J. Appl. Phys.* **54**, 5945 (1983).
25. G. L. Hansen, J. L. Schmit, and T. N. Casselman, *J. Appl. Phys.* **53**, 7099 (1982).
26. J. Calas, J. Allgre, and C. Fau, *Phys. Status Solidi B* **107**, 275 (1981).
27. B. Jensen and A. Torabi, *J. Opt. Soc. Am. B* **6**, 857 (1986).
28. B. Jensen and A. Torabi, *J. Appl. Phys.* **54**, 2030 (1983).
29. B. Jensen and A. Torabi, *Infrared Physics* **23**, 359 (1983).
30. B. Jensen and A. Torabi, *IEEE J. Quant. Electron.* **QE-19**, 1362 (1983).
31. B. Jensen and A. Torabi, *IEEE J. Quant. Electron.* **QE-20**, 618 (1984).
32. B. Jensen and A. Torabi, *Appl. Phys. Lett.* **45**, 266 (1984).
33. H. Yamamoto, M. Asada and Y. Suematsu, *J. Lightwave Technol.* **6**, 1831 (1988).
34. Y. Arakawa and A. Yariv, *IEEE J. Quant. Electron* **QE-21**, 1666 (1985).
35. P. J. Price, *Phys. Rev. B* **38**, 1994 (1988).
36. T. Ishibashi, S. Tarucha, and H. Okamoto, *Japan J. Appl. Phys.* **21**, 1476 (1982).
37. E. Finkman and Y. Nemirovsky, *J. Appl. Phys.* **50**, 4356 (1979).

# Chapter 7

# Calculation of Optical Constants, *n* and *k*, in the Interband Region

A. R. FOROUHI
Actel Corporation
Sunnyvale, California

and

I. BLOOMER
Physics Department
San José State University
San José, California

I. Introduction 151
II. The Extinction Coefficient, $k(E)$, and the Refractive Index, $n(E)$ 154
A. Derivation of $k(E)$ 154
B. Derivation of $n(E)$ 160
III. Discussion 163
A. The Parameters Involved in the Equations for $k(E)$ and $n(E)$ 163
B. k($E$) and n($E$) in the Limit $E$ Approaches Infinity 164
IV. Examples 166
A. Amorphous Semiconductors and Dielectrics 166
B. Crystalline Semiconductors and Dielectrics 169
C. Metals 171
V. Summary 174
References 175

## I INTRODUCTION

In this chapter we present a unified formulation of optical properties of materials. This formulation is applicable to amorphous semiconductor and dielectrics, crystalline semiconductors and dielectrics, and metals, throughout the fundamental optical energy range, that is, the interband region.

We use the complex index of refraction, $N = n - ik$, to describe optical properties. The real and imaginary parts of $N$ are termed refractive index


Copyright © 1991 by Academic Press.
All rights of reproduction in any form reserved.
ISBN 0-12-544422-2

and extinction coefficient, respectively. $n$ and $k$ are referred to as the optical constants of the medium. Optical constants depend on photon energy, $E = \hbar\omega$, and exhibit structure in the interband region where bound-electron transitions are dominant.

Optical constants are related to each other through the Kramers–Kronig dispersion relation. The Kramers–Kronig relation provides a simple integral formula, giving $n(E)$ as the Hilbert transform of $k(E)$. This relation is a consequence of the principle of causality, which states that no signal travels faster than the speed of light in vacuum. Therefore, any complete derivation of optical constants should be consistent with the Kramers–Kronig relation.

There are numerous other formulations of optical properties in the fundamental optical regime [1–10]. They fall into one of four categories: (1) empirical formulas; (2) harmonic-oscillator models; (3) quantum-mechanical treatments; (4) point-by-point analyses of the Brillouin zone.

Optical constants determined from empirical formulas (such as the Sellmeier dispersion equations for the refractive index and Urbach's rule for the absorption coefficient [1–4]) are not related through the Kramers–Kronig dispersion relation and are valid only over a very limited energy range.

The harmonic-oscillator model [1, 2, 10] does not incorporate the concept of an optical energy band gap, $E_g$. Thus, the optical energy band gap of semiconductors and dielectrics cannot be directly determined from this approach. Furthermore, many fitting parameters are needed to describe $n(E)$ and $k(E)$ in the fundamental energy range [10].

Quantum-mechanical treatments [1–9] involve either a quantized electromagnetic (photon) interaction where an infinite lifetime for the excited electron state is assumed, or a semiclassical (nonquantized) electromagnetic interaction where lifetime broadening assumptions are sometimes incorporated [9]. These approaches provide optical constants that are effective over only a small energy range.

Point-by-point analyses of the Brillouin zone [5, 6] do not provide equations for optical constants in closed algebraic form. Using these analyses, peaks in the optical spectra cannot be explained except by assuming the occurrence of simultaneous transitions from two singularities, that is, from two critical points, which accidentally have the same energy. Agreement with experimental results is often poor.

The formulation in this chapter is based on the quantum-mechanical theory of absorption, from which we deduce a general expression for the extinction coefficient, $k$. A finite lifetime is incorporated for the excited state to which the electron transfers, due to photon absorption. The optical energy band gap, $E_g$, is identified to be that energy for which $k(E)$ has its absolute minimum.

From the deduced equation for $k(E)$, we then derive an expression for

the refractive index, $n(E)$, via the Kramers–Kronig dispersion relation.

For particular photon energies, peaks occur in the optical spectra. We attribute these peaks to transitions of electrons from one distinguishable state to another. We define distinguishable states as either the bonding, $|\sigma\rangle$, and antibonding, $|\sigma^*\rangle$, states in the valence and conduction bands of amorphous materials [11] or critical-point, $|\mathbf{k}_{\text{crit}}\rangle$, states in the valence and conduction bands of crystalline semiconductors, dielectrics, and metals. The symbol $\mathbf{k}$ represents electron wave vector.

In the simplest case of amorphous semiconductors and dielectrics, a single peak is exhibited in the optical spectra, implying only one possible type of distinguishable transition, from $|\sigma\rangle$ to $|\sigma^*\rangle$.

For crystalline semiconductors and dielectrics, several peaks are apparent, thus indicating several possible types of distinguishable transitions, from $|\mathbf{k}^{\text{v}}_{\text{crit}}\rangle_i$ to $|\mathbf{k}^{\text{c}}_{\text{crit}}\rangle_i$. The subscript $i$ denotes the $i$th type of critical-point state and ranges over the number of observable peaks, that is, the number of types of critical-point transitions responsible for the peaks in the energy range under consideration. The superscripts v and c denote valence and conduction band, respectively.

For metals, unlike semiconductors and dielectrics, the strongest photon absorption occurs outside the fundamental range in the far- and near-infrared regime. Optical constants of metals are structureless in this energy range. Interactions involving free electrons in the partially filled conduction band contribute for the most part to their optical properties at these low energies. However, beyond the infrared regime, metals do exhibit several peaks in their optical spectra. In the fundamental optical regime, similar structure in optical constants is apparent for metals, semiconductors, and dielectrics. Therefore, we expect that optical interactions involve the same physical processes for all three types of materials. In fact we have found, as will be discussed, that in the interband region, metals can be treated as a subcase of crystalline semiconductor and dielectric materials with $E_g$ equal to zero, that is, with zero optical energy band gap.

In Section II.A we derive closed algebraic equations for $k(E)$ applicable to amorphous semiconductors and dielectrics as well as to crystalline semiconductors, dielectrics, and metals. In Section II.B we use the Kramers–Kronig dispersion relation to obtain $n(E)$ as the Hilbert transform of $k(E)$. In Section III.A we show how to determine the parameters involved in the equations that we derive, by making use of the physical significance of these parameters. In Section III.B we discuss the high energy limit of $k(E)$ and $n(E)$. In Section IV, we apply the equations that we derive for $k(E)$ and $n(E)$ to different materials to show the excellent agreement obtained with experimental data throughout the entire interband region and to show that this agreement depends on far fewer parameters in comparison to other treatments. In Section V, a summary of this chapter is presented.

## II THE EXCTINCTION COEFFICIENT, $k(E)$, AND THE REFRACTIVE INDEX, $n(E)$

### A Derivation of $k(E)$

In the fundamental optical regime, interband transitions of bound electrons are mostly responsible for optical properties. Therefore, we need to consider the relationship between photon absorption and electron transitions. Time-dependent perturbation theory provides the relation between probability per unit time that a photon is removed from an incident beam and that an electron transfers to an excited state. If we take this transition probability rate and multiply it by photon energy, $\hbar\omega$, we obtain the rate at which photon energy is absorbed from the incident intensity in the frequency range from $\omega$ to $\omega + d\omega$, which we denote by the symbol $\Phi(\omega)$.

We define the absorption coefficient, $\alpha$, as proportional to $\Phi(\omega)$. The absorption coefficient is directly related to the extinction coefficient, $k$, that is, $\alpha = (2\omega/c)k$, where $c$ is the speed of light. In addition to $\Phi$, we define the absorption coefficient as depending on the total number of ways a photon, of energy $\hbar\omega$, can be removed from the incident intensity, per unit volume in a layer of infinitesimal thickness, which we denote by the symbol $\Theta$. Thus, our definition for $\alpha$ is

$$\alpha(\omega) = \Theta\Phi/I_0, \tag{1}$$

where $I_0$ represents the incident photon intensity.

Recently, we showed [12] that the rate of energy absorbed, $\Phi(\omega)$, in the frequency range $\omega$ to $\omega + \mathrm{d}\omega$, associated with an electron transition between two arbitrary states $|a\rangle$ to $|b\rangle$ (where $E_b > E_a$), when the excited state $|b\rangle$ has a finite lifetime, $\tau = 1/\gamma$, is given by

$$\Phi(\omega) = \frac{4\pi\hbar}{3c} e^2 \omega I_0 |\langle b|\mathbf{x}|a\rangle|^2 \left\{ \frac{\gamma}{(E_b - E_a - \hbar\omega)^2 + \dfrac{\hbar^2\gamma^2}{4}} \right\}, \tag{2}$$

where $e$ stands for electron charge, $\mathbf{x}$ is the electron position vector, and $\langle b\,|\mathbf{x}|\,a\rangle$ is the dipole matrix element between initial and final states. $I_0$, the incident photon intensity, is given by

$$I_0 = (\hbar\omega)\mathcal{N}\rho c, \tag{3}$$

where $\mathcal{N}$ is photon occupation number and $\rho$ is the number of allowed photon states in the frequency range from $\omega$ to $\omega + d\omega$. All physical quantities used in Eqs. 1, 2, and 3, including $I_0$ and $c$, are taken to be at the site of the absorbing electron.

Equation 2 is based on first-order time-dependent perturbation theory, so that the electron transitions are direct; that is, there are no intermediate states involved in the transition from $|a\rangle$ to $|b\rangle$.

The finite-lifetime assumption leads to a new way of accounting for peaks in the optical spectra. It gives a Lorentzian dependence on energy in the equation for $\Phi(\omega)$ (the term in curly brackets in Eq. 2). This Lorentzian energy dependence produces a maximum in $\Phi(\omega)$ when $\hbar\omega = E_b - E_a$. Thus, the maximum probability that a photon of energy $\hbar\omega$ is removed from the incident beam occurs when $\hbar\omega = E_b - E_a$. This condition for a maximum in $\Phi(\omega)$ is analogous to resonance excitations in atomic systems [13]. And, as in the case of atomic systems, photons can still be removed from the incident beam even when the "resonant" condition is not satisfied; that is, $\Phi(\omega)$ is nonzero, even when $\hbar\omega = E_b - E_a$.

We assume that direct transitions from distinguishable states lead to peaks in optical constants. Therefore, we take $|a\rangle$ and $|b\rangle$ to be $|\sigma\rangle$ and $|\sigma^*\rangle$, with associated energies $E_\sigma$ and $E_{\sigma^*}$, respectively, in the amorphous case; we take $|a\rangle$ and $|b\rangle$ to be $|\mathbf{k}^{\mathrm{v}}_{\mathrm{crit}}\rangle_i$ and $|\mathbf{k}^{\mathrm{c}}_{\mathrm{crit}}\rangle_i$, with associated energies $E_{\mathrm{v}}(\mathbf{k}_{\mathrm{crit}})_i$ and $E_{\mathrm{c}}(\mathbf{k}_{\mathrm{crit}})_i$ in the crystalline semiconductor, dielectric, and metal case [12, 14, 15]. Accordingly, when $\hbar\omega = E_{\sigma^*} - E_\sigma$, or $\hbar\omega = E_{\mathrm{c}}(\mathbf{k}_{\mathrm{crit}})_i - E_{\mathrm{v}}(\mathbf{k}_{\mathrm{crit}})_i$, a peak in $\Phi(\omega)$ (and therefore a peak in optical constants) is expected to occur.

There is only one peak in the optical constants of amorphous semiconductors and dielectrics, indicating only one possible type of distinguishable transition. For these materials, $\Phi(\omega)$ will consist of a single term. (Amorphous materials whose optical constants exhibit more than one peak, such as amorphous silicon dioxide [1], are not discussed in this work, although the present formulation can be applied to them.) Since more than one peak occurs in the optical constants of crystalline semiconductors, dielectrics, and metals suggesting more than one type of distinguishable transition for these materials, we take $\Phi(\omega)$ to be a sum over the number of types of distinguishable transitions.

Thus, for the amorphous case,

$$\Phi(\omega) = \frac{4\pi\hbar}{3c} e^2 \omega I_0 |\langle \sigma^* | \mathbf{x} | \sigma \rangle|^2 \left\{ \frac{\gamma}{(E_{\sigma^*} - E_\sigma - \hbar\omega)^2 + \dfrac{\hbar^2\gamma^2}{4}} \right\}, \tag{4}$$

and for crystalline semiconductors, dielectrics, and metals,

$$\Phi(\omega)=\frac{4\pi\hbar}{3c}e^2\omega I_0\sum_{i=1}^{q}|\langle\mathbf{k}_{\mathrm{crit}}^{\mathrm{c}}|\mathbf{x}|\mathbf{k}_{\mathrm{crit}}^{\mathrm{v}}\rangle|^2\left\{\frac{\gamma_i}{\{[E_c(\mathbf{k}_{\mathrm{crit}})-E_{\mathrm{v}}(\mathbf{k}_{\mathrm{crit}})]_i-\hbar\omega\}^2+\dfrac{\hbar^2\gamma_i^2}{4}}\right\}. \tag{5}$$

In Eq. 4 the term $|\langle\sigma^*|\mathbf{x}|\sigma\rangle|^2$ represents the dipole matrix element squared between bonding, $|\sigma\rangle$, and antibonding, $|\sigma\rangle$, states; the term $|\langle\mathbf{k}_{\mathrm{crit}}^{\mathrm{c}}|\mathbf{x}|\mathbf{k}_{\mathrm{crit}}^{\mathrm{v}}\rangle|_i^2$ represents the dipole matrix element squared between the $i$th critical-point state in the valence band and the $i$th critical-point state in the conduction band. In Eq. 5, the integer $q$ is equal to the number of observed peaks associated with the critical-point transitions.

With $\Phi$ given by either Eq. 4 or 5, part of our task in determining the extinction coefficient, $k$, is accomplished. That is, since

$$k=\frac{c}{2\omega}\alpha=\frac{c}{2\omega}\frac{1}{I_0}\Phi\Theta, \tag{6}$$

we have, so far,

$$k_\alpha(\omega)=\Theta_\alpha\frac{2\pi\hbar}{3}e^2|\langle\sigma^*|\mathbf{x}|\sigma\rangle|^2\left\{\frac{\gamma}{(E_{\sigma^*}-E_\sigma-\hbar\omega)^2+\dfrac{\hbar^2\gamma^2}{4}}\right\}, \tag{7}$$

or

$$k_\chi(\omega)=\Theta_\chi\frac{2\pi\hbar}{3}e^2\sum_{i=1}^{q}|\langle\mathbf{k}_{\mathrm{crit}}^{\mathrm{c}}|\mathbf{x}|\mathbf{k}_{\mathrm{crit}}^{\mathrm{v}}\rangle|_i^2\left\{\frac{\gamma_i}{\{[E_{\mathrm{c}}(\mathbf{k}_{\mathrm{crit}})-E_{\mathrm{v}}(\mathbf{k}_{\mathrm{crit}})]_i-\hbar\omega\}^2+\dfrac{\hbar^2\gamma_i^2}{4}}\right\}, \tag{8}$$

or

$$k_\mu(\omega)=\Theta_\mu\frac{2\pi\hbar}{3}e^2\sum_{i=1}^{q}|\langle\mathbf{k}_{\mathrm{crit}}^{\mathrm{c}}|\mathbf{x}|\mathbf{k}_{\mathrm{crit}}^{\mathrm{v}}\rangle|_i^2\left\{\frac{\gamma_i}{\{[E_{\mathrm{c}}(\mathbf{k}_{\mathrm{crit}})-E_{\mathrm{v}}(\mathbf{k}_{\mathrm{crit}})]_i-\hbar\omega\}^2+\dfrac{\hbar^2\gamma_i^2}{4}}\right\}. \tag{9}$$

The subscripts $\alpha$, $\chi$, and $\mu$ in Eqs. 7, 8, and 9 stand for amorphous

semiconductors and dielectrics, crystalline semiconductors and dielectrics, and metals, respectively.

Our next task is to determine $\Theta$. This parameter represents the total number of ways a photon of energy $\hbar\omega$ can be removed from the incident intensity, per unit volume in an infinitesimal layer of thickness. Thus, $\Theta$ is proportional to the number of possible transitions for a given photon energy, $\hbar\omega$.

In addition to counting the number of direct transitions, we will also include the number of indirect (second-order) transitions when determining $\Theta$. Although we neglected the probability for second-order processes in our determination of $\Phi(\omega)$, we do not neglect the number of possible second-order transitions for a given $\hbar\omega$. This is because we are interested in the product of $\Phi\Theta$, which may be approximated as $\Phi\Theta \approx [\Phi_{\text{first order}} + \Phi_{\text{second order}}] \times [\Theta_{\text{first order}} + \Theta_{\text{second order}}]$. However, we assume that the probability for photon absorption via second-order processes is much smaller than the probability for photon absorption via first-order processes; that is, $\Phi_{\text{second order}} \ll \Phi_{\text{first order}}$. On the other hand, the number of possible second-order transitions for a given $\hbar\omega$ is not assumed negligible, compared with the number of first-order transitions.

Thus, $\Theta$ depends on the product of the number of occupied electron states in the valence band in the energy range $dE_v$, that is, $\eta_v(E_v)f_v(E_v)dE_v$, times the number of unoccupied electron states per energy in the conduction band, that is, $\eta_c(E_c) \times (1 - f_c(E_c))$, which are separated by an energy, $\hbar\omega$, from states in the valence band [3]. The expression $\eta_v(E_v)$ represents the density of states in the valence band, $E_v(\mathbf{k})$, and $\eta_c(E_c)$ represents the density of states in the conduction band, $E_c(\mathbf{k})$. The expression $f(E)$ represents the Fermi function. Therefore,

$$\Theta \propto \int \eta_v(E_v) f_v(E_v) \eta_c(E_v + \hbar\omega)[1 - f_c(E_v + \hbar\omega)]\, dE_v. \tag{10}$$

We assume that $f_v(E_v)$ is of order unity and $f_c(E_v + \hbar\omega)$ is of order zero. This assumption is valid for temperatures that are not too high. Then

$$\Theta \propto \int \eta_v(E_v) \eta_c(E_v + \hbar\omega)\, dE_v. \tag{11}$$

In the case of amorphous and crystalline semiconductors and dielectrics, the limits of integration range from $(E_c^{\text{bottom}} - \hbar\omega)$ to $E_v^{\text{top}}$, where $E_c^{\text{bottom}}$ and $E_v^{\text{top}}$ represent the bottommost and topmost energies of the conduction and valence bands, respectively. Then the minimum energy above which a

transition can occur, is equal to $(E_c^{\text{bottom}} - E_v^{\text{top}})$. We take the optical energy band gap, $E_g$, equal to this minimum energy, that is,

$$E_g = E_c^{\text{bottom}} - E_v^{\text{top}}. \tag{12}$$

Since $\Theta$ represents the total number of direct or indirect ways a photon can be removed, $E_g$ gives the minimum energy required for the onset of absorption.

In the case of metals, $E_c^{\text{bottom}} = E_v^{\text{top}}$, since metals are distinguished from semiconductors and dielectrics by the absence of a band gap in their electronic band structure. Therefore, we take $E_g$ equal to zero and assume that the free-electron contributions are negligible in the interband region.

In order to evaluate the integral for $\Theta$ given by Eq. 11, we need to know $\eta_v(E_v)$ and $\eta_c(E_c)$. Exact algebraic expressions for $\eta_v(E_v)$ and $\eta_c(E_c)$, however, are unknown. We will assume a parabolic approximation in all cases for these functions such that $E_v(\mathbf{k})$ and $E_c(\mathbf{k})$ are a maximum and a minimum, respectively, when $E = E_v^{\text{top}}$ and $E = E_c^{\text{bottom}}$. Accordingly, $\eta_v(E_v)$ and $\eta_c(E_c)$ are determined to be [5]

$$\eta_v(E) = \text{const}(E_v^{\text{top}} - E)^{1/2} \tag{13}$$

and

$$\eta_c(E) = \text{const}(E - E_c^{\text{bottom}})^{1/2}. \tag{14}$$

Equation 11 can then be evaluated as

$$\Theta_\alpha = \Theta_\chi = \text{const}(\hbar\omega - E_g)^2 \tag{15}$$

for amorphous and crystalline semiconductors and dielectrics. We see from Eq. 15 that $\Theta$ is a minimum, and hence $k$ is a minimum when $E = E_g$.

For metals, with $E_v^{\text{top}} = E_c^{\text{bottom}}$,

$$\Theta_\mu = \text{const}(\hbar\omega)^2. \tag{16}$$

Surprisingly, the parabolic approximation produces excellent agreement with experimental results for all cases [12, 14, 15] (see Section IV).

For the amorphous case, we insert Eq. 15 into Eq. 7:

$$k_\alpha(\omega) = \text{const}|\langle\sigma^*|\mathbf{x}|\sigma\rangle|^2 \times \left\{\frac{\gamma}{(E_{\sigma^*} - E_\sigma - \hbar\omega)^2 + \frac{\hbar^2\gamma^2}{4}}\right\}(\hbar\omega - E_g)^2. \quad (17)$$

For crystalline semiconductors and dielectrics, we insert Eq. 15 into Eq. 8:

$$k_\chi(\omega) = \text{const} \sum_{i=1}^{q} |\langle \mathbf{k}^c_{crit}|\mathbf{x}|\mathbf{k}^v_{crit}\rangle|_i^2 \times \left\{\frac{\gamma_i}{\{[E_c(\mathbf{k}_{crit}) - E_v(\mathbf{k}_{crit})]_i - \hbar\omega\}^2 + \frac{\hbar^2\gamma_i^2}{4}}\right\}(\hbar\omega - E_g)^2. \quad (18)$$

For metals, we insert Eq. 16 into Eq. 9:

$$k_\mu(\omega) = \text{const} \sum_{i=1}^{q} |\langle \mathbf{k}^c_{crit}|\mathbf{x}|\mathbf{k}^v_{crit}\rangle|_i^2 \left\{\frac{\gamma_i}{\{[E_c(\mathbf{k}_{crit}) - E_v(\mathbf{k}_{crit})]_i - \hbar\omega\}^2 + \frac{\hbar^2\gamma_i^2}{4}}\right\}(\hbar\omega)^2. \quad (19)$$

The extinction coefficient in each case can be written more compactly in the following way:

$$k_\alpha(E) = \frac{A(E - E_g)^2}{E^2 - BE + C}, \quad (20)$$

$$k_\chi(E) = \left[\sum_{i=1}^{q} \frac{A_i}{E^2 - B_iE + C_i}\right](E - E_g)^2, \quad (21)$$

$$k_\mu(E) = \left[\sum_{i=1}^{q} \frac{A_i}{E^2 - B_iE + C_i}\right](E)^2. \quad (22)$$

In the amorphous case, the parameters are given by

$$A = \text{const}|\langle\sigma^*|\mathbf{x}|\sigma\rangle|^2 \times \gamma, \quad (23)$$

$$B = 2(E_{\sigma^*} - E_\sigma), \tag{24}$$

$$C = (E_{\sigma^*} - E_\sigma)^2 + \frac{\hbar^2\gamma^2}{4}. \tag{25}$$

For crystalline semiconductors, dielectrics, and metals, the parameters are given by

$$A_i = \text{const}|\langle \mathbf{k}^{\text{c}}_{\text{crit}}|\mathbf{x}|\mathbf{k}^{\text{v}}_{\text{crit}}\rangle|_i^2 \times \gamma_i, \tag{26}$$

$$B_i = 2[E_{\text{c}}(\mathbf{k}_{\text{crit}}) - E_{\text{v}}(\mathbf{k}_{\text{crit}})]_i, \tag{27}$$

$$C_i = [E_{\text{c}}(\mathbf{k}_{\text{crit}}) - E_{\text{v}}(\mathbf{k}_{\text{crit}})]_i^2 + \frac{\hbar^2\gamma_i^2}{4}. \tag{28}$$

## B Derivation of $n(E)$

The refractive index, $n(E)$, and the extinction coefficient, $k(E)$, are related by the Kramers–Kronig dispersion relations. These relations are a consequence of the analytic behavior of the complex index of refraction, $N(E) = n(E) - ik(E)$. In turn, the analytic behavior of $N(E)$ stems from the principle of causality, which states that no signal can be transmitted through a medium at a speed greater than that of light in vacuum [16, 17].

Specifically, the necessary and sufficient condition for $N(E)$ to be a causal function is that $N(E)$ must be analytic in the lower half of the complex $E$ plane [17]. As indicated in Ref. [12], this will be the case because $A > 0$, $B > 0$, $C > 0$, and $4C - B^2 > 0$ and likewise, $A_i > 0$, $B_i > 0$, $C_i > 0$, and $4C_i - B_i^2 > 0$ (see Eqs. (23–28)).

The Kramers–Kronig dispersion relation gives $n(E)$ as the Hilbert transform of $k(E)$, that is,

$$n(E) - n(\infty) = \frac{1}{\pi} P \int_{-\infty}^{\infty} \frac{k(E') - k(\infty)}{E' - E}\, dE', \tag{29}$$

where $n(\infty) = \lim_{E\to\infty} n(E)$, and $k(\infty) = \lim_{E\to\infty} k(E)$.

In Eq. 29, $P$ denotes the Cauchy's principle-value integral, defined by

$$P\int_{-\infty}^{\infty} Z(E')\,dE' = -\sum_j (2\pi i R_j + \pi i S_j), \tag{30}$$

where $Z$ represents a general function of the complex variable $E'$, and where $R_j$ is the $j$th residue of the integrand at the $j$th pole located in the lower half of the complex $E'$ plane, and $S_j$ is the $j$th residue evaluated at the $j$th pole located along the real axis [17].

We first consider $k_\alpha(E)$, Eq. 20, consisting of a single term, and insert it into the Kramers–Kronig relation, Eq. 29:

$$n_\alpha(E) - n_\alpha(\infty) = \frac{1}{\pi} P\int_{-\infty}^{\infty} \frac{A[(B-2E_g)E' + E_g^2 - C]}{(E'^2 - BE' + C)(E' - E)}\,dE'. \tag{31}$$

The pole in the integrand of Eq. 31, located in the lower half of the complex $E'$ plane, is at $E' = B/2 - iQ$, since $Q = 1/2(4C - B^2)^{1/2} > 0$. The pole along the real axis is at $E' = E$. Applying Eq. 30 to Eq. 31, we obtain

$$n_\alpha(E) = n_\alpha(\infty) + \frac{B_\alpha E + C_\alpha}{E^2 - BE + C}, \tag{32}$$

where

$$B_\alpha = \frac{A}{Q}\left(-\frac{B^2}{2} + E_g B - E_g^2 + C\right), \tag{33}$$

$$C_\alpha = \frac{A}{Q}\left[\left(E_g^2 + C\right)\frac{B}{2} - 2E_g C\right]. \tag{34}$$

The expressions $k_\chi(E)$ and $k_\mu(E)$ consist of a sum of terms, each one having the same form as $k_\alpha(E)$. Therefore, $n_\chi(E)$ and $n_\mu(E)$ consist of a sum of terms, with each term having the same form as $n_\alpha(E)$. Inserting $k_\chi(E)$, Eq. 21, and $k_\mu(E)$, Eq. 22, into the Kramers–Kronig relation, Eq. 29,

gives

$$n_\chi(E) = n_\chi(\infty) + \sum_{i=1}^{q} \frac{B_{\chi i}E + C_{\chi i}}{E^2 - B_i E + C_i} \tag{35}$$

and

$$n_\mu(E) = n_\mu(\infty) + \sum_{i=1}^{q} \frac{B_{\mu i}E + C_{\mu i}}{E^2 - B_i E + C_i}. \tag{36}$$

The parameters $B_{\mu i}$ and $C_{\mu i}$ in the equation for $n_\mu(E)$ differ from $B_{\chi i}$ and $C_{\chi i}$ in the equation for $n_\chi(E)$ by the absence of $E_g$. Thus, for crystalline semiconductors and dielectrics,

$$B_{\chi i} = \frac{A_i}{Q_i}\left(-\frac{B_i^2}{2} + E_g B_i - E_g^2 + C_i\right) \tag{37}$$

$$C_{\chi i} = \frac{A_i}{Q_i}\left[(E_g^2 + C_i)\frac{B_i}{2} - 2E_g C_i\right]. \tag{38}$$

For metals,

$$B_{\mu i} = \frac{A_i}{Q_i}\left(-\frac{B_i^2}{2} + C_i\right) \tag{39}$$

$$C_{\mu i} = \frac{A_i B_i C_i}{2Q_i}. \tag{40}$$

$Q_i$ is the same in both cases:

$$Q_i = \tfrac{1}{2}(4C_i - B_i^2)^{1/2}. \tag{41}$$

This completes the derivation of optical constants $k_\alpha(E)$ and $n_\alpha(E)$ for amorphous semiconductors and dielectrics, Eqs. 20 and 32; $k_\chi(E)$ and $n_\chi(E)$ for crystalline semiconductors and dielectrics, Eqs. 21 and 35; and

$k_\mu(E)$ and $n_\mu(E)$ for metals, Eqs. 22 and 36. In the next section, we discuss the practical applications of these equations.

## DISCUSSION III

### The Parameters Involved in the Equations for $k(E)$ and $n(E)$ A

In the amorphous case, the energy dependence of both $k_\alpha(E)$ and $n_\alpha(E)$, given by Eqs. 20 and 32, can be fully and simultaneously determined by five parameters, $A$, $B$, $C$, $E_g$, and $n(\infty)$. Note that $B_\alpha$ and $C_\alpha$ are not independent parameters.

For crystalline semiconductors and dielectrics, each term in the sum for $k_\chi(E)$, Eq. 21, contributes either a peak or a shoulder to the $k$ spectrum and a corresponding structure to $n_\chi(E)$, Eq. 35—likewise for $k_\mu(E)$, Eq. 22, and $n_\mu(E)$, Eq. 36, for metals. Thus, the number of terms equals the number of discernible peaks and shoulders in the energy range in question.

We have found that for the most part, four terms, that is, fourteen parameters (including $E_g$ and $n(\infty)$), are sufficient to describe $k_\chi(E)$ and $n_\chi(E)$ over the interband region, indicating four types of critical-point transitions that produce spectral peaks. In the case of metals, with $E_g = 0$, we have found that three terms, that is, ten parameters (including $n(\infty)$), give an excellent fit in this region. Nevertheless, in some cases, more terms may be required to bring out the details of the spectra [14].

An important point about these parameters is that they all have physical significance, and consequently, can almost be determined by glancing at the experimental values of $k(E)$ and $n(E)$.

$E_g$, the optical energy band gap, is simply the measured energy for which $k(E)$ has its absolute minimum value. This is consistent with the experimental findings that the absolute minimum of $k(E)$ occurs at the onset of the "fundamental" absorption edge. By contrast, the values of $E_g$ quoted in the literature are obtained, usually, by extrapolating the "linear portion" of the plot of $(\alpha\hbar\omega)^{1/m}$ or $(\alpha\hbar\omega n)^{1/m}$ versus $\hbar\omega$, where $m = 1/2$, $3/2$, or 2, depending on the assumed mode of optical transition (direct, forbidden, or indirect, respectively). Examples are given in Refs. [12] and [14].

In all cases, $n(\infty)$ is approximately equal to but always greater than one, as discussed in the following section. However, if $n(\infty)$ is assumed equal to unity, reasonable agreement to experimental data is still obtained.

An uncomplicated determination of the other parameters, $A$, $B$, and $C$, associated with their physical significance, can readily be appreciated by considering the amorphous case. The value of $B/2$ is approximately equal

to the energy at which $k_\alpha(E)$ is a maximum. This is because $k_\alpha(E)$ is close to a maximum when $h\omega \approx E_{\sigma'} - E_\sigma = B/2$. The parameter $C$ depends on the energy difference between distinguishable states and on the lifetime of a distinguishable transition. To a first approximation, the lifetime contribution can be ignored so that $C \approx B^2/4$, assuming $B/2$ is equal to the peak energy (see Eqs. 24 and 25). Thus, position of the peak in the experimental $k_\alpha(E)$ spectrum provides knowledge of $B$ and $C$. The parameter $A$ is related to the dipole matrix element squared and essentially gives the strength of the peak in $k_\alpha(E)$.

Analogous statements can be made for the parameters $A_i$, $B_i$ and $C_i$ connected with crystalline semiconductors, dielectrics, and metals.

The overall fit of the equations for $k(E)$ and $n(E)$ to experimental data can be refined by means of a nonlinear, least-square, curve-fitting program, where the required preliminary values of the parameters are determined as outlined above. The values of the parameters for the crystalline materials presented in Tables I, III, IV, V, were obtained in this way. However, for the amorphous case, we used an algebraic scheme, described in Ref. [12], to determine the parameters presented in Table II.

## B $k(E)$ and $n(E)$ in the Limit $E$ Approaches Infinity

According to Eqs. 20, 21, and 22, $k(\infty)$ is a nonzero constant. Classically, (for instance, in the harmonic-oscillator model), it is expected that $k(\infty) = 0$. However, there are processes that do occur at high energies [15] that remove photons from the incident intensity and that therefore lead to a nonzero $k(\infty)$. Although our equations for $k(E)$ (as well as those based on classical models) do not describe these high-energy events, we regard $k(\infty) \neq 0$ as indicating that these events do take place.

Furthermore, in our treatment we find that $n(\infty) > 1$ for all cases, in contrast to classical dispersion theory. The values that we obtain for $n(\infty)$ and that depend on the particular material, are close to but always greater than one. Nevertheless, it should be noted that agreement with experimental results provided by our equations is not very much dependent on taking $n(\infty) > 1$. That is, if we take $n(\infty) = 1$ in our equations, we get a very slight alteration (for the worse) in our agreement with experiment. This is shown in Fig. 1a and b, for crystalline Si. The difference in fitting the experimental data to Eqs. 21 and 35 is depicted, where $n(\infty)$ is taken either as a constant equal to unity (Fig. 1a), or as a fitting parameter, determined to be 1.95 (Fig. 1b). As seen in this figure, better agreement is attained when $n(\infty)$ is not assumed a priori equal to unity. Details concerning the fit are discussed in Section IV.B.

However, we have stronger reasons (other than obtaining better agree-

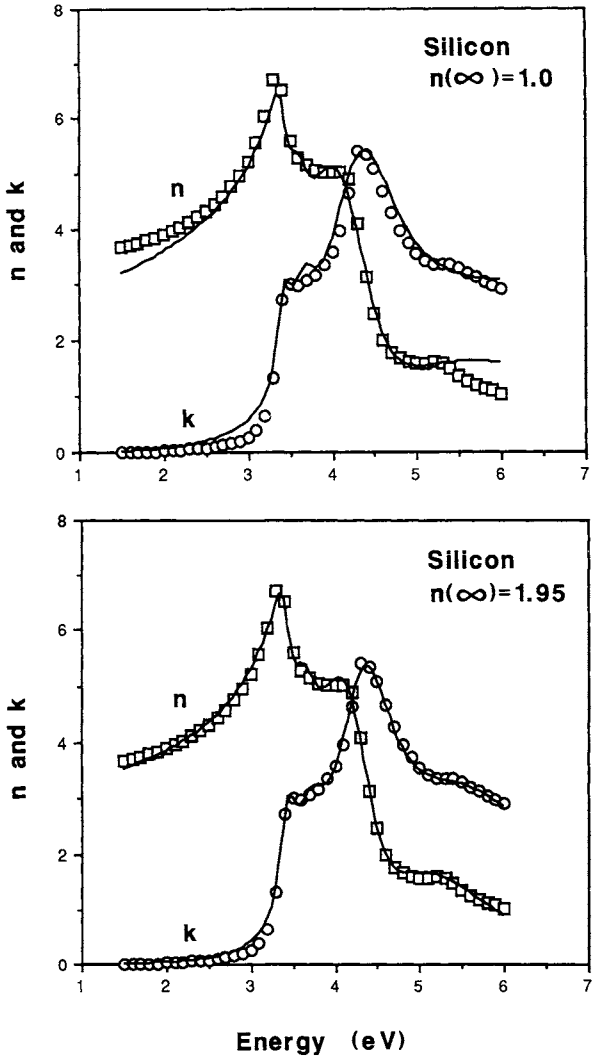


**Fig. 1.** The solid lines are the theoretical plots of $k_\chi(E)$ and $n_\chi(E)$ given by Eqs. 21 and 35 with the parameters specified in Table I for crystalline Si. Experimental data are by Aspnes and Studna [1, 21]. In (a), $n(\infty)$ is taken equal to unity, whereas in (b), $n(\infty)$ is equal to 1.95, as determined by least-square fitting of experimental data.

ment with experiment) for not assuming $n(\infty)$ equal to unity. The first reason is that J. S. Toll [16] has established mathematically that as a consequence of causality, $n(\infty) > 1$. His proof applies to the case $k(\infty) = 0$ and can trivially be extended to our case where $k(\infty) = \text{constant}$ [14]. Moreover, there is a multitude of published papers [1] by other

**TABLE I**

| | $A_i$ | $B_i$ (eV) | $C_i$ (eV$^2$) | $n(\infty)$ | $E_g$ (eV) |
|---|---|---|---|---|---|
| Si | 0.00280 | 6.873 | 11.820 | 1.00 | 1.06 |
| | 0.00769 | 7.319 | 13.429 | | |
| | 0.10213 | 8.589 | 18.705 | | |
| | 0.75064 | 10.159 | 33.183 | | |
| | 0.00405 | 6.885 | 11.864 | 1.950 | 1.06 |
| | 0.01427 | 7.401 | 13.754 | | |
| | 0.06830 | 8.634 | 18.812 | | |
| | 0.17488 | 10.652 | 29.841 | | |

Two separate sets of parameters describing the theoretial equations $k_\chi(E)$ and $n_\chi(E)$, Eqs. 21 and 35, with four terms in the sums, for crystalline Si. In both sets, values of the parameters $A_i$, $B_i$, and $C_i$ are obtained by least-square fitting of experimental data [1, 21] to the theoretical equations. However, in the first set, $n(\infty)$ is taken equal to unity, whereas in the second set, $n(\infty)$ is determined by the least-square fitting program. The optical energy band gap $E_g$, is taken as the energy at which the experimental $k$ spectrum has its absolute minimum. The corresponding plots are shown in Fig. 1a and b.

researchers, which show that $\varepsilon_1(\infty) > 1$ when experimental data are fitted to a harmonic-oscillator model or variations of a harmonic-oscillator model (where $\varepsilon_1(\infty) = n^2(\infty)$ and $k(\infty) = 0$). Finally, since the electromagnetic interaction takes place within the medium and not in a vacuum, we expect that $n_{\text{medium}}(\infty) \neq n_{\text{vacuum}}(\infty)$; that is, the presence of matter is "sensed" by electromagnetic radiation, even at high energies.

## IV EXAMPLES

As seen in the following examples, the present formulation requires far fewer parameters compared with other formulations, and at the same time it provides better agreement with experimental data. As previously noted, this approach is consistent with Kramers–Kronig analysis, and directly incorporates the concept of optical energy band gap, $E_g$.

### A Amorphous Semiconductors and Dielectrics

Our formulation for $k_\alpha(E)$ and $n_\alpha(E)$ was successfully applied to the published data of a wide class of amorphous materials, including a variety

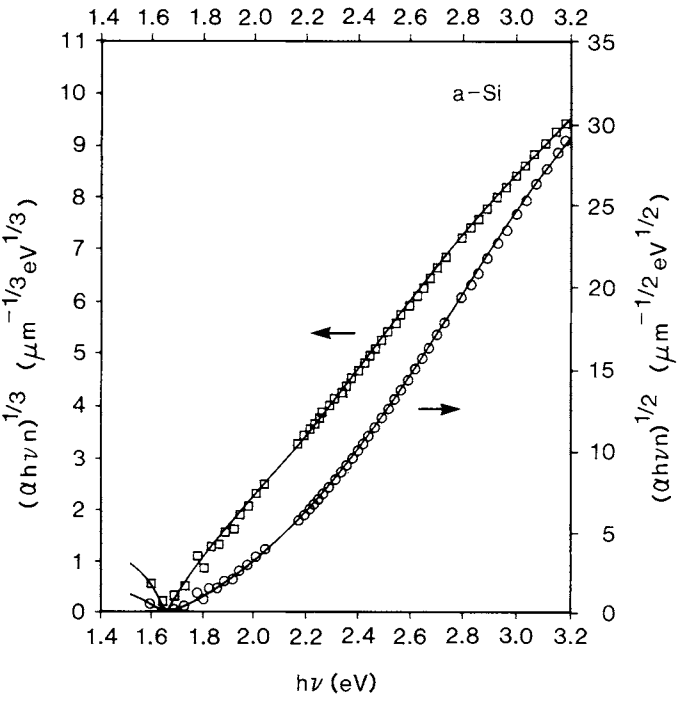


**Fig. 2.** The solid lines are the theoretical plots for a-Si representing $(\alpha h\nu n)^{1/2}$ versus $h\nu$ and $(\alpha h\nu n)^{1/3}$ versus $h\nu$, where $E = h\nu$ and $\alpha = (2\omega/c)k = 4\pi kE/hc$, with $k = k_a(E)$ given by Eq. 20 and $n = n_a(E)$ given by Eq. 32. The parameters are specified in Table II. The experimental data are from Klazes *et al.* [19] for a-Si produced by glow-discharge decomposition of $SiH_4$. (From Forouhi and Bloomer [12]).

of amorphous silicon, a-Si, and hydrogenated amorphous silicon, a-Si:H, prepared by different methods under different processing conditions [12, 18], as well as a-$Si_3N_4$ and a-$TiO_2$ [12].

**TABLE II**

| | $A$ | $B$ (eV) | $C$ (eV$^2$) | $n(\infty)$ | $E_g$ (eV) |
|---|---|---|---|---|---|
| a-Si | 1.5690 | 5.5311 | 9.6390 | 2.4330 | 1.65 |
| a-$TiO_2$ | 0.5189 | 8.1605 | 17.5291 | 1.7614 | 2.8 |

Values of the parameters describing the theoretical equations $k_a(E)$ and $n_a(E)$, Eqs 20 and 32, for amorphous silicon, a-Si, and amorphous titanium dioxide, a-$TiO_2$. The parameters are obtained by an algebraic method described in Ref. [12]. Experimental data for a-Si and a-$TiO_2$ are taken from Refs. [19] and [20], respectively. The corresponding plots are shown in Figs. 2 and 3.

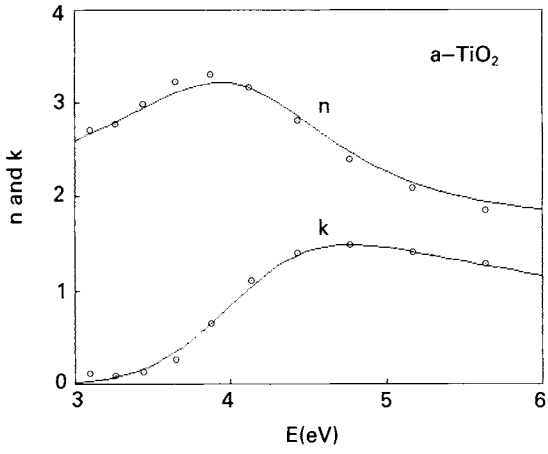


**Fig. 3.** The solid lines are the theoretical plots of $k_\alpha(E)$ and $n_\alpha(E)$ given by Eqs. 20 and 32 with the parameters specified in Table II for a-$TiO_2$. The experimental data are from Joseph [20]. (From Forouhi and Bloomer [12].)

As an example, in Fig. 2 the theoretical and experimental plots are displayed for $(\alpha h\nu n)^{1/3}$ and $(\alpha h\nu n)^{1/2}$ versus $h\nu$ for an a-Si film, where $\alpha$ denotes absorption coefficient and $h\nu$ denotes photon energy. Experimental data are from Klazes *et al.* [19]. The film was produced by capacitance rf glow-discharge decomposition of silane ($SiH_4$) diluted in argon. It was deposited on a fused-silica substrate at a deposition temperature of 370°C. Although the film is considered as a-Si in the original reference, it may be more appropriately presented as a-Si:H, since films prepared by glow-discharge decomposition of $SiH_4$ incorporate hydrogen.

The reason that consideration is given to the functions $(\alpha h\nu n)^{1/3}$ and $(\alpha h\nu n)^{1/2}$ is that Klazes *et al.* [19] argued that $(\alpha h\nu n)^{1/3} \propto (h\nu - E_g)$ provides a better fit to their experimental data than $(\alpha h\nu n)^{1/2} \propto (h\nu - E_g)$, from which they deduced $E_g$, using a linear extrapolation of $(\alpha h\nu n)^{1/3}$ as a function of $h\nu$.

The theoretical curves presented in Fig. 2 are obtained by using Eqs. 20 and 32 for $k_\alpha(E)$ and $n_\alpha(E)$ in the expressions $(\alpha h\nu n)^{1/3}$ and $(\alpha h\nu n)^{1/2}$ with the parameters $A$, $B$, $C$, $n$ ($\infty$), and $E_g$ given in Table II. As seen in this figure, a remarkably good fit is found between the experimental data and the corresponding theoretical curves. This result is in line with taking $E_g$ simply as the energy for which $k(E)$ has its absolute minimum; that is, $E_g$ need not be determined via a linear extrapolation of experimental data.

Experimental data of a-$TiO_2$ presented in Fig. 3 are from Joseph and Gagnaire [20]. The film was produced by an anodic oxidation of titanium sample. The optical constants were determined from analysis of ellipsometric measurements on a set of samples with different film thicknesses in

the wavelength range 220–720 nm, corresponding to 5.6–1.8 eV. Theoretical and experimental plots of $k_\alpha(E)$ and $n_\alpha(E)$ are shown in Fig. 3, and the parameters $A$, $B$, $C$, $n(\infty)$, and $E_g$ are given in Table II.

These two examples, as well as those given in Refs. [12] and [18], point to the fact $k_\alpha(E)$ and $n_\alpha(E)$, specified by a total of only five parameters, provide an excellent fit to measured data throughout the interband regime. As discussed in Ref. [12], this is distinctive from previous formulations, which require nine parameters to specify simultaneously $k_\alpha(E)$ and $n_\alpha(E)$ just at the absorption edge, and which furthermore do not relate $n_\alpha(E)$ to $k_\alpha(E)$ according to the Kramers–Kronig dispersion relation.

## Crystalline Semiconductors and Dielectrics B

Our formulation for $k_\chi(E)$ and $n_\chi(E)$, Eqs. 21 and 35, has been successfully applied to group IV semiconductors (Si and Ge), group III-V semiconductors (GaP, GaAs, GaSb, InP, InAs, and InSb), group IV-IV semiconductor (SiC), and crystalline insulators (cubic C and $SiO_2$) [14].

As an example, the theoretical and experimental plots of $k_\chi(E)$ and $n_\chi(E)$ for crystalline Si are shown in Fig. 1a and b. We have taken the number of terms in Eqs. 21 and 35 equal to four, corresponding to three discernable peaks and one shoulder in the experimental $k$-versus-$E$ spectrum of Si in the 1.5–6 eV range. The experimental data are by Aspnes and Studna [1, 21]. Values of the parameters, obtained by least-square fitting, are given in Table I. As discussed in Section III.B, in Fig. 1a, $n(\infty)$ is taken equal to unity, whereas in Fig. 1b, $n(\infty)$ is taken as a fitting parameter, determined equal to 1.95.

Furthermore, it should be noted that the value of the optical energy band gap, $E_g$, presented in Table I is taken as equal to 1.06 eV, corresponding to the position of the absolute minimum in the experimental values of $k(E)$. (It is not necessary to consider $E_g$ as a fitting parameter). The values that we obtain for the critical-point transition energies, $[E_c(\mathbf{k}_{crit}) - E_\gamma(\mathbf{k}_{crit})]_i = B_i/2$, are essentially the same as previously identified values of these transition energies. For example, for Si we obtain $B_1/2 \approx 3.4$ eV, $B_2/2 \approx 3.7$ eV, $B_3/2 \approx 4.3$ eV, and $B_4/2 \approx 5.3$ eV. On the other hand, from reflectance measurements, these energies are determined as $E_1 \approx 3.4$ eV, $E_0 \approx 4.0$ eV, $E_2 \approx 4.4$ eV, and $E_1' \approx 5.5$ eV [6]. (Reported values differ by a few tenths of an electron volt from one reference to another. See, for example, Refs. [5] and [6].) The notations $E_0$, $E_1$, $E_1'$, and $E_2$ refer to an identification of the critical points involved and are described in Ref. [6].

Another example is shown in Fig. 4 for crystalline $SiO_2$. Experimental data are by Philipp [1, 22]. Again, the number of terms in equations for

$k_\chi(E)$ and $n_\chi(E)$ is taken equal to four, corresponding to four distinct peaks in the experimental $k(E)$ in the 2–18 eV range. $E_g$ is taken equal to 7.0 eV, corresponding to the position of the absolute minimum in $k(E)$. We have found that the values of the parameters initially determined from the position of the peaks in the experimental $k$ versus $E$ spectrum are very close to the values obtained by a least-square, curve-fitting program (Section III.A). Experimentally, the peaks in $k$ occur at 10.45 eV, 11.7 eV, 14.3 eV, and 17.25 eV [22], whereas the least-squares fit yields $B_1/2 \approx 10.36$ eV, $B_2/2 \approx 11.64$ eV, $B_3/2 \approx 14.08$ eV, and $B_4/2 \approx 17.15$ eV. Values of the parameters are given in Table III.

These examples, as well as those given in Ref. [14], indicate that four terms in the sum for $k_\chi(E)$ and $n_\chi(E)$ are sufficient to specify simultaneously the extinction coefficient and the refractive index of crystalline semiconductors and dielectrics in the fundamental optical regime. In some cases, however, more terms may be required to bring out the details of the optical spectra [14]. Conversely, when the number of terms is reduced, fine structural details are lost and eventually one peak remains, resembling the amorphous case. This is shown for SiC in Fig. 5a, b, and c, with the number of terms equal to one, two, and four. The experimental data presented in Fig. 5 are by Leveque and Lynch [23]. Values of the parameters are given in Table IV. In the examples given in this section, as well as those in Ref.

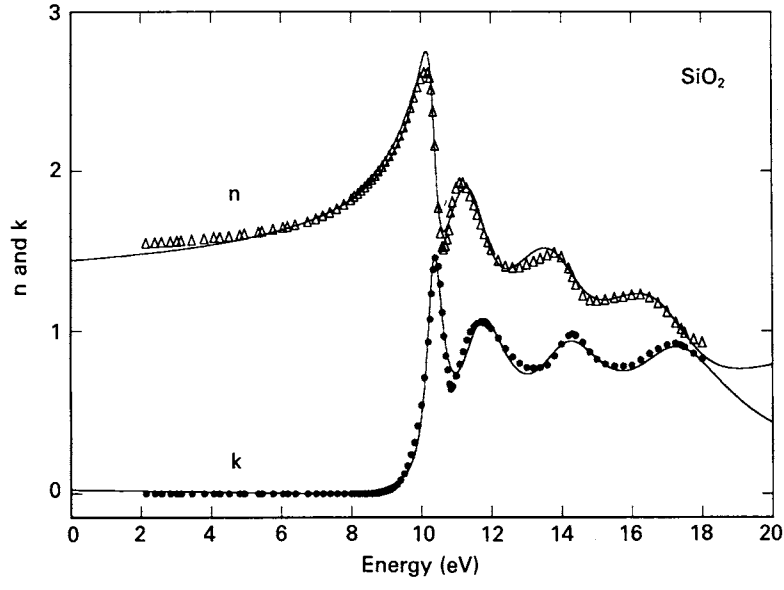


**Fig. 4.** The solid lines are the theoretical plots of $k_\chi(E)$ and $n_\chi(E)$ given by Eqs. 21 and 35 with the parameters specified in Table III for crystalline $SiO_2$. Experimental data are by Philipp [1, 22]. (From Forouhi and Bloomer [14].)

**TABLE III**

| | $A_i$ | $B_i$ (eV) | $C_i$ (eV$^2$) | $n(\infty)$ | $E_g$ (eV) |
|---|---|---|---|---|---|
| $SiO_2$ | 0.00867 | 20.729 | 107.499 | 1.226 | 7.00 |
| | 0.02948 | 23.273 | 136.132 | | |
| | 0.01908 | 28.163 | 199.876 | | |
| | 0.01711 | 34.301 | 297.062 | | |

The parameters describing the theoretical equations $k_\chi(E)$ and $n_\chi(E)$, Eqs. 21 and 35, with four terms in the sums, for crystalline $SiO_2$. Values of the parameters $A_i$, $B_i$, $C_i$, and $n(\infty)$ are obtained by least-suqare fitting of the experimental data [1, 22] to the theoretical equations. $E_g$ is taken as the energy at which the experimental $k$ spectrum has its absolute minimum. The corresponding plots are shown in Fig. 4.

[14], the number of parameters (14, including $E_g$ and $n(\infty)$) used to specify simultaneously $k_\chi(E)$ and $n_\chi(E)$, is much less than that required by other approaches. For example, the harmonic-oscillator model requires 22 parameters to fit experimental data of Si [10] in essentially the same energy range without the benefit of providing $E_g$.

## C Metals

In the case of metals, we use the example of Cu to demonstrate the applicability of $k_\mu(E)$, Eq. 22, and $n_\mu(E)$, Eq. 36. (Preliminary results indicate that they apply to other metals, such as Al and Au.) These equations, with three terms included in the sum, are fitted to the experimental values of $k_\mu(E)$ and $n_\mu(E)$ obtained by Hagemann *et al.* [24] for the energy range where interband transitions of bound electrons are predominant (see next paragraph), namely, 1.7–10 eV. Theoretical and experimental plots of $k_\mu(E)$ and $n_\mu(E)$ are shown in Fig. 6 with values of the parameters given in Table V; excellent agreement with the experimental data is achieved.

Contribution of bound electrons for $E < 1.7$ eV is overshadowed by the strength of free-electron transitions. Thus, the measured reflectance spectrum, $R(E)$, exhibits a flat, structureless plateau for $E < 1.7$ eV [25]. For $E > 1.7$ eV, bound-electron contributions prevail. Experimentally, $R(E)$ decreases sharply between 1.7 and 2.1 eV and thereafter exhibits several peaks [25].

We have extended the theoretical plots of $k_\mu(E)$ and $n_\mu(E)$ down to $E = 0$ in order to determine the interband contributions in the far-infrared regime. It should be emphasized that free-electron interactions are not

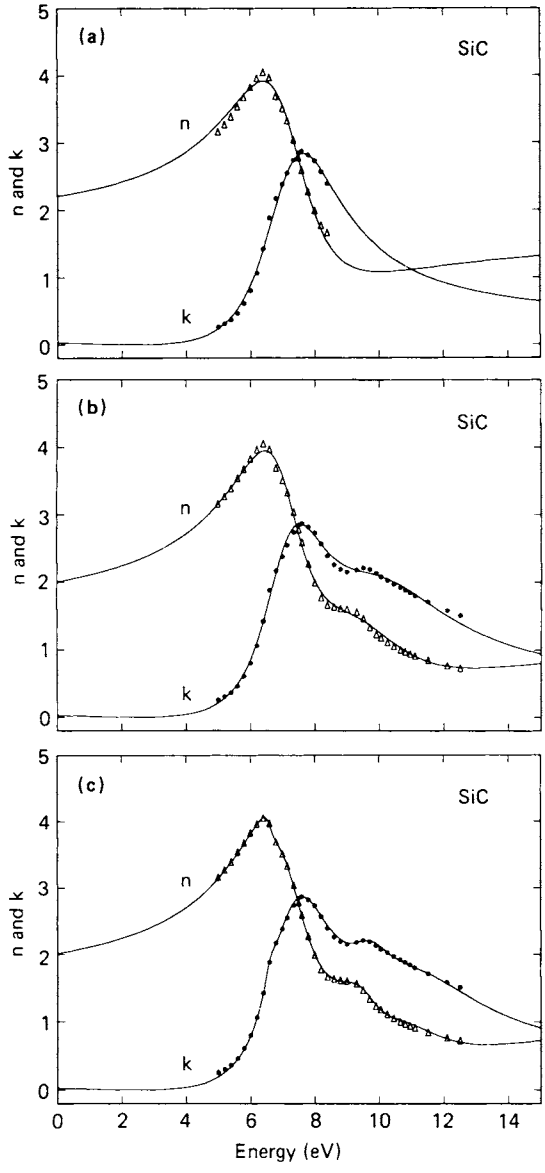


**Fig. 5.** The solid lines are the theoretical ploits of $k_\chi(E)$ and $n_\chi(E)$ given by Eqs. 21 and 35 with the parameters specified in Table IV for crystalline SiC, taking the number of terms in these equations equal to 1, 2, and 4 in (a), (b), and (c), respectively. In (a), only experimental data in the 5–8.5 eV energy range are considered. Experimental data are by Leveque and Lynch [1, 23]. (From Forouhi and Bloomer [14].)

**TABLE IV**

| | $A_i$ | $B_i$ (eV) | $C_i$ (eV$^2$) | $n(\infty)$ | $E_g$ (eV) |
|---|---|---|---|---|---|
| SiC | | | | | |
| 1 term | 0.25926 | 14.359 | 53.747 | 1.680 | 2.50 |
| 2 terms | 0.18028 | 14.222 | 52.148 | 1.337 | 2.50 |
| | 0.10700 | 19.397 | 99.605 | | |
| 4 terms | 0.00108 | 13.227 | 43.798 | 1.353 | 2.50 |
| | 0.19054 | 14.447 | 53.860 | | |
| | 0.00646 | 19.335 | 94.105 | | |
| | 0.05366 | 21.940 | 125.443 | | |

Three separate sets of parameters describing the theoretical equations $k_\chi(E)$ and $n_\chi(E)$, Eqs. 21 and 35, for crystalline SiC. The number of terms in the sums for these equations is taken equal to one, two, or four, as indicated. In all three sets, values of the parameters $A_i$, $B_i$, $C_i$, and $n(\infty)$ are obtained by least-square fitting of the experimental data [1, 23] to the theoretical equations. $E_g$ is taken as the energy at which the experimental $k$ spectrum has its absolute minimum. The corresponding plots are shown in Fig. 5a, b and c.

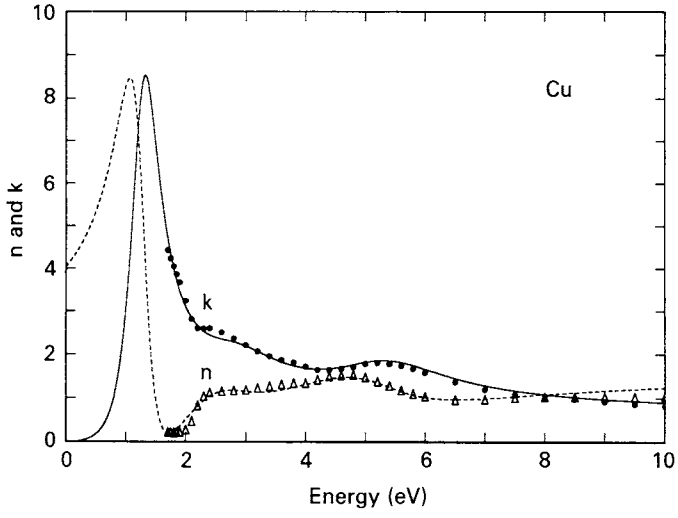


**Fig. 6.** The solid and dashed lines represent, respectively, the theoretical plots of $k_\mu(E)$ and $n_\mu(E)$ given by Eqs. 22 and 36 with the parameters specified in Table V for Cu. Experimental data are by Hagemann *et al.* [1, 24]. (From Forouhi and Bloomer [15].)

**TABLE V**

| | $A_i$ | $B_i$ (eV) | $C_i$ (eV$^2$) | $n(\infty)$ |
|---|---|---|---|---|
| Cu | 0.46531 | 2.499 | 1.652 | 1.711 |
| | 0.07489 | 5.390 | 8.010 | |
| | 0.03872 | 10.396 | 28.393 | |

The parameters describing the theoretical equations $k_\mu(E)$ and $n_\mu(E)$, Eqs. 22 and 36, with three terms in the sums, for Cu. Values of the parameters $A_i$, $B_i$, $C_i$, and $n(\infty)$ are obtained by least-square fitting of experimental data [1, 24] to the theoretical equations. The corresponding plots are shown in Fig. 6.

included in the present treatment. As expected, $k(E)\rightarrow 0$ when $E\rightarrow 0$, since bound-electron transitions are negligible at low energies where free-electron interactions dominate. (Free-electron transitions do not give rise to structure in optical constants of metals [1]). As seen in Fig. 6, a sharp peak in the theoretical curve of $k_\mu(E)$ occurs at $E\approx 1.7$ eV, indicative of a sharp peak in reflectance, $R(E)$, near this energy. This is consistent with strong reflectance of red-orange frequencies, producing the characteristic copper color. Thus, we infer that the color of Cu can be attributed to direct interband critical-point transitions of bound electrons. In fact, this was concluded by Mott and Jones [26] nearly thirty years ago.

## V SUMMARY

We have deduced equations for the extinction coefficient, $k(E)$, (Eqs. 20, 21, 22) and the refractive index, $n(E)$, (Eqs. 32, 35, 36) applicable to amorphous semiconductors and dielectrics, crystalline semiconductors and dielectrics, and metals. Amorphous semiconductors and dielectrics are distinguished from crystalline semiconductors and dielectrics and metals by the number of terms in the equations for $k(E)$ and $n(E)$, which in turn is equal to the number of spectral peaks. Metals are distinguished from crystalline semiconductors and dielectrics by the absence of $E_g$. The equations that we derive for $k(E)$ are based on direct interband transitions of bound electrons and lead to structure in optical constants through transitions of electrons from one distinguishable state to another. Distinguishable states are defined to be either the bonding and antibonding states associated with the valence and conduction bands of amorphous materials, or critical-point states associated with the valence and conduc-

tion bands of crystalline materials. The expression $n(E)$ is determined according to the Kramers–Kronig dispersion relation from the corresponding $k(E)$. These equations are applicable throughout the fundamental optical energy range. Thus, the present formulation furnishes a unified treatment of optical constants of materials in the interband region.

## REFERENCES


1. E. D. Palik, ed., "Handbook of Optical Constant Solids," Academic Press, New York (1985).
2. T. S. Moss, G. J. Burrell, and B. Ellis, "Semiconductor Opto-Electronics," Wiley, New York (1973).
3. N. F. Mott and E. A. Davis, "Electronic Processes in Non-Crystalline Materials," 2nd ed., Clarendon, Oxford (1979).
4. J. I. Pankove, "Optical Processes in Semiconductors," Dover, New York (1971).
5. D. L. Greenaway and G. Harbeke, "Optical Properties and Band Structure of Semiconductors," Pergamon, Oxford (1968).
6. J. C. Phillips, "Bonds and Bands in Semiconductors," Academic Press, New York (1973).
7. F. Stern, in "Solid State Physics" (F. Seitz and D. Turnbull, eds.), Vol. 15, Academic Press, New York, 299 (1963).
8. J. Tauc, R. Grigorovici, and A. Vancu, *Phys. Status Solidi* **15**, 627 (1966).
9. H. Ehrenreich and M. Cohen, *Phys. Rev.* **115**, 786 (1959).
10. H. W. Verleur, *J. Opt. Soc. Am.* **58**, 1356 (1968).
11. R. Zallen, "The Physics of Amorphous Solids," Wiley, New York (1983).
12. A. R. Forouhi and I. Bloomer, *Phys. Rev. B* **34**, 7018 (1986).
13. W. Heitler, "The Quantum Theory of Radiation," 3rd ed., Dover, New York (1984).
14. A. R. Forouhi and I. Bloomer, *Phys. Rev. B* **38**, 1865 (1988).
15. A. R. Forouhi and I. Bloomer, unpublished.
16. J. S. Toll, Ph.D. thesis, Princeton University, New Jersey (1952).
17. P. Roman, "Advanced Quantum Theory," Addison-Wesley, Reading, Mass. (1965).
18. A. R. Forouhi, in "Properties of Amorphous Silicon," 2nd ed., EMIS Datareview Series No. 1, INSPEC, The Institution of Electrical Engineers, London, Chapter 9, 309 (1989).
19. R. H. Klazes, M. H. L. M. van den Broek, J. Bezemer, and S. Radelaar, *Philos. Mag. B* **45**, 377 (1982).
20. J. Joseph and A. Gagnaire, *Thin Solid Films* **103**, 257 (1983).
21. D. E. Aspnes and A. A. Studna, *Phys. Rev. B* **27**, 985 (1983).
22. H. R. Philipp, *Solid State Commun.* **4**, 73 (1966); quoted in tabulated form by H. R. Philipp in Ref. 1, p. 719.
23. G. Leveque and D. A. Lynch, private communication with W. J. Choyke and E. D. Palik. See Ref. 1, p. 587.
24. H. J. Hagemann, W. Gudat, and C. Kunz, DEZY Report SR-74/7, Hamburg, (1974); H. J. Hagemann, W. Gudat, and C. Kunz, *J. Opt. Soc. Am.* **65**, 742 (1975); quoted in tabulated form by D. W. Lynch and W. R. Hunter in Ref. 1, p. 275.
25. H. Ehrenreich and H. R. Philipp, *Phys. Rev.* **128**, 1622 (1962).
26. N. F. Mott and H. Jones, "The Theory of the Properties of Metals and Alloys," Dover, New York (1958).

# Chapter 8

# Temperature Dependence of the Complex Index of Refraction

MICHAEL E. THOMAS
Applied Physics Laboratory
The Johns Hopkins University
Laurel, Maryland

I. Introduction 177
II. Temperature Dependence of $n$ and $k$ 179
A. General Remarks 179
B. One-Phonon Temperature Dependence 181
C. Absorption near Transparency 185
III. Conclusions 199
References 199

## I INTRODUCTION

Although the emphasis of *HOC I* and *HOC II* is room-temperature optical properties of materials, a discussion of temperature dependence is imperative for many current applications. A good example is thermal lensing by high-power laser windows, which requires knowledge of both absorption and index of refraction as a function of temperature. Also, the range of window materials transparency is temperature dependent. Transparency is improved by lowering temperature. For maximum sensitivity, thermal emission from a window in front of a detector must be considered. Imaging through a nonuniform hot window requires compensation of the distortions caused by the temperature-dependent index of refraction.

The intrinsic optical properties of a material are determined by three basic physical processes: free carriers, lattice vibrations, and electronic transitions. These processes were described in *HOC I*. However, the dominant physical process depends on the material. All materials have contributions to the complex index of refraction from electronic transitions. Metals and semiconductors are additionally influenced by free-


Copyright © 1991 by Academic Press.
All rights of reproduction in any form reserved.
ISBN 0-12-544422-2

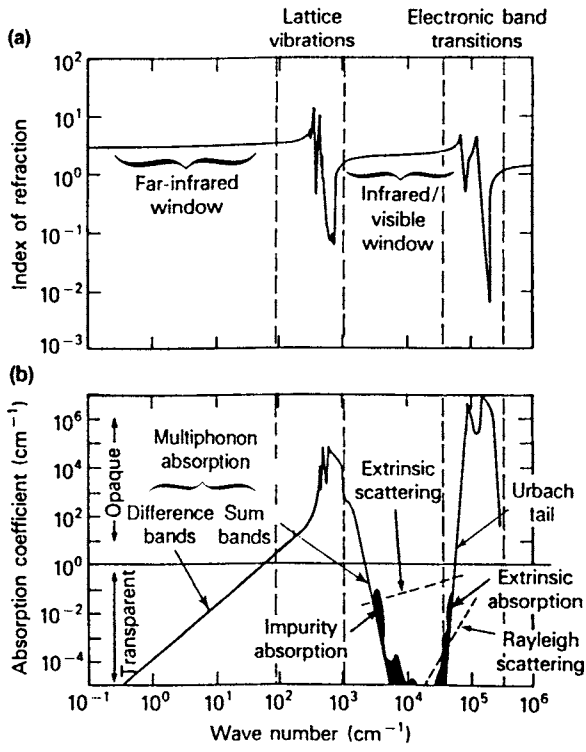


**Fig. 1.** Optical properties of a typical polar crystalline insulator.

carrier effects. The strength of this effect depends on the carrier concentration; thus, it is very important in metals. Insulators and semiconductors also require the characterization of the lattice vibrations (or phonons) to understand fully the optical properties.

In the range of transparency, more subtle processes such as impurities, defects, and scattering become important. Intrinsic Rayleigh scattering is a very weak effect, but is important in long-path optical fibers and UV transparent materials. Extrinsic scattering, caused by defects or grains in polycrystalline solids, is typically much larger than Rayleigh scattering. Impurity and defect absorption features can be of great concern depending on the spectral region, incident radiation intensity, and material temperature.

The temperature, $T$, and frequency, $\nu$ (in wave numbers), dependence of the real part of the index of refraction, $n(\nu, T)$ (index of refraction), is determined by the dominant physical processes previously mentioned. Figure 1a illustrates this point for the case of an insulating polar crystal. The value of $n(\nu, T)$ is essentially the sum of the strengths of all oscillators

with fundamental oscillation frequencies above $\nu$. Thus, the temperature dependence of those oscillations must be known to characterize $n(\nu, T)$ fully at any frequency.

The temperature and frequency dependence of the imaginary part of the index of refraction, $k(\nu, T)$ (index of extinction), is more involved and requires consideration of not only the dominant physical processes but also higher-order processes, impurities, and defects. The spectral regions of the fundamental oscillations are opaque. Transparency of an insulator is determined by three different absorption edges as illustrated in Figure 1b. Far-infrared transparency ends in the region of two-phonon difference bands and the one-phonon red wing (the low-frequency side of the absorption band). Infrared transparency begins in the region of three-phonon sum bands (essentially the third harmonic of the one-phonon bands). Visible/ultraviolet transparency ends at the Urbach tail, which can be phenomenologically interpreted as thermal fluctuations in the band-gap energy [1]. (A formula representing the Urbach tail, including temperature dependence, was given in *HOC I*, Chapter 10, by Lynch [2]). A detailed discussion of the temperature dependence of one- and multiphonon processes extends the work of Mitra in *HOC I* and is the central topic of this chapter.

The temperature dependence of intrinsic Rayleigh scattering will not be considered because it is usually too small to be of concern. Extrinsic scatter in polycrystalline materials has been observed to be constant with temperature for low-expansion materials [3], and also will not be discussed further. Impurity and defect absorption, which may be significant, are highly material and manufacturing-process dependent and will not be properly treated within the limits of this chapter.

The emphasis of this chapter is on the temperature-dependence of optical phonons. Insulators are the primary examples to be compared to the models presented.

## TEMPERATURE DEPENDENCE OF *n* AND *k* II

### General Remarks A

As an introduction to the temperature dependence of the complex index of refraction, $n^*(\nu, T) = n(\nu, T) - jk \leftarrow (\nu, T)$, consider the Lorentz–Lorenz formula,

$$\frac{n^2-1}{n^2+2} = \frac{1}{3\varepsilon_0}\rho(T)\alpha_p(\rho, T), \tag{1}$$

where $\rho$ is the number density of oscillators per unit volume and $\alpha_p$ is the polarizability. The derivative of $n$ with respect to $T$ becomes [4]

$$2n\varepsilon_0\frac{dn}{dT}=(n^2+2)(n^2-1)\left[\frac{1}{3\rho}\frac{\partial\rho}{\partial T}+\frac{1}{3\alpha_p}\left\{\left(\frac{\partial\alpha_p}{\partial\rho}\right)_T\frac{\partial\rho}{\partial T}+\left(\frac{\partial\alpha_p}{\partial T}\right)_\rho\right\}\right]. \quad (2)$$

The number density, $\rho$, is

$$\rho=N/V,$$

where $N$ is the number of oscillators per unit volume $V$. Further, the derivative of volume with respect to temperature can be written in terms of the linear coefficient of expansion, $\alpha_e$, as

$$\frac{dV}{dT}=3V\alpha_e. \quad (3)$$

Now, Eq. 2 can be rewritten in a more meaningful form

$$2n\varepsilon_0\frac{dn}{dT}=-(n^2+2)(n^2-1)\alpha_e\left[1-\frac{V}{\alpha_p}\left(\frac{\partial\alpha_p}{\partial V}\right)_T\right] + \frac{(n^2+2)(n^2-1)}{3\alpha_p}\left(\frac{\partial\alpha_p}{\partial T}\right)_V. \quad (4)$$

The first term depends on changes in volume with respect to temperature. Thermal expansion is the dominant contributor. The second term represents the temperature changes in the polarizability. Many optical materials, such as the alkali halides and the fluorides, have negative values for $dn/dT$ in the visible and infrared. Thus, for these materials, volume expansion dominates over polarizability temperature dependence. Li [5] is able to show a direct proportionality between the expansion coefficient and $dn/dT$ for the alkali halides.

The polarizability is determined by two fundamental processes in an insulating material: electronic transitions and vibrational transitions. The electronic transitions contribute to the index of refraction from the ultraviolet/visible region to DC. The vibrational transitions also contribute to the index of refraction from the far-infrared to DC. They are more

temperature sensitive than the electronic transitions; thus, $dn/dT$ in the far infrared below the optical phonons is usually positive and greater than $dn/dT$ in the visible/IR.

A more detailed discussion of the temperature dependence is given in the following sections.

## B One-Phonon Temperature Dependence

The optical properties of an insulating material can be completely specified by the complex index of refraction, $n^*(\nu, T)$, or the complex permittivity, $\varepsilon^*(\nu, T)$, where $\nu$ is the wave number (reciprocal wavelength). The relationship between $n^*$ and $\varepsilon^*$ is

$$n^*(\nu, T) = \sqrt{\varepsilon^*(\nu, T)}, \tag{5}$$

where

$$\varepsilon^*(\nu) = (n^2 - k^2) - 2jnk = \varepsilon_1 - j\varepsilon_2. \tag{6}$$

The absorption coefficient is defined by

$$\beta_a(\nu, T) = 4\pi\nu k(\nu, T). \tag{7}$$

In the following, only intrinsic absorption losses will be considered. The magnitude of the single-surface reflectance, $|R|$, of a medium (at normal incidence) is

$$|R| = \frac{(n-1)^2 + k^2}{(n+1)^2 + k^2}. \tag{8}$$

Generally, a measurement of $|R|$ is not sufficient to determine $\varepsilon^*$ (for example, both $n$ and $k$). Hence, it is necessary to describe the relationship between $n$ and $k$. The "classical pole-fit model" (see Mitra, *HOC I*)

represents $\varepsilon^*$ in terms of the lattice vibrations:

$$\varepsilon^*(\nu, T) = \varepsilon_\infty(T) + \sum_i \frac{\Delta\varepsilon_i(T)\nu_i^2(T)}{\nu_i^2(T) - \nu^2 + j\gamma_i(\nu, T)\nu}, \tag{9}$$

where $\Delta\varepsilon_i$, $\gamma_i$ and $\nu_i$ are the $j$th mode strength, line width, and long-wavelength transverse optical frequency, respectively. The sum on $i$ is over all transverse optical modes. This model is well-known to describe $n$ adequately in the infrared and radar-frequency regions [1]. Using Eq. 9, the static dielectric constant, $\varepsilon_s(T) = \varepsilon_1(0, T)$, becomes

$$\varepsilon_s(T) = \varepsilon_\infty(T) + \sum_i \Delta\varepsilon_i(T) \tag{10}$$

The implied frequency dependence of $\gamma_i$ represents a cutoff beyond the one-phonon region caused by anharmonicities of the potential. The cutoff is empirically represented by the formula [6]

$$\gamma_i(\nu, T) = \gamma_i(T) \left\{ \begin{array}{ll} 1; & \nu \leq \tilde{\nu} \\ \exp\left\{ -\alpha \left[ \left( \frac{\nu}{\tilde{\nu}} \right)^2 - 1 \right] \right\}; & \nu \geq \tilde{\nu} \end{array} \right\}, \tag{11}$$

where $\alpha$ and $\tilde{\nu}$ are arbitrary parameters. We have been most successful in this effort by choosing $\alpha = 4$ and $\tilde{\nu}$ as the highest infrared-allowed longitudinal-optical-mode frequency. Although those values for $\alpha$ and $\tilde{\nu}$ are not unique, they are adequate for the present purpose.

This model satisfies the Kramers–Kronig relationship and therefore provides the correct relationship between $\varepsilon_1$ and $\varepsilon_2$. It also allows for the construction of a physically meaningful representation of $\varepsilon^*$, using only the magnitude of $R$ as input. This point has been extremely useful in modeling efforts.

Another commonly used pole-fit model features four parameters per transition, as given by the expression [7]

$$\varepsilon^*(\nu, T) = \varepsilon_\infty(T) \prod_i \frac{\nu_{iLO}^2(T) - \nu^2 + j\nu\gamma_{iLO}(\nu, T)}{\nu_i^2(T) - \nu^2 + j\nu\gamma_i(\nu, T)}, \tag{12}$$

where the additional subscript LO indicates longitudinal-optical-mode parameters. A product instead of a sum is now used. Equation 12 in the

static limit reduces to the Lyddane–Sachs–Teller relation [8]

$$\frac{\varepsilon_s}{\varepsilon_\infty} = \prod_i \frac{\nu_{iLO}^2}{\nu_i^2}. \tag{13}$$

This is a similar statement to Eq. 10, now in the form of a product.

As Eq. 9 suggests, the reflectance is a function not only of frequency but also of temperature. Experiments reported by Jasperse *et al.* [9] have demonstrated that the optical parameters $\Delta\varepsilon_i$ and $\nu_i$ have a linear temperature dependence, and calculations by Maradudin and coworkers [10] have successfully utilized a quadratic temperature dependence for $\gamma_i$ at high temperatures. A theoretical calculation by Wallis and Maradudin [11] has shown that the temperature dependence of $\nu_i$ and $\gamma_i$ comes from cubic anharmonic terms in the lattice potential energy. The origin of the temperature dependence of the mode strengths, $\Delta\varepsilon_i$, is not well established but can be understood by considering the static dielectric constant. Szigeti [12] has shown that not only do anharmonic terms in the lattice potential energy contribute to the temperature dependence of $\varepsilon_s(T)$, but also a contribution arises from terms in the dipole moments that are of higher order in the displacement coordinates. These latter higher-order terms have their origin in the deformation of the electronic shells.

The temperature dependence of the transverse-mode frequencies, $\nu_i$, and the mode strengths, $\Delta\varepsilon_i$, can be represented by linear equations of the form

$$\nu_i(T) = \nu_i(T_0) - a_i[T - T_0] \tag{14a}$$

and

$$\Delta\varepsilon_i(T) = \Delta\varepsilon_i(T_0) + b_i[T - T_0], \tag{14b}$$

where $T_0$ is a reference temperature (typically room temperature) and $a_i$ and $b_i$ are mode- and material-specific constant coefficients. The dependence of the linewidth on temperature can be described by a quadratic equation in $T$ as

$$\frac{\gamma_i}{\nu_i}(T) = \frac{\gamma_i}{\nu_i}(T_0) + c_i[T - T_0] + d_i[T - T_0]^2, \tag{14c}$$

where $T_0$ is again a reference temperature and $c_i$ and $d_i$ are also mode- and

material-specific constant coefficients. The high-frequency permittivity, $\varepsilon_\infty$, is temperature dependent and is represented by

$$\varepsilon_\infty(T) = \varepsilon_\infty(T_0) + e_i[T - T_0]. \tag{14d}$$

Note that $e_i = d\varepsilon_\infty/dT = 2n_\infty(dn_\infty/dT)$; thus, in most cases, $e_i$ can be determined from visible $dn/dT$ measurements.

Table I lists the optical constants of $Y_2O_3$ based on the previously discussed formulas. The parameters are determined from reflection spectra as shown in Fig. 2. A comparison is made between the experimental data and the one-phonon-model representation. Other examples can be found in *HOC I*, Chapter 11. This model is important for spectral-emissivity calculations and index-of-refraction calculations from microwave to ultraviolet over a wide range of temperatures.

Differentiating Eq. 9 with respect to temperature gives an explicit formula for $dn/dT$, replacing Eq. 4 [5]. The value $\Delta\varepsilon$ depends linearly on the oscillator density and will lead to the term representing volume change with respect to temperature. Now the details of the polarizability term can be understood. For materials with strong polarizability and small volume expansion (for example, the oxides), the values of $dn/dT$ in the visible and

**TABLE I**

**Optical Constants of $Y_2O_3$**

| Mode | $\nu_i$ ($T_0$) ($cm^{-1}$) | $a_i$ ($cm^{-1}K^{-1}$) | $\Delta\varepsilon_i(T_0)$ | $b_i$ ($K^{-1}$) | $\gamma_i/\nu_i(T_0)$ | $c_i$ ($K^{-1}$) | $d_i$ ($K^{-1}$) |
|---|---|---|---|---|---|---|---|
| 1 | 120.0 | ~0.01 | 0.2 | — | 0.035 | — | — |
| 2 | 172.0 | ~0.01 | 0.1 | — | 0.025 | — | — |
| 3 | 182.0 | ~0.01 | 0.15 | — | 0.025 | — | — |
| 4 | 241.0 | 0.0072 | 0.200 | $7.10\times10^{-5}$ | 0.025 | $1.46\times10^{-5}$ | — |
| 5 | 303.0 | 0.0144 | 2.600 | $6.24\times10^{-4}$ | 0.0135 | $3.35\times10^{-5}$ | — |
| 6 | 335.0 | 0.0109 | 1.749 | $-3.55\times10^{-4}$ | 0.0115 | $2.38\times10^{-5}$ | — |
| 7 | 371.0 | 0.0109 | 2.651 | $6.38\times10^{-5}$ | 0.021 | $2.51\times10^{-5}$ | — |
| 8 | 415.0 | 0.0109 | 0.040 | $3.55\times10^{-5}$ | 0.011 | $3.24\times10^{-5}$ | — |
| 9 | 461.0 | 0.0144 | 0.050 | $3.55\times10^{-5}$ | 0.015 | $1.80\times10^{-5}$ | — |
| 10 | 490.0 | 0.0180 | 0.005 | $3.55\times10^{-6}$ | 0.018 | $2.12\times10^{-5}$ | — |
| 11 | 555.0 | 0.0210 | 0.095 | $9.36\times10^{-5}$ | 0.025 | $1.21\times10^{-5}$ | — |
| 12[b] | 72,100.0 | — | 2.579 | $1.40\times10^{-4}$ | — | — | — |

[a] $T_0 = 295$ K.
[b] Electronic transition.
$\varepsilon_\infty(T) = 1.00$.

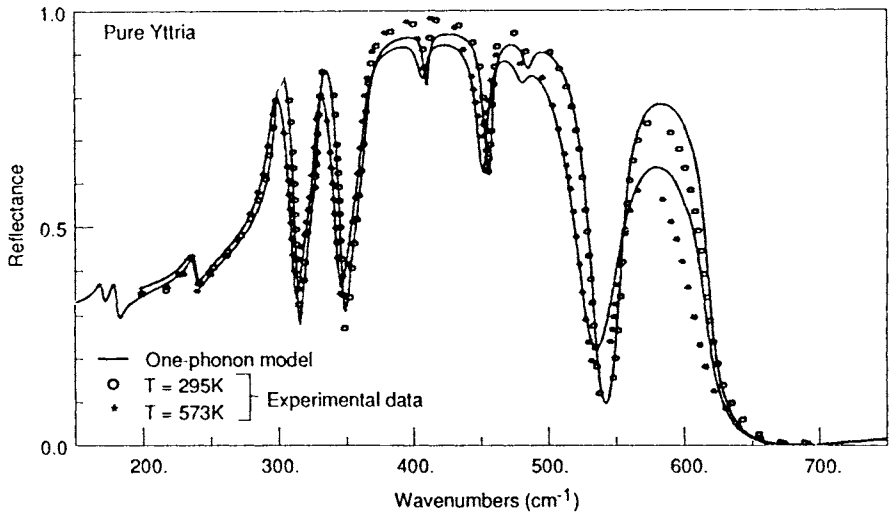


**Fig. 2.** Reflection spectra of pure yttria at two temperatures.

IR are small and positive. This is in contrast to previously discussed results for the alkali-halides and the fluorides. In the microwave region the static dielectric constant is used (see Eq. 10), which includes the contributions from the lattice vibrations. Thus, the value of the net polarizability can greatly increase, and $d\varepsilon_s/dT$ is usually positive. Figure 3 illustrates the experimental temperature dependence of $\varepsilon_s(T)$ for the ordinary-ray of sapphire [13–16]. The dashed curve shows the range of validity of the linear approximations used in obtaining Eq. 14b.

## Absorption near Transparency C

The classical pole-fit model represents the fundamental lattice vibrations or one-phonon transitions in a material. But the absorption coefficient obtained from the model is valid only in the vicinity of the one-phonon frequencies. The absorption coefficient needs to be known in the regions of transparency as well, requiring a description of multiphonon absorption bands in which more than one-phonon excitation occurs upon the absorption of a single photon. The mm-wave region is dominated by the one-phonon red wing and multiphonon difference bands. The IR region is dominated by multiphonon sum bands.

The absorption coefficient is expressed, in general, as

$$\beta_a(\nu, T) = \sum_{l} S_{lu}(T; \nu_{lu}) g(\nu, T; \nu_{lu}), \tag{15}$$

where $\nu_{lu}$ is the transition center frequency, $S_{lu}(T)$ is the transition strength, $g(\nu, T)$ is the spectral distribution function, and the sum is over all initial states. Based on the work of Kubo [17] and Van Vleck and Huber [18], the strength and shape functions are expressed as

$$S_{lu} = \frac{8\pi^3 \nu_{lu}}{3hn} \rho \frac{e^{-E_l/k_B T}}{Z(T)} (1 - e^{-hc\nu_{lu}/k_B T}) |\bar{M}|^2 \tag{16}$$

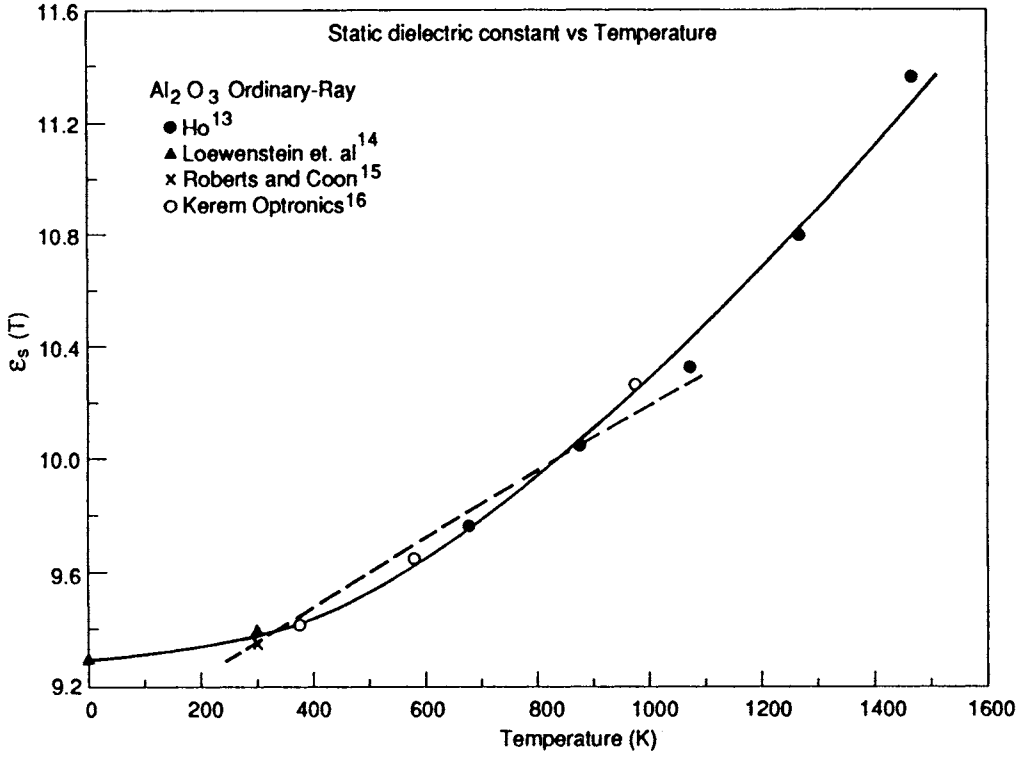


**Fig. 3.** The temperature dependence of the static dielectric constant of the ordinary-ray of $Al_2O_3$. The dash curve represents a linear approximation to the experimental data.

**TABLE II**

**The Far-Infrared Absorption-Coefficient Parameters for $T_0 = 295$ K**

| Material | $A(T_0)$ [cm] | $A_{1p}(T_0)$ [cm] | $A_{2p}$ [cm K$^{-1}$] | $A_{3p}$ [cm K$^{-2}$] |
|---|---|---|---|---|
| MgO | — | $6.1 \times 10^{-4}$ | | |
| $SiO_2$ o-ray | $1.07 \times 10^{-4}$ | $8.9 \times 10^{-5}$ | | |
| e-ray | $8.2 \times 10^{-5}$ | $1.39 \times 10^{-4}$ | | |
| $Al_2O_3$ o-ray | $9.15 \times 10^{-4}$ | $2.2 \times 10^{-4}$ | $4.7 \times 10^{-4}$ | $2.2 \times 10^{-4}$ |
| e-ray | $1.28 \times 10^{-3}$ | $8.6 \times 10^{-4}$ | | |
| $Y_2O_3$ | $2.1 \times 10^{-3}$ | $8.4 \times 10^{-4}$ | | |
| $MgAl_2O_4$ | $2.2 \times 10^{-3}$ | $1.6 \times 10^{-4}$ | | |
| ALON | $1.1 \times 10^{-3}$ | — | | |
| ZnS | $5.8 \times 10^{-4}$ | $9.8 \times 10^{-4}$ | | |
| NaCl | $1.2 \times 10^{-2}$ | $3.0 \times 10^{-3}$ | $9.0 \times 10^{-3}$ | |

and

$$g(\nu, T) = \frac{\nu}{\nu_{lu}} \frac{(1 - e^{-hc\nu/k_B T})}{(1 - e^{-hc\nu_{lu}/k_B T})} j(\nu), \tag{17}$$

where $h$ is Planck's constant, $\rho$ is the density of dipoles per unit volume, $E_l$ is the lower energy of the transition, $Z(T)$ is the partition function, $k_B$ is Boltzmann's constant, $|\bar{M}|^2$ is the dipole matrix element, and $j(\nu)$ is the Fourier transform of the dipole autocorrelation function. On the basis of this theory, the low-frequency (that is, $\leq 50\ \text{cm}^{-1}$) absorption coefficient is $\nu^2$ multiplied by the line-shape function. A simple $\nu^2$ falloff will dominate in two cases. The first is the far red wing of an absorption band and the second is for broad line-shape functions featuring very little frequency dependence throughout a band. These conditions are met for many materials of interest in the far infrared, because the absorption is dominated by intrinsic processes. Thus, the simple formula

$$\beta_a(\nu) = A\nu^2 \tag{18}$$

can be used to represent experimental data of these materials.

Based on Eq. 9, the one-phonon red wing ($\nu \to 0$) becomes

$$\beta_{1p}(\nu \to 0, T) = \left[ \frac{2\pi}{n(0, T)} \sum_i \frac{\Delta\varepsilon_i(T)\gamma_i(\nu, T)}{\nu_i^2(T)} \right] \nu^2. \tag{19}$$

Even though Eq. 9 comes from a phenomenological model, this extrapolation to the red wing works for many materials (see Table II). In addition to the one-phonon contributions, difference bands of two and three phonons must also be included. Detailed models are extremely difficult to obtain, and thus only empirical formulas are used. It is straightforward to show, however, in the high-temperature limit ($hc\nu \ll k_B T$) that the $n$-phonon difference-band temperature dependence goes as [19]

$$\beta_{np} = A_{np} T^{n-1} \nu^2. \tag{20}$$

Thus, experimental data in this high-temperature limit can be represented by the formula

$$\beta_a(\nu, T) = \sum_n \beta_{np}(\nu, T) \tag{21}$$

and

$$\beta_a(\nu, T) \underset{\nu \to 0}{=} \left[ \frac{2\pi}{n(0, T)} \sum_i \frac{\Delta\varepsilon_i(T)\gamma_i(\nu, T)}{\nu_i^2(T)} + A_{2p}T + A_{3p}T^2 \right] \nu^2 \tag{22}$$

$$= A(T)\nu^2.$$

Based on Eq. 22, the far-infrared absorption coefficient increases with increasing temperature. Temperature-dependent data are needed to determine the contributions from two-phonon and three-phonon difference bands. Figure 4 compares experimental data for sapphire [14, 15, 20] to the model based on the parameters given in Table II [14, 15, 20–22] and Eq. 22. A good fit is obtained from above 200K to 1000K for a variety of wave numbers. The fact that the absorption coefficient does not go to zero as the temperature goes to zero is a clear indication of the existence of the one-phonon red wing. The one-phonon red wing is frequently ignored in interpreting far-infrared absorption data [19], and this is not correct. Extrapolation to lower frequencies more typical of mm-wave frequencies

work reasonably well at room temperature [23]. However, the temperature dependence may change because three-phonon contributions will be greater at frequencies below two-phonon absorption than this simple model represents. This fact is demonstrated in Fig. 4; the model underestimates the experimental absorption coefficients at $50\,cm^{-1}$ at elevated temperatures. A more rapid temperature dependence is needed at $50\,cm^{-1}$ than is observed at $100\,cm^{-1}$ or $200\,cm^{-1}$. This is consistent with an increasing contribution to the absorption from three-phonon difference bands with decreasing frequency.

The absorption coefficient also increases with increasing temperature at the infrared edge of transparency. This region is dominated by multipho-

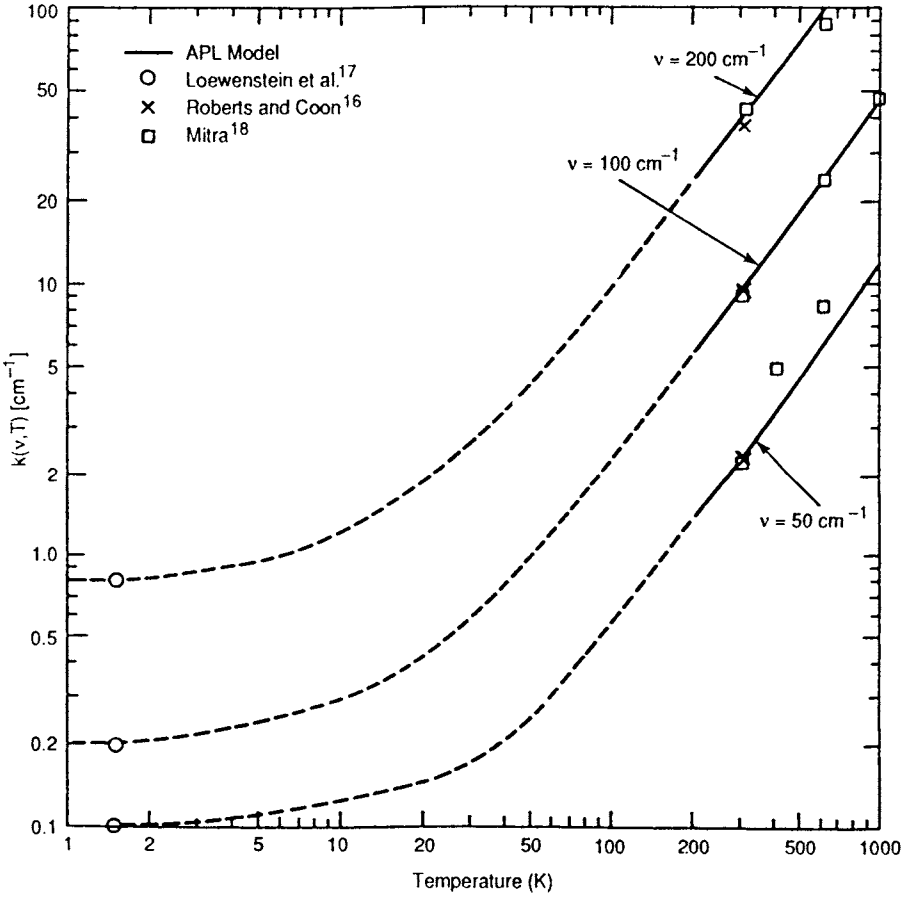


**Fig. 4.** Comparison of experimental data to the APL model for the far-infrared absorption coefficient as a function of temperature and frequency, for the ordinary-ray of $Al_2O_3$.

non sum bands. Fortunately, in this case, there are theoretical models that accurately characterize the absorption loss, and one such model requires only a few material-dependent parameters.

There are several models that have been developed to describe multiphonon absorption [24–28]. Criteria of simplicity, minimum number of parameters, and general applicability have led to models based on the Morse interatomic potential, which is given by

$$V(r) = D(1 - \exp[-a(r - r_0)])^2. \tag{23}$$

$D$ is the dissociation energy, $r_0$ is the location of the equilibrium position, $a = \omega_0(\mu/2D)^{1/2}$, $\omega_0$ is the fundamental lattice-vibration frequency, and $\mu$ is the reduced mass. Both classical [24, 25] and quantum-mechanical [26–28] models exist. The Morse potential leads to an exact solution of the Schrödinger equation and includes anharmonic effects to all orders. These characteristics greatly simplify the model. The strong anharmonic nature of the true potential means that the harmonic-oscillator perturbational approaches have questionable validity and require major correction factors.

A brief discussion of the quantum-mechanical, Morse-potential, multiphonon model is presented in the following. Assumptions used in the model, besides use of the Morse potential, are as follows:

(1) A single generalized dissociation energy is sufficient.
(2) No impurities and defects are considered.
(3) Phonon density-of-state functions quickly approach the Gaussian form dictated by the central-limit theorem as the order of the harmonic increases.

The solution of the stationary-state Schrödinger wave equation using the Morse potential results in the following energy eigenvalues [26]:

$$E_m = \hbar\omega_0\left[\left(m + \frac{1}{2}\right) - \frac{1}{J}\left(m + \frac{1}{2}\right)^2\right], \tag{24}$$

where $\hbar = h/2\pi$, $J = (4D/\hbar\omega_0)$, and $m$ is an integer, so that $m = 0, 1, 2, \ldots,$ $m_{\max} \leqslant 1/2\ (J - 1)$.

Based on Eqs. 15–17, the absorption coefficient $\beta_a$ as a function of temperature $T$ and wave number $\nu$ is

$$\beta_a(\nu, T) = \frac{8\pi^3 \rho \nu}{3hZn}[1 - \exp(-hc\nu/k_B T)]$$

$$\times \sum_{n=1}^{\infty} \sum_{m=0}^{m_{\max}-n} \exp(-E_m/k_B T)|M_{m(n+m)}|^2 j(\nu - \nu_{nm}), \qquad (25)$$

where

$$\nu_{nm} = \frac{E_{n+m} - E_m}{hc} = \nu_0 \left[ n - \frac{1}{J}(n^2 + 2nm + n) \right] = N\nu_0. \qquad (26)$$

For the case of $m \ll J$ (that is, below the material melting temperature),

$$|M_{m(n+m)}|^2 \approx \frac{e^2 h}{8\pi^2 c \nu_0 \mu} \frac{(m+n)!}{m! n^2 J^{(n-1)}}. \qquad (27)$$

Substituting this result into Eq. 25 produces

$$\beta_a(\nu, T) = K \frac{\nu[1 - \exp(-\beta)]}{\nu_0 Z'} \sum_{n=1}^{\infty} \frac{1}{n^2} J^{-(n-1)} \sum_{m=0}^{m_{\max}-n}$$

$$\times \frac{(m+n)!}{m!} \exp(-\gamma M) j(\nu - \nu_{nm}), \qquad (28)$$

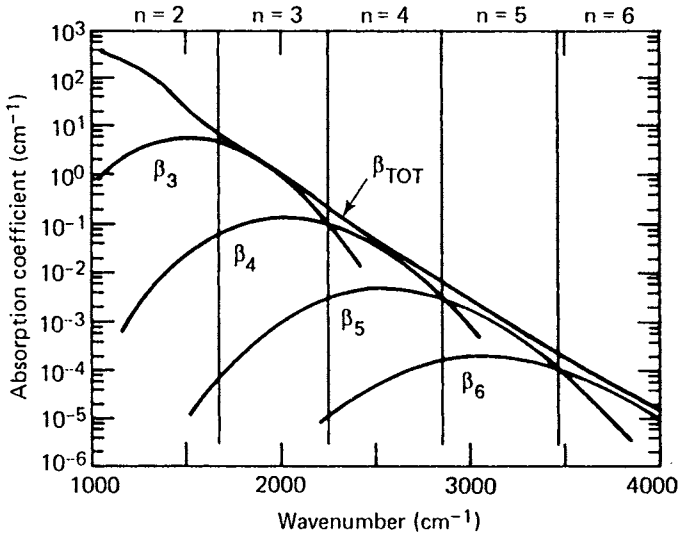


**Fig. 5.** The $n$-phonon absorption regions for room-temperature sapphire.

where

$$\beta = \frac{hc\nu}{k_B T},$$

$$Z' = \sum_{m=0}^{m_{\max}} \exp(-\gamma M),$$

$$\gamma = \frac{hc\nu_0}{k_B T},$$

$$K = \frac{\pi \rho e^2}{3c\mu n},$$

$$M = m\left(1 - \frac{1}{J}\right) - \frac{m^2}{J}.$$

In the continuum limit $J \to \infty$ ($hc\nu \ll 4D$) and for $T$ large ($\gamma \ll 1$), the

absorption coefficient reduces to

$$\beta_a(n\nu_0, T) \simeq Kn! \left(\frac{k_B T}{4D}\right)^{n-1} j(0), \tag{29}$$

which agrees with the classical result [24].

Following the development of Boyer *et al.* [26], the transition line shape $[j(\nu - \nu_{nm})]$ is considerably narrower than the density-of-states distribution and is approximated by a delta function. The net absorption is the integration over all appropriately weighted oscillators.

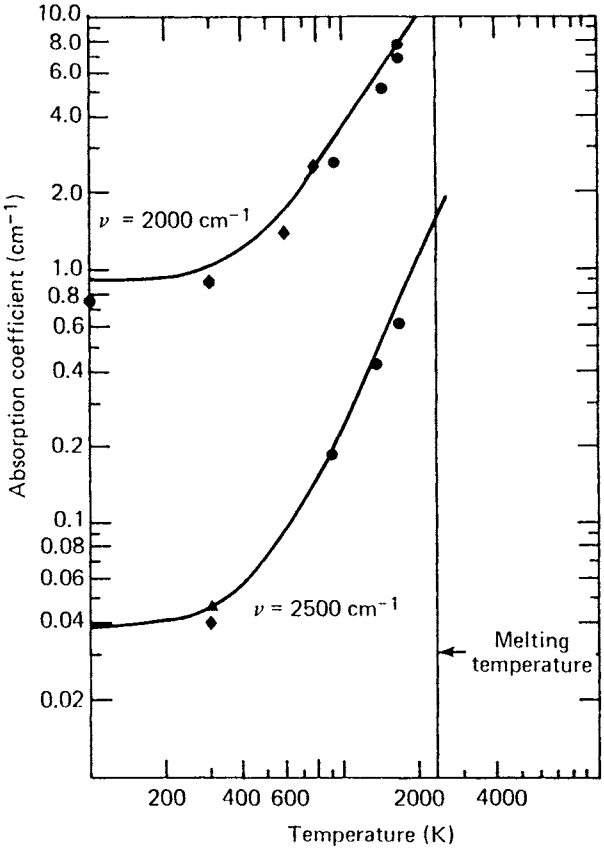


**Fig. 6.** Temperature dependence of the multiphonon absorption coefficient at fixed wave numbers for $Al_2O_3$ (▲ Deutsch [32], ● Billard *et al.* [29] and ◆ Thomas *et al.* [3]).

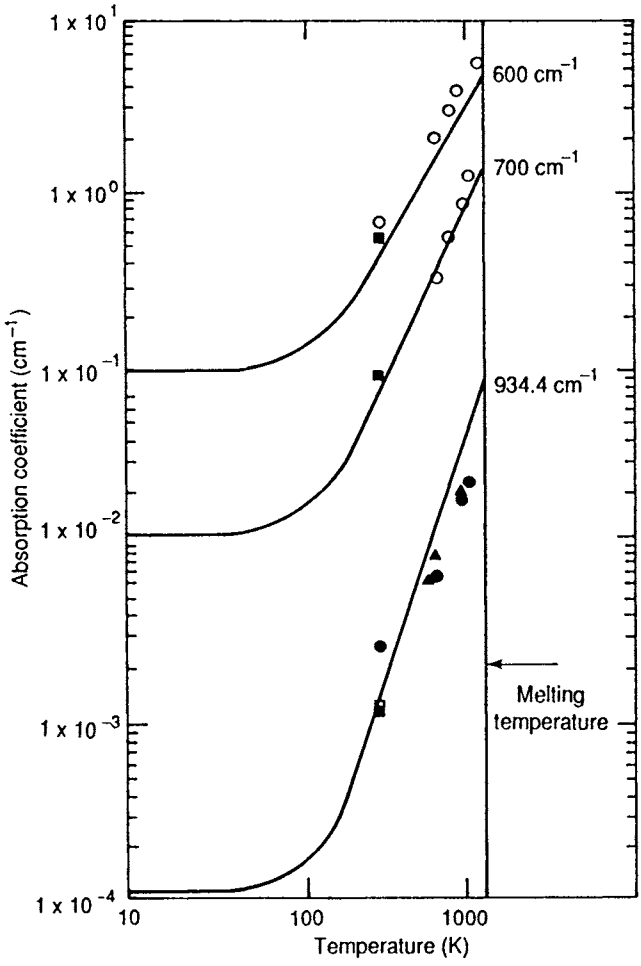


**Fig. 7.** Temperature dependence of the multiphonon absorption coefficient at fixed wave numbers for NaCl (□ Boyer *et al.* [26], ● Namjoshi and Mitra [20], ■ Deutsch [32], ○ Barker [33], and ▲ Harrington and Hass [34]).

$$\beta_{\text{tot}}(\nu, T) = \int_0^\infty d\nu_0 \beta(\nu_0, T)\rho_n(\nu_{nm})$$

$$= K[1-\exp(-\beta)] \sum_{n=1}^{\infty} \frac{\rho_n(\nu)}{n^2 Z'} \sum_{m=0}^{m_{\max}-n} \frac{(m+n)!}{m!} \frac{\exp[-\beta(M/N)}{J^{(n-1)}} \tag{30}$$

$$= \sum_{n=1}^{\infty} k_n(\nu, T),$$

where

$$Z' = \sum_{m=0}^{m_{\max}} \exp\left[-\beta\left(\frac{M}{N}\right)\right], \qquad J = \frac{4DN}{hc\nu},$$

and $\rho_n(\nu)$, the $n$-phonon density of states, is given by

$$\rho_n(\nu) = \int_0^\infty d\nu'' \int_0^\infty d\nu' \, \rho_{n-1}(\nu')\rho_1(\nu'')\delta(\nu - \nu' - \nu''), \tag{31}$$

where $\delta(\ )$ is the delta function. The value $\rho_n(\nu)$ is the probability of finding $n$-phonons in the lattice whose energies add up to $hc\nu$. It is required

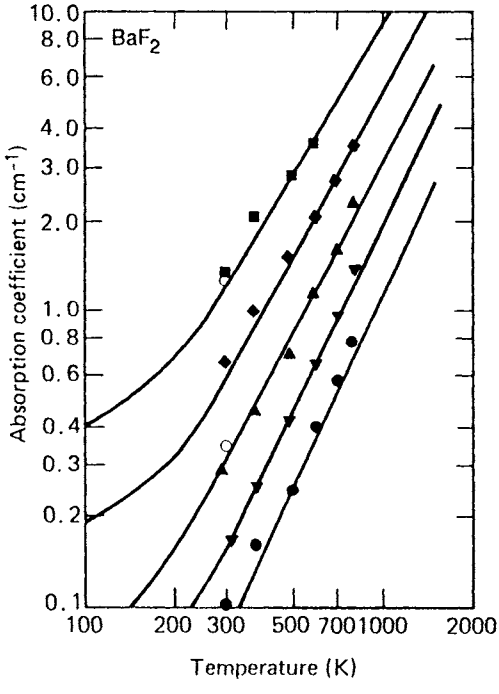


**Fig. 8.** Temperature dependence of the multiphonon absorption coefficient at fixed wave numbers for $BaF_2$ [34, 35] (○ Deutsch [32], ● $\nu = 1000\,cm^{-1}$, ▼ $\nu = 950\,cm^{-1}$, ▲ $\nu = 900\,cm^{-1}$, ◆ $\nu = 850\,cm^{-1}$, ■ $\nu = 800\,cm^{-1}$, and — multiphonon model [6]).

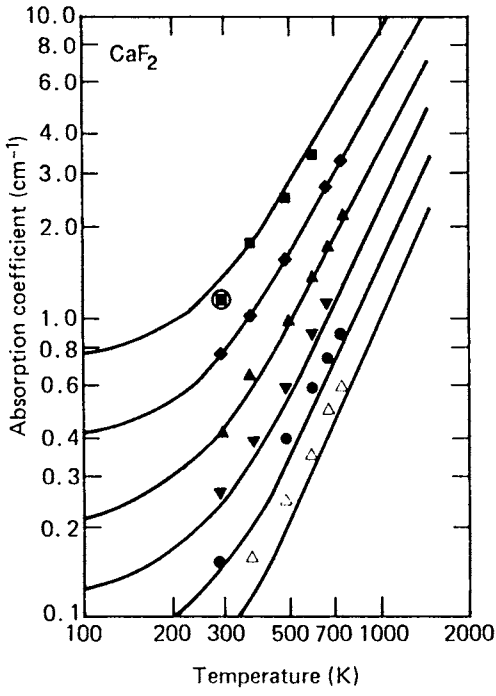


**Fig. 9.** Temperature dependence of the multiphonon absorption coefficient at fixed wave numbers for $CaF_2$ [34, 35] (○ Deutsch [32], △ $\nu = 1300\,cm^{-1}$, ● $\nu = 1050\,cm^{-1}$, ▼ $\nu = 1200\,cm^{-1}$, ▲ $\nu = 1150\,cm^{-1}$, ◆ $\nu = 1100\,cm^{-1}$, ■ $\nu = 1050\,cm^{-1}$ and — multiphonon model [6]).

that

$$\int_0^\infty \rho_1(\nu)\, d\nu = 1. \tag{32}$$

Using Eq. 31, it can be shown that all $\rho_n(\nu)$ values normalize to unity. As $n$ increases, $\rho_n(\nu)$ rapidly becomes Gaussian. This is a manifestation of the central-limit theorem. (For sapphire, even $\rho_2(\nu)$ can be somewhat approximated by a Gaussian profile [29].) Based on the results of Boyer *et al.* [26], Sparks and Sham [28], and the asymptotic expansion of the central-limit theorem [30], $\rho_n(\nu)$ can be represented by the form

$$\rho_n(\nu) = \frac{1}{\sigma'\sqrt{2\pi}}\left[1 - \frac{\alpha_3}{\sqrt{n}}(3x - x^3)\right]\exp(-x^2/2);\ n \geq 3, \tag{33}$$

where

$$x = \frac{\nu - n\alpha_1 \nu_m}{\sigma'},$$

$$\sigma' = \alpha_2 \nu_m \sqrt{n},$$

$$\alpha_1 = \frac{\langle \nu \rangle}{\nu_m},$$

$$\alpha_2 = \frac{(\langle \nu^2 \rangle - \langle \nu \rangle^2)^{1/2}}{\nu_m},$$

$$\alpha_3 = \frac{\langle \nu^3 \rangle - 3\langle \nu^2 \rangle \langle \nu \rangle + 2\langle \nu \rangle^3}{6(\langle \nu^2 \rangle - \langle \nu \rangle^2)^{3/2}},$$

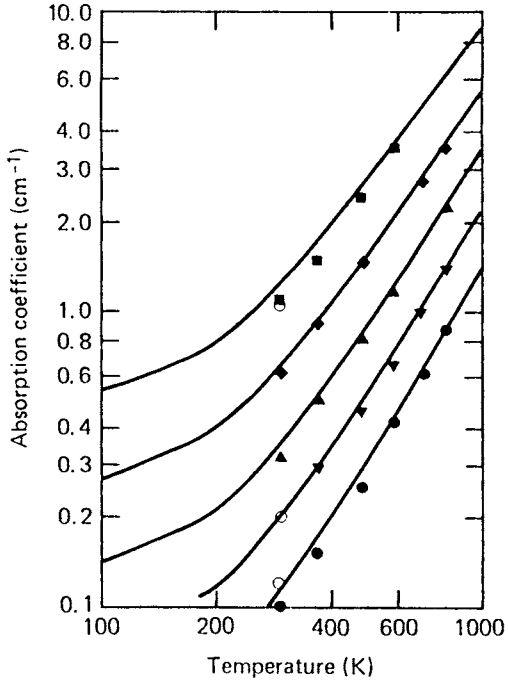


**Fig. 10.** Temperature dependence of the multiphonon absorption coefficient at fixed wave numbers for $SrF_2$ [34, 35] (○ Deutsch [32], ● $\nu = 1100\,cm^{-1}$, ▼ $\nu = 1050\,cm^{-1}$, ▲ $\nu = 1000\,cm^{-1}$, ◆ $\nu = 950\,cm^{-1}$, ■ $\nu = 900\,cm^{-1}$ and — multiphonon model [6]).

and

$$\langle \nu^r \rangle = \int_0^\infty d\nu \, \rho_1(\nu) \nu^r, \qquad r = 1, 2, 3.$$

Here $\nu_m$ is the maximum fundamental lattice-vibration frequency. It is taken to be the maximum longitudinal-optical-mode frequency of the crystal. The value of $\nu_m$ is determined experimentally for each material from the reflection spectrum. A derivative reflection-spectroscopy technique developed at The Johns Hopkins University/Applied Physics Laboratory [31] has been used to determine the values.

The shape of the distribution is determined by three parameters: $\alpha_1$, the distribution mean normalized by $\nu_m$; $\alpha_2$, the distribution standard deviation normalized by $\nu_m$; and $\alpha_3$, the distribution skewness divided by six. The parameters $\alpha_1$, $\alpha_2$, and $\alpha_3$ are directly determined from $\rho_1(\nu)$ as indicated by Billard *et al.* [29] for sapphire. The results are $\alpha_1 = 0.537$, $\alpha_2 = 0.213$, and $\alpha_3 = 0.052$. However, in practice the $\alpha_2$ parameter requires modification, because the true phonon distribution function, $\rho_n(\nu)$, goes to zero at $n\nu_m$. Thus, the value for $\alpha_2$ is too large and can artificially produce steps in the net absorption coefficient caused by the assumption of a Gaussian phonon-distribution function. Based on sapphire absorption data, a simple but effective empirical correction is used. Let $\alpha_2 = 0.153$ and multiply the strength by $N$ to correct for the increased slope in $\beta_a$ caused by the narrower $\rho_n(\nu)$. In this way, a smooth and realistic representation of the absorption coefficient is obtained.

Figure 5 illustrates the structure of $\beta_{\text{tot}}(\nu, T)$ in terms of $\beta_n(\nu, T)$, the absorption coefficient of a single $n$-phonon process. There are spectral regions in which a single $n$-phonon absorption process dominates. The individual $\beta_n$ values are nearly Gaussian in shape, yet the sum produces a nearly exponential curve for $\beta_{\text{tot}}$, as observed in experiment.

Now the temperature dependence of the multiphonon sum-band edge can be understood in a straightforward way. From very low temperature to roughly room temperature, the absorption coefficient is nearly constant, because the population of the majority of oscillators are in the ground state ($m = 0$). At high temperature, when the upper levels achieve enough population, then photon absorption for $m > 0$ becomes important. Also, the dipole matrix element increases with increasing $m$. Thus, the absorption coefficient increases with temperature basically as Eq. 29 dictates in this high-temperature regime. Figures 6–10 illustrate this point by comparing model predictions against experimental data for $Al_2O_3$ [3, 29, 32], NaCl [6, 26, 20, 32, 33, 34], $BaF_2$, $CaF_2$, and $SrF_2$ [32, 35, 36], respectively. This multiphonon sum-band model has been applied to a variety of window

materials [6]. Three parameters are needed to specify a material; $K$, the scaling constant representing the dipole density; $D$, the dissociation energy; and $\nu_m$, the maximum longitudinal-optical-mode frequency. All of these parameters can be determined from room-temperature measurements. Thus, the model provides a means of predicting $\beta_a(\nu, T)$ as a function of temperature for a material with known $\beta_a(\nu, T_0)$ at a fixed temperature $T_0$.

## CONCLUSIONS III

The previously presented models provide more than physical insight into the optical properties of materials. Because of the physical basis for the theories, meaningful interpolations and extrapolations can be made as a function of frequency and temperature. Furthermore, the models provide a precise and convenient means of communicating optical-properties data and represent an improvement over conventional figures and tables. The formulas are easily programmed on a computer, providing quick and easy access to the complex index of refraction. These results can be used further to calculate transmittance, reflectance, absorptance and emittance of bulk materials and thin films.

Efforts at JHU/APL, utilizing this approach to optical properties characterization, have resulted in the FORTRAN-based computer code PHONONB. This work is continuing and more comprehensive versions will be available in the future.

### REFERENCES

1. T. Skettrup, "Urbach's Rule Derived From Thermal Fluctuations in the Band Gap Energy," *Phys. Rev. B* **18**, 2622 (1978).
2. E. D. Palik, ed., "Handbook of Optical Constants of Solids," Academic Press, New York, (1985).
3. M. E. Thomas, R. I. Joseph, and W. J. Tropf, "Infrared Transmission Properties of Sapphire, Spinel, Yttria and ALON as a Function of Temperature and Frequency," *Appl. Opt.* **27**, 239 (1988).
4. A. J. Bosman and E. E. Havinga, "Temperature Dependence of Dielectric Constants of Cubic Ionic Compounds," *Phys. Rev.* **129**, 1593 (1963).
5. H. H. Li, "Refractive Index of Alkali Halides," *J. Phys. Chem. Ref. Data,* **5**, 329 (1976).
6. M. E. Thomas and R. I. Joseph, "A Comprehensive Model for the Intrinsic Transmission Properties of Optical Windows," in *Infrared Optical Materials, Proc. SPIE* **929**, 87 (1988).
7. F. Gervais and B. Piriou, "Temperature Dependence of Transverse- and Longitudinal-Optic Modes in $TiO_2$ (Rutile)," *Phys. Rev. B* **10** 1642 (1974).
8. R. H. Lyddane, R. G. Sachs, and E. Teller, "On the Polar Vibrations of Alkali Halides," *Phys. Rev.* **59**, 673 (1941).

9. J. R. Jasperse, A. Kahan, J. N. Plendly, and S. S. Mitra, "Temperature Dependence of Infrared Dispersion in Ionic Crystals LiF and MgO," *Phys. Rev.* **146**, 526–542 (1966).
10. A. A. Maradudin, J. P. Ipatoua, and R. F. Wallis, "Temperature Dependence of the Width of the Fundamental Lattice-Vibration Absorption Peak in Ionic Crystals II. Approximate Numerical Results," *Phys. Rev.* **155**, 882 (1967).
11. R. F. Wallis and A. A. Maradudin, "Lattice Anharmonicity and Optical Absorption in Polar Crystals: III. Quantum Mechanical Treatment in the Linear Approximation," *Phys. Rev.* **125**, 1277 (1962).
12. B. Szigeti, "Higher-Order Terms in the Dielectric Constant of Ionic Crystals," *Proc. Roy. Soc. A* **252**, 217 (1959).
13. W. W. Ho, "High-Temperature Dielectric Properties of Polycrystalline Ceramics," MRS Symposium M, April 6, 1988.
14. E. V. Loewenstein, D. R. Smith, and R. L. Morgan, "Optical Constants of Far-Infrared Materials 2: Crystalline Solids," *Appl. Opt.* **12**, 398 (1973).
15. S. Roberts and D. D. Coon, "Far-Infrared Properties of Quartz and Sapphire," *J. Opt. Soc. Am.*, **52**, 1023 (1962).
16. Kerem Optronics, Manufacturer's data sheet.
17. Kubo, R., "Lectures in theoretical physics," Vol. I, (W. E. Britten and L. G. Dunham, eds.), Interscience, New York, 151 (1959).
18. J. H. Van Vleck and D. L. Huber, "Absorption Emission and Linebreadths: A Semihistorical Perspective," *Rev. Mod. Phys.*, **49**, 939 (1977).
19. R. Stolen and K. Dransfedl, "Far-Infrared Lattice Absorption in Alkali Halide Crystals," *Phys. Rev.* **139**, 3A1295 (1965).
20. S. S. Mitra, in "Optical Properties of Nonmetallic Solids for Photon Energies Below the Fundamental Band Gap," in "Handbook of Optical Constants," (E. D. Palik, ed.), Academic Press, New York, 213 (1985).
21. M. Stead and G. Simonis, "Near Millimeter Wave Characterization of Dual Mode Materials," *Appl. Opt.* **28**, 1874 (1989).
22. J. R. Hardy and A. M. Karo, "Theoretical Study of the Long-Wavelength Optical Properties of NaCl, KCl, KBr and KI," *Phys. Rev. B* **26**, 3327 (1982).
23. M. E. Thomas, R. I. Joseph, G. J. Simonis, and M. Stead, "Characterization of the Infrared and Far-Infrared Properties of Sapphire and Quartz," in "13th International Conf. on Infrared and Millimeter Waves," (R. J. Temkin, ed.), *SPIE Conf. Digest* **1039**, 339 (1988).
24. D. L. Mills and A. A. Maradudin, "Theory of Infrared Absorption by Crystals in the High Frequency Wing of Their Fundamental Lattice Absorption," *Phys. Rev. B* **8**, 1617 (1973).
25. A. A. Maradudin and D. L. Mills, "Temperature Dependence of the Absorption Coefficient of Alkali Halides in the Multiphonon Regime," *Phys. Rev. Lett.* **31**, 718 (1973).
26. L. L. Boyer, J. A. Harrington, M. Hass, and H. B. Rosenstock, "Multiphonon Absorption in Ionic Crystals," *Phys. Rev. B* **11**, 1665–1679 (1975).
27. H. B. Rosenstock, "Multiphonon Absorption in Alkali Halides: Quantum Treatment of Morse Potential," *Phys. Rev. B* **9**, 1963 (1974).
28. M. Sparks and L. J. Sham, "Theory of Multiphonon Absorption in Insulating Crystals," *Phys. Rev. B* **8**, 3037 (1973).
29. D. Billard, F. Gervais, and B. Piriou, "Analysis of Multiphonon Absorption in Corundum," *Phys. Status Solidi B* **75**, 117 (1976).
30. H. Cramer, "Random Variables and Probability Distributions," Cambridge University Press, London (1970).
31. R. I. Joseph and M. E. Thomas, "Differential Reflection Spectroscopy: A Direct Determination of Long Wavelength Optical Mode Frequencies in Polar Crystals," *Phys. Status Solidi B* **141**, K163 (1987).

32. T. F. Deutsch, "Absorption Coefficient of Infrared Laser Window Materials," *J. Phys. Chem. Solids* **34**, 2091 (1973).
33. A. J. Barker, "The Effect of Melting on the Multiphonon Infrared Absorption Spectra of KBr, NaCl, and LiF," *J. Phys. C* **5**, 2276 (1972).
34. J. A. Harrington and M. Hass, "Temperature Dependence of Multiphonon Absorption," *Phys. Rev. Lett.* **31**, 710 (1973).
35. H. G. Lipson, B. Bendow, N. E. Massa, and S. S. Mitra, "Multiphonon Infrared Absorption in the Transparent Regime of Alkaline-Earth Fluorides," *Phys. Rev. B* **13**, 2614 (1976).
36. M. E. Thomas, "A Computer Code for Modeling Optical Properties of Window Materials," in Window and Dome Technologies and Materials, *Proc. of SPIE*, **1112**, 260–267 (1989).

# Chapter 9

# Measurement of $n$ and $k$ in the XUV by the Angle-of-Incidence, Total-External-Reflectance Method

MARION L. SCOTT
Los Alamos National Laboratory
Los Alamos, New Mexico

I. Introduction 203
II. General Considerations 204
A. Contamination and Surface Roughness 204
B. Vacuum Deposition and In Situ Reflectance Measurement 205
C. Potential Errors 206
III. Aluminum Reflectance versus Angle in UHV 206
IV. Determination of $n$ and $k$ 207
A. Thin-Film Thickness 208
B. Sensitivity to $n$ and $k$ 208
C. Results at 58.4 nm and 30.4 nm 210
V. Comparison with Other Results 210
A. Aluminum at 58.4 nm 210
B. Aluminum at 30.4 nm 211
C. Drude Free-Electron Model 211
D. Discussion 212
References 212

## I INTRODUCTION

Many methods have been developed and employed over the years to determine the optical constants of materials. Not all of these methods are useful in the extreme ultraviolet (XUV) due to the lack of appropriate optics such as quarterwave plates; the high absorption of materials; and the extreme dispersion in both $n$ and $k$ typical of this spectral region. Another complication inherent in making measurements in the XUV is the absorption of air in this spectral region, which necessitates the use of vacuum chambers for any optical measurements to be performed.

HANDBOOK OF OPTICAL CONSTANTS OF SOLIDS II

Copyright © 1991 by Academic Press.
All rights of reproduction in any form reserved.
ISBN 0-12-544422-2

The phenomenon of total external reflectance, although not unique to the XUV spectrum, is encountered in many materials in this wavelength range. This effect is analogous to total internal reflectance observed in the visible spectrum when light propagating in a dense medium (such as glass) is obliquely incident at an interface between this dense medium and a less dense medium (such as vacuum). Since the light in the less dense medium refracts away from the normal to the interface, there exists an incident angle, called the critical angle, where the refracted angle is 90 degrees. Light incident at any angle greater than this critical angle cannot be transmitted into the second medium, and in the absence of absorption, total internal reflectance is observed at the interface. If the incident-medium index of refraction is $n_1$ and the exit-medium index of refraction is $n_2$, the critical angle, $\theta_c$, is given by

$$\theta_c = \sin^{-1}[n_2/n_1]. \tag{1}$$

Total external reflectance generally occurs when light is incident in a vacuum onto a material that has the real part of its index of refraction, $n$, less than unity. The imaginary part of the complex index of refraction, $k$, which represents absorption, is never zero for these materials, but is sometimes quite small. In these cases, the critical angle is still defined by Eq. 1, but the reflectance at the interface rises to a value less than 100% at incidence angles greater than the critical angle, due to the presence of absorption. The existence of total external reflectance at a given wavelength for a specific material then implies that the complex index of refraction can be determined quite accurately by making measurements of reflectance versus angle of incidence and performing the necessary analysis. In this chapter, aluminum will be used as a specific example of this technique for the determination of $n$ and $k$.

## II GENERAL CONSIDERATIONS

There are several general considerations concerning the determination of the optical constants of a material in the XUV that should be discussed prior to a discussion of this particular method.

### A Contamination and Surface Roughness

One of the complications in using any reflection or transmission method for the determination of the optical constants of a material in the XUV is

the potential presence of contamination layers on the surface of the material. Any analysis of the reflectance data to obtain optical constants for this material must accurately include this surface contamination layer or the surface layer must be removed before measurements are attempted. The principal contamination layer on vacuum-deposited aluminum films is aluminum oxide, and a method of dealing with this oxide layer will be discussed in Section II.B.

Surface roughness of the material to be measured should be minimized for two reasons. First, surface roughness leads to optical scattering losses, which will effectively reduce the measured reflectance from the material with subsequent errors in the determination of $n$ and $k$ for the material. Second, surface roughness can cause coupling to surface plasmons in the material being measured at a characteristic wavelength. In the vicinity of this characteristic wavelength, the reflectance measurements of this material can be considerably lower than that expected from a simple interface, resulting in errors in the data analysis. Both of these effects are negligible for a thin film of material deposited on a highly polished (smooth) substrate with an rms roughness of 0.7 nm or less. These effects are discussed in detail in Ref. [1].

## B Vacuum Deposition and In Situ Reflectance Measurement

Simple vacuum deposition of a material is no guarantee that the material will not have a surface contamination layer. In particular, a monolayer of oxide will form on a freshly deposited aluminum layer exposed to $2 \times 10^{-8}$ torr of oxygen in one hour [2]. Thus, to avoid oxide formation, aluminum must be deposited in an ultrahigh-vacuum (UHV) system and maintained in this UHV environment during measurement. The system utilized in Ref. [2] for making reflectance measurements on aluminum had a base pressure of $2 \times 10^{-10}$ torr. In addition, the vacuum system should be pumped with oil-free pumps (sorption, ion, cryo) to avoid surface contamination by carbon layers.

The requirement for surface-contamination control and the consequent requirement for the maintenance of the sample in a UHV environment implies the need for an in situ XUV reflectometer to perform the reflectance measurements. This in situ reflectometer requires an XUV source, monochromator, and detector, as well as appropriate sample and detector manipulators. One method of accomplishing this would be to attach a deposition and analysis chamber to a synchrotron source, such as the SURF facility at NIST, Gaithersburg. The method utilized in Ref. [2] was to attach a capillary gas-discharge source and monochromator to a UHV deposition and analysis chamber.

### C Potential Errors

There are potential systematic errors in the measurement of $n$ and $k$ using the angle-of-incidence, total-external-reflectance (AOITER) method. An example of one of these potential errors arises from changes in beam intensity during the course of making a complete set of angular reflectance measurements. This error is minimized if the beam is measured before *and* after the angular reflectance measurements, so that a suitable average can be used to normalize the reflectance data.

The polarization of the XUV beam (if unknown) is also a potential source of error in analyzing the AOITER data for values of $n$ and $k$. In the case of a synchrotron source, the XUV beam starts out as a linearly polarized beam, and this polarization can be maintained in a carefully designed transport and monochromator system. In the case of gas-discharge sources, the XUV beam starts out as unpolarized, and some polarizing effects may be introduced by the beam-transport or monochromator system. This effect is less pronounced when the beam is incident at grazing angles on all optics.

Another example of a potential error that can occur is a spatially nonuniform detector sensitivity. This error can be minimized by always requiring that the reflected beam strike the same spot on the detector. This requirement is greatly simplified if an imaging microchannel-plate detector is used. Similarly, maintaining the same beam spot size during all measurements by keeping the source-to-detector distance the same is very important. Other potential error sources include angular misalignments, inadequate vacuum level, impurities in the evaporated material, and so on. Careful control of these potential errors will allow the measurement error to be determined primarily by the repeatability of the measurement.

## III ALUMINUM REFLECTANCE VERSUS ANGLE IN UHV

In order to describe adequately the AOITER method of determining $n$ and $k$ for a material in the XUV, aluminum will be used as an example. The reflectance versus angle of incidence for an aluminum film freshly deposited in a UHV system has been measured in situ at XUV wavelengths of 58.4 nm [2] and 30.4 nm [3]. These measurements were accomplished by rotating the coated sample and a microchannel-plate detector in synchronism to achieve an angular incidence from 10° to 85° with an interval of 5°. The sample is manipulated out of the XUV beam in order to measure the incident beam intensity. The resulting reflectance versus angle-of-

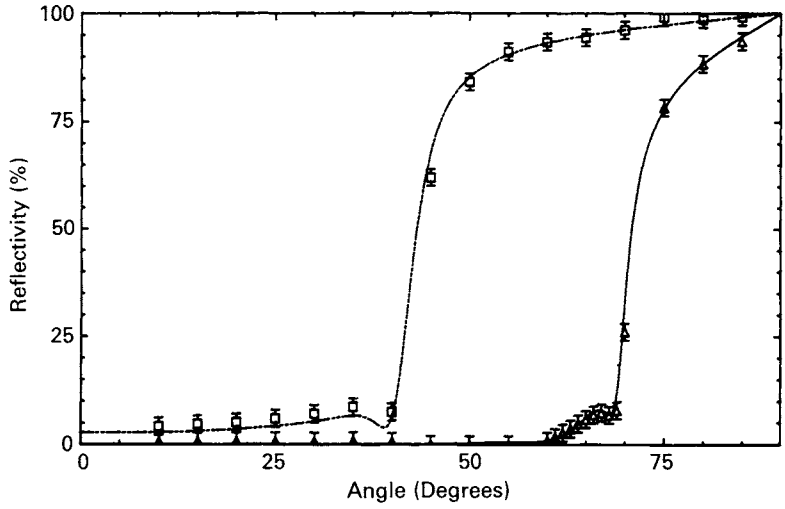


**Fig. 1.** Reflectance versus incidence angle for UHV aluminum film at 58.4 nm (squares) and at 30.4 nm (triangles). Note the rapid rise in reflectance at the critical angles (44.4 degrees for 58.4 nm and 70.7 degrees for 30.4 nm). The aluminum film thickness in these fits is 70 nm.

incidence curves for aluminum at 58.4 nm and 30.4 nm are shown in Fig. 1. The 1° increments between 60° and 70° for the 30.4 nm data clearly outline the interference "bump" that occurs with this highly transmissive sample due to the coherent addition of the reflection from the vacuum–film interface with the reflection from the film–substrate interface.

The 58.4 nm aluminum reflectance data shown in Fig. 1 clearly indicate the total-external-reflectance phenomenon that has been described here. The critical angle at which the high-reflectance onset occurs is given by Eq. 1 for a vacuum-incident medium ($n_1 = 1$),

$$\theta_c = \sin^{-1}[0.7/1] = 44.4°. \tag{2}$$

The rapid rise of the aluminum reflectance at this angle gives an unambiguous indication of the real part of the index of refraction for this wavelength. Similarly, the 30.4 nm aluminum reflectance data indicate a much greater critical angle given by

$$\theta_c = \sin^{-1}[0.944/1] = 70.7°. \tag{3}$$

## DETERMINATION OF $n$ AND $k$ IV

The actual determination of $n$ and $k$ from reflectance data such as that shown in Fig. 1 proceeds in the following manner: a computer algorithm

for the calculation of the reflectance of a substrate overcoated with one or more thin-film layers is utilized to generate reflectance curves that can be fitted to the data. This algorithm is based on the characteristic-matrix method [4] and will not be elaborated here. The $n$ and $k$ values for the substrate (silicon) must be inserted into the algorithm and previously published values [5] are available over a wide wavelength range. The thickness of the thin-film layer must also be included in the algorithm, but this value is monitored during the aluminum deposition.

## A Thin-Film Thickness

A secondary check on the accuracy of the thin-film thickness is available in the reflectance data of Fig. 1 due to the presence of interference "bumps" in the data near the onset of high reflectance. The position of these bumps is dependent on the thickness of the film, since this thickness affects the constructive and destructive interference between light reflected from the film and substrate surfaces versus angle of incidence. The appearance of these interference effects is an indication that the absorption of the thin film is very low, since the beam reflected from the second surface must traverse the thin film twice in order to interfere with the first surface reflection. The aluminum film thickness for the measurements in Fig. 1 was 70 nm.

## B Sensitivity to *n* and *k*

The AOITER method of determining the optical constants of a thin-film coating material is very useful, when conditions allow its use, due to the separation in the effects on the angular reflectance spectrum caused by changes in $n$ and $k$. The analytical formulation for the relationship between changes in the critical angle, $\Delta\theta_c$, and fractional changes in the index of refraction, $\Delta n/n$, is obtained from the derivative of Eq. 1,

$$\frac{\Delta n}{n} = \frac{\sqrt{1-n^2}}{n}\,\Delta\theta_c. \tag{4}$$

In Fig. 2, the relative changes in $n$, caused by critical-angle uncertainties, from Eq. 4, are shown for three values of $n$. It is clear from Fig. 2 that the accuracy of AOITER is better for smaller values of $n$. Using Eq. 4, we find that an index of 0.7, and a $\Delta\theta_c = \pm 0.4°$ gives a $\Delta n/n = \pm 0.007$.

For a material with $n = 0.7$, the reflectance beyond the critical angle for various values of $k$ is shown in Fig. 3. The lower values of $k$ lead to higher

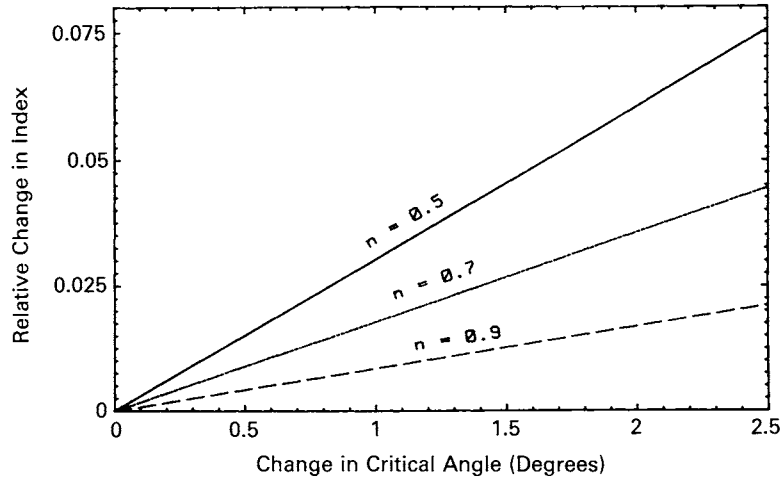


**Fig. 2.** Relative change in index of refraction, $\Delta n/n$, versus critical-angle uncertainty, $\Delta\theta_c$, for three different values of $n$.

reflectance values as one would expect. Calculations with the computer algorithm indicate that a change in $k$ of $\pm 0.003$ from a nominal value of 0.01 leads to changes in reflectance values that vary from zero to $\pm 7\%$ depending on the incidence angle. The fact that the effects due to variations in $n$ and $k$ are essentially separate means that it is very unlikely that ambiguities will occur in determining $n$ and $k$ values with AOITER.

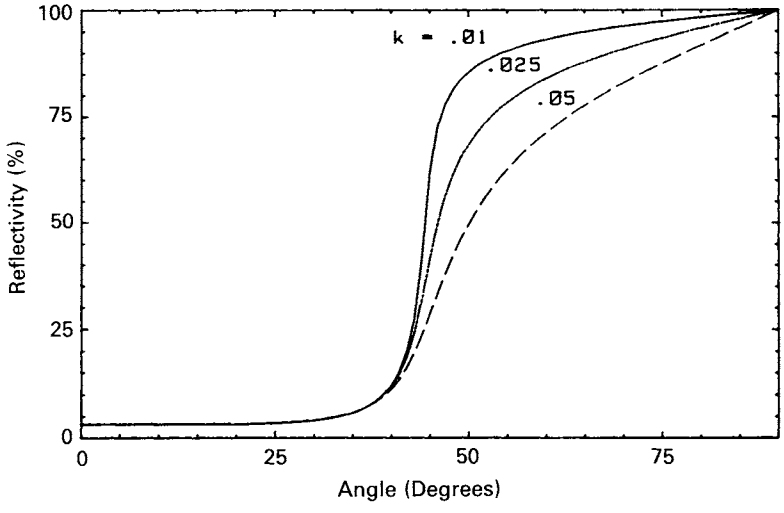


**Fig. 3.** Reflectance versus incidence angle for $n = 0.7$ and three values of $k$, the absorption index.

### C Results at 58.4 nm and 30.4 nm

With the above inputs to the reflectance calculation, the $n$ and $k$ of the aluminum thin film can be varied to get the best fit to the measured XUV reflectance data. The error in the $n$ and $k$ determined from reflectance data can be estimated from the $\pm 2\%$ reflectance error in the following way: one adds 2% to each reflectance data point to generate a new (higher) reflectance curve. This new curve is again fit to determine $n$ and $k$. One then subtracts from the original reflectance data points to generate a new (lower) reflectance curve, which is also fitted to determine $n$ and $k$. The excursion of $n$ and $k$ from the original data fit is used as the error bar on $n$ and $k$. The results of this fitting procedure for aluminum are given as the AOITER entries in Table I. In situ UHV-AOITER measurements on aluminum at other XUV wavelengths have not yet been performed.

## V COMPARISON WITH OTHER RESULTS

Other methods exist to determine the optical constants of materials in the XUV. Typically, these methods utilize reflection and/or transmission values measured at normal incidence or at more than one incident angle, to infer the optical constants of the material.

### A Aluminum at 58.4 nm

Using a combination of transmission and reflection measurements, Ditchburn and Freeman [6] determined the $n$ and $k$ of aluminum at various wavelengths. A linear interpolation of their values gives $n = 0.69$ and $k = 0.023$ at 58.4 nm. Madden, Canfield, and Hass [7] used a reflection versus time method to minimize the effects of oxidation in determining the optical constants of aluminum. The values quoted in this reference are $n = 0.71$ and $k = 0.018$ for 58.4 nm. In early work [8], Hunter used reflection measurements and determination of the critical angle to deduce the optical constants of aluminum to be $n = 0.72$ and $k = 0.018$ at 58.4 nm. In later work [9, 10], Hunter used transmission measurements to find $k$ values between 0.018 and 0.023 with a best-fit curve for multiple-wavelength data passing through $k = 0.023$ at 58.4 nm. Hass and Tousey [11] indicate that interference-fringe analysis gives $n = 0.7$ at 58.4 nm. They state that the $k$ value for aluminum at this wavelength is less than 0.04; however, the aluminum reflectance calculations in this paper were performed with

$n = 0.7$ and $k = 0.018$. The extensive compilation and analysis of aluminum optical constant data by Smith *et al.* [12] indicates that $n = 0.715$ and $k = 0.0237$ at 58.4 nm.

### Aluminum at 30.4 nm B

Fomichev and Lukirskii [13] measured absorption coefficients of thin aluminum films in the wavelength range from 2.36 nm to 41 nm. The value of $k$ linearly interpolated from this reference at 30.4 nm is $k = 0.009$. Hunter [9, 10] used the critical-angle method to determine $n$ and transmission measurements to determine $k$ at wavelengths between 10 nm and 80 nm. The approximate values from these references at 30.4 nm are $n = 0.94$ nm and $k = 0.009$ (these values were taken from the best-fit line on a graphical presentation of this multiple-wavelength data). The aluminum optical-constant data from the compilation by Smith *et al.* [12] indicates that $n = 0.943$ and $k = 0.0079$ at 30.4 nm.

### Drude Free-Electron Model C

This model utilizes only two parameters, the plasma critical wavelength and the electronic relaxation time, to characterize the optical constants of a

TABLE I

**A Comparison of the Optical Constants of Aluminum[a]**

| Source of data | $n$ | $k$ |
|---|---|---|
| 58.4 nm | | |
| AOITER | $0.700 \pm 0.005$ | $0.010 \pm 0.002$ |
| Ref. [6] | $0.69 \pm 0.02$ | $0.023 \pm 0.012$ |
| Ref. [7] | $0.71 \pm 0.02$ | $0.018 \pm 0.009$ |
| Ref. [8] | $0.72 \pm 0.015$ | $0.018 \pm 0.009$ |
| Ref. [9, 10] | $0.72 \pm 0.02$ | $0.023 \pm 0.01$ |
| Ref. [11] | $0.70 \pm 0.02$ | $0.018 \pm 0.020$ |
| Ref. [12] | $0.715 \pm 0.02$ | $0.0237 \pm 0.01$ |
| Drude model | 0.72 | 0.010 |
| 30.4 nm | | |
| AOITER | $0.944 \pm 0.002$ | $0.0055 \pm 0.0008$ |
| Ref. [13] | — | $0.009 \pm 0.004$ |
| Ref. [9, 10] | $0.94 \pm 0.03$ | $0.009 \pm 0.004$ |
| Ref. [12] | $0.943 \pm 0.03$ | $0.0079 \pm 0.004$ |
| Drude model | 0.93 | 0.001 |

[a] Errors have been estimated by the author.

given material over a wide range of wavelengths. The values of these two parameters that give the best fit [14] to available data on aluminum (in the UV and visible spectral regions) are $\lambda_{crit} = 83.7$ nm and $\tau = 1.1 \times 10^{-15}$ sec. The optical constants can be calculated in the Drude model by means of

$$\varepsilon_1 = n^2 - k^2 = 1 - [\omega_{crit}^2 \tau^2/(1+\omega^2\tau^2)], \tag{5}$$

$$\varepsilon_2 = 2nk = (\omega\tau)^{-1}[\omega_{crit}^2 \tau^2/(1+\omega^2\tau^2)], \tag{6}$$

$$\omega_{crit}^2 = 4\pi Ne^2/m = (2\pi c/\lambda_{crit})^2, \tag{7}$$

where $c$ is the speed of light, $N$ is the effective valence-electron density, $e$ is the charge of an electron and $m$ is its mass. The values for $n$ and $k$ calculated with the simple Drude model at 58.4 nm and 30.4 nm using the above values for the parameters are given in Table I along with a comparison of the various measured values discussed above.

## D Discussion

The AOITER results given in Table I are very similar to previous results, except that the AOITER values obtained for $k$ and the error bars on $n$ and $k$ are significantly smaller. The larger previous values of $k$ are presumed to arise from the presence of some oxide deposited in the coating, surface-oxide layers, surface contamination, or impurities in the starting material.

### REFERENCES

1. J. G. Endriz and W. E. Spicer, *Phys. Rev. B* **4**, 4144 (1971).
2. M. L. Scott, P. N. Arendt, B. J. Cameron, J. M. Saber, and B. E. Newnam, *Appl. Opt.* **27**, 1503 (1988).
3. M. L. Scott (unpublished).
4. M. Born and E. Wolf, "Principles of Optics," Macmillan, New York, 57 (1964).
5. D. F. Edwards, in "Handbook of Optical Constants of Solids," (E. D. Palik, ed.), Academic Press, Orlando, 547 (1985).
6. R. W. Ditchburn and G. H. C. Freeman, *Proc. R. Soc. London, Ser. a* **294**, 20 (1966).
7. R. P. Madden, L. R. Canfield, and G. Hass, *J. Opt. Soc. Am.* **53**, 620 (1963).
8. W. R. Hunter, *J. Opt. Soc. Am.* **54**, 15 (1964).
9. W. R. Hunter, *Appl. Opt.* **21**, 2103 (1982).
10. W. R. Hunter, in "Proceedings, International Colloquium on Optical Properties and Electronics Structure of Metals and Alloys," (F. Abeles, ed.), North-Holland, Amsterdam, 136 (1966).
11. G. Hass and R. Tousey, *J. Opt. Soc. Am.* **49**, 593 (1959).
12. D. Y. Smith, E. Shiles, and M. Inokuti, in "Handbook of Optical Constants of Solids," (E. D. Palik, ed.), Academic Press, Orlando, 369 (1985).
13. V. A. Fomichev and A. P. Lukirskii, *Opt. Spectrosc.* **22**, 432 (1967).
14. W. R. Hunter, *J. Appl. Phys.* **34** 1565 (1963).

# Chapter 10

# Spectroscopic Ellipsometry in the 6–35 eV Region

J. BARTH,* R. L. JOHNSON,† and M. CARDONA
Max-Planck-Institut für Festkörperforschung
D-7000 Stuttgart 80
Federal Republic of Germany

I. Introduction 213
II. The BESSY VUV Ellipsometer 217
A. Basic Experimental Considerations 217
B. Optimum Geometry 218
C. Design of the Ellipsometer 221
D. VUV Polarizers 224
E. Photodiodes as VUV-Detectors 225
III. Theory 226
A. Basic Formulas 226
B. Calibration 231
C. Error Analysis 232
IV. Results and Comparison with Reflectance Spectra 237
A. III-V Semiconductors 237
B. II-VI Compounds 238
C. Calcium Fluoride 242
V. Summary 244
Acknowledgment 245
References 245

## I INTRODUCTION

The technique of ellipsometry has experienced a renaissance recently driven by the ever-increasing demand for rapid, nondestructive analysis of surfaces and thin films. Ellipsometry enables the optical constants of

* Present address: Elektro-Optik GmbH, Fördestraße. 35, D-2392 Glücksburg, Federal Republic of Germany.
† Present address: II. Institut für Experimentalphysik, Universität Hamburg, Luruper Chaussee 149, D-2000 Hamburg 50, Federal Republic of Germany.


Copyright © 1991 by Academic Press.
All rights of reproduction in any form reserved.
ISBN 0-12-544422-2

materials to be determined with high accuracy and can therefore help to solve a wide variety of problems in different disciplines. The fact that ellipsometric measurements can be performed without a vacuum environment in the visible and near-UV regions is a definite advantage over other surface-science techniques for industrial applications. Ellipsometry is widely used in assessing the quality of semiconductor materials and oxide coatings and to characterize such diverse systems as polymers, liquid crystals, and Langmuir–Blodgett films.

There are now a number of commercial ellipsometers available that exploit recent advances in detection systems and computer technology and allow precise and rapid measurement of the optical properties of thin films and surfaces in the IR–VIS–near-UV spectral region (1.5–6.0 eV). The microscopic-imaging ellipsometer described by Beaglehole [1] is a particularly interesting instrument that enables ellipsometric measurements to be performed with a lateral resolution of about 3 $\mu$m. Given these developments and the incontestable advantages of ellipsometry for determining the optical constants of materials, it seems obvious to extend the spectral range for ellipsometry into the vacuum-ultraviolet (VUV) region. This expands the number of systems accessible for ellipsometric studies to include large-band-gap insulators and excitations from deeper valence bands and also from shallow core levels into the conduction bands.

The best light source for spectroscopic ellipsometry in the VUV region is without doubt monochromatized synchrotron radiation because of its tunability, high intensity, and natural collimation. It is also highly polarized, although the degree of linear polarization is not as high as that which can be achieved in the visible region. The possibility of carrying out ellipsometry with synchrotron radiation was demonstrated by Schledermann and Skibowski in 1970 [2, 3] at the DESY synchrotron in Hamburg. Apparently, since then no further attempts have been made despite recent advances in the development of high brightness storage rings as much more powerful sources of synchrotron radiation.

At present, reflectometry is the best-established technique for determining the optical constants in the VUV region. A detailed description of the method and data analysis has been presented by Hunter [4]. To perform such measurements, one simply measures the specularly reflected intensity from the sample using a collimated monochromatic beam of light, which has a well-defined state of polarization. Reflectometry can be performed throughout the entire VUV and X-ray regions, and by scanning the photon energy, a wealth of spectroscopic information can be obtained. The greatest uncertainty in such measurements is usually caused by variations in the intensity and spectral purity of the primary photon flux. At high energies diffuse scattering and geometrical-shadowing effects can introduce significant errors; however, by taking suitable precautions and using highly monochromatic synchrotron radiation, excellent data can be

obtained. In order to calculate the optical constants from reflectance data, it is necessary to make use of the Kramers–Kronig relation, which implies that data over a very wide energy range should be available. It is difficult to estimate the amount of uncertainty in the absolute values of the dielectric function introduced by the unavoidable extrapolation necessary for Kramers–Kronig analysis. A more complete discussion of these aspects can be found in the article by Smith [5]. The alternative method of multiple-angle reflectivity measurements is a time-consuming and laborious exercise [6].

In ellipsometry one measures the change in polarization state of the beam of light after nonnormal reflection from the sample. The polarization state is defined by two parameters, for example, the relative phase and relative amplitude of the orthogonal electric-field components of the polarized light wave. On reflection both electric-field components are modified in a linear way, so a single ellipsometric measurement provides two independent parameters. The name *ellipsometry* derives from the fact that linearly polarized light after oblique reflection becomes elliptically polarized due to the different reflection coefficients for *s*- and *p*-polarized light. By measuring the polarization ellipse, one can determine the complex dielectric function of the sample. The principles of ellipsometry were established about 100 years ago [7], but the technique only became practical with the development of the rotating-analyzer ellipsometer (RAE) [8], which makes use of digital computers to handle the rather unwieldy equations. The RAE measures continuously, so wavelength scanning or spectroscopic ellipsometry can be performed.

A conventional ellipsometer consists of a light source and a rotatable polarizer, so that the plane of polarization can be inclined to the plane of incidence. The measurement geometry is shown in Fig. 1. Polarized light falls on the sample at an angle of incidence of about 70° typically, and the reflected light is analyzed using a second rotatable polarizer and a suitable detector. The simplest ellipsometers use a single-wavelength light source and manual determination of the ellipsometric angles $\Delta$ and $\psi$ (where $\Delta$ corresponds to the phase shift and $\tan \psi = |\tilde{r}_p/\tilde{r}_s|$, the amplitude ratio of the reflected components). The measurement procedure is to locate the minimum transmission through the optical system by alternately rotating polarizer and analyzer (or equivalently polarizer and compensator). The extinction condition determines both of the ellipsometric angles; thus, a single ellipsometric measurement provides two parameters. Furthermore, since it is the polarization state and not the intensity which is being measured, the results are unaffected by source intensity fluctuations. The fact that ellipsometry simultaneously determines the relative phases and amplitudes accounts for the high sensitivity of this technique. In particular, the direct measurement of the phase changes makes ellipsometry highly surface-sensitive, and it is possible to detect extremely thin adsorbed films

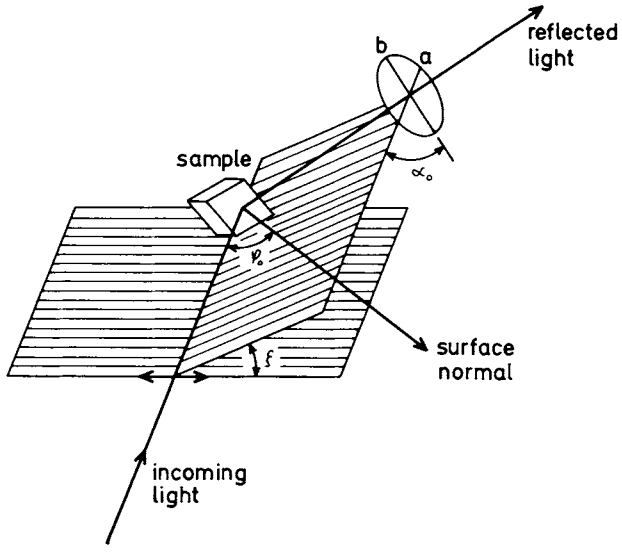


**Fig. 1.** Measurement geometry for ellipsometry: the angle of incidence is $\phi_0$, and the angle between the plane of incidence and the plane of polarization is $\xi$. The polarization ellipse of the reflected light is characterized by the ratio of the axes and the angle $\alpha_0$.

(down to 0.01 monolayer, with a good instrument). By assuming an appropriate model, the measured ellipsometric parameters can be evaluated in terms of a macroscopic refractive index with real and imaginary components. Alternatively, a single ellipsometric measurement can be used to determine the thickness and refractive index of transparent films.

The interpretation of the measured changes in polarization in terms of optical functions is a problematic aspect of ellipsometry. The simplest approach is to apply the Fresnel equations and a two-phase model to the vacuum–solid interface. The Fresnel equations are strictly applicable only to an abrupt interface between homogeneous isotropic media. In reality, no materials are perfectly isotropic and, on a microscopic scale, no interfaces are abrupt; however, the two-phase model generally provides the most useful basis for interpreting ellipsometric data. The application of the two-phase model to anisotropic media enables a "pseudodielectric function" to be calculated, which allows anisotropic samples to be characterized. A full determination of all the components of the dielectric tensor in anisotropic media is, in principle, possible by performing measurements at multiple angles of incidence for different orientations of the sample. Measurement of optical anisotropies is a challenging field of current research [9].

So far we have outlined some of the salient aspects of ellipsometry, which we can summarize as follows: spectroscopic ellipsometry is now a

well-established technique for determining the optical constants of bulk materials and thin films in the IR–VIS–near-UV spectral region over the photon-energy range 1.5–6.0 eV. It is generally accepted to be a technique with high intrinsic precision and accuracy, which allows both real and imaginary parts of the dielectric function to be measured simultaneously. In the visible, conventional instruments can yield information on samples with absorption coefficients down to typically $10^4\,cm^{-1}$, and extinction indices ~0.1. More details about conventional ellipsometry can be found in review articles [10, 11] and the proceedings of the ellipsometry conferences [12].

The purpose of this article is to introduce the concepts of VUV ellipsometry and to demonstrate that it is a viable technique to determine the optical constants of solids. There are important differences between ellipsometry in the visible and VUV regions. The fact that there are no perfect polarizers for the VUV means that all four components of the Stokes vector have to be considered in the data analysis. This, in turn, means that the full Mueller matrix notation has to be used in the theoretical description. On the experimental side it was necessary to develop new instrumentation and procedures to calibrate the imperfect polarizers and also to measure the polarization of the incident light. By making use of synchrotron radiation with its high degree of linear polarization and triple-reflection polarizers, we built an automated instrument that extends the spectral range of spectroscopic ellipsometry up to 35 eV [13]. We present data that demonstrate the usefulness of our instrument for measuring the optical constants of solids. By combining the data with theoretical calculations, new insights about the band structure of wide-band-gap semiconductors and insulators have been gained.

## THE BESSY VUV ELLIPSOMETER II

### Basic Experimental Considerations A

There are a number of different optical configurations that can be used for ellipsometry. A typical system consists of a collimated unpolarized monochromatic light source, a polarizer, a compensator, the reflecting sample under investigation, the polarization analyzer, and a detector. The modern rotating-analyzer ellipsometer has a great advantage over the older null technique in that it can be readily automated to allow the wavelength to be scanned continuously, yielding dielectric-function spectra. In a rotating-analyzer ellipsometer, the state of polarization of the

reflected light (ellipticity and orientation of the ellipse) is measured with a photodetector behind an analyzer, which rotates at a fixed frequency. Thus, the intensity at the detector has, as a function of analyzer rotation angle, $\alpha$, the form of a sinusoidal curve on a dc background, which can be written as

$$I_{\text{det}} = \text{const}(1 + a_1 \cos 2\alpha + a_2 \sin 2\alpha). \tag{1}$$

Fourier analysis yields the coefficients $a_1$ and $a_2$, which are used to determine numerically $\varepsilon_1(\hbar\omega)$ and $\varepsilon_2(\hbar\omega)$. The detected intensity is a function of $2\alpha$ because the optical cycle of the rotating analyzer corresponds to half a mechanical cycle.

The rotating analyzer is advantageous because of its higher speed of data collection, its high precision, and the fact that a compensator is not necessary. Practically all aspects of rotating-analyzer ellipsometry have been described by Aspnes [8, 10, 11, 14, 15], and our present VUV ellipsometer is based on his pioneering work.

One obstacle to performing ellipsometric measurements in the VUV is the lack of suitably intense laboratory light sources. The brightest tunable VUV light is provided by specially constructed synchrotron radiation facilities. Synchrotron radiation (SR) has the additional advantage of being highly polarized. SR extends over a broad continuum from the IR to X-ray regions, so a monochromator has to be used to filter out a narrow bandwidth. The present VUV ellipsometer at the dedicated light source BESSY in Berlin is installed on the 2m Seya–Namioka beam line, which nominally covers the photon-energy range from 5–35 eV using two gratings. The photon flux falls off rapidly near the ends of the spectral range, so it is primarily the monochromator that limits the range of the ellipsometer. In spectroscopic ellipsometry the monochromator plays a particularly important role, since alignment has to be maintained while scanning the monochromator. The present system dispenses with a polarizer before the sample and uses the fact that synchrotron radiation is linearly polarized in the plane of orbit and that the optical components in the beam line enhance the degree of polarization.

## B Optimum Geometry

In ellipsometry, linearly polarized light is incident at an oblique angle on the surface under investigation. The reflected light is in general elliptically polarized due to the differences in the complex $\tilde{r}_s$ and $\tilde{r}_p$ reflection coefficients. The complex reflection ratio can be obtained di-

rectly from the ellipsometric angles $\psi$ and $\Delta$ since, by definition, $\rho = \tilde{r}_p/\tilde{r}_s = \tan\psi \exp(i\Delta)$. The reflection coefficients depend on the angle of incidence, the photon energy, and the material properties, so it is clear that different geometrical arrangements are required to obtain the best sensitivity in ellipsometry in different spectral regions. Furthermore, different optimum geometries are to be expected for such different samples as wide-band-gap semiconductors or adsorbates on metals. A versatile instrument could be conceived with a variable angle of incidence, but it would be difficult and expensive to attain the necessary precision in ultra-high vacuum. A theoretical analysis of the optimum experimental geometry is, therefore, a prerequisite for establishing a practical design of a VUV ellipsometer.

General equations for optimizing the precision of rotating-analyzer ellipsometers have been given by Aspnes [14]. He found that for rotating-analyzer systems with an ideal detector, the angle of incidence should be as close as possible to the "principal angle." At this angle of incidence, for which $\Delta = \pm\pi/2$, linearly polarized light is generally reflected as elliptically polarized light, but when the angle between the plane of polarization and the plane of incidence is equal to $\psi$, the reflected light is circularly polarized. For spectroscopic measurements over a given spectral range, minimum uncertainty is obtained as a compromise between the conditions that yield circularly polarized light and those that maximize the transmitted flux. It is interesting to note that the optimum precision in the ideal-detector case is achieved when the measured Fourier coefficients $a_1$ and $a_2$ are zero, so the complex-reflectance ratio $\rho$ is determined purely by instrument settings. The angle of incidence is one of the most important parameters in ellipsometry and has to be determined with at least the same accuracy as the ellipsometric angles. In the principal-angle-of-incidence ellipsometer [16, 17], the rotating analyzer is used as a null detector seeking circularly polarized light. The dielectric function of the sample is determined solely by the angle of incidence and the polarizer position. The best accuracy in the determination of the optical constants is obtained at the principal angle of incidence; the linearity of the detector becomes unimportant. Hence, accurate determination of the dielectric function requires high angular precision and good mechanical stability of the ellipsometer.

Aspnes [14] applied the theory to the practical cases of silicon and gold surfaces measured with a rotating-analyzer ellipsometer and shot-noise-limited detector without using a compensator. He found that for an angle of incidence of 68 degrees, the optimum polarizer azimuth was 30 degrees over the energy range 2.5–5.5 eV.

In general, the optimum sensitivity is obtained for an angle of incidence close to the principal angle ($\Delta = \pm\pi/2$) and an optimum polarizer azimuth equal to $\psi$ (where $\tan\psi = |\rho|$). We can make use of the fact that at high photon energies $\varepsilon_1 \simeq 1$ and $\varepsilon_2 \simeq 0$ to derive the optimum experimental

geometry in the X-ray limit. In this case the optimum angle of incidence is 45°, and the optimum polarizer azimuth tends toward zero. Thus, we see that the optimum angle of incidence decreases from about 70° in the visible region to 45° in the XUV. Unfortunately, the reflectivity of the sample is reduced at the smaller angle of incidence, and this constitutes a fundamental limitation to performing ellipsometry in the soft X-ray region.

The strong dependence of the precision obtainable in ellipsometry on the measurement geometry is interesting and in some ways nonintuitive. It is somewhat paradoxical that it is necessary to know the dielectric function of the sample before one can measure it with the greatest precision by ellipsometry. It is also difficult to appreciate that the same sample will require different geometries in different wavelength regions. It is instructive to plot the variation of $\varepsilon_1$ and $\varepsilon_2$ with energy as shown in Fig. 2 and Fig. 3 for InAs. The curve A-B in Fig. 2 corresponds to photon energies from 1.5–9 eV and the curve in Fig. 3 corresponds to photon energies 14–25 eV. The optimum sensitivity is obtained when the dielectric-function curve lies in the vicinity of the principal-angle curves shown as semicircles for angles of incidence of 67.5°, 56.25°, and 45°. These figures demonstrate clearly that for InAs, the optimum angle of incidence tends rapidly toward 45°

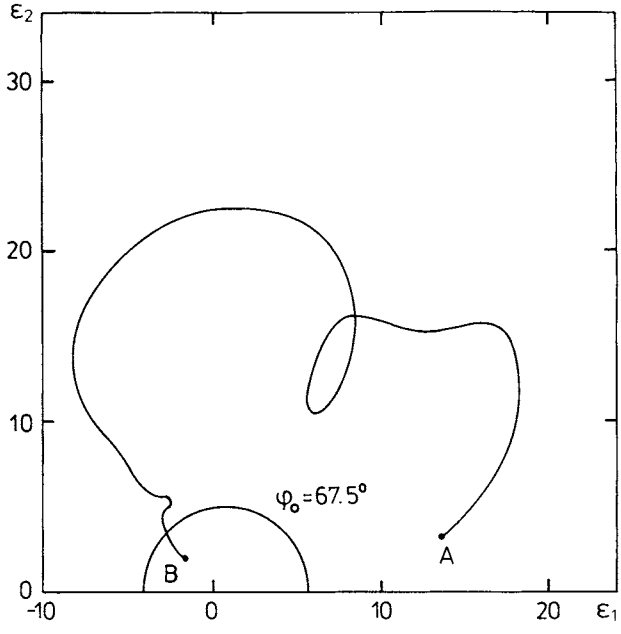


**Fig. 2.** The dielectric function of InAs from 1.5 eV (A) to 9 eV (B) plotted in the complex plane (Argand diagram). The semicircle corresponds to the values of $\varepsilon_1 + i\varepsilon_2$ for which $\Delta = -90°$ at an angle of incidence $\phi_0 = 67.5°$.

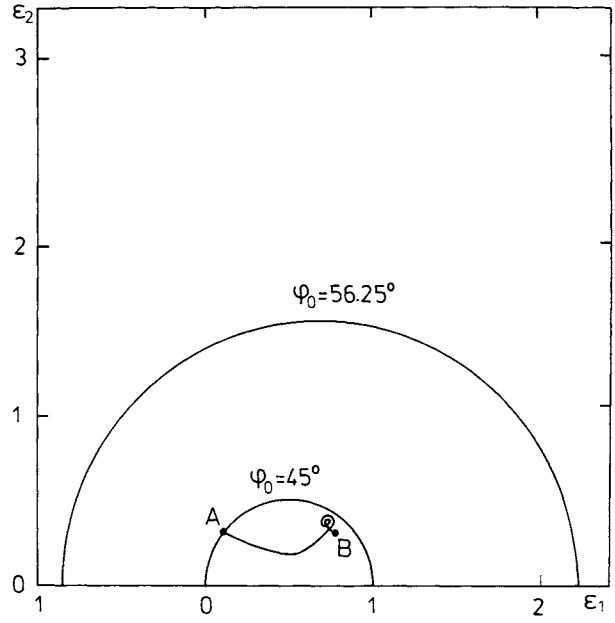


**Fig. 3.** Argand diagram for the dielectric function of InAs from 14 eV (A) to 25 eV (B). The semicircles correspond to the values of $\varepsilon_1 + i\varepsilon_2$ for which $\Delta = -90°$ at angles of incidence of 56.25° and 45°.

with increasing photon energy. Although the magnitudes of $\varepsilon_1$ and $\varepsilon_2$ become smaller at higher energies, it is important to note that good precision can be achieved by measuring with the optimum geometry.

As a compromise between optimum precision and mechanical stability, our ellipsometer provides two different angles of incidence. In the energy region 5–10 eV, the incidence angle is 67.5°, and a $MgF_2$ Rochon polarizer is used. Above 10 eV, a 45° incidence angle produces better results for most materials and only triple-reflection polarizers can be used at these energies. In practice, the two fixed angles of incidence have been found to be quite adequate, since the optimum conditions do not have to be fulfilled stringently. The two angles also provide complementary information, which is useful when studying thin films and adsorbates.

## Design of the Ellipsometer C

The basic design of the VUV ellipsometer is modular, which enables functions to be separated and individually modified and upgraded as the

system evolves. The present ellipsometer comprises of three vacuum chambers: the main UHV chamber (base pressure $10^{-10}$ mbar) around the sample manipulator, the analyzer chamber, and a preparation chamber with load-lock. In order to tilt the plane of polarization with respect to the plane of incidence, usually accomplished by turning the polarizer, the whole ellipsometer has to be rotated about the axis of the incoming light. As shown in Fig. 4, the sample is mounted on the precision manipulator in the center of the main UHV chamber. Samples are introduced via a rapid load-lock and exchanged with a transfer system and can be heated or cooled on the manipulator (77–900 K). Facilities are provided for cleaving samples and for evaporation *in situ*.

The analyzer chamber can be readily removed and positioned at ports corresponding to angles of incidence of either 67.5° or 45°. It contains the most important parts of the ellipsometer, that is, the rotating analyzer and the detector. The prealigned standardized polarizer assemblies can be easily interchanged and fit snugly inside a rotating drum, which is driven via a friction wheel by a tachogenerator-stabilized dc motor. The angular orientation of the analyzer is measured with an angle encoder (1000 pulses per revolution) mounted directly on the drum. The pulses from the angle

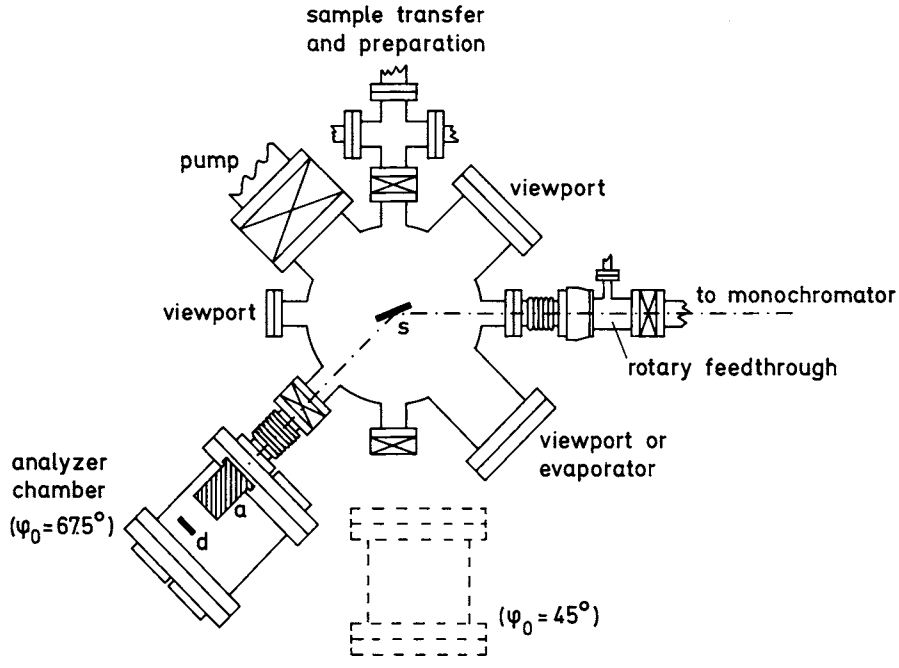


**Fig. 4.** Schematic diagram of the VUV-ellipsometer (s = sample, a = rotating analyzer, d = photodiode detector).

encoder trigger the readout of the detector 50 times per optical cycle. Two photodiode detectors—one for lower energies and one for higher energies—are mounted on a linear-motion feedthrough perpendicular to the axis of the analyzer. This enables the detector to be moved out of the optical path and allows direct visual adjustment of the polarizer by viewing the zero-order light through a window on the end of the analyzer chamber. The mounting of the analyzer chamber allows precision adjustment of the axis of the analyzer onto the beam reflected from the sample. For triple-reflection polarizers the adjustment is extremely critical and requires experience. The visual adjustment is essential to obtain correct prealignment; the final adjustment is performed using the photodiode signal at a convenient photon energy. The adjustment is optimal when the signal is sinusoidal, as a function of analyzer angle with equal intensity in both optical cycles. The photodiode signal is continuously displayed on both an oscilloscope and the computer terminal.

The ellipsometer at BESSY is installed on the 2m Seya–Namioka beamline, which contains three mirrors in addition to the spherical diffraction grating. The light from the ring is focused by a Pt-coated toroidal mirror and an Au-cylindrical mirror before being dispersed using either a 610 l/mm mechanically ruled grating coated with $Al + MgF_2$, or a Pt-coated 1200 l/mm holographic grating. The monochromatic light is brought to a stigmatic focus with an additional Au-coated cylindrical mirror. The grating can be masked down in both vertical and horizontal directions to enhance the degree of linear polarization. The monochromator can achieve high resolution ($\lambda/\delta\lambda = 4000$ at 180 nm with 50 $\mu$m slits and 610 l/mm grating), but for ellipsometry a high photon flux and linearly polarized light are the primary requirements.

Although the light from the 2 m Seya–Namioka monochromator is highly linearly polarized, it may still contain components of elliptically and unpolarized light at the level of a few percent. The proportion of these components can vary as the monochromator is scanned, and this should be taken into account when evaluating the data. Similarly, the triple-reflection analyzer has nonideal polarization characteristics, so the experimental Fourier coefficients have to be corrected for the polarization properties of the analyzer before accurate values of the dielectric function can be obtained. By mounting the analyzer chamber at the exit of the monochromator, we can directly characterize the polarization properties of the monochromator. Figure 5 shows three results of such measurements performed at different times on two different 610 l/mm gratings coated with $Al + MgF_2$. The lowest curve was recorded from the grating originally installed in the monochromator and exhibits a pronounced dip near 12 eV and a steady decline above 16 eV. A new grating was installed and the measurement was repeated, yielding the upper curve with a higher polarization and a smaller dip at 12 eV, but still with a decrease at higher photon

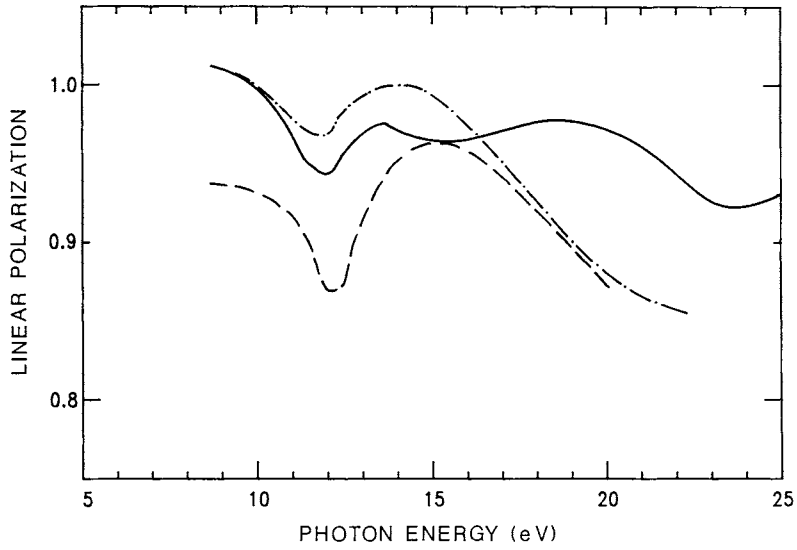


**Fig. 5.** Degree of linear polarization of light from the monochromator. The three curves were recorded at different times: the dashed line was recorded when grating was originally installed in monochromator; the dash-dot line was recorded after replacement of grating; the solid line indicates measurement with new reflection polarizer five months later.

energies. The characterization was repeated five months later with a new analyzer. The dip at 12 eV had increased again, and we attribute this to radiation-induced degradation of the monochromator grating. The decrease in the polarization at higher photon energies is no longer apparent with the new analyzer. Thus, it is clear that the optical elements in both the monochromator and the ellipsometer deteriorate with time.

## D VUV Polarizers

Rochon polarizers made from $MgF_2$ are the best polarizers to use in the photon energy range 5–10 eV. The upper limit is determined by the quality of the $MgF_2$. The long optical path through the prism (~27 mm) means that the absorption due to impurities can be significant. Since the ordinary beam passes undeviated along the axis, the Rochon polarizer is achromatic. The extraordinary beam is refracted away from the axis of rotation and is absorbed in a mask placed before the photodiode. The extinction coefficient of Rochon polarizers that we use is $10^5$, which means they can be treated as being essentially perfect.

From the considerations about the optimum geometry for ellipsometry, it is clear that reflection polarizers can only be optimized for high transmission and good polarization over a limited photon-energy range. However, for spectroscopic measurements a wide range is necessary. As shown by Hamm *et al.* [18, 19] a triple-reflection polarizer with gold-coated mirrors represents a suitable compromise. The triple-reflection polarizer we use consists of a 135° prism and a plane mirror with gold coatings [20]. A minimum of three reflections is necessary to avoid a net deviation of the transmitted light beam from the optical axis. Using literature values for the optical constants of gold [21], we have calculated the transmission and degree of polarization that we expect from our reflection polarizer. The results are shown in Fig. 6.

## Photodiodes as VUV-Detectors E

Semiconductor photodiodes have numerous advantages over other detectors. They are inexpensive, compact, easy to use, highly linear (over 10 orders of magnitude), UHV-compatible and insensitive to contamination. For ellipsometry, the good linearity, lack of polarization dependence, and uniform response over the active area make these detectors particularly attractive. The stability, quantum efficiency, and responsivity of

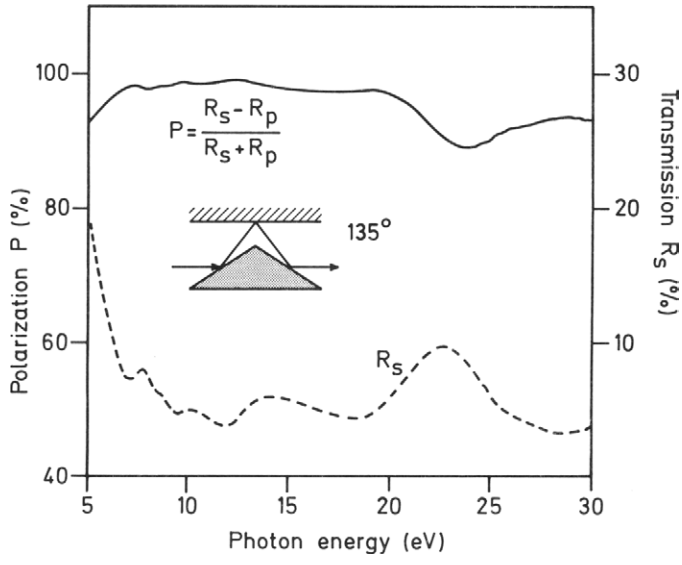


**Fig. 6.** Calculated degree of polarization and transmission of the triple-reflection polarizer.

various photodiodes have already been reported [22, 23]. In the ellipsometer, we use diffused silicon diodes with a thin oxide overlayer in conjunction with the $MgF_2$ polarizer. The standard silicon diodes have a high quantum efficiency, but are not as stable as GaAsP or GaP Schottky diodes. A particular problem with the Si diodes is charge-trapping in the silicon-dioxide layer, which can lead to a complete loss in sensitivity if the diode is inadvertently exposed to high-energy radiation (for example, zero-order light from the monochromator). Recently, a new type of inversion-layer silicon photodiode has been developed [24], which has good stability and an extremely high quantum efficiency. These are the best detectors for VUV ellipsometry. In the past, we used GaP Schottky diodes and Si diodes covered only with a thin natural-oxide layer for photon energies above 10 eV.

The rapid increase in the quantum efficiency of photodiodes with increasing photon energy enhances the contributions of higher harmonics from the monochromator. Unfortunately, there are very few filters available for the photon-energy region 5–35 eV, so it is not always easy to eliminate unwanted higher harmonics.

## III THEORY

### A Basic Formulas

Compared with conventional ellipsometry, the conditions under which we perform our measurements in the VUV are significantly less than ideal in two respects. First, the light emerging from the monochromator may contain elliptically polarized and unpolarized components at the level of a few percent, which vary as the monochromator is scanned. In principle, these unwanted components may be suppressed by an additional reflection polarizer but only at the expense of intensity. We decided to measure the complete state of polarization of the incident light and to use these reference data to evaluate $\varepsilon_1(\hbar\omega)$ and $\varepsilon_2(\hbar\omega)$ with the "Mueller matrix formalism" [29], which is a more general formalism than that usually applied. Second, for the analyzer we can use only conventional birefringent transmission polarizers for the very near VUV range. Rochon-type $MgF_2$ polarizers can be obtained with a cutoff energy between 9 eV and 10 eV depending on the optical quality. At higher photon energies, reflection polarizers have to be used, which are less ideal. Consequently, a careful characterization of these polarizers is necessary for a correct data evaluation.

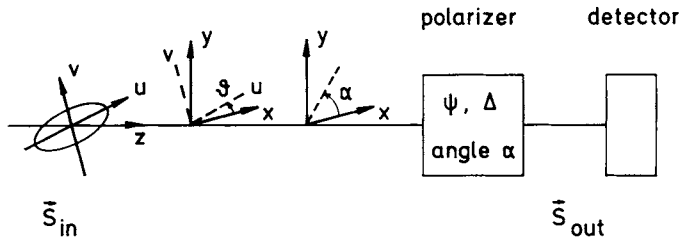


**Fig. 7.** Schematic drawing of system for analyzing polarized light.

Only very few polarimetry experiments have been conducted previously in the VUV region. The obvious difficulty is to measure the polarization of the light with a polarizer of unknown characteristics (which need to be determined at the same time). Without relying on other input parameters such as the optical constants of the polarizer surfaces, such a measurement requires the use of two sequential polarizers, which can be rotated independently [3, 25, 26, 27]. In the present experiment, however, the sample itself may be regarded as a polarizer, and by using all the mechanical degrees of freedom of our ellipsometer, we are able to perform all characterization measurements without any additional optical elements. To understand the measurement procedure, it is necessary first to deduce some relations between the measured detector signal and the parameters of the light, sample, and polarizer in the Mueller matrix formalism.

Consider the situation of Fig. 7, where light is incident on a polarizer and the intensity of the transmitted fraction is detected. The polarization of the incoming light is conveniently described by its Stokes vector in the $u$, $v$, $z$ coordinate frame with the $z$-axis being the direction of propagation and the $u$, $v$-axes coincident with the main axes $a$ and $b$ of the polarization ellipse [28]:

$$\mathbf{S}_{in} = \begin{pmatrix} I \\ IP\cos 2\varepsilon \\ 0 \\ IP\sin 2\varepsilon \end{pmatrix}. \tag{2}$$

Here $I$ denotes the light intensity, $P$ the degree of total polarization, and $\varepsilon$ the ellipticity with $\tan \varepsilon = b/a$. In Fig. 7, $\theta$ defines a tilt angle of the $u$, $v$, $z$ frame with respect to an $x$, $y$, $z$ laboratory frame, and $\alpha$ is the angle of rotation of the polarizer; both rotations are about the (common) $z$-axis.

The Stokes vector of the transmitted light in the laboratory frame is then calculated by multiplication of the Stokes vector of the incoming light with

$4 \times 4$ real Mueller matrices [29],

$$\mathbf{S}_{\text{out}} = R_{-\alpha} M_{\text{pol}} R_{\alpha} R_{-\theta} \mathbf{S}_{\text{in}}, \tag{3}$$

where $R$ represents a rotation by an angle indicated as a subscript and $M_{\text{pol}}$ represents a polarizer. Since our detector is insensitive to polarization, we measure only the intensity of the outgoing light, which is given by the first component of the Stokes vector. This component remains unchanged under rotation of the vector about the $z$-axis, so we can omit the rotation matrix $R_{-\alpha}$ and calculate the intensity using

$$\mathbf{S}_{\text{out}} = M_{\text{pol}} R_{\alpha-\theta} \mathbf{S}_{\text{in}}$$

$$\mathbf{S}_{\text{out}} = \text{const} \begin{pmatrix} 1 & \cos 2\psi_A & 0 & 0 \\ \cos 2\psi_A & 1 & 0 & 0 \\ 0 & 0 & \sin 2\psi_A \cos \Delta_A & \sin 2\psi_A \sin \Delta_A \\ 0 & 0 & -\sin 2\psi_A \sin \Delta_A & \sin 2\psi_A \cos \Delta_A \end{pmatrix}$$

$$\times \begin{pmatrix} 1 & 0 & 0 & 0 \\ 0 & \cos 2(\alpha-\theta) & \sin 2(\alpha-\theta) & 0 \\ 0 & -\sin 2(\alpha-\theta) & \cos 2(\alpha-\theta) & 0 \\ 0 & 0 & 0 & 1 \end{pmatrix} \begin{pmatrix} I \\ IP \cos 2\varepsilon \\ 0 \\ IP \sin 2\varepsilon \end{pmatrix} \tag{4}$$

and further,

$$I_{\text{det}} = I_0(1 + P \cos 2\varepsilon \cos 2\psi_A \cos 2\theta \cos 2\alpha + P \cos 2\varepsilon \cos 2\psi_A \sin 2\theta \sin 2\alpha). \tag{5}$$

The parameters $\psi_A$ and $\Delta_A$ are related to the complex transmittance of the polarizer for the electric-field vector of the light in $s$ and $p$ geometry [28]:

$$\tan \psi_A e^{i\Delta_A} = (t_p/t_s) e^{i(\delta_p - \delta_s)} \tag{6}$$

Note that frequently used "polarization" or "fractional polarization" of the polarizer follows as

$$\frac{T_s - T_p}{T_s + T_p} = \frac{1 - \tan^2 \psi_A}{1 + \tan^2 \psi_A} = \cos 2\psi_A, \tag{7}$$

with $T_{s,p}=t_{s,p}^2$ as the transmittance of the polarizer for the light intensity in $s$ and $p$ geometry. By comparison of Eqs. 1 and 5, we find the following relations using the Fourier coefficients $a_1$ and $a_2$:

$$P\cos 2\varepsilon\cos 2\psi_A=\sqrt{a_1^2+a_2^2}$$

$$\tan 2\theta=a_2/a_1. \tag{8}$$

Thus, the angle $\theta$ of the polarization plane is determined directly from $a_2/a_1$, but no independent information on the total polarization, ellipticity, and polarization of the polarizer is obtained.

Figure 8 illustrates the situation for an ellipsometry experiment. The incoming light is now incident on a sample with angle $\xi$ between the plane of incidence and the plane of polarization. The reflected light passes through a reflection polarizer and is subsequently detected. The measured intensity may be calculated from

$$\mathbf{S}_{\text{out}}=M_{\text{pol}}R_{\alpha}M_{\text{sample}}R_{-(\xi-\theta)}\mathbf{S}_{\text{in}}. \tag{9}$$

The Mueller matrix $M_{\text{sample}}$ represents the reflection at the sample and is

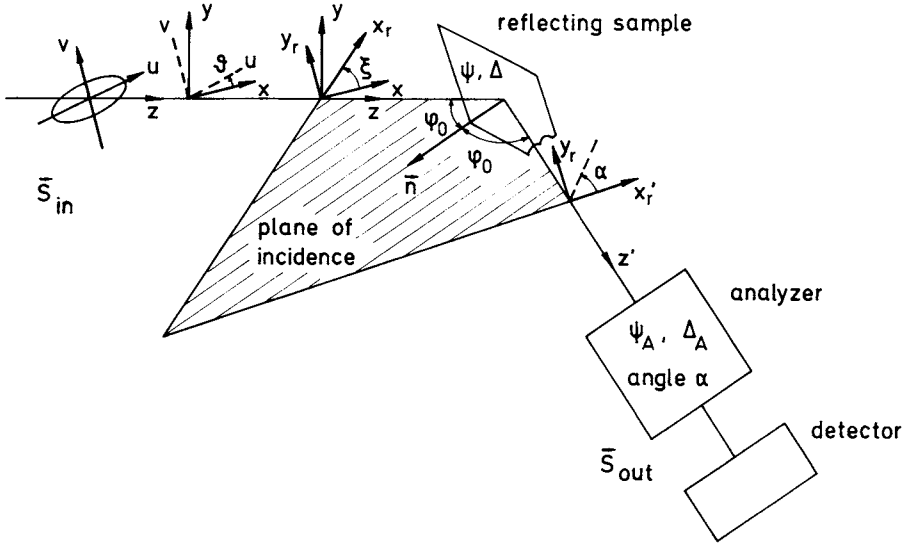


**Fig. 8.** Diagram showing coordinate systems and parameters of ellipsometer.

analogous to that of the reflection polarizer [28],

$$M_{\text{sample}} = \begin{pmatrix} 1 & -\cos 2\psi & 0 & 0 \\ -\cos 2\psi & 1 & 0 & 0 \\ 0 & 0 & \sin 2\psi \cos \Delta & \sin 2\psi \sin \Delta \\ 0 & 0 & -\sin 2\psi \sin \Delta & \sin 2\psi \cos \Delta \end{pmatrix}. \quad (10)$$

The first component of the Stokes vector $\mathbf{S}_{\text{out}}$ gives the detected intensity again, which has the general form of Eq. 1 with the Fourier coefficients

$$a_1 = \frac{P \cos 2\varepsilon \cos 2(\xi - \theta) - \cos 2\psi}{1 - P \cos 2\varepsilon \cos 2(\xi - \theta) \cos 2\psi} \cos 2\psi_A$$

$$a_2 = \frac{P \sin 2\varepsilon \sin \Delta + P \cos 2\varepsilon \sin 2(\xi - \theta) \cos \Delta}{1 - P \cos 2\varepsilon \cos 2(\xi - \theta) \cos 2\psi} \sin 2\psi \cos 2\psi_A. \quad (11)$$

From these two expressions the complex reflectance, $\rho = \tan \psi e^{i\Delta}$, of the sample can be calculated, provided we know the total polarization, $P$, ellipticity, $\varepsilon$, and orientation of the polarization plane, $\theta$, of the input light, and the polarization, $\cos 2\psi_A$, of the analyzer. We may then proceed to calculate the complex dielectric constant, for example, using Fresnel's formula for the two-phase model [28]:

$$\tilde{\varepsilon}_s = \tilde{\varepsilon}_0 (\sin^2 \phi_0 + \left(\frac{1-\rho}{1+\rho}\right)^2 \sin^2 \phi_0 \tan^2 \phi_0), \quad (12)$$

with $\tilde{\varepsilon}_0$ as the dielectric constant of the ambient and $\phi_0$ as the angle of incidence.

Some remarks are in order regarding the relation between the Fourier coefficients and the complex reflectivity $\rho$ of the sample, Eq. 11. Under ideal conditions, that is, $P = 1$, $\varepsilon = 0$, $\cos 2\psi_A = 1$, we obtain the magnitude and phase of the complex reflectance as

$$\tan \psi = \sqrt{\frac{1 + a_1}{1 - a_1}} |\tan(\xi - \theta)|$$

$$\cos \Delta = \frac{a_2}{\sqrt{1 - a_1^2}} \operatorname{sgn}(\xi - \theta), \quad (13)$$

which are the well-known formulas from conventional ellipsometry [8]. The correction for an ellipticity $\varepsilon$ gives only a second-order contribution to the Fourier coefficient $a_1$ and hence also to tan $\psi$, but may influence the coefficient $a_2$ drastically depending on the value of $\Delta$. The polarization of the analyzer enters as a multiplicative parameter in both Fourier coefficients and can thus be taken into account in exactly the same manner as the electronic attenuation factor for the difference in amplification of the ac versus the dc part of the signal [8]. Observe further that $a_1$ is an even function of the effective tilt angle $(\xi - \theta)$ of the ellipsometer; $a_2$ is an odd function of $(\xi - \theta)$ only if the ellipticity is zero, and otherwise it contains an offset.

## B Calibration

The calibration procedure is performed to establish the reference azimuthal angles for the plane of polarization of the incident light and for the analyzer. The procedure has been described in detail by Aspnes [8] and relies on the fact that linearly polarized light, reflected at an oblique angle, remains linearly polarized only if the plane of polarization is either parallel or perpendicular to the plane of incidence. The plane of polarization is determined accurately by measuring the Fourier coefficients for a range of angles about the horizontal, and then fitting a parabola to the residuals of the polarization. The minimum of the parabola gives the plane of polarization, and the analyzer azimuth and electronic attenuation factor can then be readily determined from the Fourier coefficients.

In practice, the calibration defines the condition for $p$-polarization, and the reflected light is linearly polarized, so from Eqs. 1 and 8 the Fourier coefficients are given by

$$1 - a_1^2 - a_2^2 = 0 \tag{14}$$

$$1/2 \arctan(a_2/a_1) = 0. \tag{15}$$

The residuum given by Eq. 14, when plotted as a function of the ellipsometer tilt angle, $\xi$, can be approximated by a parabola for small values of $\xi$. Equation 15, which determines the analyzer offset angle, is linear in $\xi$ [8].

The sum of the squared Fourier coefficients may deviate from unity even for exactly linear-polarized light due to electronic attenuation of the ac component relative to the dc component of the signal. However, the

"zero" position for the ellipsometer tilt angle is unambiguously identified by the minimum value of the residuum. At this position, the "zero" of the analyzer angle is fixed also, and the electronic attenuation factor can be determined [8].

Under nonideal polarization conditions, we have to analyze the expressions in Eqs. 14 and 15 using Eq. 11 for the Fourier coefficients. To simplify the calculation, only first-order terms of the ellipticity $\varepsilon$ and the fraction of unpolarized light, $1-P$, are taken into account. A power-series expansion in the effective ellipsometer tilt angle, $\xi-\theta$, then leads to the expressions

$$\begin{aligned} 1-a_1^2-a_2^2 &= 1-\cos^2 2\psi_A + 2(1-P)\cot^2\psi\cos^2 2\psi_A \\ &\quad + 8\varepsilon\cot^2\psi\sin\Delta\cos\Delta\cos^2 2\psi_A(\xi-\theta) \\ &\quad + 4\cot^2\psi(\sin^2\Delta-(1-P)\cot^2\psi)\cos^2 2\psi_A(\xi-\theta)^2 \\ 1/2\arctan(a_2/a_1) &= \varepsilon\cot\psi\sin\Delta+\cot\psi\cos\Delta(\xi-\theta). \end{aligned} \tag{16}$$

The minimum of the residuum is obtained at

$$\xi_0=\theta+\varepsilon\cot\Delta, \tag{17}$$

and the measured analyzer offset angle at this position is

$$\frac{1}{2}\arctan\frac{a_2}{a_1}=\varepsilon\frac{\cot\psi}{\sin\Delta}. \tag{18}$$

For $P=1$ and $\cos 2\psi_A=1$, Eqs. 17 and 18 are identical with those given by Aspnes for totally polarized light containing ellipticity [15]. We find that the angular position of the minimum of the residuum is displaced by the ellipticity, and its value at the minimum is changed by unpolarized light and nonideal polarization of the polarizer.

## C Error Analysis

Figure 9 shows the variation of the Fourier coefficients $a_1$ and $a_2$ as a function of the angle $\xi$ between the plane of polarization and the plane of reflection (polarizer angle). The sample is a ZnS single crystal, the photon energy is set to 5 eV, and the angle of incidence is 67.5°. The crosses

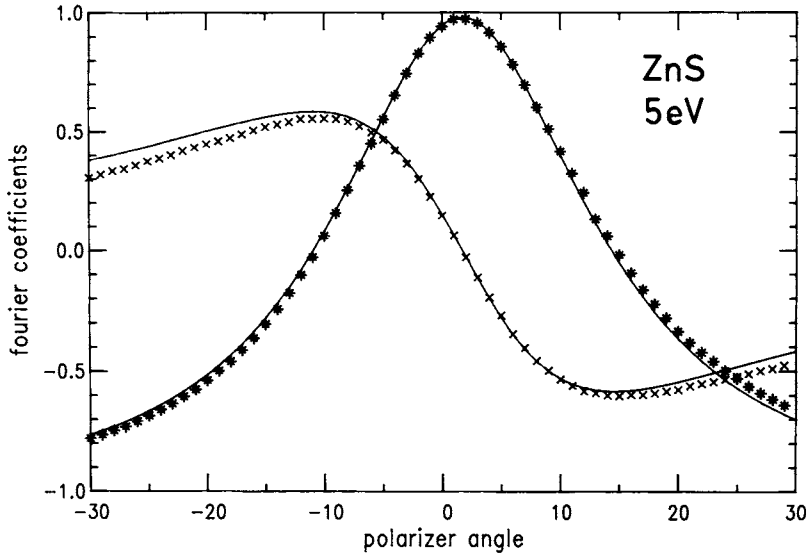


**Fig. 9.** Variation of the Fourier coefficients $a_1$ (stars) and $a_2$ (crosses) versus polarizer angle at fixed photon energy ($\hbar\omega = 5$ eV, $\phi_0 = 67.5°$).

indicate the Fourier coefficients measured with a conventional laboratory ellipsometer corrected with the appropriate analyzer and polarizer offset angles from the calibration. The solid lines are fits to the experimental values according to Eq. 11. Such measurements are extremely useful in estimating the accuracy of the experiment. In this particular case there is a significant discrepancy between the experimental data and the fit at large angles, which cannot be eliminated by varying the parameters of Eq. 11. Fitting the data separately for positive or negative $\xi$ changes the fit parameters $\psi$ by 0.3° and $\Delta$ by 0.5°. This difference can be compensated by a change in the angle of incidence on the sample of $\pm 0.2°$ as the polarizer is rotated, to yield approximately the same values of $\varepsilon_1$ and $\varepsilon_2$ as for the fit in Fig. 9.

This example demonstrates that in addition to the statistical variations in the measured Fourier coefficients, systematic errors in the angles which determine the experimental geometry set limits on the accuracy of the measured dielectric function. Now we will examine the influence of these errors, assuming that we have the optimum geometry so $\xi = \psi$ and $\Delta = -90°$. The variation of the dielectric function due to changes in the Fourier coefficients is then given by

$$\delta\tilde{\varepsilon} = \left(\frac{\partial\tilde{\varepsilon}}{\partial\psi}\bigg|_{\substack{\Delta=-90° \\ \psi=\xi}}\right)\left(\frac{\partial\psi}{\partial a_1}\delta a_1\right) + \left(\frac{\partial\tilde{\varepsilon}}{\partial\Delta}\bigg|_{\substack{\Delta=-90° \\ \psi=\xi}}\right)\left(\frac{\partial\Delta}{\partial a_2}\delta a_2\right) \tag{19}$$

$$\delta\varepsilon_1 = \left(\frac{\sin 2\psi}{4} - 4\sin^2\psi\cos^2 2\psi\right)\delta a_1 + \left(\frac{1}{2} + \sin 2\psi\cos 4\psi\right)\delta a_2 \quad (20)$$

$$\delta\varepsilon_2 = \sin 2\psi(\cos^2 2\psi - \sin^2 2\psi)\delta a_1 + 2\sin^2 2\psi\cos 2\psi\delta a_2. \quad (21)$$

For a value of $\psi = 15°$, we obtain

$$\delta\varepsilon_1 = -0.08\delta a_1 + 0.75\delta a_2, \qquad \delta\varepsilon_2 = 0.25\delta a_1 + 0.43\delta a_2.$$

Thus, an uncertainty in the measured Fourier coefficients introduces an error of the same absolute magnitude in the dielectric function. The experimental error is typically of the order of 0.01, and is therefore negligible, provided the dielectric function is large. In the VUV region, this is usually not the case and furthermore, for samples with low reflectance, the limited primary intensity can lead to an adverse signal-to-noise ratio.

Errors in the analyzer angle and polarizer angle are directly related to uncertainties in the Fourier coefficients, but are typically lower than the statistical uncertainty. The variation of the dielectric function with the uncertainty in the angle of incidence can be calculated from Eq. 12 to be

$$\delta\tilde{\varepsilon} = \frac{2}{\sin\phi_0\cos\phi_0}[(1+\cos^2\phi_0)\tilde{\varepsilon} - \sin^2\phi_0]\delta\phi_0. \quad (22)$$

This error depends on the magnitude of the dielectric function and the angle of incidence. If we assume typical values in the visible and near-UV region of $\tilde{\varepsilon} = 5 + i10$ and $\phi_0 = 67.5°$, we obtain

$$\delta\varepsilon_1 = 30\delta\phi_0; \qquad \delta\varepsilon_2 = 60\delta\phi_0.$$

Typical values for the VUV range ($\tilde{\varepsilon} = 1 + i0.2$ and $\phi_0 = 45°$) yield

$$\delta\varepsilon_1 = 4\delta\phi_0; \qquad \delta\varepsilon_2 = 1.2\delta\phi_0.$$

Thus, the absolute magnitude of this systematic error is reduced by about the same amount as the change in the absolute magnitude of the dielectric function. We conclude that the systematic errors limit the accuracy of ellipsometry at low photon energies, whereas statistical errors

due to diminishing reflected signal limit the accuracy at high photon energies.

Figure 10 shows the Fourier coefficients plotted against polarizer angle $\xi$ for ZnS at 8 eV measured with the synchrotron-radiation ellipsometer. Note that $\Delta$ is close to $-90°$ in this example, so the optimum angle of incidence is 67.5°. The quality of the fit indicates that it is in fact possible to obtain accuracies with this UHV system comparable to those routinely achieved with standard ellipsometers. It is necessary, however, to perform a rather time-consuming adjustment procedure to establish all the angular settings to an accuracy of a few tenths of a degree, and the storage ring must operate stably over this period of time.

Figure 11 shows results obtained at higher photon energies using a reflection polarizer. These measurements can be used not only to determine the ellipsometric angles with good accuracy, but can also be used to determine the polarization of the incoming light and the polarization properties of the polarizer. The data analysis indicates that the output of the monochromator contains negligible contributions of elliptically polarized light, but unpolarized light must be taken into account at high photon energies. In the energy range below 12 eV it was not possible to obtain satisfactory fits for measurements with the reflection polarizer, most probably due to second-order light from the monochromator grating. At higher energies, the second-order radiation is adequately suppressed by

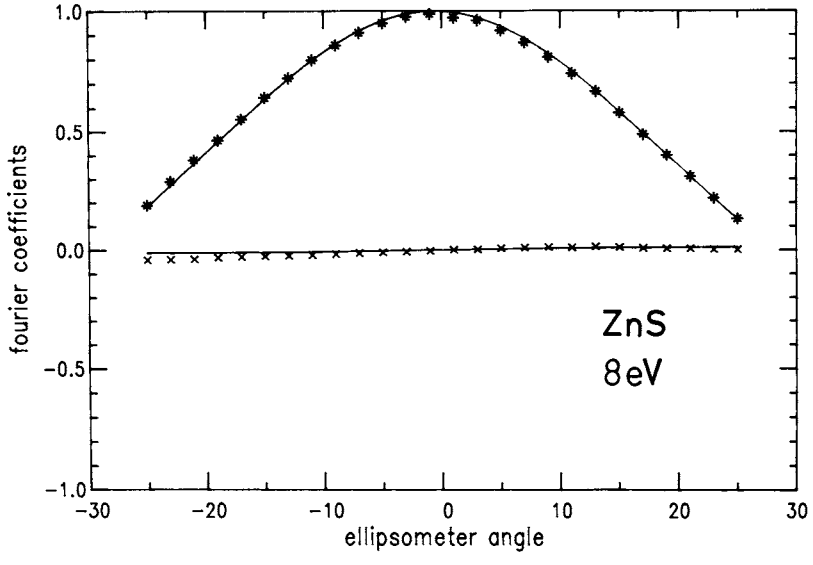


**Fig. 10.** Variation of the Fourier coefficients $a_1$ (stars) and $a_2$ (crosses) versus polarizer angle at fixed photon energy ($\hbar\omega = 8$ eV, $\phi_0 = 67.5°$).

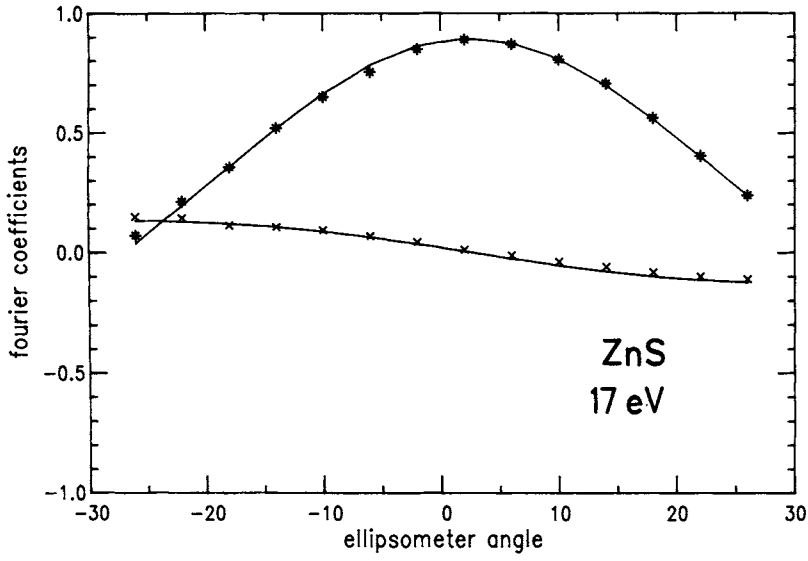


**Fig. 11.** Variation of the Fourier coefficients $a_1$ (stars) and $a_2$ (crosses) versus polarizer angle at fixed photon energy ($\hbar\omega = 17$ eV, $\phi_0 = 45°$).

the monochromator, and below 10 eV we use a $MgF_2$ Rochon polarizer, which absorbs all radiation above 11.2 eV, so second-order light is transmitted only for $\hbar\omega < 5.6$ eV.

The results of all the fits of the Fourier coefficients versus polarizer angle for ZnS are compiled in Table I. The sample was cleaved in air and

**TABLE I**

**The Dielectric Function of Cleaved ZnS(110) at Room Temperature, Determined by Stepwise Rotation of the Plane of Polarization at Fixed Photon Energies**

| $\hbar\omega$ | $\varepsilon_1$ | $\varepsilon_2$ | $\hbar\omega$ | $\varepsilon_1$ | $\varepsilon_2$ |
|---|---|---|---|---|---|
| 4.0 | 7.06 | 3.16 | 9.5 | −1.47 | 3.74 |
| 5.0 | 7.04 | 5.58 | 12.0 | 0.46 | 0.43 |
| 6.5 | 3.32 | 7.36 | 14.0 | 0.08 | 0.82 |
| 7.0 | −0.57 | 10.13 | 15.0 | −0.06 | 0.66 |
| 8.0 | −1.17 | 4.31 | 17.0 | 0.19 | 0.55 |
| 9.0 | −0.55 | 4.35 | 20.0 | 0.45 | 0.38 |

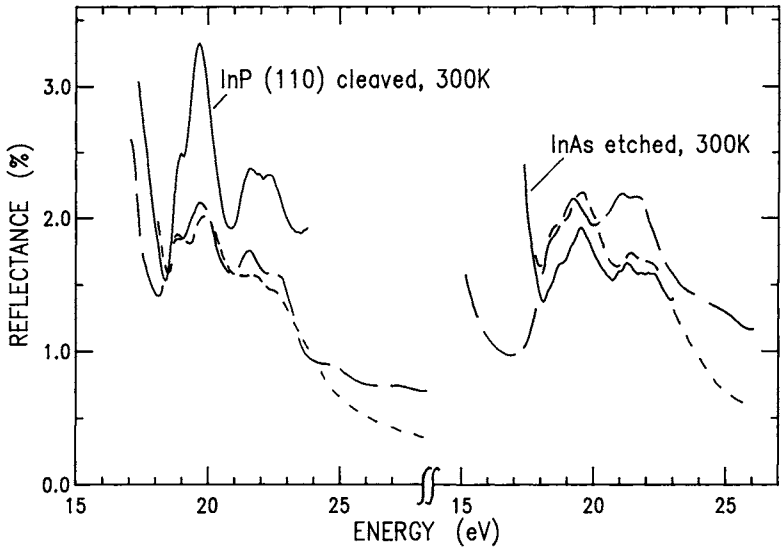


**Fig. 12.** Reflectance of InP and InAs at the In 4d edge, calculated from ellipsometric data (solid curves). For comparison the reflectance calculated by Kramers–Kronig analysis of absorption data (short dashed lines) and directly measured (long dashed lines) are included from Ref. [31].

subsequently introduced into the UHV system. The data at 4 eV and 5 eV were obtained on the same sample using a rotating-analyzer ellipsometer at our institute in Stuttgart. We estimate the uncertainty in the dielectric function to be about 0.5 for measurements below 10 eV and 0.1 for $\hbar\omega > 10$ eV in both $\varepsilon_1$ and $\varepsilon_2$.

## IV RESULTS AND COMPARISON WITH REFLECTANCE SPECTRA

### A III-V Semiconductors

The optical constants of the III-V compounds in the energy range of about 20 eV are interesting because the threshold for core *d*-level excitation lies in this region. Reflectance spectra have been reported in Refs. [31] and [32], and the data for InP and InAs are shown in Fig. 12 together with the reflectance calculated from our ellipsometrically determined dielectric function. The InAs sample was chemically etched to strip off the surface oxides following the recipe described by Aspnes [32] and was introduced into the UHV chamber after etching. The InP sample was

cleaved in situ along the (110) plane. All the reflectance spectra in [32] were measured on chemically etched samples. The absolute reflectances all compare very well; however, the spectral features at the In 3d edge are much more pronounced for the sample that was cleaved in situ. It is our experience that the structures are most clearly observed from single crystals cleaved in situ. It is important to note that ellipsometry can be carried out with a reasonable signal-to-noise ratio even when the absolute reflectivity of the sample is only about 1%.

Figures 13, 14, and 15 show the dielectric function of GaP, GaAs, and InP in the photon energy region 15–30 eV. All the samples are single crystals cleaved in situ and cooled to liquid-nitrogen temperature to enhance the weak structures at the Ga 3d and In 4d edges. These results are summarized in Ref. [30], which should be consulted for more details.

## B II-VI Compounds

### 1 *ZnS*

Figures 16 and 17 show the dielectric function of cubic ZnS at room temperature over the photon-energy range 3–22 eV, with the data from

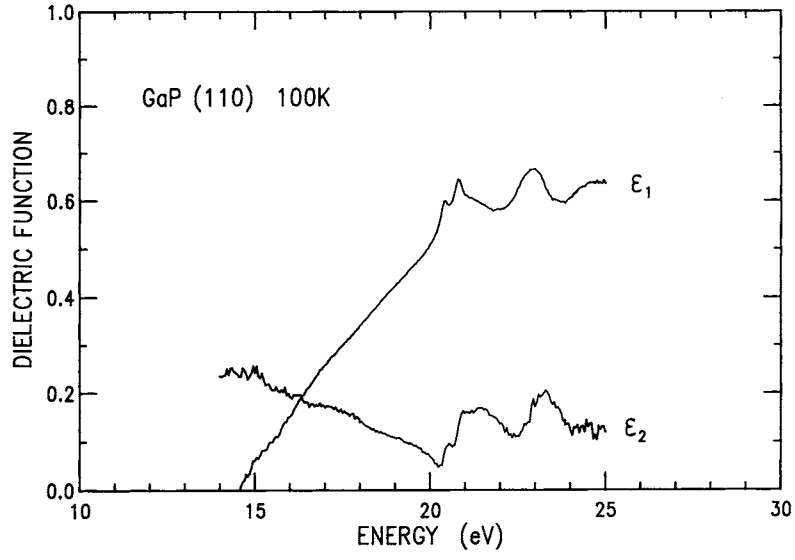


**Fig. 13.** Dielectric function of cleaved GaP(110) at 100 K.

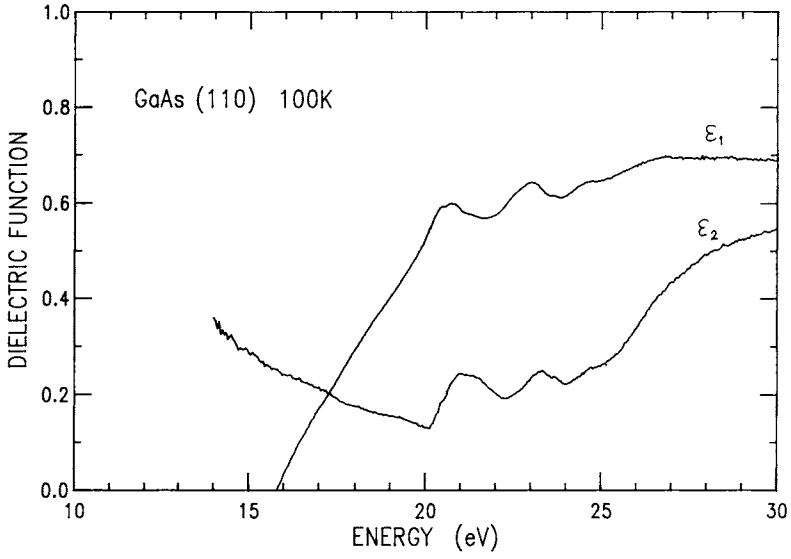


**Fig. 14.** Dielectric function of cleaved GaAs(110) at 100 K.

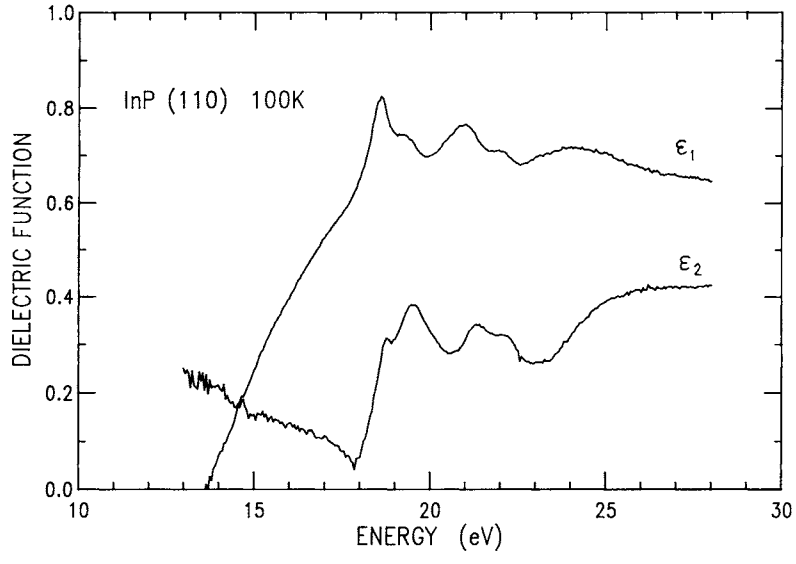


**Fig. 15.** Dielectric function of cleaved InP(110) at 100 K.

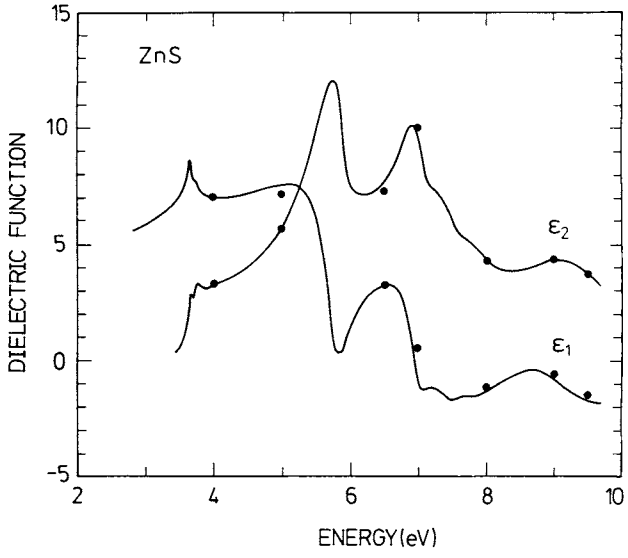


**Fig. 16.** Dielectric function of cleaved ZnS(110) at room temperature. The dots are the data from Table I.

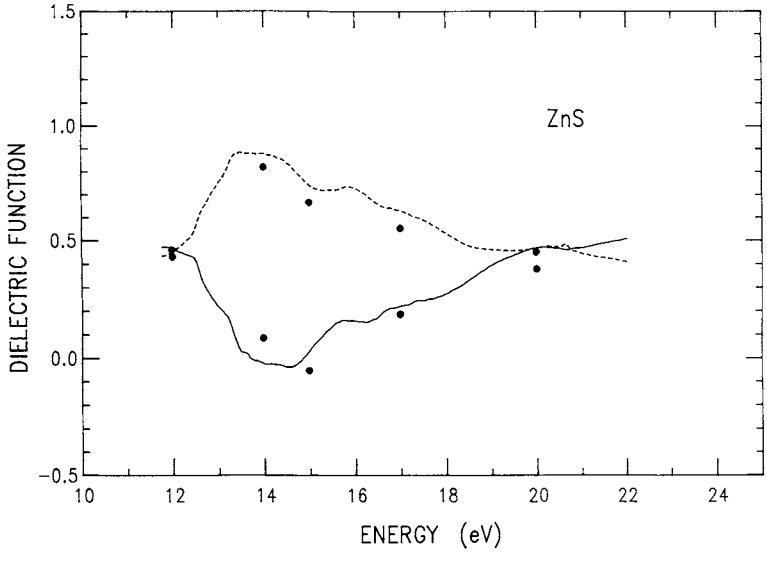


**Fig. 17.** Dielectric function of cleaved ZnS(110) at room temperature. ($\varepsilon_1$, solid line; $\varepsilon_2$, dashed line). The dots are the data from Table I.

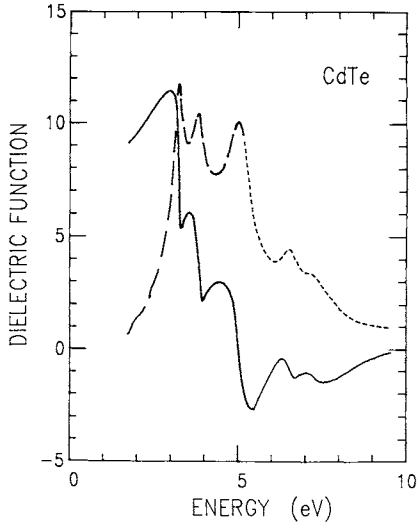


**Fig. 18.** Dielectric function of cleaved CdTe(110) at room temperature. ($\varepsilon_1$, solid line; $\varepsilon_2$, dashed line).

Table I included for comparison. The data below 5.6 eV were obtained with an ellipsometer at the Max-Planck-Institute in Stuttgart on samples previously measured at BESSY. Both natural ZnS and laboratory-grown single crystals were measured, some of which were cleaved in air and some in situ. In the photon-energy region below 10 eV, no significant differences were observed between different samples. Above 12 eV, the structures in the dielectric function were most pronounced for the natural crystal cleaved in situ. The structures in this energy range originate from transitions of Zn 3d electrons into the conduction band. By differentiating such spectra, the energies of conduction-band critical points can be readily determined. It is interesting to note that although the magnitudes of $\varepsilon_1$ and $\varepsilon_2$ are greatly reduced in the VUV compared with the visible region, detailed information can be derived from the ellipsometric data.

## *CdTe* 2

Figures 18 and 19 show the dielectric function of CdTe with the data from Lautenschlager *et al.* [34] included below $\hbar\omega = 5.6$ eV. In this case the samples are all etched single crystals measured at room temperature, so it is likely that the data in the energy range above 12 eV are influenced by a surface layer on the sample. The fine structures in the high-energy spectrum are due to transitions of Cd 4d electrons into the conduction band.

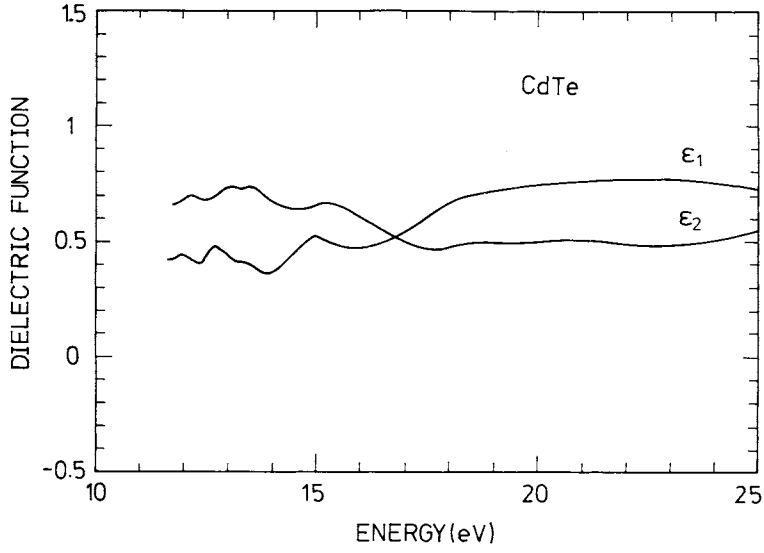


**Fig. 19.** Dielectric function of cleaved CdTe(110) at room temperature for energies above the Cd 4d threshold.

From our ellipsometrically determined dielectric-function data, it is straightforward to calculate a reflectance curve, which can be directly compared with experimental reflectivity data. In Fig. 20 we compare our calculated reflectance with the data measured by Jung [35], and the agreement is excellent. The Kramers–Kronig analysis of the reflectance data, however, yields values for $\varepsilon_2$ that differ by about 25% from the ellipsometrically measured value. In view of the excellent agreement of the reflectivity calculated from the dielectric function and the directly measured reflectance data, the discrepancy in $\varepsilon_2$ can probably be attributed to incorrect extrapolation of the reflectance when performing the Kramers–Kronig analysis. This example demonstrates nicely how ellipsometric measurements can augment reflectivity data. In the VUV region, where sample surface conditions play a particularly important role, it is advantageous to be able to compare data from two independent measurement techniques.

## C Calcium Fluoride

Another example of the type of data that can be obtained from the VUV ellipsometer is the dielectric function from a cleaved $CaF_2$ (111) crystal at

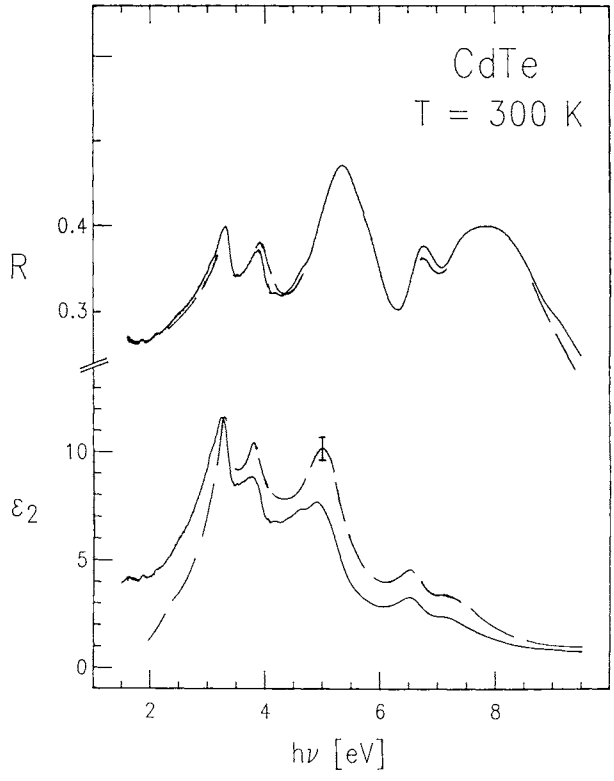


**Fig. 20.** Reflectance spectrum of CdTe and imaginary part of the dielectric function obtained by Kramers–Kronig analysis [35] (solid curves), compared to the reflectivity calculated from ellipsometric data (dashed curve) and the directly measured $\varepsilon_2$ spectrum (dashed curve).

room temperature, shown in Fig. 21. This spectrum covers the photon-energy range 10–35 eV and indicates the power of spectroscopic ellipsometry using synchrotron radiation for studying the optical properties of insulators. Considerable structure is observed throughout the entire energy range due to interband transitions between the F 2p derived valence and the Ca 4s and 3d derived conduction bands, but the threshold structures at 11.2 eV are obscured by second-order light from the monochromator grating. Above 27 eV, excitation of the 3p core electrons dominate the spectrum. In the lower energy region the spectrum is fairly well described by a recent band-structure calculation [36]. At higher energies, there is a plethora of excitonic lines associated with transitions from the Ca 3p core level; a more complete data analysis can be found in Ref. [37].

There are discrepancies of up to a factor of two between previous reflectance and energy-loss measurements on $CaF_2$, so we also performed

reflectance measurements in our ellipsometer. In Fig. 22 the direct measurement is compared to the reflectance calculated from our dielectric-function data, and it can be seen that the results agree to within the experimental error.

## V SUMMARY

Ellipsometry has developed into a standard technique for studying the optical constants of solids in the NIR-VIS-UV spectral region with high precision. With our present instrument we have demonstrated the feasibility of performing ellipsometry in the VUV and have obtained useful data from a range of samples. The examples shown here illustrate the variety of optical excitations in solids that can be studied in this spectral range. Valence excitations can be followed to energies far above the absorption threshold, and structures due to core-level excitations can be resolved in detail. For insulators with large band gaps, VUV ellipsometry is a very promising technique for band-structure investigations.

The accuracy of our results is comparable to the best reflectance data, but ellipsometry has the advantage of directly determining both real and imaginary parts of the dielectric function, and thus avoids the uncertainty

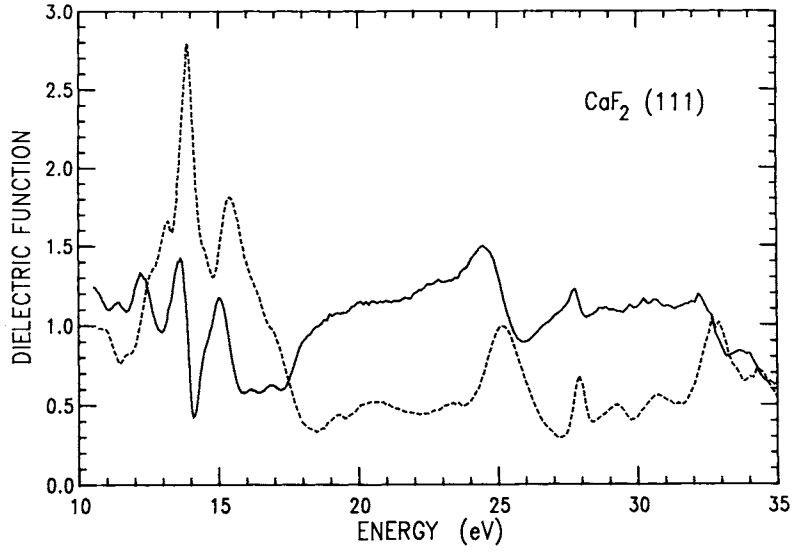


**Fig. 21.** The dielectric function of cleaved $CaF_2(111)$ at room temperature ($\varepsilon_1$, solid line, $\varepsilon_2$, dashed line).

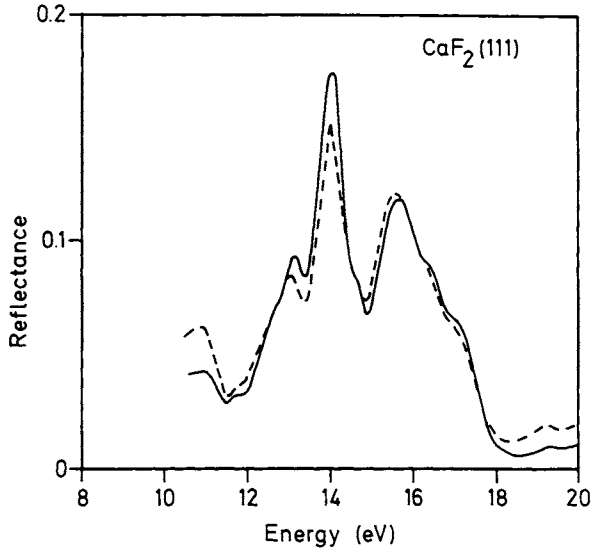


**Fig. 22.** Reflectance of $CaF_2$ at room temperature: the dashed line indicates directly measured reflectance; the solid line indicates reflectivity calculated from ellipsometric dielectric function.

associated with a Kramers–Kronig analysis. Ellipsometry is therefore potentially a more powerful technique for determining the optical constants of solids. It is to be expected that instruments with higher mechanical precision and stability, using improved polarizers and monochromators with better spectral purity, will be constructed in the near future, which will be able to obtain optical constants with enhanced precision up to even higher photon energies.

## ACKNOWLEDGEMENT

This work was supported under project no. 05 490CAB by the German Federal Minister for Research and Technology (BMFT).

## REFERENCES

1. D. Beaglehole, *Rev. Sci. Instr.* **59**, 2557 (1988).
2. M. Schledermann, DESY Internal Report 70/28 (1970).
3. M. Schledermann and M. Skibowski, *Appl. Opt.* **10**, 321 (1971).
4. W. R. Hunter in "Handbook of Optical Constants of Solids," (E. D. Palik, ed.), Academic Press, Orlando (1985).
5. D. Y. Smith in "Handbook of Optical Constants of Solids," (E. D. Palik, ed.), Academic Press, Orlando (1985).
6. D. W. Lynch in "Handbook on Synchrotron Radiation," Vol. 2, (G. V. Marr, ed.), North-Holland, Amsterdam (1987).

7. P. Drude, *Ann. d. Phys. u. Chem.* **36**, 532 (1889); **39**, 481 (1890).
8. D. E. Aspnes and A. A. Studna, *Appl. Opt.* **14**, 220 (1975).
9. S. Logothetidis, L. Viña, and M. Cardona, *Phys. Rev.* **31**, 2180 (1985).
10. D. E. Aspnes in "Optical Properties of Solids: New Developments," (B. O. Seraphin, ed.), North-Holland, Amsterdam (1976).
11. D. E. Aspnes in "Handbook of Optical Constants of Solids," (E. D. Palik, ed.), Academic Press, Orlando (1985).
12. Proc. Int. Conf. on Ellipsometry, published as Vols. 16, 56, 96 of *Surf. Sci.*
13. R. L. Johnson, J. Barth, M. Cardona, D. Fuchs, and A. M. Bradshaw, *Rev. Sci. Instr.* **60**, 2209 (1989).
14. D. E. Aspnes, *J. Opt. Soc. Am.* **64**, 639 (1974).
15. D. E. Aspnes, *J. Opt. Soc. Am.* **64**, 812 (1974).
16. M. Yamamoto and O. S. Heavens, *Surf. Sci.* **96**, 202 (1980).
17. D. Chandler-Horowitz and G. A. Candela, *Appl. Opt.* **21**, 2972 (1982).
18. R. N. Hamm, R. A. MacRae, and E. T. Arakawa, *J. Opt. Soc. Am.* **55**, 1460 (1965).
19. V. G. Horton, E. T. Arakawa, R. N. Hamm, and M. W. Williams, *Appl. Opt.* **8**, 667 (1969).
20. The triple-reflection polarizers were supplied by B. Halle Nachfolger GmbH, Berlin.
21. C. G. Olson and D. W. Lynch, tabulated optical data for Au in "Optical Properties of Metals II," (J. H. Weaver, C. Krafka, D. W. Lynch, and E. E. Koch, eds.), Fachinformationszentrum, Karlsruhe (1981).
22. J. Barth, E. Tegeler, M. Krisch, and R. Wolf in "Soft X-ray Optics and Technology," (E. E. Koch and G. Schmahl, eds.), *Proc. SPIE* **733**, 481 (1986).
23. M. Krumrey, E. Tegeler, J. Barth, M. Krisch, F. Schaefers, and R. Wolf, *Appl. Opt.* **27**, 4336 (1988).
24. R. Korde, L. R. Canfield, and B. Wallis, in "Ultraviolet Technology II," *Proc. SPIE* **932**, 153 (1988).
25. W. B. Westerveld, K. Becker, P. W. Zetner, J. J. Corr and J. W. McConkey, *Appl. Opt.* **24**, 2256 (1985).
26. A. Gaupp and W. B. Peatman in "Soft X-ray Optics and Technology," (E. E. Koch and G. Schmahl, eds.), *Proc. SPIE* **733**, 272 (1986).
27. J. Barth, R. L. Johnson, S. Logothetidis, M. Cardona, D. Fuchs and A. M. Bradshaw in "Soft X-ray Optics and Technology," (E. E. Koch and G. Schmahl, eds.), *Proc. SPIE* **733**, 265 (1986).
28. R. M. A. Azzam and N. M. Bashara, "Ellipsometry and Polarized Light," North-Holland, Amsterdam (1977).
29. H. Mueller, *J. Opt. Soc. Am.* **38**, 661 (1948).
30. J. Barth, R. L. Johnson, M. Cardona, D. Fuchs and A. M. Bradshaw, *Proc. 19th Int. Conf. Phys. of Semicond.*, Warsaw, 1988, (W. Zawadski, ed.), Institute of Physics, Polish Academy of Sciences, Warsaw, 885 (1988).
31. W. Gudat, E. E. Koch, P. Y. Yu, M. Cardona, and C. M. Penchina, *Phys. Status Solidi (b)* **52**, 505 (1972).
32. D. E. Aspnes, M. Cardona, V. Saile, M. Skibowski, and G. Sprüssel, *Solid State Commun.* **31**, 99 (1979).
33. D. E. Aspnes and A. A. Studna, *Phys. Rev. B* **27**, 985 (1983).
34. P. Lautenschlager, S. Logothetidis, L. Viña, and M. Cardona, *Phys. Rev. B* **32**, 3811 (1985).
35. C. Jung, private communication.
36. R. A. Heaton and C. C. Lin, *Phys. Rev. B* **22**, 3629 (1980).
37. J. Barth, R. L. Johnson, M. Cardona, D. Fuchs and A. M. Bradshaw, *Phys. Rev. B* **41**, 3291 (1990).

# Chapter 11

# Methods Based on Multiple-Slit Fourier Transform Interferometry for Determining Thin-Film Optical Constants in the VUV/Soft X-Ray Range

ROMAN TATCHYN*
Stanford Synchrotron Radiation Laboratory
Stanford University
Stanford, California
and
Institute of Theoretical Science
University of Oregon
Eugene, Oregon

I. Introduction to MSFTI 247
II. Fundamental Dimensional Constraints and Inequalities 253
III. Relationship of MSFTI to Alternative Metrological Techniques 254
IV. General Experimental Equations and Sensitivity Analysis 258
V. A Characterization of the Optical Constants of Au Using MSFTI in the 280–640 eV Range 265
VI. Problems and Prospects in Sample Preparation 270
VII. Prospects for MSFTI in Other Spectral Regimes 272
VIII. Summary 273
Acknowledgments 274
References 274

## I. INTRODUCTION TO MSFTI

We begin with an elementary discussion of the physical principles on which the metrological technique of multiple-slit Fourier transform

* Affiliate Member, Center for X-Ray Optics, Lawrence Berkeley Laboratory, Berkeley, California 94720.


Copyright © 1991 by Academic Press.
All rights of reproduction in any form reserved.
ISBN 0-12-544422-2

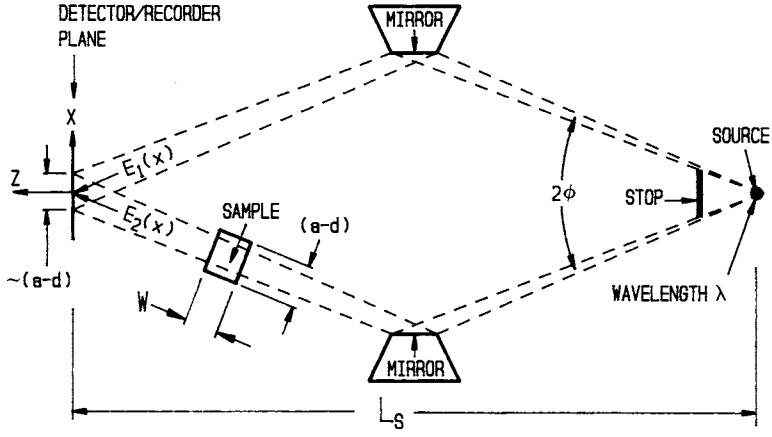


**Fig. 1.** Elementary split-beam interferometer configuration excited by a monochromatic point source. The mirrors are symmetrically positioned midway between the source and detector planes. For sufficiently small $\lambda$, $\lambda/(a-d)$, and sufficiently long beam path lengths, the wave fronts impinging on the detector can be assumed to be planar.

interferometry (MSFTI), or transmission-diffraction interferometry [1–3], is based. This will provide a foundation for the more detailed discussions to follow, and will also enable us to classify this still relatively new method with reference to the large number of alternative or complementary techniques reviewed elsewhere [4–8].

As a starting point, we consider the basic configuration of a symmetric split-beam interferometer of the direct-field type [9], shown schematized in Fig. 1. The depicted source is assumed to be monochromatic with wavelength $\lambda$. An isotropic, homogeneous, and uniformly thick sample characterized by the complex index of refraction $\hat{n}(\lambda) = (1 - \delta(\lambda)) + ik(\lambda)$, where $\delta$ and $k$ are the $\lambda$-dependent phase and absorption components [10, 11], intercepts the lower beam at normal incidence. Approximating both beams by plane waves of unit amplitude and assuming complete cancellation of surface phase shifts and negligible multiple scattering (that is, reflection) [12] within the sample, we can straightforwardly determine the intensity distribution generated on the recorder–detector plane by the two interfering wavefronts to be

$$|E_1(x) + E_2(x)|^2 = (1 + e^{-4\pi Wk}) + 2e^{-2\pi Wk} \cos(2\pi[2x \sin \phi + W\delta]). \quad (1)$$

Here all the length dimensions have been normalized into units of

"numbers of wavelengths $\lambda$," a convention to be used throughout this chapter. From Eq. 1 it is evident that by interchanging two or more samples with different $W$s, $\delta$ and $k$ can be recovered from measurements of the interference pattern's fringe-shift, $W\delta/2 \sin\phi$, and contrast ratio $[2\exp(-2\pi Wk)/(1+\exp(-2\pi Wk)]^2$.

Now consider the case depicted in Fig. 2, in the limit where the two mirrors are removed and the beam stop height is reduced to zero, allowing the adjacent beam boundaries to just touch each other. It is clear that in this limit the two independent wavefronts can at best be made to illuminate *contiguous* regions on the detector plane, apparently leaving no direct way to discern a measurable interference pattern.

We note, in passing, that the removal of the mirrors from the apparatus in Fig. 1 has resulted in a configuration of utmost simplicity, that is to say, the precisely configured interferometer has been reduced to nothing more than a point source, a sample, and an aperture in the detector plane. As indicated, the sample has been advanced forward to the original detector plane, since in the eikonal[1] approximation [13] (which is conventionally assumed for the direct-field interferometric technique under discussion), the sample's distance from the detector plane does not alter the amplitude or phase modulation of the transmitted light reaching the plane. We will henceforth refer to the plane at which the sample is located as the *sample plane*.

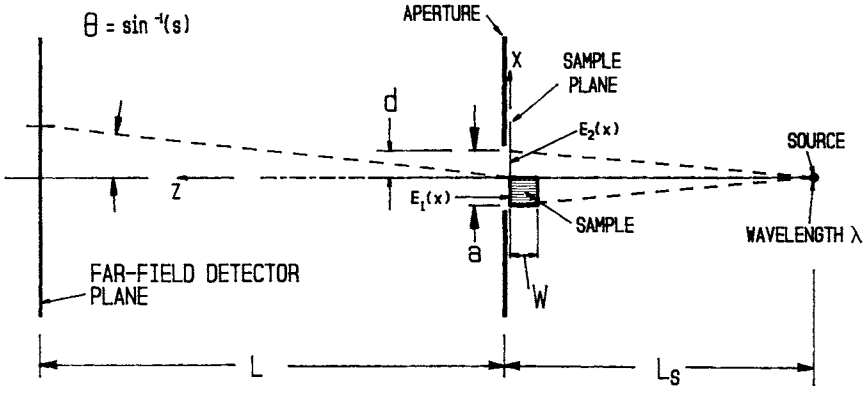


**Fig. 2.** Elementary configuration for Fourier transform interferometry viewed as a limiting case of a conventional split-beam interferometer. The width of the sample in the $x$ direction is $(a-d)$.

[1] The meaning of this term, as we use it here and throughout this chapter, is that diffraction is assumed to be negligible *over the limited distance of light travel through the medium in question*. In the far field, we assume that diffraction will *always* manifest itself. In quantitative terms, we do not actually take the wavelength limit to zero, but simply assume it to be sufficiently smaller than the minimum lateral dimension of the optical neighborhood in question.

The configuration of Fig. 2 in fact provides a convenient starting point for implementing techniques based on Fourier transform interferometry (FTI). To wit, we simply move into the far field [14], away from the sample plane, and the two apparently disparate electrical-field distributions, $E_1(x)$ and $E_2(x)$, will generate an interference pattern given by the absolute value squared of the Fourier transform of their sum. Under the restriction (which will be relaxed later) that the sample width be equal to the aperture width, that is, that $a = 2d$, this far-field intensity pattern is straightforwardly found to be

$$|\overline{E_1(x) + E_2(x)}|^2 = \left| \int_0^d dx e^{-2\pi i s x} + \int_{-d}^0 dx e^{-2\pi i W[\delta - ik]} e^{-2\pi i s x} \right|^2$$

$$= (d)^2 \operatorname{sinc}^2(ds)[(1 + e^{-4\pi k W}) + 2e^{-2\pi k W} \cos(2\pi[ds - W\delta])]. \tag{2}$$

In Eq. 2 we have utilized the notation $\operatorname{sinc}(x)$ to represent the quantity $\sin(\pi x)/\pi x$, and an overbar to represent the Fourier transformation. We point out (with reference to Fig. 2) that $s$ can be interpreted as the sine of the angle with respect to the axis of symmetry of the system (the $z$ axis) [15].

We now systematically compare Eq. 2 with Eq. 1. First, apart from the $\operatorname{sinc}^2$ factor in Eq. 2 and an inessential sign reversal, the expression in square brackets is identical in form to the right-hand side of Eq. 1. In this sense, we have established that the basic FTI approach allows us to regain valid analytical terms from which the optical constants of the sample material can in principle be unfolded. Second, we note that even for the simple configuration being considered, the FTI technique already exhibits certain decisive advantages over the direct-field method. The first of these is the greatly simplified physical arrangement upstream of the sample plane in Fig. 2. The second stems from the fact that we can now place our detector at arbitrarily large distances from the sample in the far field, and provided we do not lose sensitivity to the transmitted signal altogether, we can in principle resolve the measured features of the intensity spectrum with superior precision.

Having isolated these two evident advantages, we are now in turn forced to recognize that the $\operatorname{sinc}^2$ factor in Eq. 2 constitutes a potentially troublesome difference with respect to Eq. 1. By virtue of possessing a period comparable to the half-width of the cos term on its right, this factor is capable of distorting both the shapes and locations of the salient intensity maxima associated with the term in square brackets. It is clear that this "damping" modulation (whose direct-field analog is ordinarily negligible

[16]), can render the unambiguous characterization of the far-field spectrum problematical. In this fashion we come face-to-face with essentially two basic possibilities for mitigating this problem. In both instances, the basic idea is to sharpen the salient maxima of the intensity pattern with respect to the fixed $\text{sinc}^2$ pattern: in the first case by greatly reducing the period of the cos term in Eq. 2, and in the second by greatly compressing, or sharpening, the angular width of its intensity peaks.

The first approach is readily implemented by introducing an axially centered displacement $D'$ between the two contiguous illuminated strips at the sample plane in Fig. 2. This modification is trivially incorporated into Eq. 2 by suitably changing the integral limits, and the resulting expression for the intensity assumes the same form as Eq. 2, with the period of the cos term replaced by $[1/(d+D')]$, QED. This approach, which was in fact originally employed for measuring optical phase constants by Rayleigh [17], is in many respects analogous to Young's original double-slit configuration [18]. Its primary disadvantage is that it greatly increases the number of fringes in the far field without significantly adding to the information content associated with any fringe pair. In this respect it is highly wasteful of source light, a potentially limiting factor under certain circumstances.

A second drawback, especially troublesome in the soft X-ray range, is that even a significant attenuation of either beam will only weakly affect the contrast ratio of the intensity pattern. In fact, as may be verified by applying the sensitivity operator defined in Section IV, the sensitivities of the contrast ratio and the intensity peaks to incremental changes in $Wk$ actually vanish when the two beams become equal (that is, when $Wk \dot{\rightarrow} 0$), mandating the accurate measurement of the (nearly evanescent) intensity minima for the determination of $k$. In view of fundamental signal-to-noise limitations, this tends to make split-beam configurations significantly less flexible for measuring absorption than for phase delay.

A schematized version of the second approach is depicted in Fig. 3. The basic idea is to set up an alternating periodic array of $N$ samples and open apertures, that is to say, to configure a diffraction grating out of the material to be measured. This multiplicity of (nominally identical) periods and open apertures underlies our addition of the *multiple-slit* qualifier to the name of the basic FTI method. From elementary Fourier theory, we observe that the $N$-fold increase in the number of periods will indeed compress the angular widths of the far-field intensity peaks in inverse proportion to $N$, making the identification and measurement of the sharpened maxima highly insensitive to the attenuating $\text{sinc}^2$ factor. In addition, two other significant advantages can be shown to accrue [1, 2]:

(i) By selecting the dimensions and the number of periods of the grating structure properly, the effects of both $\delta$ and $k$ on the far-field intensity maxima can be individually controlled. MSFTI can consequently

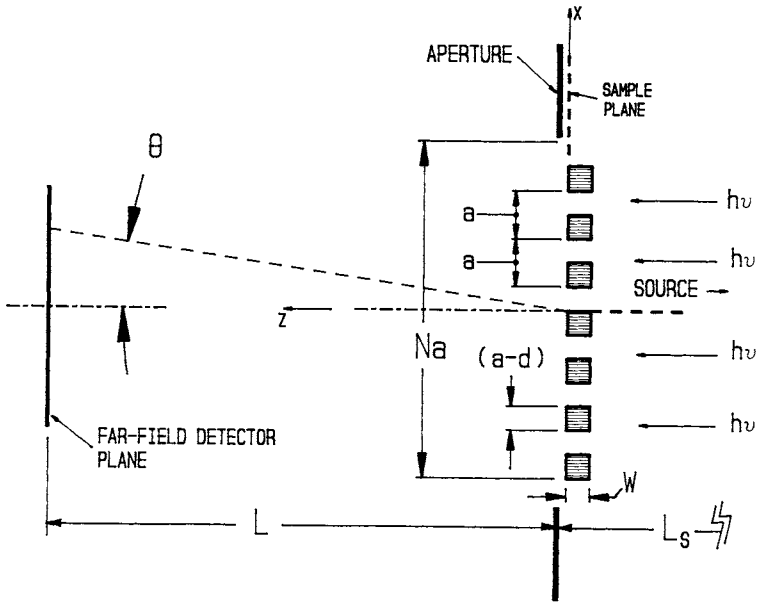


**Fig. 3.** Simplified version of the full MSFTI configuration. The incoming light waves are assumed to be planar.

be optimized for measuring both parts of the complex index of refraction with flexible accuracy.

(ii) Small-scale imperfections in the grating (sample) material, by virtue of generating much more spread-out spectra than the grating lattice, exert a proportionally diluted effect on the salient intensity peaks in the far field, minimizing the effect of such imperfections on the measured accuracy of $\hat{n}$.[2]

It is instructive to assess the basic principles underlying the MSFTI technique from the point of view of physical optics. Perhaps the most natural interpretation of the method is to view the periodic sample array as two interleaved diffraction gratings, one consisting of opaque apertures alternating with bars composed of the sample material and the other consisting of opaque bars alternating with open apertures. In this picture, each grating generates its own diffracted amplitude pattern in the far field,

[2] This phenomenon, which also helps in suppressing the effects of edge imperfections in the grating bars, can be interpreted as an illustrative case of Ernst Abbe's diffractive imaging theory [19].

and since these patterns are shift-invariant with respect to the grating's lateral positions, they interfere additively (that is, as if the gratings were situated on top of one another at the sample plane). Thus, to the extent that all the grating bars are identical, MSFTI can be viewed as being analogous to the direct-field (that is, split-beam) interferometric techniques cited above. From an alternative point of view, the radiation passing through the open apertures can be regarded as constituting a reference beam, and the resulting far-field pattern as an in-line (Gabor) hologram [20] of the sample structure. This picture becomes the more orthodox one as the number of bars and slits in the grating is reduced to one (Fig. 2).

## FUNDAMENTAL DIMENSIONAL CONSTRAINTS AND INEQUALITIES II

It will be of interest at this point to analyze the dimensional constraints on the MSFTI configuration that are required to make its practical performance consistent with the analysis in Section I. In allowing for minimal complexity in the soft X-ray range, no focusing or collimating optics are assumed.

We first note, in view of the assumption that the radiation emanates from an effective point source, that the wavefronts impinging on the sample will have the divergence angle $Na/L_s$ (see Figs. 2 and 3). To enforce a significant peak separation, our first requirement on this angle is that it leads to a peak width at the detector plane significantly smaller than $L/a$. If the natural $1/aN$ width of the peak profiles needs to be preserved, the tighter constraint $(1 + L/L_s)Na \ll L/Na$ must be established. As an intermediate criterion, we can specify a marginal restriction of

$$L_s \gg a^2 N^{3/2}. \tag{3}$$

If the source has a height $\Delta_s$ in the plane of dispersion such that $\Delta_s \geqslant Na$, the above restriction should be tightened to

$$L_s \gg aN^{1/2}(\Delta_s + Na). \tag{4}$$

The next constraint on $L_s$ is dictated by our approximation of the wavefronts by plane waves. Given the assumed point source, we can require the maximum phase variation of the light irradiating the sample to

be significantly less than one equivalent wavelength over its surface. This leads to

$$L_s > N^2 a^2, \tag{5}$$

an inequality that will typically dominate the lower bounds of the "intermediate" cases (Eqs. 3 and 4).

Moving downstream of the sample plane, the establishment of "far-field" conditions on $L$ for Fraunhofer diffraction can readily be shown [14] to be equivalent to the physical argument underlying Eq. 5; thus, we obtain a constraint of

$$L > N^2 a^2 \tag{6}$$

on the distance of the detector plane from the sample.

These relations, while explicitly restricting $L$ and $L_s$ in terms of $N$ and $a$, also strongly indicate the motivation for keeping the product $Na$ as small as possible. In this regard, we note that $a$ is restricted from below by the eikonal assumption (as outlined in Section I) and the applicability of scalar diffraction formalism. If we conservatively assume these two conditions to be very well fulfilled by the inequality $a > 100$, we can use the constraint given in Eq. 6 to define a dimensional range for nominally acceptable values of $a$, namely,

$$100 < a < L^{1/2}/N. \tag{7}$$

This inequality is useful in estimating the allowable period and size of a sample grating when $L$ is defined by extraneous factors.

## III RELATIONSHIP OF MSFTI TO ALTERNATIVE METROLOGICAL TECHNIQUES

In view of the background concepts developed in Section I, multiple-slit Fourier transform interferometry can be characterized as a photometric [21] technique that is based on normal-incidence[3] transmission and multiple-beam interference. In its usual application to nominally isotropic and homogeneous materials, it is insensitive to polarization effects and is

[3] See, however, Ref. [22].

therefore unrelated to ellipsometric [7] or polarimetric methods. In attempting to assess its range of utility within contemporary optical metrology, several issues that have a bearing on the suitability of any experimental technique need to be considered. Among these are: requirements on sample preparation; the spectral range of interest; physical properties of available light sources; requirements on detectors; experimental complexity with respect to available technology; and the merits of competing techniques. We will begin by enumerating some of the experimental requirements for MSFTI, most of which follow from the elementary analyses in Sections I and II:

(1) In the soft X-ray range ($\simeq$4–120 Å), sample structures will ordinarily be characterized by small dimensions and laterally microscopic features. This need not necessarily be the case in the visible, where lenses and collimators can be employed.

(2) In order to ensure effective planarity of the incoming wave fronts, the sample has to be located at a sufficiently far distance from the source, particularly in spectral ranges where compact optical collimators or lenses are unavailable.

(3) The detector has to be in the far field with respect to the sample, which in the soft X-ray range typically translates into distances of several to several tens of meters.

(4) In view of requirement 2, and more particularly requirement 3, which can reduce effective light flux by as much as the square of the distance from the sample (see Fig. 3), highly collimated and intense light sources are required.

(5) Additional requirements for high intensity and collimation can arise when the samples are mounted on substrates whose marginal absorption is significant.

(6) Depending on the spectral range, operation of the entire MSFTI apparatus within a hard vacuum may be required. In the soft X-ray range, operation inside a vacuum is unavoidable.

With these prolegomena, we can now systematically compare the respective merits of MSFTI with those of other metrological techniques that are used, or that could in principle be adopted, for characterizing the optical constants of thin-film samples in the VUV–soft X-ray range. In the discussions to follow, it is worthwhile to keep in mind that even very thin films in the 100–3000 eV range can exhibit high absorption [6, 23], and that naturally occurring Bragg or Laue diffractors are unavailable over large spectral regions.

As MSFTI is an interferometric method, we have listed it, along with a selected set of alternative techniques of the same class, in Table I. The configurations identified as "direct-field, split-beam" are known to be well-suited for the visible range, in which they have in fact evolved. Beginning

with Lloyd's mirror, perhaps the simplest of all direct-field interferometers, the remaining instruments become progressively more sophisticated, with the Mach–Zehnder interferometer requiring precise beam-splitters and lenses, elements that have as yet no equally viable or efficient analogs in the soft X-ray range [24, 25]. Even if Lloyd's mirror (or Fresnel's mirrors) by virtue of their simplicity could be considered as potential competitors in the soft X-ray range at a given wavelength, spanning more than a limited wavelength range would in all likelihood necessitate the eventual manipulation of their reflecting facets, leading back to an increase in system complexity (exacerbated by operation inside a vacuum). Apart from this, existing soft X-ray sources such as conventional undulators [26] are still much too limited in terms of coherent output power to give split-beam configurations [27]—which, as was pointed out in Section I, are much more wasteful of interfering photons than the multiple-slit configuration—any significant advantage in comparison to MSFTI.

Irrespective of these observations, it is noteworthy that interferometers of the split-beam type shown in Fig. 1 have nevertheless been developed for the hard X-ray range,[4] where absorption is much less severe, and diffracting-crystal arrays instead of mirrors can be used to steer the beams. These hybrid configurations, ably pioneered in the metrology of X-ray optical constants by Bonse *et al.* [4, 28] and Hart [5], can utilize diffraction to maintain the angles of the intersecting beams constant, minimizing configurational complexity. Inasmuch, however, as they employ diffracting crystals, their range of operation cannot at present be extended downward to fully encompass the soft X-ray range.

Next, the alternative multiple-beam, direct-field configurations in the visible range, typified, for example, by the Fabry–Perot interferometer, cannot be employed in the 100–3000 eV range with anywhere near the efficiency or finesse [29] that they exhibit in the visible. This is due primarily to the practically unavoidable confinement of the interfering light within media that exhibit relatively high absorption at soft X-ray wavelengths. Again, however, we note that multilayer analogs of the Fabry–Perot etalon for the lower end of the hard X-ray range (Table I) have been developed [30] and indeed proposed for characterizing optical constants. However, in view of the fact that such systems are composed of at least two different materials, and inasmuch as the dynamics of multiple scattering are highly sensitive to the sample quality and absorptance [31], the associated experimental schemes would in general need to be more intricate than for MSFTI, and therefore inferior to it.

Concluding, on the basis of Section I and the above discussions, that MSFTI in fact exhibits a number of advantages in the soft X-ray range with

[4] At energies in excess of 3–5 KeV, operation inside a vacuum is not obligatory, a simplifying factor in high-precision experimental work.

respect to alternative interferometric techniques, we next contrast it with the purely photometric method of normal-incidence absorption measurement, a technique applied in recent years to the characterizations of thin films in the VUV and soft X-ray ranges [32]. This method, based on measuring the transmittance of thin films [33], depends on accurate total-flux measurements of beams impinging on, and then passing through, a sample. The necessity for integrating all the flux, including that *scattered* by both sample surfaces, places stringent requirements on the detector quality and configuration, factors that can lead to a heightened susceptibility to systematic errors. In contrast to MSFTI, which is to a significant extent self-filtering against the presence of small-scale imperfections (see Sections I and IV), integrated absorption measurements can also be extremely sensitive to small-scale imperfections in the sample's thickness profile for

**TABLE I**

**A Classification of Selected Interferometric Configurations Used in Optical Metrology**

| | Interferometer | |
|---|---|---|
| Types | Split-beam[a] | Multiple-beam[b] |
| Direct field[c] (*specular reflection, refraction*) | Lloyd's Mirror[f] Fresnel's Mirrors[f] Mach–Zehnder[f] | Fabry-Perot[f] |
| Fourier transform[d] (diffraction) | **Rayleigh**[f,g] | **Multiple-Slit FT**[h] |
| Hybrid[e] | Bonse–Hart[i] | Multilayer Etalon[j] |

[a] Configurations based on interference between two beams.
[b] Configurations based on interference among more than two beams.
[c] Based on interference of deflected beams for which diffraction can be disregarded. Configurations utilize reflection (and refraction in the visible and infrared ranges) to steer the beams.
[d] Based on interference of diffracted beams. Configurations utilize diffraction through slits. The diffractive metrological techniques in boldface are typified by unmatched systemic simplicity, a critical consideration in certain spectral ranges.
[e] Based on direct-field interference of beams that have been steered by Bragg or Laue diffraction.
[f] Described in Ref. [9], Chapter 7.
[g] According to Rayleigh [17], first explored by Fraunhofer.
[h] Multiple-slit Fourier Transform configuration, described in Refs. [1–3] and this chapter.
[i] Used primarily from the hard X-ray range down to the higher end of the soft X-ray range.
[j] X-ray analog of Fabry–Perot etalon with multilayer (Bragg-diffracting) facets.

unfavorable values of $k$ and $W$. The latter parameter in particular tends to be unfavorable in the soft X-ray range, as the typically acceptable thicknesses ($\simeq$500–5000 Å) in that region are conducive to the generation of small-scale bulk and surface asperities during the preparation of samples [33, 34]. Additionally, only the absorption constant gets measured; the phase constant must subsequently be unfolded from a typically discrete set of $k$ values via Kramers–Kronig analysis [35], an abstraction that is not always comparable in validity to a direct measurement [2, 36].

In view of these observations, we can underscore the following two potential advantages in addition to those itemized in Section I:

(iii) In contrast to alternative techniques, MSFTI apparently requires by far the least complex experimental arrangement in the soft X-ray range. Apart from the detector and source, all the high-precision aspects of the configuration inhere in the sample, which is small, accepts the probe radiation at normal incidence, and requires no manipulation in a vacuum environment.

(iv) With respect to the detector, no absolute *or* total-flux measurements are required. All that is required is a detector that is *linear* over the typically small [2] dynamic range represented by the ratios of the first to zeroth orders.

In contrast to these favorable conditions, however, it is evident that the requirement of a precisely fabricated, high-quality sample grating with microscopic features represents a significantly more demanding requirement for MSFTI than for competing techniques. This fact perhaps provides a clue as to the apparent absence of MSFTI from the soft X-ray scene prior to the relatively recent advent of reliable microfabrication technology [37, 38, 39]. Indeed, as will be discussed in Section VI, the requirement for high-quality microstructures is still perhaps the central issue in determining the future status of MSFTI in soft X-ray metrology. The second necessary requirement for MSFTI, namely, intense and highly collimated X-ray sources, has undoubtedly been fulfilled to a certain extent by the relatively recent advent of synchrotron storage rings and insertion devices [26]. Assuming the continued evolution of these two technological underpinnings, as well as the validity of the advantages (i–iv) posited above, the characterization of soft X-ray optical constants of thin films would seem to represent an optimal niche for MSFTI within the realm of optical metrology.

## IV GENERAL EXPERIMENTAL EQUATIONS AND SENSITIVITY ANALYSIS

In this section we present the basic experimental equations of the MSFTI method, including expressions for evaluating the sensitivities of the experi-

mental quantities with respect to $\delta(\lambda)$ and $k(\lambda)$. These expressions are not the most general ones possible and are based on the following simplifying assumptions:

(1) No support structure is assumed for the free-standing diffracting bars in Fig. 3.

(2) The bars are assumed to be plane-parallel, congruent, homogeneous, and isotropic samples of the test material.

(3) The surfaces of the bars are assumed to be perfectly planar.

(4) Surface phase shifts and multiple reflections are ignored.

(5) The source radiation is assumed to be monochromatic and planar at the sample plane.

(6) The aperture and bar dimensions $d$ and $(a\text{-}d)$ are assumed to be large enough for the eikonal approximation to apply in transmission through the grating bars. Additionally, all the conditions for the validity of scalar diffraction theory are assumed to hold [40]. As opposed to assumptions 1–5, these idealizations are to be considered as prerequisites for all valid MSFTI implementations.

Although this is evidently a large set of idealizations, departures from most of the listed assumptions have been analyzed in prior work and the results are available in the literature [1–3]. In most practical cases the corresponding corrections in the soft X-ray range can be expressed quantitatively as simple correcting terms or factors in the basic equations. In view of the referential purpose of this handbook chapter, some of the more important of these will be included in this section.

We begin by quantifying the notion of sensitivity, whose physical meaning can be interpreted as the "fractional change in a parameter $x$ induced by a fractional change in a parameter $y$." Analytically, the differential form of this quantity is given by

$$S_y^x = \frac{y}{x}\left(\frac{\partial x}{\partial y}\right) \equiv \frac{\partial(\ln x)}{\partial(\ln y)}. \tag{8}$$

Referring to Fig. 3, we can now write out the expression for the magnitude squared of the Fourier transform of the electric field $x$-distribution along the sample plane in direct analogy to Eq. 2. For the intensity of the $m$th peak in the far field, this expression reduces to [41]

$$I^{(m)} = \left(\frac{\sin(\pi m N)}{\sin(\pi m)}\right)^2 |\bar{M} + e^{\pi i m}\bar{A}|^2, \qquad m = 0, \pm 1, \pm 2, \ldots, \tag{9}$$

where $\bar{M}$ and $\bar{A}$ are, respectively, the Fourier transforms of the electric

field distributions across a bar surface and an open aperture. For a given period $a$ and an arbitrary aperture dimension $d$, we obtain the following expression for the ratio of the $m$th order peak intensity to the zeroth order peak intensity:

$$\frac{I^{(m)}}{I^{(0)}} = \frac{[1 - 2e^{-2\pi W k(\lambda)} \cos 2\pi W \delta(\lambda) + e^{-4\pi W k(\lambda)}] \operatorname{sinc}^2(md/a)}{[1 + 2(a/d - 1)e^{-2\pi W k(\lambda)} \cos 2\pi W \delta(\lambda) + (a/d - 1)^2 e^{-4\pi W k(\lambda)}]}, \qquad m \neq 0. \tag{10}$$

This expression demonstrates that for the assumed rectangular bar cross-section, the peak intensity ratios among orders other than the first will be independent of $k(\lambda)$ and $\delta(\lambda)$, and that the entire effect of $\hat{n}$ on the far-field intensity spectrum can be deduced solely from the ratio $I^{(1)}/I^{(0)}$. The establishment of the experimental equations based on Eq. 10 is immediate. If we choose two gratings of the same material and of parameters $a_1$, $d_1$, $W_1$, and $a_2$, $d_2$, $W_2$ and denote the corresponding intensity ratios by

$$I_i^{(1)}/I_i^{(0)} = R_i, \qquad i = 1, 2, \tag{11}$$

we get

$$\cos 2\pi W_i \delta(\lambda) - \frac{1}{1 + A_i} \cosh 2\pi W_i k(\lambda) + \frac{A_i}{1 + A_i} \cosh[2\pi W_i k(\lambda) + r_i] = 0, \tag{12}$$

where

$$A_i = R_i \tfrac{1}{4}\pi^2 [\sin(\pi\eta_i) \cosh(\tfrac{1}{2} r_i)]^{-2}, \tag{13}$$

$$\eta_i = d_i/a_i, \tag{14}$$

and

$$r_i = \ln\left(\frac{\eta_i}{1 - \eta_i}\right), \tag{15}$$

It is evident that accurate measurements of the *lengths* $a_i$, $d_i$, $W_i$ and the far-field *intensities* $I_i^{(0)}$ and $I_i^{(1)}$ constitute, in principle, a sufficient data set for iterating the values of $k$ and $|\delta|$ out of Eq. 12.

The sensitivities of the measured peak-intensity ratios $R_i$ to the sample grating parameters are straightforwardly derived by directly applying Eq. 8 to Eq. 12. The results are

$$S_\delta^{R_i} = \left(\frac{2\pi W_i\delta \sin 2\pi W_i\delta}{\cosh 2\pi W_i k - \cos 2\pi W_i\delta}\right)\left(\frac{\cosh 2\pi W_i k + \cosh(2\pi W_i k + r_i)}{\cosh(2\pi W_i k + r_i) + \cos 2\pi W_i\delta}\right), \quad (16)$$

$$S_k^{R_i} = \left(\frac{2\pi W_i k \sinh 2\pi W_i k}{\cosh 2\pi W_i k - \cos 2\pi W_i\delta}\right)$$

$$\times \left(\frac{2\cos 2\pi W_i\delta + \cosh(2\pi W_i k + r_i) - \cosh 2\pi W_i k}{\cosh(2\pi W_i k + r_i) + \cos 2\pi W_i\delta}\right), \quad (17)$$

$$S_{W_i}^{R_i} = [2\pi W_i\delta \sin 2\pi W_i\delta(\cosh(2\pi W_i k + r_i) + \cosh 2\pi W_i k)$$

$$+ 2\pi W_i k \cosh 2\pi W_i\delta(\sinh(2\pi W_i k + r_i)$$

$$+ \sinh 2\pi W_i k) - 2\pi W_i k \sinh 2\pi W_i k]$$

$$\div [(\cosh(2\pi W_i k + r_i) + \cos 2\pi W_i\delta)(\cosh 2\pi W_i k - \cos 2\pi W_i\delta)], \quad (18)$$

and

$$S_{\eta_i}^{R_i} = 2([\pi\eta_i \cot \pi\eta_i] - 1)$$

$$+ \left[\frac{2\eta_i(e^{-2\pi W_i k} + (\eta_i^{-1} - 1)^{-1}\cos 2\pi W_i\delta)}{((\eta_i^{-1} - 1)^{-1}e^{2\pi W_i k} + (\eta_i^{-1} - 1)e^{-2\pi W_i k} + 2\cos 2\pi W_i\delta)}\right]. \quad (19)$$

Equations 11–15 constitute the basic experimental relations for a minimal set of two gratings. Utilizing more than two gratings in an experimental determination will, as expected, result in the statistical reduction of the uncertainties stemming from random errors. For example, if $M'$ gratings are used, there will be $M'(M'-1)/2$ cross-correlated calculations of $\delta$ and $k$, and the sensitivity equations must then be employed in an iterative rondo with Eqs. 11–15 to make all the calculated values of $\delta$ and $k$ consistent with each other and the known systematic errors [2]. The second, evident use of the sensitivity equations is to help choose optimal parameters or parameter ranges for sample gratings to be fabricated for an experiment, provided some initial knowledge of the actual values of the constants exists.

We next turn to the question of corrections to the basic experimental

equations, which can arise from departures from the ideal conditions assumed at the outset of this section. We will focus on those corrections liable to be of immediate concern for preliminary evaluations of MSFTI experiments. More complete treatments of nonideal experimental conditions have been cited above. The first important modification arises when multiple reflections in the grating bars have to be taken into account (as in the visible and UV [6] ranges), or when the phase shifts induced by the sample surfaces do not all cancel (as can happen, for instance, when the sample bars are deposited on a plane–parallel substrate). If we can represent all these effects by applying a complex factor, $\tau \exp(i\Phi)$, to $\bar{M}$ in Eq. 9, we arrive at the following modified version of Eq. 10, wherein we have introduced the quantity $\Omega = -\frac{1}{2}\ln(\tau)$ and utilized the (unindexed) Eq. 15:

$$\frac{I'^{(1)}}{I'^{(0)}} = e^r \operatorname{sinc}^2\left(\frac{d}{a}\right) \frac{\cosh(2\pi W k + \Omega) - \cos(2\pi W\delta - \Phi)}{\cosh(2\pi W k + r + \Omega) + \cos(2\pi W\delta - \Phi)}. \tag{20}$$

We see immediately that since both $\tau$ and $\Phi$ depend on both $\delta$ and $k$ [2, 10], the establishment of an equation separable in $\delta$ and $k$ (such as Eq. 15) will not in general be possible when $\tau$ differs from 1 and/or $\Phi$ from 0. This can in certain instances lead to an enhanced sensitivity of the experimental results to systematic errors, thereby degrading the validity and reliability of computed results. This fact highlights one of the more important potential advantages of MSFTI in the 100–3000 eV region, which we herewith add to those already listed in Sections I and III:

(v) For many materials throughout broad portions of the VUV–soft X-ray range, $\Omega$ and $\Phi$ are often close enough to zero to be ignored, a factor underlying the simplicity of the basic experimental formalism of MSFTI. This in effect can reduce the number of physical variables influencing measurements, enhancing the validity of MSFTI in the corresponding spectral region.

The following modifications of the ideal experimental equations are based on the statistical departure of real-life sample bars from cross-sectional rectangularity, dimensional congruency, and surface perfection. To generate readily interpreted worst-case corrections, we assume that the bars' total thickness $W$ varies randomly in the $x$–$y$ plane over a range $[-b, b]$; the bars' positions in the $x$ direction vary randomly over a range $[-g, g]$; and the bars' widths vary randomly over a range $[-c, c]$, all with associated uniform probability density functions.[5] Under a broad range of

[5] The general case based on arbitrary probability density functions is treated in Ref. [2].

circumstances, the primary effect of the variability of $W$ will be to alter the ratio $I^{(1)}/I^{(0)}$ *by adding the terms*

$$[e^{-2\pi\langle W\rangle k}(Q_4-1)-2(Q_1-1)\cos 2\pi\langle W\rangle\delta+2Q_3\sin 2\pi\langle W\rangle\delta] \tag{21}$$

and

$$(\eta^{-1}-1)[e^{-2\pi\langle W\rangle k}(\eta^{-1}-1)(Q_4-1)+2(Q_1-1)\cos 2\pi\langle W\rangle\delta-Q_3\sin 2\pi\langle W\rangle\delta] \tag{22}$$

into, respectively, the bracketed numerator and denominator of the right side of Eq. 10. Here we have utilized the unindexed Eq. 14, represented the average bar thickness by $\langle W\rangle$, and employed shorthand symbols $Q_j$ $(j=1,3,4)$ for

$$Q_1=\frac{k\cos 2\pi\delta b\sinh 2\pi kb+\delta\sin 2\pi\delta b\cosh 2\pi kb}{2b\pi(k^2+\delta^2)}, \tag{23}$$

$$Q_3=\frac{\delta\cos 2\pi\delta b\sinh 2\pi kb-k\sin 2\pi\delta b\cosh 2\pi kb}{2b\pi(k^2+\delta^2)}, \tag{24}$$

$$Q_4=\frac{(\cos 2\pi\delta b\sinh 2\pi kb)^2+(\sin 2\pi\delta b\cosh 2\pi kb)^2}{4b^2\pi^2(k^2+\delta^2)}. \tag{25}$$

Equations 21–25 are useful in estimating acceptable limits on both the large- and small-scale surface roughness of a sample material for use in an MSFTI experiment, particularly when prior estimates of its actual optical constants are available.

The effect of the laterally random variations is primarily to modulate the diffracted nonzero orders [1]. If we express $g$ and $c$ as fractional lengths of the grating period $a$, the ideal $I^{(1)}/I^{(0)}$ ratio in Eq. 10 is transformed into

$$\frac{I^{(1)}}{I^{(0)}}\rightarrow\left(\frac{I^{(1)}}{I^{(0)}}\right)\left[\operatorname{sinc}^2\left(\frac{2g}{a}\right)\operatorname{sinc}^2\left(\frac{c}{a}\right)\right]. \tag{26}$$

The $\operatorname{sinc}^2$ factors can be used to estimate acceptable limits on the lateral mechanical distortions that will be present, to a greater or lesser degree, in all sample grating structures. Conversely, accurate characterizations of the

lateral distortions of a sample grating can be used to correct the measured intensity ratios.

The final important departure from ideality that should be taken into account is the effect of nonrectangular bar edges. The issues to be covered in a comprehensive treatment are detailed, covering a wide range of cases and assumptions [2], and we must consequently restrict ourselves here to the brief derivation of an approximate worst-case criterion. We first assign a length parameter $\Delta_E$ to the grating structure in the $x$ direction, which we center on the nominally ideal edge locations of each bar. We then assume that over the extent of this length, each edge can assume an arbitrary thickness profile, and we represent the effect of its shape by adding the decremental electric field profile transmitted through it to the ideal field distribution in the sample plane. This procedure generates two periodic field distributions, one associated with each set of (imperfect) edges of the grating bars. Clearly, as $\Delta_E \to 0$, the ideal field distribution is recovered. We now assume that each edge-transmitted field has twice the amplitude of the field transmitted by the ideal bars. Next, we appeal to elementary diffraction theory [19] and Eq. 10 to postulate that the angular spread of the edge spectra in the far field will be greater than the primary spectral spread by the approximate factor $\Delta_E/d$. In this picture, the field amplitude transmitted by the ideal grating is taken to be proportional to $[d+(a-d)\exp(-2\pi Wk)]$ and the corresponding amplitude from the edges to $[2\Delta_E \exp(-\pi Wk)]$. A factor describing the worst-case relative intensity perturbation of, say, the first order can then be approximated by the expression

$$\left(\frac{2\Delta_E e^{-\pi Wk}(\Delta_E/d)+[d+(a-d)e^{-2\pi Wk}]}{[d+(a-d)e^{-2\pi Wk}]}\right)^2. \tag{27}$$

Assuming the representative conditions $2\pi Wk \simeq 1$ and $a \simeq 2d$, we find the perturbation on the first order to be given approximately by $[4\Delta^2{}_E/(d^2(1+\sqrt{e}))]$, and assuming (again as a worst case) an equal perturbation of the zeroth order, we arrive at a maximal perturbation on the unindexed ratio $R$ (defined by Eq. 11) of

$$\Delta R \simeq 3\left(\frac{\Delta_E}{d}\right)^2. \tag{28}$$

Perhaps the most important practical implication of Eq. 28 is that real-life experimental grating bars in the MSFTI technique should be chosen with

aspect ratios $(a-d)/W$ as large as possible, since for most fabrication techniques this will be naturally conducive to the minimization of $\Delta_E/d$.

## A CHARACTERIZATION OF THE OPTICAL CONSTANTS OF Au USING MSFTI IN THE 280–640 eV RANGE V

In this section we will augment the predominantly theoretical discussions of the prior sections by briefly reviewing the implementation and results of an actual MSFTI experiment performed on Au [3] in the 280–640 eV range.

The radiation source employed for the experiment was a bending magnet on SPEAR,[6] the storage ring at the Stanford Synchrotron Radiation Laboratory (SSRL) [42]. The radiation, which is characterized by a broad and smooth spectrum [43], was monochromatized with a 1m Rowland-circle monochromator, whose details and performance characteristics are described elsewhere [44]. For our present purposes we require the fact that this single-grating instrument, when tuned to a given photon energy, is also capable of transmitting the higher diffracted orders of shorter-wavelength radiation emanating from a broadband source.

The sample gratings for the experiment were fabricated at IBM's Thomas J. Watson Research Center, using combinations of wet and dry etching and vacuum deposition techniques. Several of the technical aspects and developments associated with this work have been described in the literature [45]. In particular, in view of the generation of the initial grating pattern as a holographic interferogram, the grating period $a$ is defined with exceptional precision. A micrograph of a typical sample grating is shown in Fig. 4. As can be seen, the grating bars are supported on a grid structure constituted of much thicker bars, and that support grid is itself supported on a tertiary grid (not shown) with proportionately coarser features. Apart from the micrographs, which were taken *following* the MSFTI experiment, the gratings' dimensional parameters were initially characterized with an inverse application of the formulas in Section IV. To wit, a set of values of $\delta$ and $k$ was selected in the 100–160 eV range that had earlier been found to corroborate the measured performance of other well-characterized Au gratings at SSRL [46, 47], and applied to unfold $d$ and $W$ from the measured intensity ratios $R$. The basic parameters of the final set of three gratings selected to measure $\hat{n}$ are listed in Table II. To be noted are the fairly high values of $(a-d)/W$, stipulated by the analytical results of Section IV.

[6] Stanford Positron Electron Asymmetric Ring.

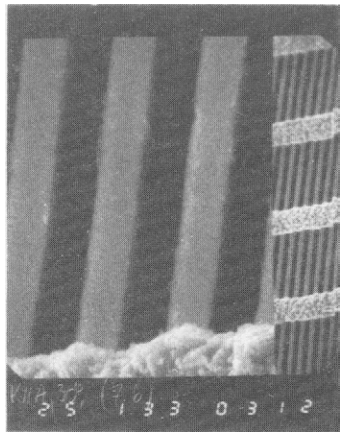

**Fig. 4.** Electromicrograph of an Au sample grating structure used in an initial version of an MSFTI experiment. The period of the free-standing bars is 2.5 μ and their width-to-thickness ratio $(a-d)/W$ is approximately 10. Portions of the supporting structure for the sample bars are visible in the demagnified structure on the right. During the experiment, the support structures face the source and intercept a significant fraction of the probe light.

A typical MSFTI spectrum, drawn from the prior characterization of the gratings' dimensions, is shown in Fig. 5. The profile reveals both spectral and line-shape anomalies, both of which typify the kinds of systematic errors that can arise in an actual experiment. In the example shown, the anomalous peaks between the zeroth and first orders stem from the harmonics transmitted by the monochromator, and it is apparent that the spectral components with which they are associated contribute to both the zeroth and first orders of the primary spectrum. The peak shape distortions are related to the shadowing effects of the structural grids sup-

**TABLE II**

**Selected Parameters of Sample Au Gratings Used in an MSFTI Experiment**

| Grating | $W$ (Å) | $d/a$ | $a$ (μm) |
|---|---|---|---|
| K12A[a] | 969.5 | 0.312 | 2.5 |
| 13F[a] | 1774.6 | 0.565 | 2.5 |
| K4[a] | 1067.0 | 0.350 | 2.5 |

[a] Grating identification codes.

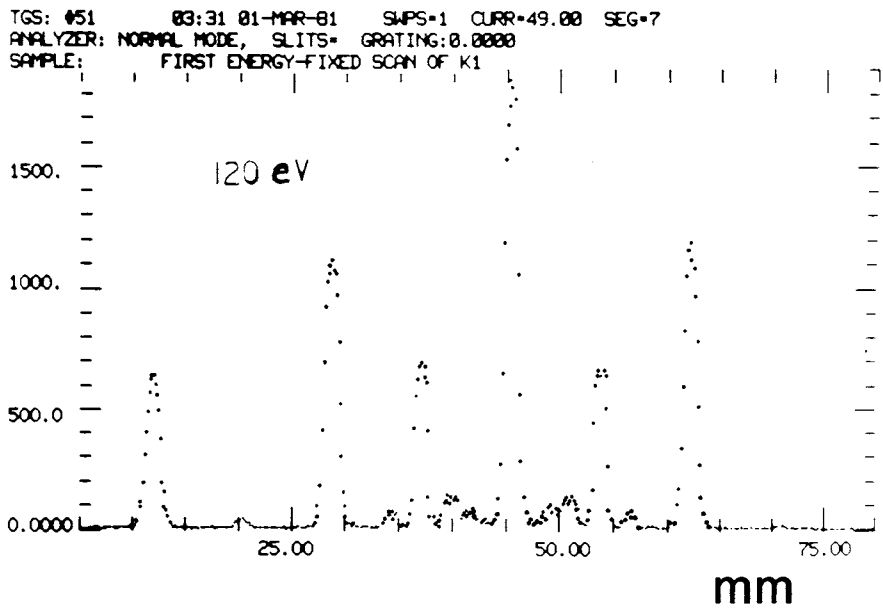


**Fig. 5.** Experimental transmission diffraction spectrum generated by an Au sample grating structure. The source radiation is monochromatized synchrotron light from a bending magnet. The 120 eV first and negative first orders are located at 28 mm and 62.5 mm.

porting the grating bars, and the slight asymmetry in the peak values is traceable in part to misalignments in detector motion [2].

Following measurements of the diffracted spectra, the data were analyzed and corrected for systematic errors, including those associated with the imperfections of the grating structures and their support grids, and the values of $\delta$ and $k$ were generated as described in Section IV. Particularly troublesome was the task of numerically separating the spectra of interest from the anomalous higher-energy diffraction patterns, which are themselves model-dependent. In all these calculations the sensitivity expressions (Eqs. 16–19) were utilized to converge on self-consistent values of $\hat{n}$ among the three sets of grating pairs, and to estimate the final error limits. A set of sensitivity curves based on the final computed constants for one of the gratings is displayed in Fig. 6. Above 640 eV and below 280 eV, the curves are smoothly adjusted to optical constants reported elsewhere [32]. The final experimental values of $\delta$ and $k$ are listed in the fourth and sixth columns of Table III.

A brief assessment of the displayed constants is in order. In the literature, Au has been particularly noted for the significant variation in the values of both its measured and calculated constants [48, 49]. These discrepancies have been associated with the apparently wide variability in the physical parameters of thin gold films prepared via different techniques

[50], or with postulated physical differences between the surface and interior regions of ordinary samples [51]. In view of these considerations, it is of interest to contrast the MSFTI constants with those measured or derived by alternative techniques.

In the fifth and seventh columns of Table III we have listed the corresponding optical constants for Au compiled by Henke *et al.* [23]. These values, based on first-principle calculations fitted to available (and very sparse) experimental data, can be used as an arbitrary referent for our purposes. We note fairly good agreement for $k$, with the exception of 640 eV and the 280–360 eV interval. Regarding these discrepancies, partial corroboration is available for the MSFTI results in the theoretical *atomic* absorption cross-sections compiled by Plechaty, Cullen, and Howerton [52], who identify strong resonances both at $\simeq$320 eV and 600 eV, the latter being clearly associated with Au's $N$ edge. A corresponding interpretation for the large discrepancy with Henke's $\delta$, however, which is based largely on Kramers–Kronig analysis of the absorption data, has proved elusive. The technique most closely related to MSFTI in terms of sample penetration, that of thin-film absorption, has been utilized by Hagemann, Gudat, and Kunz [32] to measure $k$ for Au over this region. Their films were prepared by evaporation from resistance-heated crucibles onto mesh-supported polymer substrates, which were subsequently etched away outside of the vacuum. Their measured $k$ values, interpolated, agree with both Henke's and MSFTI's to within the cited error bounds. Their primary

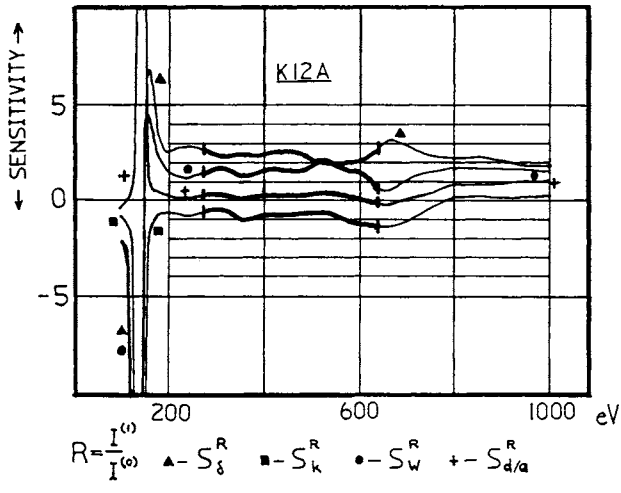


**Fig. 6.** Sensitivity curves for a typical sample grating (code number K12A) used to measure optical constants via MSFTI. Bold curve segments denote the 280–640 eV measurement interval. For this particular grating, the diffracted order ratio $R$ is seen to be minimally sensitive to the aperture-to-period ratio $d/a$.

**TABLE III**

**Optical Constants of Gold (Au) as Determined by the MSFTI Method and by Henke *et al.* [23].**

| eV | $cm^{-1}$ | μm | $1-n$ (MSFTI) | $1-n$ (Henke) | $k$ (MSFTI) | $k$ (Henke) |
|---|---|---|---|---|---|---|
| 280 | — | 0.00443 | 0.0119 | 0.00732 | 0.00762 | 0.101 |
| 320 | — | 0.00389 | 0.0109 | 0.00649 | 0.00790 | 0.00892 |
| 360 | — | 0.00344 | 0.00959 | 0.00592 | 0.00762 | 0.00797 |
| 400 | — | 0.00310 | 0.00872 | 0.00580 | 0.00672 | 0.00710 |
| 440 | — | 0.00282 | 0.00798 | 0.00552 | 0.00574 | 0.00594 |
| 480 | — | 0.00258 | 0.00729 | 0.00514 | 0.00506 | 0.00501 |
| 520 | — | 0.00238 | 0.00695 | 0.00472 | 0.00427 | 0.00426 |
| 560 | — | 0.00241 | 0.00648 | 0.00430 | 0.00378 | 0.00361 |
| 600 | — | 0.00207 | 0.00596 | 0.00385 | 0.00329 | 0.00328 |
| 640 | — | 0.00194 | 0.00500 | 0.00365 | 0.00463 | 0.00294 |

The average error bounds for the MSFTI values, dominated in large part by systematic errors, are estimated to be about ±18% for $k$ and ±10% for $\delta$ ($\delta \equiv 1-n$).

data points, however, are too sparse for resolving the two absorption anomalies observed with MSFTI. With respect to $\delta$, Hagemann *et al.*'s Kramers–Kronig analysis produces values that are closer to MSFTI's than to Henke *et al.*'s in the 280–400 eV range, but closer to Henke *et al.*'s from 400–640 eV. A set of characterizations of $\delta$ and $k$ for Au based on multiple-reflectivity measurements in the soft X-ray range has recently been reported by Windt *et al.* [53]. Their sample surfaces were prepared by *e*-beam evaporation of Au onto polished Si wafers, and their measurements extended up to ≈520 eV, with only three data points reported in the 280–520 eV interval. Their $k$ value of 0.0042 at 385 eV is noticeably lower than in all the previous compilations cited, and their $\delta$ values of 0.0069 at 280 eV and 0.00418 at 385 eV are also significantly lower than Henke *et al.*'s. On the other hand, their values compare, by and large, favorably with Lukirskii *et al.* [51], who also employed a reflectivity-based technique (at virtually the same three energy points) in an experiment reported in 1964. In still other compilations reviewed for this chapter, for example, Zombeck [54], data for the 280–640 eV range are either drawn from some of the above sources or generally fall within the same range of values.

This wide-ranging spectrum of results clearly underscores the still-unsettled status of current experimental knowledge of the optical constants of Au in the soft X-ray range, and of their systematic relationship to the surface or bulk properties of samples. Whereas some degree of correlation is perhaps apparent among the *measured* constants acquired with reflection- versus transmission-dependent techniques, the sparseness of actual measurements of *both* components of $\hat{n}$, by whatever technique, is clearly still too inhibitive to permit reliable conclusions to be drawn. This

state of affairs is no doubt partially due to the enhanced difficulty of optical experimentation in ultra-high vacuum, and to the still-extant lack of instrumentation comparable in quality or sophistication to that available in other spectral regions. In this respect, the development of a technique such as MSFTI, which is both experimentally simple and can measure both $\delta$ and $k$ directly with optimal sensitivity, could prove essential in helping to identify and resolve the issues involved.

## VI PROBLEMS AND PROSPECTS IN SAMPLE PREPARATION

Perhaps the most pertinent question that can be raised at this point concerning the present and future utility of multiple-slit Fourier transform interferometry is whether high-quality samples constructed out of materials other than Au can be prepared. It is clear that the long-term import of this metrological technique will depend directly on its ability to accommodate a wide variety of elements and materials, enabling intercomparisons and correlations with data taken by other methods.

From our present perspective, we can remark that the preparation of samples of the type used in the first experiments, namely, free-standing, grid-supported diffraction gratings, out of a wide variety of materials other than Au, does not appear overly promising. This is due in large part to the complexity of the associated fabrication processes [37, 45], which utilize sequences of several in- and out-of-vacuum procedures of both a chemical and mechanical nature. Thus, the quality and integrity of the bars in the final grating structure can strongly depend on the chemical and mechanical properties of the element or material being used, necessitating the programmatic exploration of various fabrication procedures for virtually each material of interest. To date, for example, successful results have been reported for Ag [55], whereas preliminary attempts with Ni and Cu have been inconclusive [56].

Based on this state of affairs, it seems apparent that samples of less complex construction must be made amenable to the MSFTI technique if it is to become widely applied. To this end, we can consider two simpler alternatives. First, we consider the structure in Fig. 7a [57]. Its preparation is based on the deposition of a thin film onto a substrate, and a subsequent inscription of a periodic groove structure into its surface. Due to the mechanical support of the substrate and the reduced number of fabrication steps, it can be expected that a much larger class of materials could be prepared for MSFTI in this way. Indeed, this expectation is corroborated by ongoing work in associated areas of microfabrication technology [58]. We note that the analytical formalism developed in this chapter is entirely

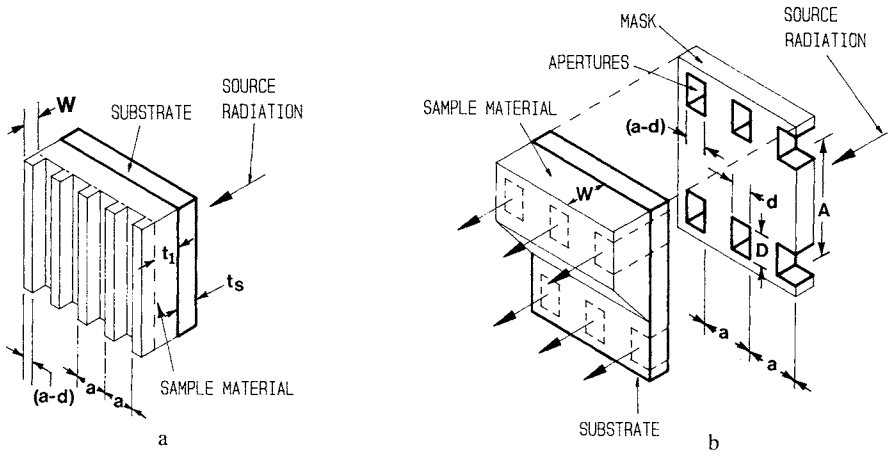


**Fig. 7.** Two alternative sample configurations (a and b) for probing the optical constants of a wide range of metallic and nonmetallic thin films in the soft X-ray range with the technique of MSFTI. The essential notion behind both configurations is to bypass the potentially problematical fabrication of free-standing diffraction gratings out of unsuitable materials. In configuration b, all microfabrication or micromachining of the sample material can in principle be avoided.

applicable to the depicted configuration, since the plane-parallel substrate (thickness $t_s$) and subsequent sample slab (thickness $t_1$) modulate the probe wavefronts homogeneously. Experimentally, the configuration is superior in avoiding the systematic errors introduced by a support grid; on the other hand, it will in general place significantly higher demands on the intensity of the radiation source.

An alternative technique that would demand an even greater source intensity, but that would in principle allow the MSFTI characterization of any material that can be deposited in thin-film form—and this includes most of the elements—is shown in Fig. 7b. Here the periodic sample bars are defined by a sequence of channels of width $a-d$ and height $D$ cut or etched into an opaque mask; the apertures are defined by a second sequence of width $d$ located at a distance $A$ below. $A$ must be chosen large enough to occlude the edge region of the thin film to ensure the homogeneity of both the defined bars and apertures. During operation, the mask is adjoined to the substrate and the two grating structures are defined (in the eikonal approximation) by the radiation passing through the apertures. With regard to the viability of this approach, we note that Si structures such as the depicted mask have recently been implemented, with smoothnesses approaching the *atomic* level [59]. This suggests that spectra of the highest quality could be generated with such configurations. Feasibility studies of sample preparation using this approach, as well as the develop-

ment of the analytical formalism for the mask/thin-film geometry, which in certain respects differs from that outlined in Sections I and IV, are currently in progress.

## VII PROSPECTS FOR MSFTI IN OTHER SPECTRAL REGIMES

It is of interest to inquire into the applicability of MSFTI in spectral regimes outside of the VUV/soft X-ray range. Just as in the comparisons drawn in Section II, the central issue is whether alternative techniques can produce superior results, and at what cost. As a specific example, consider the sensitivities defined in Section IV (Eqs. 16–18), in the limits $r \to 0$ and $W \to 0$. These become $[1+(k/\delta)^2]^{-1}$, $[1+(\delta/k)^2]^{-1}$, and $\{1+[1+(k/\delta)^2]^{-1}\}$, respectively. As opposed to the corresponding sensitivities of a split-beam interferometer, they are all seen to be independent of $W$. Thus, in regions where $k$ is of the same order of magnitude as $\delta$, and where surface phase-shift and reflectivity effects can be accounted for, MSFTI would appear to offer advantages for the testing of even extremely thin films in transmission. Based on existing tabulations of $k$ and $\delta$ [60–62], we can consequently infer that this form of MSFTI could in principle be applied to a significant number of materials in regions of the IR–visible–UV range. A practical factor that could enhance the applicability of MSFTI at these lower energies is the ready selection of focusing and collimating optics (namely, lenses), the judicious use of which would permit significantly shorter source/sample/detector lengths and coarser gratings. Such structures could consequently be imbued with higher quality, enhancing the experimental reliability even further. On the other hand, in cases where only $\delta$ was required, ordinary split-beam interferometry, or even the FTI scheme employed by Rayleigh, would probably remain preferable, since—as was discussed earlier—the simpler sample structures and the ready availability of highly intense and tunable coherent photon sources in the lower energy regimes would more than compensate for their relative inefficiency.

At energies well in excess of 3–5 KeV, the natural crystal structures of most materials begin imposing their own modulation on the light transmitted into the far-field (via Bragg or Laue diffraction), and numerous higher-energy scattering mechanisms (for example, Compton) start manifesting themselves [63]. In view of this, the additional modulation of a high-energy diffraction pattern by an array of bars of the material in question might not necessarily prove to be of value. One possibly useful interpretation of MSFTI in this regime would be to view the individual atomic planes as the "bars" of a grating, and the interplane spacings (with their lower electron densities) as the "apertures". Such a configuration could conceivably be

employed to help characterize inner-shell scattering coefficients at the appropriate absorption edges in the 10 KeV–1 MeV range, and even of nuclear cross-sections at absorption edges in the 100 KeV+ energy domain. Although the quality, alignment, and photon flux requirements for a sample structure of this type would evidently be severe, recent technological developments have shown that both of these requirements could in fact be duly met [64, 65].

A final question, of possible importance at sub-VUV energies, is whether MSFTI configurations based on reflection could be implemented. A general assessment of the analytical formalism of MSFTI clearly shows that this would indeed be possible. On the other hand, configurational problems such as the copositioning of a reference interference pattern, or the variation of the incidence and reflection angles to establish multiple equations in $\delta$ and $k$ (when only one material is being used), would seem to imply a considerably higher degree of experimental complexity. In view of the complicated dependence of the reflectivity on $\hat{n}$ (see the discussion in Sections I and IV), the analytical complexity of the experimental equations could in general be expected to be greater as well. As in all proposed applications of MSFTI (reflection- or transmission-based), the bottom-line question of whether the anticipated complexity is justified for a given material would need to be answered with a careful case-by-case analysis of the attainable precision in comparison to alternative techniques.

## SUMMARY VIII

The VUV/soft X-ray range is currently perhaps the least developed in terms of versatile coherence techniques and a broad range of sophisticated optical instrumentation. An inhibiting factor to progress in these two areas has undoubtedly been our limited knowledge and understanding of the optical constants of candidate materials. In this chapter we have reviewed MSFTI, a method for determining optical constants that is based on the interference of multiple diffracted beams following transmission. It was shown to feature a number of advantages for characterizing the complex index of refraction $\hat{n}$ of thin films in the 0.1–3 KeV range; in particular, certain troublesome errors associated with alternative techniques in this region can be minimized or avoided. In broad terms, the technique has been made possible only recently due to significant advances in high-brightness, soft X-ray sources and the advent of reliable microfabrication technology. With additional directed development of these two resources, such as was outlined in Section VI, it is expected that the method could eventually be made applicable to a wide variety of materials, enabling the

programmatic characterization of their optical constants in thin-film form. Such an experimental program would provide data complementary to that acquired with reflectivity-based techniques, enabling us, perhaps for the first time, to begin systematizing our knowledge and understanding of $\hat{n}$ in the soft X-ray range.

## ACKNOWLEDGMENTS

The author would like to acknowledge critical support from Elisabeth Källne, Ingolf Lindau, and Eberhard Spiller during the initial experimental implementations of the MSFTI technique. The tabulated optical constants were characterized at the Stanford Synchrotron Radiation Laboratory (SSRL), which is operated by the Department of Energy, Office of Basic Energy Research, Division of Chemical Sciences. That office's Division of Materials Science is acknowledged for support for this undertaking.

## REFERENCES

1. R. Tatchyn, I. Lindau, and E. Källne, "Analysis of a new method for determining optical constants in the soft x-ray region," *Optica Acta* **27**, 1505 (1980).
2. R. Tatchyn, "The Introduction and Development of a New Method for Measuring the Optical Constants of Metals in the Soft X-Ray Range," Doctoral thesis, Stanford University, SSRL Report No. 82/02 (1982).
3. R. Tatchyn, I. Lindau, E. Källne, and E. Spiller, "Derivation of the Optical Constants of Gold from Transmission Diffraction Measurements in the 280–640 eV Range," *Phys. Rev. Lett.* **53**, 1264 (1984).
4. U. Bonse and W. Graeff, "X-Ray and Neutron Interferometry," in "X-Ray Optics," (H.-J. Queisser, ed.), *Topics in Applied Physics*, Vol. 22, Springer-Verlag, Berlin, 93 (1977).
5. M. Hart, "The Application of Synchrotron Radiation to X-Ray Interferometry," *Nucl. Instr. Meth.* **172**, 209 (1980).
6. W. R. Hunter, "Measurements of Optical Constants in the Vacuum Ultraviolet Spectral Region," in "Handbook of Optical Constants of Solids," (E. D. Palik, ed.), Academic Press, New York, Chap. 4 (1985).
7. D. E. Aspnes, "The Accurate Determination of Optical Properties by Ellipsometry," op. cit., Chap. 5.
8. J. Shamir, "Interferometric Methods for the Determination of Thin-Film Parameters," op. cit., Chap. 6.
9. M. Born and E. Wolf, "Principles of Optics," Pergamon, Oxford, Chap. 7.3.2 (1980).
10. op. cit., Chap. 13.
11. B. L. Henke, "Low Energy X-Ray Interactions: Photoionization, Scattering, Specular and Bragg Reflection," in *AIP Proceedings No. 75*, (D. T. Attwood and B. L. Henke, eds.), 146 (1981).
12. Born and Wolf, op. cit. Chap. 7.6.
13. op. cit. Chap. 3.
14. op. cit. Chap. 8.3.3.
15. R. Bracewell, "The Fourier Transform and Its Applications," McGraw-Hill, New York, Chap. 13 (1965).
16. Born and Wolf, op. cit. Chap. 7.2.
17. Lord Rayleigh, "On some Physical Properties of Argon and Helium," *Proc. Roy. Soc. London* **59**, 198 (1896).
18. Born and Wolf, op. cit. Chap. 7.3.

19. Born and Wolf, op. cit. Chap. 8.6.
20. H. M. Smith, "Principles of Holography," Wiley-Interscience, New York, Chap. 6.1 (1969).
21. J. H. Weaver, C. Krafka, D. W. Lynch, and E. E. Koch, "Physik Daten, Physics Data," "Optical Properties of Metals," Vol. 18-2, Fach-informations-zentrum, Karlsruhe, 12 (1981).
22. R. Tatchyn and I. Lindau, "An Extended Maximization Technique for Measuring Optical Constants Using Transmission Gratings in the Soft X-Ray Range," in *AIP Proceedings No. 75*, (D. T. Attwood and B. L. Henke, eds.), 323 (1981).
23. B. L. Henke, P. Lee, T. J. Tanaka, R. L. Shimabukuro, and B. K. Fujikawa, "The Atomic Scattering Factor, $f_1 + if_2$, for 94 Elements and for the 100 to 2000 eV Photon Energy Region," (Appendix), in *AIP Proceedings No. 75*, (D. T. Attwood and B. L. Henke, eds.), 340 (1981).
24. A. G. Michette, "Optical Systems for X-Rays," Plenum, New York, 28 (1986).
25. A. M. Hawryluk, N. M. Ceglio, D. G. Stearns, K. Danzmann, M. Kühne, P. Müller, and B. Wende, "Soft x-ray beamsplitters and highly dispersive multilayer mirrors for use as soft x-ray laser cavity components," *SPIE Proceedings* **688**, 81 (1987).
26. H. Winick and J. E. Spencer, "Wiggler Magnets at SSRL—Present Experience and Future Plans," *Nucl. Instr. Meth.* **172**, 45 (1980).
27. R. Tatchyn, E. Källne, A. Toor, T. Cremer, and P. Csonka, "Operation of a normal-incidence transmission grating monochromator at ALLADIN," *Rev. Sci. Instrum.* **60**, 1579 (1989).
28. U. Bonse, P. Spieker, J.-T. Hein, and G. Materlik, "Measurement of K-Edge Dispersion Anomalies with the New X-Ray Interferometer at DORIS," *Nucl. Instr. Meth.* **172**, 223 (1980).
29. G. R. Fowles, "Introduction to Modern Optics," Holt, Rhinehart and Winston, New York, Chap. 4.1 (1975).
30. T. Barbee, Jr., and J. Underwood, "Solid Fabry-Perot Etalons for X-Rays," *Opt. Commun.* **48**, 161 (1983).
31. A. E. Rosenbluth and J. M. Forsyth, "The Reflecting Properties of Soft X-Ray Multilayers," in *AIP Proceedings No. 75*, (D. T. Attwood and B. L. Henke, eds.), 280 (1981).
32. H.-J. Hagemann, W. Gudat, and C. Kunz, "Optical Constants from the Far Infrared to the X-Ray Region: Mg, Al, Cu, Ag, Au, Bi, C, and $Al_2O_3$," *J. Opt. Soc. Am.* **65**, 742 (1975); DESY-Report SR-74/77, DESY, Hamburg, Federal Republic of Germany, (1974).
33. Hunter, op. cit. p. 81*ff*.
34. Aspnes, op. cit. p. 96*ff*.
35. D. Y. Smith, "Dispersion Theory, Sum Rules, and Their Application to the Analysis of Optical Data," in "Handbook of Optical Constants of Solids," (E. D. Palik, ed.), Academic Press, New York, Chap. 3 (1985).
36. Barbee and Underwood, op. cit. pp. 17–18.
37. H. I. Smith, "Fabrication Techniques for Surface-Acoustic-Wave and Thin-Film Optical Devices," *Proc. IEEE* **62**, 1361 (1974).
38. J. Dijkstra, "X-Ray Transmission Optics," *Space Sci. Instrum.* **2**, 363 (1976).
39. K. P. Beuermann, R. Lenzen, and H. Bräuninger, "Properties of a transmission grating behind a grazing incidence telescope for cosmic x-ray spectroscopy," *Appl. Opt.* **16**, 1425 (1977).
40. Born and Wolf, op. cit. Chap. 11.
41. H. W. Schnopper, L. P. Van Speybroeck, J. P. Delvaille, A. Epstein, E. Källne, R. Z. Bachrach, J. Dijkstra, and L. Lantward, "Diffraction grating transmission efficiencies for XUV and soft x-rays," *Appl. Opt.* **16**, 1088 (1977).

42. A. Bienenstock, "An Overview of the Stanford Synchrotron Radiation Laboratory," *Nucl. Instr. Meth.* **172**, 13 (1980).
43. S. Krinsky, M. L. Perlman, and R. E. Watson, "Characteristics of Synchrotron Radiation and of Its Sources," in "Handbook on Synchrotron Radiation," (E.-E. Koch, ed.), Vol. 1A, North-Holland, Amsterdam, 65 (1983).
44. F. C. Brown, R. Z. Bachrach, and N. Lien, "The SSRL Ultrahigh Vacuum Grazing Incidence Monochromator: Design Considerations and Operating Experience," *Nucl. Instr. Meth.* **152**, 73 (1978).
45. Y. Vladimirsky, E. Källne, and E. Spiller, "Fabrication of free-standing x-ray transmission gratings and zone plates," *SPIE Proceedings* **44**, 25 (1984).
46. R. Tatchyn, "*Planar Transmission Gratings Compatible with Synchrotron Radiation Sources: Analysis, Computer Modelling, Testing, and Design*," Engineer's thesis, Stanford University, 1980.
47. J. P. Delvaille, H. W. Schnopper, E. Källne, I. Lindau, R. Tatchyn, R. A. Gutcheck, R. Z. Bachrach, and J. H. Dijkstra, "Diffraction Efficiencies of Holographic Transmission Gratings in the Region 80 eV–1300 eV," *Nucl. Instr. Meth.* **172**, 281 (1980).
48. H.-J. Hagemann, W. Gudat, and C. Kunz, "Optical Constants from the Far Infrared to the X-Ray Region: Mg, Al, Cu, Ag, Au, Bi, C, and $Al_2O_3$," DESY-Report SR-74/77, DESY, Hamburg, Federal Republic of Germany 17 (1974).
49. D. W. Lynch and W. R. Hunter, "Comments on the Optical Constants of Metals and an Introduction to the Data for Several Metals," in "Handbook of Optical Constants of Solids," (E. D. Palik, ed.) Academic Press, New York, 286 (1985).
50. D. E. Aspnes, E. Kinsbron, and D. D. Bacon, "Optical properties of Au: Sample effects," *Phys. Rev.* **B21**, 3290 (1980).
51. A. P. Lukirskii, E. P. Savinov, O. A. Ershov, and Yu. F. Shepelev, "Reflection Coefficients of Radiation in the Wavelength Range from 23.6 to 113 Å for a Number of Elements and Substances and the Determination of the Refractive Index and Absorption Coefficient," *Opt. and Spectrosc.* **16**, 168 (1964).
52. E. F. Plechaty, D. E. Cullen, and R. J. Howerton, "Tables and Graphs of Photon-Interaction Cross Sections from 0.1 keV to 100 MeV Derived from the LLL Evaluated-Nuclear-Data Library," University of California Research Report UCRL-50400, **6**, Rev. 3, 398 (1981).
53. David L. Windt, Webster C. Cash, Jr., M. Scott, P. Arendt, B. Newnam, R. F. Fisher, and A. B. Swartzlander, "Optical Constants for thin films of Ti, Zr, Nb, Mo, Ru, Rh, Pd, Ag, Hf, Ta, W, Re, Ir, OS, Pt, and Au from 24 Å to 1216 Å," *Appl. Opt.* **27**, 246 (1988).
54. M. V. Zombeck, "Optical Constants and Reflectivities for Nickel, Gold, and Platinum in the X-Ray Region of the Spectrum (0.1–10 KeV)," AXAF Interim Report, Nos. SAO-AXAF-83-015 and SAO-AXAF-83-016, Smithsonian Institution Astrophysical Observatory, Cambridge, Mass., January–March (1983).
55. N. M. Ceglio, "Recent Advances in X-Ray Optics," in "X-Ray Microscopy," (G. Schmahl and D. Rudolph, eds.), *Springer Series in Optical Sciences*, Vol. 43, Berlin, 97 (1984).
56. E. Källne, private communication.
57. R. Tatchyn, unpublished, (1984).
58. H. I. Smith, E. H. Anderson, A. M. Hawryluk, and M. L. Schattenburg, "Planar Techniques for Fabricating X-Ray Diffraction Gratings and Zone Plates," in "X-Ray Microscopy," (G. Schmahl and D. Rudolph, eds.), *Springer Series in Optical Sciences*, Vol. 43, Berlin, 51 (1984).
59. D. Ciarlo and D. E. Miller, "Silicon diffraction gratings for multilayer structures," *SPIE Proceedings* **688**, 163 (1987).
60. Lynch and Hunter, op. cit. pp. 275–367. Energy ranges over which $|\delta| < k$ are tabulated for Cu, Au, Ir, Mo, Ni, Os, Pt, Rh, Ag, and W.

61. D. Y. Smith, E. Shiles, and M. Inokuti, "The Optical Properties of Aluminum," in "Handbook of Optical Constants of Solids," (E. D. Palik, ed.), Academic Press, New York, 369 (1985).
62. E. D. Palik, "Cadmium Telluride (CdTe)," in "Handbook of Optical Constants of Solids," (E. D. Palik, ed.), Academic Press, New York, 409 (1985).
63. Plechaty *et al.*, op. cit. pp. vii–xii.
64. R. Coisson and H. Winick, eds., "Workshop on PEP as a Synchrotron Radiation Source," SSRL, 10/20–21/87.
65. R. Tatchyn, P. Csonka, and A. Toor, "Perspectives on micropole undulators in synchrotron radiation technology," *Rev. Sci. Instrum.* **60**, 1796 (1989).

# Chapter 12

# Determination of Optical Constants from Angular-Dependent, Photoelectric-Yield Measurements

H.-G. BIRKEN, C. BLESSING, and C. KUNZ
II. Institut für Experimentalphysik
Universität Hamburg
D-2000 Hamburg 50
Federal Republic of Germany

I. Introduction 279
II. Theoretical Background 280
III. Experimental Details 285
IV. Examples 286
V. Conclusions and Future Prospects 289
References 292

## INTRODUCTION I

Although optical constants ordinarily are determined by measuring the primary interaction of photons with matter, we describe here a method that relies on the measurement of a secondary process, namely photoemission. The determination of the total photoelectric yield as a function of the angle of incidence on a mirror made of a conducting material, or of a thin film of such a material on a well-defined substrate, is sufficiently specific to obtain accurate optical constants. Pepper [1] has given a simple but very successful model, which yields an analytic expression for the photoelectric yield of a bulk conductor and also of a thin conducting film on a substrate if the optical constants of the materials involved, the film thickness, and the average escape depth of the photoelectrons are known. This model is based on the description of photoemission as a four-step process: primary excitation, multiplication by inelastic scattering, migration to the surface,


Copyright © 1991 by Academic Press.
All rights of reproduction in any form reserved.
ISBN 0-12-544422-2

and penetration through the surface into the vacuum. The factor that describes the penetration of photoelectrons through the surface barrier and some other constant factors cancel out if only the relative photoelectric yield for different angles of incidence is of interest. This model can be used in reverse to fit experimental angular-dependent, photoelectric-yield measurements and to determine optical constants, film thickness, and electron escape depth as fitting parameters.

Although the method is applicable only at photon energies above the photoemission threshold, no limitations other than practical ones appear to exist for higher photon energies. This method gives excellent results in those cases that have been investigated up to now. It was originally applied by Arakawa *et al.* [2, 3] with the primary interest of obtaining electron escape depths of Al at 21.1 eV and of C at 20–64 eV photon energy. In addition, the real part of the index of refraction was obtained. There are also some other investigations based on Pepper's [1] and similar formalisms [4]. In combination with synchrotron radiation, the method was explored thoroughly by Birken *et al.* [5] with Al films evaporated in ultra-high vacuum. In this case, a measurement of multiangle reflectances was performed on the same films without breaking the vacuum. Both methods yielded optical constants in excellent agreement with each other. The method was extended later at the HASYLAB reflectometer [7, 8] to copper, platinum, and Kanigen, a nickel alloy used as a polishable mirror material. Some of these unpublished results are included in this chapter. In Section II, the theoretical background is presented in detail, then the fairly simple experimental setup is described in Section III, taking as a model case the arrangement as it was used at HASYLAB. Section IV gives the examples, and finally, Section V points out future prospects of the method.

## II THEORETICAL BACKGROUND

We consider a linearly polarized light wave incident on a film of thickness $d$, which is supported by a substrate. The angle of incidence is measured relative to the normal to the film surface, and the optical properties of the film (1) and the substrate (2) are characterized by the complex dielectric functions $\varepsilon_1$ and $\varepsilon_2$, respectively, Fig. 1. $\varepsilon$ is related to the complex index of refraction by $N = n + i\kappa = \sqrt{\varepsilon}$. The central assumption in describing the photoelectric yield is that the contribution of an infinitesimal volume element of the film to the total number of escaping electrons is proportional to the photon energy absorbed within that volume element. The electromagnetic-field distribution inside the film is thus responsible for the primary excitation of photoelectrons. On the other hand, the dielectric functions $\varepsilon_1$ and $\varepsilon_2$, together with the boundary conditions, determine this field.

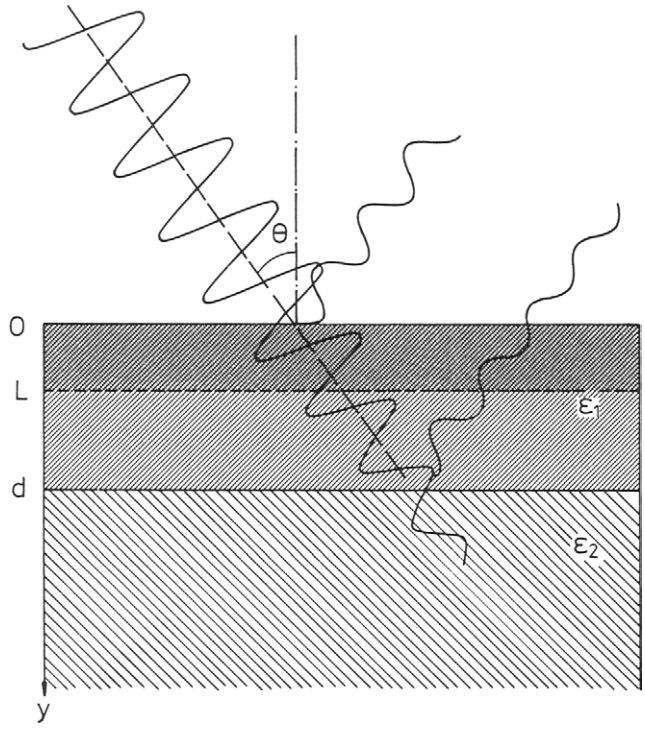


**Fig. 1.** Schematic representation of the optical system composed of a film (1) with thickness $d$, which is supported by a substrate (2). $\theta$ is the angle of incidence of the incoming light beam, and $\varepsilon_{1,2}$ denote the dielectric functions of the film and the substrate, respectively. The vacuum dielectric function $\varepsilon_0$ is unity. $L$ is the mean electron escape length.

In calculating the photoelectric yield, diffusion of the primarily excited photoelectron to the surface, multiplication due to electron–electron scattering along its path, and escape through the surface potential barrier are all condensed in the simple function $Ce^{-y/L}$. The factor $C$ takes into account the multiplication of the primary electron through electron–electron scattering and the probability of penetration through the surface potential barrier for the secondary electrons. $L(\hbar\omega)$ denotes the photon-energy-dependent electron escape depth. This is a complicated function of the mean-free paths for both elastic electron–phonon and inelastic electron–electron scattering averaged over the whole spectrum of kinetic energies. The introduction of such an exponential escape function is a simple approximation, which cannot be expected to describe perfectly this intricate escape and multiplication mechanism. Nevertheless, for our present application it turns out to be adequate.

If the contribution of the substrate to the total yield is negligible, that is,

$L \ll d$, the expression for the total yield may be written as

$$Y = C \int_0^d e^{-y/L} \eta(y)\, dy = CF(L), \tag{1}$$

where $\eta(y)$ is the volume absorptance, which is proportional to the negative divergence of the Poynting vector. This approximation, however, is no longer applicable if the film thickness becomes comparable to the electron escape depth, since then the photoelectrons arising from the substrate region must also be taken into account. This holds even in the case where the substrate is an insulating material. For electrons excited within the substrate, an analogous escape probability function $C_s e^{-y/Ls}$ may be assumed, but the values of $C_s$ and $L_s$ might be very different from those pertaining to the film. Within the frame of this chapter, we do not wish to expand Pepper's model further for such a case. In principle, however, this appears to be possible with the disadvantage that electron escape will require two (or more) additional parameters.

Defining the quantity $G(\theta) = Y(\theta)/Y(0)$ as the relative angular-dependent total yield and neglecting electrons from the substrate, the factor $C$ cancels out, since it does not depend on the angle of incidence $\theta$ of the incoming photons. Pepper has calculated analytic expressions for the absorption of energy per unit volume as well as for the reflectance and the transmittance for a system, which is composed of a film on a substrate [1]. The film and the substrate are allowed to be absorbing, homogeneous, and uniaxially anisotropic media, with their optical axes in the direction normal to the boundaries. Here, Pepper's equations for the case of a film on a substrate with homogeneous, isotropic, optical properties are reproduced for completeness:

$$\begin{aligned}
F_s(L) = {} & \frac{(1-|r_{1,s}|^2)\alpha}{|1+r_{1,s}\exp(2id\xi_1)|^2}\left\{\frac{1-\exp(-(\alpha+1/L)d)}{\alpha+1/L}\right. \\
& + |r_{2,s}|^2 \exp(-2\alpha d)\frac{1-\exp(-(1/L-\alpha)d)}{1/L-\alpha} \\
& \left. + 2\exp(-\alpha d)\,\mathrm{Re}\left[\frac{r_{2,s}(\exp(2i\xi_1' d)-\exp(-d/L))}{2i\xi_1'+1/L}\right]\right\} \\
F_p(L) = {} & \frac{(1-|r_{1,p}|^2)\alpha}{|1+r_{1,p}r_{2,p}\exp(2id\xi_1)|^2}\left\{\frac{1-\exp(-(\alpha+1/L)d)}{\alpha+1/L}\right. \\
& + |r_{2,p}|^2 \exp(-2\alpha d)\frac{1-\exp(-(1/L-\alpha)d)}{1/L-\alpha} \\
& \left. + 2\exp(-\alpha d)\,\mathrm{Re}\left[\frac{r_{2,p}(\exp(2i\xi_1' d)-\exp(-d/L))}{2i\xi_1'+1/L}\right]\frac{\xi_1'\,\mathrm{Im}(\varepsilon_1^*\xi_1)}{\xi_1''\,\mathrm{Re}(\varepsilon_1^*\xi_1)}\right\}
\end{aligned} \tag{2}$$

$$r_{j,s}=\frac{\xi_{j-1}-\xi_j}{\xi_{j-1}+\xi_j}, \qquad r_{j,p}=\frac{\varepsilon_j\xi_{j-1}-\varepsilon_{j-1}\xi_j}{\varepsilon_j\xi_{j-1}+\varepsilon_{j-1}\xi_j}, \qquad (j=1,2),$$

where $\xi_j=2\pi/\lambda\sqrt{\varepsilon_j-\sin^2\theta}(j=0,1,2)$ are the $y$ components of the wave vector within the three media. The indices $s$ and $p$ refer to incident light with $s$- and $p$-polarization, respectively, and $r_j(j=1,2)$ are the Fresnel amplitude reflectance coefficients of the two boundaries. $\xi_1'$ and $\xi''_1$ are abbreviations for the real and imaginary parts of $\xi_1$, respectively, and * denotes complex conjugate. The quantity $\alpha=2\xi''_1$ is the effective absorption coefficient of the film that depends on the angle of incidence. If the film thickness approaches infinity, these equations reduce to those which describe the relative total yield from a bulk system:

$$F_i(L)=(1-|r_{1,i}|^2)\frac{\alpha}{\alpha+1/L}, \qquad (i=s,p). \tag{3}$$

Eqs. 2 and 3 may be used in a least-squares-fit procedure in order to determine the optical constants, film thickness, and the electron escape depth. Therefore, a $\chi^2$ function

$$\chi^2=\sum_{i=1}^{n}\frac{1}{\sigma_i^2}[G_{\text{exp}}(\theta_i)-G_{\text{theo}}(\theta_i,\varepsilon_1,\varepsilon_2,d,L)]^2, \tag{4}$$

has to be minimized, while the optical constants, the film thickness, and the escape depth serve as fit parameters. $\sigma_i$ denotes the statistical error of each experimental point.

In the following, the sensitivity of $G(\theta)$ spectra to changes in $\varepsilon=\varepsilon'+i\varepsilon''$ is analyzed. Since by definition $G=1$ at normal incidence, the information on $\varepsilon=\varepsilon'+i\varepsilon''$ is contained mainly in the angular region around the critical angle of incidence of the material under investigation. In the XUV spectral range, the values $|1-\varepsilon'|$ and $\varepsilon''$ typically are less than 0.1 for many materials. Critical angles therefore are close to $\theta=90°$, mostly above $\theta=80°$. The individual shapes of the $G(\theta)$ spectra are due to two competing mechanisms:

(1) Since $n<1$, the penetrating wave is always refracted away from the surface normal. At the critical angle $\theta=\theta_c$, the refracted wave propagates parallel to the surface, and the power deposited in the material is concentrated in a small layer below the surface. Consequently, the total yield is

much higher than at normal incidence, where the energy is deposited in deeper regions of the sample.

(2) As the angle of incidence is further increased, the energy flux into the sample decreases at the expense of the increasing reflectance of the sample, which is unity at $\theta = 90°$. Thus, as $\theta$ approaches 90°, the total yield vanishes. The shape of the $G(\theta)$ curve is mainly determined by $\varepsilon''$, whereas the position of the maximum in $G(\theta)$ yields information predominantly on $\varepsilon'$.

The left upper part of Fig. 2 shows calculated $G(\theta)$ spectra between 60° and 90° angles of incidence for three different values of ratio $L/\lambda$ and *s*-polarized light. The arrows indicate the maximum of each $G(\theta)$ curve.

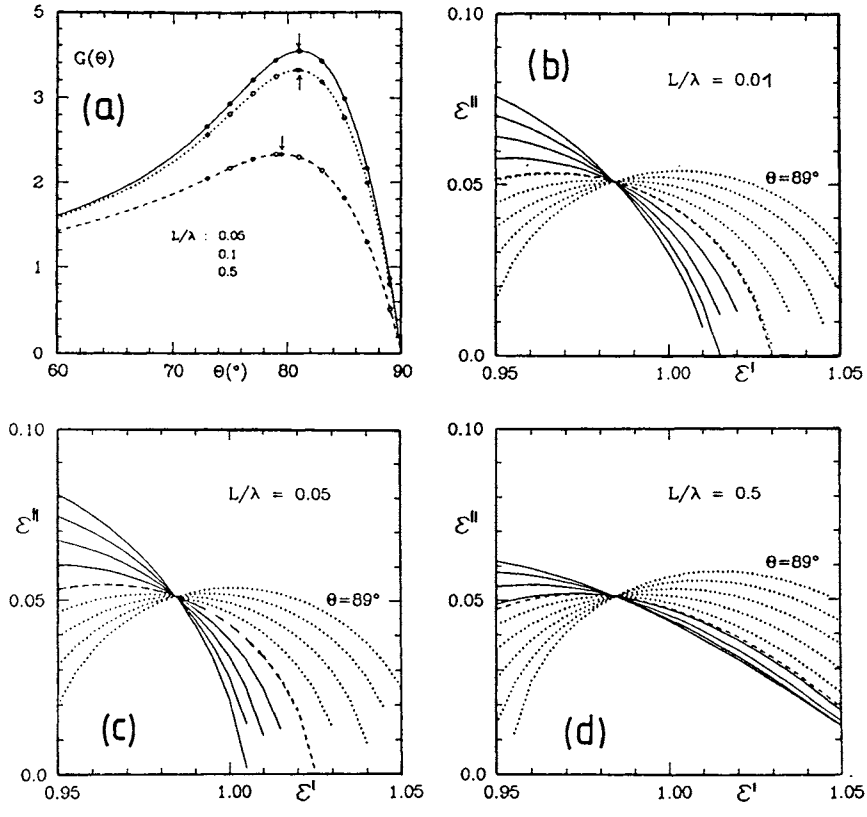


**Fig. 2.** Calculated relative angular-dependent total photoelectron yield from a bulk system for three different ratios $L/\lambda$ (a) and curves of constant $G(\theta)$ (b, c, d), corresponding to the $G(\theta)$ points in (a) as marked by circles. The dashed curves of constant $G(\theta)$ in (b, c, d) correspond to the maxima of the $G(\theta)$ spectra in (a). Consecutive curves of constant $G(\theta)$ differ from each other by $\Delta\theta = -2°$.

Also plotted in Fig. 2 are curves of constant $G(\theta)$ within the complex-$\varepsilon$ plane corresponding to the marked points on the angular-dependent $G(\theta)$ curves. Consecutive curves of constant $G(\theta)$ differ from each other by $\Delta\theta = -2°$, and the dashed lines correspond to the points at the maximum of the $G(\theta)$ curves. In principle, the point of intersection of two curves of constant $G(\theta)$ determines a value for $\varepsilon = \varepsilon' + i\varepsilon''$. An indication of the sensitivity of $G(\theta)$ spectra to changes in $\varepsilon$ is the angle of intersection of the curves of constant $G(\theta)$. Usually the $G(\theta)$ values have an uncertainty due to experimental errors. As a consequence, the curves of constant $G(\theta)$ will be shifted parallel to themselves by an amount that depends on the magnitude as well as on the sign of the error. From this it follows that the uncertainty of the value of $\varepsilon$ determined from $G(\theta)$ spectra increases with decreasing angle of intersection of different curves of constant $G(\theta)$. As long as the wavelength $\lambda$ is much larger than the electron escape depth $L(\hbar\omega)$, the curves fan out equally on both sides of the critical angle. If the wavelength becomes comparable to the electron escape depth or smaller, the curves of constant $G(\theta)$ for angles smaller than the critical angle are less separated than those for larger angles of incidence. In this case, the decrease of $G(\theta)$ above the critical angle of incidence, which originates from the loss of penetrating intensity due to the increasing reflectance, is decisive in determining the optical constants. Although surface roughness strongly influences reflectance measurements, its influence on total-yield measurements may be less important. This conjecture stems from the fact that in the case of not-too-large surface roughness and a large correlation length of the roughness profile, the sum of the specularly and diffusely reflected light is practically equal to the specularly reflected light from the corresponding perfectly smooth sample [6].

## EXPERIMENTAL DETAILS III

The principle of the setup of a sample holder for measuring angular-dependent total yield is shown in Fig. 3. The sample, either a film prepared on a substrate or a bulk material, is mounted (electrically insulated) on a holder, which allows precise rotations around an axis that lies in the surface of the sample. An anode, which is fixed to the sample holder and has slits for the incoming and reflected radiation, surrounds the sample. In this way, the anode is moved rigidly with the rotating sample, and the collection efficiency for the photoelectrons is independent of the angle of rotation. A potential difference of 15 V between the anode and the photoemitter has been shown to suffice to extract practically all photoelectrons. Thus, the signal-to-noise ratio is kept high, although the measured currents through the samples are typically on the order of 0.1 nA or less. A

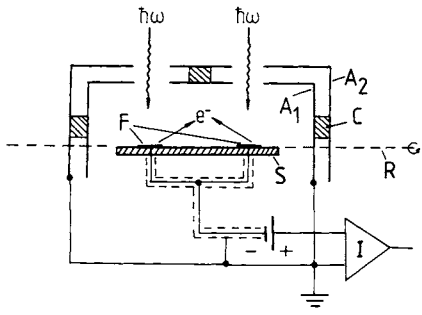


**Fig. 3.** Schematic diagram of the total-yield sample holder and electron collector ($A1$ anode, $A2$ shield anode, $F$ film, $S$ substrate, $R$ axis of rotation, $C$ insulating ceramics).

second shield is used to prevent the collection of electrons not resulting from photoemission from the sample. This setup permits total yield as well as reflectance measurements as a function of the angle of incidence of the incoming light.

The measurements described in this chapter have been performed at the UHV reflectometer at HASYLAB (DORIS II). The reflectometer [7] is equipped with 360° rotatable feedthroughs for sample and detector with rotational increments of 0.005° and an uncertainty of 0.03°. An adequate angular resolution and accuracy of the measurements is essential considering the importance of fast changes in intensity in the region around the maximum of the yield spectrum for the determination of the optical constants. In addition, the sample and the detector can be translated axially by up to 70 mm, allowing for measurements on two different samples.

An electron-beam gun and an oscillating quartz thickness monitor for *in situ* evaporation of films are installed in the reflectometer chamber. After baking, a base pressure of less than $3 \times 10^{-8}$ Pa is reached. The experiment is supplied with monoenergetic radiation from the monochromator "Bumble Bee" in the energy range 40–1000 eV. More details on the monochromator can be found in Ref. [8].

## IV EXAMPLES

Photoelectric-yield measurements have been performed with a 770 Å-thick Al film on borosilicate glass at 40–600 eV photon energy [5]. Fig. 4 shows a plot of the measured $G(\theta)$ curve of the Al film at 65.3 eV photon energy together with the fitted theoretical $G(\theta)$ curve. The strong interference pattern of the $G(\theta)$ curve, which allows the determination of the film

thickness $d$ from the fit with high accuracy, is typical of photon energies below the Al–$L_{2,3}$ edge. The theoretical expression of $G(\theta)$ depends on six adjustable parameters, the optical constants $\varepsilon_{Al}$ and the thickness $d$ of the Al film, the optical constants $\varepsilon_{Sub}$ of the substrate, and the electron escape depth $L$. Values for the optical constants of the substrate, determined from multiple-angle reflectance measurements of the substrate before evaporating the Al film, were treated as fixed fit parameters. Above the Al–$L_{2,3}$ edge, the interferences in the $G(\theta)$ spectra vanished, and the theoretical expression of $G(\theta)$ for a bulk system according to Eq. 3 was used to determine $\varepsilon_{Al}$ and the electron escape length $L$ of the Al film. As an example, Fig. 5 shows a plot of the measured $G(\theta)$ curve of the same sample as in Fig. 4 at 122.9 eV photon energy, together with the fitted theory. In addition, the reflectance versus angle of incidence for a large number of angles of the same Al film was measured. Fitting of these reflectance spectra to Fresnel's equations yielded values for $\varepsilon_{Al}$ and the thickness of the Al film, and therefore enabled a direct comparison of the two methods applied to the same sample. Figures 6 and 7 summarize the fit results of $\varepsilon_{Al}$ obtained by both the total yield and the reflectance measure-

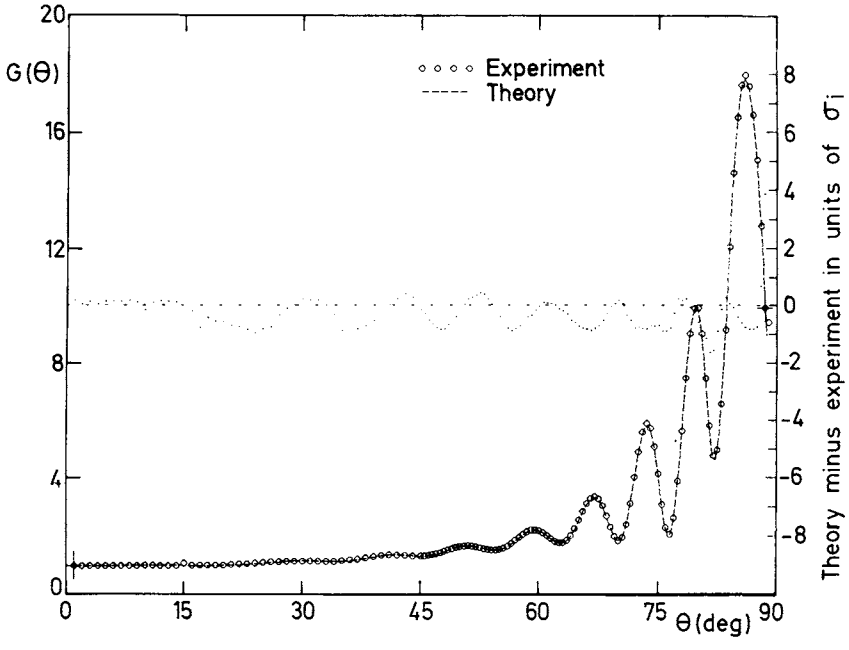


**Fig. 4.** Total yield versus angle of incidence normalized to the yield at normal incidence at 65.3 eV photon energy of an 770 Å-thick Al film. At this energy, strong interference patterns are visible in the $G(\theta)$ spectra. The dotted line in the middle of the figure shows the deviation of theory and experiment in units of the experimental error $\sigma_i$, which was estimated to be 1% of the experimental $G(\theta)$ value. For more details, see text.

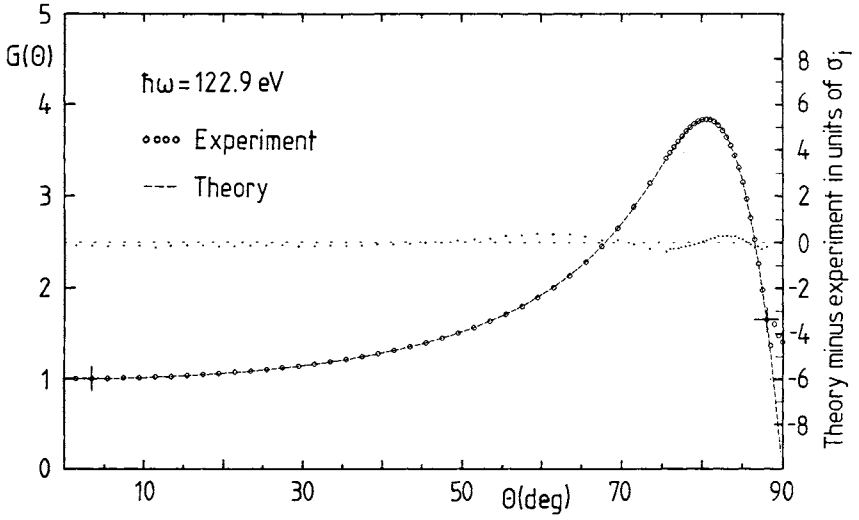


**Fig. 5.** Relative total photoelectric-yield $G(\theta)$ versus angle of incidence $\theta$ at $\hbar\omega = 122.9$ eV. This spectrum was obtained from the same Al film as the spectrum in Fig. 4. The fitted curve (dashed line) is based on the assumption of a bulk material, because the film appears to be opaque above the Al-$L_{2,3}$ edge.

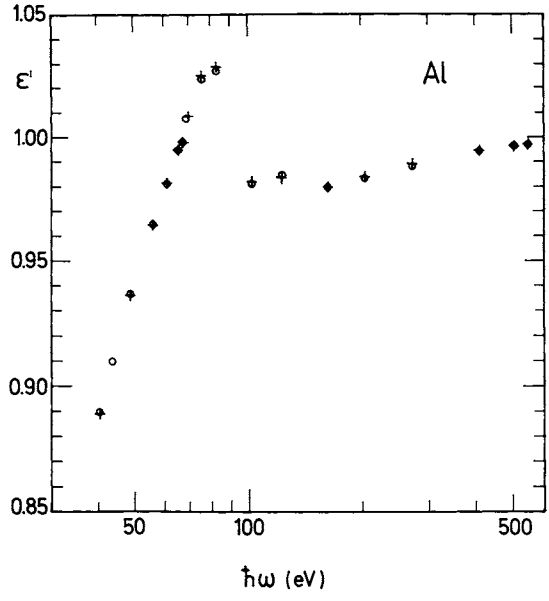


**Fig. 6.** Real part $\varepsilon'$ of the dielectric function $\varepsilon_{Al}$ versus photon energy $\hbar\omega$. The crosses denote the fit results of the total-yield method, whereas the circles refer to the reflectance measurements.

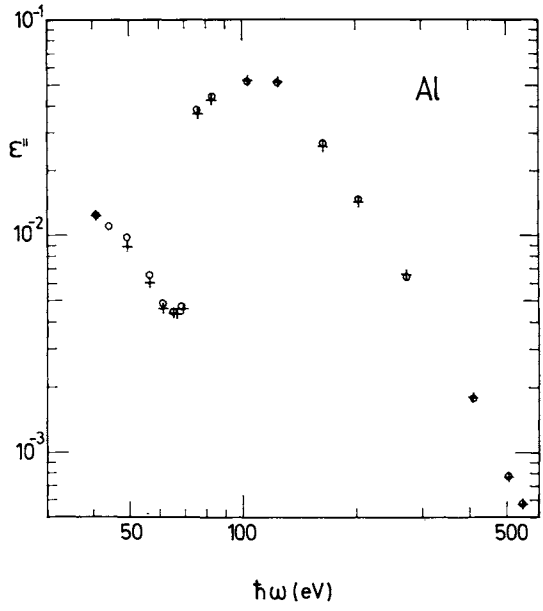


**Fig. 7.** Imaginary part $\varepsilon''$ of the dielectric function $\varepsilon_{Al}$ versus photon energy $\hbar\omega$ (compare with Fig. 6).

ments. The value of the film thickness determined from the yield method is $d = 773 \pm 9$ Å, whereas the reflectance measurements yielded $d = 768 \pm 10$ Å. The error is determined by averaging results over a range of photon energies. The smallness of the statistical spread is an additional indication of the applicability of the whole procedure.

Similar investigations have been performed on thin copper films on glass substrates in the range of 50–900 eV [10]. An example of a measurement on Cu at 644 eV photon energy is given in Fig. 8. Figures 9 and 10 show the optical constants of two films as determined from reflectance (open symbols) and total-yield measurements (closed symbols). The thicknesses of the films have been determined to be $225 \pm 5$ Å (circles) and $317 \pm 6$ Å (diamonds) from both types of measurements. For comparison, values of $\varepsilon_{Cu}$ have been calculated from atomic scattering factors given by Henke *et al.* [9] and are included in Figs. 9 and 10.

## CONCLUSIONS AND FUTURE PROSPECTS V

In this chapter it is demonstrated that angular-dependent photoelectric yield contains sufficiently detailed information, at least in the spectral

range $\hbar\omega = 20$–$1000$ eV, to extract accurate values for the optical constants. Up to now the method was applied only to a few substances, all of them metals, and in most cases they were supported by a glass substrate. The measurement of a thin layer on a substrate has the advantage of producing very pronounced interference structures, by which the sensitivity of the fits appears to be considerably increased. On the other hand, a fairly powerful computer system is needed to calculate the best fit in a reasonable time. For bulk materials the mathematical procedure is much simpler.

At first glance, the method appears to be applicable only to conducting materials, including doped semiconductors. If films are used, their thicknesses have to be so large that practically no electrons emerging from the substrate penetrate the film and contribute to the yield. The reason is that such a contribution is not included in the theory, as outlined in Section II. With materials such as metals, having mean-free paths of the order of 20 Å, a film thickness on the order of 100 Å suffices. As a matter of fact, we even had good results with a 51 Å Pt film on glass [11].

Would it also be possible to measure optical constants of insulating materials in this way? It is well-known that films with thicknesses on the order of a few hundred angstroms show no serious charging problems. Actually, CsI is used above 1000 Å as a photocathode material. In this case, the problem arises from the very large mean-free paths for slow secondary electrons. Since electron–electron scattering is not possible when the kinetic energy of the electrons is less than roughly the band gap above the conduction-band minimum, only inelastic impurity scattering

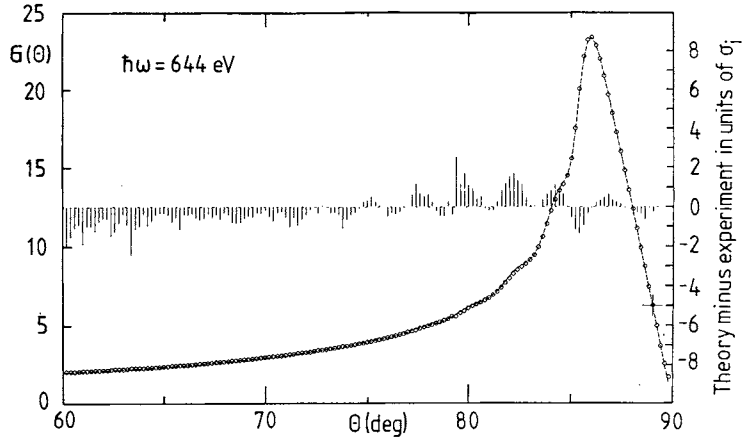


**Fig. 8.** Relative total yield $G(\theta)$ of a Cu film of 225 Å thickness on white crown glass at $\hbar\omega = 644$ eV. In addition to the experimental $G(\theta)$ spectrum (open circles), the fitted theoretical curve (dashed line) and the deviation between the theoretical and the measured spectra in units of $\sigma_i = 0.01 \times G_{\text{exp}}(\theta_i)$ (vertical bars) are plotted.

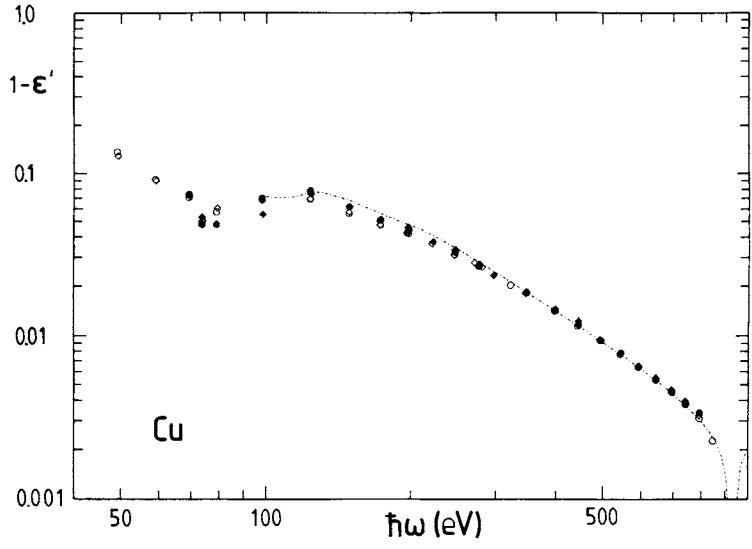


**Fig. 9.** Real part of the dielectric function $\varepsilon_{Cu}$ plotted as $1-\varepsilon'$ versus photon energy $\hbar\omega$. Full symbols result from reflectance measurements, open symbols from total-yield measurements on two samples of 225±5 Å (circles) and 317±6 Å (diamonds). The dash-dotted line represents values calculated from atomic scattering factors according to Henke *et al.* [9].

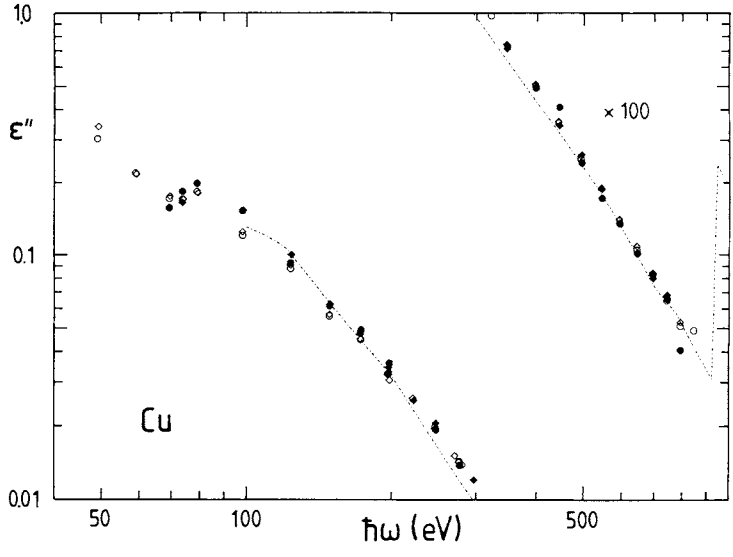


**Fig. 10.** Imaginary part $\varepsilon''$ of the dielectric function $\varepsilon_{Cu}$. Symbols are as in Fig. 9.

and a slow energy loss due to electron–phonon scattering remains. As a consequence, electrons originating from the substrate, which needs to be a conductor, can contribute to the total yield. A fairly realistic theoretical treatment of such a system appears to be possible. One or two additional parameters for the electron transport would enter the equations. They would have to be fitted together with the other parameters. Their correlation with the other parameters (optical constants) might not be very large, since the characteristic shape of the $G(\theta)$ curves close to the peak would be determined, to a large extent, by the optical constants of the insulator under investigation. Therefore, such a program could yield satisfactory results for this class of materials also. In this case, the method would be expanded beyond its present limitations.

## REFERENCES

1. S. V. Pepper, *J. Opt. Soc. Amer.* **60**, 805 (1970).
2. T. F. Gesell and E. T. Arakawa, *Phys. Rev. Lett.* **26**, 377 (1971).
3. E. T. Arakawa, R. N. Hamm, and M. W. Williams, *J. Opt. Soc. Amer.* **63**, 1131 (1973); E. T. Arakawa, M. W. Williams, R. N. Hamm, R. D. Birkhoff, and A. J. Braundmeier, "Proc. IV Int. Conf. on VUV Radiation Physics, Hamburg 1974," (E. E. Koch, R. Haensel, C. Kunz, eds.), Pergamon/Vieweg, Braunschweig, 580 (1974).
4. P. J. Vernier, J. P. Goudonnet, G. Chabrier, and J. Cornaz, *J. Opt. Soc. Amer.* **53**, 620 (1971); J. Peisner, A. Quemerais, M. Priol and S. Robin, *J. Phys. (France)* **34**, C6 (1973); A. Quemerais, J. Peisner, M. Priol, and S. Robin, *Comp. Rend. (Paris)* **276B**, 753 (1973).
5. H.-G. Birken, W. Jark, C. Kunz, and R. Wolf, *Nucl. Instr. and Meth. A* **253**, 166 (1986).
6. J. M. Elson, J. P. Rahn, and J. M. Bennett, *Appl. Opt.* **22**, 3207 (1983).
7. H. Hogrefe, D. Giesenberg, R. P. Haelbich, and C. Kunz, *Nucl. Instr. and Meth.* **208**, 415 (1983).
8. W. Jark and C. Kunz, *Nucl. Instr. and Meth. A* **246**, 320 (1986).
9. B. L. Henke, P. Lee, T. J. Tanaka, R. L. Shimabukuro, and B. K. Fujikawa, *At. Data Nucl. Data Tables* **27**, 1 (1982).
10. H.-G. Birken, C. Blessing, C. Kunz, and R. Wolf, *Rev. Sci. Instrum.* **60**, 2226 (1989).
11. C. Blessing, H.-G. Birken, C. Kunz, and R. Wolf, to be published; C. Blessing, diploma thesis, Hamburg (1988).

# Chapter 13

# Determination of Optical Constants by High-Energy, Electron-Energy-Loss Spectroscopy (EELS)

J. PFLÜGER
Hamburger Synchrotronstrahlungslabor HASYLAB at DESY
D-2000 Hamburg 52
Federal Republic of Germany

and

J. FINK
Kernforschungszentrum Karlsruhe
Institut für Nukleare Festkörperphysik
D-7500 Karlsruhe
Federal Republic of Germany

I. Introduction 293
II. Description of an EELS Experiment 295
III. Scattering Cross-Section 297
IV. Exact Determination of the Loss Function 298
V. Kramers–Kronig Analysis 299
VI. Brief Summary of the Evaluation Procedure 300
VII. Comparison with Reflectivity Measurements 300
VIII. Optical Properties of TiC, VC, TiN, and VN 303
References 310

## I INTRODUCTION

Optical properties of solids are important in the design of optical elements such as mirrors, prisms, multilayers, and so on. Optical quantities such as the complex refractive index, the reflectivity, or the absorption coefficient are also important for the investigation of the electronic structure of solids. These quantities are most commonly determined by optical


Copyright © 1991 by Academic Press.
All rights of reproduction in any form reserved.
ISBN 0-12-544422-2

methods such as reflection or absorption of light by suitable samples. The electric-field vector of a light wave is perpendicular to its **k** vector. So the electronic system is displaced transversely as a whole, and as a consequence, the electron density is not changed. Today, optical measurements are widely used and with the help of modern synchrotron-radiation sources, a very large energy range can be covered, from the far infrared up to the hard X-ray region.

A completely different method for determining optical constants is the measurement of energy losses suffered by fast electrons, with a kinetic energy of typically 50–300 keV when they are transmitted through thin solid films. In this case the electronic density is modulated longitudinally. The situation resembles the propagation of sound waves through air. The probability for energy losses is determined by the imaginary part of $-1/\varepsilon_L$, which is called the *loss function*. $\varepsilon_L(q,\omega)$ is the longitudinal $q$- and $\omega$-dependent dielectric function, which in general is different from the transverse function, which is measured by experiments involving transverse light waves. However, for $q \to 0$, $\varepsilon_T$ and $\varepsilon_L$ become identical, and thus, EELS and optical experiments give the same results. Since this contribution deals with EELS results only, we implicitly assume that only the longitudinal dielectric function $\varepsilon_L$ is involved in the formulas and drop the corresponding suffix.

Maxima in the loss function are determined by $\varepsilon_1 \simeq 0$ and $\varepsilon_2$ being "small." Such an excitation is called a plasmon [1].

More than 20 years ago, Raether's group in Hamburg [2, 3] demonstrated that dielectric properties determined by EELS can agree well with those obtained by optical methods. A compilation of older work is given in Refs. [1–4]; more recent work is reviewed in Ref. [5]. These investigations demonstrated the advantages of EELS:

1. Quite a large energy range is available starting at about 0.2 eV. The upper limit is about 2000 eV. It is, however, important to note that the accuracy of optical constants determined by EELS is reduced more and more, starting at about 30 eV, due to multiple-scattering events, which can be corrected only within a limited accuracy. This energy range is available with the help of a laboratory-scale instrument; optical methods at these energies require the use of a large synchrotron-radiation facility.
2. Only bulk properties are measured using EELS. The results are independent of surface preparation or contamination. EELS might be an alternative to optical techniques, when the preparation of an optically good surface is difficult or even impossible.
3. Since EELS is a scattering experiment, it can be performed with a momentum transfer $\hbar q$. This allows the determination of $\mathrm{Im}(-1/\varepsilon\,(q,\omega))$, which contains information about the dispersion of the electronic band structure and electron–electron correlation effects. For the determination

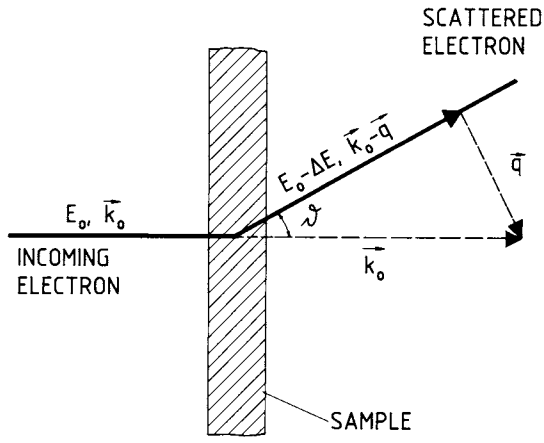


**Fig. 1.** Scattering geometry of an EELS experiment. An electron with a kinetic energy of typically 50–300 keV penetrating a sample of thickness 500–1000 Å is scattered by an angle $\vartheta$ and suffers an energy loss $\Delta E$. The scattering angles are very small, typically several mrad.

of optical constants, however, only the limit $q \rightarrow 0$ is important.

A severe problem is sample preparation, since thin self-supporting samples with a thickness of 500–2000 Å and an area of roughly 1 mm$^2$ are needed. Many techniques have been applied. A comprehensive overview of many preparation techniques is given in Ref. [5]. However, as experience shows, there is a preparation method for almost every problem. In this chapter we will restrict ourselves to the optical limit ($q \rightarrow 0$), so that the data obtained are comparable to those obtained using optical methods. The determination of optical constants from EELS data will be described in detail. The optical properties of the refractory compounds TiC, VC, TiN, and VN are discussed in detail, and for TiC, a comparison of EELS data with optical data is performed.

## DESCRIPTION OF AN EELS EXPERIMENT

The scattering geometry is shown in Fig. 1. A highly collimated beam of monochromatized electrons with a kinetic energy $E_o$ of 50–300 keV and an angular spread $\Delta\vartheta \simeq 0.3$–$0.5$ mrad penetrates a thin sample, typically 500–2000 Å thick. On its passage through the sample, the electron may be scattered inelastically by an angle $\vartheta$ and loses an amount of energy $\Delta E$.

Energy and momentum conservation require

$$\Delta E = (\hbar^2/2m)(k_o^2 - k_n^2) \tag{1}$$

$$\hbar q = \hbar(k_o - k_n). \tag{2}$$

Here, $k_o$ and $k_n$ are the wave vector of the unscattered and the scattered electrons, $\hbar$ is Planck's constant divided by $2\pi$, and $m$ is the electron mass. The transferred momentum $\hbar q$ can be decomposed into a parallel and a perpendicular component, to $k_o$, $q_\parallel$ and $q_\perp$, respectively:

$$\hbar q_\parallel = \hbar k_o \vartheta_E \tag{3}$$

with

$$\vartheta_E = \Delta E/2E_o. \tag{4}$$

This longitudinal momentum transfer is related to the energy loss only.

Similarly, the transverse momentum transfer is given by

$$\hbar q_\perp = \hbar k_o \vartheta, \tag{5}$$

which is independent of the energy loss and depends on the scattering angle only, so that the total momentum transfer is given by

$$\hbar q = \hbar k_o (\vartheta^2 + \vartheta_E^2)^{1/2}. \tag{6}$$

For scattering angles somewhat larger than $\vartheta_E$, the momentum transfer is practically determined by $\vartheta$ only. As an example, some numerical values for an electron-energy-loss experiment, used to study the optical properties of a number of refractory compounds, are given [6, 7]. The kinetic energy of the electrons was 170 keV corresponding to $k_o = 228.4$ Å$^{-1}$. At a characteristic energy loss of $\Delta E = 20$ eV, $\vartheta_E = 0.059$ mrad, which corresponds to $q_\parallel = 0.012$ Å$^{-1}$. This is, by the way, roughly the same momentum carried by a 20 eV photon (0.01 Å$^{-1}$).

## SCATTERING CROSS-SECTION III

The double-differential scattering cross-section per atom for high-energy electrons in an (infinite) solid is treated in the Born approximation and can be written as [4, 5]

$$\frac{d^2\sigma}{d\omega\, d\Omega} = \frac{4\hbar\gamma^2}{a_o^2 q^4} S(q,\omega) = \frac{\hbar\gamma^2}{(\pi e a_o)^2 N}\frac{1}{q^2}\,\mathrm{Im}(-1/\varepsilon(q,\omega)). \tag{7}$$

Here, in addition, the electron charge $e$, Bohr's radius $a_o$ and the number density of electrons $N$ per unit volume has been introduced. The factor $\gamma = 1 + E_o/m_o c^2$ makes the result relativistically invariant, where $m_o c^2 =$ 511 keV is the rest mass energy of the electron.

$S(q,\omega)$ is the dynamic structure factor originally derived by van Hove [8]. The second identity of Eq. 7, correlating the dynamic structure factor with the loss function, is derived in Ref. [9]. A derivation of the right-hand side from dielectric theory is given in Ref. [10]. Since the loss function is typically of order unity, the scattering cross-section given by Eq. 7 falls off like $1/q^2$. Using Eq. 6 gives

$$\frac{d^2\sigma}{d\omega\, d\Omega} = \frac{\hbar\gamma^2}{(\pi e a_o)^2 k_o^2}\frac{1}{\vartheta^2 + \vartheta_E^2}\,\mathrm{Im}(-1/\varepsilon(q,\omega)). \tag{8}$$

Thus, measuring the cross-section for inelastic electron scattering gives information on the loss function $\mathrm{Im}(-1/\varepsilon(q,\omega))$.

There are, however, two other contributions that might influence the accuracy of the determination of the volume loss function.

1. In a sample of finite thickness $D$, excitation of surface modes, also called *surface plasmons*, may take place, which contributes to the scattered intensity. The cross-section for surface-plasmon generation is proportional to

$$\frac{d^2\sigma}{d\omega\, d\Omega} \cong (1/q^3)\,\mathrm{Im}(-1/(\varepsilon+1)). \tag{9}$$

The function $\mathrm{Im}(-1(\varepsilon+1))$ is also called the *surface loss function*.

Surface losses are easily verified, since their cross-section varies like $1/q^3$. On the other hand, their contribution to the observed intensity decreases

as the sample thickness is increased. It was already shown by Raether [2] that even for momentum transfer $q \simeq 0.2\,\text{Å}^{-1}$, the ratio of volume-to-surface losses can be made negligibly small.

2. Radiation losses due to the emission of Cerenkov radiation can take place when the electron velocity exceeds the phase velocity of light. This might occur in highly polarizable materials. It was shown by Kröger [11] that radiation losses, like surface losses, contribute only at very small angles.

The usual way to suppress contributions from surface and radiation losses is to perform the measurements at a finite momentum transfer $q$, which is small enough so that the optical limit $q \to 0$ is still valid, but which is large enough so that only volume losses contribute. In the case of refractory compounds reported later in this article, $q = 0.1$–$0.15\,\text{Å}^{-1}$ was found sufficiently small.

## IV EXACT DETERMINATION OF THE LOSS FUNCTION

To determine the exact loss function from a spectrum measured at small $q$, as described in the preceeding section, corrections for finite spectrometer resolution and multiple scattering have to be applied. Both energy and angular resolution of a spectrometer are finite, and therefore the observed intensity at some energy and angle is a convolution of Eq. 8 with the energy- and angular-resolution function. The problem is simplified on assuming that $\text{Im}(-1/\varepsilon(q,\omega))$ is constant over the resolution interval. This assumption is fulfilled, since energy resolution typically is of the order of 0.1 eV, and the momentum transfer resolution is typically $<0.05\,\text{Å}^{-1}$. Then the convolution problem leads to a correction factor $F(\Delta E)$, which depends on the energy loss only. The whole procedure has already been described in detail in Ref. [3]. To make all corrections properly, the energy and angular resolution are recorded before each measurement, in order to calculate $F(\Delta E)$ exactly. For the spectrometer resolution given previously, the correction by $F(\Delta E)$ is below 10% and does not vary much with the energy loss.

The scattering cross-section for highly energetic electrons in solids is very high, and mean free paths are of the order of a few hundred angstroms. Therefore, there exists a probability that an electron undergoes more than one scattering event on traversing the sample. In the range of roughly twice the plasma energy, up to energy losses of 40–50 eV, only double scattering events contribute significantly and therefore have to be corrected for.

Double scattering can be described as a convolution of a "true" single-scattering spectrum with itself. In this way dominant structures like volume plasmons are also found at twice the single-energy loss. Triple losses lead to losses at three times the single-loss energy, and so on.

Several numerical deconvolution schemes have been developed [12] and applied to EELS data [3, 4, 13, 14]. Following Ref. [3], double scattering can be calculated starting at low-energy losses up to about 1–2 eV, where double scattering is negligibly small. Then, the double-scattering contribution can be calculated at slightly higher energies and subtracted from the uncorrected spectrum. By this step-by-step method, the whole spectrum can be corrected. At the end of the procedure, the loss function is determined experimentally except for a multiplicative constant. It is possible to measure the absolute value of the loss function experimentally [2, 3] but this method is not very accurate. Instead, it is preferable to use a suitable sum rule derived from the Kramers–Kronig relations for normalization.

## KRAMERS–KRONIG ANALYSIS V

The causality principle connects imaginary and real parts of a complex function via the Kramers–Kronig (K–K) integrals. Many optical spectroscopies make use of these relations. In the case of EELS at small momentum transfer ($q \to 0$), the K–K transform is given by

$$\mathrm{Re}(-1/\varepsilon(\omega)) - 1 = \frac{2}{\pi} P \int_0^\infty \mathrm{Im}(-1/\varepsilon(\omega')) \frac{\omega' \, d\omega'}{\omega'^2 - \omega^2}. \tag{10}$$

where $P$ denotes the Cauchy principal value of the integral. Two extrapolations are necessary in order to perform the integral form zero to infinity. From zero to about 0.5 eV the loss function is interpolated linearly starting at zero, since in the original data this region is obscured by the primary beam. At higher energies, above 40–50 eV, the loss function is extrapolated proportional to $\omega^{-3}$, which is the loss function of a free-electron gas. The proper normalization of the loss function can be obtained from Eq. 10 by setting $\omega = 0$:

$$\mathrm{Re}(-1/\varepsilon(\omega = 0)) - 1 = \frac{2}{\pi} P \int_0^\infty \mathrm{Im}(-1/\varepsilon(\omega')) \frac{d\omega'}{\omega'}. \tag{11}$$

For metals, $1/\varepsilon(\omega=0)=0$. For insulators and semiconductors $\varepsilon$ is real below the band gap and can be obtained from the refractive index by $\varepsilon_1=n^2$. The advantage of using Eq. 11 for normalization is this: the measured spectrum is weighted inversely proportional to the energy loss. Thus, the energy region is weighted most where multiple losses contribute only little and the loss function is therefore determined with the highest accuracy. The well-known $f$-sum rule,

$$\int_0^\infty \mathrm{Im}(-1/\varepsilon)\omega \, d\omega = \pi/2\omega_p^2. \tag{12}$$

which in principle can also be used for normalization of $\mathrm{Im}(-1/\varepsilon)$, weights the loss function proportional to $\omega$. In addition, an assumption for the electron density $N$, which enters into the plasma frequency

$$\omega_p=(4\pi Ne^2/m)^{1/2} \tag{13}$$

has to be made. This can be avoided by using Eq. 11.

## VI BRIEF SUMMARY OF THE EVALUATION PROCEDURE

To give an overview over the evaluation procedure, the five steps leading to readily evaluated data from EELS measurements will be briefly summarized.

(1) Measurement of the angular- and energy-resolution functions.
(2) Measurement of the loss spectrum.
(3) Angular and energy deconvolution.
(4) After correction for double scattering, the unnormalized loss function $\mathrm{Im}(-1/\varepsilon)$ is obtained.
(5) Kramérs–Kronig analysis and normalization of the loss function using Eq. 11. Calculation of $\varepsilon_1$, $\varepsilon_2$, $n$, $k$, and so on.

## VII COMPARISON WITH REFLECTIVITY MEASUREMENTS

During the last years, EELS has been used by the Karlsruhe group in a number of experiments to elucidate the dielectric properties in the energy

range 0.5–40 eV. Examples include the study of the binding states in amorphous hydrogenated carbon coatings [15], conducting polymers [16–22], carbides and nitrites of 3d and 4d transition metals [6, 7], A-15 superconductors [23], and, most recently, ceramic superconductors [24–26].

As an illustrative and representative example, the dot-dashed curve in Fig. 2 shows the measured loss function of TiN after the elastic line has been subtracted, and the energy and angular deconvolution was performed. The energy range extends from 0–40 eV. The solid line shows the influence of the double-scattering correction as described in Ref. [3]. It is seen that at higher energies this correction is quite substantial, whereas below about 20 eV it is less important. The maximum of the curves is arbitrarily normalized to 25. The solid curve is the input spectrum for the K–K analysis. The normalization of the loss function is then performed using Eq. 11.

In Fig. 3, optical data are shown for TiC obtained with different methods. A comparison is made between the optical constants derived by the procedure described above taken from Pflüger *et al.* [6] with data from Lynch *et al.* [27] deduced from reflectivity measurements using synchrotron radiation in the energy range 0.1–30 eV. To our knowledge, these are the only available optical measurements on refractory compounds over a large energy range comparable to that covered by EELS. The upper part of Fig. 3 shows the measured reflectance from Ref. [27] versus reflectance derived

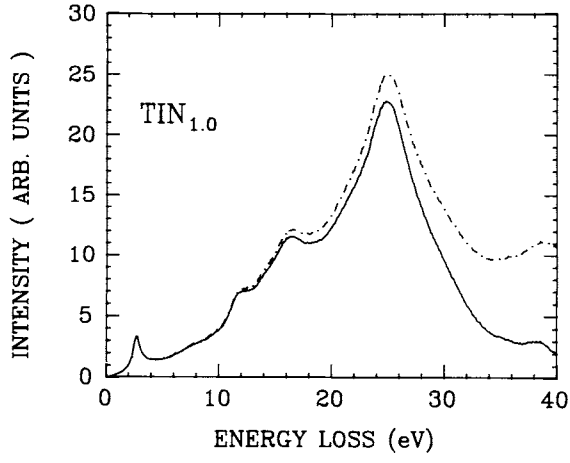


**Fig. 2.** Energy-loss intensity of TiN after the elastic line has been subtracted and angular deconvolution has been applied. The dot-dashed curve is without correction for double scattering. The solid curve is corrected for double scattering. Above about 20 eV, the correction becomes substantial.

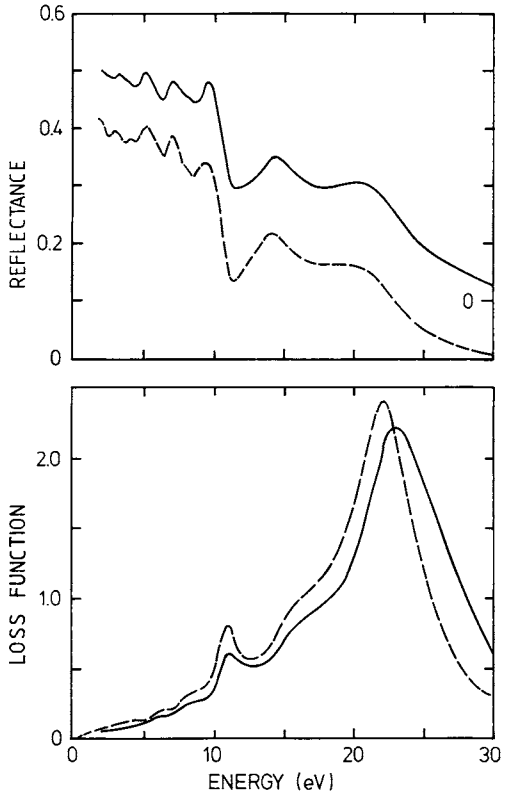


**Fig. 3.** Comparison of optical constants obtained with EELS taken from Ref. [6] with those obtained with reflectance measurements from Ref. [27]. Solid lines indicate data derived from EELS measurements. Dashed lines indicate data derived from reflectance measurements. Note the 0.1 upward shift of the solid-line curve in the upper figure.

from EELS data. Note that the scale of the EELS curve is shifted upward by one tick mark. The lower part of Fig. 3 shows the opposite comparison. The loss function calculated from reflectivity data, reproduced in Ref. [27], is compared to the loss function measured by EELS.

The data obtained by the two methods agree remarkably well. Generally the reflectance obtained by EELS differs less than reflectance data for TiC published earlier [28, 29].

Each method shows its particular strength and weakness. At about 25 eV, the EELS reflectivity seems to be too high compared with the optical data, whereas the EELS volume plasmon, at 23.5 eV, is slightly higher than that derived from optical data. Also, some structures in the EELS spectra are broader and less pronounced than in the optical curves. One possible explanation for this is the completely different method of

sample preparation. Large, carefully polished zone-melted single crystals were used by Lynch *et al.* Thin, self-supported 770 Å-thick polycrystalline films of TiC were prepared by reactive sputtering for the EELS measurements. In both groups great care was taken for a good characterization of the samples.

## VIII OPTICAL PROPERTIES OF TiC, VC, TiN, AND VN

In this section we briefly review the dielectric properties of the refractory compounds TiC, VC, TiN, and VN as determined by EELS [6]. Similar experiments were also performed on ZrN, NbC, and NbN [7]. For a complete description the reader is referred to these references.

The properly normalized loss functions together with the real and imaginary parts of the dielectric function are shown in Fig. 4 for TiC, VC, TiN, and VN. One realizes that maxima in the loss functions correspond to $\varepsilon_1 \simeq 0$ and small $\varepsilon_2$. The better this condition is fulfilled, the more pronounced is the structure of the loss function. The real and the imaginary part of the refractive index of these compounds is given in Tables I–IV.

The dominant feature in all loss spectra is the volume plasmon, the collective oscillation of all valence electrons, found at 23.5, 24.9, 24.9, and 26.3 eV for TiC, VC, TiN, and VN, respectively. These values might be compared to the plasma energy defined by Eq. 13 taking into account the metal 4s and 3d and the nonmetal 2s and 2p orbitals. One obtains 23.3, 25.5, 25.5, and 28.0 eV, which is in quite satisfactory agreement.

Apart from the main plasmon peak, there are other excitations that are caused by interband transitions, and therefore might be termed interband plasmons. Spectra of the carbides and nitrides look quite different, but there is some similarity between TiC and VC and between TiN and VN. These differences between carbides and nitrides are, however, closely related to the electronic structure of these compounds.

In the vicinity of the Fermi level, the electronic states of the refractory compounds consist of bonding nonmetal p orbitals strongly hybridized with metal d orbitals below, and antibonding d orbital hybridized with nonmetal orbitals above $E_F$ [30]. Hybridization is stronger for the carbides than for the nitrides. The Fermi level is determined by the number of available valence electrons. For TiC it lies in the very minimum between p and d states, whereas for VC, TiN, and VN it is shifted more and more upward into the d bands.

Many features of the loss spectra can be understood from details of the electronic structure. For a comparison with calculated band-structure data,

the optical joint density of states (OJDS), which is defined as [31]

$$I_1(\omega) = 2\omega\varepsilon_2(\omega)/\pi\omega_p^2 \tag{14}$$

was calculated from $\varepsilon_2$ as derived from the K–K analysis.

Fig. 5 shows a comparison between the OJDS (solid curve) and joint densities of states (dashed curve) derived from self-consistent Gaussian LCAO band-structure data [32]. The joint density of states gives a measure for the probability of interband transitions when matrix elements as well as lifetime effects are neglected. Many structures seen in the OJDS are also reflected by the calculations. The maximum (around 7 eV), which is present in all compounds, can be attributed to transitions between the

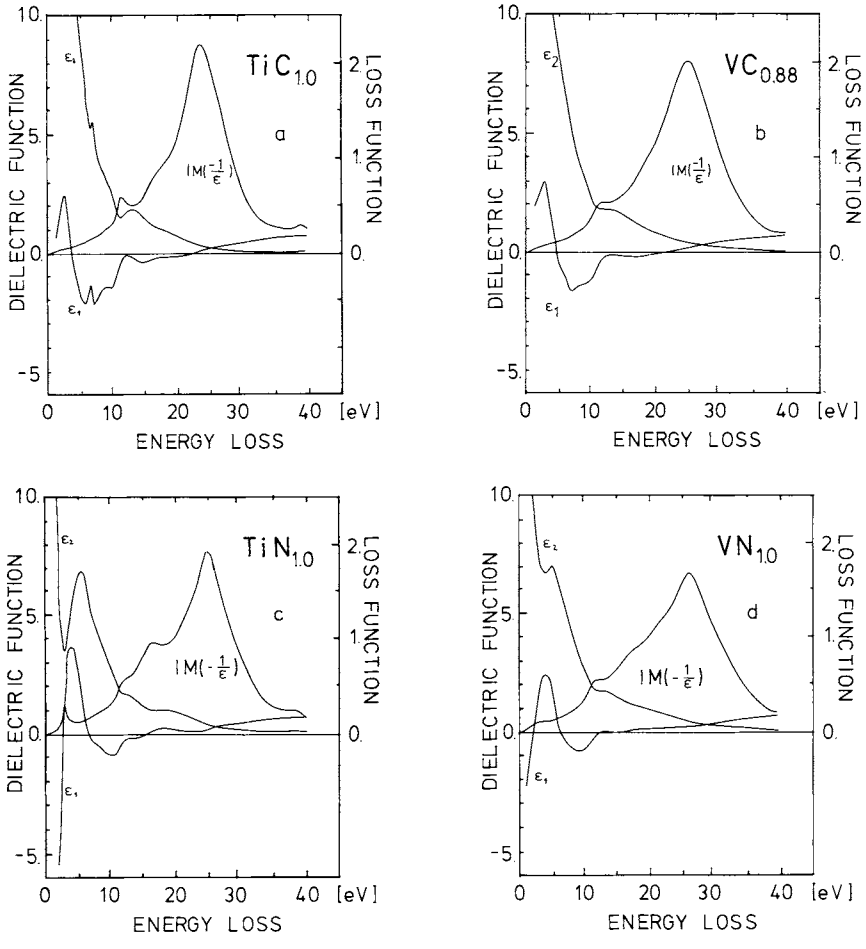


**Fig. 4.** Loss functions and Kramers–Kronig-derived real and imaginary parts of the dielectric function $\varepsilon_1$, $\varepsilon_2$ for (a) $TiC_{1.0}$, (b) $VC_{0.88}$, (c) $TiN_{1.0}$, (d) $VN_{1.0}$.

**TABLE I**

**Values of $n$ and $k$ for TiC Obtained by EELS**

| eV | $cm^{-1}$ | Å | $n$ | $k$ |
|---|---|---|---|---|
| 0.5 | 4032.7 | 24797 | $5.44 \times 10^{0}$ | $5.54 \times 10^{0}$ |
| 1.0 | 8065.5 | 12399 | 3.97 | 3.78 |
| 1.5 | 12098 | 8266 | 3.51 | 3.07 |
| 2.0 | 16131 | 6199 | 3.05 | 2.67 |
| 2.5 | 20164 | 4959 | 2.95 | 2.38 |
| 3.0 | 24169 | 4133 | 2.78 | 2.43 |
| 3.5 | 28229 | 3542 | 2.57 | 2.34 |
| 4.0 | 32262 | 3100 | 2.30 | 2.33 |
| 4.5 | 36295 | 2755 | 2.16 | 2.31 |
| 5.0 | 40327 | 2480 | 1.96 | 2.25 |
| 5.5 | 44360 | 2254 | 1.74 | 2.20 |
| 6.0 | 48393 | 2066 | 1.52 | 2.02 |
| 6.5 | 52426 | 1907 | 1.43 | 1.86 |
| 7.0 | 56458 | 1771 | 1.42 | 1.89 |
| 7.5 | 60491 | 1653 | 1.21 | 1.84 |
| 8.0 | 64524 | 1550 | 1.12 | 1.69 |
| 8.5 | 68557 | 1459 | 1.07 | 1.63 |
| 9.0 | 72589 | 1378 | $1.00 \times 10^{0}$ | 1.55 |
| 9.5 | 76622 | 1305 | $9.55 \times 10^{-1}$ | 1.50 |
| 10.0 | 80655 | 1240 | 8.01 | 1.44 |
| 10.5 | 84688 | 1181 | 7.25 | 1.25 |
| 11.0 | 88720 | 1127 | 7.45 | 1.06 |
| 11.5 | 92753 | 1078 | 8.67 | 0.96 |
| 12.0 | 96785 | 1033 | 9.42 | 0.98 |
| 13.0 | | 953.7 | 9.59 | 1.02 |
| 14.0 | | 885.6 | 8.70 | $1.03 \times 10^{0}$ |
| 15.0 | | 826.6 | 7.47 | $9.62 \times 10^{-1}$ |
| 16.0 | | 774.9 | 7.23 | 8.59 |
| 17.0 | | 729.3 | 7.06 | 8.01 |
| 18.0 | | 688.8 | 6.88 | 7.50 |
| 19.0 | | 652.6 | 6.57 | 7.29 |
| 20.0 | | 619.9 | 6.03 | 6.75 |
| 21.0 | | 590.4 | 5.51 | 6.04 |
| 22.0 | | 563.6 | 5.23 | 5.16 |
| 23.0 | | 539.1 | 5.23 | 4.21 |
| 24.0 | | 516.6 | 5.47 | 3.44 |
| 25.0 | | 495.9 | 5.79 | 2.91 |
| 26.0 | | 476.9 | 6.03 | 2.48 |
| 27.0 | | 459.2 | 6.27 | 2.10 |
| 28.0 | | 442.8 | 6.54 | 1.74 |
| 29.0 | | 427.5 | 6.79 | 1.45 |
| 30.0 | | 413.3 | 7.09 | 1.23 |
| 31.0 | | 400.0 | 7.34 | $1.07 \times 10^{-1}$ |
| 32.0 | | 387.5 | 7.62 | $8.92 \times 10^{-2}$ |
| 33.0 | | 375.7 | 7.85 | 8.30 |
| 34.0 | | 364.7 | 8.08 | 8.10 |
| 35.0 | | 354.2 | 8.26 | 7.95 |
| 36.0 | | 344.4 | 8.39 | 7.97 |
| 37.0 | | 335.1 | 8.53 | 8.41 |
| 38.0 | | 326.3 | 8.63 | 8.96 |
| 39.0 | | 317.9 | 8.53 | 1.01 |
| 39.9 | | 310.7 | 8.40 | 5.05 |

**TABLE II**

**Values of $n$ and $k$ for VC Obtained by EELS**

| eV | $cm^{-1}$ | Å | $n$ | $k$ |
|---|---|---|---|---|
| 0.5 | 4032.7 | 24797 | $4.86\times10^{0}$ | $5.34\times10^{0}$ |
| 1.0 | 8065.5 | 12399 | 3.66 | 3.42 |
| 1.5 | 12098 | 8266 | 3.37 | 2.88 |
| 2.0 | 16131 | 6199 | 3.01 | 2.51 |
| 2.5 | 20164 | 4959 | 2.84 | 2.21 |
| 3.0 | 24196 | 4133 | 2.77 | 2.16 |
| 3.5 | 28229 | 3542 | 2.59 | 2.12 |
| 4.0 | 32262 | 3100 | 2.47 | 2.15 |
| 4.5 | 36295 | 2755 | 2.27 | 2.18 |
| 5.0 | 40327 | 2480 | 2.04 | 2.13 |
| 5.5 | 44360 | 2254 | 1.86 | 2.04 |
| 6.0 | 48393 | 2066 | 1.74 | 2.00 |
| 6.5 | 52426 | 1907 | 1.62 | 1.97 |
| 7.0 | 56458 | 1771 | 1.42 | 1.92 |
| 7.5 | 60491 | 1653 | 1.32 | 1.83 |
| 8.0 | 64524 | 1550 | 1.22 | 1.73 |
| 8.5 | 68557 | 1459 | 1.13 | 1.64 |
| 9.0 | 72589 | 1378 | $1.07\times10^{0}$ | 1.59 |
| 9.5 | 76622 | 1305 | $9.58\times10^{-1}$ | 1.51 |
| 10.0 | 80655 | 1240 | 8.65 | 1.41 |
| 10.5 | 84688 | 1181 | 8.27 | 1.28 |
| 11.0 | 88720 | 1127 | 8.20 | 1.14 |
| 11.5 | 92753 | 1078 | 8.58 | 1.04 |
| 12.0 | 96785 | 1033 | 9.17 | 0.99 |
| 13.0 | | 953.7 | 9.56 | $1.00\times10^{0}$ |
| 14.0 | | 885.6 | 9.04 | $9.96\times10^{-1}$ |
| 15.0 | | 826.6 | 8.57 | 9.58 |
| 16.0 | | 774.9 | 8.03 | 9.33 |
| 17.0 | | 729.3 | 7.28 | 8.72 |
| 18.0 | | 688.8 | 6.89 | 7.99 |
| 19.0 | | 652.6 | 6.65 | 7.30 |
| 20.0 | | 619.9 | 6.37 | 6.86 |
| 21.0 | | 590.4 | 6.06 | 6.33 |
| 22.0 | | 563.6 | 5.78 | 5.68 |
| 23.0 | | 539.1 | 5.61 | 4.99 |
| 24.0 | | 516.6 | 5.60 | 4.33 |
| 25.0 | | 495.9 | 5.64 | 3.71 |
| 26.0 | | 476.9 | 5.82 | 3.16 |
| 27.0 | | 459.2 | 6.01 | 2.68 |
| 28.0 | | 442.8 | 6.23 | 2.31 |
| 29.0 | | 427.5 | 6.45 | 1.99 |
| 30.0 | | 413.3 | 6.68 | 1.72 |
| 31.0 | | 400.0 | 6.87 | 1.52 |
| 32.0 | | 387.5 | 7.06 | 1.29 |
| 33.0 | | 375.7 | 7.25 | $1.13\times10^{-1}$ |
| 34.0 | | 364.7 | 7.42 | $9.82\times10^{-2}$ |
| 35.0 | | 354.2 | 7.60 | 8.57 |
| 36.0 | | 344.4 | 7.76 | 7.27 |
| 37.0 | | 335.1 | 7.95 | 6.33 |
| 38.0 | | 326.3 | 8.14 | 5.76 |
| 39.0 | | 317.9 | 8.30 | 5.89 |
| 39.9 | | 310.7 | 8.37 | 6.42 |

**TABLE III**

**Values of $n$ and $k$ for TiN Obtained by EELS**

| eV | $cm^{-1}$ | Å | $n$ | $k$ |
|---|---|---|---|---|
| 0.5 | 4032.7 | 24797 | $4.52 \times 10^{0}$ | $8.25 \times 10^{0}$ |
| 1.0 | 8065.5 | 12399 | 2.69 | 5.04 |
| 1.5 | 12098 | 8266 | 1.82 | 3.81 |
| 2.0 | 16131 | 6199 | 1.32 | 2.69 |
| 2.5 | 20164 | 4959 | 1.20 | 1.65 |
| 3.0 | 24196 | 4133 | 1.74 | 1.04 |
| 3.5 | 28229 | 3542 | 2.14 | 1.06 |
| 4.0 | 32262 | 3100 | 2.27 | 1.23 |
| 4.5 | 36295 | 2755 | 2.31 | 1.38 |
| 5.0 | 40327 | 2480 | 2.25 | 1.54 |
| 5.5 | 44360 | 2254 | 2.06 | 1.64 |
| 6.0 | 48393 | 2066 | 1.85 | 1.71 |
| 6.5 | 52426 | 1907 | 1.69 | 1.66 |
| 7.0 | 56458 | 1771 | 1.55 | 1.64 |
| 7.5 | 60491 | 1653 | 1.46 | 1.58 |
| 8.0 | 64524 | 1550 | 1.38 | 1.53 |
| 8.5 | 68557 | 1459 | 1.28 | 1.49 |
| 9.0 | 72589 | 1378 | 1.19 | 1.49 |
| 9.5 | 76622 | 1305 | 1.09 | 1.43 |
| 10.0 | 80655 | 1240 | $1.00 \times 10^{0}$ | 1.38 |
| 11.0 | 88720 | 1127 | $8.23 \times 10^{-1}$ | $1.17 \times 10^{0}$ |
| 12.0 | 96785 | 1033 | 8.55 | $9.76 \times 10^{-1}$ |
| 13.0 | | 953.7 | 8.60 | 9.48 |
| 14.0 | | 885.6 | 7.93 | 8.74 |
| 15.0 | | 826.6 | 7.59 | 7.95 |
| 16.0 | | 774.9 | 7.47 | 6.89 |
| 17.0 | | 729.3 | 7.91 | 6.34 |
| 18.0 | | 688.8 | 8.11 | 6.28 |
| 19.0 | | 652.6 | 7.93 | 6.27 |
| 20.0 | | 619.9 | 7.49 | 6.22 |
| 21.0 | | 590.4 | 7.02 | 5.87 |
| 22.0 | | 563.6 | 6.67 | 5.45 |
| 23.0 | | 539.1 | 6.28 | 4.97 |
| 24.0 | | 516.6 | 5.89 | 4.31 |
| 25.0 | | 495.9 | 5.83 | 3.48 |
| 26.0 | | 476.9 | 6.02 | 2.78 |
| 27.0 | | 459.2 | 6.33 | 2.31 |
| 28.0 | | 442.8 | 6.58 | 2.00 |
| 29.0 | | 427.5 | 6.81 | 1.72 |
| 30.0 | | 413.3 | 6.98 | 1.48 |
| 31.0 | | 400.0 | 7.15 | 1.24 |
| 32.0 | | 387.5 | 7.37 | $1.02 \times 10^{-1}$ |
| 33.0 | | 375.7 | 7.60 | $8.63 \times 10^{-2}$ |
| 34.0 | | 364.7 | 7.81 | 7.67 |
| 35.0 | | 354.2 | 8.01 | 7.39 |
| 36.0 | | 344.4 | 8.15 | 7.07 |
| 37.0 | | 335.1 | 8.31 | 7.03 |
| 38.0 | | 326.3 | 8.34 | 7.31 |
| 39.0 | | 317.9 | 8.31 | 6.49 |
| 39.9 | | 310.7 | 8.40 | 5.05 |

**TABLE IV**

**Values of $n$ and $k$ for VN Obtained by EELS**

| eV | $cm^{-1}$ | Å | $n$ | $k$ |
|---|---|---|---|---|
| 0.5 | 4032.7 | 24797 | $4.23 \times 10^{0}$ | $6.13 \times 10^{0}$ |
| 1.0 | 8065.5 | 12399 | 3.19 | 3.66 |
| 1.5 | 12098 | 8266 | 2.73 | 2.92 |
| 2.0 | 16131 | 6199 | 2.35 | 2.47 |
| 2.5 | 20164 | 4959 | 2.17 | 1.98 |
| 3.0 | 24196 | 4133 | 2.13 | 1.70 |
| 3.5 | 28229 | 3542 | 2.18 | 1.58 |
| 4.0 | 32262 | 3100 | 2.20 | 1.54 |
| 4.5 | 36295 | 2755 | 2.19 | 1.56 |
| 5.0 | 40327 | 2480 | 2.10 | 1.64 |
| 5.5 | 44360 | 2254 | 1.98 | 1.70 |
| 6.0 | 48393 | 2066 | 1.82 | 1.74 |
| 6.5 | 52426 | 1907 | 1.66 | 1.68 |
| 7.0 | 56458 | 1771 | 1.56 | 1.65 |
| 7.5 | 60491 | 1653 | 1.46 | 1.60 |
| 8.0 | 64524 | 1550 | 1.36 | 1.57 |
| 8.5 | 68557 | 1459 | 1.25 | 1.51 |
| 9.0 | 72589 | 1378 | 1.17 | 1.46 |
| 9.5 | 76622 | 1305 | $1.07 \times 10^{0}$ | 1.39 |
| 10.0 | 80655 | 1240 | $9.82 \times 10^{-1}$ | 1.31 |
| 10.5 | 84688 | 1181 | 9.22 | 1.20 |
| 11.0 | 88720 | 1127 | 8.96 | 1.10 |
| 11.5 | 92753 | 1078 | 9.03 | $1.00 \times 10^{0}$ |
| 12.0 | 96785 | 1033 | 9.31 | $9.46 \times 10^{-1}$ |
| 13.0 | | 953.7 | 9.73 | 9.24 |
| 14.0 | | 885.6 | 9.22 | 9.02 |
| 15.0 | | 826.6 | 8.73 | 8.65 |
| 16.0 | | 774.9 | 8.29 | 8.06 |
| 17.0 | | 729.3 | 8.03 | 7.34 |
| 18.0 | | 688.8 | 7.97 | 6.91 |
| 19.0 | | 652.6 | 7.82 | 6.67 |
| 20.0 | | 619.9 | 7.59 | 6.35 |
| 21.0 | | 590.4 | 7.36 | 5.98 |
| 22.0 | | 563.6 | 7.14 | 5.60 |
| 23.0 | | 539.1 | 6.95 | 5.30 |
| 24.0 | | 516.6 | 6.63 | 4.95 |
| 25.0 | | 495.9 | 6.34 | 4.43 |
| 26.0 | | 476.9 | 6.19 | 3.81 |
| 27.0 | | 459.2 | 6.28 | 3.18 |
| 28.0 | | 442.8 | 6.44 | 2.70 |
| 29.0 | | 427.5 | 6.65 | 2.35 |
| 30.0 | | 413.3 | 6.83 | 2.09 |
| 31.0 | | 400.0 | 6.96 | 1.86 |
| 32.0 | | 387.5 | 7.12 | 1.62 |
| 33.0 | | 375.7 | 7.27 | 1.40 |
| 34.0 | | 364.7 | 7.41 | 1.22 |
| 35.0 | | 354.2 | 7.58 | $1.06 \times 10^{-1}$ |
| 36.0 | | 344.4 | 7.72 | $9.26 \times 10^{-2}$ |
| 37.0 | | 335.1 | 7.88 | 7.90 |
| 38.0 | | 326.3 | 8.05 | 7.22 |
| 39.0 | | 317.9 | 8.23 | 6.49 |
| 39.9 | | 310.7 | 8.33 | 6.71 |

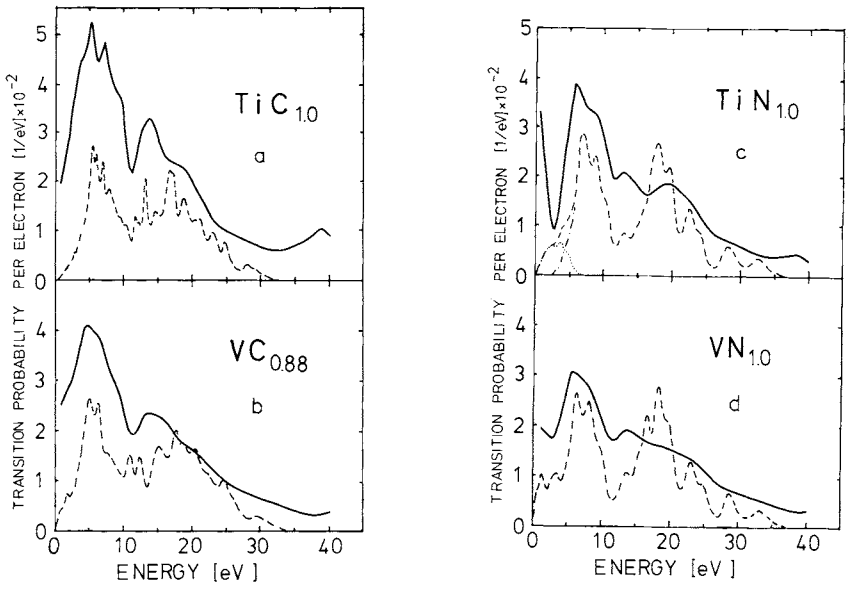


**Fig. 5.** Kramers–Kronig-derived optical joint densities of states of the stochiometric compounds (solid lines) and joint densities of states from our band-structure calculation (dashed lines) for (a) $TiC_{1.0}$, (b) $VC_{0.88}$, (c) $TiN_{1.0}$, (d) $VN_{1.0}$. In the TiN curves, the joint density of states for transitions between d bands and without d-d transitions are shown separately (dotted and dotted-dashed lines, respectively).

occupied p to unoccupied d states. Especially in the nitrites, the Fermi level lies well within the d bands. Transitions between these d states are dipole-forbidden. Thus, up to about 2.5–3 eV, interband damping is very weak. This is most clearly seen in the TiN curve. To emphasize this, the contribution of d-d transitions to the joint density of states for TiN in Fig. 5 is also shown (dotted curve in Fig. 5c). The onset of strong p-d transitions is observed above 2.8 eV. Below 2.8 eV the OJDS in Fig. 5 is dominated by intraband transitions. The strong minimum at 2.8 eV is, of course, also seen in $\varepsilon_2$. This weak interband damping (small $\varepsilon_2$) at this energy therefore ensures that the Drude plasmon (the collective oscillation of the free electrons, which is shifted down by strong interband transitions at higher energies) can be observed at 2.8 eV in TiN, and from the OJDS curve, Drude parameters that agree well with other published data can also be obtained [6, 33–35]. This low-energy plasma excitation is also observed in VN, but there much more damping occurs.

Since in the carbides $E_F$ lies in the middle between p and d states, interband transitions down to very low energies are possible. Therefore, $\varepsilon_2$ is high in that energy range so that collective oscillations are strongly damped. The same observation was also made by Lynch *et al.* on TiC [27].

This example shows how optical properties determined by EELS can be

used for a detailed comparison with theoretical band-structure data and thus can help to understand the electronic structure of these compounds.

## REFERENCES


1. H. Raether, "Excitation of Plasmons and Interband Transitions by Electrons," Springer Tracts in Modern Physics, Vol. 38, Springer, Berlin (1980).
2. H. Raether, in "Springer Tracts in Modern Physics," Vol. 28, Springer, Berlin (1965).
3. J. Daniels, C. V. Festenberg, H. Raether, and K. Zeppenfeld, in "Springer Tracts in Modern Physics," Vol. 54, Springer, Berlin (1970).
4. S. E. Schnatterly, in "Solid State Physics," Vol. 34, Academic Press, New York (1979).
5. J. Fink, "Electronics and Electron Physics," Vol. 75, Academic Press, Orlando, 121 (1988).
6. J. Pflüger, J. Fink, W. Weber, K. P. Bohnen, and G. Crecelins, *Phys. Rev. B* **30**, 1155 (1984).
7. J. Pflüger, J. Fink, W. Weber, K. P. Bohnen, and G. Crecelins, *Phys. Rev. B* **31**, 1244 (1985).
8. L. van Hove, *Phys. Rev.* **95**, 249 (1954).
9. P. M. Platzmann and P. A. Wolf, "Waves and Interactions in Solid State Plasmas," Academic Press, New York (1982).
10. J. Geiger, "Elektronen und Festkörper," Vieweg und Sohn, Braunschweig (1968).
11. E. Kröger, *Z. Physik* **216**, 115 (1968).
12. A. F. Corley and R. W. Joyner, *J. Electr. Spectroscopy and Related Phenomena* **16**, 1 (1979).
13. P. Schattschneider, F. Foedermayer, and D. S. Su, *Scanning Microscopy*, Suppl. 2, 255 (1988).
14. P. Livius, T. Aton, and S. E. Schnatterly, *Phys. Rev. B* **38**, 5511 (1989).
15. J. Fink, T. Müller-Heinzerling, J. Pflüger, B. Scheerer, B. Dischler, P. Koidl, A. Bubenzer, and R. E. Sah, *Phys. Rev. B* **30**, 4713 (1984).
16. J. J. Ritsko, G. Crecelius, and J. Fink, *Phys. Rev. B* **27**, 4902 (1983).
17. J. Fink, B. Scheerer, M. Stamm, B. Thicke, B. Kanellakopulos, and E. Dornberger, *Phys. Rev. B* **30**, 4867 (1984).
18. J. Fink, B. Scheerer, W. Wernet, M. Monkenbusch, G. Wegner, H.-J. Freund, and H. Gonska, *Phys. Rev. B* **34**, 1101 (1986).
19. J. Fink and G. Leising, *Phys. Rev. B* **34**, 5320 (1986).
20. J. Fink, *Synth. Metals* **21**, 87 (1987).
21. H. Fritzsche, N. Nücker, B. Scheerer, J. Fink, and G. Leising, *Synth. Metals* **28**, D237 (1989).
22. H. Fritzsche, J. Fink, N. Nücker, B. Scheerer, and G. Leising, to be published.
23. T. Müller-Heinzerling, J. Fink, and W. Weber, *Phys. Rev. B* **32**, 1850 (1985).
24. J. Fink, J. Pflüger, T. Müller-Heinzerling, N. Nücker, B. Scheerer, H. Romberg, M. Alexander, R. Manzke, T. Buslaps, R. Claessen, and M. Skibowski, Proc. of the Internat. Conf. of Materials Science and Technology, July 4–16, 1989. To be published in "Earlier and Recent Aspects of Superconductivity," (K. A. Müller and G. Bednorz, eds.), Springer Series in Solid-State Science, Springer, Berlin (1990).
25. N. Nücker, H. Romberg, S. Nakai, B. Scheerer, J. Fink, Y. F. Yan, and Z. X. Zhao, *Phys. Rev. B* **39**, 12379 (1989).
26. H. Romberg, N. Nücker, J. Fink, T. Wolf, X. X. Xi, B. Koch, H. P. Geserich, M. Durrler, W. Assmus, and B. Gegenheimer, *Z. Phys.*, submitted.
27. D. W. Lynch, C. G. Olsen, and D. J. Peterman, *Phys. Rev. B* **22**, 3991 (1980).
28. R. Lye, E. M. Logothetis, *Phys. Rev.* **147**, 622 (1966).

29. J. F. Alward, C. Y. Fong, M. El-Batanouny, and F. Wooten, *Phys. Rev. B* **12**, 1105 (1974).
30. A. Neckel, *Int. J. Quantum Chem.* **23**, 1317 (1983).
31. W. Y. Liang and A. R. Beal, *J. Phys. C* **9**, 2823 (1976).
32. J. A. Appelbaum and D. R. Hamann, in "Proc. of the Internat. Conf. on the Physics of Transition Metals, Toronto 1977," (M. J. G. Lee, J. M. Perz, E. Fawcett, eds.), IOP, London, 111 (1978).
33. J. Rivory, J. M. Behaghel, S. Berthier, and J. Lafait, *Thin Solid Films* **78**, 161 (1981).
34. A. Schlegel, P. Wachter, J. J. Nicke, and H. Lingh, *J. Phys. C* **10**, 4889 (1977).
35. B. Karlsson, J.-E. Sundgren, and B.-O. Johansson, *Thin Solid Films* **87**, 181 (1982).

# Chapter 14

# Optical Parameters for the Materials in *HOC I* and *HOC II*

EDWARD D. PALIK
Institute for Physical Science and Technology
University of Maryland
College Park, Maryland

I. Introduction 313
II. The Parameters 313
References 334

## INTRODUCTION I

We have collected several optical parameters that are useful in characterizing the materials in *HOC I* and *HOC II*. Some of these parameters were obtained directly from the critiques; others were found in references given in the critiques; still others were found in other references, in review articles, and in other general references such as handbooks. Some of these articles, review articles, and handbook articles are listed in the references [1–11]. Especially useful has been Ref. [4]. It was not feasible to list the many specific original references for each material, although a few have been included as Refs. [13–35].

## THE PARAMETERS II

The column headings in Table I are as follows:

(1) *Chemical formula of material.*

(2) *Most common crystallographic form of the material at room temperature.* The materials fall into many of the 32 point groups (crystal classes) and the 14 Bravais lattice classifications shown in Fig. 1.

(3) and (4) *The space group in the X-ray and spectroscopic notation.*


Copyright © 1991 by Academic Press.
All rights of reproduction in any form reserved.
ISBN 0-12-544422-2

(5) *The dimensions of the unit cell.* This will include an angle when it is not 90°. Figure 1 will suggest if the angle is not 90°.

(6) The number of molecular units in the unit cell.

(7) *The number of molecular units in the primitive (Bravais) cell.* This number is important in determining the total number of optic modes, $3N$-3, where $N$ is the number of atoms in the primitive cell. We will generally use the term *optic* mode to rhyme with *acoustic* mode.

(8) *The irreducible representation.* Each term designates one of the

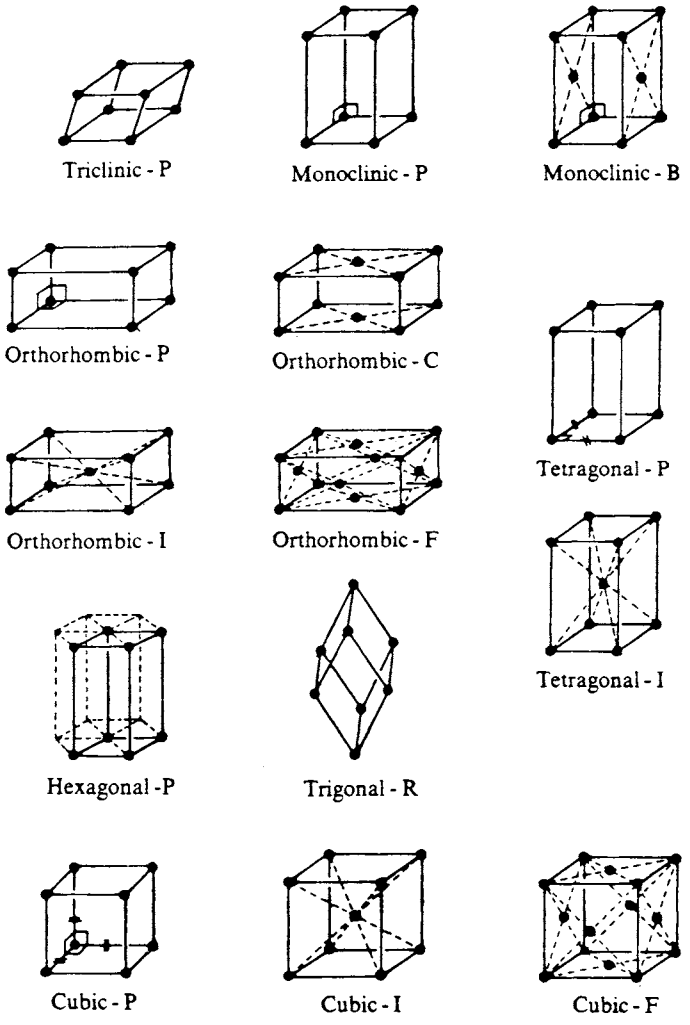


**Fig. 1.** The unit cell for each of the 14 Bravais lattices (from Burns and Glazer [5], copyright 1978, Academic Press).

types of optic modes allowed; IR, R, and O represent infrared, Raman, and silent activity. A and B have single degeneracy, $E$ has double degeneracy, and F has triple degeneracy. In most cases subscripts u and g specify IR and R activity, respectively. The three acoustic modes have already been subtracted off.

(9) *Total number of optic modes in the crystal as obtained from* $3N$*-3 or from examination of the irreducible representation.*

(10) *Transverse optic* (TO) *phonon frequencies with their species and ordinary (o)/extraordinary (e) designations.* Generally, group-theory analysis is done on the basis of the symmetry transformation properties of the $e_x$, $e_y$, and $e_z$ displacements of the atoms from their equilibrium positions. The members of the irreducible representation that are IR-active are associated with the transverse optic phonons with displacements in the $x$, $y$, $z$ directions, but the directions of propagation are not necessarily specified.

(11) *Longitudinal optic* (LO) *phonon frequencies with their species and ordinary (o)/extraordinary (e) designations.* The radiation electric field is $\|$ to the optic axis ($e$) or $\perp$ to the optic axis ($o$). In the irreducible representation for a cubic material, we can associate any particular IR term ($F$, for example) with two TO modes and one LO mode, thinking of them as propagating in the same direction as the direction of the EM wave with which we measure them. This suggests that the LO mode should be IR active. But it does not produce absorption, except in a special case of a thin sample measured at nonnormal incidence with $p$-polarization [12]. In this case the component of E$\perp$ to the film can drive (couple to) the long-wavelength LO phonons (propagating $\perp$ to the film surface), and an absorption line appears. This is related to the fact that the dipole matrix element for LO phonons in bulk materials is zero, although the mode (or rather its displacement direction) is IR-active. The activity becomes apparent in the nonnormal-incidence case. For nonpolar crystals such as Si, all three modes are degenerate, IR-inactive and R-active. For polar cubic crystals such as GaAs, the LO mode is raised slightly in frequency above the two still-degenerate TO modes; the two TO and one LO modes are IR-active and R-active, also. (Notice that the LO mode is not seen directly in IR as an absorption line for the reasons discussed above.)

For some simple cubic crystals, large anharmonic effects produce multiple structure in the reststrahlen spectrum above TO, which precludes a Lorentz-oscillator fit and obscures the LO frequency. We can still choose the $n = k$ wavelength farthest above TO (but not to the band gap yet) as the definition of LO and list this number in parentheses in Table I. Otherwise, the LO frequency is directly obtained from a simple Lorentz-oscillator fit (where $n = k$) or from Raman measurement (if selection rules permit). In studying the literature, we have found that values of TO and LO from R and IR data often vary by 5 $cm^{-1}$ from lab to lab. This is disquieting, suggesting poor spectroscopic calibration for R and IR experiments and/or

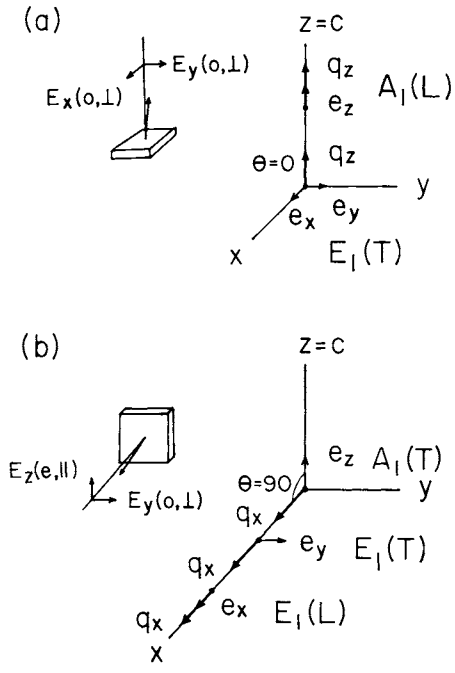


**Fig. 2.** (a) Wave vector $q_z$ for a transverse optic mode $E_1(T)$ with its accompanying lattice displacement $e_x$ and $e_y$; and wave vector $q_z$ for a longitudinal optic mode $A_1(L)$ and its accompanying lattice displacement $e_z$. The inset shows the sample with $E_x(o, \perp)$ and $E_y(o, \perp)$ electric fields. Direction of phonon propagation is parallel to the $z=c$ optic axis for $\theta=0$. (b) Wave vector $q_x$ for a transverse optic mode $A_1(T)$ with its accompanying lattice displacement $e_z$; wave vector $q_x$ for a transverse optic mode $E_1(T)$ with its lattice displacement $e_y$; wave vector $q_x$ for a longitudinal optic mode $E_1(L)$ with its lattice displacement $e_x$. The inset shows the sample with $E_x$ $(e, \|)$ and $Ey(o, \perp)$ electric fields. Direction of phonon propagation is perpendicular to the $z=c$ axis for $\theta=90°$.

poor material or poor model analysis for IR. It is not obvious that recent data are calibrated any better than older data.

For a uniaxial crystal (all noncubic crystals in Table I are uniaxial except for $As_2S_3$, $As_2Se_3$, $ThF_4$ and CuO), the situation is more complicated. For wurtzite structure for phonon wave vector $q(z)$ parallel to the $z=c$ optic axis ($\theta=0$), the degenerate TO modes ($E_1(T)$, lattice displacement $e\|x, \|y$) and the LO mode ($A_1(L)$, lattice displacement $e\|z$) appear in the Raman experiment when the appropriate polarizations for incident and scattered light are used. They also appear in the IR experiment with the proper polarization (Fig. 2a). They are designated as $E_1(T)$, $E_1(T)$ and $A_1(L)$. For phonon wave vector $q(x)$ perpendicular to the $z=c$ axis ($\theta=90°$), the nondegenerate TO mode ($E_1(T)$, $e\|y$) and the LO mode ($E_1(L)$, $e\|x$) can

appear in R, as well as the TO mode ($A_1(T)$, $e\|z$). They also appear in the IR experiment with the proper polarization (Fig. 2b). They are designated as $E_1(L)$, $E_1(T)$, $A_1(T)$. A number of uniaxial materials have been studied for wave vectors varying from $\theta = 0$ to $\theta = 90°$. Such a measurement reveals how the modes shift in frequency and symmetry as the direction of phonon propagation changes. In the Tables a–p accompanying Table I, we have tried to indicate this behavior by listing the TO and LO frequencies of each symmetry for $\theta = 0$ and $\theta = 90°$. An arrow then indicates how a given mode shifts in frequency and symmetry as the direction of propagation changes. This is relatively simple for wurtzite crystals but complicated for $x$-$SiO_2$, for example. Luckily, most wurtzite crystals have small force-constant anisotropies for directions of vibration $\|$ and $\perp$ to the $c$ axis, and the symmetry-species designations in Table d hold. For large force-constant anisotropies, the assignment of symmetry species can be quite different. This hinges on whether as the **q** vector is "tipped" from $\theta = 0$ to $\theta = 90°$, the lattice displacement can also "tip," or remains along the same direction.

Modes only R-active or O-silent are listed at the bottom of the TO column (they do not affect the optical constants). These are often TO modes not accompanied by an LO mode (as are the polar modes discussed above), but LO modes are often Raman-active, also.

If the modes are both R- and IR-active, the pertinent reststrahlen reflection spectrum can be "constructed" approximately from the TO and LO frequencies (and their line widths) determined from Raman scattering. For wurtzite crystals, the $\theta = 0$, $E_1(T)$ mode has an accompanying $\theta = 90°$, $E_1(L)$ mode forming the reststrahlen peak for the $E \perp c$ ordinary-ray polarization with sample plane $\perp c$. This LO mode is to the right and one line down from the TO mode in the Table d listing. Of course, an $E \perp c$ spectrum can also be obtained from a sample cut with the $c$ axis in the plane of the sample. Such a sample then allows the $E\|c$ spectrum to be measured, also. Now the $\theta = 90°$, $A_1(T)\|$ mode has an accompanying $\theta = 0$, $A_1(L)\|$ mode (one column to the right and one row down) forming the reststrahlen peak for the $E\|c$ extraordinary-ray polarization. Thus, a Lorentz-model analysis of the reflection spectrum gives $A_1(T)\|$ with $e\|z$ (direction of vibration of the transverse mode) and $A_1(L)\|$ with $e\|z$ (now the direction of vibration of the longitudinal mode). Of course, no absorption line is seen at $\omega_L$ where $\varepsilon_1 = n^2 - k^2 = 0$. By and large, independent measurements of R and IR spectra in various labs give results in agreement within $10\,cm^{-1}$. This again indicates the wide variations in measured frequencies from lab to lab.

In more complicated systems such as $x$-$SiO_2$ (Table m) for the pairs of $T$ and $L$ modes, the $L$ mode is adjacent to the $T$ mode on the same line or the $L$ mode is one line down, depending on the pairing scheme.

Some types of uniaxial crystals have not been studied in detail by Raman scattering for wave vectors varying from $\theta = 0$ to $\theta = 90°$, perhaps because

## TABLE I

### Collected Optical Parameters

| Material | Crystal structure | Space group | | Unit cell dimensions (Å) | Molecular units per Unit cell | Molecular units per Primative cell | No. of optic modes | Total irreducible representation | $\omega_T$ ($cm^{-1}$) | $\omega_L$ ($cm^{-1}$) | $\omega_P$ Drude (eV) | $n=k$ (eV) | $E_g$ (eV) | $\varepsilon_0$ |
|---|---|---|---|---|---|---|---|---|---|---|---|---|---|---|
| Cu | fcc | Fm3m | $O_h^5$ | 3.6149 | 4 | 1 | 0 | None | None | None | 7.4 | 8.0 | None | −65000 |
| Au | | | | 4.0782 | | | | | | | 9.0 | 5.5 | | −110000 |
| Ir | | | | 3.8394 | | | | | | | | 7.8 | | |
| | | | | | | | | | | | | 20.5 | | |
| Ni | | | | 3.5238 | | | | | | | 4.9 | 9.4 | | −13000 |
| Pt | | | | 3.9231 | | | | | | | 5.1 | 6.1 | | −5500 |
| | | | | | | | | | | | | 19.6 | | |
| | | | | | | | | | | | | 24.9 | | |
| Rh | | | | 3.8031 | | | | | | | | 8.5 | | |
| Ag | | | | 4.0862 | | | | | | | 3.8 | 3.8 | | −250000 |
| | | | | | | | | | | | 9.0 | 4.8 | | |
| | | | | | | | | | | | | 7.3 | | |
| Al | | | | 4.0495 | | | | | | | 14.8 | 15 | | −34000 |
| Pd | | | | 3.8898 | | | | | | | 5.5 | 7.7 | | −150000 |
| PbS | cubic NaCl | Fm3m | $O_h^5$ | 5.936 | 4 | 1 | 3 | $F_{1u}$(IR) | 71 IR | 212 | | 3.25 | 0.41(d) | 169 |
| | | | | | | | | | | | | 14 | | |
| PbSe | | | | 6.124 | | | | | 39 | 111 | | 2.5 | 0.278(d) | 210 |
| | | | | | | | | | | | | 7.0 | | |
| PbTe | | | | 6.46 | | | | | 32 | 112 | | 1.7 | 0.31(d) | 414 |
| | | | | | | | | | | | | 9 | | |
| SnTe | | | | 6.313 | | | | | | | | 1.7 | 0.19(d) | 1770 |
| | | | | | | | | | | | | 5.5 | | |
| | | | | | | | | | | | | 12.0 | | |
| | | | | | | | | | | | | 12.4 | | |
| NaCl | | | | 5.64 | | | | | 164 | (266) | | ---- | 8.6 | 5.90 |
| KCl | | | | 6.2929 | | | | | 142 | (213) | | 7.8 | 8.5 | 4.4 |
| | | | | | | | | | | | | 9.45 | | |
| | | | | | | | | | | | | 9.75 | | |
| | | | | | | | | | | | | 12.6 | | |
| LiF | | | | 4.0263 | | | | | 307 | 501 | | 12.8 | 14.2(d) | 9.06 |

| | | | | | | | | | | | | | | |
|---|---|---|---|---|---|---|---|---|---|---|---|---|---|---|
| KBr | | | | 6.6000 | | | | | 113 | (155) | | ---- | 7.8 | 4.8 |
| NaF | | | | 4.620 | | | | | 246 | (420) | | | 10.5 | ~5.7 |
| MgO | | | | 4.215 | | | | | 396 | 729 | | 13.2 | 7.8(d) | 9.8 |
| | | | | | | | | | | | | 13.9 | | |
| | | | | | | | | | | | | 17.5 | | |
| | | | | | | | | | | | | 21.6 | | |
| $CaF_2$ | cubic fluorite | Fm3m | $O_h^5$ | 5.4629 | 4 | 1 | 6 | $F_{1u}(IR) + F_{2g}(R)$ | 258 IR<br>322 R | 473 | | ---- | ~11 | 6.7 |
| Mo | bcc | Im3m | $O_h^9$ | 3.1473 | 2 | 1 | 0 | None | None | None | 7.5 | 2.3 | None | −21000 |
| | | | | | | | | | | | | 10.4 | | |
| W | | | | 3.1646 | | | | | | | 6.4 | 1.3 | | −13000 |
| | | | | | | | | | | | | 5.2 | | |
| | | | | | | | | | | | | 24.7 | | |
| Fe | | | | 2.8665 | | | | | | | 4.1 | 0.99 | | −50000 |
| Cr | | | | 2.8839 | | | | | | | | 1.51 | | |
| | | | | | | | | | | | | 9.05 | | |
| | | | | | | | | | | | | 10.3 | | |
| Nb | | | | 3.3004 | | | | | | | | 1.32 | | |
| | | | | | | | | | | | | 2.43 | | |
| | | | | | | | | | | | | 3.32 | | |
| | | | | | | | | | | | | 4.38 | | |
| | | | | | | | | | | | | 9.76 | | |
| | | | | | | | | | | | | 14.6 | | |
| | | | | | | | | | | | | 19.1 | | |
| K | | | | 5.2 | | | | | | | 4.25 | 3.8 | | |
| Na | | | | 4.2906 | | | | | | | 5.91 | ~5.9 | | |
| Li | | | | 3.5902 | | | | | | | | 6.66 | | |
| Ta | | | | 3.3058 | | | | | | | 6.2 | 2.04 | | |
| | | | | | | | | | | | | 5.27 | | |
| | | | | | | | | | | | | 19.9 | | |
| V | | | | 3.0240 | | | | | | | 5.2 | 1.24 | | −7200 |
| | | | | | | | | | | | | 2.63 | | |
| $Y_2O_3$ | bcc | Ia3 | $T_h^7$ | 10.604 | 16 | 8 | 117 | $4A_g(R) + 5A_u(O) + 4E_g(R) + 5E_u(O) + 14F_g(R) + 16F_u(IR)$ | See Table a | | | | 12.4<br>14.2 | ~6 | 11.4 |
| Si | cubic diamond | Fd3m | $O_h^7$ | 5.4307 | 4 | 1 | 3 | $F_{2g}(R)$ | 521 R | 521 R | | 4.22<br>16.3 | 1.1(i) | 11.6 |

*(continued)*

TABLE I (continued)

**Collected Optical Parameters**

| Material | Crystal structure | Space group | | Unit cell dimensions (Å) | Molecular units per Unit cell | Molecular units per Primative cell | No. of optic modes | Total irreducible representation | $\omega_T$ ($cm^{-1}$) | $\omega_L$ ($cm^{-1}$) | $\omega_P$ Drude (eV) | $n=k$ (eV) | $E_g$ (eV) | $\epsilon_\sigma$ |
|---|---|---|---|---|---|---|---|---|---|---|---|---|---|---|
| Ge | | | | 5.6573 | | | | | 301 | 301 | | 4.14<br>9.5 | 0.66(i) | 16.0 |
| C | | | | 3.5667 | | | | | 1332 | 1332 | | 11.8<br>30 | 5.2(i) | 5.6 |
| $Al_2MgO_4$ | cubic | Fd3m | $Oh^7$ | 8.0800 | 8 | 2 | 39 | $A_{1g}(R)+2A_{2u}(O)+Eg(R)+2Eu(O)+F_{1g}(O)+4F_{1u}(IR)+3F_{2g}(R)+2F_{2u}(O)$ | See Table b | | | | ~8 | 8.29 |
| ZnS | cubic zincblende | F$\bar{4}$3m | $Td^2$ | 5.4093 | 4 | 1 | 3 | $F_2$(R, IR) | 279 IR, R | 351 R | | 7<br>15 | 3.68(d) | 8.35 |
| ZnSe | | | | 5.6676 | | | | | 206 | 252 | | | 2.83(d) | 9.0 |
| ZnTe | | | | 6.089 | | | | | 179 | 206 | | 4.96 | 2.3(d) | 9.8 |
| CdTe | | | | 6.480 | | | | | 141 | 169 | | | 1.5(d) | 10.2 |
| GaAs | | | | 5.6535 | | | | | 269 | 292 | | 4.7<br>10.7 | 1.42(d) | 13.0 |
| GaP | | | | 5.4506 | | | | | 367 | 403 | | 5.0<br>13.5 | 2.27(i) | 11.1 |
| InAs | | | | 6.0585 | | | | | 218 | 240 | | 4.47<br>11.9 | 0.35(d) | 14.1 |
| InSb | | | | 6.4782 | | | | | 179 | 190 | | 3.82<br>9.5 | 0.18(d) | 17.7 |
| InP | | | | 5.8688 | | | | | 304 | 345 | | 4.73<br>14.3 | 1.34(d) | 12.4 |
| SiC $\beta$ | | | | 4.348 | | | | | 796 | 972 | | | 2.86 | 9.72 |
| GaSb | | | | 6.118 | | | | | 227 | 237 | | | 0.75 | 15.7 |
| AlSb | | | | 6.1347 | | | | | 318 | 340 | | | 1.61(i) | 11.2 |
| AlAs | | | | 5.62 | | | | | 362 | 404 | | 4.7 | 2.15(i) | 10.06 |
| HgTe | | | | 6.460 | | | | | 116 | 139 | | | 0 | |
| CsI | cubic CsCl | Pm3m | $O_h^1$ | 4.5667 | 1 | 1 | 3 | $F_{1u}$(IR) | 62 IR | 93 | | ---- | 6.4(d) | 6.54 |

| | | | | | | | | | | | | | | |
|---|---|---|---|---|---|---|---|---|---|---|---|---|---|---|
| $SrTiO_3$ | cubic perovskite | Pm3m | $O_h^1$ | 3.9051 | 1 | 1 | 12 | $3F_{1u}(IR) + F_{2u}(IR)$ | See Table c | | | 26.4<br>28.8 | 3.4 | 311 |
| $Cu_2O$ | cubic | Pn3m | $O_h^1$ | 4.2696 | 2 | 2 | 15 | $A_{2u}(O) + E_u(O) + F_{2u}(O) +$<br>$2F_{1u}(IR) + F_{2g}(R)$ | 613 IR<br>146 IR<br>110 R $E_u$<br>300 R $A_{2u}$ | 638<br>149 | | | 2.17(d) | ~7.5 |
| $Al_{23}O_{27}N_5$ | cubic | | | 7.948 | | | | | | | | | | |
| ZnS | hexagonal wurzite | $P6_3mc$ | $C_{6v}^4$ | a = 3.811<br>c = 6.234 | 2 | 2 | 9 | $A_1(R, IR\|) + 2B_1(O) +$<br>$E_1(R, IR\perp) + 2E_2(R)$ | See Table d | | | ××××<br>××××<br>××××<br>××××<br>7.45<br>21.7 | 3.91<br>2.55(d)<br>1.75(d)<br>9.4<br>3.1 | 9.6(o)<br>10.7(e)<br>9.29(o)<br>10.16(e)<br>6.94(o)<br>7.65(e)<br>9.7(o)<br>10.0(e) |
| CdS | | | | a = 4.1348<br>c = 6.7490 | | | | | | | | | | |
| CdSe | | | | a = 4.2999<br>c = 7.0109 | | | | | | | | | | |
| BeO | | | | a = 2.698<br>c = 4.380 | | | | | | | | | | |
| SiC 6H, $\alpha$II | | | | a = 3.076<br>c = 5.048 | | | | | | | | | | |
| Os | hcp | $P6_3/mmc$ | $D_{6h}^4$ | a = 2.7352<br>c = 4.3190 | 2 | 2 | 3 | $A_{1u}(O) + E_{2g}(R)$ | | | | 9.6<br>17.5 | None | |
| Co | | | | a = 2.5071<br>c = 4.0686 | | | | | | | 4.0 | 7.75 | | − 12000 |
| Be | | | | a = 2.2866<br>c = 3.5833 | | | | | 463 R | | | | | |
| C graphite | hexagonal | $P6_3/mmc$ | $D_{6h}^4$ | 2.456<br>6.696 | 4 | 4 | 9 | $2B_{2g}(O) + A_{2u}(IR\|) +$<br>$E_1(IR\perp) + 2E_{2g}(R)$ | See Table e | | | 4.5(o)<br>6.8(o)<br>14.4(o)<br>25.0(o)<br>6.85(e)<br>25(e) | | 5.7(e) |
| $TiO_2$ | tetragonal $SnO_2$ | $P4_2/mnm$ | $D_{4h}^{14}$ | a = 4.5937<br>c = 2.9581 | 2 | 2 | 15 | $A_{1g}(R) + A_{2g}(O) + 2A_{2u}(IR\|) +$<br>$B_{1g}(R) + 2B_{1u}(O) + B_{2g}(R) +$<br>$E_g(R) + 3E_u(IR\perp) +$ | See Table f | | | 6.5(o)<br>7.3(o)<br>4.3(e) | 3.06(d,o)<br>4.3(d, e) | 83.7(o)<br>165(e) |

(*continued*)

**TABLE I (continued)**

**Collected Optical Parameters**

| Material | Crystal structure | Space group | Unit cell dimensions (Å) | Molecular units per Unit cell | Molecular units per Primative cell | No. of optic modes | Total irreducible representation | $\omega_T$ ($cm^{-1}$) | $\omega_L$ ($cm^{-1}$) | $\omega_P$ Drude (eV) | $n=k$ (eV) | $E_g$ (eV) | $\epsilon_0$ |
|---|---|---|---|---|---|---|---|---|---|---|---|---|---|
| $MgF_2$ | | | a = 4.623<br>c = 3.052 | | | | | | | | ---- | 11 | 5.47(o)<br>4.62(e) |
| $BaTiO_3$ | tetragonal | P4mm | $C_{4v}^1$<br>a = 3.9920<br>c = 4.0361 | 1 | 1 | 12 | $3A_1(R, IR\|) + B_1(R) + 4E(R, IR\perp)$ | See Table g | | | 22.1<br>25.4 | ~3.5 | 31.5(e) |
| $KH_2PO_4$ | tetragonal | $I\bar{4}2d$ | $D_{2d}^{12}$<br>$V_d^{12}$<br>a = 7.448<br>c = 6.977 | 4 | 2 | 45 | $4A_1(R) + 5A_2(O) + 6B_1(R) +$<br>$6B_2(R, IR\|) + 12E(R, IR\perp)$ | See Table h | | | | 4.96 | ~44(o)<br>~21(e) |
| $NH_4H_2PO_4$ | tetragonal | $I\bar{4}2d$ | $D_{2d}^{12}$<br>$V_d^{12}$<br>a = 7.510<br>c = 7.564 | 4 | 2 | 69 | $7A_1(R) + 7A_2(O) + 9B_1(R) +$<br>$8B_2(R, IR\|) + 19E(R, IR\perp)$ | See Table i | | | | 9.92 | ~56(o)<br>~15(e) |
| $LiNbO_3$ | trigonal | R3c | $C_{3v}^6$<br>a = 5.47<br>$\alpha = 55°43'$ | 2 | 2 | 27 | $4A_1(R, IR\|) + 5A_2(O) + 9E(R, IR\perp)$ | See Table j | | | | ~4.2 | 43.7(o)<br>25.6(e) |
| $Al_2O_3$ | trigonal | $R\bar{3}c$ | $D_{3d}^6$<br>a = 5.128<br>$\alpha = 55°20'$ | 2 | 2 | 27 | $2A_{1g}(R) + 3A_{2g}(O) + 2A_{1u}(O) +$<br>$2A_{2u}(IR\|) + 5E_g(R) + 4E_u(IR\perp)$ | See Table k | | | ---- | 8.3 | 9.49(o)<br>11.4(e) |
| Se | trigonal | $P3_121$ | ${}_1D_3^4$<br>a = 4.3551<br>c = 4.9494 | 3 | 3 | 6 | $A_1(R) + A_2(IR\|) + 2E(R, IR\perp)$ | See Table l | | | | ~1.6(i) | 7.40(o)<br>12.2(e) |
| Te | | $P3_221$ | ${}_1D_3^6$<br>a = 4.4469<br>c = 5.9149 | | | | | | | | 2.5(o)<br>4.5(o)<br>2.0(e)<br>5.0(e) | 0.33(d) | 30(o)<br>43(e) |
| $SiO_2$ | trigonal | $P3_121$ | ${}_1D_3^4$<br>a = 4.9130<br>c = 5.4046 | 3 | 3 | 24 | $4A_1(R) + 4A_2(IR\|) + 8E(R, IR\perp)$ | See Table m | | | ---- | ~9 | 4.41(o)<br>4.62(e) |
| $As_2S_3$ | monoclinic (unit cell) | $P2_1/b,c$ | $C_{2h}^5$<br>a = 11.475<br>b = 9.577<br>c = 4.256<br>$\beta = 90°41'$ | 4 | 4 | 57 | $15A_g(R) + 15B_g(R) +$<br>$14A_u(IR) + 13B_u(IR)$ | See Table n | | | | 2.43(a, d)<br>2.45(c, d) | 15.2(a)<br>6.25(b)<br>13.0(c) |

| | | | | | | | | | | | |
|---|---|---|---|---|---|---|---|---|---|---|---|
| $As_2Se_3$ | orthorhombic (layer) | $Pnm2_1$ | $C_{2v}^7$ | a = 12.053<br>b = 9.890<br>c = 4.277<br>$\beta = 90°28'$ | 2 | 2 | 27 | $7A_1(R, IRc) + 6B_2(R, IRa) + 7A_2(R) + 7B_1(R, IRb)$ | | | ~2 | 14.4(a)<br>13.0(c) |
| CuO | monoclinic | B2/b<br>C2/c | $C_{2h}^6$ | a = 4.6837<br>b = 3.4226<br>C = 5.1288<br>$\beta = 99°29'$ | 4 | 2 | 9 | $A_g(R) + 3A_u(IR) + 2B_g(R) + 3B_u(IR)$ | See Table o | | ~1.3i | |
| $ThF_4$ | monoclinic | B2/b | $C_{2h}^6$ | a = 12.90<br>b = 10.93<br>c = 8.58<br>$\beta = 126.4°$ | 12 | 6 | 87 | | | | | |
| $(CH_2)_n$ | orthorhombic | Pnam | $V_h^{16}$<br>$D_{2h}^{16}$ | a = 7.40<br>b = 4.93<br>c = 2.534 | 4 | 4 | 33 | $6A_g(R) + 3A_u(O) + 3B_{1g}(R) + 5B_{1u}(IRc) + 3B_{2g}(R) + 5B_{2u}(IRb) + 6B_{3g}(R) + 2B_{3u}(IRa)$ | See Table p | | | 2.29(b)<br>2.32(c) |
| (AlGaAs)<br>(HgCdTe)<br>(PbSnTe)<br>(Ge-Si) | alloy | | | | | | | | | | | |
| (a-Si) | amorphous | | | | | | | | | 3.9 | 1.77 | 13.7 |
| (a-$SiO_2$) | | | | | | | | | 469<br>800<br>1094 | | ~9 | 3.8 |
| (a-SiO) | | | | | | | | | 1020 | | ~6 | 4.0 |
| (a-$Si_3N_4$) | | | | | | | | | | | | 3.6 |
| (a-$As_2S_3$) | | | | | | | | | | | | 7.45 |
| (a-$As_2Se_3$) | | | | | | | | | | | | 9.0 |
| (a-$ThF_4$) | | | | | | | | | | | | |
| (a-C:H) | | | | | | | | | | | | |
| Hg | liquid | | | | | | | | | | | |
| $H_2O$ | | | | | | | | | | | | 78.3 |

**TABLE a**

**$Y_2O_3$**

| $F_{1u}$(T)(IR) | $F_{1u}$(L)(IR) |
|---|---|
| 120 | 121 |
| 172 | 173 |
| 182 | 183 |
| 241 | 242 |
| 303 | 315 |
| 335 | 359 |
| 371 | 412 |
| 415 | 456 |
| 461 | 486 |
| 490 | 535 |
| 555 | 620 |

331 $E_g$ (R)
431 $F_g$
469 $F_g$
595 $F_g$
830 $E_g$
948 $E_g$
1184 $A_g$

**TABLE b**

**$Al_2MgO_4$**

| $F_{1u}$(T)(IR) | $F_{1u}$(L)(IR) |
|---|---|
| 307 | 311 |
| 482 | 497 |
| 675 | 800 |

311 $F_{2g}$ (R)
492 $F_{2g}$
611 $F_{2g}$
410 $E_g$
772 $A_{1g}$

**TABLE c**

**$SrTiO_3$**

| $F_{1u}$(T)(IR) | $F_{1u}$(L)(IR) |
|---|---|
| 88 | 173 |
| 178 | 473 |
| 544 | 804 |

No (R)

**TABLE d**

**ZnS [2]**

| $\theta = 0$ | 90° | 90° | 0 |
|---|---|---|---|
| $E_1(T)(R, IR \perp)$ | $E_1(L)(R, IR \perp)$ | $A_1(T)(R, IR\|\|)$ | $A_1(L)(R, IR\|\|)$ |
| 274 → | | → 274 | |
| | 352 ← | | ← 352 |

55 $E_2$ (R)
280 $E_2$

CdS [2]

| | | | |
|---|---|---|---|
| 243 → | | → 234 | |
| | 307 ← | | ← 305 |

43 $E_2$ (R)
170 $B_1$ (O)
256 $E_2$ (R)

CdSe [2]

| | | | |
|---|---|---|---|
| 171 → | | → 165 | |
| | ← | | ← 208 |

34 $E_2$ (R)

BeO [2]

| | | | |
|---|---|---|---|
| 722 → | | → 678 | |
| | 1095 ← | | ← 1085 |

340 $E_2$ (R)
684 $E_2$

SiC (6H): Because of polytype structure, the 6H crystal stacks up in 6-atomic-layer sequences. See Ref. [28] for complicated Raman spectrum due to effective zone folding.

| | | | |
|---|---|---|---|
| 794 → | | → 785 | |
| | ~970 ← | | ← 970 |

**TABLE e**

**C Graphite [21]**

| $\theta = 0$ | 90° | 90° | 0 |
|---|---|---|---|
| $E_{1u}(T)(IR \perp)$ | $E_{1u}(L)(IR \perp)$ | $A_{2u}(T)(IR\|\|)$ | $A_{2u}(L)(IR\|\|)$ |
| 1587.0 | 1587.5 | 867.8 | 868.1 |

42 $E_{2g}$ (R)
127 $B_{2g}$ (O)
1575 $E_{2g}$ (R)

**TABLE f**

**$TiO_2$ [2, 20]**

| $\theta = 0$ | 90° | 90° | 0 |
|---|---|---|---|
| $E_u(T)(IR \perp)$ | $E_u(L)(IR \perp)$ | $A_{2u}(T)(IR\|\|)$ | $A_{2u}(L)(IR\|\|)$ |
| 183 | 373 | 167 | 811 |
| 388 | 458 | | |
| 500 | 806 | | |

113 $B_{1u}$ (O)
143 $B_{1g}$ (R)
447 $E_g$ (R)
612 $A_{1g}$ (R)
653 $A_{2g}$ (O)
826 $B_{2g}$ (R)

$MgF_2$ [2,20]

| | | | |
|---|---|---|---|
| 247 | 303 | 399 | 625 |
| 410 | 415 | | |
| 450 | 617 | | |

92 $B_{1g}$ (R)
295 $E_g$ (R)
326 $A_{2g}$ (O)
410 $A_{1g}$ (R)
515 $B_{2g}$ (R)

**TABLE g**

**$BaTiO_3$ [14]**

| $\theta = 0$ | 90° | 90° | 0 |
|---|---|---|---|
| E(T)(R, IR ⊥) | E(L)(R, IR ⊥) | $A_1$(T)(R, IR‖) | $A_1$(L)(R, IR‖) |
| 38 → | → | → 179 | |
| 180 → | → 180 | | |
| | | 276 ← | ← 189 |
| 308 → | → 308 | | |
| | 466 ← | ← | ← 471 |
| 498 → | → | → 515 | |
| | 722 ← | ← | ← 725 |
| 305$B_1$ (R) | | | |

**TABLE h**

**$KH_2PO_4$; R and IR Values from Three References for Comparison**

| $A_1$ (R) | | $B_1$ (R) | | $B_2$ (R) | | (IR‖) | | E(R) | | (IR ⊥) | |
|---|---|---|---|---|---|---|---|---|---|---|---|
| [29] | [30] | [29] | [30] | [29] | [30] | [30] | [31] | [29] | [30] | [30] | [31] |
| 360 | 365 | 156 | 155 | 80 | 100 | 60 | 52 | 75 | | 86 | 90 |
| 514 | | 479 | 473 | 174 | 183 | 178 | 185 | 95 | 96 | 102 | 106 |
| 918 | 918 | 570 | 540 | * | | | | 113 | 116 | 122 | 123 |
| | | | | | | | | | | 152 | 152 |
| 2700 | | 1366 | | 386 | | | | 190 | 192 | 206 | 200 |
| | | 1806 | | 510 | | | 470 | 320 | | | |
| | | 2390 | | 1350 | | | | 490 | | | |
| | | | | | | | | 530 | 533 | 526 | 540 |
| | | | | | | | | 568 | | | |
| | | | | | | | | 960 | | | |
| | | | | | | | | 1145 | | | |
| | | | | | | | | * | | | |
| | | | | | | | | 1325 | | | |

Above the Curie temperature (123 K), the crystal is paraelectric (tetragonal); below $T_c$, it is ferroelectric (orthorhombic).

**TABLE i**

**$NH_4H_2PO_4$; R and IR Values from Two References for Comparison**

| $A_1$ (R) | | $B_1$ (R) | | $B_2$ (R) | | (IR‖) | E(R) | (IR ⊥) | |
|---|---|---|---|---|---|---|---|---|---|
| [29] | [30] | [29] | [30] | [29] | [30] | [30] | [29] | [30] | [30] |
| 337 | 341 | 178 | 182 | 80 | 100 | 76 | 100 | 68 | 51 |
| | | | | | | | | | 70 |
| 520 | | 474 | 476 | 185 | 204 | 198 | 120 | 125 | |
| | | | | | | | | 140 | 150 |
| 918 | 922 | 541 | | * | | | 172 | 175 | 164 |
| 2700 | | 1298 | | 397 | 401 | 450 | 268 | | |
| | | 1750 | | 547 | | | 390 | | 350 |
| | | 2370 | | 1320 | | | 470 | | |
| | | | | | | | 538 | 542 | 540 |
| | | | | | | | 568 | | |
| | | | | | | | 960 | | |
| | | | | | | | 1106 | | |
| | | | | | | | * | | |
| | | | | | | | 1338 | | |

Above the Curie temperature (148K), the crystal is paraelectric (tetragonal); below $T_c$, it is antiferroelectric (orthorhombic).

**TABLE j**

**$LiNbO_3$[18]**

| $\theta = 0$ | 90° | 90° | 0 |
|---|---|---|---|
| E(T)(R, IR ⊥) | E(L)(R, IR ⊥) | $A_1$(T)(R, IR‖) | $A_1$(L)(R, IR‖) |
| 155 → | → 198 | | |
| 238 → | → 243 | | |
| 265 → | | → 255 | |
| | | 276 ← | ← 275 |
| 325 → | → 295 | | |
| | | 334 ← | ← 333 |
| 371 → | → 371 | | |
| 431 → | → 428 | | |
| | 454 ← | | ← 436 |
| 582 → | | → 633 | |
| 668 → | → 668 | | |
| 743 → | → 739 | | |
| | 880 ← | | ← 876 |

**TABLE k**

**$Al_2O_3$ [22]**

| $\theta = 0$ | 90° | 90° | 0 |
|---|---|---|---|
| $E_u(T)(IR \perp)$ | $E_u(L)(IR \perp)$ | $A_{2u}(T)(IR\|)$ | $A_{2u}(L)(IR\|)$ |
| 385<br>442<br>569<br>635 | 388<br>480<br>625<br>900 | 400<br>583 | 512<br>871 |

378 $E_g$ (R)
418 $A_{1g}$
432 $E_g$
451 $E_g$
578 $E_g$
645 $A_{1g}$
751 $E_g$

**TABLE l**

**Se [2, 23]**

| $\theta = 0$ | 90° | 90° | 0 |
|---|---|---|---|
| $E(T)(R, IR \perp)$ | $E(L)(R, IR \perp)$ | $A_2(T)(IR\|)$ | $A_2(L)(IR\|)$ |
| 144<br>225 | 150<br>225 | 102 | 106 |

237 $A_1$ (R)

Te

| | | | |
|---|---|---|---|
| 92<br>144 | 106<br>145 | 90 | 96 |

120 $A_1$ (R)

**TABLE m**

**$SiO_2$ [17]**

| $\theta = 0$ | 90° | 90° | 0 |
|---|---|---|---|
| E(T)(R, IR ⊥) | E(L)(R, IR ⊥) | $A_2$(T)(IR‖) | $A_2$(L)(IR‖) |
| 127 → | → 129 | | |
| 265 → | → 270 | | |
| | | 364 ← | ← 387 |
| 394 → | → 403 | | |
| 450 → | → | → 489 | |
| | 510 ← | ← | ← 547 |
| 697 → | → 699 | | |
| | | 777 ← | ← 789 |
| 796 → | → 809 | | |
| 1076 → | → | → 1080 | |
| 1161 → | → 1161 | | |
| | 1236 ← | ← | ← 1240 |

207 $A_1$ (R)
356 $A_1$
464 $A_1$
1085 $A_1$

**TABLE n**

**$As_2S_3$; The Layer Symmetry Properties Dominate the *R* and IR Spectra [27]**

| E‖a | | E‖b | | E‖c | |
|---|---|---|---|---|---|
| T | L | T | L | T | L |
| 182 | 189 | 186 | | 140 | 148 |
| 246 | | 386 | 392 | 159 | 165 |
| 279 | | | | 185 | 189 |
| 293 | 328 | | | 201 | 203 |
| 348 | 354 | | | 260 | |
| 354 | 369 | | | 278 | |
| 369 | 370 | | | 307 | 326 |
| 384 | 390 | | | 355 | 368 |
| | | | | 385 | 390 |
| $As_2Se_3$ | | | | | |
| 106 | 108 | | | 94 | 97 |
| 132 | 134 | | | 105 | 108 |
| 201 | 209 | | | 132 | 136 |
| 224 | 238 | | | 217 | 232 |
| 249 | | | | 248 | 250 |
| | | | | 268 | |

**TABLE o**

**CuO: Spectra Were Not Necessarily Obtained for *E*-field Polarization (IR) and/or Wave Vector (*R*) Parallel to the *a*, *b*, *c* Axes [25]**

| $A_u$(T)(IR) | (L) | $B_u$(T)(IR) | (L) |
|---|---|---|---|
| 164 | 165 | 145 | 147 |
| 355 | | 480 | 593 |
| (421) | | 603 | 624 |

296 $A_g$ (R)
346 $B_g$
636 $B_g$

**TABLE p**

**$(CH_2)n$: The Formula for Polyethylene Is Designated by the Molecular Unit $CH_2$, Four of Which Are in the Unit Cell and in the Primitive Cell**

| | (IR) | | (R) |
|---|---|---|---|
| Translation *x* | 0 $B_{3u}$ | Libration | 101 $B_{3g}$ |
| Translation *y* | 0 $B_{2u}$ | Libration | 141 $A_g$ |
| Translation *z* | 0 $B_{1u}$ | Optical skeletal | 1066 $B_{1g}$ |
| Translatory | 86 $B_{1u}$ | Optical skeletal | 1070 $B_{2g}$ |
| Translatory | 109 $B_{2u}$ | Optical skeletal | 1137 $B_{3g}$ |
| $CH_2$ rocking | 721 $B_{2u}$ | Optical skeletal | 1138 $A_g$ |
| $CH_2$ rocking | 736 $B_{1u}$ | $CH_2$ rocking | 1175 $A_g$ |
| $CH_2$ twisting | 1043 $B_{3u}$ | $CH_2$ rocking | 1176 $B_{3g}$ |
| $CH_2$ wagging | 1177 $B_{3u}$ | $CH_2$ twisting | 1293 $B_{2g}$ |
| $CH_2$ scissors | 1472 $B_{2u}$ | $CH_2$ twisting | 1297 $B_{1g}$ |
| $CH_2$scissors | 1478 $B_{1u}$ | $CH_2$ wagging | 1371 $B_{1g}$ |
| C-H sym stretch | 2851 $B_{1u}$ | $CH_2$ wagging | 1373 $B_{2g}$ |
| C-H sym stretch | 2853 $B_{2u}$ | $CH_2$ scissors | 1445 $A_g$ |
| C-H asym stretch | 2921 $B_{1u}$ | $CH_2$ scissors | 1458 $B_{3g}$ |
| C-H asym stretch | 2922 $B_{2u}$ | C-H sym stretch | 2850 $B_{3g}$ |
| | | C-H sym stretch | 2855 $A_g$ |
| | (O) | C-H asym stretch | 2885 $A_g$ |
| Translatory | 55 $A_u$ | C-H asym stretch | 2889 $B_{3g}$ |
| $CH_2$ twisting | 1041 $A_u$ | | |
| $CH_2$ wagging | 1181 $A_u$ | | |

These calculated frequencies are usually within 5 $cm^{-1}$ of the observed frequencies. The translation modes (acoustic phonons) $B_{3u} + B_{2u} + B_{1u}$ are included in this example but not in the irreducible representation. While the acoustic-phonon modes are not IR-active, they are included in the IR column because of the *u* subscript. They should be active in Brillouin scattering, however. Most of the other observed modes in the IR are combination bands of these fundamentals [32–34].

the IR-active modes are not also R-active. In this case we state only the $T$ and $L$ modes omitting the arrows.

It is interesting to note the differences in R and IR experiments. Raman measurements are very specific as to which phonon mode is being measured because of the constraints on wave vector and energy. Infrared measurements do not have the constraint of wave-vector conservation. Therefore, for the configuration of Fig. 2b, many TO phonons traveling in many directions in the $x, y$ plane (and for that matter, other directions having a component of dipole moment $\|E$) contribute to the absorption line seen for $E\|c$ (they may not all have the same frequency). The imaginary part of the IR transverse dielectric function ($\varepsilon_2 = 2nk$) has a peak at $\omega_T$. The real part of the transverse dielectric function ($\varepsilon_1 = n^2 - k^2$) usually has a zero very near here, and it usually has a second zero above $\omega_T$ at $\omega_L$. This zero is presumably at the frequency of the LO phonon propagating $\|c$.

If the unit cell has a center of symmetry, modes are mutually exclusive; an R-active mode is not also IR-active and vice versa.

In the optic frequency Tables a–p, a notation such as $E(L)(\text{IR}\perp)$, $A(L)(\text{IR}\|)$ indicates that the $E$ and $A$ modes are IR-active (their transverse members are seen; the longitudinal members are not seen because of dipole-moment, matrix-element considerations, but we can obtain their values from an oscillator fit of the reststrahlen reflectivity by finding where $\varepsilon_1 = 0$).

(12) and (13) *Plasma frequency.* Metals have plasma frequencies typically in the VIS–UV because of their large free-carrier (usually electron) densities ($10^{22}$–$10^{23}\,\text{cm}^{-1}$). Since semiconductors can be doped with controlled amounts of impurities, their free-carrier plasma frequencies can be varied. We therefore omit this parameter for semiconductors. The Drude plasma frequency $\omega_P^2$ (rad/s) is given by the formula $\omega_P^2 = 4\pi Ne^2/m^*\varepsilon$ with $N$ in $\text{cm}^{-3}$; $e = 4.77 \times 10^{-10}$ esu; $m^*$ is the effective mass compared to the free-electron mass of $9.10 \times 10^{-28}$ gm; $\varepsilon$ is the background lattice dielectric constant at the plasma frequency. The values of $\omega_P$ for a given material obtained from different laboratories often vary by tens of percent, so we use the fewest possible number of significant figures, namely two. A polariton composed of a coupled EM wave and the plasmon can exist in the region where $\varepsilon_1$ is negative (from 0 to $\omega_P$) and is measurable by a total internal reflection technique in $\omega$–$q$ space, where $q$ is the polariton wave vector.

Three ways of determining $\omega_P$ are fitting the reflectivity with a Drude model; measuring the energy loss of an electron beam passing through a thin layer; and determining where the real part of the dielectric function is zero ($\varepsilon_1 = n^2 - k^2 = 0$). This last criterion is easy to determine for the metals in the Tables in *HOC I* and *HOC II*. When interband absorption effects are small, $n$ crosses $k$ at only one point in the VIS–UV and this point often agrees with a Drude-model fit (which ignores interband effects). However,

for some metals, $n = k$ occurs at two, three, or four wavelengths, and the definition is obscured. This is usually due to strong interband transitions giving strong absorption/dispersion effects.

For metals, semiconductors, and insulators the valence (bound) electrons also produce a plasma effect in the interband region usually at a frequency higher than the free-electron plasma frequency for a metal. For a metal the first zero should locate the free-electron plasma frequency and the third should locate the valence plasma frequency. Between the second and third zeros, $\varepsilon_1$ is negative and a valence plasma polariton should be definable just as a free-electron plasma polariton in $\omega$–$q$ space is definable from 0 to $\omega_P$. Ideally for a semiconductor or insulator, this valence plasma frequency is at the second zero (above the band gap). The polariton mode is confined between the first and second zeros in $\varepsilon_1$ above the band gap in the spectral region where $\varepsilon_1$ is negative. These frequencies are listed in the $n = k$ column, although with overlapping interband effects, the valence plasma frequency may not be pinpointed by the second zero (higher-energy zero) of each pair of zeros. In Table I, in the $n = k$ column for some of the materials, there is no crossing (dashed line); in other cases there are two sets of data that differ, and the crossing cannot be pinpointed (crosses); in still other cases, no data are available in the interband region, and the space is left blank.

In addition to a phonon resonance producing a zero in $\varepsilon_1$ very close to $\omega_T$ for a semiconductor and insulator, the zero somewhat above the resonance allows a longitudinal mode to exist: $\omega_L$, for example. This idea is straightforward for lattice vibrations. It also holds for the free-carriers in metals and doped semiconductors, which have a resonant frequency at $\omega = 0$ and an $\omega_P$ (a longitudinal propagating plasmon) at $\varepsilon_1 = 0$. However, the interband region (especially at the second of each pair of zeros) and the nature of the longitudinal mode are not so clear.

(14) *The fundamental band gap $E_g$ of semiconductors and insulators.* The analysis of the absorption coefficient to extract $E_g$ is model-dependent for indirect (i) and direct (d) energy gaps. In lieu of a model fit, some investigators just define $E_g$ as the point at which the absorption coefficient $\alpha = 4\pi k/\lambda = 100$–$1000\ \mathrm{cm}^{-1}$.

(15) *The dc dielectric constant $\varepsilon_0$.* The real part of $\varepsilon_0$ near $\omega = 0$ for insulators is a positive number, which is straightforwardly determined from low-frequency optical or capacity experiments. However, for doped semiconductors and metals $\varepsilon_0$ tends to large, negative values because of the free-carrier dispersion. According to the Drude model, $\varepsilon = \varepsilon_1 + i\varepsilon_2$ contains components $\varepsilon_1 = \varepsilon_\infty\,[1 - \omega_P^2/(\omega^2 + w_\tau^2)]$ and $\varepsilon_2 = \varepsilon_\infty\,\omega_P^2\,\omega_\tau/\omega(\omega^2 + \omega_\tau^2)$ with $\omega_\tau(s^{-1}) = 1/\tau$, where $\tau(s)$ is the free-carrier lifetime and $\omega_\tau$ is the damping constant. However, $\varepsilon_2$ approaches infinity as $\omega \to 0$. To escape this "dilemma," we can switch our attention to the real part of the electrical conductivity. Since $\sigma = -i\varepsilon\omega/4\pi$, then $\sigma_1 = \varepsilon_2\,\omega/4\pi = \varepsilon_\infty\,\omega_P^2\,\omega_\tau/4\pi(\omega^2 + \omega_\tau^2)$. The dc conductivity is given by $\sigma_0(s^{-1}) = \varepsilon_\infty\,\omega_P^2/4\pi\omega_\tau$, a finite num-

ber. The resistivity $\rho_0(s) = 1/\sigma_0$; $\rho_0(\text{ohm cm}) = 9 \times 10^{11}\ \rho_0(s)$. For metals $\varepsilon_\infty = 1$; for semiconductors $\varepsilon_\infty \simeq 4 - 16$.

We do not include the high-frequency dielectric constant $\varepsilon_\infty$. The real part of $\varepsilon_\infty$ for a metal is generally taken as unity in the X-ray region. For a semiconductor or insulator it is usually defined in connection with the Lorentz-model fit to reststrahlen reflectivity data; it is the value of $\varepsilon_1$ below the fundamental band gap where $\varepsilon_1$ is nearly a constant before the lattice-vibration dispersion begins to decrease $\varepsilon_1$ significantly.

## REFERENCES


1. H. P. R. Frederikse, in "AIP Handbook," (D. E. Gray, ed.), 3rd ed., McGraw-Hill, New York, 9–56 (1972).
2. G. R. Wilkinson, in "Raman Effect," (A. Anderson, ed.), Marcel Dekker, New York, 811 (1973).
3. G. F. Koster, J. O. Dimmock, R. G. Wheeler, and H. Statz, "Properties of the Thirty-Two Point Groups," MIT Press, Cambridge, Mass. (1963).
4. K.-H. Hellewege and D. O. Madelung, eds. "Landolt–Börnstein Numerical Data and Functional Relationships in Science and Technology," Springer-Verlag, New York (1985).
5. G. Burns and A. M. Glazer, "Space Groups for Solid State Scientists," Academic Press, New York (1978).
6. R. W. G. Wyckoff, "Crystal Structures," Vols. 1–4, Interscience, New York, (1965).
7. R. Loudon, *Adv. Phys.* **13**, 423 (1964).
8. W. G. Fateley, F. R. Dollish, N. T. McDevitt, and F. F. Bentley, "Infrared and Raman Selection Rules for Molecular and Lattice Vibrations: The Correlation Method," Wiley-Interscience, New York (1972).
9. H. Poulet and J. P. Mathieu, "Vibration Spectrum and Symmetry of Crystals," Gordon and Breach, Paris (1976).
10. W. Hayes and R. Loudon, "Scattering of Light by Crystals," Wiley-Interscience, New York (1978).
11. S. S. Mitra and S. Nudelman, eds., "Far-Infrared Properties of Solids," Plenum, New York (1970).
12. D. W. Berreman, *Phys. Rev.* **130**, 2193 (1963).
13. R. Dalven, *Infrared Phys.* **9**, 141 (1969); PbS, PbSe, PbTe.
14. A. Scalabrin, A. S. Chaves, D. S. Shin, and S. P. S. Porto, *Phys. Stat. Sol. B* **79**, 731 (1977); $BaTiO_3$.
15. M. A. Ordal, R. J. Bell, R. W. Alexander, Jr., L. L. Long, and M. R. Querry, *Appl. Opt.* **26**, 744 (1987); several metals.
16. J. L. Servoin, R. Gervais, A. M. Quittet and Y. Luspin, *Phys. Rev. B* **21**, 2038 (1980); Ref. [2], p. 872; $SrTiO_3$.
17. S. M. Shapiro and J. D. Axe, *Phys. Rev.* **B6**, 2420 (1972); $SiO_2$.
18. R. Claus, *Z. Naturforsch.* **27A**, 1187 (1972); $LiNbO_3$.
19. Ref. [7], p. 172; Ref. [2], p. 861; wurzite semiconductors.
20. S. P. S. Porto, P. A. Fleury, and T. C. Damen, *Phys. Rev.* **154**, 522 (1967); Ref. [2], p. 878; $TiO_2$, $MgF_2$.
21. F. Tuinstra and J. L. Koenig, *J. Chem. Phys.* **53**, 1126 (1970); graphite.
22. S. P. S. Porto and R. S. Krishnan, *J. Chem. Phys.* **47**, 1009 (1967); Ref. [2], p. 894; $Al_2O_3$.
23. G. Lucovsky, A. Mooradian, W. Taylor, G. B. Wright, and R. C. Keezer, *Solid State Commun.* **5**, 113 (1967); Ref. [2], p. 851; Se.

24. P. Dawson, M. M. Hargreave, and G. R. Wilkinson, *J. Phys. Chem. Solids* **34**, 2201 (1973); $Cu_2O$.
25. S. Guha, D. Peebles, and T. J. Wieting, *Bull. Amer. Phys. Soc.* **35**, 293, 782 (1990); *Phys. Rev.* (in press), *Bull. Mater. Sci.* (in press); CuO.
26. Ref. [2], p. 859; Zinc blende semiconductors.
27. R. Zallen, M. L. Slade, and A. T. Ward, *Phys. Rev.* **B3**, 4257 (1971); $As_2S_3$, $As_2Se_3$.
28. D. W. Feldman, J. H. Parker, W. J. Choyke, and L. Patrick, *Phys. Rev.* **170**, 698 (1968); *Phys. Rev.* **173**, 787 (1968); SiC.
29. D. K. Agrawal and C. H. Perry, in "Proc. 2nd Inter. Conf. Light Scattering in Solids," (M. Balkanski, ed.), Flammarion, Paris, 429 (1971); KDP, ADP.
30. T. Kawamura and A. Mitsuishi, *Technology Reports, Osaka University* **23**, 365 (1973); KDP, ADP.
31. F. Onyango, W. Smith, and J. F. Angress, *J. Phys. Chem. Solids* **36**, 309 (1975); KDP.
32. J. R. Nielsen and A. H. Wollett, *J. Chem. Phys.* **26**, 1391 (1957); $(CH_2)_n$.
33. R. Zbinden, "Infrared Spectroscopy of High Polymers," Academic Press, New York (1964); $(CH_2)_n$.
34. P. C. Painter, M. M. Coleman, and J. L. Koenig, "The Theory of Vibrational Spectroscopy and its Application to Polymer Materials," Wiley, New York, 1982; $(CH_2)_n$.
35. L. M. Fraas and S. P. S. Porto, *Solid State Commun.* **8**, 803 (1970); Be.

# An Introduction to the Data for Several Metals

DAVID W. LYNCH
Department of Physics and Ames Laboratory
Institue for Physical Research and Technology
Iowa State University
Ames, Iowa
and
W. R. HUNTER
SFA, Inc.
Landover, Maryland

## INTRODUCTION I

We present data below for several metals: the alkali metals Li, Na, and K, and the transition metals Cr, Fe, Nb, and Ta. There are some other data compilations that it may be useful to consult. Weaver *et al.* [1] present optical data for noble metals, transition metals, lanthanides, actinides, and a few other metals. They present plots that show the agreement, or lack thereof, of data from many investigators. The spectral region covered is usually up to 200 eV or less. Henke *et al.* [2, 3] present calculated atomic scattering factors, and derive an empirical set of data based on experimental results. The spectra range is 10–10,000 eV. Actual data do not exist over most of this range, and some of the data presented were taken on atoms (vapor samples) and some on solids.

### REFERENCES

1. J. H. Weaver, C. Krafka, D. W. Lynch, and E.-E. Koch, "Optical Properties of Metals," Parts I and II (Physics Data Series No. 18-1 and 18-2, Fachinformationszentrum Energie Physik Mathematik, Karlsruhe, 1981).
2. B. L. Henke, P. Lee, T. J. Tanaka, R. L. Shimabukuro, and B. K. Fujikawa, *Atomic Data and Nucl. Data Tables* **27**, 1 (1982).
3. B. L. Henke, J. C. Davis, E. M. Gullikson, and R. C. C. Perera, Lawrence Berkeley Laboratory Report No. LBL-26259 (1988).


Copyright © 1991 by Academic Press.
All rights of reproduction in any form reserved.
ISBN 0-12-544422-2

## II ALKALI METALS

The alkali metals are the simplest of all metals, and their dielectric functions the simplest and best understood. The nearly-free-electron model should be valid. The Fermi level should lie about in the middle of the lowest conduction band, and the gap between the bands at the zone boundaries should be small. The Fermi surface should be spherical, and all interband optical transitions should occur in a central spherical region of the Brillouin zone. The interband optical properties should be accurately calculable by perturbation theory [1–3]. Indeed this might be the case for all alkali metals except Li. Li has only three electrons per atom, with a $1s^2 2s$ configuration. In a pseudopotential approach, there are no core p electrons to which the 2p part of the valence electrons can be orthogonalized. Consequently, the pseudopotential is not as small as for other alkali metals, and the band gap is larger. The Fermi level then comes closer to the zone boundary, and the Fermi surface is distorted from a sphere. Another view is that the screening of the core potential by the single 2s valence electron of the atom is less effective in Li than by the corresponding electrons in the other alkali metals, and the gap is consequently larger. Thus, Li is expected to be somewhat different from the other alkali metals, and this is borne out by experiment.

In fact, however, recent photoemission measurements [4, 5] show that the apparent filled region of the valence band in Na and K (and presumably other alkali metals) is narrower than band-structure calculations show. This is an effect of the response of the conduction electrons to the photohole, that is, one should not interpret photoelectron spectra (or optical spectra) on the basis of the one-electron density of states, but rather the spectral density of the interacting system of electrons. An equivalent picture is to augment the calculated one-electron band structure by the (complex) self energy, which shifts bands nonuniformly and broadens them [6–9].

The experimental situation is complicated by several factors. The alkali metals are reactive. They have low melting points, and relatively high diffusion rates at room temperature, leading to surfaces that are possibly rough. A number of measurements were taken not at free metal surfaces, but at quartz–alkali metal interfaces to avoid contamination, even in ultra-high vacuum, and to yield a smooth interface. The roles of interfacial grain structure, reactions, and strain are unknown. A number of years ago, a significant peak in the optical conductivity was reported for several alkali metals, with potassium being the most studied [10, 11]. The peak occurred at an energy lower than the threshold for interband absorption. Many theoretical explanations were proposed in the ensuing years, but that peak was not found in many subsequent measurements, especially, but not

exclusively, those made on the quartz–metal interface. The best early explanation was that it arose because of roughness at the alkali metal–vacuum interface [12]. Some experiments showed that it may be present only when water is adsorbed on the alkali metal surface [13]. This led to a new interpretation, that it arose from charge-density waves, at least in potassium [14, 15]. Subsequent measurements did not confirm the predicted optical structures [16]. A final complication is the fact that at low temperatures both Na and Li undergo a structural phase transition from their normal body-centered cubic structure.

There are not many measurements in the infrared on alkali metals. They should behave as free-electron gases in this region, for there is a threshold energy of the order of 1 eV for direct interband absorption. The measurements are difficult, for the reflectance is very high, and one needs great precision and accuracy, of the order of four decimal places in the reflectance. Ellipsometry, using several reflections, has often been used for metals in the infrared, but again the measurement is difficult, for the real part of the ratio of p- to s-polarized electric-field reflection coefficients is very close to one, and the phase shift is very close to 180°. One really needs the difference between the optical properties of the metal and those of a perfect conductor in such cases, and few measurements have been made at wavelengths longer than 2.5 μm for any alkali metal. Intrinsic surface states have been calculated to be present on alkali metals, and to contribute significantly to the infrared optical properties [17–21], in contrast to their contribution in noble metals, for example Ag, where such states contribute effects of only about a part in $10^4$. The large predicted effects have not been seen, but there are really no data in the right spectral region on clean samples.

Since there may be interest in infrared optical properties, and the only such measurements do not tie in well with those in the visible, the only option is to use a nearly-free-electron (Drude) model. The parameters in this model may be obtained from data in the near infrared. In the discussion of each alkali metal, we give those parameters that have been extracted from experimental data, but there is considerable scatter in them. The real and imaginary parts of the refractive indices can be obtained from the real and imaginary parts of the Drude dielectric function from

$$2n^2 = +\varepsilon_1 + (\varepsilon_1^2 + \varepsilon_2^2)^{1/2}$$

$$2k^2 = -\varepsilon_1 + (\varepsilon_1^2 + \varepsilon_2^2)^{1/2},$$

with

$$\varepsilon_1 = 1 + \varepsilon_{xx} - \omega_p^2 \tau^2 / (1 + (\omega\tau)^2)$$

$$\varepsilon_2 = \omega_p^2 \tau / \omega (1 + (\omega\tau)^2).$$

$\varepsilon_{xx}$ is the contribution of high-energy interband transitions to the low-frequency dielectric function, $\omega_p$ is the plasma frequency, given in cgs units

by $\omega_p^2 = 4\pi Ne^2/m^*$, with $N$ the number density of electrons and $m^*$ their effective mass. $\tau$ is the relaxation time. However, to obtain a good fit to data, $\tau$ must be frequency-dependent, in the form

$$1/\tau = 1/\tau_0 + \beta\omega^2.$$

Thus, to characterize the infrared optical properties, we must know four parameters. Note that $\omega_p$ and $\tau_o$ should give the correct static conductivity, $\omega_p\tau_o/4\pi$. (Sometimes data taken above the lowest interband absorption are fit to a Drude expression. However, in such cases the relaxation time will be different, and the plasma frequency should contain the free-electron mass, or an effective mass closer to it than the infrared value.)

The following critiques, tables, and graphs contain what we consider to be the most useful $n$ and $k$ values for the chosen metals. One of the steps in producing the tables containing $E$ (energy), $\lambda$ (wavelength), $n$ (index of refraction), and $k$ (extinction coefficient) is to convert $E$ (usually the experimental units in eV) to $\lambda$ by means of the formula $E\,(\text{eV})\lambda\,(\text{Å}) = 12{,}398.42$. This was done and the values subsequently rounded to those found in the table (usually to four figures). After rounding, however, $E\lambda$ may not give the original conversion factor to four significant figures. Thus, if $E$ from the table is converted to $\lambda$ using the above conversion factor, the result may not equal the wavelength value in the table and vice versa. This slight discrepancy happens most often in the data taken from Henke *et al.* but should produce no practical problems.

## REFERENCES


1. A. H. Wilson, "The Theory of Metals," Cambridge University Press, Cambridge, 133 (1936).
2. P. N. Butcher, *Proc. Phys. Soc. (London)* **A64**, 50 (1951).
3. N. W. Ashcroft and K. Sturm, *Phys. Rev.* **B3**, 1898 (1971).
4. E. Jensen and E. W. Plummer, *Phys. Rev. Lett.* **55**, 1912 (1985).
5. I.-W. Lyo and E. W. Plummer, *Phys. Rev. Lett.* **60**, 1558 (1988).
6. J. E. Northrup, M. S. Hybertsen, and S. G. Louie, *Phys. Rev. Lett.* **59**, 819 (1987).
7. K. W. Shung, B. E. Sernelius, and G. D. Mahan, *Phys. Rev.* **B36**, 4499 (1987).
8. K. W. Shung and G. D. Mahan, *Phys. Rev.* **B38**, 3856 (1988).
9. J. E. Northrup, M. S. Hybertsen, and S. G. Louie, *Phys. Rev.* **B39**, 8198 (1989).
10. H. Mayer and M. H. El Naby, *Z. Physik* **174**, 269 (1963).
11. H. Mayer and B. Heitel in "Optical Properties of Solids," (F. Abeles, ed.), North-Holland, Amsterdam, 47 (1972).
12. J. P. Marton, *Appl. Phys. Lett.* **18**, 140 (1971).
13. P. Harms, dissertation, Clausthal, 1972.
14. A. W. Overhauser and N. R. Butler, *Phys. Rev.* **B14**, 3371 (1976).
15. F. E. Fragachan and A. W. Overhauser, *Phys. Rev.* **B31**, 4802 (1985).
16. L. H. Dubois and N. V. Smith, *J. Phys. F Met. Phys.* **17**, L7 (1987).
17. R. Garron, *Surf. Sci.* **79**, 489 (1979).
18. R. Garron, *Surf. Sci.* **91**, 358 (1980).
19. R. Garron and H. Roubaud, *Surf. Sci.* **92**, 593 (1980).

20. R. Garron and H. Roubaud, *Surf. Sci.* **146**, 527 (1984).
21. R. Garron, *Appl. Opt.* **20**, 1747 (1981).

## LITHIUM (Li) III

Lithium is a reactive material, and generally only data taken under ultrahigh-vacuum conditions will be mentioned. Li is normally body-centered cubic, but at low temperatures there is a transition to a phase often reported to be hexagonal, a phase with different optical properties. It is the stable phase below about 80 K. However, the phase transition is sluggish, and a low-temperature sample may be a mixture of phases. In fact, the early reports of this transition stated the low-temperature phase was hexagonal close packed [1, 2], but more recent descriptions [3] are 9*R*, a closed-packed stacking that is mixed fcc and hcp. We report only data on the bcc phase. We do not consider data taken in arbitrary units, for example, optical density of a film or electron-energy-loss spectra without suitable normalization, unless those are the only data available in a particular wavelength region. In such a case, we give only a reference to the original work.

The first modern measurements on Li are those of Hodgson [4]. Although the films were not prepared in ultrahigh vacuum, the ellipsometric measurements were made on an Li-silica interface, which remained stable for about a day. The data, taken in the 0.22–2 μm region and at two temperatures, were fit to a free-electron model in the longer-wavelength region. To obtain a good fit, the relaxation time had to depend on frequency. The interband-absorption threshold was not well-defined. Bösenberg [5, 6] made attenuated-total-reflectance measurements on films deposited in better vacuum, using the Li-sapphire interface. His data, covering the range of 2–3.8 eV, are not in good agreement with Hodgson's, but agree better with data taken later by other groups.

Myers and coworkers [7–9] made ellipsometric measurements at the vacuum–metal interface in the range 0.6–4 eV. They evaporated films on several substrates at several temperatures, obtaining different results. There were changes in the spectra with time after deposition. Others (see below) also observed time-dependence. For what was believed to be bcc Li, the first interband threshold was at 2.6 eV. At lower energies, the data were fitted to a free-electron model, but to obtain a fit it was necessary that the relaxation time depend on frequency. Table I lists Drude parameters from several references. Table II lists values of $n$ and $k$. Figure 1 plots $n$ and $k$ versus μm. Myers and Sixtensson [9] also reported the optical constants of hexagonal Li. Rasigni and Rasigni [10] measured the transmittance of Li films of varying thickness, from which measurements they

extracted the optical conductivity. They covered the 1–6 eV region and found two interband peaks. The one with a threshold at about 2.6 eV was the expected interband peak, whereas the anomalous one peaked between 1.5 and 2.6 eV. Films giving the latter were found to be grainier, either discontinuous grains on the substrate or a distribution of grains on a smoother Li film on the substrate. They made additional studies of the nature of the surfaces of films evaporated on substrates at different temperatures, correlating them with optical spectra [11–15]. They were able to eliminate the anomalous peak in later work [16], in which they give optical constants in the 0.15–10.7 eV range, obtained by Kramers–Kronig analysis of their reflectance measurements in the range 0.5–6 eV [13], and the reflectance of Callcott and Arakawa [17] from 3–10.7 eV. Inagaki *et al.* [18] measured the optical properties of Li in the 0.6–3.8 eV region by ellipsometry on the Li–silica interface. They obtained the anomalous absorption mentioned earlier after allowing their films to stand for a day in UHV, even though their measurements were at the Li–silica interface. The data that they took before the growth of this peak do not agree well with those of Myers *et al.*, but the reflectance calculated from their data agrees with that of Rasigni and Rasigni [13].

The spectra of $k$ from the papers mentioned earlier agree reasonably well, but there are large differences in the $n$ spectra. $n$ has a minimum near 0.5 μm, and the values at this minimum range from 0.13 to 0.21. The data of Rasigni and Rasigni exhibit a local maximum in $n$ at about 0.33 μm not apparent in the other spectra (which end at about 0.33 μm). There are also discrepancies at both ends of the range of these measurements, either in the magnitudes of $n$, the slopes $dn/d\lambda$, or both. There are no data further into the infrared, and the only data at shorter wavelengths are described in the next paragraph. Of the measurements described in the previous paragraph, only those of Rasigni and Rasigni [16] are close to matching the only data set to shorter wavelengths, and this matching was part of their own data analysis. This does not mean these are the best data, but this matching is the only criterion we can use for having selected them for the table. The data sets are too limited in range to test for consistency by sum rules. Moreover, not all authors report the frequency-dependence of the relaxation time necessary for an extrapolation of their data to longer wavelengths. The discrepancies probably result from differences in samples, either the possible occurrence of two phases, differences in surface roughness, or both. (There may be voids at the Li–substrate interface, which would appear as roughness in measurements made on that interface.)

Callcott and Arakawa [17] determined the optical constants of Li films in the 3–10.7 eV region by multiple-angle reflectance measurements. They worked on the Li–vacuum interface and the Li–substrate ($MgF_2$) interface, getting agreement in the optical constants only for energies above 6 eV.

Discrepancies below 6 eV were assigned to substrate roughness and structural effects in the film. Below 6 eV, they chose no best set of data, and only results above 6 eV are tabulated.

There are no absolute measurements at energies above 10.7 eV. Haensel *et al.* [19] presented the results of transmission measurements in the 60–149 eV region. They show considerable structure at and above the Li 1s absorption edge, structure that will appear prominently in the $k$ spectrum, but very weakly in that of $n$.

Extrapolation to the infrared may be made from the Drude parameters, but in the case of Li, those reported are not in good agreement with each other. We list many of them in Table I. (The fact that the effective-mass values are considerably larger than unity is a consequence of the distortion of the Fermi surface mentioned earlier). The first interband transition begins at about 2.6 eV. The Drude parameters may be used to obtain $\varepsilon_2$ for energies below this, but the interband contribution to $\varepsilon_2$ will persist several tenths of an eV below 2.6 eV. Thus, Drude values of $n$ and $k$ would be reliable below about 2 eV, except that a reliable set of parameters cannot be chosen rationally. (Values of the Drude parameters determined from data in the spectral region above the interband absorption are not given in Table I. Such data yield a smaller effective mass, not suitable for extrapolation in the infrared).

We have calculated $n$ and $k$ in the 1.24–240 Å (10,000–51.5 eV) region using the model of Henke *et al.* [20]. The atomic absorption edge is $K$ (55 eV) [21].

We used 8065.48 $cm^{-1}$/eV to convert among the units of [20], whereas the conversion factor varies by a digit or so for [16]. This should give no problems among the units until the fourth figure.

## REFERENCES


1. C. S. Barrett, *Phys. Rev.* **72**, 245 (1947).
2. C. S. Barrett, *Acta. Cryst.* **9**, 671 (1956).
3. References to the recent structural literature may be found in R. J. Gooding and J. A. Krumhansl, *Phys. Rev.* **B38**, 1695 (1988).
4. J. N. Hodgson in "Optical Properties and Electronic Structure of Metals and Alloys," (F. Abeles, ed.), North-Holland, Amsterdam, 60 (1966).
5. J. Bösenberg, *Phys. Lett.* **41A**, 185 (1972).
6. J. Bösenberg, *Z. Physik B* **22**, 261 (1975).
7. A. G. Mathewson and H. P. Myers, *Physica Scripta* **4**, 291 (1971).
8. A. G. Mathewson and H. P. Myers, *Phil. Mag.* **25**, 853 (1972).
9. H. P. Myers and P. Sixtensson, *J. Phys. F* **6**, 2023 (1976).
10. M. Rasigni and G. Rasigni, *J. Opt. Soc. Am.* **63**, 775 (1973).
11. M. Rasigni and G. Rasigni, *J. Opt. Soc. Am.* **62**, 1033 (1972).
12. M. Rasigni, G. Rasigni, and J. P. Palmari, *Phil. Mag.* **31**, 1307 (1975).
13. M. Rasigni and G. Rasigni, *J. Opt. Soc. Am.* **66**, 826 (1976).
14. M. Rasigni, J. P. Gasparini, G. Rasigni, and R. Fraisse, *Solid State Commun.* **18**, 629 (1976).

15. M. Rasigni, G. Rasigni, J. P. Gasparini, and R. Fraisse, *J. Appl. Phys.* **47**, 1757 (1976).
16. M. Rasigni and G. Rasigni, *J. Opt. Soc. Am.* **67**, 54 (1977).
17. T. A. Callcott and E. T. Arakawa, *J. Opt. Soc. Am.* **64**, 839 (1974).
18. T. Inagaki, L. C. Emerson, E. T. Arakawa, and M. W. Williams, *Phys. Rev.* **B13**, 2305 (1976).
19. R. Haensel, G. Keitel, B. Sonntag, C. Kunz, and P. Schreiber, *Phys. Stat. Solidi (a)* **2**, 85 (1970).
20. B. L. Henke, J. C. Davis, E. M. Gullikson, and R. C. C. Perera, Lawrence Berkeley Laboratory Report No. LBL-26259 (1988).
21. K. Siegbahn, C. Nordling, A. Fahlman, R. Nordberg, K. Hamrin, J. Hedman, G. Johansson, T. Bergmark, S.-E. Karlsson, I. Lindgren, and B. Lindberg, in "Nova Acta Regiae Societatis Scientiarum Upsaliensis," Ser. IV, Vol. 20, Almqvist and Wiksells Boktryckeri, Uppsala, (1967).

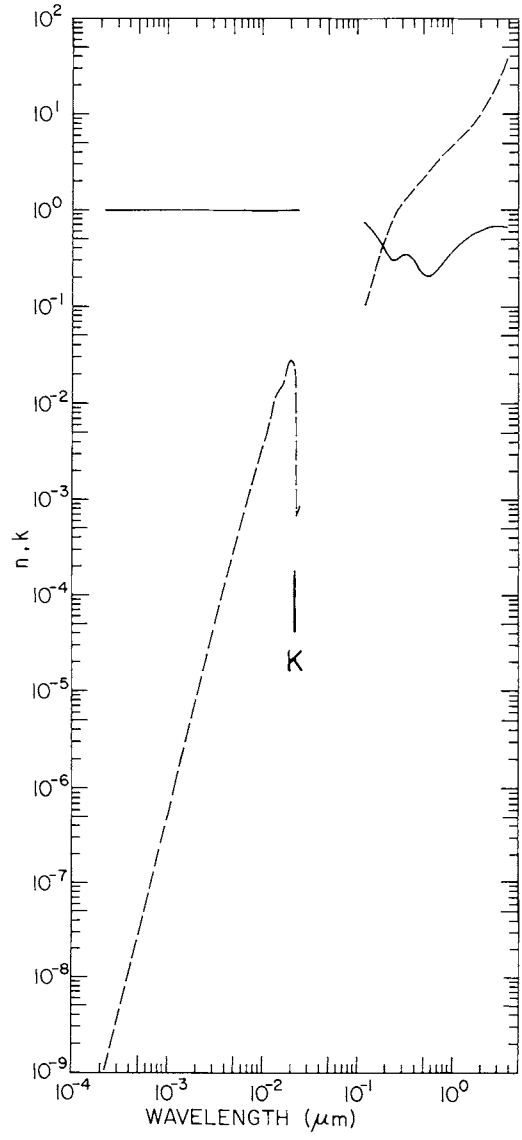


**Fig. 1.** Log–log plot of $n$ (solid line) and $k$ (dashed line) versus wavelength in micrometers for lithium.

**TABLE I**

**Drude-Model Parameters from Various References**

| Ref. | $\varepsilon_\infty$ | $\tau$ ($10^{-14}$ sec) | $\beta$ ($10^{-14}$ sec eV$^{-2}$) | $\omega_p$ (eV) | $m^*/m$ |
|---|---|---|---|---|---|
| [4] | 1.0 | | | 6.4 | 1.57 |
| [5] | 0.8 | | | | 1.47 |
| [6] | 0.75 | | | 6.2 | 1.68 |
| [8] | | | | 6.94 | 1.33 |
| [9] | <1 | 2.06 | 0.285 | 6.58 | 1.52 |
| [16] | 0 | | | | 1.80 |
| [18] | | | | | 1.61 |

**TABLE II**

**Values of $n$ and $k$ Obtained from Various References for Lithium[a]**

| eV | $cm^{-1}$ | Å | $n$ | $k$ |
|---|---|---|---|---|
| 10000 | | 1.240 | 0.9999990 [20] | 1.14E-10 [20] |
| 9549 | | 1.298 | 0.9999989 | 1.35E-10 |
| 9117 | | 1.360 | 0.9999989 | 1.60E-10 |
| 8706 | | 1.424 | 0.9999987 | 1.90E-10 |
| 8313 | | 1.492 | 0.9999986 | 2.28E-10 |
| 7937 | | 1.562 | 0.9999985 | 2.75E-10 |
| 7579 | | 1.636 | 0.9999983 | 3.31E-10 |
| 7237 | | 1.713 | 0.9999982 | 3.94E-10 |
| 6910 | | 1.794 | 0.9999980 | 4.67E-10 |
| 6598 | | 1.879 | 0.9999978 | 5.55E-10 |
| 6300 | | 1.968 | 0.9999976 | 6.59E-10 |
| 6015 | | 2.061 | 0.9999974 | 7.82E-10 |
| 5744 | | 2.159 | 0.9999971 | 9.29E-10 |
| 5484 | | 2.261 | 0.9999968 | 1.11E-09 |
| 5237 | | 2.368 | 0.9999965 | 1.34E-09 |
| 5000 | | 2.480 | 0.9999962 | 1.61E-09 |
| 4775 | | 2.597 | 0.9999958 | 1.94E-09 |
| 4559 | | 2.720 | 0.9999954 | 2.35E-09 |
| 4353 | | 2.848 | 0.9999949 | 2.83E-09 |
| 4157 | | 2.983 | 0.9999945 | 3.41E-09 |
| 3969 | | 3.124 | 0.9999939 | 4.12E-09 |
| 3790 | | 3.272 | 0.9999933 | 4.96E-09 |
| 3619 | | 3.426 | 0.9999927 | 5.98E-09 |
| 3455 | | 3.588 | 0.9999920 | 7.21E-09 |
| 3299 | | 3.758 | 0.9999912 | 8.69E-09 |
| 3150 | | 3.936 | 0.9999903 | 1.05E-08 |
| 3008 | | 4.122 | 0.9999894 | 1.26E-08 |
| 2872 | | 4.317 | 0.9999884 | 1.52E-08 |
| 2742 | | 4.521 | 0.9999872 | 1.84E-08 |
| 2619 | | 4.735 | 0.9999860 | 2.24E-08 |
| 2500 | | 4.959 | 0.9999846 | 2.71E-08 |
| 2387 | | 5.193 | 0.9999831 | 3.28E-08 |
| 2280 | | 5.439 | 0.9999815 | 3.98E-08 |
| 2177 | | 5.696 | 0.9999797 | 4.82E-08 |
| 2078 | | 5.965 | 0.9999777 | 5.84E-08 |
| 1985 | | 6.248 | 0.9999755 | 7.08E-08 |
| 1895 | | 6.543 | 0.9999731 | 8.56E-08 |
| 1809 | | 6.852 | 0.9999705 | 1.01E-07 |
| 1728 | | 7.176 | 0.9999676 | 1.22E-07 |
| 1650 | | 7.516 | 0.9999645 | 1.48E-07 |
| 1575 | | 7.871 | 0.9999610 | 1.80E-07 |
| 1504 | | 8.244 | 0.9999572 | 2.18E-07 |
| 1436 | | 8.633 | 0.9999530 | 2.65E-07 |
| 1371 | | 9.041 | 0.9999484 | 3.21E-07 |

[a]The references from which the values were extracted are given in brackets.

TABLE II (*Continued*)

Lithium

| eV | $cm^{-1}$ | Å | $n$ | $k$ |
|---|---|---|---|---|
| 1309 | | 9.469 | 0.9999434 | 3.88E-07 |
| 1250 | | 9.917 | 0.9999379 | 4.70E-07 |
| 1194 | | 10.39 | 0.9999318 | 5.68E-07 |
| 1140 | | 10.88 | 0.9999251 | 6.87E-07 |
| 1088 | | 11.39 | 0.9999177 | 8.30E-07 |
| 1039 | | 11.93 | 0.9999097 | 1.00E-06 |
| 992.3 | | 12.49 | 0.9999008 | 1.21E-06 |
| 947.5 | | 13.09 | 0.999891 | 1.46E-06 |
| 904.7 | | 13.70 | 0.999880 | 1.77E-06 |
| 863.9 | | 14.35 | 0.999869 | 2.14E-06 |
| 824.9 | | 15.03 | 0.999856 | 2.58E-06 |
| 787.7 | | 15.74 | 0.999841 | 3.12E-06 |
| 752.1 | | 16.49 | 0.999825 | 3.76E-06 |
| 718.1 | | 17.27 | 0.999808 | 4.54E-06 |
| 685.7 | | 18.08 | 0.999789 | 5.45E-06 |
| 654.7 | | 18.94 | 0.999768 | 6.59E-06 |
| 625.1 | | 19.83 | 0.999745 | 7.98E-06 |
| 610.9 | | 20.30 | 0.999733 | 8.75E-06 |
| 596.9 | | 20.77 | 0.999720 | 9.61E-06 |
| 583.3 | | 21.26 | 0.999706 | 1.05E-05 |
| 570.0 | | 21.75 | 0.999692 | 1.16E-05 |
| 544.0 | | 22.78 | 0.999661 | 1.39E-05 |
| 519.7 | | 23.86 | 0.999627 | 1.67E-05 |
| 496.2 | | 24.99 | 0.999590 | 2.01E-05 |
| 473.8 | | 26.17 | 0.999549 | 2.42E-05 |
| 452.4 | | 27.41 | 0.999504 | 2.92E-05 |
| 432.9 | | 28.70 | 0.999454 | 3.50E-05 |
| 412.5 | | 30.06 | 0.999399 | 4.20E-05 |
| 393.8 | | 31.48 | 0.999339 | 5.04E-05 |
| 376.1 | | 32.97 | 0.999273 | 6.03E-05 |
| 359.1 | | 34.53 | 0.999200 | 7.21E-05 |
| 342.9 | | 36.16 | 0.999120 | 8.61E-05 |
| 327.4 | | 37.87 | 0.999031 | 1.03E-04 |
| 312.6 | | 39.66 | 0.99893 | 1.23E-04 |
| 298.5 | | 41.54 | 0.99883 | 1.47E-04 |
| 285.0 | | 43.50 | 0.99871 | 1.76E-04 |
| 272.1 | | 45.56 | 0.99858 | 2.10E-04 |
| 259.9 | | 47.71 | 0.99844 | 2.49E-04 |
| 248.1 | | 49.97 | 0.99828 | 2.96E-04 |
| 236.9 | | 52.33 | 0.99811 | 3.52E-04 |
| 226.2 | | 54.81 | 0.99793 | 4.19E-04 |
| 216.0 | | 57.40 | 0.99772 | 4.98E-04 |
| 206.2 | | 60.12 | 0.99750 | 5.89E-04 |
| 196.9 | | 62.96 | 0.99726 | 6.96E-04 |
| 188.0 | | 65.94 | 0.99699 | 8.24E-04 |

(*Continued*)

TABLE II (*Continued*)

Lithium

| eV | $cm^{-1}$ | Å | $n$ | $k$ |
|---|---|---|---|---|
| 179.6 | | 69.05 | 0.99671 | 9.75E-04 |
| 171.4 | | 72.32 | 0.99640 | 1.14E-03 |
| 163.7 | | 75.74 | 0.99607 | 1.35E-03 |
| 156.3 | | 79.32 | 0.99571 | 1.58E-03 |
| 149.3 | | 83.07 | 0.99532 | 1.86E-03 |
| 142.5 | | 87.00 | 0.99489 | 2.18E-03 |
| 136.1 | | 91.11 | 0.99444 | 2.57E-03 |
| 129.9 | | 95.42 | 0.99398 | 3.02E-03 |
| 124.1 | | 99.94 | 0.99349 | 3.53E-03 |
| 118.5 | | 104.7 | 0.99297 | 4.13E-03 |
| 113.1 | | 109.6 | 0.99245 | 4.81E-03 |
| 108.0 | | 114.8 | 0.99181 | 5.58E-03 |
| 103.1 | | 120.2 | 0.99108 | 6.63E-03 |
| 98.47 | | 125.9 | 0.99057 | 8.05E-03 |
| 94.03 | | 131.9 | 0.99025 | 9.81E-03 |
| 89.78 | | 138.1 | 0.99065 | 1.18E-02 |
| 85.73 | | 144.6 | 0.99152 | 1.31E-02 |
| 81.85 | | 151.5 | 0.99210 | 1.40E-02 |
| 78.16 | | 158.6 | 0.99233 | 1.47E-02 |
| 74.63 | | 166.1 | 0.99202 | 1.60E-02 |
| 71.26 | | 174.0 | 0.99169 | 1.85E-02 |
| 68.04 | | 182.2 | 0.99257 | 2.28E-02 |
| 64.97 | | 190.8 | 0.99707 | 2.66E-02 |
| 62.04 | | 199.9 | 1.003 | 2.74E-02 |
| 59.24 | | 209.3 | 1.019 | 2.66E-02 |
| 56.56 | | 219.2 | 1.017 | 2.36E-02 |
| 55.27 | | 224.3 | 1.026 | 2.18E-02 |
| 54.01 | | 229.6 | 1.021 | 6.86E-04 |
| 52.77 | | 234.9 | 1.014 | 7.23E-04 |
| 51.57 | | 240.4 | 1.010 | 7.91E-04 |
| eV | $cm^{-1}$ | μm | $n$ | $k$ |
| 10.6 | 85897 | 0.1164 | 0.753 [16] | 8.00E-02 [16] |
| 10.4 | 83478 | 0.1198 | 0.743 | 0.102 |
| 10.1 | 81058 | 0.1234 | 0.726 | 0.108 |
| 9.75 | 78638 | 0.1272 | 0.708 | 0.119 |
| 9.45 | 76219 | 0.1312 | 0.680 | 0.130 |
| 9.15 | 73799 | 0.1355 | 0.657 | 0.144 |
| 8.85 | 71379 | 0.1401 | 0.624 | 0.163 |
| 8.55 | 68960 | 0.1450 | 0.601 | 0.189 |
| 8.25 | 66540 | 0.1503 | 0.572 | 0.214 |
| 7.95 | 64121 | 0.1560 | 0.545 | 0.246 |
| 7.65 | 61701 | 0.1621 | 0.517 | 0.282 |
| 7.35 | 59281 | 0.1687 | 0.492 | 0.320 |

(*Continued*)

TABLE II (*Continued*)

Lithium

| eV | $cm^{-1}$ | μm | *n* | *k* |
|---|---|---|---|---|
| 7.95 | 64121 | 0.1560 | 0.545 | 0.246 |
| 7.65 | 61701 | 0.1621 | 0.517 | 0.282 |
| 7.35 | 59281 | 0.1687 | 0.492 | 0.320 |
| 7.05 | 56862 | 0.1759 | 0.466 | 0.364 |
| 6.75 | 54442 | 0.1837 | 0.440 | 0.407 |
| 6.45 | 52022 | 0.1922 | 0.408 | 0.460 |
| 6.15 | 49603 | 0.2016 | 0.376 | 0.522 |
| 5.85 | 47183 | 0.2119 | 0.342 | 0.594 |
| 5.55 | 44763 | 0.2234 | 0.310 | 0.688 |
| 5.25 | 42344 | 0.2362 | 0.299 | 0.795 |
| 4.95 | 39924 | 0.2505 | 0.302 | 0.906 |
| 4.65 | 37504 | 0.2666 | 0.317 | 1.01 |
| 4.35 | 35085 | 0.2850 | 0.333 | 1.11 |
| 4.05 | 32665 | 0.3061 | 0.346 | 1.21 |
| 3.75 | 30246 | 0.3306 | 0.345 | 1.32 |
| 3.45 | 27826 | 0.3594 | 0.334 | 1.45 |
| 3.15 | 25406 | 0.3936 | 0.304 | 1.60 |
| 2.85 | 22987 | 0.4350 | 0.247 | 1.82 |
| 2.55 | 20567 | 0.4862 | 0.217 | 2.11 |
| 2.25 | 18147 | 0.5510 | 0.206 | 2.48 |
| 1.95 | 15728 | 0.6358 | 0.221 | 2.94 |
| 1.65 | 13308 | 0.7514 | 0.265 | 3.55 |
| 1.35 | 10888 | 0.9184 | 0.338 | 4.36 |
| 1.05 | 8469 | 1.181 | 0.448 | 5.58 |
| 0.750 | 6049 | 1.653 | 0.561 | 7.68 |
| 0.540 | 4355 | 2.296 | 0.661 | 12.6 |
| 0.140 | 1129 | 8.856 | 0.659 | 38.0 |

## IV SODIUM (Na)

The optical properties of sodium have been measured with more consistency than those of Li, but the agreement among measurements is still not satisfying. Na is normally body-centered cubic, but it also has a low-temperature hexagonal phase. However, the phase transition sets in at 51 K if aided by plastic deformation, and at 36 K upon simply cooling [1]. This means that evaporated-film samples of Na condensed on substrates at liquid-nitrogen temperatures are probably single-phase films, unlike films of Li condensed under similar circumstances. Na films are similarly likely to be rough, however, and Na is a reactive material.

The first modern measurements on Na were those of Hodgson [2, 3] and Mayer and Heitel [4]. Hodgson made ellipsometric measurements from 0.65 μm to 2.5 μm on the Na–silica interface of films evaporated in less than ultrahigh-vacuum conditions. He reported that his spectra of the optical

conductivity (hence, in this case, of $k$) were not reproducible from sample to sample, whereas those of $\varepsilon_1$ (essentially $n^2$) were. This is a similar problem to that encountered in Li. Mayer and Heitel made ellipsometric measurements from 0.3 μm to 2.5 μm on the Na–vacuum interface in ultrahigh vacuum. The real part of the dielectric function was fit to a Drude expression. The imaginary part of the dielectric function, or the optical conductivity, or the $k$ spectrum, exhibited a Drude region and the expected weak interband-absorption threshold at about 2 eV, but there was a lower-energy, temperature-dependent absorption threshold and peak, at about 1.2 and 1.8 eV, respectively. This anomalous peak has proven to be only intermittently reproducible over the years. For example, Payan and Roux [5] found such a peak in Na films, and the peak position depended on film thickness and temperature. Many of the references cited here did not find this peak, although not all carried their measurements to long-enough wavelengths. This peak is discussed in a previous section on alkali metals in general, and we view it here as anomalous, and possibly spurious, despite the extensive theoretical effort it engendered.

Althoff and Hertz [6] made the only measurements to date at wavelengths longer than 2.5 μm, using an ellipsometric method on the Na–NaCl interface over the 2.5–10 μm region. However, their samples were evaporated in vacua of $10^{-6}$ torr, and their spectra do not agree well with any spectra measured at shorter wavelengths on samples prepared in ultrahigh vacuum.

Smith [7] measured the optical properties of Na films at the Na–silica interface by ellipsometry in the 0.5–4.0 eV spectral region. The interband-absorption threshold was found to be 2.0 eV. Drude parameters were obtained at lower energies. There was no anomalous absorption structure, but the fit to the Drude parameters required a scattering rate that had a term that increased with photon energy, but when plotted as a function of the square of the energy, the expected straight line did not result. Drude parameters are listed in Table I.

Palmer and Schnatterly [8] also used an ellipsometric method on films condensed on sapphire substrates at 77 K. (Other substrates gave rough surfaces that obviously scattered incident light.) They covered the spectral range 1.75–4.5 eV. They also fit $\varepsilon_1$ data to the Drude model. Their optical-conductivity data resembled those of Smith, but agreement was not good in both the Drude and interband regions. They made some measurements at the Na–glass interface. The resultant conductivity spectrum resembled that of Smith more closely in both spectral shape and magnitude. The difference between data at the Na–vacuum and Na–silica or glass interface thus appears to be real, and the explanation is likely to be found in an effective-medium approach to both sets of data. The free surface may be rough to a degree depending on the substrate materials and temperature. The Na–substrate interface may have regions of low density or even

voids between grains nucleated at separate sites.

Monin and Boutry [9] made ellipsometric measurements between 0.24 μm and 0.63 μm on the vacuum–Na interface of films that were condensed at 77 K. They found that upon warming to room temperature, then cooling to 77 K, the optical properties at this temperature had changed irreversibly, evidently due to annealing at room temperature, which led to increased grain size. Their results for both $n$ and $k$ are quite close to those of Smith, although they used the Na–vacuum interface, unlike Smith.

Bösenberg [10] made measurements on the Na–silica interface by attenuated total reflection in the 2–3.8 eV region. His optical-conductivity spectrum does not show much evidence for the expected interband transitions beginning at about 2 eV. Inagaki *et al.* [11] also made ellipsometric measurements on the Na–silica interface in the 0.6–3.8 eV region. Their results are close to those of Smith. Their interband peak in the optical conductivity is somewhat higher and narrower than Smith's.

Sutherland *et al.* [12, 13] made measurements in the vacuum ultraviolet. They first measured spectra of $n$ on the Na–vacuum interface in the region 420–2000 Å by fitting the reflected radiation near the critical angle ($n$ is less than unity in this spectral region) as a function of angle to the Fresnel equations and by using interference fringes in the reflected signal [12]. These data do not scatter much about a curve drawn through them. They then determined the $k$ spectrum of semitransparent Na films from transmission measurements in the region of 2.8–11 eV [13]. At the longer wavelengths, their data are significantly lower than those of Smith and the later data of Inagaki *et al.* Above 6 eV, there is a great deal of scatter in the $k$ spectrum, and its general shape does not interpolate well between the spectra of Smith and Inagaki *et al.* at longer wavelengths, and of Sato *et al.* [14] at shorter.

Sato *et al.* [14] measured the absorption coefficient of Na films in the 10–35 eV region. By assuming $n$ is unity throughout this region, an assumption good to within a few percent in this region [12], they obtained an optical-conductivity spectrum, hence a spectrum of $k$. We reproduce their values in our tables, but with one exception. Between 30 and 31 eV, there is a sharp absorption edge terminating in two sharp peaks arising from the excitation of the spin-orbit-split $2p$ electrons. We do not reproduce these narrow features in Table II and Fig. 1.

The infrared data of Althoff and Hertz do not match any of the other data in the region of overlap around 2 μm. In particular, at 2 μm there is a jump in the value of $k$ from about 9 in the data of Smith and of Inagaki *et al.* to 11 in the data of Althoff and Hertz. Thus, there are no recommended infrared data, and one must resort to the Drude parameters of Table I. These do not scatter badly, but at increasing wavelength the optical constants calculated from different sets will diverge somewhat. No reliable

values of the scattering time exist, for these have been sample-dependent. Without such data one can calculate only $\varepsilon_1 = n^2 - k^2$. Since $k \gg n$ in this region, one can calculate $k$ but not $n$ from the parameters in Table I. As with Li, Drude parameters determined from data in the ultraviolet are not given below.

In the visible region, we believe the data of Smith and Inagaki *et al.* are the most reliable and physically reasonable. They differ primarily in the height and width of the weak interband-absorption peak in the optical conductivity. We list those of Smith. At shorter wavelengths, the $n$ data of Sutherland *et al.* are listed, but not their $k$ values, which scatter considerably and do not match with other data at either end of their spectral range. At the shortest wavelengths, the $k$ data of Sato *et al.* are listed, assuming $n$ is within a few percent of unity. There are no data at all in the 2000–3000 Å region, and the data sets listed do not extrapolate toward each other satisfactorily across this gap, especially the $n$ spectrum, which has a minimum in the region for which no data exist.

We have calculated $n$ and $k$ in the 1.24–240 Å (10,000–51.5 eV) region using the model of Henke *et al.* [15]. The atomic absorption edges are $K$ (1072 eV), $L_1$ (63 eV), $L_{2,3}$ (31 eV). Some of these features are indicated in Fig. 1.

We used 8065.48 $cm^{-1}/eV$ to convert between units in [15]. Note that the conversion factors for [7], [12], [14] are slightly different by a digit or two in the fourth significant figure.

## REFERENCES


1. C. S. Barrett, *Acta Cryst.* **9**, 671 (1956).
2. J. N. Hodgson, *J. Phys. Chem. Solids* **24**, 1213 (1963).
3. J. N. Hodgson, *Phys. Lett.* **7**, 300 (1963).
4. H. Mayer and B. Heitel, in "Proceedings of the International Colloquium on the Optical Properties and Electronic Structure of Metals and Alloys," (F. Abeles, ed.), North-Holland, Amsterdam, 47 (1966).
5. R. Payan and D. Roux, *Opt. Commun.* **1**, 37 (1969).
6. R. Althoff and J. H. Hertz, *Infrared Physics* **7**, 11 (1967).
7. N. V. Smith, *Phys. Rev.* **183**, 634 (1969).
8. R. E. Palmer and S. E. Schnatterly, *Phys. Rev.* **B4**, 2329 (1971).
9. J. Monin and G.-A. Boutry, *Phys. Rev.* **B9**, 1309 (1974).
10. J. Bösenberg, *Z. Physik* **22**, 261 (1975).
11. T. Inagaki, L. T. Emerson, E. T. Arakawa, and M. W. Williams, *Phys. Rev.* **B13**, 2305 (1976).
12. J. C. Sutherland, E. T. Arakawa, and R. Hamm, *J. Opt. Soc. Am.* **57**, 645 (1967).
13. J. C. Sutherland, R. N. Hamm, and E. T. Arakawa, *J. Opt. Soc. Am.* **59**, 1581 (1969).
14. S. Sato, T. Miyahara, T. Hanyu, S. Yamaguchi, and T. Ishii, *J. Phys. Soc. Japan* **47**, 846 (1979).
15. B. L. Henke, J. C. Davis, E. M. Gullikson and R. C. C. Perera, Lawrence Berkeley Laboratory Report No. LBL-26259 (1988).

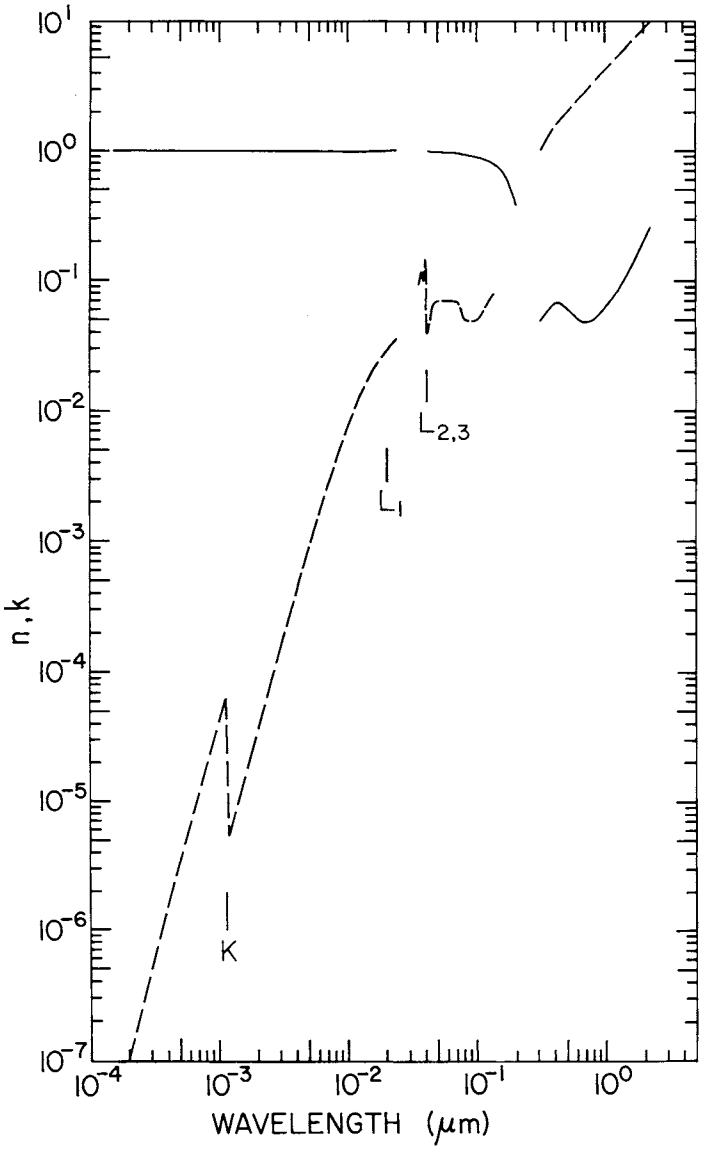


**Fig. 1.** Log–log plot of $n$ (solid line) and $k$ (dashed line) versus wavelength in micrometers for sodium.

**TABLE I**

**Drude-Model Parameters from Various References**

| Ref. | $\varepsilon_\infty$ | $\tau$ ($10^{-14}$ sec) | $\beta$ ($10^{-14}$ sec eV$^{-2}$) | $\omega_p$ (eV) | $m^*/m$ |
|---|---|---|---|---|---|
| [2,3] | 0.1 | 2.45 | | 5.94 | 1.08 |
| [4] | 0.15 | | | | 1.27 |
| [6] | | 1.85 | | | 0.99 |
| [7] | 0 | 2.4 | [a] | 5.65 | 1.13 |
| [8] | 0.34 | 2.4 | | 5.4 | 1.00 |
| [9] | 0.04 | | | 5.61 | 1.07 |
| [10] | 0.15 | | | 5.77 | 1.09 |
| [11] | 0.1 | | | 5.6 | 1.07 |

[a] A plot of $\tau$ versus $\omega$ is given, but replotting shows that the scattering rate does not increase as the square of the frequency, but somewhat faster.

**TABLE II**

**Values of $n$ and $k$ Obtained from Various References for Sodium[a]**

| eV | $cm^{-1}$ | Å | $n$ | $k$ |
|---|---|---|---|---|
| 10000 | | 1.240 | 0.9999980 [15] | 1.38E-08 [15] |
| 9549 | | 1.298 | 0.9999979 | 1.66E-08 |
| 9117 | | 1.360 | 0.9999977 | 2.00E-08 |
| 8706 | | 1.424 | 0.9999974 | 2.41E-08 |
| 8313 | | 1.492 | 0.9999972 | 2.91E-08 |
| 7937 | | 1.562 | 0.9999969 | 3.50E-08 |
| 7579 | | 1.636 | 0.9999966 | 4.21E-08 |
| 7237 | | 1.713 | 0.9999962 | 5.07E-08 |
| 6910 | | 1.794 | 0.9999959 | 6.09E-08 |
| 6598 | | 1.879 | 0.9999955 | 7.33E-08 |
| 6300 | | 1.968 | 0.9999951 | 8.81E-08 |
| 6015 | | 2.061 | 0.9999946 | 1.06E-07 |
| 5744 | | 2.159 | 0.9999940 | 1.27E-07 |
| 5484 | | 2.261 | 0.9999934 | 1.53E-07 |
| 5237 | | 2.368 | 0.9999928 | 1.83E-07 |
| 5000 | | 2.480 | 0.9999921 | 2.20E-07 |
| 4775 | | 2.597 | 0.9999914 | 2.64E-07 |
| 4559 | | 2.720 | 0.9999905 | 3.16E-07 |
| 4353 | | 2.848 | 0.9999896 | 3.79E-07 |
| 4157 | | 2.983 | 0.9999885 | 4.54E-07 |
| 3969 | | 3.124 | 0.9999874 | 5.44E-07 |
| 3790 | | 3.272 | 0.9999862 | 6.52E-07 |
| 3619 | | 3.426 | 0.9999848 | 7.80E-07 |
| 3455 | | 3.588 | 0.9999833 | 9.32E-07 |
| 3299 | | 3.758 | 0.9999816 | 1.12E-06 |
| 3150 | | 3.936 | 0.9999799 | 1.33E-06 |
| 3008 | | 4.122 | 0.9999779 | 1.59E-06 |
| 2872 | | 4.317 | 0.9999757 | 1.90E-06 |
| 2742 | | 4.521 | 0.9999734 | 2.26E-06 |
| 2619 | | 4.735 | 0.9999708 | 2.70E-06 |
| 2500 | | 4.959 | 0.9999680 | 3.22E-06 |
| 2387 | | 5.193 | 0.9999649 | 3.83E-06 |
| 2280 | | 5.439 | 0.9999616 | 4.55E-06 |
| 2177 | | 5.696 | 0.9999579 | 5.41E-06 |
| 2078 | | 5.965 | 0.9999539 | 6.43E-06 |
| 1985 | | 6.248 | 0.9999496 | 7.62E-06 |
| 1895 | | 6.543 | 0.9999450 | 9.02E-06 |
| 1809 | | 6.852 | 0.9999400 | 1.07E-05 |
| 1728 | | 7.176 | 0.9999346 | 1.26E-05 |
| 1650 | | 7.516 | 0.9999289 | 1.49E-05 |
| 1575 | | 7.871 | 0.9999228 | 1.76E-05 |
| 1504 | | 8.244 | 0.9999164 | 2.08E-05 |
| 1436 | | 8.633 | 0.9999099 | 2.45E-05 |
| 1371 | | 9.041 | 0.9999032 | 2.88E-05 |

[a]The references from which the values were extracted are given in brackets.

TABLE II (*Continued*)

Sodium

| eV | $cm^{-1}$ | Å | *n* | *k* |
|---|---|---|---|---|
| 1309 | | 9.469 | 0.999897 | 3.40E-05 |
| 1250 | | 9.917 | 0.999891 | 4.01E-05 |
| 1194 | | 10.39 | 0.999887 | 4.73E-05 |
| 1140 | | 10.88 | 0.999888 | 5.58E-05 |
| 1114 | | 11.13 | 0.999893 | 6.06E-05 |
| 1088 | | 11.39 | 0.9999092 | 6.58E-05 |
| 1064 | | 11.66 | 0.9999223 | 4.76E-06 |
| 1039 | | 11.93 | 0.999891 | 5.20E-06 |
| 1016 | | 12.21 | 0.999874 | 5.68E-06 |
| 992.3 | | 12.49 | 0.999861 | 6.21E-06 |
| 947.5 | | 13.09 | 0.999838 | 7.42E-06 |
| 904.7 | | 13.70 | 0.999816 | 8.84E-06 |
| 863.9 | | 14.35 | 0.999793 | 1.05E-05 |
| 824.9 | | 15.03 | 0.999769 | 1.25E-05 |
| 787.7 | | 15.74 | 0.999743 | 1.48E-05 |
| 752.1 | | 16.49 | 0.999715 | 1.76E-05 |
| 718.1 | | 17.27 | 0.999684 | 2.09E-05 |
| 685.7 | | 18.08 | 0.999651 | 2.47E-05 |
| 654.7 | | 18.94 | 0.999614 | 2.93E-05 |
| 625.1 | | 19.83 | 0.999574 | 3.47E-05 |
| 596.9 | | 20.77 | 0.999530 | 4.07E-05 |
| 570.0 | | 21.75 | 0.999482 | 4.80E-05 |
| 544.0 | | 22.78 | 0.999429 | 5.65E-05 |
| 519.7 | | 23.86 | 0.999371 | 6.66E-05 |
| 496.2 | | 24.99 | 0.999306 | 7.85E-05 |
| 473.8 | | 26.17 | 0.999236 | 9.25E-05 |
| 452.4 | | 27.41 | 0.999159 | 1.09E-04 |
| 432.9 | | 28.70 | 0.999074 | 1.29E-04 |
| 412.5 | | 30.06 | 0.99898 | 1.52E-04 |
| 393.8 | | 31.48 | 0.99888 | 1.80E-04 |
| 376.1 | | 32.97 | 0.99877 | 2.12E-04 |
| 359.1 | | 34.53 | 0.99865 | 2.50E-04 |
| 342.9 | | 36.16 | 0.99851 | 2.95E-04 |
| 327.4 | | 37.87 | 0.99837 | 3.46E-04 |
| 312.6 | | 39.66 | 0.99821 | 4.06E-04 |
| 298.5 | | 41.54 | 0.99804 | 4.77E-04 |
| 285.0 | | 43.50 | 0.99785 | 5.60E-04 |
| 272.1 | | 45.56 | 0.99765 | 6.58E-04 |
| 259.9 | | 47.71 | 0.99744 | 7.71E-04 |
| 248.1 | | 49.97 | 0.99720 | 8.98E-04 |
| 236.9 | | 52.33 | 0.99695 | 1.04E-03 |
| 226.2 | | 54.81 | 0.99667 | 1.22E-03 |
| 216.0 | | 57.40 | 0.99638 | 1.41E-03 |
| 206.2 | | 60.12 | 0.99607 | 1.64E-03 |
| 196.9 | | 62.96 | 0.99575 | 1.91E-03 |

(*Continued*)

TABLE II (*Continued*)

Sodium

| eV | $cm^{-1}$ | Å | $n$ | $k$ |
|---|---|---|---|---|
| 188.0 | | 65.94 | 0.99540 | 2.20E-03 |
| 179.6 | | 69.05 | 0.99503 | 2.53E-03 |
| 171.4 | | 72.32 | 0.99463 | 2.91E-03 |
| 163.7 | | 75.74 | 0.99422 | 3.35E-03 |
| 156.3 | | 79.32 | 0.99380 | 3.85E-03 |
| 149.3 | | 83.07 | 0.99339 | 4.43E-03 |
| 142.5 | | 87.00 | 0.99298 | 5.03E-03 |
| 136.1 | | 91.11 | 0.99254 | 5.69E-03 |
| 129.9 | | 95.42 | 0.99209 | 6.45E-03 |
| 124.1 | | 99.94 | 0.99163 | 7.31E-03 |
| 118.5 | | 104.7 | 0.99119 | 8.27E-03 |
| 113.1 | | 109.6 | 0.99076 | 9.35E-03 |
| 108.0 | | 114.8 | 0.99040 | 1.06E-02 |
| 103.1 | | 120.2 | 0.99012 | 1.20E-02 |
| 98.47 | | 125.9 | 0.99009 | 1.34E-02 |
| 94.03 | | 131.9 | 0.99008 | 1.48E-02 |
| 89.78 | | 138.1 | 0.99011 | 1.64E-02 |
| 85.73 | | 144.6 | 0.99037 | 1.81E-02 |
| 81.85 | | 151.5 | 0.99082 | 1.96E-02 |
| 78.16 | | 158.6 | 0.99122 | 2.12E-02 |
| 74.63 | | 166.1 | 0.99173 | 2.29E-02 |
| 71.26 | | 174.0 | 0.99247 | 2.48E-02 |
| 68.04 | | 182.2 | 0.99376 | 2.65E-02 |
| 64.97 | | 190.8 | 0.99485 | 2.78E-02 |
| 62.04 | | 199.9 | 0.99591 | 2.92E-02 |
| 59.24 | | 209.3 | 0.99705 | 3.05E-02 |
| 56.56 | | 219.2 | 0.99825 | 3.21E-02 |
| 54.01 | | 229.6 | 0.999606 | 3.36E-02 |
| 51.57 | | 240.4 | 1.001 | 3.52E-02 |
| 34.0 | | 364.7 | | 1.0E-02 [14] |
| 33.0 | | 375.7 | | 1.0E-02 |
| 32.5 | | 381.5 | | 1.1E-02 |
| 32.3 | | 383.9 | | 1.2E-02 |
| 32.0 | | 387.5 | | 1.0E-02 |
| 31.6 | | 392.4 | | 1.0E-02 |
| 31.5 | | 393.6 | | 1.0E-02 |
| 31.0 | | 399.9 | | 1.2E-02 |
| 30.9 | | 401.2 | | 1.4E-02 |
| 30.8 | | 402.5 | | 1.2E-02 |
| 30.6 | | 405.2 | | 1.0E-02 |
| 30.0 | | 413.3 | | 4E-03 |
| 29.5 | | 420.3 | | 5E-03 |
| 29.0 | | 427.5 | | 5E-03 |
| 28.0 | | 443.0 | | 5E-03 |
| 27.0 | | 459.2 | | 6E-03 |

(*Continued*)

TABLE II (*Continued*)

Sodium

| eV | $cm^{-1}$ | Å | *n* | *k* |
|---|---|---|---|---|
| 26.5 | | 467.9 | | 7E-03 |
| 26.0 | | 476.9 | | 7E-03 |
| 25.0 | | 495.9 | | 7E-03 |
| 24.0 | | 516.6 | | 7E-03 |
| 23.0 | | 539.1 | | 7E-03 |
| 22.0 | | 563.6 | | 7E-03 |
| 21.0 | | 590.4 | | 7E-03 |
| 20.0 | | 619.9 | | 7E-03 |
| 19.0 | | 652.5 | | 7E-03 |
| 18.0 | | 688.8 | | 7E-03 |
| 17.0 | | 729.3 | | 7E-03 |
| 16.5 | | 751.4 | | 7E-03 |
| 16.0 | | 774.9 | | 6E-03 |
| 15.0 | | 826.6 | | 5E-03 |
| 14.0 | | 885.6 | | 5E-03 |
| 13.0 | | 953.7 | | 5E-03 |
| eV | $cm^{-1}$ | μm | *n* | *k* |
| 12.0 | 96786 | 0.1033 | | 5E-03 |
| 11.0 | 88720 | 0.1127 | | 6E-03 |
| 10.0 | 80655 | 0.1240 | | 7E-03 |
| 9.00 | 72589 | 0.1378 | | 8E-03 |
| 29.52 | | 0.0420 | 1.02 [12] | |
| 28.37 | | 0.0437 | 1.01 | |
| 27.68 | | 0.0448 | 1.01 | |
| 26.95 | | 0.0460 | 1.00 | |
| 25.51 | | 0.0486 | 0.993 | |
| 21.12 | | 0.0587 | 0.979 | |
| 18.10 | | 0.0685 | 0.964 | |
| 16.21 | | 0.0765 | 0.948 | |
| 15.46 | | 0.0802 | 0.942 | |
| 15.05 | | 0.0824 | 0.936 | |
| 14.83 | | 0.0836 | 0.934 | |
| 14.07 | | 0.0881 | 0.922 | |
| 13.73 | | 0.0903 | 0.917 | |
| 13.42 | | 0.0924 | 0.914 | |
| 13.05 | | 0.0950 | 0.913 | |
| 12.73 | | 0.0974 | 0.907 | |
| 11.83 | 95420 | 0.1048 | 0.887 | |
| 11.08 | 89366 | 0.1119 | 0.870 | |
| 10.20 | 82237 | 0.1216 | 0.843 | |
| 9.709 | 78309 | 0.1277 | 0.819 | |
| 9.143 | 73746 | 0.1357 | 0.800 | |
| 8.634 | 69638 | 0.1437 | 0.762 | |

(*Continued*)

TABLE II (*Continued*)

**Sodium**

| eV | $cm^{-1}$ | μm | *n* | *k* |
|---|---|---|---|---|
| 8.015 | 64641 | 0.1548 | 0.710 | |
| 7.847 | 63291 | 0.1579 | 0.700 | |
| 7.583 | 61162 | 0.1636 | 0.674 | |
| 7.328 | 59102 | 0.1691 | 0.641 | |
| 7.130 | 57504 | 0.1739 | 0.616 | |
| 6.888 | 55555 | 0.1799 | 0.574 | |
| 6.702 | 54054 | 0.1851 | 0.533 | |
| 6.526 | 52632 | 0.1899 | 0.485 | |
| 6.358 | 51282 | 0.1949 | 0.454 | |
| 6.199 | 50000 | 0.2000 | 0.390 | |
| 3.97 | 32020 | 0.3123 | 0.49E-01 [7] | 1.01 [7] |
| 3.71 | 29923 | 0.3342 | 0.55E-01 | 1.13 |
| 3.40 | 27423 | 0.3647 | 0.61E-01 | 1.33 |
| 3.20 | 25810 | 0.3875 | 0.65E-01 | 1.47 |
| 3.06 | 24680 | 0.4052 | 0.69E-01 | 1.54 |
| 2.95 | 23793 | 0.4203 | 0.68E-01 | 1.63 |
| 2.82 | 22745 | 0.4397 | 0.68E-01 | 1.76 |
| 2.64 | 21293 | 0.4696 | 0.66E-01 | 1.88 |
| 2.45 | 19760 | 0.5061 | 0.63E-01 | 2.07 |
| 2.27 | 18309 | 0.5462 | 0.59E-01 | 2.23 |
| 2.07 | 16696 | 0.5990 | 0.53E-01 | 2.48 |
| 1.87 | 15082 | 0.6630 | 0.49E-01 | 2.76 |
| 1.65 | 13308 | 0.7514 | 0.50E-01 | 3.22 |
| 1.44 | 11614 | 0.8610 | 0.53E-01 | 3.72 |
| 1.23 | 9921 | 1.008 | 0.64E-01 | 4.35 |
| 1.05 | 8469 | 1.181 | 0.78E-01 | 5.11 |
| 0.920 | 7420 | 1.348 | 0.99E-01 | 5.82 |
| 0.810 | 6533 | 1.531 | 0.123 | 6.67 |
| 0.730 | 5888 | 1.698 | 0.147 | 7.42 |
| 0.670 | 5404 | 1.851 | 0.175 | 8.09 |
| 0.630 | 5081 | 1.968 | 0.207 | 8.80 |
| 0.580 | 4678 | 2.138 | 0.241 | 9.45 |
| 0.550 | 4436 | 2.254 | 0.262 | 9.97 |

## V POTASSIUM (K)

Potassium is a reactive metal that does not have a phase transition at low temperature. However, it has a low melting point. Room temperature is adequate for significant atomic motion to take place, which reduces strains at the surface, but may roughen the surface.

The first modern measurements on K were those of Hodgson [1], Mayer and El Naby [2, 3], and Mayer and Heitel [4]. Hodgson made ellipsometric measurements between 0.6 μm and 2.5 μm on the K–silica interface. He

fitted the real part of the dielectric function to a Drude model. The imaginary part varied by about a factor of two from film to film. He did not see the anomalous, low-energy, interband peak reported by Mayer *et al.*, who made ellipsometric measurements on the K-vacuum interface of bulk K samples. Mayer *et al.* fitted the real part of the dielectric function to a Drude expression. The imaginary part, or the optical conductivity, became well-known for many years because of a strong anomalous structure, an apparent interband-absorption peak beginning at about 1 eV, in addition to the expected one, which begins near 2.5 eV. Further discussion appears in the section on alkali metals. We consider the peak anomalous.

Althoff and Hertz [5] made the only measurements to date at wavelengths longer than 2.5 μm, using an ellipsometric method on K–NaCl and K–KBr interfaces over the 2.5–10 μm region. However, their samples were evaporated in vacua of $10^{-6}$ torr, and their spectra do not agree well with any spectra measured at shorter wavelengths on samples prepared in ultrahigh vacuum.

Smith [6] made ellipsometric measurements between 0.5 and 4.0 eV on the K–silica interface and obtained no anomalous peak. The interband threshold was at 1.3 eV, and the interband-absorption spectrum was in accord with theoretical expectations. Drude parameters were obtained from the data at lower energy. A frequency-dependent scattering rate resulted, but it increased with increasing photon energy faster than the expected second power.

Palmer and Schnatterly [7] also used an ellipsometric method between 1.75 and 4.5 eV on the K–vacuum interface. Their data do not agree well with those of Smith. They did not go to low enough energy to see the interband-absorption threshold.

Yamaguchi and Hanyu [8] made photometric measurements in the 2.07–6.2 eV region on semitransparent films. They measured the transmission and the reflectance from both the K–vacuum and K–silica sides, using polarized radiation and several angles of incidence. Their Drude parameters are listed here. The optical conductivity depended somewhat on sample thickness, but generally was close to that of Smith. The low-energy limit did not permit measurements at the interband threshold.

Harms [9] repeated the measurements of El Naby [3], using essentially the same techniques. The measurements spanned the 0.25–2.5 μm range. He did not find the anomalous peak in most of his measurements, but did detect it when some water vapor had been admitted to the vacuum. His and others' Drude parameters are listed in Table I. The interband conductivity was close to that of Smith; Harm's interband peak was a bit less sharp.

Monin and Boutry [10] made ellipsometric measurements on the K–silica interface in the 2500–6300 Å range. Their lowest energy is not low enough to allow observing the interband threshold, but their data appear

to have a threshold, and certainly a peak, in the interband region much higher in energy than expected and much higher than in Smith's data.

Sutherland and Arakawa [11] measured $n$ in the 3.96–9.69 eV region by the critical-angle method on the K–quartz and K–fluorite interfaces. Sutherland *et al.* [12] measured the $k$ spectrum from transmission measurements of K films on quartz of LiF substrates. They report only a few points between 3.9 eV and 7.1 eV. Their work was superseded by that of Whang *et al.* [13], who covered the 3.3–10.7 eV range. They measured reflectance versus angle of incidence on the K–$MgF_2$ interface, and transmission of semitransparent films. Their optical-conductivity spectrum matches Smith's fairly well and lies generally somewhat below those of Palmer and Schnatterly, Sutherland, and Yamaguchi and Hanyu. A second interband-absorption structure begins at about 4 eV, and peaks at 8 eV. Its origin is likely to be transitions to $d$-like states several eV above the Fermi level, but convincing proof is lacking.

Garron [14] showed that surface states may be responsible for some of the discrepancies in the near-infrared data, in particular for differences between data on K–vacuum and K–quartz interfaces. More discussion of these surface states appears in the general section on alkali metals.

Sato *et al.* [15] measured transmission spectra, which give spectra of $k$ under the assumption that $n$ is unity, an assumption valid in the 9.5–32 eV spectral region covered. We tabulate them in Table II, but do not list points close enough together to give a good representation of the $3p$ absorption edge just above 18 eV. The $n$ and $k$ spectra are plotted in Fig. 1.

The data for wavelengths longer than 2.5 μm do not match any data at shorter wavelengths, so for this region it is necessary to extrapolate with the Drude parameters given in Table I. As with Na, this is fairly reliably done for $\varepsilon_1$, which means that the $k$ spectrum can be reliably obtained, but the $n$ spectrum cannot because of the imprecise and sample-dependent values of $\varepsilon_2$ (and, hence, the relaxation time). For the near infrared, visible, and near ultraviolet, we list Smith's data in Table II, which are close to several other spectra reported, as noted above. Further in the ultraviolet, we list the data of Whang *et al.* and Sato *et al.* Unfortunately, Smith's and Whang *et al.*'s data do not overlap. They both end at about 3250 Å, where there is a peak in $k$ and a minimum in $n$, and there are no data points at these structures.

We have calculated $n$ and $k$ in the 1.24–240 Å (10,000–51.5 eV) region using the model of Henke *et al.* [16]. The atomic absorption edges are $K$ (3608 eV), $L_1$ (377 eV), $L_{2,3}$ (297, 294 eV), $M_1$ (34 eV), $M_{2,3}$ (18 eV). Some of these features are indicated in Fig. 1.

We used 8065.48 $cm^{-1}$/eV to convert among the units of [16], whereas the conversion factor is slightly different for other data in Table II (usually by a digit or two in the fourth figure). This should not present any problems among the units until the fourth figure.

## REFERENCES


1. J. Hodgson, *Phys. Lett.* **7**, 300 (1963).
2. H. Mayer and M. H. El Naby, *Z. Physik* **174**, 269 (1963).
3. M. H. El Naby, *Z. Physik* **174**, 280 (1963).
4. H. Mayer and B. Heitel, in "Proceedings of the International Colloquium on the Optical Properties and Electronic Structure of Metals and Alloys," (F. Abeles, ed.) North-Holland, Amsterdam, 47 (1966).
5. R. Althoff and J. H. Hertz, *Infrared Phys.* **7**, 11 (1967).
6. N. V. Smith, *Phys. Rev.* **183**, 634 (1969).
7. R. E. Palmer and S. E. Schnatterly, *Phys. Rev.* **B4**, 2329 (1971).
8. S. Yamaguchi and T. Hanyu, *J. Phys. Soc. Japan* **31**, 1431 (1971).
9. P. Harms, dissertation, Technische Universitaet Clausthal, 1972.
10. J. Monin and G.-A. Boutry, *Phys. Rev.* **B9**, 1309 (1974).
11. J. C. Sutherland and E. T. Arakawa, *J. Opt. Soc. Am.* **58**, 1080 (1968).
12. J. C. Sutherland, R. N. Hamm, and E. T. Arakawa, *J. Opt. Soc. Am.* **59**, 1581 (1969).
13. U. S. Whang, E. T. Arakawa, and T. A. Callcott, *Phys. Rev.* **B6**, 2109 (1972).
14. R. Garron, *Appl. Opt.* **20**, 1747 (1981).
15. S. Sato, T. Miyahara, T. Hanyu, S. Yamaguchi, and T. Ishii, *J. Phys. Soc. Japan* **47**, 836 (1979).
16. B. L. Henke, J. C. Davis, E. M. Gullikson, and R. C. C. Perera, Lawrence Berkeley Laboratory Report No. LBL-26259 (1988).

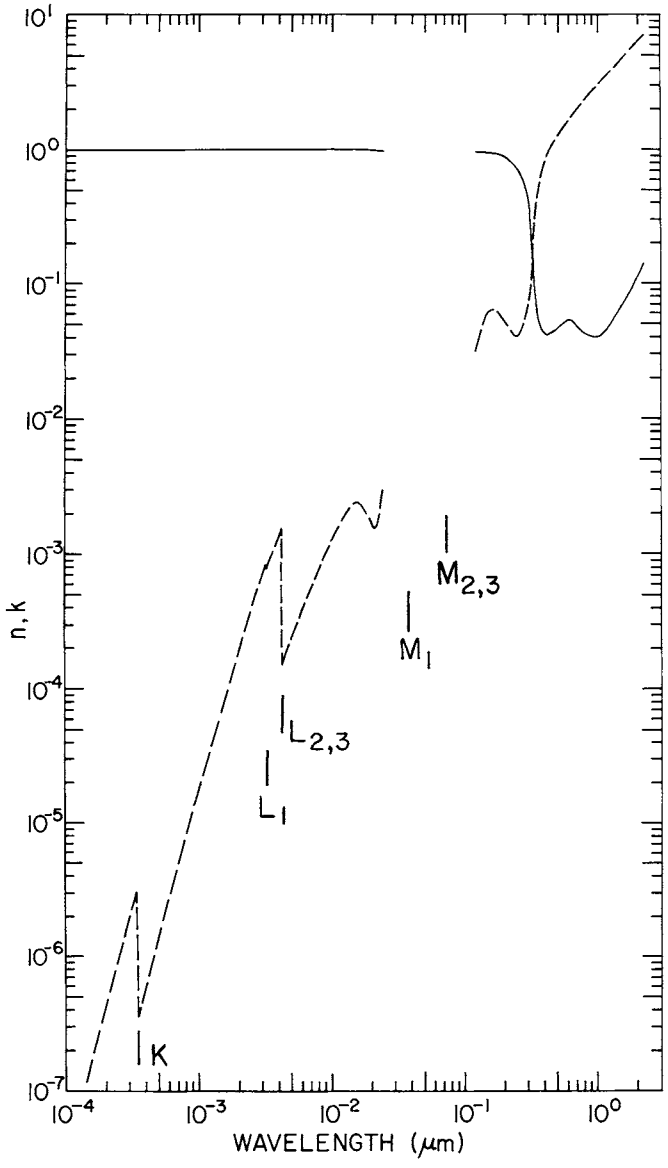


**Fig. 1.** Log–log plot of $n$ (solid line) and $k$ (dashed line) versus wavelength in micrometers for potassium.

**TABLE I**

**Drude-Model Parameters from Various References**

| Ref. | $\varepsilon_\infty$ | $\tau$ ($10^{-14}$ sec) | $\beta$ ($10^{-14}$ sec eV$^{-2}$) | $\omega_p$ (eV) | $m^*/m$ |
|---|---|---|---|---|---|
| [1] | 0 | 1.58 | | | 1.16 |
| [3] | 0.11 | | | | 1.00 |
| [5] | | 1.55 | | | 1.17 |
| [6] | 0.20 | 3.3 | [a] | 3.80 | 1.16 |
| [7] | | 3.2 | | 3.8 | 1.08 |
| [8] | 0.14 | | | 4.15 | 1.05 |
| [9] | 0.15 | 4.4 | | 3.87 | 1.11 |
| [10] | 0.20 | | | 3.79 | 1.08 |

[a] A plot of $\tau$ vs. $\omega$ is given, but replotting shows that the scattering rate does not increase as the square of the freqeuncy, but somewhat faster.

TABLE II

Values of $n$ and $k$ Obtained from Various References for Potassium[a]

| eV | $cm^{-1}$ | Å | $n$ | $k$ |
|---|---|---|---|---|
| 10000 | | 1.240 | 0.9999982 [16] | 7.02E-08 [16] |
| 9549 | | 1.298 | 0.9999980 | 8.10E-08 |
| 9117 | | 1.360 | 0.9999979 | 9.63E-08 |
| 8706 | | 1.424 | 0.9999977 | 1.15E-07 |
| 8313 | | 1.492 | 0.9999974 | 1.38E-07 |
| 7937 | | 1.562 | 0.9999972 | 1.65E-07 |
| 7579 | | 1.636 | 0.9999969 | 1.97E-07 |
| 7237 | | 1.713 | 0.9999966 | 2.34E-07 |
| 6910 | | 1.794 | 0.9999963 | 2.78E-07 |
| 6598 | | 1.879 | 0.9999959 | 3.30E-07 |
| 6300 | | 1.968 | 0.9999955 | 3.92E-07 |
| 6015 | | 2.061 | 0.9999951 | 4.66E-07 |
| 5744 | | 2.159 | 0.9999946 | 5.53E-07 |
| 5484 | | 2.261 | 0.9999942 | 6.57E-07 |
| 5237 | | 2.368 | 0.9999936 | 7.80E-07 |
| 5000 | | 2.480 | 0.9999931 | 9.25E-07 |
| 4775 | | 2.597 | 0.9999924 | 1.10E-06 |
| 4559 | | 2.720 | 0.9999918 | 1.30E-06 |
| 4353 | | 2.848 | 0.9999911 | 1.55E-06 |
| 4157 | | 2.983 | 0.9999905 | 1.83E-06 |
| 3969 | | 3.124 | 0.9999899 | 2.18E-06 |
| 3790 | | 3.272 | 0.9999895 | 2.58E-06 |
| 3703 | | 3.348 | 0.9999896 | 2.81E-06 |
| 3619 | | 3.426 | 0.9999905 | 3.06E-06 |
| 3536 | | 3.506 | 0.9999891 | 3.50E-07 |
| 3455 | | 3.588 | 0.9999880 | 3.81E-07 |
| 3299 | | 3.758 | 0.9999862 | 4.52E-07 |
| 3150 | | 3.936 | 0.9999844 | 5.35E-07 |
| 3008 | | 4.122 | 0.9999827 | 6.34E-07 |
| 2872 | | 4.317 | 0.9999808 | 7.54E-07 |
| 2742 | | 4.521 | 0.9999787 | 8.96E-07 |
| 2619 | | 4.735 | 0.9999765 | 1.07E-06 |
| 2500 | | 4.959 | 0.9999741 | 1.27E-06 |
| 2387 | | 5.193 | 0.9999714 | 1.51E-06 |
| 2280 | | 5.439 | 0.9999685 | 1.79E-06 |
| 2177 | | 5.696 | 0.9999653 | 2.12E-06 |
| 2078 | | 5.965 | 0.9999618 | 2.52E-06 |
| 1985 | | 6.248 | 0.9999579 | 2.99E-06 |
| 1895 | | 6.543 | 0.9999537 | 3.55E-06 |
| 1809 | | 6.852 | 0.9999490 | 4.21E-06 |
| 1728 | | 7.176 | 0.9999440 | 5.00E-06 |
| 1650 | | 7.516 | 0.9999384 | 5.92E-06 |
| 1575 | | 7.871 | 0.9999322 | 7.00E-06 |

[a]The references from which the values were extracted are given in brackets.

TABLE II (*Continued*)

Potassium

| eV | $cm^{-1}$ | Å | *n* | *k* |
|---|---|---|---|---|
| 1504 | | 8.244 | 0.9999255 | 8.27E-06 |
| 1436 | | 8.633 | 0.9999181 | 9.77E-06 |
| 1371 | | 9.041 | 0.9999100 | 1.15E-05 |
| 1309 | | 9.469 | 0.9999011 | 1.36E-05 |
| 1250 | | 9.917 | 0.999891 | 1.61E-05 |
| 1194 | | 10.39 | 0.999881 | 1.90E-05 |
| 1140 | | 10.88 | 0.999869 | 2.23E-05 |
| 1088 | | 11.39 | 0.999857 | 2.63E-05 |
| 1039 | | 11.93 | 0.999843 | 3.09E-05 |
| 992.3 | | 12.49 | 0.999828 | 3.64E-05 |
| 947.5 | | 13.09 | 0.999812 | 4.23E-05 |
| 904.7 | | 13.70 | 0.999794 | 4.89E-05 |
| 863.9 | | 14.35 | 0.999774 | 5.64E-05 |
| 824.9 | | 15.03 | 0.999752 | 6.66E-05 |
| 787.7 | | 15.74 | 0.999728 | 7.86E-05 |
| 752.1 | | 16.49 | 0.999703 | 9.27E-05 |
| 718.1 | | 17.27 | 0.999677 | 1.09E-04 |
| 685.7 | | 18.08 | 0.999649 | 1.29E-04 |
| 654.7 | | 18.94 | 0.999619 | 1.50E-04 |
| 625.1 | | 19.83 | 0.999587 | 1.75E-04 |
| 596.9 | | 20.77 | 0.999553 | 2.04E-04 |
| 570.0 | | 21.75 | 0.999518 | 2.38E-04 |
| 544.0 | | 22.78 | 0.999482 | 2.78E-04 |
| 519.7 | | 23.86 | 0.999447 | 3.24E-04 |
| 496.2 | | 24.99 | 0.999411 | 3.76E-04 |
| 473.8 | | 26.17 | 0.999378 | 4.38E-04 |
| 452.4 | | 27.41 | 0.999352 | 5.08E-04 |
| 432.9 | | 28.70 | 0.999331 | 5.81E-04 |
| 412.5 | | 30.06 | 0.999317 | 6.64E-04 |
| 393.8 | | 31.48 | 0.999319 | 7.59E-04 |
| 376.1 | | 32.97 | 0.999388 | 7.84E-04 |
| 359.1 | | 34.53 | 0.999331 | 9.01E-04 |
| 342.9 | | 36.16 | 0.999361 | 1.04E-03 |
| 327.4 | | 37.87 | 0.999454 | 1.19E-03 |
| 312.6 | | 39.66 | 0.999676 | 1.36E-03 |
| 305.5 | | 40.59 | 0.999883 | 1.45E-03 |
| 298.5 | | 41.54 | 1.000338 | 1.54E-03 |
| 291.7 | | 42.51 | 1.001052 | 1.53E-04 |
| 285.0 | | 43.50 | 1.000136 | 1.63E-04 |
| 278.5 | | 44.52 | 0.999882 | 1.74E-04 |
| 272.1 | | 45.56 | 0.999709 | 1.85E-04 |
| 259.9 | | 47.71 | 0.999460 | 2.10E-04 |
| 248.1 | | 49.97 | 0.999259 | 2.38E-04 |
| 236.9 | | 52.33 | 0.999077 | 2.70E-04 |
| 226.2 | | 54.81 | 0.99890 | 3.06E-04 |

(*Continued*)

TABLE II (*Continued*)

**Potassium**

| eV | $cm^{-1}$ | Å | *n* | *k* |
|---|---|---|---|---|
| 216.0 | | 57.40 | 0.99872 | 3.46E-04 |
| 206.2 | | 60.12 | 0.99854 | 3.91E-04 |
| 196.9 | | 62.96 | 0.99834 | 4.41E-04 |
| 188.0 | | 65.94 | 0.99814 | 4.96E-04 |
| 179.6 | | 69.05 | 0.99792 | 5.55E-04 |
| 171.4 | | 72.32 | 0.99769 | 6.21E-04 |
| 163.7 | | 75.74 | 0.99745 | 6.96E-04 |
| 156.3 | | 79.32 | 0.99718 | 7.76E-04 |
| 149.3 | | 83.07 | 0.99690 | 8.60E-04 |
| 142.5 | | 87.00 | 0.99659 | 9.52E-04 |
| 136.1 | | 91.11 | 0.99625 | 1.05E-03 |
| 129.9 | | 95.42 | 0.99589 | 1.17E-03 |
| 124.1 | | 99.94 | 0.99551 | 1.29E-03 |
| 118.5 | | 104.7 | 0.99510 | 1.41E-03 |
| 113.1 | | 109.6 | 0.99464 | 1.53E-03 |
| 108.0 | | 114.8 | 0.99414 | 1.67E-03 |
| 103.1 | | 120.2 | 0.99359 | 1.82E-03 |
| 98.47 | | 125.9 | 0.99301 | 1.98E-03 |
| 94.03 | | 131.9 | 0.99236 | 2.12E-03 |
| 89.78 | | 138.1 | 0.99170 | 2.30E-03 |
| 85.73 | | 144.6 | 0.99096 | 2.38E-03 |
| 81.85 | | 151.5 | 0.99011 | 2.44E-03 |
| 78.16 | | 158.6 | 0.9891 | 2.44E-03 |
| 74.63 | | 166.1 | 0.9880 | 2.40E-03 |
| 71.26 | | 174.0 | 0.9866 | 2.26E-03 |
| 68.04 | | 182.2 | 0.9849 | 2.08E-03 |
| 64.97 | | 190.8 | 0.9828 | 1.91E-03 |
| 62.04 | | 199.9 | 0.9803 | 1.68E-03 |
| 59.24 | | 209.3 | 0.9772 | 1.57E-03 |
| 56.56 | | 219.2 | 0.9733 | 1.61E-03 |
| 54.01 | | 229.6 | 0.9685 | 1.97E-03 |
| 51.57 | | 240.4 | 0.9624 | 2.97E-03 |
| 32.0 | | 387.5 | | 4.8E-02 [15] |
| 31.0 | | 399.9 | | 5.2E-02 |
| 30.0 | | 413.3 | | 5.9E-02 |
| 29.0 | | 427.5 | | 6.8E-02 |
| 28.0 | | 442.8 | | 7.9E-02 |
| 27.0 | | 459.2 | | 9.2E-02 |
| 26.0 | | 476.9 | | 9.9E-02 |
| 25.0 | | 495.9 | | 0.100 |
| 24.0 | | 516.6 | | 9.7E-02 |
| 23.0 | | 539.1 | | 8.5E-02 |
| 22.5 | | 551.0 | | 7.9E-02 |
| 22.0 | | 563.6 | | 7.5E-02 |
| 21.5 | | 576.7 | | 7.5E-02 |

(*Continued*)

**TABLE II (*Continued*)**

**Potassium**

| eV | $cm^{-1}$ | Å | *n* | *k* |
|---|---|---|---|---|
| 21.0 | | 590.4 | | 6.8E-02 |
| 20.0 | | 619.9 | | 5.4E-02 |
| 19.0 | | 652.5 | | 4.3E-02 |
| 18.8 | | 659.5 | | 4.3E-02 |
| 18.5 | | 670.2 | | 5.1E-02 |
| 18.4 | | 673.8 | | 4.2E-02 |
| 18.3 | | 677.5 | | 4.7E-02 |
| 18.0 | | 688.8 | | 1.4E-02 |
| 17.5 | | 708.5 | | 1.2E-02 |
| 17.0 | | 729.3 | | 1.2E-02 |
| 16.0 | | 774.9 | | 1.4E-02 |
| 15.0 | | 826.6 | | 1.8E-02 |
| 14.0 | | 885.6 | | 2.5E-02 |
| 13.0 | | 953.7 | | 2.3E-02 |
| eV | $cm^{-1}$ | μm | *n* | *k* |
| 12.0 | 96786 | 0.1033 | | 2.8E-02 |
| 11.0 | 88720 | 0.1127 | | 3.1E-02 |
| 10.33 | 83333 | 0.120 | 0.94 [13] | 3E-02 [13] |
| 9.919 | 80000 | 0.125 | 0.94 | 4E-02 |
| 9.537 | 76923 | 0.130 | 0.94 | 4E-02 |
| 9.50 | 76622 | 0.1305 | | 5.0E-02 [15] |
| 9.184 | 74074 | 0.135 | 0.94 [13] | 5E-02 [13] |
| 8.856 | 71429 | 0.140 | 0.94 | 5E-02 |
| 8.551 | 68966 | 0.145 | 0.94 | 6E-02 |
| 8.26 | 66667 | 0.150 | 0.94 | 6E-02 |
| 7.999 | 64516 | 0.155 | 0.94 | 6E-02 |
| 7.749 | 62500 | 0.160 | 0.94 | 6E-02 |
| 7.514 | 60606 | 0.165 | 0.93 | 6E-02 |
| 7.293 | 58824 | 0.170 | 0.93 | 6E-02 |
| 7.085 | 57143 | 0.175 | 0.92 | 6E-02 |
| 6.888 | 55555 | 0.180 | 0.92 | 6E-02 |
| 6.702 | 54054 | 0.185 | 0.91 | 6E-02 |
| 6.526 | 52632 | 0.190 | 0.90 | 6E-02 |
| 6.358 | 51282 | 0.195 | 0.88 | 5E-02 |
| 6.199 | 50000 | 0.200 | 0.87 | 5E-02 |
| 6.048 | 48780 | 0.205 | 0.85 | 5E-02 |
| 5.767 | 46512 | 0.215 | 0.83 | 5E-02 |
| 5.637 | 45455 | 0.220 | 0.81 | 5E-02 |
| 5.510 | 44444 | 0.225 | 0.79 | 5E-02 |
| 5.391 | 43478 | 0.230 | 0.78 | 4E-02 |
| 5.276 | 42553 | 0.235 | 0.76 | 4E-02 |
| 5.166 | 41667 | 0.240 | 0.74 | 4E-02 |
| 5.061 | 40816 | 0.245 | 0.72 | 4E-02 |

(*Continued*)

TABLE II (*Continued*)

Potassium

| eV | $cm^{-1}$ | μm | *n* | *k* |
|---|---|---|---|---|
| 4.959 | 40000 | 0.250 | 0.70 | 4E-02 |
| 4.862 | 39216 | 0.255 | 0.68 | 4E-02 |
| 4.769 | 38462 | 0.260 | 0.66 | 4E-02 |
| 4.679 | 37736 | 0.265 | 0.64 | 4E-02 |
| 4.592 | 37037 | 0.270 | 0.61 | 5E-02 |
| 4.509 | 36364 | 0.275 | 0.58 | 5E-02 |
| 4.428 | 35714 | 0.280 | 0.55 | 5E-02 |
| 4.350 | 35088 | 0.285 | 0.52 | 5E-02 |
| 4.275 | 34483 | 0.290 | 0.48 | 6E-02 |
| 4.203 | 33898 | 0.295 | 0.45 | 6E-02 |
| 4.133 | 33333 | 0.300 | 0.41 | 7E-02 |
| 4.065 | 32787 | 0.305 | 0.38 | 7E-02 |
| 4.000 | 32258 | 0.310 | 0.34 | 8E-02 |
| 3.97 | 32020 | 0.3123 | 0.287 [6] | 9.10E-02 [6] |
| 3.71 | 29923 | 0.3342 | 8.9E-02 | 0.288 |
| 3.40 | 27423 | 0.3647 | 5.2E-02 | 0.549 |
| 3.06 | 24680 | 0.4052 | 4.1E-02 | 0.799 |
| 2.95 | 23793 | 0.4203 | 4.1E-02 | 0.898 |
| 2.82 | 22745 | 0.4397 | 4.3E-02 | 1.02 |
| 2.64 | 21293 | 0.4696 | 4.3E-02 | 1.14 |
| 2.45 | 19760 | 0.5061 | 4.6E-02 | 1.28 |
| 2.27 | 18309 | 0.5462 | 4.9E-02 | 1.43 |
| 2.07 | 16696 | 0.5990 | 5.3E-02 | 1.62 |
| 1.87 | 15082 | 0.6630 | 5.0E-02 | 1.84 |
| 1.65 | 13308 | 0.7514 | 4.4E-02 | 2.19 |
| 1.44 | 11614 | 0.8610 | 4.0E-02 | 2.56 |
| 1.23 | 9921 | 1.008 | 4.0E-02 | 3.04 |
| 1.05 | 8469 | 1.181 | 4.4E-02 | 3.58 |
| 0.92 | 7420 | 1.348 | 5.6E-02 | 4.19 |
| 0.81 | 6533 | 1.531 | 6.6E-02 | 4.75 |
| 0.73 | 5889 | 1.698 | 7.9E-02 | 5.30 |
| 0.67 | 5404 | 1.851 | 9.1E-02 | 5.79 |
| 0.63 | 5081 | 1.968 | 0.106 | 6.32 |
| 0.58 | 4678 | 2.138 | 0.119 | 6.72 |
| 0.55 | 4436 | 2.254 | 0.139 | 7.10 |

## VI CHROMIUM (Cr)

Chromium is a body-centered cubic metal. It is antiferromagnetic below 312 K. The magnetic ordering, the spatial period of which is incommensurate with the period of the crystal lattice, introduces structure in the spectra of the optical constants in the infrared [1–4]. Since the room-temperature phase of Cr is antiferromagnetic, our data include such structure. The ordering is usually multidomained, so bulk anisotropy does not develop. A single domain of antiferromagnetic Cr is slightly tetragonal, not cubic, but the anisotropy is small. Optical anisotropies due to the ordering [2] are

neglected here. One should also note that the type of antiferromagnetism (commensurate or incommensurate) may vary with the content of impurities, especially of other transition metals, and impurity concentrations of the order of 1% may raise or lower the transition temperature by many degrees [2, 3, and references therein].

Cr oxidizes readily, but the overlayer of $Cr_2O_3$ is continuous and impermeable to Cr or O after a thickness of about 30 Å is reached, and further oxidation does not occur at room temperature. Such an overlayer may affect optical constants in the visible and near infrared obtained by ellipsometry, and by any technique in the vacuum ultraviolet. There have been few studies in which the sample was both prepared and measured in ultrahigh vacuum.

In the visible, near infrared, and near ultraviolet, we report in Table 1 and Fig. 1 the data of Bos and Lynch [3], the result of a Kramers–Kronig analysis of low-temperature absorptance data on bulk samples. They agree well with the room-temperature data of Barker and Ditzenberger [2]. The data of Johnson and Christy [5] are often quoted. They were obtained from reflectance and transmittance measurements on semitransparent films. However, later work [6] showed that these films were rather fine-grained and porous, and new data were obtained on denser, larger-grained films [7]. The reflectance spectrum calculated from these new data agrees well with that derived from the data we quote below, but there are shifts in the individual spectra of $n$ and $k$.

In the vacuum ultraviolet, we list the data of Olson and Lynch [8]. These data and others in this spectral region [9] may be affected by the presence of an oxide overlayer, but data taken in this spectral region under UHV conditions do not yet exist. In the soft X-ray region, transmission data [10–12] give spectra of $k$ under the assumption that $n$ is unity. The region of the $3p$ absorption edge has been measured. We list the data of Sonntag *et al.* [12].

The measurements of Bos and Lynch extend to 13 μm in the infrared, although their Kramers–Kronig analysis extends further. A number of measurements extend to longer wavelengths [2, 13–21]. These measurements do not agree well with each other, and some of them show weak structures which are probably spurious. Because of this, it is not possible to select long-wavelength data that are reliable. Since Cr is a transition metal, interband transitions occur at arbitrarily long wavelengths, although their strength eventually becomes negligible with respect to the Drude (interband) contribution at wavelengths longer than some value. This appears to be about 20 μm or even longer [22] and makes fits to the Drude model suspect at shorter wavelengths.

We have calculated $n$ and $k$ in the 1.24–240 Å (10,000–51.5 eV) region using the model of Henke *et al.* [23]. The atomic absorption edges are $K$ (5989 eV), $L_1$ (695 eV), $L_{2,3}$ (584, 575 eV), $M_1$ (74 eV), $M_{2,3}$ (43 eV), $M_{4,5}$

(2 eV). These features, especially at the lower energies, will be shifted due to the bonding properties of the crystal.

We used 8065.48 $cm^{-1}$/eV to convert among the units of [23], whereas the conversion factor may be different by one or two digits in the fourth figure for the other data in Table I.

We list below several other reports of quantitative optical spectra for Cr [24–28].

## REFERENCES


1. A. S. Barker, B. I. Halperin, and T. M. Rice, *Phys. Rev. Lett.* **20**, 384 (1968).
2. A. S. Barker and J. A. Ditzenberger, *Phys. Rev.* **B1**, 4378 (1970).
3. L. W. Bos and D. W. Lynch, *Phys. Rev.* **B2**, 4567 (1970).
4. M. A. Lind and J. L. Stanford, *Phys. Lett.* **39A**, 5 (1972).
5. P. B. Johnson and R. W. Christy, *Phys. Rev.* **B9**, 5056 (1974).
6. J. E. Nestell, R. W. Christy, M. Cohen, and G. C. Ruben, *J. Appl. Phys.* **51**, 655 (1980).
7. J. E. Nestell and R. W. Christy, *Phys. Rev.* **B21**, 3173 (1980).
8. C. G. Olson and D. W. Lynch, unpublished (1980).
9. P. Girault, A. Seignac, M. Priol, and S. Robin, *Compt. Rend.* **266**, 688 (1968).
10. A. P. Lukirskii, E. P. Savinov, O. A. Ershov, and Y. F. Shepelev, *Opt. Spectrosc. (USSR)* **16**, 168 (1964); *Opt. Spektrosk.* **16**, 310 (1964).
11. E. P. Savinov, L. I. Lyakhovskaya, O. A. Ershov, and E. A. Kovalyeva, *Opt. Spectrosc. (USSR)* **27**, 179 (1969); *Opt. Spektrosk.* **27**, 342 (1969).
12. B. Sonntag, R. Haensel, and C. Kunz, *Solid State Commun.* **7**, 597 (1969).
13. A. P. Lenham and D. M. Treherne, *J. Opt. Soc. Am.* **56**, 1137 (1966).
14. A. P. Lenham and D. M. Treherne, in "Optical Properties and Electronic Structure of Metals and Alloys," (F. Abeles, ed.), North-Holland, Amsterdam, 196 (1966).
15. A. P. Lenham, *J. Opt. Soc. Am.* **57**, 473 (1967).
16. R. H. W. Graves and A. P. Lenham, *J. Opt. Soc. Am.* **58**, 884 (1968).
17. M. M. Kirillova and M. M. Noskov, *Phys. Met. Metall.* **26**, 189 (1969); *Fiz. Met. Metalloved.* **26**, 592 (1968).
18. A. S. Siddiqui and D. M. Treherne, *Infrared Phys.* **17**, 33 (1975).
19. N. Fuschillo, B. Lalevic, W. Suslark, and A. Delahoy, *J. Vac. Sci. Tech.* **12**, 84 (1975).
20. M. M. Kirillova and L. V. Nomerovannaya, *Phys. Met. Metall.* **40**, 69 (1975); *Fiz. Met. Metalloved.* **40**, 983 (1975).
21. M. M. Kirillova and L. V. Nomerovannaya, *Opt. Spectrosc. (USSR)* **39**, 303 (1975); *Opt. Spektrosk.* **39**, 540 (1975).
22. J. C. Jones, D. C. Palmer, and C. L. Tien, *J. Opt. Soc. Am.* **62**, 353 (1972).
23. B. L. Henke, J. C. Davis, E. M. Gullikson, and R. C. C. Perera, Lawrence Berkeley Laboratory Report No. LBL-26259 (1988).
24. Y. P. Udoev, *Opt. Spectrosc. (USSR)* **33**, 185 (1972); *Opt. Spektrosk.* **33**, 350 (1972).
25. M. R. Steel, *J. Phys. F* **4**, 783 (1974).
26. C. Wehenkel and B. Gauthé, *Phys. Lett.* **47A**, 253 (1974).
27. C. Wehenkel and B. Gauthé, *Phys. Stat. Solidi (b)* **64**, 515 (1974).
28. P. Gravier, G. Chassaing, and M. Sigrist, *Thin Solid Films* **57**, 93 (1979).

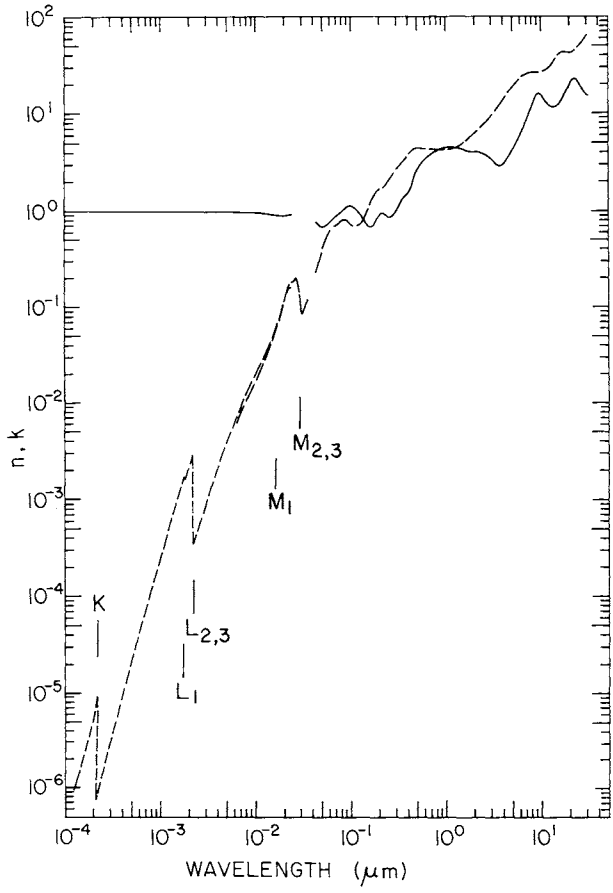


**Fig. 1.** Log–log plot of $n$ (solid line) and $k$ (dashed line) versus wavelength in micrometers for chromium.

TABLE I

Values of $n$ and $k$ Obtained from Various References for Chromium[a]

| eV | $cm^{-1}$ | Å | $n$ | $k$ |
|---|---|---|---|---|
| 10000 | | 1.240 | 0.9999862 [28] | 9.71E-07 [28] |
| 9549 | | 1.298 | 0.9999847 | 1.15E-06 |
| 9117 | | 1.360 | 0.9999833 | 1.37E-06 |
| 8706 | | 1.424 | 0.9999818 | 1.62E-06 |
| 8313 | | 1.492 | 0.9999802 | 1.92E-06 |
| 7937 | | 1.562 | 0.9999783 | 2.27E-06 |
| 7579 | | 1.636 | 0.9999764 | 2.69E-06 |
| 7237 | | 1.713 | 0.9999744 | 3.17E-06 |
| 6910 | | 1.794 | 0.9999723 | 3.74E-06 |
| 6598 | | 1.879 | 0.9999703 | 4.40E-06 |
| 6300 | | 1.968 | 0.9999686 | 5.17E-06 |
| 6156 | | 2.014 | 0.9999682 | 5.60E-06 |
| 6015 | | 2.061 | 0.9999723 | 6.06E-06 |
| 5878 | | 2.109 | 0.9999663 | 8.00E-07 |
| 5744 | | 2.159 | 0.9999633 | 8.71E-07 |
| 5613 | | 2.209 | 0.9999608 | 9.49E-07 |
| 5484 | | 2.261 | 0.9999585 | 1.03E-06 |
| 5237 | | 2.368 | 0.9999537 | 1.23E-06 |
| 5000 | | 2.480 | 0.9999486 | 1.46E-06 |
| 4775 | | 2.597 | 0.9999432 | 1.73E-06 |
| 4559 | | 2.720 | 0.9999374 | 2.05E-06 |
| 4353 | | 2.848 | 0.9999309 | 2.44E-06 |
| 4157 | | 2.983 | 0.9999238 | 2.90E-06 |
| 3969 | | 3.124 | 0.9999161 | 3.45E-06 |
| 3790 | | 3.272 | 0.9999076 | 4.10E-06 |
| 3619 | | 3.426 | 0.999898 | 4.87E-06 |
| 3455 | | 3.588 | 0.999888 | 5.80E-06 |
| 3299 | | 3.758 | 0.999877 | 6.89E-06 |
| 3150 | | 3.936 | 0.999865 | 8.20E-06 |
| 3008 | | 4.122 | 0.999851 | 9.75E-06 |
| 2872 | | 4.317 | 0.999836 | 1.16E-05 |
| 2742 | | 4.521 | 0.999820 | 1.38E-05 |
| 2619 | | 4.735 | 0.999802 | 1.64E-05 |
| 2500 | | 4.959 | 0.999782 | 1.95E-05 |
| 2387 | | 5.193 | 0.999760 | 2.32E-05 |
| 2280 | | 5.439 | 0.999737 | 2.75E-05 |
| 2177 | | 5.696 | 0.999711 | 3.27E-05 |
| 2078 | | 5.965 | 0.999682 | 3.88E-05 |
| 1985 | | 6.248 | 0.999651 | 4.60E-05 |
| 1895 | | 6.543 | 0.999616 | 5.45E-05 |
| 1809 | | 6.852 | 0.999579 | 6.46E-05 |
| 1728 | | 7.176 | 0.999538 | 7.65E-05 |
| 1650 | | 7.516 | 0.999493 | 9.05E-05 |
| 1575 | | 7.871 | 0.999445 | 1.07E-04 |

[a]The references from which the values were extracted are given in brackets.

TABLE I (*Continued*)

Chromium

| eV | $cm^{-1}$ | Å | *n* | *k* |
|---|---|---|---|---|
| 1504 | | 8.244 | 0.999392 | 1.26E-04 |
| 1436 | | 8.633 | 0.999335 | 1.49E-04 |
| 1371 | | 9.041 | 0.999273 | 1.75E-04 |
| 1309 | | 9.469 | 0.999206 | 2.06E-04 |
| 1250 | | 9.917 | 0.999133 | 2.43E-04 |
| 1194 | | 10.39 | 0.999055 | 2.85E-04 |
| 1140 | | 10.88 | 0.99897 | 3.34E-04 |
| 1088 | | 11.39 | 0.99888 | 3.93E-04 |
| 1039 | | 11.93 | 0.99879 | 4.61E-04 |
| 992.3 | | 12.49 | 0.99869 | 5.42E-04 |
| 947.5 | | 13.09 | 0.99859 | 6.39E-04 |
| 904.7 | | 13.70 | 0.99849 | 7.48E-04 |
| 863.9 | | 14.35 | 0.99839 | 8.83E-04 |
| 824.9 | | 15.03 | 0.99831 | 1.04E-03 |
| 787.7 | | 15.74 | 0.99825 | 1.20E-03 |
| 752.1 | | 16.49 | 0.99820 | 1.38E-03 |
| 734.9 | | 16.87 | 0.99819 | 1.48E-03 |
| 718.1 | | 17.27 | 0.99820 | 1.59E-03 |
| 701.7 | | 17.67 | 0.99827 | 1.71E-03 |
| 685.7 | | 18.08 | 0.99828 | 1.62E-03 |
| 670.0 | | 18.51 | 0.99822 | 1.73E-03 |
| 654.7 | | 18.94 | 0.99822 | 1.84E-03 |
| 639.8 | | 19.38 | 0.99824 | 1.97E-03 |
| 610.9 | | 20.30 | 0.99846 | 2.33E-03 |
| 596.9 | | 20.77 | 0.99879 | 2.55E-03 |
| 583.3 | | 21.26 | 0.999636 | 2.78E-03 |
| 570.0 | | 21.75 | 1.000161 | 3.41E-04 |
| 557.0 | | 22.26 | 0.999117 | 3.68E-04 |
| 544.2 | | 22.78 | 0.99862 | 3.97E-04 |
| 531.8 | | 23.31 | 0.99828 | 4.27E-04 |
| 519.7 | | 23.86 | 0.99800 | 4.58E-04 |
| 507.8 | | 24.42 | 0.99775 | 4.91E-04 |
| 484.9 | | 25.57 | 0.99728 | 5.63E-04 |
| 463.0 | | 26.78 | 0.99683 | 6.45E-04 |
| 442.1 | | 28.04 | 0.99638 | 7.37E-04 |
| 422.1 | | 29.37 | 0.99590 | 8.42E-04 |
| 403.0 | | 30.77 | 0.99538 | 9.71E-04 |
| 384.8 | | 32.22 | 0.99484 | 1.12E-03 |
| 367.5 | | 33.74 | 0.99426 | 1.31E-03 |
| 350.9 | | 35.33 | 0.99365 | 1.53E-03 |
| 335.0 | | 37.01 | 0.99301 | 1.76E-03 |
| 319.9 | | 38.76 | 0.99232 | 2.02E-03 |
| 305.5 | | 40.58 | 0.99157 | 2.31E-03 |
| 291.7 | | 42.50 | 0.99078 | 2.64E-03 |
| 278.5 | | 44.52 | 0.9899 | 3.00E-03 |

(*Continued*)

TABLE I (*Continued*)

Chromium

| eV | $cm^{-1}$ | Å | *n* | *k* |
|---|---|---|---|---|
| 265.9 | | 46.63 | 0.9890 | 3.39E-03 |
| 253.9 | | 48.83 | 0.9880 | 3.83E-03 |
| 242.5 | | 51.15 | 0.9870 | 4.32E-03 |
| 231.5 | | 53.56 | 0.9858 | 4.87E-03 |
| 221.1 | | 56.08 | 0.9846 | 5.49E-03 |
| 211.1 | | 58.73 | 0.9833 | 6.15E-03 |
| 201.5 | | 61.53 | 0.9818 | 6.86E-03 |
| 192.4 | | 64.44 | 0.9802 | 7.66E-03 |
| 183.7 | | 67.49 | 0.9785 | 8.63E-03 |
| 175.5 | | 70.69 | 0.9767 | 9.77E-03 |
| 167.5 | | 74.02 | 0.9749 | 1.11E-02 |
| 160.0 | | 77.49 | 0.9730 | 1.23E-02 |
| 152.7 | | 81.19 | 0.9710 | 1.36E-02 |
| 145.8 | | 85.04 | 0.9687 | 1.51E-02 |
| 139.3 | | 89.01 | 0.9662 | 1.67E-02 |
| 133.0 | | 93.22 | 0.9637 | 1.86E-02 |
| 127.0 | | 97.63 | 0.9611 | 2.05E-02 |
| 121.2 | | 102.3 | 0.9583 | 2.25E-02 |
| 115.8 | | 107.1 | 0.9553 | 2.45E-02 |
| 110.5 | | 112.2 | 0.9518 | 2.64E-02 |
| 105.5 | | 117.5 | 0.9476 | 2.88E-02 |
| 100.8 | | 123.0 | 0.9431 | 3.15E-02 |
| 96.22 | | 128.9 | 0.9380 | 3.48E-02 |
| 91.88 | | 134.9 | 0.9326 | 3.88E-02 |
| 87.73 | | 141.4 | 0.9270 | 4.34E-02 |
| 83.77 | | 148.0 | 0.9209 | 4.84E-02 |
| 79.99 | | 155.0 | 0.9139 | 5.43E-02 |
| 78.16 | | 158.5 | 0.9104 | 5.79E-02 |
| 76.37 | | 162.3 | 0.9068 | 6.17E-02 |
| 74.63 | | 166.2 | 0.9030 | 6.58E-02 |
| 72.92 | | 170.1 | 0.8990 | 7.08E-02 |
| 71.26 | | 173.9 | 0.8954 | 7.62E-02 |
| 69.63 | | 178.1 | 0.8918 | 8.21E-02 |
| 68.04 | | 182.3 | 0.8886 | 8.91E-02 |
| 64.97 | | 190.7 | 0.8850 | 0.104 |
| 62.04 | | 200.0 | 0.8841 | 0.120 |
| 59.24 | | 209.4 | 0.8882 | 0.136 |
| 56.56 | | 219.1 | 0.8970 | 0.150 |
| 54.01 | | 229.6 | 0.9077 | 0.157 |
| 51.57 | | 240.3 | 0.9207 | 0.159 |
| 200 | | 61.99 | | 6.0E-03 [12] |
| 150 | | 82.66 | | 1.2E-02 |
| 140 | | 88.56 | | 1.3E-02 |
| 130 | | 95.37 | | 1.6E-02 |

(*Continued*)

TABLE I (*Continued*)

Chromium

| eV | $cm^{-1}$ | Å | *n* | *k* |
|---|---|---|---|---|
| 125 | | 99.19 | | 1.7E-02 |
| 120 | | 103.3 | | 1.9E-02 |
| 115 | | 107.8 | | 2.0E-02 |
| 110 | | 112.7 | | 2.3E-02 |
| 105 | | 118.1 | | 2.60E-02 |
| 100 | | 124.0 | | 2.90E-02 |
| 95.0 | | 130.5 | | 3.20E-02 |
| 90.0 | | 137.8 | | 3.60E-02 |
| 85.0 | | 145.9 | | 4.30E-02 |
| 80.0 | | 155.0 | | 5.10E-02 |
| 75.0 | | 165.3 | | 6.20E-02 |
| 70.0 | | 177.1 | | 7.80E-02 |
| 65.0 | | 190.7 | | 0.100 |
| 60.0 | | 206.6 | | 0.132 |
| 59.0 | | 210.1 | | 0.139 |
| 58.0 | | 213.8 | | 0.148 |
| 57.0 | | 217.5 | | 0.159 |
| 56.0 | | 221.4 | | 0.167 |
| 55.0 | | 225.4 | | 0.172 |
| 54.0 | | 229.6 | | 0.177 |
| 53.0 | | 233.9 | | 0.182 |
| 52.0 | | 238.4 | | 0.182 |
| 51.0 | | 243.1 | | 0.182 |
| 50.0 | | 248.0 | | 0.184 |
| 49.0 | | 253.0 | | 0.189 |
| 48.0 | | 258.3 | | 0.195 |
| 47.0 | | 263.8 | | 0.197 |
| 46.0 | | 269.5 | | 0.195 |
| 45.0 | | 275.5 | | 0.182 |
| 44.0 | | 281.8 | | 0.164 |
| 43.0 | | 288.3 | | 9.2E-02 |
| 42.0 | | 295.2 | | 8.2E-02 |
| 41.0 | | 302.4 | | 8.3E-02 |
| 40.0 | | 310.0 | | 8.6E-02 |
| 35.0 | | 354.2 | | 0.121 |
| 29.5 | | 420.3 | 0.78 [3,8] | 0.21 [3,8] |
| 28.8 | | 430.5 | 0.77 | 0.22 |
| 28.2 | | 439.7 | 0.75 | 0.23 |
| 27.6 | | 449.2 | 0.73 | 0.25 |
| 27.0 | | 459.2 | 0.72 | 0.26 |
| 26.4 | | 469.6 | 0.71 | 0.28 |
| 25.8 | | 480.6 | 0.70 | 0.31 |
| 25.3 | | 490.1 | 0.68 | 0.33 |
| 24.8 | | 499.9 | 0.68 | 0.36 |
| 24.3 | | 510.2 | 0.67 | 0.39 |

(*Continued*)

TABLE I (*Continued*)

**Chromium**

| eV | $cm^{-1}$ | Å | *n* | *k* |
|---|---|---|---|---|
| 23.9 | | 518.8 | 0.68 | 0.43 |
| 23.4 | | 529.9 | 0.68 | 0.45 |
| 23.0 | | 539.1 | 0.69 | 0.48 |
| 22.5 | | 551.0 | 0.70 | 0.50 |
| 22.1 | | 561.0 | 0.71 | 0.52 |
| 21.8 | | 568.7 | 0.72 | 0.54 |
| 21.4 | | 579.4 | 0.73 | 0.56 |
| 21.0 | | 590.4 | 0.74 | 0.58 |
| 20.7 | | 599.0 | 0.74 | 0.60 |
| 20.3 | | 610.8 | 0.75 | 0.62 |
| 20.0 | | 619.9 | 0.77 | 0.64 |
| 19.7 | | 629.4 | 0.78 | 0.65 |
| 19.4 | | 639.1 | 0.80 | 0.67 |
| 19.1 | | 649.1 | 0.82 | 0.68 |
| 18.8 | | 659.5 | 0.83 | 0.68 |
| 18.5 | | 670.2 | 0.84 | 0.69 |
| 18.2 | | 681.2 | 0.85 | 0.70 |
| 18.0 | | 688.8 | 0.87 | 0.70 |
| 17.7 | | 700.5 | 0.87 | 0.71 |
| 17.5 | | 708.5 | 0.88 | 0.72 |
| 17.2 | | 720.8 | 0.89 | 0.72 |
| 17.0 | | 729.3 | 0.90 | 0.73 |
| 16.8 | | 738.0 | 0.90 | 0.74 |
| 16.5 | | 751.4 | 0.91 | 0.75 |
| 16.3 | | 760.6 | 0.92 | 0.76 |
| 16.1 | | 770.1 | 0.92 | 0.77 |
| 15.7 | | 789.7 | 0.95 | 0.79 |
| 15.5 | | 799.9 | 0.96 | 0.80 |
| 15.3 | | 810.4 | 0.97 | 0.80 |
| 14.9 | | 832.1 | 1.00 | 0.82 |
| 14.8 | | 837.7 | 1.01 | 0.82 |
| 14.6 | | 849.2 | 1.03 | 0.82 |
| 14.3 | | 867.0 | 1.06 | 0.82 |
| 13.9 | | 892.0 | 1.09 | 0.82 |
| 13.8 | | 898.4 | 1.10 | 0.82 |
| 13.5 | | 918.4 | 1.12 | 0.80 |
| 13.3 | | 932.2 | 1.13 | 0.80 |
| 13.1 | | 946.5 | 1.15 | 0.77 |
| 12.8 | | 968.6 | 1.15 | 0.75 |
| 12.5 | | 991.9 | 1.15 | 0.73 |
| eV | $cm^{-1}$ | μm | *n* | *k* |
| 12.3 | 99205 | 0.1008 | 1.14 | 0.71 |
| 12.0 | 96786 | 0.1033 | 1.13 | 0.70 |

(*Continued*)

TABLE I (*Continued*)

Chromium

| eV | $cm^{-1}$ | μm | $n$ | $k$ |
|---|---|---|---|---|
| 11.7 | 94366 | 0.1060 | 1.10 | 0.69 |
| 11.5 | 92753 | 0.1078 | 1.09 | 0.69 |
| 11.3 | 91140 | 0.1097 | 1.07 | 0.69 |
| 11.1 | 89527 | 0.1117 | 1.05 | 0.69 |
| 10.8 | 87107 | 0.1148 | 1.03 | 0.70 |
| 10.5 | 84688 | 0.1181 | 1.01 | 0.72 |
| 10.3 | 83074 | 0.1204 | 1.00 | 0.72 |
| 10.0 | 80655 | 0.1240 | 0.98 | 0.73 |
| 9.76 | 78719 | 0.1270 | 0.95 | 0.730 |
| 9.54 | 76945 | 0.1300 | 0.92 | 0.740 |
| 9.25 | 74606 | 0.1340 | 0.86 | 0.770 |
| 9.05 | 72993 | 0.1370 | 0.83 | 0.810 |
| 8.92 | 71944 | 0.1390 | 0.81 | 0.830 |
| 8.73 | 70412 | 0.1420 | 0.78 | 0.870 |
| 8.61 | 69444 | 0.1440 | 0.76 | 0.890 |
| 8.49 | 68476 | 0.1460 | 0.74 | 0.920 |
| 8.32 | 67105 | 0.1490 | 0.72 | 0.970 |
| 8.21 | 66218 | 0.1510 | 0.71 | 1.00 |
| 8.10 | 65330 | 0.1531 | 0.69 | 1.04 |
| 8.00 | 64524 | 0.1550 | 0.68 | 1.07 |
| 7.90 | 63717 | 0.1569 | 0.68 | 1.11 |
| 7.80 | 62911 | 0.1590 | 0.67 | 1.15 |
| 7.70 | 62104 | 0.1610 | 0.67 | 1.19 |
| 7.61 | 61378 | 0.1629 | 0.66 | 1.23 |
| 7.52 | 60652 | 0.1649 | 0.67 | 1.27 |
| 7.38 | 59523 | 0.1680 | 0.69 | 1.33 |
| 7.29 | 58797 | 0.1701 | 0.70 | 1.36 |
| 7.21 | 58152 | 0.1720 | 0.71 | 1.39 |
| 7.13 | 57507 | 0.1739 | 0.72 | 1.42 |
| 7.01 | 56539 | 0.1769 | 0.74 | 1.45 |
| 6.89 | 55571 | 0.1799 | 0.76 | 1.49 |
| 6.81 | 54926 | 0.1821 | 0.75 | 1.51 |
| 6.70 | 54039 | 0.1851 | 0.78 | 1.57 |
| 6.60 | 53232 | 0.1879 | 0.80 | 1.59 |
| 6.49 | 52345 | 0.1910 | 0.82 | 1.63 |
| 6.39 | 51538 | 0.1940 | 0.85 | 1.66 |
| 6.29 | 50732 | 0.1971 | 0.88 | 1.68 |
| 6.20 | 50006 | 0.2000 | 0.89 | 1.69 |
| 6.11 | 49280 | 0.2029 | 0.92 | 1.72 |
| 5.99 | 48312 | 0.2070 | 0.94 | 1.73 |
| 5.90 | 47586 | 0.2101 | 0.96 | 1.73 |
| 5.79 | 46699 | 0.2141 | 0.97 | 1.74 |
| 5.71 | 46054 | 0.2171 | 0.97 | 1.75 |
| 5.61 | 45247 | 0.2210 | 0.95 | 1.74 |
| 5.51 | 44441 | 0.2250 | 0.94 | 1.76 |

(*Continued*)

TABLE I (*Continued*)

**Chromium**

| eV | $cm^{-1}$ | μm | $n$ | $k$ |
|---|---|---|---|---|
| 5.39 | 43473 | 0.2300 | 0.93 | 1.80 |
| 5.30 | 42747 | 0.2339 | 0.90 | 1.83 |
| 5.21 | 42021 | 0.2380 | 0.87 | 1.87 |
| 5.10 | 41134 | 0.2431 | 0.86 | 1.94 |
| 5.00 | 40327 | 0.2480 | 0.85 | 2.01 |
| 4.90 | 39521 | 0.2530 | 0.86 | 2.07 |
| 4.80 | 38714 | 0.2583 | 0.86 | 2.13 |
| 4.70 | 37908 | 0.2638 | 0.86 | 2.21 |
| 4.60 | 37101 | 0.2695 | 0.88 | 2.28 |
| 4.50 | 36295 | 0.2755 | 0.89 | 2.35 |
| 4.40 | 35488 | 0.2818 | 0.90 | 2.42 |
| 4.32 | 34843 | 0.2870 | 0.91 | 2.49 |
| 4.22 | 34036 | 0.2938 | 0.94 | 2.58 |
| 4.13 | 33310 | 0.3002 | 0.98 | 2.67 |
| 4.03 | 32504 | 0.3077 | 1.02 | 2.76 |
| 3.92 | 31617 | 0.3163 | 1.06 | 2.85 |
| 3.83 | 30891 | 0.3237 | 1.12 | 2.95 |
| 3.72 | 30004 | 0.3333 | 1.18 | 3.04 |
| 3.63 | 29278 | 0.3416 | 1.26 | 3.12 |
| 3.53 | 28471 | 0.3512 | 1.33 | 3.18 |
| 3.42 | 27584 | 0.3625 | 1.39 | 3.24 |
| 3.33 | 26858 | 0.3723 | 1.43 | 3.31 |
| 3.22 | 25971 | 0.3850 | 1.44 | 3.40 |
| 3.13 | 25245 | 0.3961 | 1.48 | 3.54 |
| 3.03 | 24438 | 0.4092 | 1.54 | 3.71 |
| 2.92 | 23551 | 0.4246 | 1.65 | 3.89 |
| 2.83 | 22825 | 0.4381 | 1.80 | 4.06 |
| 2.72 | 21938 | 0.4558 | 1.99 | 4.22 |
| 2.63 | 21212 | 0.4714 | 2.22 | 4.36 |
| 2.53 | 20406 | 0.4901 | 2.49 | 4.44 |
| 2.42 | 19518 | 0.5123 | 2.75 | 4.46 |
| 2.33 | 18793 | 0.5321 | 2.98 | 4.45 |
| 2.22 | 17905 | 0.5585 | 3.18 | 4.41 |
| 2.13 | 17179 | 0.5821 | 3.34 | 4.38 |
| 2.03 | 16373 | 0.6108 | 3.48 | 4.36 |
| 1.77 | 14276 | 0.7005 | 3.84 | 4.37 |
| 1.52 | 12260 | 0.8157 | 4.23 | 4.34 |
| 1.50 | 12098 | 0.8266 | 4.27 | 4.33 |
| 1.46 | 11776 | 0.8492 | 4.31 | 4.32 |
| 1.44 | 11615 | 0.8610 | 4.33 | 4.32 |
| 1.40 | 11292 | 0.8856 | 4.38 | 4.31 |
| 1.36 | 10969 | 0.9116 | 4.42 | 4.30 |
| 1.32 | 10646 | 0.9393 | 4.47 | 4.29 |
| 1.28 | 10324 | 0.9686 | 4.49 | 4.28 |
| 1.24 | 10001 | 0.9999 | 4.50 | 4.28 |

(*Continued*)

TABLE I (*Continued*)

Chromium

| eV | $cm^{-1}$ | μm | *n* | *k* |
|---|---|---|---|---|
| 1.20 | 9679 | 1.033 | 4.52 | 4.29 |
| 1.16 | 9356 | 1.069 | 4.53 | 4.30 |
| 1.12 | 9033 | 1.107 | 4.53 | 4.31 |
| 1.08 | 8711 | 1.148 | 4.53 | 4.34 |
| 1.04 | 8388 | 1.192 | 4.51 | 4.36 |
| 1.00 | 8065 | 1.240 | 4.47 | 4.43 |
| 0.96 | 7743 | 1.292 | 4.47 | 4.50 |
| 0.92 | 7420 | 1.348 | 4.45 | 4.56 |
| 0.90 | 7259 | 1.378 | 4.43 | 4.60 |
| 0.86 | 6936 | 1.442 | 4.35 | 4.66 |
| 0.82 | 6614 | 1.512 | 4.24 | 4.81 |
| 0.78 | 6291 | 1.590 | 4.13 | 5.03 |
| 0.74 | 5968 | 1.675 | 4.06 | 5.30 |
| 0.70 | 5646 | 1.771 | 4.01 | 5.59 |
| 0.66 | 5323 | 1.879 | 3.96 | 5.95 |
| 0.62 | 5001 | 2.000 | 4.01 | 6.31 |
| 0.58 | 4678 | 2.138 | 4.01 | 6.65 |
| 0.54 | 4355 | 2.296 | 3.92 | 7.06 |
| 0.50 | 4033 | 2.480 | 3.83 | 7.58 |
| 0.46 | 3710 | 2.695 | 3.72 | 8.20 |
| 0.42 | 3388 | 2.952 | 3.47 | 8.97 |
| 0.38 | 3065 | 3.263 | 3.09 | 10.2 |
| 0.34 | 2742 | 3.647 | 2.89 | 12.0 |
| 0.30 | 2420 | 4.133 | 3.15 | 14.3 |
| 0.26 | 2097 | 4.769 | 3.91 | 17.1 |
| 0.22 | 1774 | 5.636 | 5.30 | 20.6 |
| 0.18 | 1452 | 6.888 | 8.73 | 25.4 |
| 0.14 | 1129 | 8.856 | 15.3 | 26.4 |
| 0.10 | 806.5 | 12.40 | 11.8 | 29.8 |
| 0.09 | 725.9 | 13.78 | 11.8 | 33.9 |
| 0.08 | 645.2 | 15.50 | 13.6 | 42.2 |
| 0.06 | 483.9 | 20.66 | 21.2 | 42.0 |
| 0.04 | 322.6 | 31.00 | 14.9 | 65.2 |

## IRON (Fe) VII

Iron is a bcc metal. It has an fcc phase at high temperatures, but we ignore that here. A single domain of cubic Fe that is magnetized is optically anisotropic; the optical dielectric function is a tensor with three independent complex components. However, the anisotropy is small, and we neglect it here. The off-diagonal anisotropy is proportional to the magnetization ($M$) and the diagonal anisotropy is proportional to its square. Iron is not a highly reactive material, but it is not inert. Several different oxides grow at rates dependent on surface quality, impurities, and ambient conditions.

We do not discuss all of the optical studies on Fe. By and large, the data in the visible and near ultraviolet are in relatively good mutual agreement. The soft X-ray data ($k$ spectrum, since $n \approx 1$) generally agree in shape above the $3p$ absorption edge, but the magnitudes do not, and the discrepancy with the longer-wavelength bulk data is in the wrong direction to be explained by a lower film density.

Values of $n$ and $k$ are given in Table I and plotted in Fig. 1. In the infrared and visible, we list the data of Weaver *et al.* [1]. These were obtained by a Kramers–Kronig analysis of absorptance data on bulk samples. They agree well, where they overlap, with the data of Johnson and Christy [2], obtained from reflectance and transmittance measurements on semitransparent films, which data we report in the ultraviolet. In the vacuum ultraviolet we use the data of Moravec *et al.* [3] obtained from Kramers–Kronig analysis of reflectance data on opaque, thin-film samples. These data show a higher reflectance, and presumably are less affected by oxides. They also match better with the soft X-ray data. At higher energies, we list $k$ spectra obtained from absorption-coefficient measurements on thin films by Sonntag *et al.* [4], using the assumption that $n$ is unity. Their data cover the region of the $3p$ absorption edge, as do those of Wehenkel and Gauthé [5, 6].

Because of the partially filled $3d$ band, interband transitions exist to arbitrarily low photon energies, although at some point they become weak. Jones *et al.* [7] showed that for wavelengths longer than about 10 μm, the interband transitions were negligible. The only infrared measurements that yield spectra of $n$ and $k$, however, appear to be those of Weaver *et al.* [1], of Lenham and Treherne [8–10], of Siddiqui and Treherne [11], and of Ordal *et al.* [12], from which we list data here. Ordal *et al.* made reflectance measurements to 55.6 μm, although details are not reported, then compared their spectra with others for consistency and fit to a set of Drude parameters. Ordal *et al.* [13] later made measurements in the 33.3–333 μm region, using a resonant cavity. This gives only one measured quantity at each point, but a reasonable approximation allows $n$ and $k$ to be extracted. We list their data in this spectral region.

We have calculated $n$ and $k$ in the 1.24–240 Å (10,000–51.5 eV) region using the model of Henke *et al.* [14]. The atomic absorption edges are $K$ (7114 eV), $L_1$ (846 eV), $L_{2,3}$ (723, 710 eV), $M_1$ (95 eV), $M_{2,3}$ (56 eV), $M_{4,5}$ (6 eV). At the lower energies these atomic features may be perturbed by the bonding properties of the crystal.

We used 8065.48 $cm^{-1}/eV$ to convert among the units of [14], whereas the conversion factor may be different by one or two digits in the fourth figure for the other data of Table I.

Finally, we list other references to optical constants of Fe [15–18]. We do not include those that give data only in arbitrary units.

## REFERENCES


1. J. H. Weaver, E. Colavita, D. W. Lynch, and R. Rosei, *Phys. Rev.* **B19**, 3850 (1979).
2. P. B. Johnson and R. W. Christy, *Phys. Rev.* **B9**, 5056 (1974).
3. T. J. Moravec, J. C. Rife, and D. L. Dexter, *Phys. Rev.* **B13**, 3297 (1976).
4. B. Sonntag, R. Haensel, and C. Kunz, *Solid State Commun.* **7**, 597 (1969).
5. C. Wehenkel and B. Gauthé, *Phys. Lett.* **47A**, 253 (1974).
6. C. Wehenkel and B. Gauthé, *Phys. Stat. Solidi (b)* **64**, 515 (1974).
7. J. C. Jones, D. C. Palmer, and C. L. Tien, *J. Opt. Soc. Am.* **62**, 353 (1972).
8. A. P. Lenham and D. M. Treherne, *J. Opt. Soc. Am.* **56**, 1137 (1966).
9. A. P. Lenham and D. M. Treherne, in "Optical Properties and Electronic Structure of Metals and Alloys," (F. Abeles, ed.), North-Holland, Amsterdam, 196 (1966).
10. A. P. Lenham, *J. Opt. Soc. Am.* **57**, 473 (1967).
11. A. S. Siddiqui and D. M. Treherne, *Infrared Phys.* **17**, 33 (1977).
12. M. A. Ordal, R. J. Bell, R. W. Alexander, L. L. Long, and M. R. Querry, *Appl. Opt.* **24**, 4493 (1985).
13. M. A. Ordal, R. J. Bell, R. W. Alexander, L. A. Newquist, and M. R. Querry, *Appl. Opt.* **27**, 1203 (1988).
14. B. L. Henke, J. C. Davis, E. M. Gullikson, and R. C. C. Perera, Lawrence Berkeley Laboratory Report No. LBL-26259 (1988).
15. H. T. Yolken and J. Kruger, *J. Opt. Soc. Am.* **55**, 842 (1965).
16. A. J. Blodgett and W. E. Spicer, *Phys. Rev.* **158**, 514 (1967).
17. G. A. Bolotin, M. M. Kirillova, and V. M. Mayevskiy, *Phys. Met. Metall.* **27**, 31 (1969); *Fiz. Met. Metalloved.* **27**, 224 (1969).
18. V. P. Shirokovskii, M. M. Kirillova, and N. A. Shilkova, *Sov. Phys. JETP* **55**, 464 (1982); *Zh. Eksp. Teor. Fiz.* **82**, 784 (1982).

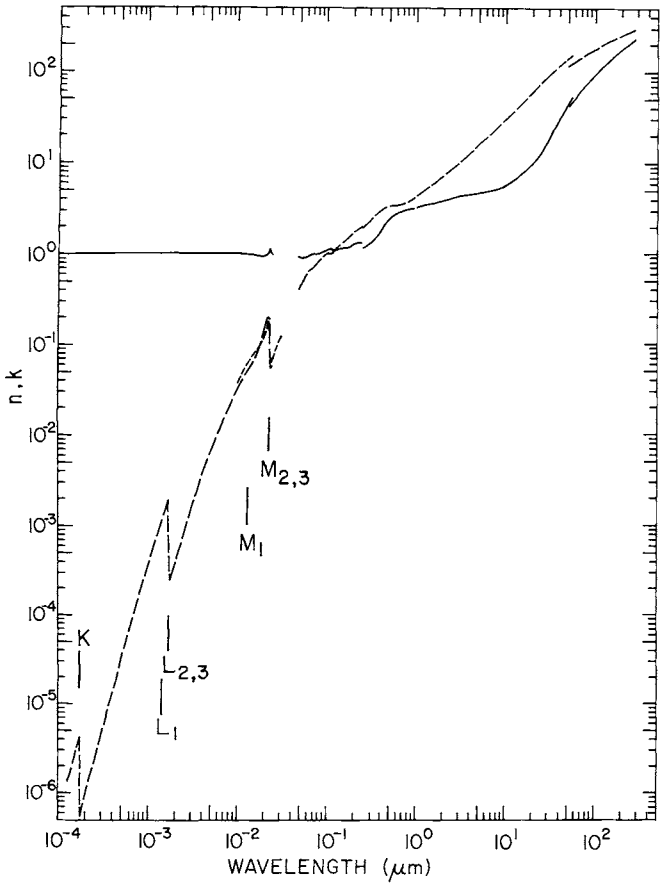


**Fig. 1.** Log–log plot of $n$ (solid line) and $k$ (dashed line) versus wavelength in micrometers for iron.

TABLE I

Values of $n$ and $k$ Obtained from Various References for Iron[a]

| eV | $cm^{-1}$ | Å | $n$ | $k$ |
|---|---|---|---|---|
| 10000 | | 1.240 | 0.9999849 [18] | 1.32E-06 [18] |
| 9549 | | 1.298 | 0.9999834 | 1.57E-06 |
| 9117 | | 1.360 | 0.9999819 | 1.86E-06 |
| 8706 | | 1.424 | 0.9999803 | 2.19E-06 |
| 8313 | | 1.492 | 0.9999787 | 2.59E-06 |
| 7937 | | 1.562 | 0.9999771 | 3.04E-06 |
| 7579 | | 1.636 | 0.9999755 | 3.58E-06 |
| 7406 | | 1.674 | 0.9999750 | 3.88E-06 |
| 7237 | | 1.713 | 0.9999750 | 4.20E-06 |
| 7071 | | 1.753 | 0.9999753 | 5.70E-07 |
| 6910 | | 1.794 | 0.9999721 | 6.21E-07 |
| 6752 | | 1.836 | 0.9999701 | 6.77E-07 |
| 6598 | | 1.879 | 0.9999682 | 7.38E-07 |
| 6300 | | 1.968 | 0.9999645 | 8.77E-07 |
| 6015 | | 2.061 | 0.9999607 | 1.04E-06 |
| 5744 | | 2.159 | 0.9999565 | 1.24E-06 |
| 5484 | | 2.261 | 0.9999520 | 1.47E-06 |
| 5237 | | 2.368 | 0.9999471 | 1.75E-06 |
| 5000 | | 2.480 | 0.9999416 | 2.08E-06 |
| 4775 | | 2.597 | 0.9999357 | 2.48E-06 |
| 4559 | | 2.720 | 0.9999293 | 2.94E-06 |
| 4353 | | 2.848 | 0.9999222 | 3.50E-06 |
| 4157 | | 2.983 | 0.9999144 | 4.16E-06 |
| 3969 | | 3.124 | 0.9999058 | 4.95E-06 |
| 3790 | | 3.272 | 0.999896 | 5.88E-06 |
| 3619 | | 3.426 | 0.999886 | 6.99E-06 |
| 3455 | | 3.588 | 0.999875 | 8.30E-06 |
| 3299 | | 3.758 | 0.999862 | 9.86E-06 |
| 3150 | | 3.936 | 0.999848 | 1.17E-05 |
| 3008 | | 4.122 | 0.999834 | 1.39E-05 |
| 2872 | | 4.317 | 0.999817 | 1.65E-05 |
| 2742 | | 4.521 | 0.999799 | 1.96E-05 |
| 2619 | | 4.735 | 0.999779 | 2.32E-05 |
| 2500 | | 4.959 | 0.999757 | 2.76E-05 |
| 2387 | | 5.193 | 0.999733 | 3.27E-05 |
| 2280 | | 5.439 | 0.999707 | 3.87E-05 |
| 2177 | | 5.696 | 0.999679 | 4.58E-05 |
| 2078 | | 5.965 | 0.999647 | 5.42E-05 |
| 1985 | | 6.248 | 0.999614 | 6.41E-05 |
| 1895 | | 6.543 | 0.999576 | 7.57E-05 |
| 1809 | | 6.852 | 0.999536 | 8.94E-05 |
| 1728 | | 7.176 | 0.999492 | 1.06E-04 |
| 1650 | | 7.516 | 0.999445 | 1.24E-04 |
| 1575 | | 7.871 | 0.999393 | 1.46E-04 |

[a]The references from which the values were extracted are given in brackets.

TABLE I (*Continued*)

**Iron**

| eV | $cm^{-1}$ | Å | $n$ | $k$ |
|---|---|---|---|---|
| 1504 | | 8.244 | 0.999337 | 1.72E-04 |
| 1436 | | 8.633 | 0.999278 | 2.03E-04 |
| 1371 | | 9.041 | 0.999214 | 2.38E-04 |
| 1309 | | 9.469 | 0.999146 | 2.79E-04 |
| 1250 | | 9.917 | 0.999075 | 3.28E-04 |
| 1194 | | 10.39 | 0.99900 | 3.84E-04 |
| 1140 | | 10.88 | 0.99892 | 4.49E-04 |
| 1088 | | 11.39 | 0.99884 | 5.26E-04 |
| 1039 | | 11.93 | 0.99876 | 6.15E-04 |
| 992.3 | | 12.49 | 0.99869 | 7.19E-04 |
| 947.5 | | 13.09 | 0.99862 | 8.38E-04 |
| 904.7 | | 13.70 | 0.99857 | 9.80E-04 |
| 884.1 | | 14.02 | 0.99856 | 1.06E-03 |
| 863.9 | | 14.35 | 0.99858 | 1.15E-03 |
| 844.2 | | 14.69 | 0.99863 | 1.10E-03 |
| 824.9 | | 15.03 | 0.99857 | 1.19E-03 |
| 806.0 | | 15.38 | 0.99856 | 1.28E-03 |
| 787.7 | | 15.74 | 0.99858 | 1.38E-03 |
| 769.7 | | 16.11 | 0.99864 | 1.50E-03 |
| 752.1 | | 16.49 | 0.99875 | 1.62E-03 |
| 734.9 | | 16.87 | 0.99897 | 1.75E-03 |
| 718.1 | | 17.27 | 0.999579 | 1.89E-03 |
| 701.7 | | 17.67 | 0.999763 | 2.40E-04 |
| 685.7 | | 18.08 | 0.999100 | 2.57E-04 |
| 670.0 | | 18.51 | 0.99876 | 2.76E-04 |
| 654.7 | | 18.94 | 0.99851 | 2.98E-04 |
| 639.8 | | 19.38 | 0.99831 | 3.22E-04 |
| 610.9 | | 20.30 | 0.99794 | 3.71E-04 |
| 583.3 | | 21.26 | 0.99759 | 4.29E-04 |
| 557.0 | | 22.26 | 0.99724 | 4.99E-04 |
| 531.8 | | 23.31 | 0.99687 | 5.80E-04 |
| 507.8 | | 24.42 | 0.99649 | 6.75E-04 |
| 484.9 | | 25.57 | 0.99608 | 7.85E-04 |
| 463.0 | | 26.78 | 0.99564 | 9.13E-04 |
| 442.1 | | 28.05 | 0.99517 | 1.06E-03 |
| 422.1 | | 29.37 | 0.99465 | 1.23E-03 |
| 403.0 | | 30.76 | 0.99411 | 1.43E-03 |
| 384.8 | | 32.22 | 0.99351 | 1.65E-03 |
| 367.5 | | 33.74 | 0.99286 | 1.93E-03 |
| 350.9 | | 35.34 | 0.99218 | 2.25E-03 |
| 335.0 | | 37.01 | 0.99147 | 2.63E-03 |
| 319.9 | | 38.76 | 0.99072 | 3.01E-03 |
| 305.5 | | 40.59 | 0.9899 | 3.44E-03 |
| 291.7 | | 42.51 | 0.9890 | 3.94E-03 |
| 278.5 | | 44.52 | 0.9881 | 4.51E-03 |

(*Continued*)

TABLE I (*Continued*)

Iron

| eV | $cm^{-1}$ | Å | *n* | *k* |
|---|---|---|---|---|
| 265.9 | | 46.63 | 0.9872 | 5.07E-03 |
| 253.9 | | 48.83 | 0.9862 | 5.68E-03 |
| 242.5 | | 51.14 | 0.9850 | 6.35E-03 |
| 231.5 | | 53.56 | 0.9838 | 7.11E-03 |
| 221.1 | | 56.09 | 0.9823 | 8.00E-03 |
| 211.1 | | 58.74 | 0.9809 | 9.09E-03 |
| 201.5 | | 61.52 | 0.9794 | 1.03E-02 |
| 192.4 | | 64.43 | 0.9779 | 1.18E-02 |
| 183.7 | | 67.48 | 0.9765 | 1.31E-02 |
| 175.5 | | 70.67 | 0.9749 | 1.45E-02 |
| 167.5 | | 74.01 | 0.9732 | 1.61E-02 |
| 160.0 | | 77.51 | 0.9713 | 1.78E-02 |
| 152.7 | | 81.17 | 0.9694 | 1.97E-02 |
| 145.8 | | 85.01 | 0.9674 | 2.18E-02 |
| 139.3 | | 89.03 | 0.9653 | 2.40E-02 |
| 133.0 | | 93.24 | 0.9631 | 2.64E-02 |
| 127.0 | | 97.66 | 0.9609 | 2.91E-02 |
| 121.2 | | 102.3 | 0.9587 | 3.17E-02 |
| 115.8 | | 107.1 | 0.9561 | 3.45E-02 |
| 110.5 | | 112.2 | 0.9534 | 3.75E-02 |
| 105.5 | | 117.5 | 0.9505 | 4.08E-02 |
| 100.8 | | 123.0 | 0.9474 | 4.43E-02 |
| 98.47 | | 125.9 | 0.9457 | 4.61E-02 |
| 96.22 | | 128.9 | 0.9440 | 4.81E-02 |
| 94.03 | | 131.9 | 0.9422 | 5.01E-02 |
| 91.88 | | 134.9 | 0.9403 | 5.22E-02 |
| 89.78 | | 138.1 | 0.9383 | 5.44E-02 |
| 87.73 | | 141.3 | 0.9363 | 5.67E-02 |
| 85.73 | | 144.6 | 0.9341 | 5.92E-02 |
| 81.85 | | 151.5 | 0.9295 | 6.44E-02 |
| 78.16 | | 158.6 | 0.9243 | 7.02E-02 |
| 74.63 | | 166.1 | 0.9172 | 7.70E-02 |
| 71.26 | | 174.0 | 0.9102 | 8.77E-02 |
| 68.04 | | 182.2 | 0.9034 | 0.100 |
| 64.97 | | 190.8 | 0.8969 | 0.121 |
| 62.04 | | 199.9 | 0.9013 | 0.149 |
| 59.24 | | 209.3 | 0.9252 | 0.179 |
| 56.56 | | 219.2 | 0.9751 | 0.191 |
| 55.27 | | 224.3 | 1.012 | 0.185 |
| 54.01 | | 229.6 | 1.109 | 0.175 |
| 52.77 | | 234.9 | 1.004 | 5.36E-02 |
| 51.57 | | 240.4 | 0.9695 | 5.44E-02 |
| 250 | | 49.59 | | 5.0E-03 [4] |
| 200 | | 61.99 | | 1.0E-02 |

(*Continued*)

TABLE I (*Continued*)

Iron

| eV | $cm^{-1}$ | Å | *n* | *k* |
|---|---|---|---|---|
| 150 | | 82.66 | | 2.3E-02 |
| 120 | | 103.3 | | 3.8E-02 |
| 115 | | 107.8 | | 4.1E-02 |
| 110 | | 112.7 | | 4.5E-02 |
| 105 | | 118.1 | | 5.0E-02 |
| 100 | | 124.0 | | 5.4E-02 |
| 95.0 | | 130.5 | | 6.0E-02 |
| 90.0 | | 137.8 | | 6.5E-02 |
| 85.0 | | 145.9 | | 7.0E-02 |
| 80.0 | | 155.0 | | 7.6E-02 |
| 75.0 | | 165.3 | | 8.4E-02 |
| 70.0 | | 177.1 | | 9.4E-02 |
| 65.0 | | 190.7 | | 0.108 |
| 60.0 | | 206.6 | | 0.130 |
| 56.0 | | 221.4 | | 0.176 |
| 52.0 | | 238.4 | | 6.0E-02 |
| 50.0 | | 248.0 | | 6.5E-02 |
| 45.0 | | 275.5 | | 9.2E-02 |
| 40.0 | | 310.0 | | 0.118 |
| 26.0 | | 476.9 | 0.890 [3] | 0.376 [3] |
| 25.8 | | 480.6 | 0.887 | 0.383 |
| 25.6 | | 484.3 | 0.886 | 0.395 |
| 25.4 | | 488.1 | 0.884 | 0.402 |
| 25.2 | | 492.0 | 0.881 | 0.408 |
| 25.0 | | 495.9 | 0.877 | 0.411 |
| 24.8 | | 499.9 | 0.874 | 0.418 |
| 24.6 | | 504.0 | 0.876 | 0.434 |
| 24.4 | | 508.1 | 0.872 | 0.436 |
| 24.2 | | 512.3 | 0.870 | 0.443 |
| 24.0 | | 516.6 | 0.867 | 0.450 |
| 23.8 | | 520.9 | 0.865 | 0.468 |
| 23.6 | | 525.4 | 0.859 | 0.477 |
| 23.4 | | 529.8 | 0.861 | 0.482 |
| 23.2 | | 534.4 | 0.862 | 0.493 |
| 23.0 | | 539.1 | 0.863 | 0.504 |
| 22.8 | | 543.8 | 0.861 | 0.511 |
| 22.6 | | 548.6 | 0.863 | 0.515 |
| 22.4 | | 553.5 | 0.862 | 0.522 |
| 22.2 | | 558.5 | 0.865 | 0.537 |
| 22.0 | | 563.6 | 0.872 | 0.556 |
| 21.8 | | 568.7 | 0.874 | 0.561 |
| 21.6 | | 574.0 | 0.875 | 0.571 |
| 21.4 | | 579.4 | 0.875 | 0.571 |
| 21.2 | | 584.8 | 0.878 | 0.575 |
| 21.0 | | 590.4 | 0.882 | 0.590 |

(*Continued*)

TABLE I (*Continued*)

**Iron**

| eV | $cm^{-1}$ | Å | $n$ | $k$ |
|---|---|---|---|---|
| 20.8 | | 596.1 | 0.892 | 0.605 |
| 20.6 | | 601.9 | 0.898 | 0.613 |
| 20.4 | | 607.8 | 0.903 | 0.620 |
| 20.2 | | 613.8 | 0.905 | 0.624 |
| 20.0 | | 619.9 | 0.910 | 0.632 |
| 19.8 | | 626.2 | 0.919 | 0.636 |
| 19.6 | | 632.6 | 0.924 | 0.644 |
| 19.4 | | 639.1 | 0.927 | 0.647 |
| 19.2 | | 645.8 | 0.933 | 0.648 |
| 19.0 | | 652.5 | 0.936 | 0.652 |
| 18.8 | | 659.5 | 0.938 | 0.656 |
| 18.6 | | 666.6 | 0.938 | 0.656 |
| 18.4 | | 673.8 | 0.941 | 0.659 |
| 18.2 | | 681.2 | 0.941 | 0.659 |
| 18.0 | | 688.8 | 0.939 | 0.665 |
| 17.8 | | 696.5 | 0.944 | 0.672 |
| 17.6 | | 704.5 | 0.946 | 0.682 |
| 17.4 | | 712.6 | 0.945 | 0.688 |
| 17.2 | | 720.8 | 0.947 | 0.697 |
| 17.0 | | 729.3 | 0.948 | 0.707 |
| 16.8 | | 738.0 | 0.952 | 0.719 |
| 16.6 | | 746.9 | 0.955 | 0.723 |
| 16.4 | | 756.0 | 0.951 | 0.731 |
| 16.2 | | 765.3 | 0.944 | 0.742 |
| 16.0 | | 774.9 | 0.940 | 0.750 |
| 15.8 | | 784.7 | 0.941 | 0.765 |
| 15.6 | | 794.8 | 0.943 | 0.774 |
| 15.4 | | 805.1 | 0.945 | 0.783 |
| 15.2 | | 815.7 | 0.949 | 0.791 |
| 15.0 | | 826.6 | 0.952 | 0.798 |
| 14.8 | | 837.7 | 0.959 | 0.824 |
| 14.6 | | 849.2 | 0.974 | 0.847 |
| 14.4 | | 861.0 | 0.988 | 0.870 |
| 14.2 | | 873.1 | 0.993 | 0.881 |
| 14.0 | | 885.6 | 1.00 | 0.889 |
| 13.8 | | 898.4 | 1.00 | 0.898 |
| 13.6 | | 911.6 | 1.01 | 0.911 |
| 13.4 | | 925.3 | 1.02 | 0.925 |
| 13.2 | | 939.3 | 1.03 | 0.935 |
| 13.0 | | 953.7 | 1.05 | 0.951 |
| 12.8 | | 968.6 | 1.06 | 0.964 |
| 12.6 | | 984.0 | 1.08 | 0.972 |
| 12.4 | | 999.9 | 1.09 | 0.968 |

(*Continued*)

TABLE I (*Continued*)

Iron

| eV | $cm^{-1}$ | μm | $n$ | $k$ |
|---|---|---|---|---|
| 12.2 | 98399 | 0.1016 | 1.10 | 0.971 |
| 12.0 | 96786 | 0.1033 | 1.10 | 0.969 |
| 11.8 | 95173 | 0.1051 | 1.11 | 0.967 |
| 11.6 | 93560 | 0.1069 | 1.12 | 0.968 |
| 11.4 | 91946 | 0.1088 | 1.11 | 0.958 |
| 11.2 | 90333 | 0.1107 | 1.11 | 0.953 |
| 11.0 | 88720 | 0.1127 | 1.11 | 0.950 |
| 10.8 | 87107 | 0.1148 | 1.10 | 0.959 |
| 10.6 | 85494 | 0.1170 | 1.07 | 0.991 |
| 10.4 | 83881 | 0.1192 | 1.07 | 1.02 |
| 10.2 | 82268 | 0.1216 | 1.06 | 1.06 |
| 10.0 | 80655 | 0.1240 | 1.05 | 1.09 |
| 9.80 | 79042 | 0.1265 | 1.08 | 1.13 |
| 9.60 | 77429 | 0.1292 | 1.09 | 1.15 |
| 9.40 | 75816 | 0.1319 | 1.10 | 1.17 |
| 9.20 | 74202 | 0.1348 | 1.12 | 1.19 |
| 9.00 | 72589 | 0.1378 | 1.12 | 1.20 |
| 8.80 | 70976 | 0.1409 | 1.13 | 1.22 |
| 8.60 | 69363 | 0.1442 | 1.13 | 1.24 |
| 8.40 | 67750 | 0.1476 | 1.13 | 1.26 |
| 8.20 | 66137 | 0.1512 | 1.13 | 1.28 |
| 8.00 | 64524 | 0.1550 | 1.13 | 1.32 |
| 7.80 | 62911 | 0.1590 | 1.15 | 1.32 |
| 7.60 | 61298 | 0.1631 | 1.15 | 1.37 |
| 7.40 | 59684 | 0.1675 | 1.15 | 1.40 |
| 7.20 | 58071 | 0.1722 | 1.13 | 1.45 |
| 7.00 | 56458 | 0.1771 | 1.15 | 1.49 |
| 6.80 | 54845 | 0.1823 | 1.20 | 1.54 |
| 6.60 | 53232 | 0.1879 | 1.22 | 1.61 |
| 6.40 | 51619 | 0.1937 | 1.23 | 1.67 |
| 6.20 | 50006 | 0.2000 | 1.28 | 1.71 |
| 6.00 | 48393 | 0.2066 | 1.30 | 1.73 |
| 5.80 | 46780 | 0.2138 | 1.32 | 1.75 |
| 5.60 | 45167 | 0.2214 | 1.32 | 1.78 |
| 5.40 | 43554 | 0.2296 | 1.31 | 1.82 |
| 5.20 | 41940 | 0.2384 | 1.32 | 1.88 |
| 5.00 | 40327 | 0.2480 | 1.31 | 1.95 |
| 1.240 | 10000 | 1.000 | 3.23 [12] | 4.35 [12] |
| 1.116 | 9000 | 1.111 | 3.32 | 4.65 |
| 0.9919 | 8000 | 1.250 | 3.42 | 5.04 |
| 0.8679 | 7000 | 1.429 | 3.53 | 5.54 |
| 0.7439 | 6000 | 1.667 | 3.67 | 6.21 |
| 0.6199 | 5000 | 2.000 | 3.84 | 7.16 |
| 0.5889 | 4750 | 2.105 | 3.92 | 7.50 |
| 0.5579 | 4500 | 2.222 | 3.98 | 7.80 |

(*Continued*)

TABLE I (*Continued*)

Iron

| eV | $cm^{-1}$ | μm | $n$ | $k$ |
|---|---|---|---|---|
| 0.5269 | 4250 | 2.353 | 4.04 | 8.18 |
| 0.4959 | 4000 | 2.500 | 4.13 | 8.59 |
| 0.4649 | 3750 | 2.667 | 4.22 | 9.02 |
| 0.4339 | 3500 | 2.857 | 4.30 | 9.55 |
| 0.4030 | 3250 | 3.077 | 4.39 | 10.1 |
| 0.3720 | 3000 | 3.333 | 4.45 | 10.8 |
| 0.3410 | 2750 | 3.636 | 4.51 | 11.6 |
| 0.3100 | 2500 | 4.000 | 4.54 | 12.6 |
| 0.2790 | 2250 | 4.444 | 4.59 | 13.8 |
| 0.2480 | 2000 | 5.000 | 4.59 | 15.4 |
| 0.2356 | 1900 | 5.263 | 4.60 | 16.2 |
| 0.2232 | 1800 | 5.555 | 4.63 | 17.1 |
| 0.2108 | 1700 | 5.882 | 4.66 | 18.1 |
| 0.1984 | 1600 | 6.250 | 4.96 | 19.2 |
| 0.1860 | 1500 | 6.667 | 4.75 | 20.5 |
| 0.1736 | 1400 | 7.143 | 4.89 | 22.0 |
| 0.1612 | 1300 | 7.692 | 5.10 | 23.7 |
| 0.1488 | 1200 | 8.333 | 5.37 | 25.6 |
| 0.1364 | 1100 | 9.091 | 5.59 | 27.8 |
| 0.1240 | 1000 | 10.00 | 5.81 | 30.4 |
| 0.1178 | 950 | 10.53 | 5.95 | 32.0 |
| 0.1116 | 900 | 11.11 | 6.12 | 33.7 |
| 0.1054 | 850 | 11.76 | 6.31 | 35.7 |
| 0.09919 | 800 | 12.50 | 6.48 | 37.7 |
| 0.09299 | 750 | 13.33 | 6.88 | 40.3 |
| 0.08679 | 700 | 14.29 | 7.30 | 43.2 |
| 0.08059 | 650 | 15.38 | 7.71 | 46.5 |
| 0.07439 | 600 | 16.67 | 8.38 | 50.3 |
| 0.06819 | 550 | 18.18 | 9.04 | 54.7 |
| 0.06199 | 500 | 20.00 | 9.87 | 60.1 |
| 0.05951 | 480 | 20.83 | 10.3 | 62.6 |
| 0.05703 | 460 | 21.74 | 10.7 | 65.4 |
| 0.05455 | 440 | 22.73 | 11.3 | 68.6 |
| 0.05207 | 420 | 23.81 | 12.0 | 71.9 |
| 0.04959 | 400 | 25.00 | 13.0 | 75.7 |
| 0.04711 | 380 | 26.32 | 14.2 | 79.8 |
| 0.04463 | 360 | 27.78 | 15.7 | 84.5 |
| 0.04215 | 340 | 29.41 | 17.7 | 89.3 |
| 0.03968 | 320 | 31.25 | 19.9 | 94.5 |
| 0.03720 | 300 | 33.33 | 22.5 | 100 |
| 0.03472 | 280 | 35.71 | 25.2 | 106 |
| 0.03224 | 260 | 38.46 | 29.1 | 114 |
| 0.02976 | 240 | 41.67 | 33.6 | 122 |
| 0.02728 | 220 | 45.45 | 38.6 | 130 |
| 0.02480 | 200 | 50.00 | 45.7 | 141 |

(*Continued*)

TABLE I (*Continued*)

Iron

| eV | $cm^{-1}$ | μm | *n* | *k* |
|---|---|---|---|---|
| | | | 43.2 [13] | 115 [13] |
| 0.02232 | 180 | 55.55 | 54.2 [12] | 152 [12] |
| 0.02170 | 175 | 57.14 | 51.2 [13] | 126 [13] |
| 0.01860 | 150 | 66.67 | 61.3 | 140 |
| 0.01550 | 125 | 80.00 | 75.2 | 158 |
| 0.01240 | 100 | 100.0 | 95.4 | 182 |
| 0.009919 | 80 | 125.0 | 120 | 207 |
| 0.008059 | 65 | 153.8 | 147 | 230 |
| 0.006199 | 50 | 200.0 | 183 | 260 |
| 0.004339 | 35 | 285.7 | 238 | 306 |

## VIII NIOBIUM (Nb)

Niobium is a body-centered cubic metal. It is not highly reactive, but a thin oxide film does form at room temperature, a film that may effect ellipsometric measurements in the visible and near ultraviolet, and all measurements further in the ultraviolet.

There are many sets of near-infrared, visible, and near-ultraviolet data [1–16]. Most of them agree in the number and position of structures in the spectra in the visible and ultraviolet, but there are large discrepancies in the magnitudes of the optical constants. Data taken on films condensed on room-temperature substrates are suspect; heated substrates must be used, and high evaporation rates are necessary to reduce surface roughness [14]. Some measurements were carried out on films prepared in UHV, but the measurements were not made in UHV. There are two vacuum-ultraviolet measurements [8, 17]. The only all-UHV studies were those of Truong *et al.* [17], and of Carroll *et al.* [18]. The former used foil samples heavily annealed in UHV. Unfortunately, their data do not match well at longer wavelengths with any other measurements, although they may be the most reliable to date at shorter wavelengths because of the possible influence of oxides on the other data. Carroll *et al.* worked with an atomically clean single-crystal surface in UHV, but their data are at only seven wavelengths in the 0.40 μm to 0.63 μm region. In this range their *n* spectrum is about 10% higher than that of Weaver *et al.* [8], and their *k* spectrum lies about 4% lower. It is not clear that these differences can be attributed exclusively to surface cleanliness. There is one measurement [19] of optical absorption in the soft X-ray region, the region of the 4*p* excitation, from which a spectrum of *k* can be obtained with the assumption that *n* is unity. However, the sample was a film condensed on a room-temperature

substrate, and its density was probably lower than bulk. The resultant $k$ spectrum is lower than expectations based on longer-wavelength data [8, 17]. Windt *et al.* [20] made multiple-angle reflectance measurements on films to obtain optical constants in the 24–1216 Å region, but all the films were produced *ex situ*.

There are discrepancies in the number and strength of interband transitions in the infrared. In the region below 1 eV, Weaver *et al.* [8] found no peaked structures, although that does not necessarily mean interband absorption is negligible. Golovashkin *et al.* [7] and Kirillova and Nomerovannaya [12] find a number of structures in $\varepsilon_2$ below 1 eV. Rashkeev *et al.* [21] calculated that there is an interband peak at 0.09 eV and a weaker one at 0.3 eV. The calculated peaks were at about the correct positions, but were considerably weaker than the experimental ones.

In Table I we list Weaver *et al.*'s data [8] for the near infrared, visible, ultraviolet, and vacuum ultraviolet. The data of Nestell and Christy [14] and of Lluesma and Aspnes [15] cover a smaller spectral region, but they result in larger values of $\varepsilon_2$, indicative of data less affected by overlayers and granularity or roughness of the sample. We do not list them, for they do not match well with the extant infrared data [7, 8, 12], which should be less sensitive to some of the problems mentioned above. The $k$ spectra we list, then, may be somewhat low in the visible, ultraviolet, and vacuum ultraviolet. We also list the soft X-ray data of Weaver and Olson [19]. Values of $n$ and $k$ are plotted in Fig. 1.

We have calculated $n$ and $k$ in the 1.24–240 Å (10,000–51.5 eV) region using the model of Henke *et al.* [22]. The absorption edges are $K$ (18 986 eV), $L_1$ (2698 eV), $L_{2,3}$ (2465, 2371 eV), $M_1$ (469 eV), $M_{2,3}$ (379, 363 eV), $M_{4,5}$ (208, 205 eV), $N_1$ (58 eV), $N_{2,3}$ (34 eV), $N_{4,5}$ (4 eV). At lower frequencies these features are perturbed by the bonding properties of the crystal.

## REFERENCES


1. M. M. Kirillova and B. A. Charikov, *Phys. Met. Metall.* **15**, 13 (1965); *Fiz. Met. Metalloved.* **15**, 495 (1965).
2. B. T. Barnes, *J. Opt. Soc. Am.* **56**, 1546 (1966).
3. A. P. Lenham and D. M. Treherne, *J. Opt. Soc. Am.* **56**, 1137 (1966).
4. A. P. Lenham and D. M. Treherne, in "Optical Properties and Electronic Structure of Metals and Alloys," (F. Abeles, ed.), North-Holland, Amsterdam, 196 (1966).
5. A. P. Lenham, *J. Opt. Soc. Am.* **57**, 473 (1967).
6. M. M. Kirillova, L. V. Nomerovannaya, G. A. Bolotin, V. M. Mayevskiy, M. M. Noskov, and M. L. Bolotina, *Phys. Met. Metall.* **25**, 81 (1968); *Fiz. Met. Metalloved.* **25**, 459 (1968).
7. A. I. Golovashkin, I. E. Leksina, G. P. Motulevich, and A. A. Shubin, *Soviet Phys. JETP* **29**, 27 (1969); *Zh. Eksp. Teor. Fiz.* **56**, 51 (1969).
8. J. H. Weaver, D. W. Lynch, and C. G. Olson, *Phys. Rev.* **B7**, 4311 (1973).
9. M. Sigrist, G. Chessaing, and P. Gravier, *Solid State Commun.* **17**, 647 (1975).

10. M. Sigrist, G. Chessaing, P. Gravier, and R. Pierrisnard, *Compt. Rend. Acad.* **280**, 413 (1975).
11. G. Chessaing, P. Gravier, and M. Sigrist, *Thin Solid Films* **35**, L25 (1976).
12. M. M. Kirillova and L. V. Nomerovannaya, *Sov. Phys. Solid State* **20**, 568 (1978); *Fiz. Tverd. Tela* **20**, 984 (1978).
13. P. Gravier, G. Chassaing, and M. Sigrist, *Thin Solid Films* **57**, 93 (1979).
14. J. E. Nestell and R. W. Christy, *Phys. Rev.* **B21**, 3173 (1980).
15. E. Lluesma and D. E. Aspnes, unpublished.
16. A. I. Golovashkin and A. L. Shelekhov, *Sov. Phys. JETP* **57**, 1246 (1983); *Zh. Eksp. Teor. Fiz.* **84**, 2141 (1983).
17. V. V. Truong, L. J. LeBlanc, and G. J. Turpin, *J. Opt. Soc. Am.* **68**, 1017 (1978).
18. J. J. Carroll, C. T. Ceyer, and A. J. Melmed, *J. Opt. Soc. Am.* **72**, 668 (1982).
19. J. H. Weaver and C. G. Olson, *Phys. Rev.* **B14**, 3251 (1976).
20. D. L. Windt, W. C. Cash, M. Scott, P. Arendt, B. Newnam, R. F. Fisher, and A. B. Swartzlander, *Appl. Opt.* **27**, 246 (1988).
21. S. N. Rashkeev, Y. A. Uspenskii, and I. I. Mazin, *Soviet Phys. JETP* **61**, 1004 (1985); *Zh. Eksp. Teor. Fiz.* **88**, 1687 (1985).
22. B. L. Henke, J. C. Davis, E. M. Gullikson, and R. C. C. Perera, Lawrence Berkeley Laboratory Report No. LBL-26259 (1988).

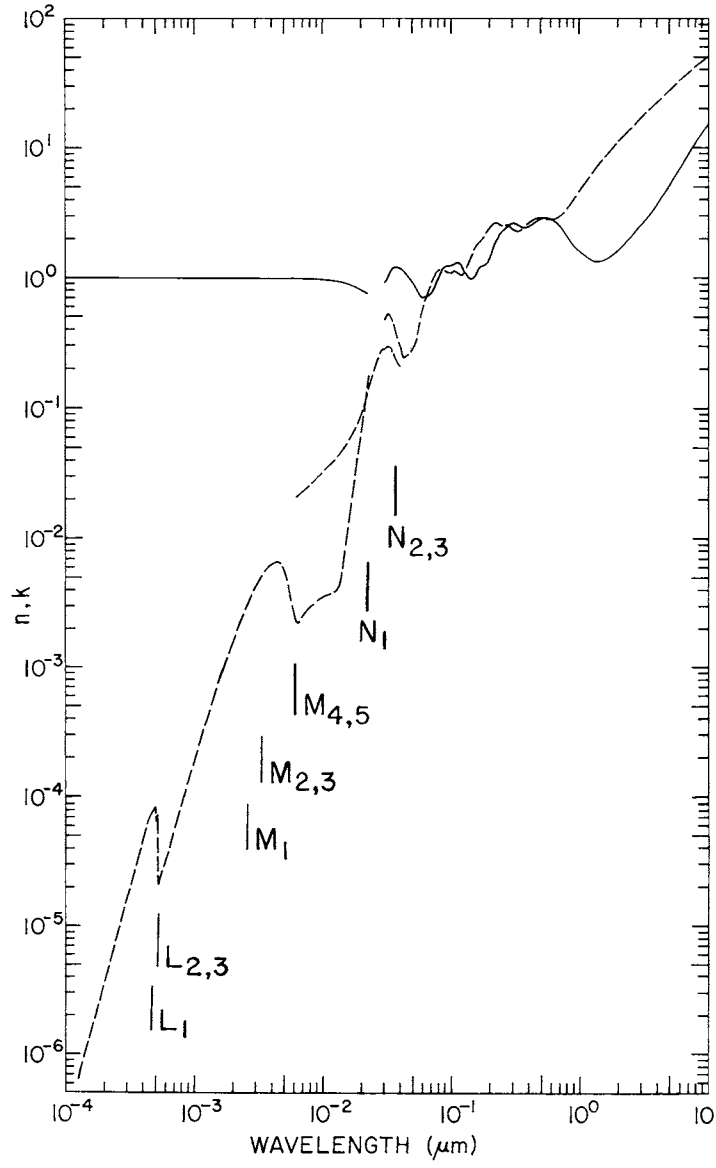


**Fig. 1.** Log–log plot of $n$ (solid line) and $k$ (dashed line) versus wavelength in micrometers for niobium.

TABLE I

Values of $n$ and $k$ Obtained from Various References for Niobium[a]

| eV | $cm^{-1}$ | Å | $n$ | $k$ |
|---|---|---|---|---|
| 10000 | | 1.240 | 0.9999845 [22] | 6.55E-07 [22] |
| 9549 | | 1.298 | 0.9999829 | 7.80E-07 |
| 9117 | | 1.360 | 0.9999812 | 9.28E-07 |
| 8706 | | 1.424 | 0.9999794 | 1.10E-06 |
| 8313 | | 1.492 | 0.9999774 | 1.31E-06 |
| 7937 | | 1.562 | 0.9999751 | 1.56E-06 |
| 7579 | | 1.636 | 0.9999726 | 1.86E-06 |
| 7237 | | 1.713 | 0.9999700 | 2.21E-06 |
| 6910 | | 1.794 | 0.9999670 | 2.62E-06 |
| 6598 | | 1.879 | 0.9999638 | 3.11E-06 |
| 6300 | | 1.968 | 0.9999602 | 3.70E-06 |
| 6015 | | 2.061 | 0.9999564 | 4.39E-06 |
| 5744 | | 2.159 | 0.9999521 | 5.21E-06 |
| 5484 | | 2.261 | 0.9999475 | 6.18E-06 |
| 5237 | | 2.368 | 0.9999425 | 7.34E-06 |
| 5000 | | 2.480 | 0.9999370 | 8.70E-06 |
| 4775 | | 2.597 | 0.9999310 | 1.03E-05 |
| 4559 | | 2.720 | 0.9999245 | 1.22E-05 |
| 4353 | | 2.848 | 0.9999175 | 1.44E-05 |
| 4157 | | 2.983 | 0.9999099 | 1.71E-05 |
| 3969 | | 3.124 | 0.9999018 | 2.02E-05 |
| 3790 | | 3.272 | 0.999893 | 2.38E-05 |
| 3619 | | 3.426 | 0.999884 | 2.81E-05 |
| 3455 | | 3.588 | 0.999874 | 3.31E-05 |
| 3299 | | 3.758 | 0.999864 | 3.90E-05 |
| 3150 | | 3.936 | 0.999854 | 4.59E-05 |
| 3008 | | 4.122 | 0.999845 | 5.39E-05 |
| 2872 | | 4.317 | 0.999836 | 6.32E-05 |
| 2807 | | 4.418 | 0.999833 | 6.84E-05 |
| 2742 | | 4.521 | 0.999832 | 7.40E-05 |
| 2680 | | 4.627 | 0.999832 | 7.02E-05 |
| 2619 | | 4.735 | 0.999826 | 7.59E-05 |
| 2559 | | 4.846 | 0.999825 | 8.21E-05 |
| 2500 | | 4.959 | 0.999831 | 8.88E-05 |
| 2443 | | 5.075 | 0.999835 | 6.97E-05 |
| 2387 | | 5.193 | 0.999839 | 7.57E-05 |
| 2333 | | 5.315 | 0.999822 | 2.21E-05 |
| 2280 | | 5.439 | 0.999795 | 2.38E-05 |
| 2228 | | 5.566 | 0.999775 | 2.58E-05 |
| 2177 | | 5.696 | 0.999757 | 2.79E-05 |
| 2078 | | 5.965 | 0.999723 | 3.26E-05 |
| 1985 | | 6.248 | 0.999688 | 3.83E-05 |
| 1895 | | 6.543 | 0.999651 | 4.49E-05 |

[a]The references from which the values were extracted are given in brackets.

TABLE I (*Continued*)

Niobium

| eV | $cm^{-1}$ | Å | *n* | *k* |
|---|---|---|---|---|
| 1809 | | 6.852 | 0.999613 | 5.27E-05 |
| 1728 | | 7.176 | 0.999570 | 6.19E-05 |
| 1650 | | 7.516 | 0.999525 | 7.29E-05 |
| 1575 | | 7.871 | 0.999475 | 8.58E-05 |
| 1504 | | 8.244 | 0.999422 | 1.01E-04 |
| 1436 | | 8.633 | 0.999364 | 1.18E-04 |
| 1371 | | 9.041 | 0.999301 | 1.38E-04 |
| 1309 | | 9.469 | 0.999232 | 1.61E-04 |
| 1250 | | 9.917 | 0.999157 | 1.88E-04 |
| 1194 | | 10.39 | 0.999076 | 2.20E-04 |
| 1140 | | 10.88 | 0.99899 | 2.56E-04 |
| 1088 | | 11.39 | 0.99889 | 2.99E-04 |
| 1039 | | 11.93 | 0.99879 | 3.47E-04 |
| 992.3 | | 12.49 | 0.99868 | 4.05E-04 |
| 947.5 | | 13.09 | 0.99856 | 4.70E-04 |
| 904.7 | | 13.70 | 0.99843 | 5.49E-04 |
| 863.9 | | 14.35 | 0.99830 | 6.47E-04 |
| 824.9 | | 15.03 | 0.99817 | 7.50E-04 |
| 787.7 | | 15.74 | 0.99803 | 8.58E-04 |
| 752.1 | | 16.49 | 0.99787 | 9.82E-04 |
| 718.1 | | 17.27 | 0.99772 | 1.12E-03 |
| 685.7 | | 18.08 | 0.99755 | 1.27E-03 |
| 654.7 | | 18.94 | 0.99737 | 1.44E-03 |
| 625.1 | | 19.83 | 0.99719 | 1.64E-03 |
| 596.9 | | 20.77 | 0.99700 | 1.86E-03 |
| 570.0 | | 21.75 | 0.99682 | 2.11E-03 |
| 544.2 | | 22.78 | 0.99666 | 2.40E-03 |
| 519.7 | | 23.86 | 0.99651 | 2.67E-03 |
| 496.2 | | 24.99 | 0.99635 | 2.96E-03 |
| 484.9 | | 25.57 | 0.99627 | 3.12E-03 |
| 473.8 | | 26.17 | 0.99620 | 3.29E-03 |
| 463.0 | | 26.78 | 0.99613 | 3.47E-03 |
| 452.4 | | 27.41 | 0.99608 | 3.65E-03 |
| 442.1 | | 28.05 | 0.99602 | 3.82E-03 |
| 432.0 | | 28.70 | 0.99596 | 4.00E-03 |
| 412.5 | | 30.06 | 0.99587 | 4.38E-03 |
| 403.0 | | 30.76 | 0.99585 | 4.59E-03 |
| 393.8 | | 31.48 | 0.99585 | 4.77E-03 |
| 384.8 | | 32.22 | 0.99584 | 4.93E-03 |
| 376.1 | | 32.97 | 0.99582 | 5.10E-03 |
| 367.5 | | 33.74 | 0.99581 | 5.28E-03 |
| 359.1 | | 34.53 | 0.99580 | 5.46E-03 |
| 350.9 | | 35.34 | 0.99580 | 5.65E-03 |
| 342.9 | | 36.16 | 0.99584 | 5.83E-03 |
| 335.0 | | 37.01 | 0.99590 | 5.97E-03 |

(*Continued*)

TABLE I (*Continued*)

Niobium

| eV | $cm^{-1}$ | Å | $n$ | $k$ |
|---|---|---|---|---|
| 319.9 | | 38.76 | 0.99597 | 6.22E-03 |
| 305.5 | | 40.58 | 0.99612 | 6.48E-03 |
| 291.7 | | 42.50 | 0.99628 | 6.48E-03 |
| 278.5 | | 44.52 | 0.99637 | 6.48E-03 |
| 265.9 | | 46.63 | 0.99663 | 6.28E-03 |
| 253.9 | | 48.83 | 0.99658 | 5.77E-03 |
| 242.5 | | 51.13 | 0.99645 | 5.06E-03 |
| 231.5 | | 53.56 | 0.99586 | 4.12E-03 |
| 221.1 | | 56.08 | 0.99472 | 3.23E-03 |
| 216.0 | | 57.40 | 0.99400 | 2.87E-03 |
| 211.1 | | 58.73 | 0.99322 | 2.62E-03 |
| 206.2 | | 60.13 | 0.99238 | 2.41E-03 |
| 201.5 | | 61.53 | 0.99149 | 2.30E-03 |
| 196.9 | | 62.97 | 0.99060 | 2.26E-03 |
| 192.4 | | 64.44 | 0.98970 | 2.29E-03 |
| 188.0 | | 65.95 | 0.9888 | 2.34E-03 |
| 179.6 | | 69.03 | 0.9871 | 2.55E-03 |
| 171.4 | | 72.34 | 0.9853 | 2.70E-03 |
| 163.7 | | 75.74 | 0.9834 | 2.86E-03 |
| 156.3 | | 79.32 | 0.9814 | 3.01E-03 |
| 149.3 | | 83.04 | 0.9791 | 3.16E-03 |
| 142.5 | | 87.01 | 0.9767 | 3.27E-03 |
| 136.1 | | 91.10 | 0.9740 | 3.40E-03 |
| 129.9 | | 95.45 | 0.9709 | 3.51E-03 |
| 124.1 | | 99.91 | 0.9676 | 3.60E-03 |
| 118.5 | | 104.6 | 0.9638 | 3.69E-03 |
| 113.1 | | 109.6 | 0.9595 | 3.75E-03 |
| 108.0 | | 114.8 | 0.9546 | 3.78E-03 |
| 103.1 | | 120.3 | 0.9490 | 3.87E-03 |
| 98.47 | | 125.9 | 0.9424 | 4.03E-03 |
| 94.03 | | 131.9 | 0.9348 | 4.69E-03 |
| 89.78 | | 138.1 | 0.9263 | 5.74E-03 |
| 85.73 | | 144.7 | 0.9164 | 7.34E-03 |
| 81.85 | | 151.5 | 0.9054 | 9.92E-03 |
| 78.16 | | 158.6 | 0.8929 | 1.35E-02 |
| 74.63 | | 166.1 | 0.8791 | 1.87E-02 |
| 71.26 | | 174.0 | 0.8643 | 2.57E-02 |
| 68.04 | | 182.2 | 0.8478 | 3.45E-02 |
| 64.97 | | 190.8 | 0.8299 | 4.62E-02 |
| 63.49 | | 195.3 | 0.8206 | 5.36E-02 |
| 62.04 | | 199.8 | 0.8113 | 6.20E-02 |
| 60.62 | | 204.5 | 0.8021 | 7.10E-02 |
| 59.24 | | 209.3 | 0.7926 | 8.12E-02 |
| 57.88 | | 214.2 | 0.7828 | 9.27E-02 |
| 56.56 | | 219.2 | 0.7732 | 0.106 |

(*Continued*)

TABLE I (*Continued*)

**Niobium**

| eV | $cm^{-1}$ | Å | *n* | *k* |
|---|---|---|---|---|
| 54.01 | | 229.6 | 0.7559 | 0.138 |
| 51.57 | | 240.4 | 0.7451 | 0.178 |
| 200 | | 61.99 | | 2.0E-02 [19] |
| 150 | | 82.66 | | 2.6E-02 |
| 100 | | 124.0 | | 3.9E-02 |
| 95.0 | | 130.5 | | 4.2E-02 |
| 90.0 | | 137.8 | | 4.4E-02 |
| 85.0 | | 145.9 | | 4.7E-02 |
| 80.0 | | 155.0 | | 5.2E-02 |
| 75.0 | | 165.3 | | 5.7E-02 |
| 70.0 | | 177.1 | | 6.5E-02 |
| 65.0 | | 190.7 | | 7.7E-02 |
| 60.0 | | 206.6 | | 9.4E-02 |
| 55.0 | | 225.4 | | 0.126 |
| 50.0 | | 248.0 | | 0.180 |
| 45.0 | | 275.5 | | 0.243 |
| 44.0 | | 281.8 | | 0.258 |
| 43.0 | | 288.3 | | 0.275 |
| 42.0 | | 295.2 | | 0.277 |
| 41.0 | | 302.4 | | 0.279 |
| 40.5 | | 306.1 | 0.920 [8] | 0.47 [8] |
| 40.0 | | 310.0 | | 0.284 [19] |
| 39.5 | | 313.9 | 0.950 [8] | 0.50 [8] |
| 39.0 | | 317.9 | | 0.291 [19] |
| 38.5 | | 322.0 | 1.00 [8] | 0.53 [8] |
| 38.0 | | 326.3 | | 0.293 [19] |
| 37.5 | | 330.6 | 1.07 [8] | 0.53 [8] |
| 37.0 | | 335.1 | | 0.291 [19] |
| 36.8 | | 336.9 | 1.11 [8] | 0.52 [8] |
| 36.4 | | 340.6 | 1.13 | 0.51 |
| 36.0 | | 344.4 | 1.15 | 0.50 |
| | | | | 0.288 [19] |
| 35.6 | | 348.3 | 1.16 [8] | 0.49 [8] |
| 35.2 | | 352.2 | 1.17 | 0.47 |
| 35.0 | | 354.2 | | 0.268 [19] |
| 34.8 | | 356.3 | 1.19 [8] | 0.46 [8] |
| 34.4 | | 360.4 | 1.20 | 0.44 |
| 34.0 | | 364.7 | 1.20 | 0.42 |
| 33.8 | | 366.8 | 1.21 | 0.41 |
| 33.6 | | 369.0 | 1.21 | 0.41 |
| 33.4 | | 371.2 | 1.21 | 0.40 |
| 33.2 | | 373.4 | 1.21 | 0.39 |
| 33.0 | | 375.7 | 1.21 | 0.38 |
| 32.8 | | 378.0 | 1.21 | 0.37 |

(*Continued*)

TABLE I (*Continued*)

Niobium

| eV | $cm^{-1}$ | Å | $n$ | $k$ |
|---|---|---|---|---|
| 32.6 | | 380.3 | 1.21 | 0.36 |
| 32.4 | | 382.7 | 1.21 | 0.35 |
| 32.2 | | 385.0 | 1.21 | 0.35 |
| 32.0 | | 387.5 | 1.20 | 0.34 |
| 31.8 | | 389.9 | 1.20 | 0.33 |
| 31.6 | | 392.4 | 1.20 | 0.32 |
| 31.4 | | 394.9 | 1.19 | 0.32 |
| 31.2 | | 397.4 | 1.18 | 0.31 |
| 31.0 | | 399.9 | 1.18 | 0.31 |
| 30.8 | | 402.5 | 1.17 | 0.31 |
| 30.6 | | 405.2 | 1.18 | 0.31 |
| 30.4 | | 407.8 | 1.18 | 0.30 |
| 30.2 | | 410.5 | 1.18 | 0.29 |
| 30.0 | | 413.3 | 1.18 | 0.28 |
| | | | | 0.207 [19] |
| 29.8 | | 416.1 | 1.17 [8] | 0.27 [8] |
| 29.6 | | 418.9 | 1.16 | 0.26 |
| 29.4 | | 421.7 | 1.15 | 0.25 |
| 29.2 | | 424.6 | 1.14 | 0.25 |
| 29.0 | | 427.5 | 1.13 | 0.25 |
| 28.8 | | 430.5 | 1.12 | 0.25 |
| 28.6 | | 433.5 | 1.11 | 0.24 |
| 28.4 | | 436.6 | 1.10 | 0.24 |
| 28.2 | | 439.7 | 1.09 | 0.24 |
| 28.0 | | 442.8 | 1.08 | 0.24 |
| 27.8 | | 446.0 | 1.07 | 0.25 |
| 27.6 | | 449.2 | 1.06 | 0.25 |
| 27.4 | | 452.5 | 1.05 | 0.25 |
| 27.2 | | 455.8 | 1.05 | 0.25 |
| 27.0 | | 459.2 | 1.04 | 0.25 |
| 26.8 | | 462.6 | 1.03 | 0.25 |
| 26.6 | | 466.1 | 1.03 | 0.25 |
| 26.4 | | 469.6 | 1.02 | 0.26 |
| 26.2 | | 473.2 | 1.01 | 0.26 |
| 26.0 | | 476.9 | 1.00 | 0.26 |
| 25.8 | | 480.6 | 0.99 | 0.26 |
| 25.6 | | 484.3 | 0.99 | 0.26 |
| 25.4 | | 488.1 | 0.98 | 0.27 |
| 25.2 | | 492.0 | 0.97 | 0.27 |
| 25.0 | | 495.9 | 0.96 | 0.27 |
| 24.8 | | 499.9 | 0.95 | 0.28 |
| 24.6 | | 504.0 | 0.94 | 0.28 |
| 24.4 | | 508.1 | 0.93 | 0.28 |
| 24.2 | | 512.3 | 0.92 | 0.29 |
| 24.0 | | 516.6 | 0.91 | 0.29 |

(*Continued*)

TABLE I (*Continued*)

**Niobium**

| eV | $cm^{-1}$ | Å | *n* | *k* |
|---|---|---|---|---|
| 23.8 | | 520.9 | 0.90 | 0.30 |
| 23.6 | | 525.4 | 0.88 | 0.30 |
| 23.4 | | 529.8 | 0.87 | 0.31 |
| 23.2 | | 534.4 | 0.86 | 0.32 |
| 23.0 | | 539.1 | 0.85 | 0.33 |
| 22.8 | | 543.8 | 0.83 | 0.34 |
| 22.6 | | 548.6 | 0.82 | 0.35 |
| 22.4 | | 553.5 | 0.81 | 0.36 |
| 22.2 | | 558.5 | 0.79 | 0.38 |
| 22.0 | | 563.6 | 0.78 | 0.40 |
| 21.8 | | 568.7 | 0.77 | 0.41 |
| 21.6 | | 574.0 | 0.75 | 0.43 |
| 21.4 | | 579.4 | 0.74 | 0.45 |
| 21.2 | | 584.8 | 0.73 | 0.47 |
| 21.0 | | 590.4 | 0.72 | 0.50 |
| 20.8 | | 596.1 | 0.72 | 0.52 |
| 20.6 | | 601.9 | 0.71 | 0.55 |
| 20.4 | | 607.8 | 0.72 | 0.57 |
| 20.2 | | 613.8 | 0.72 | 0.60 |
| 20.0 | | 619.9 | 0.72 | 0.62 |
| 19.8 | | 626.2 | 0.72 | 0.64 |
| 19.6 | | 632.6 | 0.72 | 0.66 |
| 19.4 | | 639.1 | 0.73 | 0.68 |
| 19.2 | | 645.8 | 0.73 | 0.69 |
| 19.0 | | 652.5 | 0.72 | 0.72 |
| 18.8 | | 659.5 | 0.73 | 0.74 |
| 18.6 | | 666.6 | 0.73 | 0.77 |
| 18.4 | | 673.8 | 0.73 | 0.79 |
| 18.2 | | 681.2 | 0.73 | 0.82 |
| 18.0 | | 688.8 | 0.74 | 0.85 |
| 17.8 | | 696.5 | 0.75 | 0.87 |
| 17.6 | | 704.5 | 0.76 | 0.90 |
| 17.4 | | 712.6 | 0.77 | 0.93 |
| 17.2 | | 720.8 | 0.79 | 0.96 |
| 17.0 | | 729.3 | 0.80 | 0.99 |
| 16.8 | | 738.0 | 0.82 | 1.02 |
| 16.6 | | 746.9 | 0.85 | 1.04 |
| 16.4 | | 756.0 | 0.87 | 1.06 |
| 16.2 | | 765.3 | 0.89 | 1.09 |
| 16.0 | | 774.9 | 0.92 | 1.11 |
| 15.8 | | 784.7 | 0.95 | 1.13 |
| 15.6 | | 794.8 | 0.99 | 1.14 |
| 15.4 | | 805.1 | 1.02 | 1.15 |
| 15.2 | | 815.7 | 1.05 | 1.16 |
| 15.0 | | 826.6 | 1.08 | 1.16 |

(*Continued*)

TABLE I (*Continued*)

Niobium

| eV | $cm^{-1}$ | Å | $n$ | $k$ |
|---|---|---|---|---|
| 14.8 | | 837.7 | 1.11 | 1.16 |
| 14.6 | | 849.2 | 1.14 | 1.15 |
| 14.4 | | 861.0 | 1.16 | 1.15 |
| 14.2 | | 873.1 | 1.18 | 1.14 |
| 14.0 | | 885.6 | 1.20 | 1.13 |
| 13.8 | | 898.4 | 1.22 | 1.13 |
| 13.6 | | 911.6 | 1.23 | 1.12 |
| 13.4 | | 925.3 | 1.24 | 1.10 |
| 13.2 | | 939.3 | 1.24 | 1.09 |
| 13.0 | | 953.7 | 1.24 | 1.09 |
| 12.8 | | 968.6 | 1.24 | 1.09 |
| 12.6 | | 984.0 | 1.24 | 1.09 |
| 12.4 | | 999.9 | 1.24 | 1.10 |
| eV | $cm^{-1}$ | μm | $n$ | $k$ |
| 12.2 | 98399 | 0.1016 | 1.25 | 1.11 |
| 12.0 | 96786 | 0.1033 | 1.25 | 1.12 |
| 11.8 | 95173 | 0.1051 | 1.27 | 1.13 |
| 11.6 | 93560 | 0.1069 | 1.28 | 1.13 |
| 11.4 | 91946 | 0.1088 | 1.30 | 1.13 |
| 11.3 | 91140 | 0.1097 | 1.31 | 1.12 |
| 11.2 | 90333 | 0.1107 | 1.31 | 1.12 |
| 11.1 | 89527 | 0.1117 | 1.32 | 1.11 |
| 11.0 | 88720 | 0.1127 | 1.32 | 1.10 |
| 10.9 | 87914 | 0.1137 | 1.32 | 1.09 |
| 10.8 | 87107 | 0.1148 | 1.32 | 1.08 |
| 10.7 | 86301 | 0.1159 | 1.31 | 1.07 |
| 10.6 | 85494 | 0.1170 | 1.30 | 1.06 |
| 10.5 | 84688 | 0.1181 | 1.29 | 1.05 |
| 10.4 | 83881 | 0.1192 | 1.27 | 1.04 |
| 10.3 | 83074 | 0.1204 | 1.25 | 1.04 |
| 10.2 | 82268 | 0.1216 | 1.23 | 1.04 |
| 10.1 | 81461 | 0.1228 | 1.20 | 1.04 |
| 10.0 | 80655 | 0.1240 | 1.18 | 1.05 |
| 9.9 | 79848 | 0.1252 | 1.15 | 1.06 |
| 9.8 | 79042 | 0.1265 | 1.13 | 1.09 |
| 9.7 | 78235 | 0.1278 | 1.11 | 1.11 |
| 9.6 | 77429 | 0.1292 | 1.10 | 1.13 |
| 9.5 | 76622 | 0.1305 | 1.08 | 1.15 |
| 9.4 | 75816 | 0.1319 | 1.07 | 1.18 |
| 9.3 | 75009 | 0.1333 | 1.06 | 1.19 |
| 9.2 | 74202 | 0.1348 | 1.04 | 1.22 |
| 9.1 | 73396 | 0.1362 | 1.02 | 1.25 |
| 9.0 | 72589 | 0.1378 | 1.01 | 1.29 |

(*Continued*)

TABLE I (*Continued*)

Niobium

| eV | $cm^{-1}$ | μm | *n* | *k* |
|---|---|---|---|---|
| 8.9 | 71783 | 0.1393 | 1.00 | 1.32 |
| 8.8 | 70976 | 0.1409 | 1.00 | 1.36 |
| 8.7 | 70170 | 0.1425 | 0.99 | 1.39 |
| 8.6 | 69363 | 0.1442 | 0.99 | 1.43 |
| 8.4 | 67750 | 0.1476 | 0.99 | 1.51 |
| 8.2 | 66137 | 0.1512 | 1.00 | 1.60 |
| 8.0 | 64524 | 0.1550 | 1.02 | 1.69 |
| 7.8 | 62911 | 0.1590 | 1.07 | 1.78 |
| 7.6 | 61298 | 0.1631 | 1.14 | 1.85 |
| 7.4 | 59684 | 0.1675 | 1.20 | 1.88 |
| 7.2 | 58071 | 0.1722 | 1.22 | 1.91 |
| 7.0 | 56458 | 0.1771 | 1.23 | 1.96 |
| 6.8 | 54845 | 0.1823 | 1.24 | 2.04 |
| 6.6 | 53232 | 0.1879 | 1.26 | 2.14 |
| 6.4 | 51619 | 0.1937 | 1.31 | 2.25 |
| 6.2 | 50006 | 0.2000 | 1.38 | 2.38 |
| 6.0 | 48393 | 0.2066 | 1.49 | 2.49 |
| 5.8 | 46780 | 0.2138 | 1.63 | 2.60 |
| 5.6 | 45167 | 0.2214 | 1.81 | 2.67 |
| 5.4 | 43554 | 0.2296 | 2.00 | 2.68 |
| 5.2 | 41940 | 0.2384 | 2.16 | 2.62 |
| 5.0 | 40327 | 0.2480 | 2.26 | 2.57 |
| 4.8 | 38714 | 0.2583 | 2.32 | 2.52 |
| 4.6 | 37101 | 0.2695 | 2.39 | 2.56 |
| 4.4 | 35488 | 0.2818 | 2.53 | 2.56 |
| 4.2 | 33875 | 0.2952 | 2.64 | 2.42 |
| 4.0 | 32262 | 0.3100 | 2.64 | 2.33 |
| 3.9 | 31455 | 0.3179 | 2.62 | 2.29 |
| 3.8 | 30649 | 0.3263 | 2.59 | 2.28 |
| 3.7 | 29842 | 0.3351 | 2.56 | 2.27 |
| 3.6 | 29036 | 0.3444 | 2.52 | 2.29 |
| 3.5 | 28229 | 0.3542 | 2.48 | 2.33 |
| 3.4 | 27423 | 0.3647 | 2.46 | 2.38 |
| 3.3 | 26616 | 0.3757 | 2.44 | 2.45 |
| 3.2 | 25810 | 0.3875 | 2.45 | 2.53 |
| 3.1 | 25004 | 0.3999 | 2.48 | 2.60 |
| 3.00 | 24197 | 0.4133 | 2.51 | 2.68 |
| 2.85 | 22987 | 0.4350 | 2.58 | 2.80 |
| 2.75 | 22181 | 0.4509 | 2.66 | 2.86 |
| 2.65 | 21374 | 0.4679 | 2.74 | 2.90 |
| 2.55 | 20568 | 0.4862 | 2.83 | 2.92 |
| 2.45 | 19761 | 0.5061 | 2.89 | 2.90 |
| 2.35 | 18954 | 0.5276 | 2.92 | 2.88 |
| 2.25 | 18148 | 0.5510 | 2.93 | 2.87 |
| 2.15 | 17341 | 0.5767 | 2.92 | 2.87 |

(*Continued*)

TABLE I (*Continued*)

Niobium

| eV | $cm^{-1}$ | μm | $n$ | $k$ |
|---|---|---|---|---|
| 2.05 | 16535 | 0.6048 | 2.89 | 2.87 |
| 1.95 | 15728 | 0.6358 | 2.82 | 2.86 |
| 1.85 | 14922 | 0.6702 | 2.69 | 2.89 |
| 1.75 | 14115 | 0.7085 | 2.54 | 2.99 |
| 1.65 | 13308 | 0.7514 | 2.36 | 3.13 |
| 1.55 | 12502 | 0.7999 | 2.15 | 3.37 |
| 1.45 | 11695 | 0.8551 | 1.95 | 3.68 |
| 1.35 | 10889 | 0.9184 | 1.76 | 4.13 |
| 1.25 | 10082 | 0.9919 | 1.65 | 4.63 |
| 1.15 | 9276 | 1.078 | 1.55 | 5.18 |
| 1.05 | 8469 | 1.181 | 1.44 | 5.86 |
| 0.95 | 7662 | 1.305 | 1.35 | 6.70 |
| 0.85 | 6856 | 1.459 | 1.35 | 7.74 |
| 0.75 | 6049 | 1.653 | 1.41 | 9.00 |
| 0.65 | 5243 | 1.907 | 1.57 | 10.6 |
| 0.55 | 4436 | 2.254 | 1.83 | 12.7 |
| 0.45 | 3630 | 2.755 | 2.28 | 15.6 |
| 0.35 | 2823 | 3.542 | 3.11 | 20.0 |
| 0.28 | 2258 | 4.428 | 4.26 | 25.0 |
| 0.24 | 1936 | 5.166 | 5.47 | 28.9 |
| 0.20 | 1613 | 6.199 | 7.25 | 34.1 |
| 0.16 | 1290 | 7.749 | 10.2 | 41.7 |
| 0.12 | 967.9 | 10.33 | 16.0 | 53.2 |

## IX TANTALUM (Ta)

Tantalum is a body-centered cubic metal. It is relatively nonreactive, but a thin oxide layer forms at room temperature, which may affect ellipsometric measurements in the visible and near ultraviolet and all measurements further in the ultraviolet. Very few measurements have been carried out in ultrahigh vacuum, and as for other refractory transition metals, it is difficult to make large-grained films that are of bulk density without condensation on a hot substrate. In common with other transition metals, Ta has interband transitions extending to arbitrarily low energies, making the determination of Drude parameters unreliable.

The near-infrared, visible, and near-ultraviolet data reported to date [1–11] do not agree well qualitatively, although there is agreement on structures. There are only three sets of VUV data [5, 6, 12]. They agree in magnitude, but disagree on the occurrence of a peak in $\varepsilon_2$ at about 8.5 eV. Two transmission studies have been made in the soft X-ray region [13, 14], from which $k$ spectra can be obtained. However, these spectra do not match well any of the spectra from longer wavelengths. The data listed

below for the 20–40 eV region must be considered less reliable than the other data. Finally, Windt *et al.* [15] measured multiple-angle reflectance on thin-film samples prepared ex situ, from which optical constants were derived for the 24–1216 Å region. Ordal *et al.* [16] measured the far-infrared optical properties in the 41.3–413 μm region using a cavity technique. Both optical constants were obtained from a single measurement at each wavelength by using an approximation that should be valid in this spectral region.

We list in Table I the data of Weaver *et al.* [6] for the infrared, visible, ultraviolet, and vacuum ultraviolet. These data were taken on bulk electropolished samples, and were derived by Kramers–Kronig analysis of absorptance measurements at low temperature (longer wavelengths) and room-temperature reflectance measurements (shorter wavelengths). We list the $k$ spectrum in the soft X-ray region derived from absorption (transmission) measurements [14] under the assumption that $n$ is unity. This spectrum does not join well with the higher-energy end of the data from Ref. [6], however. The discrepancy may be ascribable to the effect of an oxide overlayer on the high-energy region of the data of Ref. [6]. The spectra of $n$ and $k$ are given in Fig. 1.

We have calculated $n$ and $k$ in the 1.24–240 Å (10,000–51.5 eV) region using the model of Henke *et al.* [17]. The absorption edges are $K$ (67,417 eV), $L_1$ (11,680 eV), $L_{2,3}$ (11,156, 9881 eV), $M_1$ (2708 eV), $M_{2,3}$ (2469, 2194 eV), $M_{4,5}$ (1793, 1735 eV), $N_1$ (566 eV), $N_{2,3}$ (465, 405 eV), $N_{4,5}$ (242, 230 eV), $N_{6,7}$ (27, 25 eV), $O_1$ (71 eV), $O_{2,3}$ (45, 37 eV), $O_{4,5}$ (6 eV). At lower frequencies these atomic features are perturbed by the bonding properties of the crystal.

## REFERENCES


1. B. T. Barnes, *J. Opt. Soc. Am.* **56**, 1546 (1966).
2. A. P. Lenham and D. M. Treherne, *J. Opt. Soc. Am.* **56**, 1137 (1966).
3. A. P. Lenham, *J. Opt. Soc. Am.* **57**, 473 (1967).
4. A. P. Lenham and D. M. Treherne, in "Optical Properties and Electronic Properties of Metals and Alloys," (F. Abeles, ed.), North-Holland, Amsterdam, 196 (1966).
5. D. W. Juenker, L. J. LeBlanc, and C. R. Martin, *J. Opt. Soc. Am.* **58**, 164 (1968).
6. J. H. Weaver, D. W. Lynch, and C. G. Olson, *Phys. Rev.* **B10**, 501 (1974).
7. M. M. Kirillova, L. V. Nomerovannaya, and M. M. Noskov, *Sov. Phys. Solid State* **16**, 1425 (1975); *Fiz. Tverd. Tela* **16**, 2181 (1974).
8. L. K. Thomas and S. Thurm, *J. Phys. F* **6**, 279 (1976).
9. B. U. Habedank, L. K. Thomas and S. Thurm, *J. Phys. F* **7**, 2217 (1977).
10. P. Gravier, G. Chassaing, and M. Sigrist, *Thin Solid Films* **57**, 93 (1979).
11. J. E. Nestell and R. W. Christy, *Phys. Rev.* **B21**, 3173 (1980).
12. L. J. LeBlanc, J. S. Farrell, and D. W. Juenker, *J. Opt. Soc. Am.* **54**, 956 (1964).
13. P. Jaegle, F. Combet-Farnoux, P. Dhez, M. Cremonese, and G. Onori, *Phys. Lett.* **26A**, 364 (1968).

14. R. Haensel, K. Radler, B. Sonntag, and C. Kunz, *Solid State Commun.* **7**, 1495 (1969).
15. D. L. Windt, W. C. Cash, M. Scott, P. Arendt, B. Newnam, R. F. Fisher, and A. B. Swartzlander, *Appl. Opt.* **27**, 246 (1988).
16. M. A. Ordal, R. J. Bell, R. W. Alexander, L. A. Newquist, and M. R. Querry, *Appl. Opt.* **27**, 1203 (1988).
17. B. L. Henke, J. C. Davis, E. M. Gullikson, and R. C. C. Perera, Lawrence Berkeley Laboratory Report No. LBL-26259 (1988).

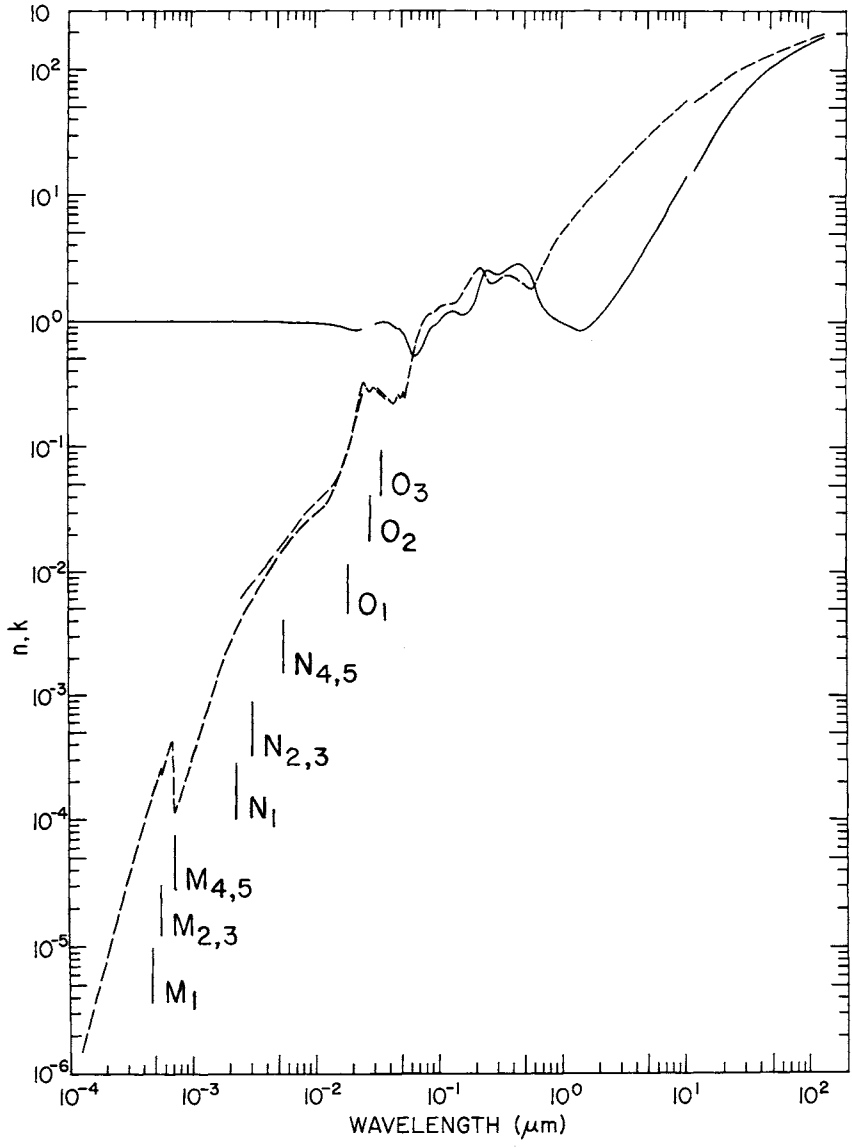


**Fig. 1.** Log–log plot of $n$ (solid line) and $k$ (dashed line) versus wavelength in micrometers for tantalum.

TABLE I

Values of $n$ and $k$ Obtained from Various References for Tantalum[a]

| eV | $cm^{-1}$ | Å | $n$ | $k$ |
|---|---|---|---|---|
| 10000 | | 1.240 | 0.9999766 [17] | 1.49E-06 [17] |
| 9772 | | 1.269 | 0.9999748 | 1.62E-06 |
| 9549 | | 1.298 | 0.9999730 | 1.75E-06 |
| 9117 | | 1.360 | 0.9999697 | 2.07E-06 |
| 8706 | | 1.424 | 0.9999664 | 2.44E-06 |
| 8313 | | 1.492 | 0.9999628 | 2.88E-06 |
| 7937 | | 1.562 | 0.9999589 | 3.39E-06 |
| 7579 | | 1.636 | 0.9999548 | 4.00E-06 |
| 7237 | | 1.713 | 0.9999501 | 4.72E-06 |
| 6910 | | 1.794 | 0.9999451 | 5.56E-06 |
| 6598 | | 1.879 | 0.9999396 | 6.55E-06 |
| 6300 | | 1.968 | 0.9999336 | 7.72E-06 |
| 6015 | | 2.061 | 0.9999270 | 9.10E-06 |
| 5744 | | 2.159 | 0.9999198 | 1.07E-05 |
| 5484 | | 2.261 | 0.9999120 | 1.26E-05 |
| 5237 | | 2.368 | 0.9999033 | 1.48E-05 |
| 5000 | | 2.480 | 0.999894 | 1.75E-05 |
| 4775 | | 2.597 | 0.999884 | 2.06E-05 |
| 4559 | | 2.720 | 0.999873 | 2.42E-05 |
| 4353 | | 2.848 | 0.999861 | 2.84E-05 |
| 4157 | | 2.983 | 0.999847 | 3.34E-05 |
| 3969 | | 3.124 | 0.999833 | 3.92E-05 |
| 3790 | | 3.272 | 0.999818 | 4.60E-05 |
| 3619 | | 3.426 | 0.999801 | 5.40E-05 |
| 3455 | | 3.588 | 0.999784 | 6.33E-05 |
| 3299 | | 3.758 | 0.999765 | 7.42E-05 |
| 3150 | | 3.936 | 0.999745 | 8.69E-05 |
| 3008 | | 4.122 | 0.999725 | 1.02E-04 |
| 2872 | | 4.317 | 0.999704 | 1.19E-04 |
| 2807 | | 4.418 | 0.999694 | 1.28E-04 |
| 2742 | | 4.521 | 0.999685 | 1.39E-04 |
| 2680 | | 4.627 | 0.999673 | 1.44E-04 |
| 2619 | | 4.735 | 0.999661 | 1.56E-04 |
| 2559 | | 4.846 | 0.999650 | 1.70E-04 |
| 2500 | | 4.959 | 0.999644 | 1.84E-04 |
| 2443 | | 5.075 | 0.999634 | 1.87E-04 |
| 2387 | | 5.193 | 0.999619 | 2.03E-04 |
| 2280 | | 5.439 | 0.999601 | 2.40E-04 |
| 2228 | | 5.566 | 0.999602 | 2.60E-04 |
| 2127 | | 5.829 | 0.999577 | 2.62E-04 |
| 2177 | | 5.696 | 0.999603 | 2.42E-04 |
| 2078 | | 5.965 | 0.999563 | 2.84E-04 |
| 1985 | | 6.248 | 0.999552 | 3.32E-04 |
| 1895 | | 6.543 | 0.999569 | 3.90E-04 |

[a]The references from which the values were extracted are given in brackets.

TABLE I (*Continued*)

**Tantalum**

| eV | $cm^{-1}$ | Å | *n* | *k* |
|---|---|---|---|---|
| 1852 | | 6.696 | 0.999604 | 4.22E-04 |
| 1809 | | 6.852 | 0.999696 | 4.21E-04 |
| 1768 | | 7.013 | 0.999757 | 3.20E-04 |
| 1728 | | 7.176 | 0.999723 | 1.14E-04 |
| 1688 | | 7.344 | 0.999592 | 1.23E-04 |
| 1650 | | 7.516 | 0.999516 | 1.32E-04 |
| 1575 | | 7.871 | 0.999405 | 1.53E-04 |
| 1504 | | 8.244 | 0.999307 | 1.78E-04 |
| 1436 | | 8.633 | 0.999212 | 2.05E-04 |
| 1371 | | 9.041 | 0.999114 | 2.37E-04 |
| 1309 | | 9.469 | 0.999012 | 2.74E-04 |
| 1250 | | 9.917 | 0.99890 | 3.16E-04 |
| 1194 | | 10.39 | 0.99879 | 3.64E-04 |
| 1140 | | 10.88 | 0.99867 | 4.19E-04 |
| 1088 | | 11.39 | 0.99854 | 4.82E-04 |
| 1039 | | 11.93 | 0.99840 | 5.54E-04 |
| 992.3 | | 12.49 | 0.99825 | 6.36E-04 |
| 947.5 | | 13.09 | 0.99809 | 7.28E-04 |
| 904.7 | | 13.70 | 0.99792 | 8.31E-04 |
| 863.9 | | 14.35 | 0.99774 | 9.48E-04 |
| 824.9 | | 15.03 | 0.99756 | 1.08E-03 |
| 787.7 | | 15.74 | 0.99736 | 1.23E-03 |
| 752.1 | | 16.49 | 0.99715 | 1.39E-03 |
| 718.1 | | 17.27 | 0.99693 | 1.58E-03 |
| 685.7 | | 18.08 | 0.99671 | 1.78E-03 |
| 654.7 | | 18.94 | 0.99646 | 2.01E-03 |
| 625.1 | | 19.83 | 0.99623 | 2.27E-03 |
| 596.9 | | 20.77 | 0.99600 | 2.56E-03 |
| 583.3 | | 21.26 | 0.99591 | 2.71E-03 |
| 570.0 | | 21.75 | 0.99583 | 2.84E-03 |
| 557.0 | | 22.26 | 0.99571 | 2.90E-03 |
| 544.2 | | 22.78 | 0.99551 | 3.03E-03 |
| 519.7 | | 23.86 | 0.99521 | 3.38E-03 |
| 496.2 | | 24.99 | 0.99491 | 3.74E-03 |
| 473.8 | | 26.17 | 0.99462 | 4.14E-03 |
| 463.0 | | 26.78 | 0.99449 | 4.35E-03 |
| 452.4 | | 27.41 | 0.99438 | 4.56E-03 |
| 442.1 | | 28.04 | 0.99427 | 4.73E-03 |
| 432.0 | | 28.70 | 0.99413 | 4.89E-03 |
| 412.5 | | 30.06 | 0.99379 | 5.22E-03 |
| 403.0 | | 30.77 | 0.99359 | 5.39E-03 |
| 393.8 | | 31.48 | 0.99334 | 5.59E-03 |
| 384.8 | | 32.22 | 0.99309 | 5.83E-03 |
| 376.1 | | 32.97 | 0.99286 | 6.09E-03 |
| 359.1 | | 34.53 | 0.99238 | 6.65E-03 |

(*Continued*)

TABLE I (*Continued*)

**Tantalum**

| eV | $cm^{-1}$ | Å | *n* | *k* |
|---|---|---|---|---|
| 342.9 | | 36.16 | 0.99191 | 7.26E-03 |
| 327.4 | | 37.87 | 0.99142 | 7.93E-03 |
| 312.6 | | 39.66 | 0.99092 | 8.66E-03 |
| 298.5 | | 41.54 | 0.99044 | 9.46E-03 |
| 285.0 | | 43.50 | 0.9900 | 1.03E-02 |
| 272.1 | | 45.56 | 0.9897 | 1.12E-02 |
| 259.9 | | 47.71 | 0.9893 | 1.19E-02 |
| 248.1 | | 49.97 | 0.9888 | 1.27E-02 |
| 242.5 | | 51.14 | 0.9885 | 1.31E-02 |
| 236.9 | | 52.33 | 0.9882 | 1.36E-02 |
| 231.5 | | 53.56 | 0.9879 | 1.40E-02 |
| 226.2 | | 54.81 | 0.9876 | 1.45E-02 |
| 221.1 | | 56.09 | 0.9873 | 1.50E-02 |
| 216.0 | | 57.40 | 0.9870 | 1.54E-02 |
| 206.2 | | 60.12 | 0.9865 | 1.64E-02 |
| 196.9 | | 62.96 | 0.9858 | 1.73E-02 |
| 188.0 | | 65.94 | 0.9852 | 1.82E-02 |
| 179.6 | | 69.05 | 0.9843 | 1.90E-02 |
| 171.4 | | 72.32 | 0.9832 | 1.99E-02 |
| 163.7 | | 75.74 | 0.9820 | 2.10E-02 |
| 156.3 | | 79.32 | 0.9807 | 2.21E-02 |
| 149.3 | | 83.07 | 0.9793 | 2.32E-02 |
| 142.5 | | 87.00 | 0.9777 | 2.45E-02 |
| 136.1 | | 91.11 | 0.9760 | 2.57E-02 |
| 129.9 | | 95.42 | 0.9740 | 2.70E-02 |
| 124.1 | | 99.94 | 0.9719 | 2.82E-02 |
| 118.5 | | 104.7 | 0.9693 | 2.92E-02 |
| 113.1 | | 109.6 | 0.9660 | 3.03E-02 |
| 108.0 | | 114.8 | 0.9621 | 3.19E-02 |
| 103.1 | | 120.2 | 0.9579 | 3.36E-02 |
| 98.47 | | 125.9 | 0.9524 | 3.55E-02 |
| 94.03 | | 131.9 | 0.9462 | 3.89E-02 |
| 89.78 | | 138.1 | 0.9398 | 4.27E-02 |
| 85.73 | | 144.6 | 0.9329 | 4.71E-02 |
| 81.85 | | 151.5 | 0.9250 | 5.20E-02 |
| 78.16 | | 158.6 | 0.9151 | 5.82E-02 |
| 74.63 | | 166.1 | 0.9047 | 6.71E-02 |
| 71.26 | | 174.0 | 0.8937 | 7.77E-02 |
| 68.04 | | 182.2 | 0.8814 | 9.22E-02 |
| 64.97 | | 190.8 | 0.8714 | 0.110 |
| 62.04 | | 200.0 | 0.8623 | 0.131 |
| 59.24 | | 209.3 | 0.8546 | 0.156 |
| 56.56 | | 219.2 | 0.8508 | 0.188 |
| 54.01 | | 229.6 | 0.8567 | 0.225 |
| 51.57 | | 240.4 | 0.8744 | 0.256 |

(*Continued*)

TABLE I (*Continued*)

**Tantalum**

| eV | $cm^{-1}$ | Å | *n* | *k* |
|---|---|---|---|---|
| 500 | | 24.80 | | 6.0E-03 [14] |
| 400 | | 31.00 | | 8.0E-03 |
| 300 | | 41.33 | | 1.2E-02 |
| 200 | | 61.99 | | 2.0E-02 |
| 190 | | 65.25 | | 2.1E-02 |
| 780 | | 15.90 | | 5.0E-03 |
| 170 | | 72.93 | | 2.4E-02 |
| 160 | | 77.49 | | 2.6E-02 |
| 150 | | 82.66 | | 2.9E-02 |
| 140 | | 88.56 | | 3.1E-02 |
| 130 | | 95.37 | | 3.4E-02 |
| 120 | | 103.3 | | 3.7E-02 |
| 110 | | 112.7 | | 4.0E-02 |
| 100 | | 124.0 | | 4.4E-02 |
| 90.0 | | 137.8 | | 5.0E-02 |
| 80.0 | | 155.0 | | 6.0E-02 |
| 70.0 | | 177.1 | | 8.0E-02 |
| 60.0 | | 206.6 | | 0.148 |
| 55.0 | | 225.4 | | 0.233 |
| 50.0 | | 248.0 | | 0.322 |
| 45.0 | | 275.5 | | 0.268 |
| 44.0 | | 281.8 | | 0.269 |
| 41.0 | | 302.4 | | 0.296 |
| 40.0 | | 310.0 | | 0.291 |
| | | | 0.95 [6] | 0.29 [6] |
| 39.5 | | 313.9 | 0.96 | 0.29 |
| 39.0 | | 317.9 | 0.97 | 0.29 |
| 38.5 | | 322.0 | 0.97 | 0.29 |
| 38.0 | | 326.3 | 0.98 | 0.28 |
| 37.5 | | 330.6 | 0.98 | 0.28 |
| 37.0 | | 335.1 | 0.99 | 0.28 |
| 36.5 | | 339.7 | 0.99 | 0.27 |
| 36.0 | | 344.4 | 0.99 | 0.27 |
| 35.5 | | 349.3 | 0.99 | 0.27 |
| 35.0 | | 354.2 | 0.99 | 0.26 |
| | | | | 0.248 [14] |
| 34.5 | | 359.4 | 0.99 [6] | 0.26 [6] |
| 34.0 | | 364.7 | 0.99 | 0.25 |
| 33.5 | | 370.1 | 0.98 | 0.25 |
| 33.0 | | 375.7 | 0.98 | 0.25 |
| | | | | 0.239 [14] |
| 32.5 | | 381.5 | 0.98 [6] | 0.24 [6] |
| 32.0 | | 387.5 | 0.98 | 0.24 |
| 31.5 | | 393.6 | 0.97 | 0.24 |
| 31.0 | | 399.9 | 0.97 | 0.23 |

(*Continued*)

TABLE I (*Continued*)

**Tantalum**

| eV | $cm^{-1}$ | Å | *n* | *k* |
|---|---|---|---|---|
| 30.5 | | 406.5 | 0.96 | 0.23 |
| 30.0 | | 413.3 | 0.95 | 0.22 |
| | | | | 0.313 [14] |
| 29.8 | | 416.1 | 0.95 [6] | 0.22 [6] |
| 29.6 | | 418.9 | 0.94 | 0.22 |
| 29.4 | | 421.7 | 0.94 | 0.22 |
| 29.2 | | 424.6 | 0.93 | 0.22 |
| 29.0 | | 427.5 | 0.92 | 0.22 |
| 28.8 | | 430.5 | 0.92 | 0.22 |
| 28.6 | | 433.5 | 0.91 | 0.22 |
| 28.4 | | 436.6 | 0.91 | 0.22 |
| 28.2 | | 439.7 | 0.90 | 0.22 |
| 28.0 | | 442.8 | 0.90 | 0.23 |
| 27.8 | | 446.0 | 0.89 | 0.23 |
| 27.6 | | 449.2 | 0.89 | 0.23 |
| 27.4 | | 452.5 | 0.88 | 0.24 |
| 27.2 | | 455.8 | 0.88 | 0.24 |
| 27.0 | | 459.2 | 0.87 | 0.25 |
| 26.8 | | 462.6 | 0.87 | 0.25 |
| 26.6 | | 466.1 | 0.87 | 0.26 |
| 26.4 | | 469.6 | 0.87 | 0.26 |
| 26.2 | | 473.2 | 0.88 | 0.26 |
| 26.0 | | 476.9 | 0.88 | 0.25 |
| 25.8 | | 480.6 | 0.87 | 0.25 |
| 25.6 | | 484.3 | 0.86 | 0.24 |
| 25.4 | | 488.1 | 0.85 | 0.24 |
| 25.2 | | 492.0 | 0.84 | 0.25 |
| 25.0 | | 495.9 | 0.83 | 0.25 |
| 24.8 | | 499.9 | 0.83 | 0.25 |
| 24.6 | | 504.0 | 0.82 | 0.25 |
| 24.4 | | 508.1 | 0.81 | 0.25 |
| 24.2 | | 512.3 | 0.80 | 0.26 |
| 24.0 | | 516.6 | 0.80 | 0.26 |
| 23.9 | | 518.8 | 0.79 | 0.27 |
| 23.8 | | 520.9 | 0.80 | 0.27 |
| 23.7 | | 523.1 | 0.80 | 0.27 |
| 23.6 | | 525.4 | 0.80 | 0.26 |
| 23.5 | | 527.6 | 0.79 | 0.25 |
| 23.4 | | 529.8 | 0.79 | 0.25 |
| 23.2 | | 534.4 | 0.76 | 0.24 |
| 23.0 | | 539.1 | 0.73 | 0.24 |
| 22.8 | | 543.8 | 0.71 | 0.26 |
| 22.6 | | 548.6 | 0.69 | 0.27 |
| 22.4 | | 553.5 | 0.68 | 0.29 |
| 22.2 | | 558.5 | 0.66 | 0.30 |

(*Continued*)

TABLE I (*Continued*)

Tantalum

| eV | $cm^{-1}$ | Å | *n* | *k* |
|---|---|---|---|---|
| 22.0 | | 563.6 | 0.64 | 0.32 |
| 21.8 | | 568.7 | 0.64 | 0.34 |
| 21.6 | | 574.0 | 0.64 | 0.34 |
| 21.4 | | 579.4 | 0.61 | 0.35 |
| 21.2 | | 584.8 | 0.59 | 0.37 |
| 21.0 | | 590.4 | 0.57 | 0.39 |
| 20.8 | | 596.1 | 0.56 | 0.42 |
| 20.6 | | 601.9 | 0.55 | 0.44 |
| 20.4 | | 607.8 | 0.55 | 0.47 |
| 20.2 | | 613.8 | 0.54 | 0.50 |
| 20.0 | | 619.9 | 0.54 | 0.52 |
| 19.8 | | 626.2 | 0.53 | 0.55 |
| 19.6 | | 632.6 | 0.53 | 0.57 |
| 19.4 | | 639.1 | 0.53 | 0.60 |
| 19.2 | | 645.8 | 0.52 | 0.63 |
| 19.0 | | 652.5 | 0.53 | 0.65 |
| 18.8 | | 659.5 | 0.53 | 0.68 |
| 18.6 | | 666.6 | 0.53 | 0.71 |
| 18.4 | | 673.8 | 0.54 | 0.73 |
| 18.2 | | 681.2 | 0.54 | 0.76 |
| 18.0 | | 688.8 | 0.55 | 0.79 |
| 17.8 | | 696.5 | 0.56 | 0.81 |
| 17.6 | | 704.5 | 0.56 | 0.84 |
| 17.4 | | 712.6 | 0.57 | 0.87 |
| 17.2 | | 720.8 | 0.58 | 0.89 |
| 17.0 | | 729.3 | 0.60 | 0.92 |
| 16.8 | | 738.0 | 0.61 | 0.94 |
| 16.6 | | 746.9 | 0.63 | 0.97 |
| 16.4 | | 756.0 | 0.64 | 0.99 |
| 16.2 | | 765.3 | 0.66 | 1.02 |
| 16.0 | | 774.9 | 0.68 | 1.04 |
| 15.8 | | 784.7 | 0.70 | 1.06 |
| 15.6 | | 794.8 | 0.72 | 1.08 |
| 15.4 | | 805.1 | 0.75 | 1.10 |
| 15 2 | | 815.7 | 0.77 | 1.12 |
| 15.0 | | 826.6 | 0.80 | 1.13 |
| 14.8 | | 837.7 | 0.82 | 1.14 |
| 14.6 | | 849.2 | 0.85 | 1.15 |
| 14.4 | | 861.0 | 0.87 | 1.15 |
| 14.2 | | 873.1 | 0.89 | 1.15 |
| 14.0 | | 885.6 | 0.90 | 1.15 |
| 13.8 | | 898.4 | 0.91 | 1.16 |
| 13.6 | | 911.6 | 0.91 | 1.16 |
| 13.4 | | 925.3 | 0.91 | 1.18 |
| 13.2 | | 939.3 | 0.92 | 1.20 |

(*Continued*)

TABLE I (*Continued*)

**Tantalum**

| eV | $cm^{-1}$ | Å | *n* | *k* |
|---|---|---|---|---|
| 13.0 | | 953.7 | 0.93 | 1.22 |
| 12.8 | | 968.6 | 0.94 | 1.24 |
| 12.6 | | 984.0 | 0.96 | 1.26 |
| 12.4 | | 999.9 | 0.98 | 1.28 |
| eV | $cm^{-1}$ | μm | *n* | *k* |
| 12.2 | 98399 | 0.1016 | 1.00 | 1.29 |
| 12.0 | 96786 | 0.1033 | 1.02 | 1.31 |
| 11.8 | 95173 | 0.1051 | 1.05 | 1.32 |
| 11.6 | 93560 | 0.1069 | 1.07 | 1.33 |
| 11.4 | 91946 | 0.1088 | 1.09 | 1.34 |
| 11.2 | 90333 | 0.1107 | 1.11 | 1.35 |
| 11.0 | 88720 | 0.1127 | 1.13 | 1.35 |
| 10.8 | 87107 | 0.1148 | 1.15 | 1.36 |
| 10.6 | 85494 | 0.1170 | 1.16 | 1.36 |
| 10.4 | 83881 | 0.1192 | 1.18 | 1.37 |
| 10.2 | 82268 | 0.1216 | 1.19 | 1.37 |
| 10.0 | 80655 | 0.1240 | 1.20 | 1.37 |
| 9.8 | 79042 | 0.1265 | 1.21 | 1.37 |
| 9.6 | 77429 | 0.1292 | 1.21 | 1.38 |
| 9.4 | 75816 | 0.1319 | 1.21 | 1.38 |
| 9.2 | 74202 | 0.1348 | 1.21 | 1.38 |
| 9.0 | 72589 | 0.1378 | 1.19 | 1.40 |
| 8.8 | 70976 | 0.1409 | 1.17 | 1.41 |
| 8.6 | 69363 | 0.1442 | 1.14 | 1.45 |
| 8.4 | 67750 | 0.1476 | 1.13 | 1.50 |
| 8.2 | 66137 | 0.1512 | 1.12 | 1.55 |
| 8.0 | 64524 | 0.1550 | 1.11 | 1.61 |
| 7.8 | 62911 | 0.1590 | 1.11 | 1.68 |
| 7.6 | 61298 | 0.1631 | 1.12 | 1.75 |
| 7.4 | 59684 | 0.1675 | 1.13 | 1.82 |
| 7.2 | 58071 | 0.1722 | 1.15 | 1.91 |
| 7.0 | 56458 | 0.1771 | 1.18 | 2.01 |
| 6.8 | 54845 | 0.1823 | 1.23 | 2.11 |
| 6.6 | 53232 | 0.1879 | 1.29 | 2.22 |
| 6.4 | 51619 | 0.1937 | 1.37 | 2.33 |
| 6.2 | 50006 | 0.2000 | 1.48 | 2.45 |
| 6.0 | 48393 | 0.2066 | 1.63 | 2.56 |
| 5.8 | 46780 | 0.2138 | 1.83 | 2.63 |
| 5.6 | 45167 | 0.2214 | 2.06 | 2.67 |
| 5.4 | 43554 | 0.2296 | 2.31 | 2.61 |
| 5.2 | 41940 | 0.2384 | 2.52 | 2.44 |
| 5.0 | 40327 | 0.2480 | 2.58 | 2.20 |
| 4.8 | 38714 | 0.2583 | 2.53 | 2.06 |

(*Continued*)

TABLE I (*Continued*)

**Tantalum**

| eV | $cm^{-1}$ | μm | *n* | *k* |
|---|---|---|---|---|
| 4.6 | 37101 | 0.2695 | 2.45 | 2.06 |
| 4.4 | 35488 | 0.2818 | 2.39 | 2.01 |
| 4.2 | 33875 | 0.2952 | 2.35 | 2.06 |
| 4.0 | 32262 | 0.3100 | 2.36 | 2.14 |
| 3.8 | 30649 | 0.3263 | 2.40 | 2.22 |
| 3.6 | 29036 | 0.3444 | 2.49 | 2.30 |
| 3.4 | 27423 | 0.3647 | 2.61 | 2.33 |
| 3.2 | 25810 | 0.3875 | 2.73 | 2.31 |
| 3.0 | 24196 | 0.4133 | 2.81 | 2.24 |
| 2.9 | 23390 | 0.4275 | 2.84 | 2.20 |
| 2.8 | 22583 | 0.4428 | 2.85 | 2.14 |
| 2.7 | 21777 | 0.4592 | 2.84 | 2.08 |
| 2.6 | 20970 | 0.4769 | 2.80 | 2.02 |
| 2.5 | 20164 | 0.4959 | 2.75 | 1.98 |
| 2.4 | 19357 | 0.5166 | 2.68 | 1.92 |
| 2.3 | 18551 | 0.5391 | 2.56 | 1.86 |
| 2.2 | 17744 | 0.5636 | 2.36 | 1.81 |
| 2.1 | 16938 | 0.5904 | 2.10 | 1.84 |
| 2.0 | 16131 | 0.6199 | 1.83 | 1.99 |
| 1.9 | 15324 | 0.6525 | 1.57 | 2.24 |
| 1.8 | 14518 | 0.6888 | 1.35 | 2.60 |
| 1.7 | 13711 | 0.7293 | 1.24 | 2.95 |
| 1.6 | 12905 | 0.7749 | 1.15 | 3.33 |
| 1.5 | 12098 | 0.8266 | 1.09 | 3.73 |
| 1.4 | 11292 | 0.8856 | 1.04 | 4.15 |
| 1.3 | 10485 | 0.9537 | 1.00 | 4.62 |
| 1.2 | 9679 | 1.033 | 0.980 | 5.14 |
| 1.1 | 8872 | 1.127 | 0.930 | 5.75 |
| 1.0 | 8065 | 1.240 | 0.890 | 6.47 |
| 0.98 | 7904 | 1.265 | 0.880 | 6.64 |
| 0.94 | 7582 | 1.319 | 0.860 | 6.99 |
| 0.90 | 7259 | 1.378 | 0.840 | 7.38 |
| 0.86 | 6936 | 1.442 | 0.850 | 7.81 |
| 0.82 | 6614 | 1.512 | 0.860 | 8.27 |
| 0.78 | 6291 | 1.590 | 0.890 | 8.77 |
| 0.74 | 5968 | 1.675 | 0.920 | 9.32 |
| 0.70 | 5646 | 1.771 | 0.960 | 9.92 |
| 0.66 | 5323 | 1.879 | 1.00 | 10.6 |
| 0.62 | 5001 | 2.000 | 1.06 | 11.4 |
| 0.58 | 4678 | 2.138 | 1.15 | 12.2 |
| 0.54 | 4355 | 2.296 | 1.25 | 13.1 |
| 0.50 | 4033 | 2.480 | 1.37 | 14.3 |
| 0.46 | 3710 | 2.695 | 1.54 | 15.6 |
| 0.42 | 3388 | 2.952 | 1.75 | 17.1 |
| 0.38 | 3065 | 3.263 | 2.03 | 18.9 |

(*Continued*)

TABLE I (*Continued*)

**Tantalum**

| eV | $cm^{-1}$ | μm | *n* | *k* |
|---|---|---|---|---|
| 0.34 | 2742 | 3.647 | 2.40 | 21.1 |
| 0.30 | 2420 | 4.133 | 2.87 | 23.9 |
| 0.28 | 2258 | 4.428 | 3.23 | 25.6 |
| 0.26 | 2097 | 4.769 | 3.67 | 27.5 |
| 0.24 | 1936 | 5.166 | 4.20 | 29.8 |
| 0.22 | 1774 | 5.636 | 4.88 | 32.4 |
| 0.20 | 1613 | 6.199 | 5.77 | 35.5 |
| 0.19 | 1533 | 6.525 | 6.29 | 37.2 |
| 0.18 | 1452 | 6.888 | 6.91 | 39.2 |
| 0.16 | 1290 | 7.749 | 8.45 | 43.7 |
| 0.15 | 1210 | 8.266 | 9.45 | 46.4 |
| 0.14 | 1129 | 8.856 | 10.6 | 49.4 |
| 0.13 | 1049 | 9.537 | 12.1 | 52.9 |
| 0.12 | 967.9 | 10.33 | 14.0 | 56.8 |
| 0.1116 | 900 | 11.11 | 15.6 [16] | 54.6 [16] |
| 0.09919 | 800 | 12.50 | 19.1 | 59.9 |
| 0.08679 | 700 | 14.29 | 24.2 | 66.4 |
| 0.07439 | 600 | 16.67 | 31.5 | 73.9 |
| 0.06199 | 500 | 20.00 | 41.7 | 82.8 |
| 0.05579 | 450 | 22.22 | 48.4 | 93.1 |
| 0.04959 | 400 | 25.00 | 56.4 | 98.9 |
| 0.04339 | 350 | 28.57 | 66.1 | 105 |
| 0.03720 | 300 | 33.33 | 77.9 | 111 |
| 0.03100 | 250 | 40.00 | 92.0 | 119 |
| 0.02790 | 225 | 44.44 | 100 | 127 |
| 0.02480 | 200 | 50.00 | 109 | 137 |
| 0.02170 | 175 | 57.14 | 119 | 143 |
| 0.01860 | 150 | 66.67 | 131 | 151 |
| 0.01550 | 125 | 80.00 | 146 | 162 |
| 0.01240 | 100 | 100.0 | 164 | 178 |
| 0.009919 | 80 | 125.0 | 184 | 197 |

# Beryllium* (Be)

E. T. ARAKAWA, T. A. CALLCOTT,† and YUN-CHING CHANG†
Health and Safety Research Division
Oak Ridge National Laboratory
Oak Ridge, Tennessee

Beryllium has many unique properties that make it of both theoretical and practical interest. As a metal, it is strikingly different both from lithium, its neighbor in the periodic table, and the higher $Z$ alkaline-earth metals magnesium and calcium, which occupy the same column of the periodic table. The density of beryllium is not only 3.5 times larger than that of lithium, but is greater than that of magnesium and calcium. Its compressibility is very low, its Debye temperature is among the highest in the periodic table, its melting temperature is much higher than the other alkaline earths, and its electronic specific heat is very low. These properties, and its hexagonal crystalline structure, have generated much theoretical interest in its electronic properties. Several authors have discussed the optical properties of Be expected from theoretical band-structure calculations [1–3].

Beryllium also has many properties that recommend it for exotic optical applications. It is relatively light compared with other metals of optical importance, offers a very high specific stiffness (ratio of Young's modulus to density), a low thermal expansion at cryogenic temperatures, a low $Z$ number, high thermal conductivity, and high reflectivity in the infrared. These properties make it particularly attractive for optical components that are intended for use in space.

In view of its many unique properties, it is surprising that no careful survey of the optical properties of Be has yet been published. In fact, only a few studies have been made, and they have produced widely different results, particularly in the visible region of the spectrum, where the methodology and instrumentation are best developed, and results are

* This research was sponsored jointly by the Office of Health and Environmental Research, U.S. Department of Energy, under contract DE-AC05-840R21400 with Martin Marietta Energy Systems, Inc. and by the Optics-MODIL under USDOE-DOD Interagency Agreement No. 1855-1562-A1.
† Also from The University of Tennessee, Physics Department, Knoxville, Tennessee


Copyright © 1991 by Academic Press.
All rights of reproduction in any form reserved.
ISBN 0-12-544422-2

normally most consistent. The variability of results may be traced to the difficulty of sample preparation. Bulk samples are usually produced by high-pressure sintering of microcrystalline powder, which results in the incorporation of significant amounts of BeO in the sample.

For many metals, oxidation problems may be overcome readily by vacuum evaporation, in which the metal evaporates, leaving the more stable oxide behind. In practice, Be is easily evaporated by subliming from the solid state at temperatures of about 900°C, well below its melting temperature at 1278°C. Our own studies suggest that the optical properties depend critically on the evaporation procedure used, and that much of the variability of the results reported in the literature can be traced to sample-preparation problems.

Published studies on the optical properties of Be date from about 50 years ago. Table I summarizes relevant facts about the more significant studies including photon-energy range, sample type, method of measurement, date of publication, and reference number. Note that all the samples in Table I except that listed as single crystal are polycrystalline.

We will discuss the available experimental data in four spectral regions. They are the soft X-ray range (SXR, $\hbar\omega > 50$ eV), the vacuum ultraviolet (VUV, $10\text{ eV} < \hbar\omega < 50$ eV), the infrared–visible–ultraviolet (IR–V–UV, $1\text{ eV} < \hbar\omega < 10$ eV), and the far infrared (FIR, $\hbar\omega < 1$ eV). These regions are chosen not to match the standard definitions of these regions, which in any case are very vague, but for convenient discussion of the available results.

Normal-incidence reflectance data for the three lowest-energy spectral regions are shown in Fig. 1. The wide range of results in the available literature is apparent, and will be the subject of further discussion. The reason for the above division into four spectral regions is also apparent. Above 10 eV, the reflectance makes the transition from reflecting to transmitting behavior at the plasmon energy. Between 1 and 10 eV, absorption by interband transitions reduces the reflectance and introduces prominent structure. Below 1 eV, the rising reflectance indicates a transition to free-electron metallic behavior.

In the SXR spectral region (>50 eV), the photon energy is above the plasmon energy (18.4 eV), and most of the interband oscillator strength is exhausted. Consequently, Be is weakly absorbing so that $n \cong \sqrt{\varepsilon_1} \approx 1$ and $\varepsilon_2 \simeq 2k \ll 1$. The only important physical process affecting the optical properties is the onset of absorption at the Be *K*-edge at 109 eV. The data available in this region are from thin-film transmittances that provide a measure of the linear absorption coefficient, $\mu = 4\pi k/\lambda_0$, where $\lambda_0$ is the wavelength of the incident radiation. The available measurements are reported in Refs. [4–7]. The measurements reported by Henke and Elgin [5] and Barstow *et al.* [6] are consistent with each other.

In the VUV spectral range (10–50 eV), the major feature of the spec-

trum is the transition from reflecting to transmitting behavior at the plasma energy (18.4 eV). Reflectance data from Seignac and Robin [8] and Toots *et al.* [9] are plotted in Fig. 1. Both sets of data were obtained on films with thickness 300–1000 Å evaporated on glass substrates and measured in vacua of $10^{-7}$ to $10^{-10}$ torr.

The reflectance data in the 1–10 eV range from Seignac and Robin [8], Hunderi and Myers [10], Weaver *et al.* [11], and Hull [12] are also plotted in Fig. 1. The most striking feature in this region is the wide range of reflectances obtained from careful studies in a spectral region where the procedures of optical measurements are usually most reliable. The two reflectance curves reported by Weaver *et al.* for the electric-field vector parallel ($E \| c$) and perpendicular ($E \perp c$) to the $c$-axis direction, were obtained on single-crystal surfaces prepared by mechanical polishing, with a subsequent chemical etch. These values are represented by the symbols (+) and (□), respectively. The reflectance data of Hull [12] were taken on the carefully polished surface of a polycrystalline mirror blank prepared by pressure sintering a low-oxygen-content (<0.5%) Be powder. This surface, intended for use as a reflector in the infrared, gives one of the highest reflectances for Be reported to date in the FIR region. However, this surface shows lower reflectance than the best evaporated films in this spectral region.

The highest reflectances reported in the visible were obtained by Seignac and Robin on Be films prepared by slow evaporation in ultrahigh vacuum (UHV). Because of the careful UHV-preparation techniques used, and because most sample preparation problems tend to reduce the measured reflectance, our initial assessment was that these data were the best available. A series of experiments performed in our laboratory confirm this initial judgment. We have been able to identify film-preparation procedures that result in lower reflectances. Thus, we adopt the reflectance values of Seignac and Robin as the best available in this spectral region. It should be noted that the reflectance values of Hunderi and Myers are substantially the same in the region of overlap. Hunderi and Myers' results are for evaporated films on sapphire prepared and measured in a vacuum of $10^{-10}$ torr.

Values of $n$ and $k$ in the visible region have been obtained by Seignac and Robin and Hunderi and Myers. Although the reflectances are very similar, there are substantial differences in the values of $n$ and $k$. Of particular significance is the crossing in the values of $n$ and $k$ in the spectral region between 1.7 eV and 3 eV in the data of Seignac and Robin, which results in the value of $\varepsilon_1$ exceeding zero over this range. Our own ellipsometric measurements on evaporated films in this spectral range confirm the crossing of the $n$ and $k$ values reported by Seignac and Robin.

The large range of reflectance values observed for samples in the visible and ultraviolet is not unprecedented. An equally large range of reflec-

tances has been reported for aluminum, depending on the method of film preparation (evaporation in UHV or normal vacuum, sputtering or mechanical polishing) [13]. It is well-known that rough surfaces not only scatter, but can couple incident light to surface-plasmon modes and reduce the reflectance [14]. It seems probable that the sensitivity of the reflectance to surface structure, and perhaps to bulk grain size, is related to coupling of light to surface- and/or bulk-plasmon modes in these samples.

In the FIR spectral region (<1 eV), Shklyarevskii and Yarovaya [15] report a full set of optical constants, and other workers [12, 16, 17] have obtained normal-incidence reflectance data. The reflectances obtained by Shklyarevskii and Yarovaya are low, which we believe to be evidence for poor film structure. The reflectances of Hull's polished bulk samples [12] are among the highest reported for this spectral region. We have measured the optical constants by ellipsometry for a number of samples in the transition region from 3 eV to 0.6 eV, and normal-incidence reflectance from 3 eV to 0.1 eV. In general, it appears that in the FIR, as in the visible region, the best samples have the highest reflectance.

From the sources described in previous paragraphs, optical constants are available that span the spectral region up to 26 eV, although only normal-incidence reflectance data are available for most of the far-infrared region. We have obtained a consistent set of optical response functions for the entire spectral range by assembling a normal-incidence reflectance $R(0)$ curve for energies of $0.06\text{ eV} < \hbar\omega < 26\text{ eV}$ from published results, extending it to zero and infinite energies using appropriate analytic functions, and performing a Kramers–Kronig (K–K) analysis on $R(0)$. The reflectance values used were obtained by drawing a smooth curve through the following data sets:

$$0.06 < \hbar\omega < 0.8\text{ eV}\ [12];$$

$$0.8 < \hbar\omega < 5.0\text{ eV}\ [10];$$

$$1.5 < \hbar\omega < 14\text{ eV}\ [8];$$

$$14 < \hbar\omega < 26\text{ eV}\ [9].$$

In regions of overlap, higher reflectance values were favored. These data sets are shown along with the fitted $R(\hbar\omega)$ curve in Fig. 1.

Below 0.06 eV, the reflectance was extrapolated to zero energy using a linear extrapolation of Hull's data. Above 26 eV the reflectance was extrapolated to infinite energy as $\hbar\omega^{-4}$, in accordance with the behavior of nearly-free-electron metal above the plasma edge. Reliable $n$ and $k$ values

could be obtained only up to 25 eV from this analysis. To obtain the optical constants above 25 eV, a second K–K analysis was carried out using the $k$ values from zero to 25 eV derived above, together with the experimental $k$ values of Henke (60–250 eV) and Barstow (41–705 eV). The structural features from 110 eV to 130 eV just above the $K$ edge were derived from the absorption data of Sagawa [18]. The $k$ values from 15 eV to 25 eV together with the experimental values from 60 eV to 190 eV were found to fit the relation $k \propto E^{-3.3}$. This relationship was used in the region of 25–60 eV where no values were available. The $k$ values above 160 eV were found to fit the relation $k \propto \hbar\omega^{-3.33}$. This analytic function was used in the high-energy extrapolation required for the K–K analysis. Finally, the initial K–K analysis on the normal-incidence reflectance $R(0)$ was refined slightly by using a high-energy extrapolation of $R(0) \propto \hbar\omega^{-4.7}$ as found from the behavior of $R(0)$ derived in the second K–K analysis of $k$. The results of these analyses are likely to be least reliable in the FIR spectral region. For example, an error of $\pm 0.005$ in the measured reflectance in this region changes the $k$ values by only a few percent but changes the $n$ values by 20–30%.

The $n$ and $k$ values derived from the K–K analysis are plotted in Fig. 2 and a numerical printout is given in Table II. These values are a combination of the results from the two types of K–K analyses. The values from 0.02 eV to 20 eV and from 26 eV to 300 eV were those derived in the analyses of $R(0)$ and $k$, respectively. The $k$ values from 20 eV to 26 eV are the same in both sets of data, whereas the $n$ values are a smooth joining of the two data sets.

The $n$ and $k$ values derived from the K–K analyses agree well with the values given by Seignac and Robin for 2–26 eV and those given by Toots *et al.* for 10–28 eV. The $k$ values from 0.6 eV to 2.5 eV agree with Hunderi and Myers' values, while the $n$ values differ somewhat. In general, the optical constants derived here for polycrystalline Be are believed to be accurate to $\pm 20\%$ over the whole energy region.

Also included here as Table III are the $n$ and $k$ values from 299 eV to 10,000 eV derived from the latest Henke-model scattering data [19]. Henke *et al.*'s values agree well with those in Table II in the region of overlap from 200 eV to 300 eV.

## REFERENCES

1. P. O. Nilsson, G. Arbman, and T. Gustafsson, *J. Phys. F: Metal Phys.* **4**, 1937 (1974).
2. M. Taut, *Phys. Status Solidi* **77**, 165 (1976); also *Phys. Status Solidi* **77**, 543 (1976).
3. P. Sinha and S. Chatterjee, *Indian J. Phys.* **52A**, 503 (1978).
4. R. W. Johnston and D. H. Tomboulian, *Phys. Rev.* **94**, 1585 (1954).
5. B. L. Henke and R. L. Elgin, *Adv. X-ray Anal.* **13**, 639 (1970).
6. M. A. Barstow, M. Lewis, and R. Petre, *J. Opt. Soc. Am.* **73**, 1220 (1983).
7. B. J. Muldar and J. J. Vrakking, *J. Phys. E: Sci. Instrum.* **11**, 743 (1978).

8. A. Seignac and S. Robin, *Solid State Commun.* **19**, 343 (1976).
9. J. Toots, H. A. Fowler, and L. Marton, *Phys. Rev.* **172**, 670 (1968).
10. O. Hunderi and H. P. Myers, *J. Phys. F: Metal Phys.* **4**, 1088 (1974).
11. J. H. Weaver, D. W. Lynch, and R. Rosei, *Phys. Rev.* **B7**, 3537 (1973).
12. Anthony B. Hull, Perkin-Elmer/Applied Optics Operations, Box 3115, Garden Grove, Calif. 92641 (private communication).
13. D. Y. Smith, E. Shiles, and Mitio Inokuti, in "Handbook of Optical Constants of Solids," (E. D. Palik, ed.), Academic Press, Orlando, 389 (1985).
14. R. H. Ritchie and R. E. Wilems, *Phys. Rev.* **178**, 372 (1969); J. Crowell and R. H. Ritchie, *J. Opt. Soc. Am.* **60**, 794 (1970); J. M. Elson and R. H. Ritchie, *Phys. Rev.* **B4**, 4129 (1971).
15. I. N. Shklyarevskii and R. G. Yarovaya, *Opt. Spect. (USSR)* **11**, 355 (1960); *Opt. Spekt.* **11**, 661 (1961).
16. H. M. O'Bryan, *J. Opt. Soc. Am.* **26**, 122 (1936).
17. R. Blickensderfer, D. K. Deardorff, and R. L. Lincoln, *J. Less Common Metals* **51**, 13 (1977).
18. T. Sagawa, in "Soft X-Ray Band Spectra," (D. J. Fabian, ed.), Academic Press, New York, 29 (1968).
19. B. L. Henke, J. C. Davis, E. M. Gullickson, and R. C. C. Perera, Lawrence Berkeley Lab Report LBL-26259 (1988).

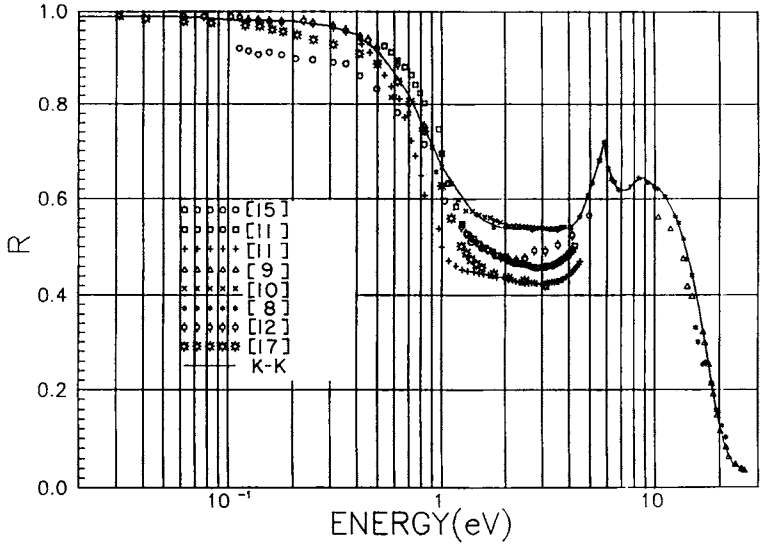


**Fig. 1.** Normal-incidence reflectances reported in the literature and reflectance data used as input for the K–K analysis.

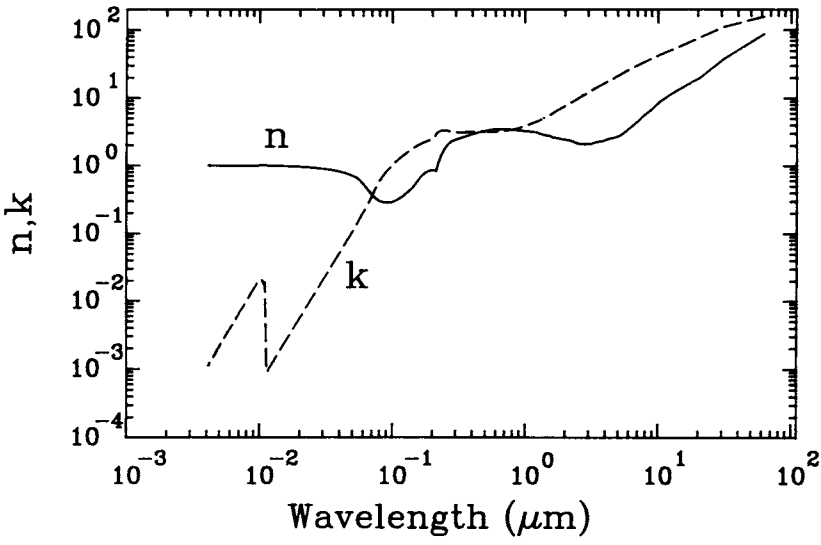


**Fig. 2.** Log–log plot of $n$ (solid line) and $k$ (dashed line) versus wavelength in micrometers for beryllium.

**TABLE I**

**Summary of Experimental Information for Significant Studies of the Optical Properties of Be**

| Ref. (date) | Range (eV) | Method | Preparation | Temp. (K) |
|---|---|---|---|---|
| [5] (1970) | 60–250 | Transmission | Evap. film | 298 |
| [6] (1983) | 41–705 | Transmission | Evap. film | 298 |
| [9] (1968) | 10–26 | $R(\Theta)$ | Evap. film | 298 |
| [8] (1976) | 2–25 | $R(0)$ and K–K | Evap. film | 298 |
| [10] (1974) | 0.5–3.8 | Ellipsometry | Evap. film | 298; 20 |
| [11] (1973) | 0.12–4.5 | Abs. and K–K | Single crystal | 4 |
| [15] (1961) | 0.11–1.5 | Ellipsometry | Evap. film | 298; 82 |
| [17] (1977) | 0.03–3.1 | $R(0)$ only | Polished bulk | 298; 82 |
| [12] (1989) | 0.06–4.8 | $R(0)$ only | Polished bulk | 298 |

$R(\Theta)$ denotes reflectance as a function of incidence angle and $R(0)$ is normal-incidence reflectance.

**TABLE II**

**Values of $n$ and $k$ for Beryllium**

| eV | $cm^{-1}$ | $\mu m$ | n | k |
|---|---|---|---|---|
| 0.02 | 161.3 | 6.199E+01 | 8.61E+01 | 1.57E+02 |
| 0.03 | 242.0 | 4.133E+01 | 5.19E+01 | 1.32E+02 |
| 0.04 | 322.6 | 3.100E+01 | 3.74E+01 | 1.10E+02 |
| 0.05 | 403.3 | 2.480E+01 | 2.47E+01 | 9.17E+01 |
| 0.06 | 483.9 | 2.066E+01 | 1.99E+01 | 7.71E+01 |
| 0.07 | 564.6 | 1.771E+01 | 1.70E+01 | 6.76E+01 |
| 0.08 | 645.2 | 1.550E+01 | 1.46E+01 | 6.04E+01 |
| 0.09 | 725.9 | 1.378E+01 | 1.27E+01 | 5.08E+01 |
| 0.1 | 806.5 | 1.240E+01 | 1.13E+01 | 5.01E+01 |
| 0.2 | 1,613 | 6.199E+00 | 3.66E+00 | 2.67E+01 |
| 0.3 | 2,420 | 4.133E+00 | 2.43E+00 | 1.73E+01 |
| 0.4 | 3,226 | 3.099E+00 | 2.07E+00 | 1.26E+01 |
| 0.5 | 4,033 | 2.480E+00 | 2.14E+00 | 9.67E+00 |
| 0.6 | 4,839 | 2.066E+00 | 2.41E+00 | 7.88E+00 |
| 0.7 | 5,646 | 1.771E+00 | 2.55E+00 | 6.64E+00 |
| 0.8 | 6,452 | 1.550E+00 | 2.74E+00 | 5.66E+00 |
| 0.9 | 7,259 | 1.378E+00 | 2.87E+00 | 5.02E+00 |
| 1.0 | 8,066 | 1.240E+00 | 3.09E+00 | 4.51E+00 |
| 1.2 | 9,679 | 1.033E+00 | 3.26E+00 | 3.96E+00 |
| 1.4 | 11,292 | 8.856E-01 | 3.35E+00 | 3.55E+00 |
| 1.6 | 12,905 | 7.749E-01 | 3.44E+00 | 3.35E+00 |
| 1.8 | 14,518 | 6.888E-01 | 3.47E+00 | 3.23E+00 |
| 2.0 | 16,132 | 6.199E-01 | 3.46E+00 | 3.18E+00 |
| 2.2 | 17,745 | 5.635E-01 | 3.39E+00 | 3.17E+00 |
| 2.4 | 19,358 | 5.166E-01 | 3.30E+00 | 3.18E+00 |
| 2.6 | 20,971 | 4.768E-01 | 3.19E+00 | 3.16E+00 |
| 2.8 | 22,584 | 4.428E-01 | 3.07E+00 | 3.16E+00 |
| 3.0 | 24,198 | 4.133E-01 | 2.95E+00 | 3.14E+00 |
| 3.2 | 25,811 | 3.874E-01 | 2.84E+00 | 3.12E+00 |
| 3.4 | 27,424 | 3.646E-01 | 2.73E+00 | 3.10E+00 |
| 3.6 | 29,037 | 3.444E-01 | 2.64E+00 | 3.08E+00 |
| 3.8 | 30,650 | 3.263E-01 | 2.55E+00 | 3.08E+00 |
| 4.0 | 32,263 | 3.100E-01 | 2.47E+00 | 3.08E+00 |
| 4.2 | 33,876 | 2.952E-01 | 2.39E+00 | 3.10E+00 |
| 4.4 | 35,490 | 2.818E-01 | 2.30E+00 | 3.15E+00 |
| 4.6 | 37,103 | 2.695E-01 | 2.17E+00 | 3.22E+00 |
| 4.8 | 38,716 | 2.583E-01 | 1.99E+00 | 3.29E+00 |
| 5.0 | 40,329 | 2.480E-01 | 1.78E+00 | 3.32E+00 |
| 5.2 | 41,942 | 2.384E-01 | 1.54E+00 | 3.30E+00 |
| 5.4 | 43,555 | 2.296E-01 | 1.31E+00 | 3.23E+00 |
| 5.6 | 45,169 | 2.214E-01 | 1.08E+00 | 3.11E+00 |
| 5.8 | 46,780 | 2.138E-01 | 8.21E-01 | 2.90E+00 |
| 6.0 | 48,393 | 2.066E-01 | 8.49E-01 | 2.64E+00 |
| 6.2 | | 2.000E-01 | 8.44E-01 | 2.52E+00 |
| 6.4 | | 1.937E-01 | 8.37E-01 | 2.42E+00 |
| 6.6 | | 1.878E-01 | 8.25E-01 | 2.34E+00 |
| 6.8 | | 1.823E-01 | 8.05E-01 | 2.28E+00 |

TABLE II (*Continued*)

**Beryllium**

| eV | $cm^{-1}$ | $\mu m$ | n | k |
|---|---|---|---|---|
| 7.0 | | 1.771E-01 | 7.78E-01 | 2.23E+00 |
| 7.2 | | 1.722E-01 | 7.44E-01 | 2.18E+00 |
| 7.4 | | 1.675E-01 | 7.07E-01 | 2.13E+00 |
| 7.6 | | 1.631E-01 | 6.71E-01 | 2.08E+00 |
| 7.8 | | 1.589E-01 | 6.28E-01 | 2.04E+00 |
| 8.0 | | 1.550E-01 | 5.88E-01 | 1.98E+00 |
| 8.2 | | 1.512E-01 | 5.51E-01 | 1.92E+00 |
| 8.4 | | 1.476E-01 | 5.18E-01 | 1.87E+00 |
| 8.6 | | 1.442E-01 | 4.90E-01 | 1.81E+00 |
| 8.8 | | 1.409E-01 | 4.63E-01 | 1.75E+00 |
| 9.0 | | 1.378E-01 | 4.45E-01 | 1.69E+00 |
| 9.2 | | 1.348E-01 | 4.27E-01 | 1.64E+00 |
| 9.4 | | 1.319E-01 | 4.12E-01 | 1.59E+00 |
| 9.6 | | 1.291E-01 | 3.98E-01 | 1.54E+00 |
| 9.8 | | 1.265E-01 | 3.85E-01 | 1.50E+00 |
| 10.0 | | 1.240E-01 | 3.73E-01 | 1.45E+00 |
| 10.5 | | 1.181E-01 | 3.45E-01 | 1.35E+00 |
| 11.0 | | 1.127E-01 | 3.24E-01 | 1.25E+00 |
| 11.5 | | 1.078E-01 | 3.09E-01 | 1.16E+00 |
| 12.0 | | 1.033E-01 | 2.98E-01 | 1.07E+00 |
| 12.5 | | 9.918E-02 | 2.87E-01 | 9.91E-01 |
| 13.0 | | 9.537E-02 | 2.84E-01 | 9.13E-01 |
| 13.5 | | 9.184E-02 | 2.83E-01 | 8.41E-01 |
| 14.0 | | 8.856E-02 | 2.84E-01 | 7.72E-01 |
| 14.5 | | 8.550E-02 | 2.87E-01 | 7.07E-01 |
| 15.0 | | 8.265E-02 | 2.93E-01 | 6.45E-01 |
| 15.5 | | 7.999E-02 | 3.00E-01 | 5.85E-01 |
| 16.0 | | 7.749E-02 | 3.12E-01 | 5.27E-01 |
| 16.5 | | 7.514E-02 | 3.26E-01 | 4.73E-01 |
| 17.0 | | 7.293E-02 | 3.42E-01 | 4.21E-01 |
| 17.5 | | 7.085E-02 | 3.61E-01 | 3.72E-01 |
| 18.0 | | 6.888E-02 | 3.82E-01 | 3.25E-01 |
| 18.5 | | 6.702E-02 | 4.07E-01 | 2.95E-01 |
| 19.0 | | 6.525E-02 | 4.36E-01 | 2.70E-01 |
| 19.5 | | 6.358E-02 | 4.68E-01 | 2.42E-01 |
| 20.0 | | 6.199E-02 | 4.96E-01 | 2.20E-01 |
| 20.5 | | 6.048E-02 | 5.26E-01 | 2.03E-01 |
| 21.0 | | 5.904E-02 | 5.55E-01 | 1.90E-01 |
| 21.5 | | 5.767E-02 | 5.83E-01 | 1.72E-01 |
| 22.0 | | 5.635E-02 | 6.11E-01 | 1.60E-01 |
| 22.5 | | 5.510E-02 | 6.32E-01 | 1.47E-01 |
| 23.0 | | 5.390E-02 | 6.53E-01 | 1.35E-01 |
| 23.5 | | 5.276E-02 | 6.68E-01 | 1.22E-01 |
| 24.0 | | 5.166E-02 | 6.84E-01 | 1.15E-01 |
| 24.5 | | 5.060E-02 | 6.97E-01 | 1.08E-01 |
| 25.0 | | 4.959E-02 | 7.10E-01 | 1.02E-01 |
| 25.5 | | 4.862E-02 | 7.22E-01 | 9.50E-02 |

TABLE II (*Continued*)

**Beryllium**

| eV | $cm^{-1}$ | $\mu m$ | n | k |
|---|---|---|---|---|
| 26 | | 4.769E-02 | 7.34E-01 | 8.95E-02 |
| 27 | | 4.592E-02 | 7.53E-01 | 8.00E-02 |
| 28 | | 4.428E-02 | 7.70E-01 | 7.05E-02 |
| 29 | | 4.275E-02 | 7.86E-01 | 6.35E-02 |
| 30 | | 4.133E-02 | 8.00E-01 | 5.65E-02 |
| 35 | | 3.542E-02 | 8.54E-01 | 3.47E-02 |
| 40 | | 3.100E-02 | 8.89E-01 | 2.24E-02 |
| 45 | | 2.755E-02 | 9.14E-01 | 1.54E-02 |
| 50 | | 2.480E-02 | 9.32E-01 | 1.10E-02 |
| 55 | | 2.254E-02 | 9.45E-01 | 8.08E-03 |
| 60 | | 2.066E-02 | 9.55E-01 | 6.09E-03 |
| 65 | | 1.907E-02 | 9.63E-01 | 4.72E-03 |
| 70 | | 1.771E-02 | 9.69E-01 | 3.71E-03 |
| 75 | | 1.653E-02 | 9.74E-01 | 2.98E-03 |
| 80 | | 1.550E-02 | 9.79E-01 | 2.42E-03 |
| 85 | | 1.459E-02 | 9.83E-01 | 2.00E-03 |
| 90 | | 1.378E-02 | 9.86E-01 | 1.66E-03 |
| 95 | | 1.305E-02 | 9.89E-01 | 1.39E-03 |
| 100 | | 1.240E-02 | 9.93E-01 | 1.18E-03 |
| 105 | | 1.181E-02 | 9.97E-01 | 1.01E-03 |
| 110 | | 1.127E-02 | 1.00E+00 | 9.43E-04 |
| 111 | | 1.117E-02 | 1.01E+00 | 1.49E-03 |
| 112 | | 1.107E-02 | 1.01E+00 | 4.87E-03 |
| 113 | | 1.097E-02 | 1.01E+00 | 1.32E-02 |
| 114 | | 1.088E-02 | 1.01E+00 | 1.88E-02 |
| 115 | | 1.078E-02 | 1.01E+00 | 1.74E-02 |
| 116 | | 1.069E-02 | 1.00E+00 | 1.79E-02 |
| 117 | | 1.060E-02 | 1.00E+00 | 1.85E-02 |
| 118 | | 1.051E-02 | 1.00E+00 | 1.99E-02 |
| 119 | | 1.042E-02 | 1.00E+00 | 2.04E-02 |
| 120 | | 1.033E-02 | 9.99E-01 | 2.04E-02 |
| 121 | | 1.025E-02 | 9.98E-01 | 2.05E-02 |
| 122 | | 1.016E-02 | 9.97E-01 | 2.05E-02 |
| 123 | | 1.008E-02 | 9.96E-01 | 2.04E-02 |
| 124 | | 9.998E-03 | 9.95E-01 | 2.02E-02 |
| 125 | | 9.918E-03 | 9.95E-01 | 2.00E-02 |
| 126 | | 9.840E-03 | 9.94E-01 | 1.99E-02 |
| 127 | | 9.762E-03 | 9.93E-01 | 1.95E-02 |
| 128 | | 9.686E-03 | 9.93E-01 | 1.90E-02 |
| 129 | | 9.611E-03 | 9.93E-01 | 1.84E-02 |
| 130 | | 9.537E-03 | 9.91E-01 | 1.80E-02 |
| 140 | | 8.856E-03 | 9.89E-01 | 1.41E-02 |
| 150 | | 8.265E-03 | 9.89E-01 | 1.12E-02 |
| 160 | | 7.749E-03 | 9.89E-01 | 9.02E-03 |
| 170 | | 7.293E-03 | 9.90E-01 | 7.37E-03 |
| 180 | | 6.888E-03 | 9.91E-01 | 6.09E-03 |
| 190 | | 6.525E-03 | 9.91E-01 | 5.09E-03 |

TABLE II (*Continued*)

**Beryllium**

| eV | $cm^{-1}$ | $\mu m$ | n | k |
|---|---|---|---|---|
| 200 | | 6.199E-03 | 9.92E-01 | 4.29E-03 |
| 210 | | 5.904E-03 | 9.92E-01 | 3.65E-03 |
| 220 | | 5.636E-03 | 9.93E-01 | 3.12E-03 |
| 230 | | 5.390E-03 | 9.94E-01 | 2.69E-03 |
| 240 | | 5.166E-03 | 9.94E-01 | 2.34E-03 |
| 250 | | 4.959E-03 | 9.94E-01 | 2.04E-03 |
| 260 | | 4.769E-03 | 9.95E-01 | 1.79E-03 |
| 270 | | 4.592E-03 | 9.95E-01 | 1.58E-03 |
| 280 | | 4.428E-03 | 9.95E-01 | 1.40E-03 |
| 290 | | 4.275E-03 | 9.96E-01 | 1.24E-03 |
| 300 | | 4.133E-03 | 9.96E-01 | 1.11E-03 |

**TABLE III**

**Optical Constants for Be from Henke Model**

| eV | Å | n | k |
|---|---|---|---|
| 299 | 4.154E+03 | 0.99586 | 1.11E-03 |
| 313 | 3.966E+03 | 0.99622 | 9.36E-04 |
| 327 | 3.787E+03 | 0.99655 | 7.92E-04 |
| 343 | 3.616E+03 | 0.99686 | 6.71E-04 |
| 359 | 3.453E+03 | 0.99713 | 5.68E-04 |
| 376 | 3.297E+03 | 0.99739 | 4.81E-04 |
| 394 | 3.148E+03 | 0.99762 | 4.06E-04 |
| 413 | 3.006E+03 | 0.99783 | 3.41E-04 |
| 432 | 2.870E+03 | 0.99802 | 2.86E-04 |
| 452 | 2.741E+03 | 0.99820 | 2.40E-04 |
| 474 | 2.617E+03 | 0.99836 | 2.01E-04 |
| 496 | 2.499E+03 | 0.99851 | 1.69E-04 |
| 520 | 2.386E+03 | 0.99865 | 1.42E-04 |
| 574 | 2.278E+03 | 0.99877 | 1.19E-04 |
| 570 | 2.175E+03 | 0.99888 | 9.94E-05 |
| 583 | 2.126E+03 | 0.99893 | 9.09E-05 |
| 597 | 2.077E+03 | 0.99898 | 8.32E-05 |
| 611 | 2.030E+03 | 0.999030 | 7.61E-05 |
| 625 | 1.983E+03 | 0.999075 | 6.96E-05 |
| 655 | 1.894E+03 | 0.999159 | 5.79E-05 |
| 686 | 1.808E+03 | 0.999236 | 4.82E-05 |
| 718 | 1.727E+03 | 0.999305 | 4.05E-05 |
| 752 | 1.649E+03 | 0.999368 | 3.37E-05 |
| 788 | 1.574E+03 | 0.999425 | 2.81E-05 |
| 825 | 1.503E+03 | 0.999477 | 2.34E-05 |
| 864 | 1.435E+03 | 0.999525 | 1.95E-05 |
| 905 | 1.370E+03 | 0.999568 | 1.63E-05 |
| 948 | 1.308E+03 | 0.999607 | 1.35E-05 |
| 992 | 1.249E+03 | 0.999642 | 1.13E-05 |
| 1039 | 1.193E+03 | 0.999674 | 9.34E-06 |
| 1088 | 1.139E+03 | 0.999704 | 7.75E-06 |
| 1140 | 1.088E+03 | 0.999730 | 6.42E-06 |
| 1194 | 1.039E+03 | 0.999755 | 5.33E-06 |
| 1250 | 9.917E+02 | 0.999777 | 4.42E-06 |
| 1309 | 9.469E+02 | 0.999797 | 3.66E-06 |
| 1371 | 9.041E+02 | 0.999815 | 3.04E-06 |
| 1436 | 8.633E+02 | 0.999832 | 2.52E-06 |
| 1504 | 8.244E+02 | 0.999847 | 2.10E-06 |
| 1575 | 7.871E+02 | 0.999860 | 1.78E-06 |
| 1650 | 7.516E+02 | 0.999873 | 1.52E-06 |
| 1728 | 7.176E+02 | 0.999884 | 1.29E-06 |
| 1809 | 6.852E+02 | 0.999895 | 1.09E-06 |
| 1895 | 6.543E+02 | 0.9999039 | 9.18E-07 |
| 1985 | 6.248E+02 | 0.9999125 | 7.70E-07 |
| 2078 | 5.965E+02 | 0.9999203 | 6.46E-07 |
| 2177 | 5.696E+02 | 0.9999273 | 5.42E-07 |
| 2280 | 5.439E+02 | 0.9999338 | 4.50E-07 |

**TABLE III** (*Continued*)

**Optical Constants for Be from Henke Model**

| eV | Å | n | k |
|---|---|---|---|
| 2387 | 5.193E+02 | 0.9999397 | 3.74E-07 |
| 2500 | 4.959E+02 | 0.9999450 | 3.11E-07 |
| 2619 | 4.735E+02 | 0.9999499 | 2.58E-07 |
| 2742 | 4.521E+02 | 0.9999544 | 2.14E-07 |
| 2872 | 4.317E+02 | 0.9999585 | 1.77E-07 |
| 3008 | 4.122E+02 | 0.9999621 | 1.46E-07 |
| 3150 | 3.936E+02 | 0.9999655 | 1.20E-07 |
| 3299 | 3.758E+02 | 0.9999685 | 9.89E-08 |
| 3455 | 3.588E+02 | 0.9999713 | 8.15E-08 |
| 3619 | 3.426E+02 | 0.9999739 | 6.71E-08 |
| 3790 | 3.272E+02 | 0.9999762 | 5.53E-08 |
| 3969 | 3.124E+02 | 0.9999783 | 4.57E-08 |
| 4157 | 2.983E+02 | 0.9999802 | 3.79E-08 |
| 4353 | 2.848E+02 | 0.9999819 | 3.14E-08 |
| 4559 | 2.720E+02 | 0.9999835 | 2.60E-08 |
| 4775 | 2.597E+02 | 0.9999850 | 2.15E-08 |
| 5000 | 2.479E+02 | 0.9999864 | 1.78E-08 |
| 5237 | 2.368E+02 | 0.9999875 | 1.48E-08 |
| 5484 | 2.261E+02 | 0.9999887 | 1.22E-08 |
| 5744 | 2.159E+02 | 0.9999896 | 1.01E-08 |
| 6015 | 2.061E+02 | 0.9999060 | 8.34E-09 |
| 6300 | 1.968E+02 | 0.99999140 | 6.89E-09 |
| 6598 | 1.879E+02 | 0.99999220 | 5.68E-09 |
| 6910 | 1.794E+02 | 0.99999280 | 4.64E-09 |
| 7237 | 1.713E+02 | 0.99999350 | 3.78E-09 |
| 7579 | 1.636E+02 | 0.99999400 | 3.09E-09 |
| 7937 | 1.562E+02 | 0.99999460 | 2.52E-09 |
| 8313 | 1.492E+02 | 0.99999510 | 2.06E-09 |
| 8706 | 1.424E+02 | 0.99999550 | 1.68E-09 |
| 9117 | 1.360E+02 | 0.99999590 | 1.37E-09 |
| 9549 | 1.298E+02 | 0.99999620 | 1.12E-09 |
| 10000 | 1.240E+02 | 0.99999660 | 9.12E-10 |

# Cobalt (Co)

L. WARD
Coventry Polytechnic
Coventry, England

Cobalt is an element with an atomic number of 27 and is one of the group of transition metals; it can readily be obtained in the form of blocks, rods, or powder, and its most common impurities are iron, nickel, sodium, and potassium. There are two allotropic forms of cobalt: close-packed hexagonal, which is stable at room temperature, and face-centered cubic, which is stable above 417 °C and which can be produced from the hexagonal form by a suitable annealing procedure. Much of the published work on solid cobalt refers to the hexagonal close-packed crystal structure, which implies that the optical properties should be different along different crystal directions. However, in most cases, authors have dealt with polycrystalline material, where the optical properties are independent of direction; only one set of results has been published for single-crystal bulk cobalt in which the optical properties along both the main crystal axes are considered. In addition, several papers have reported measurements on thin films, again mostly in the polycrystalline form.

Being metallic, cobalt, at long wavelengths in the infrared region, may be expected to behave according to the classical Drude formulas for free-electron materials, namely,

$$\varepsilon_1 = n^2 - k^2 = 1 - A\nu_c/2\pi(\nu^2 + \nu_c^2)$$

$$\varepsilon_2 = 2nk = A\nu_c^2/2\pi\nu(\nu^2 + \nu_c^2),$$

where $A$ is a constant, proportional to the dc electrical conductance, $\nu$ is the frequency and $\nu_c$ is the electron collision frequency. These formulas predict that in the infrared the optical constants $n$ and $k$ should have large values with both increasing with wavelength. This behavior is in fact observed at all wavelengths longer than about 6 μm, but below that point, there is a marked departure from the Drude equation in the form of increases in the values of both $n$ and $k$ as the wavelength decreases, producing maxima in each at about 3 μm. It is generally regarded that this


Copyright © 1991 by Academic Press.
All rights of reproduction in any form reserved.
ISBN 0-12-544422-2

anomaly is caused by the onset of interband electron transitions due to the very small energy gap (0.20 eV) between the Fermi level in the almost full d-band and the next higher s-band. However, as the wavelength continues to decrease below 1 μm, $n$ and $k$ resume their downward trend in values and ultimately $n$ becomes equal to $k$, which is the condition for plasma oscillations; this plasma resonance occurs at a frequency of $18.6 \times 10^{14}\, s^{-1}$ (0.16 μm). At very short wavelengths, $n$ becomes asymptotic to unity, while $k$ continues to fall, reaching extremely low values below 0.01 μm. However, there are further maxima in $k$, one at 0.020 μm and a second at 0.011 μm. These are due to additional electron transitions between inner levels, the first at the $M_{II,III}$ point and the second at the $M_I$ point. Beyond this wavelength, there is little published experimental optical information on cobalt, so further interband transitions have not been recorded, although X-ray data indicate $L$-edges at 0.0016 μm and 0.0013 μm and a $K$-edge at 0.00016 μm [1].

Much of the work on the optical properties of metals published before about 1950 is now regarded as unreliable because of the uncertain state of the surfaces used. Not only does mechanical polishing produce an atypical surface layer in which the crystal structure is broken down and much dislocated, but many crystals rapidly become oxidized or contaminated when exposed to air; this produces a surface layer having unknown optical properties, of which it is consequently difficult to take account when calculating $n$ and $k$. Two developments since 1950 have led to the production of reliable, clean, and reproducible crystalline surfaces, suitable for optical work: ultrahigh-vacuum conditions can be generated, which almost eliminate oxidation problems and at the same time create the conditions under which epitaxial films can be deposited; and mechanical polishing can be carefully controlled or replaced by electrochemical polishing, so that deep-seated mechanical damage may be avoided. Archard [2] has given a review of modern polishing techniques.

There have been two major reviews covering the optical constants of the transition metals, including cobalt. The first, by Weaver *et al.* [3], surveyed a large number of papers including those by Kirillova and Charikov [4], Lenham and Treherne [5], Yu *et al.* [6], Sonntag *et al.* [7], Johnson and Christy [8], Weaver *et al.* [9] and Wehenkel and Gauthe [10]. Making use mainly of their own results on single-crystal hcp cobalt, Weaver *et al.* [3] have presented sets of data of $n$ and $k$ over the wavelength range 0.15–12.44 μm for the two cases of the electric field vector of the incident radiation parallel to and perpendicular to the $c$ axis of the crystal, that is, the axis at right angles to the base of the hexagon. In the second review, Ordal *et al.* [11] collected data for cobalt over a wide range of wavelengths from 0.20–20 μm, mainly in the infrared region. The main sources of their data were Johnson and Christy [8], Weaver *et al.* [9], and Kirillova and Charikov [4]. As well as giving tables of values of $n$ and $k$ between 0.19 μm

and 20.0 μm, they have graphed $\varepsilon_1$ and $\varepsilon_2$ against wave number. A further, later review by Ordal *et al.* [12] continued the same work in the infrared and showed graphically a Drude-model fit to the various experimental results.

Values of $n$ and $k$ for cobalt from various sources are given in Table I and graphed in Fig. 1; the wavelength range covered is $6 \times 10^{-4}$–12.4 μm and, wherever possible, slight wavelength overlaps have been included between the different sets of results.

*Results for X-ray Region*

For extremely short wavelengths in the X-ray region (6–120 Å), there are no direct experimental results for the optical constants of cobalt. However, Henke [13] has shown that $n$ and $k$ in this wavelength region may be calculated from the X-ray scattering coefficients of the atoms involved. Thus, for cobalt:

$$k = 40.0\lambda^2 f_2$$

$$n = 1 - 40.0\lambda^2 f_1,$$

where $\lambda$ is the wavelength in microns and $f_1$ and $f_2$ are the appropriate scattering factors. Henke *et al.* [14] have published tables of $f_1$ and $f_2$ for many values of wavelength and photon energy for some of the atoms in the periodic table, from which the values of $n$ and $k$ for cobalt at these wavelengths have been calculated; these are tabulated at the end of this article in Table I. As expected, $n$ in this region of the spectrum is close to unity, whereas $k$ shows a definite peak at 16 Å (0.0016 μm) due to the $L_{2,3}$ transitions, and a much smaller peak at 0.00134 μm due to the $L_1$ transition.

*Results for Cobalt Films*

At slightly longer wavelengths (0.004–0.06 μm) experimental values of the absorption coefficient, $\alpha$, equal to $4\pi k/\lambda$, have been published by Sonntag *et al.* [7] and also by Wehenkel and Gauthe [10, 26]. Sonntag *et al.* used synchrotron radiation in a direct measurement of the absorption coefficient; $k$ may be easily deduced from the graphs they provide. It is assumed that $n$ is approximately equal to unity in this spectral region. Wehenkel and Gauthe measured the electron-energy-loss spectrum by bombarding thin films of cobalt by 35 keV electrons; a Kramers–Kronig summation technique was then used to calculate $\varepsilon_1$ and $\varepsilon_2$, from which $n$ and $k$ can be extracted. Both these studies revealed a maximum in $k$ at 0.020 μm and a shoulder at 0.011 μm (62.3 eV and 107 eV); these are due to the transitions $M_{II,III}$ and $M_I$, respectively. The values of $k$ deduced from

Wehenkel and Gauthe are larger than those from Sonntag *et al.*, particularly at the shorter wavelength end. Values of $k$ from both sources are presented in Table I, those of Sonntag *et al.* from 0.006–0.03 μm and the ones from Wehenkel and Gauthe between 0.035 μm and 0.31 μm. There is some wavelength overlap between these results and those calculated by Henke's method, and the agreement in the values of the optical constants is considered to be satisfactory. Fanfoni *et al.* [15], studying the electron-energy-loss spectrum up to 240 eV (0.005 μm), confirmed the $M_{II,III}$ edge at 0.018 μm but did not discover any further edges beyond that point, although a peak might have been expected at 0.011 μm.

A set of results produced by Yu *et al.* [6] is considered to be very reliable; they used specimens of polycrystalline cobalt prepared by electron-beam evaporation under ultrahigh-vacuum conditions. The optical parameter measured was the reflectance near normal incidence, and the optical constants were extracted by Kramers–Kronig analysis over the range 0.1–25 μm, although they give useful graphs only for energies greater than 0.25 eV, that is, wavelengths less than 5.0 μm; these values of $n$ and $k$ have also been tabulated in Table I and link reasonably well with those of Wehenkel and Gauthe.

Johnson and Christy [8] give a set of values of $n$ and $k$ between 0.64 eV and 6.60 eV (0.2–2.0 μm), their results being obtained from measurements of the reflectance and transmittance of thin evaporated films having thicknesses between 200 Å and 500 Å. In general, their values of both $n$ and $k$, which are presented in Table I, were smaller than those reported by Yu, possibly either because of the vacuum conditions prevailing in their equipment or the different substrate temperature used during evaporation.

Viguier *et al.* [16], using both ellipsometric and reflectance measurements, have produced values of $\varepsilon_1$ and $\varepsilon_2$ for polycrystalline cobalt films 1000 Å thick between 1 eV and 5 eV (0.25–1.25 μm). There were no distinctive optical features over this region; $\varepsilon_2$ was positive and increased steadily with wavelength, whereas $\varepsilon_1$ was negative and became more so as the wavelength increased. An accuracy of 0.2% was claimed for measurements in the visible spectrum, the greatest uncertainty being due to the surface roughness. However, the calculated values of $n$ and $k$ from this work are both at least 10% smaller than those given by Johnson and Christy. A set of their results is included in Table I, since this is one of the most recent determinations of the optical constants of cobalt.

Kudryavtsev and Lezhnenko [17] investigated cobalt films between 1 μm and 13 μm in both the hcp and the fcc crystal forms, changing from one form to the other by suitable annealing above 400 °C. Experimentally, Beattie's method [18] was used, in which the phase change on reflection was measured for several angles of incidence, which in this case were greater than 80°. The authors noted significant differences between the optical properties of the two forms of cobalt in both the intra- and

interband transition regions. In the interband region ($\lambda > 6$ μm) $n$ increased while $k$ decreased on changing from hexagonal to cubic, whereas in the interband region ($1 < \lambda < 6$ μm) both $n$ and $k$ decreased for a similar change. Because their set of results for the cubic form of cobalt is virtually unique, it has been included in Table I.

Clemens and Jaumann [19] measured the optical constants of evaporated layers of cobalt having thicknesses of about 0.03 μm and deposited on glass substrates; the wavelength range covered was 0.42–2.5 μm. The special feature of this work was that the films were magnetically saturated at right angles to their plane, and measurements were made of the reflectances and transmittances from both sides of the substrate. Both $n$ and $k$ turned out to be different as determined from the two sides, but those from the air side agreed well with the results of Weaver *et al.* [3] for the extraordinary ray. Over the spectral region investigated, both sets of optical constants increased steadily with wavelength; from the published graphs, $n$ and $k$ can be read to about ±0.01.

*Results for Bulk Cobalt*

Kirillova *et al.* [20] measured the reflectance of polycrystalline solid specimens between 0.1 μm and 0.25 μm and then used Kramers–Kronig analysis to extract $\varepsilon_1$ and $\varepsilon_2$. They noted the effects of the first quantum absorption band between 0.2 μm and 1.2 μm due to electron transitions in various directions within the Brillouin zone. However, the graphs they give are not suitable for the accurate reading of $n$ and $k$ values. Kirillova and Charikov [4] studied bulk polycrystalline cobalt by a polarimetric technique between 2.5 μm and 20.0 μm, noting the contribution from interband transitions in this region even up to 6 or 7 μm. They calculated the plasma frequency to be $18.6 \times 10^{14} s^{-1}$ (that is, the plasma wavelength = 0.162 μm) and the electron relaxation frequency as $2.5 \times 10^{14} s^{-1}$. Bolotin *et al.* [21] obtained the optical constants for a mechanically polished and then annealed polycrystalline specimen of cobalt using the method of Beattie [18]; values of $n$ and $k$ were tabulated between 0.3 μm and 17.0 μm. The classical free-electron theory provided a satisfactory model between 6 μm and 17 μm, but at shorter wavelengths the anomalous behavior described above was observed, there being a peak in the electrical conductivity at 1.5 μm. The values of $k$ reported by this group were in approximate agreement with those of Yu, but those for $n$ were considerably lower, particularly at the shorter wavelengths investigated, again probably because of the damage to the surface layer by the mechanical-polishing technique employed. However, because they are still one of the few sets of data covering this wide wavelength band, they are quoted in Table I. Afanasyeva and Kirillova [22] give data measured on polycrystalline cobalt between 0.8 μm and 3.5 μm. Using mechanically polished specimens, the measured parameter was the electrical conductivity, which as shown above

is closely related to the optical constants. They also paid particular attention to the spectral region where $n$ increased as the wavelength decreased. Their values for $k$ were comparable with those of Bolotin *et al.*, but the data for $n$ were significantly smaller, particularly at the shorter wavelengths, perhaps due to their polishing technique. Other sets of data for the infrared region (0.3–12.5 μm) have been obtained by Lenham and his collaborators [5, 23], who used an ellipsometric technique in conjunction with mechanically polished polycrystalline specimens. Their published graphs, however, are not generally suitable for the extraction of accurate values. A set of values of $n$ and $k$ for bulk cobalt at different temperatures has been published by Gushchin *et al.* [24]. Beattie's method was again the experimental method used, and the measurements were carried out between 0.4 and 3.3 μm and at temperatures of 20, 1400 and 1600 °C. The results at 20 °C are in fair agreement with those of Bolotin *et al.* taken at the same temperature, and it was also observed that both $n$ and $k$ increased with temperature up to 1400 °C. The optical constants at 1400 °C are included in Table I. Kulikov and Kulatov [25] report an interesting theoretical study of the variation of the optical properties of cobalt with pressure.

*Results for Cobalt Using Polarized Radiation*

Weaver *et al.* [9] present detailed tables of the optical constants of single-crystal cobalt between 0.15 and 12.4 μm for radiation polarized with its **E** vector parallel to and perpendicular to the $c$ axis, that is, the axis at right angles to the base of the crystalline hexagon; these being the only data to deal with both states of polarization, they are quoted extensively in Table I. Their measurements were made on electrolytically polished specimens employing reflectance for wavelengths below 0.3 μm and calorimetry for wavelengths greater than 0.3 μm. The two sets of values exhibit their greatest differences at the longer wavelengths investigated (1–6.5 μm), where $n$ for $\mathbf{E}_{\parallel c}$ $(n_e)$ is smaller than that for $\mathbf{E}_{\perp c}$ $(n_o)$; the opposite applies to the values of $k$ where $k_e$ is larger than $k_o$. For wavelengths below 0.6 μm, the separate values of $n$ and $k$ converge. At this point, the values of the optical constants are also in good agreement with those produced by Yu *et al.* and Bolotin *et al.* for the polycrystalline form of cobalt, as would be expected to happen. The results of Weaver *et al.* for the cases of polarization both parallel and perpendicular to the $c$ axis indicate maxima in $n$ at 1.7 μm and corresponding minima at 6 μm. For $k$ there is a maximum at 1.35 μm (perpendicular $c$ axis) and a much less well-defined maximum at 1.40 μm (parallel $c$ axis).

## REFERENCES

1. J. R. Beardon and A. F. Burr, *Rev. Mod. Phys.* **39**, 125 (1967).

2. J. F. Archard, *Phys. Bull.* **36**, 212 (1985).
3. J. H. Weaver, C. Krafta, D. W. Lynch, and E. E. Koch, "Physics Data, Optical Properties of Metals, Part 2," Fachsinformazionszentrum, Karlsruhe (1981).
4. M. M. Kirillova and B. A. Charikov, *Opt. and Spectros.* **17**, 134 (1964).
5. A. P. Lenham and D. M. Treherne, *J. Opt. Soc. Am.* **56**, 1076 (1966).
6. A. Y.-C. Yu, T. M. Donovan, and W. E. Spicer, *Phys. Rev.* **167**, 670 (1968).
7. B. Sonntag, R. Haensel, and C. Kunz, *Solid State Commun.* **7**, 597 (1969).
8. P. B. Johnson and R. W. Christy, *Phys. Rev.* **B9**, 5056 (1974).
9. J. H. Weaver, E. Colevita, D. W. Lynch and R. Rossi, *Phys. Rev.* **B19**, 3850 (1979).
10. C. Wehenkel and B. Gauthe, *Phys. Stat. Solidi. B* **64**, 515 (1974).
11. M. R. Ordal, L. L. Long, R. J. Bell, S. E. Bell, R. R. Bell, R. W. Alexander, and C. R. Ward, *Appl. Opt.* **22**, 1099 (1983).
12. M. R. Ordal, R. J. Bell, R. W. Alexander, L. L. Long, and M. R. Quarry, *Appl. Opt.* **24**, 4493 (1985).
13. B. L. Henke, *A.I.P. Conf. Proc. No. 75*, 146 (1981).
14. B. L. Henke, P. Lee, T. J. Tanaka, R. Shimabukaro and B. K. Fujikawa, *Atomic Data and Nuclear Data Tables* **27**, 1 (1982).
15. M. Fanfoni, S. Modesti, R. Motta, N. de Cresenta, and R. Rossi, *Phys. Rev.* **B32**, 7826 (1985).
16. C. Viguier, R. Cros, A. Humbert, C. Ferrien, O. Thomas, R. Mader, and J. P. Senateur, *Solid State Commun.* **60**, 923 (1986).
17. V. Y. Kudryavtsev and I. V. Lezhnenko, *Sov. Phys. Solid State* **21**, 249 (1981).
18. J. R. Beattie, *Phil. Mag.* **46**, 222 (1955).
19. K. H. Clemens and J. Jaumann, *Z. Physik* **173**, 135 (1963).
20. M. M. Kirillova, L. V. Nomerovannya, G. A. Bolotin, V. M. Mayevskiy, M. M. Noskov, and M. S. Bolotin, *Phys. Met. Metallog.* **25**, 81 (1969).
21. G. A. Bolotin, M. M. Noskov, and I. I. Sasovshaya, *Phys. Met. Metallog.* **35**, 24 (1973).
22. L. A. Afanasyeva and M. M. Kirillova, *Phys. Met. Metallog.* **23**, 80 (1967).
23. A. P. Lenham, *J. Opt. Soc. Am.* **57**, 473 (1967).
24. V. S. Gushchin, K. M. Shararev, B. A. Baum, and P. V. Geld, *Sov. Phys. Dokl.* **23**, 344 (1978).
25. N. I. Kulatov and E. T. Kulakov, *J. Phys. F* **12**, 2267 (1982).
26. C. Wehenkel and R. Gauthe, *Phys. Lett.* **47A**, 253 (1974).

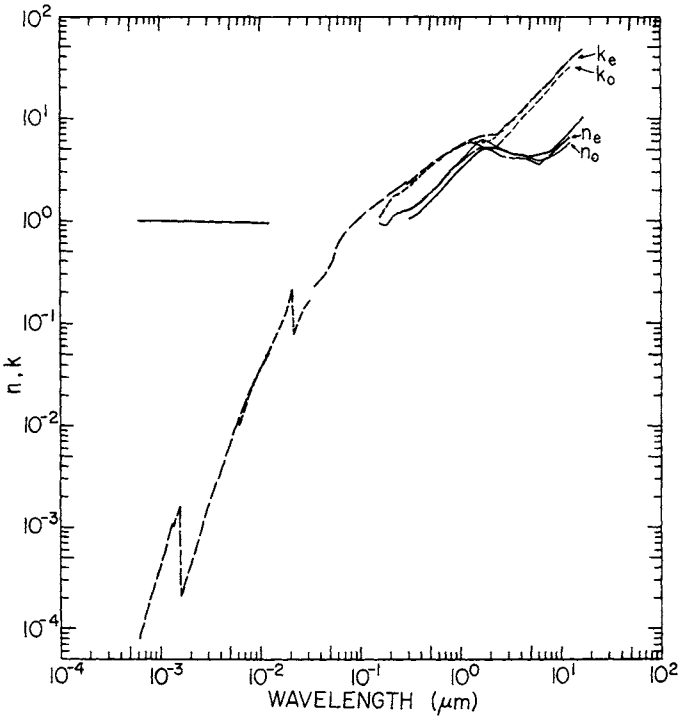


**Fig. 1.** Log–log plot of $n$ (solid line) and $k$ (dashed line) versus wavelength in micrometers for cobalt (unpolarized radiation unless specified otherwise).

**TABLE I**

**Values of *n* and *k* for Hexagonal Cobalt from Various Refs.[a]**

| eV | $cm^{-1}$ | μm | n | k |
|---|---|---|---|---|
| 2000 | 16,131,000 | 0.00062 | 0.9996 [13] | $8.0*10^{-5}$ [13] |
| 1850 | 14,921,000 | 0.00067 | 0.9996 | $1.0*10^{-4}$ |
| 1688 | 13,615,000 | 0.00073 | 0.9994 | 1.4 |
| 1609 | 12,977,000 | 0.00077 | 0.9994 | 1.6 |
| 1550 | 12,500,000 | 0.00080 | 0.9992 | 2.0 |
| 1358 | 10,953,000 | 0.00091 | 0.9992 | 3.0 |
| 1240 | 10,000,000 | 0.00100 | 0.9990 | 4.2 |
| 1148 | 9,259,300 | 0.00108 | 0.9988 | 5.2 |
| 1016 | 8,194,500 | 0.00122 | 0.9988 | 8.0 |
| 946.5 | 7,633,900 | 0.00131 | 0.9992 | 10.4 |
| 925.3 | 7,463,000 | 0.00134 | 0.9992 | 10.8 |
| 898.4 | 7,246,000 | 0.00138 | 0.9992 | 10.6 |
| 879.3 | 7,092,000 | 0.00141 | 0.9992 | 11.6 |
| 855.1 | 6,896,700 | 0.00145 | 0.9988 | 12.6 |
| 815.7 | 6,579,000 | 0.00152 | 0.9990 | 14.6 |
| 800.0 | 6,452,400 | 0.00155 | 0.9992 | 15.6 |
| 775.0 | 6,250,000 | 0.00160 | 1.0006 | 17.0 |
| 760.6 | 6,134,600 | 0.00163 | 0.9994 | 2.2 |
| 729.3 | 5,882,100 | 0.00170 | 0.9988 | 2.4 |
| 725.1 | 5,848,200 | 0.00171 | 0.9986 | 2.6 |
| 620.0 | 5,000,000 | 0.00200 | 0.9976 | 4.2 |
| 529.0 | 4,273,700 | 0.00234 | 0.9964 | 7.0 |
| 413.3 | 3,333,300 | 0.00300 | 0.9938 | 15.0 |
| 368.0 | 2,968,100 | 0.00337 | 0.9920 | 22.0 |
| 310.0 | 2,500,000 | 0.00400 | 0.9810 | 34.0 |
| 269.0 | 2,169,600 | 0.00461 | 0.9858 | 52.0 |
| 248.0 | 2,000,000 | 0.00500 | 0.9838 | 64.0 |
| 227.1 | 1,831,700 | 0.00546 | 0.9810 | $84.0*10^{-4}$ |
| 206.6 | 1,666,700 | 0.00600 | 0.9770 | $10.8*10^{-3}$ |
| 190.7 | 1,538,100 | 0.00650 | 0.9748 | 13.2 |
| 177.1 | 1,428,400 | 0.00700 | 0.9720 | 15.6 |
| 155.0 | 1,250,000 | 0.00800 | 0.9656 | 21.8 |
| 137.8 | 1,111,100 | 0.00900 | 0.9586 | 29.0 |
| 124.0 | 1,000,000 | 0.0100 | 0.9550 | 35.2 |
| 111.7 | 900,900 | 0.0111 | 0.9492 | 42.8 |
| 104.2 | 840,400 | 0.0119 | 0.9492 | 49.0 |
| 100.0 | 806,500 | 0.0124 | 0.9414 | 52.8 |

**Values of *n* and *k* for Hexagonal Cobalt Films**

| eV | $cm^{-1}$ | μm | n | k |
|---|---|---|---|---|
| 200 | 1,612,900 | 0.006200 | 1.00 [7] | $1.0*10^{-2}$ [7] |
| 172 | 1,388,900 | 0.007209 | 1.00 | 1.5 |
| 149 | 1,205,000 | 0.008322 | 1.00 | 2.3 |
| 120 | 971,100 | 0.01033 | 1.00 | 3.8 |
| 110 | 887,200 | 0.01127 | 1.00 | 4.7 |
| 106 | 854,900 | 0.01170 | 1.00 | 5.0 |
| 100 | 806,500 | 0.01240 | 1.00 | 5.5 |
| 94.7 | 763,400 | 0.01309 | 1.00 | 6.1 |
| 89.8 | 724,600 | 0.01381 | 1.00 | 7.0 |
| 80.0 | 645,200 | 0.01550 | 1.00 | $8.7*10^{-2}$ |

TABLE I (*Continued*)

**Hexagonal Cobalt**

| eV | $cm^{-1}$ | μm | n | k |
|---|---|---|---|---|
| 70.1 | 565,000 | 0.01769 | 1.00 [7] | $1.2*10^{-1}$ [7] |
| 62.0 | 500,000 | 0.02000 | 1.00 | 1.8 |
| 56.4 | 454,600 | 0.02199 | 1.00 | 0.8 |
| 49.6 | 400,000 | 0.02500 | 1.00 | 1.1 |
| 44.3 | 357,100 | 0.02805 | 1.00 | 1.4 |
| 38.8 | 312,500 | 0.03196 | 1.00 | $1.7*10^{-1}$ |
| 35.4 | 285,700 | 0.03503 | 1.00 [10] | 0.23 [10] |
| 31.0 | 250,000 | 0.04000 | 1.00 | 0.26 |
| 24.8 | 200,000 | 0.05000 | 1.00 | 0.35 |
| 20.7 | 166,300 | 0.05990 | 1.00 | 0.65 |
| 17.7 | 142,800 | 0.07006 | 1.00 | 0.77 |
| 15.5 | 125,000 | 0.08000 | 1.00 | 0.90 |
| 12.4 | 100,000 | 0.1000 | 1.00 | 1.08 |
| 10.0 | 80,650 | 0.1240 | 1.00 | 1.31 |
| 7.01 | 56,500 | 0.1769 | 1.00 | 1.68 |
| 4.00 | 32,260 | 0.3100 | 1.00 | 2.48 |
| 11.46 | 90,430 | 0.1080 | 1.096 [6] | 0.775 [6] |
| 9.69 | 78,130 | 0.1280 | 1.088 | 0.827 |
| 7.75 | 62,500 | 0.1600 | 1.049 | 1.049 |
| 5.99 | 48,310 | 0.2070 | 1.210 | 1.570 |
| 3.94 | 31,750 | 0.3150 | 1.298 | 2.118 |
| 3.00 | 24,210 | 0.4133 | 2.153 | 3.484 |
| 2.00 | 16,130 | 0.6200 | 2.486 | 4.022 |
| 1.00 | 8,065 | 1.240 | 3.639 | 6.184 |
| 0.600 | 4,839 | 2.067 | 4.708 | 8.495 |
| 0.400 | 3,226 | 3.100 | 5.301 | 11.318 |
| 6.60 | 53,230 | 0.1879 | 1.16 [8] | 1.59 [8] |
| 6.22 | 50,170 | 0.1993 | 1.29 | 1.71 |
| 5.85 | 47,180 | 0.2119 | 1.38 | 1.82 |
| 5.36 | 43,230 | 0.2313 | 1.47 | 1.87 |
| 4.98 | 40,170 | 0.2490 | 1.45 | 1.93 |
| 4.61 | 37,180 | 0.2689 | 1.44 | 2.04 |
| 4.24 | 34,200 | 0.2924 | 1.44 | 2.19 |
| 3.99 | 32,190 | 0.3107 | 1.44 | 2.31 |
| 3.74 | 30,160 | 0.3315 | 1.46 | 2.44 |
| 3.50 | 28,230 | 0.3542 | 1.49 | 2.61 |
| 3.25 | 26,710 | 0.3815 | 1.53 | 2.82 |
| 3.00 | 24,200 | 0.4133 | 1.61 | 3.05 |
| 2.75 | 22,180 | 0.4509 | 1.74 | 3.28 |
| 2.50 | 20,160 | 0.4959 | 1.88 | 3.55 |
| 2.26 | 18,180 | 0.5486 | 2.05 | 3.82 |
| 2.13 | 17,240 | 0.5821 | 2.13 | 3.96 |
| 2.01 | 16,130 | 0.6168 | 2.19 | 4.11 |
| 1.88 | 15,160 | 0.6595 | 2.25 | 4.27 |
| 1.76 | 14,280 | 0.7045 | 2.31 | 4.45 |
| 1.64 | 13,160 | 0.7560 | 2.40 | 4.64 |
| 1.51 | 12,200 | 0.8211 | 2.53 | 4.88 |
| 1.39 | 11,240 | 0.8920 | 2.65 | 5.16 |
| 1.26 | 10,200 | 0.9840 | 2.78 | 5.50 |

TABLE I (*Continued*)

**Hexagonal Cobalt**

| eV | $cm^{-1}$ | μm | n | k |
|---|---|---|---|---|
| 1.14 | 9,170 | 1.088 | 2.94 | 5.88 |
| 1.02 | 8,295 | 1.216 | 3.17 | 6.31 |
| 0.892 | 7,194 | 1.390 | 3.42 | 6.77 |
| 0.771 | 6,211 | 1.592 | 3.61 | 7.26 |
| 0.641 | 5,146 | 1.937 | 3.87 | 7.79 |
| 4.59 | 37,040 | 0.2702 | 0.87 [16] | 1.85 [16] |
| 4.00 | 32,260 | 0.3100 | 0.89 | 2.02 |
| 3.54 | 28,570 | 0.3543 | 0.96 | 2.31 |
| 3.02 | 24,390 | 0.4106 | 1.08 | 2.68 |
| 2.48 | 20,000 | 0.5000 | 1.34 | 3.23 |
| 2.00 | 16,130 | 0.6200 | 1.83 | 3.71 |
| 1.49 | 12,050 | 0.8322 | 2.34 | 4.38 |

**f.c.c. Cobalt Films**

| eV | $cm^{-1}$ | μm | n | k |
|---|---|---|---|---|
| 1.240 | 10,000 | 1.00 | 2.30 [17] | 5.27 [17] |
| 1.033 | 8,333 | 1.20 | 2.90 | 6.77 |
| 0.8856 | 7,143 | 1.40 | 3.36 | 7.39 |
| 0.7749 | 6,250 | 1.60 | 6.20 | 9.46 |
| 0.6888 | 5,555 | 1.80 | 7.80 | 8.46 |
| 0.6199 | 5,000 | 2.00 | 6.10 | 7.06 |
| 0.5636 | 4,545 | 2.20 | 4.96 | 6.75 |
| 0.5166 | 4,167 | 2.40 | 4.60 | 6.80 |
| 0.4769 | 3,846 | 2.60 | 4.68 | 7.17 |
| 0.4428 | 3,571 | 2.80 | 4.60 | 7.68 |
| 0.4133 | 3,333 | 3.00 | 4.39 | 8.13 |
| 0.3875 | 3,125 | 3.20 | 4.50 | 8.51 |
| 0.3647 | 2,941 | 3.40 | 4.77 | 9.08 |
| 0.3444 | 2,778 | 3.60 | 4.56 | 9.66 |
| 0.3263 | 2,632 | 3.80 | 4.74 | 10.16 |
| 0.3100 | 2,500 | 4.00 | 5.01 | 10.61 |
| 0.2818 | 2,273 | 4.40 | 5.45 | 11.58 |
| 0.2583 | 2,083 | 4.80 | 5.45 | 12.11 |
| 0.2384 | 1,923 | 5.20 | 5.61 | 13.48 |
| 0.2214 | 1,786 | 5.60 | 5.67 | 14.42 |
| 0.2067 | 1,667 | 6.00 | 6.13 | 15.38 |
| 0.1937 | 1,563 | 6.40 | 6.52 | 16.26 |
| 0.1771 | 1,429 | 7.00 | 6.76 | 17.22 |
| 0.1675 | 1,351 | 7.40 | 7.03 | 18.15 |
| 0.1550 | 1,250 | 8.00 | 7.36 | 19.56 |
| 0.1476 | 1,190 | 8.40 | 7.62 | 20.41 |
| 0.1376 | 1,111 | 9.00 | 7.97 | 21.64 |
| 0.1292 | 1,042 | 9.60 | 8.18 | 22.84 |
| 0.1240 | 1,000 | 10.00 | 8.42 | 23.63 |
| 0.1181 | 952 | 10.50 | 8.77 | 24.47 |
| 0.1127 | 909 | 11.00 | 9.09 | 25.16 |
| 0.1078 | 870 | 11.50 | 9.39 | 25.88 |
| 0.1033 | 833 | 12.00 | 9.70 | 26.47 |

TABLE I (*Continued*)

f.c.c. Cobalt Films

| eV | $cm^{-1}$ | μm | n | k |
|---|---|---|---|---|
| 0.09919 | 800 | 12.50 | 10.03 | 26.91 |
| 0.09537 | 769 | 13.00 | 10.30 | 27.38 |

Bulk Hexagonal Cobalt

| eV | $cm^{-1}$ | μm | n | k |
|---|---|---|---|---|
| 4.133 | 33,330 | 0.300 | 1.06 [21] | 2.29 [21] |
| 3.397 | 27,400 | 0.365 | 1.10 | 2.76 |
| 3.100 | 25,000 | 0.400 | 1.25 | 3.05 |
| 2.755 | 22,220 | 0.450 | 1.40 | 3.22 |
| 2.480 | 20,000 | 0.500 | 1.56 | 3.43 |
| 2.254 | 18,180 | 0.550 | 1.71 | 3.66 |
| 2.067 | 16,670 | 0.600 | 1.86 | 4.02 |
| 1.908 | 15,390 | 0.650 | 2.00 | 4.23 |
| 1.771 | 14,290 | 0.700 | 2.18 | 4.47 |
| 1.550 | 12,500 | 0.800 | 2.56 | 4.92 |
| 1.378 | 11,111 | 0.900 | 2.93 | 5.28 |
| 1.240 | 10,000 | 1.00 | 3.21 | 5.57 |
| 1.033 | 8,333 | 1.20 | 3.77 | 6.12 |
| 0.8866 | 7,151 | 1.40 | 4.45 | 6.52 |
| 0.7751 | 6,250 | 1.60 | 5.03 | 6.63 |
| 0.6898 | 5,564 | 1.80 | 5.25 | 6.69 |
| 0.6048 | 4,878 | 2.05 | 5.15 | 6.96 |
| 0.5391 | 4,348 | 2.30 | 5.13 | 6.90 |
| 0.4960 | 4,000 | 2.50 | 4.96 | 7.34 |
| 0.4509 | 3,636 | 2.75 | 4.75 | 8.23 |
| 0.4000 | 3,226 | 3.10 | 4.60 | 9.03 |
| 0.3543 | 2,857 | 3.50 | 4.49 | 10.06 |
| 0.3179 | 2,564 | 3.90 | 4.36 | 10.91 |
| 0.2818 | 2,273 | 4.40 | 4.25 | 12.73 |
| 0.2583 | 2,083 | 4.80 | 4.25 | 13.89 |
| 0.2384 | 1,923 | 5.20 | 4.25 | 15.13 |
| 0.2296 | 1,852 | 5.40 | 4.26 | 15.68 |
| 0.2175 | 1,754 | 5.70 | 4.37 | 16.44 |
| 0.2033 | 1,639 | 6.10 | 4.70 | 17.35 |
| 0.1907 | 1,538 | 6.50 | 4.69 | 18.71 |
| 0.1746 | 1,408 | 7.10 | 4.66 | 20.93 |
| 0.1550 | 1,250 | 8.00 | 4.89 | 23.73 |
| 0.1377 | 1,111 | 9.00 | 5.34 | 26.66 |
| 0.1240 | 1,000 | 10.0 | 5.88 | 29.37 |
| 0.1127 | 909.1 | 11.0 | 6.55 | 32.34 |
| 0.1033 | 833.3 | 12.0 | 7.20 | 35.13 |
| 0.09537 | 769.2 | 13.0 | 7.75 | 37.83 |
| 0.08856 | 714.3 | 14.0 | 8.49 | 40.81 |
| 0.08266 | 666.7 | 15.0 | 9.16 | 43.47 |
| 0.07749 | 625.0 | 16.0 | 10.11 | 46.31 |
| 0.07293 | 588.2 | 17.0 | 10.44 | 48.55 |

TABLE I (*Continued*)

**Bulk Hexagonal Cobalt**

| eV | $cm^{-1}$ | μm | n | k |
|---|---|---|---|---|
| 3.100 | 25,000 | 0.400 | 1.60 [24] | 3.30 [24] |
| 2.480 | 20,000 | 0.500 | 2.15 | 3.70 1400°C |
| 2.066 | 16,670 | 0.600 | 2.55 | 4.05 |
| 1.771 | 14,290 | 0.700 | 2.93 | 4.38 |
| 1.550 | 12,500 | 0.800 | 3.30 | 4.70 |
| 1.377 | 11,110 | 0.900 | 3.70 | 4.90 |
| 1.240 | 10,000 | 1.00 | 3.95 | 5.28 |
| 1.025 | 8,264 | 1.21 | 4.40 | 6.00 |
| 0.8266 | 6,667 | 1.50 | 5.00 | 7.00 |
| 0.7293 | 5,882 | 1.70 | 5.34 | 7.35 |
| 0.5990 | 4,831 | 2.07 | 5.50 | 7.80 |
| 0.4679 | 3,774 | 2.65 | 6.40 | 8.90 |
| 0.3657 | 2,950 | 3.39 | 8.03 | 10.28 |

TABLE I (*Continued*)

**Bulk Hexagonal Cobalt**

| eV | $cm^{-1}$ | μm | $n_e$ (‖) | $k_e$ (‖) | $n_o$ (⊥) | $k_o$ (⊥) |
|---|---|---|---|---|---|---|
| 8.00 | 64,520 | 0.1550 | 0.95[3] | 1.09[3] | 0.95[3] | 1.09 [3] |
| 7.60 | 61,350 | 0.1631 | 0.93 | 1.17 | 0.93 | 1.17 |
| 7.20 | 58,140 | 0.1722 | 0.91 | 1.26 | 0.91 | 1.26 |
| 7.00 | 56,490 | 0.1771 | 0.91 | 1.32 | 0.91 | 1.32 |
| 6.60 | 53,220 | 0.1879 | 0.91 | 1.46 | 0.91 | 1.46 |
| 6.20 | 50,000 | 0.2000 | 0.97 | 1.62 | 0.98 | 1.62 |
| 6.00 | 48,400 | 0.2066 | 1.03 | 1.68 | 1.04 | 1.69 |
| 5.50 | 44,370 | 0.2254 | 1.18 | 1.76 | 1.19 | 1.77 |
| 5.00 | 40,230 | 0.2480 | 1.22 | 1.83 | 1.24 | 1.84 |
| 4.50 | 36,300 | 0.2755 | 1.24 | 1.98 | 1.26 | 1.99 |
| 4.10 | 33,070 | 0.3024 | 1.25 | 2.15 | 1.30 | 2.17 |
| 3.80 | 30,650 | 0.3263 | 1.28 | 2.33 | 1.33 | 2.33 |
| 3.50 | 28,230 | 0.3542 | 1.34 | 2.56 | 1.39 | 2.54 |
| 3.30 | 26,620 | 0.3757 | 1.42 | 2.72 | 1.46 | 2.70 |
| 3.10 | 25,000 | 0.4000 | 1.51 | 2.88 | 1.55 | 2.86 |
| 2.80 | 22,580 | 0.4428 | 1.66 | 3.13 | 1.72 | 3.11 |
| 2.70 | 21,770 | 0.4592 | 1.73 | 3.24 | 1.79 | 3.19 |
| 2.48 | 20,000 | 0.5000 | 1.88 | 3.40 | 1.90 | 3.34 |
| 2.30 | 18,550 | 0.5391 | 2.01 | 3.59 | 1.99 | 3.56 |
| 2.10 | 16,940 | 0.5904 | 2.13 | 3.85 | 2.13 | 3.89 |
| 1.90 | 15,320 | 0.6526 | 2.31 | 4.18 | 2.41 | 4.27 |
| 1.75 | 14,120 | 0.7085 | 2.56 | 4.50 | 2.72 | 4.54 |
| 1.65 | 13,310 | 0.7514 | 2.74 | 4.66 | 2.93 | 4.66 |
| 1.55 | 12,500 | 0.8000 | 2.96 | 4.87 | 3.14 | 4.83 |
| 1.40 | 11,290 | 0.8856 | 3.37 | 5.09 | 3.55 | 5.05 |
| 1.35 | 10,890 | 0.9184 | 3.49 | 5.14 | 3.67 | 5.09 |
| 1.25 | 10,080 | 0.9919 | 3.70 | 5.28 | 3.90 | 5.25 |
| 1.10 | 8,873 | 1.127 | 4.07 | 5.61 | 4.31 | 5.60 |
| 1.00 | 8,065 | 1.240 | 4.46 | 5.86 | 4.83 | 5.94 |
| 0.90 | 7,258 | 1.378 | 4.94 | 5.95 | 5.57 | 5.93 |
| 0.80 | 6,452 | 1.550 | 5.17 | 5.89 | 6.08 | 5.61 |
| 0.70 | 5,645 | 1.771 | 5.24 | 5.85 | 6.15 | 5.12 |
| 0.65 | 5,242 | 1.908 | 5.12 | 5.93 | 5.99 | 5.10 |
| 0.60 | 4,839 | 2.067 | 4.91 | 6.13 | 5.77 | 5.17 |
| 0.55 | 4,435 | 2.255 | 4.65 | 6.56 | 5.50 | 5.36 |
| 0.50 | 4,032 | 2.480 | 4.41 | 7.19 | 5.17 | 5.75 |
| 0.45 | 3,629 | 2.756 | 4.24 | 8.12 | 4.86 | 6.46 |
| 0.40 | 3,226 | 3.100 | 4.24 | 9.13 | 4.66 | 6.46 |
| 0.35 | 2,826 | 3.543 | 4.18 | 10.38 | 4.54 | 8.47 |
| 0.30 | 2,419 | 4.133 | 4.04 | 12.16 | 4.34 | 10.01 |
| 0.25 | 2,000 | 5.000 | 3.98 | 14.59 | 4.19 | 12.12 |
| 0.20 | 1,613 | 6.200 | 3.55 | 18.78 | 3.87 | 15.53 |
| 0.17 | 1,371 | 7.294 | 4.14 | 21.81 | 4.02 | 18.08 |
| 0.15 | 1,210 | 8.267 | 4.66 | 25.47 | 4.24 | 21.37 |
| 0.13 | 1,048 | 9.538 | 5.38 | 30.52 | 4.78 | 25.88 |
| 0.10 | 806.5 | 12.400 | 6.71 | 37.87 | 5.83 | 32.36 |

[a] References are given in brackets.

# Graphite (C)

A. BORGHESI and G. GUIZZETTI
Dipartimento di Fisica "A. Volta"
and
Gruppo Nazionale di Struttura della Materia del CNR
Università di Pavia
Pavia, Italy

Graphite is a semimetal with uniaxial layered crystalline structure and is characterized by two different dielectric functions, $\tilde{\varepsilon}_\perp$ and $\tilde{\varepsilon}_\parallel$. They correspond to the electric-field vector **E** perpendicular ($\tilde{\varepsilon}_\perp$) and parallel ($\tilde{\varepsilon}_\parallel$), respectively, to the $c$ axis (symmetry axis, perpendicular to the basal plane). Therefore, $\tilde{\varepsilon}_\perp$ measures the ordinary ($o$) while $\tilde{\varepsilon}_\parallel$ the extraordinary ($e$) ray properties. Since the cleavage plane is perpendicular to the $c$ axis, $\tilde{\varepsilon}_\perp$ can easily be determined, for example, by normal-incidence reflectance measurements. $\tilde{\varepsilon}_\parallel$ cannot be obtained in a similar way, because of the difficulty of preparing suitable optical surfaces parallel to the $c$ axis.

Small, soft flakes of natural graphite are found in various rock formations, but relatively little work has been done on these crystals, since they are generally quite impure, highly twinned, and rather difficult to handle [1, 2]. After 1958, it was established that massive coherent deposition of carbon can be produced by the pyrolysis of carbonaceous vapor on a suitable substrate at temperatures of the order of 2000°C. This material, called pyrolytic graphite, consists of many small crystallites with random orientation about the $c$ axes, but with varying degrees of misorientation of $c$ axes. Successively, it was found that highly oriented (HO) material ($c$ axes aligned to within 0.2°) could be obtained if pyrolytic graphite was annealed at very high temperatures (~3000°C), particularly under applied stress [3]. HO pyrolytic graphite exhibits characteristics very similar to high-purity, natural, single crystals: in particular, their reflectance spectra coincide within experimental accuracy [3, 4]. This fact allowed the optical functions of graphite to be obtained mainly on HO pyrolytic material.

Graphite has aroused great interest from both fundamental and technological points of view, and various attempts have been made to study, experimentally and theoretically, its optical and dielectric functions [4–26]. Nevertheless, the experimental data are not yet complete and show


Copyright © 1991 by Academic Press.
All rights of reproduction in any form reserved.
ISBN 0-12-544422-2

disagreement among themselves. Overlooking the differences inherent in the techniques used (optical, photoemission, EELS), this disagreement is due to the aforesaid difficulty in obtaining good surfaces parallel to the $c$ axis, and to the fact that all optical data have been derived from reflectivity ($R$) measurements (at near-normal incidence, with subsequent Kramers–Kronig (K–K) analysis, or as a function of angle of incidence, using the Fresnel relations). Therefore, the scattering among data can be explained by errors connected to K–K analysis; the difficulty of obtaining absolute values of reflectivity, particularly at large angles of incidence; and the different surface conditions affecting $R$. The room-temperature values of $n_o$, $k_o$ and $n_e$, $k_e$ tabulated in Table I and shown in Fig. 1, were obtained from the following works and references therein: Klucker [17] from 40 eV to 5 eV; Venghaus [21] for $n_e$ and $k_e$ obtained by EELS, in the 18–2 eV range, where they substantially differ from optical data; Greenaway *et al.* [5] from 5 eV to 2 eV; Guizzetti and Piaggi [26] who K–K-transformed $R$ spectra from Refs. [5, 17, 22] from 2 to 0.02 eV for $n_o$ and $k_o$ only.

Klucker *et al.* [17, 18] measured $R$ of freshly cleaved samples ($c$ axis perpendicular to the surface) of pyrolytic graphite between 3 eV and 40 eV for different angles of incidence. The synchrotron radiation was polarized either parallel or perpendicular to the plane of incidence, with a degree of polarization between 0.9 and 0.97. The spectral resolution was better than 6 Å. Relative and absolute $R$ measurements were performed. The ratios of the reflectances for nine angles between 15° and 75°, in steps of 7.5°, were determined in the relative measurements. $\tilde{\varepsilon}_\perp$ and $\tilde{\varepsilon}_\parallel$ were then derived simultaneously by least-squares fitting $R$ with Fresnel's formula for anisotropic uniaxial crystals. Absolute $R$ at near-normal incidence (15°) was used to determine $\tilde{\varepsilon}$ by K–K analysis. The asymptotic behavior $R(\omega) \propto \omega^{-4}$ was assumed for energies above 40 eV, whereas the $R$ data from Greenaway *et al.* [5], Boyle and Nozières [6], and Sato [10] were used below 3 eV. Absolute $R$ was in good agreement with $R$ calculated from relative measurements. Moreover, the gross features in the $R$ spectrum for $E \perp c$ generally agreed well with previous spectra in [4, 5, 8] and those derived from EELS [13, 14, 21]. Two major differences were observed above 8 eV. First, the extrapolated reflectance of Taft and Philipp [4] above 25 eV, which is important for K–K analysis, was significantly lower. Second, the reflectance calculated by Zeppenfeld [14] and Venghaus [21] from EELS was lower and did not show the sharp structure between 15 and 16 eV. These differences obviously were manifested in the spectra of $\tilde{\varepsilon}_\perp$, mainly in their absolute magnitudes and in some fine structures. More significant differences occur in $\tilde{\varepsilon}_\parallel$ among results from optical measurements, EELS, and theoretical calculations, in both the overall spectral behavior and the absolute magnitude below 15 eV. In particular, EELS data [14, 21] produce a peak at 11.4 eV in $\tilde{\varepsilon}_\parallel$, which is totally absent in the Klucker *et al.* [18] spectrum. This peak is several times larger than the

estimated uncertainty in the optical spectra, which is relatively large in this region, due to uncertainty in the degree of polarization.

The electron-energy-loss spectrum was measured by Venghaus [21] on stripped pyrolytic-graphite samples about 1000 Å in thickness. The experimental conditions were as follows: 60 keV energy of the primary electrons, with 0.4 keV halfwidth in the energy distribution; $10^{-3}$ rad scattering angle; 70° angle between the $c$ axis and the direction of incoming electrons to determinate $\mathrm{Im}(-1/\tilde{\varepsilon}_{\parallel})$. Corrections for double-scattering and for $\tilde{\varepsilon}_{\perp}$ were included in the calculation of $\tilde{\varepsilon}_{\parallel}$. The resulting $\tilde{\varepsilon}_{\parallel}$ was in very good agreement with that obtained by Zeppenfeld [14]. In particular, a detailed discussion of uncertainties in the energy-loss function and in the K–K analysis led Venghaus [21] to conclude that the maximum in $\varepsilon_{2\parallel}$ near 11 eV was established beyond experimental and computational errors. No conclusive evidence in favor of or against a strong transition at ~11 eV has been provided by band-structure calculations [5, 13, 19], due to uncertainty in the calculated gaps and to the difficulty in correlating structures in the loss spectrum to specific interband transitions. Due to a lack of other evidence that could resolve the problem, we have tabulated $n_{\parallel}$ and $k_{\parallel}$, in the 2–18 eV range, both from optical and EELS measurements.

Greenaway *et al.* [5] measured reflectance of both natural and pyrolytic-graphite single crystals in the visible and UV regions. Samples of pyrolytic graphite, annealed at 3600 K, were prepared with a polished face perpendicular to the cleavage planes, by careful cutting and mechanical-polishing techniques. No etching procedure were attempted. The surface area of these samples (>1 $\mathrm{cm}^2$) and the high degree of flatness permitted accurate $R$ measurements with incidence angle as high as 88°. Laser light at three different wavelengths (4579 Å, 5145 Å, 6328 Å) yielded good absolute $R$ values, to be used as reference and to check that no significant differences existed between the optical properties of natural and pyrolytic graphite. The reflectance $R_s$ and $R_p$, corresponding to the electric field perpendicular or parallel to the plane of incidence, respectively, were measured from 1.9 to 5.15 eV at incidence angles from 10° to 80° in steps of 10°, as well as at 75°, 85°, and 87°. For small angles the results agreed well with those of Refs. [4, 18] taken at near-normal incidence. The same excellent agreement was obtained in [5] from 0.3 to 11.5 eV $R$ on cleaved natural graphite. In addition, Greenaway *et al.* [5] measured $R$ in the 2–9 eV range at near-normal incidence on polished surfaces both parallel and perpendicular to the $c$ axis. $R$ spectra of polished surfaces were not suited for deriving the optical constants through K–K transforms due to their inferior quality with respect to the cleaved surfaces; they are useful only in comparing data for $E \perp c$ and $E \| c$ under identical surface conditions. The optical constants $n_{\perp}$, $k_{\perp}$ and $n_{\parallel}$, $k_{\parallel}$ from 0.9 to 5.15 eV were obtained by a least-squares fit of $R_s$ and $R_p$ at different incidence angles with the Fresnel relations for uniaxial materials. The values of $n_{\perp}$ and $k_{\perp}$ were in close agreement (±10%) with

those of Taft and Phillip [4] obtained from K–K analysis, and with those of Klucker *et al.* [18]. We note that $n_{\parallel}$ and $k_{\parallel}$ show no structures in this region ($k_{\parallel} \approx 0$), in agreement with data of Ergun [9]. However, this is in contrast with optical properties of graphite calculated by Johnson and Dresselhaus [15], who predict a lower reflectivity with a peak near 4.3 eV. They attributed this discrepancy to experimental difficulties, for example, a slight depolarization of the light in both Greenaway *et al.*'s and Ergun's experiments [5, 9].

Guizzetti and Piaggi [26] derived $n_{\perp}$ and $k_{\perp}$ below 2 eV by K–K transforming $R$ spectra, at near-normal incidence, of Klucker [17], Greenaway *et al.* [5], and Nemanich *et al.* [22], which showed the best agreement among themselves. Moreover, the infrared $R$ values of Nemanich *et al.* [22] were much higher than those reported by Boyle and Nozières [6], Sato [10], Misu *et al.* [23], and Bowers *et al.* [24]. The extrapolation $R(\omega) \propto \omega^{-p}$ was used above 40 eV. Two different values of the exponent $p$ were used. In one case the usual value $p = 4$ was assumed. In the other case $p$ was adjusted to reproduce the values of $n_{\perp} = 2.91$ and $k_{\perp} = 1.71$, measured with an ellipsometer working at $\lambda = 6328$ Å. Although the resulting value of $p$ is 3.4, $n_{\perp}$ and $k_{\perp}$ values below 2 eV differ only by 1% from the previous ones, which are tabulated here.

Nemanich *et al.* [22] measured IR reflectivity of HO pyrolytic graphite for $E \perp c$ on a cleaved surface parallel to the layers and for $E \| c$ on a polished surface cut perpendicular to the layers. The surface damage incurred in the polishing step was accounted for by scaling the $E \| c$ spectrum with the ratio of two $E \perp c$ spectra, obtained from a cleaved and a polished surface, respectively. The $E \perp c$ spectrum exhibits a sharp weak structure at 1587 $cm^{-1}$ (attributed to the "in-plane" $E_{1u}$ symmetry vibrational mode), superimposed on a background reflectance rising slowly with decreasing frequency. The $E \| c$ spectrum displays a sharp weak structure at 868 $cm^{-1}$ (attributed to the "out-of-plane" $A_{2u}$ symmetry mode) on a constant background. These structures were well fitted by the classical oscillator model, which yields the complex dielectric function

$$\tilde{\varepsilon} = \tilde{\varepsilon}_{\infty} + \frac{S\omega_T^2}{(\omega_T^2 - \omega^2 - i\Gamma\omega)},$$

where $\omega_T$ is the phonon frequency, $\Gamma$ is the phenomenological damping constant, $S$ is the oscillator strength, and $\tilde{\varepsilon}_{\infty}$ is the complex dielectric function resulting from electronic transitions. In the range of measurement (500–4000 $cm^{-1}$) $\tilde{\varepsilon}_{\infty\parallel}$ is real with a constant value of 5.78, although theoretical calculations [15] predicted a free-carrier absorption, corresponding to a plasma frequency of ~0.1 eV. On the contrary, $\tilde{\varepsilon}_{\infty\perp}$ is really complex due

to both interband and intraband electronic transitions, which produce a positive divergence in $\varepsilon_2$ at low frequencies. The values of the real and imaginary parts of $\tilde{\varepsilon}_{\infty\perp}$ have been obtained from Table I as $\varepsilon_{1\perp} = n_\perp^2 - k_\perp^2$ and $\varepsilon_{2\perp} = 2n_\perp k_\perp$, respectively. The other oscillator parameters were as follows: for $\tilde{\varepsilon}_\parallel$, $\omega_T = 867.8\,\text{cm}^{-1}$, $\Gamma = 0.001\,\text{cm}^{-1}$, and $S = 0.004$; for $\tilde{\varepsilon}_\perp$, $\omega_T = 1587.0\,\text{cm}^{-1}$, $\Gamma = 0.003\,\text{cm}^{-1}$, and $S = 0.031$. The resulting calculated values of $n_o$, $k_o$, $n_e$, and $k_e$ are reported in Table I.

## REFERENCES


1. C. A. Klein, *Rev. Mod. Phys.* **34**, 56 (1962).
2. C. A. Klein, W. D. Straub, and R. J. Diefendorf, *Phys. Rev.* **125**, 468 (1962).
3. A. W. Moore, A. R. Ubbelohde, and D. A. Young, *Proc. Roy. Soc. (London)* **A280**, 153 (1964).
4. E. A. Taft and H. R. Philipp, *Phys. Rev.* **138**, A197 (1965).
5. D. L. Greenaway, G. Harbeke, F. Bassani, and E. Tosatti, *Phys. Rev.* **178**, 1340 (1969).
6. W. S. Boyle and P. Nozières, *Phys. Rev.* **111**, 782 (1958).
7. J. R. Nelson, *Bull. Am. Phys. Soc.* **7**, 332 (1962).
8. J. G. Carter, R. H. Huebner, R. N. Hamm, and R. D. Birkhoff, *Phys. Rev.* **137**, A639 (1965).
9. S. Ergun, *Nature* **14**, 135 (1967); S. Ergun, in "Chemistry and Physics of Carbon," (P. L. Walker, Jr., ed.), Vol. 3, M. Dekker, New York, 45 (1968).
10. Y. Sato, *J. Phys. Soc. Jpn.* **24**, 489 (1968).
11. K. Zeppenfeld, *Z. Physik* **211**, 391 (1968).
12. F. Bassani and E. Tosatti, *Phys. Lett.* **27A**, 446 (1968); *Il Nuovo Cimento* **LXV B**, 161 (1970).
13. G. S. Painter and D. E. Ellis, *Phys. Rev.* **B1**, 4747 (1970).
14. K. Zeppenfeld, *Z. Physik* **243**, 229 (1971).
15. L. G. Johnson and G. Dresselhaus, *Phys. Rev.* **B7**, 2275 (1973).
16. G. Guizzetti, L. Nosenzo, E. Reguzzoni, and G. Samoggia, *Phys. Rev. Lett.* **31**, 154 (1973).
17. R. Klucker, Interner Bericht, DESY F41-72/1 (1972).
18. R. Klucker, M. Skibowski, and W. Steinmann, *Phys. Stat. Solidi. (b)* **65**, 703 (1974).
19. R. F. Willis, B. Fitton, and G. S. Painter, *Phys. Rev.* **B9**, 1926 (1974).
20. G. Bellodi, A. Borghesi, G. Guizzetti, L. Nosenzo, E. Reguzzoni, and G. Samoggia, *Phys. Rev.* **B12**, 5951 (1975).
21. H. Venghaus, *Phys. Stat. Solidi. (b)* **71**, 609 (1975).
22. R. J. Nemanich, G. Lucovsky, and S. A. Solin, *Solid State Commun.* **23**, 117 (1977).
23. A. Misu, E. E. Mendez, and M. S. Dresselhaus, *J. Phys. Soc. Jpn.* **47**, 199 (1979).
24. C. W. Bowers, R. B. Culver, W. A. Solberg, and I. L. Spain, *Appl. Opt.* **26**, 4625 (1987).
25. N. B. Brandt, S. M. Chudinov, and Y. G. Ponomarev, in "Modern Problems in Condensed Matter Sciences, Semimetals," (V. M. Agranovich and A. A. Maradudin, eds.), Vol. 20.1, North-Holland, Amsterdam, 129 (1988).
26. G. Guizzetti and A. Piaggi, private communication (1988).

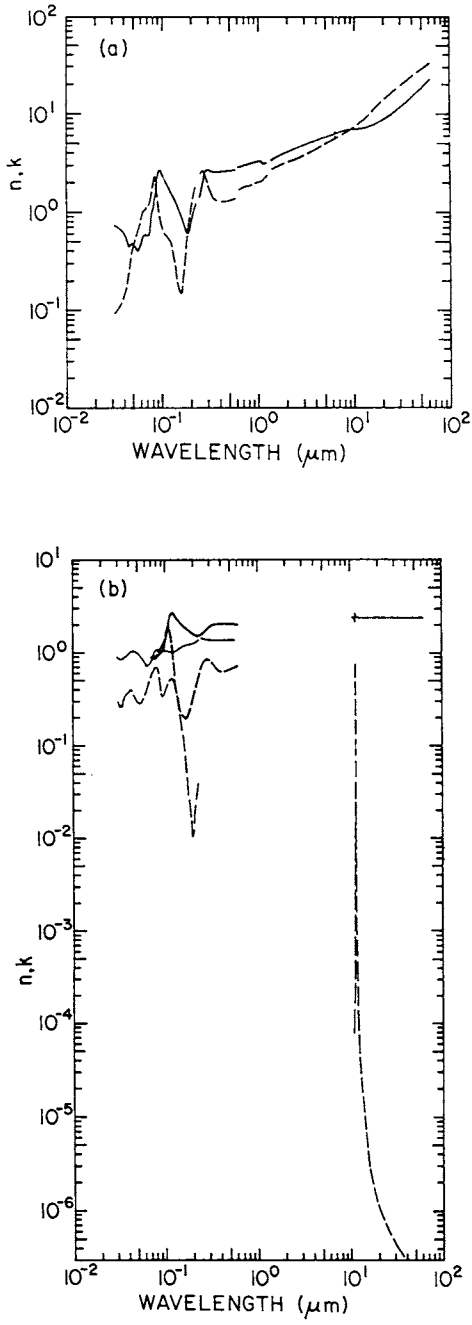


**Fig. 1.** (a) Log–log plot of $n_o$ (solid line) and $k_o$ (dashed line) versus wavelength in micrometers for graphite. (b) Log–log plot of $n_e$ (solid line) and $k_e$ (dashed line) versus wavelength in micrometers.

TABLE I

Values of $n$ and $k$ for Graphite from Various References[a]

| eV | $cm^{-1}$ | Å | $n_e$ | $n_e$ | $k_e$ | $k_e$ | $n_o$ | $k_o$ |
|---|---|---|---|---|---|---|---|---|
| 40.0 | | 309.96 | 0.91 [17] | | 0.30 [17] | | 0.75 [17] | 0.10 [17] |
| 39.5 | | 313.89 | 0.89 | | 0.29 | | 0.75 | 0.10 |
| 39.0 | | 317.91 | 0.88 | | 0.28 | | 0.75 | 0.10 |
| 38.5 | | 322.04 | 0.86 | | 0.27 | | 0.74 | 0.10 |
| 38.0 | | 326.28 | 0.85 | | 0.26 | | 0.74 | 0.10 |
| 37.5 | | 330.63 | 0.85 | | 0.26 | | 0.72 | 0.10 |
| 37.0 | | 335.10 | 0.85 | | 0.27 | | 0.72 | 0.10 |
| 36.5 | | 339.69 | 0.85 | | 0.27 | | 0.72 | 0.10 |
| 36.0 | | 344.40 | 0.84 | | 0.28 | | 0.71 | 0.10 |
| 35.5 | | 349.25 | 0.85 | | 0.30 | | 0.70 | 0.10 |
| 35.0 | | 354.24 | 0.86 | | 0.31 | | 0.68 | 0.10 |
| 34.5 | | 359.38 | 0.88 | | 0.33 | | 0.68 | 0.10 |
| 34.0 | | 364.66 | 0.89 | | 0.34 | | 0.67 | 0.12 |
| 33.5 | | 370.11 | 0.90 | | 0.35 | | 0.67 | 0.12 |
| 33.0 | | 375.71 | 0.91 | | 0.36 | | 0.66 | 0.12 |
| 32.5 | | 381.49 | 0.92 | | 0.36 | | 0.66 | 0.12 |
| 32.0 | | 387.45 | 0.93 | | 0.37 | | 0.64 | 0.13 |
| 31.5 | | 393.60 | 0.94 | | 0.37 | | 0.61 | 0.13 |
| 31.0 | | 399.95 | 0.95 | | 0.38 | | 0.60 | 0.14 |
| 30.5 | | 406.51 | 0.97 | | 0.38 | | 0.58 | 0.16 |
| 30.0 | | 413.28 | 0.99 | | 0.39 | | 0.57 | 0.16 |
| 29.5 | | 420.29 | 1.01 | | 0.40 | | 0.55 | 0.17 |
| 29.0 | | 427.54 | 1.02 | | 0.40 | | 0.52 | 0.19 |
| 28.5 | | 435.04 | 1.04 | | 0.39 | | 0.49 | 0.21 |
| 28.0 | | 442.80 | 1.05 | | 0.38 | | 0.47 | 0.24 |
| 27.5 | | 450.86 | 1.06 | | 0.37 | | 0.45 | 0.27 |

*(continued)*

TABLE I (*Continued*)

Graphite

| eV | $cm^{-1}$ | $\mu m$ | $n_e$ | $n_e$ | $k_e$ | $k_e$ | $n_o$ | $k_o$ |
|---|---|---|---|---|---|---|---|---|
| 27.0 | | 459.20 | 1.07 | | 0.35 | | 0.46 | 0.31 |
| 26.5 | | 467.87 | 1.06 | | 0.33 | | 0.47 | 0.35 |
| 26.0 | | 476.87 | 1.05 | | 0.32 | | 0.48 | 0.38 |
| 25.5 | | 486.20 | 1.03 | | 0.31 | | 0.47 | 0.43 |
| 25.0 | | 495.94 | 1.02 | | 0.30 | | 0.47 | 0.47 |
| 24.5 | | 506.06 | 1.00 | | 0.29 | | 0.46 | 0.51 |
| 24.0 | | 516.60 | 0.99 | | 0.28 | | 0.46 | 0.54 |
| 23.5 | | 527.60 | 0.97 | | 0.28 | | 0.44 | 0.56 |
| 23.0 | | 539.07 | 0.95 | | 0.28 | | 0.41 | 0.60 |
| 22.5 | | 551.05 | 0.93 | | 0.28 | | 0.40 | 0.66 |
| 22.0 | | 563.57 | 0.91 | | 0.29 | | 0.41 | 0.70 |
| 21.5 | | 576.68 | 0.88 | | 0.31 | | 0.43 | 0.76 |
| 21.0 | | 590.41 | 0.84 | | 0.33 | | 0.45 | 0.82 |
| 20.5 | | 604.81 | 0.81 | | 0.35 | | 0.51 | 0.92 |
| 20.0 | | 619.93 | 0.77 | | 0.38 | | 0.55 | 1.01 |
| 19.5 | | 635.82 | 0.74 | | 0.42 | | 0.58 | 1.05 |
| 19.0 | | 652.55 | 0.71 | | 0.47 | | 0.58 | 1.07 |
| 18.5 | | 670.19 | 0.71 | | 0.51 | | 0.58 | 1.10 |
| 18.0 | | 688.81 | 0.77 | 0.77 [21] | 0.53 | 0.75 [21] | 0.58 | 1.12 |
| 17.5 | | 708.49 | 0.85 | 0.81 | 0.56 | 0.81 | 0.58 | 1.15 |
| 17.0 | | 729.32 | 0.92 | 0.86 | 0.60 | 0.86 | 0.61 | 1.25 |
| 16.5 | | 751.43 | 0.99 | 0.90 | 0.65 | 0.87 | 0.75 | 1.36 |
| 16.0 | | 774.91 | 1.05 | 0.91 | 0.68 | 0.87 | 0.98 | 1.63 |
| 15.5 | | 799.90 | 1.10 | 0.87 | 0.71 | 0.91 | 1.09 | 1.92 |
| 15.0 | | 826.57 | 1.10 | 0.86 | 0.69 | 0.97 | 1.33 | 2.15 |
| 14.5 | | 855.07 | 1.10 | 0.91 | 0.61 | 1.04 | 1.84 | 2.25 |
| 14.0 | | 885.61 | 1.06 | 0.98 | 0.48 | 1.09 | 2.31 | 1.50 |
| 13.5 | | 918.41 | 1.02 | 1.02 | 0.34 | 1.14 | 2.72 | 1.03 |
| 13.0 | | 953.73 | 1.02 | 1.02 | 0.33 | 1.24 | 2.67 | 0.83 |
| 12.5 | | 991.88 | 1.04 | 1.07 | 0.37 | 1.36 | 2.48 | 0.70 |

| | | | | | | | | | |
|---|---|---|---|---|---|---|---|---|---|
| 12.0 | | 0.1033 | 1.06 | 1.34 | 0.42 | 1.66 | 2.25 | 0.63 | |
| 11.5 | | 0.1078 | 1.05 | 1.63 | 0.47 | 1.86 | 2.03 | 0.58 | |
| 11.0 | | 0.1127 | 1.03 | 2.30 | 0.52 | 1.78 | 1.81 | 0.57 | |
| 10.5 | | 0.1181 | 1.02 | 2.54 | 0.53 | 1.34 | 1.65 | 0.53 | |
| 10.0 | | 0.1240 | 0.98 | 2.68 | 0.50 | 0.73 | 1.52 | 0.46 | |
| 9.5 | | 0.1305 | 1.01 | 2.46 | 0.39 | 0.43 | 1.38 | 0.37 | |
| 9.0 | | 0.1378 | 1.05 | 2.27 | 0.29 | 0.31 | 1.25 | 0.27 | |
| 8.5 | | 0.1459 | 1.10 | 2.13 | 0.20 | 0.23 | 1.10 | 0.18 | |
| 8.0 | | 0.1550 | 1.15 | 1.99 | 0.12 | 0.21 | 0.96 | 0.15 | |
| 7.5 | | 0.1653 | 1.18 | 1.87 | 0.06 | 0.19 | 0.82 | 0.20 | |
| 7.0 | | 0.1771 | 1.20 | 1.73 | 0.03 | 0.22 | 0.65 | 0.44 | |
| 6.5 | | 0.1907 | 1.23 | 1.67 | 0.01 | 0.26 | 0.66 | 0.84 | |
| 6.0 | 48,393 | 0.2066 | 1.27 | 1.55 | 0.02 | 0.34 | 0.94 | 1.35 | |
| 5.5 | 44,360 | 0.2254 | 1.31 | 1.48 | 0.04 | 0.48 | 1.25 | 1.85 | |
| 5.0 | 40,327 | 0.2480 | 1.46 [12] | 1.51 | | 0.71 | 1.39 [12] | 2.48 [12] | |
| 4.9 | 39,521 | 0.2530 | 1.44 | | | | 1.66 | 2.56 | |
| 4.8 | 38,714 | 0.2583 | 1.43 | | | | 1.95 | 2.65 | |
| 4.7 | 37,908 | 0.2638 | 1.42 | | | | 2.18 | 2.64 | |
| 4.6 | 37,101 | 0.2695 | 1.41 | | | | 2.38 | 2.54 | |
| 4.5 | 36,295 | 0.2755 | 1.40 | 1.70 | | 0.84 | 2.53 | 2.41 | |
| 4.4 | 35,488 | 0.2818 | 1.40 | | | | 2.64 | 2.26 | |
| 4.3 | 34,681 | 0.2883 | 1.39 | | | | 2.71 | 2.10 | |
| 4.2 | 33,875 | 0.2952 | 1.38 | | | | 2.75 | 1.94 | |
| 4.1 | 33,068 | 0.3024 | 1.37 | | | | 2.75 | 1.79 | |
| 4.0 | 32,262 | 0.3100 | 1.37 | 1.94 | | 0.83 | 2.73 | 1.66 | |
| 3.9 | 31,455 | 0.3179 | 1.36 | | | | 2.69 | 1.56 | |
| 3.8 | 30,649 | 0.3263 | 1.36 | | | | 2.66 | 1.49 | |
| 3.7 | 29,842 | 0.3351 | 1.36 | | | | 2.64 | 1.43 | |
| 3.6 | 29,036 | 0.3444 | 1.36 | | | | 2.63 | 1.39 | |
| 3.5 | 28,229 | 0.3542 | 1.36 | 2.02 | | 0.69 | 2.62 | 1.36 | |
| 3.4 | 27,423 | 0.3647 | 1.35 | | | | 2.62 | 1.33 | |
| 3.3 | 26,616 | 0.3757 | 1.35 | | | | 2.61 | 1.31 | |
| 3.2 | 25,809 | 0.3875 | 1.35 | | | | 2.61 | 1.29 | |
| 3.1 | 25,003 | 0.4000 | 1.35 | | | | 2.62 | 1.29 | |

*(continued)*

TABLE I (*Continued*)

Graphite

| eV | $cm^{-1}$ | $\mu m$ | $n_e$ | $n_e$ | $k_e$ | $k_e$ | $n_o$ | $k_o$ |
|---|---|---|---|---|---|---|---|---|
| 3.0 | 24,196 | 0.4133 | 1.35 | 2.04 | | 0.62 | 2.62 | 1.28 |
| 2.9 | 23,390 | 0.4275 | 1.35 | | | | 2.63 | 1.28 |
| 2.8 | 22,583 | 0.4428 | 1.36 | | | | 2.63 | 1.28 |
| 2.7 | 21,777 | 0.4592 | 1.36 | | | | 2.64 | 1.28 |
| 2.6 | 20,970 | 0.4769 | 1.36 | | | | 2.64 | 1.30 |
| 2.5 | 20,164 | 0.4959 | 1.36 | 2.03 | | 0.64 | 2.65 | 1.31 |
| 2.4 | 19,357 | 0.5166 | 1.36 | | | | 2.66 | 1.33 |
| 2.3 | 18,551 | 0.5391 | 1.36 | | | | 2.67 | 1.34 |
| 2.2 | 17,744 | 0.5636 | 1.36 | | | | 2.68 | 1.36 |
| 2.1 | 16,937 | 0.5904 | 1.37 | | | | 2.70 | 1.39 |
| 2.00 | 16,131 | 0.6199 | | 2.01 | | 0.72 | 2.86 [26] | 1.73 [26] |
| 1.90 | 15,324 | 0.6526 | | | | | 2.91 | 1.77 |
| 1.80 | 14,518 | 0.6888 | | | | | 2.96 | 1.81 |
| 1.70 | 13,711 | 0.7293 | | | | | 3.01 | 1.84 |
| 1.60 | 12,905 | 0.7749 | | | | | 3.06 | 1.86 |
| 1.50 | 12,098 | 0.8266 | | | | | 3.10 | 1.90 |
| 1.40 | 11,292 | 0.8856 | | | | | 3.14 | 1.95 |
| 1.30 | 10,485 | 0.9537 | | | | | 3.20 | 2.02 |
| 1.20 | 9,679 | 1.033 | | | | | 3.25 | 2.07 |
| 1.16 | 9,356 | 1.069 | | | | | 3.33 | 2.07 |
| 1.12 | 9,033 | 1.107 | | | | | 3.19 | 2.07 |
| 1.08 | 8,711 | 1.148 | | | | | 3.16 | 2.17 |
| 1.04 | 8,388 | 1.192 | | | | | 3.16 | 2.28 |
| 1.00 | 8,065 | 1.240 | | | | | 3.18 | 2.40 |
| 0.90 | 7,259 | 1.378 | | | | | 3.39 | 2.70 |
| 0.80 | 6,452 | 1.550 | | | | | 3.69 | 2.91 |
| 0.70 | 5,646 | 1.771 | | | | | 3.94 | 3.02 |
| 0.60 | 4,839 | 2.066 | | | | | 4.24 | 3.25 |
| 0.50 | 4,033 | 2.480 | | | | | 4.50 | 3.41 |
| 0.40 | 3,226 | 3.100 | | | | | 4.83 | 3.82 |

| | | | | | | |
|---|---|---|---|---|---|---|
| 0.30 | 2,420 | 4.133 | | | 5.36 | 4.48 |
| 0.2294 | 1,850 | 5.405 | | | 5.866 [22] | 5.124 [22] |
| 0.2232 | 1,800 | 5.555 | | | 5.923 | 5.217 |
| 0.2170 | 1,750 | 5.714 | | | 6.000 | 5.318 |
| 0.2108 | 1,700 | 5.882 | | | 6.070 | 5.420 |
| 0.2046 | 1,650 | 6.061 | | | 6.129 | 5.520 |
| 0.2002 | 1,615 | 6.192 | | | 6.150 | 5.597 |
| 0.1996 | 1,610 | 6.211 | | | 6.145 | 5.611 |
| 0.1990 | 1,605 | 6.230 | | | 6.135 | 5.627 |
| 0.1984 | 1,600 | 6.250 | | | 6.120 | 5.656 |
| 0.1977 | 1,595 | 6.269 | | | 6.097 | 5.721 |
| 0.1971 | 1,590 | 6.289 | | | 6.131 | 5.948 |
| 0.1970 | 1,589 | 6.293 | | | 6.212 | 6.036 |
| 0.1969 | 1,588 | 6.297 | | | 6.378 | 6.094 |
| 0.1967 | 1,587 | 6.301 | | | 6.590 | 6.016 |
| 0.1966 | 1,586 | 6.305 | | | 6.687 | 5.813 |
| 0.1965 | 1,585 | 6.309 | | | 6.646 | 5.644 |
| 0.1959 | 1,580 | 6.329 | | | 6.371 | 5.498 |
| 0.1952 | 1,575 | 6.349 | | | 6.291 | 5.515 |
| 0.1946 | 1,570 | 6.369 | | | 6.258 | 5.530 |
| 0.1922 | 1,550 | 6.452 | | | 6.217 | 5.560 |
| 0.1860 | 1,500 | 6.666 | | | 6.205 | 5.600 |
| 0.1798 | 1,450 | 6.896 | | | 6.238 | 5.663 |
| 0.1736 | 1,400 | 7.143 | | | 6.323 | 5.775 |
| 0.1674 | 1,350 | 7.407 | | | 6.476 | 5.955 |
| 0.1612 | 1,300 | 7.692 | | | 6.712 | 6.218 |
| 0.16 | 1,290 | 7.749 | | | 6.77 [26] | 6.29 [26] |
| 0.14 | 1,129 | 8.856 | | | 6.91 | 6.63 |
| 0.12 | 968 | 10.33 | | | 6.96 | 7.38 |
| 0.1165 | 940 | 10.64 | 2.399 [22] | $3.00\times10^{-5}$ [22] | | |
| 0.1153 | 930 | 10.75 | 2.398 | 4.05 | | |
| 0.1141 | 920 | 10.87 | 2.397 | 5.75 | | |
| 0.1128 | 910 | 10.99 | 2.395 | $8.10\times10^{-5}$ | | |
| 0.1115 | 900 | 11.11 | 2.393 | $1.51\times10^{-4}$ | | |
| 0.1103 | 890 | 11.23 | 2.388 | $3.19\times10^{-4}$ | | |

*(continued)*

TABLE I (*Continued*)

Graphite

| eV | $cm^{-1}$ | $\mu m$ | $n_e$ | $n_e$ | $k_e$ | $k_e$ | $n_o$ | $k_o$ |
|---|---|---|---|---|---|---|---|---|
| 0.1091 | 880 | 11.36 | 2.374 | | $1.06\times10^{-3}$ | | | |
| 0.1085 | 875 | 11.43 | 2.353 | | 3.07 | | | |
| 0.1084 | 874 | 11.44 | 2.345 | | 4.15 | | | |
| 0.1082 | 873 | 11.45 | 2.334 | | 5.92 | | | |
| 0.1081 | 872 | 11.47 | 2.317 | | $9.11\times10^{-3}$ | | | |
| 0.1080 | 871 | 11.48 | 2.291 | | 0.015 | | | |
| 0.1079 | 870 | 11.49 | 2.241 | | 0.033 | | | |
| 0.1077 | 869 | 11.51 | 2.124 | | 0.108 | | | |
| 0.1076 | 868 | 11.52 | 2.196 | | 0.750 | | | |
| 0.1075 | 867 | 11.53 | 2.735 | | 0.166 | | | |
| 0.1074 | 866 | 11.55 | 2.587 | | 0.042 | | | |
| 0.1071 | 864 | 11.57 | 2.496 | | 0.010 | | | |
| 0.1069 | 862 | 11.60 | 2.465 | | $4.51\times10^{-3}$ | | | |
| 0.1066 | 860 | 11.63 | 2.450 | | $2.52\times10^{-3}$ | | | |
| 0.1054 | 850 | 11.76 | 2.424 | | $4.90\times10^{-4}$ | | | |
| 0.1041 | 840 | 11.90 | 2.417 | | $2.01\times10^{-4}$ | | | |
| 0.10 | 806 | 12.40 | 2.410 | | $4.08\times10^{-5}$ | | 7.14 | 8.75 |
| 0.08 | 645 | 15.50 | 2.406 | | $3.08\times10^{-6}$ | | 7.68 | 10.80 |
| 0.06 | 484 | 20.66 | 2.405 | | $9.77\times10^{-7}$ | | 8.86 | 14.02 |
| 0.04 | 323 | 30.99 | 2.405 | | 4.17 | | 11.75 | 20.00 |
| 0.02 | 161 | 61.99 | 2.404 | | $1.65\times10^{-7}$ | | 22.42 | 33.49 |

[a] The references from which the values were extracted are given in brackets.

# Liquid Mercury (Hg)*

E. T. ARAKAWA and T. INAGAKI†
Oak Ridge National Laboratory
Oak Ridge, Tennessee

The optical constants of liquid Hg at room temperature in the near infrared to the near UV have been measured extensively [1–11] by spectroscopic ellipsometry. The measurements were made both on a free surface under vacuum or inert gases [1, 4–7, 9, 10] and on a surface in contact with solid [2, 6, 8, 10, 11] or liquid [3] dielectrics. Except for the results of [2], the values of $n$ and $k$ obtained from these measurements agree in general with one another. However, the scatter of the data is far larger than the stated accuracies of individual results, which are reported with three or four significant figures. A careful recent study [11] finds no systematic difference between data obtained on a free surface and on a surface in contact with dielectrics. The measurements at wavelengths below 0.25 μm are very limited, with only two reflectance measurements at normal incidence, one on a free surface under vacuum from 0.06–0.6 μm [12] and one on a surface in contact with $MgF_2$ from 0.15–2.5 μm [8].

The room-temperature values of $n$ and $k$ are tabulated in Table I and plotted in Fig. 1. The data above 0.31 μm are from those determined by Inagaki *et al.* [11] as the mean values from the various ellipsometric measurements [1, 3–11]. The data below 0.31 μm are from the Kramers–Kronig (K–K) analysis made [11] on the normal-incidence reflectance data taken by Wilson and Rice [12] combined with the reflectance values above 0.31 μm calculated from the ellipsometric data of $n$ and $k$. We believe that the $n$ and $k$ values given in Table I are accurate to ±0.2% on an absolute scale.

As with other liquid metals, the $n$ and $k$ spectra from the infrared to the UV are nearly free-electron-like up to the plasma wavelength at 0.177 μm. However, in contrast with some other liquid metals, the $n$ and $k$ values are significantly higher in the visible region than those given by the simple Drude expressions. Two absorption features at 0.149 μm and 0.124 μm

* Sponsored by the Office of Health and Environmental Research, U.S. Department of Energy, under Contract DE-AC05-840R21400 with Martin Marietta Energy Systems, Inc.
† Permanent address: Physics Department, Osaka Kyoiku University, Osaka, Japan.


Copyright © 1991 by Academic Press.
All rights of reproduction in any form reserved.
ISBN 0-12-544422-2

were assigned to excitations from the spin-orbit split 5d band to the valence band [12]. In addition, a weak structure was noticed at 0.191 μm, for which the possibility of an exciton or a surface plasmon was suggested [8, 12].

Liquid Hg is one of the easiest metals on which an ideally smooth surface can be made in a reproducible manner. Surface contamination due to oxidation has also been believed to be less severe than for any other metal except for a few inert metals such as gold. On the other hand, many metals dissolve readily in liquid Hg, forming an amalgam. In most measurements, therefore, the sample was distilled under vacuum or under a reduced pressure [1, 3–7, 9, 10], and in some cases, directly into the sample dish [4, 9, 10]. Prior to distillation, the sample was washed in dilute solutions of KOH and/or $H_2NO_3$ and then in distilled water to remove oxides [3, 5].

For measurements on a free surface, surface oxidation was the major source of error in the measured values of $n$ and $k$. Most measurements were made under vacuum without exposing the surface to the atmosphere [1, 4–7, 9, 10]. It was reported [1], however, that the values of the optical constants in air did not change appreciably for up to 30 minutes and the changes in 60 minutes were still only of the order of the probable error. Since oxide and impurities tend to float to the surface, the overflow method was used [1, 11] to obtain clean surfaces.

Measurements on a surface in contact with dielectrics [2, 3, 6, 8, 10, 11] were relatively free from surface contamination. These measurements were also free from vibration of the liquid surface. However, two possible sources of error arose with this method. The first was due to imperfect optical contact of liquid Hg with the dielectric prism or window, and the second was due to strain in the dielectric overlayer. Schulz [13] employed the Ag-precoat method to obtain good optical contact of liquid Hg with several solid dielectrics. The liquid dielectrics used by Smith and Stromberg [3] avoided the contact and strain problems encountered with solid dielectrics.

Hodgson [1] measured a free surface by ellipsometry for the first time in an extended region from 0.365–2.40 μm using the rotating-polarizer method. The results showed unambiguously that the optical constants of liquid Hg did not agree with those given by the simple Drude formula for a nearly-free-electron metal. Lelyuk *et al.* [2] measured a sample in contact with a glass prism in the region from 0.45–1.54 μm. Multiple-reflection ellipsometry was used, and the angle of incidence was varied so that linear polarization of the incident light was restored in the reflected beam. The values of $n$ and $k$ obtained were much higher than those from the other ellipsometric measurements. This was later interpreted by Smith [5] as arising from imperfect contact between liquid Hg and the glass prism, and was reproduced experimentally by Faber and Smith [6].

Smith and Stromberg [3] measured liquid Hg in contact with three

different liquid dielectrics—cyclohexane, benzene, and distilled water—at 0.5461 μm. They used the conventional null method. The liquid Hg sample was immersed directly into the liquid dielectrics after vacuum distillation without exposure to the atmosphere. No difference was found in the $n$ and $k$ values measured under the different immersion liquids beyond the experimental accuracy of four significant figures. They analyzed theoretically the effects of surface layers, misalignment, and window birefringence on the measured values of $n$ and $k$, and evaluated the limit of accuracy of their measurements.

Smith [4] and Faber and Smith [6] measured two different surfaces, a free surface under vacuum and a surface in contact with a quartz prism, in the region from 0.4–0.7 μm. They used a variant of the null method using three polarizers, one of which rotated continuously. The $n$ and $k$ values obtained for the two different surfaces were in good agreement. The Ag-precoat method was employed to obtain good optical contact of liquid Hg with the quartz prism. They attempted to clean the free surface using argon glow discharge. This increased the $n$ and $k$ values slightly. They also measured the effects of surface contamination during several days' exposure to atmosphere.

Smith [5] measured free surfaces under vacuum and He atmosphere at 0.5461 μm. The null method was employed with a commercial ellipsometer. The surface was cleaned by moving a stainless-steel barrier along the surface. Along with the ellipsometric measurement, surface tension and contact potential were measured to ensure that the surface was free of contamination. Ellipsometric measurements were made on a free surface by Busch and Guggenheim [7] in the region from 0.47–2.32 μm and on a surface in contact with a quartz prism by Choyke *et al.* [8] at three wavelengths in the visible.

Comins [9] extended the measurement on a free surface in the infrared up to 6.3 μm. A variant of Beattie and Conn's method [14] was employed. The $n$ and $k$ values obtained were in good agreement with those given by the semiempirical formulas of Smith [15]. The formulas were derived to explain the deviations of the optical constants of liquid Hg from the simple Drude theory in terms of backscattering of the electrons. Crozier and Murphy [10] extended the measurements on a free surface down to 0.25 μm. The method of Beattie and Conn [14] was used with an ellipsometer whose entire optical assembly was enclosed in a vacuum chamber. They also measured surfaces in contact with a quartz and a glass prism. The values of $n$ and $k$ obtained for these surfaces were slightly higher than those obtained for a free surface. For the surfaces in contact with a quartz and a glass prism, $n$ and $k$ values were obtained from reflectances measured with $p$- and $s$-polarized light. The values obtained were in a good agreement with those from the ellipsometric data in the case of the quartz prism, but not in the case of the glass prism.

Inagaki *et al.* [11] measured a surface in contact with a quartz prism in the region from 0.335–2.0 μm using a method similar to the one used by Crozier and Murphy [10]. Good consistency was obtained between the $n$ and $k$ values obtained from the ellipsometric data and the reflectance data taken simultaneously on the same surface. The earlier ellipsometric values of $n$ and $k$ obtained using various contact media were analyzed and shown to be consistent with each other within the experimental accuracies. They were also shown to be internally consistent using a K–K analysis of the ellipsometric $n$ and $k$ data combined with reflectance data in the shorter-wavelength region.

Wilson and Rice [12] measured normal-incidence reflectance of a free surface under vacuum in an extended region from 0.06–0.6 μm. A K–K analysis was performed on these data to deduce $n$ and $k$ values. However, extrapolation of the reflectance data into the shorter-wavelength region was made to give agreement of the optical-constant values at 0.6 μm with those given by the simple Drude expressions. Choyke *et al.* [8] measured normal-incidence reflectance of a surface in contact with $MgF_2$ in the region from 0.15–2.5 μm. Values of $n$ and $k$ were derived from these data by a curve-fitting method [16] using classical oscillators. The results were subject to a large uncertainty.

The temperature dependences of the optical constants were measured by Hodgson [1] at three different temperatures—22°, 124° and 230 °C—in the region from 0.6–2.4 μm. Smith [5] measured $n$ and $k$ values at 0.5461 μm at a number of different temperatures between 23° and 115 °C. From these measurements he derived

$$n = [1.593 + 0.00036T] \pm 0.004$$

$$k = [4.771 - 0.00155T] \pm 0.031,$$

where $T$ was in degrees Celsius.

A few values of the optical constants have been reported [13, 17] which differ significantly from those obtained by ellipsometry. Schulz [13] reported values of $n$ and $k$ that agreed quite well with those given by the simple Drude theory in the region from 0.4–0.87 μm. However, it has been shown by the K–K analysis [11] and sum-rule calculations [7] that those values of the optical constants were questionable. The values were derived from reflectance data measured on a surface in contact with a quartz prism with unpolarized light incident at 45° and phase-shift data measured by an interferometric method for normal-incidence reflection from a surface in contact with mica. Mueller [17] also reported optical constants in the region from 0.26–2.48 μm, which were in good agreement above 0.38 μm with the simple Drude theory. The values were derived from reflectance

data measured with *s*-polarized light on a surface in contact with sapphire at normal incidence and at 45°. It was shown [11] that the precision of these reflectance measurements was far too low to permit an accurate determination of the optical constants. In addition to these two reports [13, 17], a few measurements [18, 19] of normal-incidence reflectances have been reported, which deviate slightly from those given by the $n$ and $k$ values determined by ellipsometry [1, 3–11]. The deviations were less than 0.02 in the absolute reflectance values. Bloch and Rice [19] have taken this discrepancy to be real, and proposed a model of the surface-transition zone to reconcile the discrepancy. Several papers [10, 20–24] have been developed along this line. A recent measurement made in our laboratory [25] with laser beams and with an Xe lamp at several wavelengths show that the measured values of reflectance agree well with those calculated from the optical constants determined by ellipsometry [11].

## REFERENCES


1. J. N. Hodgson, *Phil. Mag.* **4**, 183 (1959).
2. L. G. Lelyuk, I. N. Shklyarevskii, and R. G. Yarovaya, *Opt. Spect. (U.S.S.R)* **16**, 263 (1964).
3. L. E. Smith and R. R. Stromberg, *J. Opt. Soc. Am.* **56**, 1539 (1966).
4. N. V. Smith, *Adv. Phys.* **16**, 629 (1967).
5. T. Smith, *J. Opt. Soc. Am.* **57**, 1207 (1967).
6. T. E. Faber and N. V. Smith, *J. Opt. Soc. Am.* **58**, 102 (1968).
7. G. Busch and J. Guggenheim, *Helv. Phys. Acta* **41**, 401 (1968).
8. W. J. Choyke, S. H. Vosko, and T. W. O'Keeffe, *Solid State Commun.* **9**, 361 (1971).
9. N. R. Comins, *Phil. Mag.* **25**, 817 (1972).
10. E. D. Crozier and E. Murphy, *Can. J. Phys.* **50**, 1914 (1972).
11. T. Inagaki, E. T. Arakawa, and M. W. Williams, *Phys. Rev. B* **23**, 5246 (1981).
12. E. G. Wilson and S. A. Rice, *Phys. Rev.* **145**, 55 (1966).
13. L. G. Schulz, *J. Opt. Soc. Am.* **47**, 64 (1957).
14. J. R. Beattie and G. K. T. Conn, *Phil. Mag.* **46**, 222 (1955).
15. N. V. Smith, *Phys. Lett.* **26A**, 126 (1968).
16. H. W. Verleur, *J. Opt. Soc. Am.* **58**, 1356 (1968).
17. W. E. Mueller, *J. Opt. Soc. Am.* **59**, 1246 (1969).
18. J. Boiani and S. A. Rice, *Phys. Rev.* **185**, 931 (1969).
19. A. N. Bloch and S. A. Rice, *Phys. Rev.* **185**, 933 (1969).
20. H. L. Lemberg, S. A. Rice, P. H. Naylor, and A. N. Bloch, *Solid State Commun.* **14**, 1097 (1974).
21. H. L. Lemberg, S. A. Rice, and D. Guidotti, *Phys. Rev. B* **10**, 4079 (1974).
22. D. Guidotti and S. A. Rice, *Phys. Rev. B* **15**, 3796 (1977).
23. A. Tadjeddine, G. Piazza, and M. Costa, *Europhys. Lett.* **5**, 87 (1988).
24. W. L. Schaich, *Phys. Rev. B* **37**, 6193 (1988).
25. E. T. Arakawa, T. Inagaki, and P. S. Tuminello, *Bull. Am. Phys. Soc.* **33**, 422 (1988).
26. P. S. Yuminello, E. T. Arakawa, T. Inagaki, and J. E. Parks, II, *Phys. Rev. B* **40**, 11994 (1989).

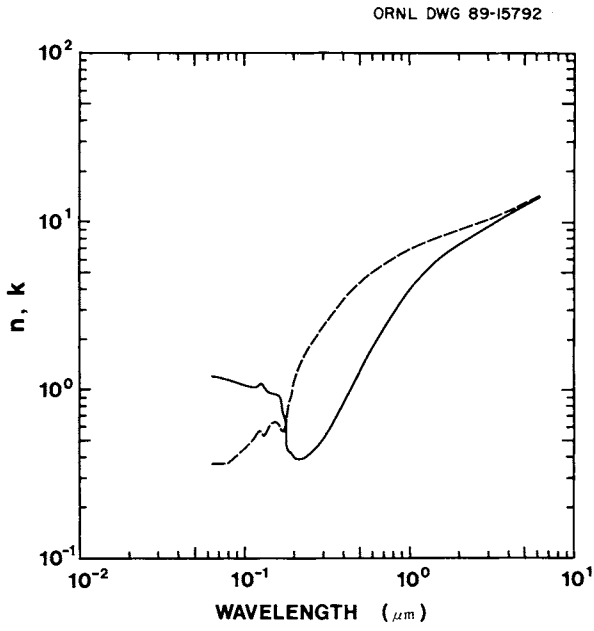


**Fig. 1.** Log–log plot of $n$ (solid line) and $k$ (dashed line) versus wavelength in micrometers for liquid mercury.

**TABLE I**

**Values of $n$ and $k$ for Liquid Mercury from Various References**

| eV | $cm^{-1}$ | $\mu m$ | n | k |
|---|---|---|---|---|
| 19.5 | | 0.06358 | 1.208 [11] | 0.364 [11] |
| 19.0 | | 0.06526 | 1.200 | 0.366 |
| 18.5 | | 0.06702 | 1.195 | 0.367 |
| 18.0 | | 0.06888 | 1.191 | 0.367 |
| 17.5 | | 0.07085 | 1.184 | 0.366 |
| 17.0 | | 0.07293 | 1.177 | 0.367 |
| 16.5 | | 0.07514 | 1.170 | 0.367 |
| 16.0 | | 0.07749 | 1.159 | 0.368 |
| 15.5 | | 0.07999 | 1.146 | 0.374 |
| 15.0 | | 0.08266 | 1.135 | 0.383 |
| 14.5 | | 0.08551 | 1.125 | 0.394 |
| 14.0 | | 0.08856 | 1.115 | 0.404 |
| 13.5 | | 0.09184 | 1.104 | 0.416 |
| 13.0 | | 0.09537 | 1.092 | 0.430 |
| 12.5 | | 0.09919 | 1.078 | 0.445 |
| 12.0 | | 0.1033 | 1.064 | 0.467 |
| 11.5 | | 0.1078 | 1.050 | 0.491 |
| 11.0 | | 0.1127 | 1.039 | 0.523 |
| 10.8 | | 0.1148 | 1.039 | 0.537 |
| 10.6 | | 0.1170 | 1.041 | 0.550 |
| 10.4 | | 0.1192 | 1.045 | 0.561 |
| 10.2 | | 0.1216 | 1.054 | 0.569 |
| 10.0 | | 0.1240 | 1.062 | 0.567 |
| 9.8 | | 0.1265 | 1.061 | 0.557 |
| 9.6 | | 0.1292 | 1.044 | 0.541 |
| 9.4 | | 0.1319 | 1.009 | 0.548 |
| 9.2 | | 0.1348 | 0.988 | 0.568 |
| 9.0 | | 0.1378 | 0.975 | 0.588 |
| 8.8 | | 0.1409 | 0.965 | 0.607 |
| 8.6 | | 0.1442 | 0.956 | 0.624 |
| 8.4 | | 0.1476 | 0.953 | 0.638 |
| 8.2 | | 0.1512 | 0.952 | 0.645 |
| 8.0 | | 0.1550 | 0.946 | 0.639 |
| 7.8 | | 0.1590 | 0.929 | 0.623 |
| 7.6 | | 0.1631 | 0.893 | 0.597 |
| 7.5 | | 0.1653 | 0.860 | 0.580 |
| 7.4 | | 0.1675 | 0.817 | 0.574 |
| 7.3 | | 0.1698 | 0.769 | 0.575 |
| 7.2 | | 0.1722 | 0.717 | 0.584 |
| 7.1 | | 0.1746 | 0.663 | 0.589 |
| 7.0 | | 0.1771 | 0.585 | 0.617 |
| 6.9 | | 0.1797 | 0.510 | 0.676 |
| 6.8 | | 0.1823 | 0.459 | 0.756 |

(continued)

TABLE I (*Continued*)

**Values of $n$ and $k$ for Liquid Mercury from Various References**

| eV | $cm^{-1}$ | $\mu m$ | n | k |
|---|---|---|---|---|
| 6.7 | | 0.1851 | 0.438 [11] | 0.836 [11] |
| 6.6 | | 0.1879 | 0.436 | 0.898 |
| 6.5 | | 0.1907 | 0.428 | 0.949 |
| 6.4 | | 0.1937 | 0.412 | 1.002 |
| 6.3 | | 0.1968 | 0.399 | 1.058 |
| 6.2 | | 0.2000 | 0.390 | 1.118 |
| 6.1 | 49,199 | 0.2033 | 0.388 | 1.176 |
| 6.0 | 48,393 | 0.2066 | 0.386 | 1.232 |
| 5.9 | 47,586 | 0.2101 | 0.385 | 1.287 |
| 5.8 | 46,780 | 0.2138 | 0.386 | 1.341 |
| 5.7 | 45,973 | 0.2175 | 0.386 | 1.396 |
| 5.6 | 45,167 | 0.2214 | 0.386 | 1.454 |
| 5.5 | 44,360 | 0.2254 | 0.390 | 1.512 |
| 5.4 | 43,554 | 0.2296 | 0.394 | 1.569 |
| 5.2 | 41,940 | 0.2384 | 0.401 | 1.687 |
| 5.0 | 40,327 | 0.2480 | 0.414 | 1.806 |
| 4.8 | 38,714 | 0.2583 | 0.431 | 1.929 |
| 4.6 | 37,101 | 0.2695 | 0.452 | 2.058 |
| 4.4 | 35,488 | 0.2818 | 0.477 | 2.195 |
| 4.2 | 33,875 | 0.2952 | 0.507 | 2.341 |
| 4.0 | 32,262 | 0.3100 | 0.542 | 2.502 |
| 3.8 | 30,649 | 0.3263 | 0.589 | 2.665 |
| 3.6 | 29,036 | 0.3444 | 0.644 | 2.860 |
| 3.4 | 27,423 | 0.3647 | 0.713 | 3.074 |
| 3.2 | 25,810 | 0.3875 | 0.798 | 3.294 |
| 3.0 | 24,196 | 0.4133 | 0.898 | 3.538 |
| 2.8 | 22,583 | 0.4428 | 1.027 | 3.802 |
| 2.6 | 20,970 | 0.4769 | 1.186 | 4.090 |
| 2.4 | 19,357 | 0.5166 | 1.384 | 4.407 |
| 2.2 | 17,744 | 0.5636 | 1.620 | 4.751 |
| 2.0 | 16,131 | 0.6199 | 1.910 | 5.150 |
| 1.8 | 14,518 | 0.6888 | 2.284 | 5.582 |
| 1.6 | 12,905 | 0.7749 | 2.746 | 6.054 |
| 1.4 | 11,292 | 0.8856 | 3.324 | 6.558 |
| 1.2 | 9,679 | 1.0332 | 4.050 | 7.082 |
| 1.0 | 8,065 | 1.240 | 4.962 | 7.643 |
| 0.8 | 6,452 | 1.550 | 6.086 | 8.312 |
| 0.6 | 4,839 | 2.066 | 7.574 | 9.195 |
| 0.5 | 4,0329 | 2.480 | 8.528 | 9.805 |
| 0.4 | 3,226 | 3.100 | 9.741 | 10.65 |
| 0.3 | 2,4197 | 4.133 | 11.37 | 11.95 |
| 0.2 | 1,613 | 6.199 | 13.99 | 14.27 |

# Palladium (Pd)

A. BORGHESI and A. PIAGGI
Dipartimento di Fisica "A. Volta"
and
Gruppo Nazionale di Struttura della Materia del CNR
Università di Pavia
Pavia, Italy

The optical properties of Pd have been studied under a variety of experimental conditions and by several techniques [1–28]. Unfortunately, many results disagree as to the actual magnitude of optical structures, although the structure energies agree in almost every case. This depends on sample preparation, accuracy of the optical measurements, and on the method by which the experimental data are analyzed.

Experimentally, Pd is difficult to study in bulk samples, since it is readily contaminated and does not electropolish easily [19]. Vacuum deposition is relatively easy, but aging effects have been shown to be significant [13]. Although Pd does not oxidize as rapidly in air as other transition metals, Pd films show a critical dependence on thickness and evaporation rate [15].

The room-temperature values of $n$ and $k$ tabulated here (Table I and Fig. 1) were obtained from the following works and references therein: Windt *et al.* [27] from 525–12.5 eV; Vehse *et al.* [13] from 12.5–6.0 eV; Johnson and Christy [15] from 6.0–0.6 eV; Weaver and Benbow and Weaver *et al.* [18, 29] from 0.6–0.1 eV. Although the optical response in the visible–UV region has been clarified by Johnson and Christy [15], experimental differences and doubts regarding higher energies and the IR region still remain to be resolved. We chose the results that were in major agreement and were reported to have comparable experimental accuracy.

Windt *et al.* [27] evaporated Pd of unknown purity with an electron-beam current of 100 mA, at a rate of 10–12 Å/s onto polished silicon (111) wafers. The pressure in the deposition system was $\sim 5 \times 10^{-6}$ torr, and the substrate temperature was 80 °C. The film thickness chosen was 1000 Å, verified using a quartz-crystal monitor during deposition. Surface roughness was 18±3 Å, measured with an optical profilometer. The Auger-electron-spectroscopy profile indicated that oxidation was confined to the film surface. Absolute-reflectance ($R$) measurements were performed at thirty-six wavelengths ($\lambda$) from 24 Å to 1216 Å, using a


Copyright © 1991 by Academic Press.
All rights of reproduction in any form reserved.
ISBN 0-12-544422-2

computer-controlled reflectometer at several incidence angles (usually sixteen angles between 10° and 85°). The incident-beam polarization was measured for $\lambda > 200$ Å using a rhodium-mirror polarization analyzer; for $\lambda \leqslant 200$ Å, the beam was assumed to be unpolarized. Although higher in overall magnitude, the shape of normal-incidence $R$ agreed with the curve of Vehse *et al.* [13], showing the characteristic peak near 600 Å and the minimum near 700 Å. Using a nonlinear, least-squares, curve-fitting technique based on the $\chi^2$ test, the values of $n$ and $k$ with their probable errors were determined from $R$ versus incidence angle. The fitting procedure accounted for the effects of beam polarization, film thickness, and surface roughness in the calculation of the model reflectance [30]. The soft X-ray data of Henke *et al.* [22], the data of Vehse *et al.* [13], and the absorptivity of Weaver and Olson [20] are in moderate agreement with Windt *et al.* [27] optical constants in the range of overlap.

In Vehse *et al.* [13], Pd films were obtained by evaporation of Pd wire of 99.9995% purity in a vacuum of $10^{-8}$ torr. The deposition rate was ~150 Å/s, and the film thickness, measured by multiple-beam interferometry, ranged from 1600–2200 Å. The near-normal-incidence $R$ was measured from 2–24 eV; in addition, $R$ was measured as a function of the angle of incidence for a few selected photon energies. Even though the measurements were made *in situ*, $R$ data were found to vary somewhat from sample to sample and to deteriorate with time; the data presented concern films with the highest $R$ measured immediately after deposition. The prevalent conditions during evaporation and the history of the sample after its preparation must account for some discrepancies in the $R$ values extending into the VUV [1–3, 7, 11]; such discrepancies occurred for all the opaque films evaporated on smooth substrates. Some scatter among data exists even for samples prepared *in situ* [11], mainly from 4 eV up to the region of the surface-plasma resonance at 7.3 eV. This probably results from surface-quality differences: the highest $R$ values of Vehse *et al.* could indicate a better surface than in Ref. [27], even though their $R$ is lower in the 10–24 eV range. In the low-energy range (4–6.5 eV) where experimental spectra overlap, $R$ agrees well with that calculated from $n$ and $k$ measured on thin semitransparent films by Johnson and Christy [15] (see below). For multiangle measurements at selected energies, $n$ and $k$ were determined by a least-squares fit to Fresnel's equations. $n$ and $k$ were determined by the Kramers–Kronig analysis of the normal-incidence $R$ spectrum from 2–24 eV. In the K–K integrals, the contribution $\Delta\theta$ to the phase change $\theta$ from the region above 24 eV was determined by interpolating the known values of $\Delta\theta$ at the selected energies mentioned above with a smoothly varying function. The results from the two methods agree within experimental error (±5%). Despite the good agreement of $R$ values, $n$ and $k$ do not agree well with Johnson and Christy's values [15] in the 4–6.5 eV range, probably due to K–K interpolations.

Johnson and Christy [15] deposited Pd onto fused-quartz substrates at room temperature by vacuum evaporation of high-purity (99.97%) material. The evaporation was performed at pressure below $3 \times 10^{-6}$ torr and at a fast rate (50 Å/s) to ensure the surface smoothness of the films. Several additional films were formed by sublimation at a rate of 0.3 Å/s. The reflectance was much higher for the quickly evaporated rather than for the sublimated films, so the optical constants determined from the former type were preferred. Moreover, annealing of the films in a nitrogen atmosphere indicated that quickly evaporated films were smooth and homogeneous, since they did not change after annealing like noble metals, whereas sublimated films changed. $n$ and $k$ as well as thickness $d$ of the films were determined at eight selected wavelengths by inverting normal-incidence $R$ and $T$ functions simultaneously with the $T$ function for $p$-polarized light incident at 60°. A three-parameter fit was used, and the resulting eight values of $d$ (which presented a scatter of ±4 Å) were averaged. Then $n$ and $k$ were determined throughout the entire 0.5–6.5 eV spectral range using only normal-incidence $R$ and $T$. The accuracy of the spectrophotometer in $R$ (or $T$) was ±0.005, ±0.001 and ±0.0005, for the ranges $R>0.2$, $0.1 \leqslant R \ll 0.2$, and $R<0.1$, respectively. $R$ spectra are in very good agreement (±0.01 in $R$) with those derived by Weaver and Benbow [18] (see below) from optical absorptivity between 0.15 and 4.4 eV. The optical constants exhibited a thickness dependence when the films were excessively thin (~100 Å). This behavior is qualitatively predicted by the Maxwell–Garnett theory [31]. $n$ and $k$ values listed are the averages of experiments on 277 and 375 Å films, which yielded results in agreement within the estimated error (less than ±1.5% in $R$ and ±4% in $n$). As stated above, $R$ processing (K–K transform) is exclusively responsible for moderate agreement of $n$ and $k$ values with those of Ref. [13]. $R$ measured by Yu and Spicer [11] on opaque films from 2.2–11.6 eV was lower, because their slowly evaporated films were probably similar in structure to slowly sublimed films. This, with additional error introduced by K–K analysis, can account for most of the differences in their $n$ and $k$ values.

Weaver and Benbow [18] Pd samples were cut from a high-purity rod, mechanically polished to obtain a specular surface, then etched in boiling aqua regia. They were then annealed at 800 °C in vacuum ($10^{-8}$ torr), followed by a high-temperature anneal under a partial pressure of He (1020 °C at $10^{-3}$ torr) to promote grain growth. Microscopic examination showed large grain (~4 mm) and an excellent work-free surface. Immediately prior to measurement, the sample was flashed in high vacuum to thermal-desorb any surface contamination. The absorptivity $A = 1 - R$ was measured at 4.2 K between 0.15 and 4.4 eV by a calorimetric technique. A K–K analysis was used to determine the optical constants [29]. For the extrapolations, a Drude form was used below 0.15 eV, and the data of Johnson and Christy [15], Vehse *et al.* [13] and Robin [7] were used from

4–50 eV. A power-law approximation $R(E) = R_o E^{-\beta}$ was used above 50 eV, with $\beta$ adjusted to fit the independently determined dielectric function of Johnson and Christy [15], whose reflectance was in very good agreement in the overlap range. Although the optical spectra of Duisebaeva *et al.* [14] also present a structure near 0.46 eV, it is approximately three times stronger than that in [18]; moreover, another structure reported in [14] between 1.5 and 3 eV was not observed in [15] and [18]. Lafait *et al.* [21] also determined the infrared optical constants of Pd, from 0.1–0.5 eV, by means of surface-plasmon excitation. Unfortunately, their data were in disagreement with those of Refs. [14] and [18]. Furthermore, their conventional measurements of near-normal $R$ and $T$ from 0.5–6 eV also disagreed with those of Refs. [15] and [18], corresponding to a systematically lower reflectance.

Very recently, Fuzi *et al.* [32] used a prism-coupling (ATR) technique to measure the surface-plasmon properties of electron-beam-evaporated Pd on a glass slide. The ATR data as a function of angle of incidence at the He/Ne laser wavelength of 3.391 μm gave average values of $\varepsilon_R = 82.6$ and $\varepsilon_I = 109.3$ for several different prism-air space thicknesses. This gives $n = 5.21$ and $k = 10.48$, compared with values interpolated from Table I of $n = 4.08$ and $k = 14.05$. Fuzi *et al.* discuss variations of $\varepsilon_R$ and $\varepsilon_I$ for different kinds of metallic thin-film samples.

## REFERENCES


1. G. B. Sabine, *Phys. Rev.* **55**, 1064 (1939).
2. D. Malé and J. Trompette, *J. de Physique et le Radium* **18**, 128 (1957).
3. P. Lostis, *J. de Physique* **25**, 118 (1964).
4. B. Dold and R. Mecke, *Optik* **22**, 435 (1965).
5. A. P. Lenham and D. M. Treherne, *J. Opt. Soc. Am.* **56**, 1137 (1966).
6. A. P. Lenham and D. M. Treherne, in "Optical Properties and Electronic Structure of Metals and Alloys," (F. Abelès ed.), North-Holland, Amsterdam, 196 (1966).
7. S. Robin, in "Optical Properties and Electronic Structure of Metals and Alloys," (F. Abelès ed.), North-Holland, Amsterdam, 202 (1966).
8. G. A. Bolotin, M. M. Kirillova, L. V. Nomerovannaya, and M. M. Noskov, *Fiz. Metal. Metalloved* **23**, 72 (1967).
9. F. I. Vilesov, A. A. Azgrubskii, and M. M. Kirillova, *Opt. Spectrosc.* **23**, 79 (1967); *Opt. Spektrosk.* **23**, 153 (1967).
10. A. P. Lenham, *J. Opt. Soc. Am.* **57**, 473 (1967).
11. A. Y-C. Yu and W. E. Spicer, *Phys. Rev.* **169**, 497 (1968).
12. J. Daniels, *Z. Physik* **227**, 234 (1969).
13. R. C. Vehse, E. T. Arakawa, and M. W. Williams, *Phys. Rev.* **B1**, 517 (1970).
14. Z. Duisebaeva, M. I. Korsunskii and G. P. Motulevich, *Opt. Spectrosc.* **34**, 307 (1973); *Opt. Spektrosk.* **34**, 535 (1973).
15. P. B. Johnson and R. W. Christy, *Phys. Rev.* **B9**, 5056 (1974).
16. Z. Duisabaeva, M. I. Korsunskii, and G. P. Motulevich, *Opt. Spectrosc.* **37**, 82 (1974); *Opt. Spektrosk.* **37**, 149 (1974).
17. C. Wehenkel and B. Gauthé, *Optics Commun.* **11**, 62 (1974).
18. J. H. Weaver and R. L. Benbow, *Phys. Rev.* **12**, 3509 (1975).

19. J. H. Weaver, *Phys. Rev.* **B11**, 1416 (1975).
20. J. H. Weaver and C. G. Olson, *Phys. Rev.* **B14**, 3251 (1976).
21. J. Lafait, F. Abelès, M. L. Theye, and G. Vuye, *J. Phys. F: Metal Phys.* **8**, 1597 (1978).
22. B. L. Henke, P. Lee, T. J. Tanaka, R. L. Shimabukuro and B. K. Fujikawa, *AIP Conf. Proc.* **75**, 340 (1981).
23. R. Riedinger and M. A. Khan, *Philos. Mag. B* **44**, 547 (1981).
24. M. A. Ordal, L. L. Long, R. J. Bell, S. E. Bell, R. W. Alexander, Jr., and C. A. Ward, *Appl. Opt.* **22**, 1099 (1983).
25. M. A. Ordal, R. J. Bell, R. W. Alexander, Jr., L. L. Long, and M. R. Querry, *Appl. Opt.* **24**, 4493 (1985).
26. G. N. Zhizhin, V. I. Silin and V. A. Yakovlev, *Sov. Phys. Solid State* **29**, 1224 (1987); *Fiz. Tverd. Tela* **29**, 231 (1987).
27. D. L. Windt, W. C. Cash, Jr., M. Scott, P. Arendt, B. Newnam, R. F. Fisher, and A. B. Swartzlander, *Appl. Opt.* **27**, 246 (1988).
28. H. Chen, N. E. Brener, and J. Callaway, *Phys. Rev.* **B40**, 1443 (1989).
29. J. H. Weaver, C. Krafka, D. W. Lynch, and E. E. Koch, in "Physik Daten, Physics Data, Optical Properties of Metals," Vol. 18-1, Fach-information zentrum, Karlsruhe, 179 (1981).
30. D. L. Windt, W. C. Cash, Jr., M. Scott, P. Arendt, B. Newnam, R. F. Fisher, A. B. Swartzlander, P. Z. Takacs, and J. M. Pinneo, *Appl. Opt.* **27**, 279 (1988).
31. O. S. Heavens, in "Optical Properties of Thin Solid Films," Dover, New York, 177 (1965).
32. Y. Fuzi, G. W. Bradberry, and J. R. Sambles, *J. Mod. Opt.* **36**, 1405 (1989).

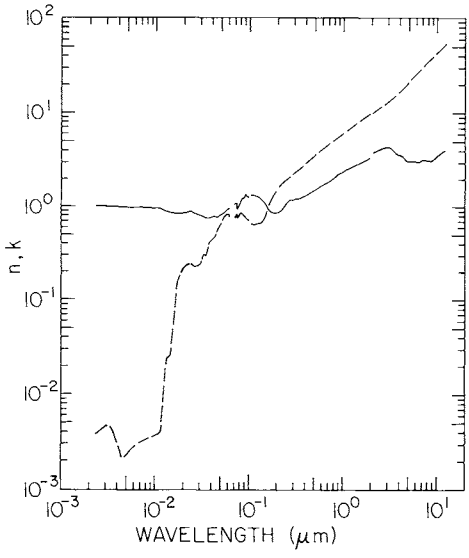


**Fig. 1.** Log–log plot of $n$ (solid line) and $k$ (dashed line) versus wavelength in micrometers for palladium.

TABLE I

Values of $n$ and $k$ for Palladium from Various References[a]

| eV | $cm^{-1}$ | Å | $n$ | $k$ |
|---|---|---|---|---|
| 525.36 | | 23.6 | 0.996 [27] | $3.8\times10^{-3}$ [27] |
| 392.36 | | 31.6 | 0.998 | 4.8 |
| 330.63 | | 37.5 | 0.995 | 3.5 |
| 277.37 | | 44.7 | 0.993 | 2.1 |
| 247.97 | | 50.0 | 0.992 | 2.3 |
| 206.64 | | 60.0 | 0.986 | 2.8 |
| 183.41 | | 67.6 | 0.982 | 3.1 |
| 165.31 | | 75.0 | 0.980 | 3.3 |
| 123.99 | | 100.0 | 0.960 | 3.7 |
| 108.76 | | 114.0 | 0.938 | 3.9 |
| 99.19 | | 125.0 | 0.910 | $9.0\times10^{-3}$ |
| 91.50 | | 135.5 | 0.871 | 0.025 |
| 82.66 | | 150.0 | 0.851 | 0.072 |
| 72.34 | | 171.4 | 0.835 | 0.148 |
| 61.99 | | 200.0 | 0.850 | 0.22 |
| 51.02 | | 243.0 | 0.879 | 0.244 |
| 48.38 | | 256.3 | 0.851 | 0.224 |
| 40.81 | | 303.8 | 0.821 | 0.247 |
| 37.92 | | 327.0 | 0.799 | 0.310 |
| 34.75 | | 356.8 | 0.758 | 0.307 |
| 32.69 | | 379.3 | 0.763 | 0.420 |
| 30.55 | | 405.9 | 0.794 | 0.451 |
| 27.69 | | 447.8 | 0.780 | 0.495 |
| 26.91 | | 460.7 | 0.765 | 0.547 |
| 25.33 | | 489.5 | 0.809 | 0.625 |
| 23.00 | | 539.1 | 0.853 | 0.763 |
| 21.22 | | 584.3 | 0.913 | 0.850 |
| 20.12 | | 616.3 | 0.990 | 0.790 |
| 18.48 | | 670.9 | 1.03 | 0.766 |
| 17.26 | | 718.5 | 1.06 | 0.778 |
| 16.85 | | 735.9 | 1.07 | 0.824 |
| 16.67 | | 743.7 | 0.94 | 0.744 |
| 14.86 | | 834.5 | 1.24 | 0.877 |
| 14.12 | | 878.0 | 1.23 | 0.815 |
| 13.48 | | 919.8 | 1.36 | 0.796 |
| 13.30 | | 932.1 | 1.30 | 0.749 |
| 12.54 | | 988.8 | 1.28 | 0.733 |
| eV | $cm^{-1}$ | $\mu$m | $n$ | $k$ |
| 12.0 | | 0.1033 | 1.34 [13] | 0.66 [13] |
| 11.5 | | 0.1078 | 1.33 | 0.65 |
| 11.0 | | 0.1127 | 1.31 | 0.65 |
| 10.5 | | 0.1181 | 1.30 | 0.66 |
| 10.0 | | 0.1240 | 1.28 | 0.66 |

[a] The references from which the values were extracted are given in brackets.

TABLE I (*Continued*)

**Palladium**

| eV | $cm^{-1}$ | $\mu m$ | $n$ | $k$ |
|---|---|---|---|---|
| 9.5 | | 0.1305 | 1.25 | 0.66 |
| 9.0 | | 0.1378 | 1.19 | 0.68 |
| 8.5 | | 0.1459 | 1.10 | 0.72 |
| 8.0 | | 0.1550 | 0.98 | 0.84 |
| 7.5 | | 0.1653 | 0.89 | 1.02 |
| 7.0 | | 0.1771 | 0.85 | 1.23 |
| 6.5 | | 0.1907 | 0.86 | 1.44 |
| 5.98 | 48,232 | 0.2073 | 0.87 [15] | 1.60 [15] |
| 5.85 | 47,183 | 0.2119 | 0.89 | 1.65 |
| 5.73 | 46,215 | 0.2164 | 0.91 | 1.70 |
| 5.60 | 45,167 | 0.2214 | 0.92 | 1.76 |
| 5.48 | 44,199 | 0.2263 | 0.94 | 1.81 |
| 5.36 | 43,231 | 0.2313 | 0.97 | 1.86 |
| 5.23 | 42,182 | 0.2371 | 1.00 | 1.91 |
| 5.11 | 41,215 | 0.2426 | 1.04 | 1.95 |
| 4.98 | 40,166 | 0.2490 | 1.08 | 1.99 |
| 4.86 | 39,198 | 0.2551 | 1.11 | 2.03 |
| 4.74 | 38,230 | 0.2616 | 1.13 | 2.07 |
| 4.61 | 37,182 | 0.2689 | 1.16 | 2.10 |
| 4.49 | 36,214 | 0.2761 | 1.19 | 2.13 |
| 4.36 | 35,165 | 0.2844 | 1.18 | 2.18 |
| 4.24 | 34,198 | 0.2924 | 1.18 | 2.23 |
| 4.12 | 33,230 | 0.3009 | 1.20 | 2.29 |
| 3.99 | 32,181 | 0.3107 | 1.21 | 2.35 |
| 3.87 | 31,213 | 0.3204 | 1.21 | 2.42 |
| 3.74 | 30,165 | 0.3315 | 1.20 | 2.50 |
| 3.62 | 29,197 | 0.3425 | 1.22 | 2.57 |
| 3.50 | 28,229 | 0.3542 | 1.23 | 2.65 |
| 3.37 | 27,181 | 0.3679 | 1.24 | 2.74 |
| 3.25 | 26,213 | 0.3815 | 1.26 | 2.83 |
| 3.12 | 25,164 | 0.3974 | 1.30 | 2.93 |
| 3.00 | 24,196 | 0.4133 | 1.33 | 3.03 |
| 2.88 | 23,229 | 0.4305 | 1.37 | 3.14 |
| 2.75 | 22,180 | 0.4509 | 1.41 | 3.26 |
| 2.63 | 21,212 | 0.4714 | 1.46 | 3.39 |
| 2.50 | 20,164 | 0.4959 | 1.52 | 3.54 |
| 2.38 | 19,196 | 0.5209 | 1.57 | 3.68 |
| 2.26 | 18,228 | 0.5486 | 1.64 | 3.84 |
| 2.13 | 17,179 | 0.5821 | 1.68 | 4.02 |
| 2.01 | 16,212 | 0.6168 | 1.75 | 4.21 |
| 1.88 | 15,163 | 0.6595 | 1.80 | 4.42 |
| 1.76 | 14,195 | 0.7045 | 1.86 | 4.65 |
| 1.64 | 13,227 | 0.7560 | 1.95 | 4.89 |
| 1.51 | 12,179 | 0.8211 | 2.06 | 5.19 |
| 1.39 | 11,211 | 0.8920 | 2.33 | 5.50 |

*(continued)*

TABLE I (*Continued*)

**Palladium**

| eV | $cm^{-1}$ | $\mu m$ | $n$ | $k$ |
|---|---|---|---|---|
| 1.26 | 10,162 | 0.9840 | 2.34 | 5.89 |
| 1.14 | 9,195 | 1.088 | 2.52 | 6.33 |
| 1.02 | 8,227 | 1.215 | 2.66 | 6.90 |
| 0.89 | 7,178 | 1.393 | 2.80 | 7.65 |
| 0.77 | 6,210 | 1.610 | 3.01 | 8.59 |
| 0.64 | 5,162 | 1.937 | 3.34 | 9.89 |
| 0.60 | 4,839 | 2.066 | 3.80 [31] | 9.96 [31] |
| 0.58 | 4,678 | 2.138 | 3.85 | 10.23 |
| 0.56 | 4,517 | 2.214 | 3.92 | 10.49 |
| 0.54 | 4,355 | 2.296 | 3.97 | 10.79 |
| 0.52 | 4,194 | 2.384 | 4.03 | 11.10 |
| 0.50 | 4,033 | 2.480 | 4.10 | 11.44 |
| 0.48 | 3,871 | 2.583 | 4.20 | 11.77 |
| 0.46 | 3,710 | 2.695 | 4.27 | 12.11 |
| 0.44 | 3,549 | 2.818 | 4.31 | 12.46 |
| 0.42 | 3,387 | 2.952 | 4.31 | 12.85 |
| 0.40 | 3,226 | 3.100 | 4.27 | 13.27 |
| 0.38 | 3,065 | 3.263 | 4.17 | 13.77 |
| 0.36 | 2,904 | 3.444 | 3.98 | 14.41 |
| 0.34 | 2,742 | 3.647 | 3.80 | 15.18 |
| 0.32 | 2,581 | 3.875 | 3.56 | 16.21 |
| 0.30 | 2,420 | 4.133 | 3.56 | 17.27 |
| 0.28 | 2,258 | 4.428 | 3.30 | 18.52 |
| 0.26 | 2,097 | 4.769 | 3.11 | 20.15 |
| 0.24 | 1,936 | 5.166 | 3.15 | 21.97 |
| 0.22 | 1,774 | 5.636 | 3.10 | 24.06 |
| 0.20 | 1,613 | 6.199 | 3.07 | 26.59 |
| 0.19 | 1,532 | 6.526 | 3.07 | 28.09 |
| 0.18 | 1,452 | 6.888 | 3.15 | 29.71 |
| 0.17 | 1,371 | 7.293 | 3.20 | 31.46 |
| 0.16 | 1,290 | 7.749 | 3.17 | 33.45 |
| 0.15 | 1,210 | 8.266 | 3.13 | 35.82 |
| 0.14 | 1,129 | 8.856 | 3.11 | 38.48 |
| 0.13 | 1,048 | 9.537 | 3.36 | 41.52 |
| 0.12 | 968 | 10.33 | 3.60 | 45.08 |
| 0.11 | 887 | 11.27 | 3.85 | 49.21 |
| 0.10 | 806 | 12.40 | 4.13 | 54.15 |

# Vanadium (V)

G. GUIZZETTI and A. PIAGGI
Dipartimento di Fisica "A. Volta"
and
Gruppo Nazionale di Struttura della Materia del CNR
Università di Pavia
Pavia, Italy

There have been many measurements of the optical properties of V [1–23]. Although in the 1960s they were generally obtained on bulk samples mechanically polished, in later years films were preferentially used. The optical properties of the V films are strongly dependent on the preparation technique and the physical-chemical conditions (in particular, deposition rate and substrate temperature). To some degree this can explain scatter among the data. Moreover, V is particularly sensitive to oxide, but no author has quantitatively estimated the oxide-coating effect on the optical response. In any case, the best films give a response very similar to the bulk.

The room-temperature values of $n$ and $k$ tabulated here (Table I and Fig. 1) were obtained from the following works and references therein: Sonntag *et al.* [7] from 300–120 eV, Wehenkel and Gauthé [13] from 120–40 eV; Seignac and Robin [8] from 40–6 eV; Nestell and Christy [19] from 6–0.5 eV; Weaver *et al.* [12] from 0.5–0.1 eV. As a general rule we preferred data that were obtained "directly," for example, from $R$ and $T$ by inverting the Fresnel relations or from ellipsometry, which do not rely on extrapolations outside the measured spectrum. However, we also considered values derived from Kramers–Kronig analysis of reflectance [12] or electron-energy-loss spectra [13], based on a very wide energy range and accurate measurements: This ensured reliable results, which were in good agreement with the others in the overlapping regions. We have disregarded data that were insufficient and ambiguous, in terms of either the sample preparation and characterization or the measurement accuracy, especially when inexplicable or in clear disagreement with other researchers. This is particularly true in the IR region, where despite numerous ellipsometric measurements, we preferred the results of calorimetry [12], although limited to 0.1 eV.


Copyright © 1991 by Academic Press.
All rights of reproduction in any form reserved.
ISBN 0-12-544422-2

In Table I we have retained three significant figures, but it is probably too generous for optical constants obtained from photometric or ellipsometric techniques.

Sonntag *et al.* [7] evaporated films onto substrates of zapon and aluminum using an electron gun. The optical absorption coefficient $\alpha$ was determined with an absolute accuracy of $\pm 20\%$, but the relative accuracy of adjacent regions was much better, about $1 \times 10^4\,\mathrm{cm}^{-1}$. The wavelength resolution in the continuous spectrum between 40 eV and ~300 eV of synchrotron light (of DESY accelerator) was better than 1 Å (0.1 eV at 40 eV, 8 eV at 300 eV). The $\alpha$ spectrum only showed an appreciable rise at 47.7 eV, while the strong oscillations reported by previous investigators [24, 25] appear to have been spurious. Above 200 eV, $\alpha$ quasi-linearly decreases to the value of $0.9 \times 10^5\,\mathrm{cm}^{-1}$ at 300 eV. The absolute magnitude of $\alpha$ was checked by performing oscillator sums to produce the expected value of $N_{\mathrm{eff}} \approx 8$ electrons.

Wehenkel and Gauthé [13] deposited V films by clean-vacuum ($10^{-8}$–$10^{-7}$ torr) evaporation from bulk material on freshly cleaved rocksalt and floated off on distilled water. Film thicknesses from 200–400 Å were determined with an accuracy of about $\pm 10\%$, by weighing the substrate before and after evaporation. Electron-energy-loss spectra were obtained by transmission of 35 keV electrons in the 2–120 eV range with an accuracy better or equal to $\pm 0.5$ eV and constant through the whole spectral range. To achieve statistical accuracy, a large number of spectra were recorded, using different specimens of different thicknesses. Through Ritchie's formula [26], the single-scattering volume losses were separated from the surface losses. Then $\varepsilon_1$, $\varepsilon_2$, and thickness were calculated by means of Kramers–Kronig relations. The energy-loss function was extrapolated by setting $\mathrm{Im}(-1/\tilde{\varepsilon}) = 0$ at $E = 0$ and assuming that it varies as $E^{-2.5}$ at high energies. In the superposition region (40–120 eV), the $\alpha$ spectrum derived is in good accord with that directly measured by Sontagg *et al.* [7]. In particular the peak at 47.7 eV differs only 3% in the energy position, although it is ~30% higher. So we report Kramers–Kronig-derived $n$ values in the range 40–120 eV.

Seignac and Robin [8] evaporated V buttons of high purity (99.98%) with an electron gun onto mica and pyrex substrates, heated to a temperature between 350 and 400 °C. The films, grown at a rate of ≈5 Å/s, had thicknesses of 900–1400 Å. The optical constants were determined by both $R$ measurements at two angles of incidence in the 4–50 eV range, and by Kramers–Kronig transforms; as far as the structure positions are concerned, the results were equivalent. The optical spectra in [8] are comparable with those of Ref. [7, 12, 19] in the respective superposition ranges; in particular, $R$ is lower than in Ref. [19], and the $\alpha$ spectrum at high energy is flatter than in [7].

Nestell and Christy [19] evaporated polycrystalline thin films in a

vacuum system (the pressure was in the range $2–5 \times 10^{-7}$ torr) onto fused-quartz substrates heated to high temperature (550–700 °C). The evaporation rates were 200–800 Å/s for opaque films, and 20 Å/s for thin films of ~200 Å. X-ray analysis showed that the films were well crystallized with a lattice constant approximately 1% smaller than bulk value (due to uniform strain) and a grain size of 150 Å. Transmittance and absolute reflectance measurements were made in the 0.5–6.5 eV range with a double-beam spectrophotometer. The accuracy was about $\pm 0.005$ in $R$. The reflectance of opaque films showed a strong evaporation-rate dependence; high rates avoid surface roughness, producing the most highly reflecting films (for example, at 6 eV, $R$ increased ~6% when the evaporation rate was increased from 21 to 317 Å/s). The reflectance of rapidly evaporated opaque films was in quite good agreement with bulk-sample results [12], but it was much higher above 5 eV and lower below 1 eV. In the UV this discrepancy is attributed to surface roughness of the bulk samples, resulting from etching; in the IR it may be due to the different measurement technique used (calorimetry; see in the following). The optical constants $n$ and $k$ as well as the film thickness were determined by inverting the normal-incidence $R$ and $T$ along with the $p$-polarized $T$ at a 60° angle of incidence, with $R$ measured from opaque films. The estimate of instrumental error was ~1% in $k$ and ~2% in $n$ over most of the spectral range. The aforesaid differences in $R$ between [19] and [8, 12] involve discontinuities in $n$ and $k$ at 0.5 eV and 6 eV, respectively.

In Weaver *et al.* [12], samples of V were spark-cut from electron-beam-melted buttons of high-purity material; then they were successively macroetched, mechanically polished, carefully electropolished, and finally very slightly polished with 0.3 μm diameter $Al_2O_3$. An X-ray Laue-gram indicated an unstrained surface. Although the samples were not single crystals, most or all of the illuminated surface was a single crystallite. A calorimetric method was used between 0.1 and 4.88 eV to determine the absorptivity $A = 1 - R$ at 4.2 K and a 15° angle of incidence. Room-temperature $R$ measurements were made at 10°, 45°, and 60° for $s$- and $p$-polarized synchrotron radiation from 3.1–35 eV. A comparison of low-energy absorptivities with those calculated from the $n$ and $k$ values of Bolotin *et al.* [1] show good qualitative agreement, although $A$ values are considerably lower in magnitude (that is, $R$ was higher). Instead, above 5–6 eV $R$ was lower than that of Seignac and Robin [8], probably due to an oxide layer. Optical constants were determined by Kramers–Kronig analysis: at low energy a Drudelike behavior was introduced; at high-energy, Sonntag *et al.* [10] absorption measurements were used to 300 eV; the range was extended up to 1000 eV (where $R = 1.4 \times 10^{-8}$) assuming $R(E) = R_o E^{-\beta}$ (with $\beta = 4.1$, from fitting $R$ at 190 and 300 eV). The very wide energy range used in Kramers–Kronig analysis and the quite good agreement below 5 eV with the data of Nestell and Christy [19] make the $n$ and $k$

values here reported in the 0.1–0.5 eV range more reliable than those obtained by ellipsometry [1–6, 22].

## REFERENCES


1. G. A. Bolotin, A. N. Voloshinskii, M. M. Kirillova, M. M. Noskov, A. V. Solokov, and B. A. Charikov, *Phys. Met. Metall.* **13**, 24 (1962).
2. M. M. Kirillova and B. A. Charikov, *Phys. Met. Metall.* **19**, 13 (1965).
3. A. P. Lenham and D. M. Treherne, in "Optical Properties and Electronic Structures of Metals and Alloys," (F. Abelès, ed.), North-Holland, Amsterdam, 196 (1966).
4. A. P. Lenham and D. M. Treherne, *J. Opt. Soc. Am.* **56**, 1076 (1966).
5. A. P. Lenham and D. M. Treherne, *J. Opt. Soc. Am.* **56**, 1137 (1966).
6. A. P. Lenham, *J. Opt. Soc. Am.* **57**, 473 (1967).
7. B. Sonntag, R. Haensel, and C. Kunz, *Solid State Commun.* **7**, 597 (1969).
8. A. Seignac and S. Robin, *C. R. Acad. Sc. Paris* **B271**, 919 (1970).
9. G. W. Simmons and E. J. Scheibner, *J. Appl. Phys.* **43**, 693 (1972).
10. P. B. Johnson and R. W. Christy, *Phys. Rev.* **B9**, 5056 (1974).
11. C. Wehenkel and B. Gauthé, *Phys. Lett.* **47A**, 253 (1974).
12. J. H. Weaver, D. W. Lynch, and C. G. Olson, *Phys. Rev.* **B10**, 501 (1974).
13. C. Wehenkel and B. Gauthé, *Phys. Status Solidi* **B64**, 515 (1974).
14. G. Chassaing, P. Gravier, M. Sigrist, and R. Pierrisnard, *Solid State Commun.* **15**, 1613 (1974).
15. M. R. Steel, *J. Phys. F: Metal Phys.* **4**, 783 (1974).
16. G. Chassaing, P. Gravier, and M. Sigrist, *Thin Solid Films* **35**, L25 (1976); *Thin Solid Films* **57**, 93 (1979).
17. R. Blickensderfer, D. K. Deardorff, and R. L. Lincoln, *J. Less Common Metals* **51**, 13 (1977).
18. J. E. Nestell, R. W. Christy, M. Cohen, and G. C. Ruben, *J. Appl. Phys.* **51**, 655 (1980).
19. J. E. Nestell and R. W. Christy, *Phys. Rev.* **B21**, 3173 (1980).
20. T. G. Lanskaya, R. I. Lyubinskaya, S. N. Svitasheva, K. K. Svitashev, *Sov. Phys. Tech. Phys.* **26**, 1115 (1981).
21. M. A. Ordal, R. J. Bell, R. W. Alexander, Jr., L. L. Long, M. R. Querry, *Appl. Opt.* **24**, 4493 (1985).
22. S. Mahmoud and Z. S. El Mandouh, *J. Mat. Sci.* **22**, 2852 (1987).
23. G. N. Zhizhin, V. I. Silin, and V. A. Yakovlev, *Sov. Phys. Solid State* **29**, 1224 (1987).
24. B. K. Agarwal and M. P. Givens, *Phys. Rev.* **108**, 658 (1957).
25. N. N. Axelrod and M. P. Givens, *Phys. Rev.* **120**, 1205 (1960).
26. R. H. Ritchie, *Phys. Rev.* **106**, 874 (1957).

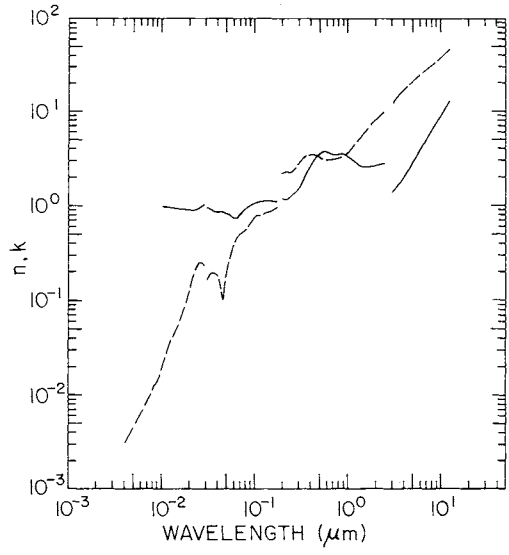


**Fig. 1.** Log–log plot of $n$ (solid line) and $k$ (dashed line) versus wavelength in micrometers for vanadium.

TABLE I

Values of $n$ and $k$ for Vanadium from Various References[a]

| eV | $cm^{-1}$ | Å | $n$ | $k$ |
|---|---|---|---|---|
| 300 | | 41.33 | | $3.0\times10^{-3}$ [7] |
| 275 | | 45.08 | | 3.9 |
| 250 | | 49.59 | | 4.8 |
| 225 | | 55.10 | | 5.7 |
| 200 | | 61.99 | | 6.6 |
| 195 | | 63.58 | | 6.9 |
| 190 | | 65.26 | | 7.2 |
| 185 | | 67.02 | | 7.6 |
| 180 | | 68.88 | | 8.0 |
| 175 | | 70.85 | | 8.5 |
| 170 | | 72.93 | | 8.9 |
| 165 | | 75.14 | | $9.5\times10^{-3}$ |
| 160 | | 77.49 | | $1.00\times10^{-2}$ |
| 155 | | 79.99 | | 1.08 |
| 150 | | 82.66 | | 1.14 |
| 145 | | 85.51 | | 1.22 |
| 140 | | 88.56 | | 1.29 |
| 135 | | 91.84 | | 1.38 |
| 130 | | 95.37 | | 1.46 |
| 125 | | 99.19 | | 1.67 |
| 120.0 | | 103.32 | 0.96 [13] | 1.96 [13] |
| 117.5 | | 105.52 | 0.96 | 2.09 |
| 115.0 | | 107.81 | 0.95 | 2.36 |
| 112.5 | | 110.21 | 0.95 | 2.50 |
| 110.0 | | 112.71 | 0.95 | 2.63 |
| 107.5 | | 115.34 | 0.95 | 2.77 |
| 105.0 | | 118.08 | 0.94 | 2.91 |
| 102.5 | | 120.96 | 0.94 | 3.19 |
| 100.0 | | 123.99 | 0.94 | 3.33 |
| 97.5 | | 127.16 | 0.94 | 3.74 |
| 95.0 | | 130.51 | 0.93 | 3.88 |
| 92.5 | | 134.04 | 0.93 | 4.04 |
| 90.0 | | 137.76 | 0.93 | 4.32 |
| 87.5 | | 141.70 | 0.92 | 4.60 |
| 85.0 | | 145.86 | 0.92 | 4.90 |
| 82.5 | | 150.29 | 0.92 | 5.19 |
| 80.0 | | 154.98 | 0.91 | 5.48 |
| 77.5 | | 159.98 | 0.91 | 6.06 |
| 75.0 | | 165.31 | 0.90 | 6.65 |
| 72.5 | | 171.01 | 0.90 | 7.24 |
| 70.0 | | 177.12 | 0.90 | 8.07 |
| 67.5 | | 183.68 | 0.89 | $9.29\times10^{-2}$ |
| 65.0 | | 190.75 | 0.88 | 0.10 |
| 62.5 | | 198.38 | 0.88 | 0.12 |
| 60.0 | | 206.64 | 0.87 | 0.14 |

[a] The references from which the values were extracted are given in brackets.

TABLE I (*Continued*)

Vanadium

| eV | $cm^{-1}$ | Å | $n$ | $k$ |
|---|---|---|---|---|
| 57.5 | | 215.63 | 0.86 | 0.16 |
| 55.0 | | 225.43 | 0.87 | 0.19 |
| 52.5 | | 236.16 | 0.89 | 0.22 |
| 50.0 | | 247.97 | 0.91 | 0.24 |
| 47.5 | | 261.02 | 0.94 | 0.25 |
| 45.0 | | 275.52 | 0.98 | 0.25 |
| 42.5 | | 291.73 | 1.01 | 0.23 |
| 40 | | 309.96 | 0.94 [8] | 0.16 [8] |
| 39 | | 317.91 | 0.93 | 0.17 |
| 38 | | 326.28 | 0.92 | 0.18 |
| 36 | | 344.40 | 0.89 | 0.19 |
| 35 | | 354.24 | 0.88 | 0.19 |
| 34 | | 364.66 | 0.86 | 0.19 |
| 33 | | 375.71 | 0.83 | 0.19 |
| 32 | | 387.45 | 0.83 | 0.18 |
| 31 | | 399.95 | 0.84 | 0.18 |
| 30 | | 413.28 | 0.84 | 0.16 |
| 29 | | 427.54 | 0.84 | 0.15 |
| 28 | | 442.80 | 0.84 | 0.12 |
| 27 | | 459.20 | 0.83 | 0.10 |
| 26 | | 476.87 | 0.83 | 0.13 |
| 25 | | 495.94 | 0.81 | 0.17 |
| 24 | | 516.60 | 0.80 | 0.22 |
| 23 | | 539.07 | 0.78 | 0.25 |
| 22 | | 563.57 | 0.76 | 0.29 |
| 21 | | 590.41 | 0.71 | 0.35 |
| 20 | | 619.93 | 0.71 | 0.42 |
| 19 | | 652.55 | 0.72 | 0.44 |
| 18 | | 688.81 | 0.78 | 0.48 |
| 17 | | 729.32 | 0.83 | 0.51 |
| 16 | | 774.91 | 0.87 | 0.52 |
| 15 | | 826.57 | 0.92 | 0.56 |
| 14 | | 885.61 | 0.97 | 0.61 |
| 13 | | 953.73 | 1.02 | 0.67 |
| eV | $cm^{-1}$ | $\mu$m | $n$ | $k$ |
| 12 | | 0.1033 | 1.04 | 0.72 |
| 11 | | 0.1127 | 1.08 | 0.76 |
| 10 | | 0.1240 | 1.10 | 0.80 |
| 9 | | 0.1378 | 1.11 | 0.83 |
| 8 | | 0.1550 | 1.10 | 0.87 |
| 7 | | 0.1771 | 1.09 | 0.95 |
| 6.0 | 48,393 | 0.2066 | 1.14 [19] | 2.18 [19] |
| 5.9 | 47,586 | 0.2101 | 1.14 | 2.20 |

*(continued)*

TABLE I (*Continued*)

Vanadium

| eV | $cm^{-1}$ | $\mu m$ | $n$ | $k$ |
|---|---|---|---|---|
| 5.8 | 46,780 | 0.2138 | 1.13 | 2.21 |
| 5.7 | 45,973 | 0.2175 | 1.12 | 2.22 |
| 5.6 | 45,167 | 0.2214 | 1.12 | 2.22 |
| 5.5 | 44,360 | 0.2254 | 1.13 | 2.21 |
| 5.4 | 43,554 | 0.2296 | 1.14 | 2.21 |
| 5.3 | 42,747 | 0.2339 | 1.16 | 2.21 |
| 5.2 | 41,940 | 0.2384 | 1.17 | 2.21 |
| 5.1 | 41,134 | 0.2431 | 1.20 | 2.18 |
| 5.0 | 40,327 | 0.2480 | 1.23 | 2.19 |
| 4.9 | 39,521 | 0.2530 | 1.26 | 2.20 |
| 4.8 | 38,714 | 0.2583 | 1.30 | 2.20 |
| 4.7 | 37,908 | 0.2638 | 1.30 | 2.29 |
| 4.6 | 37,101 | 0.2695 | 1.32 | 2.35 |
| 4.5 | 36,295 | 0.2755 | 1.34 | 2.42 |
| 4.4 | 35,488 | 0.2818 | 1.39 | 2.50 |
| 4.3 | 34,682 | 0.2883 | 1.41 | 2.57 |
| 4.2 | 33,875 | 0.2952 | 1.46 | 2.65 |
| 4.1 | 33,068 | 0.3024 | 1.51 | 2.73 |
| 4.0 | 32,262 | 0.3100 | 1.56 | 2.81 |
| 3.9 | 31,455 | 0.3179 | 1.64 | 2.89 |
| 3.8 | 30,649 | 0.3263 | 1.73 | 2.97 |
| 3.7 | 29,842 | 0.3351 | 1.84 | 3.06 |
| 3.6 | 29,036 | 0.3444 | 1.96 | 3.14 |
| 3.5 | 28,230 | 0.3542 | 2.07 | 3.22 |
| 3.4 | 27,423 | 0.3647 | 2.18 | 3.26 |
| 3.3 | 26,616 | 0.3757 | 2.30 | 3.31 |
| 3.2 | 25,809 | 0.3875 | 2.42 | 3.33 |
| 3.1 | 25,003 | 0.4000 | 2.55 | 3.38 |
| 3.0 | 24,196 | 0.4133 | 2.71 | 3.38 |
| 2.9 | 23,390 | 0.4275 | 2.84 | 3.42 |
| 2.8 | 22,583 | 0.4428 | 3.03 | 3.40 |
| 2.7 | 21,777 | 0.4592 | 3.19 | 3.38 |
| 2.6 | 20,970 | 0.4769 | 3.36 | 3.33 |
| 2.5 | 20,164 | 0.4959 | 3.53 | 3.26 |
| 2.4 | 19,357 | 0.5166 | 3.63 | 3.15 |
| 2.3 | 18,551 | 0.5391 | 3.68 | 3.05 |
| 2.2 | 17,744 | 0.5636 | 3.68 | 2.98 |
| 2.1 | 16,937 | 0.5904 | 3.65 | 2.94 |
| 2.0 | 16,131 | 0.6199 | 3.55 | 2.93 |
| 1.9 | 15,324 | 0.6526 | 3.50 | 2.99 |
| 1.8 | 14,518 | 0.6888 | 3.43 | 3.05 |
| 1.7 | 13,711 | 0.7293 | 3.41 | 3.08 |
| 1.6 | 12,905 | 0.7749 | 3.42 | 3.14 |
| 1.5 | 12,098 | 0.8266 | 3.47 | 3.18 |
| 1.4 | 11,292 | 0.8856 | 3.43 | 3.22 |

*(continued)*

TABLE I (*Continued*)

Vanadium

| eV | $cm^{-1}$ | $\mu m$ | $n$ | $k$ |
|---|---|---|---|---|
| 1.3 | 10,485 | 0.9537 | 3.38 | 3.31 |
| 1.2 | 9,679 | 1.0332 | 3.19 | 3.54 |
| 1.1 | 8,872 | 1.1271 | 2.95 | 3.87 |
| 1.0 | 8,065 | 1.2399 | 2.69 | 4.43 |
| 0.9 | 7,259 | 1.3776 | 2.56 | 5.02 |
| 0.8 | 6,452 | 1.5498 | 2.52 | 5.77 |
| 0.7 | 5,646 | 1.7712 | 2.56 | 6.83 |
| 0.6 | 4,840 | 2.0664 | 2.62 | 8.19 |
| 0.5 | 4,033 | 2.4797 | 2.72 | 9.73 |
| 0.40 | 3,226 | 3.100 | 1.38 [12] | 11.90 [12] |
| 0.36 | 2,904 | 3.440 | 1.57 | 13.32 |
| 0.32 | 2,581 | 3.875 | 1.79 | 15.08 |
| 0.28 | 2,258 | 4.428 | 2.13 | 17.35 |
| 0.24 | 1,936 | 5.166 | 2.82 | 20.32 |
| 0.20 | 1,613 | 6.199 | 3.90 | 24.30 |
| 0.16 | 1,290 | 7.749 | 5.77 | 30.03 |
| 0.12 | 968 | 10.332 | 9.51 | 38.97 |
| 0.10 | 806 | 12.400 | 12.83 | 45.89 |

# Aluminum Arsenide (AlAs)

EDWARD D. PALIK
Institute for Physical Science and Technology
University of Maryland
College Park, Maryland

O. J. GLEMBOCKI
Naval Research Laboratory
Washington, D.C.
and

KENICHI TAKARABE
Department of Natural Science
Okayama University of Science
Okayama-City
Okayama 700, Japan

Although AlAs is one end of the important superlattice material $Al_xGa_{1-x}As$, it has not been investigated nearly as much because of its hydroscopic nature. This has necessitated some care in experiment often with a thin capping of GaAs, especially for superlattice structures containing alternate layers of AlAs and GaAs. Such a multilayer sample is more complicated to analyze if one wishes to extract $n$ and $k$ from spectroscopic ellipsometry or reflection–transmission experiments. The data chosen for this critique are listed in Table I and plotted in Fig. 1. Because there are several sources of data in a given energy range, we have chosen to list these separately rather than interspersing the data. Thus, in Table I the eV scale does not run consecutively but sometimes backs up to introduce new data with a bracket reference. This is usually indicated with a space.

At high energy we have used values of $n$ and $k$ obtained from a Henke-model calculation [1, 2] in the range 10,000–51.57 eV (1.240–240.4 Å). The atomic absorption edges are found at $K(\mathrm{Al}) = 1559.8$ eV, $K(\mathrm{As}) = 11{,}865$ eV, $L_1(\mathrm{Al}) = 87.01$ eV, $L_1(\mathrm{As}) = 1529.3$ eV, $L_{2,3}(\mathrm{Al}) = 72.78$ eV, $L_2(\mathrm{As}) = 1358.7$ eV, $L_3(\mathrm{As}) = 1323.5$ eV.

A gap appears to exist in experimental reflectivity data between 51 and ~6 eV, so no $n$ and $k$ data are available.

The region 5.6–1.7 eV has been studied with spectroscopic ellipsometry by Garriga *et al.* [3]. The AlAs sample was 1 μm thick, grown on a GaAs


Copyright © 1991 by Academic Press.
All rights of reproduction in any form reserved.
ISBN 0-12-544422-2

(100) substrate; it was capped with a 17 Å GaAs layer. A multilayer model was used to extract the optical constants. A 6 Å oxide layer was assumed on top of the GaAs capping layer. We have read an expanded graph of $\varepsilon_1$ and $\varepsilon_2$ and calculated $n$ and $k$ using the equations

$$2n^2 = \varepsilon_1 + \sqrt{\varepsilon_1^2 + \varepsilon_2^2}$$

$$2k^2 = -\varepsilon_1 + \sqrt{\varepsilon_1^2 + \varepsilon_2^2}.$$

We carry three figures, but the data are surely not that good. The direct gap at 3.0 eV was defined in a fit of the absorption coefficient $\alpha$ versus eV, assuming a lineshape of a broadened two-dimensional interband minimum. These data are significantly different from data of Yim [4], who measured the transmission of bulk platelets of AlAs and determined both the indirect gap at 2.14 and the direct gap at 3.14 eV; this latter value is significantly different from that of Garriga *et al.*, and the $k$ values are over an order of magnitude different; $k = 6.38 \times 10^{-2}$ at 3.0 eV [3] and $k = 1.79 \times 10^{-3}$ at 3.0 eV [4]. We have not found other measurements of $k$ at the direct gap for comparison. To interpret the systematic variation of photoluminescence peak energies of GaAs/AlAs short-period superlattices, Nakayama *et al.* [5] cited values of 2.223 eV for the indirect gap and 3.125 eV for the direct gap of AlAs at 77 K.

An example of accuracy in reading two different graphs in the same paper is given for the values of $k$ at 3.0 eV [3]: $5.3 \times 10^{-2}$ from a graph of $\varepsilon_1$, $\varepsilon_2$ and $6.38 \times 10^{-2}$ from a graph of $\alpha$. This represents a 20% variation.

The 300 K values of index of refraction for energies below the direct gap has been measured by Fern and Onton [6] using the minimum-deviation method and a wedge-shaped sample (20°) of multigrained material. The experimental data were fit with the equation

$$\varepsilon = \varepsilon_r - i\varepsilon_i = \varepsilon_x + \frac{S_1 E_1^2}{E_1^2 - E^2 + iE\gamma_1} + \frac{S_2 E_2^2}{E_2^2 - E^2 + iE\gamma_2},$$

where $\varepsilon_x$ represents the contribution to the dielectric constant by higher energy processes above the $E_1$ and $E_2$ interband transitions, and $S_i$ and $\gamma_i$ are the oscillator strength and damping constant of the $E_1$ and $E_2$ "oscillators." Finally, $n$ is determined from $n = \mathrm{Re}[\varepsilon^{1/2}]$. This approximation is possible because in the spectral range of the measurements (<2.218 eV) the contribution from $\varepsilon_i$ is very small. The fitting process reproduced the experimental data for $n$ to $\pm 0.008$ by using $E_1 = 3.9$ eV, $E_2 = 4.54$ eV, $S_1 = 3.019$, $S_2 = 3.030$, $\gamma_1 = 0.503$ eV, $\gamma_2 = 2.101$ eV, and $\varepsilon_x = 2.114$.

Monemar [7] used interference fringes to obtain 300 K values of $n$ below the band gap for bulk samples. However, these values are considerably smaller (about $-0.06$) than those of Fern and Onton. A model of Adachi [8] for the system $Al_xGa_{1-x}As$ gives values of $n$ much closer to Fern and Onton (presumably because the adjustable constants were chosen to fit these data) as does an extrapolation of the values for $Al_xGa_{1-x}As$ by Aspnes *et al.* [9]; for example, at 1.5 eV $n=2.995$ [6], 2.936 [7], 3.01 [8], and ~3.01 [9]. We elect to stress the experimental data of Fern and Onton but also show the calculated data [8] over a somewhat wider spectral range. Lorenz [10] measured $n=3.3$ at 2.2 eV, this number being about $+0.1$ larger than that of Fern and Onton at 2.2 eV. Such variations are probably due to the quality of the various samples.

In the lattice-vibration region, the reststrahlen spectrum has been measured by Rheinlander and Neumann [11] for bulk thin plates, but no optical constants were obtained by fitting an oscillator model to the data. The data of Minden [12] do not appear to be consistent with the results of Ref. [11], which we must attribute to the quality of the epilayers used in Ref. [12]. Minden measured $R$ and $T$ in the 1300–1400 $cm^{-1}$ region for an epitaxial layer of AlAs grown on a GaAs substrate. The sample oxidized rapidly when brought out into the laboratory, and the data, which took several hours to obtain, surely contained effects of this layer. Although we expect an oxidation layer to be thin and transparent and not to perturb the results in the long-wave infrared, it is not clear what sort of material the hydroscopic nature of AlAs will produce on the surface.

Perkowitz *et al.* and Sudharsanan *et al.* [13, 14] have measured a heterostructure consisting of several layers of GaAs and AlAs. The substrate was 350 μm of undoped GaAs; on this were a 1 μm epitaxial layer of GaAs, a 0.2 μm layer of undoped AlAs, a 1 μm layer of Si-doped AlAs (the sample) and a capping layer of 250 Å of undoped GaAs. Measurements of reflectivity were performed from 200–450 $cm^{-1}$ with reststrahlen peaks of AlAs and GaAs appearing along with interference fringes. Although the fit with a multilayer model was qualitatively good, the magnitudes were not matched very well except at the reststrahlen peaks. The parameters for GaAs were assumed to be known. The parameters for AlAs for a Lorentz-oscillator model of the form

$$\varepsilon = \varepsilon_\infty + \frac{S\nu_T^2}{\nu_T^2 - \nu^2 - i\nu\gamma}$$

were determined to be $\nu_T = 361.8\ cm^{-1}$, $S = 1.9$, $\gamma = 8.0\ cm^{-1}$, $\varepsilon_\infty = 8.2$. At low frequency, the dc dielectric constant is $\varepsilon_o = 10.1$.

Interestingly, the Raman spectrum yields most of the parameters needed

to calculate the IR spectrum. From Raman data, Onton [15] determined $\nu_T = 361.8\ \text{cm}^{-1}$, $S = 1.90$, and $\gamma = 0.97\ \text{cm}^{-1}$, and chose $\varepsilon_\infty = 7.8$. These can be used in the above formula to determine $n$ and $k$ also. The only drastic difference in the two sets of parameters is in the values of $\gamma$; the line width $0.97\ \text{cm}^{-1}$ seems too small [15], while the line width $8.0\ \text{cm}^{-1}$ seems too large [13, 14] for typical semiconductors. We calculated the reflectivity with both sets and found that the parameters of Perkowitz *et al.* give a better fit to the reflectivity in Ref. [11], agreeing with the experimental $R$ within a few reflectivity percentage units almost everywhere; this assumes an uncertainty of a few $\text{cm}^{-1}$ in the wave number axis as well. We did not attempt to refit the $R$ data to obtain independent values of $n$ and $k$, however. Therefore, we have listed these values [13, 14] in Table I.

Experimental transmission data for the two-phonon spectrum above $\nu_T$ were not found.

**ACKNOWLEDGMENTS**

We thank W. R. Hunter for providing the $n$ and $k$ values calculated from the Henke model.

**REFERENCES**

1. B. L. Henke, P. Lee, T. J. Tanaka, R. L. Shimabukuro, and B. K. Fujikama, *At. Data Nucl. Data Tables* **27**, 1 (1982).
2. B. L. Henke, J. C. Davis, E. M. Gullickson, and R. C. C. Perera, Lawrence Berkeley Laboratory Report No. LBL-26259 (1988).
3. M. Garriga, P. Lautenschlager, M. Cardona, and K. Ploog, *Solid State Commun.* **61**, 157 (1987).
4. W. M. Yim, *J. Appl. Phys.* **42**, 2854 (1971).
5. M. Nakayama, I. Tanaka, I. Kimura, and H. Nishimura, *Jpn. J. Appl. Phys.* **29**, 41 (1990).
6. R. E. Fern and A. Onton, *J. Appl. Phys.* **42**, 3499 (1971).
7. B. Monemar, *Solid State Commun.* **8**, 2121 (1970).
8. S. Adachi, *J. Appl. Phys.* **58**, R1 (1985).
9. D. E. Aspnes, S. M. Kelso, R. A. Logan and R. Bhat, *J. Appl. Phys.* **60**, 754 (1986).
10. M. R. Lorenz, R. Chicotka, and G. D. Pettit, *Solid State Commun.* **8**, 693 (1970).
11. B. Rheinlander and H. Neumann, *Phys. Status Solidi* **(b)45**, K9 (1971).
12. H. T. Minden, *Appl. Phys. Lett.* **17**, 358 (1970).
13. S. Perkowitz, R. Sudharsanan, S. S. Yom, and T. J. Drummond, *Solid State Commun.* **62**, 645 (1987).
14. R. Sudharsanan, S. Perkowitz, S. S. Yom, and T. J. Drummond, *Proc. SPIE* **794**, 197 (1987).
15. A. Onton, in "Proc. 10th Intern. Conf. on the Physics of Semiconductors," U.S. Atomic Energy Commission, Washington, 107 (1970).

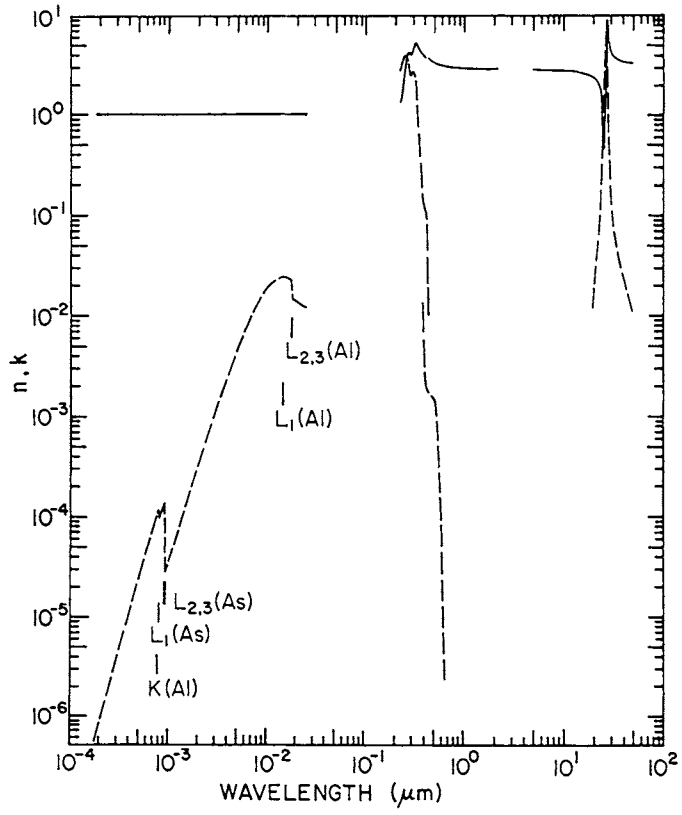


**Fig. 1.** Log–log plot of $n$ (solid line) and $k$ (dashed line) versus wavelength in micrometers for aluminum arsenide.

TABLE I

Values of $n$ and $k$ for Aluminum Arsenide Obtained from Various References[a]

| eV | $cm^{-1}$ | Å | n | k |
|---|---|---|---|---|
| 10000 | | 1.240 | 0.99999320[1] | $1.33 \times 10^{-7}$[1] |
| 9772 | | 1.269 | 0.99999280 | 1.45 |
| 9331 | | 1.329 | 0.99999210 | 1.73 |
| 8909 | | 1.392 | 0.99999130 | 2.07 |
| 8507 | | 1.458 | 0.99999050 | 2.47 |
| 8123 | | 1.526 | 0.9999895 | 2.94 |
| 7756 | | 1.599 | 0.9999884 | 3.50 |
| 7406 | | 1.674 | 0.9999873 | 4.18 |
| 7072 | | 1.753 | 0.9999861 | 4.97 |
| 6752 | | 1.836 | 0.9999846 | 5.92 |
| 6447 | | 1.923 | 0.9999831 | 7.05 |
| 6156 | | 2.014 | 0.9999815 | 8.40 |
| 5878 | | 2.109 | 0.9999796 | $9.99 \times 10^{-7}$ |
| 5613 | | 2.209 | 0.9999776 | $1.19 \times 10^{-6}$ |
| 5359 | | 2.314 | 0.9999754 | 1.41 |
| 5117 | | 2.423 | 0.9999730 | 1.68 |
| 4886 | | 2.538 | 0.9999703 | 2.00 |
| 4665 | | 2.658 | 0.9999674 | 2.38 |
| 4455 | | 2.783 | 0.9999642 | 2.83 |
| 4254 | | 2.915 | 0.9999607 | 3.36 |
| 4062 | | 3.053 | 0.9999568 | 3.99 |
| 3878 | | 3.197 | 0.9999526 | 4.74 |
| 3703 | | 3.348 | 0.9999480 | 5.63 |
| 3536 | | 3.506 | 0.9999429 | 6.67 |
| 3376 | | 3.672 | 0.9999374 | 7.92 |
| 3224 | | 3.846 | 0.9999313 | $9.39 \times 10^{-6}$ |
| 3078 | | 4.028 | 0.9999248 | $1.11 \times 10^{-5}$ |
| 2939 | | 4.218 | 0.9999176 | 1.32 |
| 2807 | | 4.418 | 0.9999099 | 1.56 |
| 2680 | | 4.627 | 0.9999015 | 1.84 |
| 2559 | | 4.846 | 0.999893 | 2.18 |
| 2443 | | 5.075 | 0.999883 | 2.58 |
| 2333 | | 5.315 | 0.999872 | 3.04 |
| 2228 | | 5.566 | 0.999861 | 3.59 |
| 2127 | | 5.829 | 0.999850 | 4.22 |
| 2031 | | 6.105 | 0.999838 | 4.97 |
| 1939 | | 6.394 | 0.999825 | 5.83 |
| 1852 | | 6.696 | 0.999813 | 6.85 |
| 1768 | | 7.013 | 0.999802 | 8.03 |
| 1688 | | 7.344 | 0.999792 | $9.40 \times 10^{-5}$ |
| 1650 | | 7.516 | 0.999789 | $1.02 \times 10^{-4}$ |
| 1612 | | 7.691 | 0.999788 | 1.10 |
| 1575 | | 7.871 | 0.999796 | 1.19 |
| 1539 | | 8.055 | 0.999794 | $1.03 \times 10^{-4}$ |
| 1504 | | 8.244 | 0.999782 | $9.80 \times 10^{-5}$ |
| 1470 | | 8.436 | 0.999771 | $1.06 \times 10^{-4}$ |
| 1436 | | 8.633 | 0.999766 | 1.14 |
| 1403 | | 8.835 | 0.999765 | 1.22 |

TABLE I (*Continued*)

Aluminumn Arsenide

| eV | $cm^{-1}$ | Å | n | k |
|---|---|---|---|---|
| 1371 | | 9.041 | 0.999772 | 1.32 |
| 1340 | | 9.253 | 0.999811 | $1.42 \times 10^{-4}$ |
| 1309 | | 9.469 | 0.999801 | $2.76 \times 10^{-5}$ |
| 1280 | | 9.690 | 0.999749 | 2.99 |
| 1250 | | 9.917 | 0.999716 | 3.23 |
| 1222 | | 10.15 | 0.999688 | 3.50 |
| 1167 | | 10.63 | 0.999639 | 4.10 |
| 1114 | | 11.13 | 0.999590 | 4.80 |
| 1064 | | 11.66 | 0.999539 | 5.62 |
| 1016 | | 12.21 | 0.999486 | 6.58 |
| 969.7 | | 12.79 | 0.999429 | 7.70 |
| 925.9 | | 13.39 | 0.999367 | $9.01 \times 10^{-5}$ |
| 884.1 | | 14.02 | 0.999299 | $1.05 \times 10^{-4}$ |
| 844.2 | | 14.69 | 0.999226 | 1.23 |
| 806.0 | | 15.38 | 0.999147 | 1.44 |
| 769.7 | | 16.11 | 0.999060 | 1.68 |
| 734.9 | | 16.87 | 0.99897 | 1.95 |
| 701.7 | | 17.67 | 0.99886 | 2.27 |
| 670.0 | | 18.51 | 0.99875 | 2.63 |
| 639.8 | | 19.38 | 0.99863 | 3.08 |
| 610.9 | | 20.30 | 0.99850 | 3.58 |
| 583.3 | | 21.26 | 0.99836 | 4.16 |
| 557.0 | | 22.26 | 0.99820 | 4.83 |
| 531.8 | | 23.31 | 0.99803 | 5.59 |
| 507.8 | | 24.42 | 0.99785 | 6.47 |
| 484.9 | | 25.57 | 0.99766 | 7.47 |
| 463.0 | | 26.78 | 0.99745 | 8.63 |
| 442.1 | | 28.05 | 0.99722 | $9.95 \times 10^{-4}$ |
| 422.1 | | 29.37 | 0.99699 | $1.14 \times 10^{-3}$ |
| 403.0 | | 30.76 | 0.99673 | 1.32 |
| 384.8 | | 32.22 | 0.99646 | 1.51 |
| 367.5 | | 33.74 | 0.99617 | 1.71 |
| 350.9 | | 35.34 | 0.99585 | 1.96 |
| 335.0 | | 37.01 | 0.99552 | 2.23 |
| 319.9 | | 38.76 | 0.99516 | 2.55 |
| 305.5 | | 40.59 | 0.99479 | 2.92 |
| 291.7 | | 42.51 | 0.99441 | 3.34 |
| 278.5 | | 44.52 | 0.99404 | 3.81 |
| 265.9 | | 46.63 | 0.99368 | 4.33 |
| 253.9 | | 48.83 | 0.99330 | 4.87 |
| 242.5 | | 51.14 | 0.99289 | 5.48 |
| 231.5 | | 53.56 | 0.99250 | 6.16 |
| 221.1 | | 56.09 | 0.99210 | 6.95 |
| 211.1 | | 58.74 | 0.99182 | 7.83 |
| 201.5 | | 61.52 | 0.99156 | 8.65 |
| 192.4 | | 64.43 | 0.99126 | $9.58 \times 10^{-3}$ |
| 183.7 | | 67.48 | 0.99106 | $1.06 \times 10^{-2}$ |
| 175.5 | | 70.67 | 0.99101 | 1.17 |
| 167.5 | | 74.01 | 0.99093 | 1.26 |

TABLE I (*Continued*)

Aluminumn Arsenide

| eV | $cm^{-1}$ | Å | n | k |
|---|---|---|---|---|
| 160.0 | | 77.51 | 0.99087 | 1.37 |
| 152.7 | | 81.17 | 0.99086 | 1.48 |
| 149.3 | | 83.07 | 0.99092 | 1.54 |
| 145.8 | | 85.01 | 0.99102 | 1.60 |
| 142.5 | | 87.00 | 0.99112 | 1.65 |
| 139.3 | | 89.03 | 0.99119 | 1.71 |
| 136.1 | | 91.11 | 0.99128 | 1.76 |
| 133.0 | | 93.24 | 0.99139 | 1.82 |
| 129.9 | | 95.42 | 0.99153 | 1.88 |
| 127.0 | | 97.66 | 0.99176 | 1.94 |
| 124.1 | | 99.94 | 0.99212 | 2.00 |
| 121.2 | | 102.3 | 0.99248 | 2.04 |
| 118.5 | | 104.7 | 0.99273 | 2.07 |
| 115.8 | | 107.1 | 0.99294 | 2.10 |
| 113.1 | | 109.6 | 0.99312 | 2.14 |
| 110.5 | | 112.2 | 0.99330 | 2.17 |
| 108.0 | | 114.8 | 0.99349 | 2.20 |
| 105.5 | | 117.5 | 0.99368 | 2.24 |
| 103.1 | | 120.2 | 0.99389 | 2.27 |
| 100.8 | | 123.0 | 0.99411 | 2.30 |
| 98.47 | | 125.9 | 0.99435 | 2.33 |
| 96.22 | | 128.9 | 0.99461 | 2.36 |
| 94.03 | | 131.9 | 0.99484 | 2.38 |
| 91.88 | | 134.9 | 0.99506 | 2.40 |
| 89.78 | | 138.1 | 0.99532 | 2.42 |
| 87.73 | | 141.3 | 0.99567 | 2.44 |
| 85.73 | | 144.6 | 0.99627 | 2.44 |
| 83.77 | | 148.0 | 0.99664 | 2.41 |
| 81.85 | | 151.5 | 0.99686 | 2.38 |
| 79.99 | | 155.0 | 0.99704 | 2.35 |
| 78.16 | | 158.6 | 0.99726 | 2.32 |
| 76.37 | | 162.3 | 0.99762 | 2.29 |
| 74.63 | | 166.1 | 0.99847 | 2.26 |
| 72.92 | | 170.0 | 1.00073 | 2.23 |
| 71.26 | | 174.0 | 0.99803 | 1.43 |
| 69.63 | | 178.1 | 0.99493 | 1.43 |
| 68.04 | | 182.2 | 0.99292 | 1.42 |
| 66.49 | | 186.5 | 0.99125 | 1.41 |
| 64.97 | | 190.8 | 0.98960 | 1.39 |
| 63.49 | | 195.3 | 0.98799 | 1.37 |
| 62.04 | | 199.9 | 0.98635 | 1.35 |
| 60.62 | | 204.5 | 0.98469 | 1.32 |
| 59.24 | | 209.3 | 0.98292 | 1.30 |
| 57.88 | | 214.2 | 0.98103 | 1.27 |
| 56.56 | | 219.2 | 0.97903 | 1.25 |
| 55.27 | | 224.3 | 0.97692 | 1.23 |
| 54.01 | | 229.6 | 0.97470 | 1.21 |
| 52.77 | | 234.9 | 0.97236 | 1.20 |
| 51.57 | | 240.4 | 0.96977 | $1.18 \times 10^{-2}$ |

TABLE I (*Continued*)

Aluminumn Arsenide

| eV | $cm^{-1}$ | μm | n | k |
|---|---|---|---|---|
| 5.6 | 45,167 | 0.2214 | 1.36[3] | 2.75[3] |
| 5.5 | 44,360 | 0.2254 | 1.36 | 2.89 |
| 5.4 | 43,554 | 0.2296 | 1.36 | 3.12 |
| 5.3 | 42,747 | 0.2339 | 1.53 | 3.40 |
| 5.2 | 41,940 | 0.2384 | 1.77 | 3.65 |
| 5.1 | 41,134 | 0.2431 | 2.16 | 3.86 |
| 5.0 | 40,327 | 0.2480 | 2.48 | 3.95 |
| 4.9 | 39,521 | 0.2630 | 2.92 | 4.04 |
| 4.8 | 38,714 | 0.2583 | 3.48 | 4.02 |
| 4.7 | 37,908 | 0.2638 | 3.96 | 3.70 |
| 4.6 | 37,101 | 0.2695 | 4.22 | 3.09 |
| 4.5 | 36,295 | 0.2755 | 4.18 | 2.63 |
| 4.4 | 35,088 | 0.2818 | 4.04 | 2.52 |
| 4.3 | 34,682 | 0.2883 | 4.01 | 2.52 |
| 4.2 | 33,875 | 0.2952 | 4.11 | 2.63 |
| 4.1 | 33,068 | 0.3024 | 4.47 | 2.68 |
| 4.0 | 32,262 | 0.3100 | 4.92 | 2.49 |
| 3.9 | 31,455 | 0.3179 | 5.35 | 2.15 |
| 3.8 | 30,649 | 0.3263 | 5.39 | 1.30 |
| 3.7 | 29,842 | 0.3351 | 4.99 | 0.752 |
| 3.6 | 29,036 | 0.3444 | 4.72 | 0.519 |
| 3.5 | 28,229 | 0.3542 | 4.48 | 0.334 |
| 3.4 | 27,423 | 0.3647 | 4.30 | 0.233 |
| 3.3 | 26,616 | 0.3757 | 4.13 | 0.139 |
| 3.2 | 25,810 | 0.3875 | 3.93 | 0.115 |
| 3.1 | 25,003 | 0.4000 | 3.77 | 0.113 |
| 3.0 | 24,196 | 0.4133 | 3.77 | $5.3 \times 10^{-2}$ |
| 3.15 | 25,406 | 0.3936 | | 0.119[3] |
| 3.12 | 25,205 | 0.3968 | | 0.115 |
| 3.10 | 25,003 | 0.4000 | | 0.113 |
| 3.075 | 24,801 | 0.4032 | | 0.110 |
| 3.05 | 24,600 | 0.4065 | | 0.106 |
| 3.025 | 24,398 | 0.4099 | | $9.98 \times 10^{-2}$ |
| 3.00 | 24,196 | 0.4133 | | 6.38 |
| 2.975 | 23,995 | 0.4168 | | 3.15 |
| 2.95 | 23,793 | 0.4203 | | 1.89 |
| 2.925 | 23,592 | 0.4239 | | 1.18 |
| 2.90 | 23,390 | 0.4275 | | 1.05 |
| 2.875 | 23,188 | 0.4313 | | $1.03 \times 10^{-2}$ |
| 2.85 | 22,987 | 0.4305 | | $9.93 \times 10^{-3}$ |
| 3.35 | 27,019 | 0.3701 | | $1.38 \times 10^{-2}$[4] |
| 3.3 | 26,616 | 0.3757 | | $3.81 \times 10^{-3}$ |
| 3.25 | 26,213 | 0.3815 | | 3.21 |
| 3.2 | 25,810 | 0.3875 | | 2.43 |
| 3.1 | 25,003 | 0.4000 | | 1.94 |
| 3.0 | 24,196 | 0.4133 | | 1.79 |
| 2.9 | 23,390 | 0.4275 | 3.919[8] | 1.67 |

TABLE I (*Continued*)

Aluminumn Arsenide

| eV | $cm^{-1}$ | μm | n | k |
|---|---|---|---|---|
| 2.8 | 22,583 | 0.4428 | 3.703 | 1.61 |
| 2.7 | 21,777 | 0.4592 | 3.570 | 1.56 |
| 2.6 | 20,970 | 0.4769 | 3.472 | 1.53 |
| 2.5 | 20,164 | 0.4959 | 3.394 | $1.25 \times 10^{-3}$ |
| 2.4 | 19,357 | 0.5166 | 3.329 | $6.82 \times 10^{-4}$ |
| 2.3 | 18,551 | 0.5391 | 3.273 | $2.75 \times 10^{-4}$ |
| 2.2 | 17,744 | 0.5636 | 3.225 | $4.04 \times 10^{-5}$ |
| 2.1 | 16,938 | 0.5904 | 3.183 | $2.30 \times 10^{-6}$ |
| 2.0 | 16,131 | 0.6199 | 3.145 | |
| 1.9 | 15,324 | 0.6526 | 3.112 | |
| 1.8 | 14,518 | 0.6888 | 3.082 | |
| 1.7 | 13,711 | 0.7293 | 3.056 | |
| 1.6 | 12,905 | 0.7749 | 3.032 | |
| 1.5 | 12,098 | 0.8266 | 3.010 | |
| 1.4 | 11,292 | 0.8856 | 2.990 | |
| 1.3 | 10,485 | 0.9537 | 2.973 | |
| 1.2 | 9,679 | 1.033 | 2.957 | |
| 1.1 | 8,872 | 1.127 | 2.943 | |
| 1.0 | 8,065 | 1.157 | 2.930 | |
| 0.9 | 7,259 | 1.378 | 2.919 | |
| 0.8 | 6,452 | 1.550 | 2.909 | |
| 0.7 | 5,646 | 1.771 | 2.901 | |
| 0.6 | 4,839 | 2.066 | 2.894 | |
| 0.5 | 4,033 | 2.480 | 2.888 | |
| 2.218 | 17,889 | 0.5590 | 3.201[6] | |
| 2.187 | 17,639 | 0.5669 | 3.189 | |
| 2.053 | 16,558 | 0.6039 | 3.139 | |
| 1.934 | 15,599 | 0.6411 | 3.102 | |
| 1.831 | 14,768 | 0.6771 | 3.072 | |
| 1.741 | 14,042 | 0.7121 | 3.049 | |
| 1.660 | 13,389 | 0.7469 | 3.029 | |
| 1.583 | 12,768 | 0.7832 | 3.012 | |
| 1.573 | 12,687 | 0.7882 | 3.009 | |
| 1.550 | 12,501 | 0.7999 | 3.005 | |
| 1.517 | 12,235 | 0.8173 | 2.999 | |
| 1.506 | 12,147 | 0.8233 | 2.995 | |
| 1.447 | 11,671 | 0.8568 | 2.983 | |
| 1.374 | 11,082 | 0.9024 | 2.970 | |
| 1.312 | 10,582 | 0.9450 | 2.960 | |
| 1.256 | 10,130 | 0.9871 | 2.951 | |
| 1.240 | 10,001 | 0.9999 | 2.948 | |
| 1.192 | 9,614 | 1.040 | 2.942 | |
| 1.033 | 8,332 | 1.200 | 2.919 | |
| 0.775 | 6,251 | 1.600 | 2.892 | |
| 0.620 | 5,001 | 2.000 | 2.876 | |
| 0.564 | 4,549 | 2.198 | 2.875 | |
| 0.2480 | 2,000 | 5.000 | 2.85[13,14] | |
| 0.1860 | 1,500 | 6.667 | 2.84 | |

TABLE I (*Continued*)

Aluminumn Arsenide

| eV | $cm^{-1}$ | μm | n | k |
|---|---|---|---|---|
| 0.1240 | 1,000 | 10.00 | 2.81 | |
| 0.1116 | 900 | 11.11 | 2.80 | |
| 0.09919 | 800 | 12.50 | 2.78 | |
| 0.08679 | 700 | 14.29 | 2.74 | $2.0 \times 10^{-3}$ [13,14] |
| 0.07439 | 600 | 16.67 | 2.67 | $4.3 \times 10^{-3}$ |
| 0.06199 | 500 | 20.00 | 2.47 | $1.4 \times 10^{-2}$ |
| 0.05579 | 450 | 22.22 | 2.18 | $4.0 \times 10^{-2}$ |
| 0.05331 | 430 | 23.26 | 1.90 | $7.7 \times 10^{-2}$ |
| 0.05207 | 420 | 23.81 | 1.67 | 0.12 |
| 0.05145 | 415 | 24.10 | 1.50 | 0.16 |
| 0.05083 | 410 | 24.39 | 1.27 | 0.23 |
| 0.05021 | 405 | 24.69 | 0.95 | 0.38 |
| 0.04959 | 400 | 25.00 | 0.60 | 0.78 |
| 0.04897 | 395 | 25.32 | 0.46 | 1.33 |
| 0.04835 | 390 | 25.64 | 0.45 | 1.87 |
| 0.04773 | 385 | 25.97 | 0.51 | 2.44 |
| 0.04711 | 380 | 26.32 | 0.63 | 3.12 |
| 0.04649 | 375 | 26.67 | 0.90 | 4.00 |
| 0.04587 | 370 | 27.03 | 1.57 | 5.25 |
| 0.04525 | 365 | 27.40 | 3.78 | 6.90 |
| 0.04486 | 361.8 | 27.64 | 6.87 | 6.25 |
| 0.04463 | 360 | 27.78 | 7.84 | 4.57 |
| 0.04401 | 355 | 28.17 | 6.99 | 1.59 |
| 0.04339 | 350 | 28.57 | 5.95 | 0.75 |
| 0.04215 | 340 | 29.41 | 4.90 | 0.29 |
| 0.04092 | 330 | 30.30 | 4.40 | 0.15 |
| 0.03968 | 320 | 31.25 | 4.11 | $9.5 \times 10^{-2}$ |
| 0.03844 | 310 | 32.26 | 3.91 | $6.5 \times 10^{-2}$ |
| 0.03720 | 300 | 33.33 | 3.78 | $4.7 \times 10^{-2}$ |
| 0.03100 | 250 | 40.00 | 3.44 | $1.5 \times 10^{-2}$ |
| 0.02480 | 200 | 50.00 | 3.31 | $7.3 \times 10^{-3}$ |

[a] References are indicated in brackets.

# Aluminum Antimonide (AlSb)

DAVID F. EDWARDS and RICHARD H. WHITE
University of California
Lawrence Livermore National Laboratory
Livermore, California

The refractive index, $n$, and the extinction coefficient, $k$, of AlSb have been measured for a limited number of samples. The two main reasons for this are that large high-quality single crystals are difficult to grow, and the surface of AlSb reacts rapidly with the atmosphere to produce a relatively thick contaminated layer.

One method for measuring the optical properties ($n$ and $k$) of semiconductors, especially for the UV and visible regions, is spectroscopic ellipsometry. However, as pointed out by Aspnes and Studna [1] and Zollner *et al.* [2], contamination-free surfaces are needed for precise ellipsometric measurements. Using the wet-chemical etching procedures of Ref. [1], Zollner *et al.* have obtained AlSb surfaces of sufficient quality for ellipsometric measurements at room temperature from 5.8–1.4 eV. They report $n$ and $k$ values calculated from the measured pseudo-dielectric function. This is called the pseudo-dielectric function because no corrections were made for any surface overlayers that may be present. For surfaces free of these overlayers or by making the appropriate corrections, the ellipsometric measurements would give the "true" dielectric function. In either case, the $n$ and $k$ values for the near UV and visible regions are calculated from the ellipsometric measurements.

Strossner *et al.* [3] have measured the dependence of the energy gap absorptance of AlSb at room temperature for hydrostatic pressures from atmospheric up to the phase change at about 8 GPa. We have extracted the extinction coefficient from the atmospheric-pressure absorption coefficient for the energy range 2.2–1.4 eV.

Oswald and Schade [4] were among the first to report $n$ and $k$ value for AlSb in the infrared region. They simultaneously measured the transmittance and reflectance of a 1 Ω-cm $p$-type sample from about 1–15 μm. From these data they calculated $n$ and $k$. They make no report of surface contamination effects and give only a plot of $n$ and $k$. Their $k$ values increase monotonically with wavelength indicating free-carrier absorption.


Copyright © 1991 by Academic Press.
l rights of reproduction in any form reserved.
ISBN 0-12-544422-2

This, coupled with the small resistivity and possible surface contamination are reasons for excluding the Oswald–Schade data from the table that follows.

Turner and Reese [5] have measured the reflectance of room-temperature AlSb between 16 μm and 40 μm, which includes the infrared lattice reflectance band. By fitting their reflectance data to the classical dispersion theory [6], they calculated $n$ and $k$ values for the 20–38 μm spectral region. Their method is similar to that used by Spitzer, Kleinman, and Walsh [7] for SiC, and by Kleinman and Spitzer [8] for GaP. In the classical dispersion theory of solids [6], the susceptibility $\chi$ and conductivity $\sigma$ in the neighborhood of a resonance frequency $\nu_o$ are given by

$$\chi = \rho \frac{1-\nu^2}{(1-\nu^2)^2+(\gamma\nu)^2} \tag{1}$$

and

$$\frac{\sigma}{\nu} = 2\pi\rho \frac{\gamma\nu}{(1-\nu^2)^2+(\gamma\nu)^2}, \tag{2}$$

where $\nu$ is the measured frequency divided by $\nu_o$, $\sigma$ is the conductivity divided by $\nu_o$, and $\gamma$ and $\rho$ are dimensionless parameters. In the Lorentz theory, $\rho$ is given by

$$\rho = \frac{Ne^2}{4\pi^2 m^* \nu_0^2}, \tag{3}$$

where $N$ is the concentration of ion pairs, and $m^*$ is their reduced mass. The dielectric constant is

$$\varepsilon = \varepsilon_0 + 4\pi\chi, \tag{4}$$

where $\varepsilon_o$ is the high-frequency ($\nu >> 1$) dielectric constant. The four parameters ($\varepsilon_o$, $\nu_o$, $\rho$, $\gamma$) were adjusted [5] for the best least-squares fit of the reflectance data to a single resonance. From these parameters the index of refraction and the extinction coefficient, $n$ and $k$, are calculated from

$$n^2 = \tfrac{1}{2}[\varepsilon^2 + 4(\sigma/\nu)^2]^{1/2} + \varepsilon \tag{5}$$

and

$$k^2 = \tfrac{1}{2}[\varepsilon^2 + 4(\sigma/\nu)^2]^{12} - \varepsilon. \tag{6}$$

Turner and Reese [5] give the following values for their four parameters:

$$\nu_0 = (9.564 \pm 0.019) \times 10^{12}\ \text{sec}^{-1}$$

$$\rho = 0.1060 \pm 0.0005$$

$$\gamma = 0.0059 \pm 0.0005$$

$$\varepsilon_0 = 9.880 \pm 0.12.$$

Hass and Henvis [9] measured the fundamental reflection band of six III-V compound semiconductors at liquid helium-temperature. AlSb was one of the materials measured. They evaluated the oscillator parameters by comparing their measured reflectance with that calculated using the classical dispersion theory of Born and Huang [10]. The four parameters as found by Hass and Henvis are

$$\omega_0 = 318\ \text{cm}^{-1}$$

$$\varepsilon_\infty = 10.24$$

$$\varepsilon_0 - \varepsilon_\infty = 1.8$$

$$\gamma/\omega_0 = 0.02.$$

The $n$ and $k$ values are calculated using these parameters and the dispersion formulas of Ref. [10].

Pikhtin and Yas'kov [11] report a semiempirical method for calculating the dispersion of the refractive index using three adjustable parameters associated with the energy-band structure. For AlSb they use the data of Oswald and Schade [4] to evaluate the three adjustable parameters. Test calculations by one of us [12] and a comparison of their predictions to the data of Refs. [5] and [9] indicate that the indices are sensitively dependent on the values of the three parameters. It appears that indices over a spectral range broader than that of Ref. [4] are needed to improve the accuracy of the Pikhtin–Yas'kov calculated data for AlSb.

The indices of refraction and extinction coefficients for AlSb are given in

Table I and plotted in Fig. 1. Most of the data are for room temperature except those of Hass and Henvis [9], which are at liquid-helium temperature. The $n$ and $k$ values from 5.8 eV to 2.1 eV are the ellipsometrically measured data of Zollner *et al.* [2]. The $k$ values for the absorption-edge region (2.2–1.4 eV) are calculated from the measured absorption coefficients of Strossner *et al.* [3]. The $n$ values from 2.1 eV to 0.529 eV [0.5905 μm to 23 μm) were calculated from a Herzberger-type dispersion formula fit to the data of Refs. [2] and [5]. A total of 16 data points were used. As seen in Table I below, the index data in the 2.3–2.1 eV region has a slope discontinuity due to an interband critical point [2]. Data for energies greater than 2.1 eV were therefore not included in the dispersion-formula fit. The indices for wavelengths greater than 23 μm were also not included in the fit because of the onset of the infrared lattice band.

The Herzberger-type dispersion formula is [13]

$$n = A + BL + CL^2 + D\lambda^2 + E\lambda^4,$$

where $L = 1/(\lambda^2 - 2.8 \times 10^6)$ with the wavelength in angstroms. As explained by Herzberger and Salzberg [13], $2.8 \times 10^6$ is the square of the mean asymptote for the short-wavelength abrupt increase in the index for 14 materials (AlSb not included). For the 16 points from 0.5905 μm to 23 μm and at room temperature, the coefficients are

$$A = 3.204093$$

$$B = 1.874871 \times 10^7$$

$$C = 2.205306 \times 10^{14}$$

$$D = -4.144419 \times 10^{12}$$

$$E = -3.199325 \times 10^{-23}$$

The RMS error between the measured values and the dispersion-formula calculated indices is 0.179%.

For the reader's convenience, the same 16 indices were also fit to the modified Sellmeier-type dispersion formula [14]:

$$n^2 = 1 + A/(\lambda^2 - B) + C\lambda^2/(\lambda^2 - D),$$

where the wavelength $\lambda$ is in angstroms. For the 16 data points, the coefficients are

$$A = 4.094753 \times 10^{-5}$$

$$B = -7.086745 \times 10^{-5}$$

$$C = 4.198623$$

$$D = 1.925813 \times 10^{-9}.$$

The RMS error is 0.371%.

The room-temperature $n$ and $k$ values of Table I from 25 μm to 100 μm were calculated from Eqs. 1–6 using the four parameters of Ref. [5]. These calculations were extended beyond the range of measurement to 100 μm in order to estimate $\varepsilon_o$ ($=n^2$). The room-temperature measurements of Ref. [5] give $\varepsilon_o = 9.88$, compared with $n^2 = 11.36$ at 100 μm. At liquid-helium temperature (Ref. [9]) the parameter fit gives $\varepsilon_o = 12.04$, compared with $n^2 = 12.24$ at 100 μm.

Ghosh *et al.* [15] have developed a simple model for predicting the temperature and pressure coefficients of the refractive index of some zinc-blende semiconductors, AlSb included. They predict the temperature coefficient at constant pressure to be

$$\left(\frac{dn}{dT}\right)_p = 1.19 \times 10^{-4}\,\mathrm{K}^{-1}.$$

No wavelength or temperature range is given.

The pressure coefficient is predicted to be

$$-\left(\frac{dn}{dP}\right)_T = 34.10 \times 10^{-3}\,\mathrm{GPa}^{-1}.$$

No wavelength or pressure range is given. They have no measured data with which they can evaluate the accuracy of these predictions.

## REFERENCES

1. D. E. Aspnes and A. A. Studna, "Dielectric Functions and Optical Parameters of Si, Ge, GaP, GaAs, GaSb, InP, InAs, and InSb from 1.5 to 6.0 eV," *Phys. Rev.* **B27**, 985 (1983).

2. S. Zollner, C. Lin, E. Schönherr, A. Böhringer, and M. Cardona, "The Dielectric Function of AlSb from 1.4 to 5.8 eV Determined by Spectroscopic Ellipsometry," *J. Appl. Phys.* **66**, 383 (1989).
3. K. Strossner, S. Ves, Chul Koo Kim, and M. Cardona, "Dependence of the Direct and Indirect Gap of AlSb on Hydrostatic Pressure," *Phys. Rev. B* **33** (6), 4044 (1986).
4. F. Oswald and R. Schade, "Über die Bestimmung der Optischen Kunstanten von Halbleitern des Typus $A^{III}B^{V}$ in Infraroten," *Z. Naturforsch.* **9a**, 611 (1954).
5. W. J. Turner and W. E. Reese, "Infrared Lattice Bands in AlSb," *Phys. Rev.* **127** (1), 126 (1962).
6. F. Seitz, "Modern Theory of Solids," McGraw-Hill, New York, Chap. 17 (1940).
7. W. G. Spitzer, D. Kleinman, and D. Walsh, "Infrared Properties of Hexagonal Silicon Carbide," *Phys. Rev.* **113** (1), 127 (1959).
8. D. A. Kleinman and W. G. Spitzer, "Infrared Lattice Absorption of GaP," *Phys. Rev.* **118** (1), 110 (1960).
9. M. Hass and B. W. Henvis, "Infrared Lattice Reflectance Spectra of III-V Compound Semiconductors," *J. Phys. Chem. Solids* **23**, 1099 (1962).
10. M. Born and K. Huang, "Dynamical Theory of Crystal Lattices," University Press, Oxford, Chap. II (1954).
11. A. N. Pikhtin and A. D. Yas'kov, "Dispersion of the Refractive Index of Semiconductors with Diamond and Zinc-blende Structures," *Sov. Phys. Semicond.* **12**, 622 (1978).
12. D. F. Edwards, 1989 (unpublished).
13. M. Herzberger and C. D. Salzberg, "Refractive Indices of Infrared Optical Materials and Color Correction of Infrared Lenses," *J. Opt. Soc. Am.* **52**, 420 (1962); M. Herzberger, "Colour Correction in Optical Systems and a New Dispersion Formula," *Opt. Acta* **6**, 197 (1959).
14. D. F. Edwards and R. H. White, see KDP in this volume.
15. D. K. Ghosh, L. K. Samanata, and G. C. Bahr, "The Temperature and Pressure Dependence of Refractive Indices of Some III-V and II-VI Binary Semiconductors," *Infrared Physics* **26**, 111 (1986).

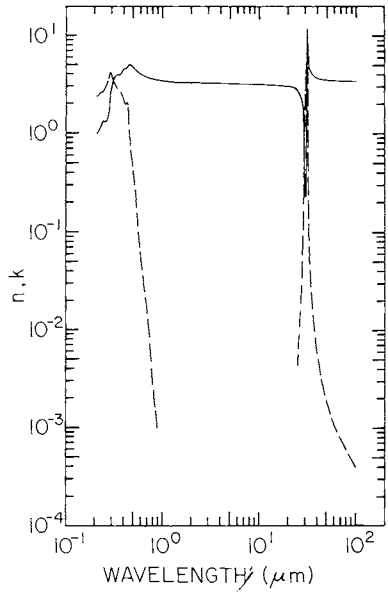


**Fig. 1.** Log–log plot of $n$ (solid line) and $k$ (dashed line) versus wavelength in micrometers for aluminum antimonide.

**TABLE I**

**Values of *n* and *k* for Aluminum Antimonide at 300 K from Various References[a]**

| eV | $cm^{-1}$ | μm | n | $n_c$ | k | k |
|---|---|---|---|---|---|---|
| 5.8 | 46,774 | 0.2138 | 1.00[2] | | 2.40[2] | |
| 5.7 | 45,968 | 0.2175 | 1.01 | | 2.42 | |
| 5.6 | 45,161 | 0.2214 | 1.04 | | 2.46 | |
| 5.5 | 44,355 | 0.2255 | 1.09 | | 2.52 | |
| 5.4 | 43,548 | 0.2296 | 1.17 | | 2.58 | |
| 5.3 | 42,742 | 0.2340 | 1.26 | | 2.59 | |
| 5.2 | 41,935 | 0.2385 | 1.31 | | 2.58 | |
| 5.1 | 41,129 | 0.2431 | 1.31 | | 2.59 | |
| 5.0 | 40,323 | 0.2480 | 1.30 | | 2.64 | |
| 4.9 | 39,516 | 0.2531 | 1.29 | | 2.72 | |
| 4.8 | 38,710 | 0.2583 | 1.30 | | 2.84 | |
| 4.7 | 37,903 | 0.2638 | 1.33 | | 2.99 | |
| 4.6 | 37,097 | 0.2696 | 1.38 | | 3.16 | |
| 4.5 | 36,290 | 0.2756 | 1.45 | | 3.39 | |
| 4.4 | 35,484 | 0.2818 | 1.59 | | 3.70 | |
| 4.3 | 34,677 | 0.2884 | 1.96 | | 4.07 | |
| 4.2 | 33,871 | 0.2952 | 2.60 | | 4.22 | |
| 4.1 | 33,065 | 0.3024 | 3.15 | | 4.00 | |
| 4.0 | 32,258 | 0.3100 | 3.50 | | 3.71 | |
| 3.9 | 31,452 | 0.3179 | 3.71 | | 3.40 | |
| 3.8 | 30,645 | 0.3263 | 3.81 | | 3.16 | |
| 3.7 | 29,839 | 0.3351 | 3.93 | | 2.97 | |
| 3.6 | 29,032 | 0.3444 | 3.96 | | 2.81 | |
| 3.5 | 28,226 | 0.3543 | 3.95 | | 2.69 | |
| 3.4 | 27,419 | 0.3647 | 3.97 | | 2.64 | |
| 3.3 | 26,613 | 0.3758 | 4.14 | | 2.69 | |
| 3.2 | 25,806 | 0.3875 | 4.51 | | 2.47 | |
| 3.1 | 25,000 | 0.4000 | 4.57 | | 2.12 | |

| | | | | | | |
|---|---|---|---|---|---|---|
| 3.0 | 24,194 | 0.4133 | 4.52 | | 1.97 | |
| 2.9 | 23,387 | 0.4276 | 4.66 | | 2.06 | |
| 2.8 | 22,581 | 0.4429 | 5.27 | | 1.58 | |
| 2.7 | 21,774 | 0.4593 | 5.08 | | 0.92 | |
| 2.6 | 20,968 | 0.4769 | 4.81 | | 0.63 | |
| 2.5 | 20,161 | 0.4960 | 4.61 | | 0.46 | |
| 2.4 | 19,355 | 0.5167 | 4.44 | | 0.33 | |
| 2.3 | 18,548 | 0.5391 | 4.31 | | 0.24 | |
| 2.2 | 17,742 | 0.5636 | 4.20 | | $1\times10^{-2}$ | $1.2\times10^{-2}$ [3] |
| 2.1 | 16,935 | 0.5905 | 4.01 | | $6\times10^{-3}$ | $6.2\times10^{-3}$ |
| 2.0 | 16,129 | 0.6200 | | 3.9036 | $4\times10^{-3}$ | $3.9\times10^{-3}$ |
| 1.9 | 15,323 | 0.6526 | | 3.8143 | $3\times10^{-3}$ | $2.3\times10^{-3}$ |
| 1.8 | 14,516 | 0.6889 | | 3.7343 | $2\times10^{-3}$ | $1.4\times10^{-3}$ |
| 1.7 | 13,710 | 0.7294 | | 3.6626 | $1\times10^{-3}$ | $6.3\times10^{-4}$ |
| 1.6 | 12,903 | 0.7750 | | 3.5985 | $3\times10^{-4}$ | $3.1\times10^{-4}$ |
| 1.5 | 12,097 | 0.8267 | | 3.5412 | $2\times10^{-4}$ | $3.3\times10^{-4}$ |
| 1.4 | 11,290 | 0.8857 | | 3.4901 | $1\times10^{-4}$ | |
| 1.3 | 10,484 | 0.9538 | | 3.4447 | | |
| 1.2 | 9,677 | 1.033 | | 3.4044 | | |
| 1.1 | 8,871 | 1.127 | | 3.3687 | | |
| 1.0 | 8,064 | 1.240 | | 3.3373 | | |
| 0.9 | 7,258 | 1.378 | | 3.3099 | | |
| 0.8 | 6,452 | 1.550 | | 3.2860 | | |
| 0.7 | 5,645 | 1.771 | | 3.2654 | | |
| 0.6 | 4,839 | 2.067 | | 3.2477 | | |
| 0.5 | 4,032 | 2.480 | | 3.2327 | | |
| 0.4 | 3,226 | 3.100 | | 3.2199 | | |
| 0.3 | 2,419 | 4.133 | | 3.2080 | | |
| 0.2 | 1,613 | 6.200 | | 3.1926 | | |
| 0.1 | 806.5 | 12.40 | | 3.1340 | | |
| 0.09 | 725.9 | 13.78 | | 3.1149 | | |
| 0.08 | 645.2 | 15.50 | | 3.0868 | | |
| 0.07 | 564.6 | 17.71 | | 3.0431 | | |
| 0.06 | 483.9 | 20.67 | | 2.9692 | | |
| 0.05 | 403.3 | 24.80 | | 2.8285 | | |

*(continued)*

**TABLE I (*Continued*)**

**Aluminumn Antimonide**

| eV | $cm^{-1}$ | μm | n | $n_c$ | k | k |
|---|---|---|---|---|---|---|
| 0.04959 | 400.0 | 25.0 | 2.75 [5] | | $5.4 \times 10^{-3}$ [5] | |
| 0.04769 | 384.6 | 26.0 | 2.64 | | $8.7 \times 10^{-3}$ | |
| 0.04592 | 370.4 | 27.0 | 2.46 | 2.28 [9] | 0.0151 | 0.0719 [9] |
| 0.04558 | 367.6 | 27.2 | 2.42 | 2.22 | 0.0172 | 0.0824 |
| 0.04525 | 365.0 | 27.4 | 2.37 | 2.15 | 0.0197 | 0.0952 |
| 0.04492 | 362.3 | 27.6 | 2.31 | 2.06 | 0.0227 | 0.111 |
| 0.04460 | 359.7 | 27.8 | 2.24 | 1.96 | 0.0265 | 0.132 |
| 0.04428 | 357.1 | 28.0 | 2.16 | 1.85 | 0.0313 | 0.159 |
| 0.04397 | 354.6 | 28.2 | 2.07 | 1.72 | 0.0375 | 0.196 |
| 0.04336 | 352.1 | 28.4 | 1.96 | 1.55 | 0.0457 | 0.249 |
| 0.04347 | 359.7 | 28.6 | 1.83 | 1.35 | 0.0572 | 0.331 |
| 0.04305 | 347.2 | 28.8 | 1.66 | 1.11 | 0.0742 | 0.475 |
| 0.04275 | 344.8 | 29.0 | 1.44 | 0.840 | 0.102 | 0.740 |
| 0.04246 | 342.5 | 29.2 | 1.13 | 0.663 | 0.157 | 1.12 |
| 0.04217 | 340.1 | 29.4 | 0.633 | 0.594 | 0.344 | 1.53 |
| 0.04189 | 337.8 | 29.6 | 0.276 | 0.583 | 0.992 | 1.93 |
| 0.04161 | 335.6 | 29.8 | 0.225 | 0.610 | 1.56 | 2.34 |
| 0.04133 | 333.3 | 30.0 | 0.224 | 0.669 | 2.09 | 2.77 |
| 0.04106 | 331.1 | 30.2 | 0.247 | 0.769 | 2.64 | 3.24 |
| 0.04079 | 328.9 | 30.4 | 0.294 | 0.925 | 3.25 | 3.78 |
| 0.04052 | 326.8 | 30.6 | 0.382 | 1.18 | 4.01 | 4.41 |
| 0.04026 | 324.7 | 30.8 | 0.557 | 1.60 | 5.02 | 5.17 |
| 0.04013 | 323.6 | 30.9 | 0.718 | 1.93 | 5.70 | 5.62 |
| 0.04000 | 322.6 | 31.0 | 0.987 | 2.39 | 6.58 | 6.09 |
| 0.03987 | 321.5 | 31.1 | 1.50 | 3.04 | 7.80 | 6.58 |
| 0.03974 | 320.5 | 31.2 | 2.67 | 3.95 | 9.56 | 6.98 |
| 0.03962 | 319.5 | 31.3 | 6.13 | 5.16 | 11.7 | 7.12 |
| 0.03949 | 318.5 | 31.4 | 12.1 | 6.53 | 8.43 | 6.74 |
| 0.03937 | 317.5 | 31.5 | 11.3 | 7.62 | 3.37 | 5.75 |

| | | | | | | |
|---|---|---|---|---|---|---|
| 0.03924 | 316.5 | 31.6 | 9.57 | 8.13 | 1.67 | 4.50 |
| 0.03912 | 315.5 | 31.7 | 8.39 | 8.13 | 1.00 | 3.39 |
| 0.03899 | 314.5 | 31.8 | 7.60 | 7.88 | 0.676 | 2.57 |
| 0.03887 | 313.5 | 31.9 | 7.02 | 7.55 | 0.491 | 1.98 |
| 0.03875 | 312.5 | 32.0 | 6.59 | 7.23 | 0.376 | 1.57 |
| 0.03757 | 303.0 | 33.0 | 4.86 | 5.40 | 0.0824 | 0.361 |
| 0.03647 | 294.1 | 34.0 | 4.34 | 4.75 | 0.0377 | 0.165 |
| 0.03542 | 285.7 | 35.0 | 4.08 | 4.42 | 0.0223 | 0.0977 |
| 0.03444 | 277.8 | 36.0 | 3.93 | 4.22 | 0.0150 | 0.0660 |
| 0.03351 | 270.3 | 37.0 | 3.82 | 4.09 | 0.0110 | 0.0484 |
| 0.03262 | 263.2 | 38.0 | 3.75 | 3.99 | $8.5\times10^{-3}$ | 0.0375 |
| 0.03100 | 250.0 | 40.0 | 3.65 | 3.87 | $5.7\times10^{-3}$ | 0.0250 |
| 0.02755 | 222.2 | 45.0 | 3.53 | 3.71 | $2.9\times10^{-3}$ | 0.0129 |
| 0.02480 | 200.0 | 50.0 | 3.48 | 3.64 | $1.9\times10^{-3}$ | $8.5\times10^{-3}$ |
| 0.02066 | 166.7 | 60.0 | 3.42 | 3.57 | $1.1\times10^{-3}$ | $5.0\times10^{-3}$ |
| 0.01771 | 142.9 | 70.0 | 3.40 | 3.53 | $8.1\times10^{-4}$ | $3.6\times10^{-3}$ |
| 0.01550 | 125.0 | 80.0 | 3.38 | 3.52 | $6.4\times10^{-4}$ | $2.8\times10^{-3}$ |
| 0.01378 | 111.1 | 90.0 | 3.38 | 3.51 | $5.2\times10^{-4}$ | $2.3\times10^{-3}$ |
| 0.01240 | 100.0 | 100.0 | 3.37 | 3.50 | $4.5\times10^{-4}$ | $2.0\times10^{-3}$ |

[a] The column headed $n_c$ contains refractive index values calculated with the Herzberger-type formula. The bracketed numbers indicate the reference to the data.

# Aluminum Gallium Arsenide ($Al_xGa_{1-x}As$)

O. J. GLEMBOCKI
Naval Research Laboratory
Washington, D.C.
and
KENICHI TAKARABE
Department of Natural Science
Okayama University of Science
Okayama-City
Okayama 700, Japan

The $Al_xGa_{1-x}As$ system is technologically one of the most important alloy systems, especially when combined with GaAs. It forms the basis of quantum-well, superlattice, and single-barrier device structures, which in turn have a significant effect on high-speed electro-optics. Because of this, it would be of the utmost importance to have the optical constants, $n$ and $k$, over a wide spectral range and over the concentration range of $x=0$ to $x=1$, in as narrowly spaced $x$ intervals as possible, preferably $\Delta x=0.1$. This, however, is not the case. In fact, we could find only bits and pieces of data at almost random values of $x$ over narrow spectral ranges, except for $x=0.3$.

There is, however, a fair amount of information about other physical parameters such as lattice constant, density, band gap, and phonon frequency. Because these parameters are useful in many applications, we list Adachi's values [1] for these most commonly used ones:

1. Lattice constant (Å) $a=5.6533+0.0078x$;
2. Density (gm/cm$^3$) $g=5.36-1.6x$;
3. Band gap (eV) $E_g=1.424+1.247x \quad (0<x<0.45)$
$=1.900+0.125x+0.143x^2 \quad (0.45<x<1.0)$;
4. LO phonon energy (meV) $\hbar\omega(\text{GaAs})=36.25-6.55x+1.79x^2$
$\hbar\omega(\text{AlAs})=44.63+8.78x-3.32x^2$;
5. TO phonon energy (meV) $\hbar\omega(\text{GaAs})=33.29-0.64x-1.16x^2$
$\hbar\omega(\text{AlAs})=44.63+0.55x-0.30x^2$.

We were able to find only one value of $x=0.3$ (within a typical


Copyright © 1991 by Academic Press.
All rights of reproduction in any form reserved.
ISBN 0-12-544422-2

uncertainty of ±0.01) where UV, VIS, and IR data have been analyzed to give $n$ and $k$. Otherwise, there are spectroscopic-ellipsometry data for $n$ and $k$ in the range of 6–1.5 eV for a number of $x$ values near tenths [2], IR reststrahlen data for $n$ and $k$ from 1000–100 $cm^{-1}$ for other values of $x$ [3] and some measurements [4] and calculations [1, 5] of $n$ from 2.5–0.5 eV. In Table I we display the values of $x$ for which we found spectroscopic data in the various photon-energy ranges. It is clear that near $x = 0.3$, we have data for a wide wavelength range, but for other values of $x$, only data in the visible or IR are available.

In Table II we list $n$ and $k$ data for the values of $x$ noted in Table I. In Fig. 1 we have plotted the values of the optical constants for $x = 0.3$. It is important to note that the end member GaAs ($x = 0$) was previously treated in *HOC I* [6], and that AlAs ($x = 1$) is discussed separately in this volume [7].

In the X-ray region from 10,000–51.5 eV (1.24–240 Å) there are no experimental data. The numbers for $x = 0.3$ listed in Table II were calculated using the Henke model [8, 9]. This model, based on calculated atomic scattering cross-sections, requires a knowledge of the density of $Al_{0.3}Ga_{0.7}As$, which is given by Adachi [1] to be $g(0.3) = 4.88$. The absorption edges of the atomic constituents are $K(\text{Al}) = 1559.88$ eV, $K(\text{Ga}) = 10368.2$ eV, $K(\text{As}) = 11865$ eV, $L_1(\text{Al}) = 87.01$ eV, $L_1(\text{As}) = 1529.3$ eV, $L_{2,3}(\text{Al}) = 72.78$ eV, $L_{2,3}(\text{Ga}) = 1145.0$, 1116.9 eV, $L_{2,3}(\text{As}) = 1358.7$, 1323.5 eV. The lower-lying energies may be perturbed by the bonding properties of the crystal material. It should be noted that this calculation can be used for any value of $x$ provided that the parameters listed above are appropriately adjusted.

There appear to be no reflectivity data that would yield $n$ and $k$ in the ultraviolet down to 6 eV.

Aspnes *et al.* [2] measured $n$ and $k$ from 6–1.5 eV by spectroscopic ellipsometry from samples close to tenths in $x$. Values of $x$ are usually determined by X-ray analysis to ±0.01. Care was taken to remove or account for the native oxide on the surface.

Interestingly, we find little data for the absorption coefficient at the band edge, presumably because the alloy samples are always on a GaAs substrate with a band gap smaller than the alloy film. This requires a reflection experiment or, for transmission, an etching process to remove the substrate but still support the film.

Below the fundamental band gap $E_g$, $n$ has been measured for a number of $x$ values [4]. Jensen [5] has developed a model to calculate $n$ in the transparent region for ternary and quaternary semiconductors. Adachi [1] has used a different model to calculate $n$ below the band gap. We have used both models for $x = 0.14$ to determine $n$ and list the values in Table II. In the overlap region (1.2–1.5 eV) agreement is to ~1% at lower energies and increases to ~2% at higher energies. The Adachi calculation does not

seem to work well as $E_g$ is neared, whereas the Jensen calculation is applicable much closer to $E_g$, even showing a plateauing of the $n$ values. In addition, we have used the latter model [1] to calculate $n$ below the respective band gaps for the tenth values of $x$, and we list them in Table II. It is also reported that the $n$ values at 0.9 μm below all the band gaps vary linearly with $x$; $\Delta n = n(Al_xGa_{1-x}As) - n(GaAs) = 0.62x$ [10].

The $n$ and $k$ values in the far infrared for $Al_xGa_{1-x}As$ were obtained by fitting the reflectivity data [3] taken near normal incidence, that is, within approximately a 10° angle of incidence. The $Al_xGa_{1-x}As$ samples were grown by an isothermal liquid-phase-epitaxy (LPE) technique for $x$ values ranging from 0 to 0.54. All materials had $n$-type carrier concentrations of less than $5 \times 10^{16}\,cm^{-3}$. The free-carrier plasma edge was not observed for $v > 50\,cm^{-1}$. The alloy compositions were evaluated by analysis of X-ray emission produced from the layer by the electron beam of an ARL model EMX-SM electron-probe microanalyzer. The accuracy of the composition measured was estimated to be within 2%; for example, $\Delta x = \pm 0.01$ for $x = 0.54$.

The optical phonons of the $Al_xGa_{1-x}As$ behave as the two-mode type [11–13]. The $n$ and $k$ values were calculated by the factorized form of the classical dispersion equation

$$(v) = (n + ik)^2 = \frac{(v_{11}^2 - v^2 - iv\gamma_{11})(v_{12}^2 - v^2 - iv\gamma_{12})}{(v_{t1}^2 - v^2 - iv\gamma_{t1})(v_{t2}^2 - v^2 - iv\gamma_{t2})}$$

where $v_{ti}$, $v_{li}$, $\gamma_{ti}$, and $\gamma_{li}$ denote TO frequency, LO frequency, TO damping constant, and LO damping constant, respectively. The indexes $i = 1$ and $i = 2$ identify the parameters for the GaAs-like and the AlAs-like modes, respectively. Those values referred to are shown in Table III [10]. The $n$ and $k$ values are tabulated in the region of 5–100 μm in Table II.

## ACKNOWLEDGMENTS

We thank W. R. Hunter for the calculation of $n$ and $k$ in the X-ray region with the Henke model.

## REFERENCES

1. S. Adachi, *J. Appl. Phys.* **58**, R1 (1985).
2. D. E. Aspnes, S. M. Kelso, R. A. Logan, and R. Bhat, *J. Appl. Phys.* **60**, 754 (1986).
3. O. K. Kim and W. G. Spitzer, *J. Appl. Phys.* **50**, 4362 (1979).
4. H. C. Casey, Jr., D. D. Sell, and M. B. Panish, *Appl. Phys. Lett.* **24**, 63 (1974).
5. B. Jensen, chapter in this volume and references therein.
6. E. D. Palik, in "Handbook of Optical Constants of Solids," (E. D. Palik, ed.), Academic Press, Orlando, 429 (1985).

7. E. D. Palik, O. J. Glembocki, and K. Takarabe, AlAs critique in this volume.
8. B. L. Henke, P. Lee, T. J. Tanaka, R. L. Shimabukuro, and B. K. Fujikama, *At. Data Nucl. Data Tables* **27**, 1 (1982).
9. B. L. Henke, J. C. Davis, E. M. Gullikson, and R. C. C. Perera, Lawrence Berkeley Laboratory Report No. LBL-26259 (1988).
10. H. Kressel and J. K. Butler, in "Semiconductors Lasers and Heterojunction LED's," Academic Press, New York, 413 (1977).
11. D. W. Taylor, in "Optical Properties of Mixed Crystals," (R. J. Elliot and I. P. Ipotova, eds.), North-Holland, Amsterdam, 35 (1988).
12. R. Bonneville, *Phys. Rev.* **B29**, 907 (1984).
13. A. S. Barker, Jr., and A. J. Sievers, *Rev. Mod. Phys.* **47**, Suppl. No. 2, S143 (1975).

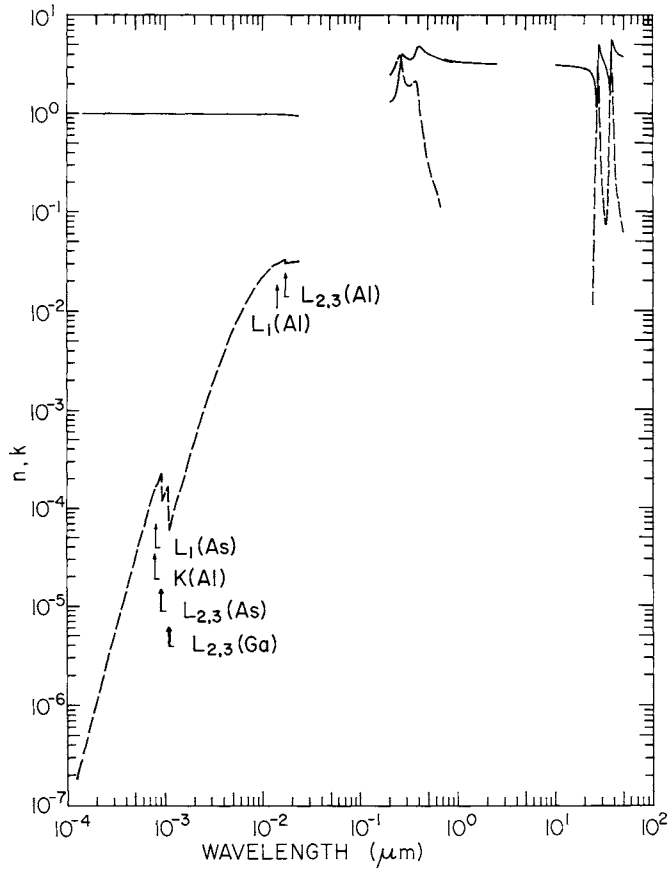


**Fig. 1.** Log–log plot of $n$ (solid line) and $k$ (dashed line) versus wavelength in micrometers for $Al_xGa_{1-x}As$ with $x = 0.31 \pm 0.01$.

**TABLE I**

**Values of $x$ for Which Spectroscopic Data for $n$ and $k$ Are Presented in the Various References**

| x | X-RAY-UV (10000–51 eV) $n$ & $k$ | UV-VIS (6–1.5 eV) $n$ & $k$ | Near IR (2.7–0.5 eV) $n$ | Far IR (1000–200 $cm^{-1}$) $n$ & $k$ |
|---|---|---|---|---|
| 0 | [6] | [6] | [6] | [6] See *HOC I* |
| 0.099 | | [2] | | |
| 0.1 | | | [1] | |
| 0.14 | | | [1, 5] | [3] |
| 0.18 | | | | [3] |
| 0.198 | | [2] | | |
| 0.2 | | | [1] | |
| 0.30 | [8, 9] | | [1] | [3] |
| 0.315 | | [2] | | |
| 0.36 | | | | [3] |
| 0.4 | | | [1] | |
| 0.419 | | [2] | | |
| 0.44 | | | | [3] |
| 0.491 | | [2] | | |
| 0.5 | | | [1] | |
| 0.54 | | | | [3] |
| 0.590 | | [2] | | |
| 0.6 | | | [1] | |
| 0.700 | | [2] | [1] | |
| 0.8 | | | [1] | |
| 0.804 | | [2] | | |
| 0.9 | | | [1] | |
| 1.0 | [7] | [7] | [7] | [7] See *HOC II* |

TABLE II

Value of n and k for $Al_{0.3}Ga_{0.7}As$ (X-RAY-UV) from Various References[a]

| eV | $cm^{-1}$ | Å | n | k |
|---|---|---|---|---|
| 10000 | | 1.240 | 0.99999150[8,9] | $1.74 \times 10^{-7}$[8,9] |
| 9772 | | 1.269 | 0.99999110 | 1.90 |
| 9331 | | 1.329 | 0.99999010 | 2.27 |
| 8909 | | 1.392 | 0.9999891 | 2.71 |
| 8507 | | 1.458 | 0.9999880 | 3.23 |
| 8123 | | 1.526 | 0.9999868 | 3.85 |
| 7756 | | 1.599 | 0.9999854 | 4.59 |
| 7406 | | 1.674 | 0.9999840 | 5.46 |
| 7072 | | 1.753 | 0.9999824 | 6.50 |
| 6752 | | 1.836 | 0.9999806 | 7.73 |
| 6447 | | 1.923 | 0.9999787 | $9.20 \times 10^{-7}$ |
| 6156 | | 2.014 | 0.9999766 | $1.09 \times 10^{-6}$ |
| 5878 | | 2.109 | 0.9999743 | 1.30 |
| 5613 | | 2.209 | 0.9999717 | 1.55 |
| 5359 | | 2.314 | 0.9999689 | 1.84 |
| 5117 | | 2.423 | 0.9999658 | 2.18 |
| 4886 | | 2.538 | 0.9999624 | 2.59 |
| 4665 | | 2.658 | 0.9999587 | 3.08 |
| 4455 | | 2.783 | 0.9999546 | 3.66 |
| 4254 | | 2.915 | 0.9999501 | 4.34 |
| 4062 | | 3.053 | 0.9999452 | 5.15 |
| 3878 | | 3.197 | 0.9999399 | 6.11 |
| 3703 | | 3.348 | 0.9999340 | 7.24 |
| 3536 | | 3.506 | 0.9999275 | $8.59 \times 10^{-6}$ |
| 3376 | | 3.672 | 0.9999205 | $1.02 \times 10^{-5}$ |
| 3224 | | 3.846 | 0.9999128 | 1.21 |
| 3078 | | 4.028 | 0.9999044 | 1.43 |
| 2939 | | 4.218 | 0.999895 | 1.69 |
| 2807 | | 4.418 | 0.999885 | 2.00 |
| 2680 | | 4.627 | 0.999875 | 2.37 |
| 2559 | | 4.846 | 0.999863 | 2.80 |
| 2443 | | 5.075 | 0.999850 | 3.30 |
| 2333 | | 5.315 | 0.999837 | 3.90 |
| 2228 | | 5.566 | 0.999822 | 4.60 |
| 2127 | | 5.829 | 0.999807 | 5.42 |
| 2031 | | 6.105 | 0.999791 | 6.38 |
| 1939 | | 6.394 | 0.999774 | 7.49 |
| 1852 | | 6.696 | 0.999757 | $8.80 \times 10^{-5}$ |
| 1768 | | 7.013 | 0.999739 | $1.03 \times 10^{-4}$ |
| 1688 | | 7.344 | 0.999723 | 1.21 |
| 1612 | | 7.691 | 0.999710 | 1.42 |
| 1575 | | 7.871 | 0.999708 | 1.53 |
| 1539 | | 8.055 | 0.999706 | 1.58 |
| 1504 | | 8.244 | 0.999697 | 1.58 |
| 1470 | | 8.436 | 0.999687 | 1.70 |
| 1436 | | 8.633 | 0.999683 | 1.83 |
| 1403 | | 8.835 | 0.999683 | 1.98 |
| 1371 | | 9.041 | 0.999692 | 2.14 |
| 1340 | | 9.253 | 0.999735 | 2.31 |

TABLE II (*Continued*)

$Al_{0.3}Ga_{0.7}As$ (X-RAY-UV)

| eV | $cm^{-1}$ | Å | n | k |
|---|---|---|---|---|
| 1309 | | 9.469 | 0.999732 | 1.23 |
| 1280 | | 9.690 | 0.999684 | 1.21 |
| 1250 | | 9.917 | 0.999652 | 1.29 |
| 1222 | | 10.15 | 0.999629 | 1.38 |
| 1194 | | 10.39 | 0.999612 | 1.47 |
| 1167 | | 10.63 | 0.999601 | 1.57 |
| 1140 | | 10.88 | 0.999603 | $1.67 \times 10^{-4}$ |
| 1114 | | 11.13 | 0.999635 | $6.37 \times 10^{-5}$ |
| 1088 | | 11.39 | 0.999554 | 6.88 |
| 1064 | | 11.66 | 0.999503 | 7.43 |
| 1039 | | 11.93 | 0.999461 | 8.02 |
| 1016 | | 12.21 | 0.999421 | $8.66 \times 10^{-5}$ |
| 969.7 | | 12.79 | 0.999342 | $1.01 \times 10^{-4}$ |
| 925.9 | | 13.39 | 0.999261 | 1.18 |
| 884.1 | | 14.02 | 0.999175 | 1.38 |
| 844.2 | | 14.69 | 0.999083 | 1.61 |
| 806.0 | | 15.38 | 0.99898 | 1.88 |
| 769.7 | | 16.11 | 0.99888 | 2.21 |
| 734.9 | | 16.87 | 0.99876 | 2.59 |
| 701.7 | | 17.67 | 0.99863 | 3.03 |
| 670.0 | | 18.51 | 0.99850 | 3.54 |
| 639.8 | | 19.38 | 0.99835 | 4.12 |
| 610.9 | | 20.30 | 0.99819 | 4.79 |
| 583.3 | | 21.26 | 0.99802 | 5.55 |
| 557.0 | | 22.26 | 0.99784 | 6.43 |
| 531.8 | | 23.31 | 0.99764 | 7.45 |
| 507.8 | | 24.42 | 0.99743 | 8.59 |
| 484.9 | | 25.57 | 0.99720 | $9.89 \times 10^{-4}$ |
| 463.0 | | 26.78 | 0.99695 | $1.14 \times 10^{-3}$ |
| 442.1 | | 28.05 | 0.99669 | 1.31 |
| 422.1 | | 29.37 | 0.99641 | 1.50 |
| 403.0 | | 30.76 | 0.99611 | 1.73 |
| 384.8 | | 32.22 | 0.99581 | 1.97 |
| 367.5 | | 33.74 | 0.99548 | 2.24 |
| 350.9 | | 35.34 | 0.99513 | 2.55 |
| 335.0 | | 37.01 | 0.99476 | 2.90 |
| 319.9 | | 38.76 | 0.99438 | 3.30 |
| 305.5 | | 40.59 | 0.99401 | 3.75 |
| 291.7 | | 42.51 | 0.99361 | 4.23 |
| 278.5 | | 44.52 | 0.99321 | 4.77 |
| 265.9 | | 46.63 | 0.99283 | 5.36 |
| 253.9 | | 48.83 | 0.99243 | 6.00 |
| 242.5 | | 51.14 | 0.99203 | 6.69 |
| 231.5 | | 53.56 | 0.99163 | 7.44 |
| 221.1 | | 56.09 | 0.99125 | 8.29 |
| 211.1 | | 58.74 | 0.99096 | $9.20 \times 10^{-3}$ |
| 201.5 | | 61.52 | 0.99069 | $1.01 \times 10^{-2}$ |
| 192.4 | | 64.43 | 0.99035 | 1.10 |
| 183.7 | | 67.48 | 0.99008 | 1.20 |
| 175.5 | | 70.67 | 0.98988 | 1.31 |

TABLE II (*Continued*)

$Al_{0.3}Ga_{0.7}As$ (X-RAY-UV)

| eV | $cm^{-1}$ | Å | n | k |
|---|---|---|---|---|
| 167.5 | | 74.01 | 0.98966 | 1.41 |
| 160.0 | | 77.51 | 0.98947 | 1.53 |
| 152.7 | | 81.17 | 0.98931 | 1.65 |
| 149.3 | | 83.07 | 0.98928 | 1.71 |
| 145.8 | | 85.01 | 0.98930 | 1.78 |
| 142.5 | | 87.00 | 0.98933 | 1.84 |
| 139.3 | | 89.03 | 0.98937 | 1.90 |
| 136.1 | | 91.11 | 0.98941 | 1.95 |
| 133.0 | | 93.24 | 0.98942 | 2.01 |
| 129.9 | | 95.42 | 0.98944 | 2.07 |
| 127.0 | | 97.66 | 0.98948 | 2.13 |
| 124.1 | | 99.94 | 0.98956 | 2.19 |
| 121.2 | | 102.3 | 0.98967 | 2.24 |
| 118.5 | | 104.7 | 0.98972 | 2.30 |
| 115.8 | | 107.1 | 0.98978 | 2.35 |
| 113.1 | | 109.6 | 0.98985 | 2.40 |
| 110.5 | | 112.2 | 0.98994 | 2.45 |
| 108.0 | | 114.8 | 0.98999 | 2.50 |
| 105.5 | | 117.5 | 0.99001 | 2.54 |
| 103.1 | | 120.2 | 0.99002 | 2.59 |
| 100.8 | | 123.0 | 0.99003 | 2.64 |
| 98.47 | | 125.9 | 0.99005 | 2.68 |
| 96.22 | | 128.9 | 0.99007 | 2.72 |
| 94.03 | | 131.9 | 0.99002 | 2.76 |
| 91.88 | | 134.9 | 0.98995 | 2.80 |
| 89.78 | | 138.1 | 0.98988 | 2.84 |
| 87.73 | | 141.3 | 0.98983 | 2.89 |
| 85.73 | | 144.6 | 0.98987 | 2.92 |
| 83.77 | | 148.0 | 0.98978 | 2.95 |
| 81.85 | | 151.5 | 0.98962 | 2.97 |
| 79.99 | | 155.0 | 0.98942 | 3.00 |
| 78.16 | | 158.6 | 0.98924 | 3.03 |
| 76.37 | | 162.3 | 0.98909 | 3.06 |
| 74.63 | | 166.1 | 0.98911 | 3.09 |
| 72.92 | | 170.0 | 0.98957 | 3.12 |
| 71.26 | | 174.0 | 0.98850 | 2.91 |
| 69.63 | | 178.1 | 0.98727 | 2.94 |
| 68.04 | | 182.2 | 0.98637 | 2.97 |
| 66.49 | | 186.5 | 0.98554 | 2.99 |
| 64.97 | | 190.8 | 0.98462 | 3.00 |
| 63.49 | | 195.3 | 0.98370 | 3.01 |
| 62.04 | | 199.9 | 0.98272 | 3.02 |
| 60.62 | | 204.5 | 0.98162 | 3.02 |
| 59.24 | | 209.3 | 0.98038 | 3.01 |
| 57.88 | | 214.2 | 0.97898 | 3.01 |
| 56.56 | | 219.2 | 0.97746 | 3.01 |
| 55.27 | | 224.3 | 0.97582 | 3.02 |
| 54.01 | | 229.6 | 0.97407 | 3.03 |
| 52.77 | | 234.9 | 0.97221 | 3.03 |
| 51.57 | | 240.4 | 0.970077 | $3.05 \times 10^{-2}$ |

TABLE II (*Continued*)

$Al_{0.099}Ga_{0.901}As$ (UV-VIS)

| eV | $cm^{-1}$ | μm | n | k |
|---|---|---|---|---|
| 6.0 | 48393 | 0.2066 | 1.311[2] | 2.457[2] |
| 5.9 | 47586 | 0.2101 | 1.318 | 2.538 |
| 5.8 | 46780 | 0.2138 | 1.330 | 2.608 |
| 5.7 | 45973 | 0.2175 | 1.345 | 2.698 |
| 5.6 | 45167 | 0.2214 | 1.371 | 2.800 |
| 5.5 | 44360 | 0.2254 | 1.408 | 2.921 |
| 5.4 | 43554 | 0.2296 | 1.459 | 3.059 |
| 5.3 | 42747 | 0.2339 | 1.531 | 3.223 |
| 5.2 | 41940 | 0.2384 | 1.634 | 3.433 |
| 5.1 | 41134 | 0.2431 | 1.819 | 3.704 |
| 5.0 | 40327 | 0.2480 | 2.207 | 3.983 |
| 4.9 | 39521 | 0.2530 | 2.772 | 4.036 |
| 4.8 | 38714 | 0.2583 | 3.267 | 3.846 |
| 4.7 | 37908 | 0.2638 | 3.611 | 3.536 |
| 4.6 | 37101 | 0.2695 | 3.829 | 3.229 |
| 4.5 | 36295 | 0.2755 | 4.010 | 2.876 |
| 4.4 | 35488 | 0.2818 | 4.017 | 2.507 |
| 4.3 | 34682 | 0.2883 | 3.922 | 2.240 |
| 4.2 | 33875 | 0.2952 | 3.801 | 2.074 |
| 4.1 | 33068 | 0.3024 | 3.697 | 1.983 |
| 4.0 | 32262 | 0.3100 | 3.618 | 1.937 |
| 3.9 | 31455 | 0.3179 | 3.566 | 1.920 |
| 3.8 | 30649 | 0.3263 | 3.537 | 1.924 |
| 3.7 | 29842 | 0.3351 | 3.532 | 1.945 |
| 3.6 | 29036 | 0.3444 | 3.552 | 1.979 |
| 3.5 | 28229 | 0.3542 | 3.601 | 2.030 |
| 3.4 | 27423 | 0.3647 | 3.690 | 2.100 |
| 3.3 | 26616 | 0.3757 | 3.864 | 2.203 |
| 3.2 | 25810 | 0.3875 | 4.253 | 2.187 |
| 3.1 | 25003 | 0.4000 | 4.460 | 1.949 |
| 3.0 | 24196 | 0.4133 | 4.838 | 1.836 |
| 2.9 | 23390 | 0.4275 | 4.968 | 1.126 |
| 2.8 | 22583 | 0.4428 | 4.725 | 0.763 |
| 2.7 | 21777 | 0.4592 | 4.518 | 0.575 |
| 2.6 | 20970 | 0.4769 | 4.353 | 0.462 |
| 2.5 | 20164 | 0.4959 | 4.220 | 0.382 |
| 2.4 | 19357 | 0.5166 | 4.111 | 0.320 |
| 2.3 | 18551 | 0.5391 | 4.018 | 0.276 |
| 2.2 | 17744 | 0.5636 | 3.940 | 0.237 |
| 2.1 | 16938 | 0.5904 | 3.876 | 0.199 |
| 2.0 | 16131 | 0.6199 | 3.820 | 0.171 |
| 1.9 | 15324 | 0.6526 | 3.775 | 0.127 |
| 1.8 | 14518 | 0.6889 | 3.716 | 0.099 |
| 1.7 | 13711 | 0.7293 | 3.678 | 0.082 |
| 1.6 | 12905 | 0.7749 | 3.661 | 0.059 |
| 1.5 | 12098 | 0.8266 | 3.572 | |

TABLE II (*Continued*)

$Al_{0.198}Ga_{0.802}As$ (UV-VIS)

| eV | $cm^{-1}$ | μm | n | k |
|---|---|---|---|---|
| 6.0 | 48393 | 0.2066 | 1.333[2] | 2.457[2] |
| 5.9 | 47586 | 0.2101 | 1.339 | 2.531 |
| 5.8 | 46780 | 0.2138 | 1.349 | 2.600 |
| 5.7 | 45973 | 0.2175 | 1.366 | 2.688 |
| 5.6 | 45167 | 0.2214 | 1.393 | 2.794 |
| 5.5 | 44360 | 0.2254 | 1.433 | 2.912 |
| 5.4 | 43554 | 0.2296 | 1.490 | 3.049 |
| 5.3 | 42747 | 0.2339 | 1.567 | 3.208 |
| 5.2 | 41940 | 0.2384 | 1.677 | 3.407 |
| 5.1 | 41134 | 0.2431 | 1.860 | 3.654 |
| 5.0 | 40327 | 0.2480 | 2.210 | 3.914 |
| 4.9 | 39521 | 0.2530 | 2.734 | 3.997 |
| 4.8 | 38714 | 0.2583 | 3.238 | 3.867 |
| 4.7 | 37908 | 0.2638 | 3.638 | 3.575 |
| 4.6 | 37101 | 0.2695 | 3.924 | 3.223 |
| 4.5 | 36295 | 0.2755 | 4.053 | 2.803 |
| 4.4 | 35488 | 0.2818 | 4.018 | 2.449 |
| 4.3 | 34682 | 0.2883 | 3.911 | 2.206 |
| 4.2 | 33875 | 0.2952 | 3.795 | 2.059 |
| 4.1 | 33068 | 0.3024 | 3.701 | 1.976 |
| 4.0 | 32262 | 0.3100 | 3.633 | 1.933 |
| 3.9 | 31455 | 0.3179 | 3.588 | 1.917 |
| 3.8 | 30649 | 0.3263 | 3.568 | 1.922 |
| 3.7 | 29842 | 0.3351 | 3.572 | 1.942 |
| 3.6 | 29036 | 0.3444 | 3.602 | 1.979 |
| 3.5 | 28229 | 0.3542 | 3.668 | 2.034 |
| 3.4 | 27423 | 0.3647 | 3.792 | 2.115 |
| 3.3 | 26616 | 0.3757 | 4.084 | 2.180 |
| 3.2 | 25810 | 0.3875 | 4.379 | 1.978 |
| 3.1 | 25003 | 0.4000 | 4.607 | 1.857 |
| 3.0 | 24196 | 0.4133 | 4.943 | 1.322 |
| 2.9 | 23390 | 0.4275 | 4.757 | 0.865 |
| 2.8 | 22583 | 0.4428 | 4.547 | 0.636 |
| 2.7 | 21777 | 0.4592 | 4.375 | 0.499 |
| 2.6 | 20970 | 0.4769 | 4.235 | 0.409 |
| 2.5 | 20164 | 0.4959 | 4.118 | 0.341 |
| 2.4 | 19357 | 0.5166 | 4.022 | 0.288 |
| 2.3 | 18551 | 0.5391 | 3.940 | 0.242 |
| 2.2 | 17744 | 0.5636 | 3.871 | 0.202 |
| 2.1 | 16938 | 0.5904 | 3.815 | 0.165 |
| 2.0 | 16131 | 0.6199 | 3.759 | 0.118 |
| 1.9 | 15324 | 0.6526 | 3.700 | 0.094 |
| 1.8 | 14518 | 0.6889 | 3.662 | 0.082 |
| 1.7 | 13711 | 0.7293 | 3.635 | 0.002 |
| 1.6 | 12905 | 0.7749 | 3.536 | 0.002 |
| 1.5 | 12098 | 0.8266 | 3.457 | |

TABLE II (*Continued*)

$Al_{0.315}Ga_{0.685}As$ (UV-VIS)

| eV | $cm^{-1}$ | μm | n | k |
|---|---|---|---|---|
| 6.0 | 48393 | 0.2066 | 1.347[2] | 2.443[2] |
| 5.9 | 47586 | 0.2101 | 1.338 | 2.502 |
| 5.8 | 46780 | 0.2138 | 1.352 | 2.577 |
| 5.7 | 45973 | 0.2175 | 1.367 | 2.669 |
| 5.6 | 45167 | 0.2214 | 1.393 | 2.776 |
| 5.5 | 44360 | 0.2254 | 1.437 | 2.893 |
| 5.4 | 43554 | 0.2296 | 1.497 | 3.030 |
| 5.3 | 42747 | 0.2339 | 1.581 | 3.187 |
| 5.2 | 41940 | 0.2384 | 1.696 | 3.376 |
| 5.1 | 41134 | 0.2431 | 1.878 | 3.604 |
| 5.0 | 40327 | 0.2480 | 2.198 | 3.845 |
| 4.9 | 39521 | 0.2530 | 2.684 | 3.957 |
| 4.8 | 38714 | 0.2583 | 3.196 | 3.881 |
| 4.7 | 37908 | 0.2638 | 3.669 | 3.617 |
| 4.6 | 37101 | 0.2695 | 3.982 | 3.177 |
| 4.5 | 36295 | 0.2755 | 4.062 | 2.733 |
| 4.4 | 35488 | 0.2818 | 3.999 | 2.393 |
| 4.3 | 34682 | 0.2883 | 3.883 | 2.172 |
| 4.2 | 33875 | 0.2952 | 3.772 | 2.040 |
| 4.1 | 33068 | 0.3024 | 3.686 | 1.966 |
| 4.0 | 32262 | 0.3100 | 3.625 | 1.927 |
| 3.9 | 31455 | 0.3179 | 3.588 | 1.914 |
| 3.8 | 30649 | 0.3263 | 3.575 | 1.921 |
| 3.7 | 29842 | 0.3351 | 3.589 | 1.946 |
| 3.6 | 29036 | 0.3444 | 3.633 | 1.988 |
| 3.5 | 28229 | 0.3542 | 3.724 | 2.054 |
| 3.4 | 27423 | 0.3647 | 3.922 | 2.134 |
| 3.3 | 26616 | 0.3757 | 4.246 | 2.041 |
| 3.2 | 25810 | 0.3875 | 4.456 | 1.879 |
| 3.1 | 25003 | 0.4000 | 4.825 | 1.558 |
| 3.0 | 24196 | 0.4133 | 4.781 | 1.012 |
| 2.9 | 23390 | 0.4275 | 4.582 | 0.722 |
| 2.8 | 22583 | 0.4428 | 4.404 | 0.556 |
| 2.7 | 21777 | 0.4592 | 4.258 | 0.446 |
| 2.6 | 20970 | 0.4769 | 4.135 | 0.367 |
| 2.5 | 20164 | 0.4959 | 4.032 | 0.305 |
| 2.4 | 19357 | 0.5166 | 3.945 | 0.258 |
| 2.3 | 18551 | 0.5391 | 3.872 | 0.227 |
| 2.2 | 17744 | 0.5636 | 3.815 | 0.202 |
| 2.1 | 16938 | 0.5904 | 3.750 | 0.167 |
| 2.0 | 16131 | 0.6199 | 3.690 | 0.145 |
| 1.9 | 15324 | 0.6526 | 3.650 | 0.111 |
| 1.8 | 14518 | 0.6889 | 3.592 | 0.008 |
| 1.7 | 13711 | 0.7293 | 3.509 | |
| 1.6 | 12905 | 0.7749 | 3.456 | |
| 1.5 | 12098 | 0.8266 | 3.404 | |

TABLE II (*Continued*)

$Al_{0.419}Ga_{0.581}As$ (UV-VIS)

| eV | $cm^{-1}$ | μm | n | k |
|---|---|---|---|---|
| 6.0 | 48393 | 0.2066 | 1.353[2] | 2.440[2] |
| 5.9 | 47586 | 0.2101 | 1.350 | 2.507 |
| 5.8 | 46780 | 0.2138 | 1.357 | 2.574 |
| 5.7 | 45973 | 0.2175 | 1.377 | 2.675 |
| 5.6 | 45167 | 0.2214 | 1.406 | 2.783 |
| 5.5 | 44360 | 0.2254 | 1.456 | 2.908 |
| 5.4 | 43554 | 0.2296 | 1.523 | 3.047 |
| 5.3 | 42747 | 0.2339 | 1.613 | 3.201 |
| 5.2 | 41940 | 0.2384 | 1.740 | 3.384 |
| 5.1 | 41134 | 0.2431 | 1.926 | 3.598 |
| 5.0 | 40327 | 0.2480 | 2.234 | 3.822 |
| 4.9 | 39521 | 0.2530 | 2.695 | 3.937 |
| 4.8 | 38714 | 0.2583 | 3.200 | 3.909 |
| 4.7 | 37908 | 0.2638 | 3.733 | 3.646 |
| 4.6 | 37101 | 0.2695 | 4.054 | 3.157 |
| 4.5 | 36295 | 0.2755 | 4.103 | 2.691 |
| 4.4 | 35488 | 0.2818 | 4.014 | 2.363 |
| 4.3 | 34682 | 0.2883 | 3.897 | 2.161 |
| 4.2 | 33875 | 0.2952 | 3.794 | 2.040 |
| 4.1 | 33068 | 0.3024 | 3.719 | 1.971 |
| 4.0 | 32262 | 0.3100 | 3.667 | 1.936 |
| 3.9 | 31455 | 0.3179 | 3.640 | 1.924 |
| 3.8 | 30649 | 0.3263 | 3.640 | 1.931 |
| 3.7 | 29842 | 0.3351 | 3.668 | 1.958 |
| 3.6 | 29036 | 0.3444 | 3.736 | 2.005 |
| 3.5 | 28229 | 0.3542 | 3.887 | 2.071 |
| 3.4 | 27423 | 0.3647 | 4.172 | 2.042 |
| 3.3 | 26616 | 0.3757 | 4.401 | 1.870 |
| 3.2 | 25810 | 0.3875 | 4.706 | 1.640 |
| 3.1 | 25003 | 0.4000 | 4.778 | 1.119 |
| 3.0 | 24196 | 0.4133 | 4.605 | 0.786 |
| 2.9 | 23390 | 0.4275 | 4.430 | 0.596 |
| 2.8 | 22583 | 0.4428 | 4.280 | 0.472 |
| 2.7 | 21777 | 0.4592 | 4.154 | 0.385 |
| 2.6 | 20970 | 0.4769 | 4.047 | 0.319 |
| 2.5 | 20164 | 0.4959 | 3.957 | 0.268 |
| 2.4 | 19357 | 0.5166 | 3.881 | 0.219 |
| 2.3 | 18551 | 0.5391 | 3.820 | 0.178 |
| 2.2 | 17744 | 0.5636 | 3.747 | 0.134 |
| 2.1 | 16938 | 0.5904 | 3.686 | 0.100 |
| 2.0 | 16131 | 0.6199 | 3.664 | 0.059 |
| 1.9 | 15324 | 0.6526 | 3.559 | 0.003 |
| 1.8 | 14518 | 0.6889 | 3.479 | |
| 1.7 | 13711 | 0.7293 | 3.422 | |
| 1.6 | 12905 | 0.7749 | 3.378 | |
| 1.5 | 12098 | 0.8266 | 3.341 | |

TABLE II (*Continued*)

$Al_{0.491}Ga_{0.509}As$ (UV-VIS)

| eV | $cm^{-1}$ | μm | n | k |
|---|---|---|---|---|
| 6.0 | 48393 | 0.2066 | 1.366[2] | 2.418[2] |
| 5.9 | 47586 | 0.2101 | 1.363 | 2.490 |
| 5.8 | 46780 | 0.2138 | 1.364 | 2.572 |
| 5.7 | 45973 | 0.2175 | 1.379 | 2.666 |
| 5.6 | 45167 | 0.2214 | 1.412 | 2.780 |
| 5.5 | 44360 | 0.2254 | 1.462 | 2.903 |
| 5.4 | 43554 | 0.2296 | 1.532 | 3.045 |
| 5.3 | 42747 | 0.2339 | 1.632 | 3.199 |
| 5.2 | 41940 | 0.2384 | 1.763 | 3.378 |
| 5.1 | 41134 | 0.2431 | 1.951 | 3.579 |
| 5.0 | 40327 | 0.2480 | 2.250 | 3.787 |
| 4.9 | 39521 | 0.2530 | 2.686 | 3.904 |
| 4.8 | 38714 | 0.2583 | 3.187 | 3.899 |
| 4.7 | 37908 | 0.2638 | 3.731 | 3.645 |
| 4.6 | 37101 | 0.2695 | 4.072 | 3.147 |
| 4.5 | 36295 | 0.2755 | 4.107 | 2.668 |
| 4.4 | 35488 | 0.2818 | 4.009 | 2.351 |
| 4.3 | 34682 | 0.2883 | 3.894 | 2.159 |
| 4.2 | 33875 | 0.2952 | 3.798 | 2.046 |
| 4.1 | 33068 | 0.3024 | 3.730 | 1.980 |
| 4.0 | 32262 | 0.3100 | 3.688 | 1.945 |
| 3.9 | 31455 | 0.3179 | 3.671 | 1.933 |
| 3.8 | 30649 | 0.3263 | 3.680 | 1.942 |
| 3.7 | 29842 | 0.3351 | 3.724 | 1.969 |
| 3.6 | 29036 | 0.3444 | 3.822 | 2.017 |
| 3.5 | 28229 | 0.3542 | 4.034 | 2.049 |
| 3.4 | 27423 | 0.3647 | 4.294 | 1.922 |
| 3.3 | 26616 | 0.3757 | 4.525 | 1.748 |
| 3.2 | 25810 | 0.3875 | 4.753 | 1.340 |
| 3.1 | 25003 | 0.4000 | 4.654 | 0.926 |
| 3.0 | 24196 | 0.4133 | 4.483 | 0.684 |
| 2.9 | 23390 | 0.4275 | 4.328 | 0.534 |
| 2.8 | 22583 | 0.4428 | 4.195 | 0.429 |
| 2.7 | 21777 | 0.4592 | 4.081 | 0.355 |
| 2.6 | 20970 | 0.4769 | 3.985 | 0.292 |
| 2.5 | 20164 | 0.4959 | 3.903 | 0.245 |
| 2.4 | 19357 | 0.5166 | 3.838 | 0.205 |
| 2.3 | 18551 | 0.5391 | 3.761 | 0.164 |
| 2.2 | 17744 | 0.5636 | 3.696 | 0.133 |
| 2.1 | 16938 | 0.5904 | 3.665 | 0.088 |
| 2.0 | 16131 | 0.6199 | 3.558 | 0.002 |
| 1.9 | 15324 | 0.6526 | 3.477 | |
| 1.8 | 14518 | 0.6889 | 3.417 | |
| 1.7 | 13711 | 0.7293 | 3.368 | |
| 1.6 | 12905 | 0.7749 | 3.329 | |
| 1.5 | 12098 | 0.8266 | 3.283 | |

TABLE II (*Continued*)

$Al_{0.590}Ga_{0.410}As$ (UV-VIS)

| eV | $cm^{-1}$ | μm | n | k |
|---|---|---|---|---|
| 6.0 | 48393 | 0.2066 | 1.385[2] | 2.420[2] |
| 5.9 | 47586 | 0.2101 | 1.370 | 2.485 |
| 5.8 | 46780 | 0.2138 | 1.370 | 2.565 |
| 5.7 | 45973 | 0.2175 | 1.389 | 2.669 |
| 5.6 | 45167 | 0.2214 | 1.422 | 2.785 |
| 5.5 | 44360 | 0.2254 | 1.475 | 2.915 |
| 5.4 | 43554 | 0.2296 | 1.553 | 3.059 |
| 5.3 | 42747 | 0.2339 | 1.661 | 3.217 |
| 5.2 | 41940 | 0.2384 | 1.805 | 3.392 |
| 5.1 | 41134 | 0.2431 | 2.007 | 3.581 |
| 5.0 | 40327 | 0.2480 | 2.304 | 3.772 |
| 4.9 | 39521 | 0.2530 | 2.740 | 3.881 |
| 4.8 | 38714 | 0.2583 | 3.221 | 3.866 |
| 4.7 | 37908 | 0.2638 | 3.762 | 3.617 |
| 4.6 | 37101 | 0.2695 | 4.120 | 3.107 |
| 4.5 | 36295 | 0.2755 | 4.127 | 2.616 |
| 4.4 | 35488 | 0.2818 | 4.015 | 2.318 |
| 4.3 | 34682 | 0.2883 | 3.903 | 2.142 |
| 4.2 | 33875 | 0.2952 | 3.815 | 2.038 |
| 4.1 | 33068 | 0.3024 | 3.758 | 1.978 |
| 4.0 | 32262 | 0.3100 | 3.729 | 1.947 |
| 3.9 | 31455 | 0.3179 | 3.725 | 1.935 |
| 3.8 | 30649 | 0.3263 | 3.750 | 1.944 |
| 3.7 | 29842 | 0.3351 | 3.822 | 1.973 |
| 3.6 | 29036 | 0.3444 | 3.977 | 2.002 |
| 3.5 | 28229 | 0.3542 | 4.224 | 1.924 |
| 3.4 | 27423 | 0.3647 | 4.429 | 1.754 |
| 3.3 | 26616 | 0.3757 | 4.665 | 1.450 |
| 3.2 | 25810 | 0.3875 | 4.649 | 1.028 |
| 3.1 | 25003 | 0.4000 | 4.497 | 0.754 |
| 3.0 | 24196 | 0.4133 | 4.343 | 0.584 |
| 2.9 | 23390 | 0.4275 | 4.208 | 0.468 |
| 2.8 | 22583 | 0.4428 | 4.092 | 0.384 |
| 2.7 | 21777 | 0.4592 | 3.992 | 0.317 |
| 2.6 | 20970 | 0.4769 | 3.909 | 0.262 |
| 2.5 | 20164 | 0.4959 | 3.837 | 0.205 |
| 2.4 | 19357 | 0.5166 | 3.758 | 0.157 |
| 2.3 | 18551 | 0.5391 | 3.690 | 0.126 |
| 2.2 | 17744 | 0.5636 | 3.658 | 0.063 |
| 2.1 | 16938 | 0.5904 | 3.546 | 0.005 |
| 2.0 | 16131 | 0.6199 | 3.467 | |
| 1.9 | 15324 | 0.6526 | 3.405 | |
| 1.8 | 14518 | 0.6889 | 3.354 | |
| 1.7 | 13711 | 0.7293 | 3.313 | |
| 1.6 | 12905 | 0.7749 | 3.274 | |
| 1.5 | 12098 | 0.8266 | 3.237 | |

TABLE II (*Continued*)

$Al_{0.700}Ga_{0.300}As$ (UV-VIS)

| eV | $cm^{-1}$ | μm | n | k |
|---|---|---|---|---|
| 6.0 | 48393 | 0.2066 | 1.377[2] | 2.426[2] |
| 5.9 | 47586 | 0.2101 | 1.366 | 2.493 |
| 5.8 | 46780 | 0.2138 | 1.365 | 2.581 |
| 5.7 | 45973 | 0.2175 | 1.375 | 2.688 |
| 5.6 | 45167 | 0.2214 | 1.407 | 2.809 |
| 5.5 | 44360 | 0.2254 | 1.462 | 2.946 |
| 5.4 | 43554 | 0.2296 | 1.545 | 3.098 |
| 5.3 | 42747 | 0.2339 | 1.662 | 3.269 |
| 5.2 | 41940 | 0.2384 | 1.829 | 3.445 |
| 5.1 | 41134 | 0.2431 | 2.049 | 3.620 |
| 5.0 | 40327 | 0.2480 | 2.354 | 3.788 |
| 4.9 | 39521 | 0.2530 | 2.777 | 3.873 |
| 4.8 | 38714 | 0.2583 | 3.214 | 3.853 |
| 4.7 | 37908 | 0.2638 | 3.758 | 3.637 |
| 4.6 | 37101 | 0.2695 | 4.144 | 3.150 |
| 4.5 | 36295 | 0.2755 | 4.142 | 2.645 |
| 4.4 | 35488 | 0.2818 | 4.028 | 2.365 |
| 4.3 | 34682 | 0.2883 | 3.932 | 2.206 |
| 4.2 | 33875 | 0.2952 | 3.868 | 2.111 |
| 4.1 | 33068 | 0.3024 | 3.835 | 2.055 |
| 4.0 | 32262 | 0.3100 | 3.836 | 2.023 |
| 3.9 | 31455 | 0.3179 | 3.868 | 2.009 |
| 3.8 | 30649 | 0.3263 | 3.947 | 2.006 |
| 3.7 | 29842 | 0.3351 | 4.103 | 1.993 |
| 3.6 | 29036 | 0.3444 | 4.319 | 1.877 |
| 3.5 | 28229 | 0.3542 | 4.502 | 1.678 |
| 3.4 | 27423 | 0.3647 | 4.665 | 1.357 |
| 3.3 | 26616 | 0.3757 | 4.615 | 0.980 |
| 3.2 | 25810 | 0.3875 | 4.471 | 0.735 |
| 3.1 | 25003 | 0.4000 | 4.325 | 0.574 |
| 3.0 | 24196 | 0.4133 | 4.196 | 0.460 |
| 2.9 | 23390 | 0.4275 | 4.084 | 0.374 |
| 2.8 | 22583 | 0.4428 | 3.987 | 0.307 |
| 2.7 | 21777 | 0.4592 | 3.906 | 0.245 |
| 2.6 | 20970 | 0.4769 | 3.823 | 0.184 |
| 2.5 | 20164 | 0.4959 | 3.746 | 0.129 |
| 2.4 | 19357 | 0.5166 | 3.696 | 0.069 |
| 2.3 | 18551 | 0.5391 | 3.595 | 0.002 |
| 2.2 | 17744 | 0.5636 | 3.500 | |
| 2.1 | 16938 | 0.5904 | 3.425 | |
| 2.0 | 16131 | 0.6199 | 3.361 | |
| 1.9 | 15324 | 0.6526 | 3.306 | |
| 1.8 | 14518 | 0.6889 | 3.261 | |
| 1.7 | 13711 | 0.7293 | 3.225 | |
| 1.6 | 12905 | 0.7749 | 3.188 | |
| 1.5 | 12098 | 0.8266 | 3.153 | |

TABLE II (*Continued*)

$Al_{0.804}Ga_{0.196}As$ (UV-VIS)

| eV | $cm^{-1}$ | μm | n | k |
|---|---|---|---|---|
| 6.0 | 48393 | 0.2066 | 1.368[2] | 2.409[2] |
| 5.9 | 47586 | 0.2101 | 1.360 | 2.473 |
| 5.8 | 46780 | 0.2138 | 1.354 | 2.560 |
| 5.7 | 45973 | 0.2175 | 1.370 | 2.667 |
| 5.6 | 45167 | 0.2214 | 1.399 | 2.792 |
| 5.5 | 44360 | 0.2254 | 1.447 | 2.935 |
| 5.4 | 43554 | 0.2296 | 1.528 | 3.104 |
| 5.3 | 42747 | 0.2339 | 1.661 | 3.293 |
| 5.2 | 41940 | 0.2384 | 1.857 | 3.475 |
| 5.1 | 41134 | 0.2431 | 2.110 | 3.635 |
| 5.0 | 40327 | 0.2480 | 2.426 | 3.763 |
| 4.9 | 39521 | 0.2530 | 2.833 | 3.815 |
| 4.8 | 38714 | 0.2583 | 3.233 | 3.765 |
| 4.7 | 37908 | 0.2638 | 3.751 | 3.582 |
| 4.6 | 37101 | 0.2695 | 4.107 | 3.128 |
| 4.5 | 36295 | 0.2755 | 4.112 | 2.639 |
| 4.4 | 35488 | 0.2818 | 4.004 | 2.389 |
| 4.3 | 34682 | 0.2883 | 3.928 | 2.256 |
| 4.2 | 33875 | 0.2952 | 3.893 | 2.183 |
| 4.1 | 33068 | 0.3024 | 3.904 | 2.144 |
| 4.0 | 32262 | 0.3100 | 3.962 | 2.119 |
| 3.9 | 31455 | 0.3179 | 4.078 | 2.092 |
| 3.8 | 30649 | 0.3263 | 4.267 | 2.013 |
| 3.7 | 29842 | 0.3351 | 4.462 | 1.820 |
| 3.6 | 29036 | 0.3444 | 4.613 | 1.561 |
| 3.5 | 28229 | 0.3542 | 4.667 | 1.199 |
| 3.4 | 27423 | 0.3647 | 4.562 | 0.890 |
| 3.3 | 26616 | 0.3757 | 4.413 | 0.685 |
| 3.2 | 25810 | 0.3875 | 4.277 | 0.541 |
| 3.1 | 25003 | 0.4000 | 4.155 | 0.437 |
| 3.0 | 24196 | 0.4133 | 4.050 | 0.353 |
| 2.9 | 23390 | 0.4275 | 3.961 | 0.276 |
| 2.8 | 22583 | 0.4428 | 3.872 | 0.205 |
| 2.7 | 21777 | 0.4592 | 3.787 | 0.161 |
| 2.6 | 20970 | 0.4769 | 3.738 | 0.104 |
| 2.5 | 20164 | 0.4959 | 3.635 | 0.013 |
| 2.4 | 19357 | 0.5166 | 3.519 | 0.004 |
| 2.3 | 18551 | 0.5391 | 3.440 | 0.003 |
| 2.2 | 17744 | 0.5636 | 3.378 | |
| 2.1 | 16938 | 0.5904 | 3.322 | |
| 2.0 | 16131 | 0.6199 | 3.277 | |
| 1.9 | 15324 | 0.6526 | 3.236 | |
| 1.8 | 14518 | 0.6889 | 3.202 | |
| 1.7 | 13711 | 0.7293 | 3.173 | |
| 1.6 | 12905 | 0.7749 | 3.147 | |
| 1.5 | 12098 | 0.8266 | 3.124 | |

TABLE II (*Continued*)

$Al_{0.1}Ga_{0.9}As$ (VIS-Near IR)

| eV | $cm^{-1}$ | μm | n |
|---|---|---|---|
| 1.5 | 12098 | 0.8266 | 3.618[1] |
| 1.4 | 11292 | 0.8856 | 3.531 |
| 1.3 | 10485 | 0.9537 | 3.484 |
| 1.2 | 9679 | 1.033 | 3.452 |
| 1.1 | 8872 | **1.127** | 3.428 |
| 1.0 | 8065 | **1.240** | 3.409 |
| 0.9 | 7259 | **1.378** | 3.395 |
| 0.8 | 6452 | 1.550 | 3.383 |
| 0.7 | 5646 | 1.771 | 3.373 |
| 0.6 | 4839 | 2.066 | 3.365 |
| 0.5 | 4033 | 2.480 | 3.359 |
| | $Al_{0.14}Ga_{0.86}As$ (VIS- Near IR) | | |
| 1.5 | 12098 | 0.8266 | 3.570[1] |
| 1.4 | 11292 | 0.8856 | 3.503 |
| 1.3 | 10485 | 0.9537 | 3.461 |
| 1.2 | 9679 | 1.033 | 3.431 |
| 1.1 | 8872 | **1.127** | 3.408 |
| 1.0 | 8065 | **1.240** | 3.390 |
| 0.9 | 7259 | **1.378** | 3.375 |
| 0.8 | 6452 | 1.550 | 3.363 |
| 0.7 | 5646 | 1.771 | 3.353 |
| 0.6 | 4839 | 2.066 | 3.345 |
| 0.5 | 4033 | 2.480 | 3.338 |
| 1.71 | 13792 | 0.7251 | 3.640[5] |
| 1.70 | 13711 | 0.7293 | 3.642 |
| 1.69 | 13631 | 0.7336 | 3.642 |
| 1.68 | 13550 | 0.7380 | 3.642 |
| 1.67 | 13469 | 0.7424 | 3.643 |
| 1.66 | 13389 | 0.7469 | 3.643 |
| 1.65 | 13308 | 0.7514 | 3.643 |
| 1.64 | 13227 | 0.7560 | 3.644 |
| 1.63 | 13147 | 0.7606 | 3.606 |
| 1.62 | 13066 | 0.7653 | 3.591 |
| 1.61 | 12985 | 0.7701 | 3.579 |
| 1.60 | 12905 | 0.7749 | 3.569 |
| 1.55 | 12501 | 0.7999 | 3.532 |
| 1.50 | 12098 | 0.8266 | 3.505 |
| 1.45 | 11695 | 0.8551 | 3.482 |
| 1.40 | 11292 | 0.8856 | 3.463 |
| 1.35 | 10888 | 0.9184 | 3.445 |
| 1.30 | 10485 | 0.9537 | 3.429 |
| 1.25 | 10082 | 0.9919 | 3.414 |
| 1.20 | 9679 | 1.033 | 3.400 |

TABLE II (*Continued*)

| eV | $cm^{-1}$ | μm | n |
|---|---|---|---|
| | | $Al_{0.2}Ga_{0.8}As$ (VIS-Near IR) | |
| 1.6 | 12905 | 0.7749 | 3.603[1] |
| 1.5 | 12098 | 0.8266 | 3.516 |
| 1.4 | 11292 | 0.8856 | 3.464 |
| 1.3 | 10485 | 0.9537 | 3.428 |
| 1.2 | 9679 | 1.033 | 3.400 |
| 1.1 | 8872 | 1.127 | 3.377 |
| 1.0 | 8065 | 1.240 | 3.359 |
| 0.9 | 7259 | 1.378 | 3.345 |
| 0.8 | 6452 | 1.550 | 3.333 |
| 0.7 | 5646 | 1.771 | 3.323 |
| 0.6 | 4839 | 2.066 | 3.314 |
| 0.5 | 4033 | 2.480 | 3.308 |
| | | $Al_{0.3}Ga_{0.7}As$ (VIS-Near IR) | |
| 1.8 | 14518 | 0.6888 | 3.797[1] |
| 1.7 | 13711 | 0.7293 | 3.580 |
| 1.6 | 12905 | 0.7749 | 3.498 |
| 1.5 | 12098 | 0.8266 | 3.443 |
| 1.4 | 11292 | 0.8856 | 3.403 |
| 1.3 | 10485 | 0.9537 | 3.372 |
| 1.2 | 9679 | 1.033 | 3.346 |
| 1.1 | 8872 | 1.127 | 3.326 |
| 1.0 | 8065 | 1.240 | 3.308 |
| 0.9 | 7259 | 1.378 | 3.294 |
| 0.8 | 6452 | 1.550 | 3.282 |
| 0.7 | 5646 | 1.771 | 3.271 |
| 0.6 | 4839 | 2.066 | 3.263 |
| 0.5 | 4033 | 2.480 | 3.256 |
| | | $Al_{0.4}Ga_{0.6}As$ (VIS-Near IR) | |
| 1.9 | 15324 | 0.6526 | 3.693[1] |
| 1.8 | 14518 | 0.6888 | 3.554 |
| 1.7 | 13711 | 0.7293 | 3.475 |
| 1.6 | 12905 | 0.7749 | 3.420 |
| 1.5 | 12098 | 0.8266 | 3.377 |
| 1.4 | 11292 | 0.8856 | 3.343 |
| 1.3 | 10485 | 0.9537 | 3.315 |
| 1.2 | 9679 | 1.033 | 3.292 |
| 1.1 | 8872 | 1.127 | 3.273 |
| 1.0 | 8065 | 1.240 | 3.256 |
| 0.9 | 7259 | 1.378 | 3.242 |
| 0.8 | 6452 | 1.550 | 3.230 |
| 0.7 | 5646 | 1.771 | 3.220 |
| 0.6 | 4839 | 2.066 | 3.212 |
| 0.5 | 4033 | 2.480 | 3.205 |

TABLE II (*Continued*)

| eV | $cm^{-1}$ | μm | n |
|---|---|---|---|
| | | $Al_{0.5}Ga_{0.5}As$ (VIS-Near IR) | |
| 2.0 | 16131 | 0.6199 | 3.635[1] |
| 1.9 | 15324 | 0.6526 | 3.523 |
| 1.8 | 14518 | 0.6888 | 3.449 |
| 1.7 | 13711 | 0.7293 | 3.393 |
| 1.6 | 12905 | 0.7749 | 3.350 |
| 1.5 | 12098 | 0.8266 | 3.314 |
| 1.4 | 11292 | 0.8856 | 3.284 |
| 1.3 | 10485 | 0.9537 | 3.259 |
| 1.2 | 9679 | 1.033 | 3.238 |
| 1.1 | 8872 | 1.127 | 3.219 |
| 1.0 | 8065 | 1.240 | 3.190 |
| 0.9 | 7259 | 1.378 | 3.190 |
| 0.8 | 6452 | 1.550 | 3.178 |
| 0.7 | 5646 | 1.771 | 3.168 |
| 0.6 | 4839 | 2.066 | 3.160 |
| 0.5 | 4033 | 2.480 | 3.153 |
| | | $Al_{0.6}Ga_{0.4}As$ (VIS-Near IR) | |
| 2.2 | 17744 | 0.5636 | 3.749[1] |
| 2.1 | 16938 | 0.5904 | 3.585 |
| 2.0 | 16131 | 0.6199 | 3.489 |
| 1.9 | 15324 | 0.6526 | 3.419 |
| 1.8 | 14518 | 0.6888 | 3.365 |
| 1.7 | 13711 | 0.7293 | 3.320 |
| 1.6 | 12905 | 0.7749 | 3.284 |
| 1.5 | 12098 | 0.8266 | 3.252 |
| 1.4 | 11292 | 0.8856 | 3.226 |
| 1.3 | 10485 | 0.9537 | 3.202 |
| 1.2 | 9679 | 1.033 | 3.182 |
| 1.1 | 8872 | 1.127 | 3.165 |
| 1.0 | 8065 | 1.240 | 3.150 |
| 0.9 | 7259 | 1.378 | 3.137 |
| 0.8 | 6452 | 1.550 | 3.125 |
| 0.7 | 5646 | 1.771 | 3.116 |
| 0.6 | 4839 | 2.066 | 3.107 |
| 0.5 | 4033 | 2.480 | 3.101 |
| | | $Al_{0.7}Ga_{0.3}As$ (VIS-Near IR) | |
| 2.4 | 19357 | 0.5166 | 3.918[1] |
| 2.3 | 18551 | 0.5391 | 3.661 |
| 2.2 | 17744 | 0.5636 | 3.538 |
| 2.1 | 16938 | 0.5904 | 3.452 |
| 2.0 | 16131 | 0.6199 | 3.386 |
| 1.9 | 15324 | 0.6526 | 3.333 |
| 1.8 | 14518 | 0.6888 | 3.289 |
| 1.7 | 13711 | 0.7293 | 3.252 |
| 1.6 | 12905 | 0.7749 | 3.219 |
| 1.5 | 12098 | 0.8266 | 3.191 |

TABLE II (*Continued*)

| eV | $cm^{-1}$ | μm | n |
|---|---|---|---|
| | | $Al_{0.7}Ga_{0.3}As$ (VIS-Near IR) | |
| 1.4 | 11292 | 0.8856 | 3.167 |
| 1.3 | 10485 | 0.9537 | 3.146 |
| 1.2 | 9679 | 1.033 | 3.127 |
| 1.1 | 8872 | 1.127 | 3.110 |
| 1.0 | 8065 | 1.240 | 3.096 |
| 0.9 | 7259 | 1.378 | 3.083 |
| 0.8 | 6452 | 1.550 | 3.072 |
| 0.7 | 5646 | 1.771 | 3.063 |
| 0.6 | 4839 | 2.066 | 3.055 |
| 0.5 | 4033 | 2.480 | 3.048 |
| | | $Al_{0.8}Ga_{0.2}As$ (VIS-Near IR) | |
| 2.5 | 20164 | 0.4959 | 3.746[1] |
| 2.4 | 19357 | 0.5166 | 3.592 |
| 2.3 | 18551 | 0.5391 | 3.490 |
| 2.2 | 17744 | 0.5636 | 3.413 |
| 2.1 | 16938 | 0.5904 | 3.351 |
| 2.0 | 16131 | 0.6199 | 3.299 |
| 1.9 | 15324 | 0.6526 | 3.256 |
| 1.8 | 14518 | 0.6888 | 3.218 |
| 1.7 | 13711 | 0.7293 | 3.185 |
| 1.6 | 12905 | 0.7749 | 3.156 |
| 1.5 | 12098 | 0.8266 | 3.131 |
| 1.4 | 11292 | 0.8856 | 3.108 |
| 1.3 | 10485 | 0.9537 | 3.088 |
| 1.2 | 9679 | 1.033 | 3.071 |
| 1.1 | 8872 | 1.127 | 3.055 |
| 1.0 | 8065 | 1.240 | 3.041 |
| 0.9 | 7259 | 1.378 | 3.029 |
| 0.8 | 6452 | 1.550 | 3.018 |
| 0.7 | 5646 | 1.771 | 3.009 |
| 0.6 | 4839 | 2.066 | 3.002 |
| 0.5 | 4033 | 2.480 | 2.995 |
| | | $Al_{0.9}Ga_{0.1}As$ (VIS-Near IR) | |
| 2.7 | 21777 | 0.4592 | 3.834[1] |
| 2.6 | 20970 | 0.4769 | 3.649 |
| 2.5 | 20164 | 0.4959 | 3.531 |
| 2.4 | 19357 | 0.5166 | 3.442 |
| 2.3 | 18551 | 0.5391 | 3.372 |
| 2.2 | 17744 | 0.5636 | 3.313 |
| 2.1 | 16938 | 0.5904 | 3.263 |
| 2.0 | 16131 | 0.6199 | 3.220 |
| 1.9 | 15324 | 0.6526 | 3.183 |
| 1.8 | 14518 | 0.6888 | 3.149 |
| 1.7 | 13711 | 0.7293 | 3.120 |
| 1.6 | 12905 | 0.7749 | 3.094 |
| 1.5 | 12098 | 0.8266 | 3.070 |

TABLE II (*Continued*)

$Al_{0.9}Ga_{0.1}As$ (VIS-Near IR)

| eV | $cm^{-1}$ | μm | n |
|---|---|---|---|
| 1.4 | 11292 | 0.8856 | 3.049 |
| 1.3 | 10485 | 0.9537 | 3.031 |
| 1.2 | 9679 | 1.033 | 3.014 |
| 1.1 | 8872 | 1.127 | 2.999 |
| 1.0 | 8065 | 1.240 | 2.986 |
| 0.9 | 7259 | 1.378 | 2.974 |
| 0.8 | 6452 | 1.550 | 2.964 |
| 0.7 | 5646 | 1.771 | 2.955 |
| 0.6 | 4839 | 2.066 | 2.948 |
| 0.5 | 4033 | 2.480 | 2.942 |

* References are indicated in brackets.

TABLE II (*Continued*)

Values of n and k for $Al_{0.14}Ga_{0.86}As$ from Various References[a]

| eV | $cm^{-1}$ | $\mu m$ | n | k |
|---|---|---|---|---|
| 0.2480 | 2000 | 5.00 | 3.244[3] | $1.99 \times 10^{-5}$[3] |
| 0.2066 | 1667 | 6.00 | 3.240 | 2.81 |
| 0.1771 | 1429 | 7.00 | 3.236 | 2.74 |
| 0.1550 | 1250 | 8.00 | 3.232 | $7.43 \times 10^{-5}$ |
| 0.1378 | 1111 | 9.00 | 3.226 | $1.43 \times 10^{-4}$ |
| 0.1240 | 1000 | 10.00 | 3.219 | 2.38 |
| 0.1227 | 990 | 10.10 | 3.219 | 2.49 |
| 0.1215 | 980 | 10.20 | 3.218 | 2.61 |
| 0.1203 | 970 | 10.31 | 3.217 | 2.74 |
| 0.1190 | 960 | 10.42 | 3.216 | 2.87 |
| 0.1178 | 950 | 10.53 | 3.215 | 3.01 |
| 0.1165 | 940 | 10.64 | 3.215 | 3.16 |
| 0.1153 | 930 | 10.75 | 3.214 | 3.32 |
| 0.1141 | 920 | 10.87 | 3.213 | 3.48 |
| 0.1128 | 910 | 10.99 | 3.212 | 3.66 |
| 0.1116 | 900 | 11.11 | 3.211 | 3.85 |
| 0.1103 | 890 | 11.24 | 3.210 | 4.04 |
| 0.1091 | 880 | 11.36 | 3.209 | 4.25 |
| 0.1079 | 870 | 11.49 | 3.208 | 4.47 |
| 0.1066 | 860 | 11.63 | 3.206 | 4.71 |
| 0.1054 | 850 | 11.76 | 3.205 | 4.96 |
| 0.1041 | 840 | 11.90 | 3.204 | 5.23 |
| 0.1029 | 830 | 12.05 | 3.203 | 5.51 |
| 0.1017 | 820 | 12.20 | 3.201 | 5.82 |
| 0.1004 | 810 | 12.35 | 3.200 | 6.14 |
| 0.0992 | 800 | 12.50 | 3.198 | 6.49 |
| 0.0979 | 790 | 12.66 | 3.197 | 6.87 |
| 0.0967 | 780 | 12.82 | 3.195 | 7.27 |
| 0.0955 | 770 | 12.99 | 3.193 | 7.70 |
| 0.0942 | 760 | 13.16 | 3.191 | 8.16 |
| 0.0930 | 750 | 13.33 | 3.189 | 8.66 |
| 0.0917 | 740 | 13.51 | 3.187 | 9.20 |
| 0.0905 | 730 | 13.70 | 3.185 | $9.78 \times 10^{-4}$ |
| 0.0893 | 720 | 13.89 | 3.183 | $1.04 \times 10^{-3}$ |
| 0.0880 | 710 | 14.08 | 3.180 | 1.11 |
| 0.0868 | 700 | 14.29 | 3.178 | 1.18 |
| 0.0855 | 690 | 14.49 | 3.175 | 1.27 |
| 0.0843 | 680 | 14.71 | 3.172 | 1.35 |
| 0.0831 | 670 | 14.93 | 3.169 | 1.45 |
| 0.0818 | 660 | 15.15 | 3.166 | 1.56 |
| 0.0806 | 650 | 15.38 | 3.163 | 1.68 |
| 0.0793 | 640 | 15.63 | 3.159 | 1.81 |
| 0.0781 | 630 | 15.87 | 3.155 | 1.95 |
| 0.0769 | 620 | 16.13 | 3.151 | 2.11 |
| 0.0756 | 610 | 16.39 | 3.146 | 2.29 |
| 0.0744 | 600 | 16.67 | 3.141 | 2.49 |
| 0.0731 | 590 | 16.95 | 3.136 | 2.71 |
| 0.0719 | 580 | 17.24 | 3.130 | 2.97 |
| 0.0707 | 570 | 17.54 | 3.124 | 3.26 |
| 0.0694 | 560 | 17.86 | 3.117 | 3.59 |

TABLE II (*Continued*)

$Al_{0.14}Ga_{0.86}As$

| eV | $cm^{-1}$ | $\mu$m | n | k |
|---|---|---|---|---|
| 0.0682 | 550 | 18.18 | 3.110 | 3.97 |
| 0.0669 | 540 | 18.52 | 3.101 | 4.41 |
| 0.0657 | 530 | 18.87 | 3.092 | 4.92 |
| 0.0645 | 520 | 19.23 | 3.082 | 5.53 |
| 0.0632 | 510 | 19.61 | 3.071 | 6.25 |
| 0.0620 | 500 | 20.00 | 3.058 | 7.12 |
| 0.0608 | 490 | 20.41 | 3.044 | 8.17 |
| 0.0595 | 480 | 20.83 | 3.028 | $9.48\times10^{-3}$ |
| 0.0583 | 470 | 21.28 | 3.009 | $1.11\times10^{-2}$ |
| 0.0570 | 460 | 21.74 | 2.987 | 1.32 |
| 0.0558 | 450 | 22.22 | 2.961 | 1.60 |
| 0.0555 | 448 | 22.32 | 2.955 | 1.67 |
| 0.0553 | 446 | 22.42 | 2.949 | 1.74 |
| 0.0550 | 444 | 22.52 | 2.943 | 1.82 |
| 0.0548 | 442 | 22.62 | 2.936 | 1.90 |
| 0.0546 | 440 | 22.73 | 2.930 | 1.99 |
| 0.0543 | 438 | 22.83 | 2.922 | 2.08 |
| 0.0541 | 436 | 22.94 | 2.915 | 2.18 |
| 0.0538 | 434 | 23.04 | 2.907 | 2.29 |
| 0.0536 | 432 | 23.15 | 2.899 | 2.40 |
| 0.0533 | 430 | 23.26 | 2.891 | 2.53 |
| 0.0531 | 428 | 23.36 | 2.882 | 2.67 |
| 0.0528 | 426 | 23.47 | 2.872 | 2.81 |
| 0.0526 | 424 | 23.58 | 2.862 | 2.98 |
| 0.0523 | 422 | 23.70 | 2.852 | 3.15 |
| 0.0521 | 420 | 23.81 | 2.841 | 3.34 |
| 0.0518 | 418 | 23.92 | 2.829 | 3.56 |
| 0.0516 | 416 | 24.04 | 2.817 | 3.79 |
| 0.0513 | 414 | 24.15 | 2.803 | 4.05 |
| 0.0511 | 412 | 24.27 | 2.789 | 4.34 |
| 0.0508 | 410 | 24.39 | 2.774 | 4.66 |
| 0.0506 | 408 | 24.51 | 2.758 | 5.02 |
| 0.0503 | 406 | 24.63 | 2.741 | 5.43 |
| 0.0501 | 404 | 24.75 | 2.722 | 5.89 |
| 0.0498 | 402 | 24.88 | 2.702 | 6.42 |
| 0.0496 | 400 | 25.00 | 2.680 | 7.02 |
| 0.0493 | 398 | 25.13 | 2.656 | 7.73 |
| 0.0491 | 396 | 25.25 | 2.630 | 8.54 |
| 0.0488 | 394 | 25.38 | 2.601 | $9.51\times10^{-2}$ |
| 0.0486 | 392 | 25.51 | 2.569 | $1.07\times10^{-1}$ |
| 0.0484 | 390 | 25.64 | 2.533 | 1.20 |
| 0.0481 | 388 | 25.77 | 2.493 | 1.37 |
| 0.0479 | 386 | 25.91 | 2.448 | 1.58 |
| 0.0476 | 384 | 26.04 | 2.396 | 1.84 |
| 0.0474 | 382 | 26.18 | 2.337 | 2.18 |
| 0.0471 | 380 | 26.32 | 2.270 | 2.62 |
| 0.0469 | 378 | 26.46 | 2.191 | 3.22 |
| 0.0466 | 376 | 26.60 | 2.102 | 4.04 |
| 0.0464 | 374 | 26.74 | 2.002 | 5.21 |
| 0.0461 | 372 | 26.88 | 1.900 | 6.92 |

TABLE II (*Continued*)

$Al_{0.14}Ga_{0.86}As$

| eV | $cm^{-1}$ | $\mu m$ | n | k |
|---|---|---|---|---|
| 0.0459 | 370 | 27.03 | 1.819 | $9.36x10^{-1}$ |
| 0.0456 | 368 | 27.17 | 1.805 | $1.26x10^{0}$ |
| 0.0454 | 366 | 27.32 | 1.913 | 1.65 |
| 0.0451 | 364 | 27.47 | 2.194 | 2.05 |
| 0.0449 | 362 | 27.62 | 2.694 | 2.36 |
| 0.0446 | 360 | 27.78 | 3.380 | 2.41 |
| 0.0444 | 358 | 27.93 | 4.003 | 2.07 |
| 0.0441 | 356 | 28.09 | 4.291 | 1.52 |
| 0.0439 | 354 | 28.25 | 4.293 | $1.05x10^{0}$ |
| 0.0436 | 352 | 28.41 | 4.177 | $7.25x10^{-1}$ |
| 0.0434 | 350 | 28.57 | 4.037 | 5.19 |
| 0.0431 | 348 | 28.74 | 3.906 | 3.84 |
| 0.0429 | 346 | 28.90 | 3.791 | 2.94 |
| 0.0426 | 344 | 29.07 | 3.691 | 2.31 |
| 0.0424 | 342 | 29.24 | 3.604 | 1.86 |
| 0.0422 | 340 | 29.41 | 3.527 | 1.53 |
| 0.0419 | 338 | 29.59 | 3.459 | 1.29 |
| 0.0417 | 336 | 29.76 | 3.397 | $1.10x10^{-1}$ |
| 0.0414 | 334 | 29.94 | 3.341 | $9.55x10^{-2}$ |
| 0.0412 | 332 | 30.12 | 3.288 | 8.43 |
| 0.0409 | 330 | 30.30 | 3.238 | 7.56 |
| 0.0407 | 328 | 30.49 | 3.191 | 6.88 |
| 0.0404 | 326 | 30.67 | 3.144 | 6.37 |
| 0.0402 | 324 | 30.86 | 3.099 | 5.99 |
| 0.0399 | 322 | 31.06 | 3.054 | 5.73 |
| 0.0397 | 320 | 31.25 | 3.008 | 5.57 |
| 0.0394 | 318 | 31.45 | 2.962 | 5.51 |
| 0.0392 | 316 | 31.65 | 2.914 | 5.54 |
| 0.0389 | 314 | 31.85 | 2.864 | 5.67 |
| 0.0387 | 312 | 32.05 | 2.812 | 5.90 |
| 0.0384 | 310 | 32.26 | 2.756 | 6.24 |
| 0.0382 | 308 | 32.47 | 2.696 | 6.72 |
| 0.0379 | 306 | 32.68 | 2.630 | 7.35 |
| 0.0377 | 304 | 32.89 | 2.558 | 8.18 |
| 0.0374 | 302 | 33.11 | 2.478 | $9.26x10^{-2}$ |
| 0.0372 | 300 | 33.33 | 2.388 | $1.07x10^{-1}$ |
| 0.0369 | 298 | 33.56 | 2.283 | 1.25 |
| 0.0367 | 296 | 33.78 | 2.162 | 1.51 |
| 0.0365 | 294 | 34.01 | 2.017 | 1.87 |
| 0.0362 | 292 | 34.25 | 1.841 | 2.39 |
| 0.0360 | 290 | 34.48 | 1.620 | 3.23 |
| 0.0357 | 288 | 34.72 | 1.338 | 4.73 |
| 0.0355 | 286 | 34.97 | 1.013 | $7.69x10^{-1}$ |
| 0.0352 | 284 | 35.21 | 0.786 | $1.25x10^{0}$ |
| 0.0350 | 282 | 35.46 | 0.715 | 1.77 |
| 0.0347 | 280 | 35.71 | 0.734 | 2.31 |
| 0.0345 | 278 | 35.97 | 0.822 | 2.88 |
| 0.0342 | 276 | 36.23 | 0.992 | 3.51 |
| 0.0340 | 274 | 36.50 | 1.299 | 4.27 |
| 0.0337 | 272 | 36.76 | 1.882 | 5.18 |

TABLE II (*Continued*)

$Al_{0.14}Ga_{0.86}As$

| eV | $cm^{-1}$ | $\mu m$ | n | k |
|---|---|---|---|---|
| 0.0335 | 270 | 37.04 | 3.097 | 6.23 |
| 0.0332 | 268 | 37.31 | 5.523 | 6.60 |
| 0.0330 | 266 | 37.59 | 7.692 | 4.63 |
| 0.0327 | 264 | 37.88 | 7.611 | 2.49 |
| 0.0325 | 262 | 38.17 | 6.944 | $1.44 \times 10^{0}$ |
| 0.0322 | 260 | 38.46 | 6.375 | $9.23 \times 10^{-1}$ |
| 0.0320 | 258 | 38.76 | 5.947 | 6.45 |
| 0.0317 | 256 | 39.06 | 5.623 | 4.78 |
| 0.0315 | 254 | 39.37 | 5.371 | 3.70 |
| 0.0312 | 252 | 39.68 | 5.172 | 2.96 |
| 0.0310 | 250 | 40.00 | 5.009 | 2.43 |
| 0.0304 | 245 | 40.82 | 4.711 | 1.61 |
| 0.0298 | 240 | 41.67 | 4.507 | $1.16 \times 10^{-1}$ |
| 0.0291 | 235 | 42.55 | 4.360 | $8.78 \times 10^{-2}$ |
| 0.0285 | 230 | 43.48 | 4.247 | 6.92 |
| 0.0279 | 225 | 44.44 | 4.159 | 5.61 |
| 0.0273 | 220 | 45.45 | 4.087 | 4.66 |
| 0.0267 | 215 | 46.51 | 4.028 | 3.93 |
| 0.0260 | 210 | 47.62 | 3.978 | 3.37 |
| 0.0254 | 205 | 48.78 | 3.936 | 2.92 |
| 0.0248 | 200 | 50.00 | 3.899 | 2.56 |
| 0.0207 | 167 | 60.00 | 3.745 | $1.26 \times 10^{-2}$ |
| 0.0177 | 143 | 70.00 | 3.684 | $8.38 \times 10^{-3}$ |
| 0.0155 | 125 | 80.00 | 3.653 | 6.35 |
| 0.0138 | 111 | 90.00 | 3.634 | 5.14 |
| 0.0124 | 100 | 100.00 | 3.621 | 4.35 |

TABLE II (*Continued*)

Values of n and k for $Al_{0.18}Ga_{0.82}As$ from Various References[a]

| eV | $cm^{-1}$ | $\mu m$ | n | k |
|---|---|---|---|---|
| 0.2480 | 2000 | 5.00 | 3.228[3] | |
| 0.2066 | 1667 | 6.00 | 3.225 | |
| 0.1771 | 1429 | 7.00 | 3.221 | |
| 0.1550 | 1250 | 8.00 | 3.216 | |
| 0.1378 | 1111 | 9.00 | 3.210 | |
| 0.1240 | 1000 | 10.00 | 3.203 | |
| 0.1227 | 990 | 10.10 | 3.202 | |
| 0.1215 | 980 | 10.20 | 3.202 | |
| 0.1203 | 970 | 10.31 | 3.201 | |
| 0.1190 | 960 | 10.42 | 3.200 | |
| 0.1178 | 950 | 10.53 | 3.199 | |
| 0.1165 | 940 | 10.64 | 3.198 | |
| 0.1153 | 930 | 10.75 | 3.197 | |
| 0.1141 | 920 | 10.87 | 3.196 | |
| 0.1128 | 910 | 10.99 | 3.195 | |
| 0.1116 | 900 | 11.11 | 3.194 | |
| 0.1103 | 890 | 11.24 | 3.193 | |
| 0.1091 | 880 | 11.36 | 3.192 | |
| 0.1079 | 870 | 11.49 | 3.191 | |
| 0.1066 | 860 | 11.63 | 3.190 | |
| 0.1054 | 850 | 11.76 | 3.188 | |
| 0.1041 | 840 | 11.90 | 3.187 | |
| 0.1029 | 830 | 12.05 | 3.186 | |
| 0.1017 | 820 | 12.20 | 3.184 | |
| 0.1004 | 810 | 12.35 | 3.183 | |
| 0.0992 | 800 | 12.50 | 3.181 | |
| 0.0979 | 790 | 12.66 | 3.179 | |
| 0.0967 | 780 | 12.82 | 3.178 | |
| 0.0955 | 770 | 12.99 | 3.176 | |
| 0.0942 | 760 | 13.16 | 3.174 | |
| 0.0930 | 750 | 13.33 | 3.172 | |
| 0.0917 | 740 | 13.51 | 3.170 | |
| 0.0905 | 730 | 13.70 | 3.168 | |
| 0.0893 | 720 | 13.89 | 3.165 | |
| 0.0880 | 710 | 14.08 | 3.163 | |
| 0.0868 | 700 | 14.29 | 3.160 | |
| 0.0855 | 690 | 14.49 | 3.157 | |
| 0.0843 | 680 | 14.71 | 3.154 | |
| 0.0831 | 670 | 14.93 | 3.151 | |
| 0.0818 | 660 | 15.15 | 3.147 | |
| 0.0806 | 650 | 15.38 | 3.144 | |
| 0.0793 | 640 | 15.63 | 3.140 | |
| 0.0781 | 630 | 15.87 | 3.136 | |
| 0.0769 | 620 | 16.13 | 3.131 | |
| 0.0756 | 610 | 16.39 | 3.126 | |
| 0.0744 | 600 | 16.67 | 3.121 | |
| 0.0731 | 590 | 16.95 | 3.115 | |
| 0.0719 | 580 | 17.24 | 3.109 | |
| 0.0707 | 570 | 17.54 | 3.103 | |
| 0.0694 | 560 | 17.86 | 3.095 | |

TABLE II (*Continued*)

$Al_{0.18}Ga_{0.82}As$

| eV | $cm^{-1}$ | $\mu$m | n | k |
|---|---|---|---|---|
| 0.0682 | 550 | 18.18 | 3.087 | |
| 0.0669 | 540 | 18.52 | 3.078 | |
| 0.0657 | 530 | 18.87 | 3.069 | |
| 0.0645 | 520 | 19.23 | 3.058 | |
| 0.0632 | 510 | 19.61 | 3.045 | |
| 0.0620 | 500 | 20.00 | 3.031 | |
| 0.0608 | 490 | 20.41 | 3.016 | |
| 0.0595 | 480 | 20.83 | 2.997 | |
| 0.0583 | 470 | 21.28 | 2.976 | |
| 0.0570 | 460 | 21.74 | 2.951 | |
| 0.0558 | 450 | 22.22 | 2.921 | |
| 0.0555 | 448 | 22.32 | 2.915 | |
| 0.0553 | 446 | 22.42 | 2.908 | |
| 0.0550 | 444 | 22.52 | 2.900 | |
| 0.0548 | 442 | 22.62 | 2.893 | |
| 0.0546 | 440 | 22.73 | 2.885 | |
| 0.0543 | 438 | 22.83 | 2.876 | |
| 0.0541 | 436 | 22.94 | 2.868 | |
| 0.0538 | 434 | 23.04 | 2.859 | |
| 0.0536 | 432 | 23.15 | 2.849 | |
| 0.0533 | 430 | 23.26 | 2.839 | |
| 0.0531 | 428 | 23.36 | 2.828 | |
| 0.0528 | 426 | 23.47 | 2.817 | |
| 0.0526 | 424 | 23.58 | 2.805 | |
| 0.0523 | 422 | 23.70 | 2.792 | |
| 0.0521 | 420 | 23.81 | 2.779 | |
| 0.0518 | 418 | 23.92 | 2.764 | |
| 0.0516 | 416 | 24.04 | 2.749 | |
| 0.0513 | 414 | 24.15 | 2.733 | |
| 0.0511 | 412 | 24.27 | 2.716 | |
| 0.0508 | 410 | 24.39 | 2.697 | |
| 0.0506 | 408 | 24.51 | 2.677 | |
| 0.0503 | 406 | 24.63 | 2.655 | |
| 0.0501 | 404 | 24.75 | 2.631 | |
| 0.0498 | 402 | 24.88 | 2.605 | |
| 0.0496 | 400 | 25.00 | 2.576 | $1.56 \times 10^{-2}$ [3] |
| 0.0493 | 398 | 25.13 | 2.545 | 2.29 |
| 0.0491 | 396 | 25.25 | 2.511 | 3.17 |
| 0.0488 | 394 | 25.38 | 2.472 | 4.26 |
| 0.0486 | 392 | 25.51 | 2.429 | 5.59 |
| 0.0484 | 390 | 25.64 | 2.380 | 7.27 |
| 0.0481 | 388 | 25.77 | 2.325 | $9.40 \times 10^{-2}$ |
| 0.0479 | 386 | 25.91 | 2.262 | $1.21 \times 10^{-1}$ |
| 0.0476 | 384 | 26.04 | 2.189 | 1.58 |
| 0.0474 | 382 | 26.18 | 2.105 | 2.07 |
| 0.0471 | 380 | 26.32 | 2.007 | 2.75 |
| 0.0469 | 378 | 26.46 | 1.895 | 3.72 |
| 0.0466 | 376 | 26.60 | 1.772 | 5.15 |
| 0.0464 | 374 | 26.74 | 1.653 | $7.25 \times 10^{-1}$ |
| 0.0461 | 372 | 26.88 | 1.576 | $1.02 \times 10^{0}$ |

TABLE II (*Continued*)

$Al_{0.18}Ga_{0.82}As$

| eV | $cm^{-1}$ | $\mu m$ | n | k |
|---|---|---|---|---|
| 0.0459 | 370 | 27.03 | 1.589 | 1.38 |
| 0.0456 | 368 | 27.17 | 1.726 | 1.78 |
| 0.0454 | 366 | 27.32 | 2.012 | 2.16 |
| 0.0451 | 364 | 27.47 | 2.471 | 2.47 |
| 0.0449 | 362 | 27.62 | 3.090 | 2.60 |
| 0.0446 | 360 | 27.78 | 3.731 | 2.41 |
| 0.0444 | 358 | 27.93 | 4.165 | 1.96 |
| 0.0441 | 356 | 28.09 | 4.321 | 1.47 |
| 0.0439 | 354 | 28.25 | 4.299 | $1.08\times10^{0}$ |
| 0.0436 | 352 | 28.41 | 4.203 | $8.01\times10^{-1}$ |
| 0.0434 | 350 | 28.57 | 4.089 | 6.06 |
| 0.0431 | 348 | 28.74 | 3.978 | 4.70 |
| 0.0429 | 346 | 28.90 | 3.876 | 3.72 |
| 0.0426 | 344 | 29.07 | 3.785 | 2.99 |
| 0.0424 | 342 | 29.24 | 3.704 | 2.44 |
| 0.0422 | 340 | 29.41 | 3.632 | 2.01 |
| 0.0419 | 338 | 29.59 | 3.566 | 1.68 |
| 0.0417 | 336 | 29.76 | 3.506 | 1.41 |
| 0.0414 | 334 | 29.94 | 3.451 | 1.19 |
| 0.0412 | 332 | 30.12 | 3.400 | $1.00\times10^{-1}$ |
| 0.0409 | 330 | 30.30 | 3.351 | $8.51\times10^{-2}$ |
| 0.0407 | 328 | 30.49 | 3.304 | 7.22 |
| 0.0404 | 326 | 30.67 | 3.259 | 6.13 |
| 0.0402 | 324 | 30.86 | 3.216 | 5.20 |
| 0.0399 | 322 | 31.06 | 3.172 | 4.40 |
| 0.0397 | 320 | 31.25 | 3.129 | 3.72 |
| 0.0394 | 318 | 31.45 | 3.085 | 3.14 |
| 0.0392 | 316 | 31.65 | 3.040 | 2.66 |
| 0.0389 | 314 | 31.85 | 2.994 | 2.26 |
| 0.0387 | 312 | 32.05 | 2.946 | 1.96 |
| 0.0384 | 310 | 32.26 | 2.895 | 1.75 |
| 0.0382 | 308 | 32.47 | 2.841 | 1.63 |
| 0.0379 | 306 | 32.68 | 2.782 | 1.64 |
| 0.0377 | 304 | 32.89 | 2.719 | 1.78 |
| 0.0374 | 302 | 33.11 | 2.649 | 2.09 |
| 0.0372 | 300 | 33.33 | 2.571 | 2.63 |
| 0.0369 | 298 | 33.56 | 2.482 | 3.46 |
| 0.0367 | 296 | 33.78 | 2.380 | 4.72 |
| 0.0365 | 294 | 34.01 | 2.261 | 6.59 |
| 0.0362 | 292 | 34.25 | 2.119 | $9.43\times10^{-2}$ |
| 0.0360 | 290 | 34.48 | 1.944 | $1.39\times10^{-1}$ |
| 0.0357 | 288 | 34.72 | 1.724 | 2.12 |
| 0.0355 | 286 | 34.97 | 1.439 | 3.48 |
| 0.0352 | 284 | 35.21 | 1.089 | $6.36\times10^{-1}$ |
| 0.0350 | 282 | 35.46 | 0.840 | $1.16\times10^{0}$ |
| 0.0347 | 280 | 35.71 | 0.802 | 1.74 |
| 0.0345 | 278 | 35.97 | 0.889 | 2.31 |
| 0.0342 | 276 | 36.23 | 1.079 | 2.90 |
| 0.0340 | 274 | 36.50 | 1.409 | 3.53 |
| 0.0337 | 272 | 36.76 | 1.971 | 4.20 |

TABLE II (*Continued*)

$Al_{0.18}Ga_{0.82}As$

| eV | $cm^{-1}$ | $\mu$m | n | k |
|---|---|---|---|---|
| 0.0335 | 270 | 37.04 | 2.919 | 4.79 |
| 0.0332 | 268 | 37.31 | 4.321 | 4.91 |
| 0.0330 | 266 | 37.59 | 5.634 | 4.13 |
| 0.0327 | 264 | 37.88 | 6.135 | 2.94 |
| 0.0325 | 262 | 38.17 | 6.049 | 2.02 |
| 0.0322 | 260 | 38.46 | 5.795 | 1.44 |
| 0.0320 | 258 | 38.76 | 5.534 | $1.08\times10^{0}$ |
| 0.0317 | 256 | 39.06 | 5.307 | $8.41\times10^{-1}$ |
| 0.0315 | 254 | 39.37 | 5.117 | 6.80 |
| 0.0312 | 252 | 39.68 | 4.959 | 5.65 |
| 0.0310 | 250 | 40.00 | 4.826 | 4.79 |
| 0.0304 | 245 | 40.82 | 4.574 | 3.41 |
| 0.0298 | 240 | 41.67 | 4.397 | 2.61 |
| 0.0291 | 235 | 42.55 | 4.267 | 2.09 |
| 0.0285 | 230 | 43.48 | 4.167 | 1.73 |
| 0.0279 | 225 | 44.44 | 4.088 | 1.47 |
| 0.0273 | 220 | 45.45 | 4.023 | 1.27 |
| 0.0267 | 215 | 46.51 | 3.970 | $1.11\times10^{-1}$ |
| 0.0260 | 210 | 47.62 | 3.924 | $9.87\times10^{-2}$ |
| 0.0254 | 205 | 48.78 | 3.886 | 8.85 |
| 0.0248 | 200 | 50.00 | 3.853 | 7.99 |
| 0.0207 | 167 | 60.00 | 3.710 | 4.58 |
| 0.0177 | 143 | 70.00 | 3.654 | 3.30 |
| 0.0155 | 125 | 80.00 | 3.625 | 2.62 |
| 0.0138 | 111 | 90.00 | 3.607 | 2.19 |
| 0.0124 | 100 | 100.00 | 3.595 | 1.89 |

TABLE II (*Continued*)

Values of n and k for $Al_{0.30}Ga_{0.70}As$ from Various References[a]

| eV | $cm^{-1}$ | $\mu$m | n | k |
|---|---|---|---|---|
| 0.2480 | 2000 | 5.00 | 3.179[3] | |
| 0.2066 | 1667 | 6.00 | 3.175 | |
| 0.1771 | 1429 | 7.00 | 3.170 | |
| 0.1550 | 1250 | 8.00 | 3.164 | |
| 0.1378 | 1111 | 9.00 | 3.157 | |
| 0.1240 | 1000 | 10.00 | 3.150 | |
| 0.1227 | 990 | 10.10 | 3.149 | |
| 0.1215 | 980 | 10.20 | 3.148 | |
| 0.1203 | 970 | 10.31 | 3.147 | |
| 0.1190 | 960 | 10.42 | 3.146 | |
| 0.1178 | 950 | 10.53 | 3.145 | |
| 0.1165 | 940 | 10.64 | 3.144 | |
| 0.1153 | 930 | 10.75 | 3.143 | |
| 0.1141 | 920 | 10.87 | 3.142 | |
| 0.1128 | 910 | 10.99 | 3.140 | |
| 0.1116 | 900 | 11.11 | 3.139 | |
| 0.1103 | 890 | 11.24 | 3.138 | |
| 0.1091 | 880 | 11.36 | 3.137 | |
| 0.1079 | 870 | 11.49 | 3.135 | |
| 0.1066 | 860 | 11.63 | 3.134 | |
| 0.1054 | 850 | 11.76 | 3.132 | |
| 0.1041 | 840 | 11.90 | 3.131 | |
| 0.1029 | 830 | 12.05 | 3.129 | |
| 0.1017 | 820 | 12.20 | 3.127 | |
| 0.1004 | 810 | 12.35 | 3.126 | |
| 0.0992 | 800 | 12.50 | 3.124 | |
| 0.0979 | 790 | 12.66 | 3.122 | |
| 0.0967 | 780 | 12.82 | 3.120 | |
| 0.0955 | 770 | 12.99 | 3.117 | |
| 0.0942 | 760 | 13.16 | 3.115 | |
| 0.0930 | 750 | 13.33 | 3.113 | |
| 0.0917 | 740 | 13.51 | 3.110 | |
| 0.0905 | 730 | 13.70 | 3.107 | |
| 0.0893 | 720 | 13.89 | 3.104 | |
| 0.0880 | 710 | 14.08 | 3.101 | |
| 0.0868 | 700 | 14.29 | 3.098 | |
| 0.0855 | 690 | 14.49 | 3.095 | |
| 0.0843 | 680 | 14.71 | 3.091 | |
| 0.0831 | 670 | 14.93 | 3.087 | |
| 0.0818 | 660 | 15.15 | 3.083 | |
| 0.0806 | 650 | 15.38 | 3.079 | |
| 0.0793 | 640 | 15.63 | 3.074 | |
| 0.0781 | 630 | 15.87 | 3.069 | |
| 0.0769 | 620 | 16.13 | 3.063 | |
| 0.0756 | 610 | 16.39 | 3.057 | |
| 0.0744 | 600 | 16.67 | 3.051 | |
| 0.0731 | 590 | 16.95 | 3.044 | |
| 0.0719 | 580 | 17.24 | 3.036 | |
| 0.0707 | 570 | 17.54 | 3.028 | |
| 0.0694 | 560 | 17.86 | 3.018 | |

TABLE II (*Continued*)

$Al_{0.30}Ga_{0.70}As$

| eV | $cm^{-1}$ | $\mu$m | n | k |
|---|---|---|---|---|
| 0.0682 | 550 | 18.18 | 3.008 | |
| 0.0669 | 540 | 18.52 | 2.997 | |
| 0.0657 | 530 | 18.87 | 2.984 | |
| 0.0645 | 520 | 19.23 | 2.970 | |
| 0.0632 | 510 | 19.61 | 2.954 | |
| 0.0620 | 500 | 20.00 | 2.936 | |
| 0.0608 | 490 | 20.41 | 2.915 | |
| 0.0595 | 480 | 20.83 | 2.891 | |
| 0.0583 | 470 | 21.28 | 2.862 | |
| 0.0570 | 460 | 21.74 | 2.828 | |
| 0.0558 | 450 | 22.22 | 2.786 | |
| 0.0555 | 448 | 22.32 | 2.777 | |
| 0.0553 | 446 | 22.42 | 2.767 | |
| 0.0550 | 444 | 22.52 | 2.757 | |
| 0.0548 | 442 | 22.62 | 2.746 | |
| 0.0546 | 440 | 22.73 | 2.734 | |
| 0.0543 | 438 | 22.83 | 2.722 | |
| 0.0541 | 436 | 22.94 | 2.710 | |
| 0.0538 | 434 | 23.04 | 2.696 | |
| 0.0536 | 432 | 23.15 | 2.682 | |
| 0.0533 | 430 | 23.26 | 2.668 | |
| 0.0531 | 428 | 23.36 | 2.652 | |
| 0.0528 | 426 | 23.47 | 2.635 | |
| 0.0526 | 424 | 23.58 | 2.617 | |
| 0.0523 | 422 | 23.70 | 2.598 | |
| 0.0521 | 420 | 23.81 | 2.578 | |
| 0.0518 | 418 | 23.92 | 2.557 | |
| 0.0516 | 416 | 24.04 | 2.533 | $1.12 \times 10^{-2}$ [3] |
| 0.0513 | 414 | 24.15 | 2.508 | 1.50 |
| 0.0511 | 412 | 24.27 | 2.481 | 1.95 |
| 0.0508 | 410 | 24.39 | 2.452 | 2.46 |
| 0.0506 | 408 | 24.51 | 2.420 | 3.06 |
| 0.0503 | 406 | 24.63 | 2.385 | 3.76 |
| 0.0501 | 404 | 24.75 | 2.346 | 4.59 |
| 0.0498 | 402 | 24.88 | 2.304 | 5.58 |
| 0.0496 | 400 | 25.00 | 2.257 | 6.78 |
| 0.0493 | 398 | 25.13 | 2.205 | $8.24 \times 10^{-2}$ |
| 0.0491 | 396 | 25.25 | 2.146 | $1.00 \times 10^{-1}$ |
| 0.0488 | 394 | 25.38 | 2.080 | 1.23 |
| 0.0486 | 392 | 25.51 | 2.005 | 1.51 |
| 0.0484 | 390 | 25.64 | 1.918 | 1.89 |
| 0.0481 | 388 | 25.77 | 1.818 | 2.38 |
| 0.0479 | 386 | 25.91 | 1.702 | 3.06 |
| 0.0476 | 384 | 26.04 | 1.567 | 4.03 |
| 0.0474 | 382 | 26.18 | 1.418 | 5.44 |
| 0.0471 | 380 | 26.32 | 1.270 | $7.52 \times 10^{-1}$ |
| 0.0469 | 378 | 26.46 | 1.158 | $1.03 \times 10^{0}$ |
| 0.0466 | 376 | 26.60 | 1.114 | 1.37 |
| 0.0464 | 374 | 26.74 | 1.144 | 1.72 |
| 0.0461 | 372 | 26.88 | 1.246 | 2.10 |

TABLE II (*Continued*)

$Al_{0.30}Ga_{0.70}As$

| eV | $cm^{-1}$ | $\mu m$ | n | k |
|---|---|---|---|---|
| 0.0459 | 370 | 27.03 | 1.427 | 2.49 |
| 0.0456 | 368 | 27.17 | 1.712 | 2.89 |
| 0.0454 | 366 | 27.32 | 2.142 | 3.27 |
| 0.0451 | 364 | 27.47 | 2.761 | 3.56 |
| 0.0449 | 362 | 27.62 | 3.560 | 3.62 |
| 0.0446 | 360 | 27.78 | 4.356 | 3.28 |
| 0.0444 | 358 | 27.93 | 4.869 | 2.65 |
| 0.0441 | 356 | 28.09 | 5.025 | 2.00 |
| 0.0439 | 354 | 28.25 | 4.964 | 1.48 |
| 0.0436 | 352 | 28.41 | 4.820 | $1.11\times10^{0}$ |
| 0.0434 | 350 | 28.57 | 4.658 | $8.59\times10^{-1}$ |
| 0.0431 | 348 | 28.74 | 4.505 | 6.79 |
| 0.0429 | 346 | 28.90 | 4.367 | 5.49 |
| 0.0426 | 344 | 29.07 | 4.245 | 4.53 |
| 0.0424 | 342 | 29.24 | 4.137 | 3.80 |
| 0.0422 | 340 | 29.41 | 4.042 | 3.23 |
| 0.0419 | 338 | 29.59 | 3.957 | 2.78 |
| 0.0417 | 336 | 29.76 | 3.880 | 2.42 |
| 0.0414 | 334 | 29.94 | 3.811 | 2.12 |
| 0.0412 | 332 | 30.12 | 3.748 | 1.88 |
| 0.0409 | 330 | 30.30 | 3.689 | 1.68 |
| 0.0407 | 328 | 30.49 | 3.634 | 1.51 |
| 0.0404 | 326 | 30.67 | 3.583 | 1.36 |
| 0.0402 | 324 | 30.86 | 3.534 | 1.24 |
| 0.0399 | 322 | 31.06 | 3.486 | 1.13 |
| 0.0397 | 320 | 31.25 | 3.441 | $1.04\times10^{-1}$ |
| 0.0394 | 318 | 31.45 | 3.396 | $9.66\times10^{-2}$ |
| 0.0392 | 316 | 31.65 | 3.352 | 9.02 |
| 0.0389 | 314 | 31.85 | 3.308 | 8.49 |
| 0.0387 | 312 | 32.05 | 3.263 | 8.06 |
| 0.0384 | 310 | 32.26 | 3.218 | 7.74 |
| 0.0382 | 308 | 32.47 | 3.171 | 7.52 |
| 0.0379 | 306 | 32.68 | 3.122 | 7.41 |
| 0.0377 | 304 | 32.89 | 3.071 | 7.43 |
| 0.0374 | 302 | 33.11 | 3.017 | 7.59 |
| 0.0372 | 300 | 33.33 | 2.958 | 7.91 |
| 0.0369 | 298 | 33.56 | 2.894 | 8.44 |
| 0.0367 | 296 | 33.78 | 2.823 | $9.24\times10^{-2}$ |
| 0.0365 | 294 | 34.01 | 2.743 | $1.04\times10^{-1}$ |
| 0.0362 | 292 | 34.25 | 2.653 | 1.21 |
| 0.0360 | 290 | 34.48 | 2.548 | 1.44 |
| 0.0357 | 288 | 34.72 | 2.425 | 1.78 |
| 0.0355 | 286 | 34.97 | 2.277 | 2.29 |
| 0.0352 | 284 | 35.21 | 2.094 | 3.09 |
| 0.0350 | 282 | 35.46 | 1.868 | 4.41 |
| 0.0347 | 280 | 35.71 | 1.598 | $6.77\times10^{-1}$ |
| 0.0345 | 278 | 35.97 | 1.347 | $1.09\times10^{0}$ |
| 0.0342 | 276 | 36.23 | 1.247 | 1.66 |
| 0.0340 | 274 | 36.50 | 1.334 | 2.28 |
| 0.0337 | 272 | 36.76 | 1.606 | 2.94 |

**TABLE II (*Continued*)**

$Al_{0.30}Ga_{0.70}As$

| eV | $cm^{-1}$ | $\mu$m | n | k |
|---|---|---|---|---|
| 0.0335 | 270 | 37.04 | 2.134 | 3.62 |
| 0.0332 | 268 | 37.31 | 3.055 | 4.18 |
| 0.0330 | 266 | 37.59 | 4.381 | 4.22 |
| 0.0327 | 264 | 37.88 | 5.496 | 3.42 |
| 0.0325 | 262 | 38.17 | 5.831 | 2.36 |
| 0.0322 | 260 | 38.46 | 5.705 | 1.60 |
| 0.0320 | 258 | 38.76 | 5.467 | $1.13x10^{0}$ |
| 0.0317 | 256 | 39.06 | 5.237 | $8.40x10^{-1}$ |
| 0.0315 | 254 | 39.37 | 5.042 | 6.53 |
| 0.0312 | 252 | 39.68 | 4.879 | 5.25 |
| 0.0310 | 250 | 40.00 | 4.744 | 4.34 |
| 0.0304 | 245 | 40.82 | 4.492 | 2.95 |
| 0.0298 | 240 | 41.67 | 4.320 | 2.19 |
| 0.0291 | 235 | 42.55 | 4.194 | 1.72 |
| 0.0285 | 230 | 43.48 | 4.099 | 1.40 |
| 0.0279 | 225 | 44.44 | 4.025 | 1.18 |
| 0.0273 | 220 | 45.45 | 3.964 | $1.01x10^{-1}$ |
| 0.0267 | 215 | 46.51 | 3.914 | $8.80x10^{-2}$ |
| 0.0260 | 210 | 47.62 | 3.872 | 7.78 |
| 0.0254 | 205 | 48.78 | 3.836 | 6.94 |
| 0.0248 | 200 | 50.00 | 3.805 | 6.25 |
| 0.0207 | 167 | 60.00 | 3.671 | 3.57 |
| 0.0177 | 143 | 70.00 | 3.618 | 2.57 |
| 0.0155 | 125 | 80.00 | 3.590 | 2.04 |
| 0.0138 | 111 | 90.00 | 3.573 | 1.70 |
| 0.0124 | 100 | 100.00 | 3.561 | 1.47 |

TABLE II (*Continued*)

Values of n and k for $Al_{0.36}Ga_{0.64}As$ from Various References[a]

| eV | $cm^{-1}$ | $\mu m$ | n | k |
|---|---|---|---|---|
| 0.2480 | 2000 | 5.00 | 3.160[3] | |
| 0.2066 | 1667 | 6.00 | 3.155 | |
| 0.1771 | 1429 | 7.00 | 3.150 | |
| 0.1550 | 1250 | 8.00 | 3.144 | |
| 0.1378 | 1111 | 9.00 | 3.137 | |
| 0.1240 | 1000 | 10.00 | 3.129 | |
| 0.1227 | 990 | 10.10 | 3.128 | |
| 0.1215 | 980 | 10.20 | 3.127 | |
| 0.1203 | 970 | 10.31 | 3.126 | |
| 0.1190 | 960 | 10.42 | 3.125 | |
| 0.1178 | 950 | 10.53 | 3.124 | |
| 0.1165 | 940 | 10.64 | 3.123 | |
| 0.1153 | 930 | 10.75 | 3.122 | |
| 0.1141 | 920 | 10.87 | 3.121 | |
| 0.1128 | 910 | 10.99 | 3.120 | |
| 0.1116 | 900 | 11.11 | 3.118 | |
| 0.1103 | 890 | 11.24 | 3.117 | |
| 0.1091 | 880 | 11.36 | 3.116 | |
| 0.1079 | 870 | 11.49 | 3.114 | |
| 0.1066 | 860 | 11.63 | 3.113 | |
| 0.1054 | 850 | 11.76 | 3.111 | |
| 0.1041 | 840 | 11.90 | 3.109 | |
| 0.1029 | 830 | 12.05 | 3.108 | |
| 0.1017 | 820 | 12.20 | 3.106 | |
| 0.1004 | 810 | 12.35 | 3.104 | |
| 0.0992 | 800 | 12.50 | 3.102 | |
| 0.0979 | 790 | 12.66 | 3.100 | |
| 0.0967 | 780 | 12.82 | 3.098 | |
| 0.0955 | 770 | 12.99 | 3.095 | |
| 0.0942 | 760 | 13.16 | 3.093 | |
| 0.0930 | 750 | 13.33 | 3.090 | |
| 0.0917 | 740 | 13.51 | 3.088 | |
| 0.0905 | 730 | 13.70 | 3.085 | |
| 0.0893 | 720 | 13.89 | 3.082 | |
| 0.0880 | 710 | 14.08 | 3.079 | |
| 0.0868 | 700 | 14.29 | 3.075 | |
| 0.0855 | 690 | 14.49 | 3.071 | |
| 0.0843 | 680 | 14.71 | 3.068 | |
| 0.0831 | 670 | 14.93 | 3.063 | |
| 0.0818 | 660 | 15.15 | 3.059 | |
| 0.0806 | 650 | 15.38 | 3.054 | |
| 0.0793 | 640 | 15.63 | 3.049 | |
| 0.0781 | 630 | 15.87 | 3.044 | |
| 0.0769 | 620 | 16.13 | 3.038 | |
| 0.0756 | 610 | 16.39 | 3.032 | |
| 0.0744 | 600 | 16.67 | 3.025 | |
| 0.0731 | 590 | 16.95 | 3.017 | |
| 0.0719 | 580 | 17.24 | 3.009 | |
| 0.0707 | 570 | 17.54 | 3.000 | |
| 0.0694 | 560 | 17.86 | 2.990 | |

TABLE II (*Continued*)

$Al_{0.36}Ga_{0.64}As$

| eV | $cm^{-1}$ | $\mu$m | n | k |
|---|---|---|---|---|
| 0.0682 | 550 | 18.18 | 2.979 | |
| 0.0669 | 540 | 18.52 | 2.967 | |
| 0.0657 | 530 | 18.87 | 2.954 | |
| 0.0645 | 520 | 19.23 | 2.939 | |
| 0.0632 | 510 | 19.61 | 2.921 | |
| 0.0620 | 500 | 20.00 | 2.902 | |
| 0.0608 | 490 | 20.41 | 2.879 | |
| 0.0595 | 480 | 20.83 | 2.853 | |
| 0.0583 | 470 | 21.28 | 2.822 | |
| 0.0570 | 460 | 21.74 | 2.784 | |
| 0.0558 | 450 | 22.22 | 2.738 | |
| 0.0555 | 448 | 22.32 | 2.728 | |
| 0.0553 | 446 | 22.42 | 2.717 | |
| 0.0550 | 444 | 22.52 | 2.706 | |
| 0.0548 | 442 | 22.62 | 2.694 | |
| 0.0546 | 440 | 22.73 | 2.681 | |
| 0.0543 | 438 | 22.83 | 2.668 | |
| 0.0541 | 436 | 22.94 | 2.654 | |
| 0.0538 | 434 | 23.04 | 2.639 | |
| 0.0536 | 432 | 23.15 | 2.623 | |
| 0.0533 | 430 | 23.26 | 2.607 | |
| 0.0531 | 428 | 23.36 | 2.589 | |
| 0.0528 | 426 | 23.47 | 2.570 | |
| 0.0526 | 424 | 23.58 | 2.550 | |
| 0.0523 | 422 | 23.70 | 2.529 | |
| 0.0521 | 420 | 23.81 | 2.506 | |
| 0.0518 | 418 | 23.92 | 2.482 | |
| 0.0516 | 416 | 24.04 | 2.455 | |
| 0.0513 | 414 | 24.15 | 2.427 | |
| 0.0511 | 412 | 24.27 | 2.396 | |
| 0.0508 | 410 | 24.39 | 2.362 | |
| 0.0506 | 408 | 24.51 | 2.325 | |
| 0.0503 | 406 | 24.63 | 2.285 | |
| 0.0501 | 404 | 24.75 | 2.241 | $1.53 \times 10^{-2}$ [3] |
| 0.0498 | 402 | 24.88 | 2.191 | 2.56 |
| 0.0496 | 400 | 25.00 | 2.136 | 3.84 |
| 0.0493 | 398 | 25.13 | 2.075 | 5.42 |
| 0.0491 | 396 | 25.25 | 2.005 | 7.41 |
| 0.0488 | 394 | 25.38 | 1.925 | $9.96 \times 10^{-2}$ |
| 0.0486 | 392 | 25.51 | 1.834 | $1.33 \times 10^{-1}$ |
| 0.0484 | 390 | 25.64 | 1.727 | 1.78 |
| 0.0481 | 388 | 25.77 | 1.602 | 2.41 |
| 0.0479 | 386 | 25.91 | 1.456 | 3.32 |
| 0.0476 | 384 | 26.04 | 1.290 | 4.70 |
| 0.0474 | 382 | 26.18 | 1.121 | 6.82 |
| 0.0471 | 380 | 26.32 | 0.995 | $9.74 \times 10^{-1}$ |
| 0.0469 | 378 | 26.46 | 0.946 | $1.31 \times 10^{0}$ |
| 0.0466 | 376 | 26.60 | 0.967 | 1.67 |
| 0.0464 | 374 | 26.74 | 1.049 | 2.03 |
| 0.0461 | 372 | 26.88 | 1.191 | 2.40 |

TABLE II (*Continued*)

$Al_{0.36}Ga_{0.4}As$

| eV | $cm^{-1}$ | $\mu m$ | n | k |
|---|---|---|---|---|
| 0.0459 | 370 | 27.03 | 1.411 | 2.79 |
| 0.0456 | 368 | 27.17 | 1.736 | 3.19 |
| 0.0454 | 366 | 27.32 | 2.213 | 3.56 |
| 0.0451 | 364 | 27.47 | 2.887 | 3.83 |
| 0.0449 | 362 | 27.62 | 3.733 | 3.84 |
| 0.0446 | 360 | 27.78 | 4.545 | 3.44 |
| 0.0444 | 358 | 27.93 | 5.043 | 2.76 |
| 0.0441 | 356 | 28.09 | 5.182 | 2.08 |
| 0.0439 | 354 | 28.25 | 5.109 | 1.55 |
| 0.0436 | 352 | 28.41 | 4.955 | $1.17\times10^{0}$ |
| 0.0434 | 350 | 28.57 | 4.787 | $9.04\times10^{-1}$ |
| 0.0431 | 348 | 28.74 | 4.627 | 7.15 |
| 0.0429 | 346 | 28.90 | 4.483 | 5.77 |
| 0.0426 | 344 | 29.07 | 4.355 | 4.74 |
| 0.0424 | 342 | 29.24 | 4.243 | 3.95 |
| 0.0422 | 340 | 29.41 | 4.143 | 3.33 |
| 0.0419 | 338 | 29.59 | 4.055 | 2.83 |
| 0.0417 | 336 | 29.76 | 3.975 | 2.43 |
| 0.0414 | 334 | 29.94 | 3.903 | 2.09 |
| 0.0412 | 332 | 30.12 | 3.837 | 1.81 |
| 0.0409 | 330 | 30.30 | 3.776 | 1.58 |
| 0.0407 | 328 | 30.49 | 3.720 | 1.37 |
| 0.0404 | 326 | 30.67 | 3.667 | 1.20 |
| 0.0402 | 324 | 30.86 | 3.617 | $1.04\times10^{-1}$ |
| 0.0399 | 322 | 31.06 | 3.569 | $9.11\times10^{-2}$ |
| 0.0397 | 320 | 31.25 | 3.523 | 7.93 |
| 0.0394 | 318 | 31.45 | 3.478 | 6.88 |
| 0.0392 | 316 | 31.65 | 3.434 | 5.95 |
| 0.0389 | 314 | 31.85 | 3.390 | 5.12 |
| 0.0387 | 312 | 32.05 | 3.347 | 4.39 |
| 0.0384 | 310 | 32.26 | 3.303 | 3.74 |
| 0.0382 | 308 | 32.47 | 3.258 | 3.18 |
| 0.0379 | 306 | 32.68 | 3.211 | 2.71 |
| 0.0377 | 304 | 32.89 | 3.163 | 2.33 |
| 0.0374 | 302 | 33.11 | 3.112 | 2.04 |
| 0.0372 | 300 | 33.33 | 3.057 | 1.87 |
| 0.0369 | 298 | 33.56 | 2.998 | 1.84 |
| 0.0367 | 296 | 33.78 | 2.934 | 2.00 |
| 0.0365 | 294 | 34.01 | 2.863 | 2.38 |
| 0.0362 | 292 | 34.25 | 2.782 | 3.10 |
| 0.0360 | 290 | 34.48 | 2.691 | 4.28 |
| 0.0357 | 288 | 34.72 | 2.584 | 6.14 |
| 0.0355 | 286 | 34.97 | 2.457 | $9.06\times10^{-2}$ |
| 0.0352 | 284 | 35.21 | 2.303 | $1.37\times10^{-1}$ |
| 0.0350 | 282 | 35.46 | 2.113 | 2.14 |
| 0.0347 | 280 | 35.71 | 1.875 | 3.49 |
| 0.0345 | 278 | 35.97 | 1.590 | $6.03\times10^{-1}$ |
| 0.0342 | 276 | 36.23 | 1.346 | $1.06\times10^{0}$ |
| 0.0340 | 274 | 36.50 | 1.306 | 1.67 |
| 0.0337 | 272 | 36.76 | 1.485 | 2.30 |

TABLE II (*Continued*)

$Al_{0.36}Ga_{0.64}As$

| eV | $cm^{-1}$ | $\mu$m | n | k |
|---|---|---|---|---|
| 0.0335 | 270 | 37.04 | 1.879 | 2.90 |
| 0.0332 | 268 | 37.31 | 2.539 | 3.41 |
| 0.0330 | 266 | 37.59 | 3.473 | 3.63 |
| 0.0327 | 264 | 37.88 | 4.436 | 3.33 |
| 0.0325 | 262 | 38.17 | 5.024 | 2.65 |
| 0.0322 | 260 | 38.46 | 5.187 | 1.98 |
| 0.0320 | 258 | 38.76 | 5.132 | 1.48 |
| 0.0317 | 256 | 39.06 | 5.005 | $1.14x10^{0}$ |
| 0.0315 | 254 | 39.37 | 4.869 | $9.03x10^{-1}$ |
| 0.0312 | 252 | 39.68 | 4.743 | 7.38 |
| 0.0310 | 250 | 40.00 | 4.632 | 6.18 |
| 0.0304 | 245 | 40.82 | 4.414 | 4.30 |
| 0.0298 | 240 | 41.67 | 4.259 | 3.25 |
| 0.0291 | 235 | 42.55 | 4.144 | 2.58 |
| 0.0285 | 230 | 43.48 | 4.056 | 2.13 |
| 0.0279 | 225 | 44.44 | 3.986 | 1.81 |
| 0.0273 | 220 | 45.45 | 3.929 | 1.56 |
| 0.0267 | 215 | 46.51 | 3.882 | 1.37 |
| 0.0260 | 210 | 47.62 | 3.842 | 1.22 |
| 0.0254 | 205 | 48.78 | 3.808 | $1.10x10^{-1}$ |
| 0.0248 | 200 | 50.00 | 3.779 | $9.92x10^{-2}$ |
| 0.0207 | 167 | 60.00 | 3.651 | 5.77 |
| 0.0177 | 143 | 70.00 | 3.599 | 4.19 |
| 0.0155 | 125 | 80.00 | 3.572 | 3.34 |
| 0.0138 | 111 | 90.00 | 3.555 | 2.80 |
| 0.0124 | 100 | 100.00 | 3.544 | 2.42 |

TABLE II (*Continued*)

Values of n and k for $Al_{0.44}Ga_{0.56}As$ from Various References[a]

| eV | $cm^{-1}$ | $\mu m$ | n | k |
|---|---|---|---|---|
| 0.2480 | 2000 | 5.00 | 3.127[3] | |
| 0.2066 | 1667 | 6.00 | 3.122 | |
| 0.1771 | 1429 | 7.00 | 3.117 | |
| 0.1550 | 1250 | 8.00 | 3.110 | |
| 0.1378 | 1111 | 9.00 | 3.102 | |
| 0.1240 | 1000 | 10.00 | 3.093 | |
| 0.1227 | 990 | 10.10 | 3.092 | |
| 0.1215 | 980 | 10.20 | 3.091 | |
| 0.1203 | 970 | 10.31 | 3.090 | |
| 0.1190 | 960 | 10.42 | 3.089 | |
| 0.1178 | 950 | 10.53 | 3.088 | |
| 0.1165 | 940 | 10.64 | 3.086 | |
| 0.1153 | 930 | 10.75 | 3.085 | |
| 0.1141 | 920 | 10.87 | 3.084 | |
| 0.1128 | 910 | 10.99 | 3.082 | |
| 0.1116 | 900 | 11.11 | 3.081 | |
| 0.1103 | 890 | 11.24 | 3.080 | |
| 0.1091 | 880 | 11.36 | 3.078 | |
| 0.1079 | 870 | 11.49 | 3.076 | |
| 0.1066 | 860 | 11.63 | 3.075 | |
| 0.1054 | 850 | 11.76 | 3.073 | |
| 0.1041 | 840 | 11.90 | 3.071 | |
| 0.1029 | 830 | 12.05 | 3.069 | |
| 0.1017 | 820 | 12.20 | 3.067 | |
| 0.1004 | 810 | 12.35 | 3.065 | |
| 0.0992 | 800 | 12.50 | 3.063 | |
| 0.0979 | 790 | 12.66 | 3.060 | |
| 0.0967 | 780 | 12.82 | 3.058 | |
| 0.0955 | 770 | 12.99 | 3.055 | |
| 0.0942 | 760 | 13.16 | 3.053 | |
| 0.0930 | 750 | 13.33 | 3.050 | |
| 0.0917 | 740 | 13.51 | 3.047 | |
| 0.0905 | 730 | 13.70 | 3.044 | |
| 0.0893 | 720 | 13.89 | 3.040 | |
| 0.0880 | 710 | 14.08 | 3.037 | |
| 0.0868 | 700 | 14.29 | 3.033 | |
| 0.0855 | 690 | 14.49 | 3.029 | |
| 0.0843 | 680 | 14.71 | 3.024 | |
| 0.0831 | 670 | 14.93 | 3.020 | |
| 0.0818 | 660 | 15.15 | 3.015 | |
| 0.0806 | 650 | 15.38 | 3.009 | |
| 0.0793 | 640 | 15.63 | 3.004 | |
| 0.0781 | 630 | 15.87 | 2.997 | |
| 0.0769 | 620 | 16.13 | 2.991 | |
| 0.0756 | 610 | 16.39 | 2.984 | |
| 0.0744 | 600 | 16.67 | 2.976 | |
| 0.0731 | 590 | 16.95 | 2.967 | |
| 0.0719 | 580 | 17.24 | 2.958 | |
| 0.0707 | 570 | 17.54 | 2.948 | |
| 0.0694 | 560 | 17.86 | 2.936 | |

TABLE II (*Continued*)

$Al_{0.44}Ga_{0.56}As$

| eV | $cm^{-1}$ | $\mu m$ | n | k |
|---|---|---|---|---|
| 0.0682 | 550 | 18.18 | 2.924 | |
| 0.0669 | 540 | 18.52 | 2.910 | |
| 0.0657 | 530 | 18.87 | 2.895 | |
| 0.0645 | 520 | 19.23 | 2.877 | |
| 0.0632 | 510 | 19.61 | 2.857 | |
| 0.0620 | 500 | 20.00 | 2.834 | |
| 0.0608 | 490 | 20.41 | 2.808 | |
| 0.0595 | 480 | 20.83 | 2.777 | |
| 0.0583 | 470 | 21.28 | 2.741 | |
| 0.0570 | 460 | 21.74 | 2.697 | |
| 0.0558 | 450 | 22.22 | 2.642 | |
| 0.0555 | 448 | 22.32 | 2.630 | |
| 0.0553 | 446 | 22.42 | 2.617 | |
| 0.0550 | 444 | 22.52 | 2.603 | |
| 0.0548 | 442 | 22.62 | 2.589 | |
| 0.0546 | 440 | 22.73 | 2.574 | |
| 0.0543 | 438 | 22.83 | 2.558 | |
| 0.0541 | 436 | 22.94 | 2.541 | |
| 0.0538 | 434 | 23.04 | 2.523 | |
| 0.0536 | 432 | 23.15 | 2.504 | |
| 0.0533 | 430 | 23.26 | 2.484 | |
| 0.0531 | 428 | 23.36 | 2.463 | $1.07 \times 10^{-2}$[3] |
| 0.0528 | 426 | 23.47 | 2.440 | 1.34 |
| 0.0526 | 424 | 23.58 | 2.415 | 1.64 |
| 0.0523 | 422 | 23.70 | 2.389 | 1.98 |
| 0.0521 | 420 | 23.81 | 2.361 | 2.37 |
| 0.0518 | 418 | 23.92 | 2.331 | 2.81 |
| 0.0516 | 416 | 24.04 | 2.298 | 3.31 |
| 0.0513 | 414 | 24.15 | 2.263 | 3.89 |
| 0.0511 | 412 | 24.27 | 2.224 | 4.57 |
| 0.0508 | 410 | 24.39 | 2.182 | 5.35 |
| 0.0506 | 408 | 24.51 | 2.135 | 6.27 |
| 0.0503 | 406 | 24.63 | 2.084 | 7.37 |
| 0.0501 | 404 | 24.75 | 2.027 | $8.68 \times 10^{-2}$ |
| 0.0498 | 402 | 24.88 | 1.963 | $1.03 \times 10^{-1}$ |
| 0.0496 | 400 | 25.00 | 1.891 | 1.22 |
| 0.0493 | 398 | 25.13 | 1.809 | 1.47 |
| 0.0491 | 396 | 25.25 | 1.715 | 1.79 |
| 0.0488 | 394 | 25.38 | 1.607 | 2.21 |
| 0.0486 | 392 | 25.51 | 1.480 | 2.79 |
| 0.0484 | 390 | 25.64 | 1.331 | 3.63 |
| 0.0481 | 388 | 25.77 | 1.160 | 4.90 |
| 0.0479 | 386 | 25.91 | 0.983 | 6.84 |
| 0.0476 | 384 | 26.04 | 0.844 | $9.53 \times 10^{-1}$ |
| 0.0474 | 382 | 26.18 | 0.770 | $1.26 \times 10^{0}$ |
| 0.0471 | 380 | 26.32 | 0.751 | 1.58 |
| 0.0469 | 378 | 26.46 | 0.774 | 1.91 |
| 0.0466 | 376 | 26.60 | 0.832 | 2.25 |
| 0.0464 | 374 | 26.74 | 0.930 | 2.61 |
| 0.0461 | 372 | 26.88 | 1.077 | 3.01 |

TABLE II (*Continued*)

$Al_{0.44}Ga_{0.56}As$

| eV | $cm^{-1}$ | $\mu m$ | n | k |
|---|---|---|---|---|
| 0.0459 | 370 | 27.03 | 1.297 | 3.44 |
| 0.0456 | 368 | 27.17 | 1.632 | 3.92 |
| 0.0454 | 366 | 27.32 | 2.156 | 4.43 |
| 0.0451 | 364 | 27.47 | 2.984 | 4.89 |
| 0.0449 | 362 | 27.62 | 4.188 | 5.02 |
| 0.0446 | 360 | 27.78 | 5.463 | 4.43 |
| 0.0444 | 358 | 27.93 | 6.135 | 3.28 |
| 0.0441 | 356 | 28.09 | 6.146 | 2.24 |
| 0.0439 | 354 | 28.25 | 5.884 | 1.55 |
| 0.0436 | 352 | 28.41 | 5.578 | $1.11\times10^{0}$ |
| 0.0434 | 350 | 28.57 | 5.299 | $8.23\times10^{-1}$ |
| 0.0431 | 348 | 28.74 | 5.060 | 6.32 |
| 0.0429 | 346 | 28.90 | 4.859 | 4.99 |
| 0.0426 | 344 | 29.07 | 4.689 | 4.03 |
| 0.0424 | 342 | 29.24 | 4.543 | 3.31 |
| 0.0422 | 340 | 29.41 | 4.417 | 2.76 |
| 0.0419 | 338 | 29.59 | 4.307 | 2.32 |
| 0.0417 | 336 | 29.76 | 4.210 | 1.98 |
| 0.0414 | 334 | 29.94 | 4.124 | 1.69 |
| 0.0412 | 332 | 30.12 | 4.046 | 1.46 |
| 0.0409 | 330 | 30.30 | 3.975 | 1.27 |
| 0.0407 | 328 | 30.49 | 3.910 | $1.10\times10^{-1}$ |
| 0.0404 | 326 | 30.67 | 3.850 | $9.61\times10^{-2}$ |
| 0.0402 | 324 | 30.86 | 3.793 | 8.41 |
| 0.0399 | 322 | 31.06 | 3.740 | 7.37 |
| 0.0397 | 320 | 31.25 | 3.690 | 6.47 |
| 0.0394 | 318 | 31.45 | 3.642 | 5.69 |
| 0.0392 | 316 | 31.65 | 3.595 | 5.01 |
| 0.0389 | 314 | 31.85 | 3.550 | 4.42 |
| 0.0387 | 312 | 32.05 | 3.506 | 3.91 |
| 0.0384 | 310 | 32.26 | 3.461 | 3.48 |
| 0.0382 | 308 | 32.47 | 3.417 | 3.12 |
| 0.0379 | 306 | 32.68 | 3.372 | 2.84 |
| 0.0377 | 304 | 32.89 | 3.326 | 2.64 |
| 0.0374 | 302 | 33.11 | 3.279 | 2.52 |
| 0.0372 | 300 | 33.33 | 3.229 | 2.50 |
| 0.0369 | 298 | 33.56 | 3.177 | 2.59 |
| 0.0367 | 296 | 33.78 | 3.121 | 2.83 |
| 0.0365 | 294 | 34.01 | 3.060 | 3.25 |
| 0.0362 | 292 | 34.25 | 2.993 | 3.90 |
| 0.0360 | 290 | 34.48 | 2.919 | 4.89 |
| 0.0357 | 288 | 34.72 | 2.834 | 6.32 |
| 0.0355 | 286 | 34.97 | 2.737 | $8.43\times10^{-2}$ |
| 0.0352 | 284 | 35.21 | 2.623 | $1.15\times10^{-1}$ |
| 0.0350 | 282 | 35.46 | 2.486 | 1.63 |
| 0.0347 | 280 | 35.71 | 2.320 | 2.37 |
| 0.0345 | 278 | 35.97 | 2.114 | 3.59 |
| 0.0342 | 276 | 36.23 | 1.868 | 5.75 |
| 0.0340 | 274 | 36.50 | 1.628 | $9.58\times10^{-1}$ |
| 0.0337 | 272 | 36.76 | 1.533 | $1.52\times10^{0}$ |

TABLE II (*Continued*)

$Al_{0.44}Ga_{0.56}As$

| eV | $cm^{-1}$ | $\mu$m | n | k |
|---|---|---|---|---|
| 0.0335 | 270 | 37.04 | 1.674 | 2.16 |
| 0.0332 | 268 | 37.31 | 2.068 | 2.79 |
| 0.0330 | 266 | 37.59 | 2.770 | 3.30 |
| 0.0327 | 264 | 37.88 | 3.761 | 3.46 |
| 0.0325 | 262 | 38.17 | 4.695 | 3.03 |
| 0.0322 | 260 | 38.46 | 5.156 | 2.29 |
| 0.0320 | 258 | 38.76 | 5.211 | 1.64 |
| 0.0317 | 256 | 39.06 | 5.100 | $1.20\times10^{0}$ |
| 0.0315 | 254 | 39.37 | 4.951 | $9.11\times10^{-1}$ |
| 0.0312 | 252 | 39.68 | 4.808 | 7.16 |
| 0.0310 | 250 | 40.00 | 4.682 | 5.80 |
| 0.0304 | 245 | 40.82 | 4.439 | 3.80 |
| 0.0298 | 240 | 41.67 | 4.271 | 2.74 |
| 0.0291 | 235 | 42.55 | 4.149 | 2.12 |
| 0.0285 | 230 | 43.48 | 4.057 | 1.70 |
| 0.0279 | 225 | 44.44 | 3.985 | 1.42 |
| 0.0273 | 220 | 45.45 | 3.927 | 1.21 |
| 0.0267 | 215 | 46.51 | 3.878 | $1.04\times10^{-1}$ |
| 0.0260 | 210 | 47.62 | 3.838 | $9.18\times10^{-2}$ |
| 0.0254 | 205 | 48.78 | 3.803 | 8.16 |
| 0.0248 | 200 | 50.00 | 3.773 | 7.32 |
| 0.0207 | 167 | 60.00 | 3.644 | 4.09 |
| 0.0177 | 143 | 70.00 | 3.591 | 2.92 |
| 0.0155 | 125 | 80.00 | 3.563 | 2.30 |
| 0.0138 | 111 | 90.00 | 3.547 | 1.92 |
| 0.0124 | 100 | 100.00 | 3.535 | 1.65 |

TABLE II (*Continued*)

Values of n and k for $Al_{0.54}Ga_{0.46}As$ from Various References[a]

| eV | $cm^{-1}$ | $\mu m$ | n | k |
|---|---|---|---|---|
| 0.2480 | 2000 | 5.00 | 3.088[3] | |
| 0.2066 | 1667 | 6.00 | 3.083 | |
| 0.1771 | 1429 | 7.00 | 3.078 | |
| 0.1550 | 1250 | 8.00 | 3.071 | |
| 0.1378 | 1111 | 9.00 | 3.062 | |
| 0.1240 | 1000 | 10.00 | 3.053 | |
| 0.1227 | 990 | 10.10 | 3.052 | |
| 0.1215 | 980 | 10.20 | 3.051 | |
| 0.1203 | 970 | 10.31 | 3.049 | |
| 0.1190 | 960 | 10.42 | 3.048 | |
| 0.1178 | 950 | 10.53 | 3.047 | |
| 0.1165 | 940 | 10.64 | 3.046 | |
| 0.1153 | 930 | 10.75 | 3.044 | |
| 0.1141 | 920 | 10.87 | 3.043 | |
| 0.1128 | 910 | 10.99 | 3.042 | |
| 0.1116 | 900 | 11.11 | 3.040 | |
| 0.1103 | 890 | 11.24 | 3.039 | |
| 0.1091 | 880 | 11.36 | 3.037 | |
| 0.1079 | 870 | 11.49 | 3.035 | |
| 0.1066 | 860 | 11.63 | 3.033 | |
| 0.1054 | 850 | 11.76 | 3.032 | |
| 0.1041 | 840 | 11.90 | 3.030 | |
| 0.1029 | 830 | 12.05 | 3.028 | |
| 0.1017 | 820 | 12.20 | 3.025 | |
| 0.1004 | 810 | 12.35 | 3.023 | |
| 0.0992 | 800 | 12.50 | 3.021 | |
| 0.0979 | 790 | 12.66 | 3.018 | |
| 0.0967 | 780 | 12.82 | 3.016 | |
| 0.0955 | 770 | 12.99 | 3.013 | |
| 0.0942 | 760 | 13.16 | 3.010 | |
| 0.0930 | 750 | 13.33 | 3.007 | |
| 0.0917 | 740 | 13.51 | 3.004 | |
| 0.0905 | 730 | 13.70 | 3.000 | |
| 0.0893 | 720 | 13.89 | 2.997 | |
| 0.0880 | 710 | 14.08 | 2.993 | |
| 0.0868 | 700 | 14.29 | 2.989 | |
| 0.0855 | 690 | 14.49 | 2.985 | |
| 0.0843 | 680 | 14.71 | 2.980 | |
| 0.0831 | 670 | 14.93 | 2.975 | |
| 0.0818 | 660 | 15.15 | 2.970 | |
| 0.0806 | 650 | 15.38 | 2.964 | |
| 0.0793 | 640 | 15.63 | 2.958 | |
| 0.0781 | 630 | 15.87 | 2.951 | |
| 0.0769 | 620 | 16.13 | 2.944 | |
| 0.0756 | 610 | 16.39 | 2.936 | |
| 0.0744 | 600 | 16.67 | 2.928 | |
| 0.0731 | 590 | 16.95 | 2.919 | |
| 0.0719 | 580 | 17.24 | 2.908 | |
| 0.0707 | 570 | 17.54 | 2.897 | |
| 0.0694 | 560 | 17.86 | 2.885 | |

TABLE II (*Continued*)

$Al_{0.54}Ga_{0.46}As$

| eV | $cm^{-1}$ | $\mu$m | n | k |
|---|---|---|---|---|
| 0.0682 | 550 | 18.18 | 2.871 | |
| 0.0669 | 540 | 18.52 | 2.856 | |
| 0.0657 | 530 | 18.87 | 2.839 | |
| 0.0645 | 520 | 19.23 | 2.820 | |
| 0.0632 | 510 | 19.61 | 2.798 | |
| 0.0620 | 500 | 20.00 | 2.772 | |
| 0.0608 | 490 | 20.41 | 2.743 | |
| 0.0595 | 480 | 20.83 | 2.708 | |
| 0.0583 | 470 | 21.28 | 2.667 | |
| 0.0570 | 460 | 21.74 | 2.616 | |
| 0.0558 | 450 | 22.22 | 2.553 | $1.10x10^{-2}$[3] |
| 0.0555 | 448 | 22.32 | 2.539 | 1.25 |
| 0.0553 | 446 | 22.42 | 2.524 | 1.41 |
| 0.0550 | 444 | 22.52 | 2.508 | 1.59 |
| 0.0548 | 442 | 22.62 | 2.491 | 1.78 |
| 0.0546 | 440 | 22.73 | 2.473 | 2.00 |
| 0.0543 | 438 | 22.83 | 2.454 | 2.23 |
| 0.0541 | 436 | 22.94 | 2.434 | 2.48 |
| 0.0538 | 434 | 23.04 | 2.413 | 2.77 |
| 0.0536 | 432 | 23.15 | 2.391 | 3.08 |
| 0.0533 | 430 | 23.26 | 2.367 | 3.43 |
| 0.0531 | 428 | 23.36 | 2.341 | 3.81 |
| 0.0528 | 426 | 23.47 | 2.313 | 4.24 |
| 0.0526 | 424 | 23.58 | 2.284 | 4.73 |
| 0.0523 | 422 | 23.70 | 2.252 | 5.27 |
| 0.0521 | 420 | 23.81 | 2.218 | 5.89 |
| 0.0518 | 418 | 23.92 | 2.180 | 6.60 |
| 0.0516 | 416 | 24.04 | 2.140 | 7.41 |
| 0.0513 | 414 | 24.15 | 2.096 | 8.34 |
| 0.0511 | 412 | 24.27 | 2.047 | $9.43x10^{-2}$ |
| 0.0508 | 410 | 24.39 | 1.994 | $1.07x10^{-1}$ |
| 0.0506 | 408 | 24.51 | 1.934 | 1.23 |
| 0.0503 | 406 | 24.63 | 1.868 | 1.41 |
| 0.0501 | 404 | 24.75 | 1.793 | 1.64 |
| 0.0498 | 402 | 24.88 | 1.709 | 1.92 |
| 0.0496 | 400 | 25.00 | 1.612 | 2.28 |
| 0.0493 | 398 | 25.13 | 1.501 | 2.76 |
| 0.0491 | 396 | 25.25 | 1.372 | 3.41 |
| 0.0488 | 394 | 25.38 | 1.224 | 4.35 |
| 0.0486 | 392 | 25.51 | 1.061 | 5.74 |
| 0.0484 | 390 | 25.64 | 0.905 | $7.76x10^{-1}$ |
| 0.0481 | 388 | 25.77 | 0.790 | $1.03x10^{0}$ |
| 0.0479 | 386 | 25.91 | 0.728 | 1.31 |
| 0.0476 | 384 | 26.04 | 0.707 | 1.60 |
| 0.0474 | 382 | 26.18 | 0.717 | 1.90 |
| 0.0471 | 380 | 26.32 | 0.753 | 2.20 |
| 0.0469 | 378 | 26.46 | 0.815 | 2.53 |
| 0.0466 | 376 | 26.60 | 0.910 | 2.88 |
| 0.0464 | 374 | 26.74 | 1.047 | 3.27 |
| 0.0461 | 372 | 26.88 | 1.249 | 3.70 |

TABLE II (*Continued*)

$Al_{0.54}Ga_{0.46}As$

| eV | $cm^{-1}$ | $\mu$m | n | k |
|---|---|---|---|---|
| 0.0459 | 370 | 27.03 | 1.552 | 4.20 |
| 0.0456 | 368 | 27.17 | 2.028 | 4.75 |
| 0.0454 | 366 | 27.32 | 2.802 | 5.32 |
| 0.0451 | 364 | 27.47 | 4.038 | 5.69 |
| 0.0449 | 362 | 27.62 | 5.623 | 5.32 |
| 0.0446 | 360 | 27.78 | 6.702 | 4.02 |
| 0.0444 | 358 | 27.93 | 6.825 | 2.66 |
| 0.0441 | 356 | 28.09 | 6.500 | 1.74 |
| 0.0439 | 354 | 28.25 | 6.105 | $1.19\times10^{0}$ |
| 0.0436 | 352 | 28.41 | 5.751 | $8.54\times10^{-1}$ |
| 0.0434 | 350 | 28.57 | 5.454 | 6.35 |
| 0.0431 | 348 | 28.74 | 5.208 | 4.86 |
| 0.0429 | 346 | 28.90 | 5.003 | 3.81 |
| 0.0426 | 344 | 29.07 | 4.831 | 3.04 |
| 0.0424 | 342 | 29.24 | 4.684 | 2.46 |
| 0.0422 | 340 | 29.41 | 4.557 | 2.00 |
| 0.0419 | 338 | 29.59 | 4.446 | 1.65 |
| 0.0417 | 336 | 29.76 | 4.348 | 1.36 |
| 0.0414 | 334 | 29.94 | 4.261 | $1.12\times10^{-1}$ |
| 0.0412 | 332 | 30.12 | 4.183 | $9.28\times10^{-2}$ |
| 0.0409 | 330 | 30.30 | 4.112 | 7.63 |
| 0.0407 | 328 | 30.49 | 4.047 | 6.24 |
| 0.0404 | 326 | 30.67 | 3.987 | 5.03 |
| 0.0402 | 324 | 30.86 | 3.932 | 3.99 |
| 0.0399 | 322 | 31.06 | 3.880 | 3.08 |
| 0.0397 | 320 | 31.25 | 3.831 | 2.29 |
| 0.0394 | 318 | 31.45 | 3.785 | $1.58\times10^{-2}$ |
| 0.0392 | 316 | 31.65 | 3.741 | $9.54\times10^{-3}$ |
| 0.0389 | 314 | 31.85 | 3.699 | $3.97\times10^{-3}$ |
| 0.0387 | 312 | 32.05 | 3.658 | $9.83\times10^{-4}$ |
| 0.0384 | 310 | 32.26 | 3.617 | $5.38\times10^{-3}$ |
| 0.0382 | 308 | 32.47 | 3.578 | $9.25\times10^{-3}$ |
| 0.0379 | 306 | 32.68 | 3.539 | $1.26\times10^{-2}$ |
| 0.0376 | 304 | 32.89 | 3.499 | 1.55 |
| 0.0374 | 302 | 33.11 | 3.460 | 1.78 |
| 0.0372 | 300 | 33.33 | 3.419 | 1.95 |
| 0.0369 | 298 | 33.56 | 3.377 | 2.05 |
| 0.0367 | 296 | 33.78 | 3.333 | 2.07 |
| 0.0365 | 294 | 34.01 | 3.286 | 1.98 |
| 0.0362 | 292 | 34.25 | 3.237 | 1.76 |
| 0.0360 | 290 | 34.48 | 3.183 | $1.36\times10^{-2}$ |
| 0.0357 | 288 | 34.72 | 3.123 | $7.14\times10^{-3}$ |
| 0.0355 | 286 | 34.97 | 3.057 | $2.81\times10^{-3}$ |
| 0.0352 | 284 | 35.21 | 2.982 | $1.78\times10^{-2}$ |
| 0.0350 | 282 | 35.46 | 2.896 | 4.03 |
| 0.0347 | 280 | 35.71 | 2.795 | $7.45\times10^{-2}$ |
| 0.0345 | 278 | 35.97 | 2.674 | $1.27\times10^{-1}$ |
| 0.0342 | 276 | 36.23 | 2.531 | 2.12 |
| 0.0340 | 274 | 36.50 | 2.362 | 3.51 |
| 0.0337 | 272 | 36.76 | 2.183 | 5.86 |

TABLE II (*Continued*)

$Al_{0.54}Ga_{0.46}As$

| eV | $cm^{-1}$ | $\mu$m | n | k |
|---|---|---|---|---|
| 0.0335 | 270 | 37.04 | 2.056 | $9.63 \times 10^{-1}$ |
| 0.0332 | 268 | 37.31 | 2.104 | $1.46 \times 10^{0}$ |
| 0.0330 | 266 | 37.59 | 2.407 | 1.96 |
| 0.0327 | 264 | 37.88 | 2.949 | 2.30 |
| 0.0325 | 262 | 38.17 | 3.606 | 2.33 |
| 0.0322 | 260 | 38.46 | 4.145 | 2.05 |
| 0.0320 | 258 | 38.76 | 4.430 | 1.64 |
| 0.0317 | 256 | 39.06 | 4.514 | $1.27 \times 10^{0}$ |
| 0.0315 | 254 | 39.37 | 4.495 | $9.91 \times 10^{-1}$ |
| 0.0312 | 252 | 39.68 | 4.436 | 7.88 |
| 0.0310 | 250 | 40.00 | 4.367 | 6.42 |
| 0.0304 | 245 | 40.82 | 4.208 | 4.20 |
| 0.0298 | 240 | 41.67 | 4.084 | 3.02 |
| 0.0291 | 235 | 42.55 | 3.991 | 2.32 |
| 0.0285 | 230 | 43.48 | 3.919 | 1.86 |
| 0.0279 | 225 | 44.44 | 3.862 | 1.54 |
| 0.0273 | 220 | 45.45 | 3.815 | 1.30 |
| 0.0267 | 215 | 46.51 | 3.775 | $1.12 \times 10^{-2}$ |
| 0.0260 | 210 | 47.62 | 3.742 | 9.82 |
| 0.0254 | 205 | 48.78 | 3.713 | 8.70 |
| 0.0248 | 200 | 50.00 | 3.688 | 7.77 |
| 0.0207 | 167 | 60.00 | 3.578 | 4.26 |
| 0.0177 | 143 | 70.00 | 3.532 | 3.01 |
| 0.0155 | 125 | 80.00 | 3.508 | 2.37 |
| 0.0138 | 111 | 90.00 | 3.493 | 1.96 |
| 0.0124 | 100 | 100.00 | 3.483 | 1.69 |

[a]References are indicated in brackets.

**TABLE III**

**Oscillator Parameters Obtained from the Curve Fitting by Using a Factorized Form of a Dielectric Function; ν and γ in $cm^{-1}$**

| $x$ | $\nu_{t1}$ | $\nu_{l1}$ | $\gamma_{t1}$ | $\gamma_{l1}$ | $\nu_{t2}$ | $\nu_{l2}$ | $\gamma_{t2}$ | $\gamma_{l2}$ | $\varepsilon$ |
|---|---|---|---|---|---|---|---|---|---|
| 0.14 | 267.1 | 285.7 | 5.67 | 4.85 | 358.8 | 369.0 | 10.56 | 11.31 | 10.57 |
| 0.18 | 266.9 | 283.4 | 8.76 | 4.24 | 360.1 | 372.4 | 12.20 | 10.24 | 10.47 |
| 0.30 | 265.2 | 278.3 | 8.64 | 6.15 | 360.2 | 379.1 | 12.10 | 9.42 | 10.16 |
| 0.36 | 264.5 | 276.5 | 10.69 | 5.58 | 360.4 | 381.3 | 12.23 | 8.08 | 10.04 |
| 0.44 | 262.9 | 273.7 | 10.05 | 6.44 | 360.2 | 385.4 | 9.55 | 7.90 | 9.84 |
| 0.54 | 261.8 | 269.8 | 12.43 | 7.97 | 361.5 | 390.1 | 8.75 | 8.68 | 9.60 |

# Cadmium Selenide (CdSe)

H. PILLER
Louisiana State University
Baton Rouge, Louisiana

Cadmium selenide is a tetrahedral semiconductor with wurtzite structure in the hexagonal modification. CdSe is an optically uniaxial semiconductor with two components of the dielectric function. Measurements of the reflectivity spectra of CdSe crystals with polarized light have shown strong differences for the electric vector parallel ($\mathbf{E} \| c$) and perpendicular ($\mathbf{E} \perp c$) to the hexagonal axis. The room-temperature reflectivity of hexagonal CdSe was measured by Cardona and Harbeke [1] in the 0.8–12 eV region with linearly polarized light. Measurements were performed with the electric vector parallel and perpendicular to the $c$ axis of the crystal. From these reflection measurements, extended with unpolarized light to the region between 11.3 and 22.5 eV, the optical constants were determined by means of the Kramers–Kronig technique. The crystals were polished in a crystal plane containing the hexagonal axis; however, no satisfactory etchant was found. The measurements were performed on polished, unetched surfaces; hence, the spectra obtained must be somewhat smeared out. The orientation of the $c$ axis was determined by X-ray diffraction. The optical constants $n$ and $k$, as read from the graph, are listed in Table I and plotted in Fig. 1 for both the ordinary ($o$) and extraordinary ($e$) rays. The numbers are probably correct to two figures.

Logothetidis *et al.* [2] investigated the real and imaginary parts of the ordinary and extraordinary dielectric functions of CdSe as a function of temperature with a scanning rotating-analyzer ellipsometer in the spectral range 1.3–5.5 eV. The measurements were made at 15, 210, 400, and 550 K. Automatic spectroscopic ellipsometry is an excellent technique to measure the real and imaginary parts of the dielectric function. On-line digitization of the data permits a fast and efficient analysis of the optical response of the semiconductor crystal. Ellipsometry is a sensitive technique used to investigate the optical response as it yields information on both the amplitude and the phase of the reflected polarized light beam. The data show strong structures in the optical spectra in the 4–5.5 eV region. For $\mathbf{E} \| c$ only one peak is seen, whereas three peaks are observed for $\mathbf{E} \perp c$. The absorption edge of CdSe exhibits three excitonic structures.


Copyright © 1991 by Academic Press.
All rights of reproduction in any form reserved.
ISBN 0-12-544422-2

The lowest excitation energy is 1.741 eV at 295 K. These peaks have been interpreted in terms of interband transitions modified by excitonic interaction. The spectra of the dielectric function were obtained using the two-phase model (ambient and uniaxially anisotropic substrate) of the interface. No additional corrections for possible surface overlayers or roughness were made (for the edge excitons, three-phase models were used to take exciton-free layers into account). All measurements were made at an angle of incidence of 67.5°. The sample surface treatment included mechanical lapping and polishing with Syton (Monsanto Chemical Co.) in a plane surface parallel to the $c$ axis. Chemical etching was used to remove the distorted layer produced by the mechanical polishing. The maximization of the real part of the complex dielectric constant, $\varepsilon_1$, around the $E_1$ structure (in the 4–5.5 eV region) was used as a criterion of quality of the surface. The method of surface preparation involved the cleaning of a surface growth with methanol and distilled water, while the sample was kept under the flow of dry nitrogen. This method gave the highest values of $\varepsilon_1$. No systematic investigation of the effect of a possible residual oxide layer was made. The values of $n_{o,e}$ and $k_{o,e}$ were calculated from the values of $\varepsilon_1$ and $\varepsilon_2$ as read from the graphs. The tabulated data are for 210 K (except the $n_o$ and $k_o$ values in the photon-energy range 1.3–2 eV, which were measured at 330 K). The numbers are listed in Table I and are plotted in Fig. 1 for both $o$ and $e$ rays.

The absorption spectra of undoped semi-insulating CdSe were measured from 0.6–1.8 eV by Rosen *et al.* [3]. The absorption spectra showed indirect absorption from energy levels of the shallow-acceptor defect, including a possible deep level at 1.3 eV. The absorption (of sample $H_1$) was fitted with the following expression for the absorption coefficient $\alpha$:

$$\alpha(\hbar\omega) = A + B(\hbar\omega - E_0),$$

where $\hbar\omega$ is the photon energy, $T = 293$ K, $A = 2.5\,\mathrm{cm}^{-1}$, $B = 6.1 \times 10^{-3}\,\mathrm{meV}^{-2}\,\mathrm{cm}^{-1}$, and $E_0 = 110$ meV. $E_0$ is the threshold energy, $A$ is the deep-state absorption near $E_0$, and $B$ is an indirect absorption parameter. The slopes of the absorption components were nearly temperature-independent. The deep-level absorption changed with temperature, indicating association with the shallow acceptor. The undoped samples of CdSe were made semi-insulating by treatment with Se vapor. The thickness of the samples were in the 1.55–2 mm. The $c$ axis of the samples was perpendicular to the surface. The absorption coefficient was calculated at each wavelength and corrected for reflection at the two surfaces. We calculated the imaginary part of the complex refractive index $k$ from the absorption data given in the graph [3, Fig. 7]. The results are listed in Table I and are plotted in Fig. 1.

Beserman [4] measured the infrared absorption by pure CdSe platelets

in the range of frequencies $300\,cm^{-1}$–$465\,cm^{-1}$. The experiments were performed at room temperature with an experimental resolution of approximately $1\,cm^{-1}$. The observed main absorption peaks in the range of combination of optical modes are at 329, 354, 365, and $371\,cm^{-1}$. Raman-scattering measurements were made on the same platelets. The following phonon frequencies ($cm^{-1}$) were obtained from the infrared absorption and Raman data: $TA = 43.5$, $LO_\Gamma = 210$, $TO_\Gamma = 168$. Table I lists $k$ as calculated from the data given in the graph in Beserman [4, Fig. 1]. Fig. 1 shows $k$.

The spectral dependence of the refractive index and birefringence of CdSe single crystals was investigated in a wide temperature and wavelength range by Lisita *et al.* [5]. The single crystals were grown by sublimation from the gaseous phase and had a conductivity in the range $10^{-10}$–$10^{-11}\,\Omega^{-1}\,cm^{-1}$. The direction of the $c$ axis was determined by using X-ray analysis with an accuracy of 20 min. In the spectral region between the fundamental absorption edge and $\nu = 5000\,cm^{-1}$, the refractive index was determined by the prism method. Prisms were cut in such a way that the optical axis of the crystal was parallel to the refracting edge. The absolute error in determining $n$ was about $5 \times 10^{-4}$. In the spectral region $\nu < 5000\,cm^{-1}$, the interference method was used to determine the refractive index $n_o$ of the ordinary beam. The corresponding values of $n_e$ were calculated according to the equation $n_e = n_o + \Delta n$. The absolute error in determining $n_o$ using the interference method was about $5 \times 10^{-3}$. The dispersion of the birefringence was measured by the method of interference of polarized beams. The absolute error in determining $\Delta n$ was between $2 \times 10^{-5}$ and $4 \times 10^{-5}$. The measurements were performed in a temperature interval between 100 and 600 K. The room-temperature measurements show that $n_e > n_o$ for all crystals. The numerical values of $n_o$ and $n_e$ are in good agreement with the data by Bond [6]. We have listed the values of $n_o$ and $n_e$ in Table I. Pikhtin and Yas'kov [7] have refitted the data with an oscillator-model formula obtained from the Kramers–Kronig dispersion relations. Additional data points listed in Table I and plotted in Fig. 1 were calculated using these analytic expressions [7].

Transmission and reflection spectra were measured on CdSe single crystals in the region of 3.6–5.9 eV at 109 K and at room temperature by Lange and Iliev [8]. The optical constants were calculated from these data and agree well with the data of Ludeke and Paul [9] on CdSe thin films and agree semiquantitatively with those obtained by ellipsometry [2]. The plate-shaped, single-crystal samples were grown from the vapor phase. Thickness of the samples was measured by means of an interference microscope and ranged between 100 and 150 nm. The in-out technique was used in the optical experiments. The multiple internal reflections in the sample were neglected in calculating the absorption coefficient and the refractive index from experimental spectra.

Polarized synchrotron radiation was used by Freeouf [10] to measure the reflectance spectra for photon energies between 0.6 and 30 eV at temperatures between 90 and 400 K. The optical constants were determined by Kramers–Kronig analysis. Synchrotron radiation provides an intense polarized continuum spectrum of light throughout the ultraviolet spectral region. The reflectance was measured by the rotating-light-pipe, scanning-reflectometer technique. The precision of the reflectance measurements was lower for photon energies larger than 8 eV. The single crystals of CdSe were cleaved just prior to mounting in the experimental system.

Terekhova *et al.* [11] measured the ordinary and extraordinary refractive index in the photon-energy region of 1.88–1.76 eV using two-beam interferometry at 5 K. The observed dispersion in the refractive indices was interpreted in terms of exciton states.

Beserman and Balkanski [12] measured the vibrational properties of CdSe at room temperature. The reflectivity was measured on a single crystal of CdSe containing 0.5% S, for $\mathbf{E} \perp \mathbf{c}$ and $\mathbf{E} \| \mathbf{c}$, in the frequency range 100–350 $\text{cm}^{-1}$. The resolution was 1 $\text{cm}^{-1}$ in the entire range studied. The real and imaginary parts of the dielectric constant were deduced from the reflectance data by means of the Kramers–Kronig relations in the frequency range 100–300 $\text{cm}^{-1}$. The optical-mode frequencies were calculated from the following equations:

$$\omega_{TO} = \varepsilon_{i\,\max} = 2nk_{\max}$$

$$\omega_{\text{LO}} = \text{Im}(-1/\varepsilon)_{\max} = [2nk/(n^2 + k^2)]_{\max}$$

For each polarization two types of oscillators were observed: the TO mode of pure CdSe, whose frequencies are, for $\mathbf{E} \| c$, $\omega_{\text{TO}} = 166.5\ \text{cm}^{-1}$, and for $\mathbf{E} \perp c$, $\omega_{\text{TO}} = 169\ \text{cm}^{-1}$; and the localized-mode frequencies of S in CdSe. In both polarizations, two localized modes were observed: for $\mathbf{E} \| \mathbf{c}$, 262 $\text{cm}^{-1}$ and 266.5 $\text{cm}^{-1}$; for $\mathbf{E} \perp c$, 263 $\text{cm}^{-1}$ and 269 $\text{cm}^{-1}$. The LO-mode frequencies were calculated either from $\varepsilon_r = 0$ ($\varepsilon_r$ is the real part of the dielectric constant) or from $\text{Im}(-1/\varepsilon) = \max$. Two sets of LO modes were observed: for pure CdSe, $\omega_{\text{LO}} = 210\ \text{cm}^{-1}$ ($\mathbf{E} \| c$) and $\omega_{\text{LO}} = 212\ \text{cm}^{-1}$ ($\mathbf{E} \perp c$); for *S* in CdSe, $\omega_{\text{LO}} = 262.5\ \text{cm}^{-1}$, $268.5\ \text{cm}^{-1}$ ($\mathbf{E} \| c$), and $\omega_{\text{LO}} = 263.5\ \text{cm}^{-1}$, $270.5\ \text{cm}^{-1}$ ($\mathbf{E} \perp c$). We calculated the real and imaginary parts of the complex refractive index from the corresponding real and imaginary parts of the dielectric constant for the ordinary and extraordinary rays from the experimental data given in the graphs [12, Figs. 2 and 3]. The results are listed in Table I and plotted in Fig. 1.

Geick, Perry, and Mitra [13] measured the reflectivity of single-crystal CdSe with linearly polarized light at room temperature and at liquid-nitrogen temperature. The reflectivity was measured in the spectral region

from 70 $cm^{-1}$ to 375 $cm^{-1}$. Transmission measurements were made with unpolarized light on polycrystalline samples. The extinction coefficient $k$ was determined from the experimental results for the spectral region from 80 $cm^{-1}$ to 500 $cm^{-1}$. The spectra were analyzed by means of an optimum fit with a classical dispersion formula. The transmission measurements showed several multiphonon peaks, which were interpreted in terms of four representative phonon energies for the edge of the Brillouin zone.

Verleur and Barker [14] measured the infrared reflectivity over the frequency range from 100 $cm^{-1}$ to 400 $cm^{-1}$ at 15 and 300 K with polarized light. A resolution of 2.5 $cm^{-1}$ was maintained over the entire frequency range. Agreement between different runs on the same specimen was within 1%. "Pure" CdSe was found to contain up to 2% S. A single-crystal specimen containing 1.5% sulphur was used in the reflectivity measurements. Classical oscillator fits of the reflectivity spectrum were used to determine the mode parameters and related constants.

## REFERENCES


1. M. Cardona and G. Harbeke, *Phys. Rev.* **137**, 1467 (1965).
2. S. Logothetidis, M. Cardona, P. Lautenschlager, and M. Garriga, *Phys. Rev. B* **34**, 2458 (1986).
3. D. L. Rosen, Q. X. Li, and R. R. Alfano, *Phys. Rev. B* **31**, 2396 (1985).
4. R. Beserman, *Solid State Commun.* **23**, 323 (1977).
5. M. P. Lisita, L. F. Gudymenko, V. N. Malinko, and S. F. Terekhova, *Phys. Status Solidi* **31**, 389 (1969).
6. W. L. Bond, *J. Appl. Phys.* **36**, 1674 (1965).
7. A. N. Pikhtin and A. D. Yas'kov, *Sov. Phys. Semicond.* **15**, 8 (1981).
8. H. Lange and I. A. Iliev, *Phys. Status Solidi B* **84**, 569 (1977).
9. R. Ludeke and W. Paul, *Phys. Status Solidi* **23**, 413 (1967); "Proc. 7th Internat. Conf. II-VI Compounds," (D. G. Thomas ed.) Benjamin, New York, Providence, 123 (1967).
10. J. L. Freeouf, *Phys. Rev. B* **7**, 3810 (1973).
11. S. F. Terekhova, N. A. Onishchenko, O. N. Talenskii, S. A. Pendur, *Phys. Status Solidi B* **131**, 207 (1985).
12. R. Beserman and M. Balkanski, *Phys. Rev. B* **1**, 608 (1970).
13. R. Geick, C. H. Perry, and S. S. Mitra, *J. Appl. Phys.* **37**, 1994 (1966).
14. H. W. Verleur and A. S. Barker, Jr., *Phys. Rev.* **155**, 750 (1967).

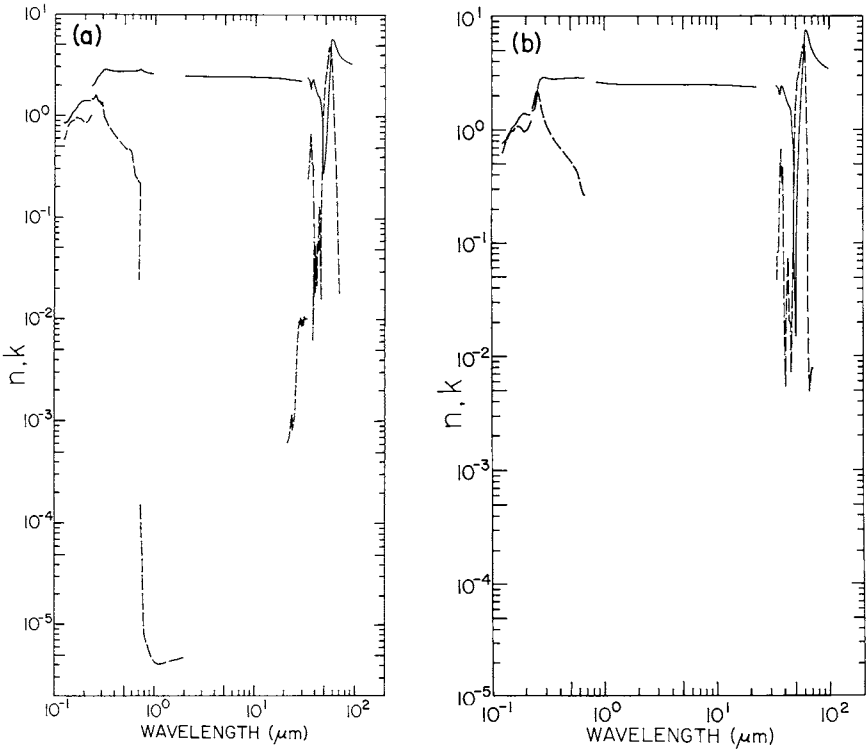


**Fig. 1.** (a) Log–log plot of $n_o$ (solid line) and $k_o$ (dashed line) versus wavelength in micrometers for cadmium selenide. (b) Log–log plot of $n_e$ (solid line) and $k_e$ (dashed line) versus wavelength in micrometers.

TABLE I

Values of $n$ and $k$ for Cadmium Selenide Obtained from Various References[a]

| eV | μm | $n_\perp$ | $k_\perp$ | $n_\parallel$ | $k_\parallel$ |
|---|---|---|---|---|---|
| 10.000 | 0.1240 | | 0.591 [1] | | 0.625 [1] |
| 9.959 | 0.1245 | 0.862 [1] | | 0.771 [1] | |
| 9.867 | 0.1257 | | | 0.774 | 0.650 |
| 9.848 | 0.1259 | | 0.599 | | |
| 9.800 | 0.1265 | 0.848 | | | |
| 9.794 | 0.1266 | | | 0.781 | |
| 9.747 | 0.1272 | 0.847 | | | 0.675 |
| 9.738 | 0.1273 | | 0.624 | | |
| 9.710 | 0.1277 | | | 0.787 | |
| 9.651 | 0.1285 | | | | 0.698 |
| 9.628 | 0.1288 | | 0.650 | | |
| 9.585 | 0.1293 | | | 0.793 | |
| 9.582 | 0.1294 | 0.846 | | | |
| 9.537 | 0.1300 | | 0.678 | | |
| 9.482 | 0.1308 | | | 0.792 | |
| 9.463 | 0.1310 | | | | 0.747 |
| 9.431 | 0.1315 | | 0.715 | | |
| 9.364 | 0.1324 | 0.851 | | 0.805 | |
| 9.311 | 0.1332 | | 0.746 | | 0.788 |
| 9.258 | 0.1339 | | | 0.811 | |
| 9.201 | 0.1348 | | 0.769 | | |
| 9.183 | 0.1350 | 0.865 | | | |
| 9.130 | 0.1358 | | | | 0.835 |
| 9.102 | 0.1362 | | 0.793 | 0.833 | |
| 8.999 | 0.1378 | | | 0.849 | |
| 8.984 | 0.1380 | | 0.819 | | |
| 8.962 | 0.1384 | | | | 0.885 |
| 8.943 | 0.1386 | 0.901 | | | |
| 8.861 | 0.1399 | | 0.840 | | |
| 8.840 | 0.1403 | | | 0.880 | |
| 8.809 | 0.1407 | | | | 0.923 |
| 8.735 | 0.1419 | | 0.859 | 0.910 | |
| 8.709 | 0.1424 | | | | 0.950 |
| 8.632 | 0.1436 | | 0.877 | | |
| 8.622 | 0.1438 | 0.968 | | | |
| 8.615 | 0.1439 | | | | 0.974 |
| 8.575 | 0.1446 | | | 0.956 | |
| 8.512 | 0.1457 | | 0.897 | | |
| 8.499 | 0.1459 | | | | 0.977 |
| 8.463 | 0.1465 | | | 0.988 | |
| 8.400 | 0.1476 | 1.016 | 0.907 | | |
| 8.308 | 0.1492 | | | | 0.972 |
| 8.301 | 0.1494 | | 0.910 | 1.034 | |
| 8.263 | 0.1500 | 1.058 | | | |
| 8.201 | 0.1512 | | 0.903 | | |

TABLE I (*Continued*)

Cadmium Selenide

| eV | μm | $n_o$ | $k_o$ | $n_e$ | $k_e$ |
|---|---|---|---|---|---|
| 8.166 | 0.1518 | | | | 0.971 |
| 8.163 | 0.1519 | | | 1.069 | |
| 8.101 | 0.1531 | 1.092 | | | |
| 8.088 | 0.1533 | | 0.900 | | |
| 8.045 | 0.1541 | | | 1.076 | |
| 7.972 | 0.1555 | | 0.910 | | |
| 7.968 | 0.1556 | | | | 0.980 |
| 7.945 | 0.1561 | 1.111 | | | |
| 7.930 | 0.1564 | | | 1.082 | |
| 7.852 | 0.1579 | | | | 1.014 |
| 7.849 | 0.1580 | | 0.935 | | |
| 7.814 | 0.1587 | | | 1.082 | |
| 7.802 | 0.1589 | 1.120 | | | |
| 7.771 | 0.1596 | | | 1.088 | |
| 7.758 | 0.1598 | | 0.955 | | |
| 7.748 | 0.1600 | | | | 1.050 |
| 7.705 | 0.1609 | | | 1.096 | |
| 7.687 | 0.1613 | | 0.967 | | |
| 7.630 | 0.1620 | 1.148 | | | |
| 7.629 | 0.1622 | | | | 1.066 |
| 7.608 | 0.1630 | | | 1.119 | |
| 7.583 | 0.1635 | | 0.976 | | |
| 7.527 | 0.1647 | | | 1.158 | |
| 7.506 | 0.1652 | | | | 1.080 |
| 7.499 | 0.1653 | | 0.968 | | |
| 7.437 | 0.1667 | 1.213 | | | |
| 7.403 | 0.1675 | | | 1.217 | |
| 7.300 | 0.1699 | 1.256 | | | 1.084 |
| 7.266 | 0.1706 | | 0.949 | | |
| 7.225 | 0.1716 | | | 1.278 | |
| 7.184 | 0.1726 | 1.288 | | | |
| 7.108 | 0.1744 | | | | 1.070 |
| 7.066 | 0.1755 | | 0.942 | | |
| 7.053 | 0.1758 | | | 1.326 | |
| 7.031 | 0.1763 | 1.325 | | | |
| 6.907 | 0.1795 | | 0.947 | | |
| 6.862 | 0.1807 | | | | 1.046 |
| 6.797 | 0.1824 | | 0.924 | | |
| 6.782 | 0.1828 | | | 1.364 | |
| 6.692 | 0.1853 | | | 1.380 | |
| 6.665 | 0.1860 | | 0.904 | | |
| 6.604 | 0.1877 | 1.394 | | | |
| 6.589 | 0.1882 | | | 1.427 | |
| 6.551 | 0.1893 | | | | 0.988 |

TABLE I (*Continued*)

Cadmium Selenide

| eV | $cm^{-1}$ | μm | $n_o$ | $k_o$ | $n_e$ | $k_e$ |
|---|---|---|---|---|---|---|
| 6.501 | | 0.1907 | | | 1.435 | |
| 6.428 | | 0.1929 | 1.420 | 0.882 | | |
| 6.402 | | 0.1937 | | | 1.423 | |
| 6.367 | | 0.1947 | | | | 0.957 |
| 6.268 | | 0.1978 | | | 1.419 | |
| 6.244 | | 0.1986 | | | | 0.957 |
| 6.233 | | 0.1989 | 1.419 | | | |
| 6.192 | | 0.2002 | | 0.865 | | |
| 6.162 | | 0.2012 | | | 1.380 | |
| 6.153 | | 0.2015 | | | | 0.978 |
| 6.111 | | 0.2029 | | | | 1.001 |
| 6.090 | | 0.2036 | 1.418 | | | |
| 6.063 | | 0.2045 | | | | 1.018 |
| 6.040 | | 0.2053 | | | 1.368 | |
| 6.001 | | 0.2066 | | | | 1.012 |
| 5.988 | 48299 | 0.2070 | | 0.870 | | |
| 5.971 | 48162 | 0.2076 | | | 1.374 | |
| 5.946 | 47960 | 0.2085 | | | | 1.011 |
| 5.912 | 47684 | 0.2097 | 1.414 | | | |
| 5.888 | 47490 | 0.2106 | | | | 1.028 |
| 5.865 | 47306 | 0.2114 | | | 1.371 | |
| 5.801 | 46786 | 0.2137 | | 0.898 | | |
| 5.781 | 46627 | 0.2145 | 1.401 | | | |
| 5.775 | 46577 | 0.2147 | | | | 1.065 |
| 5.753 | 46401 | 0.2155 | | | 1.357 | |
| 5.697 | 45948 | 0.2176 | | | 1.352 | |
| 5.694 | 45923 | 0.2178 | | | 1.354 | |
| 5.691 | 45898 | 0.2179 | | | | 1.098 |
| 5.658 | 45637 | 0.2191 | | 0.932 | | |
| 5.631 | 45420 | 0.2202 | 1.392 | | | |
| 5.620 | 45324 | 0.2206 | | | | 1.141 |
| 5.590 | 45089 | 0.2218 | | 0.958 | | |
| 5.557 | 44817 | 0.2231 | | | 1.358 | |
| 5.545 | 44724 | 0.2236 | | | | 1.170 |
| 5.506 | 44411 | 0.2252 | | | | 1.201 |
| 5.497 | 44333 | 0.2256 | | | 1.506 [2] | 1.544 [2] |
| 5.480 | 44202 | 0.2262 | | 0.989 | | |
| 5.444 | 43912 | 0.2277 | | | 1.505 | 1.566 |
| 5.432 | 43811 | 0.2283 | 1.399 | | | |
| 5.406 | 43600 | 0.2294 | | | 1.499 | 1.594 |
| 5.361 | 43237 | 0.2313 | | 1.028 | | |
| 5.353 | 43174 | 0.2316 | 1.943 [2] | 1.497 [2] | | |
| 5.350 | 43152 | 0.2317 | | | 1.499 | 1.631 |
| 5.318 | 42894 | 0.2331 | | | 1.487 | 1.679 |
| 5.291 | 42676 | 0.2343 | | | 1.481 | 1.712 |
| 5.279 | 42574 | 0.2349 | 1.957 | 1.491 | | |

TABLE I (*Continued*)

Cadmium Selenide

| eV | $cm^{-1}$ | μm | $n_o$ | $k_o$ | $n_e$ | $k_e$ |
|---|---|---|---|---|---|---|
| 5.259 | 42418 | 0.2358 | | | 1.490 | 1.763 |
| 5.231 | 42188 | 0.2370 | | | 1.487 | 1.829 |
| 5.216 | 42068 | 0.2377 | 1.969 | 1.482 | | |
| 5.190 | 41862 | 0.2389 | | | 1.526 | 1.914 |
| 5.170 | 41699 | 0.2398 | | | 1.555 | 1.959 |
| 5.145 | 41495 | 0.2410 | 1.967 | 1.481 | | |
| 5.130 | 41373 | 0.2417 | | | 1.600 | 2.020 |
| 5.080 | 40975 | 0.2441 | 1.976 | 1.480 | | |
| 5.035 | 40613 | 0.2462 | | | 1.812 | 2.178 |
| 5.021 | 40496 | 0.2469 | 1.991 | 1.528 | | |
| 5.013 | 40436 | 0.2473 | | | 1.886 | 2.196 |
| 4.998 | 40314 | 0.2481 | | | 1.939 | 2.208 |
| 4.976 | 40136 | 0.2492 | 2.020 | 1.580 | | |
| 4.965 | 40042 | 0.2497 | | | 2.046 | 2.214 |
| 4.941 | 39852 | 0.2509 | | | 2.096 | 2.217 |
| 4.931 | 39771 | 0.2514 | | | 2.121 | 2.215 |
| 4.922 | 39696 | 0.2519 | 2.062 | 1.623 | | |
| 4.910 | 39603 | 0.2525 | 2.084 | 1.639 | | |
| 4.874 | 39309 | 0.2544 | | | 2.269 | 2.198 |
| 4.857 | 39173 | 0.2553 | | | 2.320 | 2.187 |
| 4.842 | 39051 | 0.2561 | | | 2.364 | 2.178 |
| 4.828 | 38942 | 0.2568 | | | 2.399 | 2.169 |
| 4.826 | 38923 | 0.2569 | 2.229 | 1.647 | | |
| 4.822 | 38888 | 0.2572 | | | 2.425 | 2.152 |
| 4.811 | 38807 | 0.2577 | | | 2.449 | 2.143 |
| 4.800 | 38712 | 0.2583 | | | 2.486 | 2.129 |
| 4.798 | 38698 | 0.2584 | | | 2.490 | 2.126 |
| 4.786 | 38603 | 0.2591 | | | 2.515 | 2.113 |
| 4.768 | 38454 | 0.2601 | | | 2.556 | 2.088 |
| 4.756 | 38359 | 0.2607 | 2.344 | 1.580 | 2.581 | 2.070 |
| 4.751 | 38318 | 0.2610 | | | 2.593 | 2.063 |
| 4.734 | 38182 | 0.2619 | | | 2.626 | 2.040 |
| 4.729 | 38141 | 0.2622 | | | 2.639 | 2.027 |
| 4.710 | 37992 | 0.2632 | | | 2.675 | 1.999 |
| 4.695 | 37870 | 0.2641 | | | 2.694 | 1.983 |
| 4.690 | 37829 | 0.2644 | | | 2.705 | 1.972 |
| 4.673 | 37693 | 0.2653 | | | 2.714 | 1.956 |
| 4.666 | 37631 | 0.2657 | 2.436 | 1.491 | | |
| 4.663 | 37612 | 0.2659 | | | 2.745 | 1.930 |
| 4.646 | 37476 | 0.2668 | | | 2.774 | 1.889 |
| 4.635 | 37381 | 0.2675 | | | 2.787 | 1.869 |
| 4.625 | 37299 | 0.2681 | | | 2.808 | 1.858 |
| 4.613 | 37204 | 0.2688 | | | 2.817 | 1.833 |
| 4.600 | 37098 | 0.2696 | 2.443 | 1.434 | | |
| 4.588 | 37001 | 0.2703 | | | 2.834 | 1.773 |
| 4.571 | 36865 | 0.2713 | | | 2.850 | 1.745 |

TABLE I (*Continued*)

Cadmium Selenide

| eV | $cm^{-1}$ | μm | $n_o$ | $k_o$ | $n_e$ | $k_e$ |
|---|---|---|---|---|---|---|
| 4.562 | 36791 | 0.2718 | 2.438 | 1.408 | | |
| 4.556 | 36743 | 0.2722 | | | 2.870 | 1.708 |
| 4.530 | 36539 | 0.2737 | | | 2.885 | 1.664 |
| 4.525 | 36498 | 0.2740 | 2.421 | 1.392 | | |
| 4.512 | 36390 | 0.2748 | | | 2.892 | 1.631 |
| 4.502 | 36308 | 0.2754 | | | 2.910 | 1.609 |
| 4.478 | 36118 | 0.2769 | | | 2.919 | 1.571 |
| 4.474 | 36085 | 0.2771 | 2.435 | 1.429 | | |
| 4.443 | 35832 | 0.2791 | 2.462 | 1.454 | | |
| 4.441 | 35819 | 0.2792 | | | 2.914 | 1.502 |
| 4.407 | 35548 | 0.2813 | | | 2.915 | 1.450 |
| 4.375 | 35285 | 0.2834 | 2.575 | 1.419 | | |
| 4.365 | 35208 | 0.2840 | | | 2.911 | 1.392 |
| 4.335 | 34965 | 0.2860 | 2.624 | 1.370 | | |
| 4.318 | 34828 | 0.2871 | | | 2.904 | 1.337 |
| 4.299 | 34672 | 0.2884 | 2.621 | 1.332 | | |
| 4.266 | 34407 | 0.2906 | | | 2.897 | 1.274 |
| 4.251 | 34286 | 0.2917 | 2.607 | 1.302 | | |
| 4.216 | 34006 | 0.2941 | 2.593 | 1.313 | | |
| 4.195 | 33833 | 0.2956 | 2.616 | 1.349 | | |
| 4.192 | 33810 | 0.2958 | | | 2.885 | 1.203 |
| 4.173 | 33659 | 0.2971 | 2.673 | 1.370 | | |
| 4.147 | 33446 | 0.2990 | 2.735 | 1.381 | | |
| 4.140 | 33389 | 0.2995 | | | 2.865 | 1.163 |
| 4.124 | 33260 | 0.3007 | 2.779 | 1.322 | | |
| 4.091 | 32993 | 0.3031 | 2.837 | 1.260 | | |
| 4.066 | 32791 | 0.3050 | | | 2.845 | 1.109 |
| 4.063 | 32767 | 0.3052 | 2.854 | 1.201 | | |
| 4.010 | 32340 | 0.3092 | 2.870 | 1.114 | | |
| 3.992 | 32194 | 0.3106 | | | 2.830 | 1.069 |
| 3.965 | 31980 | 0.3127 | 2.871 | 1.054 | | |
| 3.935 | 31741 | 0.3151 | 2.869 | 1.010 | | |
| 3.916 | 31583 | 0.3166 | | | 2.813 | 1.027 |
| 3.904 | 31487 | 0.3176 | 2.864 | 0.981 | | |
| 3.869 | 31208 | 0.3204 | 2.854 | 0.952 | | |
| 3.831 | 30901 | 0.3236 | 2.843 | 0.922 | | |
| 3.797 | 30621 | 0.3266 | 2.834 | 0.893 | | |
| 3.795 | 30605 | 0.3267 | | | 2.793 | 0.964 |
| 3.740 | 30168 | 0.3315 | 2.818 | 0.859 | | |
| 3.715 | 29967 | 0.3337 | | | 2.787 | 0.936 |
| 3.691 | 29768 | 0.3359 | 2.804 | 0.838 | | |
| 3.640 | 29355 | 0.3407 | 2.791 | 0.809 | | |
| 3.635 | 29315 | 0.3411 | | | 2.777 | 0.902 |
| 3.567 | 28769 | 0.3476 | 2.778 | 0.782 | | |
| 3.540 | 28555 | 0.3502 | | | 2.767 | 0.850 |
| 3.511 | 28316 | 0.3532 | 2.764 | 0.760 | | |

TABLE I (*Continued*)

Cadmium Selenide

| eV | $cm^{-1}$ | μm | $n_o$ | $k_o$ | $n_e$ | $k_e$ |
|---|---|---|---|---|---|---|
| 3.434 | 27700 | 0.3610 | | | 2.765 | 0.817 |
| 3.423 | 27610 | 0.3622 | 2.751 | 0.736 | | |
| 3.364 | 27130 | 0.3686 | 2.740 | 0.714 | | |
| 3.335 | 26899 | 0.3718 | | | 2.763 | 0.781 |
| 3.258 | 26277 | 0.3806 | 2.724 | 0.682 | | |
| 3.256 | 26260 | 0.3808 | | | 2.763 | 0.761 |
| 3.165 | 25527 | 0.3917 | | | 2.762 | 0.731 |
| 3.131 | 25251 | 0.3960 | 2.710 | 0.649 | | |
| 3.089 | 24916 | 0.4014 | | | 2.762 | 0.709 |
| 3.046 | 24571 | 0.4070 | 2.704 | 0.630 | | |
| 3.019 | 24346 | 0.4108 | | | 2.764 | 0.688 |
| 2.977 | 24012 | 0.4165 | 2.703 | 0.615 | | |
| 2.966 | 23925 | 0.4180 | | | 2.763 | 0.675 |
| 2.919 | 23545 | 0.4247 | 2.698 | 0.602 | | |
| 2.879 | 23219 | 0.4307 | | | 2.764 | 0.649 |
| 2.842 | 22919 | 0.4363 | 2.695 | 0.581 | | |
| 2.822 | 22757 | 0.4394 | | | 2.771 | 0.635 |
| 2.774 | 22372 | 0.4470 | 2.696 | 0.566 | | |
| 2.758 | 22241 | 0.4496 | | | 2.773 | 0.619 |
| 2.695 | 21733 | 0.4601 | 2.694 | 0.546 | | |
| 2.677 | 21589 | 0.4632 | | | 2.780 | 0.596 |
| 2.594 | 20924 | 0.4779 | | | 2.785 | 0.583 |
| 2.586 | 20853 | 0.4796 | 2.703 | 0.523 | | |
| 2.503 | 20191 | 0.4953 | | | 2.796 | 0.551 |
| 2.465 | 19881 | 0.5030 | 2.708 | 0.496 | | |
| 2.429 | 19593 | 0.5104 | | | 2.802 | 0.524 |
| 2.362 | 19050 | 0.5249 | | | 2.812 | 0.506 |
| 2.331 | 18801 | 0.5319 | 2.728 | 0.478 | | |
| 2.269 | 18303 | 0.5464 | | | 2.829 | 0.482 |
| 2.234 | 18015 | 0.5551 | 2.760 | 0.481 | | |
| 2.202 | 17760 | 0.5631 | | | 2.853 | 0.440 |
| 2.196 | 17708 | 0.5647 | 2.765 | 0.459 | | |
| 2.175 | 17543 | 0.5700 | | | 2.866 | 0.402 |
| 2.163 | 17448 | 0.5731 | | | 2.885 | 0.422 |
| 2.131 | 17189 | 0.5818 | 2.758 | 0.427 | | |
| 2.125 | 17136 | 0.5836 | | | 2.874 | 0.391 |
| 2.076 | 16742 | 0.5973 | | | 2.853 | 0.344 |
| 2.022 | 16307 | 0.6132 | | | 2.837 | 0.311 |
| 1.972 | 15904 | 0.6288 | 2.740 | 0.275 | | |
| 1.934 | 15599 | 0.6411 | 2.733 | 0.257 | | |
| 1.916 | 15452 | 0.6472 | | | 2.834 | 0.268 |
| 1.891 | 15253 | 0.6556 | 2.733 | 0.242 | | |
| 1.877 | 15140 | 0.6605 | 2.739 | 0.247 | | |
| 1.861 | 15010 | 0.6662 | 2.741 | 0.250 | | |
| 1.840 | 14841 | 0.6738 | | | 2.862 | 0.270 |
| 1.827 | 14737 | 0.6786 | 2.755 | 0.231 | | |

TABLE I (*Continued*)

Cadmium Selenide

| eV | $cm^{-1}$ | μm | $n_o$ | $k_o$ | $n_e$ | $k_e$ |
|---|---|---|---|---|---|---|
| 1.811 | 14608 | 0.6846 | 2.765 | 0.233 | | |
| 1.799 | 14507 | 0.6893 | 2.778 | 0.231 | | |
| 1.783 | 14383 | 0.6953 | 2.797 | 0.230 | | |
| 1.768 | 14257 | 0.7014 | 2.812 | 0.230 | | |
| 1.756 | 14166 | 0.7059 | 2.832 | 0.228 | | |
| 1.750 | 14115 | 0.7085 | 2.845 | 0.217 | | |
| 1.738 | 14016 | 0.7135 | 2.856 | 0.162 | | |
| 1.727 | 13926 | 0.7181 | 2.864 | 0.025 | | |
| 1.716 | 13838 | 0.7226 | 2.856 | | | |
| 1.706 | 13758 | 0.7269 | 2.841 | | | |
| 1.697 | 13689 | 0.7306 | 2.821 | | | |
| 1.691 | 13641 | 0.7331 | | 1.55E-04 [3] | | |
| 1.690 | 13632 | 0.7336 | 2.807 | | | |
| 1.683 | 13571 | 0.7369 | | 1.24E-04 | | |
| 1.677 | 13526 | 0.7393 | 2.780 | | | |
| 1.676 | 13514 | 0.7400 | | 1.00E-04 | | |
| 1.667 | 13447 | 0.7437 | | 7.88E-05 | | |
| 1.665 | 13425 | 0.7449 | 2.761 | | | |
| 1.659 | 13384 | 0.7472 | | 6.21E-05 | | |
| 1.655 | 13348 | 0.7492 | 2.746 | | | |
| 1.652 | 13324 | 0.7505 | | 5.04E-05 | | |
| 1.649 | 13297 | 0.7520 | 2.660 | [5] | | |
| 1.647 | 13286 | 0.7527 | 2.738 | | | |
| 1.640 | 13229 | 0.7559 | | 3.67E-05 | | |
| 1.639 | 13216 | 0.7567 | 2.727 | | | |
| 1.633 | 13172 | 0.7592 | | 2.96E-05 | | |
| 1.632 | 13164 | 0.7596 | 2.721 | | | |
| 1.626 | 13112 | 0.7627 | | 2.35E-05 | | |
| 1.623 | 13092 | 0.7638 | 2.712 | | | |
| 1.614 | 13017 | 0.7682 | | 1.74E-05 | | |
| 1.603 | 12927 | 0.7736 | 2.691 | | | |
| 1.602 | 12922 | 0.7739 | | 1.32E-05 | | |
| 1.593 | 12852 | 0.7781 | | 9.93E-06 | | |
| 1.590 | 12822 | 0.7799 | | 8.58E-06 | | |
| 1.584 | 12777 | 0.7826 | | 7.50E-06 | | |
| 1.573 | 12689 | 0.7881 | 2.673 | | | |
| 1.567 | 12642 | 0.7910 | 2.635 | | | |
| 1.560 | 12580 | 0.7949 | | 7.07E-06 | | |
| 1.552 | 12514 | 0.7991 | 2.659 | | | |
| 1.530 | 12341 | 0.8103 | 2.646 | | | |
| 1.528 | 12325 | 0.8113 | | 6.69E-06 | | |
| 1.497 | 12075 | 0.8282 | 2.634 | | | |
| 1.494 | 12051 | 0.8298 | | 6.33E-06 | | |
| 1.475 | 11897 | 0.8406 | 2.625 | | | |
| 1.459 | 11765 | 0.8500 | 2.608 | | 2.626 [5] | |
| 1.453 | 11719 | 0.8534 | | 5.83E-06 | | |

TABLE I (*Continued*)

Cadmium Selenide

| eV | $cm^{-1}$ | μm | $n_o$ | $k_o$ | $n_e$ | $k_e$ |
|---|---|---|---|---|---|---|
| 1.442 | 11633 | 0.8596 | 2.612 | | | |
| 1.418 | 11435 | 0.8746 | 2.602 | | | |
| 1.417 | 11427 | 0.8752 | | 5.51E-06 | | |
| 1.386 | 11182 | 0.8943 | 2.592 | | | |
| 1.379 | 11122 | 0.8991 | | 5.16E-06 | | |
| 1.354 | 10921 | 0.9157 | 2.583 | | | |
| 1.352 | 10905 | 0.9171 | | 4.94E-06 | | |
| 1.328 | 10709 | 0.9338 | 2.576 | | | |
| 1.321 | 10655 | 0.9386 | | 4.67E-06 | | |
| 1.314 | 10600 | 0.9434 | 2.573 | | | |
| 1.293 | 10425 | 0.9592 | | 4.47E-06 | | |
| 1.265 | 10205 | 0.9799 | | 4.23E-06 | | |
| 1.248 | 10066 | 0.9935 | | 4.15E-06 | | |
| 1.240 | 10000 | 1.000 | 2.547 | | 2.566 | |
| 1.229 | 9916 | 1.009 | | 4.11E-06 | | |
| 1.195 | 9641 | 1.037 | | 4.14E-06 | | |
| 1.164 | 9389 | 1.065 | | 4.10E-06 | | |
| 1.127 | 9089 | 1.100 | | 4.11E-06 | | |
| 1.080 | 8712 | 1.148 | | 4.13E-06 | | |
| 1.069 | 8619 | 1.160 | 2.524 | | | |
| 1.044 | 8423 | 1.187 | | 4.12E-06 | | |
| 1.010 | 8143 | 1.228 | | 4.13E-06 | | |
| 0.9659 | 7791 | 1.284 | | 4.17E-06 | | |
| 0.9269 | 7476 | 1.338 | | 4.20E-06 | | |
| 0.9239 | 7452 | 1.342 | 2.500 | | | |
| 0.8811 | 7107 | 1.407 | | 4.26E-06 | | |
| 0.8396 | 6772 | 1.477 | | 4.31E-06 | | |
| 0.8266 | 6667 | 1.500 | 2.484 | | 2.504 | |
| 0.8019 | 6467 | 1.546 | | 4.36E-06 | | |
| 0.7647 | 6168 | 1.621 | | 4.41E-06 | | |
| 0.7421 | 5986 | 1.671 | 2.469 | | | |
| 0.7238 | 5838 | 1.713 | | 4.51E-06 | | |
| 0.6864 | 5536 | 1.806 | | 4.60E-06 | | |
| 0.6790 | 5477 | 1.826 | 2.465 | | | |
| 0.6551 | 5284 | 1.893 | | 4.70E-06 | | |
| 0.6328 | 5104 | 1.959 | | 4.77E-06 | | |
| 0.6199 | 5000 | 2.000 | 2.468 | | 2.488 | |
| 0.5298 | 4273 | 2.340 | 2.459 | | | |
| 0.4623 | 3728 | 2.682 | 2.453 | | | |
| 0.3997 | 3223 | 3.102 | 2.451 | | | |
| 0.3519 | 2839 | 3.523 | 2.448 | | | |
| 0.3040 | 2452 | 4.000 | 2.449 | | 2.469 | |
| 0.2679 | 2161 | 4.627 | 2.443 | | | |
| 0.2292 | 1848 | 5.410 | 2.441 | | | |
| 0.2066 | 1666 | 6.000 | 2.445 | | 2.466 | |
| 0.1764 | 1422 | 7.030 | 2.438 | | | |

TABLE I (*Continued*)

Cadmium Selenide

| eV | $cm^{-1}$ | μm | $n_o$ | $k_o$ | $n_e$ | $k_e$ |
|---|---|---|---|---|---|---|
| 0.1544 | 1245 | 8.033 | 2.432 | | | |
| 0.1353 | 1091 | 9.164 | 2.429 | | | |
| 0.1240 | 1000 | 10.00 | 2.431 | | 2.452 | |
| 0.1072 | 864.6 | 11.57 | 2.413 | | | |
| 0.09733 | 785.0 | 12.74 | 2.419 | | | |
| 0.08860 | 714.6 | 13.99 | 2.410 | | 2.431 | |
| 0.07750 | 625.1 | 16.00 | 2.399 | | 2.419 | |
| 0.06874 | 554.4 | 18.04 | 2.385 | | | |
| 0.06200 | 500.1 | 20.00 | 2.376 | | 2.389 | |
| 0.05763 | 464.8 | 21.52 | | 6.35E-04 [4] | | |
| 0.05687 | 458.7 | 21.80 | | 6.51E-04 | | |
| 0.05630 | 454.1 | 22.02 | 2.339 | | 2.351 | |
| 0.05627 | 453.8 | 22.04 | | 6.61E-04 | | |
| 0.05495 | 443.2 | 22.57 | | 6.77E-04 | | |
| 0.05422 | 437.3 | 22.87 | | 7.94E-04 | | |
| 0.05359 | 432.2 | 23.14 | | 9.39E-04 | | |
| 0.05311 | 428.4 | 23.34 | | 1.12E-03 | | |
| 0.05274 | 425.4 | 23.51 | | 1.20E-03 | | |
| 0.05254 | 423.8 | 23.60 | | 1.18E-03 | | |
| 0.05241 | 422.7 | 23.66 | | 1.11E-03 | | |
| 0.05210 | 420.2 | 23.80 | | 9.74E-04 | | |
| 0.05182 | 417.9 | 23.93 | | 8.43E-04 | | |
| 0.05157 | 415.9 | 24.04 | | 8.08E-04 | | |
| 0.05120 | 412.9 | 24.22 | | 8.21E-04 | | |
| 0.05099 | 411.3 | 24.32 | 2.291 | | | |
| 0.05075 | 409.3 | 24.43 | | 8.37E-04 | | |
| 0.05035 | 406.1 | 24.62 | | 8.35E-04 | | |
| 0.05008 | 403.9 | 24.76 | | 9.25E-04 | | |
| 0.04987 | 402.2 | 24.86 | | 1.07E-03 | | |
| 0.04956 | 399.7 | 25.00 | | 1.31E-03 | | |
| 0.04914 | 396.3 | 25.23 | | 1.71E-03 | | |
| 0.04876 | 393.3 | 25.43 | | 2.10E-03 | | |
| 0.04832 | 389.7 | 25.66 | | 2.64E-03 | | |
| 0.04799 | 387.1 | 25.84 | | 3.28E-03 | | |
| 0.04773 | 384.9 | 25.98 | | 3.86E-03 | | |
| 0.04757 | 383.7 | 26.06 | | 4.59E-03 | | |
| 0.04741 | 382.4 | 26.15 | | 5.13E-03 | | |
| 0.04727 | 381.2 | 26.23 | | 5.76E-03 | | |
| 0.04705 | 379.5 | 26.35 | | 6.41E-03 | | |
| 0.04688 | 378.1 | 26.45 | | 6.96E-03 | | |
| 0.04678 | 377.3 | 26.51 | | 7.51E-03 | | |
| 0.04655 | 375.5 | 26.63 | | 8.11E-03 | | |
| 0.04646 | 374.7 | 26.69 | | 8.50E-03 | | |
| 0.04641 | 374.3 | 26.72 | | 8.69E-03 | | |
| 0.04630 | 373.4 | 26.78 | 2.280 | | | |
| 0.04618 | 372.5 | 26.85 | | 8.78E-03 | | |

TABLE I (*Continued*)

Cadmium Selenide

| eV | $cm^{-1}$ | μm | $n_o$ | $k_o$ | $n_e$ | $k_e$ |
|---|---|---|---|---|---|---|
| 0.04603 | 371.2 | 26.94 | | 8.87E-03 | | |
| 0.04600 | 371.0 | 26.95 | | 8.96E-03 | | |
| 0.04591 | 370.3 | 27.01 | | 9.30E-03 | | |
| 0.04580 | 369.4 | 27.07 | | 9.66E-03 | | |
| 0.04570 | 368.6 | 27.13 | | 9.86E-03 | | |
| 0.04555 | 367.4 | 27.22 | | 9.96E-03 | | |
| 0.04544 | 366.5 | 27.28 | | 9.90E-03 | | |
| 0.04541 | 366.2 | 27.31 | | 9.84E-03 | | |
| 0.04529 | 365.3 | 27.38 | | 9.71E-03 | | |
| 0.04518 | 364.4 | 27.44 | | 9.55E-03 | | |
| 0.04497 | 362.7 | 27.57 | | 9.48E-03 | | |
| 0.04480 | 361.3 | 27.68 | | 9.67E-03 | | |
| 0.04461 | 359.8 | 27.79 | | 1.00E-02 | | |
| 0.04448 | 358.8 | 27.87 | | 1.04E-02 | | |
| 0.04431 | 357.4 | 27.98 | | 1.07E-02 | | |
| 0.04413 | 355.9 | 28.10 | | 1.09E-02 | | |
| 0.04397 | 354.6 | 28.20 | | 1.08E-02 | | |
| 0.04387 | 353.9 | 28.26 | | 1.07E-02 | | |
| 0.04370 | 352.5 | 28.37 | | 1.06E-02 | | |
| 0.04361 | 351.7 | 28.43 | | 1.02E-02 | | |
| 0.04350 | 350.9 | 28.50 | | 9.66E-03 | | |
| 0.04343 | 350.2 | 28.55 | | 9.15E-03 | | |
| 0.04331 | 349.3 | 28.63 | | 8.70E-03 | | |
| 0.04300 | 346.8 | 28.83 | | 8.63E-03 | | |
| 0.04275 | 344.8 | 29.00 | | 8.78E-03 | | |
| 0.04269 | 344.3 | 29.05 | 2.253 | | | |
| 0.04267 | 344.2 | 29.06 | | 8.95E-03 | | |
| 0.04258 | 343.4 | 29.12 | | 9.26E-03 | | |
| 0.04248 | 342.6 | 29.19 | | 9.55E-03 | | |
| 0.04241 | 342.1 | 29.24 | | 9.87E-03 | | |
| 0.04228 | 341.0 | 29.33 | | 1.02E-02 | | |
| 0.04211 | 339.6 | 29.45 | | 1.04E-02 | | |
| 0.04196 | 338.4 | 29.55 | | 1.03E-02 | | |
| 0.04187 | 337.7 | 29.61 | | 1.02E-02 | | |
| 0.04178 | 336.9 | 29.68 | | 1.01E-02 | | |
| 0.04172 | 336.5 | 29.72 | 2.239 | | | |
| 0.04170 | 336.3 | 29.74 | | 9.81E-03 | | |
| 0.04156 | 335.2 | 29.83 | | 9.31E-03 | | |
| 0.04151 | 334.8 | 29.87 | | 9.03E-03 | | |
| 0.04126 | 332.8 | 30.05 | | 9.34E-03 | | |
| 0.04120 | 332.3 | 30.10 | | 9.68E-03 | | |
| 0.04118 | 332.2 | 30.11 | | 1.01E-02 | | |
| 0.04112 | 331.6 | 30.16 | | 1.05E-02 | | |
| 0.04110 | 331.5 | 30.17 | | 1.08E-02 | | |
| 0.04106 | 331.2 | 30.19 | | 1.12E-02 | | |
| 0.04098 | 330.6 | 30.25 | | 1.16E-02 | | |

TABLE I (*Continued*)

**Cadmium Selenide**

| eV | $cm^{-1}$ | μm | $n_e$ | $k_e$ | $n_\perp$ | $k_\perp$ |
|---|---|---|---|---|---|---|
| 0.04079 | 329.0 | 30.40 | | 1.08E-02 | | |
| 0.04067 | 328.0 | 30.49 | | 1.06E-02 | | |
| 0.04055 | 327.0 | 30.58 | | 1.04E-02 | | |
| 0.04047 | 326.4 | 30.64 | | 1.05E-02 | | |
| 0.04046 | 326.3 | 30.65 | | 1.06E-02 | | |
| 0.04040 | 325.9 | 30.69 | | 1.09E-02 | | |
| 0.04035 | 325.4 | 30.73 | | 1.12E-02 | | |
| 0.04011 | 323.5 | 30.91 | | 1.14E-02 | | |
| 0.04001 | 322.7 | 30.99 | | 1.12E-02 | | |
| 0.03992 | 321.9 | 31.06 | | 1.10E-02 | | |
| 0.03988 | 321.6 | 31.09 | | 1.08E-02 | | |
| 0.03978 | 320.9 | 31.17 | | 1.05E-02 | | |
| 0.03974 | 320.6 | 31.20 | | 1.03E-02 | | |
| 0.03953 | 318.8 | 31.36 | | 1.02E-02 | | |
| 0.03940 | 317.8 | 31.47 | | 1.03E-02 | | |
| 0.03920 | 316.2 | 31.63 | | 1.05E-02 | | |
| 0.03895 | 314.2 | 31.83 | | 1.07E-02 | | |
| 0.03885 | 313.3 | 31.92 | | 1.04E-02 | | |
| 0.03870 | 312.1 | 32.04 | | 1.04E-02 | | |
| 0.03856 | 310.9 | 32.16 | | 1.05E-02 | | |
| 0.03825 | 308.5 | 32.41 | | 1.07E-02 | | |
| 0.03811 | 307.4 | 32.54 | | 1.07E-02 | | |
| 0.03800 | 306.5 | 32.63 | | 1.07E-02 | | |
| 0.03784 | 305.2 | 32.76 | | 1.06E-02 | | |
| 0.03750 | 302.5 | 33.06 | | 1.05E-02 | | |
| 0.03625 | 292.4 | 34.21 | | | 2.384[12] | 4.64E-02[12] |
| 0.03623 | 292.2 | 34.22 | 2.411[12] | 2.40E-01[12] | | |
| 0.03586 | 289.2 | 34.58 | | | 2.386 | 4.66E-02 |
| 0.03577 | 288.5 | 34.67 | 2.400 | 2.98E-01 | | |
| 0.03539 | 285.5 | 35.03 | 2.394 | 3.54E-01 | | |
| 0.03539 | 285.4 | 35.04 | | | 2.369 | 8.25E-02 |
| 0.03500 | 282.3 | 35.43 | | | 2.287 | 8.73E-02 |
| 0.03498 | 282.2 | 35.44 | 2.288 | 5.13E-01 | | |
| 0.03461 | 279.1 | 35.83 | | | 2.185 | 2.07E-01 |
| 0.03452 | 278.4 | 35.92 | 2.160 | 6.74E-01 | | |
| 0.03419 | 275.8 | 36.26 | | | 2.017 | 4.18E-01 |
| 0.03413 | 275.3 | 36.33 | 1.961 | 6.27E-01 | | |
| 0.03381 | 272.7 | 36.67 | | | 2.078 | 6.99E-01 |
| 0.03379 | 272.6 | 36.69 | 1.887 | 4.09E-01 | | |
| 0.03343 | 269.6 | 37.09 | | | 2.245 | 4.80E-01 |
| 0.03341 | 269.5 | 37.11 | 2.006 | 3.38E-01 | | |
| 0.03306 | 266.6 | 37.51 | | | 2.399 | 3.44E-01 |
| 0.03304 | 266.5 | 37.53 | 2.215 | 3.42E-01 | | |
| 0.03263 | 263.2 | 38.00 | 2.268 | 3.30E-01 | 2.447 | 4.67E-01 |
| 0.03220 | 259.7 | 38.51 | | | 2.556 | 2.69E-01 |

TABLE I (*Continued*)

Cadmium Selenide

| eV | $cm^{-1}$ | μm | $n_\perp$ | $k_\perp$ | $n_\parallel$ | $k_\parallel$ |
|---|---|---|---|---|---|---|
| 0.03214 | 259.2 | 38.58 | 2.341 | 2.16E-01 | | |
| 0.03182 | 256.6 | 38.96 | | | 2.366 | 1.38E-01 |
| 0.03176 | 256.1 | 39.04 | 2.363 | 7.55E-03 | | |
| 0.03133 | 252.7 | 39.58 | | | 2.220 | 2.55E-03 |
| 0.03132 | 252.6 | 39.59 | 2.221 | 7.16E-03 | | |
| 0.03102 | 250.2 | 39.97 | | | 2.144 | 3.83E-03 |
| 0.03099 | 249.9 | 40.01 | 2.134 | 3.23E-02 | | |
| 0.03065 | 247.2 | 40.45 | | | 2.047 | 1.00E-03 |
| 0.03064 | 247.1 | 40.47 | 2.052 | 5.67E-02 | | |
| 0.03033 | 244.6 | 40.88 | | | 1.995 | 2.97E-02 |
| 0.03031 | 244.5 | 40.90 | 1.993 | 1.88E-02 | | |
| 0.02996 | 241.6 | 41.39 | | | 1.883 | 5.35E-03 |
| 0.02990 | 241.1 | 41.47 | 1.909 | 4.23E-02 | | |
| 0.02956 | 238.4 | 41.95 | 1.806 | 3.01E-02 | | |
| 0.02955 | 238.3 | 41.96 | | | 1.837 | 2.30E-02 |
| 0.02911 | 234.7 | 42.59 | 1.704 | 2.21E-02 | | |
| 0.02909 | 234.6 | 42.62 | | | 1.736 | 3.34E-02 |
| 0.02879 | 232.2 | 43.07 | | | 1.721 | 4.90E-02 |
| 0.02874 | 231.8 | 43.14 | 1.685 | 5.54E-02 | | |
| 0.02832 | 228.4 | 43.77 | | | 1.649 | 7.44E-02 |
| 0.02829 | 228.2 | 43.82 | 1.590 | 4.79E-02 | | |
| 0.02795 | 225.4 | 44.37 | | | 1.628 | 4.08E-02 |
| 0.02787 | 224.8 | 44.48 | 1.612 | 7.60E-02 | | |
| 0.02752 | 221.9 | 45.05 | | | 1.581 | 2.05E-02 |
| 0.02749 | 221.7 | 45.09 | 1.555 | 9.72E-02 | | |
| 0.02715 | 218.9 | 45.68 | | | 1.481 | 2.01E-02 |
| 0.02712 | 218.7 | 45.72 | 1.442 | 1.36E-01 | | |
| 0.02675 | 215.8 | 46.35 | | | 1.329 | 1.96E-02 |
| 0.02674 | 215.7 | 46.37 | 1.343 | 4.59E-02 | | |
| 0.02642 | 213.1 | 46.93 | | | 1.298 | 7.12E-03 |
| 0.02640 | 212.9 | 46.97 | 1.203 | 1.59E-02 | | |
| 0.02599 | 209.6 | 47.71 | | | 0.801 | 3.33E-02 |
| 0.02596 | 209.4 | 47.75 | 0.714 | 1.83E-01 | | |
| 0.02559 | 206.4 | 48.45 | | | 0.159 | 2.82E-01 |
| 0.02555 | 206.0 | 48.53 | 0.274 | 7.53E-01 | | |
| 0.02518 | 203.1 | 49.23 | | | 0.095 | 9.81E-01 |
| 0.02515 | 202.8 | 49.30 | 0.298 | 1.34E+00 | | |
| 0.02483 | 200.3 | 49.93 | | | 0.023 | 1.41E+00 |
| 0.02479 | 200.0 | 50.01 | 0.285 | 1.78E+00 | | |
| 0.02449 | 197.5 | 50.63 | | | 0.015 | 1.91E+00 |
| 0.02447 | 197.4 | 50.66 | 0.381 | 2.08E+00 | | |
| 0.02412 | 194.5 | 51.41 | 0.401 | 2.40E+00 | | |
| 0.02411 | 194.4 | 51.43 | | | 0.110 | 2.24E+00 |
| 0.02375 | 191.5 | 52.21 | | | 0.333 | 2.65E+00 |
| 0.02371 | 191.3 | 52.29 | 0.582 | 2.72E+00 | | |
| 0.02348 | 189.3 | 52.81 | | | 0.624 | 2.95E+00 |

TABLE I (*Continued*)

**Cadmium Selenide**

| eV | $cm^{-1}$ | μm | $n_o$ | $k_o$ | $n_e$ | $k_e$ |
|---|---|---|---|---|---|---|
| 0.02341 | 188.8 | 52.97 | 0.655 | 3.07E+00 | | |
| 0.02295 | 185.1 | 54.03 | 1.168 | 3.61E+00 | | |
| 0.02294 | 185.0 | 54.05 | | | 0.934 | 3.54E+00 |
| 0.02261 | 182.3 | 54.85 | 1.696 | 4.12E+00 | | |
| 0.02257 | 182.0 | 54.94 | | | 1.244 | 3.95E+00 |
| 0.02217 | 178.8 | 55.93 | 2.308 | 4.65E+00 | | |
| 0.02212 | 178.4 | 56.06 | | | 1.662 | 4.53E+00 |
| 0.02179 | 175.7 | 56.90 | | | 2.314 | 4.98E+00 |
| 0.02174 | 175.3 | 57.03 | 3.238 | 4.74E+00 | | |
| 0.02142 | 172.8 | 57.87 | 4.858 | 3.89E+00 | | |
| 0.02137 | 172.4 | 58.01 | | | 3.081 | 5.38E+00 |
| 0.02125 | 171.4 | 58.34 | | | 3.664 | 5.66E+00 |
| 0.02124 | 171.3 | 58.38 | 5.439 | 3.75E+00 | | |
| 0.02101 | 169.5 | 59.00 | 5.702 | 3.34E+00 | | |
| 0.02100 | 169.3 | 59.05 | | | 4.396 | 5.60E+00 |
| 0.02076 | 167.4 | 59.73 | 5.964 | 2.75E+00 | | |
| 0.02075 | 167.3 | 59.74 | | | 5.724 | 5.75E+00 |
| 0.02055 | 165.8 | 60.32 | 5.848 | 2.17E+00 | | |
| 0.02052 | 165.6 | 60.41 | | | 6.554 | 5.19E+00 |
| 0.02035 | 164.1 | 60.92 | 5.682 | 1.68E+00 | | |
| 0.02030 | 163.7 | 61.09 | | | 7.307 | 4.01E+00 |
| 0.02012 | 162.3 | 61.61 | 5.719 | 1.35E+00 | | |
| 0.02008 | 162.0 | 61.73 | | | 7.633 | 3.05E+00 |
| 0.01998 | 161.1 | 62.07 | 5.667 | 1.07E+00 | | |
| 0.01990 | 160.5 | 62.31 | | | 7.413 | 1.45E+00 |
| 0.01976 | 159.4 | 62.75 | 5.414 | 8.70E-01 | | |
| 0.01966 | 158.6 | 63.06 | | | 7.389 | 6.18E-01 |
| 0.01940 | 156.5 | 63.91 | 5.062 | 5.47E-01 | | |
| 0.01929 | 155.6 | 64.28 | | | 6.926 | 1.61E-01 |
| 0.01897 | 153.0 | 65.36 | 4.711 | 3.69E-01 | | |
| 0.01893 | 152.7 | 65.49 | | | 5.903 | 1.65E-02 |
| 0.01863 | 150.2 | 66.56 | 4.484 | 2.50E-01 | | |
| 0.01860 | 150.0 | 66.68 | | | 5.506 | 4.90E-03 |
| 0.01826 | 147.2 | 67.92 | 4.282 | 1.54E-01 | | |
| 0.01822 | 146.9 | 68.05 | | | 5.257 | 5.97E-03 |
| 0.01788 | 144.2 | 69.36 | 4.136 | 7.89E-02 | | |
| 0.01782 | 143.7 | 69.56 | | | 4.999 | 7.09E-03 |
| 0.01750 | 141.2 | 70.84 | 4.016 | 4.05E-02 | | |
| 0.01748 | 140.9 | 70.95 | | | 4.800 | 7.97E-03 |
| 0.01710 | 137.9 | 72.49 | 3.877 | 1.78E-02 | | |
| 0.01705 | 137.5 | 72.70 | | | 4.624 | |
| 0.01670 | 134.7 | 74.26 | 3.791 | | | |
| 0.01664 | 134.2 | 74.51 | | | 4.430 | |
| 0.01631 | 131.6 | 76.01 | 3.708 | | | |
| 0.01629 | 131.4 | 76.10 | | | 4.327 | |
| 0.01589 | 128.2 | 78.02 | 3.630 | | | |

TABLE I (*Continued*)

**Cadmium Selenide**

| eV | $cm^{-1}$ | μm | $n_o$ | $k_o$ | $n_e$ | $k_e$ |
|---|---|---|---|---|---|---|
| 0.01587 | 128.0 | 78.12 | | | 4.178 | |
| 0.01555 | 125.4 | 79.76 | 3.576 | | | |
| 0.01549 | 124.9 | 80.05 | | | 4.063 | |
| 0.01515 | 122.2 | 81.84 | 3.532 | | | |
| 0.01511 | 121.8 | 82.06 | | | 3.967 | |
| 0.01471 | 118.6 | 84.29 | 3.469 | | | |
| 0.01464 | 118.1 | 84.69 | | | 3.838 | |
| 0.01437 | 115.9 | 86.27 | 3.416 | | | |
| 0.01433 | 115.6 | 86.54 | | | 3.745 | |
| 0.01395 | 112.5 | 88.86 | 3.405 | | | |
| 0.01394 | 112.4 | 88.94 | | | 3.688 | |
| 0.01359 | 109.6 | 91.25 | 3.377 | | | |
| 0.01355 | 109.3 | 91.49 | | | 3.609 | |
| 0.01321 | 106.6 | 93.82 | 3.352 | | | |
| 0.01314 | 106.0 | 94.33 | | | 3.538 | |
| 0.01278 | 103.1 | 97.03 | 3.340 | | | |
| 0.01275 | 102.8 | 97.26 | | | 3.474 | |
| 0.01245 | 100.4 | 99.55 | 3.335 | | 3.474 | |

[a] References are indicated in brackets.

# Cadmium Sulphide (CdS)

L. WARD
Coventry Polytechnic
Coventry, England

Cadmium sulphide is a member of the II-VI group of semiconducting compounds formed by alloying one element from group II of the periodic table with another from group VI. The energy gap between the valence and conduction bands is about 2.4 eV and CdS has been used extensively in photoconducting cells, being effective in the ultraviolet and blue parts of the spectrum. In addition, there is a strong absorption band in the infrared due to lattice vibrations (phonons). At short wavelengths there are also absorption bands due to electron transitions involving inner energy levels. The normal crystal structure is hexagonal close-packed (wurtzite), which is in space group C6mc, and most of the reported values of the optical constants of CdS have been for this form of the compound. However, a face-centered cubic form of CdS can also be prepared (zinc-blende structure, space group $F\bar{4}3m$), and a few results for this material are also available. In dealing with hexagonal CdS, the optical properties of the single crystals depend on whether the electric vector of the incident radiation is vibrating perpendicular to or parallel to the $c$ axis, that is, the axis at a right angle to the crystal hexagon. The main impurities occurring in CdS are iron, potassium, and sodium; it is possible to obtain material where all the impurities total less than 0.01%. Values of $n$ and $k$ for CdS are given in Table I and graphed in Fig. 1; the wavelength range covered is $6 \times 10^{-4}$ to 1000 μm and, wherever possible, slight wavelength overlaps have been included between the different sets of results.

*Hexagonal Cadmium Sulphide*

Henke [1] has described a method of calculating optical constants at X-ray wavelengths (0.0006–0.0124 μm) from X-ray scattering data; the scattering coefficients $f_1$ and $f_2$ for all elements are given in detail by Henke *et al.* [2]. For CdS, the following relationships apply;

$$n = 1 - 4.45\lambda^2(f_{1\mathrm{Cd}} + f_{1\mathrm{S}})$$
$$k = 4.45\lambda^2(f_{2\mathrm{Cd}} + f_{2\mathrm{S}}),$$

where $\lambda$ is the wavelength in μm.


Copyright © 1991 by Academic Press.
All rights of reproduction in any form reserved.
ISBN 0-12-544422-2

The calculated values of $n$ in this region, which are given in Table I, were generally just less than unity, whereas peaks in $k$ were produced at 0.0075 μm ($L_{II,III}$ transition in S) and 0.0028 μm ($M_V$ in Cd). Cardona and Haensel [3] made a direct measurement of the absorption coefficient, $\alpha$, between 36 and 120 eV (0.01–0.34 μm) of evaporated thin films of CdS; $k$ may then be calculated from the relationship, $k = \alpha\lambda/4\pi$, a peak being observed at 0.0225 μm (55 eV). Where overlap occurs, there is reasonably good agreement between the values of $k$ from Henke and those of Cardona and Haensel.

Cardona and Harbeke [4] measured the reflectances $R_p$ and $R_s$ between 2 and 12 eV (0.1–0.62 μm) of platelets of CdS grown from the vapor phase, although they claimed that similar results could be obtained from etched solid material; they used a Kramers–Kronig (K–K) analysis to calculate $n$ and $k$ for the cases of both $\mathbf{E}_{\parallel c}$ and $\mathbf{E}_{\perp c}$. Peaks were observed in $n$ at 0.490, 0.264, and 0.143 μm (both states of polarization) and at 0.234 μm ($\mathbf{E}_{\perp c}$) and 0.175 μm ($\mathbf{E}_{\parallel c}$); there were peaks in $k$ at 0.490, 0.225, 0.155, and 0.136 μm (both) and at 0.200 μm ($\mathbf{E}_{\parallel c}$) and 0.253 μm ($\mathbf{E}_{\perp c}$); the peaks at 0.490 μm correspond to the main energy gap (2.53 eV). The authors were able to correlate all these peaks with different electron transitions within the energy-band structure of cadmium sulphide. Their values of $n$ and $k$ for both states of polarization are included in Table I. Balkanski and Petroff [5] determined $\varepsilon_1$ and $\varepsilon_2$ between 1 and 20 eV (0.06–1.24 μm) using measurements of reflectance from the natural faces of CdS crystals. They found a similar set of absorption peaks to those of Cardona and Harbeke with the addition of a further peak at 14.5 eV (0.0855 μm). Freeout [6] used synchrotron radiation to measure the reflectance of the natural faces of CdS crystals between 0.04 and 2.0 μm using a rotating-light-pipe scanning reflectometer originally devised by Gerhardt and Rubloff [7]. He presented graphs of $\varepsilon_1$ and $\varepsilon_2$ versus wavelength, finding a strong absorption doublet at 13.5 eV (0.092 μm), which is close to the $M_1$ transition in sulphur; he suggested that this doublet was produced by spin-orbit splitting of this transition.

In the region around 0.5 μm, which includes the main absorption band due to electron transitions between the valence and conduction bands, Brodin and his collaborators have made important contributions. Brodin and Strashnikova [8] determined $n$ for single-crystal CdS films by an interference technique; for radiation polarized with the **E** vector perpendicular to the $c$ axis, there was a single absorption peak at about 0.48 μm, whereas for the **E** vector parallel to the $c$ axis, there were two close peaks centered about the same wavelength. In addition, there was also a wide absorption band near 0.28 μm, present in both states of polarization. Brodin *et al.* [9] also measured the reflectance of single-crystal material but at a temperature of 4.2 K; for **E** vibrations that were polarized parallel to the $c$ axis, a single absorption maximum was found at 0.483 μm; for

polarization at right angles to the $c$ axis, two maxima were discovered at 0.487 and 0.463 μm. Brodin [10] has published values of $n$ versus wavelength between 0.5 and 0.65 μm for monocrystals of CdS at temperatures of 20 K and 290 K. He measured the reflectance and used K–K analysis to find $n$ for **E** both parallel and perpendicular to the $c$ axis; over the range of wavelengths studied, $n_e$ ($\|$) was always about 2% larger than $n_o$ ($\perp$).

Kreisel *et al.* [11] studied CdS in the range of 0.5–0.7 μm under different levels of light excitation and at low temperatures (5 K). At low excitation levels, excitons (see below) were observed, but at high levels of excitation, an electron-hole plasma was produced. $n_o$ was larger than $n_e$ up to 0.510 μm, but at the longer wavelengths this situation was reversed. When the CdS contained free-carrier impurities ($2 \times 10^{18}\,\text{cm}^{-3}$), the value of $n$ at the absorption peak was reduced from 5.0 to 3.5. Lampicki [12] found three peaks in his reflectance curves at 0.4874, 0.4844, and 0.4731 μm, which he identified with electron transitions between the valence and conduction bands in the Γ direction in the Brillouin zone. All three peaks were present for $\mathbf{E}_{\perp c}$ but only the two at lower wavelengths for $\mathbf{E}_{\|c}$; these results are similar to those found by Brodin. Gobrecht and Bartschat [13] determined $n$ and $k$ by Denton's method [14], which required a knowledge of both the reflectance and transmittance and yielded values for both the *o*- and *e*-rays between 0.49 and 0.65 μm at both 20°C and −180°C. For the longer wavelengths, $n_o$ was smaller than $n_e$, but there was a crossover at about 0.51 μm. They concluded that just beyond the absorption edge at 0.485 μm, CdS shows evidence of direct electron transitions between the valence and conduction bands. At higher photon energies, the form of the absorption curve was probably determined by the combined effects of indirect transitions and direct transitions between nonparabolic energy bands.

Bienewski and Czyzek [15] and also Czyzek *et al.* [16] have made measurements of $n$ between 0.5 and 1.4 μm at 298 K using the minimum-deviation method reported by Czyzek *et al.* [17] in which the chopped radiation was detected by a thermocouple; tables of values for both the *o*- and *e*-rays ($\mathbf{E}_{\perp c}$ and $\mathbf{E}_{\|c}$) were produced in which $n$ is quoted to three decimal places. These values are reproduced in Table I. Using a nonlinear regression technique, Sanchez-Gomez *et al.* [18] claimed to have refined these results of Bienewski and Czyzek for the dispersion of CdS and were also able to calculate the residuals for each wavelength. However, this process made little difference to the original values of $n$, causing only small alterations in the third decimal place. Another investigator in this part of the spectrum was Devore [19] who also used the prism technique and was able to produce Sellmeier-type equations for both the *e*- and *o*-rays. Reynolds *et al.* [20] have also published graphs of $n$ and $\alpha$ against wavelength between 0.5 and 1.0 μm for single-crystal cadmium sulphide.

Francis and Carlson [21] have published a set of results for $n$ measured

on polycrystalline cadmium sulphide between 1 and 14 μm determined by the minimum-deviation method involving a narrow-angled prism of the material. They did not distinguish between the *o*- and *e*-rays, but their values of $n$ link well with those of Bienewski and Czyzek for *e*-rays; they have been quoted extensively in Table I.

Vitrikhovskii *et al.* [22], using single crystals of CdS, have investigated the variation of $n$ with temperature over the range 100–600 K. The refractive index was measured between 0.5 and 1.6 μm by the prism technique and by an interference method; there was good agreement between their published values and those of Bienewski and Czyzek at 300 K. Both $n_o$ and $n_e$ increased with temperature, $dn/dT$ being about $8 \times 10^{-5}$/°C.

*Thin Films*

Gottesmann and Ferguson [23] measured the reflectance of thin films of CdS between 0.4 and 0.75 μm finding an absorption edge at 0.52 μm. The most rapid deposition rate that they used (90 Å/min) produced the highest values of $n$, but these were still less than those for bulk material, presumably because of the low packing density of the film particles. Hall [24], who measured the reflectance and transmittance of thin films on quartz substrates between 0.2 and 0.6 μm at different deposition rates, observed peaks in $n$ at 0.25 and 0.5 μm and in $k$ at 0.23 μm. The absorption maximum occurred close to the s–p transition wavelength of sulphur at 0.229 μm. $n$ was found to be proportional to the deposition rate up to 0.40 μm but not at the higher wavelengths, whereas $k$ did not appear to be affected by the deposition rate. There was a region of anomalous dispersion between 0.40 and 0.50 μm due to the excitation of electrons from the valence to the conduction band; the absorption edge was measured at 0.51 μm.

De la Plaza *et al.* [25] studied RF sputtered films of CdS and published values of $n$ versus wavelength over the narrow range 0.5–0.7 μm for different sputtering pressures. The largest values of $n$ were obtained at the lowest deposition pressure, but again these were less than those for crystalline cadmium sulphide. Strashnikova *et al.* [26] using a prism of very small angle ($0.75 \times 10^{-4}$ rad), noted that $n$ increased slightly with the thickness of the prism up to 4 μm thick at wavelengths between 0.46 and 0.49 μm. In another paper, Strashnikova *et al.* [27] studied the variation of the wavelength of the inversion point (where $n$ is the same for both *o*- and *e*-rays) with film thickness. The inversion wavelength decreased from 0.510 μm for films thicker than 1.5 μm, to 0.498 μm at a thickness of 0.5 μm, the authors claiming that this effect was due to the decreasing oscillator strength of the exciton.

Khawaja and Tomlin [28] measured both the reflectance and transmittance of thin films deposited on quartz wedges with 3° angles to eliminate

reflection from the back of the substrate. The wavelength range covered was 0.3–2.0 μm and three substrate temperatures were used: 20, 140, and 180°C. The highest substrate temperature generated the largest values of $n$ and $k$, presumably because the higher mobilities of the deposited particles produced a more densely packed film, but the values of $n$ were still lower than those for bulk materials. Wohlegemutt *et al.* [29] also measured the normal-incidence reflectance and transmittance up to a wavelength of 1.0 μm for both polycrystalline and amorphous CdS films deposited on sapphire; they compared their results with those of Cardona and Harbeke [4], Khawaja and Tomlin [28] and Kuwabara [34], noting a peak in $n$ at about 0.5 μm in all the sets of results. However, the curves of $n$ versus wavelength produced by Wohlegemutt *et al.* were at all points lower than those by the other authors; on the other hand, the values of $k$ were in much better agreement. $n$ initially fell as the wavelength decreased over the anomalous-dispersion region, but commenced to increase again as the wavelength approached 0.3 μm. The results of Khawaja and Tomlin are regarded as being the best in this region of the spectrum, and they are given in Table I.

Shklyarevskii *et al.* [30] working between 0.45 and 0.65 μm used ellipsometry to measure the optical constants of a thin film of CdS deposited on a chromium substrate. $n$ was found to be a function of both the film thickness and the wavelength, but all the curves showed a maximum at about 0.485 μm; $k$, however, was independent of thickness and increased with decreasing wavelength. Czyzek *et al.* [17] have reported studies on synthetic CdS from the visible region up to 1.4 μm. Over this limited wavelength range, the following Sellmeier-type equations were derived for $n_o$ and $n_e$:

$$n_0^2 = 5.235 + 1.819 \times 10^7/(\lambda^2 - 1.651 \times 10^7)$$

$$n_e^2 = 5.239 + 2.076 \times 10^7/(\lambda^2 - 1.651 \times 10^7).$$

Measurements on polycrystalline films of CdS have been made by Soera and Serdyuk [31]. A complicated structure in the reflectance curve near the absorption edge was attributed to layers of excitons and possibly also to lattice defects. Nolly *et al.* [32] have carried out an ellipsometric study of spray-pyrolized thin films of CdS over the visible spectrum. Hall and Ferguson [33] determined the optical constants of films of CdS from measurements of reflectance and transmittance between 0.6 and 14 μm; $n$ was found to be independent of the deposition rate and also decreased monotonically with wavelength from 2.52 at 0.6 μm to 2.26 at 14.0 μm, whereas $k$ showed a linear increase with wavelength and was also dependent on the deposition rate up to 7 μm, being largest for the highest rates. Their values of $n$ agree reasonably well with those of Bienewski and

Czyzek. As examples of the optical constants of thin films in this spectral region, Hall and Ferguson's results are reproduced in Table I.

Kuwabara [34] worked with polycrystalline evaporated films between 0.4 and 1.0 μm finding a maximum in $n$ of 2.65 at 0.5 μm where $k$ was equal to 0.18; the absorption edge, corresponding to electron transitions from the valence to the conduction band, occurred at the same wavelength. He claimed that the optical properties of the films were similar to those for a single crystal, but his values for $n$ were significantly smaller than those of Khawaja and Tomlin for similar films. Elizelde and Rueda [35] measured the reflectance and transmittance of thin-film specimens and, using the exact equations for these parameters produced by Bauer [36] (which take account of both faces of the substrate), calculated the optical constants between 0.5 and 2.5 μm. Between 0.5 and 10.0 μm, Miloslavski [37], working with layers of single-crystal CdS of thickness 2–3 μm deposited on a sodium-chloride substrate, measured the transmittance, from which $n$ could be calculated. He was interested in the effect on $n$ of the presence of impurities and noted that as the proportion of impurities was increased up to $1.2 \times 10^{18}$ carriers/cm$^{-3}$, the values of $n$ between 5 and 18 μm decreased by about 2.5%.

*Infrared region*

In the spectral region from 10–50 μm several studies of the optical properties of cadmium sulphide have been made. Collins [38] has reported reflectance values for unpolarized radiation measured on a single crystal between 20 and 48 μm; these showed a minimum reflectance at 32 μm followed by a peak at 38 μm. Taking the value of the dielectric constant at very long wavelengths, $e_o$, as 9.3, the value of $e_\infty$ as 5.76, and the transverse optical phonon as 241 cm$^{-1}$ (41.5 μm), the wave number of the longitudinal optical phonon was deduced from a Lorentz-type equation to be 305 cm$^{-1}$ (37.8 μm). Balkanski and Besson [39] measured the reflectance between 15 and 30 μm at both 293 K and 80 K and found that their results could be explained in terms of multiple-phonon processes, that is, two or three phonons being excited by the absorption of a single photon. Values of $k$ over this wavelength range calculated from their absorption-coefficient graph are incorporated in Table I. Deutsch [40] also studied the infrared absorption of CdS between 10 and 25 μm, finding bands at 22.55 and 23.15 μm when the **E** vector of the incident radiation was parallel to the $c$ axis of the crystal, and at 19.95 μm when the **E** vector was perpendicular to the $c$ axis; he needed four phonons to explain his results. As the absorption curves were determined in more detail, extra phonons had to be invoked to explain all the peaks; for example, Marshall and Mitra [41] needed six phonons, and Balkanski *et al.* [42] required ten. Balkanski *et al.* also measured the absorption coefficient $\alpha$ of CdS between 27 and 120 μm and have presented a graph of $\alpha$ against wave number from which values of $k$

over this spectral region have been calculated and are presented in Table I. Because a logarithmic scale was used for $\alpha$, it is difficult to take precise readings from this graph, and the estimated accuracy in $k$ is no better than the second decimal place. In their experiment CdS was deposited on silicon whose (111) axis was at right angles to the surface; the layers were then found to have their $c$ axes also at right angles to the substrate. For radiation vibrating parallel to the $c$ axis, the transverse optical phonon, $\nu_t$, was at 233.5 $cm^{-1}$ (42.8 μm) and the longitudinal optical phonon, $\nu_l$, was at 305 $cm^{-1}$ (32.8 μm); radiation vibrating at right angles to the $c$ axis gave a transverse optical phonon at 242 $cm^{-1}$ with the longitudinal phonon being unchanged.

Balkanski [43] has given a graph of $n$ versus wave number covering the range of wavelengths between 27 and 60 μm. Values of $n$ read from this graph are incorporated in Table I.

Manabe *et al.* [44] measured the reflectance of polished specimens of CdS at wavelengths between 20 and 100 μm and at temperatures of 100 and 300 K; they calculated $n$ and $k$ using the following version of the Lorentz dispersion formulas:

$$n^2 - k^2 = \varepsilon_\infty + N(\nu_t^2 - \nu^2)/((\nu_t^2 - \nu^2)^2 + \gamma^2\nu^2)$$

$$2nk = N(\gamma\nu)/((\nu_t^2 - \nu^2)^2 + \gamma^2\nu^2).$$

For $\mathbf{E}_{\parallel c}$, they used $\varepsilon_\infty = 5.4$, $N = 1.92 \times 10^5$ $cm^{-2}$, $\nu_t = 234$ $cm^{-1}$, $\nu_l = 300$ $cm^{-1}$ and $\gamma = 3.98$ $cm^{-1}$; for $\mathbf{E}_{\perp c}$ the constants were 5.3, $1.82 \times 10^5$ $cm^{-2}$, 241 $cm^{-1}$, 306 $cm^{-1}$, and 5.54 $cm^{-1}$ at 300 K. Their values for $n$ and $k$ are those quoted in Table I to represent this part of the spectrum; from their published graphs, it is just possible to read off the values to the second decimal place.

Barker and Summers [45] have reported values for the dielectric constants both parallel and perpendicular to the $c$ axis of platelets of single-crystal CdS measured by an interference method between 70 and 330 μm. Their results are given in Table I.

The refractive index of CdS between 100 and 1000 μm was determined by Hattori *et al.* [46] using a channel-spectrum technique in conjunction with a Michelson interferometer coupled to a germanium bolometer. The refractive index was calculated from the transmission interference maxima and minima. $n$ for CdS appeared to be constant over this range of wavelengths: 3.27±3% for $\mathbf{E}_{\parallel c}$ and 3.11±2% for $\mathbf{E}_{\perp c}$. Both these values were up to 10% higher than those produced by other authors such as Berlincourt *et al.* [47], Verleur and Barker [48], and Barker and Summers [45] who have also made measurements in this spectral region.

*Excitons*

Gross *et al.* [49] investigated the presence of excitons, that is, electron-hole pairs having energy levels within the energy gap, at 4.2 K, finding 13 narrow emission lines between 4853.5 and 4889.5 Å near the main absorption edge. They also found a series of equally spaced lines between 5150 and 5600 Å, which were ascribed to electron transitions involving phonons. From their results, an absorption peak could be predicted in the infrared at 47 μm, compared with the now-accepted value of 42.25 μm. Pevtsov and his colleagues [50, 51] carried out thorough investigations on two types of excitons, specified as type A and type B, due to the double degeneracy of the valence band. Another group that studied excitons was Henneberger *et al.* [52], who used artificially grown platelets of CdS and measured the transmission between crossed polaroids. Voigt *et al.* [53] studied the energy spectra of type A and B excitons by reflectance and transmittance measurements on very thin but highly perfect crystals at 1.8 K. Exciton studies were also carried out by Lambe *et al.* [54] and by Thomas and Hopfield 55, 56, 57]. The properties of excitons in semiconductors has been well-covered in a review article by Thomas and Timofiev [58].

*Cubic Cadmium Sulphide*

Cubic cadmium sulphide was studied by Cardona [59], who measured the normal-incidence reflectance of epitaxial films deposited onto the (111) face of GaAs. He noted that most of the peaks in the reflectance spectrum occurred at the same wavelengths as those for the hexagonal form, although the peak at 7.12 eV (0.174 μm) was missing, and the one at 5.49 eV (0.226 μm) was not split, as it was in the hexagonal case. No values of $n$ and $k$ are available for cubic cadmium sulphide.

## REFERENCES

1. B. L. Henke, *A.I.P. Conf. Proc. No. 75*, 146 (1981).
2. B. L. Henke, P. Lee, T. J. Tanoka, R. Shimabukura and B. K. Fujikawa, *Atomic Data and Nuclear Data Tables* **27**, 1 (1982).
3. M. Cardona and R. Haensel, *Phys. Rev.* **B1**, 2605 (1970).
4. M. Cardona and G. Harbeke, *Phys. Rev.* **A137**, 1467 (1965).
5. M. Balkanski and Y. Petroff, in "Int. Conf. Phys. Semicond. Paris," Dunod, Paris, and Academic Press, New York, 245 (1964).
6. J. L. Freeout, *Phys. Rev.* **B7**, 3810 (1973).
7. U. Gerhardt and G. W. Rubloff, *Appl. Opt.* **8**, 305 (1969).
8. M. S. Brodin and M. I. Strashnikova, *Sov. Phys. Sol. State* **8**, 549 (1966).
9. M. S. Brodin, A. V. Kritskii, and M. I. Strasnikova, *Sov. Phys. Sol. State* **13**, 475 (1971).
10. M. S. Brodin, *Sov. Phys. Sol. State* **2**, 1926 (1960); 2292 (1961).
11. A. Kreisel, K. Bohnert, V. G. Lyssenko, and C. Klingsheim, *Phys. Stat. Solidi* **B114**, 537 (1982).
12. A. Lampicki, *Proc. Phys. Soc.* **74**, 138 (1959).

13. H. Gobrecht and A. Bartschat, in "*Int. Conf. Phys. Semicond., Paris*," Dunod, Paris, and Academic Press, New York, 245 (1964).
14. R. E. Denton, R. D. Campbell, and S. G. Tomlin, *J. Phys. D* **5**, 872 (1972).
15. T. M. Bienewski and S. J. Czyzek, *J. Opt. Soc. Am.* **53**, 496 (1963).
16. S. J. Czyzek, R. C. Crane, and T. M. Bienewski, *J. Opt. Soc. Am.* **49**, 485 (1959).
17. S. J. Czyzek, W. M. Baker, R. C. Crane, and J. B. Howe, *J. Opt. Soc. Am.* **47**, 240 (1957).
18. M. Sanchez-Gomez, J. M. Guerra, and F. Vitches, *Appl. Opt.* **24**, 1147 (1985).
19. J. R. Devore, *J. Opt. Soc. Am.* **41**, 416 (1951).
20. D. C. Reynolds, S. J. Crzyzek, R. C. Allen, and C. C. Reynolds, *J. Opt. Soc. Am.* **45**, 136 (1955).
21. A. B. Francis and A. J. Carlson, *J. Opt. Soc. Am.* **50**, 118 (1960).
22. N. I. Vitrikhovskii, L. F. Gudymenko, and A. F. Maznichenko, *Sov. Phys. Semicond.* **2**, 732 (1968).
23. J. Gottesmann and W. F. C. Ferguson, *J. Opt. Soc. Am.* **44**, 368 (1954).
24. J. F. Hall, *J. Opt. Soc. Am.* **46**, 1013 (1956).
25. I. M. De la Plaza, G. Gonzales-Diaz, E. Sanchez-Quesada, and M. Rodriguez-Vidal, *Thin Solid Films* **120**, 31 (1984).
26. M. I. Strashnikova, V. Y. Resnichenko, and V. V. Cherny, *Phys. Stat. Solidi* **141**, K153 (1987).
27. M. I. Strashnikova, V. Y. Resnichenko, and V. V. Cherny, *Solid State Commun.* **47**, 375 (1983).
28. E. E. Khawaja and S. G. Tomlin, *J. Phys. D* **8**, 581 (1975).
29. J. H. Wohlgemutt, D. E. Brodie, and P. C. Eastman, *Can. J. Phys.* **54**, 785 (1976).
30. I. N. Shklyarevskii, A. F. A. El Shazli, R. G. Yarovaya, and V. P. Kostyuk, *Opt. Spectrosc.* **36**, 116 (1974).
31. T. Y. Soera and V. V. Serdyuk, *Opt. Spectrosc.* **9**, 210 (1960).
32. J. Nolly, K. K. Abadullah and K. P. Vyayakumar, *Phys. Stat. Solidi A* **101**, K35 (1987).
33. J. F. Hall and W. F. C. Ferguson, *J. Opt. Soc. Am.* **45**, 714 (1955).
34. S. Kuwabara, *J. Phys. Soc. Japan* **9**, 97 (1954).
35. E. Elizelde and F. Rueda, *Thin Solid Films* **122**, 45 (1984).
36. J. Bauer, *Exp. Tech. Phys.* **25**, 105 (1972).
37. J. K. Miloslavski, *Opt. Spectrosc.* **14**, 280 (1963).
38. R. T. Collins, *J. Appl. Phys.* **30**, 1135 (1959).
39. M. Balkanski and J. M. Besson, *J. Appl. Phys.* **32**, 2292 (1961).
40. T. Deutsch, *J. Appl. Phys.* **33**, 751 (1962).
41. R. Marshall and S. S. Mitra, *Phys. Rev.* **134**, 1019 (1964).
42. M. Balkanski, J. M. Besson, and R. Le Toullec, in "Int. Conf. Phys. Semicond., Paris," Dunod, Paris, and Academic Press, New York, 1091 (1964).
43. M. Balkanski, in "Optical Properties of Solids," (F. Abèles, ed.), North-Holland, Amsterdam, 529 (1972).
44. A. Manabe, A. Mitsuishi, and H. Yoshinga, *Jap. J. Appl. Phys.* **6**, 593 (1967).
45. A. S. Barker and C. J. Summers, *J. Appl. Phys.* **41**, 3552 (1970).
46. T. Hattori, Y. Homma, A. Mitsuishi, and M. Tacke, *Opt. Comm.* **7**, 229 (1971).
47. D. Berlincourt, H. Jaffe, and L. R. Shiozawa, *Phys. Rev.* **129**, 1009 (1963).
48. H. W. Verleur and A. S. Barker, *Phys. Rev.* **155**, 750 (1967).
49. E. F. Gross, B. S. Razbirin, and M. A. Iacobson, *Sov. Phys. Tech. Phys.* **2**, 2014 (1957).
50. A. B. Pevtsov, S. A. Permogorov, S. R. Salfullnev, and A. V. Sel'kin, *Sov. Phys. Sol. State* **22**, 1396 (1980).
51. A. B. Pevtsov and A. V. Sel'kin, *Sov. Phys. Sol. State* **25**, 85 (1983).
52. F. Henneberger, J. Puls, H. Rossmann, and I. N. Uraltsov., *Phys. Stat. Solidi* **B121**, K191 (1984).

53. J. Voigt, F. Spiegelberg, and M. Senomer, *Phys. Stat. Solidi* **B91**, 189 (1979).
54. J. J. Lambe, C. C. Klick, and D. L. Dexter, *Phys. Rev.* **103**, 1715 (1956).
55. D. G. Thomas and J. J. Hopfield, *Phys. Rev.* **116**, 573 (1959).
56. D. G. Thomas, J. J. Hopfield, and M. Power, *Phys. Rev.* **119**, 570 (1960).
57. D. G. Thomas and J. J. Hopfield, *Phys. Rev.* **128**, 2135 (1969).
58. G. A. Thomas and V. B. Timofiev, "Handbook on Semiconductors," (T. S. Moss, ed.) Vol. 2, North-Holland, Amsterdam, 45 (1984).
59. M. Cardona, *Phys. Rev.* **129**, 1068 (1963).

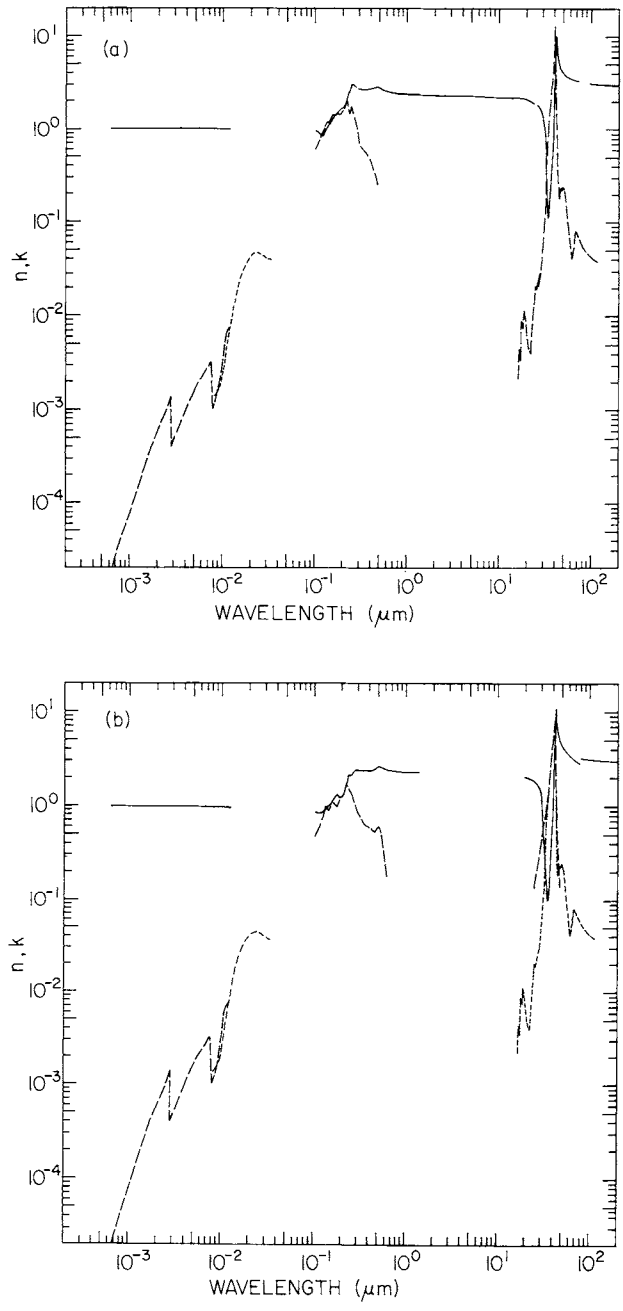


**Fig. 1.** (a) Log–log plot of $n_o$ (solid line) and $k_o$ (dashed line) versus wavelength in micrometers for cadmium sulphide. (b) Log–log plot of $n_e$ (solid line) and $k_e$ (dashed line) versus wavelength in micrometers.

TABLE I

Values of $n$ and $k$ for Hexagonal CdS from Various References[a]

| eV | $cm^{-1}$ | μm | n | k |
|---|---|---|---|---|
| 2000 | 16,131,000 | 0.000620 | 0.9999 [1] | $2.0*10^{-5}$ [1] |
| 1850 | 14,925,000 | 0.000670 | 0.9999 | 2.0 |
| 1688 | 13,614,000 | 0.000734 | 0.9999 | 3.0 |
| 1609 | 12,977,000 | 0.000771 | 0.9998 | 3.0 |
| 1358 | 10,953,000 | 0.000913 | 0.9998 | 6.0 |
| 1233 | 9,944,700 | 0.00100 | 0.9997 | $8.0*10^{-5}$ |
| 1147 | 9,251,000 | 0.00108 | 0.9997 | $1.0*10^{-4}$ |
| 946.5 | 7,634,000 | 0.00131 | 0.9996 | 1.8 |
| 855.1 | 6,896,800 | 0.00145 | 0.9995 | 2.5 |
| 826.6 | 6,666.700 | 0.00150 | 0.9995 | 2.8 |
| 815.7 | 6,579,000 | 0.00152 | 0.9995 | 2.9 |
| 760.6 | 6,134,600 | 0.00163 | 0.9994 | 3.6 |
| 725.1 | 5,848,300 | 0.00171 | 0.9994 | 4.0 |
| 620.0 | 5,000,000 | 0.00200 | 0.9993 | 6.0 |
| 529.9 | 4,273,900 | 0.00234 | 0.9992 | $8.3*10^{-4}$ |
| 496.0 | 4,000,500 | 0.00250 | 0.9992 | $1.0*10^{-3}$ |
| 469.6 | 3,787,900 | 0.00264 | 0.9993 | 1.2 |
| 447.6 | 3,613,100 | 0.00277 | 0.9994 | $1.4*10^{-3}$ |
| 436.6 | 3,516,100 | 0.00284 | 1.0002 | $4.0*10^{-4}$ |
| 426.0 | 3,436,000 | 0.00291 | 0.9995 | 4.2 |
| 413.3 | 3,333,300 | 0.00300 | 0.9993 | 5.0 |
| 368.0 | 2,968,100 | 0.00337 | 0.9987 | $6.3*10^{-4}$ |
| 310.0 | 2,500,000 | 0.00400 | 0.9981 | $1.0*10^{-3}$ |
| 269.0 | 2,169,600 | 0.00461 | 0.9976 | 1.3 |
| 248.0 | 2,000,000 | 0.00500 | 0.9974 | 1.6 |
| 227.1 | 1,831,700 | 0.00546 | 0.9969 | 2.0 |
| 206.6 | 1,666,700 | 0.00600 | 0.9965 | 2.2 |
| 190.7 | 1,538,100 | 0.00650 | 0.9949 | 2.6 |
| 177.1 | 1,428,400 | 0.00700 | 0.9960 | 2.9 |
| 165.3 | 1,333,300 | 0.00750 | 0.9975 | 3.3 |
| 162.1 | 1,307,200 | 0.00765 | 0.9963 | 0.94 |
| 155.0 | 1,250,000 | 0.00800 | 0.9946 | 1.0 |
| 136.3 | 1,099,300 | 0.00910 | 0.9910 | 1.7 |
| 124.0 | 1,000,000 | 0.0100 | 0.9885 | 3.4 |
| 118.1 | 951,530 | 0.0105 | 0.9870 | 5.7 |
| 111.7 | 900,910 | 0.0111 | 0.9852 | 7.0 |
| 104.2 | 833,330 | 0.0120 | 0.9833 | 7.5 |
| 100.0 | 806,550 | 0.0124 | 0.9823 | 8.0 |
| 149 | 1,201,800 | 0.008321 | 1.0000 [3] | $1.4*10^{-3}$ [3] |
| 139 | 1,121,100 | 0.008920 | 1.0000 | 1.5 |
| 135 | 1,088,400 | 0.009184 | 1.0000 | 1.6 |
| 131 | 1,056,600 | 0.009469 | 1.0000 | 1.7 |
| 125 | 1,008,200 | 0.009919 | 1.0000 | 2.0 |
| 115 | 927,530 | 0.01078 | 1.0000 | 3.9 |
| 110 | 887,200 | 0.01127 | 1.0000 | 5.0 |
| 100 | 806,550 | 0.01240 | 1.0000 | $8.9*10^{-3}$ |
| 90.0 | 725,890 | 0.01378 | 1.0000 | $1.5*10^{-2}$ |
| 80.0 | 645,240 | 0.01550 | 1.0000 | 2.4 |
| 70.0 | 564,840 | 0.01771 | 1.0000 | 3.4 |

TABLE I (*Continued*)

**Hexagonal Cadmium Sulphide**

| eV | $cm^{-1}$ | μm | n | k |
|---|---|---|---|---|
| 65.0 | 524,260 | 0.01908 | 1.0000 [3] | $3.8*10^{-2}$ [3] |
| 60.0 | 483,930 | 0.02067 | 1.0000 | 4.1 |
| 55.0 | 443,600 | 0.02254 | 1.0000 | 4.5 |
| 50.0 | 403,270 | 0.02480 | 1.0000 | 4.3 |
| 40.0 | 322,620 | 0.03100 | 1.0000 | 3.8 |
| 37.5 | 302,460 | 0.03306 | 1.0000 | $3.8*10^{-2}$ |

| eV | $cm^{-1}$ | μm | $n_e$ ( ‖ ) | $k_e$ ( ‖ ) |
|---|---|---|---|---|
| 12.0 | 96,786 | 0.1033 | 0.88 [4] | 0.48 [4] |
| 11.0 | 88,720 | 0.1127 | 0.84 | 0.56 |
| 10.0 | 80,655 | 0.1240 | 0.76 | 0.75 |
| 9.3 | 75,010 | 0.1333 | 0.92 | 1.00 |
| 9.1 | 72,990 | 0.1362 | 0.95 | 0.96 |
| 8.7 | 69,940 | 0.1425 | 1.00 | 0.92 |
| 8.0 | 64,524 | 0.1550 | 1.10 | 1.12 |
| 7.6 | 60,610 | 0.1631 | 1.28 | 1.08 |
| 7.2 | 58,070 | 0.1722 | 1.29 | 1.04 |
| 7.0 | 56,460 | 0.1771 | 1.36 | 1.00 |
| 6.5 | 52,426 | 0.1907 | 1.22 | 1.18 |
| 6.0 | 48,390 | 0.2066 | 1.26 | 1.30 |
| 5.5 | 44,360 | 0.2254 | 1.72 | 1.76 |
| 5.4 | 43,551 | 0.2216 | 1.83 | 1.68 |
| 5.3 | 42,750 | 0.2339 | 1.96 | 1.66 |
| 5.2 | 41,940 | 0.2384 | 2.20 | 1.56 |
| 5.1 | 41,134 | 0.2431 | 2.20 | 1.52 |
| 5.0 | 40,330 | 0.2480 | 2.16 | 1.44 |
| 4.7 | 37,910 | 0.2638 | 2.34 | 1.24 |
| 4.4 | 35,490 | 0.2818 | 2.48 | 1.04 |
| 4.0 | 32,260 | 0.3100 | 2.40 | 0.81 |
| 3.75 | 30,245 | 0.3306 | 2.38 | 0.74 |
| 3.5 | 28,230 | 0.3542 | 2.38 | 0.65 |
| 3.25 | 26,213 | 0.3815 | 2.36 | 0.61 |
| 3.0 | 24,196 | 0.4133 | 2.37 | 0.56 |
| 2.7 | 21,780 | 0.4592 | 2.47 | 0.54 |
| 2.5 | 20,164 | 0.4959 | 2.62 | 0.60 |
| 2.25 | 18,147 | 0.5510 | 2.53 | 0.26 |
| 2.0 | 16,130 | 0.6199 | 2.44 | 0.18 |
| 1.5 | 12,098 | 0.8266 | 2.36 | |

| eV | $cm^{-1}$ | μm | $n_o$ ( ⊥ ) | $k_o$ ( ⊥ ) |
|---|---|---|---|---|
| 12.0 | 96,786 | 0.1033 | 0.95 [4] | 0.60 [4] |
| 11.0 | 88,720 | 0.1127 | 0.87 | 0.72 |
| 10.0 | 80,655 | 0.1240 | 0.82 | 0.92 |
| 9.0 | 72,589 | 0.1377 | 1.00 | 1.19 |
| 8.7 | 70,170 | 0.1425 | 1.08 | 1.15 |
| 8.0 | 64,524 | 0.1550 | 1.20 | 1.40 |
| 7.5 | 60,490 | 0.1653 | 1.40 | 1.36 |

TABLE I (*Continued*)

Hexagonal Cadmium Sulphide

| eV | cm$^{-1}$ | μm | $n_o$ (⊥) | $k_o$ (⊥) |
|---|---|---|---|---|
| 7.1 | 57,265 | 0.1746 | 1.44 [4] | 1.47 [4] |
| 7.0 | 56,460 | 0.1771 | 1.50 | 1.45 |
| 6.5 | 52,450 | 0.1907 | 1.60 | 1.40 |
| 6.0 | 48,390 | 0.2067 | 1.74 | 1.56 |
| 5.5 | 44,360 | 0.2254 | 1.84 | 1.96 |
| 5.4 | 43,550 | 0.2296 | 2.30 | 1.83 |
| 5.3 | 42,750 | 0.2339 | 2.49 | 1.68 |
| 5.2 | 41,940 | 0.2384 | 2.40 | 1.52 |
| 5.1 | 41,130 | 0.2431 | 2.48 | 1.48 |
| 5.0 | 40,330 | 0.2480 | 2.57 | 1.60 |
| 4.9 | 39,530 | 0.2530 | 2.92 | 1.73 |
| 4.8 | 38,760 | 0.2583 | 3.04 | 1.64 |
| 4.0 | 32,260 | 0.3100 | 2.64 | 0.64 |
| 3.75 | 30,245 | 0.3306 | 2.64 | 0.62 |
| 3.5 | 28,230 | 0.3542 | 2.62 | 0.56 |
| 3.25 | 26,213 | 0.3815 | 2.62 | 0.49 |
| 3.0 | 24,196 | 0.4133 | 2.63 | 0.44 |
| 2.75 | 22,180 | 0.4509 | 2.70 | 0.41 |
| 2.5 | 20,164 | 0.4959 | 2.81 | 0.36 |
| 2.25 | 18,147 | 0.5510 | 2.57 | 0.04 |
| 2.0 | 16,130 | 0.6199 | 2.48 | 0.02 |
| 1.5 | 12,098 | 0.8206 | 2.40 | |

| eV | cm$^{-1}$ | μm | $n_o$ (⊥) | $n_e$ (∥) |
|---|---|---|---|---|
| 2.408 | 19,420 | 0.515 | 2.726 [15] | 2.743 [15] |
| 2.255 | 18,190 | 0.550 | 2.593 | 2.580 |
| 2.067 | 16,670 | 0.600 | 2.511 | 2.493 |
| 1.908 | 15,390 | 0.650 | 2.463 | 2.446 |
| 1.771 | 14,280 | 0.700 | 2.432 | 2.414 |
| 1.653 | 13,330 | 0.750 | 2.409 | 2.390 |
| 1.550 | 12,500 | 0.800 | 2.392 | 2.374 |
| 1.459 | 11,770 | 0.850 | 2.378 | 2.361 |
| 1.378 | 11,110 | 0.900 | 2.368 | 2.350 |
| 1.305 | 10,530 | 0.950 | 2.359 | 2.341 |
| 1.240 | 10,000 | 1.00 | 2.352 | 2.334 |
| 1.181 | 9,525 | 1.05 | 2.346 | 2.328 |
| 1.127 | 9,091 | 1.10 | 2.340 | 2.324 |
| 1.078 | 8,696 | 1.15 | 2.336 | 2.320 |
| 1.033 | 8,333 | 1.20 | 2.332 | 2.316 |
| 0.9919 | 8,000 | 1.25 | 2.329 | 2.312 |
| 0.9538 | 7,694 | 1.30 | 2.326 | 2.309 |
| 0.9184 | 7,408 | 1.35 | 2.323 | 2.306 |
| 0.8856 | 7,143 | 1.40 | 2.321 | 2.304 |

| eV | cm$^{-1}$ | μm | n(polycryst) | k |
|---|---|---|---|---|
| 1.550 | 12,500 | 0.80 | 2.38 [21] | |
| 1.240 | 10,000 | 1.00 | 2.33 | |
| 0.8266 | 6,667 | 1.50 | 2.29 | |

TABLE I (*Continued*)

**Hexagonal Cadmium Sulphide**

| eV | cm$^{-1}$ | μm | n | k(both axes) |
|---|---|---|---|---|
| 0.6200 | 5,000 | 2.00 | 2.280 [21] | |
| 0.4959 | 4,000 | 2.50 | 2.275 | |
| 0.4133 | 3,333 | 3.00 | 2.270 | |
| 0.3100 | 2,500 | 4.00 | 2.265 | |
| 0.2480 | 2,000 | 5.00 | 2.260 | |
| 0.2067 | 1,667 | 6.00 | 2.255 | |
| 0.1771 | 1,429 | 7.00 | 2.250 | |
| 0.1550 | 1,250 | 8.00 | 2.245 | |
| 0.1378 | 1,111 | 9.00 | 2.235 | |
| 0.1240 | 1,000 | 10.00 | 2.230 | |
| 0.1127 | 909.1 | 11.00 | 2.215 | |
| 0.1033 | 823.3 | 12.00 | 2.205 | |
| 0.09537 | 769.3 | 13.00 | 2.190 | |
| 0.08856 | 714.3 | 14.00 | 2.175 | |
| 0.08266 | 666.7 | 15.00 | 2.175 | |
| 0.07438 | 600 | 16.67 | | 0.0022[39] |
| 0.07290 | 588 | 17.01 | | 0.0044 |
| 0.07191 | 580 | 17.24 | | 0.0034 |
| 0.06993 | 564 | 17.73 | | 0.0067 |
| 0.06894 | 556 | 17.86 | | 0.0087 |
| 0.06670 | 538 | 18.59 | | 0.0074 |
| 0.06532 | 526 | 19.00 | | 0.011 |
| 0.06199 | 500 | 20.00 | | 0.0080 |
| 0.05889 | 475 | 21.05 | | 0.0047 |
| 0.05579 | 450 | 22.22 | | 0.0039 |
| 0.05269 | 425 | 23.53 | | 0.0075 |
| 0.04959 | 400 | 25.00 | | 0.020 |
| 0.04811 | 388 | 25.77 | | 0.019 |
| 0.04339 | 350 | 28.57 | | 0.029 |

| eV | cm$^{-1}$ | μm | $n_e$ ( ∥ ) | $k_e$ ( ∥ ) | $n_o$ ( ⊥ ) | $k_o$ ( ⊥ ) |
|---|---|---|---|---|---|---|
| 0.06200 | 500.1 | 20.0 | 2.10[44] | | 2.10[44] | |
| 0.04959 | 400.0 | 25.0 | 1.90 | 0.14[44] | 1.85 | 0.10[44] |
| 0.04133 | 333.3 | 30.0 | 1.33 | 0.43 | 1.33 | 0.43 |
| 0.03542 | 285.7 | 35.0 | 0.10 | 1.28 | 0.10 | 1.78 |
| 0.03100 | 250.0 | 40.0 | 0.58 | 4.35 | 2.03 | 6.03 |
| 0.03024 | 243.9 | 41.0 | 1.55 | 5.95 | 3.10 | 8.99 |
| 0.02988 | 241.0 | 41.5 | 2.00 | 6.70 | 4.28 | 8.35 |
| 0.02931 | 236.6 | 42.3 | 5.50 | 8.12 | 9.71 | 5.90 |
| 0.02870 | 231.5 | 43.2 | 11.16 | 3.20 | 7.20 | 3.10 |
| 0.02818 | 227.3 | 44.0 | 7.85 | 1.22 | 5.65 | 1.05 |
| 0.02755 | 222.2 | 45.0 | 6.67 | 0.64 | 5.07 | 0.23 |
| 0.02638 | 212.8 | 47.0 | 5.23 | 0.14 | 4.30 | |
| 0.02480 | 200.0 | 50.0 | 4.29 | | 3.77 | |
| 0.02067 | 166.7 | 60.0 | 3.48 | | 3.19 | |
| 0.01771 | 142.8 | 70.0 | 3.04 | | 3.04 | |
| 0.01653 | 133.3 | 75.0 | 2.90 | | 2.90 | |
| 0.01550 | 125.0 | 80.0 | 2.90 | | 2.90 | |

TABLE I (*Continued*)

Hexagonal Cadmium Sulphide

| eV | $cm^{-1}$ | μm | $n_e$ ( ∥ ) | $n_o$ ( ⊥ ) |
|---|---|---|---|---|
| 0.01550 | 125 | 80.00 | 3.27 [45] | 3.14 [45] |
| 0.01240 | 100 | 100.0 | 3.18 | 3.06 |
| 0.009300 | 75.0 | 133.3 | 3.11 | 3.00 |
| 0.006199 | 50.0 | 200.0 | 3.07 | 2.97 |
| 0.01240 | 100.0 | 100 | 3.27 [46] | 3.11 [46] |
| 0.001240 | 10.00 | 1000 | 3.27 | 3.11 |
| | | >1000 | 3.00 [47] | 3.09 [47] |
| | | >1000 | 2.90 [48] | 2.90 [48] |

| eV | $cm^{-1}$ | μm | $n_o$ ( ⊥ ) | k(both) |
|---|---|---|---|---|
| 0.04563 | 368 | 27.17 | 1.78 [43] | 0.02 [42] |
| 0.04377 | 353 | 28.35 | 1.68 | 0.03 |
| 0.04104 | 331 | 30.21 | 1.37 | 0.05 |
| 0.03968 | 320 | 31.25 | 1.16 | 0.08 |
| 0.03831 | 309 | 32.36 | 0.96 | 0.13 |
| 0.03794 | 306 | 32.68 | 0.82 | 0.16 |
| 0.03769 | 304 | 32.89 | 0.77 | 0.26 |
| 0.03695 | 298 | 33.56 | 0.33 | 0.53 |
| 0.03596 | 290 | 34.48 | 0.14 | 0.82 |
| 0.03434 | 277 | 36.10 | 0.15 | 1.44 |
| 0.03174 | 256 | 39.01 | 0.55 | 3.11 |
| 0.03062 | 247 | 40.49 | 1.12 | 6.45 |
| 0.03025 | 244 | 40.98 | 2.03 | 9.77 |
| 0.03000 | 242 | 41.33 | 3.42 | 13.15 |
| 0.02963 | 239 | 41.84 | 4.45 | 10.01 |
| 0.02950 | 238 | 42.02 | 6.16 | 6.69 |
| 0.02926 | 236 | 42.37 | 10.0 | 3.38 |
| 0.02901 | 234 | 42.74 | 7.81 | 1.70 |
| 0.02889 | 233 | 42.92 | 7.29 | 1.02 |
| 0.02876 | 232 | 43.10 | 6.84 | 0.69 |
| 0.02814 | 227 | 44.05 | 5.82 | 0.35 |
| 0.02690 | 217 | 46.08 | 4.62 | 0.18 |
| 0.02591 | 209 | 47.85 | 4.10 | 0.23 |
| 0.02542 | 205 | 48.78 | 4.04 | 0.22 |
| 0.02505 | 202 | 49.51 | 4.10 | 0.23 |
| 0.02443 | 197 | 50.76 | 3.73 | 0.24 |
| 0.02368 | 191 | 52.36 | 3.70 | 0.21 |
| 0.02219 | 179 | 55.87 | 3.63 | 0.13 |
| 0.02182 | 176 | 56.82 | 3.49 | 0.09 |
| 0.01947 | 157 | 63.69 | 3.42 | 0.04 |
| 0.01798 | 145 | 68.97 | 3.34 | 0.08 |
| 0.01624 | 131 | 76.34 | 3.29 | 0.06 |
| 0.01277 | 103 | 97.09 | | 0.04 |
| 0.01030 | 83 | 120.3 | | 0.04 |

TABLE I (*Continued*)

**Cadmium Sulphide (Thin Films)**

| eV | $cm^{-1}$ | μm | n | k |
|---|---|---|---|---|
| 4.133 | 33,330 | 0.30 | 2.68[28] | >0.70 [28] |
| 3.543 | 28,580 | 0.35 | 2.58 | >0.70 |
| 3.100 | 25,000 | 0.40 | 2.55 | >0.70 |
| 2.480 | 20,000 | 0.50 | 2.72 | 0.70 |
| 2.067 | 16,670 | 0.60 | 2.40 | 0.54 |
| 1.771 | 14,280 | 0.70 | 2.35 | 0.47 |
| 1.550 | 12,500 | 0.80 | 2.32 | 0.43 |
| 1.378 | 11,110 | 0.90 | 2.30 | 0.40 |
| 1.240 | 10,000 | 1.0 | 2.28 | 0.37 |
| 1.127 | 9,091 | 1.1 | 2.28 | 0.33 |
| 1.033 | 8,333 | 1.20 | 2.27 | 0.28 |
| 0.9538 | 7,693 | 1.30 | 2.27 | 0.15 |
| 0.8856 | 7,143 | 1.40 | 2.26 | 0.04 |
| 0.8266 | 6,667 | 1.50 | 2.25 | |
| 0.7749 | 6,250 | 1.60 | 2.25 | |
| 0.6888 | 5,556 | 1.80 | 2.24 | |
| 0.6200 | 5,000 | 2.00 | 2.23 | |
| 0.6200 | 5,000 | 2.00 | 2.300 [33] | |
| 0.4133 | 3,333 | 3.00 | 2.284 | |
| 0.3100 | 2,500 | 4.00 | 2.277 | |
| 0.2067 | 1,667 | 6.00 | 2.271 | |
| 0.1550 | 1,250 | 8.00 | 2.267 | |
| 0.1240 | 1,000 | 10.00 | 2.263 | |
| 0.1033 | 833.3 | 12.00 | 2.260 | |
| 0.08856 | 714.3 | 14.00 | 2.255 | |

[a] References are indicated in brackets.

# Gallium Antimonide (GaSb)

DAVID F. EDWARDS and RICHARD H. WHITE
University of California
Lawrence Livermore National Laboratory
Livermore, California

Few reports can be found in the literature of the fundamental optical properties of GaSb. Research-sized crystals are relatively easy to grow, but GaSb has developed little technical interest. Aspnes and Studna [1] report $n$ and $k$ values calculated from pseudo-dielectric functions measured by spectroscopic ellipsometry. They call this the pseudo-dielectric function because no corrections were made for possible surface overlayers or subsurface damage effects. For surfaces free of these defects or by making the appropriate corrections, the ellipsometric measurements would give the "true" dielectric function. In either case they calculate the $n$ and $k$ values from the ellipsometric measurements.

As pointed out by Aspnes and Studna [1], three recent technical advances have been made that allow for more accurate determination of the optical properties of semiconductors, GaSb included. The first and most important is the development of their new etching and cleanup procedures [2]. These procedures minimize the thickness of the undesirable surface layer that forms on semiconductors. As a result, their ellipsometric measurements and calculated pseudo-dielectric functions more accurately represent the intrinsic bulk values. The second advance is the development of the automatic spectroscopic ellipsometer. This instrument determines both components of the complex pseudo-dielectric function over a broad spectral range. No wavelength extrapolations are needed as in the Kramers–Kronig analysis of reflectance data. The third is the development of unambiguous criteria for optically determining the best surfaces. These "best" surfaces are the ones most free of roughness, unintentional overlayers, absorbed contaminants, and subsurface damage. Aspnes and Studna have been leaders in this field of the ellipsometric determination of the optical properties of solids.

Several reports have been made of the reflectance in the near-UV and visible regions. Seraphin and Bennett [3] list the reflectance data of Cardona [4] for the 4–0.5 eV spectral range. Tauc and Abraham [5] report reflectance for the same spectral region. The objective of both reports was


Copyright © 1991 by Academic Press.
All rights of reproduction in any form reserved.
ISBN 0-12-544422-2

an investigation of the band structure of GaSb, and no extraction of $n$ and $k$ values was made.

Johnson, Filinski, and Fan [6] measured the absorption coefficient in a $p$-type undoped GaSb sample at 1.7 K in the region of the intrinsic energy gap. ($E_g = 0.8100$ eV at 1.7 K). They observed three sharp bands. The highest energy band (0.8100 eV) they identify as due to an exciton absorption. The two bands of lower energy (0.8049 eV and 0.7958 eV) they attribute to exciton-impurity complexes. They report their data in a curve of absorption coefficient ($cm^{-1}$) as a function of photon energy. From their curve we have extracted the $k$ values. The three exciton peaks are designated $\alpha$, $\beta$, and $\gamma$ in Table I.

Edwards and Hayne [7], using the angle-of-minimum-deviation technique, measured the near-IR index of refraction from 1.8–2.5 μm (about 0.7–0.5 eV). Oswald and Schade [8] were among the first to report $n$ and $k$ values for the infrared region. They calculated $n$ and $k$ values from the measured reflectance and transmittance for a GaSb sample with a resistivity of only 0.08 Ω cm. This small resistivity and the monotonically increasing $k$ values with wavelength indicate free-carrier absorption. As a result, the Oswald and Schade data are not given in the table that follows. Wynne and Bloembergen [9] calculated the indices of refraction at 5.3 μm and 10.6 μm from the measured transmittance and coherence length for second-harmonic generation in GaSb with a $CO_2$ laser. These data are not included in our tabulation because of the inconsistencies with the data of other sources and the lack of precision of their method for extracting index values.

Hass and Henvis [10] measured the fundamental lattice reflection bands of several III-V compound semiconductors including GaSb. These measurements were made at liquid-helium temperature using a grating spectrometer for increased spectral resolution. By comparing the observed reflectance spectrum with that calculated using a single classical oscillator [11], they obtained the "best" values of the oscillator parameters. From these parameters we calculated the $n$ and $k$ values for the 29–100 μm spectral region.

Pikhtin and Yas'kov [12] report a semi-empirical method for calculating the dispersion of the refractive index using three adjustable parameters associated with the energy-band structure. For those materials where extensive data are available, their predictions accurately fit the indices. For GaSb they use the data of Refs. [7] and [8], which do not have the spectral breadth necessary for the accurate determination of their three parameters. Test calculations [13] for wavelengths longer than those of Ref. [7] indicate the values of the indices are sensitively dependent on the values of these adjustable parameters. It appears that indices over a broad spectral range are needed to improve the accuracy of the Pikhtin–Yas'kov calculated data for GaSb.

The indices of refraction and extinction coefficients for GaSb are given in Table I and plotted in Fig. 1. Most of the data are for room temperature except where noted. The $n$ and $k$ values from 6.0 eV to 2.1 eV are the measured data of Aspnes and Studna [1]. The $k$ values for the absorption-edge region are calculated from the measured absorption coefficients of Johnson *et al.* [6]. The $n$ values from 2.0 eV to 0.0443 eV (0.62–28 μm) were calculated from a Herzberger-type dispersion formula fit to the measured data of various references [1, 7, 10]. These same data were also fit to a modified Sellmeier-type dispersion formula. This was done for convenience to the reader, but the Sellmeier values are not given in Table I. A total of 28 data points were used for these fittings. As seen in Fig. 1, the indices between 6.0 eV and 2.1 eV (0.2067 μm and 0.5905 μm) do not lend themselves to Herzberger- or Sellmeier-type, curve-fitting routines.

The Herzberger-type dispersion formula [14] is

$$n = A + BL + CL^2 + D\lambda^2 + E\lambda^4,$$

where $L = 1/(\lambda^2 - 2.8 \times 10^6)$ with the wavelength $\lambda$ in Å, and $2.8 \times 10^6$ is the square of the mean asymptote for the short-wavelength abrupt rise in index for 14 materials (GaSb not included) [14]. For the 28 points from 0.62 μm to 28 μm, and room temperature, the coefficients are

$$A = 3.850787$$

$$B = 2.024481 \times 10^7$$

$$C = 1.079226 \times 10^{15}$$

$$D = -4.397689 \times 10^{-11}$$

$$E = 3.527494 \times 10^{-19}.$$

The RMS error between the reported indices and the values calculated from the dispersion formula is 0.192%.

For the reader's convenience, the modified Sellmeier-type dispersion formula [15] is

$$n^2 = 1 + A/(\lambda^2 - B) + C\lambda^2/(\lambda^2 - D),$$

where the wavelength $\lambda$ is in Å. For the 28 data points, the coefficients are

$$A = 3.779678 \times 10^{-8}$$

$$B = 1.558825 \times 10^{-9}$$

$$C = 1.266738 \times 10^{1}$$

$$D = -1.013537 \times 10^{-9}.$$

The RMS error is 0.226%.

In Table I the $n$ and $k$ values from 29 μm to 100 μm were calculated from the lattice band parameters of Ref. [10] and are for liquid-helium temperature. These calculations were extended beyond the range of measurement to 100 μm, in order to estimate $\varepsilon_0$, the low frequency dielectric constant. Hass and Henvis [10] report $\varepsilon_o = 15.69$ compared with $n^2 = 15.98$ at 100 μm.

Cardona [16] reports the measured temperature coefficient of the refractive index of GaSb to be

$$\frac{1}{n}\frac{\mathrm{d}n}{\mathrm{d}T} = 8.1 \pm 0.2 \times 10^{-5}\,\mathrm{K}^{-1}$$

for the 5–10 μm spectral region. This coefficient was determined from changes in the interference patterns produced by multiple internal reflections in single crystals with low impurity concentrations. He reports that the results are independent of free-carrier effects for the temperature range of about 85–415 K.

Ghosh *et al.* [17] have developed a simple model for predicting the temperature and pressure coefficients of the refractive index of some zinc-blende semiconductors, GaSb included. They predict the temperature coefficient at constant pressure to be

$$\left(\frac{\mathrm{d}n}{\mathrm{d}T}\right)_{\mathrm{P}} = 1.47 \times 10^{-4}\,\mathrm{K}^{-1}$$

at 3.7 μm for the range −173–127 °C. They compare this with experimental values of $3.11\text{–}3.05 \times 10^{-4}\,\mathrm{K}^{-1}$. Their predicted pressure coefficient is

$$-\left(\frac{\mathrm{d}n}{\mathrm{d}P}\right)_{\mathrm{T}} = 44.5 - 52.8 \times 10^{-3}\,\mathrm{GPa}^{-1}.$$

They have no experimental data for comparison nor do they give a wavelength or pressure range.

## REFERENCES


1. D. E. Aspnes and A. A. Studna, "Dielectric Functions and Optical Parameters of Si, Ge, GaP, GaAs, GaSb, InP, InAs, and InSb from 1.5 to 6.0 eV," *Phys. Rev. B* **27**, 985 (1983).
2. D. E. Aspnes and A. A. Studna, *SPIE Proc.* **276**, 227 (1981); *Appl. Phys. Lett.* **39**, 316 (1981).
3. B. O. Seraphin and H. E. Bennett, in "Optical Properties of III-V Compounds," (R. K. Willardson and A. C. Beer, eds.), Academic Press, New York, 499 (1967).
4. M. Cardona, "Optical Investigation of the Band Structure of GaSb," *Z. Phys.* **161**, 99 (1961); "Fundamental Reflectivity Spectrum of Semiconductors with Zinc-Blende Structure," *J. Appl. Phys.* **32**, Suppl., 2151 (1961).
5. J. Tauc and A. Abraham, "Reflection Spectra of Semiconductors with Diamond and Sphalerite Structures," "Proc. Int. Conf. Semicond. Phys., Prague, 1960," (K. Zaveta, ed.), Czech. Acad. Sci., Prague, and Academic Press, New York, 375 (1961).
6. E. J. Johnson, I. Filinski, and H. Y. Fan, "Absorption and Emission of Excitons and Impurities in GaSb," "Proc. Intern. Conf. Phys. Semicond. 6th, Exeter, 1962," The Institute of Physics and the Physical Society, London, 375 (1962).
7. D. F. Edwards and G. S. Hayne, "Optical Properties of Gallium Antimonide," *J. Opt. Soc. Am.* **49**, 414 (1959).
8. F. Oswald and R. Schade, "Uber die Bestimmung der Optischen Konstanten von Halbleitern des Typus $A^{III}B^{V}$ in Infraroten," *Z. Naturforschg.* **9a**, 611 (1954).
9. J. J. Wynne and N. Bloembergen, Measurement of the Lowest Order Nonlinear Susceptibility in III-V Semiconductors by Second-Harmonic Generation with a $CO_2$ Laser," *Phys. Rev.* **188**, 1211 (1969); Erratum, *Phys. Rev.* **B2**, 4306 (1970).
10. M. Hass and B. W. Henvis, "Infrared Lattice Refraction Spectra of III-V Compound Semiconductors," *J. Phys. Chem. Solids* **23**, 1099 (1962).
11. M. Born and K. Huang, "Dynamical Theory of Crystal Lattices," University Press, Oxford, Chap. 2 (1954).
12. A. N. Pikhtin and A. D. Yas'kov, "Dispersion of the Refractive Index of Semiconductors with Diamond and Zinc-blende Structures," *Sov. Phys. Semicond.* **12**, 622 (1978).
13. D. F. Edwards, 1989 (unpublished).
14. M. Herzberger and C. D. Salzberg, "Refractive Indices of Infrared Optical Materials and Color Correction of Infrared Lens," *J. Opt. Soc. Am.* **52**, (4), 420 (1962); M. Herzberger, "Colour Corrections in Optical Systems and a New Dispersion Formula," *Opt. Acta* **6**, 197 (1959).
15. D. F. Edwards and R. H. White, see KDP in this volume.
16. M. Cardona, "Temperature Dependence of the Refractive Index and the Polarizability of Free Carriers in Some III-V Semiconductors, "Proc. Intern. Conf. Semicond. Phys., Prague, 1960," Czech. Acad. Sci., Prague, and Academic Press, New York, 388 (1961).
17. D. K. Ghosh, L. K. Samanta, and G. C. Bhar, "The Temperature and Pressure Dependence of Refractive Indices of Some III-V and II-VI Binary Semiconductors," *Infrared Physics* **26**, 111 (1986).

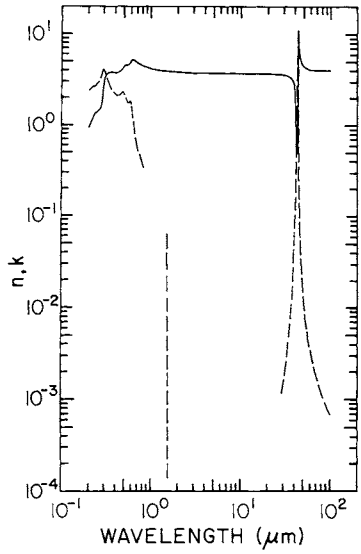


**Fig. 1.** Log–log plot of $n$ (solid line) and $k$ (dashed line) versus wavelength in micrometers for gallium antimonide.

TABLE I

Values of $n$ and $k$ for Gallium Antimonide Obtained from Various References[a]

| eV | $cm^{-1}$ | μm | $n$ | $n_c$ | $k$ |
|---|---|---|---|---|---|
| 6.00 | 48,387 | 0.2067 | 0.935 [1] | | 2.416 [1] |
| 5.90 | 47,581 | 0.2102 | 0.985 | | 2.444 |
| 5.80 | 46,774 | 0.2138 | 1.022 | | 2.479 |
| 5.70 | 45,968 | 0.2175 | 1.062 | | 2.535 |
| 5.60 | 45,161 | 0.2214 | 1.127 | | 2.602 |
| 5.50 | 44,355 | 0.2255 | 1.212 | | 2.645 |
| 5.40 | 43,548 | 0.2296 | 1.299 | | 2.653 |
| 5.30 | 42,742 | 0.2340 | 1.345 | | 2.638 |
| 5.20 | 41,935 | 0.2385 | 1.356 | | 2.645 |
| 5.10 | 41,129 | 0.2431 | 1.358 | | 2.685 |
| 5.00 | 40,323 | 0.2480 | 1.369 | | 2.751 |
| 4.90 | 39,516 | 0.2531 | 1.387 | | 2.829 |
| 4.80 | 38,710 | 0.2583 | 1.408 | | 2.928 |
| 4.70 | 37,903 | 0.2638 | 1.444 | | 3.055 |
| 4.60 | 37,097 | 0.2696 | 1.503 | | 3.208 |
| 4.50 | 36,290 | 0.2756 | 1.586 | | 3.392 |
| 4.40 | 35,484 | 0.2818 | 1.723 | | 3.628 |
| 4.30 | 34,677 | 0.2884 | 1.989 | | 3.923 |
| 4.20 | 33,871 | 0.2952 | 2.522 | | 4.130 |
| 4.10 | 33,065 | 0.3024 | 3.100 | | 3.976 |
| 4.00 | 32,258 | 0.3100 | 3.450 | | 3.643 |
| 3.90 | 31,452 | 0.3179 | 3.620 | | 3.323 |
| 3.80 | 30,645 | 0.3263 | 3.701 | | 3.069 |
| 3.70 | 29,839 | 0.3351 | 3.748 | | 2.862 |
| 3.60 | 29,032 | 0.3444 | 3.774 | | 2.690 |
| 3.50 | 28,226 | 0.3543 | 3.785 | | 2.545 |
| 3.40 | 27,419 | 0.3647 | 3.794 | | 2.430 |
| 3.30 | 26,613 | 0.3758 | 3.808 | | 2.319 |
| 3.20 | 25,806 | 0.3875 | 3.800 | | 2.210 |
| 3.10 | 25,000 | 0.4000 | 3.766 | | 2.134 |
| 3.00 | 24,194 | 0.4133 | 3.732 | | 2.109 |
| 2.90 | 23,387 | 0.4276 | 3.728 | | 2.121 |
| 2.80 | 22,581 | 0.4429 | 3.760 | | 2.157 |
| 2.70 | 21,774 | 0.4593 | 3.836 | | 2.211 |
| 2.60 | 20,968 | 0.4769 | 3.984 | | 2.280 |
| 2.50 | 20,161 | 0.4960 | 4.312 | | 2.285 |
| 2.40 | 19,355 | 0.5167 | 4.513 | | 1.962 |
| 2.30 | 18,548 | 0.5391 | 4.492 | | 1.789 |
| 2.20 | 17,742 | 0.5636 | 4.521 | | 1.747 |
| 2.10 | 16,935 | 0.5905 | 4.705 | | 1.803 |
| 2.000 | 16,129 | 0.620 | | 5.2496 | 1.378 |
| 1.938 | 15,625 | 0.640 | | 5.1058 | |
| 1.900 | 15,323 | 0.6526 | | | 0.829 |
| 1.879 | 15,152 | 0.660 | | 4.9812 | |
| 1.824 | 14,706 | 0.680 | | 4.8724 | |
| 1.800 | 14,516 | 0.6889 | | | 0.611 |
| 1.771 | 14,286 | 0.700 | | 4.7771 | |

**TABLE I (*Continued*)**

**Gallium Antimonide**

| eV | $cm^{-1}$ | μm | $n$ | $n_c$ | $k$ |
|---|---|---|---|---|---|
| 1.722 | 13,889 | 0.720 | | 4.6929 | |
| 1.700 | 13,710 | 0.7294 | | | 0.485 |
| 1.676 | 13,514 | 0.740 | | 4.6184 | |
| 1.632 | 13,158 | 0.760 | | 4.5521 | |
| 1.600 | 12,903 | 0.7750 | | | 0.416 |
| 1.590 | 12,821 | 0.780 | | 4.4928 | |
| 1.550 | 12,500 | 0.800 | | 4.4396 | |
| 1.512 | 12,195 | 0.820 | | 4.3916 | |
| 1.500 | 12,096 | 0.8267 | | | 0.344 |
| 1.476 | 11,905 | 0.840 | | 4.3483 | |
| 1.442 | 11,628 | 0.860 | | 4.3090 | |
| 1.409 | 11,364 | 0.880 | | 4.2733 | |
| 1.378 | 11,111 | 0.900 | | 4.2406 | |
| 1.348 | 10,870 | 0.920 | | 4.2108 | |
| 1.319 | 10,638 | 0.940 | | 4.1834 | |
| 1.292 | 10,417 | 0.960 | | 4.1583 | |
| 1.265 | 10,204 | 0.980 | | 4.1351 | |
| 1.240 | 10,000 | 1.000 | | 4.1137 | |
| 0.6199 | 5,000 | 2.0 | | 3.7883 | |
| 0.4133 | 3,333 | 3.0 | | 3.7421 | |
| 0.3100 | 2,500 | 4.0 | | 3.7285 | |
| 0.2480 | 2,000 | 5.0 | | 3.7241 | |
| 0.2066 | 1,667 | 6.0 | | 3.7236 | |
| 0.1771 | 1,429 | 7.0 | | 3.7251 | |
| 0.1550 | 1,250 | 8.0 | | 3.7278 | |
| 0.1378 | 1,111 | 9.0 | | 3.7313 | |
| 0.1240 | 1,000 | 10.0 | | 3.7352 | |
| 0.1127 | 909.1 | 11.0 | | 3.7395 | |
| 0.1033 | 833.3 | 12.0 | | 3.7438 | |
| 0.09537 | 769.2 | 13.0 | | 3.7481 | |
| 0.08856 | 714.3 | 14.0 | | 3.7521 | |
| 0.08266 | 666.7 | 15.0 | | 3.7557 | |
| 0.07749 | 625.0 | 16.0 | | 3.7586 | |
| 0.07293 | 588.2 | 17.0 | | 3.7608 | |
| 0.06889 | 555.6 | 18.0 | | 3.7620 | |
| 0.06526 | 526.3 | 19.0 | | 3.7620 | |
| 0.06199 | 500.0 | 20.0 | | 3.7605 | |
| 0.05904 | 476.2 | 21.0 | | 3.7574 | |
| 0.05636 | 454.5 | 22.0 | | 3.7524 | |
| 0.05391 | 434.8 | 23.0 | | 3.7453 | |
| 0.05166 | 416.7 | 24.0 | | 3.7357 | |
| 0.04959 | 400.0 | 25.0 | | 3.7235 | |
| 0.04769 | 384.6 | 26.0 | | 3.7083 | |
| 0.04592 | 370.4 | 27.0 | | 3.6898 | |
| 0.04428 | 357.1 | 28.0 | | 3.6677 | |
| 0.04275 | 344.8 | 29.0 | | 3.66 [10] | $1.2 \times 10^{-3}$ [10] |
| 0.04133 | 333.3 | 30.0 | | 3.65 | $1.5 \times 10^{-3}$ |

TABLE I (*Continued*)

**Gallium Antimonide**

| eV | $cm^{-1}$ | μm | $n$ | $n_c$ | $k$ |
|---|---|---|---|---|---|
| 0.04000 | 322.6 | 31.0 | | 3.62 | $1.8 \times 10^{-3}$ |
| 0.03875 | 312.5 | 32.0 | | 3.60 | $2.3 \times 10^{-3}$ |
| 0.03757 | 303.0 | 33.0 | | 3.57 | $3.0 \times 10^{-3}$ |
| 0.03647 | 294.1 | 34.0 | | 3.53 | $4.0 \times 10^{-3}$ |
| 0.03542 | 285.7 | 35.0 | | 3.48 | $5.4 \times 10^{-3}$ |
| 0.03444 | 277.8 | 36.0 | | 3.42 | $7.5 \times 10^{-3}$ |
| 0.03351 | 270.3 | 37.0 | | 3.33 | $1.09 \times 10^{-2}$ |
| 0.03263 | 263.2 | 38.0 | | 3.21 | $1.69 \times 10^{-2}$ |
| 0.03179 | 256.4 | 39.0 | | 3.03 | $2.85 \times 10^{-2}$ |
| 0.03100 | 250.0 | 40.0 | | 2.71 | $5.61 \times 10^{-2}$ |
| 0.03024 | 243.9 | 41.0 | | 2.02 | 0.160 |
| 0.02952 | 238.1 | 42.0 | | 0.484 | 2.06 |
| 0.02945 | 237.5 | 42.1 | | 0.485 | 2.39 |
| 0.02938 | 237.0 | 42.2 | | 0.502 | 2.73 |
| 0.02931 | 236.4 | 42.3 | | 0.531 | 3.08 |
| 0.02924 | 235.8 | 42.4 | | 0.575 | 3.45 |
| 0.02917 | 235.3 | 42.5 | | 0.637 | 3.86 |
| 0.02910 | 234.7 | 42.6 | | 0.723 | 4.31 |
| 0.02904 | 234.2 | 42.7 | | 0.844 | 4.82 |
| 0.02897 | 233.6 | 42.8 | | 1.02 | 5.41 |
| 0.02890 | 233.1 | 42.9 | | 1.28 | 6.12 |
| 0.02883 | 232.6 | 43.0 | | 1.70 | 6.98 |
| 0.02877 | 232.0 | 43.1 | | 2.43 | 8.07 |
| 0.02870 | 231.5 | 43.2 | | 3.84 | 9.36 |
| 0.02863 | 230.9 | 43.3 | | 6.65 | 10.3 |
| 0.02857 | 230.4 | 43.4 | | 10.3 | 8.56 |
| 0.02850 | 229.9 | 43.5 | | 11.2 | 5.04 |
| 0.02844 | 229.4 | 43.6 | | 10.4 | 2.87 |
| 0.02837 | 228.8 | 43.7 | | 9.39 | 1.81 |
| 0.02831 | 228.3 | 43.8 | | 8.62 | 1.24 |
| 0.02824 | 227.8 | 43.9 | | 8.03 | 0.907 |
| 0.02818 | 227.3 | 44.0 | | 7.57 | 0.694 |
| 0.02755 | 222.2 | 45.0 | | 5.66 | 0.148 |
| 0.02695 | 217.4 | 46.0 | | 5.07 | $6.64 \times 10^{-2}$ |
| 0.02638 | 212.8 | 47.0 | | 4.78 | $3.85 \times 10^{-2}$ |
| 0.02583 | 208.3 | 48.0 | | 4.61 | $2.56 \times 10^{-2}$ |
| 0.02530 | 204.1 | 49.0 | | 4.50 | $1.84 \times 10^{-2}$ |
| 0.02480 | 200.00 | 50.0 | | 4.42 | $1.41 \times 10^{-2}$ |
| 0.02066 | 166.67 | 60.0 | | 4.13 | $3.4 \times 10^{-3}$ |
| 0.01771 | 142.86 | 70.0 | | 4.058 | $1.8 \times 10^{-3}$ |
| 0.01550 | 125.00 | 80.0 | | 4.026 | $1.2 \times 10^{-3}$ |
| 0.01378 | 111.11 | 90.0 | | 4.008 | $8.9 \times 10^{-4}$ |
| 0.01240 | 100.00 | 100.0 | | 3.997 | $7.2 \times 10^{-4}$ |
| 0.8166 | 6,585.5 | 1.5185 | | | $5.08 \times 10^{-2}$ [6] |
| 0.8145 | 6,568.5 | 1.5224 | | | 4.85 |
| 0.8128 | 6,554.8 | 1.5256 | | | 4.86 |
| 0.8120 | 6,548.4 | 1.5271 | | | 5.10 |
| 0.8112 | 6,541.9 | 1.5286 | | | 5.11 |

TABLE I (*Continued*)

**Gallium Antimonide**

| eV | $cm^{-1}$ | μm | $n$ | $n_c$ | $k$ |
|---|---|---|---|---|---|
| 0.8109 | 6,539.5 | 1.5292 | | | 5.35 |
| 0.8105 | 6,536.3 | 1.5299 | | | 5.84 |
| 0.8100 | 6,532.3 | 1.5309 | | | α 6.33 |
| 0.8095 | 6,528.2 | 1.5318 | | | 5.73 |
| 0.8094 | 6,527.4 | 1.5320 | | | 4.88 |
| 0.8087 | 6,521.8 | 1.5333 | | | 2.5 |
| 0.8085 | 6,520.2 | 1.5337 | | | 1.35 |
| 0.8080 | 6,516.1 | 1.5347 | | | $1.07\times10^{-2}$ |
| 0.8075 | 6,512.1 | 1.5356 | | | $9.65\times10^{-3}$ |
| 0.8068 | 6,506.5 | 1.5369 | | | 9.05 |
| 0.8061 | 6,500.8 | 1.5383 | | | 9.06 |
| 0.8055 | 6,496.0 | 1.5394 | | | $9.80\times10^{-3}$ |
| 0.8053 | 6,494.4 | 1.5398 | | | $1.10\times10^{-2}$ |
| 0.8049 | 6,491.1 | 1.5406 | | | β 1.23 |
| 0.8045 | 6,487.9 | 1.5413 | | | $1.03\times10^{-2}$ |
| 0.8040 | 6,483.9 | 1.5423 | | | $8.10\times10^{-3}$ |
| 0.8036 | 6,480.6 | 1.5431 | | | 5.16 |
| 0.8034 | 6,479.0 | 1.5434 | | | 3.93 |
| 0.8030 | 6,475.8 | 1.5442 | | | 2.70 |
| 0.8022 | 6,469.4 | 1.5457 | | | 1.66 |
| 0.8016 | 6,464.5 | 1.5469 | | | 1.23 |
| 0.8012 | 6,461.3 | 1.5477 | | | $1.05\times10^{-3}$ |
| 0.8005 | 6,455.6 | 1.5490 | | | $8.63\times10^{-4}$ |
| 0.7996 | 6,448.4 | 1.5508 | | | 6.54 |
| 0.7990 | 6,443.5 | 1.5519 | | | 5.31 |
| 0.7980 | 6,435.5 | 1.5339 | | | 3.59 |
| 0.7970 | 6,427.4 | 1.5558 | | | 3.10 |
| 0.7965 | 6,423.4 | 1.5568 | | | 3.34 |
| 0.7964 | 6,422.6 | 1.5570 | | | 4.09 |
| 0.7962 | 6,421.0 | 1.5574 | | | 4.71 |
| 0.7958 | 6,417.7 | 1.5582 | | | γ 4.96 |
| 0.7957 | 6,416.9 | 1.5584 | | | 4.34 |
| 0.7954 | 6,414.5 | 1.5590 | | | 2.73 |
| 0.7950 | 6,411.3 | 1.5597 | | | 2.23 |
| 0.7946 | 6,408.1 | 1.5605 | | | 1.74 |
| 0.7940 | 6,403.2 | 1.5617 | | | 1.49 |
| 0.7932 | 6,396.8 | 1.5633 | | | 1.49 |
| 0.7922 | 6,388.7 | 1.5653 | | | 1.5 |
| 0.7906 | 6,375.8 | 1.5684 | | | $1.4\times10^{-4}$ |

[a] The column headed $n_c$ contains refractive-index values calculated with the Herzberger-type formula. The bracketed numbers indicate the reference to the data. Near 1.54 μm excitonic peaks are designated α, β, γ.

# Silicon–Germanium Alloys ($Si_xGe_{1-x}$)

J. HUMLÍČEK, F. LUKEŠ, and E. SCHMIDT
Department of Solid State Physics
Masaryk University
Brno, Czechoslovakia

Silicon and germanium form a continuous series of crystalline alloys, $Si_xGe_{1-x}$, from $x=0$ to $x=1$. Optical constants of both constituents have been critiqued extensively by Potter [1] and Edwards [2] in *HOC I*. Optical response of the alloy varies continuously over the entire range of compositions $x$, providing a suitable degree of freedom in tailoring the material for possible optical applications. On the other hand, the alloy is a very good object for physical studies of disorder-induced effects in electron and phonon structure of crystalline solids. It has also been studied in order to understand better the electron band structure of the pure constituents. In spite of numerous studies devoted to this alloy system, the number of papers allowing reasonable extraction of the optical constants is somewhat limited.

In the present critique, we compile the optical data for three compositions, representative of Si-rich ($x\approx0.80$), Ge-rich ($x\approx0.25$), and nearly-equal-content ($x\approx0.50$) alloys. This particular choice was influenced by the requirement of nearly coinciding compositions for data available from various sources. With one exception, we did not interpolate the composition dependence at fixed wavelengths to match the chosen values of $x$; instead, we have tabulated the original data obtained for slightly different compositions. It should be pointed out that the three spectra are a rather limited data base with respect to possible accurate interpolation for other alloy compositions. Data are listed in Table I and plotted in Fig. 1.

Early measurements of the energy position of the intrinsic optical absorption edge were reported in 1954 by Johnson and Christian [3]. The near-infrared absorption spectra were subsequently studied in detail by Braunstein *et al.* [4] in wide ranges of composition and temperature. Bulk samples were single crystals in the range of 0–20% and 90–100% Si;


Copyright © 1991 by Academic Press.
All rights of reproduction in any form reserved.
ISBN 0-12-544422-2

intermediate compositions were polycrystals. The alloy composition was determined by spectrographic techniques to ±5% of the content of silicon (for 0–70% Si) or germanium (for 70–100% Si). Fluctuations in composition between slices from the same ingot are mentioned; consequently, the spectra of absorption coefficient $\alpha$ were taken on the same sample thinned progressively from 500 to 5 μm. Higher values of $\alpha$ might be influenced by the inferior quality reported for some of the thinnest alloy samples. Special care was taken to ensure that all the light transmitted through the sample was collected on the detector. This indicates problems with scattered light, which we also mention below in the discussion of phonon spectra. Room temperature was specified to be 296 K; this is fairly important, since the band edge shifts strongly with temperature. The refractive index needed for calculations of $\alpha$ from measured transmittances was obtained from the transmission at long wavelengths.

The extensive work of Braunstein *et al.* [4] provides no spectra for the representative compositions of 25%, 50%, and 80% Si; therefore, we used their results in the following interpolation scheme. The absorption coefficient was fitted in Ref. [4] to the Macfarlane–Roberts expression:

$$\alpha(E, T) = A\left[\frac{(E-E_g-k\theta)^2}{1-\exp(-\theta/T)} + \frac{(E-E_g+k\theta)^2}{\exp(\theta/T)-1}\right], \tag{1}$$

where $E$ is the photon energy, $k\theta$ the phonon energy ($k$ is the Boltzmann constant, not to be confused with the extinction coefficient), $E_g$ the energy gap, $T$ the temperature, and $A$ a temperature-independent factor. The first term in square brackets of Eq. 1 is to be included for $E > E_g + k\theta$, the second for $E > E_g - k\theta$; $\alpha = 0$ below $E_g - k\theta$. A detailed compositional dependence of the best-fit values of $E_g(x)$ and the phonon equivalent temperature $\theta(x)$ is given by Braunstein *et al.* [4]. We have read their room-temperature spectra from graphs and determined the remaining parameter $A$ that fits them best with appropriate values of $E_g$ and $\theta$. Interpolated values of all of the three parameters were inserted in Eq. 1 to generate the $\alpha(E)$ spectra for $T = 296$ K. We have limited the spectral range so as to obtain the $\alpha$ values from 1 to 1000 $cm^{-1}$. The corresponding extinction coefficient is shown in the tables. The results of the interpolation procedure agree to about ±20% with values obtained by interpolating the experimental spectra either in compositions for fixed photon energies or vice versa. Because of the smoothing action of Eq. 1, the precision of the tabular data is limited only by the three decimals shown. The accuracy, however, is probably much lower. A factor-of-two difference, which is rather typical of various sources for pure Si and Ge [1, 2], is probably hard to achieve in the case of an alloy.

Reflectance measurements in the spectral range of strong absorption above the band gap, aiming at the identification of several interband thresholds, were performed by Tauc and Abrahám [5]. Schmidt [6] measured the reflectance in the energy region from 1–13 eV on a number of alloy samples. Three of them had compositions suitable for our tabulation. The compositions were determined by X-ray diffraction; the mean error of $x$ was $\pm 0.004$. The polycrystalline samples were mechanically polished and chemically etched. The thickness of surface oxides was estimated ellipsometrically to be between 2 and 4 nm. No correction was performed for the overlayers. The optical constants were computed from Kramers–Kronig (K–K) relations, using a combination of exponential (13–18 eV) and constant (above 18 eV) extrapolation of the reflectance. The K–K analysis of these data was repeated with a modified extrapolation, and the accuracy of the dielectric functions was tested for pure Si and Ge by Humlíček *et al.* [7]. We tabulate the room-temperature (300 K) results of the latter K–K computations for selected photon energies. Since the low values of the extinction coefficient $k$ at the red side of the spectral region are very unreliable, only values where $k>0.4$ are given.

Very recently, ellipsometry has been used to measure the optical response from 1.66–5.7 eV by Humlíček *et al.* [8]. Two series of samples were studied. Bulk polycrystals were Syton-polished; no polishing was used for single-crystal epitaxial layers. The epilayers were strain-free; the lattice mismatch was relaxed by misfit dislocations extending less than about 100 nm into the layers of total thickness of several micrometers. All samples were measured under flowing dry nitrogen, after a wet chemical treatment was used to remove the surface overlayers. The alloy compositions were determined from the energy position of the strong $E_1$ interband threshold; the mean error of $x$ was about $\pm 0.003$. The accuracy of the dielectric functions was estimated by examining trends in the data at fixed wavelengths as a function of alloy composition for 20 different samples. In spite of the care taken to avoid both surface damage and overlayers, the surface quality was found to be the limiting factor in the accuracy. In the nine spectra selected for tabulation in Ref. [8], the errors of both real and imaginary parts of the dielectric function are estimated to be a few tenths throughout the whole composition and spectral range. We have not tabulated the uncertain values of $k$ less than 0.3 on the low-energy side of the ellipsometric spectra, because of the poor accuracy and precision of the method in this case [8].

There is a fairly good agreement of the reflectance and ellipsometric results in the energy position of all spectral structures. In particular, the $E_1$ absorption edge shifts from 2.1 eV in Ge to 3.4 eV in Si; this offers a convenient way to determine accurately the alloy composition, provided the bowing of the concentration dependence is taken into account [8]. A slight blue shift of the reflectance spectrum of Table I b with respect to the

ellipsometric one in the region around 2.7 eV is due to the difference of the compositions. The systematic trends in the differences of both sets of $n$ and $k$ are obviously due to the thicker surface films in the reflectance measurements. The refractive indices agree to two figures in the near infrared. The agreement of extinction coefficients above 5 eV is also satisfactory. The most pronounced failure of the reflectance data is the systematically lower values of $n$ on the high-energy side of the overlap with the ellipsometric spectra. The discrepancy becomes more pronounced for Ge-rich alloys, in accordance with increasing optical thickness of the overlayers with increasing Ge content.

For both Ge and Si, refractive indices in the transparent region below the intrinsic absorption gap were measured with high precision by angle of minimum-deviation and channel-spectra techniques [1, 2]. We have not found analogous data for the alloys, obviously because of the problems in obtaining sufficiently homogeneous crystals of high optical quality. We have chosen the values based on the reflectance measured by Schmidt [6]. The $R$ values were fitted with refractive coefficients given by the polynomial

$$n(E) = n_0 + n_1 E^2 \tag{2}$$

for the photon energy $E$ from 1–1.5 eV, neglecting extinction indices $k$. The two coefficients $n_0$ and $n_1$ were determined from the least-squares fit for each alloy composition. The extrapolation of Eq. 2 below 1 eV is tabulated here. The values are probably accurate to a few hundredths, as indicated by a reasonable agreement of the results for pure Si and Ge.

Infrared lattice absorption in the alloys has been measured by Braunstein [9] throughout the whole range of compositions. However, most of his spectra for a silicon content of 22–81% showed a strong background absorption due to free carriers. Cosand and Spitzer [10] studied the lattice modes for Ge-rich ($x \leqslant 0.12$) and Si-rich ($x \geqslant 0.88$) alloys in the wavenumber region from 100–700 $cm^{-1}$. They identified two-phonon bands analogous to those of pure Si and Ge. In addition, several temperature-independent bands are interpreted as being due to single-phonon processes. The latter are not seen in perfect homopolar lattices of Si and Ge, since the single-phonon excitations produce no dipole moment. Unpublished spectra of Humlíček [11] were measured in the 180–1500 $cm^{-1}$ range at 300 K. The samples were of $p$-type conductivity with about $10^{15}$ free holes per $cm^3$. No Drude-like background is observable for this low level of doping. The alloy compositions (determined from spectral positions of the $E_1$ interband thresholds [8]) are fairly close to the three target values of the present tabulation. The observed transmission in the transparent region above 1500 $cm^{-1}$ was found to be lower than the

value predicted by reflection losses of the thick slab of nonabsorbing material:

$$T|_{k=0} = \frac{1-R}{1+R}, \qquad R = \left(\frac{n-1}{n+1}\right)^2, \tag{3}$$

where $n$ is the refractive index. This is obviously due to the scattering of the probing beam by inhomogeneities in the composition, which prevents a part of the transmitted light from reaching the detector. The tabular $k$ values were obtained from the transmittances normalized to the maximum value of Eq. 3 in the region above 1500 $cm^{-1}$. For $x = 0.8$, two strong peaks near 400 and 480 $cm^{-1}$ emerge; they are related to the analogous bands observed for Si-rich alloys by Cosand and Spitzer [10]. For higher Ge content, the band near 400 $cm^{-1}$ dominates the absorption spectrum with peak values of the absorption coefficient, $\alpha = 4\pi k/\lambda$, above 10 $cm^{-1}$. The phonon absorption is related to inevitable spectral variations of the refractive index. However, the magnitude of the changes from any smooth dispersion curve of the Eq. 2 type is expected to be less than a few thousandths, as found for silicon by Humlíček and Vojtěchovský [12]. Because of the rich spectral structure changing strongly with the composition, this spectral region is most difficult for dealing with the wavenumber- and composition-dependent extinction coefficients.

## REFERENCES


1. R. F. Potter, in "Handbook of Optical Constants of Solids," (E. D. Palik, ed.), Academic Press, Orlando, 465 (1985).
2. D. F. Edwards, ibid., p. 547.
3. E. R. Johnson and S. M. Christian, *Phys. Rev.* **95**, 560 (1954).
4. R. Braunstein, A. R. Moore, and F. Herman, *Phys. Rev.* **109**, 695 (1958).
5. J. Tauc and A. Abrahám, *J. Phys. Chem. Solids* **20**, 190 (1961).
6. E. Schmidt, *Phys. Status Solidi* **27**, 57 (1968).
7. J. Humlíček, F. Lukeš, E. Schmidt, M. G. Kekoua, and E. Khoutsishvili, *Phys. Rev.* **B33**, 1092 (1986).
8. J. Humlíček, M. Garriga, M. I. Alonso, and M. Cardona, *J. Appl. Phys.* **65**, 2827 (1989).
9. R. Braunstein, *Phys. Rev.* **130**, 879 (1963).
10. A. E. Cosand and W. G. Spitzer, *J. Appl. Phys.* **42**, 5241 (1971).
11. J. Humlíček, unpublished data (1989).
12. J. Humlíček and K. Vojtěchovský, *Phys. Status Solidi (a)* **92**, 249 (1985).

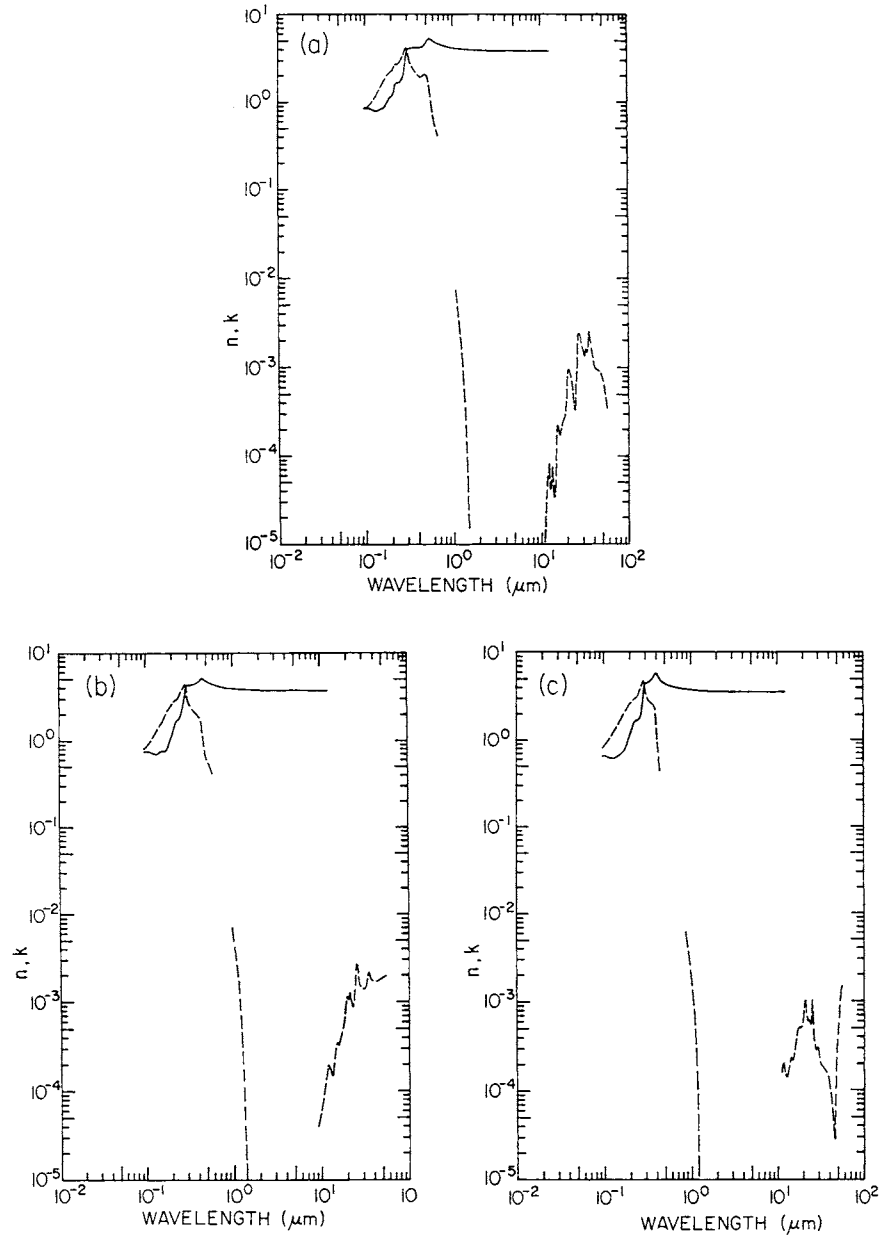


**Fig. 1.** Log–log plot of $n$ (solid line) and $k$ (dashed line) versus wavelength in micrometers. (a) For $Si_xGe_{1-x}$, $x = 0.25$. (b) For $Si_xGe_{1-x}$, $x = 0.50$. (c) For $Si_xGe_{1-x}$, $x = 0.80$.

**TABLE I(a)**

**Values of $n$ and $k$ for $Si_xGe_{1-x}$, $x=0.25$, from Various References[a]**

| eV | $cm^{-1}$ | $\mu m$ | $n$ | $n$ | $k$ | $k$ |
|---|---|---|---|---|---|---|
| 12.8 | | 0.09686 | 0.85 [6] | | 0.84 [6] | |
| 12.6 | | 0.09840 | 0.85 | | 0.85 | |
| 12.2 | | 0.1016 | 0.85 | | 0.88 | |
| 12.0 | | 0.1033 | 0.85 | | 0.90 | |
| 11.8 | | 0.1051 | 0.85 | | 0.92 | |
| 11.4 | | 0.1088 | 0.85 | | 0.95 | |
| 11.0 | | 0.1127 | 0.84 | | 0.99 | |
| 10.6 | | 0.1170 | 0.83 | | 1.02 | |
| 10.2 | | 0.1216 | 0.81 | | 1.09 | |
| 10.0 | | 0.1240 | 0.80 | | 1.13 | |
| 9.80 | | 0.1265 | 0.79 | | 1.17 | |
| 9.40 | | 0.1319 | 0.79 | | 1.26 | |
| 9.00 | | 0.1378 | 0.80 | | 1.36 | |
| 8.80 | | 0.1409 | 0.81 | | 1.40 | |
| 8.60 | | 0.1442 | 0.82 | | 1.45 | |
| 8.40 | | 0.1476 | 0.82 | | 1.50 | |
| 8.20 | | 0.1512 | 0.82 | | 1.57 | |
| 8.00 | | 0.1550 | 0.83 | | 1.64 | |
| 7.90 | | 0.1569 | 0.83 | | 1.68 | |
| 7.80 | | 0.1590 | 0.84 | | 1.72 | |
| 7.70 | | 0.1610 | 0.85 | | 1.77 | |
| 7.60 | | 0.1631 | 0.87 | | 1.81 | |
| 7.50 | | 0.1653 | 0.89 | | 1.85 | |
| 7.40 | | 0.1675 | 0.91 | | 1.90 | |
| 7.30 | | 0.1698 | 0.93 | | 1.95 | |
| 7.20 | | 0.1722 | 0.96 | | 1.99 | |
| 7.10 | | 0.1746 | 0.99 | | 2.03 | |
| 7.00 | | 0.1771 | 1.03 | | 2.08 | |
| 6.90 | | 0.1797 | 1.08 | | 2.10 | |
| 6.80 | | 0.1823 | 1.11 | | 2.11 | |
| 6.70 | | 0.1851 | 1.12 | | 2.12 | |
| 6.60 | | 0.1879 | 1.12 | | 2.15 | |
| 6.50 | | 0.1907 | 1.12 | | 2.20 | |
| 6.40 | | 0.1937 | 1.13 | | 2.26 | |
| 6.30 | | 0.1968 | 1.15 | | 2.32 | |
| 6.20 | | 0.2000 | 1.17 | | 2.39 | |
| 6.10 | **49,200** | 0.2033 | 1.20 | | 2.48 | |
| 6.00 | **48,390** | 0.2066 | 1.27 | | 2.58 | |
| 5.90 | 47,580 | 0.2101 | 1.36 | | 2.66 | |
| 5.80 | 46,780 | 0.2138 | 1.48 | | 2.70 | |
| 5.70 | 45,970 | 0.2175 | 1.58 | | 2.69 | |
| 5.60 | 45,160 | 0.2214 | 1.64 | 1.28 [8] | 2.66 | 2.89 [8] |
| 5.50 | 44,360 | 0.2254 | 1.65 | 1.33 | 2.66 | 2.87 |
| 5.40 | 43,550 | 0.2296 | 1.65 | 1.34 | 2.68 | 2.87 |
| 5.30 | 42,740 | 0.2339 | 1.64 | 1.33 | 2.74 | 2.90 |
| 5.20 | **41,940** | 0.2384 | 1.66 | 1.33 | 2.83 | 2.96 |
| 5.18 | **41,780** | 0.2394 | | 1.32 | | 2.98 |

TABLE I(a) (*Continued*)

$Si_xGe_{1-x}$, $x = 0.25$

| eV | $cm^{-1}$ | $\mu m$ | $n$ | $n$ | $k$ | $k$ |
|---|---|---|---|---|---|---|
| 5.16 | 41,610 | 0.2403 | | 1.33 | | 3.00 |
| 5.14 | 41,450 | 0.2412 | | 1.33 | | 3.01 |
| 5.12 | 41,290 | 0.2422 | | 1.33 | | 3.04 |
| 5.10 | 41,130 | 0.2431 | 1.69 | 1.33 | 2.93 | 3.06 |
| 5.08 | 40,970 | 0.2441 | | 1.33 | | 3.08 |
| 5.06 | 40,810 | 0.2450 | | 1.34 | | 3.10 |
| 5.04 | 40,650 | 0.2460 | | 1.34 | | 3.12 |
| 5.02 | 40,480 | 0.2470 | | 1.35 | | 3.15 |
| 5.00 | 40,320 | 0.2480 | | 1.35 | | 3.17 |
| 4.98 | 40,160 | 0.2490 | | 1.36 | | 3.20 |
| 4.96 | 40,000 | 0.2500 | | 1.37 | | 3.22 |
| 4.94 | 39,840 | 0.2510 | | 1.37 | | 3.25 |
| 4.92 | 39,680 | 0.2520 | | 1.38 | | 3.28 |
| 4.90 | 39,520 | 0.2530 | 1.80 | 1.40 | 3.19 | 3.31 |
| 4.88 | 39,360 | 0.2541 | | 1.40 | | 3.34 |
| 4.86 | 39,190 | 0.2551 | | 1.42 | | 3.37 |
| 4.84 | 39,030 | 0.2562 | | 1.43 | | 3.40 |
| 4.82 | 38,870 | 0.2572 | | 1.44 | | 3.44 |
| 4.80 | 38,710 | 0.2583 | 1.89 | 1.45 | 3.34 | 3.47 |
| 4.78 | 38,550 | 0.2594 | | 1.47 | | 3.50 |
| 4.76 | 38,390 | 0.2605 | | 1.48 | | 3.54 |
| 4.75 | 38,310 | 0.2610 | 1.95 | | 3.43 | |
| 4.74 | 38,230 | 0.2616 | | 1.50 | | 3.58 |
| 4.72 | 38,060 | 0.2627 | | 1.52 | | 3.62 |
| 4.70 | 37,900 | 0.2638 | 2.02 | 1.54 | 3.51 | 3.66 |
| 4.68 | 37,740 | 0.2649 | | 1.56 | | 3.70 |
| 4.66 | 37,580 | 0.2661 | | 1.58 | | 3.74 |
| 4.65 | 37,500 | 0.2666 | 2.09 | | 3.61 | |
| 4.64 | 37,420 | 0.2672 | | 1.61 | | 3.79 |
| 4.62 | 37,260 | 0.2684 | | 1.64 | | 3.84 |
| 4.60 | 37,100 | 0.2695 | 2.19 | 1.67 | 3.72 | 3.89 |
| 4.58 | 36,940 | 0.2707 | 2.23 | 1.71 | 3.77 | 3.94 |
| 4.56 | 36,770 | 0.2719 | 2.28 | 1.74 | 3.82 | 3.99 |
| 4.54 | 36,610 | 0.2731 | 2.33 | 1.79 | 3.87 | 4.05 |
| 4.52 | 36,450 | 0.2743 | 2.39 | 1.84 | 3.92 | 4.10 |
| 4.50 | 36,290 | 0.2755 | 2.47 | 1.89 | 3.97 | 4.16 |
| 4.48 | 36,130 | 0.2768 | 2.55 | 1.95 | 4.03 | 4.23 |
| 4.46 | 35,970 | 0.2780 | 2.64 | 2.02 | 4.07 | 4.29 |
| 4.44 | 35,810 | 0.2792 | 2.74 | 2.10 | 4.12 | 4.35 |
| 4.42 | 35,640 | 0.2805 | 2.85 | 2.19 | 4.15 | 4.41 |
| 4.40 | 35,480 | 0.2818 | 2.97 | 2.30 | 4.18 | 4.46 |
| 4.38 | 35,320 | 0.2831 | 3.11 | 2.42 | 4.18 | 4.51 |
| 4.36 | 35,160 | 0.2844 | 3.24 | 2.54 | 4.17 | 4.54 |
| 4.34 | 35,000 | 0.2857 | 3.38 | 2.68 | 4.14 | 4.55 |
| 4.32 | 34,840 | 0.2870 | 3.52 | 2.81 | 4.09 | 4.54 |
| 4.30 | 34,680 | 0.2883 | 3.64 | 2.95 | 4.02 | 4.51 |
| 4.28 | 34,520 | 0.2897 | 3.75 | 3.08 | 3.93 | 4.48 |

**TABLE I(a) (*Continued*)**

**$Si_xGe_{1-x}$, $x = 0.25$**

| eV | $cm^{-1}$ | $\mu$m | $n$ | $n$ | $k$ | $k$ |
|---|---|---|---|---|---|---|
| 4.26 | 34,350 | 0.2910 | | 3.19 | | 4.42 |
| 4.25 | 34,270 | 0.2917 | 3.87 | | 3.79 | |
| 4.24 | 34,190 | 0.2924 | | 3.29 | | 4.35 |
| 4.22 | 34,030 | 0.2938 | 3.96 | 3.38 | 3.65 | 4.29 |
| 4.20 | 33,870 | 0.2952 | | 3.46 | | 4.21 |
| 4.19 | 33,790 | 0.2959 | 4.02 | | 3.51 | |
| 4.18 | 33,710 | 0.2966 | | 3.52 | | 4.14 |
| 4.16 | 33,550 | 0.2980 | 4.05 | 3.58 | 3.38 | 4.06 |
| 4.14 | 33,390 | 0.2995 | | 3.62 | | 3.99 |
| 4.13 | 33,310 | 0.3002 | 4.07 | | 3.27 | |
| 4.12 | 33,230 | 0.3009 | | 3.67 | | 3.92 |
| 4.10 | 33,060 | 0.3024 | 4.09 | 3.70 | 3.17 | 3.85 |
| 4.08 | 32,900 | 0.3039 | | 3.72 | | 3.79 |
| 4.06 | 32,740 | 0.3054 | | 3.75 | | 3.73 |
| 4.05 | 32,660 | 0.3061 | 4.09 | | 3.02 | |
| 4.04 | 32,580 | 0.3069 | | 3.77 | | 3.68 |
| 4.02 | 32,420 | 0.3084 | | 3.79 | | 3.63 |
| 4.00 | 32,260 | 0.3100 | 4.09 | 3.80 | 2.91 | 3.58 |
| 3.98 | 32,100 | 0.3115 | | 3.82 | | 3.53 |
| 3.96 | 31,930 | 0.3131 | | 3.83 | | 3.49 |
| 3.95 | 31,850 | 0.3139 | 4.09 | | 2.81 | |
| 3.94 | 31,770 | 0.3147 | | 3.84 | | 3.45 |
| 3.92 | 31,610 | 0.3163 | | 3.86 | | 3.41 |
| 3.90 | 31,450 | 0.3179 | 4.09 | 3.87 | 2.72 | 3.37 |
| 3.88 | 31,290 | 0.3195 | | 3.88 | | 3.34 |
| 3.86 | 31,130 | 0.3212 | | 3.89 | | 3.30 |
| 3.85 | 31,050 | 0.3220 | 4.08 | | 2.64 | |
| 3.84 | 30,970 | 0.3229 | | 3.90 | | 3.27 |
| 3.82 | 30,810 | 0.3246 | | 3.92 | | 3.24 |
| 3.80 | 30,640 | 0.3263 | 4.08 | 3.92 | 2.58 | 3.22 |
| 3.78 | 30,480 | 0.3280 | | 3.93 | | 3.19 |
| 3.76 | 30,320 | 0.3297 | | 3.95 | | 3.16 |
| 3.75 | 30,240 | 0.3306 | 4.08 | | 2.53 | |
| 3.74 | 30,160 | 0.3315 | | 3.96 | | 3.13 |
| 3.72 | 30,000 | 0.3333 | | 3.96 | | 3.11 |
| 3.70 | 29,840 | 0.3351 | 4.08 | 3.98 | 2.48 | 3.09 |
| 3.68 | 29,680 | 0.3369 | | 3.99 | | 3.06 |
| 3.66 | 29,520 | 0.3388 | | 4.00 | | 3.04 |
| 3.65 | 29,430 | 0.3397 | 4.09 | | 2.43 | |
| 3.64 | 29,350 | 0.3406 | | 4.01 | | 3.02 |
| 3.62 | 29,190 | 0.3425 | | 4.02 | | 3.00 |
| 3.60 | 29,030 | 0.3444 | 4.10 | 4.03 | 2.39 | 2.98 |
| 3.58 | 28,870 | 0.3463 | | 4.04 | | 2.96 |
| 3.56 | 28,710 | 0.3483 | | 4.05 | | 2.94 |
| 3.55 | 28,630 | 0.3493 | 4.11 | | 2.35 | |
| 3.54 | 28,550 | 0.3502 | | 4.06 | | 2.93 |
| 3.52 | 28,390 | 0.3522 | | 4.08 | | 2.91 |

TABLE I(a) (*Continued*)

$Si_xGe_{1-x}$, $x=0.25$

| eV | $cm^{-1}$ | $\mu m$ | $n$ | $n$ | $k$ | $k$ |
|---|---|---|---|---|---|---|
| 3.50 | 28,220 | 0.3542 | 4.13 | 4.09 | 2.31 | 2.89 |
| 3.48 | 28,060 | 0.3563 | | 4.11 | | 2.87 |
| 3.46 | 27,900 | 0.3583 | | 4.13 | | 2.85 |
| 3.45 | 27,820 | 0.3594 | 4.14 | | 2.27 | |
| 3.44 | 27,740 | 0.3604 | | 4.14 | | 2.84 |
| 3.42 | 27,580 | 0.3625 | | 4.16 | | 2.82 |
| 3.40 | 27,420 | 0.3647 | 4.16 | 4.18 | 2.24 | 2.80 |
| 3.38 | 27,260 | 0.3668 | | 4.20 | | 2.78 |
| 3.36 | 27,100 | 0.3690 | | 4.21 | | 2.76 |
| 3.35 | 27,010 | 0.3701 | 4.19 | | 2.19 | |
| 3.34 | 26,930 | 0.3712 | | 4.23 | | 2.75 |
| 3.32 | 26,770 | 0.3734 | | 4.25 | | 2.72 |
| 3.30 | 26,610 | 0.3757 | 4.21 | 4.27 | 2.14 | 2.70 |
| 3.28 | 26,450 | 0.3780 | | 4.28 | | 2.68 |
| 3.26 | 26,290 | 0.3803 | | 4.30 | | 2.65 |
| 3.25 | 26,210 | 0.3815 | 4.23 | | 2.09 | |
| 3.24 | 26,130 | 0.3827 | | 4.31 | | 2.62 |
| 3.22 | 25,970 | 0.3850 | | 4.32 | | 2.60 |
| 3.20 | 25,810 | 0.3875 | 4.24 | 4.34 | 2.03 | 2.57 |
| 3.18 | 25,640 | 0.3899 | | 4.35 | | 2.55 |
| 3.16 | 25,480 | 0.3924 | | 4.35 | | 2.52 |
| 3.15 | 25,400 | 0.3936 | 4.23 | | 1.98 | |
| 3.14 | 25,320 | 0.3949 | | 4.36 | | 2.49 |
| 3.12 | 25,160 | 0.3974 | | 4.36 | | 2.47 |
| 3.10 | 25,000 | 0.4000 | 4.21 | 4.36 | 1.94 | 2.45 |
| 3.08 | 24,840 | 0.4025 | | 4.36 | | 2.43 |
| 3.06 | 24,680 | 0.4052 | | 4.36 | | 2.41 |
| 3.05 | 24,600 | 0.4065 | 4.19 | | 1.92 | |
| 3.04 | 24,510 | 0.4078 | | 4.36 | | 2.40 |
| 3.02 | 24,350 | 0.4105 | | 4.36 | | 2.39 |
| 3.00 | 24,190 | 0.4133 | 4.17 | 4.36 | 1.91 | 2.38 |
| 2.98 | 24,030 | 0.4161 | | 4.36 | | 2.38 |
| 2.96 | 23,870 | 0.4189 | | 4.37 | | 2.38 |
| 2.95 | 23,790 | 0.4203 | 4.16 | | 1.92 | |
| 2.94 | 23,710 | 0.4217 | | 4.38 | | 2.38 |
| 2.92 | 23,550 | 0.4246 | | 4.38 | | 2.38 |
| 2.90 | 23,390 | 0.4275 | 4.17 | 4.40 | 1.94 | 2.39 |
| 2.88 | 23,220 | 0.4305 | | 4.42 | | 2.39 |
| 2.86 | 23,060 | 0.4335 | | 4.43 | | 2.40 |
| 2.85 | 22,980 | 0.4350 | 4.19 | | 1.97 | |
| 2.84 | 22,900 | 0.4366 | | 4.45 | | 2.41 |
| 2.82 | 22,740 | 0.4397 | | 4.48 | | 2.41 |
| 2.80 | 22,580 | 0.4428 | 4.23 | 4.50 | 2.01 | 2.42 |
| 2.78 | 22,420 | 0.4460 | | 4.54 | | 2.42 |
| 2.76 | 22,260 | 0.4492 | | 4.57 | | 2.43 |
| 2.75 | 22,180 | 0.4509 | 4.30 | | 2.04 | |
| 2.74 | 22,090 | 0.4525 | | 4.62 | | 2.44 |

**TABLE I(a) (*Continued*)**

**$Si_xGe_{1-x}$, $x = 0.25$**

| eV | $cm^{-1}$ | $\mu m$ | $n$ | $n$ | $k$ | $k$ |
|---|---|---|---|---|---|---|
| 2.72 | 21,930 | 0.4558 | | 4.66 | | 2.45 |
| 2.70 | 21,770 | 0.4592 | 4.38 | 4.72 | 2.07 | 2.45 |
| 2.68 | 21,610 | 0.4626 | | 4.78 | | 2.45 |
| 2.66 | 21,450 | 0.4661 | | 4.85 | | 2.45 |
| 2.65 | 21,370 | 0.4679 | 4.50 | | 2.09 | |
| 2.64 | 21,290 | 0.4696 | | 4.92 | | 2.44 |
| 2.62 | 21,130 | 0.4732 | | 5.00 | | 2.42 |
| 2.60 | 20,970 | 0.4769 | 4.64 | 5.07 | 2.09 | 2.39 |
| 2.58 | 20,800 | 0.4806 | 4.72 | 5.15 | 2.08 | 2.35 |
| 2.56 | 20,640 | 0.4843 | 4.79 | 5.23 | 2.05 | 2.30 |
| 2.54 | 20,480 | 0.4881 | 4.86 | 5.30 | 2.02 | 2.24 |
| 2.52 | 20,320 | 0.4920 | 4.92 | 5.37 | 1.97 | 2.18 |
| 2.50 | 20,160 | 0.4959 | 4.97 | 5.45 | 1.92 | 2.11 |
| 2.48 | 20,000 | 0.4999 | 5.03 | 5.53 | 1.87 | 2.03 |
| 2.46 | 19,840 | 0.5040 | 5.08 | 5.59 | 1.83 | 1.93 |
| 2.44 | 19,680 | 0.5081 | 5.14 | 5.65 | 1.77 | 1.82 |
| 2.42 | 19,510 | 0.5123 | 5.20 | 5.70 | 1.71 | 1.70 |
| 2.40 | 19,350 | 0.5166 | 5.28 | 5.72 | 1.64 | 1.57 |
| 2.38 | 19,190 | 0.5209 | 5.33 | 5.74 | 1.53 | 1.43 |
| 2.36 | 19,030 | 0.5254 | 5.37 | 5.72 | 1.41 | 1.30 |
| 2.34 | 18,870 | 0.5299 | 5.37 | 5.69 | 1.30 | 1.17 |
| 2.32 | 18,710 | 0.5344 | 5.37 | 5.65 | 1.18 | 1.08 |
| 2.30 | 18,550 | 0.5391 | 5.34 | 5.60 | 1.07 | 0.98 |
| 2.28 | 18,380 | 0.5438 | 5.30 | 5.55 | 0.98 | 0.89 |
| 2.26 | 18,220 | 0.5486 | 5.25 | 5.49 | 0.91 | 0.81 |
| 2.24 | 18,060 | 0.5535 | 5.20 | 5.44 | 0.84 | 0.75 |
| 2.22 | 17,900 | 0.5585 | | 5.39 | | 0.67 |
| 2.20 | 17,740 | 0.5636 | 5.11 | 5.33 | 0.74 | 0.64 |
| 2.18 | 17,580 | 0.5687 | | 5.29 | | 0.58 |
| 2.16 | 17,420 | 0.5740 | | 5.23 | | 0.54 |
| 2.15 | 17,340 | 0.5767 | 5.00 | | 0.65 | |
| 2.14 | 17,260 | 0.5794 | | 5.19 | | 0.49 |
| 2.12 | 17,090 | 0.5848 | | 5.15 | | 0.46 |
| 2.10 | 16,930 | 0.5904 | 4.91 | 5.11 | 0.58 | 0.43 |
| 2.08 | 16,770 | 0.5961 | | 5.07 | | 0.38 |
| 2.06 | 16,610 | 0.6019 | | 5.03 | | 0.37 |
| 2.05 | 16,530 | 0.6048 | 4.82 | | 0.53 | |
| 2.04 | 16,450 | 0.6078 | | 5.00 | | 0.35 |
| 2.02 | 16,290 | 0.6138 | | 4.96 | | 0.33 |
| 2.00 | 16,130 | 0.6199 | 4.77 | 4.93 | 0.50 | |
| 1.98 | 15,970 | 0.6262 | | 4.90 | | 0.30 |
| 1.96 | 15,800 | 0.6326 | | 4.87 | | |
| 1.95 | 15,720 | 0.6358 | 4.72 | | 0.46 | |
| 1.94 | 15,640 | 0.6391 | | 4.83 | | |
| 1.92 | 15,480 | 0.6458 | | 4.81 | | |
| 1.90 | 15,320 | 0.6526 | 4.67 | 4.78 | 0.41 | |
| 1.88 | 15,160 | 0.6595 | | 4.75 | | |

TABLE I(a) (*Continued*)

$Si_xGe_{1-x}$, $x = 0.25$

| eV | $cm^{-1}$ | $\mu$m | $n$ | $n$ | $k$ | $k$ |
|---|---|---|---|---|---|---|
| 1.86 | 15,000 | 0.6666 | | 4.72 | | |
| 1.85 | 14,920 | 0.6702 | 4.62 | | | |
| 1.84 | 14,840 | 0.6738 | | 4.69 | | |
| 1.82 | 14,670 | 0.6812 | | 4.67 | | |
| 1.80 | 14,510 | 0.6888 | 4.58 | 4.65 | | |
| 1.78 | 14,350 | 0.6965 | | 4.63 | | |
| 1.76 | 14,190 | 0.7045 | | 4.60 | | |
| 1.74 | 14,030 | 0.7126 | | 4.58 | | |
| 1.72 | 13,870 | 0.7208 | | 4.56 | | |
| 1.70 | 13,710 | 0.7293 | 4.49 | 4.54 | | |
| 1.68 | 13,550 | 0.7380 | | 4.51 | | |
| 1.66 | 13,380 | 0.7469 | | 4.49 | | |
| 1.60 | 12,900 | 0.7749 | 4.42 | | | |
| 1.50 | 12,090 | 0.8266 | 4.36 | | | |
| 1.40 | 11,290 | 0.8856 | 4.30 | | | |
| 1.30 | 10,480 | 0.9537 | 4.23 | | | |
| 1.22 | 9,840 | 1.016 | | | | 7.69E-03 [4] |
| 1.21 | 9,759 | 1.024 | | | | 7.29E-03 |
| 1.20 | 9,679 | 1.033 | 4.17 | | | 6.91E-03 |
| 1.19 | 9,598 | 1.041 | | | | 6.53E-03 |
| 1.18 | 9,517 | 1.050 | | | | 6.16E-03 |
| 1.17 | 9,437 | 1.059 | | | | 5.80E-03 |
| 1.16 | 9,356 | 1.068 | | | | 5.45E-03 |
| 1.15 | 9,275 | 1.078 | | | | 5.11E-03 |
| 1.14 | 9,195 | 1.087 | | | | 4.77E-03 |
| 1.13 | 9,114 | 1.097 | | | | 4.44E-03 |
| 1.12 | 9,033 | 1.107 | | | | 4.13E-03 |
| 1.11 | 8,953 | 1.116 | | | | 3.82E-03 |
| 1.10 | 8,872 | 1.127 | 4.12 | | | 3.52E-03 |
| 1.09 | 8,791 | 1.137 | | | | 3.23E-03 |
| 1.08 | 8,711 | 1.148 | | | | 2.95E-03 |
| 1.07 | 8,630 | 1.158 | | | | 2.68E-03 |
| 1.06 | 8,549 | 1.169 | | | | 2.43E-03 |
| 1.05 | 8,469 | 1.180 | | | | 2.18E-03 |
| 1.04 | 8,388 | 1.192 | | | | 1.95E-03 |
| 1.03 | 8,307 | 1.203 | | | | 1.72E-03 |
| 1.02 | 8,227 | 1.215 | | | | 1.51E-03 |
| 1.01 | 8,146 | 1.227 | | | | 1.31E-03 |
| 1.00 | 8,065 | 1.239 | 4.06 | | | 1.13E-03 |
| 0.99 | 7,985 | 1.252 | | | | 9.55E-04 |
| 0.98 | 7,904 | 1.265 | | | | 7.96E-04 |
| 0.97 | 7,824 | 1.278 | | | | 6.51E-04 |
| 0.96 | 7,743 | 1.291 | | | | 5.21E-04 |
| 0.95 | 7,662 | 1.305 | | | | 4.06E-04 |
| 0.94 | 7,582 | 1.318 | | | | 3.06E-04 |
| 0.93 | 7,501 | 1.333 | | | | 2.22E-04 |
| 0.92 | 7,420 | 1.347 | | | | 1.54E-04 |

TABLE I(a) (*Continued*)

$Si_xGe_{1-x}$, $x = 0.25$

| eV | $cm^{-1}$ | $\mu m$ | $n$ | $n$ | $k$ | $k$ |
|---|---|---|---|---|---|---|
| 0.91 | 7,340 | 1.362 | | | | 1.04E-04 |
| 0.90 | 7,259 | 1.377 | 4.02 | | | 7.04E-05 |
| 0.89 | 7,178 | 1.393 | | | | 4.75E-05 |
| 0.88 | 7,098 | 1.408 | | | | 2.89E-05 |
| 0.87 | 7,017 | 1.425 | | | | 1.48E-05 |
| 0.80 | 6,452 | 1.549 | 3.97 | | | |
| 0.70 | 5,646 | 1.771 | 3.94 | | | |
| 0.60 | 4,839 | 2.066 | 3.90 | | | |
| 0.50 | 4,033 | 2.479 | 3.88 | | | |
| 0.40 | 3,226 | 3.099 | 3.86 | | | |
| 0.30 | 2,420 | 4.132 | 3.84 | | | |
| 0.20 | 1,613 | 6.199 | 3.83 | | | |
| 0.1239 | 1,000 | 10.00 | | | | 8.35E-06 [11] |
| 0.1178 | 950 | 10.52 | | | | 1.10E-05 |
| 0.1147 | 925 | 10.81 | | | | 1.83E-05 |
| 0.1116 | 900 | 11.11 | | | | 3.34E-05 |
| 0.1091 | 880 | 11.36 | | | | 4.96E-05 |
| 0.1066 | 860 | 11.62 | | | | 7.28E-05 |
| 0.1041 | 840 | 11.90 | | | | 7.74E-05 |
| 0.1017 | 820 | 12.19 | | | | 4.21E-05 |
| 0.1000 | 807 | 12.39 | 3.82 | | | |
| 0.09919 | 800 | 12.49 | | | | 4.88E-05 |
| 0.09671 | 780 | 12.82 | | | | 7.41E-05 |
| 0.09423 | 760 | 13.15 | | | | 5.75E-05 |
| 0.09175 | 740 | 13.51 | | | | 3.46E-05 |
| 0.08927 | 720 | 13.88 | | | | 3.56E-05 |
| 0.08679 | 700 | 14.28 | | | | 8.94E-05 |
| 0.08431 | 680 | 14.70 | | | | 2.09E-04 |
| 0.08307 | 670 | 14.92 | | | | 2.21E-04 |
| 0.08183 | 660 | 15.15 | | | | 2.07E-04 |
| 0.07935 | 640 | 15.62 | | | | 1.78E-04 |
| 0.07687 | 620 | 16.12 | | | | 1.75E-04 |
| 0.07439 | 600 | 16.66 | | | | 2.27E-04 |
| 0.07191 | 580 | 17.24 | | | | 2.55E-04 |
| 0.06943 | 560 | 17.85 | | | | 2.64E-04 |
| 0.06695 | 540 | 18.51 | | | | 3.66E-04 |
| 0.06447 | 520 | 19.23 | | | | 6.90E-04 |
| 0.06323 | 510 | 19.60 | | | | 8.96E-04 |
| 0.06199 | 500 | 20.00 | | | | 9.58E-04 |
| 0.06075 | 490 | 20.40 | | | | 8.90E-04 |
| 0.05951 | 480 | 20.83 | | | | 8.05E-04 |
| 0.05703 | 460 | 21.74 | | | | 7.04E-04 |
| 0.05455 | 440 | 22.72 | | | | 4.34E-04 |
| 0.05331 | 430 | 23.25 | | | | 3.37E-04 |
| 0.05207 | 420 | 23.81 | | | | 3.81E-04 |
| 0.05083 | 410 | 24.39 | | | | 5.14E-04 |
| 0.04959 | 400 | 25.00 | | | | 1.62E-03 |

**TABLE I(a) (*Continued*)**

**$Si_xGe_{1-x}$, $x=0.25$**

| eV | $cm^{-1}$ | $\mu$m | $n$ | $n$ | $k$ | $k$ |
|---|---|---|---|---|---|---|
| 0.04835 | 390 | 25.64 | | | | 2.25E-03 |
| 0.04711 | 380 | 26.31 | | | | 2.34E-03 |
| 0.04587 | 370 | 27.02 | | | | 2.35E-03 |
| 0.04463 | 360 | 27.78 | | | | 2.11E-03 |
| 0.04339 | 350 | 28.57 | | | | 1.72E-03 |
| 0.04215 | 340 | 29.41 | | | | 1.55E-03 |
| 0.04092 | 330 | 30.29 | | | | 1.35E-03 |
| 0.03968 | 320 | 31.24 | | | | 1.46E-03 |
| 0.03906 | 315 | 31.74 | | | | 1.63E-03 |
| 0.03844 | 310 | 32.25 | | | | 1.62E-03 |
| 0.03782 | 305 | 32.78 | | | | 1.46E-03 |
| 0.03720 | 300 | 33.33 | | | | 1.92E-03 |
| 0.03596 | 290 | 34.47 | | | | 2.50E-03 |
| 0.03472 | 280 | 35.70 | | | | 2.11E-03 |
| 0.03348 | 270 | 37.03 | | | | 1.54E-03 |
| 0.03224 | 260 | 38.45 | | | | 1.18E-03 |
| 0.02976 | 240 | 41.66 | | | | 9.36E-04 |
| 0.02728 | 220 | 45.44 | | | | 9.28E-04 |
| 0.02480 | 200 | 50.00 | | | | 7.10E-04 |
| 0.02232 | 180 | 55.54 | | | | 3.48E-04 |

[a]The reference from which the values were extracted is given in brackets next to the first value. The nominal alloy compositions are: x=0.246 [6], x=0.250 [8], x=0.250 obtained by interpolating the data of Braunstein et al. [4], x=0.260 [11].

**TABLE I(b)**

**Values of $n$ and $k$ for $Si_xGe_{1-x}$, $x = 0.50$, from Various References[a]**

| eV | $cm^{-1}$ | $\mu m$ | $n$ | $n$ | $k$ | $k$ |
|---|---|---|---|---|---|---|
| 12.8 | | 0.09686 | 0.75 [6] | | 0.81 [6] | |
| 12.4 | | 0.09999 | 0.75 | | 0.85 | |
| 12.0 | | 0.1033 | 0.75 | | 0.88 | |
| 11.6 | | 0.1069 | 0.75 | | 0.92 | |
| 11.2 | | 0.1107 | 0.74 | | 0.96 | |
| 10.8 | | 0.1148 | 0.73 | | 1.01 | |
| 10.4 | | 0.1192 | 0.72 | | 1.07 | |
| 10.0 | | 0.1240 | 0.70 | | 1.15 | |
| 9.80 | | 0.1265 | 0.70 | | 1.19 | |
| 9.60 | | 0.1292 | 0.70 | | 1.23 | |
| 9.20 | | 0.1348 | 0.71 | | 1.32 | |
| 8.80 | | 0.1409 | 0.72 | | 1.42 | |
| 8.40 | | 0.1476 | 0.74 | | 1.53 | |
| 8.00 | | 0.1550 | 0.76 | | 1.63 | |
| 7.80 | | 0.1590 | 0.75 | | 1.70 | |
| 7.60 | | 0.1631 | 0.75 | | 1.78 | |
| 7.40 | | 0.1675 | 0.76 | | 1.88 | |
| 7.20 | | 0.1722 | 0.77 | | 2.00 | |
| 7.00 | | 0.1771 | 0.82 | | 2.13 | |
| 6.90 | | 0.1797 | 0.86 | | 2.19 | |
| 6.80 | | 0.1823 | 0.90 | | 2.24 | |
| 6.70 | | 0.1851 | 0.95 | | 2.29 | |
| 6.60 | | 0.1879 | 0.99 | | 2.33 | |
| 6.50 | | 0.1907 | 1.02 | | 2.38 | |
| 6.40 | | 0.1937 | 1.05 | | 2.42 | |
| 6.30 | | 0.1968 | 1.08 | | 2.48 | |
| 6.20 | | 0.2000 | 1.11 | | 2.55 | |
| 6.10 | 49,200 | 0.2033 | 1.16 | | 2.62 | |
| 6.00 | 48,390 | 0.2066 | 1.22 | | 2.70 | |
| 5.90 | 47,580 | 0.2101 | 1.29 | | 2.77 | |
| 5.80 | 46,780 | 0.2138 | 1.37 | | 2.83 | |
| 5.70 | 45,970 | 0.2175 | 1.47 | | 2.88 | |
| 5.60 | 45,160 | 0.2214 | 1.56 | 1.32 [8] | 2.91 | 2.87 [8] |
| 5.50 | 44,360 | 0.2254 | 1.64 | 1.37 | 2.91 | 2.88 |
| 5.40 | 43,550 | 0.2296 | 1.70 | 1.39 | 2.91 | 2.88 |
| 5.30 | 42,740 | 0.2339 | 1.71 | 1.39 | 2.93 | 2.91 |
| 5.28 | 42,580 | 0.2348 | | 1.39 | | 2.91 |
| 5.26 | 42,420 | 0.2357 | | 1.39 | | 2.93 |
| 5.24 | 42,260 | 0.2366 | | 1.39 | | 2.93 |
| 5.22 | 42,100 | 0.2375 | | 1.40 | | 2.95 |
| 5.20 | 41,940 | 0.2384 | 1.72 | 1.40 | 3.00 | 2.96 |
| 5.18 | 41,780 | 0.2394 | | 1.40 | | 2.98 |
| 5.16 | 41,610 | 0.2403 | | 1.40 | | 2.99 |
| 5.14 | 41,450 | 0.2412 | | 1.39 | | 3.01 |
| 5.12 | 41,290 | 0.2422 | | 1.40 | | 3.03 |
| 5.10 | 41,130 | 0.2431 | 1.75 | 1.40 | 3.11 | 3.05 |
| 5.08 | 40,970 | 0.2441 | | 1.41 | | 3.07 |

TABLE I(b) (*Continued*)

$Si_xGe_{1-x}$, $x = 0.50$

| eV | $cm^{-1}$ | $\mu$m | $n$ | $n$ | $k$ | $k$ |
|---|---|---|---|---|---|---|
| 5.06 | 40,810 | 0.2450 | | 1.41 | | 3.09 |
| 5.04 | 40;650 | 0.2460 | | 1.41 | | 3.11 |
| 5.02 | 40,480 | 0.2470 | | 1.42 | | 3.13 |
| 5.00 | 40,320 | 0.2480 | 1.81 | 1.43 | 3.24 | 3.16 |
| 4.98 | 40,160 | 0.2490 | | 1.43 | | 3.19 |
| 4.96 | 40,000 | 0.2500 | | 1.44 | | 3.21 |
| 4.94 | 39,840 | 0.2510 | | 1.45 | | 3.24 |
| 4.92 | 39,680 | 0.2520 | | 1.46 | | 3.26 |
| 4.90 | 39,520 | 0.2530 | 1.90 | 1.47 | 3.36 | 3.30 |
| 4.88 | 39,360 | 0.2541 | | 1.48 | | 3.32 |
| 4.86 | 39,190 | 0.2551 | | 1.49 | | 3.36 |
| 4.84 | 39,030 | 0.2562 | | 1.51 | | 3.39 |
| 4.82 | 38,870 | 0.2572 | | 1.52 | | 3.42 |
| 4.80 | 38,710 | 0.2583 | 2.00 | 1.54 | 3.51 | 3.46 |
| 4.78 | 38,550 | 0.2594 | | 1.55 | | 3.49 |
| 4.76 | 38,390 | 0.2605 | | 1.57 | | 3.52 |
| 4.75 | 38,310 | 0.2610 | 2.07 | | 3.59 | |
| 4.74 | 38,230 | 0.2616 | | 1.59 | | 3.56 |
| 4.72 | 38,060 | 0.2627 | | 1.60 | | 3.60 |
| 4.70 | 37,900 | 0.2638 | 2.14 | 1.63 | 3.67 | 3.64 |
| 4.68 | 37,740 | 0.2649 | | 1.66 | | 3.68 |
| 4.66 | 37,580 | 0.2661 | | 1.68 | | 3.72 |
| 4.65 | 37,500 | 0.2666 | 2.22 | | 3.78 | |
| 4.64 | 37,420 | 0.2672 | | 1.71 | | 3.77 |
| 4.62 | 37,260 | 0.2684 | | 1.74 | | 3.82 |
| 4.60 | 37,100 | 0.2695 | 2.33 | 1.77 | 3.89 | 3.87 |
| 4.58 | 36,940 | 0.2707 | 2.38 | 1.81 | 3.93 | 3.91 |
| 4.56 | 36,770 | 0.2719 | 2.44 | 1.85 | 3.98 | 3.97 |
| 4.54 | 36,610 | 0.2731 | 2.50 | 1.89 | 4.03 | 4.02 |
| 4.52 | 36,450 | 0.2743 | 2.57 | 1.95 | 4.07 | 4.07 |
| 4.50 | 36,290 | 0.2755 | 2.64 | 2.00 | 4.12 | 4.13 |
| 4.48 | 36,130 | 0.2768 | 2.72 | 2.06 | 4.16 | 4.18 |
| 4.46 | 35,970 | 0.2780 | 2.81 | 2.13 | 4.20 | 4.23 |
| 4.44 | 35,810 | 0.2792 | 2.91 | 2.21 | 4.24 | 4.29 |
| 4.42 | 35,640 | 0.2805 | 3.02 | 2.30 | 4.27 | 4.34 |
| 4.40 | 35,480 | 0.2818 | 3.14 | 2.40 | 4.29 | 4.39 |
| 4.38 | 35,320 | 0.2831 | 3.27 | 2.51 | 4.30 | 4.43 |
| 4.36 | 35,160 | 0.2844 | 3.41 | 2.63 | 4.31 | 4.46 |
| 4.34 | 35,000 | 0.2857 | 3.56 | 2.76 | 4.27 | 4.47 |
| 4.32 | 34,840 | 0.2870 | 3.70 | 2.90 | 4.22 | 4.46 |
| 4.30 | 34,680 | 0.2883 | 3.83 | 3.02 | 4.15 | 4.44 |
| 4.28 | 34,520 | 0.2897 | 3.94 | 3.15 | 4.05 | 4.40 |
| 4.26 | 34,350 | 0.2910 | 4.03 | 3.26 | 3.96 | 4.34 |
| 4.24 | 34,190 | 0.2924 | 4.11 | 3.36 | 3.87 | 4.28 |
| 4.22 | 34,030 | 0.2938 | 4.17 | 3.45 | 3.78 | 4.21 |
| 4.20 | 33,870 | 0.2952 | 4.25 | 3.53 | 3.70 | 4.14 |
| 4.18 | 33,710 | 0.2966 | 4.33 | 3.59 | 3.58 | 4.06 |

TABLE I(b) (*Continued*)

$Si_xGe_{1-x}$, $x = 0.50$

| eV | $cm^{-1}$ | $\mu m$ | $n$ | $n$ | $k$ | $k$ |
|---|---|---|---|---|---|---|
| 4.16 | 33,550 | 0.2980 | 4.34 | 3.65 | 3.41 | 3.99 |
| 4.14 | 33,390 | 0.2995 | 4.29 | 3.70 | 3.32 | 3.92 |
| 4.12 | 33,230 | 0.3009 | 4.30 | 3.74 | 3.31 | 3.85 |
| 4.10 | 33,060 | 0.3024 | 4.33 | 3.77 | 3.24 | 3.79 |
| 4.08 | 32,900 | 0.3039 | | 3.80 | | 3.73 |
| 4.06 | 32,740 | 0.3054 | | 3.82 | | 3.67 |
| 4.05 | 32,660 | 0.3061 | 4.34 | | 3.06 | |
| 4.04 | 32,580 | 0.3069 | | 3.84 | | 3.61 |
| 4.02 | 32,420 | 0.3084 | | 3.86 | | 3.56 |
| 4.00 | 32,260 | 0.3100 | 4.34 | 3.87 | 2.92 | 3.52 |
| 3.98 | 32,100 | 0.3115 | | 3.89 | | 3.47 |
| 3.96 | 31,930 | 0.3131 | | 3.90 | | 3.42 |
| 3.95 | 31,850 | 0.3139 | 4.32 | | 2.81 | |
| 3.94 | 31,770 | 0.3147 | | 3.92 | | 3.39 |
| 3.92 | 31,610 | 0.3163 | | 3.93 | | 3.35 |
| 3.90 | 31,450 | 0.3179 | 4.31 | 3.94 | 2.72 | 3.31 |
| 3.88 | 31,290 | 0.3195 | | 3.95 | | 3.28 |
| 3.86 | 31,130 | 0.3212 | | 3.97 | | 3.25 |
| 3.85 | 31,050 | 0.3220 | 4.30 | | 2.64 | |
| 3.84 | 30,970 | 0.3229 | | 3.98 | | 3.22 |
| 3.82 | 30,810 | 0.3246 | | 3.99 | | 3.19 |
| 3.80 | 30,640 | 0.3263 | 4.30 | 4.00 | 2.57 | 3.16 |
| 3.78 | 30,480 | 0.3280 | | 4.01 | | 3.14 |
| 3.76 | 30,320 | 0.3297 | | 4.02 | | 3.11 |
| 3.75 | 30,240 | 0.3306 | 4.29 | | 2.51 | |
| 3.74 | 30,160 | 0.3315 | | 4.04 | | 3.09 |
| 3.72 | 30,000 | 0.3333 | | 4.04 | | 3.06 |
| 3.70 | 29,840 | 0.3351 | 4.30 | 4.06 | 2.46 | 3.04 |
| 3.68 | 29,680 | 0.3369 | | 4.07 | | 3.02 |
| 3.66 | 29,520 | 0.3388 | | 4.08 | | 3.00 |
| 3.65 | 29,430 | 0.3397 | 4.30 | | 2.41 | |
| 3.64 | 29,350 | 0.3406 | | 4.10 | | 2.98 |
| 3.62 | 29,190 | 0.3425 | | 4.11 | | 2.96 |
| 3.60 | 29,030 | 0.3444 | 4.31 | 4.12 | 2.37 | 2.94 |
| 3.58 | 28,870 | 0.3463 | | 4.14 | | 2.93 |
| 3.56 | 28,710 | 0.3483 | | 4.15 | | 2.91 |
| 3.55 | 28,630 | 0.3493 | 4.32 | | 2.34 | |
| 3.54 | 28,550 | 0.3502 | | 4.16 | | 2.89 |
| 3.52 | 28,390 | 0.3522 | | 4.19 | | 2.88 |
| 3.50 | 28,220 | 0.3542 | 4.34 | 4.20 | 2.30 | 2.87 |
| 3.48 | 28,060 | 0.3563 | | 4.22 | | 2.85 |
| 3.46 | 27,900 | 0.3583 | | 4.24 | | 2.83 |
| 3.45 | 27,820 | 0.3594 | 4.37 | | 2.27 | |
| 3.44 | 27,740 | 0.3604 | | 4.26 | | 2.82 |
| 3.42 | 27,580 | 0.3625 | | 4.28 | | 2.81 |
| 3.40 | 27,420 | 0.3647 | 4.40 | 4.31 | 2.24 | 2.79 |
| 3.38 | 27,260 | 0.3668 | | 4.33 | | 2.77 |

TABLE I(b) (*Continued*)

$Si_xGe_{1-x}$, $x=0.50$

| eV | $cm^{-1}$ | $\mu m$ | $n$ | $n$ | $k$ | $k$ |
|---|---|---|---|---|---|---|
| 3.36 | 27,100 | 0.3690 | | 4.35 | | 2.76 |
| 3.35 | 27,010 | 0.3701 | 4.44 | | 2.20 | |
| 3.34 | 26,930 | 0.3712 | | 4.38 | | 2.74 |
| 3.32 | 26,770 | 0.3734 | | 4.41 | | 2.72 |
| 3.30 | 26,610 | 0.3757 | 4.48 | 4.43 | 2.15 | 2.69 |
| 3.28 | 26,450 | 0.3780 | | 4.46 | | 2.67 |
| 3.26 | 26,290 | 0.3803 | | 4.48 | | 2.65 |
| 3.25 | 26,210 | 0.3815 | 4.52 | | 2.10 | |
| 3.24 | 26,130 | 0.3827 | | 4.51 | | 2.62 |
| 3.22 | 25,970 | 0.3850 | | 4.53 | | 2.60 |
| 3.20 | 25,810 | 0.3875 | 4.55 | 4.55 | 2.05 | 2.57 |
| 3.18 | 25,640 | 0.3899 | | 4.56 | | 2.55 |
| 3.16 | 25,480 | 0.3924 | | 4.58 | | 2.52 |
| 3.15 | 25,400 | 0.3936 | 4.57 | | 2.00 | |
| 3.14 | 25,320 | 0.3949 | | 4.60 | | 2.50 |
| 3.12 | 25,160 | 0.3974 | | 4.61 | | 2.48 |
| 3.10 | 25,000 | 0.4000 | 4.61 | 4.63 | 1.97 | 2.46 |
| 3.08 | 24,840 | 0.4025 | 4.62 | 4.64 | 1.96 | 2.45 |
| 3.06 | 24,680 | 0.4052 | 4.64 | 4.66 | 1.95 | 2.44 |
| 3.04 | 24,510 | 0.4078 | 4.66 | 4.68 | 1.94 | 2.43 |
| 3.02 | 24,350 | 0.4105 | 4.69 | 4.71 | 1.94 | 2.42 |
| 3.00 | 24,190 | 0.4133 | 4.73 | 4.74 | 1.93 | 2.42 |
| 2.98 | 24,030 | 0.4161 | 4.77 | 4.78 | 1.91 | 2.41 |
| 2.96 | 23,870 | 0.4189 | 4.80 | 4.82 | 1.89 | 2.41 |
| 2.94 | 23,710 | 0.4217 | 4.85 | 4.87 | 1.87 | 2.40 |
| 2.92 | 23,550 | 0.4246 | 4.90 | 4.92 | 1.84 | 2.39 |
| 2.90 | 23,390 | 0.4275 | 4.95 | 4.98 | 1.80 | 2.38 |
| 2.88 | 23,220 | 0.4305 | 5.01 | 5.05 | 1.75 | 2.35 |
| 2.86 | 23,060 | 0.4335 | | 5.12 | | 2.32 |
| 2.84 | 22,900 | 0.4366 | 5.09 | 5.19 | 1.62 | 2.28 |
| 2.82 | 22,740 | 0.4397 | 5.13 | 5.27 | 1.55 | 2.23 |
| 2.80 | 22,580 | 0.4428 | 5.16 | 5.34 | 1.46 | 2.16 |
| 2.78 | 22,420 | 0.4460 | | 5.42 | | 2.09 |
| 2.76 | 22,260 | 0.4492 | | 5.48 | | 2.00 |
| 2.75 | 22,180 | 0.4509 | 5.17 | | 1.24 | |
| 2.74 | 22,090 | 0.4525 | | 5.55 | | 1.90 |
| 2.72 | 21,930 | 0.4558 | | 5.60 | | 1.79 |
| 2.70 | 21,770 | 0.4592 | 5.10 | 5.64 | 1.04 | 1.66 |
| 2.68 | 21,610 | 0.4626 | | 5.65 | | 1.53 |
| 2.66 | 21,450 | 0.4661 | | 5.65 | | 1.40 |
| 2.65 | 21,370 | 0.4679 | 5.01 | | 0.89 | |
| 2.64 | 21,290 | 0.4696 | | 5.63 | | 1.28 |
| 2.62 | 21,130 | 0.4732 | | 5.59 | | 1.17 |
| 2.60 | 20,970 | 0.4769 | 4.91 | 5.55 | 0.79 | 1.07 |
| 2.58 | 20,800 | 0.4806 | | 5.50 | | 0.99 |
| 2.56 | 20,640 | 0.4843 | | 5.45 | | 0.91 |
| 2.55 | 20,560 | 0.4862 | 4.82 | | 0.72 | |

**TABLE I(b) (*Continued*)**

**$Si_xGe_{1-x}$, $x = 0.50$**

| eV | $cm^{-1}$ | $\mu m$ | $n$ | $n$ | $k$ | $k$ |
|---|---|---|---|---|---|---|
| 2.54 | 20,480 | 0.4881 | | 5.40 | | 0.83 |
| 2.52 | 20,320 | 0.4920 | | 5.34 | | 0.77 |
| 2.50 | 20,160 | 0.4959 | 4.74 | 5.29 | 0.66 | 0.72 |
| 2.48 | 20,000 | 0.4999 | | 5.24 | | 0.66 |
| 2.46 | 19,840 | 0.5040 | | 5.19 | | 0.61 |
| 2.45 | 19,760 | 0.5061 | 4.67 | | 0.62 | |
| 2.44 | 19,680 | 0.5081 | | 5.15 | | 0.58 |
| 2.42 | 19,510 | 0.5123 | | 5.10 | | 0.52 |
| 2.40 | 19,350 | 0.5166 | 4.61 | 5.06 | 0.58 | 0.49 |
| 2.38 | 19,190 | 0.5209 | | 5.01 | | 0.46 |
| 2.36 | 19,030 | 0.5254 | | 4.97 | | 0.44 |
| 2.35 | 18,950 | 0.5276 | 4.56 | | 0.55 | |
| 2.34 | 18,870 | 0.5299 | | 4.93 | | 0.41 |
| 2.32 | 18,710 | 0.5344 | | 4.89 | | 0.40 |
| 2.30 | 18,550 | 0.5391 | 4.52 | 4.85 | 0.52 | 0.35 |
| 2.28 | 18,380 | 0.5438 | | 4.81 | | 0.36 |
| 2.26 | 18,220 | 0.5486 | | 4.77 | | 0.34 |
| 2.25 | 18,140 | 0.5510 | 4.47 | | 0.49 | |
| 2.24 | 18,060 | 0.5535 | | 4.74 | | 0.30 |
| 2.22 | 17,900 | 0.5585 | | 4.71 | | |
| 2.20 | 17,740 | 0.5636 | 4.44 | 4.67 | 0.46 | |
| 2.18 | 17,580 | 0.5687 | | 4.64 | | |
| 2.16 | 17,420 | 0.5740 | | 4.61 | | |
| 2.15 | 17,340 | 0.5767 | 4.41 | | 0.44 | |
| 2.14 | 17,260 | 0.5794 | | 4.58 | | |
| 2.12 | 17,090 | 0.5848 | | 4.55 | | |
| 2.10 | 16,930 | 0.5904 | 4.38 | 4.52 | 0.41 | |
| 2.08 | 16,770 | 0.5961 | | 4.50 | | |
| 2.06 | 16,610 | 0.6019 | | 4.47 | | |
| 2.05 | 16,530 | 0.6048 | 4.35 | | | |
| 2.04 | 16,450 | 0.6078 | | 4.45 | | |
| 2.02 | 16,290 | 0.6138 | | 4.42 | | |
| 2.00 | 16,130 | 0.6199 | 4.32 | 4.40 | | |
| 1.98 | 15,970 | 0.6262 | | 4.38 | | |
| 1.96 | 15,800 | 0.6326 | | 4.36 | | |
| 1.95 | 15,720 | 0.6358 | 4.29 | | | |
| 1.94 | 15,640 | 0.6391 | | 4.34 | | |
| 1.92 | 15,480 | 0.6458 | | 4.32 | | |
| 1.90 | 15,320 | 0.6526 | 4.26 | 4.30 | | |
| 1.88 | 15,160 | 0.6595 | | 4.28 | | |
| 1.86 | 15,000 | 0.6666 | | 4.26 | | |
| 1.85 | 14,920 | 0.6702 | 4.24 | | | |
| 1.84 | 14,840 | 0.6738 | | 4.25 | | |
| 1.82 | 14,670 | 0.6812 | | 4.23 | | |
| 1.80 | 14,510 | 0.6888 | 4.21 | 4.21 | | |
| 1.78 | 14,350 | 0.6965 | | 4.20 | | |
| 1.76 | 14,190 | 0.7045 | | 4.18 | | |

TABLE I(b) (*Continued*)

$Si_xGe_{1-x}$, $x = 0.50$

| eV | $cm^{-1}$ | $\mu$m | $n$ | $n$ | $k$ | $k$ |
|---|---|---|---|---|---|---|
| 1.74 | 14,030 | 0.7126 | | 4.16 | | |
| 1.72 | 13,870 | 0.7208 | | 4.14 | | |
| 1.70 | 13,710 | 0.7293 | 4.16 | 4.13 | | |
| 1.68 | 13,550 | 0.7380 | | 4.11 | | |
| 1.66 | 13,380 | 0.7469 | | 4.09 | | |
| 1.60 | 12,900 | 0.7749 | 4.11 | | | |
| 1.50 | 12,090 | 0.8266 | 4.06 | | | |
| 1.40 | 11,290 | 0.8856 | 4.01 | | | |
| 1.30 | 10,480 | 0.9537 | 3.96 | | | 7.24E-03 [4] |
| 1.29 | 10,400 | 0.9611 | | | | 6.91E-03 |
| 1.28 | 10,320 | 0.9686 | | | | 6.59E-03 |
| 1.27 | 10,240 | 0.9763 | | | | 6.27E-03 |
| 1.26 | 10,160 | 0.9840 | | | | 5.96E-03 |
| 1.25 | 10,080 | 0.9919 | | | | 5.66E-03 |
| 1.24 | 10,000 | 0.9999 | | | | 5.36E-03 |
| 1.23 | 9,921 | 1.008 | | | | 5.07E-03 |
| 1.22 | 9,840 | 1.016 | | | | 4.78E-03 |
| 1.21 | 9,759 | 1.024 | | | | 4.50E-03 |
| 1.20 | 9,679 | 1.033 | 3.92 | | | 4.23E-03 |
| 1.19 | 9,598 | 1.041 | | | | 3.96E-03 |
| 1.18 | 9,517 | 1.050 | | | | 3.70E-03 |
| 1.17 | 9,437 | 1.059 | | | | 3.44E-03 |
| 1.16 | 9,356 | 1.068 | | | | 3.20E-03 |
| 1.15 | 9,275 | 1.078 | | | | 2.96E-03 |
| 1.14 | 9,195 | 1.087 | | | | 2.73E-03 |
| 1.13 | 9,114 | 1.097 | | | | 2.51E-03 |
| 1.12 | 9,033 | 1.107 | | | | 2.29E-03 |
| 1.11 | 8,953 | 1.116 | | | | 2.08E-03 |
| 1.10 | 8,872 | 1.127 | 3.88 | | | 1.88E-03 |
| 1.09 | 8,791 | 1.137 | | | | 1.69E-03 |
| 1.08 | 8,711 | 1.148 | | | | 1.51E-03 |
| 1.07 | 8,630 | 1.158 | | | | 1.34E-03 |
| 1.06 | 8,549 | 1.169 | | | | 1.18E-03 |
| 1.05 | 8,469 | 1.180 | | | | 1.02E-03 |
| 1.04 | 8,388 | 1.192 | | | | 8.81E-04 |
| 1.03 | 8,307 | 1.203 | | | | 7.48E-04 |
| 1.02 | 8,227 | 1.215 | | | | 6.26E-04 |
| 1.01 | 8,146 | 1.227 | | | | 5.14E-04 |
| 1.00 | 8,065 | 1.239 | 3.84 | | | 4.14E-04 |
| 0.99 | 7,985 | 1.252 | | | | 3.25E-04 |
| 0.98 | 7,904 | 1.265 | | | | 2.47E-04 |
| 0.97 | 7,824 | 1.278 | | | | 1.82E-04 |
| 0.96 | 7,743 | 1.291 | | | | 1.30E-04 |
| 0.95 | 7,662 | 1.305 | | | | 9.07E-05 |
| 0.94 | 7,582 | 1.318 | | | | 6.48E-05 |
| 0.93 | 7,501 | 1.333 | | | | 4.67E-05 |
| 0.92 | 7,420 | 1.347 | | | | 3.14E-05 |

**TABLE I(b) (*Continued*)**

**$Si_xGe_{1-x}$, $x = 0.50$**

| eV | $cm^{-1}$ | $\mu m$ | $n$ | $n$ | $k$ | $k$ |
|---|---|---|---|---|---|---|
| 0.91 | 7,340 | 1.362 | | | | 1.90E-05 |
| 0.90 | 7,259 | 1.377 | 3.80 | | | 9.66E-06 |
| 0.80 | 6,452 | 1.549 | 3.77 | | | |
| 0.70 | 5,646 | 1.771 | 3.75 | | | |
| 0.60 | 4,839 | 2.066 | 3.72 | | | |
| 0.50 | 4,033 | 2.479 | 3.70 | | | |
| 0.40 | 3,226 | 3.099 | 3.69 | | | |
| 0.30 | 2,420 | 4.132 | 3.67 | | | |
| 0.20 | 1,613 | 6.199 | 3.67 | | | |
| 0.1363 | 1,100 | 9.091 | | | | 3.92E-05 [11] |
| 0.1301 | 1,050 | 9.524 | | | | 4.84E-05 |
| 0.1239 | 1,000 | 10.00 | | | | 5.87E-05 |
| 0.1178 | 950 | 10.52 | | | | 8.49E-05 |
| 0.1116 | 900 | 11.11 | | | | 1.29E-04 |
| 0.1091 | 880 | 11.36 | | | | 1.54E-04 |
| 0.1066 | 860 | 11.62 | | | | 1.89E-04 |
| 0.1041 | 840 | 11.90 | | | | 1.97E-04 |
| 0.1017 | 820 | 12.19 | | | | 1.81E-04 |
| 0.1000 | 807 | 12.39 | 3.66 | | | |
| 0.09919 | 800 | 12.49 | | | | 1.77E-04 |
| 0.09671 | 780 | 12.82 | | | | 1.73E-04 |
| 0.09423 | 760 | 13.15 | | | | 1.45E-04 |
| 0.09175 | 740 | 13.51 | | | | 1.32E-04 |
| 0.08927 | 720 | 13.88 | | | | 1.61E-04 |
| 0.08679 | 700 | 14.28 | | | | 2.32E-04 |
| 0.08431 | 680 | 14.70 | | | | 3.26E-04 |
| 0.08183 | 660 | 15.15 | | | | 3.49E-04 |
| 0.07935 | 640 | 15.62 | | | | 3.28E-04 |
| 0.07687 | 620 | 16.12 | | | | 3.33E-04 |
| 0.07439 | 600 | 16.66 | | | | 3.84E-04 |
| 0.07191 | 580 | 17.24 | | | | 4.55E-04 |
| 0.06943 | 560 | 17.85 | | | | 5.20E-04 |
| 0.06695 | 540 | 18.51 | | | | 6.31E-04 |
| 0.06447 | 520 | 19.23 | | | | 9.62E-04 |
| 0.06323 | 510 | 19.60 | | | | 1.13E-03 |
| 0.06199 | 500 | 20.00 | | | | 1.16E-03 |
| 0.06075 | 490 | 20.40 | | | | 1.02E-03 |
| 0.05951 | 480 | 20.83 | | | | 1.24E-03 |
| 0.05827 | 470 | 21.27 | | | | 1.30E-03 |
| 0.05703 | 460 | 21.74 | | | | 1.15E-03 |
| 0.05455 | 440 | 22.72 | | | | 9.01E-04 |
| 0.05207 | 420 | 23.81 | | | | 8.89E-04 |
| 0.05083 | 410 | 24.39 | | | | 1.12E-03 |
| 0.04959 | 400 | 25.00 | | | | 2.30E-03 |
| 0.04835 | 390 | 25.64 | | | | 2.62E-03 |
| 0.04711 | 380 | 26.31 | | | | 2.26E-03 |
| 0.04587 | 370 | 27.02 | | | | 1.87E-03 |

**TABLE I(b) (*Continued*)**

**$Si_xGe_{1-x}$, $x=0.50$**

| eV | $cm^{-1}$ | $\mu m$ | $n$ | $n$ | $k$ | $k$ |
|---|---|---|---|---|---|---|
| 0.04463 | 360 | 27.78 | | | | 1.47E-03 |
| 0.04215 | 340 | 29.41 | | | | 1.43E-03 |
| 0.03968 | 320 | 31.24 | | | | 1.39E-03 |
| 0.03720 | 300 | 33.33 | | | | 1.57E-03 |
| 0.03596 | 290 | 34.47 | | | | 2.11E-03 |
| 0.03472 | 280 | 35.70 | | | | 2.13E-03 |
| 0.03348 | 270 | 37.03 | | | | 1.80E-03 |
| 0.03224 | 260 | 38.45 | | | | 1.71E-03 |
| 0.02976 | 240 | 41.66 | | | | 1.70E-03 |
| 0.02728 | 220 | 45.44 | | | | 1.70E-03 |
| 0.02480 | 200 | 50.00 | | | | 1.81E-03 |
| 0.02232 | 180 | 55.54 | | | | 1.95E-03 |

[a]The reference from which the values were extracted is given in brackets next to the first value. The nominal alloy compositions are: x=0.551 [6], x=0.487 [8], x=0.500 obtained by interpolating the data of Braunstein et al. [4], x=0.450 [11].

**TABLE I(c)**

**Values of $n$ and $k$ for $Si_xGe_{1-x}$, $x = 0.80$, from Various References[a]**

| eV | $cm^{-1}$ | $\mu m$ | $n$ | $n$ | $k$ | $k$ |
|---|---|---|---|---|---|---|
| 12.8 | | 0.09686 | 0.64 [6] | | 0.78 [6] | |
| 12.6 | | 0.09840 | 0.65 | | 0.80 | |
| 12.2 | | 0.1016 | 0.65 | | 0.84 | |
| 11.8 | | 0.1051 | 0.64 | | 0.88 | |
| 11.4 | | 0.1088 | 0.63 | | 0.92 | |
| 11.0 | | 0.1127 | 0.62 | | 0.98 | |
| 10.6 | | 0.1170 | 0.61 | | 1.04 | |
| 10.2 | | 0.1216 | 0.60 | | 1.11 | |
| 9.80 | | 0.1265 | 0.60 | | 1.20 | |
| 9.40 | | 0.1319 | 0.60 | | 1.29 | |
| 9.00 | | 0.1378 | 0.60 | | 1.40 | |
| 8.60 | | 0.1442 | 0.63 | | 1.51 | |
| 8.20 | | 0.1512 | 0.65 | | 1.63 | |
| 7.90 | | 0.1569 | 0.67 | | 1.73 | |
| 7.80 | | 0.1590 | 0.67 | | 1.76 | |
| 7.40 | | 0.1675 | 0.69 | | 1.95 | |
| 7.00 | | 0.1771 | 0.77 | | 2.18 | |
| 6.90 | | 0.1797 | 0.82 | | 2.25 | |
| 6.80 | | 0.1823 | 0.87 | | 2.30 | |
| 6.70 | | 0.1851 | 0.91 | | 2.34 | |
| 6.60 | | 0.1879 | 0.95 | | 2.38 | |
| 6.50 | | 0.1907 | 0.99 | | 2.42 | |
| 6.40 | | 0.1937 | 1.02 | | 2.45 | |
| 6.30 | | 0.1968 | 1.05 | | 2.51 | |
| 6.20 | | 0.2000 | 1.08 | | 2.57 | |
| 6.10 | 49,200 | 0.2033 | 1.12 | | 2.64 | |
| 6.00 | 48,390 | 0.2066 | 1.18 | | 2.71 | |
| 5.90 | 47,580 | 0.2101 | 1.24 | | 2.78 | |
| 5.70 | 45,970 | 0.2175 | 1.40 | | 2.89 | |
| 5.60 | 45,160 | 0.2214 | 1.48 | 1.28 [8] | 2.92 | 3.06 [8] |
| 5.50 | 44,360 | 0.2254 | 1.56 | 1.35 | 2.95 | 3.11 |
| 5.40 | 43,550 | 0.2296 | 1.62 | 1.43 | 2.96 | 3.13 |
| 5.30 | 42,740 | 0.2339 | 1.66 | 1.47 | 2.98 | 3.14 |
| 5.28 | 42,580 | 0.2348 | | 1.47 | | 3.15 |
| 5.26 | 42,420 | 0.2357 | | 1.48 | | 3.15 |
| 5.24 | 42,260 | 0.2366 | | 1.48 | | 3.16 |
| 5.22 | 42,100 | 0.2375 | | 1.48 | | 3.17 |
| 5.20 | 41,940 | 0.2384 | 1.67 | 1.48 | 3.01 | 3.18 |
| 5.18 | 41,780 | 0.2394 | | 1.48 | | 3.20 |
| 5.16 | 41,610 | 0.2403 | | 1.48 | | 3.21 |
| 5.14 | 41,450 | 0.2412 | | 1.48 | | 3.23 |
| 5.12 | 41,290 | 0.2422 | | 1.48 | | 3.25 |
| 5.10 | 41,130 | 0.2431 | 1.67 | 1.45 | 3.08 | 3.27 |
| 5.08 | 40,970 | 0.2441 | | 1.48 | | 3.29 |
| 5.06 | 40,810 | 0.2450 | | 1.48 | | 3.31 |
| 5.04 | 40,650 | 0.2460 | | 1.49 | | 3.34 |
| 5.02 | 40,480 | 0.2470 | | 1.49 | | 3.37 |

**TABLE I(c) (*Continued*)**

**$Si_xGe_{1-x}$, $x = 0.80$**

| eV | $cm^{-1}$ | $\mu m$ | $n$ | $n$ | $k$ | $k$ |
|---|---|---|---|---|---|---|
| 5.00 | 40,320 | 0.2480 | 1.67 | 1.50 | 3.19 | 3.39 |
| 4.98 | 40,160 | 0.2490 | | 1.50 | | 3.42 |
| 4.96 | 40,000 | 0.2500 | | 1.51 | | 3.45 |
| 4.94 | 39,840 | 0.2510 | | 1.51 | | 3.48 |
| 4.92 | 39,680 | 0.2520 | | 1.52 | | 3.52 |
| 4.90 | 39,520 | 0.2530 | 1.69 | 1.53 | 3.36 | 3.55 |
| 4.88 | 39,360 | 0.2541 | | 1.54 | | 3.59 |
| 4.86 | 39,190 | 0.2551 | | 1.55 | | 3.62 |
| 4.84 | 39,030 | 0.2562 | | 1.57 | | 3.66 |
| 4.82 | 38,870 | 0.2572 | | 1.58 | | 3.70 |
| 4.80 | 38,710 | 0.2583 | 1.75 | 1.60 | 3.56 | 3.74 |
| 4.78 | 38,550 | 0.2594 | | 1.61 | | 3.78 |
| 4.76 | 38,390 | 0.2605 | | 1.63 | | 3.83 |
| 4.75 | 38,310 | 0.2610 | 1.81 | | 3.68 | |
| 4.74 | 38,230 | 0.2616 | | 1.65 | | 3.88 |
| 4.72 | 38,060 | 0.2627 | | 1.68 | | 3.93 |
| 4.70 | 37,900 | 0.2638 | 1.88 | 1.70 | 3.80 | 3.98 |
| 4.68 | 37,740 | 0.2649 | | 1.73 | | 4.03 |
| 4.66 | 37,580 | 0.2661 | | 1.76 | | 4.08 |
| 4.65 | 37,500 | 0.2666 | 1.95 | | 3.95 | |
| 4.64 | 37,420 | 0.2672 | | 1.79 | | 4.14 |
| 4.62 | 37,260 | 0.2684 | | 1.83 | | 4.20 |
| 4.60 | 37,100 | 0.2695 | 2.07 | 1.87 | 4.10 | 4.26 |
| 4.58 | 36,940 | 0.2707 | 2.12 | 1.92 | 4.16 | 4.33 |
| 4.56 | 36,770 | 0.2719 | 2.19 | 1.97 | 4.23 | 4.39 |
| 4.54 | 36,610 | 0.2731 | 2.25 | 2.03 | 4.29 | 4.46 |
| 4.52 | 36,450 | 0.2743 | 2.33 | 2.10 | 4.35 | 4.52 |
| 4.50 | 36,290 | 0.2755 | 2.41 | 2.18 | 4.41 | 4.59 |
| 4.48 | 36,130 | 0.2768 | 2.51 | 2.26 | 4.47 | 4.66 |
| 4.46 | 35,970 | 0.2780 | 2.60 | 2.35 | 4.52 | 4.72 |
| 4.44 | 35,810 | 0.2792 | 2.71 | 2.45 | 4.58 | 4.78 |
| 4.42 | 35,640 | 0.2805 | 2.83 | 2.56 | 4.62 | 4.84 |
| 4.40 | 35,480 | 0.2818 | 2.96 | 2.68 | 4.66 | 4.90 |
| 4.38 | 35,320 | 0.2831 | 3.10 | 2.81 | 4.70 | 4.94 |
| 4.36 | 35,160 | 0.2844 | 3.25 | 2.96 | 4.72 | 4.98 |
| 4.34 | 35,000 | 0.2857 | 3.41 | 3.13 | 4.72 | 5.00 |
| 4.32 | 34,840 | 0.2870 | 3.59 | 3.30 | 4.70 | 5.00 |
| 4.30 | 34,680 | 0.2883 | 3.76 | 3.48 | 4.64 | 4.97 |
| 4.28 | 34,520 | 0.2897 | 3.92 | 3.64 | 4.54 | 4.91 |
| 4.26 | 34,350 | 0.2910 | 4.04 | 3.80 | 4.44 | 4.83 |
| 4.24 | 34,190 | 0.2924 | 4.15 | 3.93 | 4.34 | 4.73 |
| 4.22 | 34,030 | 0.2938 | 4.23 | 4.03 | 4.23 | 4.62 |
| 4.20 | 33,870 | 0.2952 | 4.32 | 4.13 | 4.14 | 4.51 |
| 4.18 | 33,710 | 0.2966 | 4.40 | 4.20 | 4.03 | 4.40 |
| 4.16 | 33,550 | 0.2980 | 4.45 | 4.25 | 3.89 | 4.30 |
| 4.14 | 33,390 | 0.2995 | 4.47 | 4.29 | 3.78 | 4.21 |
| 4.12 | 33,230 | 0.3009 | 4.49 | 4.33 | 3.69 | 4.11 |

**TABLE I(c) (*Continued*)**

**$Si_xGe_{1-x}$, $x = 0.80$**

| eV | $cm^{-1}$ | $\mu m$ | $n$ | $n$ | $k$ | $k$ |
|---|---|---|---|---|---|---|
| 4.10 | 33,060 | 0.3024 | 4.51 | 4.36 | 3.60 | 4.03 |
| 4.08 | 32,900 | 0.3039 | 4.52 | 4.38 | 3.52 | 3.95 |
| 4.06 | 32,740 | 0.3054 | 4.52 | 4.40 | 3.45 | 3.88 |
| 4.04 | 32,580 | 0.3069 | 4.53 | 4.41 | 3.38 | 3.81 |
| 4.02 | 32,420 | 0.3084 | 4.53 | 4.43 | 3.32 | 3.75 |
| 4.00 | 32,260 | 0.3100 | 4.53 | 4.44 | 3.26 | 3.69 |
| 3.98 | 32,100 | 0.3115 | | 4.45 | | 3.64 |
| 3.96 | 31,930 | 0.3131 | | 4.46 | | 3.59 |
| 3.95 | 31,850 | 0.3139 | 4.54 | | 3.13 | |
| 3.94 | 31,770 | 0.3147 | | 4.47 | | 3.55 |
| 3.92 | 31,610 | 0.3163 | | 4.48 | | 3.50 |
| 3.90 | 31,450 | 0.3179 | 4.54 | 4.50 | 3.03 | 3.46 |
| 3.88 | 31,290 | 0.3195 | | 4.51 | | 3.42 |
| 3.86 | 31,130 | 0.3212 | | 4.52 | | 3.39 |
| 3.85 | 31,050 | 0.3220 | 4.54 | | 2.95 | |
| 3.84 | 30,970 | 0.3229 | | 4.53 | | 3.36 |
| 3.82 | 30,810 | 0.3246 | | 4.54 | | 3.32 |
| 3.80 | 30,640 | 0.3263 | 4.55 | 4.56 | 2.88 | 3.30 |
| 3.78 | 30,480 | 0.3280 | | 4.57 | | 3.27 |
| 3.76 | 30,320 | 0.3297 | | 4.59 | | 3.24 |
| 3.75 | 30,240 | 0.3306 | 4.57 | | 2.81 | |
| 3.74 | 30,160 | 0.3315 | | 4.60 | | 3.21 |
| 3.72 | 30,000 | 0.3333 | | 4.62 | | 3.19 |
| 3.70 | 29,840 | 0.3351 | 4.60 | 4.64 | 2.76 | 3.16 |
| 3.68 | 29,680 | 0.3369 | | 4.65 | | 3.14 |
| 3.66 | 29,520 | 0.3388 | | 4.67 | | 3.12 |
| 3.65 | 29,430 | 0.3397 | 4.63 | | 2.71 | |
| 3.64 | 29,350 | 0.3406 | | 4.69 | | 3.10 |
| 3.62 | 29,190 | 0.3425 | | 4.71 | | 3.08 |
| 3.60 | 29,030 | 0.3444 | 4.66 | 4.73 | 2.67 | 3.06 |
| 3.58 | 28,870 | 0.3463 | | 4.75 | | 3.05 |
| 3.56 | 28,710 | 0.3483 | | 4.77 | | 3.03 |
| 3.55 | 28,630 | 0.3493 | 4.71 | | 2.64 | |
| 3.54 | 28,550 | 0.3502 | | 4.81 | | 3.05 |
| 3.52 | 28,390 | 0.3522 | | 4.82 | | 3.01 |
| 3.50 | 28,220 | 0.3542 | 4.77 | 4.86 | 2.61 | 3.00 |
| 3.48 | 28,060 | 0.3563 | 4.80 | 4.90 | 2.61 | 2.99 |
| 3.46 | 27,900 | 0.3583 | 4.84 | 4.94 | 2.60 | 2.98 |
| 3.44 | 27,740 | 0.3604 | 4.88 | 4.98 | 2.59 | 2.97 |
| 3.42 | 27,580 | 0.3625 | 4.92 | 5.03 | 2.58 | 2.96 |
| 3.40 | 27,420 | 0.3647 | 4.98 | 5.09 | 2.57 | 2.95 |
| 3.38 | 27,260 | 0.3668 | 5.03 | 5.15 | 2.55 | 2.93 |
| 3.36 | 27,100 | 0.3690 | 5.10 | 5.21 | 2.53 | 2.91 |
| 3.34 | 26,930 | 0.3712 | 5.17 | 5.29 | 2.50 | 2.89 |
| 3.32 | 26,770 | 0.3734 | 5.24 | 5.37 | 2.46 | 2.86 |
| 3.30 | 26,610 | 0.3757 | 5.32 | 5.46 | 2.42 | 2.82 |
| 3.28 | 26,450 | 0.3780 | 5.40 | 5.55 | 2.36 | 2.76 |

TABLE I(c) (*Continued*)

$Si_xGe_{1-x}$, $x = 0.80$

| eV | $cm^{-1}$ | $\mu m$ | $n$ | $n$ | $k$ | $k$ |
|---|---|---|---|---|---|---|
| 3.26 | 26,290 | 0.3803 | 5.48 | 5.64 | 2.28 | 2.70 |
| 3.24 | 26,130 | 0.3827 | 5.55 | 5.73 | 2.19 | 2.61 |
| 3.22 | 25,970 | 0.3850 | 5.62 | 5.82 | 2.10 | 2.52 |
| 3.20 | 25,810 | 0.3875 | 5.68 | 5.89 | 1.99 | 2.41 |
| 3.18 | 25,640 | 0.3899 | 5.73 | 5.96 | 1.87 | 2.30 |
| 3.16 | 25,480 | 0.3924 | 5.76 | 6.01 | 1.75 | 2.17 |
| 3.14 | 25,320 | 0.3949 | 5.79 | 6.06 | 1.62 | 2.03 |
| 3.12 | 25,160 | 0.3974 | 5.80 | 6.10 | 1.48 | 1.88 |
| 3.10 | 25,000 | 0.4000 | 5.79 | 6.11 | 1.34 | 1.73 |
| 3.08 | 24,840 | 0.4025 | | 6.11 | | 1.58 |
| 3.06 | 24,680 | 0.4052 | | 6.08 | | 1.44 |
| 3.05 | 24,600 | 0.4065 | 5.66 | | 1.03 | |
| 3.04 | 24,510 | 0.4078 | | 6.04 | | 1.30 |
| 3.02 | 24,350 | 0.4105 | | 5.99 | | 1.17 |
| 3.00 | 24,190 | 0.4133 | 5.49 | 5.92 | 0.81 | 1.06 |
| 2.98 | 24,030 | 0.4161 | | 5.86 | | 0.95 |
| 2.96 | 23,870 | 0.4189 | | 5.78 | | 0.87 |
| 2.95 | 23,790 | 0.4203 | 5.32 | | 0.65 | |
| 2.94 | 23,710 | 0.4217 | | 5.71 | | 0.79 |
| 2.92 | 23,550 | 0.4246 | | 5.64 | | 0.73 |
| 2.90 | 23,390 | 0.4275 | 5.15 | 5.57 | 0.55 | 0.66 |
| 2.88 | 23,220 | 0.4305 | | 5.50 | | 0.60 |
| 2.86 | 23,060 | 0.4335 | | 5.44 | | 0.56 |
| 2.85 | 22,980 | 0.4350 | 5.00 | | 0.47 | |
| 2.84 | 22,900 | 0.4366 | | 5.38 | | 0.51 |
| 2.82 | 22,740 | 0.4397 | | 5.32 | | 0.48 |
| 2.80 | 22,580 | 0.4428 | 4.88 | 5.26 | 0.43 | 0.44 |
| 2.78 | 22,420 | 0.4460 | | 5.21 | | 0.42 |
| 2.76 | 22,260 | 0.4492 | | 5.16 | | 0.39 |
| 2.75 | 22,180 | 0.4509 | 4.76 | | | |
| 2.74 | 22,090 | 0.4525 | | 5.11 | | 0.37 |
| 2.72 | 21,930 | 0.4558 | | 5.06 | | 0.34 |
| 2.70 | 21,770 | 0.4592 | 4.65 | 5.02 | | 0.32 |
| 2.68 | 21,610 | 0.4626 | | 4.97 | | 0.30 |
| 2.66 | 21,450 | 0.4661 | | 4.93 | | |
| 2.65 | 21,370 | 0.4679 | 4.56 | | | |
| 2.64 | 21,290 | 0.4696 | | 4.89 | | |
| 2.62 | 21,130 | 0.4732 | | 4.85 | | |
| 2.60 | 20,970 | 0.4769 | 4.50 | 4.82 | | |
| 2.58 | 20,800 | 0.4806 | | 4.78 | | |
| 2.56 | 20,640 | 0.4843 | | 4.75 | | |
| 2.55 | 20,560 | 0.4862 | 4.44 | | | |
| 2.54 | 20,480 | 0.4881 | | 4.71 | | |
| 2.52 | 20,320 | 0.4920 | | 4.68 | | |
| 2.50 | 20,160 | 0.4959 | 4.39 | 4.65 | | |
| 2.48 | 20,000 | 0.4999 | | 4.62 | | |
| 2.46 | 19,840 | 0.5040 | | 4.59 | | |

TABLE I(c) (*Continued*)

$Si_xGe_{1-x}$, $x = 0.80$

| eV | $cm^{-1}$ | $\mu m$ | $n$ | $n$ | $k$ | $k$ |
|---|---|---|---|---|---|---|
| 2.45 | 19,760 | 0.5061 | 4.35 | | | |
| 2.44 | 19,680 | 0.5081 | | 4.57 | | |
| 2.42 | 19,510 | 0.5123 | | 4.54 | | |
| 2.40 | 19,350 | 0.5166 | 4.30 | 4.51 | | |
| 2.38 | 19,190 | 0.5209 | | 4.49 | | |
| 2.36 | 19,030 | 0.5254 | | 4.46 | | |
| 2.34 | 18,870 | 0.5299 | | 4.44 | | |
| 2.32 | 18,710 | 0.5344 | | 4.41 | | |
| 2.30 | 18,550 | 0.5391 | 4.23 | 4.39 | | |
| 2.28 | 18,380 | 0.5438 | | 4.37 | | |
| 2.26 | 18,220 | 0.5486 | | 4.35 | | |
| 2.24 | 18,060 | 0.5535 | | 4.33 | | |
| 2.22 | 17,900 | 0.5585 | | 4.31 | | |
| 2.20 | 17,740 | 0.5636 | 4.16 | 4.29 | | |
| 2.18 | 17,580 | 0.5687 | | 4.27 | | |
| 2.16 | 17,420 | 0.5740 | | 4.25 | | |
| 2.14 | 17,260 | 0.5794 | | 4.23 | | |
| 2.12 | 17,090 | 0.5848 | | 4.21 | | |
| 2.10 | 16,930 | 0.5904 | 4.11 | 4.19 | | |
| 2.08 | 16,770 | 0.5961 | | 4.18 | | |
| 2.06 | 16,610 | 0.6019 | | 4.16 | | |
| 2.04 | 16,450 | 0.6078 | | 4.14 | | |
| 2.02 | 16,290 | 0.6138 | | 4.13 | | |
| 2.00 | 16,130 | 0.6199 | 4.05 | 4.11 | | |
| 1.98 | 15,970 | 0.6262 | | 4.10 | | |
| 1.96 | 15,800 | 0.6326 | | 4.08 | | |
| 1.94 | 15,640 | 0.6391 | | 4.07 | | |
| 1.92 | 15,480 | 0.6458 | | 4.05 | | |
| 1.90 | 15,320 | 0.6526 | 4.00 | 4.04 | | |
| 1.88 | 15,160 | 0.6595 | | 4.03 | | |
| 1.86 | 15,000 | 0.6666 | | 4.01 | | |
| 1.84 | 14,840 | 0.6738 | | 4.00 | | |
| 1.82 | 14,670 | 0.6812 | | 3.99 | | |
| 1.80 | 14,510 | 0.6888 | 3.96 | 3.98 | | |
| 1.78 | 14,350 | 0.6965 | | 3.97 | | |
| 1.76 | 14,190 | 0.7045 | | 3.95 | | |
| 1.74 | 14,030 | 0.7126 | | 3.94 | | |
| 1.72 | 13,870 | 0.7208 | | 3.93 | | |
| 1.70 | 13,710 | 0.7293 | 3.91 | 3.92 | | |
| 1.68 | 13,550 | 0.7380 | | 3.91 | | |
| 1.66 | 13,380 | 0.7469 | | 3.90 | | |
| 1.60 | 12,900 | 0.7749 | 3.87 | | | |
| 1.50 | 12,090 | 0.8266 | 3.84 | | | |
| 1.49 | 12,010 | 0.8321 | | | | 6.43E-03 [4] |
| 1.48 | 11,930 | 0.8377 | | | | 6.19E-03 |
| 1.47 | 11,850 | 0.8434 | | | | 5.96E-03 |
| 1.46 | 11,770 | 0.8492 | | | | 5.73E-03 |

**TABLE I(c) (*Continued*)**

**$Si_xGe_{1-x}$, $x = 0.80$**

| eV | $cm^{-1}$ | $\mu m$ | $n$ | $n$ | $k$ | $k$ |
|---|---|---|---|---|---|---|
| 1.45 | 11,690 | 0.8551 | | | | 5.50E-03 |
| 1.44 | 11,610 | 0.8610 | | | | 5.28E-03 |
| 1.43 | 11,530 | 0.8670 | | | | 5.06E-03 |
| 1.42 | 11,450 | 0.8731 | | | | 4.84E-03 |
| 1.41 | 11,370 | 0.8793 | | | | 4.63E-03 |
| 1.40 | 11,290 | 0.8856 | 3.80 | | | 4.42E-03 |
| 1.39 | 11,210 | 0.8920 | | | | 4.21E-03 |
| 1.38 | 11,130 | 0.8984 | | | | 4.01E-03 |
| 1.37 | 11,050 | 0.9050 | | | | 3.81E-03 |
| 1.36 | 10,960 | 0.9117 | | | | 3.61E-03 |
| 1.35 | 10,880 | 0.9184 | | | | 3.42E-03 |
| 1.34 | 10,800 | 0.9253 | | | | 3.23E-03 |
| 1.33 | 10,720 | 0.9322 | | | | 3.05E-03 |
| 1.32 | 10,640 | 0.9393 | | | | 2.87E-03 |
| 1.31 | 10,560 | 0.9465 | | | | 2.70E-03 |
| 1.30 | 10,480 | 0.9537 | 3.76 | | | 2.53E-03 |
| 1.29 | 10,400 | 0.9611 | | | | 2.36E-03 |
| 1.28 | 10,320 | 0.9686 | | | | 2.20E-03 |
| 1.27 | 10,240 | 0.9763 | | | | 2.04E-03 |
| 1.26 | 10,160 | 0.9840 | | | | 1.89E-03 |
| 1.25 | 10,080 | 0.9919 | | | | 1.74E-03 |
| 1.24 | 10,000 | 0.9999 | | | | 1.60E-03 |
| 1.23 | 9,921 | 1.008 | | | | 1.47E-03 |
| 1.22 | 9,840 | 1.016 | | | | 1.33E-03 |
| 1.21 | 9,759 | 1.024 | | | | 1.21E-03 |
| 1.20 | 9,679 | 1.033 | 3.73 | | | 1.09E-03 |
| 1.19 | 9,598 | 1.041 | | | | 9.73E-04 |
| 1.18 | 9,517 | 1.050 | | | | 8.64E-04 |
| 1.17 | 9,437 | 1.059 | | | | 7.61E-04 |
| 1.16 | 9,356 | 1.068 | | | | 6.64E-04 |
| 1.15 | 9,275 | 1.078 | | | | 5.74E-04 |
| 1.14 | 9,195 | 1.087 | | | | 4.90E-04 |
| 1.13 | 9,114 | 1.097 | | | | 4.13E-04 |
| 1.12 | 9,033 | 1.107 | | | | 3.42E-04 |
| 1.11 | 8,953 | 1.116 | | | | 2.79E-04 |
| 1.10 | 8,872 | 1.127 | 3.69 | | | 2.22E-04 |
| 1.09 | 8,791 | 1.137 | | | | 1.74E-04 |
| 1.08 | 8,711 | 1.148 | | | | 1.32E-04 |
| 1.07 | 8,630 | 1.158 | | | | 9.89E-05 |
| 1.06 | 8,549 | 1.169 | | | | 7.34E-05 |
| 1.05 | 8,469 | 1.180 | | | | 5.63E-05 |
| 1.04 | 8,388 | 1.192 | | | | 4.55E-05 |
| 1.03 | 8,307 | 1.203 | | | | 3.61E-05 |
| 1.02 | 8,227 | 1.215 | | | | 2.76E-05 |
| 1.01 | 8,146 | 1.227 | | | | 2.02E-05 |
| 1.00 | 8,065 | 1.239 | 3.65 | | | 1.39E-05 |
| 0.99 | 7,985 | 1.252 | | | | 8.76E-06 |

TABLE I(c) (*Continued*)

$Si_xGe_{1-x}$, $x = 0.80$

| eV | $cm^{-1}$ | $\mu m$ | $n$ | $n$ | $k$ | $k$ |
|---|---|---|---|---|---|---|
| 0.90 | 7,259 | 1.377 | 3.63 | | | |
| 0.80 | 6,452 | 1.549 | 3.60 | | | |
| 0.70 | 5,646 | 1.771 | 3.58 | | | |
| 0.60 | 4,839 | 2.066 | 3.56 | | | |
| 0.50 | 4,033 | 2.479 | 3.55 | | | |
| 0.40 | 3,226 | 3.099 | 3.53 | | | |
| 0.30 | 2,420 | 4.132 | 3.52 | | | |
| 0.20 | 1,613 | 6.199 | 3.52 | | | |
| 0.1487 | 1,200 | 8.333 | | | | 1.05E-05 [11] |
| 0.1463 | 1,180 | 8.474 | | | | 1.48E-05 |
| 0.1438 | 1,160 | 8.620 | | | | 1.92E-05 |
| 0.1413 | 1,140 | 8.772 | | | | 2.53E-05 |
| 0.1388 | 1,120 | 8.928 | | | | 3.18E-05 |
| 0.1363 | 1,100 | 9.091 | | | | 3.85E-05 |
| 0.1339 | 1,080 | 9.259 | | | | 3.77E-05 |
| 0.1314 | 1,060 | 9.434 | | | | 3.36E-05 |
| 0.1289 | 1,040 | 9.615 | | | | 2.78E-05 |
| 0.1264 | 1,020 | 9.804 | | | | 2.51E-05 |
| 0.1239 | 1,000 | 10.00 | | | | 3.22E-05 |
| 0.1215 | 980 | 10.20 | | | | 6.47E-05 |
| 0.1190 | 960 | 10.41 | | | | 9.31E-05 |
| 0.1165 | 940 | 10.63 | | | | 1.05E-04 |
| 0.1141 | 920 | 10.86 | | | | 1.27E-04 |
| 0.1116 | 900 | 11.11 | | | | 1.53E-04 |
| 0.1091 | 880 | 11.36 | | | | 1.91E-04 |
| 0.1066 | 860 | 11.62 | | | | 2.06E-04 |
| 0.1041 | 840 | 11.90 | | | | 1.84E-04 |
| 0.1017 | 820 | 12.19 | | | | 1.52E-04 |
| 0.1000 | 807 | 12.39 | 3.51 | | | |
| 0.09919 | 800 | 12.49 | | | | 1.41E-04 |
| 0.09671 | 780 | 12.82 | | | | 1.45E-04 |
| 0.09423 | 760 | 13.15 | | | | 1.59E-04 |
| 0.09175 | 740 | 13.51 | | | | 1.80E-04 |
| 0.08927 | 720 | 13.88 | | | | 2.15E-04 |
| 0.08679 | 700 | 14.28 | | | | 2.37E-04 |
| 0.08555 | 690 | 14.49 | | | | 2.37E-04 |
| 0.08431 | 680 | 14.70 | | | | 2.28E-04 |
| 0.08183 | 660 | 15.15 | | | | 2.21E-04 |
| 0.07935 | 640 | 15.62 | | | | 2.63E-04 |
| 0.07687 | 620 | 16.12 | | | | 3.63E-04 |
| 0.07439 | 600 | 16.66 | | | | 4.46E-04 |
| 0.07191 | 580 | 17.24 | | | | 5.00E-04 |
| 0.07067 | 570 | 17.54 | | | | 5.13E-04 |
| 0.06943 | 560 | 17.85 | | | | 5.17E-04 |
| 0.06695 | 540 | 18.51 | | | | 5.16E-04 |
| 0.06447 | 520 | 19.23 | | | | 5.30E-04 |
| 0.06199 | 500 | 20.00 | | | | 7.53E-04 |

**TABLE I(c) (*Continued*)**

**$Si_xGe_{1-x}$, $x=0.80$**

| eV | $cm^{-1}$ | $\mu m$ | $n$ | $n$ | $k$ | $k$ |
|---|---|---|---|---|---|---|
| 0.06075 | 490 | 20.40 | | | | 9.45E-04 |
| 0.05951 | 480 | 20.83 | | | | 1.01E-03 |
| 0.05827 | 470 | 21.27 | | | | 9.21E-04 |
| 0.05703 | 460 | 21.74 | | | | 6.81E-04 |
| 0.05579 | 450 | 22.22 | | | | 6.06E-04 |
| 0.05455 | 440 | 22.72 | | | | 6.33E-04 |
| 0.05331 | 430 | 23.25 | | | | 5.97E-04 |
| 0.05207 | 420 | 23.81 | | | | 5.61E-04 |
| 0.05145 | 415 | 24.09 | | | | 5.55E-04 |
| 0.05083 | 410 | 24.39 | | | | 6.93E-04 |
| 0.05021 | 405 | 24.69 | | | | 9.63E-04 |
| 0.04959 | 400 | 25.00 | | | | 1.06E-03 |
| 0.04897 | 395 | 25.31 | | | | 8.23E-04 |
| 0.04835 | 390 | 25.64 | | | | 6.58E-04 |
| 0.04711 | 380 | 26.31 | | | | 4.42E-04 |
| 0.04587 | 370 | 27.02 | | | | 3.16E-04 |
| 0.04463 | 360 | 27.78 | | | | 2.91E-04 |
| 0.04339 | 350 | 28.57 | | | | 3.11E-04 |
| 0.04215 | 340 | 29.41 | | | | 2.85E-04 |
| 0.03968 | 320 | 31.24 | | | | 1.98E-04 |
| 0.03720 | 300 | 33.33 | | | | 1.88E-04 |
| 0.03472 | 280 | 35.70 | | | | 1.64E-04 |
| 0.03224 | 260 | 38.45 | | | | 1.24E-04 |
| 0.02976 | 240 | 41.66 | | | | 7.93E-05 |
| 0.02728 | 220 | 45.44 | | | | 2.84E-05 |
| 0.02604 | 210 | 47.61 | | | | 2.68E-04 |
| 0.02480 | 200 | 50.00 | | | | 4.28E-04 |
| 0.02356 | 190 | 52.62 | | | | 1.24E-03 |
| 0.02232 | 180 | 55.54 | | | | 1.49E-03 |

[a]The reference from which the values were extracted is given in brackets next to the first value. The nominal alloy compositions are: x=0.803 [6], x=0.782 [8], x=0.800 obtained by interpolating the data of Braunstein et al. [4], x=0.800 [11].

# Lead Tin Telluride (PbSnTe)

H. PILLER
Louisiana State University
Baton Rouge, Louisiana

There are many alloys of $Pb_{1-x}Sn_xTe$. We can tabulate data only for a very few on the Pb-rich side. Also, it is not possible to find the same $x$ value over a wide spectral range. The reflectivity of the lead-salt narrow-gap alloy PbSnTe was studied by Korn and Braunstein [1, 2]. Measurements of near-normal reflectivity were made at room temperature in the photon-energy range of 0.5–13 eV. Czochralski-grown $p$-type bulk samples were used in the measurements. Samples were cut, ground, and hand-polished to produce optical-quality surfaces. After an electrochemical etch, samples were immediately placed in a vacuum (at least $10^{-5}$ torr), and spectral scans were begun. Consistent results were obtained upon repreparation of sample surfaces. The maximum estimated absolute reflectance error throughout the spectral range was at most 2%. The optical constants $n$ and $k$ were obtained through a Kramers–Kronig computation. $Pb_{1-x}Sn_xTe$ can be grown throughout the range $0 \leqslant x \leqslant 1$. PbTe and SnTe both crystallize in the rocksalt structure, and both have interband optical transitions at the $L$ point in the Brillouin zone. The width of the direct energy gap changes with the composition of the alloy; as $x$ increases, the band gap first decreases and then increases. The optical constants are listed in Table II. Columns 4 and 5 show $n$ and $k$ for $x = 0.17$ and columns 6 and 7 for $x = 0.09$. Both samples were $p$-type single crystals. Values of $n$ and $k$ for $x = 0.19 \pm 0.02$ are plotted in Fig. 1.

Drabkin *et al.* [3] measured the variation of the absorption coefficient in $Pb_{1-x}Sn_xTe$ for $x = 0.2$ and $x = 0.1$ with carrier densities $n_e = 8 \times 10^{17}$ and $n_p = 2.5 \times 10^{18}\ cm^{-3}$, respectively. The measurements were made in the photon-energy region 0.2–0.8 eV. The data were obtained from epitaxial films at 300 K. The films were single crystals. The lattice constants of the films were identical with the constants of the bulk samples, which shows that the evaporation did not alter the composition. The thicknesses of the samples were 1.92 and 1.48 μm, respectively. The $k$ data were calculated from the absorption coefficients given in the graph [3], which are readable to three figures. The corresponding $k$ values for $x = 0.2$ and $x = 0.1$ are


Copyright © 1991 by Academic Press.
All rights of reproduction in any form reserved.
ISBN 0-12-544422-2

listed in Table II (columns 5 and 7) and $k$ for $x=0.2$ is plotted in Fig. 1. Good agreement with experiment was found by calculating the data from a two-band Kane model. The following energy gaps were used in the calculations: 0.207 eV for $x=0.2$ and 0.25 eV for $x=0.1$.

McKnight and El-Rayess [4] measured the far-infrared reflectivity of films of indium-doped $Pb_{1-x}Sn_xTe$ from 40–240 $cm^{-1}$. The films were grown from sources with $x=0.21$ and 0.25 on $BaF_2$ substrates. The measurements were made at 300, 150, 80, 25, 20, 15, and 8 K. Both samples were doped with In at levels above 0.5 atomic percent. In "sufficiently doped" samples, the indium centers pin the Fermi level by binding carriers usually present because of deviations from metal-chalcogenide stochiometry. The sample with $x=0.21$ was estimated to be 15 μm thick and the sample with $x=0.25$ was 19 μm thick. Data were ratioed versus a coin-silver mirror of near-unit reflectivity. Multiple runs were made and the data averaged to achieve a standard deviation of about 1%. A fit to the reflectivity of the $x=0.21$ sample at 300 K was made assuming a film dielectric function, based on a classical two-oscillator (plasmon–phonon) model of the following form:

$$\varepsilon(\omega)=\varepsilon_\infty\left[\frac{(\omega_L^2-\omega^2)}{(\omega_T^2-\omega^2-i\Gamma\omega)}\right]-\frac{\omega_p^2}{\omega(\omega+i/\tau)}.$$

Here $\omega_T$ and $\omega_L$ are the transverse and longitudinal optical phonon frequencies, respectively. $\omega_P$ is the plasma frequency. A very good fit to the experimental reflectivity was obtained with the following parameters: $\omega_T=32\ cm^{-1}$, $\omega_L=111\ cm^{-1}$, $\omega_P=402\ cm^{-1}$, $1/\tau=88.4\ cm^{-1}$, $\Gamma=17.2\ cm^{-1}$, $\varepsilon_\infty=42.5$. The carrier concentration was estimated to be below $10^{17}\ cm^{-3}$. We calculated the optical constants $n$ and $k$ from the dielectric constant using the parameters given above. These data are listed in Table II. A smooth plot of the $n$ and $k$ data is given in Fig. 1.

McKnight and El-Rayess [5] measured also the far-infrared reflectivity of indium-doped $Pb_{1-x}Sn_xTe$ films with $x=0.25$ and $x=0.21$ under high hydrostatic pressure. The measurements were made in the region 50–200 $cm^{-1}$. The primary effect of the hydrostatic pressure is to decrease the band gap by about 7.4 meV/kbar. An increase in the plasma frequency was observed with increasing hydrostatic pressure. This is consistent with the observed large relative decrease in the narrow band gap and hence the effective mass. Carrier freeze-out and semi-insulating behavior was observed at low temperatures.

Takaoka *et al.* [6] measured the far-infrared magnetoplasma spectra in 1 at.% indium-doped $Pb_{1-x}Sn_xTe$ single crystals across the band-inversion region between $x=0.15$ and 0.40 at temperatures between 4.2 and 20 K. They observed that the band-edge masses and the energy gaps seem not to reach zero at the band-inversion tin composition ($x=0.35$) [7].

Takaoka and Murase [8] observed the local vibration mode of indium atoms in $Pb_{1-x}Sn_xTe$ at 160 $cm^{-1}$ by far-infrared absorption measurements.

Dornhaus *et al.* [9] reviewed the optical properties, including dielectric properties and phonon spectra. The dielectric properties of the mixed-crystal $Pb_{1-x}Sn_xTe$ were extensively investigated. They are characterized by large static and optical dielectric constants. Lehmann *et al.* [10] measured the dielectric properties of epitaxial $Pb_{1-x}Sn_xTe$ layers in a range between $x=0$ and 0.225 at 9 GHz. Their results show that the static dielectric constant ($\varepsilon_s$) does not depend on the effective band gap. The authors measured $\varepsilon_s=230$ in an *n*-type sample with $x=0.2$ with a carrier concentration of $2\times10^{17}$ $cm^{-3}$ at 300 K and $\varepsilon_s=1850$ with a carrier concentration of $0.14\times10^{17}$ $cm^{-3}$ at 77 K. The temperature dependence of the static dielectric constant and of the TO phonon energy was investigated in many experiments, including neutron scattering experiments [9].

Table I is a summary of the *n* and *k* data for various values of *x*. We have plotted *n* and *k* only for $x=0.19\pm0.02$ over the widest possible spectral range, thus omitting plots for other *x* values in Table II.

## REFERENCES


1. D. M. Korn, thesis (UCLA, 1971) (unpublished).
2. D. M. Korn and R. Braunstein, *Phys. Rev. B* **5**, 4837 (1972).
3. I. A. Drabkin, L. Ya. Morgovsky, I. V. Nelson, Yu. I. Ravich, *Sov. Phys. Semicond.* **6**, 1156 (1973).
4. S. W. McKnight and M. K. El-Rayess, *Solid State Commun.* **49**, 1001 (1984).
5. S. W. McKnight and M. K. El-Rayess, "Proc. Int. Conf. Semicond. Phys., San Francisco," 1984, Springer-Verlag, New York, 1389 (1984).
6. S. Takaoka, S. Shimomura, H. Takahashi, and K. Murase, *Phys. Rev. B* **40**, 5642 (1989).
7. J. F. Butler, *Solid State Commun.* **7**, 909 (1969).
8. S. Takaoka and K. Murase, *J. Phys. Soc. Jpn.* **52**, 25 (1983).
9. R. Dornhaus, G. Nimtz, and B. Schlicht, in "Narrow-Gap Semiconductors," Springer-Verlag, Berlin, (1983).
10. H. Lehmann, G. Nimtz, L. D. Haas, and T. Jakobus, *Appl. Phys.* **25**, 291 (1981).

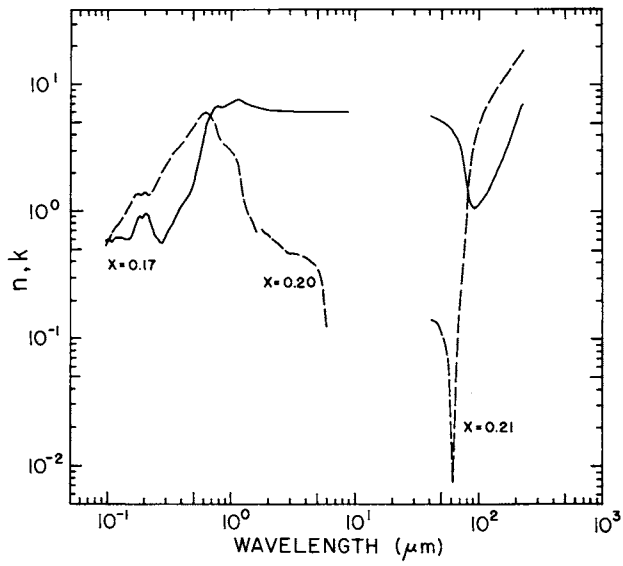


**Fig. 1.** Log–log plot of $n$ (solid line) and $k$ (dashed line) versus wavelength in micrometers for $Pb_{1-x}Sn_xTe$ with $x = 0.19 \pm 0.02$.

**TABLE I**

**Values of $x$ for Which Data for $n$ and $k$ Are Presented in Table II**

| $x$ | UV–VIS (13–0.5 eV) $n$ & $k$ | Near IR (0.8–0.2 eV) $k$ | Far IR (240–40 $cm^{-1}$) $n$ & $k$ |
|---|---|---|---|
| 0 | See PbTe *HOC I* | | |
| 0.09 | *X* | | |
| 0.1 | | *X* | |
| 0.17[a] | *X* | | |
| 0.2[a] | | *X* | |
| 0.21[a] | | | *x* |
| 1 | See SnTe *HOC II* | | |

[a] Plotted in Fig. 1.

**TABLE II**

**Values of $n$ and $k$ for $Pb_{1-x}Sn_xTe$ Obtained from Various References[a]**

| eV | μm | n | k | n | k |
|---|---|---|---|---|---|
| | | x = 0.17 | | x = 0.09 | |
| 12.86 | 0.0964 | | | 0.597 [1] | |
| 12.84 | 0.0966 | | 0.531 [1] | | |
| 12.82 | 0.0967 | 0.606 [1] | | | 0.461 [1] |
| 12.75 | 0.0972 | | 0.527 | 0.598 | |
| 12.74 | 0.0973 | 0.608 | | | |
| 12.71 | 0.0975 | | | | 0.462 |
| 12.66 | 0.0980 | | 0.528 | | |
| 12.64 | 0.0981 | 0.574 | | | |
| 12.62 | 0.0982 | | | | 0.495 |
| 12.59 | 0.0985 | | | 0.600 | |
| 12.50 | 0.0992 | | | | 0.497 |
| 12.43 | 0.0998 | 0.578 | 0.566 | | |
| 12.41 | 0.0999 | | | 0.602 | |
| 12.30 | 0.1008 | 0.580 | | | |
| 12.27 | 0.1010 | | | | 0.505 |
| 12.25 | 0.1012 | | | 0.589 | |
| 12.20 | 0.1016 | | 0.597 | | |
| 12.12 | 0.1023 | 0.583 | | | |
| 12.07 | 0.1027 | | | | 0.530 |
| 12.03 | 0.1031 | | 0.618 | 0.572 | |
| 11.92 | 0.1040 | 0.603 | | | |
| 11.91 | 0.1041 | | | | 0.532 |
| 11.83 | 0.1048 | | 0.613 | 0.574 | |
| 11.79 | 0.1052 | | | | 0.562 |
| 11.76 | 0.1055 | 0.606 | | | |
| 11.62 | 0.1067 | | | 0.577 | 0.557 |
| 11.55 | 0.1073 | | 0.648 | | |
| 11.54 | 0.1074 | 0.574 | | | |
| 11.45 | 0.1083 | | | | 0.583 |
| 11.43 | 0.1085 | | 0.650 | | |
| 11.39 | 0.1089 | | | 0.579 | |
| 11.33 | 0.1095 | 0.578 | | | |
| 11.23 | 0.1104 | | | | 0.610 |
| 11.21 | 0.1106 | | | 0.581 | |
| 11.19 | 0.1108 | | 0.683 | | |
| 11.12 | 0.1115 | 0.582 | | | |
| 11.04 | 0.1124 | | | | 0.645 |
| 11.02 | 0.1125 | | 0.716 | | |
| 10.96 | 0.1131 | | | 0.600 | |
| 10.93 | 0.1135 | 0.585 | | | |
| 10.89 | 0.1139 | | | | 0.675 |
| 10.86 | 0.1142 | | 0.741 | | |
| 10.81 | 0.1146 | 0.617 | | | |

**TABLE II (*Continued*)**

**$Pb_{1-x}Sn_xTe$**

| eV | μm | n | k | n | k |
|---|---|---|---|---|---|
| 10.78 | 0.1151 | | | 0.625 | |
| 10.71 | 0.1157 | | 0.760 | | |
| 10.67 | 0.1162 | 0.619 | | | 0.678 |
| 10.58 | 0.1172 | | | 0.659 | |
| 10.54 | 0.1176 | | 0.762 | | |
| 10.49 | 0.1182 | 0.623 | | | 0.665 |
| 10.41 | 0.1192 | | | 0.674 | |
| 10.33 | 0.1200 | | 0.785 | | |
| 10.32 | 0.1202 | | | | 0.658 |
| 10.31 | 0.1203 | 0.607 | | | |
| 10.22 | 0.1213 | | | 0.659 | |
| 10.15 | 0.1222 | | | | 0.662 |
| 10.12 | 0.1225 | 0.610 | | | |
| 10.10 | 0.1228 | | 0.788 | | |
| 9.973 | 0.1243 | | | 0.660 | |
| 9.970 | 0.1244 | 0.613 | | | |
| 9.930 | 0.1249 | | | | 0.665 |
| 9.898 | 0.1253 | | 0.818 | | |
| 9.789 | 0.1267 | 0.626 | | | |
| 9.750 | 0.1272 | | | 0.630 | |
| 9.706 | 0.1277 | | 0.834 | | |
| 9.706 | 0.1278 | | | | 0.668 |
| 9.593 | 0.1292 | 0.606 | | | |
| 9.549 | 0.1298 | | | 0.600 | |
| 9.509 | 0.1304 | | | | 0.671 |
| 9.455 | 0.1311 | 0.613 | | | |
| 9.454 | 0.1312 | | 0.865 | | |
| 9.328 | 0.1329 | | | | 0.705 |
| 9.303 | 0.1333 | | | 0.556 | |
| 9.284 | 0.1336 | | 0.901 | | |
| 9.270 | 0.1338 | 0.616 | | | |
| 9.158 | 0.1354 | | | | 0.756 |
| 9.101 | 0.1362 | | 0.927 | | |
| 9.089 | 0.1364 | 0.619 | | | |
| 9.059 | 0.1369 | | | 0.531 | |
| 8.996 | 0.1378 | | | | 0.786 |
| 8.948 | 0.1386 | | 0.954 | | |
| 8.866 | 0.1398 | 0.593 | | | |
| 8.861 | 0.1399 | | | 0.508 | |
| 8.765 | 0.1415 | | 1.005 | | |
| 8.746 | 0.1418 | | | | 0.819 |
| 8.670 | 0.1430 | 0.596 | | | |
| 8.602 | 0.1441 | | | 0.494 | |
| 8.575 | 0.1446 | | 1.033 | | |
| 8.525 | 0.1454 | | | | 0.878 |
| 8.449 | 0.1467 | 0.600 | | | |

**TABLE II (*Continued*)**

**$Pb_{1-x}Sn_xTe$**

| eV | μm | n | k | n | k |
|---|---|---|---|---|---|
| 8.405 | 0.1475 | | | 0.496 | |
| 8.398 | 0.1476 | | 1.095 | | |
| 8.336 | 0.1487 | | | | 0.961 |
| 8.298 | 0.1494 | 0.601 | | | |
| 8.274 | 0.1498 | | 1.093 | | |
| 8.246 | 0.1504 | | | 0.492 | |
| 8.155 | 0.1520 | | | | 1.001 |
| 8.149 | 0.1522 | 0.604 | | | |
| 8.079 | 0.1535 | | 1.157 | | |
| 8.041 | 0.1542 | | | | 1.062 |
| 8.025 | 0.1545 | | | 0.495 | |
| 7.990 | 0.1552 | 0.619 | | | |
| 7.915 | 0.1566 | | 1.219 | | |
| 7.894 | 0.1571 | | | 0.530 | |
| 7.875 | 0.1574 | | | | 1.105 |
| 7.821 | 0.1585 | 0.658 | | | |
| 7.736 | 0.1603 | | 1.259 | | |
| 7.730 | 0.1604 | | | | 1.141 |
| 7.648 | 0.1621 | 0.695 | | | |
| 7.632 | 0.1625 | | | 0.553 | |
| 7.544 | 0.1644 | | | | 1.212 |
| 7.509 | 0.1651 | | 1.325 | | |
| 7.465 | 0.1661 | 0.743 | | | |
| 7.406 | 0.1674 | | | 0.619 | 1.244 |
| 7.356 | 0.1686 | | 1.370 | | |
| 7.310 | 0.1696 | 0.800 | | | |
| 7.262 | 0.1707 | | | | 1.266 |
| 7.199 | 0.1722 | | | 0.653 | |
| 7.162 | 0.1731 | 0.823 | | | |
| 7.133 | 0.1738 | | 1.382 | | |
| 7.088 | 0.1749 | | | | 1.269 |
| 7.038 | 0.1762 | | | 0.702 | |
| 6.997 | 0.1772 | 0.890 | | | |
| 6.954 | 0.1783 | | 1.369 | | |
| 6.903 | 0.1796 | | | 0.737 | |
| 6.895 | 0.1798 | 0.903 | | | |
| 6.871 | 0.1805 | | | | 1.292 |
| 6.774 | 0.1830 | | 1.325 | | |
| 6.718 | 0.1846 | | | 0.739 | |
| 6.714 | 0.1847 | 0.910 | | | |
| 6.673 | 0.1858 | | | | 1.291 |
| 6.611 | 0.1875 | | 1.327 | | |
| 6.543 | 0.1895 | 0.886 | | | |
| 6.533 | 0.1898 | | | 0.741 | |
| 6.496 | 0.1909 | | | | 1.353 |
| 6.467 | 0.1917 | | 1.355 | | |

TABLE II (*Continued*)

$Pb_{1-x}Sn_xTe$

| eV | $cm^{-1}$ | μm | n | k | n | k |
|---|---|---|---|---|---|---|
| 6.368 | | 0.1947 | 0.889 | | | |
| 6.355 | | 0.1951 | | | 0.743 | 1.344 |
| 6.342 | | 0.1955 | | 1.394 | | |
| 6.202 | | 0.1999 | | 1.390 | | |
| 6.198 | | 0.2000 | 0.939 | | | |
| 6.186 | | 0.2004 | | | 0.752 | |
| 6.180 | | 0.2006 | | | | 1.410 |
| 6.059 | | 0.2046 | 0.955 | | | |
| 6.037 | | 0.2054 | | | 0.802 | |
| 6.019 | | 0.2060 | | 1.407 | | |
| 5.976 | 48197 | 0.2075 | | | | 1.386 |
| 5.945 | 47949 | 0.2086 | | | 0.803 | |
| 5.941 | 47915 | 0.2087 | 0.947 | | | |
| 5.850 | 47184 | 0.2119 | | 1.359 | | |
| 5.796 | 46751 | 0.2139 | 0.916 | | | |
| 5.757 | 46436 | 0.2154 | | | 0.779 | |
| 5.752 | 46396 | 0.2155 | | | | 1.344 |
| 5.683 | 45839 | 0.2182 | | 1.327 | | |
| 5.663 | 45678 | 0.2189 | 0.900 | | | |
| 5.582 | 45025 | 0.2221 | | | 0.706 | |
| 5.549 | 44754 | 0.2235 | | | | 1.369 |
| 5.534 | 44635 | 0.2240 | | 1.361 | | |
| 5.492 | 44296 | 0.2258 | 0.819 | | | |
| 5.393 | 43494 | 0.2299 | | | | 1.444 |
| 5.379 | 43388 | 0.2305 | | | 0.644 | |
| 5.357 | 43206 | 0.2315 | 0.752 | 1.395 | | |
| 5.216 | 42071 | 0.2377 | | | 0.616 | |
| 5.209 | 42010 | 0.2380 | | | | 1.548 |
| 5.174 | 41733 | 0.2396 | 0.704 | | | |
| 5.139 | 41452 | 0.2413 | | 1.504 | | |
| 5.062 | 40829 | 0.2449 | | | 0.582 | |
| 5.046 | 40698 | 0.2457 | 0.631 | | | |
| 5.017 | 40466 | 0.2471 | | | | 1.642 |
| 4.967 | 40060 | 0.2496 | | 1.613 | | |
| 4.867 | 39258 | 0.2547 | | | 0.584 | |
| 4.859 | 39189 | 0.2552 | 0.614 | | | |
| 4.848 | 39103 | 0.2557 | | | | 1.743 |
| 4.764 | 38428 | 0.2602 | | 1.739 | | |
| 4.727 | 38128 | 0.2623 | | | | 1.797 |
| 4.678 | 37732 | 0.2650 | | | 0.586 | |
| 4.632 | 37359 | 0.2677 | 0.569 | | | |
| 4.629 | 37339 | 0.2678 | | 1.862 | | |
| 4.597 | 37079 | 0.2697 | | | | 1.871 |
| 4.498 | 36280 | 0.2756 | | 1.982 | | |
| 4.489 | 36206 | 0.2762 | | | 0.588 | |
| 4.467 | 36031 | 0.2775 | 0.553 | | | |

**TABLE II (*Continued*)**

**$Pb_{1-x}Sn_xTe$**

| eV | $cm^{-1}$ | μm | n | k | n | k |
|---|---|---|---|---|---|---|
| 4.434 | 35763 | 0.2796 | | | | 1.987 |
| 4.346 | 35056 | 0.2853 | 0.584 | | | |
| 4.337 | 34982 | 0.2859 | | 2.130 | | |
| 4.304 | 34711 | 0.2881 | | | 0.590 | |
| 4.295 | 34641 | 0.2887 | | | | 2.083 |
| 4.245 | 34238 | 0.2921 | | 2.224 | | |
| 4.184 | 33744 | 0.2964 | | | | 2.159 |
| 4.168 | 33616 | 0.2975 | 0.634 | | | |
| 4.106 | 33119 | 0.3019 | | 2.355 | | |
| 4.082 | 32923 | 0.3037 | | | | 2.246 |
| 4.077 | 32882 | 0.3041 | | | 0.581 | |
| 4.038 | 32569 | 0.3070 | 0.688 | | | |
| 3.982 | 32119 | 0.3114 | | | | 2.346 |
| 3.971 | 32032 | 0.3122 | | 2.491 | | |
| 3.907 | 31509 | 0.3174 | | | 0.609 | |
| 3.864 | 31162 | 0.3209 | | | | 2.434 |
| 3.860 | 31129 | 0.3213 | 0.735 | | | |
| 3.821 | 30821 | 0.3245 | | 2.602 | | |
| 3.766 | 30378 | 0.3292 | | | 0.633 | |
| 3.760 | 30327 | 0.3297 | | | | 2.532 |
| 3.729 | 30079 | 0.3325 | 0.767 | | | |
| 3.690 | 29762 | 0.3360 | | 2.719 | | |
| 3.641 | 29363 | 0.3406 | | | | 2.687 |
| 3.623 | 29218 | 0.3423 | | | 0.670 | |
| 3.598 | 29021 | 0.3446 | | 2.855 | | |
| 3.590 | 28958 | 0.3453 | 0.833 | | | |
| 3.526 | 28443 | 0.3516 | | | | 2.832 |
| 3.468 | 27968 | 0.3576 | | | 0.717 | |
| 3.465 | 27947 | 0.3578 | | 2.977 | | |
| 3.461 | 27912 | 0.3583 | 0.897 | | | |
| 3.413 | 27524 | 0.3633 | | | | 2.989 |
| 3.360 | 27099 | 0.3690 | | 3.096 | | |
| 3.331 | 26869 | 0.3722 | | | 0.773 | |
| 3.296 | 26587 | 0.3761 | | | | 3.125 |
| 3.294 | 26570 | 0.3764 | 0.999 | | | |
| 3.240 | 26132 | 0.3827 | | 3.230 | | |
| 3.186 | 25697 | 0.3892 | 1.091 | | | 3.266 |
| 3.182 | 25668 | 0.3896 | | | 0.857 | |
| 3.098 | 24983 | 0.4003 | | 3.355 | | |
| 3.074 | 24790 | 0.4034 | | | | 3.400 |
| 3.017 | 24330 | 0.4110 | | | 0.941 | |
| 2.982 | 24049 | 0.4158 | | 3.514 | | |
| 2.959 | 23869 | 0.4190 | 1.185 | | | |
| 2.954 | 23827 | 0.4197 | | | | 3.570 |
| 2.877 | 23207 | 0.4309 | | 3.693 | | |
| 2.867 | 23121 | 0.4325 | | | | 3.739 |

**TABLE II (*Continued*)**

**$Pb_{1-x}Sn_xTe$**

| eV | $cm^{-1}$ | μm | n | k | n | k |
|---|---|---|---|---|---|---|
| 2.845 | 22945 | 0.4358 | | | 0.995 | |
| 2.817 | 22718 | 0.4402 | 1.255 | | | |
| 2.788 | 22486 | 0.4447 | | 3.874 | | |
| 2.772 | 22354 | 0.4474 | | | | 3.901 |
| 2.729 | 22009 | 0.4544 | | | | 4.066 |
| 2.720 | 21941 | 0.4558 | | | 1.100 | |
| 2.715 | 21897 | 0.4567 | | 4.021 | | |
| 2.690 | 21695 | 0.4609 | 1.373 | | | |
| 2.662 | 21472 | 0.4657 | | | | 4.263 |
| 2.642 | 21312 | 0.4692 | | 4.203 | | |
| 2.607 | 21030 | 0.4755 | | | 1.223 | |
| 2.599 | 20958 | 0.4771 | 1.493 | | | |
| 2.597 | 20948 | 0.4774 | | | | 4.441 |
| 2.569 | 20719 | 0.4827 | | 4.455 | | |
| 2.519 | 20318 | 0.4922 | | | | 4.621 |
| 2.498 | 20150 | 0.4963 | 1.635 | 4.641 | | |
| 2.484 | 20033 | 0.4992 | | | 1.396 | |
| 2.482 | 20021 | 0.4995 | | | | 4.808 |
| 2.444 | 19711 | 0.5073 | | 4.791 | | |
| 2.434 | 19630 | 0.5094 | 1.798 | | | |
| 2.407 | 19410 | 0.5152 | | | | 5.024 |
| 2.394 | 19312 | 0.5178 | | | 1.632 | |
| 2.379 | 19188 | 0.5212 | 1.978 | | | |
| 2.374 | 19147 | 0.5223 | | 5.030 | | |
| 2.364 | 19070 | 0.5244 | | | | 5.226 |
| 2.342 | 18891 | 0.5294 | | 5.182 | | |
| 2.340 | 18874 | 0.5298 | | | 1.812 | |
| 2.324 | 18742 | 0.5336 | | | | 5.402 |
| 2.317 | 18687 | 0.5351 | 2.167 | | | |
| 2.279 | 18383 | 0.5440 | | 5.382 | | |
| 2.278 | 18376 | 0.5442 | | | 2.000 | |
| 2.275 | 18347 | 0.5451 | 2.430 | | | |
| 2.261 | 18232 | 0.5485 | | | | 5.579 |
| 2.245 | 18107 | 0.5523 | | | 2.205 | |
| 2.236 | 18037 | 0.5544 | | | | 5.728 |
| 2.229 | 17978 | 0.5562 | | 5.565 | | |
| 2.218 | 17890 | 0.5590 | 2.613 | | | |
| 2.195 | 17707 | 0.5648 | | | 2.477 | 5.865 |
| 2.183 | 17603 | 0.5681 | 2.823 | | | |
| 2.170 | 17500 | 0.5715 | | 5.754 | | |
| 2.158 | 17407 | 0.5745 | 3.033 | | | |
| 2.150 | 17340 | 0.5767 | | | | 5.980 |
| 2.142 | 17273 | 0.5790 | | | 2.705 | |
| 2.126 | 17150 | 0.5831 | 3.242 | | | |
| 2.125 | 17141 | 0.5834 | | | 2.932 | |
| 2.113 | 17045 | 0.5867 | | 5.884 | | |

**TABLE II** (*Continued*)

**$Pb_{1-x}Sn_xTe$**

| eV | $cm^{-1}$ | μm | n | k | n | k |
|---|---|---|---|---|---|---|
| 2.104 | 16972 | 0.5892 | | | | 6.064 |
| 2.103 | 16963 | 0.5895 | | | 3.145 | |
| 2.098 | 16918 | 0.5911 | 3.419 | | | |
| 2.073 | 16720 | 0.5981 | 3.618 | | | |
| 2.071 | 16705 | 0.5986 | | | 3.315 | |
| 2.071 | 16704 | 0.5987 | | | | 6.100 |
| 2.070 | 16692 | 0.5991 | | | 3.513 | |
| 2.064 | 16646 | 0.6008 | | 5.963 | | |
| 2.062 | 16627 | 0.6014 | 3.814 | | | |
| 2.026 | 16337 | 0.6121 | 4.004 | | | |
| 2.017 | 16271 | 0.6146 | | 5.986 | | |
| 2.014 | 16241 | 0.6157 | | | 3.722 | |
| 2.000 | 16130 | 0.6200 | | | | 6.101 |
| 1.986 | 16022 | 0.6242 | 4.226 | | | |
| 1.986 | 16018 | 0.6243 | | | 3.940 | |
| 1.982 | 15985 | 0.6256 | | 5.992 | | |
| 1.972 | 15908 | 0.6286 | | | 4.249 | |
| 1.962 | 15823 | 0.6320 | 4.420 | | | |
| 1.954 | 15758 | 0.6346 | 4.601 | | | |
| 1.946 | 15693 | 0.6372 | | 5.942 | | |
| 1.939 | 15641 | 0.6394 | | | | 6.042 |
| 1.937 | 15619 | 0.6403 | 4.795 | | | |
| 1.919 | 15478 | 0.6461 | | | 4.521 | |
| 1.908 | 15386 | 0.6500 | 4.960 | | | |
| 1.907 | 15383 | 0.6501 | | | | 5.893 |
| 1.892 | 15259 | 0.6554 | | | 4.786 | |
| 1.891 | 15249 | 0.6558 | 5.168 | | | |
| 1.858 | 14984 | 0.6674 | | 5.784 | | |
| 1.855 | 14959 | 0.6685 | 5.358 | | | |
| 1.851 | 14929 | 0.6698 | | | 4.996 | |
| 1.845 | 14878 | 0.6722 | | | | 5.683 |
| 1.824 | 14712 | 0.6797 | | | 5.285 | |
| 1.824 | 14710 | 0.6798 | 5.512 | | | |
| 1.815 | 14642 | 0.6830 | 5.672 | | | |
| 1.809 | 14590 | 0.6854 | | | | 5.532 |
| 1.801 | 14522 | 0.6886 | | 5.546 | | |
| 1.791 | 14446 | 0.6922 | | | 5.533 | |
| 1.788 | 14425 | 0.6933 | 5.845 | | | |
| 1.784 | 14385 | 0.6952 | | | | 5.316 |
| 1.770 | 14275 | 0.7006 | | 5.333 | | |
| 1.747 | 14089 | 0.7098 | 6.027 | | | |
| 1.745 | 14072 | 0.7106 | | | 5.755 | |
| 1.728 | 13934 | 0.7177 | | 5.094 | | |
| 1.725 | 13912 | 0.7188 | | | | 5.128 |
| 1.723 | 13896 | 0.7196 | 6.269 | | | |
| 1.698 | 13693 | 0.7303 | | | | 4.920 |

**TABLE II (*Continued*)**

**$Pb_{1-x}Sn_xTe$**

| eV | $cm^{-1}$ | μm | n | k | n | k |
|---|---|---|---|---|---|---|
| 1.688 | 13613 | 0.7346 | | 4.900 | | |
| 1.686 | 13602 | 0.7352 | | | 5.915 | |
| 1.673 | 13490 | 0.7413 | 6.486 | | | |
| 1.660 | 13385 | 0.7471 | | | | 4.724 |
| 1.650 | 13306 | 0.7515 | 6.574 | | | |
| 1.646 | 13275 | 0.7533 | | 4.685 | | |
| 1.633 | 13168 | 0.7595 | 6.661 | | | |
| 1.632 | 13162 | 0.7598 | | 4.464 | | |
| 1.612 | 12998 | 0.7694 | | | 6.099 | |
| 1.602 | 12918 | 0.7741 | | 4.283 | | |
| 1.594 | 12858 | 0.7777 | 6.710 | | | |
| 1.591 | 12831 | 0.7794 | | | | 4.480 |
| 1.570 | 12659 | 0.7900 | | 4.106 | | |
| 1.569 | 12655 | 0.7902 | 6.660 | | | |
| 1.545 | 12461 | 0.8025 | | 3.942 | | |
| 1.531 | 12348 | 0.8099 | | | | 4.339 |
| 1.520 | 12256 | 0.8159 | | | 6.259 | |
| 1.512 | 12197 | 0.8199 | | 3.714 | | |
| 1.486 | 11985 | 0.8344 | 6.609 | | | |
| 1.468 | 11841 | 0.8445 | | | | 4.260 |
| 1.437 | 11589 | 0.8629 | | 3.516 | | |
| 1.432 | 11551 | 0.8657 | | | 6.496 | |
| 1.421 | 11465 | 0.8722 | 6.661 | | | |
| 1.403 | 11315 | 0.8838 | | | | 4.137 |
| 1.390 | 11211 | 0.8920 | | 3.354 | | |
| 1.379 | 11125 | 0.8989 | 6.710 | | | |
| 1.371 | 11059 | 0.9043 | | | 6.744 | |
| 1.338 | 10789 | 0.9269 | | | 6.951 | |
| 1.335 | 10770 | 0.9285 | | | | 3.985 |
| 1.326 | 10692 | 0.9353 | 6.848 | | | |
| 1.303 | 10513 | 0.9512 | | 3.164 | | |
| 1.297 | 10460 | 0.9560 | | | | 3.777 |
| 1.295 | 10442 | 0.9577 | | | 7.131 | |
| 1.274 | 10274 | 0.9734 | | | 7.285 | |
| 1.262 | 10178 | 0.9825 | 7.051 | | | |
| 1.251 | 10091 | 0.9910 | | 3.014 | | |
| 1.246 | 10049 | 0.9952 | | | | 3.598 |
| 1.240 | 10004 | 0.9997 | | | 7.486 | |
| 1.231 | 9929 | 1.007 | | | 7.674 | |
| 1.208 | 9743 | 1.026 | | | | 3.419 |
| 1.197 | 9652 | 1.036 | | | | 3.278 |
| 1.190 | 9599 | 1.042 | 7.221 | | | |
| 1.190 | 9598 | 1.042 | | | | 3.054 |
| 1.187 | 9574 | 1.044 | | 2.822 | | |
| 1.183 | 9543 | 1.048 | | | 7.933 | |
| 1.179 | 9511 | 1.051 | | | 8.094 | |

**TABLE II (*Continued*)**

**$Pb_{1-x}Sn_xTe$**

| eV | $cm^{-1}$ | μm | n | k | n | k |
|---|---|---|---|---|---|---|
| 1.174 | 9472 | 1.056 | | | | 2.873 |
| 1.172 | 9456 | 1.058 | | | | 2.716 |
| 1.147 | 9247 | 1.081 | | | 8.190 | |
| 1.146 | 9243 | 1.082 | | | | 2.563 |
| 1.143 | 9220 | 1.085 | | | | 2.356 |
| 1.138 | 9178 | 1.090 | | | 8.260 | |
| 1.134 | 9145 | 1.093 | 7.423 | | | |
| 1.132 | 9130 | 1.095 | | 2.602 | | |
| 1.119 | 9022 | 1.108 | | | | 2.198 |
| 1.117 | 9008 | 1.110 | | | | 2.069 |
| 1.097 | 8850 | 1.130 | | 2.374 | | |
| 1.096 | 8842 | 1.131 | 7.517 | | | |
| 1.093 | 8813 | 1.135 | | | | 1.795 |
| 1.087 | 8763 | 1.141 | | | 8.183 | |
| 1.075 | 8667 | 1.154 | | 2.198 | | |
| 1.074 | 8659 | 1.155 | 7.609 | | | |
| 1.061 | 8558 | 1.168 | | | 8.080 | |
| 1.061 | 8554 | 1.169 | | 1.972 | | |
| 1.060 | 8549 | 1.170 | | | 7.972 | |
| 1.043 | 8415 | 1.188 | | | | 1.607 |
| 1.040 | 8387 | 1.192 | | 1.813 | | |
| 1.037 | 8368 | 1.195 | 7.570 | | | |
| 1.033 | 8330 | 1.201 | | | | 1.373 |
| 1.023 | 8252 | 1.212 | 7.496 | | | |
| 1.017 | 8202 | 1.219 | | | 7.803 | |
| 1.011 | 8156 | 1.226 | | 1.467 | | |
| 1.006 | 8114 | 1.232 | | 1.649 | | |
| 0.9968 | 8040 | 1.244 | 7.382 | | | |
| 0.9949 | 8024 | 1.246 | | | | 1.202 |
| 0.9739 | 7855 | 1.273 | | | 7.624 | |
| 0.9713 | 7834 | 1.277 | | 1.256 | | |
| 0.9696 | 7820 | 1.279 | | | | 0.990 |
| 0.9545 | 7699 | 1.299 | 7.206 | | | |
| 0.9419 | 7597 | 1.316 | | | 7.439 | |
| 0.9363 | 7552 | 1.324 | | 1.004 | | |
| 0.9199 | 7419 | 1.348 | | | 7.298 | |
| 0.9089 | 7330 | 1.364 | | | | 0.787 |
| 0.9005 | 7263 | 1.377 | 6.998 | | | |
| 0.8766 | 7070 | 1.414 | | | 7.106 | |
| 0.8596 | 6933 | 1.442 | | 0.850 | | |
| 0.8543 | 6890 | 1.451 | 6.811 | | | |
| 0.8330 | 6718 | 1.488 | | | 6.876 | |
| 0.8221 | 6631 | 1.508 | | | | 0.600 |
| 0.7769 | 6266 | 1.596 | | 0.660 | | |
| 0.7732 | 6237 | 1.603 | | | 6.717 | |
| 0.7537 | 6079 | 1.645 | 6.612 | | | |

**TABLE II (*Continued*)**

**$Pb_{1-x}Sn_xTe$**

| eV | $cm^{-1}$ | μm | n | k | n | k |
|---|---|---|---|---|---|---|
| 0.7417 | 5982 | 1.672 | | | | 0.463 |
| | | | | x = 0.2 | | x = 0.1 |
| 0.7119 | 5742 | 1.741 | | | | 0.607 [3] |
| 0.7052 | 5688 | 1.758 | | 0.718 [3] | | |
| 0.6990 | 5638 | 1.774 | 6.476 [1] | | | |
| 0.6913 | 5575 | 1.794 | | 0.672 | | |
| 0.6909 | 5573 | 1.794 | | | | 0.633 |
| 0.6849 | 5524 | 1.810 | | | 6.514 [1] | |
| 0.6750 | 5444 | 1.837 | | 0.665 | | |
| 0.6744 | 5439 | 1.838 | | | | 0.632 |
| 0.6582 | 5308 | 1.884 | | 0.676 | | |
| 0.6554 | 5286 | 1.892 | | | | 0.621 |
| 0.6433 | 5189 | 1.927 | | 0.659 | | |
| 0.6429 | 5185 | 1.929 | | | | 0.636 |
| 0.6287 | 5071 | 1.972 | | 0.638 | | |
| 0.6270 | 5057 | 1.978 | | | | 0.619 |
| 0.6255 | 5045 | 1.982 | 6.332 | | | |
| 0.6119 | 4935 | 2.026 | | | | 0.656 |
| 0.6116 | 4933 | 2.027 | | 0.632 | | |
| 0.6022 | 4857 | 2.059 | | | 6.312 | |
| 0.5993 | 4834 | 2.069 | | | | 0.623 |
| 0.5970 | 4815 | 2.077 | | 0.610 | | |
| 0.5857 | 4724 | 2.117 | | | | 0.624 |
| 0.5798 | 4677 | 2.138 | | 0.601 | | |
| 0.5738 | 4628 | 2.161 | 6.258 | | | |
| 0.5703 | 4600 | 2.174 | | | | 0.602 |
| 0.5644 | 4552 | 2.197 | | 0.590 | | |
| 0.5579 | 4499 | 2.222 | | | | 0.591 |
| 0.5472 | 4414 | 2.266 | | | | 0.587 |
| 0.5457 | 4401 | 2.272 | | 0.570 | | |
| 0.5309 | 4282 | 2.335 | | | | 0.591 |
| 0.5207 | 4200 | 2.381 | | | | 0.564 |
| 0.5183 | 4180 | 2.392 | | 0.558 | | |
| 0.5149 | 4153 | 2.408 | | | 6.204 | |
| 0.5110 | 4121 | 2.427 | | | | 0.574 |
| 0.5014 | 4044 | 2.473 | | | | 0.557 |
| 0.4989 | 4024 | 2.485 | | 0.548 | | |
| 0.4902 | 3954 | 2.529 | | | | 0.574 |
| 0.4812 | 3881 | 2.576 | | | | 0.585 |
| 0.4772 | 3849 | 2.598 | | 0.519 | | |
| 0.4715 | 3803 | 2.630 | | | | 0.551 |
| 0.4684 | 3777 | 2.647 | | | | 0.507 |
| 0.4676 | 3772 | 2.651 | 6.171 | | | |

**TABLE II (*Continued*)**

**$Pb_{1-x}Sn_xTe$**

| eV | $cm^{-1}$ | μm | n | k | n | k |
|---|---|---|---|---|---|---|
| 0.4617 | 3724 | 2.685 | | 0.495 | | |
| 0.4569 | 3685 | 2.714 | | 0.472 | | |
| 0.4547 | 3668 | 2.727 | | | | 0.570 |
| 0.4458 | 3595 | 2.781 | | | | 0.478 |
| 0.4367 | 3522 | 2.839 | | 0.470 | | |
| 0.4319 | 3484 | 2.871 | | | | 0.565 |
| 0.4225 | 3408 | 2.935 | | 0.470 | | |
| 0.4222 | 3405 | 2.937 | | | | 0.482 |
| 0.4164 | 3359 | 2.977 | | | 6.100 | |
| 0.4109 | 3314 | 3.017 | | | | 0.498 |
| 0.4074 | 3286 | 3.044 | | 0.464 | | |
| 0.4013 | 3236 | 3.090 | | | | 0.486 |
| 0.3920 | 3162 | 3.163 | | | | 0.483 |
| 0.3908 | 3152 | 3.172 | | 0.459 | | |
| 0.3830 | 3089 | 3.237 | | | | 0.474 |
| 0.3758 | 3031 | 3.299 | | | | 0.461 |
| 0.3745 | 3021 | 3.310 | | 0.464 | | |
| 0.3645 | 2940 | 3.401 | | | | 0.446 |
| 0.3615 | 2916 | 3.430 | | 0.454 | | |
| 0.3543 | 2858 | 3.500 | | | | 0.465 |
| 0.3486 | 2812 | 3.557 | 6.095 | | | |
| 0.3480 | 2806 | 3.563 | | | | 0.426 |
| 0.3451 | 2783 | 3.593 | | 0.448 | | |
| 0.3411 | 2751 | 3.635 | | | | 0.432 |
| 0.3319 | 2677 | 3.736 | | | | 0.417 |
| 0.3281 | 2647 | 3.779 | | 0.441 | | |
| 0.3215 | 2593 | 3.856 | | | | 0.423 |
| 0.3154 | 2543 | 3.932 | | 0.433 | | |
| 0.3143 | 2535 | 3.945 | | | | 0.393 |
| 0.3046 | 2457 | 4.071 | | | | 0.383 |
| 0.3009 | 2427 | 4.121 | | 0.421 | | |
| 0.2993 | 2414 | 4.143 | | | 6.004 | |
| 0.2897 | 2336 | 4.280 | | 0.408 | | |
| 0.2853 | 2301 | 4.346 | | | | 0.322 |
| 0.2794 | 2253 | 4.438 | | 0.400 | | |
| 0.2764 | 2229 | 4.486 | | | | 0.323 |
| 0.2734 | 2205 | 4.535 | | | | 0.288 |
| 0.2705 | 2182 | 4.583 | | 0.386 | | |
| 0.2683 | 2164 | 4.621 | | | | 0.256 |
| 0.2644 | 2132 | 4.689 | | | | 0.229 |
| 0.2634 | 2124 | 4.707 | | | 5.976 | |
| 0.2609 | 2104 | 4.752 | | | | 0.210 |
| 0.2596 | 2094 | 4.777 | | | | 0.194 |
| 0.2545 | 2053 | 4.872 | | 0.367 | | |
| 0.2542 | 2050 | 4.877 | | | | 0.167 |
| 0.2476 | 1997 | 5.008 | | 0.351 | | |

**TABLE II (*Continued*)**

**$Pb_{1-x}Sn_xTe$**

| eV | $cm^{-1}$ | μm | n | k | n | k |
|---|---|---|---|---|---|---|
| 0.2408 | 1942 | 5.149 | | 0.317 | | |
| 0.2325 | 1875 | 5.334 | | 0.286 | | |
| 0.2283 | 1841 | 5.431 | 6.052 | | | |
| 0.2265 | 1827 | 5.475 | | 0.252 | | |
| 0.2220 | 1791 | 5.584 | | 0.215 | | |
| 0.2189 | 1766 | 5.664 | | 0.177 | | |
| 0.2175 | 1754 | 5.701 | | 0.157 | | |
| 0.2138 | 1725 | 5.799 | | 0.135 | | |
| 0.2123 | 1712 | 5.841 | | 0.123 | | |
| 0.1349 | 1088 | 9.190 | 6.053 | | | |
| 0.08708 | 702 | 14.24 | | | 5.956 | |
| | | | x = 0.21 | | | |
| 0.02976 | 240 | 41.67 | 5.602 [4] | 0.139 [4] | | |
| 0.02926 | 236 | 42.37 | 5.568 | 0.138 | | |
| 0.02876 | 232 | 43.10 | 5.533 | 0.137 | | |
| 0.02827 | 228 | 43.86 | 5.495 | 0.135 | | |
| 0.02777 | 224 | 44.64 | 5.456 | 0.133 | | |
| 0.02728 | 220 | 45.46 | 5.413 | 0.131 | | |
| 0.02678 | 216 | 46.30 | 5.368 | 0.128 | | |
| 0.02628 | 212 | 47.17 | 5.320 | 0.125 | | |
| 0.02579 | 208 | 48.08 | 5.269 | 0.121 | | |
| 0.02529 | 204 | 49.02 | 5.214 | 0.117 | | |
| 0.02480 | 200 | 50.00 | 5.156 | 0.111 | | |
| 0.02430 | 196 | 51.02 | 5.093 | 0.106 | | |
| 0.02381 | 192 | 52.08 | 5.025 | 0.0989 | | |
| 0.02331 | 188 | 53.19 | 4.952 | 0.0911 | | |
| 0.02281 | 184 | 54.35 | 4.873 | 0.0820 | | |
| 0.02232 | 180 | 55.56 | 4.788 | 0.0715 | | |
| 0.02182 | 176 | 56.82 | 4.695 | 0.0592 | | |
| 0.02133 | 172 | 58.14 | 4.593 | 0.0448 | | |
| 0.02083 | 168 | 59.52 | 4.482 | 0.0280 | | |
| 0.02033 | 164 | 60.98 | 4.360 | 0.0080 | | |
| 0.01984 | 160 | 62.50 | 4.224 | 0.0157 | | |
| 0.01934 | 156 | 64.10 | 4.074 | 0.0442 | | |
| 0.01885 | 152 | 65.79 | 3.905 | 0.0789 | | |
| 0.01835 | 148 | 67.57 | 3.714 | 0.122 | | |
| 0.01785 | 144 | 69.45 | 3.497 | 0.176 | | |
| 0.01736 | 140 | 71.43 | 3.247 | 0.246 | | |
| 0.01686 | 136 | 73.53 | 2.955 | 0.341 | | |
| 0.01637 | 132 | 75.76 | 2.608 | 0.478 | | |
| 0.01587 | 128 | 78.13 | 2.194 | 0.691 | | |
| 0.01537 | 124 | 80.65 | 1.731 | 1.055 | | |
| 0.01488 | 120 | 83.33 | 1.345 | 1.622 | | |

**TABLE II (*Continued*)**

**$Pb_{1-x}Sn_xTe$**

| eV | $cm^{-1}$ | μm | n | k | n | k |
|---|---|---|---|---|---|---|
| 0.01438 | 116 | 86.21 | 1.145 | 2.264 | | |
| 0.01389 | 112 | 89.29 | 1.066 | 2.876 | | |
| 0.01339 | 108 | 92.59 | 1.047 | 3.455 | | |
| 0.01289 | 104 | 96.16 | 1.062 | 4.015 | | |
| 0.01240 | 100 | 100.0 | 1.100 | 4.570 | | |
| 0.01190 | 96 | 104.2 | 1.156 | 5.129 | | |
| 0.01141 | 92 | 108.7 | 1.229 | 5.702 | | |
| 0.01091 | 88 | 113.6 | 1.321 | 6.299 | | |
| 0.01041 | 84 | 119.0 | 1.432 | 6.928 | | |
| 0.009919 | 80 | 125.0 | 1.566 | 7.600 | | |
| 0.009423 | 76 | 131.6 | 1.730 | 8.325 | | |
| 0.008927 | 72 | 138.9 | 1.930 | 9.118 | | |
| 0.008431 | 68 | 147.1 | 2.180 | 9.997 | | |
| 0.007935 | 64 | 156.2 | 2.498 | 10.984 | | |
| 0.007439 | 60 | 166.7 | 2.912 | 12.109 | | |
| 0.006943 | 56 | 178.6 | 3.471 | 13.409 | | |
| 0.006447 | 52 | 192.3 | 4.253 | 14.934 | | |
| 0.005951 | 48 | 208.3 | 5.405 | 16.735 | | |
| 0.005465 | 44 | 227.3 | 7.195 | 18.840 | | |

The references are given in brackets.

# Mercury Cadmium Telluride ($Hg_{1-x}Cd_xTe$)

P. M. AMIRTHARAJ
U.S. Army Center for Night Vision and Electro-Optics
Fort Belvoir, Virginia

Mercury cadmium telluride is a II-VI ternary alloy semiconductor that belongs to the zinc-blende family and hence has much in common with other, better known semiconductors such as GaAs and InP. The overall shape of the dielectric functions $\varepsilon_1$ and $\varepsilon_2$ are similar for most of the materials of the same family, but the precise energy positions of the various spectroscopic features vary from one material to the other. The uniqueness of $Hg_{1-x}Cd_xTe$ arises from the fact that the direct gap can be varied all the way from $0(x \simeq 0.15)$ to 1.6 eV ($x = 1$). The band gap can therefore be reduced below the lowest limit attainable within the III-V family. Hence, $Hg_{1-x}Cd_xTe$ has found widespread use in the fabrication of quantum infrared detectors and is currently the leading candidate. In order of technological importance, it is perhaps next only to Si and GaAs.

The optical properties of $Hg_{1-x}Cd_xTe$ has been investigated by many investigators ever since the very first reported study by Lawson *et al.* [1]. However, the main thrust of the early work was in using spectroscopic features for obtaining information regarding the electronic band structure. Hence, the photometric accuracy available in the reports on the measurement of reflection and transmission spectra was limited, and consequently, the precision of the optical constants determined is not completely satisfactory. More recent investigations, particularly using scanning ellipsometry, have yielded optical data with substantially improved accuracy.

One must also take note of the advances in materials technology. The more recent reports of absorption measurements performed on epitaxial films with well-controlled properties, in particular $x$ and its uniformity, are clearly more dependable than the earliest reports. Hence, values compiled in this review are weighted toward the more recent papers and those that are expected to possess greater intrinsic accuracy. Comparisons to earlier work are made where warranted; the remaining earlier studies are referenced without an evaluation of the dependability and accuracy of the data.


Copyright © 1991 by Academic Press.
All rights of reproduction in any form reserved.
ISBN 0-12-544422-2

The review by Dornhaus and Nimtz [2], the compilation of several parameter values by Brice and Capper [3], and the comprehensive collection of $n$ and $k$ values of CdTe by Palik [4] are earlier works to which the reader is referred for additional information. Table I displays a summary of the data included in this review, and Fig. 1 shows a graphical plot of the variation of $n$ and $k$ for one representative alloy composition, namely $x = 0.2 \pm 0.01$. The complex forms of the dielectric function, $\varepsilon$, and the refractive index, $\mathbf{n}$, the absorption coefficient $\alpha$ and the reflectivity $R$ are reproduced below for later reference:

$$\varepsilon = \varepsilon_1 + i\varepsilon_2 \tag{1}$$

$$\mathbf{n} = n + ik \tag{2}$$

$$\mathbf{n} = \sqrt{\varepsilon} = \sqrt{(\varepsilon_1 + i\varepsilon_2)} \tag{3}$$

$$R = |(\mathbf{n}-1)/(\mathbf{n}+1)|^2 = \{(n-1)^2 + k^2\}/\{(n+1)^2 + k^2\} \tag{4}$$

$$\alpha = 4\pi k/\lambda. \tag{5}$$

The units of energy ($E$), frequency ($\omega$), and wavelength ($\lambda$) throughout this review will be eV, $cm^{-1}$, and μm, respectively.

*The Ultraviolet, Visible, and Near-Infrared Range (6–1.5 eV)*

The most complete and dependable set of ellipsometric measurements in the near-ultraviolet, visible, and near-infrared region on $Hg_{1-x}Cd_xTe$ have been reported by Arwin and Aspnes [5] and Viña *et al.* [6]. Arwin and Aspnes [5] measured $\varepsilon_1$ and $\varepsilon_2$ in the visible and near-visible energy region from 6–1.5 eV of crystalline HgTe, $Hg_{0.8}Cd_{0.2}Te$, $Hg_{0.71}Cd_{0.29}Te$ and CdTe. The samples were prepared by zone refining and were $n$-type. A detailed investigation was undertaken of the surface modifications introduced by the most commonly used chemical treatment, namely etching in a solution of $Br_2/CH_3OH$ as well as other etching procedures. A residual layer of amorphous Te ($\alpha$-Te), approximately 7 Å thick, was observed to be present on the $Br_2/CH_3OH$-treated surfaces. Figures 1 and 2 in Ref. [5] display the values of $\varepsilon_1$ and $\varepsilon_2$ corrected for the presence of the overlayers; an electronic computer record provided by Aspnes [7] was used to calculate the $n$ and $k$ values shown in Table II. The presented values are rounded off to three decimal places. Some variation can be seen in the last significant digit due to random noise. The overall absolute accuracy is ~2%. However, the ability to calculate third derivatives (to simulate electroreflectance data) suggests that the precision or relative accuracy is significantly better than that.

The ellipsometric measurements of Viña *et al.* [6] reported the $\varepsilon_1$ and $\varepsilon_2$ values for seven values of $x$: 0, 0.2, 0.43, 0.76, 0.86, 0.91, and 1.0. The samples were grown by the traveling-heater method using Te as a solvent, and sample surfaces were prepared using a chemomechanical polish of $Br_2/CH_3OH$. $\varepsilon_1$ and $\varepsilon_2$ were measured in the 5.5–1.7 eV energy region. Large figures provided by Cardona [8] were digitized using an electronic digitizer, the $n$ and $k$ values were computed, and they are displayed in Table III for all except the $x = 0.2$ sample. The digitization error in $\varepsilon_1$ and $\varepsilon_2$ is expected to be $\pm 1\%$ or $\pm 0.02$, whichever is greater. The worst errors are likely to occur in the vicinity of the zero crossing of $\varepsilon_1$ and at the smallest values of $k$. Values for the endpoint binaries, HgTe and CdTe, are included for completeness as well as to provide the reader with a standard of comparison. The numerical procedures for correcting the data for the presence of the $\alpha$-Te overlayer has been discussed by Aspnes and Arwin [9] and may be carried out where warranted.

For HgTe, the $n$ and $k$ values presented in Table III agree with those in Table II to better than ~3%, except for the $k$ values at the lowest energies, which deviate by ~10%. The CdTe values, on the other hand, display a maximum deviation of ~10% for both $n$ and $k$. In addition, a comparison of the values of Viña *et al.* [6] with those obtained from Arwin *et al.* [10] that were not corrected for the presence of the surface $\alpha$-Te layer indicates a deviation of only ~5%, half of that for the previous comparison. Hence, at least part of the disagreement between the values quoted in Table II and III is probably due to the ~7 Å-thick surface $\alpha$-Te layer. The $n$ and $k$ values in Table III are both more accurate for HgTe than for CdTe. For $x$ values of 0.43, 0.76, 0.86, and 0.91, the values presented in Table III are likely to be reliable to better than ~3% for the low-$x$ value; however, the error for the high-$x$ samples may be as high as ~10% in the worst case.

The first scanning ellipsometric measurements for HgTe were reported by Moritani *et al.* [11]. Their uncorrected $n$ and $k$ values deviate approximately 10% from those in Table II; the corrections attempted by them to account for a thin overlayer actually make the deviation much larger. The $n$ and $k$ values for CdTe were compiled earlier by Palik [4]. The values for the 1.5–4.9 eV range were obtained from the ellipsometric results of Marple and Ehrenreich [12] and the reflection and transmission investigation of Myers *et al.* [13]. Marple and Ehrenreich's [12] results agree to within ~3% of those in Table II for $n$ in the near-infrared and visible range of 1.5–3.2 eV but deviate by as much as 15% in the higher energy ultraviolet region, that is, 3.2–4.9 eV; the opposite seems to hold for $k$, with the UV values agreeing to better than ~10% but deviating much more for the visible and near IR. Both the $n$ and $k$ values of Myers *et al.* fall within 10% of those of Table II.

Single-wavelength measurements of $\varepsilon_1$ and $\varepsilon_2$ have been reported by Korsak *et al.* [14] for the He–Ne laser wavelength of 0.6328 μm for the

following $x$ values: 0, ~0.16, 0.2, ~0.29, ~0.65, and 1.0. These measurements were conducted using ellipsometry with chemomechanically polished samples; allowance was made for a naturally occurring native-oxide layer. The graphs presented in the paper were digitized and $n$ and $k$ values calculated for all but the $x = 0.2$ sample, whose values were quoted in the paper; they are presented in Table IV. The $n$ values, where a direct comparison could be made, agree to better than ~3% with those in Table II; the $k$ values for the endpoint binaries, HgTe and CdTe, agree within ~10%, but those for the alloys indicate large differences, being greater than a factor of two for $x = 0.29$.

The dominant shape of the variation of $\varepsilon_1$ and $\varepsilon_2$ with the energy is determined by transitions between the various electronic bands. The main spectroscopic features in the 6–1.5 eV range are labeled $E_1$, $E_1 + \Delta_1$ and $E_2$. The variation of these transitions with the Cd mole fraction, $x$, have been investigated by Viña *et al.* [6] and are reproduced below:

$$E_1\,(\text{eV}) = (2.147 \pm 0.005) + (0.44 \pm 0.02)x + (0.7 \pm 0.1)x^2 \tag{6}$$

$$E_1 + \Delta_1\,(\text{eV}) = (2.778 \pm 0.005) + (0.47 \pm 0.02)x + (0.6 \pm 0.1)x^2 \tag{7}$$

$$E_2\,(\text{eV}) = \pm(4.468 \pm 0.003) + (0.66 \pm 0.01)x - (0.06 \pm 0.08)x^2. \tag{8}$$

The $E_2$ feature has been shown to comprise four transitions [5]. However, these can be resolved only in the derivative spectra [5] and not directly in the shape of $\varepsilon_1$ and $\varepsilon_2$.

Reflectivity measurements have been conducted for both the endpoint binaries and the alloy for energies above 6 eV, but no published results of Kramers–Kronig analysis exists. As noted earlier, the driving force behind the reflectivity measurements was the understanding of the electronic band structure, and hence the photometric accuracy of the results is less than that required to extract reliable $n$ and $k$ values. However, a short review of the reflectivity analysis is presented in the interest of completeness.

Room-temperature reflectivity measurements up to 22 eV have been reported by Cardona and Greenaway [15]. The measurements were performed on cleaved bulk crystals of CdTe and HgTe; the difficulty of obtaining crystals that were of sufficient size and flatness in the case of HgTe led to an error that could be as large ±10%. Shay and Spicer [16] have reported reflectivity measurements on CdTe in the 6–10 eV range. Low-temperature reflectivity for HgTe and CdTe measured at 10 and 15 K, respectively, in the 2.5–8 eV range has been published by Chadi *et al.* [17]. For the alloy, reflectivity measurements have been performed by Rodzik and Kisiel [18] in the energy range of 2–8.5 eV for the following thirteen alloy $x$ values: 0, 0.02, 0.04, 0.095, 0.12, 0.155, 0.35, 0.37, 0.47, 0.5, 0.58,

0.62, and 1.0; the measurements were conducted in the 115–300 K temperature range, and the temperature coefficients of the various critical-point energies were computed.

*The Band-Edge and Subband-Gap Region (~1.5 $E_g$–0.1 eV)*

The energy region in the vicinity of the direct gap has, by far, commanded the most attention due to its obvious importance in electro-optic device applications. The dependence of the energy gap, $E_g$, on the alloy composition $x$ has been reviewed by Hansen *et al.* [19], and more recently by Seiler *et al.* [20]. The relationship between $E_g$ and $x$ from Ref. [19], which is valid for the entire range of $x$ for the temperature range 4.2–300 K, is given below:

$$E_g(x) = -0.302 + 1.93x + 5.35(1-2x)(10^{-4})T - 0.81x^2 + 0.832x^3. \quad (9)$$

The standard error in the calculation was estimated to be 0.013 eV [19]. A modification of the above equation that more accurately represents $E_g(x)$ for $0.2 \leqslant x \leqslant 0.3$ for low temperatures has been proposed in Ref. [20] and is shown below:

$$E_g(x) = -0.302 + 1.93x + 5.35(1-2x)(10^{-4})[(-1822 + T^3)/(255.2 + T^2)]$$
$$- 0.81x^2 + 0.832x^3. \quad (10)$$

A large number of infrared absorption measurements have been reported for the alloy beginning with the first report by Lawson *et al.* [1]. This review is limited to the more recent efforts, particularly those that report $n$ and $k$ and those for which a reasonable estimate of $n$ can be carried out using the interpolation procedure described in the next section.

Many of the infrared optical studies in $Hg_{1-x}Cd_xTe$ have been limited to an analysis of the details of the absorption mechanisms and consequently report only the absorption coefficient, $\alpha(E)$. Fortunately, however, some exceptions exist. Kucera [21] has measured the value of $n$ in the subband-gap energy region extending down to ~0.045 eV for $x$ values of 0.18, 0.292, 0.39, 0.397, 0.459, 0.461, 0.522, and 1.0 at 80 and 300 K using the spacing of the interference fringes. Samples used in the study were grown using the Bridgman technique and annealed in Hg vapor to produce $n$-type conductivity except for the endpoint binary, CdTe, which was $p$-type and grown using a directional-freezing procedure. The observed $n$ values at 300 K

were computer-fitted to the Sellmeier form with two resonances as shown:

$$n^2(\lambda) = a_0 + a_1/(1-(a_2/\lambda)^2) + a_3/(1-(a_4/\lambda)^2), \tag{11}$$

where $\lambda$ is the wavelength in μm.

The parameters determined from the computer fit are presented in Table V. An interpolation procedure was also established to express the empirical $x$ dependence of each of the parameters in Eq. 12 as shown below:

$$a_i = A_i + B_i x + C_i x^2. \tag{12}$$

The values of $A_i$, $B_i$, and $C_i$ determined from a computer fit are presented in Table VI. In addition, Kucera [21] has measured the dispersion of $n$ at 80 K and analyzed both the 80 and 300 K data using the semiempirical theory of Pikhtin and Yaskov [22]. Jensen and Torabi [23] have calculated the value of $n$ from first principles for the whole alloy range, $0 \leqslant x \leqslant 1$. The calculations agree with the interpolated values of Kucera [21] to within ~3% for both high $x$ values and low energies but deviate by 10% for energies close to the band gap for the low $x$ alloys. The reader is referred to Refs. [21–23] for further details.

The behavior of $n$ and $k$ has been investigated by Finkman and Nemirovsky [24] for $0.205 \leqslant x \leqslant 0.220$ and by Finkman and Schacham [25] for $x = 0.29$ and 1.0. The refractive index was established using the interference fringes at energies below $E_g$, and the absorption coefficient in the vicinity of $E_g$ was measured using straightforward reflection and transmission studies. The samples used were grown using the solid-state recrystallization method or the Bridgman technique and were $n$-type with carrier concentrations in the range of $1 \times 10^{15}$ to $3 \times 10^{15}$ cm$^{-3}$ and mobilities in the range of $0.3 \times 10^5$ to $1 \times 10^5$ cm$^2$/Vs; the CdTe sample was semi-insulating. The $x$ value was measured to an accuracy of better than $\pm 0.005$.

The values of $n$ were computer-fitted to a modified Sellmeier form with a $\lambda^2$ and a $\lambda^4$ correction term as shown below:

$$n^2(\lambda) = a_0 + a_1/(1-(a_2/\lambda)^2) + c\lambda^2 + d\lambda^4, \tag{13}$$

where $\lambda$ is the wavelength in μm. The values of the parameters $a_0$, $a_1$, $a_2$, $c$, and $d$ for $x = 0.205$, 0.29, and 1 are presented in Table V. The authors estimate the error in Eq. 13 to be less than ±2% and ±0.5%, respectively, for the absolute and relative values. The change in $n$ when the temperature was reduced from 300 K to 80 K is estimated to be less than 3% [24, 25]. A comparison between the values reported by Finkman and Schacham [25]

and those obtained from Kucera [21] for $x = 0.29$ shows that the latter is systematically lower by ~1% for energies up to $\sim 0.75E_g$, above which it is lower by as much as 3%.

The dispersion of $n$ is less than ±1% for the energy range $\sim 0.75E_g \leqslant E \leqslant 0.1$ eV for $0.29 \leqslant x \leqslant 0.522$ and for the energy range $\sim 0.5E_g \leqslant E \leqslant 0.1$ eV for CdTe. Hence, a consideration of the mean value of $n$ in this region, namely $n_{av}$, is appropriate. A computation of $n$ using the results from Refs. [21] and [25] and a computer fit, with the condition that the variation with $x$ be monotonic, leads to the following simple empirical relationship:

$$n_{av} = 2.65 + 1.17(1-x)^2 \qquad 0.29 \leqslant x \leqslant 1. \tag{14}$$

The estimated errors are approximately ±2%. Values calculated using Eq. 14 for $x$ ranging from 0.3–1 are displayed in Table VII; these values are lower by 5–8% than $\sqrt{\varepsilon_\infty}$ determined from the far-infrared measurements of Baars and Sorger [26].

Absorption measurements for HgTe, the endpoint binary, which is semimetallic with a band gap of $\sim -0.3$ eV, have been reported by Szuszkiewicz [27] in the 0.05–0.625 eV region. Optical measurements were conducted at 10 K using thin sample plates 10 μm thick, obtained by crystallization of HgTe on an Hg solution. The samples were further thinned using chemical etching. Figures provided in Ref. [27] were digitized, and the $k$ values calculated are displayed in Table VIII; a constant value of 3.74 was assumed for $n$ in calculating the absorption coefficient from the measured reflection and transmission spectra.

The absorption coefficient, $\alpha(E)$, in the vicinity of $E_g$ was also studied by Finkman and Nemirovsky [24], Finkman and Schacham [25], and Schacham and Finkman [28] in the temperature range of ~85–300 K for the same samples used for determining $n$. The behavior of $\alpha(E)$ below the band gap was described by a modified form of the Urbach rule [24, 25] as shown:

$$\alpha(E) = \alpha_0 \exp[\sigma(E - E_0)/w] \tag{15}$$

$$w = T + T_0. \tag{16}$$

$T$ is the lattice temperature of the specimen, and the parameters $\alpha_0$, $\sigma$, $E_0$, and $T_0$ were determined using a computer fit to the measured $\alpha(E)$. For $x = 0.205$, the values of $\alpha_0$, $\sigma$, $E_0$, and $T_0$ are $4 \times 10^{-5}$ cm$^{-1}$; 5.65 K/cm$^{-1}$; 263.3 cm$^{-1}$, and 80.5 K, respectively [24]. A simultaneous computer fit to

two samples with $x = 0.215$ and 0.29 led to the following empirical dependence of the various parameters on the alloy composition, $x$ [25]:

$$\alpha_0 = \exp(53.61.x - 18.88) \tag{17a}$$

$$E_0\,(\text{eV}) = 1.838.x - 0.3434\ \text{eV} \tag{17b}$$

$$\sigma(K/\text{eV}) = 3.267 \times 10^4 (1+x) K/\text{eV} \tag{17c}$$

$$T_0(K) = 81.9K. \tag{17d}$$

At energy values exceeding the band gap, direct optical transitions will occur between the valence and conduction bands. The large values of $\alpha(E)$ exceeding $10^3\,\text{cm}^{-1}$ require the use of very thin samples, and hence, relatively few results have been reported [28, 30]. However, Schacham and Finkman [28] have established the following approximate simple relationship to describe the behavior of $\alpha(E)$:

$$\alpha(E) = \beta(E - E_g)^{1/2} \tag{18a}$$

$$\beta = 2.109 \times 10^5 [(1+x)/(T+81.9)] \tag{18b}$$

with the band gap, $E_g$, being defined as that energy at which $\alpha(E) = 500\,\text{cm}^{-1}$ with Eq. 18a valid for $\alpha(E) > 800\,\text{cm}^{-1}$. The estimated values compared favorably for $E_g = 0.15$ eV with the theoretical calculation based on the Kane model by Anderson [29]. The values of $E_g$ from $\alpha(E) = 500\,\text{cm}^{-1}$ deviate by ~10 meV from those calculated using Eq. 9 [25]. The values of $\alpha(E)$, and hence $k$, were calculated for $x = 0.205$ and 0.29 using the appropriate parameter values for the Urbach region and estimated for the band-to-band region up to $1.5E_g$ using the relationship shown in Eq. 18a. These $k$ values along with the value of $n$ for $x = 0.205$ and $x = 0.29$ are displayed in Tables IX and X, respectively, for temperatures of ~80 and 300 K; the values of $E_g$ given in Refs. [24, 25] are indicated in the tables.

In the case of $p$-type samples and samples at high temperatures with a significant hole density, the intervalence-band transitions between the light- and the heavy-hole bands will cause additional absorption and hence a larger value of $k$. The values of $k$ for $E \geqslant E_g$ and $n$ are not likely to be affected significantly. Mroczkowski and Nelson [31] and Mroczkowski *et al.* [32] have reported $\alpha(E)$ for $p$-type samples with $x$ values of 0.2 and 0.3 and acceptor density in the range of $1.2 \times 10^{17}$ to $2.8 \times 10^{17}\,\text{cm}^{-3}$. Bulk samples grown using a quench-anneal process were thinned and transmission and reflection measurements made to establish the absorption

coefficient. Figures provided in Ref. [31] were digitized and interpolated to determine the appropriate values of $k$; they are presented in Tables IX and X for $x=0.2$ and 0.3, respectively. For energies below the fundamental gap, $E_g$, the $k$ values in $p$-type samples are significantly larger than those in $n$-type samples.

Chu *et al.* [30] have also reported $\alpha(E)$ results for the $x=0.2$ value at 300 K. Compared with the values from Ref. [24], their values of $\alpha(E)$, and hence $k$, are twice as large for $E>E_g$ and nearly an order of magnitude greater at 0.12 eV. The lack of well-defined standards for measuring $x$ and $E_g$ as well as sample differences make it difficult to explain the disagreement. However, the $k$ values presented in Tables IX and X are probably reliable only up to a factor of two. As indicated earlier, a comparison between the $n$ values reported by Finkman and Schacham [25] and those obtained from Kucera [21] for $x=0.29$ shows that the latter is systematically lower by ~1% for energies up to $\sim 0.75E_g$, above which it is lower by as much as 3%.

The absorption behavior for $E \leqslant E_g$ can also be affected significantly by other sample-dependent properties: the presence of a large density of free electrons will affect the band edge through the Burstein–Moss shift [33], which is particularly important in small-band-gap $Hg_{1-x}Cd_xTe$. Chu *et al.* [33] have investigated the influence of the Burstein–Moss effect in samples with $0.165 \leqslant x \leqslant 0.194$ and electron density in the range of $0.4 \times 10^{17}$ to $7 \times 10^{17}\ cm^{-3}$. For energies lower than $E_g$, free-carrier absorption will also play a part as shown by Qian *et al.* [34]; their absorption coefficient for a sample with $x=0.19$ and free-electron density of $7 \times 10^{17}\ cm^{-3}$ and impurity density of $3.4 \times 10^{18}\ cm^{-3}$ ranged from ~30 to ~200 $cm^{-1}$ in the 9–15 μm wavelength region. Optical transitions between energy levels associated with impurity levels may also influence the $k$ values in the subband-gap region.

The $n$ values are not likely to change significantly with the electronic properties. For high temperatures approaching 300 K and above, the intrinsic carriers are likely to dominate [2], and hence, the optical absorption will be influenced by both the Burstein–Moss effect and the intervalence-band mechanisms.

The $n$ and $k$ values obtained at 300 K for $x=0.443$ are presented in Table XI. The $k$ values were obtained by digitizing the appropriate $\alpha(E)$ curve provided in Ref. [30], and the value of $n$ was calculated using the interpolation procedure established by Kucera [21].

*Far-Infrared and Reststrahlen Region (0.05–0.0001 eV)*

The optical behavior in the far-infrared (FIR) and reststrahlen region is determined by the lattice oscillations, free-carrier properties, impurity transitions, and band-to-band transitions in the narrow-gap alloys. Of these, the free-carrier and impurity-related behavior are extrinsic and can

vary significantly from sample to sample. Hence, the optical constants reported are confined to those determined at low temperatures using reflection spectroscopy, where the free-carrier and impurity contributions are expected to be small. Methods of estimating the free-carrier contribution and references to both free-carrier and impurity-related FIR investigations are provided for further information.

The FIR reflectivity spectrum of HgTe was studied by Grynberg *et al.* [35] in the frequency range extending from 80–250 $cm^{-1}$ at temperatures ranging from 8–300 K. The samples were crystalline slabs, approximately 60 μm in thickness and were fabricated using liquid-phase deposition by slow cooling of Te in an Hg bath. At 4.2 K the samples were *n*-type with free-carrier densities and mobilities of $\sim 6 \times 10^{15}$ $cm^{-3}$ and $\sim 6 \times 10^{5}$ $cm^2/Vs$, respectively. The dielectric function was determined using the Kramers–Kronig (K–K) analysis. The low-temperature values of $n$ and $k$ reported in Table XII were determined from digitized values of the $\mathrm{Im}(\varepsilon)$ and $\mathrm{Im}(-1/\varepsilon)$ curves presented in Ref. [35]. The approximate positions of the zeros in $\mathrm{Re}(\varepsilon)$ were estimated from the theory and the values of various parameters provided in Ref. [35]. The limited accuracy available in the procedure described confines the range of $n$ and $k$ to 110–161 $cm^{-1}$ which overlaps the reststrahlen region extending from the transverse optical (TO) phonon frequency at $\sim 118$ $cm^{-1}$ to the longitudinal optical (LO) phonon frequency at $\sim 139$ $cm^{-1}$ [36]. Grynberg *et al.* have described the FIR behavior using a model of $\varepsilon(\omega)$ that accounts for the band-to-band transitions in addition to the well-known free-carrier and lattice-oscillation contributions. The functional form of the latter two are discussed in the following paragraphs.

The FIR reflectivity spectrum measured at a temperature of ~5 K and the associated K–K analysis results for *n*- and *p*-type samples with $x \simeq 0.21$ have recently been reported by Amirtharaj *et al.* [37]. The samples were grown using the solid-state recrystallization method, which usually yields *p*-type crystals; conversion to *n*-type was induced using an Hg vapor annealing procedure. The free-carrier densities were $\sim 4 \times 10^{17}$ and $3 \times 10^{14}$ $cm^{-3}$ in the *p*- and *n*-type samples, respectively, at low temperatures. The reflectivity spectrum measured in the 10–400 $cm^{-1}$ frequency range was analyzed using the K–K procedure to determine the optical constants $n$ and $k$ presented in Table XII. The large differences in the values of $n$ and $k$ between the *n*- and *p*-type samples are expected to be due to the presence of the hole plasma, intervalence-band transitions, as well as possible impurity transitions in the *p*-type samples.

In samples with a large value of $x$ and low impurity and hole density, the band-to-band and intervalence band transitions as well as impurity-related transitions can be neglected. In this case, the FIR behavior can be satisfactorily described using the well-known classical form shown below [38]:

$$\varepsilon(\omega) = \varepsilon_\infty + \Sigma_j\{S_j(\omega_j)^2\}/\{(\omega_j)^2 - \omega^2 - i\omega\Gamma_j\} - (\omega_p)^2\varepsilon_\infty/\{\omega(\omega + i/\tau)\}, \quad (19)$$

where $\omega$ is the frequency and the lattice oscillations are treated as damped oscillators with strength $S_j$, frequency $\omega_j$, and damping $\Gamma_j$, and $\varepsilon_\infty$ is the value of $\varepsilon(\omega)$ at frequencies much larger than the lattice oscillations in the absence of free carriers. The last term describes the contribution of the free carriers, where $\omega_p$ is the plasma frequency and $\tau$ is the scattering time. $\omega_p$ and $\tau$ are related to the free carrier density, $N$, and mobility, $\mu$, through the following relations:

$$\omega_p = 4\pi Ne^2/m^*\varepsilon_\infty \quad (20a)$$

$$\tau = \mu m^*/e, \quad (20b)$$

where $m^*$ is the effective mass of the charge carrier and $e$ its electronic charge.

Shen and Chu [39] have analyzed the FIR reflectivity of an $x = 0.45$ sample using the classical form of $\varepsilon(\omega)$ shown in Eq. 19. The reflection spectrum was measured at a temperature of 35 K in the frequency range of 50–210 $cm^{-1}$. Seven lattice oscillators with the following parameters were used to computer fit the spectrum with all the observed fine structure: $\omega_j$, $S_j$, $\Gamma_j$,

(1) 110 $cm^{-1}$, 0.3, 10 $cm^{-1}$
(2) 123 $cm^{-1}$, 5.6, 2.8 $cm^{-1}$
(3) 134 $cm^{-1}$, 0.7, 9 $cm^{-1}$
(4) 141 $cm^{-1}$, 0.15, 6 $cm^{-1}$
(5) 149 $cm^{-1}$, 0.9, 4 $cm^{-1}$
(6) 153 $cm^{-1}$, 0.35, 6 $cm^{-1}$
(7) 157 $cm^{-1}$, 0.15, 4 $cm^{-1}$.

The 110 $cm^{-1}$ feature has been assigned to a two-phonon process. The HgTe- and the CdTe-like TO phonons occur at 123 and 149 $cm^{-1}$, respectively. The fine structure in the measured spectrum described by the remaining oscillators has been tentatively assigned to originate in optically active vibrational modes of the various combinations of anions and cations in the alloy lattice. The value of $\varepsilon_\infty$ needed to fit the measurements is ~16. The values of $n$ and $k$ determined using Eq. 19 and the parameters mentioned above are displayed in Table XIII along with $\sqrt{\varepsilon_\infty}$ reported by Baars and Sorger [26].

The values of $n$ and $k$ for alloy compositions where the band gap occurs above the FIR region can be estimated if the lattice-oscillator and free-

carrier parameters are known. The two main optical phonons, namely the CdTe- ($TO_1$ and $LO_1$) and the HgTe-like ($TO_2$ and $LO_2$) phonons, have been investigated using both FIR reflectivity and Raman scattering by many investigators [2, 26, 40–43]. The variation of the optical phonons with $x$, the Cd mole fraction, is nearly linear. The CdTe-like phonons, $TO_1$ and $LO_1$ converge to $\sim 152\,\text{cm}^{-1}$ as $x$ approaches 0, which is the frequency of the local vibrational mode of Cd in HgTe; and the HgTe-like modes, $TO_2$ and $LO_2$, converge to $\sim 131\,\text{cm}^{-1}$ at $x=1$, which is the gap mode related to Cd oscillations in HgTe [40]. Talwar and Vandevyer [40] have used a random-element isodisplacement model to describe the $x$ dependence of the optical phonons, and the fitted values of the various parameters may be found in Ref. [40].

Absorption due to electronic transitions associated with impurities at energies below the reststrahlen region has been reported by Scott [44] and Dornhaus [45]. Impurity-related vibrational features have been investigated by Talwar and Vandevyer [40], and Shen and Chu [46] have measured low-frequency absorption and interpreted it as originating in impurity- and disorder-activated phonons.

## Conclusion

The optical constants, $n$ and $k$, of the semiconducting alloy, $Hg_{1-x}Cd_xTe$, have been reviewed. Since $Hg_{1-x}Cd_xTe$ has been known and investigated only since 1959, the relevant published literature is less extensive and thorough than that of Si and GaAs. However, the technological importance of $Hg_{1-x}Cd_xTe$ is well recognized, and hence, it is hoped that this review is timely and will be helpful to researchers as well as engineers who are mainly concerned with the design and production of electro-optic devices.

The values of $n$ and $k$ included have been confined to the more recent reports and those that are, in the author's opinion, more reliable. Although a reasonable effort was made to study and evaluate all the published literature, inadvertent omissions are possible, particularly with papers published in languages other than English. The lack of measurements in the 1.5 eV to $\sim 1.5\,E_g$ energy region is a significant absence and needs to be addressed.

## ACKNOWLEDGMENTS

The author wishes to thank Dr. D. E. Aspnes of Bellcore, Redbank, N.J., U.S.A. for the electronic record of $\varepsilon_1$ and $\varepsilon_2$ data and Prof. M. Cardona of the Max Planck Institute,

Stuttgart, Germany, for the expanded figures from Ref. [6]. The assistance provided by Mr. E. Kelso of the U.S. Army Center for Night Vision and Electro-Optics with the literature search is gratefully acknowledged.

## REFERENCES

1. W. D. Lawson, S. Nielsen, E. H. Putley, and A. S. Young, *J. Phys. Chem. Solids* **9**, 325 (1959).
2. R. Dornhaus and G. Nimtz, "Narrow-Gap Semiconductors, Springer Tracts in Modern Physics," (G. Hohler and E. A. Niekisch, eds.), Vol. 98, Springer-Verlag, Berlin, 119 (1983).
3. J. Brice and P. Capper, eds., "Properties of Mercury Cadmium Telluride," Inst. of Electrical Engineers, London, 1987.
4. E. D. Palik, in "Handbook of Optical Constants of Solids," (E. D. Palik, ed.), Academic Press, New York, 409 (1985).
5. H. Arwin and D. E. Aspnes, *J. Vac. Sci. Technol. A* **2**, 1316 (1984).
6. L. Viña, C. Umbach, M. Cardona, and L. Vodopyanov, *Phys. Rev. B* **29**, 6752 (1984).
7. D. E. Aspnes, private communication.
8. M. Cardona, private communication.
9. D. E. Aspnes and H. Arwin, *J. Vac. Sci. Technol. A* **2**, 1309 (1984).
10. H. Arwin, D. E. Aspnes, and D. R. Rhiger, *J. Appl. Phys.* **54**, 7132 (1983).
11. A. Moritani, H. Sekiya, K. Taniguchi, C. Hamaguchi, J. Nakai, and R. Makabe, *Jpn. J. Appl. Phys.* **10**, 1410 (1971).
12. D. T. F. Marple and H. Ehrenreich, *Phys. Rev. Lett.* **8**, 87 (1962).
13. T. H. Myers, S. W. Edwards, and J. F. Schetzina, *J. Appl. Phys.* **52**, 4231 (1981).
14. T. E. Korsak, N. P. Sysoeva, B. M. Ayupov, V. V. Antonov, A. V. Voltsekhovskii, and E. F. Tivota, *Sov. Phys. Semicond.* **19**, 222 (1985).
15. M. Cardona and D. L. Greenaway, *Phys. Rev.* **131**, 98 (1963).
16. J. L. Shay and W. E. Spicer, *Phys. Rev.* **161**, 799 (1967).
17. D. J. Chadi, J. P. Walter, M. L. Cohen, Y. Petroff, and M. Balkanski, *Phys. Rev.* **5**, 3058 (1972).
18. A. Rodzik and A. Kisiel, *J. Phys. C.* **16**, 203 (1983).
19. G. L. Hansen, J. L. Schmit, and T. N. Casselman, *J. Appl. Phys.* **53**, 7099 (1982).
20. D. G. Seiler, J. R. Lowney, C. L. Littler, and M. R. Loloee, *J. Vac. Sci. Technol. A.* **8**, 1237 (1990).
21. Z. Kucera, *Phys. Status Solidi (a)* **100**, 659 (1987).
22. A. N. Pikhtin and A. D. Yaskov, *Sov. Phys. Semicond.* **15**, 8 (1981). See also V. G. Sredin, *Sov. Phys. Semicond.* **17**, 328 (1983).
23. B. Jensen and A. Torabi, *J. Appl. Phys.* **54**, 5945 (1983). See also chapter by B. Jensen, this volume.
24. E. Finkman and Y. Nemirovsky, *J. Appl. Phys.* **50**, 4356 (1979).
25. E. Finkman and S. E. Schacham, *J. Appl. Phys.* **56**, 2896 (1984).
26. J. Baars and F. Sorger, *Solid State Commun.* **10**, 875 (1972). See also Ref. [2].
27. W. Szuszkiewicz, *Phys. Status Solidi (b)* **79**, 691 (1977).
28. S. E. Schacham and E. Finkman, *J. Appl. Phys.* **57**, 2001 (1985).
29. W. W. Anderson, *Infrared Phys.* **20**, 363 (1980).
30. J. Chu, S. Xu, H. Ji, W. Zhang, C. Shiwei, and R. Jiang, *Chinese J. Infrared Res.* **4**, 255 (1985).
31. J. A. Mroczkowski and D. A Nelson, *J. Appl. Phys.* **54**, 2041 (1983).
32. J. A. Mroczkowski, D. A. Nelson, R. Murosako, and P. H. Zimmermann, *J. Vac. Sci. Technol. A* **1**, 1756 (1983).
33. J. Chu, D. Qian, and D. Tang, *Physica Scripta* **T14**, 37 (1986).

34. D. Qian, W. Tang, J. Shen, J. Chu, and G. Zheng, *Solid State Commun.* **56**, 813 (1985).
35. M. Grynberg, R. Le Toullec, and M. Balkanski, *Phys. Rev. B* **9**, 517 (1974).
36. P. M. Amirtharaj, K. K. Tiong, P. Parayanthal, F. H. Pollak, and J. K. Furdyna, *J. Vac. Sci. Technol. A* **3**, 226 (1985).
37. P. M. Amirtharaj, N. K. Dhar, J. Baars, and H. Seelewind, *Semiconductor Sci. Technol.* **5**, S68 (1990).
38. S. Perkowitz, "Infrared and Millimeter Waves," (K. J. Button, ed.), Vol. 8, Academic Press, New York, 71 (1983).
39. X. C. Shen and J. H. Chu, *Acta Physica Sinica* **34**, 56 (1985).
40. D. N. Talwar and M. Vandevyer, *J. Appl. Phys.* **56**, 1601 (1984).
41. S. P. Kozyrev, L. D. Vodopyanov, and R. Triboulet, *Solid State Commun.* **45**, 383 (1983).
42. A. Ksendzov, F. H. Pollak, P. M. Amirtharaj, and J. A. Wilson, *Semiconductor Sci. Technol.* **5**, S78 (1990).
43. A. Lusson and J. Wagner, *Phys. Rev. B* **38**, 10064 (1988).
44. W. Scott, E. L. Stelzer and R. J. Hager, *J. Appl. Phys.* **47**, 1408 (1976).
45. R. Dornhaus, G. Nimtz, W. Schlabitz, and H. Burkhard, *Solid State Commun.* **17**, 837 (1975).
46. S. C. Shen and J. H. Chu, *Solid State Commun.* **48**, 1017 (1983).

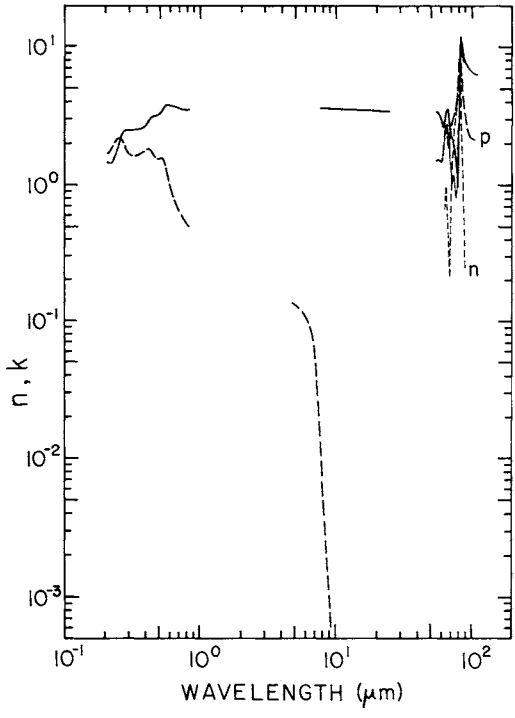


**Fig. 1.** Log–log plot of $n$ (solid line) and $k$ (dashed line) versus wavelength in μm are for $Hg_{1-x}Cd_xTe$ with $x=0.2$. The ultraviolet, visible, and near-infrared data are for $x=0.2$, $n$-type at room temperature. The IR data in the vicinity of $E_g$ and lower energies are for $x\simeq 0.2$, $n$-type at room temperature. The far-infrared data are for $x=0.21$ at 5 K, $n$- and $p$-type. Free-carrier effects appear minimal in the $n$-type data.

TABLE I

**Values of $n$ and $k$ of $Hg_{1-x}Cd_xTe$ – Synopsis of x values included in this review**

| x | UV, Visible and Near IR (6 - 1.5 eV) | Band Edge and Subband gap (~$1.5E_g$ - 0.1 eV) | Far Infrared and Reststrahlen (~0.05 - ~0.001 eV) |
|---|---|---|---|
| 0 | X | X | X |
| 0.16 | X[a] | | |
| 0.18 | | X[b] | |
| 0.20 | X | X | |
| 0.205 | | X | |
| 0.21 | | | X |
| 0.29 | X | X | |
| 0.292 | | X[b] | |
| 0.3 | | X | |
| 0.39 | | X[b] | |
| 0.397 | | X[b] | |
| 0.4 | | X[c] | |
| 0.43 | X | | |
| 0.443 | | X | |
| 0.45 | | | X |
| 0.459 | | X[b] | |
| 0.5 | | X[c] | |
| 0.522 | | X[b] | |
| 0.6 | | X[c] | |
| 0.65 | X[a] | | |
| 0.7 | | X[c] | |
| 0.76 | X | | |
| 0.8 | | X[c] | |
| 0.86 | X | | |
| 0.9 | | X[c] | |
| 0.91 | X | | |
| 1.0 | X | X[c], Ref. [4] | Ref. [4] |

[a] Measurements were made at the He-Ne laser wavelength of 0.6328 $\mu$m.
[b] n was measured in the subband gap region and computer fitted to the Sellmeier equation [21].
[c] Average values of n for the subband gap region ($0.75E_g$ to 0.1 eV) computed using an interpolation routine are presented.

TABLE II

Values of $n$ and $k$ for $Hg_{1-x}Cd_xTe$ (Ref. [5])

| | | | x=0 | | 0.20 | | 0.29 | | 1.0 | |
|---|---|---|---|---|---|---|---|---|---|---|
| eV | $cm^{-1}$ | $\mu m$ | n | k | n | k | n | k | n | k |
| 6.000 | 48395 | 0.2066 | 1.435 | 1.747 | 1.450 | 1.702 | 1.384 | 1.712 | 1.191 | 1.831 |
| 5.982 | 48249 | 0.2073 | 1.437 | 1.704 | 1.413 | 1.722 | 1.383 | 1.710 | 1.250 | 1.842 |
| 5.964 | 48103 | 0.2079 | 1.433 | 1.717 | 1.438 | 1.691 | 1.409 | 1.717 | 1.259 | 1.821 |
| 5.946 | 47958 | 0.2085 | 1.435 | 1.716 | 1.418 | 1.707 | 1.380 | 1.729 | 1.240 | 1.860 |
| 5.928 | 47812 | 0.2092 | 1.434 | 1.706 | 1.437 | 1.706 | 1.390 | 1.722 | 1.269 | 1.883 |
| 5.910 | 47666 | 0.2098 | 1.437 | 1.708 | 1.429 | 1.721 | 1.396 | 1.729 | 1.270 | 1.906 |
| 5.892 | 47520 | 0.2104 | 1.440 | 1.709 | 1.420 | 1.713 | 1.386 | 1.736 | 1.265 | 1.920 |
| 5.873 | 47375 | 0.2111 | 1.426 | 1.709 | 1.413 | 1.728 | 1.384 | 1.744 | 1.265 | 1.945 |
| 5.855 | 47229 | 0.2117 | 1.427 | 1.713 | 1.419 | 1.724 | 1.383 | 1.752 | 1.273 | 1.957 |
| 5.837 | 47083 | 0.2124 | 1.431 | 1.712 | 1.414 | 1.735 | 1.382 | 1.761 | 1.278 | 1.977 |
| 5.819 | 46937 | 0.2131 | 1.426 | 1.710 | 1.413 | 1.740 | 1.377 | 1.775 | 1.279 | 1.998 |
| 5.801 | 46791 | 0.2137 | 1.424 | 1.713 | 1.411 | 1.742 | 1.376 | 1.775 | 1.295 | 2.011 |
| 5.783 | 46646 | 0.2144 | 1.416 | 1.721 | 1.413 | 1.757 | 1.378 | 1.788 | 1.298 | 2.035 |
| 5.765 | 46500 | 0.2151 | 1.415 | 1.724 | 1.409 | 1.759 | 1.379 | 1.800 | 1.310 | 2.054 |
| 5.747 | 46354 | 0.2157 | 1.421 | 1.730 | 1.409 | 1.768 | 1.377 | 1.808 | 1.319 | 2.065 |
| 5.729 | 46208 | 0.2164 | 1.416 | 1.734 | 1.410 | 1.781 | 1.380 | 1.819 | 1.327 | 2.091 |
| 5.711 | 46063 | 0.2171 | 1.416 | 1.740 | 1.411 | 1.786 | 1.382 | 1.833 | 1.334 | 2.113 |
| 5.693 | 45917 | 0.2178 | 1.411 | 1.749 | 1.413 | 1.797 | 1.382 | 1.843 | 1.345 | 2.133 |
| 5.675 | 45771 | 0.2185 | 1.413 | 1.756 | 1.413 | 1.812 | 1.386 | 1.855 | 1.356 | 2.145 |
| 5.657 | 45625 | 0.2192 | 1.410 | 1.765 | 1.413 | 1.822 | 1.391 | 1.870 | 1.364 | 2.168 |
| 5.639 | 45480 | 0.2199 | 1.409 | 1.772 | 1.419 | 1.834 | 1.395 | 1.885 | 1.378 | 2.186 |
| 5.620 | 45334 | 0.2206 | 1.412 | 1.779 | 1.421 | 1.843 | 1.400 | 1.895 | 1.387 | 2.210 |
| 5.602 | 45188 | 0.2213 | 1.413 | 1.788 | 1.429 | 1.856 | 1.408 | 1.913 | 1.403 | 2.233 |
| 5.584 | 45042 | 0.2220 | 1.414 | 1.799 | 1.432 | 1.867 | 1.414 | 1.926 | 1.414 | 2.254 |
| 5.566 | 44896 | 0.2227 | 1.415 | 1.808 | 1.438 | 1.881 | 1.421 | 1.939 | 1.428 | 2.282 |
| 5.548 | 44751 | 0.2235 | 1.417 | 1.820 | 1.444 | 1.892 | 1.430 | 1.953 | 1.450 | 2.307 |
| 5.530 | 44605 | 0.2242 | 1.420 | 1.829 | 1.450 | 1.905 | 1.439 | 1.967 | 1.464 | 2.336 |
| 5.512 | 44459 | 0.2249 | 1.424 | 1.839 | 1.457 | 1.916 | 1.449 | 1.980 | 1.490 | 2.365 |
| 5.494 | 44313 | 0.2257 | 1.426 | 1.849 | 1.465 | 1.930 | 1.459 | 1.994 | 1.513 | 2.389 |
| 5.476 | 44168 | 0.2264 | 1.431 | 1.860 | 1.473 | 1.942 | 1.471 | 2.008 | 1.544 | 2.416 |
| 5.458 | 44022 | 0.2272 | 1.434 | 1.871 | 1.483 | 1.953 | 1.482 | 2.020 | 1.572 | 2.447 |
| 5.440 | 43876 | 0.2279 | 1.441 | 1.882 | 1.491 | 1.966 | 1.495 | 2.034 | 1.608 | 2.470 |
| 5.422 | 43730 | 0.2287 | 1.445 | 1.892 | 1.504 | 1.978 | 1.510 | 2.046 | 1.646 | 2.494 |
| 5.404 | 43585 | 0.2294 | 1.453 | 1.904 | 1.515 | 1.989 | 1.525 | 2.058 | 1.688 | 2.515 |
| 5.386 | 43439 | 0.2302 | 1.459 | 1.916 | 1.530 | 2.002 | 1.540 | 2.068 | 1.729 | 2.536 |
| 5.367 | 43293 | 0.2310 | 1.467 | 1.928 | 1.541 | 2.013 | 1.557 | 2.079 | 1.772 | 2.552 |
| 5.349 | 43147 | 0.2318 | 1.475 | 1.939 | 1.555 | 2.023 | 1.572 | 2.088 | 1.821 | 2.567 |
| 5.331 | 43001 | 0.2326 | 1.483 | 1.949 | 1.569 | 2.033 | 1.589 | 2.097 | 1.870 | 2.576 |
| 5.313 | 42856 | 0.2333 | 1.493 | 1.960 | 1.584 | 2.042 | 1.606 | 2.106 | 1.921 | 2.585 |
| 5.295 | 42710 | 0.2341 | 1.502 | 1.972 | 1.596 | 2.050 | 1.621 | 2.114 | 1.973 | 2.587 |
| 5.277 | 42564 | 0.2349 | 1.513 | 1.981 | 1.611 | 2.058 | 1.638 | 2.122 | 2.022 | 2.587 |
| 5.259 | 42418 | 0.2357 | 1.524 | 1.992 | 1.626 | 2.066 | 1.656 | 2.130 | 2.070 | 2.583 |
| 5.241 | 42273 | 0.2366 | 1.534 | 2.001 | 1.640 | 2.074 | 1.672 | 2.138 | 2.122 | 2.578 |
| 5.223 | 42127 | 0.2374 | 1.544 | 2.011 | 1.654 | 2.083 | 1.691 | 2.145 | 2.169 | 2.568 |

TABLE II (*Continued*)

| | | | x=0 | | 0.20 | | 0.29 | | 1.0 | |
|---|---|---|---|---|---|---|---|---|---|---|
| eV | $cm^{-1}$ | μm | n | k | n | k | n | k | n | k |
| 5.205 | 41981 | 0.2382 | 1.555 | 2.019 | 1.668 | 2.090 | 1.707 | 2.152 | 2.217 | 2.556 |
| 5.187 | 41835 | 0.2390 | 1.566 | 2.029 | 1.683 | 2.098 | 1.726 | 2.158 | 2.264 | 2.542 |
| 5.169 | 41690 | 0.2399 | 1.577 | 2.037 | 1.699 | 2.106 | 1.745 | 2.166 | 2.310 | 2.525 |
| 5.151 | 41544 | 0.2407 | 1.587 | 2.047 | 1.715 | 2.113 | 1.764 | 2.172 | 2.356 | 2.507 |
| 5.133 | 41398 | 0.2416 | 1.598 | 2.057 | 1.731 | 2.120 | 1.783 | 2.176 | 2.400 | 2.483 |
| 5.114 | 41252 | 0.2424 | 1.610 | 2.067 | 1.749 | 2.128 | 1.802 | 2.181 | 2.446 | 2.458 |
| 5.096 | 41107 | 0.2433 | 1.622 | 2.079 | 1.766 | 2.136 | 1.822 | 2.185 | 2.487 | 2.430 |
| 5.078 | 40961 | 0.2441 | 1.635 | 2.089 | 1.785 | 2.142 | 1.842 | 2.188 | 2.527 | 2.399 |
| 5.060 | 40815 | 0.2450 | 1.649 | 2.101 | 1.803 | 2.149 | 1.862 | 2.191 | 2.562 | 2.362 |
| 5.042 | 40669 | 0.2459 | 1.664 | 2.112 | 1.822 | 2.153 | 1.882 | 2.194 | 2.598 | 2.325 |
| 5.024 | 40523 | 0.2468 | 1.680 | 2.123 | 1.843 | 2.157 | 1.903 | 2.196 | 2.627 | 2.285 |
| 5.006 | 40378 | 0.2477 | 1.697 | 2.134 | 1.862 | 2.164 | 1.923 | 2.198 | 2.655 | 2.242 |
| 4.988 | 40232 | 0.2486 | 1.715 | 2.145 | 1.881 | 2.166 | 1.943 | 2.200 | 2.675 | 2.201 |
| 4.970 | 40086 | 0.2495 | 1.734 | 2.154 | 1.902 | 2.170 | 1.965 | 2.201 | 2.692 | 2.160 |
| 4.952 | 39940 | 0.2504 | 1.754 | 2.162 | 1.922 | 2.173 | 1.987 | 2.201 | 2.704 | 2.116 |
| 4.934 | 39795 | 0.2513 | 1.774 | 2.171 | 1.942 | 2.175 | 2.008 | 2.202 | 2.714 | 2.076 |
| 4.916 | 39649 | 0.2522 | 1.795 | 2.177 | 1.964 | 2.177 | 2.031 | 2.202 | 2.721 | 2.038 |
| 4.898 | 39503 | 0.2531 | 1.817 | 2.184 | 1.985 | 2.178 | 2.054 | 2.201 | 2.724 | 2.002 |
| 4.880 | 39357 | 0.2541 | 1.838 | 2.188 | 2.007 | 2.179 | 2.077 | 2.199 | 2.725 | 1.966 |
| 4.861 | 39212 | 0.2550 | 1.860 | 2.193 | 2.029 | 2.180 | 2.100 | 2.197 | 2.723 | 1.936 |
| 4.843 | 39066 | 0.2560 | 1.882 | 2.196 | 2.051 | 2.180 | 2.121 | 2.194 | 2.722 | 1.904 |
| 4.825 | 38920 | 0.2569 | 1.904 | 2.199 | 2.074 | 2.179 | 2.146 | 2.190 | 2.718 | 1.875 |
| 4.807 | 38774 | 0.2579 | 1.926 | 2.201 | 2.097 | 2.177 | 2.169 | 2.185 | 2.713 | 1.849 |
| 4.789 | 38628 | 0.2589 | 1.949 | 2.203 | 2.121 | 2.174 | 2.194 | 2.180 | 2.709 | 1.825 |
| 4.771 | 38483 | 0.2599 | 1.971 | 2.204 | 2.144 | 2.170 | 2.218 | 2.173 | 2.702 | 1.802 |
| 4.753 | 38337 | 0.2608 | 1.994 | 2.203 | 2.168 | 2.166 | 2.243 | 2.164 | 2.696 | 1.780 |
| 4.735 | 38191 | 0.2618 | 2.017 | 2.202 | 2.191 | 2.160 | 2.267 | 2.155 | 2.689 | 1.762 |
| 4.717 | 38045 | 0.2628 | 2.041 | 2.201 | 2.215 | 2.153 | 2.291 | 2.145 | 2.681 | 1.742 |
| 4.699 | 37900 | 0.2639 | 2.065 | 2.198 | 2.239 | 2.145 | 2.315 | 2.132 | 2.675 | 1.725 |
| 4.681 | 37754 | 0.2649 | 2.088 | 2.194 | 2.262 | 2.136 | 2.338 | 2.117 | 2.668 | 1.710 |
| 4.663 | 37608 | 0.2659 | 2.111 | 2.189 | 2.286 | 2.125 | 2.361 | 2.101 | 2.659 | 1.696 |
| 4.645 | 37462 | 0.2669 | 2.135 | 2.183 | 2.309 | 2.114 | 2.381 | 2.084 | 2.653 | 1.682 |
| 4.627 | 37317 | 0.2680 | 2.158 | 2.177 | 2.332 | 2.101 | 2.400 | 2.066 | 2.645 | 1.670 |
| 4.608 | 37171 | 0.2690 | 2.180 | 2.169 | 2.353 | 2.086 | 2.418 | 2.047 | 2.638 | 1.659 |
| 4.590 | 37025 | 0.2701 | 2.203 | 2.161 | 2.373 | 2.070 | 2.435 | 2.028 | 2.630 | 1.649 |
| 4.572 | 36879 | 0.2712 | 2.225 | 2.151 | 2.393 | 2.054 | 2.449 | 2.008 | 2.624 | 1.640 |
| 4.554 | 36733 | 0.2722 | 2.246 | 2.141 | 2.409 | 2.036 | 2.462 | 1.988 | 2.617 | 1.632 |
| 4.536 | 36588 | 0.2733 | 2.267 | 2.130 | 2.427 | 2.018 | 2.475 | 1.969 | 2.611 | 1.625 |
| 4.518 | 36442 | 0.2744 | 2.287 | 2.117 | 2.441 | 1.999 | 2.485 | 1.948 | 2.604 | 1.619 |
| 4.500 | 36296 | 0.2755 | 2.307 | 2.104 | 2.454 | 1.980 | 2.494 | 1.928 | 2.598 | 1.613 |
| 4.482 | 36150 | 0.2766 | 2.325 | 2.089 | 2.466 | 1.961 | 2.502 | 1.908 | 2.592 | 1.608 |
| 4.464 | 36005 | 0.2777 | 2.343 | 2.075 | 2.477 | 1.942 | 2.508 | 1.888 | 2.586 | 1.605 |
| 4.446 | 35859 | 0.2789 | 2.360 | 2.059 | 2.487 | 1.923 | 2.513 | 1.870 | 2.582 | 1.602 |
| 4.428 | 35713 | 0.2800 | 2.375 | 2.043 | 2.495 | 1.904 | 2.517 | 1.852 | 2.576 | 1.599 |
| 4.410 | 35567 | 0.2812 | 2.388 | 2.026 | 2.503 | 1.886 | 2.519 | 1.835 | 2.571 | 1.596 |
| 4.392 | 35422 | 0.2823 | 2.401 | 2.009 | 2.508 | 1.867 | 2.520 | 1.818 | 2.566 | 1.596 |

TABLE II (*Continued*)

| | | | x=0 | | 0.20 | | 0.29 | | 1.0 | |
|---|---|---|---|---|---|---|---|---|---|---|
| eV | $cm^{-1}$ | μm | n | k | n | k | n | k | n | k |
| 4.373 | 35276 | 0.2835 | 2.413 | 1.992 | 2.513 | 1.849 | 2.521 | 1.803 | 2.562 | 1.595 |
| 4.355 | 35130 | 0.2847 | 2.423 | 1.975 | 2.517 | 1.831 | 2.521 | 1.789 | 2.558 | 1.596 |
| 4.337 | 34984 | 0.2858 | 2.433 | 1.959 | 2.519 | 1.814 | 2.522 | 1.775 | 2.555 | 1.596 |
| 4.319 | 34839 | 0.2870 | 2.441 | 1.942 | 2.521 | 1.798 | 2.521 | 1.762 | 2.551 | 1.598 |
| 4.301 | 34693 | 0.2882 | 2.449 | 1.926 | 2.521 | 1.783 | 2.521 | 1.751 | 2.548 | 1.600 |
| 4.283 | 34547 | 0.2895 | 2.456 | 1.910 | 2.521 | 1.768 | 2.520 | 1.740 | 2.546 | 1.603 |
| 4.265 | 34401 | 0.2907 | 2.462 | 1.894 | 2.521 | 1.756 | 2.520 | 1.729 | 2.543 | 1.607 |
| 4.247 | 34255 | 0.2919 | 2.467 | 1.879 | 2.519 | 1.743 | 2.519 | 1.719 | 2.541 | 1.612 |
| 4.229 | 34110 | 0.2932 | 2.472 | 1.864 | 2.518 | 1.732 | 2.519 | 1.710 | 2.539 | 1.617 |
| 4.211 | 33964 | 0.2944 | 2.475 | 1.848 | 2.517 | 1.722 | 2.518 | 1.701 | 2.539 | 1.623 |
| 4.193 | 33818 | 0.2957 | 2.478 | 1.834 | 2.516 | 1.712 | 2.518 | 1.693 | 2.538 | 1.630 |
| 4.175 | 33672 | 0.2970 | 2.479 | 1.820 | 2.514 | 1.703 | 2.516 | 1.685 | 2.538 | 1.638 |
| 4.157 | 33527 | 0.2983 | 2.481 | 1.807 | 2.513 | 1.695 | 2.516 | 1.678 | 2.537 | 1.647 |
| 4.139 | 33381 | 0.2996 | 2.481 | 1.794 | 2.512 | 1.687 | 2.515 | 1.671 | 2.537 | 1.658 |
| 4.120 | 33235 | 0.3009 | 2.481 | 1.782 | 2.511 | 1.680 | 2.514 | 1.664 | 2.538 | 1.670 |
| 4.102 | 33089 | 0.3022 | 2.480 | 1.771 | 2.510 | 1.673 | 2.514 | 1.658 | 2.540 | 1.685 |
| 4.084 | 32944 | 0.3035 | 2.479 | 1.761 | 2.509 | 1.666 | 2.513 | 1.653 | 2.543 | 1.703 |
| 4.066 | 32798 | 0.3049 | 2.478 | 1.752 | 2.508 | 1.661 | 2.513 | 1.647 | 2.548 | 1.724 |
| 4.048 | 32652 | 0.3063 | 2.476 | 1.744 | 2.507 | 1.655 | 2.512 | 1.642 | 2.557 | 1.748 |
| 4.030 | 32506 | 0.3076 | 2.475 | 1.736 | 2.506 | 1.650 | 2.512 | 1.638 | 2.571 | 1.776 |
| 4.012 | 32360 | 0.3090 | 2.474 | 1.729 | 2.506 | 1.645 | 2.511 | 1.634 | 2.593 | 1.806 |
| 3.994 | 32215 | 0.3104 | 2.473 | 1.722 | 2.505 | 1.641 | 2.510 | 1.630 | 2.624 | 1.834 |
| 3.976 | 32069 | 0.3118 | 2.471 | 1.716 | 2.504 | 1.637 | 2.511 | 1.626 | 2.665 | 1.859 |
| 3.958 | 31923 | 0.3133 | 2.470 | 1.711 | 2.503 | 1.633 | 2.510 | 1.622 | 2.715 | 1.876 |
| 3.940 | 31777 | 0.3147 | 2.470 | 1.706 | 2.503 | 1.629 | 2.510 | 1.619 | 2.768 | 1.881 |
| 3.922 | 31632 | 0.3161 | 2.469 | 1.701 | 2.502 | 1.626 | 2.510 | 1.617 | 2.822 | 1.875 |
| 3.904 | 31486 | 0.3176 | 2.468 | 1.697 | 2.502 | 1.623 | 2.510 | 1.614 | 2.873 | 1.860 |
| 3.886 | 31340 | 0.3191 | 2.468 | 1.693 | 2.502 | 1.621 | 2.510 | 1.612 | 2.917 | 1.838 |
| 3.867 | 31194 | 0.3206 | 2.467 | 1.690 | 2.502 | 1.619 | 2.511 | 1.610 | 2.956 | 1.809 |
| 3.849 | 31049 | 0.3221 | 2.467 | 1.687 | 2.502 | 1.617 | 2.511 | 1.609 | 2.988 | 1.778 |
| 3.831 | 30903 | 0.3236 | 2.467 | 1.684 | 2.502 | 1.615 | 2.511 | 1.607 | 3.015 | 1.745 |
| 3.813 | 30757 | 0.3251 | 2.467 | 1.681 | 2.502 | 1.614 | 2.511 | 1.606 | 3.035 | 1.712 |
| 3.795 | 30611 | 0.3267 | 2.467 | 1.679 | 2.502 | 1.613 | 2.512 | 1.605 | 3.052 | 1.679 |
| 3.777 | 30465 | 0.3282 | 2.466 | 1.677 | 2.502 | 1.612 | 2.512 | 1.606 | 3.063 | 1.648 |
| 3.759 | 30320 | 0.3298 | 2.467 | 1.675 | 2.503 | 1.612 | 2.513 | 1.606 | 3.071 | 1.618 |
| 3.741 | 30174 | 0.3314 | 2.467 | 1.674 | 2.503 | 1.612 | 2.514 | 1.606 | 3.077 | 1.591 |
| 3.723 | 30028 | 0.3330 | 2.467 | 1.673 | 2.504 | 1.612 | 2.515 | 1.607 | 3.080 | 1.566 |
| 3.705 | 29882 | 0.3346 | 2.467 | 1.672 | 2.505 | 1.613 | 2.517 | 1.608 | 3.082 | 1.542 |
| 3.687 | 29737 | 0.3363 | 2.468 | 1.672 | 2.506 | 1.614 | 2.518 | 1.609 | 3.081 | 1.521 |
| 3.669 | 29591 | 0.3379 | 2.469 | 1.671 | 2.508 | 1.614 | 2.520 | 1.611 | 3.080 | 1.503 |
| 3.651 | 29445 | 0.3396 | 2.470 | 1.671 | 2.509 | 1.616 | 2.522 | 1.613 | 3.077 | 1.486 |
| 3.633 | 29299 | 0.3413 | 2.470 | 1.671 | 2.511 | 1.617 | 2.525 | 1.615 | 3.074 | 1.472 |
| 3.614 | 29154 | 0.3430 | 2.472 | 1.672 | 2.513 | 1.619 | 2.527 | 1.617 | 3.070 | 1.459 |
| 3.596 | 29008 | 0.3447 | 2.473 | 1.673 | 2.515 | 1.621 | 2.530 | 1.619 | 3.066 | 1.448 |
| 3.578 | 28862 | 0.3465 | 2.474 | 1.674 | 2.517 | 1.624 | 2.533 | 1.622 | 3.060 | 1.439 |
| 3.560 | 28716 | 0.3482 | 2.476 | 1.675 | 2.519 | 1.626 | 2.536 | 1.625 | 3.054 | 1.434 |

TABLE II (*Continued*)

| | | | x=0 | | 0.20 | | 0.29 | | 1.0 | |
|---|---|---|---|---|---|---|---|---|---|---|
| eV | $cm^{-1}$ | μm | n | k | n | k | n | k | n | k |
| 3.542 | 28570 | 0.3500 | 2.478 | 1.677 | 2.522 | 1.629 | 2.540 | 1.629 | 3.047 | 1.430 |
| 3.524 | 28425 | 0.3518 | 2.480 | 1.679 | 2.525 | 1.633 | 2.544 | 1.632 | 3.040 | 1.430 |
| 3.506 | 28279 | 0.3536 | 2.481 | 1.681 | 2.529 | 1.636 | 2.548 | 1.636 | 3.032 | 1.434 |
| 3.488 | 28133 | 0.3555 | 2.484 | 1.683 | 2.532 | 1.640 | 2.553 | 1.640 | 3.023 | 1.445 |
| 3.470 | 27987 | 0.3573 | 2.487 | 1.686 | 2.536 | 1.644 | 2.557 | 1.645 | 3.016 | 1.463 |
| 3.452 | 27842 | 0.3592 | 2.489 | 1.689 | 2.540 | 1.648 | 2.563 | 1.649 | 3.013 | 1.490 |
| 3.434 | 27696 | 0.3611 | 2.492 | 1.692 | 2.545 | 1.652 | 2.568 | 1.654 | 3.019 | 1.528 |
| 3.416 | 27550 | 0.3630 | 2.495 | 1.696 | 2.549 | 1.657 | 2.574 | 1.659 | 3.040 | 1.575 |
| 3.398 | 27404 | 0.3649 | 2.499 | 1.699 | 2.555 | 1.662 | 2.580 | 1.665 | 3.085 | 1.626 |
| 3.380 | 27259 | 0.3669 | 2.502 | 1.703 | 2.560 | 1.667 | 2.587 | 1.670 | 3.158 | 1.667 |
| 3.361 | 27113 | 0.3688 | 2.506 | 1.707 | 2.566 | 1.673 | 2.595 | 1.676 | 3.251 | 1.683 |
| 3.343 | 26967 | 0.3708 | 2.510 | 1.712 | 2.572 | 1.679 | 2.603 | 1.682 | 3.350 | 1.668 |
| 3.325 | 26821 | 0.3728 | 2.515 | 1.716 | 2.579 | 1.685 | 2.612 | 1.689 | 3.441 | 1.625 |
| 3.307 | 26676 | 0.3749 | 2.520 | 1.722 | 2.586 | 1.691 | 2.621 | 1.696 | 3.515 | 1.561 |
| 3.289 | 26530 | 0.3769 | 2.525 | 1.727 | 2.594 | 1.697 | 2.630 | 1.703 | 3.569 | 1.489 |
| 3.271 | 26384 | 0.3790 | 2.530 | 1.732 | 2.602 | 1.704 | 2.641 | 1.710 | 3.605 | 1.416 |
| 3.253 | 26238 | 0.3811 | 2.536 | 1.738 | 2.610 | 1.711 | 2.652 | 1.717 | 3.627 | 1.345 |
| 3.235 | 26092 | 0.3833 | 2.542 | 1.743 | 2.620 | 1.718 | 2.664 | 1.725 | 3.639 | 1.277 |
| 3.217 | 25947 | 0.3854 | 2.548 | 1.750 | 2.630 | 1.726 | 2.676 | 1.732 | 3.643 | 1.213 |
| 3.199 | 25801 | 0.3876 | 2.555 | 1.756 | 2.640 | 1.733 | 2.691 | 1.741 | 3.641 | 1.154 |
| 3.181 | 25655 | 0.3898 | 2.563 | 1.763 | 2.652 | 1.742 | 2.706 | 1.749 | 3.634 | 1.101 |
| 3.163 | 25509 | 0.3920 | 2.570 | 1.770 | 2.664 | 1.750 | 2.723 | 1.758 | 3.625 | 1.051 |
| 3.145 | 25364 | 0.3943 | 2.578 | 1.777 | 2.677 | 1.759 | 2.741 | 1.766 | 3.613 | 1.007 |
| 3.127 | 25218 | 0.3965 | 2.587 | 1.784 | 2.691 | 1.767 | 2.761 | 1.774 | 3.600 | 0.9661 |
| 3.108 | 25072 | 0.3989 | 2.596 | 1.792 | 2.706 | 1.776 | 2.782 | 1.781 | 3.587 | 0.9297 |
| 3.090 | 24926 | 0.4012 | 2.606 | 1.800 | 2.722 | 1.785 | 2.806 | 1.788 | 3.572 | 0.8963 |
| 3.072 | 24781 | 0.4035 | 2.616 | 1.808 | 2.740 | 1.794 | 2.832 | 1.793 | 3.558 | 0.8639 |
| 3.054 | 24635 | 0.4059 | 2.627 | 1.816 | 2.759 | 1.804 | 2.861 | 1.795 | 3.543 | 0.8345 |
| 3.036 | 24489 | 0.4083 | 2.639 | 1.825 | 2.781 | 1.813 | 2.891 | 1.795 | 3.528 | 0.8078 |
| 3.018 | 24343 | 0.4108 | 2.651 | 1.834 | 2.804 | 1.822 | 2.922 | 1.790 | 3.513 | 0.7819 |
| 3.000 | 24197 | 0.4133 | 2.664 | 1.844 | 2.831 | 1.829 | 2.953 | 1.782 | 3.498 | 0.7588 |
| 2.982 | 24052 | 0.4158 | 2.678 | 1.853 | 2.860 | 1.835 | 2.983 | 1.770 | 3.484 | 0.7362 |
| 2.964 | 23906 | 0.4183 | 2.694 | 1.863 | 2.891 | 1.838 | 3.010 | 1.756 | 3.470 | 0.7148 |
| 2.946 | 23760 | 0.4209 | 2.710 | 1.873 | 2.923 | 1.837 | 3.034 | 1.740 | 3.457 | 0.6955 |
| 2.928 | 23614 | 0.4235 | 2.727 | 1.883 | 2.957 | 1.833 | 3.056 | 1.722 | 3.444 | 0.6762 |
| 2.910 | 23469 | 0.4261 | 2.746 | 1.893 | 2.991 | 1.823 | 3.075 | 1.703 | 3.430 | 0.6589 |
| 2.892 | 23323 | 0.4288 | 2.768 | 1.904 | 3.023 | 1.810 | 3.091 | 1.684 | 3.418 | 0.6419 |
| 2.873 | 23177 | 0.4315 | 2.790 | 1.914 | 3.052 | 1.793 | 3.105 | 1.666 | 3.405 | 0.6252 |
| 2.855 | 23031 | 0.4342 | 2.816 | 1.924 | 3.078 | 1.774 | 3.118 | 1.648 | 3.393 | 0.6105 |
| 2.837 | 22886 | 0.4370 | 2.844 | 1.933 | 3.101 | 1.754 | 3.129 | 1.631 | 3.381 | 0.5956 |
| 2.819 | 22740 | 0.4398 | 2.874 | 1.940 | 3.120 | 1.734 | 3.138 | 1.616 | 3.369 | 0.5824 |
| 2.801 | 22594 | 0.4426 | 2.908 | 1.945 | 3.136 | 1.713 | 3.146 | 1.602 | 3.358 | 0.5690 |
| 2.783 | 22448 | 0.4455 | 2.945 | 1.946 | 3.150 | 1.694 | 3.154 | 1.589 | 3.347 | 0.5552 |
| 2.765 | 22302 | 0.4484 | 2.983 | 1.942 | 3.162 | 1.675 | 3.161 | 1.576 | 3.336 | 0.5428 |
| 2.747 | 22157 | 0.4513 | 3.020 | 1.932 | 3.172 | 1.658 | 3.167 | 1.566 | 3.326 | 0.5306 |
| 2.729 | 22011 | 0.4543 | 3.056 | 1.917 | 3.181 | 1.642 | 3.174 | 1.555 | 3.315 | 0.5192 |

TABLE II (*Continued*)

| | | | x=0 | | 0.20 | | 0.29 | | 1.0 | |
|---|---|---|---|---|---|---|---|---|---|---|
| eV | $cm^{-1}$ | μm | n | k | n | k | n | k | n | k |
| 2.711 | 21865 | 0.4573 | 3.088 | 1.898 | 3.190 | 1.627 | 3.181 | 1.546 | 3.305 | 0.5089 |
| 2.693 | 21719 | 0.4604 | 3.115 | 1.877 | 3.197 | 1.613 | 3.187 | 1.539 | 3.296 | 0.4995 |
| 2.675 | 21574 | 0.4635 | 3.138 | 1.856 | 3.203 | 1.601 | 3.193 | 1.533 | 3.286 | 0.4895 |
| 2.657 | 21428 | 0.4667 | 3.159 | 1.833 | 3.210 | 1.590 | 3.201 | 1.527 | 3.276 | 0.4800 |
| 2.639 | 21282 | 0.4699 | 3.175 | 1.812 | 3.216 | 1.581 | 3.207 | 1.524 | 3.269 | 0.4702 |
| 2.620 | 21136 | 0.4731 | 3.190 | 1.791 | 3.222 | 1.572 | 3.216 | 1.520 | 3.259 | 0.4607 |
| 2.602 | 20991 | 0.4764 | 3.203 | 1.771 | 3.229 | 1.564 | 3.225 | 1.517 | 3.252 | 0.4507 |
| 2.584 | 20845 | 0.4797 | 3.214 | 1.753 | 3.236 | 1.558 | 3.236 | 1.515 | 3.243 | 0.4421 |
| 2.566 | 20699 | 0.4831 | 3.223 | 1.736 | 3.242 | 1.554 | 3.246 | 1.516 | 3.237 | 0.4337 |
| 2.548 | 20553 | 0.4865 | 3.231 | 1.721 | 3.251 | 1.549 | 3.259 | 1.517 | 3.230 | 0.4248 |
| 2.530 | 20407 | 0.4900 | 3.239 | 1.707 | 3.259 | 1.546 | 3.274 | 1.518 | 3.223 | 0.4169 |
| 2.512 | 20262 | 0.4935 | 3.245 | 1.695 | 3.268 | 1.545 | 3.290 | 1.522 | 3.217 | 0.4080 |
| 2.494 | 20116 | 0.4971 | 3.252 | 1.683 | 3.278 | 1.544 | 3.310 | 1.525 | 3.211 | 0.3978 |
| 2.476 | 19970 | 0.5007 | 3.259 | 1.674 | 3.290 | 1.545 | 3.333 | 1.530 | 3.204 | 0.3900 |
| 2.458 | 19824 | 0.5044 | 3.265 | 1.665 | 3.303 | 1.546 | 3.360 | 1.534 | 3.197 | 0.3789 |
| 2.440 | 19679 | 0.5082 | 3.272 | 1.658 | 3.318 | 1.549 | 3.393 | 1.537 | 3.190 | 0.3681 |
| 2.422 | 19533 | 0.5120 | 3.279 | 1.653 | 3.335 | 1.553 | 3.433 | 1.536 | 3.182 | 0.3574 |
| 2.404 | 19387 | 0.5158 | 3.287 | 1.647 | 3.355 | 1.558 | 3.479 | 1.529 | 3.174 | 0.3475 |
| 2.386 | 19241 | 0.5197 | 3.294 | 1.644 | 3.379 | 1.564 | 3.527 | 1.514 | 3.165 | 0.3390 |
| 2.367 | 19096 | 0.5237 | 3.303 | 1.641 | 3.407 | 1.570 | 3.576 | 1.487 | 3.157 | 0.3315 |
| 2.349 | 18950 | 0.5277 | 3.313 | 1.641 | 3.442 | 1.576 | 3.621 | 1.450 | 3.148 | 0.3244 |
| 2.331 | 18804 | 0.5318 | 3.324 | 1.640 | 3.485 | 1.579 | 3.658 | 1.406 | 3.139 | 0.3189 |
| 2.313 | 18658 | 0.5360 | 3.335 | 1.642 | 3.536 | 1.574 | 3.688 | 1.358 | 3.131 | 0.3134 |
| 2.295 | 18513 | 0.5402 | 3.349 | 1.645 | 3.591 | 1.559 | 3.709 | 1.309 | 3.123 | 0.3080 |
| 2.277 | 18367 | 0.5445 | 3.364 | 1.649 | 3.648 | 1.530 | 3.724 | 1.261 | 3.116 | 0.3024 |
| 2.259 | 18221 | 0.5488 | 3.382 | 1.653 | 3.699 | 1.488 | 3.733 | 1.213 | 3.108 | 0.2970 |
| 2.241 | 18075 | 0.5532 | 3.402 | 1.660 | 3.741 | 1.437 | 3.738 | 1.167 | 3.102 | 0.2917 |
| 2.223 | 17929 | 0.5577 | 3.425 | 1.668 | 3.772 | 1.383 | 3.739 | 1.125 | 3.095 | 0.2854 |
| 2.205 | 17784 | 0.5623 | 3.454 | 1.677 | 3.794 | 1.328 | 3.738 | 1.085 | 3.089 | 0.2813 |
| 2.187 | 17638 | 0.5670 | 3.488 | 1.687 | 3.808 | 1.275 | 3.734 | 1.047 | 3.083 | 0.2734 |
| 2.169 | 17492 | 0.5717 | 3.532 | 1.696 | 3.816 | 1.224 | 3.729 | 1.011 | 3.076 | 0.2708 |
| 2.151 | 17346 | 0.5765 | 3.586 | 1.700 | 3.819 | 1.175 | 3.722 | 0.9776 | 3.070 | 0.2682 |
| 2.133 | 17201 | 0.5814 | 3.650 | 1.694 | 3.818 | 1.131 | 3.714 | 0.9480 | 3.064 | 0.2651 |
| 2.114 | 17055 | 0.5863 | 3.719 | 1.670 | 3.814 | 1.090 | 3.706 | 0.9190 | 3.059 | 0.2608 |
| 2.096 | 16909 | 0.5914 | 3.785 | 1.626 | 3.809 | 1.050 | 3.696 | 0.8924 | 3.054 | 0.2600 |
| 2.078 | 16763 | 0.5965 | 3.838 | 1.569 | 3.803 | 1.014 | 3.688 | 0.8664 | 3.048 | 0.2576 |
| 2.060 | 16618 | 0.6018 | 3.876 | 1.507 | 3.795 | 0.9795 | 3.678 | 0.8430 | 3.044 | 0.2508 |
| 2.042 | 16472 | 0.6071 | 3.901 | 1.443 | 3.786 | 0.9476 | 3.669 | 0.8201 | 3.040 | 0.2497 |
| 2.024 | 16326 | 0.6125 | 3.917 | 1.382 | 3.776 | 0.9175 | 3.659 | 0.7979 | 3.035 | 0.2450 |
| 2.006 | 16180 | 0.6180 | 3.925 | 1.325 | 3.766 | 0.8887 | 3.649 | 0.7780 | 3.031 | 0.2403 |
| 1.988 | 16034 | 0.6237 | 3.929 | 1.272 | 3.756 | 0.8630 | 3.641 | 0.7573 | 3.027 | 0.2338 |
| 1.970 | 15889 | 0.6294 | 3.929 | 1.222 | 3.745 | 0.8380 | 3.631 | 0.7401 | 3.023 | 0.2314 |
| 1.952 | 15743 | 0.6352 | 3.924 | 1.176 | 3.735 | 0.8145 | 3.621 | 0.7218 | 3.019 | 0.2249 |
| 1.934 | 15597 | 0.6411 | 3.919 | 1.134 | 3.724 | 0.7936 | 3.612 | 0.7053 | 3.016 | 0.2201 |
| 1.916 | 15451 | 0.6472 | 3.911 | 1.094 | 3.714 | 0.7725 | 3.603 | 0.6901 | 3.013 | 0.2182 |
| 1.898 | 15306 | 0.6534 | 3.903 | 1.058 | 3.703 | 0.7530 | 3.594 | 0.6745 | 3.009 | 0.2186 |

TABLE II (*Continued*)

| | | | x=0 | | 0.20 | | 0.29 | | 1.0 | |
|---|---|---|---|---|---|---|---|---|---|---|
| eV | $cm^{-1}$ | $\mu m$ | n | k | n | k | n | k | n | k |
| 1.880 | 15160 | 0.6596 | 3.892 | 1.024 | 3.691 | 0.7356 | 3.584 | 0.6616 | 3.005 | 0.2171 |
| 1.861 | 15014 | 0.6660 | 3.882 | 0.9923 | 3.682 | 0.7181 | 3.576 | 0.6486 | 3.002 | 0.2144 |
| 1.843 | 14868 | 0.6726 | 3.870 | 0.9642 | 3.671 | 0.7025 | 3.566 | 0.6368 | 3.000 | 0.2138 |
| 1.825 | 14723 | 0.6792 | 3.860 | 0.9358 | 3.661 | 0.6860 | 3.558 | 0.6253 | 2.997 | 0.2109 |
| 1.807 | 14577 | 0.6860 | 3.848 | 0.9107 | 3.652 | 0.6733 | 3.550 | 0.6136 | 2.995 | 0.2085 |
| 1.789 | 14431 | 0.6930 | 3.837 | 0.8863 | 3.643 | 0.6568 | 3.541 | 0.6022 | 2.994 | 0.2025 |
| 1.771 | 14285 | 0.7000 | 3.826 | 0.8633 | 3.633 | 0.6429 | 3.534 | 0.5914 | 2.992 | 0.1972 |
| 1.753 | 14139 | 0.7072 | 3.815 | 0.8419 | 3.624 | 0.6307 | 3.527 | 0.5802 | 2.990 | 0.1984 |
| 1.735 | 13994 | 0.7146 | 3.805 | 0.8226 | 3.617 | 0.6157 | 3.520 | 0.5703 | 2.990 | 0.1908 |
| 1.717 | 13848 | 0.7221 | 3.795 | 0.8024 | 3.608 | 0.6026 | 3.514 | 0.5586 | 2.989 | 0.1865 |
| 1.699 | 13702 | 0.7298 | 3.786 | 0.7828 | 3.600 | 0.5915 | 3.508 | 0.5512 | 2.989 | 0.1808 |
| 1.681 | 13556 | 0.7377 | 3.776 | 0.7644 | 3.593 | 0.5792 | 3.500 | 0.5415 | 2.989 | 0.1780 |
| 1.663 | 13411 | 0.7457 | 3.767 | 0.7474 | 3.585 | 0.5691 | 3.498 | 0.5344 | 2.990 | 0.1747 |
| 1.645 | 13265 | 0.7539 | 3.756 | 0.7351 | 3.576 | 0.5594 | 3.491 | 0.5229 | 2.991 | 0.1718 |
| 1.627 | 13119 | 0.7622 | 3.747 | 0.7225 | 3.570 | 0.5502 | 3.484 | 0.5147 | 2.992 | 0.1727 |
| 1.608 | 12973 | 0.7708 | 3.738 | 0.7097 | 3.562 | 0.5423 | 3.478 | 0.5073 | 2.997 | 0.1761 |
| 1.590 | 12828 | 0.7796 | 3.729 | 0.6957 | 3.554 | 0.5344 | 3.473 | 0.5019 | 3.004 | 0.1650 |
| 1.572 | 12682 | 0.7885 | 3.719 | 0.6864 | 3.548 | 0.5273 | 3.465 | 0.4966 | 3.012 | 0.1578 |
| 1.554 | 12536 | 0.7977 | 3.711 | 0.6716 | 3.541 | 0.5197 | 3.462 | 0.4845 | 3.021 | 0.1506 |
| 1.536 | 12390 | 0.8071 | 3.702 | 0.6600 | 3.533 | 0.5062 | 3.451 | 0.4905 | 3.033 | 0.1249 |
| 1.518 | 12244 | 0.8167 | 3.691 | 0.6552 | 3.524 | 0.5078 | 3.446 | 0.4793 | 3.037 | 0.1475 |
| 1.500 | 12099 | 0.8265 | 3.685 | 0.6382 | 3.518 | 0.4999 | 3.442 | 0.4716 | 3.037 | 0.0998 |

TABLE III

Values of $n$ and $k$ for $Hg_{1-x}Cd_xTe$ (Ref. [6])

| | | | x=0 | | 0.43 | | 0.76 | | 0.86 | | 0.91 | | 1.0 | |
|---|---|---|---|---|---|---|---|---|---|---|---|---|---|---|
| eV | $cm^{-1}$ | $\mu m$ | n | k | n | k | n | k | n | k | n | k | n | k |
| 5.50 | 44362 | 0.2254 | 1.42 | 1.75 | 1.41 | 1.94 | 1.39 | 2.06 | 1.41 | 2.05 | 1.41 | 2.10 | 1.35 | 2.12 |
| 5.46 | 44039 | 0.2271 | 1.42 | 1.77 | 1.43 | 1.96 | 1.40 | 2.09 | 1.42 | 2.08 | 1.43 | 2.13 | 1.40 | 2.18 |
| 5.42 | 43717 | 0.2287 | 1.43 | 1.79 | 1.46 | 1.99 | 1.44 | 2.12 | 1.47 | 2.11 | 1.46 | 2.16 | 1.44 | 2.22 |
| 5.38 | 43394 | 0.2304 | 1.44 | 1.81 | 1.49 | 2.01 | 1.49 | 2.15 | 1.51 | 2.13 | 1.50 | 2.19 | 1.50 | 2.26 |
| 5.34 | 43071 | 0.2322 | 1.45 | 1.83 | 1.53 | 2.04 | 1.54 | 2.18 | 1.56 | 2.16 | 1.57 | 2.22 | 1.58 | 2.29 |
| 5.30 | 42749 | 0.2339 | 1.46 | 1.85 | 1.57 | 2.06 | 1.58 | 2.20 | 1.62 | 2.18 | 1.62 | 2.24 | 1.65 | 2.32 |
| 5.26 | 42426 | 0.2357 | 1.48 | 1.87 | 1.61 | 2.06 | 1.63 | 2.21 | 1.68 | 2.21 | 1.68 | 2.25 | 1.73 | 2.33 |
| 5.22 | 42104 | 0.2375 | 1.50 | 1.88 | 1.65 | 2.08 | 1.68 | 2.23 | 1.74 | 2.22 | 1.75 | 2.25 | 1.84 | 2.32 |
| 5.18 | 41781 | 0.2393 | 1.51 | 1.91 | 1.70 | 2.09 | 1.76 | 2.26 | 1.81 | 2.21 | 1.85 | 2.25 | 1.94 | 2.31 |
| 5.14 | 41458 | 0.2412 | 1.54 | 1.94 | 1.74 | 2.11 | 1.82 | 2.25 | 1.91 | 2.23 | 1.95 | 2.23 | 2.03 | 2.29 |
| 5.10 | 41136 | 0.2431 | 1.56 | 1.95 | 1.78 | 2.12 | 1.90 | 2.25 | 1.99 | 2.22 | 2.03 | 2.21 | 2.10 | 2.29 |
| 5.06 | 40813 | 0.2450 | 1.58 | 1.97 | 1.82 | 2.12 | 1.97 | 2.26 | 2.06 | 2.22 | 2.10 | 2.20 | 2.18 | 2.27 |
| 5.02 | 40490 | 0.2470 | 1.61 | 1.99 | 1.87 | 2.13 | 2.06 | 2.22 | 2.14 | 2.19 | 2.19 | 2.14 | 2.26 | 2.22 |
| 4.98 | 40168 | 0.2490 | 1.65 | 2.01 | 1.92 | 2.13 | 2.14 | 2.18 | 2.21 | 2.14 | 2.28 | 2.08 | 2.34 | 2.15 |
| 4.94 | 39845 | 0.2510 | 1.69 | 2.03 | 1.97 | 2.13 | 2.20 | 2.14 | 2.25 | 2.11 | 2.33 | 2.04 | 2.38 | 2.10 |
| 4.90 | 39523 | 0.2530 | 1.72 | 2.05 | 2.01 | 2.13 | 2.24 | 2.10 | 2.29 | 2.06 | 2.37 | 1.99 | 2.42 | 2.04 |
| 4.86 | 39200 | 0.2551 | 1.76 | 2.06 | 2.07 | 2.11 | 2.27 | 2.05 | 2.32 | 2.01 | 2.40 | 1.94 | 2.44 | 1.98 |
| 4.82 | 38877 | 0.2572 | 1.81 | 2.07 | 2.14 | 2.11 | 2.30 | 2.00 | 2.33 | 1.95 | 2.42 | 1.89 | 2.45 | 1.93 |
| 4.78 | 38555 | 0.2594 | 1.86 | 2.07 | 2.20 | 2.08 | 2.31 | 1.95 | 2.35 | 1.90 | 2.43 | 1.85 | 2.45 | 1.87 |
| 4.74 | 38232 | 0.2616 | 1.90 | 2.07 | 2.24 | 2.05 | 2.33 | 1.91 | 2.36 | 1.87 | 2.44 | 1.82 | 2.44 | 1.83 |
| 4.70 | 37909 | 0.2638 | 1.94 | 2.07 | 2.29 | 2.01 | 2.34 | 1.87 | 2.36 | 1.84 | 2.45 | 1.79 | 2.44 | 1.79 |
| 4.66 | 37587 | 0.2661 | 2.00 | 2.07 | 2.32 | 1.98 | 2.34 | 1.84 | 2.37 | 1.80 | 2.45 | 1.76 | 2.43 | 1.75 |
| 4.62 | 37264 | 0.2684 | 2.05 | 2.05 | 2.35 | 1.94 | 2.35 | 1.81 | 2.37 | 1.77 | 2.45 | 1.74 | 2.42 | 1.72 |
| 4.58 | 36941 | 0.2707 | 2.10 | 2.04 | 2.38 | 1.90 | 2.36 | 1.78 | 2.37 | 1.75 | 2.45 | 1.72 | 2.41 | 1.70 |
| 4.54 | 36619 | 0.2731 | 2.13 | 2.03 | 2.38 | 1.87 | 2.36 | 1.76 | 2.37 | 1.73 | 2.44 | 1.70 | 2.40 | 1.69 |
| 4.50 | 36296 | 0.2755 | 2.17 | 2.01 | 2.40 | 1.83 | 2.36 | 1.75 | 2.36 | 1.71 | 2.44 | 1.69 | 2.40 | 1.67 |
| 4.46 | 35974 | 0.2780 | 2.21 | 1.98 | 2.41 | 1.80 | 2.36 | 1.72 | 2.37 | 1.69 | 2.44 | 1.67 | 2.39 | 1.66 |
| 4.42 | 35651 | 0.2805 | 2.24 | 1.95 | 2.41 | 1.77 | 2.37 | 1.71 | 2.37 | 1.68 | 2.43 | 1.66 | 2.38 | 1.66 |
| 4.38 | 35328 | 0.2831 | 2.27 | 1.92 | 2.41 | 1.74 | 2.37 | 1.70 | 2.38 | 1.67 | 2.43 | 1.66 | 2.37 | 1.65 |
| 4.34 | 35006 | 0.2857 | 2.29 | 1.89 | 2.42 | 1.73 | 2.37 | 1.69 | 2.38 | 1.67 | 2.43 | 1.65 | 2.37 | 1.65 |
| 4.30 | 34683 | 0.2883 | 2.31 | 1.86 | 2.42 | 1.71 | 2.37 | 1.68 | 2.38 | 1.66 | 2.43 | 1.65 | 2.36 | 1.65 |
| 4.26 | 34360 | 0.2910 | 2.33 | 1.83 | 2.42 | 1.69 | 2.38 | 1.67 | 2.39 | 1.66 | 2.43 | 1.66 | 2.36 | 1.66 |
| 4.22 | 34038 | 0.2938 | 2.34 | 1.81 | 2.42 | 1.67 | 2.38 | 1.66 | 2.39 | 1.65 | 2.44 | 1.66 | 2.36 | 1.67 |
| 4.18 | 33715 | 0.2966 | 2.35 | 1.78 | 2.42 | 1.67 | 2.38 | 1.66 | 2.40 | 1.65 | 2.44 | 1.66 | 2.35 | 1.68 |
| 4.14 | 33392 | 0.2995 | 2.35 | 1.76 | 2.42 | 1.66 | 2.38 | 1.66 | 2.40 | 1.65 | 2.44 | 1.67 | 2.35 | 1.69 |
| 4.10 | 33070 | 0.3024 | 2.35 | 1.73 | 2.43 | 1.65 | 2.39 | 1.66 | 2.41 | 1.65 | 2.45 | 1.68 | 2.34 | 1.72 |
| 4.06 | 32747 | 0.3054 | 2.35 | 1.71 | 2.43 | 1.64 | 2.40 | 1.66 | 2.42 | 1.66 | 2.47 | 1.69 | 2.35 | 1.76 |
| 4.02 | 32425 | 0.3084 | 2.35 | 1.70 | 2.43 | 1.64 | 2.40 | 1.66 | 2.42 | 1.66 | 2.48 | 1.70 | 2.36 | 1.79 |
| 3.98 | 32102 | 0.3115 | 2.35 | 1.68 | 2.43 | 1.63 | 2.41 | 1.66 | 2.43 | 1.67 | 2.49 | 1.72 | 2.39 | 1.85 |
| 3.94 | 31779 | 0.3147 | 2.35 | 1.67 | 2.43 | 1.63 | 2.42 | 1.66 | 2.45 | 1.67 | 2.51 | 1.73 | 2.51 | 1.89 |
| 3.90 | 31457 | 0.3179 | 2.35 | 1.66 | 2.44 | 1.62 | 2.43 | 1.67 | 2.47 | 1.68 | 2.56 | 1.74 | 2.66 | 1.90 |
| 3.86 | 31134 | 0.3212 | 2.36 | 1.66 | 2.44 | 1.62 | 2.45 | 1.67 | 2.49 | 1.69 | 2.60 | 1.76 | 2.75 | 1.88 |
| 3.82 | 30811 | 0.3246 | 2.36 | 1.65 | 2.44 | 1.62 | 2.46 | 1.68 | 2.51 | 1.70 | 2.63 | 1.77 | 2.82 | 1.84 |
| 3.78 | 30489 | 0.3280 | 2.36 | 1.65 | 2.45 | 1.62 | 2.48 | 1.68 | 2.53 | 1.71 | 2.68 | 1.78 | 2.87 | 1.79 |

TABLE III (*Continued*)

| | | | x=0 | | 0.43 | | 0.76 | | 0.86 | | 0.91 | | 1.0 | |
|---|---|---|---|---|---|---|---|---|---|---|---|---|---|---|
| eV | $cm^{-1}$ | μm | n | k | n | k | n | k | n | k | n | k | n | k |
| 3.74 | 30166 | 0.3315 | 2.36 | 1.65 | 2.45 | 1.62 | 2.50 | 1.69 | 2.56 | 1.72 | 2.75 | 1.77 | 2.90 | 1.74 |
| 3.70 | 29844 | 0.3351 | 2.37 | 1.65 | 2.46 | 1.62 | 2.52 | 1.71 | 2.60 | 1.73 | 2.81 | 1.74 | 2.91 | 1.68 |
| 3.66 | 29521 | 0.3387 | 2.37 | 1.65 | 2.47 | 1.62 | 2.55 | 1.72 | 2.64 | 1.73 | 2.84 | 1.72 | 2.92 | 1.64 |
| 3.62 | 29198 | 0.3425 | 2.38 | 1.65 | 2.47 | 1.63 | 2.57 | 1.72 | 2.67 | 1.74 | 2.88 | 1.69 | 2.92 | 1.60 |
| 3.58 | 28876 | 0.3463 | 2.38 | 1.66 | 2.48 | 1.64 | 2.61 | 1.73 | 2.73 | 1.73 | 2.91 | 1.65 | 2.92 | 1.58 |
| 3.54 | 28553 | 0.3502 | 2.39 | 1.66 | 2.50 | 1.65 | 2.66 | 1.74 | 2.79 | 1.70 | 2.94 | 1.62 | 2.91 | 1.56 |
| 3.50 | 28230 | 0.3542 | 2.39 | 1.67 | 2.51 | 1.66 | 2.71 | 1.75 | 2.82 | 1.68 | 2.96 | 1.60 | 2.89 | 1.56 |
| 3.46 | 27908 | 0.3583 | 2.39 | 1.68 | 2.53 | 1.67 | 2.75 | 1.73 | 2.86 | 1.65 | 2.98 | 1.58 | 2.87 | 1.58 |
| 3.42 | 27585 | 0.3625 | 2.40 | 1.68 | 2.55 | 1.69 | 2.80 | 1.71 | 2.88 | 1.62 | 3.00 | 1.56 | 2.85 | 1.62 |
| 3.38 | 27262 | 0.3668 | 2.41 | 1.69 | 2.57 | 1.70 | 2.84 | 1.68 | 2.91 | 1.59 | 3.01 | 1.55 | 2.94 | 1.72 |
| 3.34 | 26940 | 0.3712 | 2.42 | 1.70 | 2.60 | 1.72 | 2.87 | 1.65 | 2.94 | 1.57 | 3.04 | 1.55 | 3.18 | 1.76 |
| 3.30 | 26617 | 0.3757 | 2.43 | 1.71 | 2.63 | 1.74 | 2.90 | 1.61 | 2.96 | 1.55 | 3.07 | 1.55 | 3.39 | 1.73 |
| 3.26 | 26295 | 0.3803 | 2.44 | 1.73 | 2.66 | 1.75 | 2.93 | 1.59 | 2.98 | 1.53 | 3.11 | 1.54 | 3.50 | 1.62 |
| 3.22 | 25972 | 0.3850 | 2.46 | 1.74 | 2.71 | 1.76 | 2.95 | 1.56 | 3.00 | 1.52 | 3.16 | 1.53 | 3.54 | 1.50 |
| 3.18 | 25649 | 0.3899 | 2.48 | 1.76 | 2.78 | 1.76 | 2.98 | 1.54 | 3.03 | 1.50 | 3.24 | 1.50 | 3.56 | 1.31 |
| 3.14 | 25327 | 0.3948 | 2.50 | 1.78 | 2.85 | 1.76 | 3.00 | 1.53 | 3.07 | 1.49 | 3.31 | 1.46 | 3.55 | 1.20 |
| 3.10 | 25004 | 0.3999 | 2.51 | 1.79 | 2.89 | 1.74 | 3.02 | 1.52 | 3.09 | 1.48 | 3.36 | 1.42 | 3.54 | 1.12 |
| 3.06 | 24681 | 0.4052 | 2.54 | 1.81 | 2.93 | 1.71 | 3.04 | 1.51 | 3.13 | 1.47 | 3.42 | 1.33 | 3.52 | 1.04 |
| 3.02 | 24359 | 0.4105 | 2.57 | 1.84 | 2.98 | 1.67 | 3.07 | 1.50 | 3.18 | 1.45 | 3.47 | 1.22 | 3.50 | 0.965 |
| 2.98 | 24036 | 0.4160 | 2.60 | 1.86 | 3.01 | 1.64 | 3.10 | 1.50 | 3.26 | 1.41 | 3.50 | 1.12 | 3.48 | 0.893 |
| 2.94 | 23714 | 0.4217 | 2.64 | 1.89 | 3.03 | 1.61 | 3.14 | 1.49 | 3.31 | 1.35 | 3.50 | 1.04 | 3.45 | 0.839 |
| 2.90 | 23391 | 0.4275 | 2.67 | 1.91 | 3.06 | 1.58 | 3.18 | 1.47 | 3.35 | 1.29 | 3.49 | 0.981 | 3.43 | 0.793 |
| 2.86 | 23068 | 0.4335 | 2.72 | 1.93 | 3.08 | 1.56 | 3.25 | 1.43 | 3.38 | 1.21 | 3.48 | 0.923 | 3.41 | 0.747 |
| 2.82 | 22746 | 0.4396 | 2.79 | 1.95 | 3.10 | 1.54 | 3.33 | 1.36 | 3.41 | 1.12 | 3.47 | 0.857 | 3.39 | 0.702 |
| 2.78 | 22423 | 0.4460 | 2.89 | 1.95 | 3.11 | 1.53 | 3.37 | 1.27 | 3.44 | 1.04 | 3.45 | 0.799 | 3.36 | 0.654 |
| 2.74 | 22100 | 0.4525 | 2.96 | 1.93 | 3.13 | 1.52 | 3.39 | 1.20 | 3.45 | 0.983 | 3.44 | 0.770 | 3.34 | 0.621 |
| 2.70 | 21778 | 0.4592 | 3.01 | 1.90 | 3.15 | 1.52 | 3.42 | 1.12 | 3.45 | 0.918 | 3.43 | 0.731 | 3.33 | 0.585 |
| 2.66 | 21455 | 0.4661 | 3.07 | 1.85 | 3.19 | 1.52 | 3.43 | 1.05 | 3.45 | 0.864 | 3.41 | 0.688 | 3.31 | 0.547 |
| 2.62 | 21132 | 0.4732 | 3.11 | 1.80 | 3.25 | 1.53 | 3.43 | 0.974 | 3.43 | 0.807 | 3.39 | 0.644 | 3.29 | 0.510 |
| 2.58 | 20810 | 0.4805 | 3.15 | 1.76 | 3.31 | 1.53 | 3.42 | 0.917 | 3.42 | 0.759 | 3.38 | 0.611 | 3.28 | 0.476 |
| 2.54 | 20487 | 0.4881 | 3.17 | 1.73 | 3.37 | 1.51 | 3.41 | 0.875 | 3.41 | 0.714 | 3.36 | 0.582 | 3.26 | 0.447 |
| 2.50 | 20165 | 0.4959 | 3.19 | 1.70 | 3.47 | 1.47 | 3.40 | 0.828 | 3.40 | 0.672 | 3.35 | 0.547 | 3.25 | 0.418 |
| 2.46 | 19842 | 0.5040 | 3.21 | 1.68 | 3.54 | 1.36 | 3.39 | 0.780 | 3.38 | 0.629 | 3.33 | 0.516 | 3.23 | 0.390 |
| 2.42 | 19519 | 0.5123 | 3.23 | 1.67 | 3.60 | 1.25 | 3.37 | 0.731 | 3.37 | 0.590 | 3.31 | 0.485 | 3.21 | 0.357 |
| 2.38 | 19197 | 0.5209 | 3.25 | 1.66 | 3.63 | 1.17 | 3.36 | 0.696 | 3.35 | 0.558 | 3.29 | 0.455 | 3.20 | 0.338 |
| 2.34 | 18874 | 0.5298 | 3.28 | 1.66 | 3.65 | 1.08 | 3.35 | 0.662 | 3.34 | 0.529 | 3.28 | 0.429 | 3.19 | 0.313 |
| 2.30 | 18551 | 0.5390 | 3.30 | 1.67 | 3.64 | 1.00 | 3.33 | 0.629 | 3.33 | 0.498 | 3.26 | 0.405 | 3.18 | 0.290 |
| 2.26 | 18229 | 0.5486 | 3.34 | 1.68 | 3.63 | 0.923 | 3.32 | 0.598 | 3.32 | 0.461 | 3.24 | 0.379 | 3.16 | 0.271 |
| 2.22 | 17906 | 0.5585 | 3.39 | 1.70 | 3.62 | 0.864 | 3.31 | 0.571 | 3.30 | 0.431 | 3.23 | 0.353 | 3.15 | 0.252 |
| 2.18 | 17583 | 0.5687 | 3.45 | 1.72 | 3.60 | 0.814 | 3.30 | 0.545 | 3.29 | 0.404 | 3.21 | 0.333 | 3.14 | 0.238 |
| 2.14 | 17261 | 0.5793 | 3.54 | 1.74 | 3.59 | 0.763 | 3.29 | 0.522 | 3.28 | 0.376 | 3.20 | 0.314 | 3.13 | 0.226 |
| 2.10 | 16938 | 0.5904 | 3.68 | 1.69 | 3.56 | 0.711 | 3.27 | 0.497 | 3.27 | 0.343 | 3.19 | 0.298 | 3.11 | 0.210 |
| 2.06 | 16616 | 0.6018 | 3.77 | 1.52 | 3.54 | 0.664 | 3.26 | 0.469 | 3.25 | 0.313 | 3.18 | 0.285 | 3.10 | 0.196 |
| 2.02 | 16293 | 0.6138 | 3.84 | 1.39 | 3.52 | 0.637 | 3.24 | 0.444 | 3.24 | 0.287 | 3.16 | 0.279 | 3.09 | 0.186 |
| 1.98 | 15970 | 0.6262 | 3.89 | 1.27 | 3.51 | 0.607 | 3.23 | 0.421 | 3.23 | 0.268 | 3.15 | 0.272 | 3.08 | 0.177 |
| 1.94 | 15648 | 0.6391 | 3.90 | 1.16 | 3.49 | 0.580 | 3.22 | 0.400 | 3.22 | 0.251 | 3.14 | 0.263 | 3.08 | 0.171 |

TABLE III (*Continued*)

| | | | x=0 | | 0.43 | | 0.76 | | 0.86 | | 0.91 | | 1.0 | |
|---|---|---|---|---|---|---|---|---|---|---|---|---|---|---|
| eV | $cm^{-1}$ | $\mu m$ | n | k | n | k | n | k | n | k | n | k | n | k |
| 1.90 | 15325 | 0.6525 | 3.88 | 1.09 | 3.47 | 0.553 | 3.21 | 0.377 | 3.21 | 0.239 | 3.12 | 0.260 | 3.06 | 0.169 |
| 1.86 | 15002 | 0.6666 | 3.86 | 1.05 | 3.45 | 0.534 | 3.20 | 0.362 | 3.19 | 0.238 | 3.12 | 0.259 | 3.05 | 0.170 |
| 1.82 | 14680 | 0.6812 | 3.84 | 1.02 | 3.44 | 0.519 | 3.19 | 0.351 | 3.18 | 0.239 | 3.11 | 0.258 | 3.04 | 0.173 |
| 1.78 | 14357 | 0.6965 | 3.82 | 0.989 | 3.42 | 0.508 | 3.18 | 0.346 | 3.17 | 0.241 | 3.09 | 0.260 | 3.03 | 0.178 |
| 1.74 | 14035 | 0.7125 | 3.80 | 0.969 | 3.40 | 0.498 | 3.17 | 0.341 | 3.16 | 0.244 | 3.08 | 0.263 | 3.03 | 0.184 |
| 1.70 | 13712 | 0.7293 | 3.77 | 0.951 | 3.39 | 0.487 | 3.16 | 0.336 | 3.16 | 0.246 | 3.07 | 0.266 | 3.02 | 0.189 |

TABLE IV

Values of $n$ and $k$ for $Hg_{1-x}Cd_xTe$ (Ref. [14])

| | | | x=0 | | ~0.16 | | 0.2 | | ~0.29 | | ~0.65 | | 1.0 | |
|---|---|---|---|---|---|---|---|---|---|---|---|---|---|---|
| eV | $cm^{-1}$ | $\mu m$ | n | k | n | k | n | k | n | k | n | k | n | k |
| 1.959 | 15803 | 0.6328 | 4.00 | 1.06 | 3.94 | 0.74 | 3.87 | 0.66 | 3.34 | 0.32 | 3.30 | 0.28 | 3.14 | 0.24 |

TABLE V

Sellmeier Parameters for $Hg_{1-x}Cd_xTe - 300K$

| x | $a_0$ | $a_1$ | $a_2(\mu m)$ | $a_3$ | $a_4(\mu m)$ | c | d |
|---|---|---|---|---|---|---|---|
| 0.18[a] | 13.337. | 0.3890 | 8.628 | 10.067 | 65.63 | | |
| 0.292 | 10.539 | 0.4792 | 3.75 | 6.063 | 74.29 | | |
| 0.390 | 8.600 | 0.6029 | 2.333 | 3.698 | 77.97 | | |
| 0.397 | 8.595 | 0.5954 | 2.304 | 3.785 | 75.20 | | |
| 0.459 | 7.919 | 0.6816 | 1.843 | 3.414 | 75.80 | | |
| 0.461 | 7.802 | 0.6968 | 1.820 | 3.418 | 76.14 | | |
| 0.522 | 7.310 | 0.8223 | 1.413 | 2.209 | 67.74 | | |
| 0.205[b] | 12.33 | 0.2167 | 6.568 | | | $-1.102\times10^{-3}$ | $-3.065\times10^{-7}$ |
| 0.29 | 10.91 | 0.3437 | 3.752 | | | $-9.661\times10^{-4}$ | $-1.956\times10^{-8}$ |
| 1.0 | 5.304 | 1.899 | 0.5713 | | | $-4.188\times10^{-4}$ | $-2.391\times10^{-7}$ |

[a] The first seven values for $0.18 \le x \le 0.522$ are from Ref. [21].
[b] The next three values for x=0.205, 0.29 and 1.0 are from Ref. [26].

TABLE VI

**Quadratic Interpolation Sellmeier Coefficients**

| | $A_i$ | $B_i$ | $C_i$ |
|---|---|---|---|
| $a_0$ | 19.76 | -41.82 | 34.5 |
| $a_1$ | 0.373 | -0.281 | 2.153 |
| $a_2(\mu m)$ | -200.0 | 2.841 | 1.897 |
| $a_3$ | 18.79* | -58.4* | 52.41* |
| $a_4(\mu m)$ | 73.25* | 73.25* | 73.25* |

* The mean value of 73.25 $\mu$m was used.

TABLE VII

**$n_{av}$ – Mean Value of $n$ for the Subband-Gap Region in $Hg_{1-x}Cd_xTe$ – 300K[a]**

| x | 0.3 | 0.4 | 0.5 | 0.6 | 0.7 | 0.8 | 0.9 | 1.0 |
|---|---|---|---|---|---|---|---|---|
| $n_{av}$ | 3.22 | 3.07 | 2.94 | 2.84 | 2.76 | 2.70 | 2.66 | 2.72 |

[a] $n_{av}$ values are computed using interpolation procedure described in the section on the visible and near visible behavior and are valid for the energy range $0.75E_g \leq E \leq 0.1$ eV for $0.3 \leq x \leq 0.5$ and for $0.5E_g \leq E \leq 0.1$ eV for $0.5 \leq x \leq 1$

TABLE VIII

Values of n and k for HgTe – 10K (Ref. [27])

| eV | $cm^{-1}$ | $\mu m$ | n | k |
|---|---|---|---|---|
| 0.60 | 4839 | 2.066 | 3.74[a] | 0.258 |
| 0.59 | 4759 | 2.101 | | 0.261 |
| 0.58 | 4678 | 2.138 | | 0.264 |
| 0.57 | 4598 | 2.175 | | 0.267 |
| 0.56 | 4517 | 2.214 | | 0.270 |
| 0.55 | 4436 | 2.254 | | 0.269 |
| 0.54 | 4356 | 2.296 | | 0.273 |
| 0.53 | 4275 | 2.339 | | 0.277 |
| 0.52 | 4194 | 2.384 | | 0.280 |
| 0.51 | 4114 | 2.431 | | 0.284 |
| 0.50 | 4033 | 2.480 | | 0.287 |
| 0.49 | 3952 | 2.530 | | 0.291 |
| 0.48 | 3872 | 2.583 | | 0.296 |
| 0.47 | 3791 | 2.638 | | 0.299 |
| 0.46 | 3710 | 2.695 | | 0.304 |
| 0.45 | 3630 | 2.755 | | 0.309 |
| 0.44 | 3549 | 2.818 | | 0.313 |
| 0.43 | 3468 | 2.883 | | 0.316 |
| 0.42 | 3388 | 2.952 | | 0.321 |
| 0.41 | 3307 | 3.024 | | 0.325 |
| 0.40 | 3226 | 3.100 | | 0.331 |
| 0.39 | 3146 | 3.179 | | 0.335 |
| 0.38 | 3065 | 3.263 | | 0.341 |
| 0.37 | 2984 | 3.351 | | 0.344 |
| 0.36 | 2904 | 3.444 | | 0.350 |
| 0.35 | 2823 | 3.542 | | 0.351 |
| 0.34 | 2742 | 3.646 | | 0.358 |
| 0.33 | 2662 | 3.757 | | 0.357 |
| 0.32 | 2581 | 3.874 | | 0.358 |
| 0.31 | 2500 | 3.999 | | 0.354 |
| 0.30 | 2420 | 4.133 | | 0.350* |
| 0.29 | 2339 | 4.275 | | 0.358 |
| 0.28 | 2258 | 4.428 | | 0.364 |
| 0.27 | 2178 | 4.592 | | 0.371 |
| 0.26 | 2097 | 4.768 | | 0.378 |
| 0.25 | 2016 | 4.959 | | 0.385 |
| 0.24 | 1936 | 5.166 | | 0.390 |
| 0.23 | 1855 | 5.390 | | 0.399 |
| 0.22 | 1774 | 5.635 | | 0.410 |
| 0.21 | 1694 | 5.904 | | 0.420 |
| 0.20 | 1613 | 6.199 | | 0.430 |
| 0.19 | 1533 | 6.525 | | 0.440 |
| 0.18 | 1452 | 6.888 | | 0.449 |
| 0.17 | 1371 | 7.293 | | 0.461 |
| 0.16 | 1291 | 7.749 | | 0.477 |

TABLE VIII (*Continued*)

| eV | $cm^{-1}$ | $\mu m$ | n | k |
|---|---|---|---|---|
| 0.15 | 1210 | 8.265 | | 0.487 |
| 0.14 | 1129 | 8.856 | | 0.506 |
| 0.13 | 1049 | 9.537 | | 0.524 |
| 0.12 | 967.9 | 10.33 | | 0.545 |
| 0.11 | 887.2 | 11.27 | | 0.574 |
| 0.10 | 806.6 | 12.40 | | 0.600 |
| 0.09 | 725.9 | 13.78 | | 0.633 |
| 0.08 | 645.3 | 15.50 | | 0.668 |
| 0.07 | 564.6 | 17.71 | | 0.712 |
| 0.06 | 483.9 | 20.66 | | 0.763 |
| 0.05 | 403.3 | 24.77 | 3.74[a] | 0.860 |

[a] A constant value was assumed to calculate $\alpha(E)$ in Ref. [27].

* The approximate position of the band-gap, $E_g$ is indicated. Note that the value of $E_g$ is negative in HgTe

TABLE IX

Values of $n$ and $k$ for $Hg_{1-x}Cd_xTe - x \simeq 0.2$ (Ref. [25] and [31])

| eV | $cm^{-1}$ | $\mu m$ | n | n-type (x=0.205) k (300K) | n-type (x=0.205) k (80K) | p-type (x=0.2) k (295K) | p-type (x=0.2) k (90K) |
|---|---|---|---|---|---|---|---|
| 0.260 | 2097 | 4.768 | | 0.134 | | | |
| 0.255 | 2057 | 4.862 | | 0.133 | | | |
| 0.250 | 2016 | 4.959 | | 0.131 | | | |
| 0.245 | 1976 | 5.060 | | 0.130 | | | |
| 0.240 | 1936 | 5.166 | | 0.128 | | | |
| 0.235 | 1895 | 5.276 | | 0.126 | | | |
| 0.230 | 1855 | 5.390 | | 0.123 | | | |
| 0.225 | 1815 | 5.510 | | 0.121 | | | |
| 0.220 | 1774 | 5.635 | | 0.117 | | | |
| 0.215 | 1734 | 5.767 | | 0.114 | | | |
| 0.210 | 1694 | 5.904 | | 0.110 | | | |
| 0.205 | 1653 | 6.048 | | 0.105 | | | |
| 0.200 | 1613 | 6.199 | | $0.992 \times 10^{-1}$ | | | |
| 0.195 | 1573 | 6.358 | | 0.924 | | | |
| 0.190 | 1533 | 6.525 | | 0.843 | | | |
| 0.185 | 1492 | 6.702 | | 0.741 | | | |
| 0.180 | 1452 | 6.888 | | 0.607 | | | |
| 0.175 | 1412 | 7.085 | | 0.408 | | | |
| 0.170 | 1371 | 7.293 | | 0.324* | | - * - | |
| 0.165 | 1331 | 7.514 | | 0.183 | | | |
| 0.160 | 1291 | 7.749 | 3.610 | 0.104 | | | |
| 0.155 | 1250 | 7.999 | 3.595 | $0.589 \times 10^{-2}$ | | $0.155 \times 10^{-1}$ | |
| 0.150 | 1210 | 8.265 | 3.583 | 0.334 | | 0.127 | |
| 0.145 | 1170 | 8.550 | 3.574 | 0.190 | | 0.102 | |
| 0.140 | 1129 | 8.856 | 3.567 | 0.108 | 0.280 | $0.899 \times 10^{-2}$ | |
| 0.135 | 1089 | 9.184 | 3.561 | $0.616 \times 10^{-3}$ | 0.275 | 0.832 | |
| 0.130 | 1049 | 9.537 | 3.555 | | 0.268 | 0.797 | |
| 0.125 | 1008 | 9.918 | 3.550 | | 0.260 | 0.760 | |
| 0.120 | 967.9 | 10.33 | 3.546 | | 0.249 | 0.773 | |
| 0.115 | 927.6 | 10.78 | 3.542 | | 0.235 | 0.787 | |
| 0.110 | 887.2 | 11.27 | 3.537 | | 0.216 | 0.803 | |
| 0.105 | 846.9 | 11.81 | 3.533 | | 0.191 | 0.843 | |
| 0.100 | 806.6 | 12.40 | 3.529 | | 0.155 | 0.899 | - * - |
| 0.095 | 766.3 | 13.05 | 3.525 | | $0.935 \times 10^{-1}$ | 0.961 | |
| 0.090 | 725.9 | 13.78 | 3.520 | | 0.519* | $0.103 \times 10^{-1}$ | |
| 0.085 | 685.6 | 14.59 | 3.515 | | 0.133 | 0.112 | $0.259 \times 10^{-1}$ |
| 0.080 | 645.3 | 15.50 | 3.509 | | $0.341 \times 10^{-2}$ | 0.123 | 0.274 |
| 0.075 | 604.9 | 16.53 | 3.502 | | $0.880 \times 10^{-3}$ | 0.141 | 0.297 |
| 0.070 | 564.6 | 17.71 | 3.494 | | | 0.164 | 0.323 |
| 0.065 | 524.3 | 19.07 | 3.483 | | | 0.186 | 0.352 |
| 0.060 | 483.9 | 20.66 | 3.471 | | | 0.215 | 0.390 |
| 0.055 | 443.6 | 22.54 | 3.454 | | | 0.258 | 0.441 |
| 0.050 | 403.3 | 24.80 | 3.431 | | | 0.311 | |

* The position of the band-gap, $E_g$, estimated in Ref. [25] and [31] is indicated.

TABLE X

Values of $n$ and $k$ for $Hg_{1-x}Cd_xTe - x \simeq 0.3$ (Ref. [26] and [31])

| eV | $cm^{-1}$ | $\mu m$ | n | n-type (x=0.29) k (300K) | n-type (x=0.29) k (85K) | p-type (x=0.3) k (295K) | p-type (x=0.3) k (90K) |
|---|---|---|---|---|---|---|---|
| 0.420 | 3388 | 2.952 | | 0.108 | | | |
| 0.415 | 3347 | 2.987 | | 0.108 | | | |
| 0.410 | 3307 | 3.024 | | 0.107 | | | |
| 0.405 | 3267 | 3.061 | | 0.106 | | | |
| 0.400 | 3226 | 3.100 | | 0.106 | | | |
| 0.395 | 3186 | 3.139 | | 0.105 | | | |
| 0.390 | 3146 | 3.179 | | 0.104 | | | |
| 0.385 | 3105 | 3.220 | | 0.103 | | | |
| 0.380 | 3065 | 3.263 | | 0.102 | | | |
| 0.375 | 3025 | 3.306 | | 0.100 | | | |
| 0.370 | 2984 | 3.351 | | $0.991 \times 10^{-1}$ | | | |
| 0.365 | 2944 | 3.397 | | 0.977 | | | |
| 0.360 | 2904 | 3.444 | | 0.962 | | | |
| 0.355 | 2863 | 3.492 | | 0.945 | | | |
| 0.350 | 2823 | 3.542 | | 0.927 | | | |
| 0.345 | 2783 | 3.594 | | 0.907 | | | |
| 0.340 | 2742 | 3.646 | | 0.886 | 0.179 | | |
| 0.335 | 2702 | 3.701 | | 0.862 | 0.177 | | |
| 0.330 | 2662 | 3.757 | | 0.836 | 0.176 | | |
| 0.325 | 2621 | 3.815 | | 0.807 | 0.174 | | |
| 0.320 | 2581 | 3.874 | | 0.775 | 0.172 | | |
| 0.315 | 2541 | 3.936 | | 0.739 | 0.170 | | |
| 0.310 | 2500 | 3.999 | | 0.698 | 0.167 | - * - | |
| 0.305 | 2460 | 4.065 | | 0.652 | 0.165 | | |
| 0.300 | 2420 | 4.133 | | 0.598 | 0.162 | | |
| 0.295 | 2379 | 4.203 | | 0.535 | 0.159 | | |
| 0.290 | 2339 | 4.275 | | 0.458 | 0.155 | | |
| 0.285 | 2299 | 4.350 | | 0.357 | 0.151 | | |
| 0.280 | 2258 | 4.428 | 3.480 | 0.241* | 0.147 | | - * - |
| 0.275 | 2218 | 4.508 | 3.465 | 0.142 | 0.142 | | |
| 0.270 | 2178 | 4.592 | 3.453 | $0.830 \times 10^{-2}$ | 0.136 | | |
| 0.265 | 2137 | 4.678 | 3.443 | 0.487 | 0.130 | | |
| 0.260 | 2097 | 4.768 | 3.434 | 0.286 | 0.123 | $0.336 \times 10^{-2}$ | |
| 0.255 | 2057 | 4.862 | 3.426 | 0.168 | 0.115 | 0.337 | |
| 0.250 | 2016 | 4.959 | 3.419 | $0.987 \times 10^{-3}$ | 0.105 | 0.339 | |
| 0.245 | 1976 | 5.060 | 3.413 | 0.580 | $0.933 \times 10^{-1}$ | 0.345 | |
| 0.240 | 1936 | 5.166 | 3.407 | 0.341 | 0.785 | 0.356 | |
| 0.235 | 1895 | 5.276 | 3.403 | | 0.584 | 0.368 | |
| 0.230 | 1855 | 5.390 | 3.398 | | 0.319* | 0.380 | |
| 0.225 | 1815 | 5.510 | 3.394 | | $0.921 \times 10^{-2}$ | 0.393 | |
| 0.220 | 1774 | 5.635 | 3.391 | | 0.267 | 0.407 | $0.624 \times 10^{-2}$ |
| 0.215 | 1734 | 5.767 | 3.387 | | $0.772 \times 10^{-3}$ | 0.421 | 0.645 |
| 0.210 | 1694 | 5.904 | 3.384 | | | 0.435 | 0.668 |
| 0.205 | 1653 | 6.048 | 3.381 | | | 0.451 | 0.695 |

TABLE X (*Continued*)

| eV | $cm^{-1}$ | μm | n | n-type (x=0.29 k (300K) | n-type (x=0.29 k (85K) | p-type (x=0.3) k (295K) | p-type (x=0.3) k (90K) |
|---|---|---|---|---|---|---|---|
| 0.200 | 1613 | 6.199 | 3.379 | | | 0.468 | 0.727 |
| 0.195 | 1573 | 6.358 | 3.376 | | | 0.486 | 0.762 |
| 0.190 | 1533 | 6.525 | 3.374 | | | 0.505 | 0.798 |
| 0.185 | 1492 | 6.702 | 3.372 | | | 0.525 | 0.835 |
| 0.180 | 1452 | 6.888 | 3.369 | | | 0.546 | 0.875 |
| 0.175 | 1412 | 7.085 | 3.367 | | | 0.568 | 0.918 |
| 0.170 | 1371 | 7.293 | 3.365 | | | 0.591 | 0.963 |
| 0.165 | 1331 | 7.514 | 3.364 | | | 0.616 | $0.101 \times 10^{-1}$ |
| 0.160 | 1291 | 7.749 | 3.362 | | | 0.643 | 0.106 |
| 0.155 | 1250 | 7.999 | 3.360 | | | 0.671 | 0.112 |
| 0.150 | 1210 | 8.265 | 3.358 | | | 0.712 | 0.120 |
| 0.145 | 1170 | 8.550 | 3.356 | | | 0.755 | 0.128 |
| 0.140 | 1129 | 8.856 | 3.355 | | | 0.801 | 0.138 |
| 0.135 | 1089 | 9.184 | 3.353 | | | 0.851 | 0.148 |
| 0.130 | 1049 | 9.537 | 3.351 | | | 0.904 | 0.159 |
| 0.125 | 1008 | 9.918 | 3.349 | | | 0.962 | 0.170 |
| 0.120 | 967.9 | 10.33 | 3.347 | | | $0.102 \times 10^{-1}$ | 0.183 |
| 0.115 | 927.6 | 10.78 | 3.345 | | | 0.109 | 0.197 |
| 0.110 | 887.2 | 11.27 | 3.343 | | | 0.117 | 0.212 |
| 0.105 | 846.9 | 11.81 | 3.340 | | | 0.125 | 0.228 |
| 0.100 | 806.6 | 12.40 | 3.338 | | | 0.135 | 0.251 |
| 0.095 | 766.3 | 13.05 | 3.335 | | | 0.148 | 0.280 |
| 0.090 | 725.9 | 13.78 | 3.331 | | | 0.163 | 0.313 |
| 0.085 | 685.6 | 14.59 | 3.327 | | | 0.179 | 0.349 |
| 0.080 | 645.3 | 15.50 | 3.323 | | | 0.200 | 0.388 |
| 0.075 | 604.9 | 16.53 | 3.318 | | | 0.227 | 0.431 |
| 0.070 | 564.6 | 17.71 | 3.311 | | | 0.257 | 0.481 |
| 0.065 | 524.3 | 19.07 | 3.304 | | | 0.287 | 0.538 |
| 0.060 | 483.9 | 20.66 | 3.294 | | | 0.319 | |
| 0.055 | 443.6 | 22.54 | 3.281 | | | 0.357 | |
| 0.050 | 403.3 | 24.80 | 3.265 | | | | |

* The position of the band-gap, $E_g$ estimated in Ref. [26] and [31] is indicated.

**TABLE XI**

**Values of $n$ and $k$ for $Hg_{1-x}Cd_xTe - x = 0.443$, 300K (Ref. [21] and [30])**

| eV | $cm^{-1}$ | $\mu m$ | n | k |
|---|---|---|---|---|
| 0.625 | 5041 | 1.984 | | 0.147 |
| 0.620 | 5001 | 2.000 | | 0.144 |
| 0.615 | 4960 | 2.016 | | 0.141 |
| 0.610 | 4920 | 2.032 | | 0.138 |
| 0.605 | 4880 | 2.049 | | 0.135 |
| 0.600 | 4839 | 2.066 | | 0.133 |
| 0.595 | 4799 | 2.084 | | 0.131 |
| 0.590 | 4759 | 2.101 | | 0.130 |
| 0.585 | 4719 | 2.119 | | 0.128 |
| 0.580 | 4678 | 2.138 | | 0.125 |
| 0.575 | 4638 | 2.156 | | 0.122 |
| 0.570 | 4598 | 2.175 | | 0.120 |
| 0.565 | 4557 | 2.194 | | 0.119 |
| 0.560 | 4517 | 2.214 | | 0.117 |
| 0.555 | 4477 | 2.234 | | 0.113 |
| 0.550 | 4436 | 2.254 | | 0.110 |
| 0.545 | 4396 | 2.275 | | 0.105 |
| 0.540 | 4356 | 2.296 | | 0.101 |
| 0.535 | 4315 | 2.317 | | $0.953 \times 10^{-1}$ |
| 0.530 | 4275 | 2.339 | | 0.885 |
| 0.525 | 4235 | 2.362 | | 0.815 |
| 0.520 | 4194 | 2.384 | | 0.660 |
| 0.515 | 4154 | 2.407 | | 0.574 |
| 0.510 | 4114 | 2.431 | | 0.456 |
| 0.505 | 4073 | 2.455 | | 0.308 |
| 0.500 | 4033 | 2.480 | 3.107 | 0.225* |
| 0.495 | 3993 | 2.505 | 3.101 | 0.155 |
| 0.490 | 3952 | 2.530 | 3.092 | $0.941 \times 10^{-2}$ |
| 0.485 | 3912 | 2.556 | 3.085 | 0.620 |
| 0.480 | 3872 | 2.583 | 3.080 | 0.349 |
| 0.470 | 3791 | 2.638 | 3.068 | |
| 0.460 | 3710 | 2.695 | 3.057 | |
| 0.450 | 3630 | 2.755 | 3.048 | |
| 0.440 | 3549 | 2.818 | 3.040 | |
| 0.430 | 3468 | 2.883 | 3.033 | |
| 0.420 | 3388 | 2.952 | 3.026 | |
| 0.410 | 3307 | 3.024 | 3.020 | |
| 0.400 | 3226 | 3.100 | 3.013 | |
| 0.380 | 3065 | 3.263 | 3.003 | |
| 0.360 | 2904 | 3.444 | 2.995 | |
| 0.340 | 2742 | 3.646 | 2.987 | |
| 0.320 | 2581 | 3.874 | 2.980 | |
| 0.300 | 2420 | 4.133 | 2.975 | |

TABLE XI (*Continued*)

| eV | $cm^{-1}$ | $\mu m$ | n | k |
|---|---|---|---|---|
| 0.250 | 2016 | 4.959 | 2.963 | |
| 0.200 | 1613 | 6.199 | 2.953 | |
| 0.150 | 1210 | 8.265 | 2.945 | |
| 0.100 | 806.6 | 12.40 | 2.932 | |
| 0.050 | 403.3 | 24.80 | 2.875 | |

* The position of the band-gap, $E_g$ estimated in Ref. [30] is indicated.

TABLE XII

Values of $n$ and $k$ for $Hg_{1-x}Cd_xTe - x = 0$ (Ref. [35]) and $x \simeq 0.21$ (Ref. [37])

| | | | x=0 | | x≃0.21 | | | |
|---|---|---|---|---|---|---|---|---|
| | | | | | n-type | | p-type | |
| eV | $cm^{-1}$ | μm | n | k | n | k | n | k |
| | | | (8K) | | (~5K) | | (~5K) | |
| 0.02256 | 182 | 54.95 | | | | | 3.42 | 1.52 |
| 0.02219 | 179 | 55.87 | | | | | 3.39 | 1.51 |
| 0.02182 | 176 | 56.82 | | | | | 3.36 | 1.54 |
| 0.02145 | 173 | 57.80 | | | | | 3.32 | 1.55 |
| 0.02108 | 170 | 58.82 | | | | | 3.28 | 1.52 |
| 0.02070 | 167 | 59.88 | | | | | 3.18 | 1.53 |
| 0.02033 | 164 | 60.98 | | | | | 2.96 | 1.51 |
| 0.01996 | 161 | 62.11 | 3.22 | 0.350 | | | 2.66 | 1.69 |
| 0.01959 | 158 | 63.29 | 3.17 | 0.376 | 1.91 | 0.672 | 2.76 | 2.15 |
| 0.01922 | 155 | 64.52 | 3.18 | 0.431 | 2.60 | 0.958 | 3.28 | 2.49 |
| 0.01884 | 152 | 65.79 | 3.15 | 0.491 | 2.72 | 0.722 | 3.41 | 2.48 |
| 0.01847 | 149 | 67.11 | 3.12 | 0.567 | 2.79 | 0.369 | 3.54 | 2.11 |
| 0.01810 | 146 | 68.49 | 3.05 | 0.660 | 2.10 | 0.219 | 3.06 | 1.89 |
| 0.01773 | 143 | 69.93 | 2.96 | 0.786 | 1.75 | 0.558 | 2.68 | 2.07 |
| 0.01736 | 140 | 71.43 | 2.85 | 0.935 | 1.03 | 1.53 | 2.23 | 2.74 |
| 0.01699 | 137 | 72.99 | 2.74 | 1.15 | 1.19 | 1.65 | 2.20 | 2.92 |
| 0.01661 | 134 | 74.63 | 2.64 | 1.40 | 1.01 | 2.14 | 1.96 | 3.28 |
| 0.01624 | 131 | 76.34 | 2.51 | 1.79 | 0.809 | 3.09 | 1.69 | 3.74 |
| 0.01587 | 128 | 78.13 | 2.09 | 3.04 | 1.08 | 4.56 | 1.26 | 4.52 |
| 0.01550 | 125 | 80.00 | 2.19 | 4.25 | 1.93 | 6.63 | 0.967 | 6.27 |
| 0.01513 | 122 | 81.97 | 3.26 | 6.33 | 5.60 | 10.2 | 1.83 | 10.3 |
| 0.01475 | 119 | 84.03 | 7.95 | 7.95 | 11.5 | 2.47 | 11.3 | 8.47 |
| 0.01438 | 116 | 86.21 | 9.97 | 2.49 | 9.52 | 0.595 | 9.43 | 4.63 |
| 0.01401 | 113 | 88.50 | 8.97 | 0.868 | 7.77 | 0.247 | 8.42 | 3.55 |
| 0.01364 | 110 | 90.91 | 9.61 | 0.503 | | | 7.70 | 2.81 |
| 0.01327 | 107 | 93.46 | | | | | 7.33 | 2.62 |
| 0.01289 | 104 | 96.15 | | | | | 7.07 | 2.37 |
| 0.01252 | 101 | 99.01 | | | | | 6.78 | 2.18 |
| 0.01215 | 98 | 102.0 | | | | | 6.51 | 2.18 |
| 0.01178 | 95 | 105.3 | | | | | 6.45 | 2.18 |
| 0.01141 | 92 | 108.7 | | | | | 6.34 | 2.11 |

TABLE XIII

Values of $n$ and $k$ for $Hg_{1-x}Cd_xTe - x = 0.45$ (Ref. [39])

| eV | $cm^{-1}$ | $\mu m$ | n | k |
|---|---|---|---|---|
| 0.04959 | 400 | 25.00 | 3.42[a] | |
| 0.02703 | 218 | 45.87 | 3.41 | $0.197 \times 10^{-1}$ |
| 0.02666 | 215 | 46.51 | 3.38 | $0.215 \times 10^{-1}$ |
| 0.02628 | 212 | 47.17 | 3.35 | $0.235 \times 10^{-1}$ |
| 0.02591 | 209 | 47.85 | 3.31 | $0.259 \times 10^{-1}$ |
| 0.02554 | 206 | 48.54 | 3.27 | $0.286 \times 10^{-1}$ |
| 0.02517 | 203 | 49.26 | 3.23 | $0.318 \times 10^{-1}$ |
| 0.02480 | 200 | 50.00 | 3.18 | $0.356 \times 10^{-1}$ |
| 0.02442 | 197 | 50.76 | 3.13 | $0.402 \times 10^{-1}$ |
| 0.02405 | 194 | 51.55 | 3.07 | $0.456 \times 10^{-1}$ |
| 0.02368 | 191 | 52.36 | 3.00 | $0.524 \times 10^{-1}$ |
| 0.02331 | 188 | 53.19 | 2.93 | $0.609 \times 10^{-1}$ |
| 0.02294 | 185 | 54.05 | 2.83 | $0.718 \times 10^{-1}$ |
| 0.02256 | 182 | 54.95 | 2.73 | $0.862 \times 10^{-1}$ |
| 0.02219 | 179 | 55.87 | 2.60 | 0.106 |
| 0.02182 | 176 | 56.82 | 2.44 | 0.134 |
| 0.02145 | 173 | 57.80 | 2.23 | 0.178 |
| 0.02108 | 170 | 58.82 | 1.96 | 0.254 |
| 0.02070 | 167 | 59.88 | 1.58 | 0.410 |
| 0.02033 | 164 | 60.98 | 1.07 | 0.839 |
| 0.01996 | 161 | 62.11 | 0.807 | 1.68 |
| 0.01959 | 158 | 63.29 | 0.923 | 2.59 |
| 0.01922 | 155 | 64.52 | 1.49 | 3.54 |
| 0.01884 | 152 | 65.79 | 2.44 | 4.06 |
| 0.01847 | 149 | 67.11 | 4.65 | 4.17 |
| 0.01810 | 146 | 68.49 | 4.38 | 1.70 |
| 0.01773 | 143 | 69.93 | 3.09 | 1.59 |
| 0.01736 | 140 | 71.43 | 2.58 | 2.07 |
| 0.01699 | 137 | 72.99 | 2.17 | 2.79 |
| 0.01661 | 134 | 74.63 | 2.29 | 3.45 |
| 0.01624 | 131 | 76.34 | 1.88 | 4.17 |
| 0.01587 | 128 | 78.13 | 1.78 | 6.31 |
| 0.01550 | 125 | 80.00 | 4.04 | 10.3 |
| 0.01513 | 122 | 81.97 | 13.4 | 6.20 |
| 0.01475 | 119 | 84.03 | 10.1 | 1.43 |
| 0.01438 | 116 | 86.21 | 8.36 | 0.696 |
| 0.01401 | 113 | 88.50 | 7.47 | 0.519 |
| 0.01364 | 110 | 90.91 | 7.01 | 0.473 |
| 0.01327 | 107 | 93.46 | 6.73 | 0.353 |
| 0.01289 | 104 | 96.15 | 6.46 | 0.236 |
| 0.01252 | 101 | 99.01 | 6.23 | 0.166 |
| 0.01215 | 98 | 102.0 | 6.04 | 0.124 |
| 0.01178 | 95 | 105.3 | 5.89 | $0.977 \times 10^{-1}$ |
| 0.01141 | 92 | 108.7 | 5.76 | $0.793 \times 10^{-1}$ |
| 0.01103 | 89 | 112.4 | 5.66 | $0.660 \times 10^{-1}$ |

**TABLE XIII (*Continued*)**

| eV | $cm^{-1}$ | $\mu m$ | n | k |
|---|---|---|---|---|
| 0.01066 | 86 | 116.3 | 5.57 | $0.559 \times 10^{-1}$ |
| 0.01029 | 83 | 120.5 | 5.49 | $0.480 \times 10^{-1}$ |
| 0.00992 | 80 | 125.0 | 5.42 | $0.416 \times 10^{-1}$ |
| 0.000124 | 10 | 1000.0 | 4.91[b] | |

[a] $\sqrt{\epsilon_\infty}$, from Ref. [26].
[b] $\sqrt{\epsilon_0}$, where $\epsilon_0 = \epsilon_\infty + \Sigma_j S_j$, from Ref. [39].

# Selenium (Se)

EDWARD D. PALIK
Institute for Physical Science and Technology
University of Maryland
College Park, Maryland

The trigonal form of Se is birefringent with an optical $c$ axis. Light polarized perpendicular to $c$ is termed ordinary ($o$), and light polarized parallel to $c$ is termed extraordinary ($e$). This leads to one of the applications of Se for second-harmonic generation of IR light [1, 2]. Se is a direct-band-gap semiconductor ($E_{g\perp} = 1.98$ eV; $E_{g\parallel} = 2.11$ eV). In addition to the IR spectrum (to be discussed), the Raman spectrum has been studied in some detail [3, 4]. A good collection of many of the properties of Se is given in Ref. [5].

The room-temperature $n$ and $k$ values chosen in this critique are listed in Table II. These are plotted in Fig. 1.

Starting at the long wavelength of 3.3 cm, permittivity measurements have been done by Sicha *et al.* [6] using a cavity-resonance method. A rectangular resonator with a $TE_{101}$ mode had a resonance frequency of $\sim 9.1 \times 10^9$ Hz ($\sim$3.3 cm). A needle-shaped Se crystal with $c$ along the long direction was inserted at a point of maximum electric-field intensity, and the change of resonant frequency was measured. Some analysis of the resonant frequency as a function of electric field across the cavity, depolarization factor for $\mathbf{E}\|c$, and $\varepsilon$ for polycrystalline material, finally yielded $\varepsilon_\parallel = 9.3$ and $\varepsilon_\perp = 8.0$. These numbers prove to be in poor agreement with reststrahlen-data analysis and extrapolation ($\varepsilon_{o\parallel} = 12.2$, $\varepsilon_{o\perp} = 7.4$), and we do not weight them heavily. Other data of Salo *et al.* [7] give $\varepsilon_\parallel = 21$ and $\varepsilon_\perp = 11$, also much different. It seems that reflectivity to long wavelength (100–1000 μm) is a better way to determine $\varepsilon_o$ as long as the free-carrier concentration is low. This question of the free-carrier contribution to the low-frequency dielectric function is important to consider and should be answered, based on the measured free-carrier concentration and conductivity.

Danielewicz and Coleman [8] have collected several sets of data in the spectral range 10–$10^4$ $cm^{-1}$, and we have used these as a basis set of data, adding other data for comparison and overlap. The extinction-coefficient


Copyright © 1991 by Academic Press.
All rights of reproduction in any form reserved.
ISBN 0-12-544422-2

data are extracted from absorption-constant data for the multiphonon region [9]. The fundamental transverse optic phonon absorption was obtained from a Lorentz-oscillator fit of the reststrahlen reflectivity. Similar results were obtained by Lucovsky *et al.* [10] and Geick *et al.* [9]. All these workers used equivalent models, except that Danielewicz and Coleman used UV interband oscillators to account for $\varepsilon_\infty$ better. In their notation,

$$\varepsilon = \varepsilon_1 - i\varepsilon_2 = (n - ik)^2 = 1 + \sum \frac{Se_j ve_j^2}{ve_j - v^2} + \sum \frac{So_j vo_j^2}{vo_j - v^2 + i\gamma_j v},$$

but we have omitted their free-carrier term. Note that they have chosen the negative sign in defining $\varepsilon$. $Se_j$ and $So_j$ are the strengths for electronic and vibrational oscillators, respectively, for each polarization. $ve_j$ and $vo_j$ are the resonant frequencies for the electronic and vibrational oscillators, respectively, for each polarization. $\gamma_j$ is the phonon line width (damping constant) for each polarization. We list these parameters in Table I.

The oscillator fit was used to calculate $n$ from 10,000–10 $cm^{-1}$, but the near-IR data of Gampel and Johnson [11] are implicit in the tabulation. This fit also provided the $k$ values in the vicinity of the phonon frequencies $v_T(\perp) = 140$ and $v_T(\parallel) = 102\ cm^{-1}$ but did not consider the multiphonon absorption.

Measurements of the IR refractive index by minimum-deviation and interference-fringe techniques yielded values from 3.2–3.7 for $n_\parallel$ and 2.5–2.9 for $n_\perp$, suggesting material and sample-preparation problems. We accept the values given by the fit of Danielewicz and Coleman, which are essentially those of Gampel and Johnson [11]; the results of Caldwell and Fan [12] are in reasonable agreement to one unit in the first decimal place; the results of Gobrecht and Tausend [13] are within two units in the first decimal place. Although the data of Ref. [13] fill in a gap from 1.0–0.7 μm, we have not tabulated it because it fails to join on to $n$ values at either end. Gampel and Johnson discuss such variations in $n$ among several groups.

Henrion [14] has measured the transmission of thin-plate samples at various temperatures between 400 K and 90 K. Analysis of $\alpha$ versus $hv$ yielded a straight line indicating a direct band gap $E_{g\parallel} = 2.11$ eV and $E_{g\perp} = 1.98$ eV at 300 K. Exponential tail absorption at lower energy was shown to be due to charged impurities.

Several reflection experiments have been performed at and above the fundamental band gap [15, 16]. Absorption peaks have been correlated to band-structure calculation. The Kramers–Kronig (K–K) analysis of such data in the 4–14 eV region by Leiga [15] and in the 2–5 eV region by Tutihasi *et al.* [16] have been combined for Table II. Tutihasi *et al.*

performed standard reflection experiments from cleaved/acid-etched surfaces using Glan-prism linear polarizers. Prisms of silica and flint glass were used in the monochromator. The reflection standard was an Al mirror.

Leiga used a vacuum UV monochromator with hydrogen, neon, or helium discharges as the light source. Only cleaved or as-grown surfaces were used because chemical etching affected the reflectivity results. The angle of incidence was 20°. Two types of samples were used: one with the $c$ axis perpendicular to the surface and one with the $c$ axis in the surface. Measurements (with the partially polarized light from the monochromator) on both kinds of samples for two positions of each sample 90° apart (about the incident-beam direction) could be algebraically unsorted to give $R_\perp$ and $R_\parallel$. K–K analysis involved some assumptions and use of other researchers' data to cover the entire spectrum.

Bammes *et al.* [17] used synchrotron radiation to measure reflectivity from 3–30 eV for samples with the $c$ axis in the plane. Since the synchrotron radiation was nearly linearly polarized to start, and further linearly polarized by a premirror and grating, the sample/detector could be rotated to change the angle of incidence and the sample could be rotated to measure $\mathbf{E} \perp c$ and $\mathbf{E} \parallel c$. This, along with the work of Liega, dramatically illustrates how to do polarization experiments when there are no polarizers at high photon energies!

The $\varepsilon_1$ and $\varepsilon_2$ dielectric-function data were plotted in small figures, which had to be expanded in order to read the values. Therefore, in addition to the errors in measuring $R$ and performing K–K analysis, there are now errors due to graph reading. Since peaks are well-defined in the $\varepsilon$ versus eV plots, however, we keep two to three significant figures for $n$ and $k$ to show the peaks in most instances.

We have found no data above 30 eV until the absorption edges are reached. Since X-ray scattering cross-sections have been determined for many elemental materials, we have used the model of Henke *et al.* [18] to calculate $n$ and $k$ from 4–250 Å. The X-ray absorption edges as listed in Ref. [19] are $K$(12.654 keV), $L_1$(1.652 keV), $L_2$(1.474 keV), $L_3$(1.434 keV), $M_5$(0.05443 keV), and most of these appear in Fig. 1 (remember the conversion factor 8065.48 $\text{cm}^{-1}$/eV). Still-lower-energy transitions are merged into the band structure. Although there is no overlap with the data of Bammes *et al.*, extrapolation of both sets of data toward each other seems to be feasible.

**ACKNOWLEDGMENTS**

We thank W. R. Hunter for calculating optical constants in the X-ray region. V. Saile kindly provided unpublished data in the visible–UV regions.

## REFERENCES


1. G. W. Day, *Appl. Phys. Lett.* **18**, 347 (1971).
2. G. H. Sherman and P. D. Coleman, *J. Appl. Phys.* **44**, 238 (1973).
3. G. Lucovsky, A. Mooradian, W. Taylor, G. B. Wright, and R. C. Keezer, *Solid State Comm.* **5**, 113 (1967).
4. A. Mooradian and G. B. Wright, in "Physics of Selenium and Tellurium," (W. C. Cooper, ed.), Pergamon, New York, 296 (1969).
5. G. Weiser, in "Landolt–Börnstein Numerical Data and Functional Relationships in Science and Technology," (K.-H. Hellewege, ed.), Vol. 17, Springer-Verlag, Berlin, 86 (1983).
6. M. Sicha, J. Studnicka, V. Prosser, and B. Gruber, *Phys. Stat. Solidi* **7**, 1045 (1964).
7. T. Salo, T. Stubb, and E. Suosara, in "The Physics of Selenium and Tellurium," (W. C. Cooper, ed.), Pergamon, New York, 335 (1969).
8. E. J. Danielewicz and P. D. Coleman, *Appl. Opt.* **13**, 1164 (1974).
9. R. Geick, U. Schröder, and J. Stuke, *Phys. Stat. Solidi* **24**, 99 (1967).
10. G. Lucovsky, R. C. Keezer, and E. Burstein, *Solid State Comm.* **5**, 439 (1967).
11. L. Gampel and F. M. Johnson, *J. Opt. Soc. Am.* **59**, 72 (1969).
12. R. S. Caldwell and H. Y. Fan, *Phys. Rev.* **114**, 664 (1959).
13. H. Gorbrecht and A. Tausend, *Z. Physik* **161**, 205 (1961).
14. W. Henrion, in "Physics of Selenium and Tellurium," (W. C. Cooper, ed.), Pergamon, New York, 75 (1969); *Phys. Stat. Solidi* **12,** K113 (1965).
15. A. G. Leiga, *J. Opt. Soc. Am.* **58**, 880 (1968).
16. S. Tutihasi and I. Chen, *Phys. Rev.* **158**, 623 (1967).
17. P. Bammes, R. Klucker, E. E. Koch, and T. Tuomi, *Phys. Stat. Solidi (b)* **49**, 561 (1972); private communication from V. Saile.
18. B. L. Henke, P. Lee, T. J. Tanaka, R. L. Shimabukuro, and B. K. Fujikama, *At. Data Nucl. Data Tables* **27**, 1 (1982).
19. D. E. Gray, ed. "American Institute of Physics Handbook," Third Edition, McGraw-Hill, New York, 7–120 (1982).

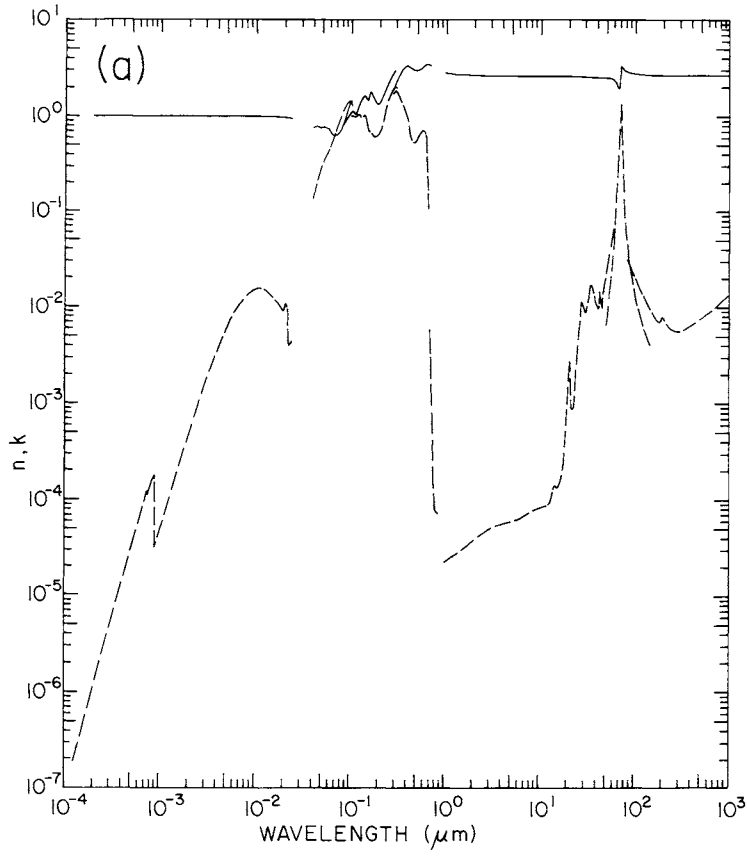


**Fig. 1.** (a) Log–log plot of $n_o$ (solid line) and $k_o$ (dashed line) versus wavelength in micrometers for selenium. (b) Log–log plot of $n_e$ (solid line) and $k_e$ (dashed line) versus wavelength in micrometers.

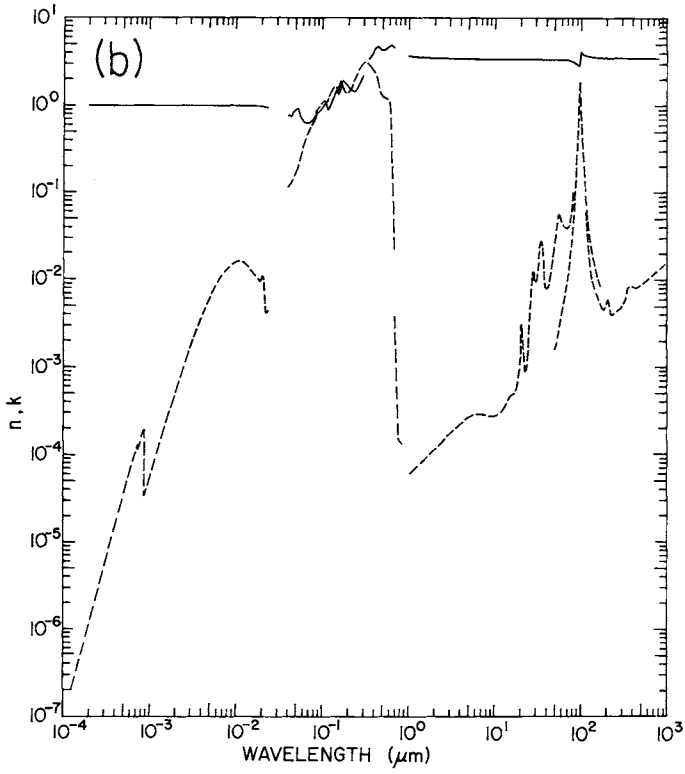


**TABLE I**

**Oscillator Parameters for Se at 300 K**

| | $ve_j(\text{cm}^{-1})$ | $Se_j$ | $vo_j(\text{cm}^{-1})$ | $So_j$ | $\gamma_j(\text{cm}^{-1})$ |
|---|---|---|---|---|---|
| ∥ | 27,422.6 | 10.62 | 102.0 | 0.62 | 7.15 |
| ⊥ | 30,648.7 | 5.79 | 231.0 | 0.01 | 9.0 |
| | 12,904.8 | 0.18 | 140.0 | 0.45 | 8.0 |

TABLE II

Values of $n$ and $k$ for Selenium from Various References[a]

| eV | $cm^{-1}$ | Å | n | k |
|---|---|---|---|---|
| 9972 | | 1.243 | 0.99999190[18] | $1.90 \times 10^{-7}$[18] |
| 9331 | | 1.329 | 0.99999110 | $2.47 \times 10^{-7}$ |
| 8909 | | 1.392 | 0.99999020 | $2.94 \times 10^{-7}$ |
| 8507 | | 1.458 | 0.9999892 | $3.50 \times 10^{-7}$ |
| 8123 | | 1.526 | 0.9999881 | $4.17 \times 10^{-7}$ |
| 7756 | | 1.599 | 0.9999869 | $4.96 \times 10^{-7}$ |
| 7406 | | 1.674 | 0.9999856 | $5.90 \times 10^{-7}$ |
| 7072 | | 1.753 | 0.9999841 | $7.02 \times 10^{-7}$ |
| 6752 | | 1.836 | 0.9999826 | $8.34 \times 10^{-7}$ |
| 6447 | | 1.923 | 0.9999809 | $9.92 \times 10^{-7}$ |
| 6156 | | 2.014 | 0.9999790 | $1.18 \times 10^{-6}$ |
| 5878 | | 2.109 | 0.9999769 | $1.41 \times 10^{-6}$ |
| 5613 | | 2.209 | 0.9999746 | $1.67 \times 10^{-6}$ |
| 5359 | | 2.314 | 0.9999720 | $1.98 \times 10^{-6}$ |
| 5117 | | 2.423 | 0.9999693 | $2.35 \times 10^{-6}$ |
| 4886 | | 2.538 | 0.9999663 | $2.79 \times 10^{-6}$ |
| 4665 | | 2.658 | 0.9999630 | $3.32 \times 10^{-6}$ |
| 4455 | | 2.783 | 0.9999593 | $3.94 \times 10^{-6}$ |
| 4254 | | 2.915 | 0.9999554 | $4.67 \times 10^{-6}$ |
| 4062 | | 3.053 | 0.9999509 | $5.54 \times 10^{-6}$ |
| 3878 | | 3.197 | 0.9999462 | $6.57 \times 10^{-6}$ |
| 3703 | | 3.348 | 0.9999410 | $7.79 \times 10^{-6}$ |
| 3536 | | 3.506 | 0.9999353 | $9.23 \times 10^{-6}$ |
| 3376 | | 3.672 | 0.9999290 | $1.09 \times 10^{-5}$ |
| 3324 | | 3.846 | 0.9999223 | $1.29 \times 10^{-5}$ |
| 3078 | | 4.028 | 0.9999149 | $1.53 \times 10^{-5}$ |
| 2939 | | 4.218 | 0.9999070 | $1.81 \times 10^{-5}$ |
| 2807 | | 4.418 | 0.999898 | $2.14 \times 10^{-5}$ |
| 2680 | | 4.627 | 0.999889 | $2.53 \times 10^{-5}$ |
| 2559 | | 4.846 | 0.999879 | $2.98 \times 10^{-5}$ |
| 2443 | | 5.075 | 0.999869 | $3.52 \times 10^{-5}$ |
| 2333 | | 5.315 | 0.999857 | $4.14 \times 10^{-5}$ |
| 2228 | | 5.566 | 0.999846 | $4.88 \times 10^{-5}$ |
| 2127 | | 5.829 | 0.999834 | $5.73 \times 10^{-5}$ |
| 2031 | | 6.105 | 0.999821 | $6.73 \times 10^{-5}$ |
| 1939 | | 6.394 | 0.999809 | $7.87 \times 10^{-5}$ |
| 1852 | | 6.696 | 0.999798 | $9.22 \times 10^{-5}$ |
| 1768 | | 7.013 | 0.999789 | $1.08 \times 10^{-4}$ |
| 1728 | | 7.176 | 0.999787 | $1.17 \times 10^{-4}$ |
| 1688 | | 7.344 | 0.999788 | $1.26 \times 10^{-4}$ |
| 1650 | | 7.516 | 0.999817 | $1.20 \times 10^{-4}$ |
| 1612 | | 7.691 | 0.999779 | $1.29 \times 10^{-4}$ |
| 1575 | | 7.871 | 0.999778 | $1.39 \times 10^{-4}$ |
| 1539 | | 8.055 | 0.999781 | $1.50 \times 10^{-4}$ |
| 1504 | | 8.244 | 0.999791 | $1.62 \times 10^{-4}$ |
| 1470 | | 8.436 | 0.999818 | $1.74 \times 10^{-4}$ |
| 1436 | | 8.633 | 0.9999337 | $1.88 \times 10^{-4}$ |
| 1403 | | 8.835 | 0.999811 | $3.29 \times 10^{-5}$ |

TABLE II (*Continued*)

**Selenium**

| eV | $cm^{-1}$ | Å | n | k |
|---|---|---|---|---|
| 1371 | | 9.041 | 0.999767 | $3.55\times10^{-5}$ |
| 1340 | | 9.253 | 0.999736 | $3.84\times10^{-5}$ |
| 1280 | | 9.690 | 0.999684 | $4.49\times10^{-5}$ |
| 1222 | | 10.15 | 0.999637 | $5.25\times10^{-5}$ |
| 1167 | | 10.63 | 0.999588 | $6.13\times10^{-5}$ |
| 1114 | | 11.13 | 0.999538 | $7.17\times10^{-5}$ |
| 1064 | | 11.66 | 0.999485 | $8.38\times10^{-5}$ |
| 1016 | | 12.21 | 0.999427 | $9.76\times10^{-5}$ |
| 969.7 | | 12.77 | 0.999366 | $1.14\times10^{-4}$ |
| 925.9 | | 13.39 | 0.999299 | $1.34\times10^{-4}$ |
| 884.1 | | 14.02 | 0.999226 | $1.55\times10^{-4}$ |
| 844.2 | | 14.69 | 0.999148 | $1.81\times10^{-4}$ |
| 806.0 | | 15.38 | 0.999063 | $2.10\times10^{-4}$ |
| 769.7 | | 16.11 | 0.99897 | $2.44\times10^{-4}$ |
| 734.9 | | 16.87 | 0.99887 | $2.84\times10^{-4}$ |
| 701.7 | | 17.67 | 0.99876 | $3.28\times10^{-4}$ |
| 670.0 | | 18.51 | 0.99864 | $3.79\times10^{-4}$ |
| 639.8 | | 19.38 | 0.99852 | $4.41\times10^{-4}$ |
| 610.9 | | 20.30 | 0.99838 | $5.10\times10^{-4}$ |
| 583.3 | | 21.26 | 0.99823 | $5.89\times10^{-4}$ |
| 557.0 | | 22.26 | 0.99808 | $6.80\times10^{-4}$ |
| 531.8 | | 23.31 | 0.99791 | $7.83\times10^{-4}$ |
| 507.8 | | 24.42 | 0.99773 | $8.99\times10^{-4}$ |
| 484.9 | | 25.57 | 0.99753 | $1.03\times10^{-3}$ |
| 463.0 | | 26.78 | 0.99733 | $1.19\times10^{-3}$ |
| 442.1 | | 28.05 | 0.99711 | $1.36\times10^{-3}$ |
| 422.1 | | 29.37 | 0.99689 | $1.56\times10^{-3}$ |
| 403.0 | | 30.76 | 0.99665 | $1.78\times10^{-3}$ |
| 384.8 | | 32.22 | 0.99642 | $2.02\times10^{-3}$ |
| 367.5 | | 33.74 | 0.99616 | $2.29\times10^{-3}$ |
| 350.9 | | 35.34 | 0.99589 | $2.59\times10^{-3}$ |
| 335.0 | | 37.01 | 0.99561 | $2.92\times10^{-3}$ |
| 319.9 | | 38.76 | 0.99533 | $3.30\times10^{-3}$ |
| 305.5 | | 40.59 | 0.99505 | $3.74\times10^{-3}$ |
| 291.7 | | 42.51 | 0.99478 | $4.22\times10^{-3}$ |
| 278.5 | | 44.52 | 0.99455 | $4.76\times10^{-3}$ |
| 265.9 | | 46.63 | 0.99437 | $5.27\times10^{-3}$ |
| 253.9 | | 48.83 | 0.99415 | $5.81\times10^{-3}$ |
| 242.5 | | 51.14 | 0.99392 | $6.40\times10^{-3}$ |
| 231.5 | | 53.56 | 0.99371 | $7.05\times10^{-3}$ |
| 221.1 | | 56.09 | 0.99353 | $7.76\times10^{-3}$ |
| 211.1 | | 58.74 | 0.99343 | $8.54\times10^{-3}$ |
| 201.5 | | 61.52 | 0.99339 | $9.30\times10^{-3}$ |
| 192.4 | | 64.43 | 0.99347 | $1.01\times10^{-2}$ |
| 183.7 | | 67.48 | 0.99354 | $1.08\times10^{-2}$ |
| 175.5 | | 70.67 | 0.99359 | $1.15\times10^{-2}$ |
| 167.5 | | 74.01 | 0.99373 | $1.22\times10^{-2}$ |
| 160.0 | | 77.51 | 0.99385 | $1.28\times10^{-2}$ |

TABLE II (*Continued*)

Selenium

| eV | $cm^{-1}$ | Å | n | k |
|---|---|---|---|---|
| 152.7 | | 81.17 | 0.99397 | $1.35\times10^{-2}$ |
| 145.8 | | 85.01 | 0.99418 | $1.41\times10^{-2}$ |
| 139.3 | | 89.03 | 0.99435 | $1.46\times10^{-2}$ |
| 133.0 | | 93.24 | 0.99464 | $1.51\times10^{-2}$ |
| 127.0 | | 97.66 | 0.99481 | $1.55\times10^{-2}$ |
| 121.2 | | 102.3 | 0.99493 | $1.58\times10^{-2}$ |
| 115.8 | | 107.1 | 0.99515 | $1.60\times10^{-2}$ |
| 110.5 | | 112.2 | 0.99517 | $1.61\times10^{-2}$ |
| 105.5 | | 117.5 | 0.99513 | $1.61\times10^{-2}$ |
| 100.8 | | 123.0 | 0.99522 | $1.59\times10^{-2}$ |
| 96.22 | | 128.9 | 0.99486 | $1.53\times10^{-2}$ |
| 91.88 | | 134.9 | 0.99427 | $1.48\times10^{-2}$ |
| 88.73 | | 141.3 | 0.99351 | $1.40\times10^{-2}$ |
| 83.77 | | 148.0 | 0.99218 | $1.31\times10^{-2}$ |
| 79.99 | | 155.0 | 0.99042 | $1.24\times10^{-2}$ |
| 76.37 | | 162.3 | 0.98843 | $1.18\times10^{-2}$ |
| 72.92 | | 170.0 | 0.98618 | $1.12\times10^{-2}$ |
| 69.63 | | 178.1 | 0.98358 | $1.04\times10^{-2}$ |
| 66.49 | | 186.5 | 0.98040 | $9.68\times10^{-3}$ |
| 64.97 | | 190.8 | 0.97851 | $9.35\times10^{-3}$ |
| 63.49 | | 195.3 | 0.97636 | $9.33\times10^{-3}$ |
| 62.04 | | 199.9 | 0.97419 | $9.66\times10^{-3}$ |
| 60.62 | | 204.5 | 0.97294 | $1.06\times10^{-2}$ |
| 59.24 | | 209.3 | 0.97252 | $1.07\times10^{-2}$ |
| 57.88 | | 214.2 | 0.97257 | $9.39\times10^{-3}$ |
| 56.56 | | 219.2 | 0.97010 | $5.25\times10^{-3}$ |
| 55.27 | | 224.3 | 0.96510 | $4.06\times10^{-3}$ |
| 54.01 | | 229.6 | 0.96089 | $4.10\times10^{-3}$ |
| 52.77 | | 234.9 | 0.95714 | $4.23\times10^{-3}$ |
| 51.57 | | 240.4 | 0.95339 | $4.42\times10^{-3}$ |

| eV | $cm^{-1}$ | μm | $n_o$ (⊥) | $k_o$ (⊥) | $n_e$ (∥) | $k_e$ (∥) |
|---|---|---|---|---|---|---|
| 30 | | 0.04133 | 0.79[17] | 0.14[17] | 0.87[17] | 0.11[17] |
| 29 | | 0.04275 | 0.79 | 0.16 | 0.86 | 0.12 |
| 28 | | 0.04428 | 0.80 | 0.19 | 0.85 | 0.13 |
| 27 | | 0.04592 | 0.78 | 0.23 | 0.85 | 0.14 |
| 26 | | 0.04769 | 0.78 | 0.26 | 0.86 | 0.15 |
| 25 | | 0.04959 | 0.77 | 0.29 | 0.88 | 0.17 |
| 24 | | 0.05166 | 0.78 | 0.32 | 0.91 | 0.18 |
| 23 | | 0.05391 | 0.79 | 0.35 | 0.92 | 0.19 |
| 22 | | 0.05636 | 0.78 | 0.39 | 0.81 | 0.25 |
| 21 | | 0.05904 | 0.76 | 0.43 | 0.74 | 0.31 |
| 20 | | 0.06199 | 0.73 | 0.48 | 0.69 | 0.36 |
| 19 | | 0.06526 | 0.65 | 0.57 | 0.64 | 0.40 |
| 18 | | 0.06888 | 0.61 | 0.65 | 0.65 | 0.48 |
| 17 | | 0.07293 | 0.66 | 0.76 | 0.66 | 0.53 |

TABLE II (*Continued*)

Selenium

| eV | $cm^{-1}$ | μm | $n_o$ (⊥) | $k_o$ (⊥) | $n_e$ (∥) | $k_e$ (∥) |
|---|---|---|---|---|---|---|
| 16 | | 0.07749 | 0.68 | 0.96 | 0.65 | 0.61 |
| 15 | | 0.08266 | 0.78 | 1.10 | 0.70 | 0.71 |
| 14.5 | | 0.08551 | 0.80 | 1.18 | 0.60 | 0.92 |
| | | | | | 0.80[15] | 0.85[15] |
| 14 | | 0.08856 | 0.90 | 1.30 | 0.76[17] | 0.82[17] |
| | | | 0.98[15] | 0.92[15] | 0.81[15] | 0.91[15] |
| 13.5 | | 0.0918 | 1.04[17] | 1.40[17] | 0.81[17] | 0.87[17] |
| | | | 1.06[15] | 0.97[15] | 0.86[15] | 0.96[15] |
| 13 | | 0.09537 | 1.23[17] | 1.47[17] | 0.88[17] | 0.91[17] |
| | | | 1.13[15] | 1.00[15] | 0.89[15] | 1.02[15] |
| 12.5 | | 0.09919 | 1.45[17] | 1.48[17] | 0.98[17] | 0.95[17] |
| | | | 1.19[15] | 1.01[15] | 0.92[15] | 1.06[15] |
| 12 | | 0.1033 | 1.66[17] | 1.25[17] | 1.09[17] | 0.92[17] |
| | | | 1.25[15] | 1.02[15] | 1.00[15] | 1.10[15] |
| 11.5 | | 0.1078 | 1.71[17] | 1.08[17] | 1.05[17] | 0.86[17] |
| | | | 1.33[15] | 1.01[15] | 1.04[15] | 1.10[15] |
| 11 | | 0.1127 | 1.69[17] | 1.02[17] | 0.95[17] | 0.90[17] |
| | | | 1.36[15] | 1.00[15] | 1.03[15] | 1.08[15] |
| 10.7 | | 0.1153 | 1.37 | 1.04 | 0.90 | 1.16 |
| 10.5 | | 0.1181 | 1.71[17] | 0.99[17] | 0.92[17] | 0.98[17] |
| | | | 1.43[15] | 1.06[15] | 0.91[15] | 1.28[15] |
| 10.0 | | 0.1240 | 1.72[17] | 0.95[17] | 0.92[17] | 1.07[17] |
| | | | 1.56[15] | 1.03[15] | 1.03[15] | 1.46[15] |
| 9.7 | | 0.1272 | 1.57 | 0.97 | 1.11 | 1.51 |
| 9.5 | | 0.1305 | 1.57 | 0.97 | 1.18 | 1.54 |
| 9.2 | | 0.1340 | 1.58 | 1.00 | 1.25 | 1.60 |
| 9.0 | | 0.1378 | 1.66 | 1.02 | 1.35 | 1.64 |
| 8.7 | | 0.1417 | 1.75 | 1.02 | 1.46 | 1.59 |
| 8.5 | | 0.1459 | 1.82 | 0.92 | 1.48 | 1.52 |
| 8.25 | | 0.1503 | 1.84 | 0.80 | 1.38 | 1.48 |
| 8.0 | | 0.1550 | 1.81 | 0.69 | 1.35 | 1.68 |
| 7.75 | | 0.1600 | 1.73 | 0.69 | 1.58 | 1.82 |
| 7.5 | | 0.1653 | 1.71 | 0.67 | 1.84 | 1.83 |
| 7.25 | | 0.1710 | 1.69 | 0.64 | 1.96 | 1.60 |
| 7.0 | | 0.1771 | 1.62 | 0.61 | 1.84 | 1.45 |
| 6.75 | | 0.1837 | 1.57 | 0.62 | 1.83 | 1.43 |
| 6.5 | | 0.1907 | 1.51 | 0.63 | 1.72 | 1.35 |
| 6.25 | | 0.1984 | 1.41 | 0.67 | 1.62 | 1.38 |
| 6.0 | 48393 | 0.2066 | 1.32 | 0.73 | 1.57 | 1.49 |
| 5.75 | 46377 | 0.2156 | 1.28 | 0.87 | 1.51 | 1.62 |
| 5.5 | 44360 | 0.2254 | 1.22 | 1.03 | 1.47 | 1.75 |
| 5.25 | 42344 | 0.2362 | 1.21 | 1.25 | 1.43 | 2.00 |
| 5.0 | 40327 | 0.2480 | 1.25 | 1.50 | 1.50 | 2.31 |
| 4.75 | 38311 | 0.2610 | 1.41 | 1.75 | 1.69 | 2.53 |
| 4.5 | 36295 | 0.2755 | 1.75 | 1.94 | 1.92 | 2.78 |
| 4.4 | 35488 | 0.2817 | 1.89[16] | 1.72[16] | | |
| 4.25 | 34278 | 0.2917 | 2.01[15] | 2.07[15] | 2.22 | 3.06 |
| 4.2 | 33875 | 0.2952 | 2.18[16] | 1.83[16] | | |

TABLE II (*Continued*)

Selenium

| eV | $cm^{-1}$ | μm | $n_o$ (⊥) | $k_o$ (⊥) | $n_e$ (∥) | $k_e$ (∥) |
|---|---|---|---|---|---|---|
| 4.0 | 32261 | 0.3100 | 2.67[15] | 1.99[15] | | |
| | | | 2.51[16] | 1.81[16] | | |
| 3.8 | 30648 | 0.3262 | 2.84 | 1.66 | | |
| 3.6 | 29035 | 0.3444 | 3.06 | 1.47 | 3.39[16] | 3.01[16] |
| 3.4 | 27422 | 0.3646 | 3.22 | 1.24 | 3.69 | 2.76 |
| 3.2 | 25809 | 0.3874 | 3.35 | 1.01 | 3.92 | 2.59 |
| 3.0 | 24196 | 0.4132 | 3.30 | 0.70 | 4.44 | 2.29 |
| 2.8 | 22583 | 0.4428 | 3.12 | 0.58 | 4.59 | 1.70 |
| 2.6 | 20970 | 0.4769 | 3.00 | 0.53 | 4.40 | 1.32 |
| 2.4 | 19357 | 0.5166 | 2.93 | 0.61 | 4.28 | 1.21 |
| 2.2 | 17744 | 0.5635 | 3.07 | 0.73 | 4.49 | 1.19 |
| 2.0 | 16130 | 0.6199 | 3.38 | 0.65 | 4.79 | 0.76 |
| 1.8 | 14517 | 0.6888 | 3.32 | 0.11 | 4.46 | $2.2\times10^{-2}$ |
| | | | | $5.48\times10^{-3}$[14] | | |
| 1.78 | 14356 | 0.6965 | | $3.49\times10^{-3}$ | | $3.66\times10^{-3}$[14] |
| 1.76 | 14195 | 0.7045 | | $1.96\times10^{-3}$ | | $2.41\times10^{-3}$ |
| 1.74 | 14034 | 0.7126 | | $1.02\times10^{-3}$ | | $1.44\times10^{-3}$ |
| 1.72 | 13873 | 0.7208 | | $6.31\times10^{-4}$ | | $9.75\times10^{-4}$ |
| 1.70 | 13711 | 0.7293 | | $3.60\times10^{-4}$ | | $6.27\times10^{-4}$ |
| 1.68 | 13550 | 0.7380 | | $2.23\times10^{-4}$ | | $4.23\times10^{-4}$ |
| 1.66 | 13389 | 0.7469 | | $1.55\times10^{-4}$ | | $2.85\times10^{-4}$ |
| 1.64 | 13227 | 0.7560 | | $1.16\times10^{-4}$ | | $2.17\times10^{-4}$ |
| 1.62 | 13066 | 0.7653 | | $9.44\times10^{-5}$ | | $1.83\times10^{-4}$ |
| 1.60 | 12905 | 0.7749 | | $8.63\times10^{-5}$ | | $1.59\times10^{-4}$ |
| 1.58 | 12743 | 0.7847 | | $8.18\times10^{-5}$ | | $1.44\times10^{-4}$ |
| 1.56 | 12582 | 0.7948 | | $7.78\times10^{-5}$ | | $1.36\times10^{-4}$ |
| 1.54 | 12421 | 0.8051 | | $7.69\times10^{-5}$ | | $1.36\times10^{-4}$ |
| 1.52 | 12259 | 0.8157 | | $7.40\times10^{-5}$ | | $1.35\times10^{-4}$ |
| 1.50 | 12098 | 0.8266 | | $7.37\times10^{-5}$ | | $1.33\times10^{-4}$ |
| 1.48 | 11937 | 0.8377 | | $7.33\times10^{-5}$ | | $1.31\times10^{-4}$ |
| 1.46 | 11775 | 0.8429 | | $7.30\times10^{-5}$ | | $1.30\times10^{-4}$ |
| 1.240 | 10000 | 1.000 | 2.816[8] | $2.31\times10^{-5}$[8] | 3.640[8] | $5.81\times10^{-5}$[8] |
| 1.116 | 9000 | 1.111 | 2.772 | $2.48\times10^{-5}$ | 3.592 | $6.37\times10^{-5}$ |
| 0.9919 | 8000 | 1.250 | 2.739 | $2.69\times10^{-5}$ | 3.551 | $7.11\times10^{-5}$ |
| 0.8679 | 7000 | 1.429 | 2.713 | $2.96\times10^{-5}$ | 3.516 | $8.07\times10^{-5}$ |
| 0.7439 | 6000 | 1.667 | 2.692 | $3.32\times10^{-5}$ | 3.486 | $9.42\times10^{-5}$ |
| 0.6199 | 5000 | 2.000 | 2.675 | $3.82\times10^{-5}$ | 3.462 | $1.12\times10^{-4}$ |
| 0.4959 | 4000 | 2.500 | 2.654 | $4.58\times10^{-5}$ | 3.442 | $1.41\times10^{-4}$ |
| 0.3720 | 3000 | 3.333 | 2.652 | $5.44\times10^{-5}$ | 3.427 | $1.90\times10^{-4}$ |
| 0.3100 | 2500 | 4.000 | 2.648 | $5.73\times10^{-5}$ | 3.422 | $2.26\times10^{-4}$ |
| 0.2480 | 2000 | 5.000 | 2.645 | $5.97\times10^{-5}$ | 3.417 | $2.67\times10^{-4}$ |
| 0.1860 | 1500 | 6.667 | 2.642 | $6.90\times10^{-5}$ | 3.413 | $2.81\times10^{-4}$ |
| 0.1550 | 1250 | 8.000 | 2.641 | | 3.411 | |
| 0.1240 | 1000 | 10.00 | 2.639 | $8.51\times10^{-5}$ | 3.410 | $2.71\times10^{-4}$ |
| 0.1116 | 900 | 11.11 | 2.638 | $8.84\times10^{-5}$ | 3.409 | $2.87\times10^{-4}$ |
| 0.09919 | 800 | 12.50 | 2.637 | $8.95\times10^{-5}$ | 3.409 | $3.23\times10^{-4}$ |
| 0.09299 | 750 | 13.33 | | $1.04\times10^{-4}$ | | $2.44\times10^{-4}$ |
| 0.08679 | 700 | 14.29 | 2.636 | $1.42\times10^{-4}$ | 3.408 | $4.32\times10^{-4}$ |

TABLE II (*Continued*)

**Selenium**

| eV | $cm^{-1}$ | μm | $n_o(\perp)$ | $k_o(\perp)$ | $n_e(\parallel)$ | $k_e(\parallel)$ |
|---|---|---|---|---|---|---|
| 0.08059 | 650 | 15.38 | | $1.35\times10^{-4}$ | | $4.41\times10^{-4}$ |
| 0.07439 | 600 | 16.67 | 2.635 | $1.59\times10^{-4}$ | 3.407 | $4.44\times10^{-4}$ |
| 0.06819 | 550 | 18.18 | | $2.89\times10^{-4}$ | | $5.79\times10^{-4}$ |
| 0.06199 | 500 | 20.00 | 2.632 | $2.07\times10^{-3}$ | 3.405 | $1.35\times10^{-3}$ |
| 0.05951 | 480 | 20.83 | | $2.16\times10^{-3}$ | | $2.98\times10^{-3}$ |
| 0.05703 | 460 | 21.74 | | $8.65\times10^{-4}$ | | $1.56\times10^{-3}$ |
| 0.05455 | 440 | 22.73 | | $9.04\times10^{-4}$ | | $9.04\times10^{-4}$ |
| 0.05207 | 420 | 23.81 | | $1.52\times10^{-3}$ | | $1.02\times10^{-3}$ |
| 0.04959 | 400 | 25.00 | 2.627 | $3.58\times10^{-3}$ | 3.403 | $2.79\times10^{-3}$ |
| 0.04711 | 380 | 26.32 | | $7.33\times10^{-3}$ | | $5.24\times10^{-3}$ |
| 0.04463 | 360 | 27.78 | | $1.17\times10^{-2}$ | | $1.13\times10^{-2}$ |
| 0.04215 | 340 | 29.41 | | $9.36\times10^{-3}$ | | $9.36\times10^{-3}$ |
| 0.03968 | 320 | 31.25 | | $9.95\times10^{-3}$ [9] | | $9.20\times10^{-3}$ [9] |
| 0.03720 | 300 | 33.33 | 2.613 | $1.54\times10^{-2}$ | 3.397 | $1.72\times10^{-2}$ |
| 0.03472 | 280 | 35.71 | 2.607 | $1.68\times10^{-2}$ | | $2.70\times10^{-2}$ |
| 0.03224 | 260 | 38.46 | 2.598 | $1.16\times10^{-2}$ | | $8.57\times10^{-3}$ |
| 0.03100 | 250 | 40.00 | | | 3.391 | $6.26\times10^{-4}$ [8] |
| 0.02976 | 240 | 41.67 | 2.576 | $9.95\times10^{-3}$ | | $7.96\times10^{-3}$ [9] |
| 0.02914 | 235 | 42.55 | 2.568 | | | |
| 0.02876 | 232 | 43.10 | | $1.51\times10^{-2}$ | | |
| 0.02852 | 230 | 43.48 | 2.600 | | | |
| 0.02790 | 225 | 44.44 | 2.610 | | | |
| 0.02728 | 220 | 45.45 | 2.600 | $1.01\times10^{-2}$ | | $1.16\times10^{-2}$ |
| 0.02604 | 210 | 47.62 | 2.582 | | | |
| 0.02480 | 200 | 50.00 | 2.550 | $2.39\times10^{-2}$ | 3.377 | $2.39\times10^{-2}$ |
| | | | | $6.73\times10^{-3}$ [8] | | $1.56\times10^{-3}$ [8] |
| 0.02418 | 195 | 51.28 | 2.555 | $7.96\times10^{-3}$ | | |
| 0.02356 | 190 | 52.63 | 2.543 | $9.66\times10^{-3}$ | 3.372 | $1.96\times10^{-3}$ |
| 0.02294 | 185 | 54.05 | 2.530 | $1.20\times10^{-2}$ | | |
| 0.02232 | 180 | 55.56 | 2.502 | $4.42\times10^{-2}$ [9] | 3.366 | $5.31\times10^{-2}$ [9] |
| | | | | $1.53\times10^{-2}$ [8] | | $2.54\times10^{-3}$ [8] |
| 0.02170 | 175 | 57.14 | 2.491 | $2.01\times10^{-2}$ | | |
| 0.02108 | 170 | 58.82 | 2.462 | $2.76\times10^{-2}$ | 3.358 | $3.40\times10^{-3}$ |
| 0.02046 | 165 | 60.61 | 2.422 | $4.02\times10^{-2}$ | | |
| 0.01984 | 160 | 62.50 | 2.356 | $7.46\times10^{-2}$ [9] | 3.346 | $4.23\times10^{-2}$ [9] |
| | | | | $6.37\times10^{-2}$ [8] | | $4.75\times10^{-3}$ [8] |
| 0.01922 | 155 | 64.52 | 2.270 | 0.114 | | |
| 0.01860 | 150 | 66.67 | 2.111 | 0.255 | 3.330 | $7.04\times10^{-3}$ |
| 0.01798 | 145 | 68.97 | 1.964 | 0.771 | | |
| 0.01736 | 140 | 71.43 | 2.959 | 1.33 | 3.306 | $3.81\times10^{-2}$ [9] |
| | | | | | | $1.41\times10^{-2}$ [8] |
| 0.01674 | 135 | 74.07 | 3.342 | 0.466 | | |
| 0.01612 | 130 | 76.92 | 3.140 | 0.175 | 3.263 | $2.13\times10^{-3}$ |
| 0.01550 | 125 | 80.00 | 3.013 | $8.71\times10^{-2}$ | | |
| 0.01488 | 120 | 83.33 | 2.932 | $3.25\times10^{-2}$ [9] | 3.175 | $9.95\times10^{-2}$ [9] |
| | | | | $5.16\times10^{-2}$ [8] | | $5.22\times10^{-2}$ [8] |
| 0.01364 | 110 | 90.90 | 2.854 | $2.39\times10^{-2}$ | 2.914 | 0.248 |

TABLE II (*Continued*)

**Selenium**

| eV | $cm^{-1}$ | μm | $n_o(\perp)$ | $k_o(\perp)$ | $n_e(\parallel)$ | $k_e(\parallel)$ |
|---|---|---|---|---|---|---|
| 0.01302 | 105 | 95.24 | | | 2.862 | 0.891[b] |
| 0.01277 | 103 | 97.09 | | | 3.754 | 1.57 |
| 0.01265 | 102 | 98.04 | | | 3.676 | 1.70[b] |
| 0.01252 | 101 | 99.01 | | | 3.884 | 1.07 |
| 0.01240 | 100 | 100.0 | 2.805 | $2.31\times10^{-2}$[9] | 4.026 | 0.477[9] |
| | | | | $1.36\times10^{-2}$[b][8] | | 0.849[b][8] |
| 0.01215 | 98 | 102.0 | | | 3.885 | 0.514[b] |
| 0.01116 | 90 | 111.1 | 2.783 | $1.59\times10^{-2}$[9] | 3.772 | 0.128[9] |
| | | | | $8.60\times10^{-3}$[b][8] | | $9.62\times10^{-2}$[b][8] |
| 0.009919 | 80 | 125.0 | 2.761 | $1.29\times10^{-2}$[9] | 3.633 | $1.69\times10^{-2}$[9] |
| | | | | $5.86\times10^{-3}$[b][8] | | $3.10\times10^{-2}$[b][8] |
| 0.008679 | 70 | 142.9 | 2.753 | $1.05\times10^{-2}$[9] | 3.575 | $8.07\times10^{-3}$ |
| | | | | $4.15\times10^{-3}$[b][8] | | $1.48\times10^{-2}$[b] |
| 0.007439 | 60 | 166.7 | 2.740 | $7.83\times10^{-3}$ | 3.545 | $5.31\times10^{-3}$ |
| | | | | | | $8.40\times10^{-3}$[b] |
| 0.007191 | 58 | 172.4 | | | | $5.08\times10^{-3}$ |
| 0.006943 | 56 | 178.6 | | | | $4.69\times10^{-3}$ |
| 0.006819 | 55 | 181.8 | | $7.23\times10^{-3}$ | | |
| 0.006695 | 54 | 185.2 | | | | $4.49\times10^{-3}$ |
| 0.006447 | 52 | 192.3 | | | | $4.67\times10^{-3}$ |
| 0.006199 | 50 | 200.0 | 2.737 | $8.12\times10^{-3}$ | 3.526 | $5.57\times10^{-3}$ |
| 0.005951 | 48 | 208.3 | | | | $5.80\times10^{-3}$ |
| 0.005703 | 46 | 217.4 | | | | $4.15\times10^{-3}$ |
| 0.005579 | 45 | 222.2 | | $6.54\times10^{-3}$ | | |
| 0.005455 | 44 | 227.3 | | | | $3.89\times10^{-3}$ |
| 0.005207 | 42 | 238.1 | | | | $4.02\times10^{-3}$ |
| 0.004959 | 40 | 250.0 | 2.729 | $5.97\times10^{-3}$ | 3.515 | $4.18\times10^{-3}$ |
| 0.004339 | 35 | 285.7 | | | | $4.55\times10^{-3}$ |
| 0.003720 | 30 | 333.3 | 2.729 | $5.89\times10^{-3}$ | 3.507 | $5.84\times10^{-3}$ |
| 0.003410 | 27.5 | 363.6 | | | | $8.10\times10^{-3}$ |
| 0.003100 | 25 | 400.0 | | $6.84\times10^{-3}$ | | $8.28\times10^{-3}$ |
| 0.002790 | 22.5 | 444.4 | | | | $7.96\times10^{-3}$ |
| 0.002480 | 20 | 500.0 | 2.727 | $7.84\times10^{-3}$ | 3.502 | $8.55\times10^{-3}$ |
| 0.001860 | 15 | 666.7 | | $9.71\times10^{-3}$ | | $1.09\times10^{-2}$ |
| 0.001240 | 10 | 1000 | 2.724 | $1.43\times10^{-2}$ | 3.499 | $1.59\times10^{-2}$ |

[a] Various references are indicated in brackets.
[b] Values obtained from oscillator model in Ref. [8].

# Cubic Silicon Carbide ($\beta$-SiC)

SAMUEL A. ALTEROVITZ
NASA Lewis Research Center
Cleveland, Ohio
and
JOHN A. WOOLLAM
Center for Microelectronic and Optical Materials Research
and Department of Electrical Engineering
University of Nebraska
Lincoln, Nebraska

The optical constants of 6H SiC were presented by Choyke and Palik in *HOC I* [1]. The purpose of the present critique is to present optical constants of high-quality, large-area, cubic $\beta$-SiC epitaxially grown films on (100) polished silicon wafers. This epitaxy and the advance in associated technology is a relatively recent development [2, 3] and permits electronic application using these materials. Optical-properties measurements taken so far include those in Refs. [4] and [5].

There are early references to properties of various polymorphs of SiC including bulk-grown cubic SiC that may interest the reader. Most of the references were given in [1], with additional ones listed elsewhere [6–10].

Cubic SiC films were grown on silicon substrates by S. Nishino, J. A. Powell, and others using the technique described in Refs. [2–4]. Briefly, buffer layers were formed on heated Si substrates by flowing hydrocarbon gas and hydrogen over the surface. Then crystalline SiC was grown by flowing silane, hydrocarbon, and hydrogen. Table I contains original, unpublished data, taken by variable-angle spectroscopic ellipsometry (VASE) on samples grown by J. A. Powell. Measurements at up to five angles of incidence were used for each wavelength. A model of a single film on a substrate was used, thus ignoring the possibility of an interface between the film and the substrate or of an overlayer. The refractive index of these (cubic) materials was assumed to be isotropic.

Results on two samples are reported here: a thick film (of order 10 μm), and a film approximately 6000 Å thick. For the spectral range given, the


Copyright © 1991 by Academic Press.
All rights of reproduction in any form reserved.
ISBN 0-12-544422-2

extinction coefficient, $|k|$, <0.02, which is the lower limit measurable by ellipsometry. Cubic SiC has an indirect optical band gap of approximately 2.3 eV. At 3500 Å the absorption coefficient is $3 \times 10^3\,\text{cm}^{-1}$ [5], corresponding to an extinction coefficient of <0.01, below the limit of reliable measurement by ellipsometry. Thus, the data in the table below are given down to 3500 Å.

Errors in index of refraction of the thick film were ±0.01, whereas for the 6000 Å film, errors were ±0.03. The results generally agree with the data reported for $n_O$ of the 6H phase in Ref. [1]. The values of $n$ reported for the thick film were lower than $n_O$ [1] by 1%; the results for the 6000 Å film were higher than $n_O$ in [1] by 1 to 3%. The 6000 Å film results for $n$ were nearer to the values of $n_e$ reported in [1].

The growth of polycrystalline $\beta$-SiC films on Si was accomplished by Spitzer *et al.* [11, 12] as early as 1959. They deposited the films on Si (heated to 1300 °C) from a gas mixture. The infrared properties were determined by study of transmittance and reflectance. Although data were obtained from 1–15 μm, we stress only the lattice-vibration region 10.5–15 μm. An oscillator fit [11, 12] yielded the parameters $\rho = 0.263 = (\omega_L^2 - \omega_T^2)\varepsilon_\infty / 4\pi\omega_T^2$, $\gamma = 0.0107 = \Gamma/\omega_T$, $\nu_O = 2.38 \times 10^{13}$ cycles/sec (12.60 μm, $\omega_T = 793.6\,\text{cm}^{-1}$), $\varepsilon_\infty = 6.7$; these are essentially the same as those obtained for $\alpha$II-SiC (hexagonal) [12, 13] for reststrahlen reflection fits only. While the value of $\gamma$ given here for $\beta$-SiC differs substantially from the one given in HOC I for $\alpha$II-SiC ($\gamma = 0.006$, $\Gamma = 4.75\,\text{cm}^{-1}$), the effect on $n$ and $k$ is small except within $\omega_T \pm 5\,\text{cm}^{-1}$, where it can be as large as +30%. Therefore, the optical constants given by Choyke and Palik [1] for the ordinary ray (virtually the same as for the extraordinary ray) should suffice as a good first approximation for $\beta$-SiC. Note the definitions of the oscillator model parameters in Refs. [1, 11, 13].

## REFERENCES


1. W. J. Choyke and E. D. Palik, in "Handbook of Optical Constants of Solids," (E. D. Palik, ed.), and references therein, Academic Press, Orlando, 587, (1985).
2. S. Nishino, V. Hazuki, H. Matsunami, and T. Tanaka, *J. Electrochem. Soc.* **127**, 2674 (1980).
3. S. Nishino, J. A. Powell, and H. A. Will, *Appl. Phys. Lett.* **42**, 460 (1983).
4. R. T. Holm, P. H. Klein, and P. E. R. Nordquist, Jr., *J. Appl. Phys.* **60**, 1479 (1986).
5. W. L. Choyke, L. C. Feng, and J. A. Powell, *J. Appl. Phys.* **64**, 3163 (1988).
6. M. Neuberger, in "Handbook of Electronic Materials," Vol. 5, IFI/Plenum, New York, 1971.
7. R. C. Marshall, J. W. Faust, Jr. and C. E. Ryan, eds., "Silicon Carbide 1973," University of South Carolina Press, Columbia, South Carolina, (1974).
8. J. A. Powell, *J. Opt. Soc. Amer.* **62**, 3411 (1972).
9. P. T. B. Shaffer and R. G. Naum, *J. Opt. Soc. Am.* **59**, 1498 (1969).
10. G. Derst, C. Wilbertz, K. L. Bhatia, W. Kratschmer, and S. Kalbitger, *Appl. Phys. Lett.* **54**, 1722 (1989).

11. W. G. Spitzer, D. A. Kleinman, and C. J. Frosch, *Phys. Rev.* **113**, 133 (1959).
12. W. G. Spitzer, D. A. Kleinman, C. J. Frosch, and D. J. Walsh, in "Silicon Carbide, A High Temperature Semiconductor," (J. R. O'Connor and J. Smiltens, eds.), Pergamon, New York, 347 (1960).
13. W. G. Spitzer, D. A. Kleinman, and D. Walsh, *Phys. Rev.* **113**, 127 (1959).

**TABLE I**

**Index of Refraction of Epitaxially Grown Cubic SiC**

| E (eV) | $cm^{-1}$ | $\mu$m | n (10 $\mu$m film) | n (6100 Å film) |
|---|---|---|---|---|
| 3.543 | 28,576 | 0.350 | 2.828 | 2.83 |
| 3.444 | 27,777 | 0.360 | 2.800 | 2.89 |
| 3.351 | 27,027 | 0.370 | 2.780 | 2.85 |
| 3.263 | 26,318 | 0.380 | 2.763 | 2.77 |
| 3.179 | 25,640 | 0.390 | 2.749 | 2.81 |
| 3.100 | 25,003 | 0.400 | 2.738 | 2.74 |
| 3.024 | 24,390 | 0.410 | 2.727 | 2.78 |
| 2.952 | 23,809 | 0.420 | 2.719 | 2.80 |
| 2.884 | 23,261 | 0.430 | 2.710 | 2.78 |
| 2.818 | 22,729 | 0.440 | 2.702 | 2.77 |
| 2.756 | 22,228 | 0.450 | 2.693 | 2.72 |
| 2.696 | 21,745 | 0.460 | 2.687 | 2.72 |
| 2.638 | 21,277 | 0.470 | 2.680 | 2.73 |
| 2.583 | 20,833 | 0.480 | 2.673 | 2.72 |
| 2.531 | 20,414 | 0.490 | 2.664 | 2.73 |
| 2.480 | 20,000 | 0.500 | 2.664 | 2.72 |
| 2.431 | 19,607 | 0.510 | 2.658 | 2.63 |
| 2.385 | 19,236 | 0.520 | 2.654 | 2.67 |
| 2.340 | 18,873 | 0.530 | 2.650 | 2.69 |
| 2.296 | 18,518 | 0.540 | 2.645 | 2.71 |
| 2.255 | 18,188 | 0.550 | 2.640 | 2.70 |
| 2.214 | 17,857 | 0.560 | 2.636 | 2.68 |
| 2.175 | 17,542 | 0.570 | 2.632 | 2.69 |
| 2.138 | 17,244 | 0.580 | 2.630 | 2.67 |
| 2.102 | 16,954 | 0.590 | 2.621 | 2.69 |
| 2.067 | 16,667 | 0.600 | 2.621 | 2.71 |
| 2.033 | 16,397 | 0.610 | 2.617 | 2.64 |
| 2.000 | 16,131 | 0.620 | 2.613 | 2.66 |
| 1.968 | 15,873 | 0.630 | 2.613 | 2.66 |
| 1.938 | 15,631 | 0.640 | 2.608 | 2.65 |
| 1.908 | 15.389 | 0.650 | 2.604 | 2.66 |
| 1.879 | 15,155 | 0.660 | 2.605 | 2.68 |
| 1.851 | 14,929 | 0.670 | 2.606 | 2.65 |
| 1.826 | 14,728 | 0.680 | 2.599 | 2.66 |
| 1.797 | 14,494 | 0.690 | 2.594 | 2.67 |
| 1.771 | 14,286 | 0.700 | 2.588 | 2.66 |

$k < 0.01$ over the entire spectral range.

# Tellurium (Te)

EDWARD D. PALIK
Institute for Physical Science and Technology
University of Maryland
College Park, Maryland

Te has been studied in some detail because
(1) it has a small band gap (0.335 eV, comparable to that of InAs, 0.35 eV, and PbS, 0.45 eV);
(2) this trigonal crystal is birefringent, making it useful as a nonlinear crystal for producing second-harmonic generation by orientation of the index ellipsoid, so that the ordinary index ($\perp$) at the fundamental (say 10.6 μm) can be matched to the extraordinary index ($\parallel$) at 5.3 μm [1];
(3) its band structure is similar to the "classic" III-V compound semiconductor InSb.

Te is a direct-band-gap semiconductor ($E_g = 0.33$ eV), which can be doped to produce free-carrier absorption. When $p$-doped, interband transitions between the split-off valence band and the heavy- and light-hole bands can be seen peaked at 900 $cm^{-1}$ but covering a broad region of the near IR from 5–20 μm. Good collections of many of the properties of Te are given in Refs. [2, 3].

The room-temperature $n$ and $k$ values chosen in this critique are listed in Table II. These numbers are plotted in Fig. 1. The data were obtained by reading expanded graphs or tables in the original literature or from private-communication data. The references indicated in brackets in the $n$ and $k$ columns pertain down the column until a new reference appears.

Wagner [4] measured the dielectric constants of Te at two wavelengths, 3.2 cm and 8.5 mm, between $-170$ °C and room temperature. At 3.2 cm a standing-wave, node method was used in which the Te sample was placed at one end of the expandable microwave arm, sandwiched between a crystal-quartz plate and a shorting plate. At 8.5 mm a smaller, more detailed sample holder was used. After some analysis, the following low-temperature values were obtained: at 3.2 cm, $\varepsilon_\parallel = 53$ and $\varepsilon_\perp = 33$; at 8.5 mm, $\varepsilon_\parallel = 55$ and $\varepsilon_\perp = 32.5$. At 3.2 cm there seems to be a slight decrease in $\varepsilon$ as the temperature is lowered from room temperature (~13 °C is the highest value from the graphs), then a flattening out. At 8.5 mm there is a


Copyright © 1991 by Academic Press.
All rights of reproduction in any form reserved.
ISBN 0-12-544422-2

slight rise, then a plateauing or decrease in $\varepsilon$. The conductivity is observed to decrease at the same time. We must conclude that the stated hole concentration of $N = 5 \times 10^{14}\,\mathrm{cm}^{-3}$ puts the plasma frequency $\omega_p = 4\pi Ne^2/\varepsilon m^*$ near 3.6 cm, and these slight variations in $\varepsilon$ are indications that the free carriers are freezing out, revealing the dielectric constant of the lattice. (We used $e = 4.77 \times 10^{-10}$ esu, $\varepsilon_\parallel = 55$, $m^* = 0.11(9.1 \times 10^{-28}$ gm.)) Subsequent use of these (low-temperature, hole-free) $\varepsilon_{\parallel,\perp}$ values as room-temperature data must be kept in mind. All subsequent Te samples in this collection of data will have comparable or larger free-carrier concentrations.

The lattice-vibration region in the far IR from 60–500 $\mathrm{cm}^{-1}$ has been measured in reflection and transmission by Geick *et al.* [5] with a Perkin–Elmer Model 301 grating spectrometer (sample at 300 K). Similar work over a shorter spectral range has been done by Lucovsky *et al.* [6], who concentrated on the reststrahlen reflectivity. Both groups fitted their reflectivities with the same type of Lorentz-oscillator model. Although the numbers are similar, some differences occur. More recently, Rautenberg [7] has measured the far-infrared reflectivity at 300 K with a Fourier transform infrared spectrometer. We choose these more recent data as analyzed with the same oscillator model, namely

$$(n - ik)^2 = \varepsilon_1 - i\varepsilon_2 = \varepsilon = \varepsilon_\infty + \frac{\Delta\varepsilon_j \nu_{Tj}^2}{\nu_{Tj}^2 - \nu^2 + i\Gamma_j \nu}$$

for each polarization. $\varepsilon_\infty$ is the high-frequency dielectric constant at ~8 μm, $\nu_T$ is the transverse optic phonon frequency ($\mathrm{cm}^{-1}$), $\Delta\varepsilon$ is the change in dielectric function upon passing through the resonant frequency from near IR to dc (oscillator strength), and $\Gamma$ is the phonon damping constant ($\mathrm{cm}^{-1}$). These are listed in Table I. The corresponding parameters of Geick *et al.* and Lucovsky *et al.* ($4\pi\rho = \Delta\varepsilon$ and $\gamma\nu_T = \Gamma$) vary significantly from these in some cases, and we list all three sets of parameters just to illustrate typical differences between laboratories.

The difference in the corresponding parameters indicates that we cannot hope to know $n$ and $k$ to better than one or, at most, two significant figures. Such large differences suggest crystal misorientation, poor polish, or filtering problems for grating spectrometers, all of which would affect $R$.

We are also confused by the different values of $\varepsilon_\infty$ obtained by the three groups, since presumably these numbers are well known in the 5–10 μm region [8, 9], and they should have been used in the fitting process by all the groups. Caldwell and Fan [9] determined $n_\perp = 4.81$ ($\varepsilon_\perp = 23.1$) and $n_\parallel = 6.25$ ($\varepsilon_\parallel = 39.0$) at 8 μm. The fact that $\varepsilon_\parallel$ is as low as 36 suggests that the measured high-frequency reflectivity was too low.

Also of note is the dc dielectric constant obtained from each model: $\varepsilon_{o\parallel}=54.0$ and $\varepsilon_{o\perp}=34.7$ for Geick *et al.*; $\varepsilon_{o\parallel}=45.2$ and $\varepsilon_{o\perp}=30.6$ for Lucovsky *et al.*, and $\varepsilon_{o\parallel}=43.2$ and $\varepsilon_{o\perp}=30.1$ for Rautenberg. These values are to be compared with the values of Wagner: $\varepsilon_{\parallel}=54$ and $\varepsilon_{\perp}=33$. Measurement of reflectivity to 1000 μm is surely the easiest way to determine $\varepsilon_o$.

The region of multiphonon absorption above the fundamental TO frequency has been measured by Grosse and Richter [10] and Geick *et al.* [5]. Both sets of data are similar, but we chose the latter, more complete data as obtained with a Perkin–Elmer spectrophotometer Model 301 at 300 K. Polarization was obtained with polyethylene wire-grid polarizers. The $k$ data as listed in Table II have somewhat less detail than the figures of Ref. [5] because of the coarse grid we used to read the values of the absorption coefficient from expanded graphs. Since the index of refraction was not determined in these measurements, the values listed are from a Lorentz-oscillator fit [7], which ignored this small amount of multiphonon absorption. Note that the values of $k$ for the oscillator fit near $\nu_T$ are always less than the measured values of Geick *et al.*, as is to be expected.

The index of refraction has been measured in the near IR from 4–14 μm by Caldwell and Fan [9] using the minimum angle-of-deviation method for a collimated beam passing through an 8°16′ Te prism. However, it was not a single crystal but consisted of several crystallites with boundaries parallel to the $c$ axis. Since the $c$ axis was perpendicular to both the refracting edge and the base of the prism, light could be polarized $\parallel$ and $\perp$ to $c$ for the measurement. Similar prism measurements were done earlier by Hartig and Loferski [8] with Te doped to $p=10^{17}\,\mathrm{cm}^{-3}$. These values, measured to two decimal places, were about 0.04 larger for $n_\perp$ and about 0.05 smaller for $n_\parallel$. This sort of difference could be due to a slight variation of the direction of the $c$ axis, which was supposedly perpendicular to the refracting edge and the base. Note in Fig. 1 that the measured values of $n$ [9] do not join smoothly with the calculated values obtained from the oscillator model [7].

$p$-Te with $1.25\times10^{17}\,\mathrm{cm}^{-3}$ holes at 300 K shows interband hole absorption (split-off valence band to light- and heavy-hole bands) peaked near $900\,\mathrm{cm}^{-1}$ for $\mathbf{E}\parallel c$ ($\alpha_\parallel=110\,\mathrm{cm}^{-1}$) and much less absorption ($\alpha_\perp=3\,\mathrm{cm}^{-1}$) for $\mathbf{E}\perp c$. We usually would not include such structure because it is extrinsic. However, for $1.7\times10^{15}\,\mathrm{cm}^{-3}$ at 297 K the peak is much smaller and data of Caldwell and Fan are included in Table II because the hole absorption is located just between the multiphonon absorption (which is decreasing to higher frequency) and the band gap absorption (which is increasing to higher frequency). $n$-Te would not show such absorption.

The absorption in the 5–3 μm region reaches a minimum at 5 μm and begins to increase rapidly at 4 μm as the band gap is neared. The values in this minimum of absorption at 5 μm vary considerably in the literature

depending on whether the material is *n*- or *p*-type; lightly doped *n*-type or *p*-type material with less than $1\times10^{15}\,cm^{-3}$ is desirable to obtain intrinsic results. With such a small band gap, pure Te is expected to be slightly intrinsic at 300 K with electrons as the electrical conductors. As an example, at 5 μm $k_{\|}=4.4\times10^{-4}$ [2], $7.2\times10^{-5}$ [9], $3.7\times10^{-4}$ [11], $<1.1\times10^{-5}$ [12].

The band-edge and higher-energy regions have been studied by several groups by transmission of thin plates [2, 12] and by reflectivity and Kramers–Kronig analysis by Tutihasi *et al.* [12], Merdy [13], and Bammes *et al.* [14]. We have used the data of Tutihasi *et al.* as the basis data (because it represents the lowest free-carrier concentration) over the range 0.3–12 eV, and we have added other sets of data for comparison and overlap. We read expanded graphs of absorption coefficient $\alpha=4\pi k/\lambda$ and $\varepsilon_1$ and $\varepsilon_2$ [12] and calculated *n* and *k*. At the fundamental edge between 0.37 and 0.45 eV, the data of Refs. [2] and [12] obtained from transmission measurements of thin plates are in good agreement. In Ref. [2] there is a table of *n* and *k* over a part of this spectral region (1.4–3.0 eV), presumably obtained from Ref. [12], but it is not exhibited in Ref. [12]. We include both sets of data to illustrate how two separate determinations agree (or disagree). The IR data were obtained with a Leiss monochromator equipped with a LiF prism and a double-plate Si transmission polarizer utilizing Brewster's angle. The UV reflectivity data were obtained with a McPherson 0.5 m monochromator with a 600 line/mm grating blazed at 1500 Å and a biotite plate used as a Brewster-angle reflection polarizer. In the various papers there is considerable discussion of excitons, and direct and indirect gaps; since we are only interested in optical constants, these interpretations are not of primary interest.

Bammes *et al.* have made synchrotron-radiation measurements of reflectivity from 3–30 eV. However, to determine absolute reflectivity, they had to normalize their measurements between 3.5 and 6 eV to the spectra of Tutihasi *et al.* For this reason, we still stress the Tutihasi *et al.* data in Table II. The sample was cleaved with the *c* axis in the sample plane. Since the synchrotron, premirror, and grating each tended to polarize the light linearly, the sample was rotated 90° in its near-normal-incidence position to change from ∥ to ⊥. Peaks in *k* appear to be more clear-cut in the data of Tutihasi *et al.* The overlap of the data of Refs. [7] and [13] is poor, principally in the vicinity of 6 eV.

Since X-ray scattering cross-sections have been determined for many elemental materials above 30 eV, we have used the model of Henke *et al.* [15] to calculate *n* and *k* from 4–250 Å. Since the model takes into account only the number of atoms/$cm^3$ and not the lattice structure, there is no ∥ and ⊥ designation. The absorption edges of Te [16] are found at *K* (31.811 keV), $L_1$(4.939 keV), $L_2$(4.612 keV), $L_3$(4.341 keV) and most of these appear in Fig. 1. Other broader peaks are made up of many $M_3N_1$,

$M_4O_{2,3}$, $M_3M_5$ transitions. Other lower-energy transitions are merged into the band structure. Although there is no overlap with the Bammes *et al.* data, extrapolation of both sets of data until they meet seems to be feasible.

**ACKNOWLEDGMENTS**

We thank W. R. Hunter for calculating the optical constants in the X-ray region. P. Grosse and V. Saile kindly provided unpublished data in the far IR and VIS–UV regions, respectively.

**REFERENCES**

1. G. H. Sherman and P. D. Coleman, *J. Appl. Phys.* **44**, 238 (1973).
2. P. Grosse and W. Richter, in "Landolt–Börnstein Numerical Data and Functional Relationships in Science and Technology," (K.-H. Hellwege, ed.), Vol. 17, Springer-Verlag, Berlin, 106 (1983).
3. P. Grosse, in "Springer Tracts in Modern Physics," (G. Höhler, ed.), Vol. 48, Springer, Berlin, (1969).
4. H. Wagner, *Z. Physik* **193**, 218 (1966).
5. R. Geick, P. Grosse, and W. Richter, in "Physics of Selenium and Tellurium," (W. C. Cooper, ed.), Pergamon, New York, 309 (1969).
6. G. Lucovsky, R. C. Keezer, and E. Burstein, *Solid State Comm.* **5**, 439 (1967).
7. M. Rautenberg, Ph.D. thesis, Der Rheinisch-Westfäleschen Technischen Hochschule Aachen, (1977); private communication from P. Grosse.
8. P. A. Hartig and J. J. Loferski, *J. Opt. Soc. Am.* **44**, 17 (1954).
9. R. S. Caldwell and H. Y. Fan, *Phys. Rev.* **114**, 664 (1959).
10. P. Grosse and W. Richter, *Phys. Stat. Solidi* **41**, 239 (1970).
11. J. J. Loferski, *Phys. Rev.* **93**, 707 (1954).
12. S. Tutihasi, G. G. Roberts, R. C. Keezer, and R. E. Drews, *Phys. Rev.* **177**, 1143 (1969).
13. H. Merdy, *Ann. Phys. Paris* **1**, 289 (1966).
14. P. Bammes, R. Klucker, E. E. Koch, and T. Tuomi, *Phys. Stat. Solidi (b)* **49**, 561 (1972); private communication from T. Saile.
15. B. L. Henke, P. Lee, T. J. Tanaka, R. L. Shimabukuro, and B. K. Fujikama, *At. Data Nucl. Data Tables* **27**, 1 (1982).
16. D. E. Gray, ed., "American Institute of Physics Handbook," Third Edition, McGraw-Hill, New York, 7 (1982).

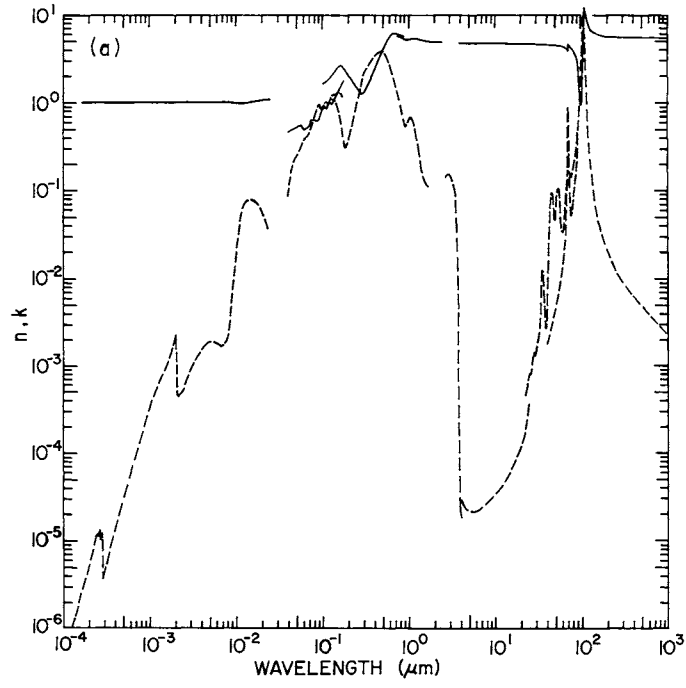


**Fig. 1.** (a) Log–log plot of $n_o$ (solid line) and $k_o$ (dashed line) versus wavelength in micrometers for tellurium. (b) Log–log plot of $n_e$ (solid line) and $k_e$ (dashed line) versus wavelength in micrometers.

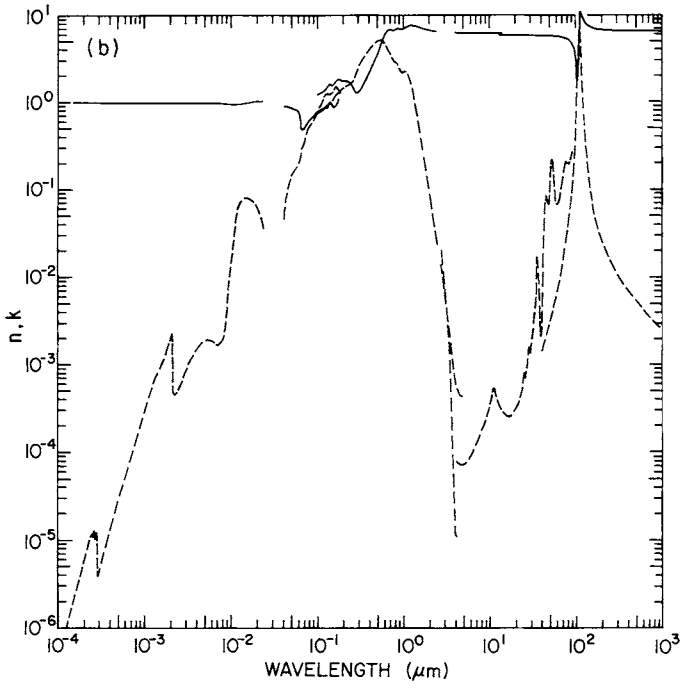


**TABLE I**

**Parameters Obtained from Fitting an Oscillator Model to Reflectivity**

| | $\Delta\varepsilon$ | | | $\nu_T(\text{cm}^{-1})$ | | | $\Gamma(\text{cm}^{-1})$ | | | $\varepsilon_\infty$ | | |
|---|---|---|---|---|---|---|---|---|---|---|---|---|
| | [7] | [5] | [6] | [7] | [5] | [6] | [7] | [5] | [6] | [7] | [5] | [6] |
| ∥ | 7.2 | 18 | 5.6 | 88.1 | 86.5 | 90 | 3.5 | 4.0 | 3.6 | 36 | 36 | 39.5 |
| ⊥ | 7.0 | 11 | 7.5 | 92.4 | 92 | 92 | 3.0 | 4.0 | 3.2 | 23 | 23 | 22.9 |
| | 0.14 | 0.73 | 0.25 | 141.1 | 142 | 144 | 2.7 | 6.5 | 5.8 | | | |

**TABLE II**

**Values of *n* and *k* for Tellurium from Various References[a]**

| eV | Å | n | k |
|---|---|---|---|
| 9972 | 1.243 | 0.9999889[15] | 1.04x10$^{-6}$[15] |
| 9331 | 1.329 | 0.9999878 | 1.23x10$^{-6}$ |
| 8909 | 1.392 | 0.9999866 | 1.46x10$^{-6}$ |
| 8507 | 1.458 | 0.9999853 | 1.73x10$^{-6}$ |
| 8123 | 1.526 | 0.9999840 | 2.05x10$^{-6}$ |
| 7756 | 1.599 | 0.9999825 | 2.43x10$^{-6}$ |
| 7406 | 1.674 | 0.9999809 | 2.87x10$^{-6}$ |
| 7072 | 1.753 | 0.9999791 | 3.40x10$^{-6}$ |
| 6752 | 1.836 | 0.9999720 | 4.01x10$^{-6}$ |
| 6447 | 1.923 | 0.9999752 | 4.73x10$^{-6}$ |
| 6156 | 2.014 | 0.9999731 | 5.58x10$^{-6}$ |
| 5878 | 2.109 | 0.9999709 | 6.57x10$^{-6}$ |
| 5613 | 2.209 | 0.9999860 | 7.73x10$^{-6}$ |
| 5359 | 2.314 | 0.9999640 | 9.08x10$^{-6}$ |
| 5117 | 2.423 | 0.9999645 | 1.07x10$^{-5}$ |
| 5000 | 2.480 | 0.9999640 | 1.15x10$^{-5}$ |
| 4886 | 2.538 | 0.9999635 | 1.10x10$^{-5}$ |
| 4775 | 2.597 | 0.9999621 | 1.19x10$^{-5}$ |
| 4665 | 2.658 | 0.9999622 | 1.30x10$^{-5}$ |
| 4559 | 2.720 | 0.9999619 | 1.03x10$^{-5}$ |
| 4455 | 2.783 | 0.9999603 | 1.12x10$^{-5}$ |
| 4353 | 2.848 | 0.9999635 | 1.21x10$^{-5}$ |
| 4254 | 2.915 | 0.9999568 | 3.84x10$^{-6}$ |
| 4157 | 2.983 | 0.9999523 | 4.17x10$^{-6}$ |
| 4062 | 3.053 | 0.9999486 | 4.53x10$^{-6}$ |
| 3878 | 3.197 | 0.9999417 | 5.34x10$^{-6}$ |
| 3703 | 3.348 | 0.9999347 | 6.30x10$^{-6}$ |
| 3536 | 3.506 | 0.9999273 | 7.42x10$^{-6}$ |
| 3376 | 3.672 | 0.9999194 | 8.75x10$^{-6}$ |
| 3224 | 3.846 | 0.9999108 | 1.03x10$^{-5}$ |
| 3078 | 4.028 | 0.9999015 | 1.22x10$^{-5}$ |
| 2939 | 4.218 | 0.999891 | 1.43x10$^{-5}$ |
| 2807 | 4.418 | 0.999880 | 1.69x10$^{-5}$ |
| 2680 | 4.627 | 0.999868 | 1.98x10$^{-5}$ |
| 2559 | 4.846 | 0.999855 | 2.34x10$^{-5}$ |
| 2443 | 5.075 | 0.999840 | 2.75x10$^{-5}$ |
| 2333 | 5.315 | 0.999825 | 3.23x10$^{-5}$ |
| 2228 | 5.557 | 0.999807 | 3.80x10$^{-5}$ |
| 2127 | 5.829 | 0.999789 | 4.46x10$^{-5}$ |
| 2031 | 6.105 | 0.999768 | 5.24x10$^{-5}$ |
| 1939 | 6.394 | 0.999745 | 6.13x10$^{-5}$ |
| 1852 | 6.696 | 0.999722 | 7.18x10$^{-5}$ |
| 1768 | 7.013 | 0.999696 | 8.42x10$^{-5}$ |
| 1688 | 7.344 | 0.999668 | 9.84x10$^{-5}$ |
| 1612 | 7.691 | 0.999637 | 1.15x10$^{-4}$ |
| 1539 | 8.055 | 0.999605 | 1.34x10$^{-4}$ |
| 1470 | 8.436 | 0.999570 | 1.56x10$^{-4}$ |
| 1403 | 8.835 | 0.999533 | 1.82x10$^{-4}$ |

**TABLE II (*Continued*)**

**Tellurium**

| eV | Å | n | k |
|---|---|---|---|
| 1340 | 9.253 | 0.999494 | $2.11\times10^{-4}$ |
| 1280 | 9.690 | 0.999452 | $2.45\times10^{-4}$ |
| 1222 | 10.15 | 0.999408 | $2.85\times10^{-4}$ |
| 1167 | 10.63 | 0.999363 | $3.31\times10^{-4}$ |
| 1114 | 11.13 | 0.999318 | $3.85\times10^{-4}$ |
| 1064 | 11.66 | 0.999274 | $4.48\times10^{-4}$ |
| 1016 | 12.21 | 0.999240 | $5.20\times10^{-4}$ |
| 969.7 | 12.79 | 0.999209 | $5.82\times10^{-4}$ |
| 925.9 | 13.39 | 0.999167 | $6.57\times10^{-4}$ |
| 884.1 | 14.02 | 0.999139 | $7.46\times10^{-4}$ |
| 844.2 | 14.69 | 0.999141 | $8.34\times10^{-4}$ |
| 806.0 | 15.38 | 0.999114 | $8.63\times10^{-4}$ |
| 769.7 | 16.11 | 0.999035 | $9.58\times10^{-4}$ |
| 734.9 | 16.87 | 0.998983 | $1.10\times10^{-3}$ |
| 701.7 | 17.67 | 0.998973 | $1.27\times10^{-3}$ |
| 670.0 | 18.51 | 0.999018 | $1.46\times10^{-3}$ |
| 639.8 | 19.38 | 0.999111 | $1.66\times10^{-3}$ |
| 610.9 | 20.30 | 0.999339 | $1.96\times10^{-3}$ |
| 596.9 | 20.77 | 0.999620 | $2.14\times10^{-3}$ |
| 583.3 | 21.26 | 1.000231 | $2.33\times10^{-3}$ |
| 570.0 | 21.75 | 1.001085 | $5.00\times10^{-4}$ |
| 557.0 | 22.26 | 1.000177 | $4.59\times10^{-4}$ |
| 531.8 | 23.31 | 0.999560 | $4.53\times10^{-4}$ |
| 507.8 | 24.42 | 0.999210 | $4.89\times10^{-4}$ |
| 484.9 | 25.57 | 0.99893 | $5.37\times10^{-4}$ |
| 463.0 | 26.78 | 0.99867 | $6.01\times10^{-4}$ |
| 442.1 | 28.05 | 0.99843 | $6.73\times10^{-4}$ |
| 422.1 | 29.37 | 0.99818 | $7.57\times10^{-4}$ |
| 403.0 | 30.76 | 0.99794 | $8.66\times10^{-4}$ |
| 384.8 | 32.22 | 0.99770 | $9.89\times10^{-4}$ |
| 367.5 | 33.74 | 0.99748 | $1.09\times10^{-3}$ |
| 350.9 | 35.34 | 0.99723 | $1.19\times10^{-3}$ |
| 335.0 | 37.01 | 0.99696 | $1.31\times10^{-3}$ |
| 319.9 | 38.76 | 0.99669 | $1.41\times10^{-3}$ |
| 305.5 | 40.59 | 0.99639 | $1.51\times10^{-3}$ |
| 291.7 | 42.51 | 0.99605 | $1.61\times10^{-3}$ |
| 278.5 | 44.52 | 0.99568 | $1.71\times10^{-3}$ |
| 265.9 | 46.63 | 0.99530 | $1.80\times10^{-3}$ |
| 253.9 | 48.83 | 0.99486 | $1.86\times10^{-3}$ |
| 242.5 | 51.14 | 0.99436 | $1.91\times10^{-3}$ |
| 231.5 | 53.56 | 0.99378 | $1.94\times10^{-3}$ |
| 221.1 | 56.09 | 0.99312 | $1.96\times10^{-3}$ |
| 211.1 | 58.74 | 0.99236 | $1.93\times10^{-3}$ |
| 201.5 | 61.52 | 0.99144 | $1.90\times10^{-3}$ |
| 192.4 | 64.43 | 0.99037 | $1.84\times10^{-3}$ |
| 183.7 | 67.48 | 0.9891 | $1.76\times10^{-3}$ |
| 175.5 | 70.67 | 0.9874 | $1.71\times10^{-3}$ |
| 167.5 | 74.01 | 0.9856 | $1.73\times10^{-3}$ |

**TABLE II (*Continued*)**

**Tellurium**

| eV | Å | n | k |
|---|---|---|---|
| 160.0 | 77.51 | 0.9833 | $1.79\times10^{-3}$ |
| 152.7 | 81.17 | 0.9805 | $1.94\times10^{-3}$ |
| 145.8 | 85.01 | 0.9768 | $2.43\times10^{-3}$ |
| 142.5 | 87.00 | 0.9747 | $2.88\times10^{-3}$ |
| 139.3 | 89.03 | 0.9724 | $3.64\times10^{-3}$ |
| 136.1 | 91.11 | 0.9699 | $4.62\times10^{-3}$ |
| 133.0 | 93.24 | 0.9673 | $5.87\times10^{-3}$ |
| 129.9 | 95.42 | 0.9644 | $7.45\times10^{-3}$ |
| 127.0 | 97.66 | 0.9614 | $9.45\times10^{-3}$ |
| 124.1 | 99.94 | 0.9581 | $1.20\times10^{-2}$ |
| 121.2 | 102.3 | 0.9547 | $1.55\times10^{-2}$ |
| 118.5 | 104.7 | 0.9515 | $2.00\times10^{-2}$ |
| 115.8 | 107.1 | 0.9493 | $2.57\times10^{-2}$ |
| 113.1 | 109.6 | 0.9483 | $3.11\times10^{-2}$ |
| 108.0 | 114.8 | 0.9469 | $4.34\times10^{-2}$ |
| 103.1 | 120.2 | 0.9522 | $5.68\times10^{-2}$ |
| 98.47 | 125.9 | 0.9600 | $6.60\times10^{-2}$ |
| 94.03 | 131.9 | 0.9680 | $7.26\times10^{-2}$ |
| 89.78 | 138.1 | 0.9767 | $7.67\times10^{-2}$ |
| 85.73 | 144.6 | 0.9854 | $7.99\times10^{-2}$ |
| 81.85 | 151.5 | 0.99376 | $8.03\times10^{-2}$ |
| 78.16 | 158.6 | 1.00126 | $7.98\times10^{-2}$ |
| 74.63 | 166.1 | 1.00741 | $7.82\times10^{-2}$ |
| 71.26 | 174.0 | 1.0140 | $7.63\times10^{-2}$ |
| 68.04 | 182.2 | 1.0193 | $7.33\times10^{-2}$ |
| 64.97 | 190.8 | 1.0250 | $6.85\times10^{-2}$ |
| 62.04 | 199.9 | 1.0278 | $6.29\times10^{-2}$ |
| 59.24 | 209.3 | 1.0311 | $5.65\times10^{-2}$ |
| 56.56 | 219.2 | 1.0302 | $4.92\times10^{-2}$ |
| 54.01 | 229.6 | 1.0286 | $4.35\times10^{-2}$ |
| 51.57 | 240.4 | 1.0265 | $3.59\times10^{-2}$ |

| eV | $cm^{-1}$ | μm | $n_o(\perp)$ | $k_o(\perp)$ | $n_e(\parallel)$ | $k_e(\parallel)$ |
|---|---|---|---|---|---|---|
| 30 | | 0.04133 | 0.46[14] | 0.088[14] | 0.90[14] | 0.045[14] |
| 29 | | 0.04275 | 0.47 | 0.13 | 0.90 | 0.067 |
| 28 | | 0.04428 | 0.48 | 0.17 | 0.89 | 0.090 |
| 27 | | 0.04592 | 0.48 | 0.19 | 0.88 | 0.10 |
| 26 | | 0.04769 | 0.50 | 0.20 | 0.87 | 0.12 |
| 25 | | 0.04959 | 0.52 | 0.23 | 0.86 | 0.14 |
| 24 | | 0.05166 | 0.54 | 0.25 | 0.85 | 0.15 |
| 23 | | 0.05391 | 0.54 | 0.26 | 0.84 | 0.16 |
| 22 | | 0.05636 | 0.56 | 0.29 | 0.83 | 0.18 |
| 21 | | 0.05904 | 0.55 | 0.33 | 0.82 | 0.18 |
| 20 | | 0.06199 | 0.50 | 0.38 | 0.74 | 0.20 |
| 19 | | 0.06526 | 0.51 | 0.40 | 0.49 | 0.30 |
| 18 | | 0.06888 | 0.52 | 0.41 | 0.48 | 0.31 |

**TABLE II (*Continued*)**

**Tellurium**

| eV | $cm^{-1}$ | μm | $n_o$ (⊥) | $k_o$ (⊥) | $n_e$ (∥) | $k_e$ (∥) |
|---|---|---|---|---|---|---|
| 17 | | 0.07293 | 0.56 | 0.46 | 0.51 | 0.39 |
| 16 | | 0.07749 | 0.64 | 0.55 | 0.59 | 0.49 |
| 15 | | 0.08266 | 0.62 | 0.70 | 0.64 | 0.55 |
| 14.5 | | 0.08551 | 0.62 | 0.76 | 0.65 | 0.57 |
| 14 | | 0.08856 | 0.59 | 0.87 | 0.67 | 0.59 |
| 13.5 | | 0.09184 | 0.61 | 0.93 | 0.71 | 0.64 |
| 13 | | 0.09537 | 0.69 | 0.94 | 0.73 | 0.69 |
| 12.5 | | 0.09919 | 0.85 | 0.85 | 0.75 | 0.72 |
| 12 | 96,786 | 0.1033 | 0.87 | 0.87 | 0.79 | 0.76 |
| | | | 1.64[12] | 0.70[12] | 1.22[12] | 0.82[12] |
| 11.5 | 92,753 | 0.1078 | 1.70 | 0.83 | 1.24 | 0.89 |
| | | | 0.84[14] | 0.90[14] | 0.79[14] | 0.75[14] |
| 11 | 88,720 | 0.1127 | 0.84 | 1.01 | 0.80 | 0.77 |
| | | | 1.74[12] | 0.92[12] | 1.26[12] | 0.95[12] |
| 10.5 | 84,688 | 0.1181 | 1.84 | 1.04 | 1.33 | 1.09 |
| | | | 0.98[14] | 0.98[14] | 0.83[14] | 0.80[14] |
| 10.0 | 80,655 | 0.1240 | 0.99 | 1.04 | 0.86 | 0.86 |
| | | | 1.93[12] | 1.06[12] | 1.36[12] | 1.21[12] |
| 9.5 | 76,622 | 0.1305 | 2.08 | 1.11 | 1.47 | 1.25 |
| | | | 0.96[14] | 1.20[14] | 0.84[14] | 0.95[14] |
| 9.0 | 72,589 | 0.1378 | 1.11 | 1.24 | 0.99 | 0.93 |
| | | | 2.27[12] | 1.12[12] | 1.60[12] | 1.25[12] |
| 8.75 | 70,573 | 0.1417 | 2.35 | 1.06 | 1.59 | 1.23 |
| 8.5 | 68,557 | 0.1459 | 2.39 | 1.00 | 1.55 | 1.23 |
| | | | 1.25[14] | 1.25[14] | 0.96[14] | 0.96[14] |
| 8.25 | 66,540 | 0.1503 | 2.45[12] | 0.96[12] | 1.54[12] | 1.30[12] |
| 8.0 | 64,524 | 0.1550 | 2.59 | 0.91 | 1.54 | 1.37 |
| | | | 1.40[14] | 1.36[14] | 0.85[14] | 1.06[14] |
| 7.75 | 62,507 | 0.1600 | 2.61[12] | 0.77[12] | 1.60[12] | 1.47[12] |
| 7.5 | 60,491 | 0.1653 | 2.60 | 0.69 | 1.72 | 1.51 |
| | | | 1.66[14] | 1.29[14] | 0.92[14] | 1.20[14] |
| 7.25 | 58,475 | 0.1710 | 2.57[12] | 0.55[12] | 1.81[12] | 1.44[12] |
| 7.0 | 56,458 | 0.1771 | 2.48 | 0.40 | 1.83 | 1.36 |
| | | | 1.81[14] | 1.18[14] | 1.08[14] | 1.29[14] |
| 6.75 | 54,442 | 0.1837 | 2.35[12] | 0.32[12] | 1.79[12] | 1.34[12] |
| 6.5 | 52,426 | 0.1907 | 2.19 | 0.32 | 1.78 | 1.36 |
| 6.25 | 50,409 | 0.1984 | 2.04 | 0.36 | 1.73 | 1.41 |
| 6.0 | 48,393 | 0.2066 | 1.94 | 0.39 | 1.73 | 1.45 |
| 5.75 | 46,377 | 0.2156 | 1.82 | 0.47 | 1.72 | 1.51 |
| 5.5 | 44,360 | 0.2254 | 1.74 | 0.51 | 1.72 | 1.57 |
| 5.25 | 42,344 | 0.2362 | 1.59 | 0.69 | 1.71 | 1.58 |
| 5.0 | 40,327 | 0.2480 | 1.47 | 0.82 | 1.63 | 1.60 |
| 4.75 | 38,311 | 0.2610 | 1.39 | 1.01 | 1.49 | 1.71 |
| 4.5 | 36,295 | 0.2755 | 1.28 | 1.28 | 1.32 | 1.96 |
| 4.25 | 34,278 | 0.2917 | 1.27 | 1.65 | 1.25 | 2.31 |
| 4.0 | 32,262 | 0.3100 | 1.32 | 2.01 | 1.33 | 2.64 |
| 3.75 | 30,246 | 0.3306 | 1.50 | 2.37 | 1.44 | 3.06 |
| 3.5 | 28,229 | 0.3542 | 1.72 | 2.70 | 1.69 | 3.44 |

**TABLE II (*Continued*)**

**Tellurium**

| eV | $cm^{-1}$ | μm | $n_o$ (⊥) | $k_o$ (⊥) | $n_e$ (∥) | $k_e$ (∥) |
|---|---|---|---|---|---|---|
| 3.25 | 26,213 | 0.3815 | 2.02 | 3.03 | 1.92 | 3.78 |
| 3.069 | 24,750 | 0.4040 | 2.37[2] | 3.29[2] | 2.22[2] | 3.96[2] |
| 3.0 | 24,196 | 0.4133 | 2.51[12] | 3.39[12] | 2.30[12] | 4.16[12] |
| 2.976 | 24,000 | 0.4167 | 2.56[2] | 3.39[2] | 2.35[2] | 4.15[2] |
| 2.883 | 23,250 | 0.4301 | 2.77 | 3.47 | 2.54 | 4.27 |
| 2.8 | 22,583 | 0.4428 | 3.03[12] | 3.63[12] | 2.73[12] | 4.42[12] |
| 2.790 | 22,500 | 0.4444 | 3.01[2] | 3.57[2] | 2.76[2] | 4.39[2] |
| 2.697 | 21,750 | 0.4598 | 3.27 | 3.66 | 2.98 | 4.52 |
| 2.604 | 21,000 | 0.4762 | 3.55 | 3.72 | 3.21 | 4.71 |
| 2.6 | 20,970 | 0.4769 | 3.57[12] | 3.75[12] | 3.25[12] | 4.77[12] |
| 2.534 | 20,440 | 0.4892 | 3.76[2] | 3.76[2] | 3.46[2] | 4.85[2] |
| 2.487 | 20,060 | 0.4985 | 3.91 | 3.77 | 3.63 | 4.93 |
| 2.441 | 19,690 | 0.5079 | 4.07 | 3.77 | 3.81 | 5.01 |
| 2.4 | 19,357 | 0.5166 | 4.24[12] | 3.77[12] | 3.94[12] | 5.08[12] |
| 2.394 | 19,310 | 0.5179 | 4.25[2] | 3.78[2] | 3.99[2] | 5.08[2] |
| 2.348 | 18,940 | 0.5280 | 4.43 | 3.76 | 4.20 | 5.16 |
| 2.301 | 18,560 | 0.5388 | 4.62 | 3.69 | 4.39 | 5.20 |
| 2.255 | 18,190 | 0.5498 | 4.81 | 3.63 | 4.65 | 5.21 |
| 2.209 | 17,820 | 0.5612 | 5.01 | 3.57 | 4.91 | 5.20 |
| 2.2 | 17,744 | 0.5636 | 5.10[12] | 3.61[12] | 4.94[12] | 5.16[12] |
| 2.162 | 17,440 | 0.5734 | 5.26[2] | 3.52[2] | 5.17[2] | 5.16[2] |
| 2.166 | 17,070 | 0.5858 | 5.49 | 3.37 | 5.45 | 5.06 |
| 2.069 | 16,690 | 0.5992 | 5.67 | 3.16 | 5.76 | 4.92 |
| 2.023 | 16,320 | 0.6127 | 5.82 | 2.94 | 6.00 | 4.77 |
| 2.0 | 16,131 | 0.6199 | 5.94[12] | 2.69[12] | 4.67[12] | 4.67[12] |
| 1.976 | 15,940 | 0.6274 | 5.97[2] | 2.70[2] | 6.21[2] | 4.60[2] |
| 1.930 | 15,570 | 0.6423 | 6.07 | 2.45 | 6.40 | 4.36 |
| 1.883 | 15,190 | 0.6583 | 6.11 | 2.25 | 6.58 | 4.10 |
| 1.837 | 14,820 | 0.6748 | 6.12 | 2.02 | 6.77 | 3.86 |
| 1.8 | 14,518 | 0.6888 | 6.10[12] | 1.80[12] | 6.89[12] | 3.70[12] |
| 1.790 | 14,440 | 0.6925 | 6.09[2] | 1.72[2] | 6.85[2] | 3.65[2] |
| 1.744 | 14,070 | 0.7107 | 6.04 | 1.52 | 6.86 | 3.47 |
| 1.697 | 13,690 | 0.7305 | 5.95 | 1.36 | 6.80 | 3.18 |
| 1.651 | 13,320 | 0.7508 | 5.87 | 1.26 | 6.78 | 3.03 |
| 1.604 | 12,940 | 0.7728 | 5.86 | 1.17 | 6.74 | 2.93 |
| 1.6 | 12,905 | 0.7749 | 5.88[12] | 1.15[12] | 6.75[12] | 2.91[12] |
| 1.557 | 12,560 | 0.7962 | 5.84[2] | 1.06[2] | 6.73[2] | 2.89[2] |
| 1.511 | 12,190 | 0.8203 | 5.78 | 0.895 | 6.81 | 2.86 |
| 1.464 | 11,810 | 0.8467 | 5.68 | 0.760 | 6.95 | 2.80 |
| 1.418 | 11,440 | 0.8741 | 5.59 | 0.659 | 7.14 | 2.56 |
| 1.4 | 11,292 | 0.8856 | 5.56[12] | 0.63[12] | 7.11[12] | 2.46[12] |
| 1.3 | 10,485 | 0.9537 | 5.36 | 0.54 | 6.87 | 2.16 |
| 1.2 | 9,679 | 1.033 | 5.17 | 0.63 | 6.99 | 2.22 |
| 1.1 | 8,872 | 1.127 | 5.33 | 0.68 | 7.51 | 2.10 |
| 1.0 | 8,065 | 1.240 | 5.35 | 0.45 | 7.70 | 1.56 |
| 0.9 | 7,259 | 1.378 | 5.22 | 0.22 | 7.48 | 0.94 |
| 0.8 | 6,452 | 1.550 | 5.10 | 0.13 | 7.23 | 0.48 |
| 0.7 | 5,646 | 1.771 | 4.95 | 0.11 | 7.00 | 0.24 |

**TABLE II (*Continued*)**

**Tellurium**

| eV | $cm^{-1}$ | μm | $n_o$ (⊥) | $k_o$ (⊥) | $n_e$ (∥) | $k_e$ (∥) |
|---|---|---|---|---|---|---|
| 0.6 | 4,839 | 2.066 | 4.93 | | 6.71 | $7.5\times10^{-2}$ |
| 0.5 | 4,033 | 2.480 | 4.90 | | 6.53 | $2.3\times10^{-2}$ |
| 0.45 | 3,629 | 2.755 | | 0.145[12] | | $2.02\times10^{-2}$[12] |
| 0.44 | 3,549 | 2.818 | | 0.150 | | $1.52\times10^{-2}$ |
| 0.43 | 3,468 | 2.883 | | 0.151 | | $1.15\times10^{-2}$ |
| 0.42 | 3,388 | 2.952 | | 0.150 | | $8.69\times10^{-3}$ |
| 0.41 | 3,307 | 3.024 | | 0.149 | | $6.74\times10^{-3}$ |
| 0.40 | 3,226 | 3.100 | | 0.148 | | $5.18\times10^{-3}$ |
| 0.39 | 3,146 | 3.179 | | 0.139 | | $3.79\times10^{-3}$ |
| 0.38 | 3,065 | 3.263 | | 0.125 | | $2.60\times10^{-3}$ |
| 0.37 | 2,984 | 3.351 | | 0.115 | | $1.65\times10^{-3}$ |
| 0.365 | 2,944 | 3.397 | | | | $1.35\times10^{-3}$ |
| 0.36 | 2,904 | 3.444 | | 0.104 | | $1.07\times10^{-3}$ |
| 0.355 | 2,863 | 3.493 | | | | $7.64\times10^{-4}$ |
| 0.35 | 2,823 | 3.542 | | $7.89\times10^{-2}$ | | $4.93\times10^{-4}$ |
| 0.345 | 2,783 | 3.594 | | $6.86\times10^{-2}$ | | $3.15\times10^{-4}$ |
| 0.34 | 2,742 | 3.647 | | $5.51\times10^{-2}$ | | $1.68\times10^{-4}$ |
| 0.335 | 2,702 | 3.701 | | $2.65\times10^{-2}$ | | $9.13\times10^{-5}$ |
| 0.33 | 2,662 | 3.757 | | $5.98\times10^{-3}$ | | $5.08\times10^{-5}$ |
| 0.325 | 2,621 | 3.815 | | $1.28\times10^{-3}$ | | $2.79\times10^{-5}$ |
| 0.32 | 2,581 | 3.875 | | $2.78\times10^{-4}$ | | $1.88\times10^{-5}$ |
| 0.315 | 2,541 | 3.936 | | $8.77\times10^{-5}$ | | $1.45\times10^{-5}$ |
| 0.31 | 2,500 | 4.000 | 4.929[9] | $3.18\times10^{-5}$ | 6.372[9] | $1.18\times10^{-5}$ |
| 0.305 | 2,460 | 4.065 | | $1.94\times10^{-5}$ | | $1.10\times10^{-5}$ |
| 0.30 | 2,420 | 4.133 | | $1.81\times10^{-5}$ | | $1.09\times10^{-5}$ |
| 0.2976 | 2,400 | 4.167 | | $2.92\times10^{-5}$[9] | | $7.96\times10^{-5}$[9] |
| 0.2728 | 2,200 | 4.545 | | $2.35\times10^{-5}$ | | $7.23\times10^{-5}$ |
| 0.2480 | 2,000 | 5.000 | 4.864 | $2.19\times10^{-5}$ | 6.316 | $7.48\times10^{-5}$ |
| 0.2232 | 1,800 | 5.556 | | $2.03\times10^{-5}$ | | $7.60\times10^{-5}$ |
| 0.2066 | 1,667 | 6 | 4.838 | | 6.286 | |
| 0.1984 | 1,600 | 6.250 | | $2.09\times10^{-5}$ | | $9.10\times10^{-5}$ |
| 0.1771 | 1,429 | 7 | 4.821 | | 6.257 | |
| 0.1736 | 1,400 | 7.143 | | $2.27\times10^{-5}$ | | $1.31\times10^{-4}$ |
| 0.1550 | 1,250 | 8 | 4.809 | | 6.253 | |
| 0.1488 | 1,200 | 8.333 | | $2.59\times10^{-5}$ | | $1.82\times10^{-4}$ |
| 0.1240 | 1,000 | 10.00 | 4.796 | $3.18\times10^{-5}$ | 6.246 | $3.34\times10^{-4}$ |
| 0.1116 | 900 | 11.11 | | $3.63\times10^{-5}$ | | $5.31\times10^{-4}$ |
| 0.1033 | 833.3 | 12 | 4.789 | | 6.237 | |
| 0.09919 | 800 | 12.50 | | $4.28\times10^{-5}$ | | $3.68\times10^{-4}$ |
| 0.09299 | 750 | 13.33 | 4.78[7] | | 5.99[7] | |
| 0.08856 | 714.3 | 14 | 4.785[9] | | 6.230[9] | |
| 0.08679 | 700 | 14.29 | | $5.34\times10^{-5}$ | | $2.96\times10^{-4}$ |
| 0.07439 | 600 | 16.67 | | $7.23\times10^{-5}$ | | $2.52\times10^{-4}$ |
| 0.06199 | 500 | 20.00 | 4.77[7] | $1.16\times10^{-4}$ | 5.98[7] | $3.09\times10^{-4}$ |
| 0.05579 | 450 | 22.22 | | $1.59\times10^{-4}$ | | $3.89\times10^{-4}$ |
| 0.05455 | 440 | 22.73 | | $4.52\times10^{-4}$[5] | | $4.16\times10^{-4}$[5] |
| 0.05331 | 430 | 23.26 | | $5.37\times10^{-4}$ | | $4.81\times10^{-4}$ |
| 0.05207 | 420 | 23.81 | | $6.06\times10^{-4}$ | | $5.87\times10^{-4}$ |

**TABLE II (*Continued*)**

**Tellurium**

| eV | $cm^{-1}$ | μm | $n_o$ (⊥) | $k_o$ (⊥) | $n_e$ (∥) | $k_e$ (∥) |
|---|---|---|---|---|---|---|
| 0.05083 | 410 | 24.39 | | $6.79\times10^{-4}$ | | $7.38\times10^{-4}$ |
| 0.04959 | 400 | 25.00 | | $7.66\times10^{-4}$ | | $8.16\times10^{-4}$ |
| | | | 4.75 | $3.58\times10^{-4}$ [9] | 5.97 | $7.36\times10^{-4}$ [9] |
| 0.04835 | 390 | 25.64 | | $7.96\times10^{-4}$ [5] | | $7.14\times10^{-4}$ [5] |
| 0.04711 | 380 | 26.32 | | $8.38\times10^{-4}$ | | $7.85\times10^{-4}$ |
| 0.04587 | 370 | 27.03 | | $1.12\times10^{-3}$ | | $1.03\times10^{-3}$ |
| 0.04463 | 360 | 27.78 | | $1.35\times10^{-3}$ | | $1.41\times10^{-3}$ |
| 0.04339 | 350 | 28.57 | 4.74 | $1.41\times10^{-3}$ | 5.96 | $1.59\times10^{-3}$ |
| 0.04215 | 340 | 29.41 | | $1.29\times10^{-3}$ | | $1.40\times10^{-3}$ |
| 0.04092 | 330 | 30.30 | | $1.47\times10^{-3}$ | | $1.93\times10^{-3}$ |
| 0.03968 | 320 | 31.25 | | $1.89\times10^{-3}$ | | $2.44\times10^{-3}$ |
| 0.03844 | 310 | 32.26 | | $2.31\times10^{-3}$ | | $3.08\times10^{-3}$ |
| 0.03720 | 300 | 33.33 | 4.71 | $2.65\times10^{-3}$ | 5.94 | $3.71\times10^{-3}$ |
| 0.03596 | 290 | 34.48 | | $8.78\times10^{-3}$ | | $5.76\times10^{-3}$ |
| 0.03472 | 280 | 35.71 | | $1.25\times10^{-2}$ | | $1.71\times10^{-2}$ |
| 0.03348 | 270 | 37.04 | | $1.03\times10^{-2}$ | | $8.84\times10^{-3}$ |
| 0.03224 | 260 | 38.46 | | $3.06\times10^{-3}$ | | $2.14\times10^{-3}$ |
| 0.03100 | 250 | 40.00 | | $3.50\times10^{-3}$ | | $2.86\times10^{-3}$ |
| | | | 4.67 | $1.76\times10^{-3}$ [7] | 5.91 | $1.38\times10^{-3}$ [7] |
| 0.02976 | 240 | 41.67 | | $2.32\times10^{-2}$ [5] | | $1.49\times10^{-2}$ [5] |
| 0.02852 | 230 | 43.48 | | $7.09\times10^{-2}$ | | $5.19\times10^{-2}$ |
| 0.02728 | 220 | 45.45 | | $8.86\times10^{-2}$ | | $8.32\times10^{-2}$ |
| 0.02604 | 210 | 47.62 | | $9.28\times10^{-2}$ | | $6.82\times10^{-2}$ |
| 0.02480 | 200 | 50.00 | | $4.58\times10^{-2}$ | | $7.16\times10^{-2}$ |
| | | | 4.58 | $4.36\times10^{-3}$ [7] | 5.85 | $3.21\times10^{-3}$ [7] |
| 0.02356 | 190 | 52.63 | | $8.80\times10^{-2}$ [5] | | 0.222[5] |
| 0.02232 | 180 | 55.56 | | 0.106 | | 0.190 |
| 0.02170 | 175 | 57.14 | 4.48 | $7.48\times10^{-3}$ [7] | | |
| 0.02108 | 170 | 58.82 | | $4.21\times10^{-2}$ [5] | | $7.49\times10^{-2}$ |
| 0.01984 | 160 | 62.50 | | $3.43\times10^{-2}$ | | $6.96\times10^{-2}$ |
| 0.01860 | 150 | 66.67 | | 0.117 | | $7.96\times10^{-2}$ |
| | | | 4.20 | $3.59\times10^{-2}$ [7] | 5.71 | $9.54\times10^{-3}$ [7] |
| 0.01835 | 148 | 67.57 | 4.15 | $5.03\times10^{-2}$ | | |
| 0.01810 | 146 | 68.49 | 4.06 | $8.31\times10^{-2}$ | | |
| 0.01785 | 144 | 69.44 | 3.92 | 0.188 | | |
| 0.01761 | 142 | 70.42 | 3.87 | 0.676 | | |
| 0.01749 | 141.1 | 70.87 | 4.30 | 0.873 | | |
| 0.01736 | 140 | 71.43 | 4.63 | 0.499 | 5.59 | $1.74\times10^{-2}$ |
| | | | | 0.171[5] | | 0.142[5] |
| 0.01711 | 138 | 72.46 | 4.48 | 0.156[7] | | |
| 0.01686 | 136 | 73.53 | 4.34 | $8.35\times10^{-2}$ | | |
| 0.01612 | 130 | 76.92 | 4.10 | $5.35\times10^{-2}$ | 5.47 | $2.78\times10^{-2}$ [7] |
| | | | | 0.141[5] | | 0.208[5] |
| 0.01550 | 125 | 80.00 | 3.90 | $6.35\times10^{-2}$ [7] | | |
| 0.01488 | 120 | 83.33 | 3.65 | $8.94\times10^{-2}$ | 5.26 | $5.05\times10^{-2}$ [7] |
| | | | | 0.206[5] | | 0.199[5] |
| 0.01426 | 115 | 86.96 | 3.28 | 0.145[7] | | |
| 0.01364 | 110 | 90.90 | 2.61 | 0.298 | 4.82 | 0.118[7] |

TABLE II (*Continued*)

Tellurium

| eV | $cm^{-1}$ | μm | $n_o$ (⊥) | $k_o$ (⊥) | $n_e$ (∥) | $k_e$ (∥) |
|---|---|---|---|---|---|---|
| | | | | 0.383[5] | | 0.268[5] |
| 0.01333 | 107.5 | 93.02 | | | 4.63 | 0.156[7] |
| 0.01302 | 105 | 95.24 | 1.16 | 1.30[7] | 4.38 | 0.218 |
| 0.01271 | 102.5 | 97.56 | | | 4.01 | 0.326 |
| 0.01240 | 100 | 100.0 | 0.980 | 4.11 | 3.46 | 0.552 |
| | | | | | | 0.446[5] |
| 0.01215 | 98 | 102.0 | 1.30 | 5.52 | 2.77 | 0.986[7] |
| 0.01190 | 96 | 104.2 | 2.12 | 7.48 | 2.00 | 2.11 |
| 0.01165 | 94 | 106.4 | 4.86 | 0.3 | 1.88 | 3.88 |
| 0.01146 | 92.4 | 108.2 | 11.0 | 9.84 | | |
| 0.01141 | 92 | 108.7 | 12.1 | 8.34 | 2.51 | 6.00 |
| 0.01116 | 90 | 111.1 | 11.4 | 2.68 | 4.75 | 8.66 |
| 0.01092 | 88.1 | 113.5 | | | 10.5 | 8.62 |
| 0.01091 | 88 | 113.6 | 9.61 | 1.17[7] | 10.8 | 8.38 |
| 0.01066 | 86 | 116.3 | 8.57 | 0.657 | 11.7 | 3.20 |
| 0.01041 | 84 | 119.0 | 7.91 | 0.422 | 10.3 | 1.37 |
| 0.01017 | 82 | 122.0 | 7.46 | 0.294 | 9.30 | 0.744 |
| 0.009819 | 80 | 125.0 | 7.13 | 0.218 | 8.69 | 0.466 |
| | | | | 0.308[5] | | 0.597[5] |
| 0.009671 | 78 | 128.2 | | | 8.28 | 0.319[7] |
| 0.009423 | 76 | 131.6 | | | 7.98 | 0.232 |
| 0.009175 | 74 | 116.3 | | | 7.76 | 0.176 |
| 0.008927 | 72 | 138.9 | | | 7.58 | 0.138 |
| 0.008679 | 70 | 142.9 | 6.29 | $7.53\times10^{-2}$[7] | 7.44 | 0.112 |
| | | | | 0.250[5] | | 0.330[5] |
| 0.007439 | 60 | 166.7 | | 0.265 | | 0.259 |
| | | | 5.94 | $3.72\times10^{-2}$[7] | 7.03 | $4.81\times10^{-2}$[7] |
| 0.006199 | 50 | 200.0 | 5.75 | $2.14\times10^{-2}$ | 6.83 | $2.58\times10^{-2}$ |
| | | | | 0.382[5] | | 0.302[5] |
| 0.004959 | 40 | 250.0 | | 0.657 | | 0.477 |
| | | | 5.64 | $1.32\times10^{-2}$[7] | 6.71 | $1.53\times10^{-2}$[7] |
| 0.003720 | 30 | 333.3 | 5.56 | $8.34\times10^{-3}$ | 6.64 | $9.38\times10^{-3}$ |
| 0.002480 | 20 | 500.0 | 5.52 | $4.94\times10^{-3}$ | 6.60 | $5.47\times10^{-3}$ |
| 0.001240 | 10 | 1000 | 5.50 | $2.31\times10^{-3}$ | 6.58 | $2.53\times10^{-3}$ |

[a] References are indicated in brackets.

# Tin Telluride (SnTe)

H. PILLER
Louisiana State University
Baton Rouge, Louisiana

The binary compound semiconductor SnTe was found to be isomorphous with rock salt. The nature of chemical binding is mixed ionic–covalent. SnTe has direct interband optical transitions at the $L$ point in the Brillouin zone. The band structure near the fundamental gap is more complicated than in the lead salts. For large hole concentrations one should observe a positive temperature coefficient of the fundamental gap. Optical experiments by Murase *et al.* [1] have shown that the temperature coefficient of the gap changes its sign from negative to positive with increasing hole concentration in the temperature region between 50 and 150 K.

The first detailed study of the reflectivity of SnTe was performed by Cardona and Greenaway [2]. The measurement of reflectivity and absorption of a semiconductor provides a direct method of studying the band structure. Epitaxial layers of SnTe on KCl were used for the reflection and transmission measurements. The SnTe layers were evaporated onto KCl single-crystal substrates, cleaved in air, and held at a temperature of approximately 573 K. X-ray results showed all the films to be single-crystal and to have the crystal orientation of the substrate: (100). No attempt was made to determine the impurity level in the samples. The thickness of the films was determined by the Tolansky interference method. The room-temperature reflectivity should be accurate to a few percent. An analysis of the reflectivity data for SnTe, using the Kramers–Kronig relation, made it possible to make a detailed comparison of the optical constants obtained from both the reflection and transmission results. The absorption constants obtained from the reflection analysis were compared with values obtained from transmission measurements on thin epitaxial films of SnTe. The agreement was shown to be excellent. The quasi-free electron region (plasma region) was also investigated. It was shown that the phenomenological scattering time required to fit the optical constants with the Drude formula [3] is $1.3 \times 10^{-16}$ sec. The plasma frequency was calculated by taking the density of the valence electrons equal to five electrons per atom.


Copyright © 1991 by Academic Press.
All rights of reproduction in any form reserved.
ISBN 0-12-544422-2

The room-temperature reflectivity measurements were made over the photon energy range 0.5–20 eV. Measurements of transmission were made in the photon energy range below 4 eV. The optical constants $n$ and $k$ are listed in the first two columns of Table I ($n$ and $k$). Figure 1 shows a plot of the data.

Korn and Braunstein [4, 5] measured the near-normal reflectivity of polycrystalline SnTe over the photon-energy range 0.5–21 eV at room temperature. The optical constants $n$ and $k$ were determined through a Kramers–Kronig computation. The samples were cut, ground, and hand-polished to produce optical-quality surfaces. After an electrochemical etch, samples were immediately placed in a vacuum (at least $10^{-5}$ torr) and spectral scans were begun. Consistent results were obtained upon repreparation of sample surfaces. The maximum absolute reflectance error throughout the spectral range was estimated to be at most 2%. The optical constants $n$ and $k$ are listed in Table I (columns 3 and 4). Figure 1 shows a plot of the data.

Burke and Riedl [6] measured the absorption coefficient and the index of refraction of SnTe at 300 K over the photon-energy range between 0.14 and 0.64 eV. The sample was a single-crystal film with a hole concentration of $3.6 \times 10^{19}\,\mathrm{cm}^{-3}$. The single crystal was epitaxially deposited to a thickness of 1.2 μm on an NaCl substrate. The room-temperature data are in good agreement with those obtained by Schoolar and Dixon [7], who measured the optical constants of $p$-type SnTe at room temperature over the spectral range from 0.1–3.8 eV. The indices of refraction and absorption coefficients were obtained from analysis of normal reflectance and transmittance measurements on epitaxial films ranging in carrier concentration from $3.6 \times 10^{19}$ to $6.8 \times 10^{20}\,\mathrm{cm}^{-3}$. At photon energies greater than 1.0 eV, the absorption spectrum agrees with the results of Cardona and Greenaway [2]. Electrical, X-ray, and optical data indicate that the films are high quality, single crystals. A "sample in, sample out" procedure was used for taking the data. The error of reflectance and transmittance is estimated to be less than ±3%. The film thickness was determined from analysis of the interference fringes. Such spectra were also used to determine the carrier concentration $p$ from the position of the plasma reflectance minimum. It was estimated that the carrier concentrations determined in this way are accurate to within ±10%. The homogeneity of the films was checked by measuring the reflectance of different areas of the films on both the front and back surfaces. Variations were less than ±3% for all the samples studied. The $n$ and $k$ values determined by Burke and Riedl [6] and Schoolar and Dixon [7] are listed in Table I and plotted in Fig. 1. These, of course, contain the effects of free holes.

Potter [8] made an ellipsometry study of SnTe in the infrared and visible spectral regions. Fukui *et al.* [9] measured the absorption spectra of crystalline SnTe films in the 2–120 eV region using synchrotron radiation at

liquid-nitrogen temperature. In the *in situ* measurements, an SnTe film was evaporated onto a collodion film cooled to about 80 K at a pressure below $10^{-8}$ torr before the absorption measurements were made. Then the film was annealed at room temperature and then again cooled to 80 K when the measurements were repeated. The absorption spectrum of SnTe in the amorphous and in the crystalline phase was measured. The structure in the absorption spectrum in the crystalline SnTe below 20 eV is in good agreement with previous results [2]. No absorption coefficient was determined from these measurements.

## REFERENCES


1. K. Murase, S. Sugai, T. Higuchi, S. Takaoka, T. Fukunaga, and H. Kawamura, "Proc. 14th Internat. Conf. Phys. Semicond.," (B. L. H. Wilson, ed.), Institute of Physics, Edinburgh, 437 (1979).
2. M. Cardona and D. L. Greenaway, *Phys. Rev.* **133**, A1685 (1964).
3. H. R. Philipp and H. Ehrenreich, *Phys. Rev.* **129**, 1550 (1963).
4. D. M. Korn, thesis, UCLA, unpublished, (1971).
5. D. M. Korn and R. Braunstein, *Phys. Rev. B* **5**, 4837 (1972).
6. J. Richard Burke, Jr., and H. R. Riedl, *Phys. Rev.* **184**, 830 (1969).
7. R. B. Schoolar and J. R. Dixon, *J. Opt. Soc.* **58**, 119 (1968).
8. R. Potter, thesis, Brown University, unpublished, (1970).
9. K. Fukui, J. Yamazaki, T. Saito, S. Kondo, and M. Watanabe, *J. Phys. Soc. Japan* **56**, 4196 (1987).


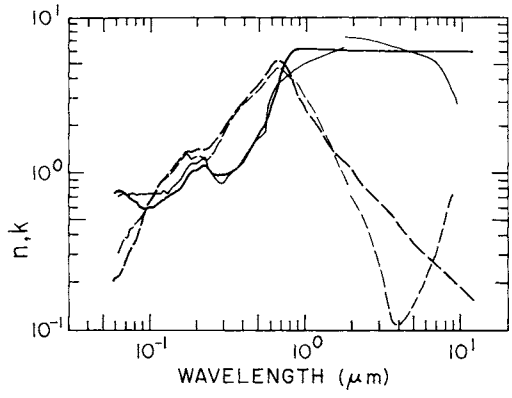


**Fig. 1.** Log–log plot of $n$ (solid line) and $k$ (dashed line) versus wavelength in micrometers for tin telluride.

**TABLE I**

**Values of *n* and *k* for Tin Telluride Obtained from Various References[a]**

| eV | μm | n | k | n | k |
|---|---|---|---|---|---|
| 21.203 | 0.05848 | | | 0.748 [4] | |
| 21.195 | 0.05850 | | | | 0.200 [4] |
| 20.949 | 0.05919 | | | | 0.215 |
| 20.824 | 0.05954 | | | 0.764 | |
| 20.652 | 0.06004 | | | | 0.216 |
| 20.411 | 0.06074 | | | | 0.216 |
| 20.400 | 0.06078 | | | 0.759 | |
| 20.204 | 0.06137 | | | | 0.217 |
| 20.021 | 0.06193 | | | 0.771 | |
| 19.979 | 0.06206 | 0.725 [2] | | | |
| 19.979 | 0.06206 | | 0.312 [2] | | |
| 19.869 | 0.06240 | | | | 0.217 |
| 19.645 | 0.06311 | | | 0.781 | |
| 19.561 | 0.06339 | | | | 0.218 |
| 19.537 | 0.06347 | 0.730 | | | |
| 19.393 | 0.06394 | | 0.342 | | |
| 19.354 | 0.06406 | | | 0.768 | |
| 19.261 | 0.06437 | | | | 0.219 |
| 19.035 | 0.06514 | | | 0.747 | |
| 19.033 | 0.06515 | 0.750 | | | |
| 18.961 | 0.06540 | | 0.357 | | |
| 18.948 | 0.06544 | | | | 0.246 |
| 18.710 | 0.06627 | | | | 0.235 |
| 18.644 | 0.06650 | | | 0.771 | |
| 18.478 | 0.06711 | 0.735 | | | |
| 18.394 | 0.06741 | | | | 0.236 |
| 18.306 | 0.06773 | | | 0.729 | |
| 18.252 | 0.06794 | | 0.393 | | |
| 18.101 | 0.06850 | | | | 0.278 |
| 17.902 | 0.06926 | | | 0.749 | |
| 17.860 | 0.06942 | | | | 0.252 |
| 17.707 | 0.07003 | 0.735 | | | |
| 17.596 | 0.07046 | | | 0.734 | |
| 17.512 | 0.07081 | | 0.383 | | |
| 17.485 | 0.07091 | | | | 0.269 |
| 17.215 | 0.07202 | | | 0.729 | |
| 17.119 | 0.07243 | | | | 0.308 |
| 17.008 | 0.07291 | 0.740 | | | |
| 16.925 | 0.07326 | | 0.448 | | |
| 16.803 | 0.07379 | | | 0.705 | |
| 16.702 | 0.07424 | | | | 0.309 |
| 16.504 | 0.07513 | 0.745 | | | |
| 16.476 | 0.07526 | | | 0.686 | |
| 16.391 | 0.07565 | | 0.443 | | |
| 16.375 | 0.07572 | | | | 0.324 |

**TABLE I (*Continued*)**

**Tin Telluride**

| eV | μm | n | k | n | k |
|---|---|---|---|---|---|
| 16.033 | 0.07733 | | | | 0.342 |
| 16.002 | 0.07748 | | | 0.671 | |
| 15.907 | 0.07795 | 0.750 | | | |
| 15.695 | 0.07900 | | | | 0.345 |
| 15.650 | 0.07923 | | 0.488 | | |
| 15.537 | 0.07980 | | | 0.665 | |
| 15.352 | 0.08077 | 0.730 | | | |
| 15.306 | 0.08101 | | | | 0.370 |
| 15.189 | 0.08163 | | | 0.650 | |
| 15.054 | 0.08236 | | | | 0.370 |
| 14.951 | 0.08294 | | 0.498 | | |
| 14.883 | 0.08331 | | | 0.657 | |
| 14.789 | 0.08384 | | | | 0.429 |
| 14.694 | 0.08439 | 0.745 | | | |
| 14.537 | 0.08529 | | | 0.610 | |
| 14.498 | 0.08552 | | | | 0.430 |
| 14.293 | 0.08676 | | 0.539 | | |
| 14.254 | 0.08699 | | | 0.614 | |
| 14.190 | 0.08738 | | | | 0.431 |
| 13.902 | 0.08919 | 0.740 | | | |
| 13.815 | 0.08975 | | | | 0.512 |
| 13.808 | 0.08979 | | | 0.596 | |
| 13.635 | 0.09094 | | 0.569 | | |
| 13.474 | 0.09202 | | | | 0.556 |
| 13.382 | 0.09265 | | | 0.590 | |
| 13.382 | 0.09265 | | | 0.590 | |
| 13.213 | 0.09384 | 0.745 | | | |
| 13.189 | 0.09401 | | | | 0.574 |
| 13.112 | 0.09456 | | | 0.606 | |
| 13.028 | 0.09518 | | 0.634 | | |
| 12.920 | 0.09596 | | | | 0.584 |
| 12.680 | 0.09778 | | | 0.619 | |
| 12.655 | 0.09798 | | | | 0.612 |
| 12.627 | 0.09820 | 0.735 | | | |
| 12.411 | 0.0999 | | 0.700 | | |
| 12.397 | 0.1000 | | | 0.610 | |
| 12.392 | 0.1001 | | | | 0.662 |
| 12.087 | 0.1026 | | | | 0.683 |
| 12.043 | 0.1030 | | | 0.623 | |
| 11.959 | 0.1037 | 0.745 | | | |
| 11.754 | 0.1055 | | | | 0.718 |
| 11.743 | 0.1056 | | 0.775 | | |
| 11.721 | 0.1058 | | | 0.619 | |
| 11.420 | 0.1086 | | | 0.630 | |
| 11.343 | 0.1093 | | | | 0.775 |
| 11.177 | 0.1109 | 0.745 | | | |

**TABLE I (*Continued*)**

**Tin Telluride**

| eV | μm | n | k | n | k |
|---|---|---|---|---|---|
| 11.097 | 0.1117 | | | 0.645 | |
| 11.092 | 0.1118 | | | | 0.819 |
| 11.064 | 0.1121 | | 0.841 | | |
| 10.842 | 0.1144 | | | 0.662 | |
| 10.770 | 0.1151 | | | | 0.838 |
| 10.684 | 0.1161 | 0.740 | | | |
| 10.560 | 0.1174 | | 0.901 | | |
| 10.488 | 0.1182 | | | 0.680 | |
| 10.474 | 0.1184 | | | | 0.869 |
| 10.247 | 0.1210 | | | 0.681 | |
| 10.174 | 0.1219 | | | | 0.907 |
| 10.170 | 0.1219 | 0.780 | | | |
| 9.995 | 0.1241 | | 0.941 | | |
| 9.898 | 0.1253 | | | 0.709 | |
| 9.842 | 0.1260 | | | | 0.942 |
| 9.589 | 0.1293 | | | 0.712 | |
| 9.542 | 0.1299 | 0.740 | | | |
| 9.514 | 0.1303 | | | | 0.974 |
| 9.481 | 0.1308 | | 1.002 | | |
| 9.176 | 0.1351 | | | 0.747 | |
| 9.137 | 0.1357 | | | | 1.024 |
| 9.039 | 0.1372 | 0.816 | | | |
| 8.936 | 0.1388 | | 1.047 | | |
| 8.876 | 0.1397 | | | 0.743 | |
| 8.813 | 0.1407 | | | | 1.077 |
| 8.603 | 0.1441 | | | 0.783 | |
| 8.474 | 0.1463 | | | | 1.144 |
| 8.452 | 0.1467 | 0.866 | | | |
| 8.452 | 0.1467 | | 1.108 | | |
| 8.286 | 0.1496 | | | 0.788 | |
| 8.133 | 0.1524 | | | | 1.205 |
| 8.051 | 0.1540 | | 1.223 | | |
| 7.979 | 0.1554 | 0.916 | | | |
| 7.924 | 0.1565 | | | 0.810 | |
| 7.840 | 0.1582 | | | | 1.243 |
| 7.733 | 0.1604 | | 1.299 | | |
| 7.642 | 0.1623 | | | 0.857 | |
| 7.572 | 0.1638 | | | | 1.313 |
| 7.506 | 0.1652 | 1.012 | | | |
| 7.445 | 0.1666 | | 1.354 | | |
| 7.348 | 0.1687 | | | 0.913 | |
| 7.290 | 0.1701 | | 1.354 | | |
| 7.272 | 0.1705 | | | | 1.377 |
| 7.208 | 0.1720 | 1.108 | | | |
| 7.105 | 0.1745 | | | 0.991 | |
| 7.054 | 0.1758 | | 1.269 | | |

**TABLE I (*Continued*)**

**Tin Telluride**

| eV | $cm^{-1}$ | μm | n | k | n | k |
|---|---|---|---|---|---|---|
| 6.993 | | 0.1773 | | | | 1.369 |
| 6.941 | | 0.1787 | 1.153 | | | |
| 6.810 | | 0.1821 | | | 1.026 | |
| 6.787 | | 0.1827 | | 1.239 | | |
| 6.663 | | 0.1861 | 1.168 | | | |
| 6.618 | | 0.1874 | | | | 1.385 |
| 6.591 | | 0.1881 | | 1.254 | | |
| 6.537 | | 0.1897 | | | 1.049 | |
| 6.406 | | 0.1936 | 1.163 | | | |
| 6.324 | | 0.1961 | | 1.299 | | |
| 6.271 | | 0.1977 | | | | 1.432 |
| 6.239 | | 0.1987 | | | 1.074 | |
| 6.057 | 48846 | 0.2047 | 1.188 | | | |
| 5.995 | 48349 | 0.2068 | | 1.304 | | |
| 5.909 | 47661 | 0.2098 | | | 1.128 | |
| 5.793 | 46720 | 0.2140 | | | | 1.433 |
| 5.707 | 46026 | 0.2173 | | 1.259 | | |
| 5.676 | 45777 | 0.2184 | | | 1.155 | |
| 5.645 | 45529 | 0.2197 | 1.228 | | | |
| 5.450 | 43953 | 0.2275 | | 1.223 | | |
| 5.443 | 43899 | 0.2278 | | | | 1.434 |
| 5.419 | 43704 | 0.2288 | 1.153 | | | |
| 5.319 | 42898 | 0.2331 | | | 1.081 | |
| 5.213 | 42046 | 0.2379 | 1.052 | | | |
| 5.183 | 41797 | 0.2393 | | 1.284 | | |
| 5.060 | 40811 | 0.2450 | | | | 1.519 |
| 4.987 | 40223 | 0.2486 | | | 1.008 | |
| 4.925 | 39724 | 0.2518 | 0.977 | | | |
| 4.905 | 39558 | 0.2528 | | 1.369 | | |
| 4.791 | 38643 | 0.2588 | | | 0.990 | |
| 4.786 | 38603 | 0.2590 | | | | 1.618 |
| 4.617 | 37236 | 0.2686 | | 1.556 | | |
| 4.599 | 37095 | 0.2696 | | | | 1.721 |
| 4.555 | 36738 | 0.2722 | 0.881 | | | |
| 4.469 | 36042 | 0.2775 | | | 0.986 | |
| 4.350 | 35080 | 0.2851 | | 1.752 | | |
| 4.281 | 34529 | 0.2896 | | | | 1.895 |
| 4.211 | 33960 | 0.2945 | | | 0.993 | |
| 4.144 | 33421 | 0.2992 | 0.876 | | | |
| 4.061 | 32752 | 0.3053 | | | | 2.046 |
| 4.031 | 32509 | 0.3076 | | 2.019 | | |
| 3.979 | 32094 | 0.3116 | 0.967 | | | |
| 3.916 | 31580 | 0.3167 | | | 1.013 | |
| 3.888 | 31359 | 0.3189 | | | | 2.195 |
| 3.763 | 30353 | 0.3295 | | 2.261 | | |
| 3.733 | 30104 | 0.3322 | 1.007 | | | |

**TABLE I (*Continued*)**

**Tin Telluride**

| eV | $cm^{-1}$ | μm | n | k | n | k |
|---|---|---|---|---|---|---|
| 3.640 | 29357 | 0.3406 | | | | 2.361 |
| 3.496 | 28194 | 0.3547 | | | 1.085 | |
| 3.486 | 28113 | 0.3557 | | 2.502 | | |
| 3.439 | 27739 | 0.3605 | | | | 2.553 |
| 3.434 | 27699 | 0.3610 | 1.103 | | | |
| 3.275 | 26415 | 0.3786 | | | | 2.756 |
| 3.229 | 26040 | 0.3840 | | 2.749 | | |
| 3.209 | 25884 | 0.3863 | | | 1.199 | |
| 3.177 | 25626 | 0.3903 | 1.228 | | | |
| 3.069 | 24753 | 0.4040 | | | | 2.962 |
| 2.992 | 24133 | 0.4144 | 1.364 | | | |
| 2.958 | 23857 | 0.4192 | | | | 3.127 |
| 2.935 | 23673 | 0.4224 | | | 1.375 | |
| 2.879 | 23221 | 0.4307 | | 3.086 | | |
| 2.800 | 22579 | 0.4429 | | | | 3.349 |
| 2.771 | 22347 | 0.4475 | | | 1.542 | |
| 2.735 | 22060 | 0.4533 | 1.551 | | | |
| 2.666 | 21504 | 0.4650 | | | | 3.555 |
| 2.577 | 20786 | 0.4811 | | | 1.745 | |
| 2.571 | 20733 | 0.4824 | | 3.378 | | |
| 2.488 | 20069 | 0.4983 | 1.702 | | | |
| 2.488 | 20069 | 0.4983 | | | | 3.805 |
| 2.401 | 19362 | 0.5165 | | | 1.943 | |
| 2.386 | 19241 | 0.5197 | | | | 3.980 |
| 2.375 | 19157 | 0.5220 | | 3.685 | | |
| 2.324 | 18742 | 0.5336 | 1.813 | | | |
| 2.317 | 18684 | 0.5352 | | | | 4.177 |
| 2.265 | 18265 | 0.5475 | | | | 4.420 |
| 2.262 | 18245 | 0.5481 | 1.878 | | | |
| 2.252 | 18162 | 0.5506 | 1.989 | | | |
| 2.242 | 18079 | 0.5532 | 2.135 | | | |
| 2.231 | 17997 | 0.5556 | | | 2.183 | |
| 2.221 | 17913 | 0.5583 | 2.442 | | | |
| 2.221 | 17913 | 0.5583 | | 4.043 | | |
| 2.190 | 17664 | 0.5662 | 2.719 | | | |
| 2.185 | 17620 | 0.5675 | | | | 4.678 |
| 2.160 | 17423 | 0.5740 | | | 2.427 | |
| 2.129 | 17167 | 0.5826 | 2.991 | | | |
| 2.087 | 16835 | 0.5940 | | 4.375 | | |
| 2.086 | 16825 | 0.5943 | | | 2.673 | |
| 2.080 | 16774 | 0.5962 | | | | 4.977 |
| 2.070 | 16692 | 0.5991 | | | 2.863 | |
| 2.056 | 16580 | 0.6031 | | 4.496 | | |
| 2.046 | 16503 | 0.6060 | 3.273 | | | |
| 2.019 | 16287 | 0.6140 | | | 3.059 | |
| 2.011 | 16216 | 0.6167 | | | | 5.144 |

**TABLE I (*Continued*)**

**Tin Telluride**

| eV | $cm^{-1}$ | μm | n | k | n | k |
|---|---|---|---|---|---|---|
| 2.003 | 16153 | 0.6191 | | | | 5.266 |
| 1.995 | 16089 | 0.6216 | 3.479 | | | |
| 1.970 | 15885 | 0.6295 | | 4.677 | | |
| 1.961 | 15813 | 0.6324 | | | 3.257 | |
| 1.932 | 15585 | 0.6417 | | | 3.472 | |
| 1.928 | 15547 | 0.6432 | | | | 5.372 |
| 1.921 | 15497 | 0.6453 | | | 3.664 | |
| 1.919 | 15474 | 0.6462 | | 4.741 | | |
| 1.913 | 15425 | 0.6483 | 3.701 | | | |
| 1.877 | 15135 | 0.6607 | | | 3.868 | |
| 1.874 | 15116 | 0.6615 | | 4.749 | | |
| 1.863 | 15025 | 0.6655 | | | 4.056 | |
| 1.834 | 14790 | 0.6761 | | 4.754 | | |
| 1.829 | 14748 | 0.6781 | | | 4.286 | |
| 1.824 | 14710 | 0.6798 | | | | 5.295 |
| 1.822 | 14697 | 0.6804 | | | 4.516 | |
| 1.820 | 14679 | 0.6813 | 3.912 | | | |
| 1.795 | 14474 | 0.6909 | | 4.687 | | |
| 1.790 | 14439 | 0.6926 | | | 4.660 | |
| 1.785 | 14399 | 0.6945 | | | 4.839 | |
| 1.767 | 14254 | 0.7016 | | | | 5.175 |
| 1.766 | 14243 | 0.7021 | | 4.621 | | |
| 1.739 | 14022 | 0.7132 | | 4.560 | | |
| 1.722 | 13887 | 0.7201 | | | | 5.032 |
| 1.719 | 13865 | 0.7212 | | | 5.001 | |
| 1.714 | 13824 | 0.7234 | | | 5.190 | |
| 1.705 | 13748 | 0.7274 | | 4.492 | | |
| 1.688 | 13612 | 0.7346 | | | | 4.912 |
| 1.684 | 13579 | 0.7364 | | 4.402 | | |
| 1.682 | 13562 | 0.7373 | | | 5.450 | |
| 1.667 | 13442 | 0.7440 | | | 5.586 | |
| 1.656 | 13352 | 0.7490 | 4.285 | | | |
| 1.651 | 13316 | 0.7510 | | 4.334 | | |
| 1.636 | 13194 | 0.7579 | | | 5.784 | |
| 1.622 | 13085 | 0.7643 | | | | 4.690 |
| 1.620 | 13064 | 0.7655 | | 4.251 | | |
| 1.610 | 12987 | 0.7700 | | | | 4.493 |
| 1.597 | 12880 | 0.7764 | | | 5.977 | |
| 1.587 | 12801 | 0.7812 | | 4.156 | | |
| 1.564 | 12617 | 0.7926 | | | | 4.256 |
| 1.556 | 12548 | 0.7969 | | 4.078 | | |
| 1.552 | 12519 | 0.7988 | | | | 4.049 |
| 1.542 | 12440 | 0.8039 | 4.541 | | | |
| 1.526 | 12306 | 0.8126 | | 4.006 | | |
| 1.520 | 12260 | 0.8156 | | | 6.221 | |
| 1.512 | 12192 | 0.8202 | | | 6.327 | |

**TABLE I (*Continued*)**

**Tin Telluride**

| eV | $cm^{-1}$ | μm | n | k | n | k |
|---|---|---|---|---|---|---|
| 1.495 | 12058 | 0.8293 | | | | 3.790 |
| 1.494 | 12053 | 0.8297 | | 3.945 | | |
| 1.480 | 11937 | 0.8377 | | | | 3.574 |
| 1.462 | 11790 | 0.8482 | | 3.898 | | |
| 1.430 | 11531 | 0.8672 | | | 6.450 | |
| 1.429 | 11527 | 0.8676 | 4.803 | | | |
| 1.429 | 11522 | 0.8679 | | | | 3.343 |
| 1.428 | 11516 | 0.8683 | | 3.861 | | |
| 1.407 | 11347 | 0.8813 | | 3.724 [7] | | |
| 1.390 | 11214 | 0.8917 | | | 6.449 | |
| 1.373 | 11070 | 0.9033 | | 3.566 | | |
| 1.368 | 11033 | 0.9064 | | | | 2.948 |
| 1.333 | 10751 | 0.9301 | | | 6.396 | |
| 1.320 | 10643 | 0.9396 | | 3.322 | | |
| 1.306 | 10532 | 0.9495 | 5.070 | | | |
| 1.277 | 10302 | 0.9706 | | | | 2.721 |
| 1.271 | 10251 | 0.9756 | | | | 2.542 |
| 1.269 | 10238 | 0.9768 | | 3.126 | | |
| 1.203 | 9706 | 1.030 | | 2.886 | | |
| 1.203 | 9703 | 1.031 | 5.312 | | | |
| 1.194 | 9634 | 1.038 | | | | 2.341 |
| 1.174 | 9467 | 1.056 | | | 6.372 | |
| 1.150 | 9279 | 1.078 | | 2.677 | | |
| 1.126 | 9085 | 1.101 | | | | 2.167 |
| 1.091 | 8801 | 1.136 | | 2.446 | | |
| 1.069 | 8625 | 1.160 | 5.573 | | | |
| 1.044 | 8424 | 1.187 | | | | 1.971 |
| 1.028 | 8291 | 1.206 | | | 6.370 | |
| 1.026 | 8273 | 1.209 | | 2.199 | | |
| 0.980 | 7907 | 1.265 | | 2.018 | | |
| 0.946 | 7630 | 1.311 | 5.865 | | | |
| 0.937 | 7556 | 1.323 | | | | 1.694 |
| 0.935 | 7541 | 1.326 | | 1.815 | | |
| 0.888 | 7165 | 1.396 | | | | 1.509 |
| 0.887 | 7152 | 1.398 | | 1.617 | | |
| 0.864 | 6966 | 1.436 | 6.102 | | | |
| 0.837 | 6753 | 1.481 | | 1.409 | | |
| 0.822 | 6632 | 1.508 | | | 6.302 | |
| 0.798 | 6432 | 1.555 | | 1.257 | | |
| 0.784 | 6322 | 1.582 | | | | 1.295 |
| 0.781 | 6303 | 1.587 | 6.314 | | | |
| 0.754 | 6085 | 1.644 | | 1.097 | | |
| 0.718 | 5794 | 1.726 | | 0.984 | | |
| 0.710 | 5722 | 1.748 | 6.545 | | | |
| 0.692 | 5583 | 1.791 | 7.681 [6] | | | |
| 0.678 | 5468 | 1.829 | | 0.864 | | |

**TABLE I (*Continued*)**

**Tin Telluride**

| eV | $cm^{-1}$ | μm | n | k | n | k |
|---|---|---|---|---|---|---|
| 0.674 | 5438 | 1.839 | | | 6.280 | |
| 0.650 | 5242 | 1.908 | | 0.731 [6] | | |
| 0.646 | 5209 | 1.920 | | | | 1.100 |
| 0.612 | 4938 | 2.025 | 7.550 | | | |
| 0.606 | 4891 | 2.045 | | 0.669 | | |
| 0.569 | 4588 | 2.180 | | 0.572 | | |
| 0.555 | 4477 | 2.234 | | | | 0.843 |
| 0.548 | 4422 | 2.262 | 7.442 | | | |
| 0.528 | 4256 | 2.350 | | 0.505 | | |
| 0.493 | 3979 | 2.513 | 7.304 | | | |
| 0.487 | 3926 | 2.547 | | 0.415 | | |
| 0.447 | 3606 | 2.773 | | 0.316 | | |
| 0.427 | 3444 | 2.904 | | 0.272 | | |
| 0.425 | 3426 | 2.919 | 7.106 | | | |
| 0.406 | 3272 | 3.057 | | 0.230 | | |
| 0.400 | 3226 | 3.100 | | 0.216 | | |
| 0.396 | 3192 | 3.133 | 6.873 | | | |
| 0.382 | 3082 | 3.245 | | 0.182 | | |
| 0.366 | 2955 | 3.384 | | 0.150 | | |
| 0.366 | 2954 | 3.385 | 6.824 | | | |
| 0.363 | 2926 | 3.418 | | 0.141 | | |
| 0.346 | 2791 | 3.583 | | 0.113 | | |
| 0.342 | 2759 | 3.625 | | | 6.225 | |
| 0.341 | 2750 | 3.636 | | | | 0.529 |
| 0.337 | 2719 | 3.678 | 6.628 | | | |
| 0.329 | 2657 | 3.764 | | 0.109 | | |
| 0.318 | 2562 | 3.903 | | 0.109 | | |
| 0.308 | 2481 | 4.031 | 6.447 | | | |
| 0.296 | 2388 | 4.188 | | 0.116 | | |
| 0.278 | 2240 | 4.465 | 6.255 | | | |
| 0.270 | 2176 | 4.595 | | 0.131 | | |
| 0.253 | 2044 | 4.892 | | | | 0.351 |
| 0.250 | 2016 | 4.960 | | 0.149 | | |
| 0.249 | 2007 | 4.982 | 6.007 | | | |
| 0.226 | 1825 | 5.481 | | 0.182 | | |
| 0.214 | 1728 | 5.786 | 5.759 | | | |
| 0.206 | 1660 | 6.022 | | 0.224 | | |
| 0.187 | 1508 | 6.632 | 5.301 | | | |
| 0.182 | 1471 | 6.799 | | 0.305 | | |
| 0.164 | 1324 | 7.550 | | 0.436 | | |
| 0.163 | 1314 | 7.608 | 4.575 | | | |
| 0.157 | 1265 | 7.904 | | 0.537 | | |
| 0.143 | 1152 | 8.680 | 3.483 | | | |
| 0.142 | 1147 | 8.722 | | 0.740 | | |

**TABLE I** (*Continued*)

**Tin Telluride**

| eV | $cm^{-1}$ | μm | n | k | n | k |
|---|---|---|---|---|---|---|
| 0.135 | 1088 | 9.187 | 2.863 | | | |
| 0.105 | 847 | 11.80 | | | 6.173 | |
| 0.104 | 841 | 11.89 | | | | 0.15 |

[a] References are indicated in brackets.

# Zinc Selenide (ZnSe)
# Zinc Telluride (ZnTe)

L. WARD
Coventry Polytechnic
Coventry, England

In optical terms these two materials have many points in common, and it is therefore proposed to deal with both in the same critique. They are both semiconductors and are members of the II-VI group formed by alloying one element from group II of the periodic table with another from group VI. Their normal crystal structure is face-centered cubic, the zinc-blende or sphalerite type ($F\bar{4}3m$), although it is also possible to grow hexagonal forms of each material (wurtzite structure, C6mc). These materials may be produced synthetically by alloying the two elements in the correct proportions; by chemical vapor deposition (CVP); or by evaporation in vacuum. In making these materials from the basic elements, there is often a tendency for the resulting compound to be zinc-ion deficient and several investigators (for example, Horikoshi *et al.* [1]) have found that this situation may be partially remedied by soaking the boule for several hours in a bath of molten zinc.

In broad terms these two materials each exhibit two main absorption bands. The first of these is in the near-ultraviolet region and arises as a result of electron excitations across the energy gap (about 2 eV) between the broad valence band and the conduction band; the second occurs in the infrared at a wavelength between 40 and 50 μm and is caused by photon resonance with lattice vibrations (transverse phonons). Through the visible spectrum and into the near-infrared region, both ZnSe and ZnTe behave as normally dispersive materials, the refractive indices decreasing monotonically with wavelength; the mean value of $n$ in this region for ZnSe is 2.5, and, that for ZnTe is 2.8. Over the same region, the extinction coefficient, $k$, is very small for each of the compounds. Consequently, both materials have been used extensively for high-refractive-index optical components and windows. In addition, many of the sets of values of the optical constants that have been published for the visible and near-infrared regions


Copyright © 1991 by Academic Press.
All rights of reproduction in any form reserved.
ISBN 0-12-544422-2

can be fitted into dispersion equations of the Sellmeier type; over the infrared absorption band, Lorentz equations for $\varepsilon_1 = (n^2 - k^2)$ and $\varepsilon_2 = 2nk$ have also been used successfully. At very short wavelengths there are further absorption bands due to the $L$ and $M$ transitions of electrons in both the elements within each of the compounds. In the X-ray region, the refractive indices approach a value of unity, whereas at very long wavelengths, $n$ is asymptotic to about 3.0 for ZnSe and to 2.9 for ZnTe.

A comprehensive review (up until 1984) of the optical properties of both these materials as well as of zinc sulphide has been given by Li [2], who also presents the results in a variety of graphical forms. In addition, Li lists some of the Sellmeier and Lorentz equations derived by different authors. Tauc [3] has also reviewed the optical properties of semiconductors in the visible and ultraviolet regions and presents tables of the main absorption peaks and their identification with various electron transitions within the Brillouin zone.

*Optical Properties of Zinc Selenide*

The $n$ and $k$ data selected in this critique are listed in Table I and graphed in Fig. 1. At wavelengths in the X-ray region, 0.0006–0.012 μm, values of $n$ and $k$ may be calculated by the method described by Henke [4] based on the X-ray scattering coefficients, $f_1$ and $f_2$, for each element; values of these coefficients are presented in another paper by Henke *et al.* [5]. For ZnSe, $n = 1 - 9.90\lambda^2 (f_{1zn} + f_{1se})$ and $k = 9.90\lambda^2 (f_{2zn} + f_{2se})$, where $\lambda$ is the wavelength in μm. Over this region, the calculated value of $n$ is close to unity, whereas $k$ shows maxima due to the $L_{II,III}$ transition in Zn (0.0012 μm) and the $L_{II,III}$ transition in Se (0.00085 μm). Values of $n$ and $k$ calculated by Henke's method are listed in Table I.

At short wavelengths (0.01–0.1 μm) the work of Freeout [6], Gautron *et al.* [7] and Cardona and Haensel [8] may be quoted. Cardona and Haensel used evaporated films and made a direct measurement of the absorption coefficient $\alpha$ using radiation from an electron synchrotron, which was dispersed by a Rowland grazing-incidence monochromator and detected by a photomultiplier. $k$ may then be found from the relationship $\alpha = 4\pi k/\lambda$, and $n$ is assumed to be equal to unity; their values of $n$ and $k$ between 0.008 and 0.033 μm are presented in Table I. They found a sharp absorption doublet at 90.6 and 93.35 eV (0.0133 and 0.0137 μm) corresponding to electron transits from the $3p$ level to the conduction band ($L$) in zinc. A less pronounced peak was caused by the $3d$ to conduction band transition ($M$) in selenium at 59 eV (0.021 μm). Where there is an overlap in wavelengths, their results are in reasonably good agreement with those calculated by the Henke method. Freeout used synchrotron radiation and a rotary light-pipe scanning reflectometer due to Gerhardt and Rubloff [9] to measure the polarization-dependent reflectance of cleaved single crystals of ZnSe. Analysis by the Kramers–Kronig (K–K) technique enabled him to

produce a graph of $\varepsilon_2$ versus energy, which showed strong structures in the valence-to-conduction-band transition region. Gautron *et al.*, using polished and etched single crystals of ZnSe, measured both the reflectance and the electrolyte electroreflectance; they also employed K–K analysis to extract $\varepsilon_1$ and $\varepsilon_2$, from which $n$ and $k$ may then be calculated over the wavelength range 0.04–1.24 μm. In their experimental technique (see Cardona *et al.* [10]), the specimen is immersed in an electrolyte and dc biased in the blocking direction; a modulating ac voltage is also applied. Monochromatic radiation is then reflected by the specimen to a photomultiplier and both the dc and ac components of the output are recorded. The dc output is proportional to the reflectance; the ratio of ac to dc outputs gives the quantity $dR/R$, which can be related to $\varepsilon_1$ and $\varepsilon_2$. Their results for $n$ and $k$, which are also quoted in Table I, match well at the shortest wavelengths with those of Cardona and Haensel, but thereafter and up to 0.02 μm, $n$ remains below 1.0, which behavior differs from that observed by other investigators, for example, Balkanski and Petroff [11]. They were also able to confirm the existence of excitons at room temperature and to correlate features in the reflectance spectrum with different band-to-band transitions within the Brillouin zone. Cardona [12] reported a series of eight peaks in the reflectance spectrum of ZnSe at room temperature between 2.0 and 14.0 eV (0.09–0.62 μm); he was able to correlate all of them with various electron transitions within the Brillouin zone.

Published results over the region of the main energy gap (0.1–0.5 μm) differ among themselves more than those for other wavelength regions; in particular, it is experimentally difficult to make accurate measurements of $n$ and $k$ at the actual absorption edge. Measuring reflectances, Balkanski and Petroff [11] obtained a peak in $n$ of 3.61 at 0.28 μm followed by a minimum of 0.80 at 0.124 μm and then a second maximum of 1.42 at 0.095 μm; $k$ showed peaks at 0.25, 0.18, and 0.13 μm. Aven *et al.* [13] made measurements of the reflectance of single-crystal zinc selenide from 0.1–0.5 μm and used K–K analysis to extract $n$ and $k$. They found a maximum in $n$ (3.24) also at 0.28 μm with peaks in $k$ at 2.7, 3.15, 4.75, and 5.1 eV (0.459, 0.394, 0.261, and 0.243 μm). The work of Gautron *et al.* [7], which has already been discussed, also extended over the energy gap and up to 1.24 μm. Their peak value for $n$ (2.68) was much smaller than that obtained by other investigators and was found at 0.41 μm, followed by a second maximum (2.57) at 0.31 μm, together with minima at 0.177 and 0.124 μm; $k$ showed maxima at 0.25 and 0.19 μm. The results of Balkanski and Petroff [11] measured between 0.06 and 1.24 μm are considered to be the most reliable of this group and have been chosen to represent this spectral region in Table I.

Over the visible and near-infrared region (0.5–10.0 μm), there have been a large number of measurements of the refractive index, and there is very

good agreement among the various results. The work of Aven *et al.* [13] with single-crystal zinc selenide was extended up to 2.5 μm, and they presented values of $\varepsilon_1$ and $\varepsilon_2$, these being determined from a K–K analysis of the reflectance taken at a temperature of 296 K. From their results, they were able to determine $\nu_t$, the transverse-optical-phonon energy, as 0.026 eV (48.5 μm) and $\nu_l$, the longitudinal-optical-phonon energy as 0.031 eV (40.0 μm); the very-long-wavelength limit of $n$ was calculated to be 2.85.

Thutupalli and Tomlin [14] have also published work in this region (0.3–2.0 μm), where they determined $n$ for films of ZnSe from measurements of reflectance and transmittance at room temperature and also at 400 °C. At room temperature, only cubic crystals were observed in the films; the hexagonal form began to appear at 100 °C becoming more prominent as the temperature increased. Both $n$ and $k$ increased with temperature, and the values of $n$ at 400 °C were in good agreement with those of Marple [15]. Ahmed and Khawaja [16] determined $n$ between 2.5 and 14 μm using a technique due to Khawaja [17], in which the transmittance at normal incidence was measured; an iteration process was then used to produce a dispersion curve and when an acceptable version of this was obtained, it yielded both $n$ and the specimen thickness. Over this region $n$ fell monotonically from 2.42 to 2.40, in good agreement with Thutupalli and Tomlin's results. Marple [15] measured the refractive index of a prism by the minimum-deviation method between 0.5 and 2.5 μm for material containing less than 30 ppm of impurities, the chief ones being phosphorus, arsenic, and cadmium. The optical material was grown as single-crystal boules by sublimation in an argon-filled quartz tube. Marple claimed an experimental error of ±0.002 and was able to fit his experimental data over this wavelength region with a Sellmeier-type dispersion equation:

$$n^2 = 4.0 + 1.90\lambda^2/(\lambda^2 - 0.113),$$

where $\lambda$ is the wavelength in μm.

An investigation covering the visible spectrum was made by Rambauske [18] using the minimum-deviation technique and Avery's method [19], in which the reflectance ratio ($R_p/R_s$) is measured. Two quite different dispersion curves were produced from two specimens of ZnSe, which had been obtained from different sources. For one specimen, the dispersion curve peaked at 0.50 μm ($n = 2.72$) and then fell rapidly as the wavelength decreased. The curve due to the second specimen closely followed those by Aven *et al.* and Thutupalli and Tomlin between 0.65 and 0.45 μm, where it peaked at $n = 2.82$. At shorter wavelengths, this curve was very different from theirs in that it fell to a value of $n$ of 2.25 at 0.40 μm, whereas theirs, after a shoulder at 0.45 μm, went on to peak at 0.30 μm. There is some

evidence that the specimens used by Rambauske were not of high purity, and the displacement of the maximum may have been caused by the presence of impurity energy levels in the energy gap. Zholkevich [20] has determined directly the absorption coefficient of ZnSe between 0.45 and 0.65 μm; the derived values of $k$ were very small, and they have been included in Table I with the values for $n$ due to Balkanski and Petroff [11]. Another set of results covering a narrow range (0.476–0.633 μm) in the visible spectrum, which did not include the absorption edge, was produced by Wunderlich and De Shazer [21] also using the minimum-deviation prism technique. Their values of $n$, which had errors of ±0.002, were very similar to those of Rambauske over the same wavelength range.

Feldman *et al.* [22] also used the minimum-deviation method to measure $n$ at room temperature for two specimens between 0.5 and 18.0 μm. Their values of $n$ were quoted to five decimal places, but the results for the two specimens were not identical, and it is considered by Li that ±0.0004 is a more realistic error. A set of mean values for $n$ calculated from the three-term dispersion formulas given by Feldman *et al.* is included in Table I, the fifth figure being given in brackets.

Measurements of $n$ and $k$ at wavelengths in the range 20–1000 μm have been performed by Manabe *et al.* [23] and by Hattori *et al.* [24]. Manabe *et al.* measured the reflectance of polished specimens between 20 and 85 μm at an angle of incidence of 12 degrees and determined $n$ and $k$ by the use of the following Lorentz-oscillator equations;

$$n^2 - k^2 = \varepsilon_\infty + N(\nu_t^2 - \nu^2)/((\nu_t^2 - \nu^2)^2 + \gamma^2\nu^2)$$

$$2nk = N\gamma\nu/((\nu_t^2 - \nu^2)^2 + \gamma^2\nu^2).$$

At 300 K, the transverse-optical-phonon frequency, $\nu_t = 207\ \text{cm}^{-1}$ (48.3 μm), the longitudinal-optical-phonon frequency, $\nu_l = 246\ \text{cm}^{-1}$ (40.7 μm), $\varepsilon_\infty = 5.4$, $N = 8.94 \times 10^5\ \text{cm}^{-2}$, and $\gamma = 3.73\ \text{cm}^{-1}$. They also produced another set of results at 100 K, where the corresponding values were $211\ \text{cm}^{-1}$, $250\ \text{cm}^{-1}$, 5.4, $9.25 \times 10^4\ \text{cm}^{-2}$, and $2.11\ \text{cm}^{-1}$. Their value of $n$ at 20 μm and at 300 K compares well with that of Feldman *et al.* [22] at 18 μm. Hattori *et al.* [24] used transmission interferometry for their measurements taken between 100 and 1000 μm and at temperatures of 2, 80, and 300 K. Specimens were grown by Bridgman's technique and ranged in thickness between 500 and 1000 μm. Again, a simple dispersion formula was used to evaluate the optical constants. Their results agreed to within a few percent with those of Manabe *et al.* in the wavelength overlap region. They found the transverse optical phonon to be at $203\ \text{cm}^{-1}$ at 300 K, $207\ \text{cm}^{-1}$ at 80 K, and $210\ \text{cm}^{-1}$ at 2 K; the extreme long-wavelength value of $n$ was 3.00 at

300 K and 2.96 at 80 K. Sets of results read from the graphs given by both Manabe *et al.* and Hattori *et al.* are quoted in Table I.

Miles [25] has published a graph of absorption coefficient versus wave number between 300 and 900 $cm^{-1}$ (11–33 μm). This shows structure attributable to multiphonon absorption, the main peaks being at 360, 415, 430, 570, and 610 $cm^{-1}$ with a shoulder at 800 $cm^{-1}$. The derived values of $k$ are small (between 0.02 and $1 \times 10^{-7}$) and do not exhibit the structure clearly. Nevertheless, some values have been included in Table I. Aven *et al.* [13] have also reported results for the absorption coefficient in this region (0.02–0.08 eV, 15.5–62 μm); these had peaks at 0.026, 0.0375, 0.046, 0.0525, and 0.073 eV. (47.7, 33.1, 27.0, 23.6, and 17.0 μm). Over the main peak at 47.7 μm, the values for $k$ agree well with those of Manabe *et al.*; other values of $k$, covering the regions of 30–40 μm and 50–60 μm are given in Table I.

At very low frequencies (20 Hz–1 mHz) Strzalkowski *et al.* [26] have measured the dielectric constant $\varepsilon$ of ZnSe by the capacitance method. At 296 K, $\varepsilon$ was equal to 9.25; that is, $n = 3.10$; $\varepsilon$ varied linearly with temperature and, when extrapolated to 0 K, $\varepsilon_o = 8.80 \pm 0.04$; that is, $n_o = 2.97 \pm 0.02$. $\varepsilon$, and therefore $n$, were independent of wavelength out to 300 m.

Thompson *et al.* [27] measured $n$ as a function of temperature at two discrete wavelengths, 3.8 and 10.8 μm, making use of the minimum-deviation method; it is possible to read values from their graphs to three decimal places. At 300 K and 3.8 μm, $n = 2.435$, whereas at 10.8 μm $n = 2.405$, both values being in very good agreement with those of Feldman *et al.* In each case, $n$ fell by 0.010 when the temperature was reduced to 75 K, giving a temperature coefficient of $1.9 \times 10^{-5}$/°C. Another investigation of the effect of temperature was carried out by Tubota *et al.* [28], who studied the variation of the position of the absorption edge over the range 295–496 K. The energy gap was found to change from 2.59 eV (0.479 μm) at 293 K to 2.47 eV at 398 K and then to 2.38 eV at 496 K.

*Excitons in ZnSe*

At low temperatures (5 K), the presence of excitons has been detected in ZnSe crystals. These are electron-hole pairs that occupy energy levels inside the fundamental energy gap just below the conduction band; some excitons are free, and others are bound to impurity atoms. Spectroscopically, they may be represented by a simple hydrogenlike energy level series. Absorption lines are observed at energies just below the main band due to the breakup of the excitons by photons of the correct energy. This dissociation may also be brought about by thermal energy, and so it is more difficult to observe excitons at higher temperatures. An account of the properties of excitons has been given by Thomas and Timofiev [29]. Hite *et al.* [30] also found evidence for the presence of

excitons in ZnSe even though the absorption spectrum they observed was dominated by the defects in their crystals. Another group that observed the presence of excitons in ZnSe for temperatures below 60 K was Tokura *et al.* [31], who used attenuated total reflection to study the coupling of photons to excitons at the semiconductor surface. Jiang *et al.* [32] found evidence for the presence of excitons in ZnSe, bound to deep impurity levels or defects.

*Irtran 4*

Commercial synthetic zinc selenide, produced by hot sintering of the polycrystalline material and known as Irtran 4, has been investigated by McCarthy [33] between 2 and 50 μm using measurements of reflectance and transmittance. He produced curves of reflectance and transmittance versus wavelength but, unfortunately, did not evaluate $n$ and $k$. Another study of Irtran 4 was made by Hilton and Jones [34] using a prism minimum-deviation technique to measure $n$ between 3 and 13 μm and at temperatures of 198 and 295 K. Both values of $n$ were presented graphically, and those for 198 K were lower by approximately 0.005 over the whole of the wavelength range covered. The temperature coefficient of $n$ at 5 μm was found to be $2.0 \times 10^{-5}\,\mathrm{K}^{-1}$. Hadni *et al.* [35] measured the reflectance and transmittance of a thin plate of Irtran 4 and also of films of ZnSe on quartz at 290 K and at liquid-nitrogen temperature. They found that their results could be explained by postulating a single Lorentzian-type oscillator with $\nu_t$ equal to $204\,\mathrm{cm}^{-1}$ (49.0 μm) and $\nu_l$, the longitudinal-optical-phonon frequency, equal to $254\,\mathrm{cm}^{-1}$ (39.4 μm) at 300 K. Their values for $n$ and $k$ were considerably smaller than those obtained by Manabe *et al.* for bulk material possibly because of the structural properties of their films. Their value of $n$ extrapolated to very long wavelengths was 3.10 at 290 K.

There is some evidence that $n$ for Irtran 4 may be sample dependent; nevertheless, results due to Hilton and Jones and to Hadni *et al.* are included in Table I.

*Optical Properties of Zinc Telluride*

The $n$ and $k$ data selected in this critique are listed in Table II and graphed in Fig. 2. Many of the authors who investigated zinc sellenide have also extended their work to cover the closely related material zinc telluride.

At wavelengths in the X-ray region, $n$ and $k$ may again be calculated by the method of Henke [4] described earlier. For ZnTe,

$$n = 1 - 7.88\lambda^2(f_{1zn} + f_{1te}),$$

where the wavelength $\lambda$ is in μm. As with ZnSe, the values of $n$ in this

region are very close to unity, and peaks in $k$ are obtained at 0.0012 μm (the $L_{II,III}$ transition point in Zn) and 0.0021 μm (the $M_{IV,V}$ transition point in Te).

In direct measurements of the absorption coefficient, Cardona and Haensel [8] found a doublet of absorption lines for ZnTe at 89.4 and 93.0 eV (0.0133 and 0.0139 μm) corresponding to the $M$-transition in Zn. However, no peak for Te was discovered right up to a wavelength of 0.3 μm. Values of $k$ for ZnTe between 0.008 and 0.033 μm, derived from $\alpha$, are presented in Table II; $n$ is assumed to be close to unity in this spectral region.

At wavelengths between 0.05 and 1.0 μm, Cardona and Greenaway [36] measured the reflectance of cleaved single-crystal ZnTe. In the region of 0.10 μm, the reflectance spectrum exhibited a number of structures that could be assigned to various electron transitions from the $d$-band to the conduction band in zinc (0.071 and 0.153 μm). The temperature coefficient of reflectance was approximately $6 \times 10^{-4}$/°C at all the wavelengths investigated. Cardona himself [37] measured the normal-incidence reflectance up to 20 eV at 300 and 77 K. He then calculated $\varepsilon_1$, $\varepsilon_2$, $n$, and $k$ by K–K analysis and determined the dielectric constant at infinite wavelength using Penn's model [38]. His values for $n$ and $k$ are included in Table II.

Cardona [12] has also reported measurements of the reflectance of ZnTe at room temperature in the ultraviolet spectrum between 0.06 and 0.59 μm where 12 peaks were observed between 2.35 and 14.6 eV, all of which were accounted for in terms of electron transitions within the Brillouin zone. Freeout [6] used synchrotron radiation to measure the reflectance of cleaved ZnTe at wavelengths in the range 0.04–2.0 μm, analyzing the results by the K–K technique. He was able to correlate the structures in the reflectance spectrum with excitations of the core electrons.

Gauthe [39] studied the energy losses in 30 keV electrons on transmission through thin evaporated films of ZnTe. He found that the loss spectra were significantly different from a simple superposition of the loss spectra due to the component elements, the main loss peaks being at 4.6 and 16.3 eV and the plasmon energy at 14 eV. Tomoda and Mannami [40] also plotted the energy-loss spectrum of thin ZnTe films, which had been deposited on cubic rock salt, thus giving the zinc-blende lattice, and then dissolving away the substrate; using 40 keV electrons, they found a series of peaks ranging from 2.5–15.3 eV and also determined the plasmon energy as 12.3 eV. Walter *et al.* [41] measured the reflectance of ZnTe specimens cleaved in air along the (110) plane and subsequently maintained in a cryostat at low pressure. Taking into account the spin–orbit interactions, they were also able to make calculations of the reflectance from the band structure and claimed good agreement between the two sets of values.

Near the fundamental energy gap, the results from various studies are

again inconsistent. Loh and Newman [42] measured the transmittance of crystals of ZnTe near the fundamental edge and deduced the absorption coefficient, which was then plotted against wavelength. It was found that the absorption edge shifted upwards by about 0.1 eV as the temperature was reduced from 300 to 77 K. By measuring the absorption coefficient of hand-polished specimens of different thicknesses, it was possible to obtain estimates for the separate bulk and surface absorptions. Brown and Brodie [43] measured the reflectance and absorption spectra of amorphous ZnTe deposited on both glass and sapphire substratres; these showed only one broad maximum centered at 4.4 eV, which was associated with electron transitions near the center of the Brillouin zone in the [111] direction, that is, $L$ direction. Their values of $k$ between 0.35 and 0.61 μm are in reasonable agreement with those of Cardona [12] over the same spectral range.

The visible and near-infrared region has been well covered in a number of publications. Sliker and Jost [44] confirmed Cardona's results [37] and also gave tabulated values of $n$ between 0.5 and 1.5 μm at 300 K. They used a single-crystal prism of undoped ZnTe cut from a boule grown by sublimation of high-purity zinc and tellurium; one face was polished using 0.3 μm alumina but because the material was cubic in structure, no attempt was made to align it crystallographically when making minimum-deviation measurements. Shiozawa *et al.* [45], also using the method of minimum deviation, have reported results in this same region (0.57–1.5 μm) for synthetic ZnTe. Aten *et al.* [46] used this particular experimental technique to produce a smooth curve of $n$ versus photon energy at 300 K; at this temperature they measured the indirect energy gap as 2.164 eV. However, it is difficult to make accurate readings from the graphs they give, and their results have not been included. Working with thin films, Marple [15] used very pure ZnTe (containing less than 30 ppm of impurities) at wavelengths up to 2.0 μm and claimed an accuracy of ±0.003 in $n$ from his minimum-deviation technique. He fitted his results into the following Sellmeier-type formula:

$$n^2 = 4.27 + 3.61/(\lambda^2 - 0.142).$$

Jensen and Torabi [47] derived a theoretical expression for the real part of the refractive index near the fundamental band edge and claimed that it gave a good fit with Marple's results. In addition, Horikoshi *et al.* [1] have reported values of $n$ between 1.6 and 2.3 eV and at temperatures of 97 and 300 K, these being determined from their spectrophotometric measurements of transmittance. There is good agreement between this set of results and those of Marple, Shiozaka *et al.*, and Sliker and Jost. Horikoshi *et al.* also presented a graph of absorption coefficient versus energy

between 0.1 and 0.6 eV (2.0–12.0 μm) from which values of $k$ may be calculated; $k$ is very small (<0.01) over this range. In Table II, the values of $n$ from Sliker and Jost and from Jensen and Torabi are presented for 300 K; Horikoshi *et al.*'s values of $k$ between 2 and 12 μm are also included, as well as those of Zholkevich [20] between 0.5 and 0.7 μm.

Miloslavskii *et al.* [48] measured the transmittance of thin films of ZnTe and used the K–K method of analysis to calculate the phase change on transmission and hence to determine $n$ and $k$. They produced a graph of $n$ and $k$ versus wave number between 10,000 and 22,500 $cm^{-1}$ (0.44 and 1.0 μm), a peak in $n$ being found at 0.526 μm. Chu *et al.* [49] also worked with films of ZnTe deposited on glass, ceramic, and tungsten, substrates at temperatures of 500–600 °C. They present a graph of the absorption coefficient squared versus energy between 2.20 and 2.28 eV for ZnTe on polished glass, and this was linear for energies just above the band gap. When extrapolated, the line intersected the energy axis at 2.25 eV, the optical band gap. Thutupalli and Tomlin's work [14] on thin films deposited at room temperature and between the wavelengths of 0.3 and 2.0 μm produced values of $n$ that were in general smaller than those quoted in Table II, but when deposition took place at a substrate temperature of 325 °C, the values of $n$ became very similar to those for the bulk material. A set of data in the near-infrared has also been published by Masso and Turner [50]. Where overlap of wavelength occurs, these data are in good agreement with those of Thutupalli and Tomlin for room-temperature deposition. For this wavelength region, Table II gives values of $n$ due to Jensen and Torabi and also a set of values due to Masso and Turner, read off from the graph given by Li.

At long wavelengths (20–85 μm), Manabe *et al.* [23] again used the Lorentz-oscillator dispersion relationship quoted earlier to calculate $n$ and $k$ from their reflectance measurements on ZnTe. At 300 K, $\nu_t = 177\ cm^{-1}$, $\nu_l = 206\ cm^{-1}$, $\varepsilon_\infty = 6.7$, $N = 7.26 \times 10^4\ cm^{-2}$, and $\gamma = 3.01\ cm^{-1}$. At 100 K, the corresponding values were $180\ cm^{-1}$, $210\ cm^{-1}$, 6.7, $7.52 \times 10^4\ cm^{-2}$, and $2.34\ cm^{-1}$. Hadni *et al.* [35] measured the reflectance and transmittance of a pellet of ZnTe in the far infrared, explaining their results in terms of a single Lorentz-oscillator; this also produced values of $177\ cm^{-1}$ for $\nu_t$ and $205\ cm^{-1}$ for $\nu_l$ at 300 K. Hattori *et al.* [24] used their transmission interference technique to make measurements of $n$ and $k$ in the range 100–1000 μm and at temperatures of 300, 80, and 2 K; they were able to express their results in the form of a simple Sellmeier dispersion formula. Extrapolated to infinitely long wavelengths, the value of $n$ became 3.15 at 300 K, 3.11 at 80 K, and 3.10 at 2 K. The corresponding values of the transverse-optical-phonon frequency were 180, 190, and $192\ cm^{-1}$, respectively. Nahory and Fan [51] presented graphs of the absorption coefficient of single crystals of ZnTe at wavelengths between the visible and 50 μm and at temperatures of 295 and 10 K. Most of the room-temperature

absorption was due to free holes, but there was some wavelength-related structure caused by lattice vibrations. Their values of $k$ at room temperature are used in Table II, which also includes the optical constants due to Manabe *et al.*, Hadni *et al.*, and Hattori *et al.*

*Excitons in ZnTe*

Kurik and Manzhara [52] studied the exciton reflectance spectra of ZnTe single crystals, also noting the effects produced by the crystal defects. Pevtsov and Sel'kin [53] obtained the spectrum of excitons at 2 K by measurements of the reflectance and the phase change on reflection in both the $s$ and $p$ states of polarization. Their results appeared to fit well with the theoretical model of Thomas and Hopfield [54].

## REFERENCES


1. Y. Horikoshi, A. Ebina, and T. Takahashi, *Japan. J. Appl. Phys.* **11**, 992 (1972).
2. H. H. Li, *J. Phys. Chem. Ref. Data* **13**, 103 (1984).
3. J. Tauc, in "Prog. in Semiconductors," (A. F. Gibson and R. E. Burgess, eds.), Vol. 9, Temple Press, London, 87 (1965).
4. B. L. Henke, *A.I.P. Conf. Proc. No 75*, 146 (1981).
5. B. L. Henke, P. Lee, T. J. Tanoka, R. Shimabukura, and B. K. Fujikawa, *Atomic Data and Nuclear Data Tables* **27**, 1, (1982).
6. J. L. Freeout, *Phys. Rev.* **B7**, 3810 (1973).
7. J. Gautron, C. Raisin, and P. Lemasson, *J. Phys. D* **15**, 153 (1982).
8. M. Cardona and R. Haensel, *Phys. Rev.* **B1**, 2605 (1970).
9. U. Gerhardt and G. W. Rubloff, *Appl. Opt.* **8**, 305 (1969).
10. M. Cardona, K. L. Shaklee, and F. H. Pollak, *Phys. Rev.* **154**, 696 (1967).
11. M. Balkanski and Y. Petroff, in "Int. Conf. Phys. Semicond., Paris, 1964," Dunod, Paris, and Academic Press, New York, 245 (1964).
12. M. Cardona, in "Int. Conf. Phys. Semicond., Paris, 1964,"Dunod, Paris, and Academic Press, New York, 181 (1964).
13. M. Aven, D. T. F. Marple, and B. Segall, *J. Appl. Phys.* **32**, 2261 (1961).
14. G. K. M. Thutupalli and S. G. Tomlin, *J. Phys. D* **9**, 1639 (1976).
15. D. T. F. Marple, *J. Appl. Phys.* **25**, 539 (1964).
16. S. Ahmed and E. E. Khawaja, *Thin Solid Films* **112**, L1 (1984).
17. E. E. Khawaja, *J. Phys. D* **9**, 1939 (1976).
18. M. R. Rambauske, *J. Appl. Phys.* **35**, 2958 (1964).
19. D. G. Avery, *Phil. Mag.* **41**, 1028 (1950).
20. G. A. Zholkevich, *Sov. Phys. Sol. State* **2**, 1009 (1960).
21. J. A. Wunderlich and L. G. De Shazer, *Appl. Opt.* **16**, 1584 (1977).
22. A. Feldman, I. Malitson, D. Horwitz, R. M. Waxler, and M. J. Dodge, Nat. Bur. Stand. (U.S.), Tech. Note 993, 63 (1979).
23. A. Manabe, A. Mitsuishi, and H. Yoshinga, *Japan J. Appl. Phys.* **6**, 593 (1967).
24. T. Hattori, Y. Homma, and A. Mitsuishi, *Opt. Commun.* **7**, 229 (1973).
25. P. A. Miles, *Appl. Opt.* **16**, 2891 (1977).
26. I. Strzalkowski, S. Joshi, and C. R. Crowell, *App. Phys. Lett.* **28**, 350 (1976).
27. C. I. C. Thompson, R. G. de Bell and W. L. Wolfe, *Appl. Opt.* **18**, 2085 (1979).
28. H. Tubota, H. Suzaki, and O. Motumba, *J. Phys. Soc. Japan* **11**, 610 (1956).
29. G. A. Thomas and V. B. Timofiev, in "Handbook on Semiconductors," (T. S. Moss, ed), North-Holland, Amsterdam, 45 (1980).

30. G. E. Hite, D. T. F. Marple, M. Aven, and B. Segall, *Phys. Rev.* **156**, 850 (1967).
31. Y. Tokura, T. Koda, I. Hirabayashi, and S. Nakada, *J. Phys. Soc. Japan* **50**, 145 (1981).
32. X. J. Jiang, T. Hisamura, Y. Nosua, and T. Goto, *J. Phys. Soc. Japan* **52**, 4008 (1983).
33. D. E. McCarthy, *Appl. Opt.* **4**, 317 (1965).
34. A. R. Hilton and C. E. Jones, *Appl. Opt.* **6**, 1513 (1967).
35. A. Hadni, J. Claudel, and P. Strimer, *Phys. Stat. Solidi* **26**, 241 (1968).
36. M. Cardona and D. L. Greenaway, *Phys. Rev.* **131**, 98 (1963).
37. M. Cardona, *J. Appl. Phys.* **36**, 2181 (1965).
38. D. R. Penn, *Phys. Rev.* **128**, 2093 (1962).
39. B. Gauthe, *Phys. Rev.* **114**, 1265 (1959).
40. T. Tomoda and M. Mannami, *J. Phys. Soc. Japan* **27**, 1204 (1969).
41. J. P. Walter, M. L. Cohen, Y. Petroff, and M. Balkanski, *Phys. Rev.* **B1**, 2261 (1970).
42. E. Loh and R. Newmann, *J. Phys. Chem. Solids* **21**, 324 (1961).
43. H. M. Brown and D. E. Brodie, *Can. J. Phys.* **50**, 2502 (1972).
44. T. Sliker and J. M. Jost, *J. Opt. Soc. Amer.* **56**, 130 (1966).
45. L. R. Shiozawa, J. L. Barrett, J. M. Jost, C. P. Chotkevys, and S. S. Devlin, "Research on II-VI Compound Semiconductors," Clevite Corp., Cleveland, Ohio, Final Report on the Office of Aerospace Research, U.S. Air Force Contract AF.33(616)-6865, (1962) [AD 287 718].
46. A. C. Aten, C. Z. Van Doorn and A. T. Vink, in "Proc. Int. Conf. Phys. Semicond. Exeter, 1962," (A. C. Stickland, ed.), Institute of Physics, London, 696 (1962).
47. B. Jensen and A. Torabi, *J. Appl. Phys.* **54**, 2030 (1983).
48. V. K. Miloslavskii and E. N. Nabockina, *Opt. and Spectros.* **38**, 565 (1975).
49. T. L. Chu, S. S. Chu, F. Firszt, and C. Herrington, *J. App. Phys.* **59**, 1259 (1986).
50. J. Masso and A. F. Turner, Bausch and Lomb Inc., Final Report on Development of Army Contract DA-44-009-AMC 124(T) (AD 600 264) (1964).
51. R. E. Nahory and H. Y. Fan, *Phys. Rev.* **156**, 825 (1967).
52. M. V. Kurik and V. S. Manzhara, *Sov. Phys. Sol. State* **18**, 1445 (1976).
53. A. B. Pevtsov and A. V. Sel'kin, *Sov. Phys. Sol. State* **23**, 1644 (1981).
54. D. G. Thomas and J. J. Hopfield, *Phys. Rev.* **128**, 2135 (1969).

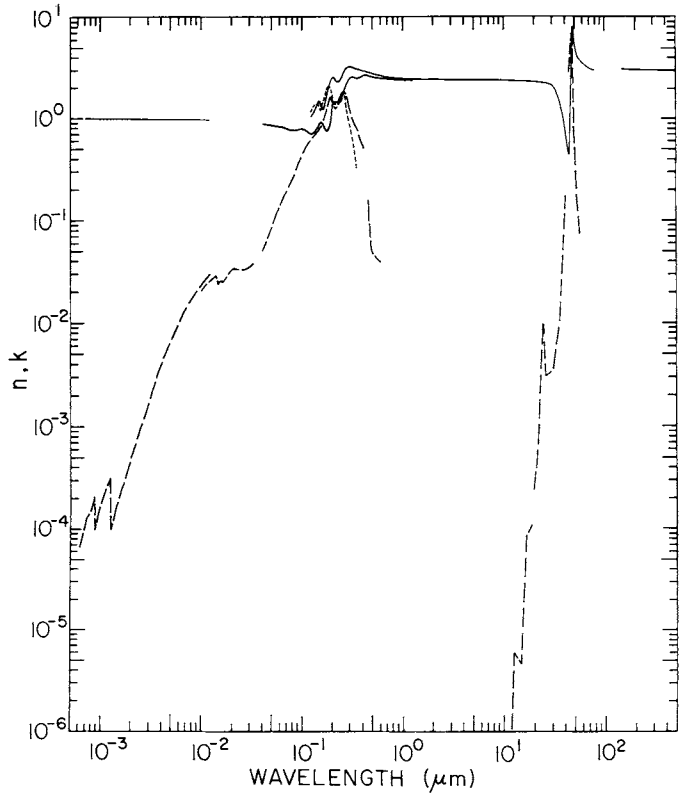


**Fig. 1.** Log–log plot of $n$ (solid line) and $k$ (dashed line) versus wavelength in micrometers for zinc selenide.

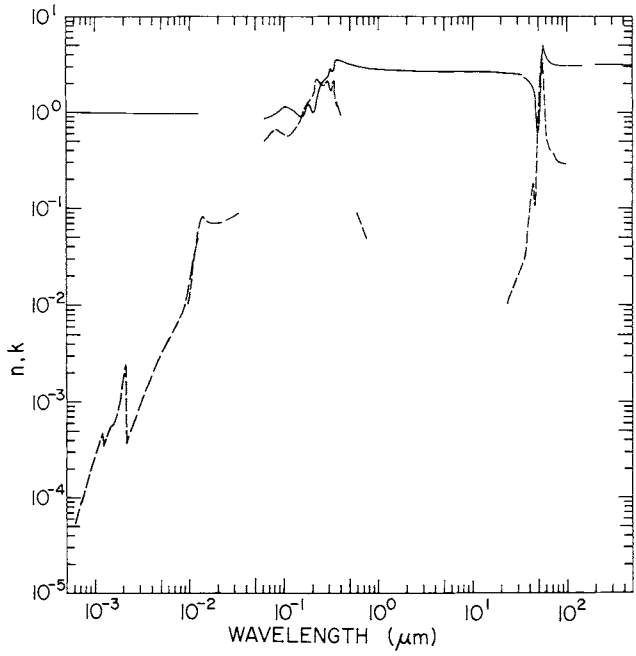


**Fig. 2.** Log–log plot of $n$ (solid line) and $k$ (dashed line) versus wavelength in micrometers for zinc telluride.

**TABLE I**

**Values of *n* and *k* for Cubic ZnSe from Various References[a]**

| eV | $cm^{-1}$ | μm | n | k |
|---|---|---|---|---|
| 2000 | 16,131,000 | 0.00062 | 0.9998 [4] | $7.0*10^{-5}$ [4] |
| 1851 | 14,929,000 | 0.00067 | 0.9998 | $9.6*10^{-5}$ |
| 1698 | 13,695,000 | 0.00073 | 0.9998 | $1.32*10^{-4}$ |
| 1610 | 12,985,000 | 0.00077 | 0.9998 | 1.44 |
| 1459 | 11,768,000 | 0.00085 | 0.9998 | 2.00 |
| 1425 | 11,493,000 | 0.00087 | 0.9998 | 0.98 |
| 1393 | 11,235,000 | 0.00089 | 0.9996 | 1.22 |
| 1363 | 10,993,000 | 0.00091 | 0.9996 | 1.32 |
| 1240 | 10,000,000 | 0.00100 | 0.9996 | 1.80 |
| 1147 | 9,251,100 | 0.00108 | 0.9996 | 2.24 |
| 1033 | 8,333,300 | 0.00120 | 0.9996 | 3.00 |
| 991.9 | 8,000,000 | 0.00125 | 0.9994 | 1.00 |
| 946.5 | 7,634,000 | 0.00131 | 0.9992 | 1.22 |
| 826.6 | 6,666,700 | 0.00150 | 0.9990 | 2.00 |
| 815.7 | 6,579,000 | 0.00152 | 0.9990 | 2.02 |
| 760.7 | 6,135,400 | 0.00163 | 0.9988 | 2.54 |
| 725.1 | 5,848,300 | 0.00171 | 0.9986 | 2.96 |
| 673.9 | 5,435,300 | 0.00184 | 0.9984 | 3.69 |
| 620.0 | 5,000,000 | 0.00200 | 0.9982 | 4.80 |
| 529.9 | 4,273,900 | 0.00234 | 0.9974 | $7.96*10^{-4}$ |
| 413.3 | 3,333,300 | 0.00300 | 0.9960 | $1.69*10^{-3}$ |
| 367.9 | 2,967,300 | 0.00337 | 0.9952 | 2.36 |
| 310.0 | 2,500,000 | 0.00400 | 0.9938 | 3.74 |
| 269.0 | 2,169,600 | 0.00461 | 0.9924 | 5.48 |
| 248.0 | 2,000,000 | 0.00500 | 0.9918 | 6.62 |
| 227.1 | 1,831,700 | 0.00546 | 0.9908 | $8.12*10^{-3}$ |
| 206.7 | 1,666,700 | 0.00600 | 0.9900 | $1.00*10^{-2}$ |
| 190.8 | 1,538,900 | 0.0065 | 0.9898 | 1.18 |
| 177.1 | 1,428,400 | 0.0070 | 0.9890 | 1.36 |
| 155.0 | 1,250,000 | 0.0080 | 0.9886 | 1.71 |
| 136.3 | 1,099,300 | 0.0091 | 0.9882 | 2.02 |
| 124.0 | 1,000,000 | 0.0100 | 0.9876 | 2.28 |
| 109.7 | 884,780 | 0.0113 | 0.9872 | 2.68 |
| 103.3 | 833,330 | 0.0120 | 0.9870 | 2.88 |
| 100.0 | 806,550 | 0.01240 | 0.9872 | 2.98 |
| 150 | 1,209,800 | 0.008226 | 1.00 [8] | 1.5*10-2 [8] |
| 140 | 1,129,200 | 0.008856 | 1.00 | 1.6 |
| 136 | 1,096,900 | 0.009116 | 1.00 | 2.0 |
| 130 | 1,048,500 | 0.009537 | 1.00 | 2.0 |
| 125 | 1,008,200 | 0.009919 | 1.00 | 2.1 |
| 120 | 967,860 | 0.01033 | 1.00 | 2.2 |
| 115 | 927,530 | 0.0108 | 1.00 | 2.3 |
| 110 | 887,200 | 0.0113 | 1.00 | 2.4 |
| 100 | 806,550 | 0.0124 | 1.00 | 2.6 |
| 93.0 | 750,090 | 0.0133 | 1.00 | 2.8 |
| 90.0 | 725,890 | 0.0138 | 1.00 | 2.9 |
| 85.0 | 685,570 | 0.0146 | 1.00 | 2.4 |
| 80.0 | 645,240 | 0.0155 | 1.00 | 2.6 |
| 75.0 | 604,910 | 0.01653 | 1.00 | 2.6 |
| 70.0 | 564,580 | 0.01771 | 1.00 | $2.7*10^{-2}$ |

**TABLE I (*Continued*)**

**ZnSe**

| eV | $cm^{-1}$ | μm | n | k |
|---|---|---|---|---|
| 60.0 | 483,930 | 0.02066 | 1.00 [8] | $3.4*10^{-2}$ |
| 50.0 | 403,270 | 0.02480 | 1.00 | 3.3 |
| 40.0 | 322,620 | 0.03100 | 1.00 | 3.5 |
| 37.5 | 302,460 | 0.03306 | 1.00 | $3.8*10^{-2}$ |
| 30.0 | 241,960 | 0.04133 | 0.90 [7] | 0.05 [7] |
| 25.0 | 201,640 | 0.04959 | 0.86 | 0.08 |
| 20.0 | 161,310 | 0.06199 | 0.84 | 0.15 |
| 15.0 | 120,980 | 0.08266 | 0.76 | 0.25 |
| 12.5 | 100,820 | 0.09919 | 0.81 | 0.43 |
| 10.0 | 80,655 | 0.1240 | 0.70 | 0.65 |
| 8.00 | 64,524 | 0.1550 | 0.92 | 0.81 |
| 7.00 | 56,458 | 0.1771 | 0.76 | 1.28 |
| 6.50 | 52,426 | 0.1907 | 0.89 | 1.65 |
| 6.00 | 48,393 | 0.2066 | 1.40 | 1.40 |
| 5.50 | 44,360 | 0.2254 | 1.46 | 1.41 |
| 5.00 | 40,327 | 0.2480 | 1.43 | 1.86 |
| 4.50 | 36,295 | 0.2755 | 2.16 | 1.73 |
| 4.00 | 32,262 | 0.3100 | 2.57 | 1.00 |
| 3.50 | 28,229 | 0.3542 | 2.43 | 0.82 |
| 3.00 | 24,196 | 0.4133 | 2.68 | 0.50 |
| 2.00 | 16,131 | 0.6199 | 2.49 | |
| 1.00 | 8,065 | 1.240 | 2.38 | |
| 10.00 | 80,655 | 0.1240 | 1.03 [11] | 1.19 [11] |
| 8.99 | 72,509 | 0.1379 | 1.26 | 1.39 |
| 8.38 | 67,588 | 0.1480 | 1.48 | 1.35 |
| 8.00 | 64,524 | 0.1550 | 1.38 | 1.21 |
| 7.52 | 60,652 | 0.1649 | 1.25 | 1.60 |
| 7.01 | 56,539 | 0.1769 | 1.56 | 1.92 |
| 6.29 | 50,731 | 0.1971 | 2.45 | 2.00 |
| 5.99 | 48,312 | 0.2070 | 2.58 | 1.39 |
| 5.51 | 44,444 | 0.2250 | 2.38 | 1.29 |
| 5.30 | 42,747 | 0.2339 | 2.33 | 1.39 |
| 4.96 | 40,000 | 0.2500 | 2.54 | 1.57 |
| 4.77 | 38,472 | 0.2599 | 2.74 | 1.82 |
| 4.43 | 35,730 | 0.2800 | 3.24 | 1.23 |
| 4.30 | 34,682 | 0.2883 | 3.26 | 0.91 |
| 4.00 | 32,262 | 0.3100 | 3.24 | 0.70 |
| 3.54 | 28,551 | 0.3503 | 3.09 | 0.32 |
| 2.82 | 22,744 | 0.4397 | 2.83 [11] | 0.16 [20] |
| 2.70 | 21,777 | 0.4592 | 2.90 | 0.16 |
| 2.48 | 20,000 | 0.5000 | 2.78 | 0.05 |
| 2.00 | 16,131 | 0.6199 | 2.61 | 0.04 |
| 1.50 | 12,097 | 0.8266 | 2.51 | |
| 1.00 | 8,065 | 1.2400 | 2.45 | |
| 2.480 | 20,000 | 0.500 | 2.742(0) [22] | |
| 1.653 | 13,333 | 0.750 | 2.578(2) | |
| 1.240 | 10,000 | 1.00 | 2.489(0) | |
| 0.9918 | 8,000 | 1.25 | 2.468(1) | |
| 0.8266 | 6,667 | 1.50 | 2.457(1) | |

**TABLE I (*Continued*)**

**ZnSe**

| eV | $cm^{-1}$ | μm | n | k |
|---|---|---|---|---|
| 0.7085 | 5,714 | 1.75 | 2.450(6) [22] | |
| 0.6199 | 5,000 | 2.00 | 2.446(2) | |
| 0.5510 | 4,444 | 2.25 | 2.443(2) | |
| 0.4959 | 4,000 | 2.50 | 2.440(9) | |
| 0.4509 | 3,636 | 2.75 | 2.439(1) | |
| 0.4133 | 3,333 | 3.00 | 2.437(6) | |
| 0.3542 | 2,857 | 3.50 | 2.435(2) | |
| 0.3100 | 2,500 | 4.00 | 2.433(1) | |
| 0.2755 | 2,222 | 4.50 | 2.431(3) | |
| 0.2480 | 2,000 | 5.00 | 2.429(5) | |
| 0.2254 | 1,818 | 5.50 | 2.427(7) | |
| 0.2066 | 1,667 | 6.00 | 2.425(8) | |
| 0.1908 | 1,538 | 6.50 | 2.423(9) | |
| 0.1771 | 1,429 | 7.00 | 2.421(8) | |
| 0.1653 | 1,333 | 7.50 | 2.419(6) | |
| 0.1550 | 1,250 | 8.00 | 2.417(3) | |
| 0.1459 | 1,176 | 8.50 | 2.414(8) | |
| 0.1378 | 1,111 | 9.00 | 2.412(2) | |
| 0.1305 | 1,053 | 9.50 | 2.409(3) | |
| 0.1240 | 1,000 | 10.00 | 2.406(5) | |
| 0.1181 | 952.5 | 10.50 | 2.403(4) | |
| 0.1127 | 909.0 | 11.00 | 2.400(1) | $1.1*10^{-7}$ [25] |
| 0.1078 | 869.5 | 11.50 | 2.396(6) | |
| 0.1033 | 833.2 | 12.00 | 2.392(9) | |
| 0.09919 | 800.0 | 12.50 | 2.389(0) | $6.0*10^{-6}$ |
| 0.09538 | 769.3 | 13.00 | 2.384(9) | |
| 0.09184 | 740.7 | 13.50 | 2.380(6) | |
| 0.08856 | 714.3 | 14.00 | 2.376(1) | |
| 0.08551 | 689.7 | 14.50 | 2.371(3) | $4.6*10^{-6}$ |
| 0.08266 | 666.7 | 15.00 | 2.366(3) | |
| 0.08000 | 645.2 | 15.50 | 2.361(0) | |
| 0.07749 | 625.0 | 16.00 | 2.355(5) | |
| 0.07515 | 606.1 | 16.50 | 2.349(6) | $8.5*10^{-5}$ |
| 0.07294 | 588.3 | 17.00 | 2.343(5) | |
| 0.07085 | 571.4 | 17.50 | 2.337(1) | |
| 0.06888 | 555.6 | 18.00 | 2.330(3) | $1.1*10^{-4}$ |
| 0.06199 | 500.0 | 20.00 | 2.33 [23] | $4.8*10^{-4}$ |
| 0.05703 | 460.0 | 21.74 | 2.30 | $1.7*10^{-3}$ |
| 0.05145 | 415.0 | 24.10 | 2.28 | $2.0*10^{-2}$ |
| 0.04959 | 400.0 | 25.00 | 2.25 | $6.0*10^{-3}$ |
| 0.04133 | 333.3 | 30.00 | 2.15 | $7.0*10^{-3}$ |
| 0.03542 | 285.7 | 35.00 | 1.60 | $2.1*10^{-2}$ |
| 0.03100 | 250.0 | 40.00 | 1.01 | $3.2*10^{-1}$ |
| 0.02755 | 222.2 | 45.00 | 0.43 | 2.90 [23] |
| 0.02695 | 217.4 | 46.00 | 0.58 | 3.62 |
| 0.02638 | 212.8 | 47.00 | 1.16 | 4.93 |
| 0.02610 | 210.5 | 47.50 | 2.10 | 6.10 |
| 0.02583 | 208.3 | 48.00 | 3.19 | 6.67 |
| 0.02556 | 206.2 | 48.50 | 3.20 | 6.20 |

TABLE I (*Continued*)

ZnSe

| eV | cm⁻¹ | μm | n | k | |
|---|---|---|---|---|---|
| 0.02530 | 204.1 | 49.00 | 7.54 | 3.62 | |
| 0.02525 | 203.7 | 49.10 | 7.68 | 2.52 | |
| 0.02505 | 202.0 | 49.50 | 6.75 | 1.83 | |
| 0.02480 | 200.0 | 50.00 | 6.09 | 0.87 | |
| 0.02431 | 196.1 | 51.00 | 5.07 | 0.58 | |
| 0.02384 | 192.3 | 52.00 | 4.64 | 0.43 | |
| 0.02339 | 188.7 | 53.00 | 4.29 | 0.23 | |
| 0.02296 | 185.2 | 54.00 | 4.00 | 0.18 | [23] |
| 0.02254 | 181.8 | 55.00 | 3.83 | 0.14 | |
| 0.02156 | 173.9 | 57.50 | 3.71 | 0.11 | |
| 0.02066 | 166.7 | 60.00 | 3.54 | 0.08 | |
| 0.01771 | 142.8 | 70.00 | 3.04 | | |
| 0.01550 | 125.0 | 80.00 | 2.90 | | |
| 0.008257 | 66.67 | 150 | 3.07 | [24] | |
| 0.006199 | 50.00 | 200 | 3.04 | | |
| 0.004959 | 40.00 | 250 | 3.03 | | |
| 0.004133 | 33.33 | 300 | 3.02 | | |
| 0.003542 | 28.57 | 350 | 3.02 | | |
| 0.003100 | 25.00 | 400 | 3.01 | | |
| 0.002755 | 22.22 | 450 | 3.01 | | |
| 0.002480 | 20.00 | 500 | 3.01 | | |
| 0.0 | 0 | >99999.99 | 3.00 | | |

Irtran 4

| eV | cm⁻¹ | μm | n | k | |
|---|---|---|---|---|---|
| 0.4133 | 3,333 | 3.0 | 2.445 | [34] | |
| 0.3100 | 2,500 | 4.0 | 2.438 | | |
| 0.2480 | 2,000 | 5.0 | 2.434 | | |
| 0.2066 | 1,667 | 6.0 | 2.430 | | |
| 0.1771 | 1,429 | 7.0 | 2.425 | | |
| 0.1550 | 1,250 | 8.0 | 2.422 | | |
| 0.1378 | 1,111 | 9.0 | 2.417 | | |
| 0.1240 | 1,000 | 10.0 | 2.410 | | |
| 0.1127 | 909.0 | 11.0 | 2.405 | | |
| 0.1033 | 833.3 | 12.0 | 2.398 | | |
| 0.09517 | 769.2 | 13.0 | 2.390 | | |
| 0.08856 | 714.3 | 14.0 | 2.380 | | |
| 0.04339 | 350 | 28.57 | 2.00 | [35] | |
| 0.03720 | 300 | 33.33 | 2.00 | | |
| 0.03100 | 250 | 40.00 | 0.20 | 1.5 | [35] |
| 0.02790 | 225 | 44.44 | 0.50 | 2.8 | |
| 0.02604 | 210 | 47.62 | 2.50 | 7.9 | |
| 0.02542 | 205 | 48.78 | 5.00 | 4.8 | |
| 0.02480 | 200 | 50.00 | 8.42 | 3.2 | |
| 0.02170 | 175 | 57.14 | 3.50 | 0.4 | |
| 0.01860 | 150 | 66.67 | 3.40 | 0.5 | |

[a] References are indicated in brackets.

**TABLE II**

**Values of *n* and *k* for Cubic ZnTe from Various References[a]**

| eV | $cm^{-1}$ | μm | n | k |
|---|---|---|---|---|
| 2000 | 16,131,000 | 0.00062 | 0.9998 [4] | $5.2*10^{-5}$ [4] |
| 1850 | 14,929,000 | 0.00067 | 0.9998 | 7.2 |
| 1698 | 13,695,000 | 0.00073 | 0.9996 | $9.8*10^{-5}$ |
| 1610 | 12,985,000 | 0.00077 | 0.9996 | $1.18*10^{-4}$ |
| 1459 | 11,768,000 | 0.00085 | 0.9996 | 1.64 |
| 1363 | 10,993,000 | 0.00091 | 0.9996 | 2.00 |
| 1147 | 9,251,100 | 0.00108 | 0.9994 | 3.60 |
| 1033 | 8,333,300 | 0.00120 | 0.9994 | 4.80 |
| 991.9 | 8,000,000 | 0.00125 | 0.9994 | 3.60 |
| 855.1 | 6,896,800 | 0.00145 | 0.9992 | 5.40 |
| 826.6 | 6,666,700 | 0.00150 | 0.9990 | 5.80 |
| 815.7 | 6,579,000 | 0.00152 | 0.9990 | 5.80 |
| 760.7 | 6,135,400 | 0.00163 | 0.9990 | 6.40 |
| 725.1 | 5,848,300 | 0.00171 | 0.9988 | $7.40*10^{-4}$ |
| 673.9 | 5,435,300 | 0.00184 | 0.9988 | $1.02*10^{-3}$ |
| 620.0 | 5,000,000 | 0.00200 | 0.9988 | 1.82 |
| 582.1 | 4,694,900 | 0.00213 | 1.0000 | 2.44 |
| 563.6 | 4,545,700 | 0.00220 | 1.0012 | 0.38 |
| 529.9 | 4,273,900 | 0.00234 | 0.9990 | 0.48 |
| 413.3 | 3,333,300 | 0.00300 | 0.9976 | 0.92 |
| 367.9 | 2,967,400 | 0.00337 | 0.9968 | 1.24 |
| 310.0 | 2,500,000 | 0.00400 | 0.9954 | 1.90 |
| 269.0 | 2,169,600 | 0.00461 | 0.9940 | 2.60 |
| 248.0 | 2,000,000 | 0.00500 | 0.9932 | 3.20 |
| 227.1 | 1,831,700 | 0.00546 | 0.9920 | 3.80 |
| 206.7 | 1,666,700 | 0.0060 | 0.9904 | 4.60 |
| 190.8 | 1,538,900 | 0.0065 | 0.9892 | 5.40 |
| 177.1 | 1,428,400 | 0.0070 | 0.9876 | 6.20 |
| 155.0 | 1,250,000 | 0.0080 | 0.9832 | $7.80*10^{-3}$ |
| 136.3 | 1,099,300 | 0.0091 | 0.9762 | $1.08*10^{-2}$ |
| 124.0 | 1,000,000 | 0.0100 | 0.9688 | 1.66 |
| 112.7 | 909,090 | 0.0110 | 0.9626 | 3.02 |
| 103.3 | 833,330 | 0.0120 | 0.9638 | 4.28 |
| 100.0 | 806,550 | 0.0124 | 0.9666 | 4.96 |
| 150 | 1,209,800 | 0.008266 | 1.00 [8] | $3.8*10^{-3}$ [8] |
| 140 | 1,129,200 | 0.008856 | 1.00 | 6.0 |
| 135 | 1,088,800 | 0.009184 | 1.00 | 7.4 |
| 130 | 1,048,500 | 0.009538 | 1.00 | $9.8*10^{-3}$ |
| 125 | 1,008,200 | 0.009919 | 1.00 | $1.2*10^{-2}$ |
| 120 | 967,860 | 0.01032 | 1.00 | 1.7 |
| 110 | 887,200 | 0.01127 | 1.00 | 3.2 |
| 100 | 806,550 | 0.01240 | 1.00 | 5.5 |
| 90.0 | 725,890 | 0.01378 | 1.00 | 8.2 |
| 80.0 | 645,240 | 0.01550 | 1.00 | 7.4 |
| 70.0 | 564,580 | 0.01771 | 1.00 | 7.2 |
| 60.0 | 483,930 | 0.02066 | 1.00 | 7.0 |
| 50.0 | 403,270 | 0.02480 | 1.00 | 7.4 |
| 37.5 | 302,460 | 0.03306 | 1.00 | $9.0*10^{-2}$ |

TABLE II (*Continued*)

ZnTe

| eV | cm$^{-1}$ | μm | n | k |
|---|---|---|---|---|
| 20.0 | 161,310 | 0.06200 | 0.87 [37] | 0.50 [37] |
| 15.0 | 120,980 | 0.08266 | 1.00 | 0.67 |
| 12.0 | 96,786 | 0.1033 | 1.17 | 0.60 |
| 11.0 | 88,720 | 0.1127 | 1.13 | 0.57 |
| 10.0 | 80,653 | 0.1240 | 1.07 | 0.64 |
| 9.0 | 72,589 | 0.1378 | 1.00 | 0.70 |
| 8.0 | 64,524 | 0.1550 | 0.90 | 0.83 |
| 7.5 | 60,491 | 0.1653 | 0.97 | 1.07 |
| 7.0 | 56,458 | 0.1771 | 1.20 | 1.20 |
| 6.0 | 48,393 | 0.2066 | 1.00 | 1.47 |
| 5.5 | 44,360 | 0.2254 | 1.43 | 2.17 |
| 5.0 | 40,327 | 0.2480 | 2.00 | 2.00 |
| 4.6 | 37,101 | 0.2695 | 2.20 | 1.90 |
| 4.3 | 34,682 | 0.2883 | 2.27 | 2.13 |
| 4.0 | 32,262 | 0.3100 | 2.80 | 2.00 |
| 3.85 | 31,052 | 0.3220 | 2.73 | 1.73 |
| 3.6 | 29,036 | 0.3444 | 3.00 | 2.10 |
| 3.5 | 28,229 | 0.3542 | 3.47 | 1.33 |
| 3.0 | 24,196 | 0.4133 | 3.40 | 0.95 |
| 2.18 | 17,583 | 0.5687 | 3.10 [15] | |
| 2.00 | 16,130 | 0.6199 | 3.00 | |
| 1.72 | 13,873 | 0.7208 | 2.90 | |
| 1.30 | 10,485 | 0.9537 | 2.80 | |
| 1.00 | 8,065 | 1.240 | 2.75 | |
| 0.50 | 4,033 | 2.480 | 2.70 | |
| 2.179 | 17,580 | 0.569 | 3.111 [44] | |
| 2.149 | 17,330 | 0.577 | 3.085 | 0.09 [20] |
| 2.141 | 17,270 | 0.579 | 3.079 | 0.09 |
| 2.105 | 16,980 | 0.589 | 3.054 | 0.09 |
| 2.066 | 16,670 | 0.600 | 3.035 | 0.09 |
| 2.013 | 16,230 | 0.616 | 3.005 | 0.08 |
| 1.908 | 15,390 | 0.650 | 2.962 | 0.07 |
| 1.771 | 14,290 | 0.700 | 2.912 | 0.06 |
| 1.710 | 13,800 | 0.725 | 2.893 | 0.06 |
| 1.653 | 13,330 | 0.750 | 2.879 | 0.05 |
| 1.610 | 12,990 | 0.770 | 2.866 | |
| 1.550 | 12,500 | 0.800 | 2.853 | |
| 1.240 | 10,000 | 1.000 | 2.790 | |
| 1.033 | 8,333 | 1.200 | 2.758 | |
| 0.8856 | 7,143 | 1.400 | 2.741 | |
| 0.8266 | 6,667 | 1.500 | 2.734 | |
| 0.8194 | 6,609 | 1.513 | 2.734 | |
| 2.066 | 16,667 | 0.60 | 3.00 [47] | |
| 1.240 | 10,000 | 1.0 | 2.82 | |
| 0.6200 | 5,000 | 2.0 | 2.73 | $2.0*10^{-4}$ [1] |
| 0.4133 | 3,333 | 3.0 | 2.69 | 4.0 |
| 0.3100 | 2,500 | 4.0 | 2.68 | $8.0*10^{-4}$ |
| 0.2480 | 2,000 | 5.0 | 2.67 | $1.6*10^{-3}$ |

TABLE II (*Continued*)

ZnTe

| eV | $cm^{-1}$ | μm | n | k |
|---|---|---|---|---|
| 0.2067 | 1,667 | 6.0 | 2.67 [47] | $2.0*10^{-3}$ [1] |
| 0.1771 | 1,429 | 7.0 | 2.66 | 3.0 |
| 0.1240 | 1,000 | 10.0 | 2.65 | $7.0*10^{-3}$ |
| 0.06199 | 500.0 | 20.0 | 2.64 | |
| 0.04133 | 333.3 | 30.0 | 2.638 | |
| 0.03100 | 250.0 | 40.0 | 2.635 | |
| 0.02480 | 200.0 | 50.0 | 2.634 | |
| 0.9465 | 7,634 | 1.31 | 2.66 [50] | |
| 0.5299 | 4,274 | 2.34 | 2.65 | |
| 0.3757 | 3,030 | 3.30 | 2.65 | |
| 0.2566 | 2,070 | 4.83 | 2.64 | |
| 0.1885 | 1,520 | 6.58 | 2.64 | |
| 0.1406 | 1,334 | 8.82 | 2.64 | |
| 0.1150 | 927.6 | 10.78 | 2.63 | |
| 0.09770 | 788.0 | 12.69 | 2.63 | |
| 0.08293 | 668.9 | 14.95 | 2.62 | |
| 0.06508 | 524.9 | 19.05 | 2.59 | |
| 0.05344 | 431.0 | 23.20 | 2.56 | 0.01 [51] |
| 0.04521 | 364.6 | 27.43 | 2.53 | 0.02 |
| 0.03887 | 313.6 | 31.90 | 2.49 | 0.02 |
| 0.03591 | 298.6 | 34.53 | 2.47 | 0.03 |
| 0.03546 | 286 | 34.97 | 2.26 [35] | 0.03 [51] |
| 0.03224 | 260 | 38.46 | 2.19 | 0.03 |
| 0.03100 | 250 | 40.00 | 2.07 | 0.09 |
| 0.02914 | 235 | 42.55 | 1.92 | 0.15 |
| 0.02790 | 225 | 44.44 | 1.90 | 0.18 |
| 0.02728 | 220 | 45.45 | 1.68 | 0.11 |
| 0.02604 | 210 | 47.62 | 0.75 | 0.18 |
| 0.02480 | 200 | 50.00 | 0.70 | 1.0 [35] |
| 0.02356 | 190 | 52.63 | 1.10 | 1.9 |
| 0.02294 | 185 | 54.05 | 1.46 | 3.1 |
| 0.02232 | 180 | 55.55 | 3.72 | 3.6 |
| 0.02207 | 178 | 56.18 | 4.00 | 3.0 |
| 0.02170 | 175 | 57.14 | 4.94 | 2.3 |
| 0.02070 | 167 | 59.88 | 3.95 | 0.6 |
| 0.01860 | 150 | 66.67 | 3.29 | 0.4 |
| 0.01773 | 143 | 69.93 | 3.14 | 0.4 |
| 0.01550 | 125 | 80.00 | 3.07 | 0.3 |
| 0.01376 | 111 | 90.09 | 3.06 | 0.3 |
| 0.01240 | 100 | 100.0 | 3.05 | 0.3 |
| 0.01116 | 90 | 111.1 | 3.04 | 0.3 |
| 0.009919 | 80 | 125.0 | 3.02 | 0.2 |
| 0.008307 | 67 | 150.0 | 3.01 | 0.2 |
| 0.06199 | 500.0 | 20.0 | 2.20 [25] | 0.01 [51] |
| 0.04133 | 333.3 | 30.0 | 2.10 | 0.03 |
| 0.03543 | 285.7 | 35.0 | 2.03 | 0.03 |
| 0.03100 | 250.0 | 40.0 | 1.74 | – |
| 0.02755 | 222.2 | 45.0 | 1.59 | – |

TABLE II (*Continued*)

ZnTe

| eV | $cm^{-1}$ | μm | n | k |
|---|---|---|---|---|
| 0.02480 | 200.0 | 50.0 | 0.23 [23] | 1.30 [23] |
| 0.02431 | 196.1 | 51.0 | 0.14 | 1.74 |
| 0.02384 | 192.3 | 52.0 | 0.14 | 2.46 |
| 0.02339 | 188.7 | 53.0 | 0.23 | 3.48 |
| 0.02296 | 185.2 | 54.0 | 0.58 | 4.35 |
| 0.02254 | 181.8 | 55.0 | 1.45 | 6.09 |
| 0.02214 | 178.6 | 56.0 | 3.48 | 6.96 |
| 0.02175 | 175.4 | 57.0 | 7.97 | 2.90 |
| 0.02156 | 173.9 | 57.5 | 9.57 | 2.32 |
| 0.02138 | 172.4 | 58.0 | 7.54 | 1.88 |
| 0.02102 | 169.5 | 59.0 | 5.80 | 0.87 |
| 0.02067 | 166.7 | 60.0 | 5.16 | 0.35 |
| 0.01771 | 142.9 | 70.0 | 3.19 | |
| 0.01550 | 125.0 | 80.0 | 2.90 | |
| 0.006199 | 50.00 | 200 | 3.20 | 0.02 [24] |
| 0.004959 | 40.00 | 250 | 3.18 | 0.02 |
| 0.004132 | 33.33 | 300 | 3.17 | 0.017 |
| 0.003100 | 25.00 | 400 | 3.16 | |

[a] References are indicated in brackets.

# Aluminum Oxide ($Al_2O_3$)

FRANÇOIS GERVAIS
Centre de Recherches sur la Physique des Hautes Températures
Centre National de la Recherche Scientifique
45071 Orléans, France

Aluminum oxide crystallizes in the corundum ($\alpha$-$Al_2O_3$) rhombohedral structure. It is also known as sapphire. The system is uniaxial and optical properties measured on a single crystal are therefore anisotropic. The structure of the oxygen sublattice is close-packed. As a result, the anisotropy of the refractive index in the visible region, mainly related to the anisotropy of the oxygen polarizability is small (less than 2%). In the millimeter-wave range, the anisotropy reaches 10%. The optical constants selected are listed in Table I and plotted in Fig. 1.

A study including original measurements and a compilation of previous data, which extends over a wide energy range, from 6 eV up to $1.6 \times 10^3$ eV, has been performed at the Deutsches Elektronen-synchrotron DESY [1]. The compilation concerns Refs. [2–5]. Although measurements have been performed on evaporated amorphous $Al_2O_3$ such that information related to anisotropy is lost, they are of practical interest. Results agree well with previous measurements at low energies but extend over a much wider energy range. Optical absorption measurements performed on single-crystal samples, but restricted to the 1–6 eV range, were reported in Refs. [6, 7]. Some anisotropy of the spectra is displayed in [6]. However, these spectra are of little practical interest, since it is difficult to extract $n$ and $k$ from the UV edge by Kramers–Kronig analysis in a too-narrow energy range where there is strong dispersion. Results of [1] are given in Table I.

The indexes of refraction of a synthetic sapphire prism measured over its entire range of transmission (0.2–6 μm) is reported in Ref. [8]. The optic axis of the prism was oriented parallel to the base and perpendicular to the apex, so that measurements refer to the ordinary ray (electric field perpendicular to the $c$ axis of the corundum structure). Results are listed in Table I.

Measurements in the infrared were reported in the literature at the beginning of this century. However, the quantitative exploitation of


Copyright © 1991 by Academic Press.
All rights of reproduction in any form reserved.
ISBN 0-12-544422-2

infrared reflectivity spectra started with the availability of computers in the 1960s. The most complete set of measurements in the infrared complemented by data processing was performed by Barker [9]. Several single crystals from different origins were compared. Measurements were performed with a prism spectrometer. Barker emphasized the large differences that may appear from one sample to another in specific spectral regions. The forbidden modes disappear after etching of the surface. Measurements analyzed in Refs. [11] and [12] were performed on a single crystal previously annealed at 1775 K, thus above 3/4 of the temperature of the melting point, to regenerate the surface partially altered by the polishing. The spectra then consist of normal vibrational modes only, and no extra modes are visible.

Surprisingly, the literature is short of data concerning $n$ and $k$ in alumina ceramics. A study of this type was published only recently [12], performed with a grating spectrometer. The hot-pressed alumina sample was as-fired. The spectrum mainly resembles that for the ordinary ray of a single crystal but of course also contains features related to the extraordinary ray. Again, the authors emphasize the influence of polishing on the appearance of forbidden modes. The authors seem to have been surprised by the existence of a weak band at approximately $500\,cm^{-1}$. This is simply the signature of the presence of the longitudinal optical mode at $514\,cm^{-1}$ for the electric field polarized parallel to the $c$ axis (extraordinary ray) in the vicinity of the LO mode at $482\,cm^{-1}$ for the ordinary ray. In randomly oriented materials, a reflection band necessarily develops between the two values that cancel the real part of the dielectric response. In other words, there is necessarily a maximum between two minima of the dielectric response. In Ref. [12], the optical constants are calculated by Kramers–Kronig relations.

In single crystals, the dielectric function can be modeled. As soon as a dielectric function model fits the infrared reflectivity, one may deduce the optical constants more accurately than with a Kramers–Kronig analysis. The absorption coefficient is found to be extremely high. The penetration depth of the infrared radiation is found currently smaller than 1 μm at a peak corresponding to a normal vibrational mode. As a result, the infrared beam in these spectral regions probes the surface of the sample rather than the bulk. The result is then very sensitive to the alterations of the crystal surface, as shown by various authors. Conversely, in the vicinity of vibrational-mode frequencies, the results reflect bulk properties on etched surfaces or annealed crystals. This is also true far from normal modes, because then the penetration depth of the infrared beam is much larger. Disorder or alteration of the sample surface increases mode damping and therefore lowers the reflectivity level. The higher the reflectivity, the better is the sample quality generally. Note that fitting the spectra minimizes the spurious effects of the surface (by comparison with a Kramers–Kronig

analysis) because the damping is averaged over a wide spectral range (with larger penetration depth on average) in the former case, instead of being determined too near the mode frequency where disorder may alter the result.

Barker [9] fitted his spectra with the dielectric-function model

$$\varepsilon = \varepsilon_\infty + \sum_j \Delta\varepsilon_j \frac{\Omega_{j\mathrm{TO}}^2}{\Omega_{j\mathrm{TO}}^2 - \omega^2 + i\gamma_{j\mathrm{TO}}\omega}. \tag{1}$$

Here $\varepsilon$ stands for the dielectric function, $\varepsilon_\infty$ is the high-frequency dielectric constant, $\Delta\varepsilon$, $\Omega$, and $\gamma$ are the oscillator strength, the frequency, and the damping of the $j$th TO (transverse optic) mode, respectively. Results have been used to calculate the $n$ and $k$ data given in Table I.

A factorization over poles and zeros of the dielectric response in the form

$$\varepsilon = \varepsilon_\infty \prod_j \frac{\Omega_{j\mathrm{LO}}^2 - \omega^2 + i_{j\mathrm{LO}}\omega}{\Omega_{j\mathrm{TO}}^2 - \omega^2 + i\gamma_{j\mathrm{TO}}\omega} \tag{2}$$

was preferred in Refs. [10] and [11]. Here the index LO refers to longitudinal optic modes. The reason invoked by the authors is that in highly polar systems where the coulombic field splits the polar modes into transverse and longitudinal components (one being possibly twice more energetic than the other), phonons have very different decays, and mode damping is possibly very different. Conversely, identical dampings are implicitly assumed for the TO and LO components by the model in Eq. 1. Results deduced from the fit to the reflectivity data with the dielectric-function model in Eq. 2 are compared with those of Barker [9] in Table I. Data are given for the electric field of infrared radiation polarized perpendicular (ordinary ray) and parallel (extraordinary ray) to the crystal $c$ axis. The overall agreement is good. Discrepancies appear in the regions of poor fitting in Eq. 1 and mainly near highly polar TO modes, where surface effects limit the penetration depth of the infrared radiation, thus giving less-sharp peaks for $n$ and $k$. Note that this fitting procedure yields better agreement to the data near the normal vibrational modes, but results far from the resonances are less reliable than those calculated with Eq. (1).

Also included in Table I are the data given in [12] for a polycrystalline sample of hot-pressed 99.9% alumina. These data have been deduced by the author of the measurements via a Kramers–Kronig analysis of his reflectivity data.

**REFERENCES**

1. H. J. Hagemann, W. Gudat, and C. Kunz, *J. Opt. Soc. Am.* **65**, 742 (1975); DESY SR-74/7 (Hamburg, 1974).
2. G. Hass, W. R. Hunter, and R. Tousey, *J. Opt. Soc. Am.* **47**, 1070 (1957).
3. W. R. Hunter, *J. Opt. Soc. Am.* **54**, 15 (1964).
4. W. A. Fomichev and A. S. Parobets, *Opt. Spectrosc.* **21**, 419 (1966).
5. V. A. Fomichev, *Sov. Phys.-Solid State* **8**, 2312 (1967).
6. E. W. J. Mitchell, J. D. Ridgen, and P. D. Townsend, *Phil. Mag.* **5**, 1013 (1960).
7. P. W. Levy, *Phys. Rev.* **123**, 1226 (1961).
8. I. H. Malitson, F. V. Murphy, and W. S. Rodeny, *J. Opt. Soc. Am.* **48**, 72 (1958).
9. A. S. Barker, *Phys. Rev.* **132**, 1474 (1963).
10. F. Gervais and B. Piriou, *J. Phys. C.-Solid St. Phys.* **7**, 2374 (1974).
11. F. Gervais, D. Billard, and B. Piriou, *Revue Internationale des Hautes Températures et des Réfractaires* **12**, 58 (1975).
12. C. A. Worrell, *J. Mat. Science* **21**, 781 (1986).

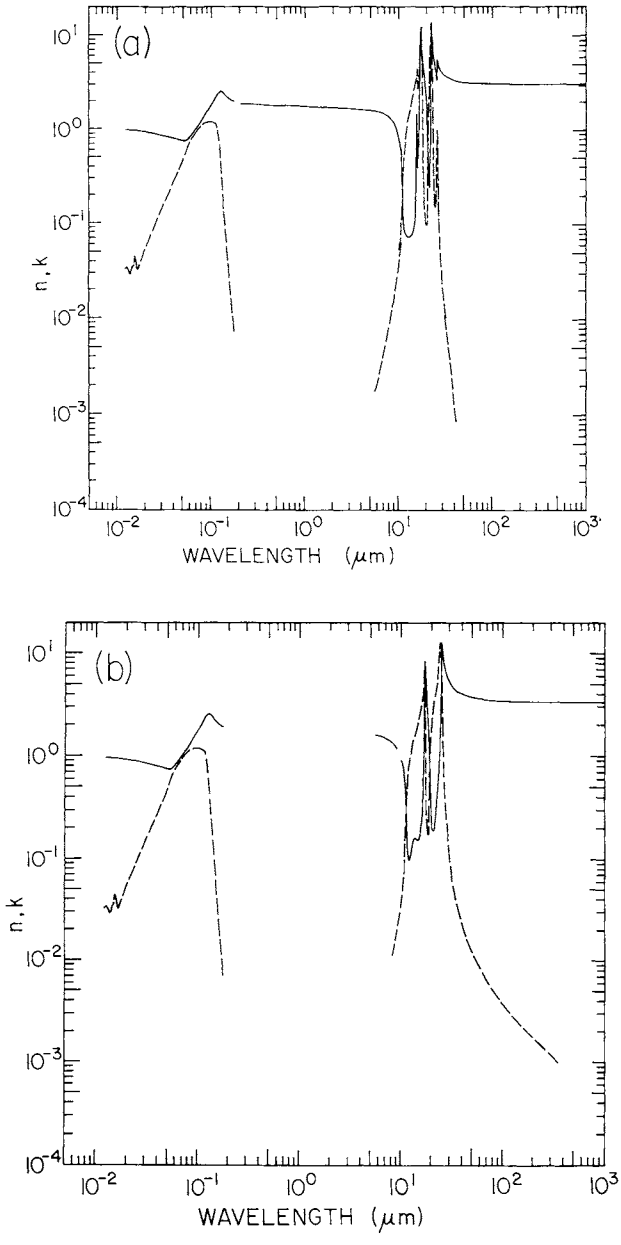


**Fig. 1.** (a) Log–log plot of $n_o$ (solid line) and $k_o$ (dashed line) versus wavelength in micrometers for aluminum oxide. (b) Log–log plot of $n_e$ (solid line) and $k_e$ (dashed line) versus wavelength in micrometers.

**TABLE I**

**Values of *n* and *k* for Aluminum Oxide Obtained from Various References[a]**

| eV | $cm^{-1}$ | μm | n | k | $n_{\perp}$ | $k_{\perp}$ | $n_{\perp}$ | $k_{\perp}$ | $n_{\parallel}$ | $k_{\parallel}$ | $n_{\parallel}$ | $k_{\parallel}$ |
|---|---|---|---|---|---|---|---|---|---|---|---|---|
| 100.0 | 806,452 | 0.01240 | 0.967 | 0.033[1] | | | | | | | | |
| 99.0 | 798,387 | 0.01252 | 0.968 | 0.034 | | | | | | | | |
| 98.0 | 790,323 | 0.01265 | 0.968 | 0.034 | | | | | | | | |
| 97.0 | 782,258 | 0.01278 | 0.968 | 0.034 | | | | | | | | |
| 96.0 | 774,194 | 0.01292 | 0.969 | 0.033 | | | | | | | | |
| 95.0 | 766,129 | 0.01305 | 0.969 | 0.033 | | | | | | | | |
| 94.0 | 758,065 | 0.01319 | 0.970 | 0.032 | | | | | | | | |
| 93.0 | 750,000 | 0.01333 | 0.969 | 0.032 | | | | | | | | |
| 92.0 | 741,935 | 0.01348 | 0.968 | 0.031 | | | | | | | | |
| 91.0 | 733,871 | 0.01363 | 0.968 | 0.030 | | | | | | | | |
| 90.0 | 725,806 | 0.01378 | 0.967 | 0.029 | | | | | | | | |
| 89.0 | 717,742 | 0.01393 | 0.966 | 0.029 | | | | | | | | |
| 88.0 | 709,677 | 0.01409 | 0.965 | 0.030 | | | | | | | | |
| 87.0 | 701,613 | 0.01425 | 0.963 | 0.031 | | | | | | | | |
| 86.0 | 693,548 | 0.01442 | 0.962 | 0.032 | | | | | | | | |
| 85.0 | 685,484 | 0.01459 | 0.961 | 0.033 | | | | | | | | |
| 84.0 | 677,419 | 0.01476 | 0.960 | 0.034 | | | | | | | | |
| 83.0 | 669,355 | 0.01494 | 0.959 | 0.035 | | | | | | | | |
| 82.0 | 661,290 | 0.01512 | 0.958 | 0.035 | | | | | | | | |
| 81.0 | 653,226 | 0.01531 | 0.955 | 0.037 | | | | | | | | |
| 80.0 | 645,161 | 0.01550 | 0.956 | 0.044 | | | | | | | | |
| 79.0 | 637,097 | 0.01570 | 0.958 | 0.042 | | | | | | | | |
| 78.0 | 629,032 | 0.01590 | 0.960 | 0.040 | | | | | | | | |
| 77.0 | 620,968 | 0.01610 | 0.961 | 0.038 | | | | | | | | |
| 76.0 | 612,903 | 0.01632 | 0.963 | 0.035 | | | | | | | | |
| 75.0 | 604,839 | 0.01653 | 0.960 | 0.030 | | | | | | | | |
| 74.0 | 596,774 | 0.01676 | 0.957 | 0.032 | | | | | | | | |
| 73.0 | 588,710 | 0.01700 | 0.954 | 0.033 | | | | | | | | |
| 72.0 | 580,645 | 0.01722 | 0.952 | 0.034 | | | | | | | | |
| 71.0 | 572,581 | 0.01746 | 0.949 | 0.036 | | | | | | | | |

**TABLE I** *(Continued)*

**Aluminum Oxide**

| eV | $cm^{-1}$ | μm | n | k | $n_\perp$ | $k_\perp$ | $n_\perp$ | $k_\perp$ | $n_{\|\|}$ | $k_{\|\|}$ | $n_{\|\|}$ | $k_{\|\|}$ |
|---|---|---|---|---|---|---|---|---|---|---|---|---|
| 70.0 | 564,516 | 0.01771 | 0.946 | 0.037 | | | | | | | | |
| 69.0 | 556,452 | 0.01797 | 0.944 | 0.038 | | | | | | | | |
| 68.0 | 548,387 | 0.01824 | 0.941 | 0.040 | | | | | | | | |
| 67.0 | 540,323 | 0.01851 | 0.938 | 0.041 | | | | | | | | |
| 66.0 | 532,258 | 0.01879 | 0.935 | 0.042 | | | | | | | | |
| 65.0 | 524,194 | 0.01908 | 0.933 | 0.044 | | | | | | | | |
| 64.0 | 516,129 | 0.01937 | 0.930 | 0.046 | | | | | | | | |
| 63.0 | 508,065 | 0.01968 | 0.928 | 0.048 | | | | | | | | |
| 62.0 | 500,000 | 0.02000 | 0.925 | 0.049 | | | | | | | | |
| 61.0 | 491,935 | 0.02033 | 0.923 | 0.051 | | | | | | | | |
| 60.0 | 483,871 | 0.02067 | 0.920 | 0.053 | | | | | | | | |
| 59.0 | 475,806 | 0.02102 | 0.917 | 0.056 | | | | | | | | |
| 58.0 | 467,742 | 0.02138 | 0.914 | 0.060 | | | | | | | | |
| 57.0 | 459,677 | 0.02175 | 0.911 | 0.063 | | | | | | | | |
| 56.0 | 451,613 | 0.02214 | 0.908 | 0.067 | | | | | | | | |
| 55.0 | 443,548 | 0.02255 | 0.905 | 0.070 | | | | | | | | |
| 54.0 | 435,484 | 0.02296 | 0.902 | 0.074 | | | | | | | | |
| 53.0 | 427,419 | 0.02340 | 0.899 | 0.077 | | | | | | | | |
| 52.0 | 419,355 | 0.02385 | 0.895 | 0.081 | | | | | | | | |
| 51.0 | 411,290 | 0.02431 | 0.892 | 0.085 | | | | | | | | |
| 50.0 | 403,226 | 0.02480 | 0.889 | 0.088 | | | | | | | | |
| 49.0 | 395,161 | 0.02531 | 0.886 | 0.092 | | | | | | | | |
| 48.0 | 387,097 | 0.02583 | 0.883 | 0.095 | | | | | | | | |
| 47.0 | 379,032 | 0.02638 | 0.879 | 0.102 | | | | | | | | |
| 46.0 | 370,968 | 0.02696 | 0.875 | 0.109 | | | | | | | | |
| 45.0 | 362,903 | 0.02756 | 0.871 | 0.115 | | | | | | | | |
| 44.0 | 354,839 | 0.02818 | 0.866 | 0.122 | | | | | | | | |
| 43.0 | 346,774 | 0.02884 | 0.862 | 0.129 | | | | | | | | |
| 42.0 | 338,710 | 0.02952 | 0.858 | 0.136 | | | | | | | | |
| 41.0 | 330,645 | 0.03024 | 0.854 | 0.143 | | | | | | | | |

**TABLE I (*Continued*)**

**Aluminum Oxide**

| eV | $cm^{-1}$ | μm | n | k | $n_{\perp}$ | $k_{\perp}$ | $n_{\perp}$ | $k_{\perp}$ | $n_{\parallel}$ | $k_{\parallel}$ | $n_{\parallel}$ | $k_{\parallel}$ |
|---|---|---|---|---|---|---|---|---|---|---|---|---|
| 40.0 | 322,581 | 0.03100 | 0.850 | 0.150 | | | | | | | | |
| 39.0 | 314,516 | 0.03179 | 0.845 | 0.159 | | | | | | | | |
| 38.0 | 306,452 | 0.03263 | 0.839 | 0.171 | | | | | | | | |
| 37.0 | 298,387 | 0.03351 | 0.834 | 0.182 | | | | | | | | |
| 36.0 | 290,323 | 0.03444 | 0.828 | 0.194 | | | | | | | | |
| 35.0 | 282,258 | 0.03543 | 0.823 | 0.205 | | | | | | | | |
| 34.0 | 274,194 | 0.03647 | 0.817 | 0.217 | | | | | | | | |
| 33.0 | 266,129 | 0.03758 | 0.812 | 0.229 | | | | | | | | |
| 32.0 | 258,065 | 0.03875 | 0.805 | 0.248 | | | | | | | | |
| 31.0 | 250,000 | 0.04000 | 0.798 | 0.266 | | | | | | | | |
| 30.0 | 241,935 | 0.04133 | 0.791 | 0.285 | | | | | | | | |
| 29.0 | 233,871 | 0.04276 | 0.782 | 0.307 | | | | | | | | |
| 28.0 | 225,806 | 0.04429 | 0.774 | 0.330 | | | | | | | | |
| 27.0 | 217,742 | 0.04593 | 0.762 | 0.362 | | | | | | | | |
| 26.0 | 209,677 | 0.04769 | 0.750 | 0.395 | | | | | | | | |
| 25.0 | 201,613 | 0.04960 | 0.737 | 0.436 | | | | | | | | |
| 24.0 | 193,548 | 0.05167 | 0.730 | 0.500 | | | | | | | | |
| 23.0 | 185,484 | 0.05391 | 0.737 | 0.574 | | | | | | | | |
| 22.0 | 177,419 | 0.05636 | 0.764 | 0.651 | | | | | | | | |
| 21.0 | 169,355 | 0.05905 | 0.805 | 0.725 | | | | | | | | |
| 20.0 | 161,290 | 0.06200 | 0.856 | 0.774 | | | | | | | | |
| 19.0 | 153,226 | 0.06526 | 0.896 | 0.832 | | | | | | | | |
| 18.0 | 145,161 | 0.06889 | 0.953 | 0.916 | | | | | | | | |
| 17.0 | 137,097 | 0.07294 | 1.037 | 0.998 | | | | | | | | |
| 16.0 | 129,032 | 0.07750 | 1.149 | 1.078 | | | | | | | | |
| 15.0 | 120,968 | 0.08267 | 1.297 | 1.135 | | | | | | | | |
| 14.0 | 112,903 | 0.08857 | 1.465 | 1.166 | | | | | | | | |
| 13.0 | 104,839 | 0.09538 | 1.657 | 1.179 | | | | | | | | |
| 12.0 | 96,774 | 0.1033 | 1.885 | 1.171 | | | | | | | | |
| 11.0 | 88,710 | 0.1127 | 2.231 | 1.109 | | | | | | | | |

**TABLE I (*Continued*)**

**Aluminum Oxide**

| eV | $cm^{-1}$ | μm | n | k | $n_\perp$ | $k_\perp$ | $n_\perp$ | $k_\perp$ | $n_\parallel$ | $k_\parallel$ | $n_\parallel$ | $k_\parallel$ |
|---|---|---|---|---|---|---|---|---|---|---|---|---|
| 10.0 | 80,645 | 0.1240 | 2.519 | 0.629 | | | | | | | | |
| 9.0 | 72,581 | 0.1378 | 2.338 | 0.108 | | | | | | | | |
| 8.0 | 64,516 | 0.1550 | 2.074 | 0.032 | | | | | | | | |
| 7.0 | 56,452 | 0.1771 | 1.939 | 0.007 | | | | | | | | |
| 6.0 | 48,387 | 0.2067 | | | 1.834[8] | | | | | | | |
| 5.9 | 47,581 | 0.2102 | | | 1.834 | | | | | | | |
| 5.8 | 46,774 | 0.2138 | | | 1.834 | | | | | | | |
| 5.7 | 45,968 | 0.2175 | | | 1.834 | | | | | | | |
| 5.6 | 45,161 | 0.2214 | | | 1.834 | | | | | | | |
| 5.5 | 44,355 | 0.2255 | | | 1.834 | | | | | | | |
| 5.4 | 43,548 | 0.2296 | | | 1.834 | | | | | | | |
| 5.3 | 42,742 | 0.2340 | | | 1.834 | | | | | | | |
| 5.2 | 41,935 | 0.2385 | | | 1.834 | | | | | | | |
| 5.1 | 41,129 | 0.2431 | | | 1.834 | | | | | | | |
| 5.0 | 40,323 | 0.2480 | | | 1.834 | | | | | | | |
| 4.9 | 39,516 | 0.2531 | | | 1.834 | | | | | | | |
| 4.8 | 38,710 | 0.2583 | | | 1.834 | | | | | | | |
| 4.7 | 37,903 | 0.2638 | | | 1.834 | | | | | | | |
| 4.6 | 37,097 | 0.2696 | | | 1.831 | | | | | | | |
| 4.5 | 36,290 | 0.2756 | | | 1.827 | | | | | | | |
| 4.4 | 35,484 | 0.2818 | | | 1.823 | | | | | | | |
| 4.3 | 34,677 | 0.2884 | | | 1.820 | | | | | | | |
| 4.2 | 33,871 | 0.2952 | | | 1.817 | | | | | | | |
| 4.1 | 33,065 | 0.3024 | | | 1.813 | | | | | | | |
| 4.0 | 32,258 | 0.3100 | | | 1.810 | | | | | | | |
| 3.9 | 31,452 | 0.3179 | | | 1.807 | | | | | | | |
| 3.8 | 30,645 | 0.3263 | | | 1.804 | | | | | | | |
| 3.7 | 29,839 | 0.3351 | | | 1.801 | | | | | | | |
| 3.6 | 29,032 | 0.3444 | | | 1.799 | | | | | | | |
| 3.5 | 28,226 | 0.3543 | | | 1.796 | | | | | | | |

**TABLE I (*Continued*)**

**Aluminum Oxide**

| eV | $cm^{-1}$ | μm | n | k | $n_{\perp}$ | $k_{\perp}$ | $n_{\perp}$ | $k_{\perp}$ | $n_{\parallel}$ | $k_{\parallel}$ | $n_{\parallel}$ | $k_{\parallel}$ |
|---|---|---|---|---|---|---|---|---|---|---|---|---|
| 3.4 | 27,419 | 0.3647 | | | 1.794 | | | | | | | |
| 3.3 | 26,613 | 0.3758 | | | 1.791 | | | | | | | |
| 3.2 | 25,806 | 0.3875 | | | 1.789 | | | | | | | |
| 3.1 | 25,000 | 0.4000 | | | 1.787 | | | | | | | |
| 3.0 | 24,194 | 0.4133 | | | 1.784 | | | | | | | |
| 2.9 | 23,387 | 0.4276 | | | 1.782 | | | | | | | |
| 2.8 | 22,581 | 0.4429 | | | 1.780 | | | | | | | |
| 2.7 | 21,774 | 0.4593 | | | 1.779 | | | | | | | |
| 2.6 | 20,968 | 0.4769 | | | 1.777 | | | | | | | |
| 2.5 | 20,161 | 0.4960 | | | 1.775 | | | | | | | |
| 2.4 | 19,355 | 0.5167 | | | 1.773 | | | | | | | |
| 2.3 | 18,548 | 0.5391 | | | 1.771 | | | | | | | |
| 2.2 | 17,742 | 0.5636 | | | 1.770 | | | | | | | |
| 2.1 | 16,935 | 0.5905 | | | 1.768 | | | | | | | |
| 2.0 | 16,129 | 0.6200 | | | 1.767 | | | | | | | |
| 1.9 | 15,323 | 0.6526 | | | 1.765 | | | | | | | |
| 1.8 | 14,516 | 0.6889 | | | 1.764 | | | | | | | |
| 1.7 | 13,710 | 0.7294 | | | 1.762 | | | | | | | |
| 1.6 | 12,903 | 0.7750 | | | 1.761 | | | | | | | |
| 1.5 | 12,097 | 0.8267 | | | 1.759 | | | | | | | |
| 1.4 | 11,290 | 0.8857 | | | 1.758 | | | | | | | |
| 1.3 | 10,484 | 0.9538 | | | 1.757 | | | | | | | |
| 1.2 | 9,677 | 1.033 | | | 1.755 | | | | | | | |
| 1.1 | 8,871 | 1.127 | | | 1.753 | | | | | | | |
| 1.0 | 8,065 | 1.240 | | | 1.751 | | | | | | | |
| 0.9 | 7,258 | 1.378 | | | 1.749 | | | | | | | |
| 0.8 | 6,452 | 1.550 | | | 1.746 | | | | | | | |
| 0.7 | 5,645 | 1.771 | | | 1.742 | | | | | | | |
| 0.6 | 4,839 | 2.067 | | | 1.736 | | | | | | | |
| 0.5 | 4,032 | 2.480 | | | 1.726 | | | | | | | |

**TABLE I (*Continued*)**

**Aluminum Oxide**

| eV | $cm^{-1}$ | μm | n | k | $n_\perp$ | $k_\perp$ | $n_\perp$ | $k_\perp$ | $n_{\|\|}$ | $k_{\|\|}$ | $n_{\|\|}$ | $k_{\|\|}$ |
|---|---|---|---|---|---|---|---|---|---|---|---|---|
| 0.48 | 3,900 | 2.564 | | | 1.723 | | | | | | | |
| 0.47 | 3,800 | 2.632 | | | 1.721 | | | | | | | |
| 0.46 | 3,700 | 2.703 | | | 1.719 | | | | | | | |
| 0.45 | 3,600 | 2.778 | | | 1.716 | | | | | | | |
| 0.43 | 3,500 | 2.857 | | | 1.714 | | | | | | | |
| 0.42 | 3,400 | 2.941 | | | 1.712 | | | | | | | |
| 0.41 | 3,300 | 3.030 | | | 1.709 | | | | | | | |
| 0.40 | 3,200 | 3.125 | | | 1.707 | | | | | | | |
| 0.38 | 3,100 | 3.226 | | | 1.705 | | | | | | | |
| 0.37 | 3,000 | 3.333 | | | 1.701 | | | | | | | |
| 0.36 | 2,900 | 3.448 | | | 1.697 | | | | | | | |
| 0.35 | 2,800 | 3.571 | | | 1.692 | | | | | | | |
| 0.33 | 2,700 | 3.704 | | | 1.687 | | | | | | | |
| 0.32 | 2,600 | 3.846 | | | 1.681 | | | | | | | |
| 0.31 | 2,500 | 4.000 | | | 1.674 | | | | | | | |
| 0.30 | 2,400 | 4.167 | | | 1.667 | | | | | | | |
| 0.29 | 2,300 | 4.348 | | | 1.658 | | | | | | | |
| 0.27 | 2,200 | 4.545 | | | 1.647 | | | | | | | |
| 0.26 | 2,100 | 4.762 | | | 1.636 | | | | | | | |
| 0.25 | 2,000 | 5.000 | | | 1.624 | | | | | | | |
| 0.24 | 1,900 | 5.263 | | | 1.607 | | | | | | | |
| 0.2232 | 1,800 | 5.556 | | | 1.624[9] | 0.002[9] | | | 1.594[9] | 0.002[9] | | |
| 0.2108 | 1,700 | 5.882 | | | 1.600 | 0.002 | | | 1.571 | 0.003 | | |
| 0.1984 | 1,600 | 6.250 | | | 1.571 | 0.003 | | | 1.542 | 0.004 | | |
| 0.1860 | 1,500 | 6.667 | | | 1.534 | 0.004 | | | 1.506 | 0.004 | | |
| 0.1736 | 1,400 | 7.143 | | | 1.485 | 0.005 | | | 1.459 | 0.006 | | |
| 0.1612 | 1,300 | 7.692 | | | 1.419 | 0.007 | | | 1.396 | 0.008 | | |
| 0.1488 | 1,200 | 8.333 | | | 1.325 | 0.011 | | | 1.307 | 0.011 | | |
| 0.1364 | 1,100 | 9.091 | | | 1.181 | 0.017 | | | 1.174 | 0.018 | | |
| 0.1240 | 1,000 | 10.00 | 0.907[12] | 0.003[12] | 0.925 | 0.034 | 0.877[10] | 0.053[10] | 0.950 | 0.033 | 0.935[11] | 0.037[11] |

**TABLE I** (*Continued*)

**Aluminum Oxide**

| eV | $cm^{-1}$ | μm | n | k | $n_{\perp}$ | $k_{\perp}$ | $n_{\perp}$ | $k_{\perp}$ | $n_{\parallel}$ | $k_{\parallel}$ | $n_{\parallel}$ | $k_{\parallel}$ |
|---|---|---|---|---|---|---|---|---|---|---|---|---|
| 0.1228 | 990 | 10.10 | 0.875 | 0.003 | 0.888 | 0.037 | 0.839 | 0.057 | 0.918 | 0.035 | 0.904 | 0.039 |
| 0.1215 | 980 | 10.20 | 0.831 | 0.003 | 0.847 | 0.041 | 0.796 | 0.062 | 0.884 | 0.038 | 0.869 | 0.042 |
| 0.1203 | 970 | 10.31 | 0.770 | 0.003 | 0.801 | 0.045 | 0.749 | 0.068 | 0.846 | 0.042 | 0.832 | 0.045 |
| 0.1190 | 960 | 10.42 | 0.709 | 0.003 | 0.750 | 0.051 | 0.696 | 0.075 | 0.805 | 0.046 | 0.791 | 0.049 |
| 0.1178 | 950 | 10.53 | 0.648 | 0.021 | 0.693 | 0.058 | 0.636 | 0.084 | 0.759 | 0.051 | 0.745 | 0.054 |
| 0.1166 | 940 | 10.64 | 0.576 | 0.041 | 0.627 | 0.067 | 0.566 | 0.097 | 0.709 | 0.057 | 0.694 | 0.061 |
| 0.1153 | 930 | 10.75 | 0.499 | 0.088 | 0.550 | 0.081 | 0.484 | 0.117 | 0.651 | 0.066 | 0.636 | 0.069 |
| 0.1141 | 920 | 10.87 | 0.423 | 0.145 | 0.456 | 0.103 | 0.384 | 0.153 | 0.585 | 0.077 | 0.569 | 0.081 |
| 0.1128 | 910 | 10.99 | 0.344 | 0.228 | 0.340 | 0.147 | 0.270 | 0.224 | 0.507 | 0.093 | 0.489 | 0.098 |
| 0.1116 | 900 | 11.11 | 0.263 | 0.339 | 0.213 | 0.249 | 0.182 | 0.344 | 0.413 | 0.121 | 0.392 | 0.128 |
| 0.1104 | 890 | 11.24 | 0.180 | 0.449 | 0.143 | 0.393 | 0.138 | 0.468 | 0.298 | 0.176 | 0.276 | 0.192 |
| 0.1091 | 880 | 11.36 | 0.125 | 0.541 | 0.115 | 0.522 | 0.116 | 0.579 | 0.193 | 0.288 | 0.181 | 0.312 |
| 0.1079 | 870 | 11.49 | 0.109 | 0.629 | 0.101 | 0.634 | 0.103 | 0.680 | 0.140 | 0.419 | 0.136 | 0.440 |
| 0.1066 | 860 | 11.63 | 0.113 | 0.717 | 0.093 | 0.737 | 0.094 | 0.774 | 0.117 | 0.535 | 0.116 | 0.553 |
| 0.1054 | 850 | 11.77 | 0.114 | 0.797 | 0.088 | 0.834 | 0.087 | 0.864 | 0.104 | 0.639 | 0.106 | 0.655 |
| 0.1042 | 840 | 11.91 | 0.115 | 0.877 | 0.085 | 0.927 | 0.083 | 0.951 | 0.096 | 0.734 | 0.101 | 0.750 |
| 0.1029 | 830 | 12.05 | 0.116 | 0.957 | 0.083 | 1.017 | 0.079 | 1.037 | 0.092 | 0.825 | 0.099 | 0.840 |
| 0.1017 | 820 | 12.20 | 0.116 | 1.036 | 0.083 | 1.107 | 0.077 | 1.122 | 0.089 | 0.912 | 0.100 | 0.927 |
| 0.1004 | 810 | 12.35 | 0.117 | 1.116 | 0.083 | 1.197 | 0.075 | 1.208 | 0.087 | 0.998 | 0.103 | 1.011 |
| 0.09920 | 800 | 12.50 | 0.118 | 1.197 | 0.084 | 1.287 | 0.074 | 1.294 | 0.086 | 1.083 | 0.108 | 1.095 |
| 0.09796 | 790 | 12.66 | 0.119 | 1.278 | 0.085 | 1.379 | 0.073 | 1.383 | 0.086 | 1.167 | 0.115 | 1.177 |
| 0.09672 | 780 | 12.82 | 0.119 | 1.360 | 0.088 | 1.473 | 0.072 | 1.473 | 0.087 | 1.253 | 0.124 | 1.258 |
| 0.09548 | 770 | 12.99 | 0.120 | 1.441 | 0.090 | 1.571 | 0.072 | 1.567 | 0.089 | 1.340 | 0.134 | 1.338 |
| 0.09424 | 760 | 13.16 | 0.121 | 1.537 | 0.094 | 1.672 | 0.072 | 1.664 | 0.091 | 1.430 | 0.143 | 1.417 |
| 0.09300 | 750 | 13.33 | 0.121 | 1.637 | 0.099 | 1.778 | 0.073 | 1.766 | 0.094 | 1.523 | 0.152 | 1.495 |
| 0.09176 | 740 | 13.51 | 0.122 | 1.736 | 0.104 | 1.890 | 0.074 | 1.873 | 0.098 | 1.620 | 0.157 | 1.575 |
| 0.09052 | 730 | 13.70 | 0.122 | 1.836 | 0.111 | 2.010 | 0.076 | 1.988 | 0.102 | 1.721 | 0.159 | 1.659 |
| 0.08928 | 720 | 13.89 | 0.124 | 1.947 | 0.120 | 2.138 | 0.078 | 2.110 | 0.108 | 1.830 | 0.159 | 1.749 |
| 0.08804 | 710 | 14.09 | 0.126 | 2.058 | 0.131 | 2.278 | 0.080 | 2.243 | 0.116 | 1.946 | 0.156 | 1.848 |
| 0.08680 | 700 | 14.29 | 0.129 | 2.169 | 0.145 | 2.433 | 0.083 | 2.389 | 0.127 | 2.073 | 0.154 | 1.958 |

**TABLE I (*Continued*)**

**Aluminum Oxide**

| eV | $cm^{-1}$ | μm | n | k | $n_\perp$ | $k_\perp$ | $n_\perp$ | $k_\perp$ | $n_{\parallel}$ | $k_{\parallel}$ | $n_{\parallel}$ | $k_{\parallel}$ |
|---|---|---|---|---|---|---|---|---|---|---|---|---|
| 0.08556 | 690 | 14.49 | 0.131 | 2.296 | 0.165 | 2.607 | 0.088 | 2.552 | 0.141 | 2.214 | 0.153 | 2.080 |
| 0.08432 | 680 | 14.71 | 0.142 | 2.441 | 0.192 | 2.807 | 0.094 | 2.739 | 0.164 | 2.375 | 0.153 | 2.216 |
| 0.08308 | 670 | 14.93 | 0.167 | 2.585 | 0.236 | 3.047 | 0.102 | 2.961 | 0.211 | 2.568 | 0.156 | 2.371 |
| 0.08184 | 660 | 15.15 | 0.192 | 2.811 | 0.317 | 3.350 | 0.118 | 3.243 | 0.358 | 2.782 | 0.163 | 2.547 |
| 0.08060 | 650 | 15.39 | 0.251 | 3.175 | 0.516 | 3.761 | 0.164 | 3.657 | 0.465 | 2.722 | 0.175 | 2.754 |
| 0.07936 | 640 | 15.63 | 0.807 | 3.642 | 1.222 | 4.181 | 0.580 | 4.557 | 0.329 | 2.951 | 0.194 | 3.004 |
| 0.07812 | 630 | 15.87 | 0.502 | 3.040 | 1.718 | 3.157 | 1.482 | 2.767 | 0.350 | 3.298 | 0.227 | 3.319 |
| 0.07688 | 620 | 16.13 | 0.361 | 3.479 | 0.852 | 3.306 | 0.474 | 3.564 | 0.449 | 3.720 | 0.286 | 3.740 |
| 0.07564 | 610 | 16.39 | 0.377 | 4.082 | 0.698 | 4.006 | 0.410 | 4.284 | 0.662 | 4.287 | 0.405 | 4.359 |
| 0.07440 | 600 | 16.67 | 0.516 | 4.784 | 0.841 | 4.789 | 0.491 | 5.099 | 1.178 | 5.123 | 0.725 | 5.428 |
| 0.07316 | 590 | 16.95 | 2.155 | 5.601 | 1.298 | 5.810 | 0.747 | 6.301 | 2.818 | 6.198 | 2.371 | 7.855 |
| 0.07192 | 580 | 17.24 | 4.935 | 7.345 | 2.636 | 7.240 | 1.690 | 8.614 | 5.915 | 4.426 | 8.501 | 3.269 |
| 0.07068 | 570 | 17.54 | 6.713 | 5.552 | 6.570 | 7.320 | 10.257 | 11.277 | 5.185 | 1.755 | 5.363 | 0.678 |
| 0.06944 | 560 | 17.86 | 7.407 | 0.816 | 7.683 | 3.150 | 9.100 | 1.534 | 4.066 | 0.949 | 3.959 | 0.313 |
| 0.06820 | 550 | 18.18 | 5.406 | 0.487 | 6.256 | 1.432 | 6.548 | 0.507 | 3.265 | 0.673 | 3.106 | 0.206 |
| 0.06696 | 540 | 18.52 | 4.391 | 0.378 | 5.206 | 0.865 | 5.280 | 0.255 | 2.631 | 0.580 | 2.449 | 0.174 |
| 0.06572 | 530 | 18.87 | 3.526 | 0.350 | 4.455 | 0.635 | 4.456 | 0.158 | 2.061 | 0.595 | 1.837 | 0.186 |
| 0.06448 | 520 | 19.23 | 2.722 | 0.357 | 3.856 | 0.545 | 3.817 | 0.115 | 1.488 | 0.738 | 1.126 | 0.278 |
| 0.06324 | 510 | 19.61 | 2.089 | 0.584 | 3.318 | 0.544 | 3.243 | 0.099 | 0.959 | 1.121 | 0.342 | 0.932 |
| 0.06200 | 500 | 20.00 | 1.674 | 1.002 | 2.774 | 0.642 | 2.636 | 0.106 | 0.680 | 1.660 | 0.213 | 1.644 |
| 0.06076 | 490 | 20.41 | 1.035 | 1.366 | 2.170 | 0.930 | 1.830 | 0.163 | 0.582 | 2.161 | 0.187 | 2.168 |
| 0.05952 | 480 | 20.83 | 0.312 | 1.879 | 1.620 | 1.635 | 0.380 | 1.028 | 0.563 | 2.627 | 0.186 | 2.636 |
| 0.05828 | 470 | 21.28 | 0.255 | 2.826 | 1.521 | 2.697 | 0.241 | 2.622 | 0.591 | 3.091 | 0.201 | 3.103 |
| 0.05704 | 460 | 21.74 | 0.337 | 3.910 | 1.989 | 3.903 | 0.323 | 4.155 | 0.663 | 3.586 | 0.229 | 3.606 |
| 0.05580 | 450 | 22.22 | 0.765 | 5.591 | 3.501 | 5.065 | 0.730 | 6.677 | 0.792 | 4.145 | 0.279 | 4.186 |
| 0.05456 | 440 | 22.73 | 5.581 | 8.162 | 6.125 | 4.255 | 10.079 | 14.014 | 1.016 | 4.813 | 0.363 | 4.906 |
| 0.05332 | 430 | 23.26 | 6.676 | 4.919 | 6.386 | 2.025 | 8.570 | 0.764 | 1.422 | 5.654 | 0.522 | 5.881 |
| 0.05208 | 420 | 23.81 | 6.185 | 2.747 | 5.683 | 1.057 | 6.356 | 0.257 | 2.247 | 6.738 | 0.889 | 7.382 |
| 0.05084 | 410 | 24.39 | 5.710 | 1.893 | 5.102 | 0.699 | 5.356 | 0.152 | 4.148 | 7.894 | 2.161 | 10.225 |
| 0.04960 | 400 | 25.00 | 5.366 | 1.769 | 4.677 | 0.612 | 4.635 | 0.156 | 7.599 | 7.167 | 11.820 | 12.959 |

**TABLE I (*Continued*)**

**Aluminum Oxide**

| eV | $cm^{-1}$ | μm | n | k | $n_{\perp}$ | $k_{\perp}$ | $n_{\perp}$ | $k_{\perp}$ | $n_{\parallel}$ | $k_{\parallel}$ | $n_{\parallel}$ | $k_{\parallel}$ |
|---|---|---|---|---|---|---|---|---|---|---|---|---|
| 0.04836 | 390 | 25.64 | 5.454 | 2.034 | 4.482 | 0.719 | 3.533 | 0.732 | 8.708 | 3.874 | 11.359 | 2.261 |
| 0.04712 | 380 | 26.32 | 5.443 | 0.381 | 4.589 | 0.634 | 5.644 | 0.552 | 7.807 | 1.991 | 8.541 | 0.804 |
| 0.04588 | 370 | 27.03 | 4.942 | 0.213 | 4.485 | 0.378 | 4.774 | 0.097 | 6.927 | 1.180 | 7.178 | 0.422 |
| 0.04464 | 360 | 27.78 | 4.635 | 0.183 | 4.302 | 0.245 | 4.438 | 0.045 | 6.279 | 0.782 | 6.364 | 0.264 |
| 0.04340 | 350 | 28.57 | 4.362 | 0.164 | 4.144 | 0.178 | 4.229 | 0.028 | 5.800 | 0.560 | 5.816 | 0.182 |
| 0.04216 | 340 | 29.41 | 4.152 | 0.144 | 4.015 | 0.139 | 4.075 | 0.020 | 5.436 | 0.422 | 5.417 | 0.133 |
| 0.04092 | 330 | 30.30 | 3.985 | 0.125 | 3.908 | 0.113 | 3.953 | 0.015 | 5.149 | 0.331 | 5.112 | 0.101 |
| 0.03968 | 320 | 31.25 | 3.863 | 0.105 | 3.818 | 0.095 | 3.852 | 0.011 | 4.918 | 0.267 | 4.871 | 0.080 |
| 0.03844 | 310 | 32.26 | 3.758 | 0.089 | 3.740 | 0.082 | 3.767 | 0.009 | 4.727 | 0.221 | 4.674 | 0.064 |
| 0.03720 | 300 | 33.33 | 3.661 | 0.074 | 3.672 | 0.071 | 3.693 | 0.007 | 4.568 | 0.185 | 4.510 | 0.053 |
| 0.03596 | 290 | 34.48 | 3.603 | 0.059 | 3.611 | 0.062 | 3.629 | | 4.431 | 0.158 | 4.371 | 0.044 |
| 0.03472 | 280 | 35.71 | 3.545 | 0.043 | 3.558 | 0.055 | 3.572 | | 4.314 | 0.136 | 4.253 | 0.037 |
| 0.03348 | 270 | 37.04 | 3.501 | 0.028 | 3.510 | 0.049 | 3.521 | | 4.212 | 0.119 | 4.150 | 0.032 |
| 0.03224 | 260 | 38.46 | 3.460 | 0.013 | 3.467 | 0.044 | 3.475 | | 4.123 | 0.104 | 4.060 | 0.027 |
| 0.03100 | 250 | 40.00 | 3.422 | 0.009 | 3.428 | 0.040 | 3.434 | | 4.044 | 0.092 | 3.980 | 0.024 |
| 0.02976 | 240 | 41.67 | | | 3.393 | 0.036 | 3.397 | | 3.973 | 0.082 | 3.910 | 0.021 |
| 0.02852 | 230 | 43.48 | | | 3.361 | 0.033 | 3.363 | | 3.911 | 0.073 | 3.847 | 0.018 |
| 0.02728 | 220 | 45.46 | | | 3.331 | 0.030 | 3.332 | | 3.854 | 0.066 | 3.791 | 0.016 |
| 0.02604 | 210 | 47.62 | | | 3.304 | 0.027 | 3.304 | | 3.804 | 0.059 | 3.741 | 0.014 |
| 0.02480 | 200 | 50.00 | | | 3.280 | 0.025 | 3.279 | | 3.758 | 0.053 | 3.695 | 0.012 |
| 0.02356 | 190 | 52.63 | | | 3.258 | 0.023 | 3.255 | | 3.717 | 0.048 | 3.654 | 0.011 |
| 0.02232 | 180 | 55.56 | | | 3.237 | 0.021 | 3.234 | | 3.680 | 0.043 | 3.617 | 0.010 |
| 0.02108 | 170 | 58.82 | | | 3.218 | 0.019 | 3.214 | | 3.646 | 0.039 | 3.583 | 0.009 |
| 0.01984 | 160 | 62.50 | | | 3.201 | 0.017 | 3.196 | | 3.615 | 0.036 | 3.553 | 0.008 |
| 0.01860 | 150 | 66.67 | | | 3.185 | 0.016 | 3.180 | | 3.588 | 0.032 | 3.525 | 0.007 |
| 0.01736 | 140 | 71.43 | | | 3.171 | 0.014 | 3.165 | | 3.562 | 0.029 | 3.501 | 0.006 |
| 0.01612 | 130 | 76.92 | | | 3.158 | 0.013 | 3.151 | | 3.540 | 0.026 | 3.478 | 0.006 |
| 0.01488 | 120 | 83.33 | | | 3.146 | 0.012 | 3.139 | | 3.519 | 0.023 | 3.458 | 0.005 |
| 0.01364 | 110 | 90.91 | | | 3.135 | 0.011 | 3.128 | | 3.501 | 0.021 | 3.440 | 0.004 |
| 0.01240 | 100 | 100.0 | | | 3.126 | 0.009 | 3.118 | | 3.485 | 0.019 | 3.424 | 0.004 |

**TABLE I (*Continued*)**

**Aluminum Oxide**

| eV | $cm^{-1}$ | μm | n | k | $n_{\perp}$ | $k_{\perp}$ | $n_{\perp}$ | $k_{\perp}$ | $n_{\parallel}$ | $k_{\parallel}$ | $n_{\parallel}$ | $k_{\parallel}$ |
|---|---|---|---|---|---|---|---|---|---|---|---|---|
| 0.01116 | 90 | 111.1 | | | 3.117 | 0.008 | 3.109 | | 3.470 | 0.016 | 3.409 | 0.003 |
| 0.009920 | 80 | 125.0 | | | 3.110 | 0.007 | 3.101 | | 3.458 | 0.014 | 3.397 | 0.003 |
| 0.008680 | 70 | 142.9 | | | 3.103 | 0.006 | 3.095 | | 3.447 | 0.012 | 3.386 | 0.002 |
| 0.007440 | 60 | 166.7 | | | 3.097 | 0.005 | 3.089 | | 3.437 | 0.010 | 3.376 | 0.002 |
| 0.006200 | 50 | 200.0 | | | 3.093 | 0.004 | 3.084 | | 3.429 | 0.009 | 3.369 | 0.002 |
| 0.004960 | 40 | 250.0 | | | 3.089 | 0.004 | 3.080 | | 3.423 | 0.007 | 3.362 | 0.001 |
| 0.003720 | 30 | 333.3 | | | 3.086 | 0.003 | 3.077 | | 3.418 | 0.005 | 3.357 | 0.001 |
| 0.002480 | 20 | 500.0 | | | 3.084 | 0.002 | 3.075 | | 3.415 | 0.003 | 3.354 | 0.001 |
| 0.001240 | 10 | 1000.0 | | | 3.083 | 0.001 | 3.073 | | 3.412 | 0.002 | 3.352 | |

[a] References are indicated in brackets.

# Aluminum Oxynitride (ALON) Spinel

WILLIAM J. TROPF and MICHAEL E. THOMAS
Applied Physics Laboratory
The Johns Hopkins University
Laurel, Maryland

Aluminum oxynitride, or ALON, is a crystal made of various amounts of aluminum oxide and aluminum nitride, with the aluminum-nitride content between 27 and 40 mole-percent. The resulting material, a nitrogen-stabilized cubic aluminum oxide, is face-centered cubic with spinel structure (see "Magnesium Aluminum Spinel," this volume). The lattice parameter of ALON varies from 7.938 (30 mole-percent AlN) to 7.951 (38 mole-percent AlN) [1]. Of particular interest is the composition of ≈35.7 mole-percent, which is equivalent to the composition $5AlN9Al_2O_3$ or $Al_{23}O_{27}N_5$. This composition has a unit cell with lattice parameter of 0.7948 nm [1]. Theoretical density of this composition is 3.71 g/cm$^3$ and melting point is 2323 K [1] to 2438±15 K [2].

Aluminum oxynitride is termed a nonstoichiometric spinel because some cation sites are occupied by vacancies. McCauley [3] proposed a formula of the form

$$Al_{(64+X)/3}\square_{(8-X)/3}O_{32-X}N_X \qquad 0 \leqslant x \leqslant 8, \tag{1}$$

where $x = 0$ corresponds to $\gamma$-alumina, and $x = 8$ is the unstable stoichiometric oxynitride $Al_3O_3N$. The symbol □ denotes cation vacancies. Since ALON exists over the range 27–40 mole-percent AlN, values of $x$ for ALON range from approximately 3.5 to 5.8. When the composition is 35.7 mole-percent AlN ($x = 5$), there is one cation vacancy per unit cell. Neutron-diffraction studies (see [2]) confirm that oxygen and nitrogen occupy the anion sites of the spinel lattice and that aluminum cations occupy both the octahedral and tetrahedral sites of the spinel ($Fd3m$) structure. Corbin [2] implies that the vacancies occur at the octahedral cation sites.

ALON can be produced by a variety of methods, including reaction sintering of alumina and aluminum nitride, simultaneous reduction and nitridation of alumina, combustionlike reaction of aluminum metal with


Copyright © 1991 by Academic Press.
All rights of reproduction in any form reserved.
ISBN 0-12-544422-2

oxygen and nitrogen, and reaction of gases [2]. Commercial optical ALON is made by reacting the raw materials, pressing into near-finished shape, and firing at high temperature to produce a fully dense, transparent ceramic [4]. The resulting high-temperature, high-strength ceramic is used for windows and optical elements where hardness and resistance to harsh environments is important. Property data for ALON are given in the literature [4–7].

ALON is transparent at 0.230 to 5.0 μm. The band gaps of the constituent materials, alumina and aluminum nitride, are 9.9 and 6.0 eV, respectively [8]. From this information we surmise a band gap of 6–7 eV.

Index-of-refraction data for ALON are very sparse. Hartnett and Gentilman give a measured value of 1.793 at 0.589 μm and an estimated value of 1.66 at 4 μm based on reflection loss [4]. Corbin [2] and Hartnett *et al.* [9] give an index of refraction from 1.770 (also see [1]) to 1.785 in the visible (0.55 μm) as the composition increases from 30% to 37.5% AlN.

Precision room-temperature index-of-refraction measurements have also been made by Scheller [10] using a prism supplied by Raytheon. These values were used to construct the following Sellmeier formula:

$$n^2 - 1 = \frac{20.32 \times 10^9}{(97{,}500)^2 - \nu^2} + \frac{1.287 \times 10^6}{(530)^2 - \nu^2}, \tag{2}$$

where $\nu$ is the frequency in wave numbers. This formula is applicable to bulk polycrystalline ALON (37.5% AlN) in the range of 0.4–2.3 μm and duplicates measurements to within ±0.0002.

The dominant loss mechanism in the visible and near-IR transparent region of polycrystalline ALON is scatter. Bulk scatter in polycrystalline ALON is low and decreases with increasing wavelength [4, 5].

Absorption at the IR edge of transparency is dominated by multiphonon absorption. A model of multiphonon absorption for ALON has been developed and validated with experimental data over a wide temperature range [11]. ALON exhibits a two-phonon structure in the 1700–1950 $cm^{-1}$ region that is not adequately represented by this multiphonon model. The fundamental (one-phonon) lattice vibrations occur in the 350–970 $cm^{-1}$ spectral region.

Table I gives the transverse and longitudinal optical frequencies of ALON [12] as determined by reflectance measurements. The transverse optical frequencies are the mode locations, and the maximum longitudinal frequency is an important parameter in the multiphonon model [11], since it designates the maximum phonon frequency.

At frequencies below the lowest fundamental optical mode, absorption decreases, and the material becomes transparent. The magnitude of absorption is thought to be a combination of contributions from both the

tail of the fundamental lattice vibrations and various multiphonon difference bands. The index of refraction now also includes the effect of lattice vibrations.

The low-frequency real index of refraction (dielectric constant) of ALON is given as 2.93 by McCauley and Corbin [1] for a composition of 30% AlN and as 3.06 by Stead and Simonis [13] for ALON with 37.5% AlN. Temperature dependence of the low-frequency index of refraction is given by Ho [14] as $2.2 \times 10^{-4}$/K (average, 23–300 °C), $2.7 \times 10^{-4}$/K (average, 23–1000 °C), and $3.0 \times 10^{-4}$/K (average, 23–1200 °C). Stead and Simonis [13] give values for the imaginary index of refraction ($k$) in the 7–16 $cm^{-1}$ region. Estimates made from the red wing of the fundamental modes (Table I) are three to four times greater than the experimental imaginary index-of-refraction value determined by Stead and Simonis [13] at 10 and 15 $cm^{-1}$. Corbin [2] also gives absorption coefficient data in the 5–40 $cm^{-1}$ range for ALON of an unreported composition. These values agree well with model predictions of $k$, but tend to have lower values at low frequency.

The high-temperature electrical conductivity of ALON was measured by Kim and Richards [15] and found to be typical of oxides. They found a correlation between the number of vacancies (see Eq. [1]) and conductivity and interpret the conductivity as ionic.

Table II was constructed from measurements reported in the literature as well as model predictions. Real-index data ($n$) in the visible and near IR are taken from the measurements by Scheller [10]. Lattice-vibration-model results [12] are used to calculate real-index data from 0–10,000 $cm^{-1}$ and imaginary-index data from 5–3300 $cm^{-1}$. Laser-calorimetry results for $k$ at 2.9 and 3.9 μm by Detrio and Greason [16] give measurements of the imaginary part of the index of refraction, based on thin samples with the lowest absorption coefficients. Note that the value at 3.9 μm agrees well with the multiphonon-absorption-model prediction [11, 12]. The measured value at 2.9 μm is much higher than the multiphonon model value because of the presence of an $OH^-$ impurity vibrational band.

Measurements of Stead and Simonis [13] are used to represent the low-frequency characteristics of ALON (37.5% AlN). In this region, one-phonon model predictions [12] of $k$ are several times the measured values [13], probably because a few wide fundamental modes are used to represent many narrower modes, and the broadness of these modes gives excessive low-frequency-wing absorption. Values of $k$ for ALON of unknown composition are also given [2]. Low-frequency index predictions are virtually the same as measurements [13]. At very low frequency, ALON exhibits considerable free-carrier absorption that increases rapidly with temperature [9]. Extrapolation of this low-frequency absorption (in the region dominated by free-carrier effects) to 100 GHz (3 $cm^{-1}$) gives a value for $k$ of $3 \times 10^{-4}$ for ALON (30 mole-percent AlN) [9], consistent

with the data given in Table II. ALON with 30 mole-percent AlN has a low-frequency index of refraction of 2.9 [9].

Index measurements by Scheller [10] are accurate to $\pm 0.00001$. Calculated index data are probably accurate to $\pm 0.01$ for $n$ (outside the range of measured values) and $\pm 5\%$ for $k$ down to $350\,\mathrm{cm}^{-1}$. Calculated values of $k$ below $350\,\mathrm{cm}^{-1}$ are too high, ultimately by a factor of four at low frequency. In all data, except $k$ below $350\,\mathrm{cm}^{-1}$, the uncertainty in the values is probably in the least significant digit reported in Table II.

Figure 1 shows a composite of the complex index of refraction based on the data of Table II.

Table III gives temperature dependence for the real part of the index of refraction. Our measurements of $dn/dT$ in the visible and those of Ho [14] at low frequency are given.

Temperature-dependent absorption computed from optical models of ALON [12] have been used to estimate total hemispherical emissivity of pure, transparent ALON over the temperature range 200–1000 K, where the models are expected to give the best results and defect absorption is believed to be insignificant. These results were obtained by estimating complex refractive index at a given temperature, calculating directional emittance for a specific slab thickness, integrating over angle, and convolving the resulting spectral hemispherical emittances with the Planck function.

Table IV gives the resulting total hemispherical emittance for semi-infinite slabs as a function of slab thickness. Since total hemispherical emissivity is an important function for radiation-relief calculations and may be needed to correct property measurements such as thermal conductivity, we have included this calculated result.

## REFERENCES

1. J. W. McCauley and N. D. Corbin, "Phase Relations and Reaction Sintering of Transparent Cubic Aluminum Oxynitride (ALON)," *J. Am. Ceram. Soc.* **62**, 476 (1979).
2. N. D. Corbin, "Aluminum Oxynitride Spinel (ALON): A Review," U.S. Army Materials Technology Laboratory Report MTL MS 87-3, July (1987).
3. J. W. McCauley, "A Simple Model for Aluminum Oxynitride Spinels," *J. Am. Ceram. Soc.* **61**, 372 (1978).
4. T. M. Hartnett and R. L. Gentilman, "Optical and Mechanical Properties of Highly Transparent Spinel and ALON Domes," *Proc. SPIE* **505**, 15 (1984).
5. R. Gentilman, E. Maguire, T. Kohane, and D. B. Valentine, "Comparison of Large ALON and Sapphire Windows," *Proc. SPIE* **1112**, 31 (1989).
6. G. D. Quinn, N. D. Corbin, and J. W. McCauley, "Thermomechanical Properties of Aluminum Oxynitride Spinel," *Bull. Am. Ceram. Soc.* **64**, 723 (1984).
7. E. K. Graham, W. C. Munly, J. W. McCauley, and N. D. Corbin, "Elastic Properties of Polycrystalline Aluminum Oxynitride Spinel and Their Dependence on Pressure, Temperature, and Composition," *J. Am. Ceram. Soc.* **71**, 807 (1988).
8. J. Bauer, L. Biste, and D. Bolze, "Optical Properties of Aluminum Nitride Prepared by Chemical and Plasmachemical Vapour Deposition," *Phys. Stat. Solidi (a)* **39**, 173 (1977).

9. T. M. Hartnett, E. A. Maguire, and R. L. Gentilman, "Aluminum Oxynitride Spinel (ALON)-A New Optical and Multimode Window Material," in "Ceramic Engineer and Science Proceedings," Vol. 3, American Ceramic Society, Columbus, Ohio, 67 (1982).
10. R. J. Scheller, Schott Glass Technologies, Inc., personal communication (Oct. 2, 1989).
11. M. E. Thomas, R. I. Joseph, and W. J. Tropf, "Infrared Transmission Properties of Sapphire, Spinel, Yttria, and ALON as a Function of Temperature and Frequency," *Appl. Opt.* **27**, 239 (1988).
12. M. E. Thomas, "A Computer Code for Modeling Optical Properties of Window Materials," *Proc. SPIE* **1112**, 260 (1989).
13. M. Stead and G. Simonis, "Near Millimeter Wave Characterization of Dual Mode Materials," *Appl. Opt.* **28**, 1874 (1989).
14. W. W. Ho, "High-Temperature Dielectric Properties of Polycrystalline Ceramics," in "MRS Symposium M," Reno, April 6 (1988).
15. I.-U. Kim and V. L. Richards, "High-Temperature Electrical Conductivity of Aluminum Oxynitride Spinel," *J. Am. Ceram. Soc.* **68**, C210 (1985).
16. J. A. Detrio and P. Greason, University of Dayton, personal communication (April 8, 1988).

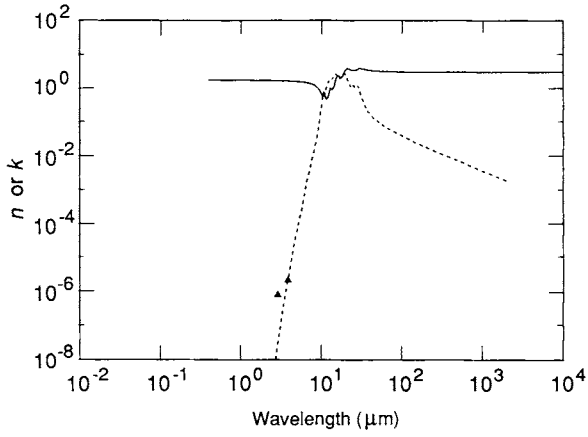


**Fig. 1.** Log–log plot of $n$ (solid line) and $k$ (dashed line) versus wavelength in micrometers for aluminum oxynitride spinel. Symbols are laser-calorimetry measurements of $k$.

## NOTES ADDED IN PROOF

The electronic structure and bang gap of ALON was recently measured by French [17]. The first UV absorption peak occurs at 7.3 eV and bandgap is approximately 6.2 eV.

Details of the measurement of $dn/dT$ at 0.6328 μm in Table III are given in [18]. Spectral and directional scatter measurement of commercial ALON are given in [19].

17. R. H. French, "Electronic Band Structure of $Al_2O_3$ with Comparison to ALON and AlN," *J. Am. Ceram. Soc.* **73**, 477–489 (1990).
18. C. H. Lange and D. D. Duncan, "Temperature Coefficient of Refractive Index for Candidate Optical Windows," *SPIE Proc.* **1326**, 71–78 (1990).
19. C. H. Lange, D. D. Duncan, and D. G. Fischer "Imaging Performance of Crystalline and Polycrystalline Oxides," *SPIE Proc.* **1326**, 59–70 (1990).

**TABLE I**

**Fundamental Infrared Lattice Vibration Parameters of ALON**[a]

| Mode | Transverse optical frequency ($cm^{-1}$) | Strength | Normalized width | Longitudinal optical frequency ($cm^{-1}$) | Refs. |
|---|---|---|---|---|---|
| 1 | 346 | 1.0 | 0.16 | — | [12] |
| 2 | 395 | 0.4 | 0.13 | — | [12] |
| 3 | 495 | 3.33 | 0.20 | 551 | [12] |
| 4 | 634 | 1.32 | 0.15 | 718 | [12] |
| 5 | 768 | 0.16 | 0.085 | 869 | [12] |
| 6 | 920 | 0.03 | 0.050 | 969 | [12] |
| | Total = 6.24 | | | | |

[a]The transverse optical frequency ($\nu_j$) is the location of the mode. The strength ($\Delta\epsilon_j$) is the contribution of the mode to the dielectric constant. The normalized width ($\gamma_j$) is the mode width divided by the mode frequency. The complex dielectric constant ($\epsilon$) is then modeled as a function of frequency ($\nu$) by:

$$\epsilon(\nu) = \epsilon_\infty + \sum_j \frac{\Delta\epsilon_j \, \nu_j^2}{\nu_j^2 - \nu^2 + i\gamma_j \nu_j \nu} ,$$

where the $\epsilon_\infty$ term (= 3.1375) represents the electronic contributions to the dielectric constant (plus one). This model has a static dielectric constant of 9.38.

**TABLE II**

**Values of $n$ and $k$ Obtained from Various References for ALON[a]**

| eV | $cm^{-1}$ | $\mu m$ | $n$ | | $k$ | | $n$ | $k$ |
|---|---|---|---|---|---|---|---|---|
| 3.064 | 24710 | 0.40466 | 1.81167 | [10] | | | | |
| 2.845 | 22944.7 | 0.43583 | 1.80562 | | | | | |
| 2.270 | 18312 | 0.54601 | 1.79218 | | | | | |
| 2.104 | 16969 | 0.5893 | 1.793 | [8] | | | | |
| 1.455 | 11735.6 | 0.85211 | 1.77758 | [10] | | | | |
| 1.240 | 10000 | 1.0000 | 1.776 | [12] | | | | |
| 1.223 | 9862.13 | 1.01398 | 1.77375 | [10] | | | | |
| 1.215 | 9800 | 1.0204 | 1.776 | [12] | | | | |
| 1.190 | 9600 | 1.0417 | 1.775 | | | | | |
| 1.165 | 9400 | 1.0638 | 1.774 | | | | | |
| 1.141 | 9200 | 1.0870 | 1.774 | | | | | |
| 1.116 | 9000 | 1.1111 | 1.773 | | | | | |
| 1.091 | 8800 | 1.1364 | 1.773 | | | | | |
| 1.066 | 8600 | 1.1628 | 1.772 | | | | | |
| 1.041 | 8400 | 1.1905 | 1.771 | | | | | |
| 1.017 | 8200 | 1.2195 | 1.771 | | | | | |
| 0.9919 | 8000 | 1.2500 | 1.770 | | | | | |
| 0.9671 | 7800 | 1.2821 | 1.769 | | | | | |
| 0.9423 | 7600 | 1.3158 | 1.769 | | | | | |
| 0.9175 | 7400 | 1.3514 | 1.768 | | | | | |
| 0.8927 | 7200 | 1.3889 | 1.767 | | | | | |
| 0.8679 | 7000 | 1.4286 | 1.766 | | | | | |
| 0.8431 | 6800 | 1.4706 | 1.766 | | | | | |
| 0.8183 | 6600 | 1.5152 | 1.765 | | | | | |
| 0.8106 | 6537.74 | 1.52958 | 1.76543 | [10] | | | | |
| 0.7935 | 6400 | 1.5625 | 1.764 | [12] | | | | |
| 0.7687 | 6200 | 1.6129 | 1.763 | | | | | |
| 0.7439 | 6000 | 1.6667 | 1.762 | | | | | |
| 0.7191 | 5800 | 1.7241 | 1.761 | | $3.9\cdot10^{-13}$ | [12] | | |
| 0.6943 | 5600 | 1.7857 | 1.759 | | $1.5\cdot10^{-12}$ | | | |
| 0.6695 | 5400 | 1.8519 | 1.758 | | $4.9\cdot10^{-12}$ | | | |
| 0.6447 | 5200 | 1.9231 | 1.756 | | $1.4\cdot10^{-11}$ | | | |
| 0.6293 | 5075.91 | 1.97009 | 1.75838 | [10] | | | | |
| 0.6199 | 5000 | 2.0000 | 1.755 | [12] | $3.5\cdot10^{-11}$ | | | |
| 0.6075 | 4900 | 2.0408 | 1.754 | | $5.5\cdot10^{-11}$ | | | |
| 0.5951 | 4800 | 2.0833 | 1.753 | | $8.4\cdot10^{-11}$ | | | |
| 0.5827 | 4700 | 2.1277 | 1.752 | | $1.3\cdot10^{-10}$ | | | |
| 0.5703 | 4600 | 2.1739 | 1.751 | | $1.9\cdot10^{-10}$ | | | |
| 0.5579 | 4500 | 2.2222 | 1.750 | | $2.9\cdot10^{-10}$ | | | |
| 0.5455 | 4400 | 2.2727 | 1.749 | | $4.4\cdot10^{-10}$ | | | |
| 0.5332 | 4300.30 | 2.32542 | 1.75268 | [10] | | | | |
| 0.5331 | 4300 | 2.3256 | 1.747 | [12] | $6.7\cdot10^{-10}$ | | | |
| 0.5207 | 4200 | 2.3810 | 1.746 | | $1.0\cdot10^{-9}$ | | | |
| 0.5083 | 4100 | 2.4390 | 1.745 | | $1.6\cdot10^{-9}$ | | | |

(*continued*)

**TABLE II** *(Continued)*

**ALON**

| eV | $cm^{-1}$ | $\mu m$ | $n$ | $k$ | $n$ | $k$ |
|---|---|---|---|---|---|---|
| 0.4959 | 4000 | 2.5000 | 1.743 | $2.4 \cdot 10^{-9}$ | | |
| 0.4835 | 3900 | 2.5641 | 1.741 | $3.7 \cdot 10^{-9}$ | | |
| 0.4711 | 3800 | 2.6316 | 1.740 | $5.7 \cdot 10^{-9}$ | | |
| 0.4587 | 3700 | 2.7027 | 1.738 | $9.0 \cdot 10^{-9}$ | | |
| 0.4463 | 3600 | 2.7778 | 1.735 | $1.4 \cdot 10^{-8}$ | | |
| 0.4339 | 3500 | 2.8571 | 1.733 | $2.3 \cdot 10^{-8}$ | | |
| 0.4275 | 3448 | 2.9000 | | | | $7.8 \cdot 10^{-7}$ [16] |
| 0.4215 | 3400 | 2.9412 | 1.731 | $3.6 \cdot 10^{-8}$ | | |
| 0.4092 | 3300 | 3.0303 | 1.728 | $5.8 \cdot 10^{-8}$ | | |
| 0.3968 | 3200 | 3.1250 | 1.725 | $9.3 \cdot 10^{-8}$ | | |
| 0.3844 | 3100 | 3.2258 | 1.722 | $1.5 \cdot 10^{-7}$ | | |
| 0.3720 | 3000 | 3.3333 | 1.718 | $2.5 \cdot 10^{-7}$ | | |
| 0.3596 | 2900 | 3.4483 | 1.714 | $4.2 \cdot 10^{-7}$ | | |
| 0.3472 | 2800 | 3.5714 | 1.709 | $7.1 \cdot 10^{-7}$ | | |
| 0.3348 | 2700 | 3.7037 | 1.704 | $1.2 \cdot 10^{-6}$ | | |
| 0.3224 | 2600 | 3.8462 | 1.698 | $2.0 \cdot 10^{-6}$ | | |
| 0.3179 | 2564 | 3.9000 | | | | $2.1 \cdot 10^{-6}$ [16] |
| 0.3100 | 2500 | 4.0000 | 1.702 | $3.3 \cdot 10^{-6}$ | | |
| 0.2976 | 2400 | 4.1667 | 1.68 | $5.8 \cdot 10^{-6}$ | | |
| 0.2852 | 2300 | 4.3478 | 1.68 | $1.0 \cdot 10^{-5}$ | | |
| 0.2728 | 2200 | 4.5455 | 1.67 | $1.9 \cdot 10^{-5}$ | | |
| 0.2604 | 2100 | 4.7619 | 1.65 | $3.4 \cdot 10^{-5}$ | | |
| 0.2480 | 2000 | 5.0000 | 1.64 | $6.0 \cdot 10^{-5}$ | | |
| 0.2418 | 1950 | 5.1282 | 1.63 | $9.0 \cdot 10^{-5}$ [11][b] | | |
| 0.2356 | 1900 | 5.2632 | 1.62 | $1.7 \cdot 10^{-4}$ | | |
| 0.2294 | 1850 | 5.4054 | 1.62 | $3.1 \cdot 10^{-4}$ | | |
| 0.2232 | 1800 | 5.5556 | 1.60 | $3.6 \cdot 10^{-4}$ | | |
| 0.2170 | 1750 | 5.7143 | 1.59 | $4.3 \cdot 10^{-4}$ | | |
| 0.2108 | 1700 | 5.8824 | 1.58 | $4.9 \cdot 10^{-4}$ | | |
| 0.2046 | 1650 | 6.0606 | 1.57 | $5.0 \cdot 10^{-4}$ [12] | | |
| 0.1984 | 1600 | 6.2500 | 1.55 | $7.4 \cdot 10^{-4}$ | | |
| 0.1922 | 1550 | 6.4516 | 1.53 | $1.1 \cdot 10^{-3}$ | | |
| 0.1860 | 1500 | 6.6667 | 1.51 | $1.6 \cdot 10^{-3}$ | | |
| 0.1798 | 1450 | 6.8966 | 1.49 | $2.4 \cdot 10^{-3}$ | | |
| 0.1736 | 1400 | 7.1429 | 1.46 | $3.6 \cdot 10^{-3}$ | | |
| 0.1674 | 1350 | 7.4074 | 1.43 | $5.2 \cdot 10^{-3}$ | | |
| 0.1612 | 1300 | 7.6923 | 1.39 | $7.5 \cdot 10^{-3}$ | | |
| 0.1550 | 1250 | 8.0000 | 1.34 | 0.011 | | |
| 0.1488 | 1200 | 8.3333 | 1.29 | 0.017 | | |
| 0.1426 | 1150 | 8.6957 | 1.21 | 0.026 | | |
| 0.1364 | 1100 | 9.0909 | 1.12 | 0.045 | | |
| 0.1302 | 1050 | 9.5238 | 0.99 | 0.088 | | |
| 0.1240 | 1000 | 10.000 | 0.80 | 0.21 | | |
| 0.1215 | 980 | 10.204 | 0.71 | 0.33 | | |

*(continued)*

**TABLE II *(Continued)***
**ALON**

| eV | $cm^{-1}$ | $\mu m$ | $n$ | $k$ | $n$ | $k$ |
|---|---|---|---|---|---|---|
| 0.1190 | 960 | 10.417 | 0.63 | 0.49 | | |
| 0.1165 | 940 | 10.638 | 0.62 | 0.69 | | |
| 0.1141 | 920 | 10.870 | 0.77 | 0.78 | | |
| 0.1116 | 900 | 11.111 | 0.74 | 0.70 | | |
| 0.1091 | 880 | 11.364 | 0.59 | 0.79 | | |
| 0.1066 | 860 | 11.628 | 0.51 | 0.98 | | |
| 0.1041 | 840 | 11.905 | 0.50 | 1.2 | | |
| 0.1017 | 820 | 12.195 | 0.54 | 1.4 | | |
| 0.0992 | 800 | 12.500 | 0.65 | 1.6 | | |
| 0.0967 | 780 | 12.821 | 0.87 | 1.7 | | |
| 0.0942 | 760 | 13.158 | 1.04 | 1.7 | | |
| 0.0917 | 740 | 13.514 | 0.98 | 1.6 | | |
| 0.0893 | 720 | 13.889 | 0.92 | 1.8 | | |
| 0.0868 | 700 | 14.286 | 1.00 | 2.1 | | |
| 0.0843 | 680 | 14.706 | 1.21 | 2.4 | | |
| 0.0818 | 660 | 15.152 | 1.57 | 2.6 | | |
| 0.0794 | 640 | 15.625 | 2.04 | 2.6 | | |
| 0.0769 | 620 | 16.129 | 2.36 | 2.3 | | |
| 0.0744 | 600 | 16.667 | 2.34 | 2.0 | | |
| 0.0719 | 580 | 17.241 | 2.16 | 1.9 | | |
| 0.0694 | 560 | 17.857 | 2.06 | 2.1 | | |
| 0.0670 | 540 | 18.519 | 2.19 | 2.5 | | |
| 0.0645 | 520 | 19.231 | 2.63 | 2.7 | | |
| 0.0620 | 500 | 20.000 | 3.28 | 2.7 | | |
| 0.0608 | 490 | 20.408 | 3.58 | 2.5 | | |
| 0.0595 | 480 | 20.833 | 3.79 | 2.2 | | |
| 0.0583 | 470 | 21.277 | 3.89 | 1.9 | | |
| 0.0570 | 460 | 21.739 | 3.90 | 1.7 | | |
| 0.0558 | 450 | 22.222 | 3.84 | 1.4 | | |
| 0.0546 | 440 | 22.727 | 3.75 | 1.3 | | |
| 0.0533 | 430 | 23.256 | 3.63 | 1.2 | | |
| 0.0521 | 420 | 23.810 | 3.52 | 1.1 | | |
| 0.0508 | 410 | 24.390 | 3.45 | 1.2 | | |
| 0.0496 | 400 | 25.000 | 3.46 | 1.2 | | |
| 0.0484 | 390 | 25.641 | 3.51 | 1.2 | | |
| 0.0471 | 380 | 26.316 | 3.51 | 1.1 | | |
| 0.0459 | 370 | 27.027 | 3.48 | 1.1 | | |
| 0.0446 | 360 | 27.778 | 3.51 | 1.2 | | |
| 0.0434 | 350 | 28.571 | 3.67 | 1.2 | | |
| 0.0422 | 340 | 29.412 | 3.86 | 1.1 | | |
| 0.0409 | 330 | 30.303 | 3.95 | 0.87 | | |
| 0.0397 | 320 | 31.250 | 3.93 | 0.66 | | |
| 0.0384 | 310 | 32.258 | 3.86 | 0.51 | | |
| 0.0372 | 300 | 33.333 | 3.78 | 0.41 | | |

*(continued)*

**TABLE II** *(Continued)*

**ALON**

| eV | $cm^{-1}$ | $\mu$m | $n$ | $k$ | $n$ | $k$ | |
|---|---|---|---|---|---|---|---|
| 0.0360 | 290 | 34.483 | 3.70 | 0.33 | | | |
| 0.0347 | 280 | 35.714 | 3.63 | 0.28 | | | |
| 0.0335 | 270 | 37.037 | 3.56 | 0.24 | | | |
| 0.0322 | 260 | 38.462 | 3.51 | 0.21 | | | |
| 0.0310 | 250 | 40.000 | 3.46 | 0.19 | | | |
| 0.0298 | 240 | 41.667 | 3.42 | 0.16 | | | |
| 0.0285 | 230 | 43.478 | 3.38 | 0.15 | | | |
| 0.0273 | 220 | 45.455 | 3.34 | 0.13 | | | |
| 0.0260 | 210 | 47.619 | 3.31 | 0.12 | | | |
| 0.0248 | 200 | 50.000 | 3.28 | 0.11 | | | |
| 0.0236 | 190 | 52.632 | 3.26 | 0.10 | | | |
| 0.0223 | 180 | 55.556 | 3.23 | 0.090 | | | |
| 0.0211 | 170 | 58.824 | 3.21 | 0.082 | | | |
| 0.0198 | 160 | 62.500 | 3.19 | 0.075 | | | |
| 0.0186 | 150 | 66.667 | 3.18 | 0.068 | | | |
| 0.0174 | 140 | 71.429 | 3.16 | 0.062 | | | |
| 0.0161 | 130 | 76.923 | 3.15 | 0.056 | | | |
| 0.0149 | 120 | 83.333 | 3.13 | 0.050 | | | |
| 0.0136 | 110 | 90.909 | 3.12 | 0.045 | | | |
| 0.0124 | 100 | 100.00 | 3.11 | 0.040 | | | |
| 0.0112 | 90 | 111.11 | 3.10 | 0.036 | | | |
| 0.0099 | 80 | 125.00 | 3.09 | 0.031 | | | |
| 0.0087 | 70 | 142.86 | 3.09 | 0.027 | | | |
| 0.0074 | 60 | 166.67 | 3.08 | 0.023 | | | |
| 0.0062 | 50 | 200.00 | 3.075 | 0.019 | | | |
| 0.0050 | 40 | 250.00 | 3.071 | 0.015 | | 0.012 | [2] |
| 0.0037 | 30 | 333.33 | 3.067 | 0.011 | | $8.8 \cdot 10^{-3}$ | |
| 0.0025 | 20 | 500.00 | 3.065 | $7.5 \cdot 10^{-3}$ | | $5.9 \cdot 10^{-3}$ | |
| 0.0019 | 15 | 666.67 | 3.064 | $5.6 \cdot 10^{-3}$ | | $1.5 \cdot 10^{-3}$ | [13] |
| 0.0012 | 10 | 1000.0 | 3.064 | $3.7 \cdot 10^{-3}$ | 3.06 [13] | $8.8 \cdot 10^{-4}$ | |
| 0.0006 | 5 | 2000.0 | 3.063 | $1.9 \cdot 10^{-3}$ | | | |
| 0.0000 | 0 | $\infty$ | 3.063 | 0.0 | | | |

[a]References are indicated in brackets.

[b]Values in the two-phonon region from 1700–1950 $cm^{-1}$ are taken from our measurements.

**TABLE III**

**Values of $dn/dT$ Obtained from Various References for ALON**

| eV | $cm^{-1}$ | $\mu m$ | $dn/dT$ (1/K) | Notes |
|---|---|---|---|---|
| 1.959 | 15803 | 0.6328 | $1.5 \cdot 10^{-5}$ | Our measurement |
| 0.310 | 2500 | 4.0000 | $2.8 \cdot 10^{-6}$ | Model [12] |
| 0.0 | 0 | $\infty$ | $2.2 \cdot 10^{-4}$ | Average, 23–300°C [14] |

**TABLE IV**

**Calculated Total Hemispherical Emissivity for ALON**

| Temperature (K) | Thickness (cm) | | | |
|---|---|---|---|---|
| | 0.10 | 0.25 | 0.50 | 1.25 |
| 200.0 | 0.62 | 0.62 | 0.62 | 0.62 |
| 300.0 | 0.65 | 0.66 | 0.66 | 0.67 |
| 400.0 | 0.64 | 0.67 | 0.69 | 0.71 |
| 500.0 | 0.59 | 0.64 | 0.67 | 0.70 |
| 600.0 | 0.53 | 0.58 | 0.62 | 0.66 |
| 700.0 | 0.46 | 0.52 | 0.56 | 0.61 |
| 800.0 | 0.40 | 0.46 | 0.50 | 0.55 |
| 900.0 | 0.35 | 0.41 | 0.45 | 0.50 |
| 1000.0 | 0.31 | 0.36 | 0.40 | 0.45 |

# Barium Titanate ($BaTiO_3$)

CHUEN WONG and YE YUNG TENG
Department of Physics and Applied Physics
University of Lowell
Lowell, Massachusetts
and
J. ASHOK and P. L. H. VARAPRASAD
Applied Physics Department
Andhra University
Visakhapatnam, India

The barium titanate crystal is ferroelectric at room temperature. The crystal structure is perovskite, cubic above the Curie temperature, and tetragonal below the Curie temperature. At room temperature, the $c$ axis is longer than the $a$ axis by 1% [1]. Practically all the barium titanate samples described in the literature were fabricated by either the flux-grown or the melt-grown method. The process of growing large single crystals of barium titanate by the top-seeded melt growth was developed by a group headed by A. Linz at MIT [2] and later transferred to Sanders Associates [3], which is presently a major commercial supplier of this crystal. The Curie temperature of melt-grown barium titanate is about 133 °C, while that of flux-grown is 120 °C. The lower Curie temperature of flux-grown barium titanate is believed to be a result of the higher impurity content, which also affects the optical constants. Recently, there has been increased interest in barium titanate, mainly due to its photorefractive properties and other associated effects and applications, such as phase conjugation, volume holography for optical storage, two-beam coupling, and optical computing.

The UV data in Table II are the result of Kramers–Kronig (K–K) analysis of reflectivity measurement on unpoled multiple-domain samples. They represent a certain weighted average of the optical constants for the ordinary (o) and extraordinary (e) rays. The o-ray is expected to dominate because it has an entire plane of polarization, whereas the e-ray has only one direction of polarization [4]. We read the $n$ and $k$ values from the graphs of Bäuerle *et al.* [5], who measured the reflectivity from 10–32 eV at room temperature, and did a K–K analysis of a combination of their own reflectivity data and Cardona's [6] 2–22 eV, room-temperature data. At 2.94 eV, these graphs give $n = 2.67$, $k = 0.05$, whereas Table II lists


Copyright © 1991 by Academic Press.
All rights of reproduction in any form reserved.
ISBN 0-12-544422-2

$n_o = 2.644$, $n_e = 2.541$ from minimum deviation and $k_o = 5.84 \times 10^{-6}$, $k_e = 6.51 \times 10^{-6}$ from absorption measurements. There is significant disagreement in the $k$ values. The reflectivity measurement of Bäuerle *et al.* [5] involved the polarized synchrotron radiation from the DORIS storage ring at Hamburg together with a modified special UHV version of the McPherson Model 225.3 monochromator with a resolution of 0.03 Å. The sample was a polished single crystal with (100) faces in the cubic phase. Cardona [6] used unpolarized light from various arc lamps, and a 1-m McPherson monochromator. The unpoled sample was polished, etched, and had random orientation for the ferroelectric domains.

For the visible region, we tabulate the room-temperature index of refraction data from Wemple *et al.* [7], covering the range 0.42–0.68 μm. Their sample was melt-grown. The method of measurement was minimum deviation. The sample was poled to a single domain, then cut with a string saw to minimize surface damage and polished with 6 and 3 μm diamond paste on a flat tin lap. The data can be represented by the following single-oscillator Sellmeier equations:

$$n_o^2 = 1 + \frac{4.219}{1 - (0.2231/\lambda)^2}$$
$$n_e^2 = 1 + \frac{4.064}{1 - (0.2109/\lambda)^2}, \tag{1}$$

where $\lambda$ is wavelength in μm. Discrepancy between Eq. 1 and the data is within 0.003 for wavelengths shorter than 0.45 μm, higher for shorter wavelengths. We read the data from the graphs in Fig. 4 of Ref. [7]. The measurements by Deshpande *et al.* [8, 9] at the wavelength of the sodium $D$ line using two different methods agree well with the data of Wemple *et al.* [7]. The first method [8] is a refinement of Duc de Chaulnes' method of image displacement. The second method [9] uses the phenomenon of polarization by reflection, and the results are $n_o = 2.428 \pm 0.002$, $n_e = 2.371 \pm 0.0045$. According to Deshpande *et al.* [8, 9], these methods can achieve accuracy better than or comparable to that of minimum deviation in the case of ferroelectric barium titanate. As for flux-grown samples, the data of Johnston [10] agree well with those of Wemple *et al.* [7] for the o-ray, although the e-ray data are slightly larger. The explanation is in the difference in polarization of the flux-grown and melt-grown samples. Johnston [10] used the method of minimum deviation and analyzed his data with a two-oscillator Sellmeier equation.

The extinction coefficient $k$ in the UV–VIS range was calculated using

the absorption coefficient data from DiDomenico and Wemple [11] and Schunemann *et al.* [12]. Both their samples were melt-grown. Schunemann *et al.* [12] prepared a particularly pure sample and made absorption measurements between 0.4 and 0.85 μm. Temperature was not mentioned, but must be room temperature. DiDomenico and Wemple [11] made their measurements at 33 °C, between 2.95 and 3.27 eV (0.38–0.42 μm), near the absorption edge. Their absorption coefficient data exhibit an exponential Urbach tail, and there is a large difference between the o- and e-rays. At about 0.4 μm, where measurements of DiDomenico and Wemple [11] and Schunemann *et al.* [12] overlap, their data agree to within 50%. The absorption coefficient was found to be very sensitive to small amounts of impurities [13]. Klein and Schwartz [14] measured the absorption coefficient between 0.44 and 0.64 μm of four samples grown by Sanders Associates [3] and obtained results from 0.16 to 2.2 $cm^{-1}$ at 0.5 μm. Flux-grown barium titanate was found to have higher absorption coefficients than those of melt-grown [11, 15].

In the near-IR region, the index of refraction between 0.85 and 2 μm was calculated using Eq. 1. Equation 1 is probably valid in this region because the value of $n_o$ at 2 μm calculated from this equation agrees with the reflectivity data of Spitzer *et al.* [16]. Furthermore, the absorption in this region is very low according to Schunemann [17] and Hilsum [18]. Schunemann [17] measured the absorption coefficient between 0.85 and 3 μm on the same very pure sample [12] using unpolarized light. The absorption coefficient reaches a minimum at about 2 μm where the extinction coefficient $k$ is about $10^{-7}$. Hilsum [18] reported transmission and absorption data between 1 and 12 μm, and the minimum absorption also occurs around 2 μm with $k$ about $10^{-5}$. Hilsum's [18] sample is a yellowish plate several millimeters square and 0.1 mm thick. Temperature was not mentioned. A plot of $\alpha$ versus wavelength from 7 to 12 μm has been used to determine $k$ as listed in Table II. No crystal orientation was specified, so we assume $k_o(\perp)$.

The index of refraction below the band gap for many covalent and ionic materials has been discussed by Wemple and DiDomenico [19], who developed a model equation of the form

$$n^2 = \frac{1 + E_d E_o}{E_o^2 - (\hbar\omega)^2}$$

to fit many materials. For $BaTiO_3$, $E_d = 24.0$ eV and $E_o = 5.63$ eV. Although this does not take into account the birefringence, it gives values closely approaching $n_o(\perp)$, so we have included these values (three significant figures) in Table II.

For the region between 10 and 1000 μm, Servoin *et al.* [20] measured the reflectivity with a Fourier-transform scanning interferometer, on a small, natural, single domain in the surface of a crystal. They fitted their data with the four-parameter factorized form of the dielectric function

$$\varepsilon = \varepsilon' \pm i\varepsilon'' = \varepsilon_\infty \prod_j \frac{\Omega_{j\mathrm{LO}}^2 - \omega^2 \mp i\gamma_{j\mathrm{LO}}\omega}{\Omega_{j\mathrm{TO}}^2 - \omega^2 \mp i\gamma_{j\mathrm{TO}}\omega}, \tag{2}$$

where $\omega$ is the frequency, $\Omega$ and $\gamma$ are the mode frequency and damping constant, respectively, and $\varepsilon_\infty$ is the high-frequency dielectric constant. Preliminary values of the mode frequencies and damping constants were obtained from Raman spectra and then fine-tuned to fit the reflectivity data. The fit is very good. In Table II, the $n$ and $k$ values from 2 to 1000 μm were calculated using Eq. 2 and the values of mode frequencies and damping constants given by Servoin *et al.* [20]. These parameters are listed in Table I. To fit the reflectivity data of Servoin *et al.* [20], we chose 5.3 to be the high-frequency dielectric constant for the o-ray, and 5.1 for the e-ray. We have extended the use of Eq. 2 to obtain the $n$ and $k$ values in the 2–10 μm region. Results from Eq. 2 in this region agree with the data of Spitzer *et al.* [16] who measured the o-ray reflectivity at room temperature from 5000 to 70 $\mathrm{cm}^{-1}$ using a double-pass prism spectrometer between 5000 and 333 $\mathrm{cm}^{-1}$ and a single-pass grating monochromator below 333 $\mathrm{cm}^{-1}$. The reflectivity data of Servoin *et al.* [20] agree with those of Spitzer *et al.* [16] to within 2–3%, and Sanjurjo *et al.* [4], except at low frequencies.

Sanjurjo *et al.* [21] fitted their room-temperature (not defined) reflectivity data for $\mathbf{E}\|c$ with a coupled-mode model, noting that real coupling (in contrast to imaginary coupling and independent oscillators) provided the best fit. They displayed graphs of $\varepsilon_1(\|)$ and $\varepsilon_2(\|)$ in a coarser grid than the calculated values of Servoin *et al.* [20], also given in Table II. We have displayed these data in a separate block at the end of Table II. Although most values of $n$ and $k$ are well within a factor of two of each other, it is interesting to note where large differences occur. Sanjurjo *et al.* [21] also performed a K–K analysis of their reflectivity data demonstrating a good qualitative agreement with the coupled-oscillator-model fit. They displayed only $\varepsilon_2(\|)$ in this case.

Ballantyne [22] measured the reflectivity of the o-ray only, from 4000 to 5 $\mathrm{cm}^{-1}$ and between 24 and 200 °C using various spectrometers, an interferometer, and a Carcinotron system, and permittivities were obtained from K–K analysis. The $n$ values, calculated from Ballantyne's [22] permittivities, agree with those of Servoin *et al.* [20] at the ends of the spectral region: within 1% at 10 $\mathrm{cm}^{-1}$ and 6% at 900 $\mathrm{cm}^{-1}$. The discrepancy increases to 24% at 600 $\mathrm{cm}^{-1}$ and 90% at 200 $\mathrm{cm}^{-1}$. There is better

agreement for the $k$ values, especially when they are larger than unity. Barker [23] measured the reflectivity between 400 and 100 $cm^{-1}$ at 300 K and 475 K on a multiple-domain sample, and the spectra resemble closely the o-ray spectra of Servoin *et al.* [20].

It is interesting to observe that an "antiresonance" occurs at 780 $cm^{-1}$ (12.82 μm) where $n_o = 1.01$ and $k_o = 9.18 \times 10^{-4}$ as shown in Table II. A similar antiresonance occurs at 800 $cm^{-1}$ (12.50 μm), where $n_e = 1.03$ and $k_e = 6.18 \times 10^{-3}$. At antiresonances, an incident ray will suffer very small reflection and absorption. Antiresonance is a quantum effect occurring when two electronic levels attempt to cross each other. The integrated absorption remains constant, but the absorption is redistributed. When two phonon levels (frequencies) attempt to cross (couple), the effect also occurs. The factorized form of Eq. 2 leads to such effects. Note that the model predicts much too much absorption in the 2.5–10 μm region compared with the measurement of Hilsum [18].

In the microwave region at a wavelength of 12 mm, we have $n_o = 39$ and $k_o = 4.7$, calculated from Ballantyne's [22] permittivity data (accuracy 20%) measured with a microwave dielectrometer. As a comparison, Eq. 2 gives, at 12.5 mm, $n_o = 46$ and $k_o = 1.6$.

Turik and Shevchenko [24] measured the permittivity along the $c$ axis in the $1 \times 10^3$ to $3 \times 10^8$ Hz frequency range using a bridge and various $Q$ meters. They found piezoelectric resonance at $10^6$–$10^7$ Hz. Permittivity data from other authors [25] were also presented. At $10^{10}$ Hz, we have $\varepsilon_{33} = 44.9$ and the loss tangent $\tan \delta = 0.24$, from which we obtain $n_e = 6.74$ and $k_e = 0.798$. At $10^4$–$10^5$ Hz, $\varepsilon_{33} = 188$, $\tan \delta = 0.027$, $n_e = 13.7$, and $k_e = 0.187$.

Papers dealing with optical properties of powders and small particles include Ruppin [26], Mara *et al.* [27], Last [28] and Demeshina and Murzin [29].

Although we have stressed room-temperature measurements, there has been much work (both IR and Raman) through the Curie temperature at 133 °C. IR data are found in Luspin *et al.* [30]. Some of the Raman data are found in DiDomenico *et al.* [31], Vogt *et al.* [32], Pinczuk *et al.* [33], and references therein.

## ACKNOWLEDGMENTS

We would like to thank the editor for valuable suggestions, D. Bäuerle for providing a larger-size graph of $n$ and $k$, and P. G. Schunemann for a copy of his thesis. The assistance of C. H. Lin, L. Li, and M. Villani in the preparation of the tables is greatly appreciated.

## REFERENCES

1. W. J. Merz, *Phys. Rev.* **76**, 1221 (1949).
2. A. Linz, V. Belruss, and C. S. Naiman, *J. Electrochem. Soc.* **112**, 60C (1965).

3. Sanders Associates, 130 Daniel Webster Highway, Merrimack, N. H., 03054, U.S.A.
4. J. A. Sanjurjo, S. P. S. Porto, and E. Silberman, *Solid State Commun.* **30**, 55 (1979).
5. D. Bäuerle, W. Braun, V. Saile, G. Sprüssel, and E. E. Koch, *Z. Physik B* **29**, 179, (1978).
6. M. Cardona, *Phys. Rev.* **140**, A651 (1965).
7. S. H. Wemple, M. DiDomenico, Jr., and I. Camlibel, *J. Phys. Chem. Solids* **29**, 1797 (1968).
8. L. V. Deshpande, M. B. Joshi, and R. B. Mishra, *J. Opt. Soc. Am.* **70**, 1160 (1980).
9. L. V. Deshpande, M. B. Joshi, and R. B. Mishra, *J. Opt. Soc. Am.* **70**, 1163 (1980).
10. A. R. Johnston, *J. Appl. Phys.* **42**, 3501 (1971).
11. M. DiDomenico, Jr., and S. H. Wemple, *Phys. Rev.* **166**, 565 (1968).
12. P. G. Schunemann, D. A. Temple, R. S. Hathcock, H. L. Tuller, H. P. Jenssen, D. R. Gabbe, and C. Ward, *J. Opt. Soc. Am. B* **5**, 1685 (1988).
13. P. G. Schunemann and T. M. Pollak, Y. Yang, Y. Y . Teng, and C. Wong, *J. Opt. Soc. Am. B* **5**, 1702 (1988).
14. M. B. Klein and R. N. Schwartz, *J. Opt. Soc. Am. B* **3**, 293 (1986).
15. R. C. Casella and S. P. Keller, *Phys. Rev.* **116**, 1469 (1959).
16. W. G. Spitzer, R. C. Miller, I. A. Kleinman, and L. E. Howarth, *Phys. Rev.* **126**, 1710 (1962).
17. P. G. Schunemann, master's thesis, Massachusetts Institute of Technology, May 8, 1987.
18. C. Hilsum, *J. Opt. Soc. Am.* **45**, 771 (1955).
19. S. H. Wemple and M. DiDomenico, Jr., *Phys. Rev. B* **3**, 1338 (1971).
20. J. L. Servoin, F. Gervais, A. M. Quittet, and Y. Luspin, *Phys. Rev. B* **21**, 2038 (1980).
21. J. A. Sanjurjo, R. S. Katiyar, and S. P. S. Porto, *Phys. Rev. B* **22**, 2396 (1980).
22. J. M. Ballantyne, *Phys. Rev.* **136**, A 429 (1964).
23. A. S. Barker, Jr., *Phys. Rev.* **145**, 391 (1966).
24. A. V. Turik and N. B. Shevchenko, *Sov. Phys. Solid State* **19**, 1644 (1977).
25. A. V. Turik and K. R. Chernyshev, *Izv. Akad. Nauk SSSR Ser. Fiz* **31**, 1775 (1967); A. V. Turik, E. N. Sidorenko, B. F. Proskuryakov, V. F. Zhestkov, and N. B. Shevchenko, in "Crystallization and Properties of Crystals" (Inter-University Collection) [in Russian], No. 2, Novocherkassk, 72 (1975).
26. R. Ruppin, *Phys. Stat. Sol. b* **64**, 701 (1974).
27. R. T. Mara, G. B. B. M. Sutherland, and H. V. Tyrell, *Phys. Rev.* **96**, 801 (1954).
28. J. T. Last, *Phys. Rev.* **105**, 1740 (1957).
29. A. I. Demeshina and V. N. Murzin, *Solid State Phys. (USSR)* **4**, 2185 (1963); *Fiz. Tverd. Tela* **4**, 2980 (1962).
30. Y. Luspin, J. L. Servoin, and F. Gervais, *J. Phys. C: Solid State Phys.* **13**, 3761 (1980).
31. M. DiDomenico, Jr., S. H. Wemple, S. P. S. Porto, and R. P. Bauman, *Phys. Rev.* **174**, 522 (1968).
32. H. Vogt, J. A. Sanjurjo, and G. Rossbroich, *Phys. Rev. B* **26**, 5904 (1982).
33. A. Pinczuk, W. Taylor, E. Burstein, and I. Lefkowitz, *Solid State Commun.* **5**, 429 (1967).

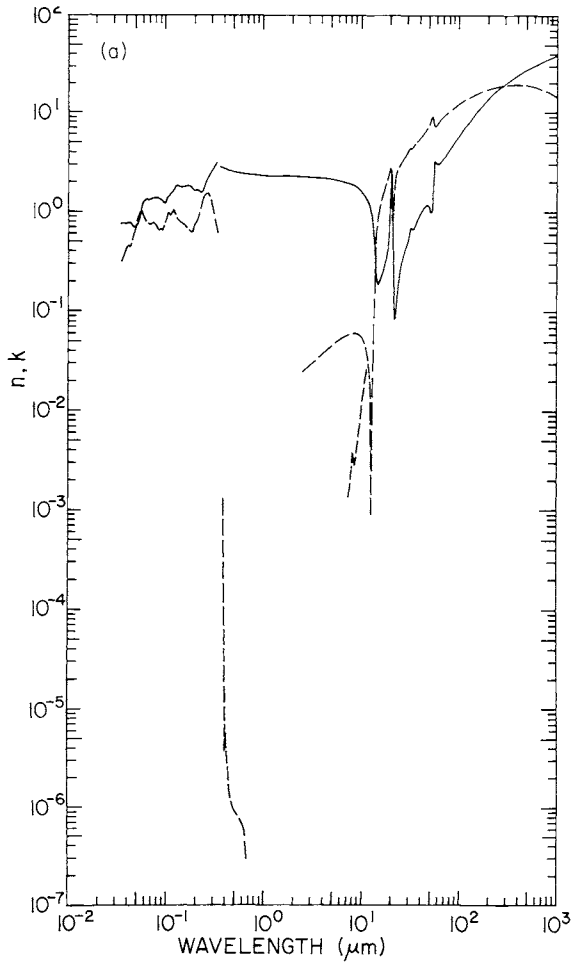


**Fig. 1.** (a) Log–log plot of $n_o$ (solid line) and $k_o$ (dashed line) versus wavelength in micrometers for barium titanate. (b) Log–log plot of $n_e$ (solid line) and $k_e$ (dashed line) versus wavelength in micrometers.

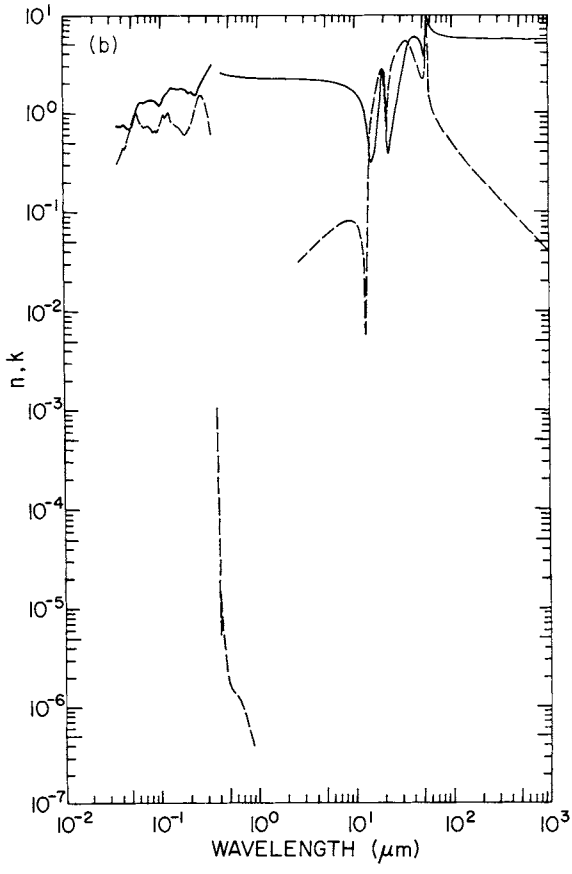


**TABLE I**

**Values of Mode Frequencies and Damping Constants for Barium Titanate[a]**

| $j$ | $\Omega_{jLO}$ | $\gamma_{jLO}$ | $\Omega_{jTO}$ | $\gamma_{jTO}$ |
|---|---|---|---|---|
| 1 | 180 | 9 | 34 | 100 |
| 2 | 305.6 | 9 | 181.8 | 2.8 |
| 3 | 465 | 5 | 306 | 9 |
| 4 | 706 | 22 | 482 | 21 |
| 1 | 187 | 9 | 180 | 4 |
| 2 | 469 | 12 | 280 | 120 |
| 3 | 729 | 34 | 507 | 45 |

[a]The data were obtained from Ref. [20]. The unit is $cm^{-1}$. The first four rows are for the ordinary ray and the last three rows are for the extraordinary ray.

TABLE II

Values of $n$ and $k$ for Barium Titanate Obtained from Various References[a]

| eV | $cm^{-1}$ | μm | $n$ | $k$ |
|---|---|---|---|---|
| 33.8 | | 0.03668 | 0.761[5] | 0.326[5] |
| 32.5 | | 0.03815 | 0.753 | 0.370 |
| 31.3 | | 0.03968 | 0.745 | 0.420 |
| 30.0 | | 0.04133 | 0.782 | 0.450 |
| 29.4 | | 0.04217 | 0.786 | 0.444 |
| 28.1 | | 0.04412 | 0.741 | 0.449 |
| 27.4 | | 0.04533 | 0.720 | 0.494 |
| 26.6 | | 0.04670 | 0.700 | 0.548 |
| 25.7 | | 0.04867 | 0.679 | 0.667 |
| 24.6 | | 0.05040 | 0.720 | 0.770 |
| 24.0 | | 0.05166 | 0.741 | 0.839 |
| 22.9 | | 0.05414 | 0.872 | 0.956 |
| 22.3 | | 0.05560 | 0.975 | 1.002 |
| 21.7 | | 0.05714 | 1.09 | 1.020 |
| 20.9 | | 0.05947 | 1.26 | 0.914 |
| 19.3 | | 0.06424 | 1.32 | 0.790 |
| 18.3 | | 0.06794 | 1.29 | 0.741 |
| 17.3 | | 0.07167 | 1.32 | 0.765 |
| 16.3 | | 0.07618 | 1.36 | 0.763 |
| 15.3 | | 0.08091 | 1.39 | 0.723 |
| 14.1 | | 0.08794 | 1.36 | 0.672 |
| 13.4 | | 0.09236 | 1.32 | 0.654 |
| 12.6 | | 0.09880 | 1.21 | 0.751 |
| 11.7 | 94,370 | 0.1060 | 1.39 | 0.985 |
| 11.1 | 89,530 | 0.1117 | 1.48 | 0.938 |
| 10.2 | 82,270 | 0.1216 | 1.65 | 1.05 |
| 9.45 | 76,220 | 0.1312 | 1.84 | 0.839 |
| 8.50 | 68,560 | 0.1459 | 1.77 | 0.760 |
| 7.68 | 61,940 | 0.1616 | 1.82 | 0.704 |
| 6.75 | 54,440 | 0.1837 | 1.78 | 0.617 |
| 6.33 | 51,050 | 0.1960 | 1.63 | 0.720 |
| 5.75 | 46,380 | 0.2156 | 1.65 | 0.844 |
| 5.25 | 42,340 | 0.2362 | 1.54 | 1.28 |
| 5.08 | 40,930 | 0.2443 | 1.72 | 1.30 |
| 4.93 | 39,760 | 0.2518 | 1.91 | 1.51 |
| 4.58 | 36,940 | 0.2707 | 2.40 | 1.40 |
| 4.00 | 32,262 | 0.3110 | 3.10[19] | |
| 3.98 | 32,100 | 0.3115 | 2.81 [5] | 1.07 |
| 3.83 | 30,890 | 0.3237 | 2.98 | 0.86 |
| 3.63 | 29,280 | 0.3420 | 3.20 | 0.62 |

*(continued)*

TABLE II (*Continued*)

**Barium Titanate**

| eV | $cm^{-1}$ | μm | $n_o(\perp)$ | $k_o(\perp)$ | $n_e(\|\|)$ | $k_e(\|\|)$ |
|---|---|---|---|---|---|---|
| 3.500 | 28,229 | 0.3542 | 2.82[19] | | | |
| 3.270 | 26,347 | 0.3792 | | | | $1.08\times10^{-3}$[11] |
| 3.180 | 25,648 | 0.3899 | | $1.33\times10^{-3}$[11] | | $1.68\times10^{-4}$ |
| 3.150 | 25,406 | 0.3936 | | $6.42\times10^{-4}$ | | $7.11\times10^{-5}$ |
| 3.100 | 25,003 | 0.4000 | | 1.91 | | 1.91 |
| | | | | | | 1.49 [12] |
| 3.050 | 24,600 | 0.4065 | | $5.53\times10^{-5}$ | | $5.53\times10^{-6}$[11] |
| 3.000 | 24,196 | 0.4133 | 2.64 | 1.38 | | |
| 2.950 | 23,793 | 0.4203 | | $3.68\times10^{-6}$ | | |
| 2.938 | 23,697 | 0.422 | 2.645[7] | $5.84\times10^{-6}$[12] | 2.541[7] | $6.51\times10^{-6}$[12] |
| 2.755 | 22,222 | 0.450 | 2.578 | 1.86 | 2.492 | 2.51 |
| 2.610 | 21,053 | 0.475 | 2.534 | 1.25 | 2.461 | 1.70 |
| 2.500 | 20,164 | 0.4959 | 2.51[19] | | | |
| 2.480 | 20,000 | 0.500 | 2.500[7] | 1.03 | 2.436 | 1.55 |
| 2.362 | 19,048 | 0.525 | 2.478 | $9.6\times10^{-7}$ | 2.416 | 1.46 |
| 2.254 | 18,182 | 0.550 | 2.459 | 8.8 | 2.400 | 1.44 |
| 2.156 | 17,391 | 0.575 | 2.442 | 7.8 | 2.385 | 1.37 |
| 2.066 | 16,667 | 0.600 | 2.430 | 7.2 | 2.372 | 1.29 |
| 2.000 | 16,131 | 0.6199 | 2.42[19] | | | |
| 1.984 | 16,000 | 0.625 | 2.416[7] | 7.0 | 2.362 | 1.14 |
| 1.907 | 15,385 | 0.650 | 2.405 | 6.2 | 2.352 | 1.03 |
| 1.837 | 14,815 | 0.675 | 2.396 | 3.8 | 2.344 | 1.02 |
| 1.797 | 14,493 | 0.690 | 2.390 | 2.8 | 2.340 | $9.6\times10^{-7}$ |
| 1.710 | 13,793 | 0.725 | 2.379 | | 2.332 | 7.5 |
| 1.653 | 13,333 | 0.750 | 2.372 | | 2.327 | 6.0 |
| 1.600 | 12,903 | 0.775 | 2.366 | | 2.321 | 5.6 |
| 1.550 | 12,500 | 0.800 | 2.361 | | 2.317 | 5.1 |
| 1.503 | 12,121 | 0.825 | 2.356 | | 2.313 | 4.8 |
| 1.500 | 12,098 | 0.8266 | 2.36[19] | | | |
| 1.459 | 11,765 | 0.850 | 2.352[7] | | 2.309 | 4.1 |
| 1.417 | 11,429 | 0.875 | 2.348 | | 2.305 | |
| 1.378 | 11,111 | 0.900 | 2.344 | | 2.302 | |
| 1.305 | 10,526 | 0.950 | 2.338 | | 2.297 | |
| 1.240 | 10,000 | 1.00 | 2.332 | | 2.292 | |
| 1.181 | 9,524 | 1.05 | 2.328 | | 2.288 | |
| 1.127 | 9,091 | 1.10 | 2.324 | | 2.284 | |
| 1.078 | 8,696 | 1.15 | 2.320 | | 2.281 | |
| 1.033 | 8,333 | 1.20 | 2.317 | | 2.279 | |
| 1.000 | 8,065 | 1.240 | 2.32[19] | | | |
| 0.9919 | 8,000 | 1.25 | 2.314[7] | | 2.277 | |

*(continued)*

TABLE II (*Continued*)

**Barium Titanate**

| eV | $cm^{-1}$ | μm | $n_o(\perp)$ | $k_o(\perp)$ | $n_e(\|\|)$ | $k_e(\|\|)$ |
|---|---|---|---|---|---|---|
| 0.9537 | 7,692 | 1.30 | 2.312[7] | | 2.275[7] | |
| 0.9184 | 7,407 | 1.35 | 2.310 | | 2.273 | |
| 0.8856 | 7,143 | 1.40 | 2.308 | | 2.271 | |
| 0.8551 | 6,897 | 1.45 | 2.307 | | 2.270 | |
| 0.8266 | 6,667 | 1.50 | 2.305 | | 2.268 | |
| 0.7999 | 6,452 | 1.55 | 2.304 | | 2.267 | |
| 0.7749 | 6,250 | 1.60 | 2.303 | | 2.266 | |
| 0.7514 | 6,061 | 1.65 | 2.301 | | 2.265 | |
| 0.75 | 6,049 | 1.653 | 2.31[19] | | | |
| 0.7293 | 5,882 | 1.70 | 2.300[7] | | 2.264 | |
| 0.7085 | 5,714 | 1.75 | 2.300 | | 2.264 | |
| 0.6888 | 5,556 | 1.80 | 2.299 | | 2.263 | |
| 0.6702 | 5,405 | 1.85 | 2.298 | | 2.262 | |
| 0.6526 | 5,263 | 1.90 | 2.297 | | 2.262 | |
| 0.6358 | 5,128 | 1.95 | 2.297 | | 2.261 | |
| 0.6199 | 5,000 | 2.00 | 2.296 | | 2.260 | |
| 0.5 | 4,033 | 2.480 | 2.30[19] | | | |
| 0.4960 | 4,000 | 2.50 | 2.27[20] | $2.48\times10^{-2}$[20] | 2.21[20] | $3.15\times10^{-2}$[20] |
| 0.4092 | 3,300 | 3.03 | 2.25 | 2.97 | 2.19 | 3.79 |
| 0.3472 | 2,800 | 3.57 | 2.23 | 3.46 | 2.18 | 4.42 |
| 0.3100 | 2,500 | 4.00 | 2.22 | 3.83 | 2.16 | 4.91 |
| 0.2728 | 2,200 | 4.55 | 2.19 | 4.28 | 2.14 | 5.51 |
| 0.2480 | 2,000 | 5.00 | 2.16 | 4.62 | 2.11 | 5.99 |
| 0.2356 | 1,900 | 5.26 | 2.15 | 4.82 | 2.10 | 6.25 |
| 0.2232 | 1,800 | 5.56 | 2.13 | 5.02 | 2.08 | 6.54 |
| 0.2108 | 1,700 | 5.88 | 2.10 | 5.23 | 2.06 | 6.84 |
| 0.1984 | 1,600 | 6.25 | 2.08 | 5.45 | 2.04 | 7.16 |
| 0.1860 | 1,500 | 6.67 | 2.04 | 5.67 | 2.00 | 7.48 |
| 0.1736 | 1,400 | 7.14 | 2.00 | $5.88\times10^{-2}$ | 1.97 | 7.81 |
| 0.1653 | 1,333 | 7.5 | | $1.37\times10^{-3}$[18] | | |
| 0.1612 | 1,300 | 7.69 | 1.95 | $6.06\times10^{-2}$[20] | 1.92 | 8.11 |
| 0.1600 | 1,290 | 7.75 | | $2.03\times10^{-3}$ | | |
| 0.1550 | 1,250 | 8.0 | | 2.93[18] | | |
| 0.1503 | 1,212 | 8.25 | | 3.87 | | |
| 0.1488 | 1,200 | 8.33 | 1.88 | $6.18\times10^{-2}$[20] | 1.85 | 8.33 |
| 0.1459 | 1,176 | 8.5 | | $3.38\times10^{-3}$[18] | | |
| 0.1417 | 1,143 | 8.75 | | 2.85 | | |
| 0.1378 | 1,111 | 9.0 | | 3.58 | | |
| 0.1364 | 1,100 | 9.09 | 1.78 | $6.15\times10^{-2}$[20] | 1.76 | 8.35 |
| 0.1305 | 1,053 | 9.5 | | $5.74\times10^{-3}$[18] | | |

*(continued)*

**TABLE II (*Continued*)**

**Barium Titanate**

| eV | $cm^{-1}$ | μm | $n_o(\perp)$ | $k_o(\perp)$ | $n_e(\|\|)$ | $k_e(\|\|)$ |
|---|---|---|---|---|---|---|
| 0.1240 | 1,000 | 10.00 | 1.65[20] | $5.81\times10^{-2}$[20] $8.75\times10^{-3}$[18] | 1.63[20] | $7.89\times10^{-2}$[20] |
| 0.1215 | 980 | 10.20 | 1.61 | $5.68\times10^{-2}$[20] | 1.59 | 7.68 |
| 0.1181 | 952.4 | 10.5 | | $1.33\times10^{-2}$[18] | | |
| 0.1203 | 970 | 10.31 | 1.60 | 5.60 [20] | 1.57 | 7.56 |
| 0.1190 | 960 | 10.42 | 1.58 | 5.51 | 1.55 | 7.42 |
| 0.1178 | 950 | 10.53 | 1.56 | 5.41 | 1.54 | 7.26 |
| 0.1116 | 940 | 10.64 | 1.54 | 5.30 | 1.51 | 7.09 |
| 0.1153 | 930 | 10.75 | 1.52 | 5.18 | 1.49 | 6.89 |
| 0.1141 | 920 | 10.87 | 1.50 | 5.05 | 1.47 | 6.66 |
| 0.1128 | 910 | 10.99 | 1.47 | 4.90 | 1.44 | 6.40 |
| 0.1127 | 909.1 | 11.0 | | 1.88 [18] | | |
| 0.1160 | 900 | 11.11 | 1.45 | 4.73 [20] | 1.42 | 6.11 |
| 0.1104 | 890 | 11.24 | 1.42 | 4.54 | 1.39 | 5.78 |
| 0.1091 | 880 | 11.36 | 1.40 | 4.34 | 1.36 | 5.41 |
| 0.1079 | 870 | 11.49 | 1.37 | 4.10 | 1.33 | 4.98 |
| 0.1078 | 869.6 | 11.5 | | 2.74 [18] | | |
| 0.1066 | 860 | 11.63 | 1.34 | 3.84 [20] | 1.30 | 4.50 |
| 0.1054 | 850 | 11.76 | 1.30 | 3.55 | 1.26 | 3.94 |
| 0.1042 | 840 | 11.90 | 1.27 | 3.22 | 1.22 | 3.29 |
| 0.1029 | 830 | 12.05 | 1.23 | 2.84 | 1.18 | 2.54 |
| 0.1017 | 820 | 12.20 | 1.20 | 2.41 | 1.14 | 1.67 |
| 0.1004 | 810 | 12.35 | 1.15 | 1.92 | 1.09 | $6.27\times10^{-3}$ |
| 0.0992 | 800 | 12.50 | 1.11 | 1.36 | 1.03 | 6.18 |
| 0.0980 | 790 | 12.66 | 1.06 | $6.92\times10^{-3}$ | 0.976 | $2.14\times10^{-2}$ |
| 0.0967 | 780 | 12.82 | 1.01 | $9.18\times10^{-4}$ | 0.911 | 4.03 |
| 0.0955 | 770 | 12.99 | 0.946 | $1.04\times10^{-2}$ | 0.837 | 6.45 |
| 0.0942 | 760 | 13.16 | 0.880 | 2.20 | 0.754 | $9.69\times10^{-2}$ |
| 0.0930 | 750 | 13.33 | 0.807 | 3.68 | 0.659 | 0.143 |
| 0.0918 | 740 | 13.51 | 0.723 | 5.65 | 0.552 | 0.212 |
| 0.0905 | 730 | 13.70 | 0.625 | 8.46 | 0.447 | 0.319 |
| 0.0893 | 720 | 13.89 | 0.508 | 0.130 | 0.372 | 0.459 |
| 0.0880 | 710 | 14.08 | 0.372 | 0.215 | 0.335 | 0.605 |
| 0.0868 | 700 | 14.29 | 0.262 | 0.364 | 0.321 | 0.741 |
| 0.0856 | 690 | 14.49 | 0.214 | 0.523 | 0.320 | 0.867 |
| 0.0843 | 680 | 14.71 | 0.197 | 0.662 | 0.326 | 0.987 |
| 0.0831 | 670 | 14.93 | 0.191 | 0.785 | 0.338 | 1.10 |
| 0.0818 | 660 | 15.15 | 0.192 | 0.898 | 0.354 | 1.21 |
| 0.0806 | 650 | 15.38 | 0.196 | 1.00 | 0.374 | 1.32 |
| 0.0794 | 640 | 15.63 | 0.202 | 1.11 | 0.399 | 1.43 |

*(continued)*

TABLE II (*Continued*)

**Barium Titanate**

| eV | $cm^{-1}$ | μm | $n_o(\perp)$ | $k_o(\perp)$ | $n_e(\|\|)$ | $k_e(\|\|)$ |
|---|---|---|---|---|---|---|
| 0.0781 | 630 | 15.87 | 0.210[20] | 1.20[20] | 0.427[20] | 1.55[20] |
| 0.0769 | 620 | 16.13 | 0.220 | 1.30 | 0.461 | 1.66 |
| 0.0756 | 610 | 16.39 | 0.232 | 1.40 | 0.501 | 1.77 |
| 0.0744 | 600 | 16.67 | 0.246 | 1.50 | 0.550 | 1.89 |
| 0.0732 | 590 | 16.95 | 0.262 | 1.59 | 0.608 | 2.02 |
| 0.0719 | 580 | 17.24 | 0.281 | 1.69 | 0.681 | 2.15 |
| 0.0707 | 570 | 17.54 | 0.304 | 1.79 | 0.773 | 2.29 |
| 0.0694 | 560 | 17.86 | 0.331 | 1.89 | 0.893 | 2.44 |
| 0.0682 | 550 | 18.18 | 0.366 | 2.01 | 1.06 | 2.59 |
| 0.0670 | 540 | 18.52 | 0.410 | 2.12 | 1.29 | 2.73 |
| 0.0657 | 530 | 18.87 | 0.471 | 2.26 | 1.63 | 2.83 |
| 0.0645 | 520 | 19.23 | 0.561 | 2.40 | 2.11 | 2.77 |
| 0.0632 | 510 | 19.61 | 0.709 | 2.58 | 2.60 | 2.36 |
| 0.0620 | 500 | 20.00 | 0.994 | 2.76 | 2.71 | 1.62 |
| 0.0608 | 490 | 20.41 | 1.63 | 2.81 | 2.32 | 0.99 |
| 0.0595 | 480 | 20.83 | 2.32 | 1.80 | 1.65 | 0.68 |
| 0.0583 | 470 | 21.28 | 1.35 | 0.69 | 0.849 | 0.81 |
| 0.0570 | 460 | 21.74 | 0.165 | 1.26 | 0.428 | 1.42 |
| 0.0558 | 450 | 22.22 | $8.56 \times 10^{-2}$ | 1.85 | 0.374 | 1.91 |
| 0.0546 | 440 | 22.73 | 0.111 | 2.17 | 0.408 | 2.27 |
| 0.0533 | 430 | 23.26 | 0.148 | 2.40 | 0.472 | 2.58 |
| 0.0521 | 420 | 23.81 | 0.185 | 2.60 | 0.555 | 2.85 |
| 0.0508 | 410 | 24.39 | 0.220 | 2.76 | 0.652 | 3.10 |
| 0.0496 | 400 | 25.00 | 0.254 | 2.92 | 0.763 | 3.34 |
| 0.0484 | 390 | 25.64 | 0.287 | 3.07 | 0.890 | 3.58 |
| 0.0471 | 380 | 26.32 | 0.320 | 3.22 | 1.04 | 3.83 |
| 0.0459 | 370 | 27.03 | 0.354 | 3.37 | 1.21 | 4.07 |
| 0.0446 | 360 | 27.78 | 0.389 | 3.52 | 1.41 | 4.32 |
| 0.0434 | 350 | 28.57 | 0.425 | 3.68 | 1.66 | 4.56 |
| 0.0422 | 340 | 29.41 | 0.464 | 3.84 | 1.95 | 4.81 |
| 0.0409 | 330 | 30.30 | 0.507 | 4.01 | 2.29 | 5.04 |
| 0.0397 | 320 | 31.25 | 0.563 | 4.20 | 2.70 | 5.23 |
| 0.0384 | 310 | 32.26 | 0.700 | 4.41 | 3.18 | 5.38 |
| 0.0372 | 300 | 33.33 | 0.691 | 4.41 | 3.72 | 5.44 |
| 0.0360 | 290 | 34.48 | 0.688 | 4.65 | 4.30 | 5.38 |
| 0.0347 | 280 | 35.71 | 0.736 | 4.88 | 4.88 | 5.17 |
| 0.0335 | 270 | 37.04 | 0.793 | 5.11 | 5.38 | 4.83 |
| 0.0322 | 260 | 38.46 | 0.855 | 5.35 | 5.77 | 4.39 |
| 0.0310 | 250 | 40.00 | 0.922 | 5.60 | 6.01 | 3.90 |
| 0.0298 | 240 | 41.67 | 0.993 | 5.87 | 6.11 | 3.42 |

*(continued)*

TABLE II (*Continued*)

**Barium Titanate**

| eV | $cm^{-1}$ | μm | $n_o(\perp)$ | $k_o(\perp)$ | $n_e(\|\|)$ | $k_e(\|\|)$ |
|---|---|---|---|---|---|---|
| 0.0285 | 230 | 43.48 | 1.07[20] | 6.18[20] | 6.08[20] | 2.99[20] |
| 0.0273 | 220 | 45.45 | 1.14 | 6.52 | 5.94 | 2.62 |
| 0.0260 | 210 | 47.62 | 1.19 | 6.92 | 5.67 | 2.34 |
| 0.0248 | 200 | 50.00 | 1.19 | 7.46 | 5.16 | 2.22 |
| 0.0242 | 195 | 51.28 | 1.14 | 7.86 | 4.68 | 2.33 |
| 0.0236 | 190 | 52.63 | 1.00 | 8.57 | 3.86 | 2.91 |
| 0.0231 | 186 | 53.76 | 0.88 | 9.96 | 3.14 | 4.62 |
| 0.0228 | 184 | 54.35 | 1.33 | 11.7 | 3.35 | 6.32 |
| 0.0227 | 183 | 54.64 | 2.57 | 13.1 | 3.88 | 7.42 |
| 0.0226 | 182 | 54.95 | 5.61 | 13.5 | 5.01 | 8.63 |
| 0.0224 | 181 | 55.25 | 7.82 | 10.8 | 7.10 | 9.46 |
| 0.0223 | 180 | 55.56 | 7.29 | 8.41 | 9.81 | 8.78 |
| 0.0221 | 178 | 56.18 | 5.41 | 6.95 | 11.3 | 4.56 |
| 0.0218 | 176 | 56.82 | 4.35 | 6.84 | 10.1 | 2.65 |
| 0.0211 | 170 | 58.82 | 3.28 | 7.32 | 8.19 | 1.44 |
| 0.0205 | 165 | 60.61 | 3.07 | 7.70 | 7.54 | 1.21 |
| 0.0198 | 160 | 62.50 | 3.04 | 8.03 | 7.17 | 1.09 |
| 0.0186 | 150 | 66.67 | 3.17 | 8.63 | 6.74 | 0.928 |
| 0.0174 | 140 | 71.43 | 3.44 | 9.22 | 6.48 | 0.811 |
| 0.0161 | 130 | 76.92 | 3.81 | 9.84 | 6.29 | 0.712 |
| 0.0149 | 120 | 83.33 | 4.28 | 10.5 | 6.16 | 0.627 |
| 0.0136 | 110 | 90.91 | 4.87 | 11.2 | 6.04 | 0.550 |
| 0.0124 | 100 | 100.0 | 5.59 | 12.0 | 5.95 | 0.482 |
| 0.0112 | 90 | 111.1 | 6.48 | 12.8 | 5.88 | 0.419 |
| 0.0099 | 80 | 125.0 | 7.59 | 13.8 | 5.81 | 0.362 |
| 0.0087 | 70 | 142.9 | 9.00 | 14.8 | 5.76 | 0.309 |
| 0.0074 | 60 | 166.7 | 10.8 | 15.9 | 5.72 | 0.259 |
| 0.0062 | 50 | 200.0 | 13.2 | 17.0 | 5.68 | 0.212 |
| 0.0050 | 40 | 250.0 | 16.4 | 18.1 | 5.65 | 0.167 |
| 0.0037 | 30 | 333.3 | 20.9 | 19.1 | 5.63 | 0.124 |
| 0.0025 | 20 | 500.0 | 27.7 | 19.0 | 5.61 | $8.20 \times 10^{-2}$ |
| 0.0012 | 10 | 1000.0 | 37.8 | 15.0 | 5.61 | $4.08 \times 10^{-2}$ |
| 0.0744 | 600 | 16.67 | | | 0.44[21] | 2.05[21] |
| 0.0719 | 580 | 17.24 | | | 0.48 | 2.29 |
| 0.0694 | 560 | 17.86 | | | 0.67 | 2.82 |
| 0.0670 | 540 | 18.52 | | | 0.99 | 3.24 |
| 0.0657 | 530 | 18.87 | | | 1.34 | 3.43 |
| 0.0645 | 520 | 19.23 | | | 2.05 | 3.42 |
| 0.0632 | 510 | 19.61 | | | 2.93 | 2.93 |
| 0.0620 | 500 | 20.00 | | | 3.60 | 1.39 |

*(continued)*

TABLE II (*Continued*)

**Barium Titanate**

| eV | $cm^{-1}$ | μm | $n_o(\perp)$ | $k_o(\perp)$ | $n_e(\|\|)$ | $k_e(\|\|)$ |
|---|---|---|---|---|---|---|
| 0.0595 | 480 | 20.83 | | | 1.39[21] | 0.65[21] |
| 0.0570 | 460 | 21.74 | | | 0.13 | 1.88 |
| 0.0546 | 440 | 22.73 | | | 0.091 | 2.74 |
| 0.0521 | 420 | 23.81 | | | 0.24 | 3.17 |
| 0.0496 | 400 | 25.00 | | | 0.27 | 3.75 |
| 0.0471 | 380 | 26.32 | | | 0.28 | 4.48 |
| 0.0446 | 360 | 27.78 | | | 0.44 | 5.12 |
| 0.0422 | 340 | 29.41 | | | 0.77 | 5.88 |
| 0.0397 | 320 | 31.25 | | | 1.35 | 7.06 |
| 0.0384 | 310 | 32.26 | | | 1.82 | 7.70 |
| 0.0372 | 300 | 33.33 | | | 2.60 | 8.47 |
| 0.0360 | 290 | 34.48 | | | 3.70 | 9.34 |
| 0.0347 | 280 | 35.71 | | | 5.36 | 9.79 |
| 0.0335 | 270 | 37.04 | | | 8.09 | 8.97 |
| 0.0322 | 260 | 38.46 | | | 9.81 | 7.44 |
| 0.0298 | 240 | 41.67 | | | 9.33 | 3.48 |
| 0.0273 | 220 | 45.45 | | | 6.08 | 2.24 |
| 0.0260 | 210 | 47.62 | | | 7.15 | 2.03 |
| 0.0248 | 200 | 50.00 | | | 5.68 | 2.29 |
| 0.0236 | 190 | 52.63 | | | 3.42 | 4.67 |
| 0.0223 | 180 | 55.55 | | | 7.52 | 13.3 |
| 0.0211 | 170 | 58.82 | | | 10.9 | 0.0046 |
| 0.0198 | 160 | 62.50 | | | 9.11 | 0.082 |
| 0.0186 | 150 | 66.67 | | | 8.37 | 0.11 |
| 0.0174 | 140 | 71.43 | | | 7.75 | 0.13 |
| 0.0149 | 120 | 83.33 | | | 7.07 | 0.13 |
| 0.0124 | 100 | 100.0 | | | 6.71 | 0.097 |

[a] The references are given in brackets at the beginning of the tabulation of $n$ and $k$ and are understood to refer to all $n$'s or all $k$'s below it until a new reference appears. When an exponent of 10 is given, all numbers below it have the same exponent until the power of 10 changes or the next number has $10^{-1}$, which is usually written as a decimal. The samples used in Refs. [7], [11] and [12] were melt-grown. Method of sample growth were not mentioned in Refs. [5] and [20]. The optical constants from Ref. [5] are for unpoled samples.

# Beryllium Oxide (BeO)

DAVID F. EDWARDS and RICHARD H. WHITE
University of California
Lawrence Livermore National Laboratory
Livermore, California

The optical properties of crystalline synthetic beryllium oxide, BeO, have been reported for a very limited number of samples. The main reasons for this lack of data are probably the toxic properties of the material and the difficulty of growing large optical-quality crystals [1]. As pointed out by Peterson and Palma [2], BeO is a useful new optical material for the vacuum UV because of its high transmittance down to about 9.4 eV (1320 Å) and its apparent resistance to UV radiation damage. In their report they show only the transmittance and, unfortunately, not enough data to estimate the $n$ and $k$ values for the 3–10 eV region. Calculations by White, Edwards, and Rathkopf [3] predict that overlayers of BeO on metallic reflectors should significantly enhance their hardness to X-ray radiation.

Natural bromellite (BeO) and synthetically grown BeO crystals are uniaxially positive. Newkirk *et al.* [4], using the angle-of-minimum-deviation technique, have measured the ordinary and extraordinary refractive indices and their dependence on temperature from 0.430 μm to 0.690 μm.

Loh [5] has evaluated the ordinary and extraordinary infrared refractive indices and extinction coefficients for BeO from their polarized reflectance spectra. The $n$ and $k$ values were derived from parameters used to fit the classical oscillator dispersion formula to the reflectance spectra. The well-known formula, as used by Loh, is

$$\varepsilon(\omega) - n_\infty^2 = (\varepsilon_0 - n_\infty^2)\omega_0^2/(\omega_0^2 - \omega^2 + i\gamma\omega),$$

where $\varepsilon_0$ is the static dielectric constant, and $n_\infty{}^2$ is the high-frequency dielectric constant. $\gamma$ is a phenomenological damping term, and $\omega_0$ is the transverse optical resonance frequency. These classical dispersion parameters are given in Table I. The $n$ and $k$ values were determined from the


Copyright © 1991 by Academic Press.
All rights of reproduction in any form reserved.
ISBN 0-12-544422-2

complex dielectric constant and are included in Table II (and Fig. 1) for the infrared region 100 to 1400 $cm^{-1}$ (100 to 7.14 μm). These calculations were extended beyond the measurement range (up to 400 $cm^{-1}$) to 100 $cm^{-1}$ in order to estimate the static dielectric constant, $\varepsilon_o$. From the classical dispersion analysis of Loh, $\varepsilon_o(\|) = 7.65$ and $\varepsilon_o(\perp) = 6.94$. From Table II, $n(\|)^2 = 7.765$ and $n(\perp)^2 = 6.96$ at 100 $cm^{-1}$.

The indices of refraction between 0.440 μm and 7.0 μm have been fit to both a Herzberger-type and a modified Sellmeier-type dispersion formula. A total of 31 and 29 wavelengths were used for fitting the ordinary and extraordinary indices, respectively. The indices for wavelengths greater than 7.0 μm are from the lattice band spectra of Loh [5] and are not included in the dispersion formulas.

The Herzberger-type dispersion formula for the index is [6]

$$n = A + BL + CL^2 + D\lambda^2 + E\lambda^4,$$

where $L = 1/(\lambda^2 - 2.80 \times 10^6)$ with $\lambda$ in angstroms. As explained by Herzberger [6], the $2.80 \times 10^6$ is the square of the mean asymptote for the short-wavelength abrupt increase in the index for 14 materials (BeO not included). The coefficients for the room-temperature ordinary indices, evaluated by least squares, are $A = 1.699773$, $B = 7.451288 \times 10^2$, $C = -4.331397 \times 10^{12}$, $D = -8.194535 \times 10^{-12}$, and $E = -1.659630 \times 10^{-20}$. The RMS error between the measured values and the dispersion formula calculated indices is 0.355% for the 0.440 to 7.0 μm range. The coefficients for the extraordinary indices are $A = 1.715140$, $B = 7.871215 \times 10^5$, $C = -4.782711 \times 10^{12}$, $D = -2.139439 \times 10^{-11}$, and $E = -1.390880 \times 10^{-20}$. The RMS error is 0.263%. The calculated $n_o$ and $n_e$ values are included in Table II.

The modified Sellmeier-type dispersion formula [7] is

$$n^2 = 1 + A/(\lambda^2 - B) + C\lambda^2/(\lambda^2 - D),$$

where the wavelength $\lambda$ is in angstroms. For the 31 ordinary and 29 extraordinary data points, the coefficients are as follows. For the ordinary index of refraction, $A = 3.698124 \times 10^{-6}$, $B = -1.878147 \times 10^{-6}$, $C = 1.953730$, and $D = 1.472502 \times 10^{-6}$. The extraordinary coefficients are $A = 3.257604 \times 10^{-6}$, $B = -1.609457 \times 10^{-6}$, $C = 1.997330$, and $D = 1.548286 \times 10^{-6}$. The RMS errors are 0.228% and 0.216% for the ordinary and extraordinary indices, respectively. The Sellmeier-calculated indices are not tabulated here but the equation and coefficients are included for completeness.

Worrell [8] has determined the infrared optical constants for commer-

cially available ceramic beryllia, BeO. He evaluated $n$ and $k$ from a Kramers–Kronig analysis of the reflectance spectrum at near normal incidence. His results for one of the two measured samples are tabulated in Table III. The data for the second sample are not listed here but have the same general features with some variation in detail. Comparisons have been made of these ceramic data with those of Loh [5] for the crystalline BeO. The ceramic beryllia is optically isotropic compared with the uniaxial crystalline BeO. Plots of the ceramic data are not shown here but a comparison with the Loh data shows that the reststrahlen band is the same for the two materials: 1200 to 600 $cm^{-1}$. The maximum reflectance at the center of this band (around 800 $cm^{-1}$) is less than that of the crystalline BeO: approximately, 84% versus 96%. This lower reflectance is attributed to a lower density and the polycrystalline nature of the ceramic relative to the crystal. Differences in band profile are noted with the appearance of shoulder bands at approximately 1070 $cm^{-1}$ and 710 $cm^{-1}$ in the ceramic materials. The peak values of the index and extinction coefficient are about 10 to 13 for the crystal and about half that for the ceramic. The $n$ and $k$ values outside of the reststrahlen band show greater variation with the Loh data. The reason is that corrections were not applied by Worrell [8] to the Kramers–Kronig analysis to account for truncations.

Newkirk *et al.* [4] measured the ordinary and extraordinary indices at five different temperatures from $-12.06\pm0.01$°C to $44.85\pm0.01$°C, at five different wavelengths from 0.450 to 0.670 μm. They found the temperature coefficient of refractive index (dn/dT) to be essentially wavelength independent and linear with temperature. They report the ordinary coefficient to be $+8.18\times10^{-6}$/°C and $+13.40\times10^{-6}$/°C for the extraordinary index.

## REFERENCES


1. S. B. Austerman, "Growth of Beryllia Crystals," *J. Am. Ceram. Soc.* **46**, 6 (1963).
2. C. W. Peterson and G. E. Palma, "BeO as a Window in the Vacuum UV," *J. Opt. Soc. Am.* **63**, 387 (1973).
3. R. H. White, D. F. Edwards, and J. A. Rathkopf, "Hardening of Optical Coatings to the Effects of X-Rays," *J. Appl. Phys.* (in press).
4. H. W. Newkirk, D. K. Smith, and J. S. Kahn, "Synthetic Bromellite III. Some Optical Properties," *Am. Mineral.* **51**, 141 (1966).
5. E. Loh, "Optical Phonons in BeO Crystals," *Phys. Rev.* **166**, 673 (1968).
6. M. Herzberger and C. D. Salzberg, "Refractive Indices of Infrared Optical Materials and Color Correction of Infrared Lenses," *J. Opt. Soc. Am.* **52** 420 (1962); M. Herzberger, "Colour Correction in Optical Systems and a New Dispersion Formula," *Opt. Acta* **6**, 197 (1959).
7. D. F. Edwards and R. H. White, see KDP in this volume.
8. C. A. Worrell, "Infrared Optical Constants for $CO_2$ Laser Waveguide Materials," *J. Mater. Sci.* **21**, 781 (1986); private communication, (1990).

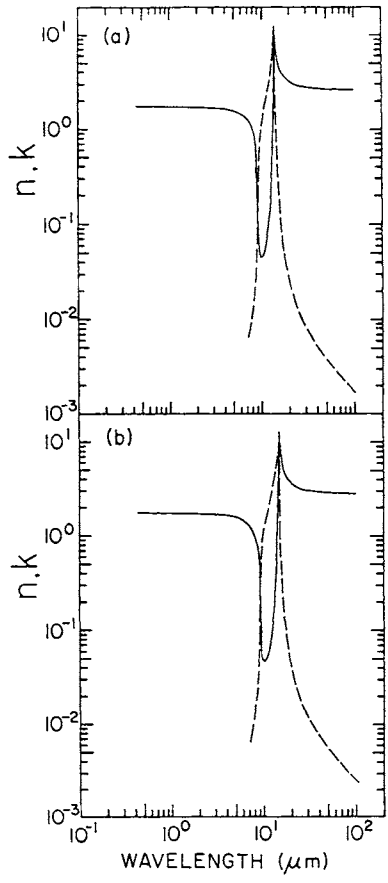


**Fig. 1.** (a) Log–log plot of $n_o$ (solid line) and $k_o$ (dashed line) versus wavelength in micrometers for beryllium oxide. (b) Log–log plot of $n_e$ (solid line) and $k_e$ (dashed line) versus wavelength in micrometers.

**TABLE I**

**Classical Dispersion Parameters for Evaluating the Infrared Optical Properties of BeO**

| | Ordinary (⊥) | Extraordinary (‖) |
|---|---|---|
| $\omega_o(cm^{-1})$ | 680 | 724 |
| $\lambda$ | 12.8 | 11.6 |
| $\varepsilon_o$ | 7.65 | 6.94 |
| $n_\infty^2$ | 2.99 | 2.95 |

**TABLE II**

**Values of *n* and *k* for Beryllium Oxide from Various References[a]**

| eV | $cm^{-1}$ | μm | $n_o$ (⊥) | $k_o$ (⊥) | $n_e$ (∥) | $k_e$ (∥) |
|---|---|---|---|---|---|---|
| 2.818 | 22,727 | 0.44 | 1.7288 [4] | | 1.7448 [4] | |
| 2.696 | 21,739 | 0.46 | 1.7273 | | 1.7434 | |
| 2.583 | 20,833 | 0.48 | 1.7258 | | 1.7419 | |
| 2.480 | 20,000 | 0.50 | 1.7243 | | 1.7403 | |
| 2.385 | 19,231 | 0.52 | 1.7229 | | 1.7389 | |
| 2.296 | 18,519 | 0.54 | 1.7216 | | 1.7375 | |
| 2.214 | 17,857 | 0.56 | 1.7203 | | 1.7362 | |
| 2.138 | 17,241 | 0.58 | 1.7191 | | 1.7349 | |
| 2.067 | 16,667 | 0.60 | 1.7180 | | 1.7337 | |
| 2.000 | 16,129 | 0.62 | 1.7169 | | 1.7326 | |
| 1.938 | 15,625 | 0.64 | 1.7160 | | 1.7316 | |
| 1.879 | 15,152 | 0.66 | 1.7151 | | 1.7306 | |
| 1.824 | 14,706 | 0.68 | 1.7142 | | 1.7297 | |
| 1.771 | 14,286 | 0.70 | 1.7134 [6] | | 1.7289 [6] | |
| 1.722 | 13,889 | 0.72 | 1.7127 | | 1.7281 | |
| 1.676 | 13,514 | 0.74 | 1.7120 | | 1.7273 | |
| 1.632 | 13,158 | 0.76 | 1.7114 | | 1.7266 | |
| 1.590 | 12,821 | 0.78 | 1.7108 | | 1.7259 | |
| 1.550 | 12,500 | 0.80 | 1.7102 | | 1.7253 | |
| 1.378 | 11,111 | 0.90 | 1.7078 | | 1.7226 | |
| 1.240 | 10,000 | 1.0 | 1.7060 | | 1.7205 | |
| 0.6199 | 5,000 | 2.0 | 1.6957 | | 1.7063 | |
| 0.4133 | 3,333 | 3.0 | 1.6798 | | 1.6855 | |
| 0.3100 | 2,500 | 4.0 | 1.6446 | | 1.6458 | |
| 0.2480 | 2,000 | 5.0 | 1.5759 | | 1.5750 | |
| 0.2067 | 1,667 | 6.0 | 1.4554 | | 1.4581 | |
| 0.1771 | 1,429 | 7.0 | 1.2613 | | 1.2765 | |
| 0.1736 | 1,400 | 7.143 | 1.230 [5] | 0.0076 [5] | 1.247 [5] | 0.007 [5] |
| 0.1674 | 1,350 | 7.407 | 1.166 | 0.008 | 1.187 | 0.008 |
| 0.1612 | 1,300 | 7.692 | 1.086 | 0.011 | 1.113 | 0.011 |
| 0.1550 | 1,250 | 8.000 | 0.981 | 0.014 | 1.018 | 0.014 |
| 0.1488 | 1,200 | 8.333 | 0.834 | 0.021 | 0.890 | 0.019 |
| 0.1457 | 1,175 | 8.511 | 0.735 | 0.026 | 0.806 | 0.024 |
| 0.1426 | 1,150 | 8.696 | 0.604 | 0.036 | 0.701 | 0.030 |
| 0.1395 | 1,125 | 8.889 | 0.411 | 0.060 | 0.562 | 0.043 |
| 0.1364 | 1,100 | 9 091 | 0.105 | 0.267 | 0.348 | 0.078 |
| 0.1333 | 1,075 | 9.302 | 0.057 | 0.568 | 0.089 | 0.344 |

**TABLE II (*Continued*)**

**Beryllium Oxide**

| eV | $cm^{-1}$ | μm | $n_o$ (⊥) | $k_o$ (⊥) | $n_e$ (∥) | $k_e$ (∥) |
|---|---|---|---|---|---|---|
| 0.1302 | 1,050 | 9.524 | 0.048 | 0.789 | 0.058 | 0.609 |
| 0.1271 | 1,025 | 9.756 | 0.045 | 0.986 | 0.050 | 0.816 |
| 0.1240 | 1,000 | 10.00 | 0.045 | 1.179 | 0.047 | 1.005 |
| 0.1209 | 975 | 10.26 | 0.047 | 1.375 | 0.047 | 1.189 |
| 0.1178 | 950 | 10.53 | 0.050 | 1.583 | 0.049 | 1.376 |
| 0.1147 | 925 | 10.81 | 0.056 | 1.810 | 0.052 | 1.573 |
| 0.1116 | 900 | 11.11 | 0.064 | 2.066 | 0.057 | 1.787 |
| 0.1085 | 875 | 11.43 | 0.076 | 2.365 | 0.065 | 2.024 |
| 0.1054 | 850 | 11.76 | 0.095 | 2.729 | 0.075 | 2.295 |
| 0.1023 | 825 | 12.12 | 0.126 | 3.196 | 0.091 | 2.617 |
| 0.09919 | 800 | 12.50 | 0.184 | 3.847 | 0.115 | 3.015 |
| 0.09609 | 775 | 12.90 | 0.321 | 4.879 | 0.157 | 3.537 |
| 0.09299 | 750 | 13.33 | 0.830 | 6.700 | 0.239 | 4.284 |
| 0.08989 | 725 | 13.79 | 10.089 | 11.834 | 0.444 | 5.523 |
| 0.08679 | 700 | 14.29 | 7.805 | 0.870 | 1.407 | 8.36 |
| 0.08369 | 675 | 14.81 | 5.725 | 0.296 | 13.180 | 7.050 |
| 0.08059 | 650 | 15.38 | 4.814 | 0.155 | 7.428 | 0.732 |
| 0.07749 | 625 | 16.00 | 4.287 | 0.097 | 5.715 | 0.289 |
| 0.07439 | 600 | 16.67 | 3.939 | 0.068 | 4.888 | 0.160 |
| 0.07129 | 575 | 17.39 | 3.689 | 0.050 | 4.389 | 0.103 |
| 0.06819 | 550 | 18.18 | 3.502 | 0.038 | 4.052 | 0.073 |
| 0.06509 | 525 | 19.05 | 3.355 | 0.030 | 3.807 | 0.054 |
| 0.06199 | 500 | 20.00 | 3.237 | 0.025 | 3.620 | 0.042 |
| 0.05889 | 475 | 21.05 | 3.141 | 0.020 | 3.474 | 0.034 |
| 0.05579 | 450 | 22.22 | 3.061 | 0.017 | 3.356 | 0.027 |
| 0.05269 | 425 | 23.53 | 2.993 | 0.014 | 3.259 | 0.023 |
| 0.04959 | 400 | 25.00 | 2.936 | 0.012 | 3.178 | 0.018 |
| 0.04339 | 350 | 28.57 | 2.845 | 9.1x10-3 | 3.052 | 0.0136 |
| 0.03720 | 300 | 33.3 | 2.776 | 6.9x10-3 | 2.960 | 0.010 |
| 0.03100 | 250 | 40 | 2.725 | 5.1x10-3 | 2.893 | 7.4x10-3 |
| 0.02480 | 200 | 50 | 2.686 | 3.8x10-3 | 2.843 | 5.4x10-3 |
| 0.01860 | 150 | 66.7 | 2.659 | 2.7x10-3 | 2.807 | 3.8x10-3 |
| 0.01240 | 100 | 100 | 2.639 | 1.7x10-3 | 2.783 | 2.4x10-3 |

[a] The $n_o$ and $n_e$ values for wavelength 7.0 μm and smaller were calculated with the Herzberger-type formula. The n and k values for wavelength greater than 7.0 μm were calculated from the reststrahlen data. The bracketed numbers indicate the reference to the data.

TABLE III

Values of $n$ and $k$ for Ceramic Beryllium Oxide [8]

| eV | $cm^{-1}$ | μm | n | k |
|---|---|---|---|---|
| 0.02244 | 181.0 | 55.25 | 2.6208 | 0.0799 |
| 0.02360 | 190.3 | 52.55 | 2.6270 | 0.0779 |
| 0.02480 | 200.0 | 50.00 | 2.6336 | 0.0784 |
| 0.02606 | 210.2 | 47.57 | 2.6410 | 0.0798 |
| 0.02740 | 221.0 | 45.25 | 2.6491 | 0.0819 |
| 0.02852 | 230.0 | 43.48 | 2.6562 | 0.0841 |
| 0.02982 | 240.5 | 41.58 | 2.6650 | 0.0871 |
| 0.03104 | 250.3 | 39.95 | 2.6735 | 0.0903 |
| 0.03230 | 260.5 | 38.39 | 2.6828 | 0.0938 |
| 0.03346 | 269.8 | 37.06 | 2.6917 | 0.0973 |
| 0.03482 | 280.8 | 35.61 | 2.7027 | 0.1018 |
| 0.03605 | 290.7 | 34.40 | 2.7131 | 0.1061 |
| 0.03715 | 299.6 | 33.38 | 2.7227 | 0.1101 |
| 0.03846 | 310.2 | 32.25 | 2.7348 | 0.1151 |
| 0.03963 | 319.6 | 31.29 | 2.7459 | 0.1198 |
| 0.04104 | 331.0 | 30.21 | 2.7599 | 0.1255 |
| 0.04209 | 339.4 | 29.46 | 2.7707 | 0.1298 |
| 0.04357 | 351.4 | 28.46 | 2.7869 | 0.1360 |
| 0.04468 | 360.3 | 27.75 | 2.8009 | 0.1397 |
| 0.04581 | 369.4 | 27.07 | 2.8138 | 0.1457 |
| 0.04723 | 380.9 | 26.25 | 2.8327 | 0.1522 |
| 0.04838 | 390.2 | 25.63 | 2.8485 | 0.1564 |
| 0.04961 | 400.1 | 24.99 | 2.8683 | 0.1602 |
| 0.05086 | 410.2 | 24.38 | 2.8905 | 0.1665 |
| 0.05214 | 420.5 | 23.78 | 2.9165 | 0.1718 |
| 0.05320 | 429.0 | 23.31 | 2.9376 | 0.1801 |
| 0.05454 | 439.8 | 22.74 | 2.9683 | 0.1928 |
| 0.05591 | 450.9 | 22.18 | 2.9961 | 0.2071 |
| 0.05704 | 460.0 | 21.74 | 3.0179 | 0.2199 |
| 0.05819 | 469.3 | 21.31 | 3.0375 | 0.2277 |
| 0.05967 | 481.2 | 20.78 | 3.0734 | 0.2323 |
| 0.06086 | 490.8 | 20.37 | 3.1129 | 0.2375 |
| 0.06209 | 500.7 | 19.97 | 3.1595 | 0.2499 |
| 0.06335 | 510.8 | 19.57 | 3.2034 | 0.2701 |
| 0.06462 | 521.1 | 19.19 | 3.2464 | 0.2892 |
| 0.06592 | 531.6 | 18.81 | 3.2978 | 0.3091 |
| 0.06691 | 539.6 | 18.53 | 3.3361 | 0.3238 |
| 0.06826 | 550.5 | 18.17 | 3.3931 | 0.3382 |

TABLE III (*Continued*)

**Beryllium Oxide**

| eV | $cm^{-1}$ | μm | n | k |
|---|---|---|---|---|
| 0.06964 | 561.6 | 17.81 | 3.4728 | 0.3566 |
| 0.07069 | 570.1 | 17.54 | 3.5387 | 0.3662 |
| 0.07212 | 581.6 | 17.19 | 3.6485 | 0.3993 |
| 0.07320 | 590.3 | 16.94 | 3.7442 | 0.4173 |
| 0.07467 | 602.2 | 16.61 | 3.9054 | 0.4786 |
| 0.07580 | 611.3 | 16.36 | 4.0367 | 0.5445 |
| 0.07694 | 620.5 | 16.12 | 4.1815 | 0.6166 |
| 0.07811 | 629.9 | 15.88 | 4.3584 | 0.7298 |
| 0.07929 | 639.4 | 15.64 | 4.5546 | 0.8448 |
| 0.08048 | 649.0 | 15.41 | 4.8086 | 1.0489 |
| 0.08169 | 658.8 | 15.18 | 5.1446 | 1.3233 |
| 0.08334 | 672.1 | 14.88 | 5.5384 | 2.0507 |
| 0.08459 | 682.2 | 14.66 | 5.6595 | 2.8332 |
| 0.08587 | 692.5 | 14.44 | 5.4389 | 3.7439 |
| 0.08673 | 699.4 | 14.30 | 5.1068 | 4.3753 |
| 0.08804 | 710.0 | 14.08 | 4.1266 | 5.1834 |
| 0.08937 | 720.7 | 13.88 | 2.9343 | 5.2651 |
| 0.09071 | 731.5 | 13.67 | 2.1243 | 4.8910 |
| 0.09208 | 742.6 | 13.47 | 1.6565 | 4.5246 |
| 0.09300 | 750.0 | 13.33 | 1.4092 | 4.3319 |
| 0.09440 | 761.3 | 13.14 | 1.0695 | 4.0385 |
| 0.09583 | 772.8 | 12.94 | 0.7918 | 3.7230 |
| 0.09678 | 780.5 | 12.81 | 0.6559 | 3.5065 |
| 0.09825 | 792.3 | 12.62 | 0.5184 | 3.2061 |
| 0.09922 | 800.2 | 12.50 | 0.4551 | 3.0236 |
| 0.1007 | 812.3 | 12.31 | 0.3912 | 2.7791 |
| 0.1017 | 820.4 | 12.19 | 0.3630 | 2.6336 |
| 0.1033 | 832.8 | 12.01 | 0.3359 | 2.4419 |
| 0.1043 | 841.2 | 11.89 | 0.3224 | 2.3282 |
| 0.1054 | 849.6 | 11.77 | 0.3125 | 2.2235 |
| 0.1069 | 862.4 | 11.60 | 0.2959 | 2.0818 |
| 0.1080 | 871.0 | 11.48 | 0.2872 | 1.9938 |
| 0.1091 | 879.8 | 11.37 | 0.2804 | 1.9097 |
| 0.1107 | 893.0 | 11.20 | 0.2704 | 1.7957 |
| 0.1118 | 902.0 | 11.09 | 0.2622 | 1.7242 |
| 0.1130 | 911.0 | 10.98 | 0.2525 | 1.6550 |
| 0.1141 | 920.2 | 10.87 | 0.2424 | 1.5876 |
| 0.1152 | 929.4 | 10.76 | 0.2320 | 1.5215 |
| 0.1170 | 943.4 | 10.60 | 0.2151 | 1.4235 |

**TABLE III (*Continued*)**

**Beryllium Oxide**

| eV | $cm^{-1}$ | μm | n | k |
|---|---|---|---|---|
| 0.1182 | 952.9 | 10.49 | 0.2032 | 1.3580 |
| 0.1193 | 962.4 | 10.39 | 0.1911 | 1.2919 |
| 0.1205 | 972.1 | 10.29 | 0.1791 | 1.2248 |
| 0.1217 | 981.8 | 10.19 | 0.1669 | 1.1556 |
| 0.1230 | 991.7 | 10.08 | 0.1564 | 1.0832 |
| 0.1242 | 1001.6 | 9.984 | 0.1488 | 1.0080 |
| 0.1254 | 1011.6 | 9.885 | 0.1453 | 0.9309 |
| 0.1267 | 1021.8 | 9.787 | 0.1466 | 0.8535 |
| 0.1280 | 1032.0 | 9.690 | 0.1510 | 0.7783 |
| 0.1293 | 1042.4 | 9.593 | 0.1531 | 0.7041 |
| 0.1305 | 1052.8 | 9.498 | 0.1507 | 0.6246 |
| 0.1319 | 1063.4 | 9.404 | 0.1463 | 0.5277 |
| 0.1332 | 1074.0 | 9.311 | 0.1602 | 0.4103 |
| 0.1345 | 1084.8 | 9.218 | 0.2098 | 0.2794 |
| 0.1352 | 1090.2 | 9.173 | 0.2469 | 0.2173 |
| 0.1365 | 1101.2 | 9.081 | 0.3590 | 0.1216 |
| 0.1379 | 1112.2 | 8.991 | 0.4797 | 0.0777 |
| 0.1393 | 1123.3 | 8.902 | 0.5733 | 0.0678 |
| 0.1414 | 1140.3 | 8.770 | 0.6778 | 0.0587 |
| 0.1428 | 1151.7 | 8.683 | 0.7388 | 0.0555 |
| 0.1442 | 1163.3 | 8.596 | 0.7874 | 0.0523 |
| 0.1457 | 1174.9 | 8.511 | 0.8354 | 0.0505 |
| 0.1464 | 1180.8 | 8.469 | 0.8586 | 0.0512 |
| 0.1479 | 1192.6 | 8.385 | 0.8996 | 0.0553 |
| 0.1494 | 1204.6 | 8.302 | 0.9347 | 0.0604 |
| 0.1501 | 1210.6 | 8.260 | 0.9476 | 0.0632 |
| 0.1516 | 1222.7 | 8.179 | 0.9770 | 0.0623 |
| 0.1524 | 1228.9 | 8.137 | 0.9900 | 0.0633 |
| 0.1539 | 1241.2 | 8.057 | 1.0180 | 0.0607 |
| 0.1554 | 1253.6 | 7.977 | 1.0484 | 0.0621 |
| 0.1562 | 1259.9 | 7.937 | 1.0621 | 0.0638 |
| 0.1578 | 1272.5 | 7.859 | 1.0858 | 0.0695 |
| 0.1594 | 1285.3 | 7.780 | 1.1072 | 0.0760 |
| 0.1602 | 1291.7 | 7.742 | 1.1169 | 0.0786 |
| 0.1618 | 1304.6 | 7.665 | 1.1369 | 0.0802 |
| 0.1626 | 1311.2 | 7.627 | 1.1469 | 0.0822 |
| 0.1642 | 1324.3 | 7.551 | 1.1670 | 0.0916 |
| 0.1650 | 1330.9 | 7.514 | 1.1744 | 0.0969 |
| 0.1667 | 1344.3 | 7.439 | 1.1850 | 0.1058 |

TABLE III (*Continued*)

**Beryllium Oxide**

| eV | $cm^{-1}$ | μm | n | k |
|---|---|---|---|---|
| 0.1675 | 1351.0 | 7.402 | 1.1900 | 0.1087 |
| 0.1692 | 1364.5 | 7.329 | 1.2002 | 0.1185 |
| 0.1701 | 1371.4 | 7.292 | 1.2040 | 0.1259 |
| 0.1718 | 1385.1 | 7.220 | 1.1972 | 0.1430 |
| 0.1726 | 1392.0 | 7.184 | 1.1838 | 0.1435 |
| 0.1735 | 1399.0 | 7.148 | 1.1714 | 0.1354 |
| 0.1752 | 1413.0 | 7.077 | 1.1636 | 0.1006 |
| 0.1761 | 1420.1 | 7.042 | 1.1711 | 0.0831 |
| 0.1779 | 1434.3 | 6.972 | 1.1968 | 0.0611 |
| 0.1787 | 1441.5 | 6.937 | 1.2132 | 0.0544 |
| 0.1823 | 1470.5 | 6.800 | 1.2617 | 0.0586 |
| 0.1917 | 1545.8 | 6.469 | 1.3150 | 0.0697 |
| 0.2015 | 1624.8 | 6.155 | 1.3571 | 0.0743 |
| 0.2226 | 1795.2 | 5.570 | 1.4255 | 0.0735 |
| 0.2460 | 1983.5 | 5.042 | 1.4726 | 0.1125 |

# Calcium Fluoride ($CaF_2$)

D. F. BEZUIDENHOUT
Division of Production Technology
Council for Scientific and Industrial Research
Pretoria, Republic of South Africa

X-ray diffraction analysis of calcium fluoride ($CaF_2$) has shown it to belong to the cubic fluorite structure. The $Ca^{2+}$ ions are arranged in a face-centered cubic lattice and the $F^-$ ions in a cubic lattice. Each fluorine ion is surrounded by four calcium ions and each calcium ion by eight fluorine ions [1, 2, 3]. The lattice constant $a_o$ is given as 0.546305 nm [4], which is slightly higher than $a_o = 0.545$ nm reported by Goldschmidt [5]. Based on symmetry considerations, $CaF_2$ is classified under the space group $Fm3m$ ($O_h^5$) [6].

An early account of the growth of "artificial" $CaF_2$ is given by Stockbarger [7]. At present, high-purity, synthetic $CaF_2$ material is readily available in cylindrical form up to 200 mm in diameter [8]. However, it has been reported that large crystals of optical quality $CaF_2$, 600 mm in diameter, have been grown by Sokolov *et al.* [9, 10]. In a more recent publication, Horowitz *et al.* gave a correlation between growth parameters and the chemical and structural quality of $CaF_2$ crystals [11]. Mechanical and thermal properties of synthetic $CaF_2$, which are relevant from an engineering point of view, are given by Combes *et al.* [12]. Because of the physical properties of calcium fluoride, both mechanical and thermal shock should be avoided during optical processing [7, 13, 14].

The wide transmission band (0.2–9 μm) of $CaF_2$ leads to a multitude of applications. These applications range from dispersive elements in infrared monochromators [15], filters for reducing stray light [16] and radiation-blocking elements [17, 18], to lenses and windows [19, 20]. When used as laser elements, the tendency of water to adsorb on $CaF_2$ surfaces should be kept in mind [21]. However, it has been found that laser-induced desorption treatment leads to passivated $CaF_2$ surfaces that are highly resistant to water adsorption at room temperature [22]. During the early 1940s, $CaF_2$ was used in thin-film form as antireflection coatings on glass lenses [23].


Copyright © 1991 by Academic Press.
All rights of reproduction in any form reserved.
ISBN 0-12-544422-2

More recent applications of $CaF_2$ include areas such as optical fibers [24] and laser host material [25].

*Synthetic Calcium Fluoride*

$CaF_2$, which is a highly ionic compound, has a wide band gap. The edge of the fundamental absorption band lies in the vacuum ultraviolet at about 12 eV [26]. Much of the X-ray and ultraviolet work has been centered on studies concerning the determination of the electronic structure of $CaF_2$ and on color-center phenomena [27, 28]. The forbidden energy band gap is formed by the $F^-$ $2p$ state and the $3d$ and $4s$ states of the $Ca^{2+}$ ions [26]. Rubloff [29] used the synchrotron radiation from a 240 MeV electron storage ring as a light source in the vacuum ultraviolet to investigate the reflectance spectrum of $CaF_2$ covering the photon energy range 6–36 eV. The characteristics of the reflection spectra above the fundamental absorption edge were divided into three regions. Peaks in region I (6–26 eV) arise from optical excitation of electrons in the valence band. The peaks at lower energy in the valence excitation region are caused by exciton absorption, whereas intraband transitions dominate at higher energies in region I. Although valence excitations may continue into regions II (26–30 eV) and III (30–36 eV) at higher photon energies, electrons are mainly excited from core states, which lie below the valence bands. A change to broader peaks occurs on passing from region II to III, where the spectral features are caused primarily by excitations of the core states of $Ca^{2+}$.

Cluster calculations on $CaF_2$ showed the influence of impurities on the position of the absorption edge: oxygen impurity caused transitions to appear in the region 4.3–5 eV [26]. However, the theoretical values for the excitation energies in $CaF_2$ associated with defects appear to be less than the experimental values [26]. The effect of impurities such as oxygen or hydroxyl ions is a sharp cutoff at 0.22 μm [30, 31].

Bontinck [32] reported on the formation of color centers in $CaF_2$. He identified a number of absorption bands in the visible and near-infrared regions after X-ray radiation or additive coloration at high temperatures. During investigation of the coloration and luminescence of $CaF_2$ crystals, Rauch *et al.* [33] found that crystals that differed relatively little as to UV absorption showed marked differences in their photoluminescence and thermoluminescence behavior. Exposure to an electric field or to X-rays also leads to a change in the absorption features of $CaF_2$ [34, 35]. De and Rao [35] subjected low-absorption $CaF_2$ crystals to a high AC (or DC) field. There seems to be a considerable interaction of the field with the crystal lattice, resulting in increased concentration of lattice defects, which increases the absorption at 0.2 μm. Furthermore, when these crystals were irradiated with X-rays, absorption bands were observed at 0.375 and 0.58 μm.

The importance of surface preparation for short-wavelength investi-

gations has been stated by two groups who have done reflectance and transmittance measurements over the absorption-edge region of $CaF_2$ (0.12–0.16 μm) [36, 37]. It was reported that as the surface polish is improved, the increase in transmission is greater at shorter rather than at longer wavelengths. Different types of abrasives did not play any significant role in the reflectance behavior of these surfaces at short wavelengths. However, it was suggested that fluorite powder be used for the final polishing step [36]. Furthermore, it was also stated that an adsorbed layer of water vapor might influence the reflective properties of a $CaF_2$ surface because the absorption of water is quite high in the 0.12–0.16 μm region.

The temperature dependence of the absorption tail was investigated over the temperature range 78–573 K [37, 38, 39]. Linear behavior was found in the shift of the absorption edge. The rate of thermal shift was expressed by Tomiki and Miyata [37] as $\Delta\lambda/\Delta T = 0.26$ Å/K at the $\alpha = 10\ cm^{-1}$ point, where $\alpha$ is the absorption coefficient. The transmission limit (that is, $T<1\%$) changed from 0.121 μm at 291 K to 0.1165 μm at 77 K, where the sample thicknesses ranged from 0.25–0.71 mm [38]. These facts should be kept in mind when $CaF_2$ is used as window material near its shortwave edge in thermal experiments. At wavelengths longer than 0.15 μm, the transmission of $CaF_2$ windows is not affected appreciably by temperatures up to 500 °C [40].

The reflecting power of a polished fluorite surface has been measured from 0.0927 μm to 0.1605 μm for angles of incidence varying from 45 to 85 degrees [41]. A vacuum spectrograph and a method of photographic photometry, using oil-sensitized photographic film were used. The oil layer on the surface of the film absorbs the incident extreme ultraviolet light completely and fluoresces in the near ultraviolet. It is this fluorescent radiation that exposes the film, and its intensity is proportional to that of the incident light reflected from the $CaF_2$ sample surface inside the spectrograph. Below 0.123 μm the reflection becomes metallic in character, and by applying the appropriate reflectance formula and a numerical method, the refractive index and extinction coefficient were determined over the 0.0927–0.119 μm region. The first absorption band below the cutoff edge of $CaF_2$ was identified in the vicinity of 0.1115 μm. This band corresponds to an energy of 11.12 eV, which is in good agreement with the results of later reports such as Rubloff [29], who found a reflection peak at 11.02 eV at 300 K.

The dispersion curve is anomalous from between 0.113 and 0.12 μm to about 0.109 μm, when crossing the center of the absorption band. It becomes normal again toward the shorter wavelengths, but appears to become anomalous again at 0.1 μm as the next absorption band is approached [41].

On the long-wave side of the cutoff edge, refractive-index values are given for wavelengths up to 0.1605 μm [41]. For longer wavelengths, the

publication by Malitson [42] is a most comprehensive report on the dispersive properties of $CaF_2$. He used a modified Gaertner precision spectrometer, fitted with reflecting optics, to measure at visible and nonvisible wavelengths. The method of minimum deviation was applied to determine refractive-index values from wavelengths of 0.2288–9.724 μm. The experimentally determined index values were fitted to a three-term Sellmeier dispersion equation of the form

$$n^2 - 1 = \sum A_j \lambda^2 / (\lambda^2 - \lambda_j^2). \tag{1}$$

The $\lambda_j$ represents ultraviolet and infrared absorption wavelengths and the $A_j$ is related to the strength of the absorption bands. The parameters of the equation are given in Table I. The dispersion formula was then used to compute the refractive index at 24 °C, at wavelengths separated by regular intervals (Table IV and Fig. 1).

Malitson [42] also investigated dispersion, chromatic abberation, and resolution. It was found that the dispersion decreases steadily with increasing wavelength, reaches a minimum at 1.5 μm, and then slowly increases again while approaching the long-wavelength cutoff. For the purpose of lens design, chromatism is therefore minimized in the region near 1.5 μm. Finally, $CaF_2$ was found to be an excellent choice as prism material in the wavelength range 4–9 μm.

The thermal coefficient of the refractive index was determined for the range 15–35 °C and for the range 35–55 °C [42]. The results can be summarized as follows:

(1) The value of $dn/dT$ is negative.

(2) The $dn/dT$ versus wavelength behavior shows a steeper slope in the ultraviolet than in the visible, indicating a shift of the ultraviolet bands toward longer wavelengths with an increase in temperature.

(3) In the visible region, increases in temperature lead to a decrease in refractive-index values.

(4) The absolute value of $dn/dT$ tends to increase with increasing wavelength and temperature.

(5) A decrease of the absolute $dn/dT$ values in the infrared indicates that the infrared absorption bands have also shifted toward longer wavelengths with increasing temperature.

(6) An average value of $-dn/dT$ for the temperature interval of 15–24 °C over the wavelength range 0.228–9.7 μm is $8.65 \times 10^{-6}$/°C.

The temperature coefficient of the refractive index was measured by Lipson *et al.* [43] using a laser interferometric method. The temperature

was varied over the 25–110 °C range, and the wavelengths used were those of He–Ne lasers radiating at 0.6328 μm, 1.15 μm, and 3.39 μm. The *dn/dT* behavior showed the same previously observed trends [42, 44]. The *dn/dT* data follow the theoretical model suggested by Tsay *et al.* [45], where *dn/dT* is given by an approximation of the form

$$\frac{dn}{dT} = \frac{\sqrt{\varepsilon_\infty}}{n(\omega)} \left[ \left( \frac{dn}{dT} \right)_e + \left( \frac{dn}{dT} \right)_l \right].$$

$(dn/dT)_e$ and $(dn/dT)_l$ are the electronic and lattice contributions to *dn/dT*. Furthermore, it was demonstrated that the slight increase in the value of *dn/dT* is comparable to the variation of the thermal expansion coefficient with temperature.

Measurements at very high temperatures in the range 293–300 K showed that the refractive index at 0.6328 μm decreased according to the relationship

$$n_T = n_r[1 - 8.07 \times 10^{-6}(T - 293) - 4.27 \times 10^{-9}(T - 293)^2],$$

where $n_r$ is the refractive index at 293 K [46]. In the same experiment it was found that the short wavelength side of the infrared band edge shifted considerably toward higher frequencies as the temperature was increased from 293 K to 1600 K. This behavior is believed to originate from a temperature broadening of the absorption band. These measurements were carried out in argon-filled chambers.

Several processes can contribute to absorption in the transparent region of a material, between the absorption edge (due to electronic transitions) on the short-wavelength side, and the reststrahlen band (due to lattice vibrations characteristic of ionic materials) on the long-wavelength side. These processes include multiphonon absorption, where a photon is absorbed and generates two or more phonons; free-carrier absorption identified by the $\lambda^2$ dependence of the absorption coefficient on the wavelength $\lambda$; impurity absorptions, which are recognized by a sharp-line structure; and the short-wavelength tail of the reststrahlen band extending into the transparent region [47].

An explanation of what may be regarded as impurity bands in $CaF_2$ has been given by Wickersheim and Hanking [48]. Absorption bands were observed at 2.74, 2.79, 6.76, 7.07, and 11.36 μm after $CaF_2$ samples were heated in air. The band at 2.74 μm was termed the infrared OH-stretching fundamental of $Ca(OH)_2$ occurring in or on the crystal. The band at 2.79 μm was identified as the stretching vibration of hydroxyl ions occur-

ring substitutionally for fluorine in $CaF_2$. The bands at 6.76, 7.07, and 12.5 μm were ascribed to a surface layer of $CaCO_3$.

An exponential frequency dependence of the infrared absorption coefficient, $\alpha$, was found at frequencies $\omega$ greater than several times the reststrahlen frequency $\omega_o$ [47, 49, 50]. In this region the value of $\alpha$ decreases from about $10\,cm^{-1}$ at a wavelength of 12.5 μm, to approximately $10^{-4}\,cm^{-1}$ at 5 μm [50]. These results were interpreted as being caused by intrinsic multiphonon absorption processes [49, 50].

Kaiser *et al.* [51] used reflection and transmission measurements to obtain information on lattice vibrations. The absorption coefficient $\alpha$ was calculated from the transmission according to the equation

$$T=(1-R)^2e^{-\alpha x}/(1-R^2e^{-2\alpha x}),$$

where $R$ is the reflectivity and $x$ the sample thickness. Over the wavelength range 16.67–8.89 μm, the value of $\alpha$ decreased from $200\,cm^{-1}$ to $0.4\,cm^{-1}$ at a temperature of 77 K.

The reflection band was analyzed using the classical dispersion theory [51]. According to this theory, the real and imaginary parts of the complex dielectric constant, $\varepsilon'$ and $\varepsilon''$, are given by

$$\varepsilon' = n^2 - k^2 = \varepsilon_\infty + \sum_j 4\pi\rho_j\nu_j^2 \frac{\nu_j^2 - \nu^2}{(\nu_j^2-\nu^2)^2 + \gamma_j^2\nu^2\nu_j^2} \tag{2}$$

and

$$\varepsilon'' = 2nk = \sum_j 4\pi\rho_j\nu_j^2 \frac{\gamma_j\nu\nu_j}{(\nu_j^2-\nu^2)^2 + \gamma_j^2\nu^2\nu_j^2}, \tag{3}$$

where $n$ is the refractive index, $k$ the extinction coefficient, $\varepsilon_\infty$ the high-frequency limiting value of the dielectric constant, $4\pi\rho_j$ the strength of the $j$th resonance, $\gamma_j$ the damping constant for the $j$th resonance, and $\nu_j$ the resonance frequency. From this analysis a strong resonance was found at 38.91 μm ($257\,cm^{-1}$) and identified as the transverse optical phonon mode [51].

At longer wavelengths the refractive index was determined from transmission interference measurements over the range 280–600 μm [52]. An average value of $n$ equal to $2.58\pm0.06$ was found with no indication of any dispersive behavior. The extinction coefficient was calculated from trans-

mission of a thick sample over the range 170–250 μm. Values obtained for $k$ were around 0.034 at 170 μm and 0.017 at 320 μm.

The optical constants of $CaF_2$ were determined from transmittance measurements on plane-parallel slabs over the wavelength band 50–200 $cm^{-1}$ [53]. Dispersion curves were found by fitting the expression

$$n(\omega) = (\varepsilon(\omega))^{1/2} = \{(\varepsilon_0 \nu_{TO}^2 - \varepsilon_\infty \omega^2)/(\omega_{TO}^2 - \omega^2)\}^{1/2} \tag{4}$$

to the experimentally obtained values. There are essentially two unknowns: $\varepsilon_o$, the static dielectric constant and $\omega_{TO}$, the vibrational frequency at zero wave vector. The values used were $\varepsilon_\infty = 2.04$, $\varepsilon_o = 6.63$, and $\omega_{TO} = 257$ $cm^{-1}$ at 300 K. Equation 4 was used to calculate $n$ at 100 and 200 μm (Table IV); however, it should be noted that Eq. 4 does not take absorption into account. The absorption coefficient was found to be strongly temperature dependent. At a wavelength of 100 μm the absorption $\alpha$ decreases from approximate values of 50 $cm^{-1}$ at 300 K to 4 $cm^{-1}$ at 80 K and less than 1 $cm^{-1}$ at 5 K [53].

Denham *et al.* [54] used a Kramers–Kronig analysis to determine the dielectric parameters $\varepsilon'$ and $\varepsilon''$ from reflection-spectra measurements over the 20–100 μm range. At 200 μm an estimated reflectivity of 19.6% leads to a refractive index $n = 2.52$. In the mm range (0.4–3 mm) the absorption of $CaF_2$ decreases with increasing wavelength (at $\lambda = 1$ mm, $k = 5 \times 10^{-3}$) [55]. A constant refractive index $n = \sqrt{\varepsilon_o} = 2.61$ is found at wavelengths beyond 0.3 mm.

The lattice vibrations in a crystal can be classified into optic and acoustic branches. For each value of the wave vector **k** there are $3N$ branches, where $N$ is the number of ions in the unit cell. Three of the $3N$ branches are acoustic and $3N$-3 are optic modes [56, 57, 58]. The minimal unit cell of $CaF_2$ is formed by two fluorine ions sitting at the center of two tetrahedra [59]. Since the unit cell contains three nonequivalent ions (one formula unit), there are nine branches in the phonon spectra of which six are due to optic modes.

A mode of vibration can absorb energy only if a mechanism exists for the coupling of vibrational motion to the electromagnetic radiation—the motion produces an oscillating dipole moment, which can be driven by the oscillating electric field of the radiation. Also, the requirements for the conservation of energy and momentum must hold [57]. To determine the optically active vibrational modes, a crystal factor group analysis [60] or the correlation method of Fately *et al.* can be used [61].

The factor group ($O_h$ in the case of $CaF_2$) leads to an identification of the species of lattice vibrations in the crystal also allowing the prediction of infrared or Raman activity. The total irreducible representation for $CaF_2$

can be written as [61]

$$\Gamma_{CaF_2} = 2F_{1u} + 1F_{2g}.$$

Both the optic and acoustic vibrations are included in the irreducible representation given above. One of the $F_{1u}$ modes represents the three acoustic branches and can be subtracted leading to [61]

$$\Gamma_{optical} = F_{iu}(ir) + F_{2g}(R).$$

The remaining $F_{1u}$ representation can be classified as a doubly degenerate transverse optic mode $\nu_{TO}$, which interacts with infrared radiation and a longitudinal mode $\nu_{LO}$ [54]. Therefore, only one (double degenerate) mode is infrared active, resulting from the sublattice of metal ions vibrating rigidly against the fluorine lattice [62]. From the measurements of Kaiser *et al.* [51], the transverse optic mode of vibration was found at $\nu_{TO} = 257\ cm^{-1}$. The frequency of the longitudinal phonon is related to the transverse vibrational mode by the Lyddane, Sacks, Teller relation [54]:

$$\nu_{LO} = \nu_{TO}(\varepsilon_0/\varepsilon_\infty)^{1/2}.$$

A value of $\upsilon_{LO} = 476 \pm 4\ cm^{-1}$ was suggested by Zernik [63].

The Raman scattering process involves the destruction of an incident photon of frequency $\omega_i$, the creation of a scattered photon of frequency $\omega_s$, and the creation or destruction of a phonon of frequency $\omega_p$ [57]. In wave-vector notation the Raman process can be expressed as $\mathbf{k}_i = \mathbf{k}_s \pm \mathbf{k}_p$. The mode of symmetry $F_{2g}$ is triply degenerate and Raman-active [54]. This mode results from a stationary cation lattice with the anions undergoing displacements against each other [58]. Using shortwave (0.488–0.6328 μm) laser light to excite $CaF_2$ crystals, the Stokes shifted component of the Raman spectrum was found at $322\ cm^{-1}$ [59, 64, 65]. It has also been pointed out that impurities might lead to fluorescent lines, which could be misinterpreted as Raman scattering [64]. The temperature dependence of the one-phonon Raman bands has been investigated using argon-ion (0.488 μm and 0.5145 μm) and He–Cd (0.4416 μm) lasers as light sources. A shift was observed from $330\ cm^{-1}$ at 15 K to about $300\ cm^{-1}$ at 1200 K [59]. Raman spectra excited by surface polaritons were produced by 0.5145 μm light and investigated at different scattering angles $\theta_s$ [66]. The angle of incidence was 35 degrees and Raman peaks were observed from $324\ cm^{-1}$ ($\theta_s = 36.5°$) to $403\ cm^{-1}$ ($\theta_s = 38.25°$). The strongest peaks were found at $371.5\ cm^{-1}$ ($\theta_s = 37°$) and $391\ cm^{-1}$ ($\theta_s = 37.25°$).

*Laser Applications*

Calcium fluoride has been considered a prime candidate for use as laser windows at both short (249 nm) [67] and long wavelengths (2.8–5.3 μm) [68]. Its sensitivity to thermal and mechanical shock led to programs for

strengthening the material without degrading the optical performance over its transparent range [68, 69, 70]. A hot-forging process was developed to produce small-grain polycrystalline blanks. Forged $CaF_2$ has shown an increase in the crystal-fracture energy in excess of five times that of single crystals, but has the disadvantage of cloudy regions within the bulk, or so-called veiling. Microscopic investigation of a veiled area has shown it to be composed of needlelike defects, which are voids lying parallel to the boundaries of elongated grains. These defects are characteristic of the forging process [68]. A hot isostatic pressing (HIP) treatment can eliminate these voids. It was postulated that the veils migrated to the surface where the bulk material collapsed in on itself [69]. It was also concluded that HIP-processed $CaF_2$ showed slightly increased absorption at 2.7 and 3.8 μm, and although the optical inhomogeneity is increased at 633 nm, it is still very low. Furthermore, the visible-scattering levels are decreased by a factor of eight compared with pre-HIP material, and the infrared scatter (at 3.7 μm) was largely unaffected.

An early attempt to determine some of the optical properties of forged $CaF_2$ is that of Dodge [71]. The index of refraction was determined by means of the minimum-deviation method. Data were obtained at 20.8 °C and 33.6 °C from 0.25–8 μm. Each set of experimental values was fitted to a three-term Sellmeier dispersion equation (Eq. 1). Emphasis was placed on obtaining a mathematical fit of the measured data, and the $\lambda_j$ and $A_j$ values are not intended to have any physical significance. These values are given in Table III. A comparison of Dodge's results [71] with those of Malitson [42] shows a minimum difference between 0.7 and 0.9 μm ($\Delta n = 0.5 \times 10^{-5}$) and a maximum difference ($\Delta n = 6.6 \times 10^{-5}$) at 0.28 μm and 4.8 μm. The index variation at 0.28 μm is attributed to a weak absorption band near 0.3 μm in the forged $CaF_2$. A possible absorption band between 4 and 5 μm was considered to be the reason for the difference at 4.8 μm. It must also be stressed that Dodge's [71] investigation should be regarded as a case study of a specific piece of $CaF_2$ material.

A photoacoustic study of the absorption properties reveals that surface absorption was found to be strongly wavelength dependent [72]. In the 2.7 μm region the surface absorption becomes dominant over bulk absorption. In another experiment both a photoacoustical and a laser-calorimetry method were used to determine bulk and surface absorption values at 1.3 μm [73]. Photoacoustic values of $\alpha_{\text{bulk}} = 6.8 \times 10^{-4}\,\text{cm}^{-1}$, $\alpha_{\text{surface}} = 4.8 \times 10^{-5}\,\text{cm}^{-1}$ compared closely with calorimetry values $\alpha_{\text{bulk}} = 6.14 \times 10^{-4}\,\text{cm}^{-1}$ and $\alpha_{\text{surface}} = 8.36 \times 10^{-5}\,\text{cm}^{-1}$ [73]. The optical absorption coefficient $\alpha$ measured at DF (3.8 μm) and HF (2.7 μm) wavelengths showed that single-crystal material has a slightly lower absorption than the forged material; the results for the absorption obtained from a variety of commercial $CaF_2$ samples indicate a variation in $\alpha$ obtained from different suppliers [74]. An investigation into the surface spectral distribution of

extrinsic absorption in highly transparent solids revealed that the atmospheric contaminants identified on $CaF_2$ surfaces could be grouped as hydrocarbons (3–4 μm), $CO_2$ (4.2 μm), liquid water (around 6 μm), and carbides (6.8 μm) [75]. The results obtained by Fernelius *et al.* [73] (that $\alpha_{surface} < \alpha_{bulk}$) might be ascribed to the fact that atmospheric contaminants at 1.3 μm are much less absorbing than at other wavelengths, such as the excimer UV region or 2.7 μm in the infrared, for example. Also, surface preparation, that is, polishing and cleaning before the tests, plays an important role in the experimental results of surface absorption measurements. In an experiment in which the absorption of $CaF_2$ was measured by laser calorimetry, it was found that hydrofluoric-acid cleaning reduced the surface absorption of the samples substantially [76]. It was suggested that contamination from the polishing process or the presence of calcium oxides on the sample surfaces led to the relatively high precleaned absorption values [76]. The presence of smooth, undamaged surface layers (<20 nm thick), which cover the subsurface damage on polished $CaF_2$, was illustrated by Law *et al.* [77].

Damage in $CaF_2$ optics used at excimer wavelengths may manifest itself in bulk and surface damage or in the generation of color centers. A laser damage experiment was carried out using a 0.249 μm, 3 ns excimer laser with an output pulse energy of around 700 mJ [67]. Work on the surface finish of $CaF_2$ surfaces indicated that the damage threshold is not as dependent on surface topography as it is on surface cleanliness, which is by far the greatest factor affecting damage thresholds [67]. For instance, it was suggested that the most important role of cracks is to act as a trap for absorbing impurities. Work done on highly pure $CaF_2$ crystals and naturally occurring fluorspar led to the conclusion that the presence of rare earth $3^+$ ions is crucial in the formation of color centers [67]. XeF laser-damage experiments were used to measure damage thresholds for bare polished crystals of $CaF_2$ [78]. Damage was induced by applying 1000 pulses ($\lambda = 0.35$ μm, 25 ns) to small sites ($0.12 \times 0.03$ cm) on the surfaces of the samples. Fluorescence-free $CaF_2$ exhibited both surface and bulk damage at 10 J cm$^{-2}$, whereas UV-grade $CaF_2$ showed only surface damage at 10 J cm$^{-2}$. From the damage morphology on the UV grade samples, it was suggested that improved polishing methods could lead to higher surface-damage thresholds. Laidler and Emmony [79] demonstrated the effect of rare-earth impurities on the ultraviolet wavelength absorption (0.339 μm) of $CaF_2$. It was found by these authors that pulsed laser damage thresholds (at 0.248 μm) indicated that the impure crystals had a higher damage threshold than the pure ones at certain dopant levels. It was suggested that the impurities, which act as electron acceptors, or holes formed by these impurities, continually trap conduction electrons and therefore hinder the buildup of an efficient electron avalanche process [79].

At infrared wavelengths the laser-damage threshold of $CaF_2$ was investi-

gated using pulsed DF laser light with three dominant lines at 3.8 μm [80]. The temporal pulse width was approximately 75 ns and a single-shot, one-site method was used. The peak on-axis intensity that damages $CaF_2$ was 25 GW/cm$^2$. What is more important, though, are the conclusions that the surface-damage thresholds are much lower than the bulk-damage thresholds, and that the damage-site morphology suggests that inclusions or defects are responsible for the damaging interaction [80].

It is clear that special attention must be given to surface preparation such as polishing and cleaning, in order to obtain $CaF_2$ laser components that will withstand high laser power densities.

*Thin Films*

Films a few thousand angstroms thick, grown by physical vapor deposition, were investigated by X-ray diffraction for a number of different coating conditions [81, 82]. It was found that when the substrate temperature was maintained at 25 °C during evaporation, the (111) planes were orientated approximately parallel to the glass substrate surface. For a substrate temperature of 110 °C the (110) planes were strongly oriented parallel to the surface, and this orientation of the (110) planes persisted for temperatures up to 310 °C [81, 82]. Stress measurements showed a high initial tensile stress, which rapidly fell to a low value as the thickness increased [83].

When the substrate temperature was kept below 100 °C during coating, the film showed a refractive index as low as about 1.26 [23]. These films tended to be very soft. At substrate temperatures between 280 and 300 °C, hard, robust films were formed with an estimated refractive index of 1.4. When the substrate temperature was 330 °C, films with a refractive index of approximately 1.42 resulted [23]. In a review of ultraviolet coating materials the refractive index of $CaF_2$ was given as 1.23–1.46 at 0.55 μm [84].

Bousquet [85] found that the reflectances of $CaF_2$ films at the half-wave positions are invariably lower than those of the substrate, where $n_f < n_s$. This result has been interpreted by Heavens and Smith as being caused by films having a gradient of refractive index normal to the substrate surface, with the index decreasing as the air–film surface is approached [86].

The laser-damage threshold of $CaF_2$ films was found to increase with an increase in both wavelength and pulse width [87]. At 0.265 μm, threshold values of 2.29 J cm$^{-2}$ (5 ns pulse width) and 3.55 J cm$^{-2}$ (15 ns pulse width) were found. Corresponding threshold values at 1.06 μm are 20 J cm$^{-2}$ and 33 J cm$^{-2}$ (pulse width 5 ns and 15 ns, respectively). These results were obtained for $\lambda/4$ films ($\lambda = 1.06$ μm).

## REFERENCES

1. W. L. Bragg, *Proc. Roy. Soc.* **A89**, 468 (1914).

2. H. Pealing, *Proc. Roy. Soc.* **33**, 297 (1920).
3. A. F. Wells, *Phil. Mag.* **37**, 217 (1946).
4. Powder Diffraction File (Joint Committee on Powder Diffraction Standards, International Centre for Diffraction Data, Swarthmore, PA) Card: 35-0816 (1986).
5. V. M. Goldschmidt, *Trans. Faraday Soc.* **25**, 253 (1929).
6. G. Burns and A. M. Glazer, "Space Groups for Solid State Scientists," Academic Press, New York, (1978).
7. D. C. Stockbarger, *J. Opt. Soc. Am.* **39**, 731 (1949).
8. J. A. Savage, "Infrared Optical Materials and their Antireflection Coatings," Adam Hilger, Bristol, (1988).
   C. W. King and O. H. Nestov, *SPIE Proceedings* **1047**, 80 (1989).
9. V. A. Sokolov, E. A. Simun, and A. N. Sinev, *Sov. J. Opt. Technol.* **46**, 279 (1979).
10. V. A. Sokolov, A. N. Sinev, I. B. Gusev, and V. I. Nikolaev, *Sov. J. Opt. Technol.* **51**, 530 (1984).
11. A. Horowitz, S. Biderman, G. Ben Amar, U. Laor, M. Weiss, and A. Stern, *J. Crystal Growth* **85**, 215 (1987).
12. L. S. Combes, S. S. Ballard, and K. A. McCarthy, *J. Opt. Soc. Am.* **41**, 215 (1951).
13. W. L. Wolfe and G. J. Zissis, "The Infrared Handbook," Environmental Research Institute of Michigan (1978).
14. G. W. Fynn and W. J. A. Powell, "The Cutting and Polishing of Electro-Optic Materials," Adam Hilger Ltd., Bristol, England, (1979).
15. R. C. Gore, R. S. McDonald, V. Z. Williams, and J. U. White, *J. Opt. Soc. Am.* **37**, 23 (1947).
16. E. K. Plyler, *Phys. Rev.* **72**, 165 (1947).
17. Y. Yamada, A. Mitsuishi, and H. Yoshinaga, *J. Opt. Soc. Am.* **52**, 17 (1962).
18. G. M. Ressler and K. D. Möller, *Appl. Opt.* **5**, 877 (1966).
19. M. Buback, E. U. Franck, and H. Lendle, *Z. Naturforsch.* **34a**, 1489 (1979).
20. D. Funnemann and H. Merz, *J. Phys. E: Sci. Instrum.* **19**, 554 (1986).
21. R. C. Estler, J. E. Anderson, E. C. Apel, and N. S. Nogar, *J. Vac. Sci. Technol.* **B5**, 1519 (1987).
22. S. D. Allen, J. O. Porteus, W. N. Faith, and J. B. Franck, *Appl. Phys. Lett.* **45**, 997 (1984).
23. J. Bannon, *Nature* **157**, 446 (1946).
24. R. S. Feigelson, W. L. Kway, and R. K. Route, *Opt. Eng.* **24**, 1102 (1985).
25. H. Marxer, B. Derighetti, and E. Brun, *Phys. Rev. Lett.* **50**, 958 (1983).
26. N. I. Medvedeva, V. A. Gubanov, A. I. Likhtenshtein, A. F. Golota, M. Y. Khodos, and F. I. Kosintsev, *J. Struct. Chem.* **25**, 649 (1984).
27. S. Muramatsu and C. Sugiura, *Phys. Rev. B.* **26**, 3092 (1982).
28. W. Hayes, A. B. Kunz, and E. E. Koch, *J. Phys. C* **4**, L 200 (1971).
29. G. W. Rubloff, *Phys. Rev. B.* **5**, 662 (1972).
30. W. Bontinck, *Physica* **24**, 650 (1958).
31. H. Bruch, P. Görlich, H. Karras, and R. Lehmann, *Phys. Stat. Solidi* **4**, 685 (1964).
32. W. Bontinck, *Physica* **24**, 639 (1958).
33. R. Rauch, R. Reimann, and G. Schwotzer, *Phys. Stat. Solidi (a)* **23**, 69 (1974).
34. F. Abba, Y. Marqueton, and E. A. Decamps, *Phys. Stat. Solidi* **35**, K129 (1969).
35. A. De and K. V. Rao, *Phys. Stat. Solidi (a)* **105**, 297 (1988).
36. W. M. Powell, *Phys. Rev.* **45**, 154 (1934).
37. T. Tomiki and T. Miyata, *J. Phys. Soc. Jap.* **27**, 658 (1969).
38. A. R. Knudson and J. E. Kupperian, *J. Opt. Soc. Am.* **47**, 440 (1957).
39. A. H. Laufer, J. A. Pirog, and J. R. McNesby, *J. Opt. Soc. Am.* **55**, 64 (1965).
40. A. Gilles and B. Vodar, *J. Opt. Soc. Am.* **42**, 783 (1952).
41. R. Tousey, *Phys. Rev.* **50**, 1057 (1936).

42. I. H. Malitson, *Appl. Opt.* **2**, 1103 (1963).
43. H. G. Lipson, Y. F. Tsay, B. Bendow, and P. A. Ligor, *Appl. Opt.* **15**, 2352 (1976).
44. T. Radhakrishnan, *Proc. Ind. Acad. Sci.* **A33**, 22 (1951).
45. Y. F. Tsay, B. Bendow, and S. S. Mitra, *Phys. Rev.* **B8**, 2688 (1973).
46. G. N. Vasil'chenko, I. E. Veneraki, A. M. Mikhal'chuk, and V. A. Sokolov, *Sov. J. Opt. Technol.* **49**, 226 (1982).
47. T. F. Deutsch, *J. Phys. Chem. Solids* **34**, 2091 (1973).
48. K. A. Wickersheim and B. M. Hanking, *Physica* **25**, 569 (1959).
49. M. Sparks and L. J. Sham, *Solid State Commun.* **11**, 1451 (1972).
50. K. V. Namjoshi, S. S. Mitra, B. Bendow, J. A. Harrington, and D. L. Stierwalt, *Appl. Phys. Lett.* **26**, 41 (1975).
51. W. Kaiser, W. G. Spitzer, R. H. Kaiser, and L. E. Howarth, *Phys. Rev.* **127**, 1950 (1962).
52. L. V. Berman and A. G. Zhukov, *Opt. Spectrosc.* **19**, 433 (1965).
53. D. R. Bosomworth, *Phys. Rev.* **157**, 709 (1967).
54. P. Denham, G. R. Field, P. L. R. Morse, and G. R. Wilkinson, *Proc. Roy. Soc. London A* **317**, 55 (1970).
55. H. Happ, H. W. Hofmann, E. Lux, and G. Seger, *Z. Physik* **166**, 510 (1962).
56. R. Loudon, *Advances in Physics* **13** (B. R. Coles ed.), 423 (1964).
57. J. T. Houghton and S. D. Smith, "Infra-red Physics," Oxford University Press, London, (1966).
58. W. Hayes and A. M. Stoneham, in "Crystals with the Fluorite Structure," (W. Hayes, ed.), Oxford University Press, London, (1974).
59. D. G. Mead and G. R. Wilkinson, *J. Phys. C: Solid State Phys.* **10**, 1063 (1977).
60. D. M. Adams and D. C. Newton, "Tables for Factor Group and Point Group Analysis," Beckman-RIII Ltd, Croydon, (1970).
61. W. G. Fateley, F. R. Dollish, N. T. McDevitt, and F. F. Bentley, "Infrared and Raman Selection Rules for Molecular and Lattice Vibrations: The Correlation Method," John Wiley, New York, (1972).
62. D. H. Martin, Advances in Physics, **14** (B. R. Coles, ed.), 39 (1965).
63. W. Zernik, *Rev. Mod. Phys.* **39**, 432 (1967).
64. A. R. Gee, D. C. O'Shea, and H. Z. Cummins, *Solid State Comm.* **4**, 43 (1965).
65. R. Srivastava, H. V. Lauer, Jr., L. L. Chase, and W. E. Bron, *Phys. Lett.* **36A**, 333 (1971).
66. Y. Q. Sheng, E. Rechnagel, A. Weidinger, Z. G. Gu, Z. Y. Lai, and Z. G. Zhurang, *Phys. Stat. Sol. (b)* **145**, 151 (1988).
67. I. Laidler and D. C. Emmony, *NBS Special Publication* **746**, 182 (1985).
68. R. H. Anderson, R. A. Skogman, J. F. Ready, and J. M. Bennett, *NBS Special Publication* **541**, 70 (1978).
69. A. K. Hopkins, R. H. Anderson, J. F. Ready, J. M. Bennett, P. C. Archibald, and D. K. Burge, *NBS Special Publication* **568**, 47 (1979).
70. C. B. Willingham, M. A. Spears, G. A. Graves, and W. L. Knecht, *NBS Special Publication* **688**, 101 (1983).
71. M. J. Dodge, *NBS Special Publication* **462**, 64 (1976).
72. A. Hordvik, B. Bendow, H. G. Lipson, L. H. Skolnik, and R. N. Brown, *NBS Special Publication* **462**, 50 (1976).
73. N. C. Fernelius, D. V. Dempsey, and D. B. O'Quinn, *NBS Special Publication* **620**, 58 (1980).
74. J. A. Harrington, D. A. Gregory, and W. F. Otto, *Appl. Opt.* **15**, 1953 (1976).
75. R. Braunstein, R. K. Kim, and M. Braunstein, *NBS Special Publication* **620**, 29 (1980).
76. D. J. Gallant, M. Law, and B. Pond, *NBS Special Publication* **752**, 159 (1986).
77. M. Law, J. Bender, and C. K. Carniglia, *NBS Special Publication* **752**, 532 (1986).

78. M. C. Staggs, D. Milam, I. M. Thomas, and J. G. Wilder, *NBS Special Publication* **746**, 404 (1985).
79. I. Laidler and D. C. Emmony, *NBS Special Publication* **752**, 151 (1986).
80. M. Bass, K. M. Leung, C. Tang, and M. J. Soileau, *NBS Special Publication* **462**, 136 (1976).
81. J. Bannon and C. E. Curnow, *Nature* **161**, 136 (1948).
82. J. Bannon and C. K. Coogan, *Nature* **163**, 62 (1949).
83. A. E. Ennos, *Appl. Opt.* **5**, 51 (1966).
84. M. L. Scott, *NBS Special Publication* **688**, 329 (1983).
85. P. Bousquet, *Compt. Rend.* **238**, 1485 (1954).
86. O. S. Heavens and S. D. Smith, *J. Opt. Soc. Am.* **47**, 469 (1957).
87. T. W. Walker, A. H. Guenther, C. G. Fray, and P. Nielson, *NBS Special Publication* **568**, 405 (1979).
88. G. Stephan, J. C. Lemonnier, Y. Le Calvez and S. Robin, *Compt. Rend.* **262** *Serie B*, 1272 (1966).
89. Landolt-Börnstein, "Physikalisch-Chemische Tabellen," (W. A. Roth and K. Scheel, eds.), Edwards Brothers, Inc., Berlin, 911 (1923).
90. F. F. Martens, *Ann. Phys.* **6**, 603 (1901).
91. J. C. Lemonnier, G. Stéphan, and S. Robin, *Compt. Rend.* **261**, 2463 (1965).

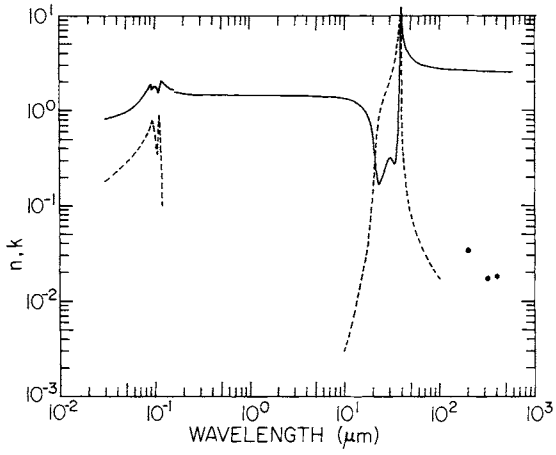


**Fig. 1.** Log–log plot of $n$ (solid line) and $k$ (dashed line) versus wavelength in micrometers for calcium fluoride.

**TABLE I**

**Constants of the Dispersion Equation Used by Malitson [42]**

| | |
|---|---|
| $\lambda_1 = 0.050263605$ | $A_1 = 0.5675888$ |
| $\lambda_2 = 0.1003909$ | $A_2 = 0.4710914$ |
| $\lambda_3 = 34.64904$ | $A_3 = 3.8484723$ |

**TABLE II**

**A List of Parameters Used to Calculate the Dispersion Values in Table IV from 1000 $cm^{-1}$ to 100 $cm^{-1}$ [51]**

| Parameter | Value |
|---|---|
| $\nu_1$ | 257 $cm^{-1}$ |
| $\gamma_1$ | 0.018 |
| $4\pi\rho_1$ | 4.2 |
| $\nu_2$ | 328 $cm^{-1}$ |
| $\gamma_2$ | 0.35 |
| $4\pi\rho_2$ | 0.4 |
| $\varepsilon_\infty$ | 2.045 |

**TABLE III**

**Constants for Dispersion Equations Used by Dodge at a temperature of 20.8 °C [71]**

| | |
|---|---|
| $\lambda_1 = 0.07218116$ | $A_1 = 0.98584551$ |
| $\lambda_2 = 0.14114719$ | $A_2 = 0.05290246$ |
| $\lambda_3 = 36.465937$ | $A_3 = 4.2816899$ |

TABLE IV

Values of $n$ and $k$ for Calcium Fluoride obtained from various references[a]

| eV | Å | n | k |
|---|---|---|---|
| 41.3285 | 300 | 0.814 [91][b] | 0.148 [91][b] |
| | | 0.82 [88] | 0.18 [88] |
| 30.9964 | 400 | 0.917 [91] | 0.284 [91] |
| 24.7971 | 500 | 1.108 | 0.433 |
| 20.6643 | 600 | 1.074 | 0.335 |
| | | 1.08 [88] | 0.34 [88] |
| 17.7122 | 700 | 0.908 [91] | 0.353 [91] |
| 15.4982 | 800 | 1.169 | 0.753 |
| 13.7762 | 900 | 1.630 | 0.675 |
| | | 1.85 [88] | 0.65 [88] |
| 13.3749 | 927 | 1.640 [41] | 0.768 [41] |
| 12.6775 | 978 | 1.780 | 0.650 |
| 12.2153 | 1,015 | 1.775 | 0.540 |
| 12.0844 | 1,026 | 1.742 | 0.517 |
| 11.9793 | 1,035 | 1.732 | 0.473 |
| 11.8420 | 1,047 | 1.725 | 0.395 |
| 11.6200 | 1,067 | 1.615 | 0.344 |
| 11.3748 | 1,090 | 1.533 | 0.600 |
| 11.2714 | 1,100 | 1.570 | 0.785 |
| 11.1098 | 1,116 | 1.775 | 0.830 |
| 10.8190 | 1,146 | 2.000 | 0.631 |
| 10.6700 | 1,162 | 2.027 | 0.490 |
| 10.5520 | 1,175 | 1.996 | 0.390 |
| 10.4190 | 1,190 | 1.983 | 0.290 |
| 10.3321 | 1,200 | 2.05 [88] | 0.1 [88] |
| 9.8872 | 1,254 | 1.888 [41] | |
| 9.7167 | 1,276 | 1.855 | |
| 9.3013 | 1,333 | 1.803 | |
| 8.6522 | 1,433 | 1.711 | |
| 7.7250 | 1,605 | 1.607 | |
| | | 1.5547 [89] | |

**TABLE IV (*Continued*)**

**Calcium Fluoride**

| eV | Å | n | k |
|---|---|---|---|
| 7.6914 | 1,612 | 1.5509 | |
| 7.5371 | 1,645 | 1.5438 | |
| 7.4199 | 1,671 | 1.5385 | |
| 7.1876 | 1,725 | 1.5289 | |
| 7.0287 | 1,764 | 1.5227 | |
| 6.8161 | 1,819 | 1.5152 | |
| 6.7019 | 1,850 | 1.51024 [90] | |
| 6.6659 | 1,860 | 1.50930 | |
| 6.4241 | 1,930 | 1.50150 | |
| 6.2937 | 1,970 | 1.49755 | |
| 6.2619 | 1,980 | 1.49643 | |
| 6.1993 | 2,000 | 1.49547 | |
| 6.0777 | 2,040 | 1.49190 | |
| 5.9609 | 2,080 | 1.48907 | |
| 5.8761 | 2,110 | 1.48705 | |
| 5.7937 | 2,140 | 1.48480 | |
| 5.6614 | 2,190 | 1.48167 | |

| eV | $cm^{-1}$ | μm | n | k |
|---|---|---|---|---|
| 5.6357 | 45,455 | 0.22 | 1.48110 [42] | |
| 5.1661 | 41,666 | 0.24 | 1.47120 | |
| 4.7687 | 38,462 | 0.26 | 1.46391 | |
| 4.4281 | 35,714 | 0.28 | 1.45836 | |
| 4.1329 | 33,333 | 0.30 | 1.45402 | |
| 3.8746 | 31,250 | 0.32 | 1.45056 | |
| 3.6466 | 29,412 | 0.34 | 1.44775 | |
| 3.4440 | 27,778 | 0.36 | 1.44548 | |
| 3.2628 | 26,316 | 0.38 | 1.44349 | |
| 3.0996 | 25,000 | 0.40 | 1.44185 | |
| 2.9520 | 23,810 | 0.42 | 1.44045 | |
| 2.8179 | 22,727 | 0.44 | 1.43924 | |
| 2.6953 | 21,739 | 0.46 | 1.43820 | |

TABLE IV (*Continued*)

**Calcium Fluoride**

| eV | $cm^{-1}$ | $\mu m$ | n | k |
|---|---|---|---|---|
| 2.5830 | 20,833 | 0.48 | 1.43728 | |
| 2.4797 | 20,000 | 0.50 | 1.43647 | |
| 2.3843 | 19,231 | 0.52 | 1.43575 | |
| 2.2960 | 18,519 | 0.54 | 1.43512 | |
| 2.2140 | 17,857 | 0.56 | 1.43454 | |
| 2.1377 | 17,241 | 0.58 | 1.43403 | |
| 2.0664 | 16,667 | 0.60 | 1.43356 | |
| 1.9998 | 16,129 | 0.62 | 1.43313 | |
| 1.9373 | 15,625 | 0.64 | 1.43275 | |
| 1.8786 | 15,152 | 0.66 | 1.43239 | |
| 1.8233 | 14,706 | 0.68 | 1.43206 | |
| 1.7712 | 14,286 | 0.70 | 1.43176 | |
| 1.7220 | 13,889 | 0.72 | 1.43148 | |
| 1.6755 | 13,514 | 0.74 | 1.43121 | |
| 1.6314 | 13,158 | 0.76 | 1.43097 | |
| 1.5896 | 12,821 | 0.78 | 1.43074 | |
| 1.5498 | 12,500 | 0.80 | 1.43052 | |
| 1.5120 | 12,195 | 0.82 | 1.43032 | |
| 1.4760 | 11,905 | 0.84 | 1.43013 | |
| 1.4417 | 11,628 | 0.86 | 1.42995 | |
| 1.4089 | 11,364 | 0.88 | 1.42977 | |
| 1.3776 | 11,111 | 0.90 | 1.42961 | |
| 1.3477 | 10,870 | 0.92 | 1.42945 | |
| 1.3190 | 10,638 | 0.94 | 1.42930 | |
| 1.2915 | 10,417 | 0.96 | 1.42915 | |
| 1.2652 | 10,204 | 0.98 | 1.42901 | |
| 1.2399 | 10,000 | 1.00 | 1.42888 | |
| 1.0332 | 8,333 | 1.20 | 1.42771 | |
| 0.8856 | 7,143 | 1.40 | 1.42672 | |
| 0.7749 | 6,250 | 1.60 | 1.42579 | |
| 0.6888 | 5,555 | 1.80 | 1.42484 | |
| 0.6199 | 5,000 | 2.00 | 1.42385 | |
| 0.5636 | 4,545 | 2.20 | 1.42280 | |

TABLE IV (*Continued*)

**Calcium Fluoride**

| eV | $cm^{-1}$ | μm | n | k |
|---|---|---|---|---|
| 0.5166 | 4,167 | 2.40 | 1.42168 | |
| 0.4769 | 3,846 | 2.60 | 1.42049 | |
| 0.4428 | 3,571 | 2.80 | 1.41921 | |
| 0.4133 | 3,333 | 3.00 | 1.41785 | |
| 0.3875 | 3,125 | 3.20 | 1.41639 | |
| 0.3647 | 2,941 | 3.40 | 1.41484 | |
| 0.3444 | 2,778 | 3.60 | 1.41320 | |
| 0.3263 | 2,632 | 3.80 | 1.41147 | |
| 0.3100 | 2,500 | 4.00 | 1.40963 | |
| 0.2952 | 2,381 | 4.20 | 1.40770 | |
| 0.2818 | 2,273 | 4.40 | 1.40567 | |
| 0.2695 | 2,174 | 4.60 | 1.40354 | |
| 0.2583 | 2,083 | 4.80 | 1.40130 | |
| 0.2480 | 2,000 | 5.00 | 1.39895 | |
| 0.2384 | 1,923 | 5.20 | 1.39650 | |
| 0.2296 | 1,852 | 5.40 | 1.39394 | |
| 0.2234 | 1,800 | 5.55 | | $3.5 \times 10^{-8}$ [50] |
| 0.2214 | 1,786 | 5.60 | 1.39127 | |
| 0.2138 | 1,724 | 5.80 | 1.38849 | |
| 0.2066 | 1,667 | 6.00 | 1.38559 | |
| 0.2000 | 1,613 | 6.20 | 1.38258 | |
| 0.1984 | 1,600 | 6.25 | | $3.5 \times 10^{-7}$ |
| 0.1937 | 1,563 | 6.40 | 1.37945 | |
| 0.1879 | 1,515 | 6.60 | 1.37620 | |
| 0.1823 | 1,471 | 6.80 | 1.37282 | |
| 0.1771 | 1,429 | 7.00 | 1.36932 | |
| 0.1737 | 1,400 | 7.14 | | $3.4 \times 10^{-6}$ |
| 0.1722 | 1,389 | 7.20 | 1.36569 | |
| 0.1676 | 1,351 | 7.40 | 1.36193 | |
| 0.1631 | 1,316 | 7.60 | 1.35804 | |
| 0.1590 | 1,282 | 7.80 | 1.35401 | |
| 0.1550 | 1,250 | 8.00 | 1.34983 | |
| 0.1512 | 1,220 | 8.20 | 1.34552 | |

TABLE IV (*Continued*)

**Calcium Fluoride**

| eV | $cm^{-1}$ | μm | n | k |
|---|---|---|---|---|
| 0.1488 | 1,200 | 8.33 | | $3.3 \times 10^{-5}$ |
| 0.1476 | 1,190 | 8.40 | 1.34106 | |
| 0.1442 | 1,163 | 8.60 | 1.33645 | |
| 0.1409 | 1,136 | 8.80 | 1.33169 | |
| 0.1378 | 1,111 | 9.00 | 1.32677 | |
| 0.1348 | 1,087 | 9.20 | 1.32168 | |
| 0.1319 | 1,064 | 9.40 | 1.31643 | |
| 0.1292 | 1,042 | 9.60 | 1.31101 | |
| 0.1265 | 1,020 | 9.80 | 1.30541 | |
| 0.1240 | 1,000 | 10.000 | 1.306 [51][c] | 0.0029 [51][c] |
| 0.1178 | 950 | 10.526 | 1.289 | 0.0035 |
| 0.1116 | 900 | 11.111 | 1.269 | 0.004 |
| 0.1054 | 850 | 11.765 | 1.247 | 0.005 |
| 0.0992 | 800 | 12.500 | 1.218 | 0.007 |
| 0.0930 | 750 | 13.333 | 1.181 | 0.009 |
| 0.0868 | 700 | 14.286 | 1.133 | 0.012 |
| 0.0806 | 650 | 15.385 | 1.067 | 0.017 |
| 0.0744 | 600 | 16.667 | 0.971 | 0.027 |
| 0.0713 | 575 | 17.391 | 0.906 | 0.035 |
| 0.0682 | 560 | 18.182 | 0.821 | 0.047 |
| 0.0651 | 525 | 19.048 | 0.707 | 0.068 |
| 0.0620 | 500 | 20.000 | 0.539 | 0.115 |
| 0.0589 | 475 | 21.053 | 0.291 | 0.280 |
| 0.0558 | 450 | 22.222 | 0.182 | 0.609 |
| 0.0527 | 425 | 23.529 | 0.174 | 0.902 |
| 0.0496 | 400 | 25.000 | 0.196 | 1.187 |
| 0.0465 | 375 | 26.667 | 0.241 | 1.488 |
| 0.0434 | 350 | 28.571 | 0.298 | 1.818 |
| 0.0403 | 325 | 30.769 | 0.317 | 2.235 |
| 0.0372 | 300 | 33.333 | 0.276 | 3.011 |
| 0.0360 | 290 | 34.483 | 0.280 | 3.565 |
| 0.0347 | 280 | 35.714 | 0.346 | 4.430 |
| 0.0335 | 270 | 37.037 | 0.639 | 6.071 |

TABLE IV (*Continued*)

Calcium Fluoride

| eV | $cm^{-1}$ | μm | n | k |
|---|---|---|---|---|
| 0.0322 | 260 | 38.462 | 3.909 | 11.146 |
| 0.0320 | 258 | 38.760 | 8.093 | 12.137 |
| 0.0319 | 257 | 38.911 | 10.876 | 10.750 |
| 0.0317 | 256 | 39.063 | 12.342 | 8.010 |
| 0.0315 | 254 | 39.370 | 11.463 | 3.831 |
| 0.0312 | 252 | 39.683 | 9.864 | 2.115 |
| 0.0310 | 250 | 40.000 | 8.673 | 1.352 |
| 0.0298 | 240 | 41.667 | 5.927 | 0.389 |
| 0.0285 | 230 | 43.478 | 4.867 | 0.206 |
| 0.0273 | 220 | 45.455 | 4.283 | 0.136 |
| 0.0260 | 210 | 47.619 | 3.907 | 0.100 |
| 0.0248 | 200 | 50.000 | 3.641 | 0.079 |
| 0.0223 | 180 | 55.556 | 3.289 | 0.053 |
| 0.0198 | 160 | 62.500 | 3.066 | 0.039 |
| 0.0174 | 140 | 71.429 | 2.914 | 0.029 |
| 0.0149 | 120 | 83.333 | 2.805 | 0.022 |
| 0.0124 | 100 | 100.00 | 2.726 | 0.017 |
| | | | 2.729 [53][d] | |
| 0.0062 | 50 | 200.00 | 2.610 | |
| | | | | 0.034 [52] |
| 0.0042 | 34.01 | 294.0 | 2.57 [52] | |
| 0.0040 | 31.85 | 314.0 | 2.55 | |
| 0.0039 | 31.25 | 320.0 | | 0.017 |
| 0.0037 | 29.41 | 340.0 | 2.55 | |
| 0.0034 | 27.62 | 362.0 | 2.49 | |
| 0.0031 | 25.32 | 395.0 | 2.47 | |
| 0.0031 | 25.00 | 400.0 | | 0.018 |
| 0.0027 | 22.08 | 453.0 | 2.55 | |
| 0.0021 | 17.24 | 580.0 | 2.54 | |

[a] References are given in brackets.

[b] Values obtained from Fig. 5 [91].

[c] Values obtained using Eqs. (2) and (3).

[d] Values obtained using Eq. (4).

# Amorphous Hydrogenated "Diamondlike" Carbon Films and Arc-Evaporated Carbon Films

SAMUEL A. ALTEROVITZ
Space Electronics Division
NASA Lewis Research Center
Cleveland, Ohio

N. SAVVIDES
CSIRO Division of Applied Physics
National Measurements Laboratory
Sydney, Australia

F. W. SMITH
Department of Physics
City College of CUNY
New York, New York
and
JOHN A. WOOLLAM
Center for Microelectronic and Optical Materials Research
and Department of Electrical Engineering
University of Nebraska
Lincoln, Nebraska

There is considerable nomenclature confusion concerning these films, which various authors have attempted to rectify. Although there is no general consensus on terminology, they are often referred to as "a-C : H" or "diamondlike" carbon or "DLC." Here we will use the terms a-C : H and DLC interchangeably. Unfortunately, they are also being confused recently with diamond films. Amorphous hydrogenated carbon (a-C : H) has 20–55 percent hydrogen, and an optical band gap (determined from Tauc plots) between 0.5 and 3.0 eV. Diamond films nominally contain no hydrogen, are polycrystalline, and form only at high temperatures. a-C : H films are typically formed by plasma or ion-beam deposition (using hydrocarbon gas) onto substrates maintained at room temperature or slightly


Copyright © 1991 by Academic Press.
All rights of reproduction in any form reserved.
ISBN 0-12-544422-2

above room temperature. There are other preparation techniques as well [1–30]. There is considerable general literature on these films, including reviews [1, 2, 5, 6, 10, 17, 26, 27]. a-C : H (DLC) films graphitize above a few hundred degrees Celcius [31].

The properties of DLC, including optical constants, depend strongly on preparation conditions. Thus, the user can prepare samples with an optical gap anywhere in the 0.5–3.0 eV range, but most easily in the 1–2 eV range. Associated with this is the control of index of refraction from approximately 1.7 to 2.2, and a related extinction-coefficient dependence.

DLC is generally transparent for wavelengths greater than mid-visible. In the infrared there are resonant hydrogen absorptions in several spectral ranges, but with minimal absorption in other ranges [1–2].

Readers should carefully compare their preparation techniques and conditions before using data from the literature or from the table displayed in this critique. We have included the dependence of optical constants on substrate and/or annealing temperature, since this is a commonly varied parameter, which results in large property changes.

We have chosen to present the optical data of plasma-deposited DLC in tabular form, as well as the constants of a fit to the experimental data according to the theory given by Forouhi and Bloomer [24, 32]. Table I gives the constants in the following equations for index of refraction $n$ and extinction coefficient $k$:

$$n(E) = n(\infty) + [B_0 E + C_0]/[E^2 - BE + C] \tag{1}$$

$$k(E) = A(E - E_g)^2/(E^2 - BE + C), \tag{2}$$

where $E$ is photon energy, and $E_g$ is the optical band gap, both in eV. Also,

$$B_0 = (A/Q)[-B^2/2 + E_g B - E_g^2 + C], \tag{3}$$

$$C_0 = (A/Q)[(E_g^2 + C)B/2 - 2E_g C], \tag{4}$$

and

$$Q = \tfrac{1}{2}(4C - B^2)^{1/2}. \tag{5}$$

The values of the constants in Table I are given for films prepared by

30 kHz plasma deposition from $CH_4$ on silicon substrates held at room temperature using powers of 50–200 W with subsequent annealing at 400, 600, and 750°C [24]. In all depositions the flowing $CH_4$ pressure was held at 315 m torr. Data were taken over the range 1.5–4.1 eV. Extensions of Eqs. 1 and 2 beyond this range should be done cautiously.

Table II gives the measured data for selected samples described above, but in tabular form. Fig. 1 is a plot of $n$ and $k$. These data were taken by variable-angle spectroscopic ellipsometry (VASE) (for which no Kramers–Kronig analysis is required), assuming a model of a single film on a substrate. These results are highly reliable with the exception of very low values of $k$; it is difficult to measure $k$ accurately by ellipsometry for values less than about 0.02.

Infrared optical-constant data for samples prepared in the same deposition system for data given in Tables I and II are given in Table III [6, 28].

For completeness, we also include optical constants of a-C:H in the 1.5–4.75 eV spectral range prepared in a dc glow discharge from $C_2H_2$ deposited on quartz held at 250°C with anneal at 350°C, as well as with no further anneal [3]. These are shown in Table IV. Fig. 2 is a plot of $n$ and $k$. In the original reference the reader can find data for samples annealed to even higher temperatures [3]. These are not repeated here, due to the expected partial graphitic transformaton of the DLC films at higher than about 400°C [31].

In addition to data presented above on plasma-deposited films, we present data in Tables V and VI on diamondlike films made by a low-energy, ion-assisted deposition (IAD) technique based on unbalanced dc magnetron sputtering. Fig. 3 is a plot of $n$ and $k$ from Table VI. Details of the preparation technique are given in Refs. [5, 33–35]. The optical properties of these films are sensitive to both the ion energy per deposited carbon atom, and (as for all diamondlike carbon) the hydrogen content. These films were deposited at 300 K onto quartz substrates, and the optical constants were determined from transmittance and near-normal reflectance measurements in the photon energy range 0.5–7.3 eV. Measurements were made at room temperature (295 K). The relative measurement accuracy is about 1% except at the UV extreme ($>6.5$ eV) where it is a bit worse. Table V gives preparation parameters for nine different samples, but detailed data are given only for sample numbers 1, 5, and 9. These three were selected because they represent a range of hydrogen concentration and therefore a range of optical properties. Notice the trend toward increasing optical band gap with increasing hydrogen content $C_H$. The original references [5, 33–35] can be consulted for information on the remaining samples.

Finally, we present in Table VII the optical constants of arc-evaporated carbon films [36, 37]. These are amorphous and nominally contain no hydrogen; these are *not* called "a-C:H," "DLC," or "diamondlike"

carbon. The reader can see from the table that these films are very different from DLC, for example, in the lack of an optical absorption edge.

## REFERENCES


1. J. C. Angus, P. Koidl, and S. Domitz, in "Plasma Deposited Thin Films," (J. Mort and F. Jansen, eds.), CRC Press, Cleveland (1986).
2. A. Bubenzer, B. Dischler, G. Brandt, and P. Koidl, *J. Appl. Phys.* **54**, 4590 (1983).
3. F. W. Smith, *J. Appl. Phys.* **55**, 764 (1984).
4. J. Fink, T. Muller-Heinzerling, J. Pfluger, B. Scheerer, B. Dischler, P. Koidl, A. Bubenzer, and R. E. Sah, *Phys. Rev.* **B30**, 4713 (1985).
5. N. Savvides, in "Properties and Characterization of Amorphous Carbon Films", (J. J. Pouch and S. A. Alterovitz, eds.), Materials Science Forum **52**, **53**, Trans Tech Publications, Zurich, Switzerland, 407 (1990).
6. J. A. Woollam, B. N. De, S. Orzeszko, N. J. Ianno, P. G. Snyder, S. A. Alterovitz, J. J. Pouch, R. L. C. Wu, and D. C. Ingram in "Properties and Characterization of Amorphous Carbon Films," (J. J. Pouch and S. A. Alterovitz, eds.), Materials Science Forum **52**, **53**, Trans Tech Publications, Zurich, Switzerland, 577 (1990).
7. B. Dischler, A. Bubenzer, and P. Koidl, *Appl. Phys. Letters* **42**, 636 (1983).
8. P. Coderc and Y. Catherine, *Thin Solid Films* **146**, 93 (1987).
9. B. Dischler, A. Bubenzer, and P. Koidl, *Solid State Commun.* **48**, 105 (1983).
10. P. Koidl, C. Wild, B. Dischler, J. Wagner, and M. Ramsteiner, in "Properties and Characterization of Amorphous Carbon Films," (J. J. Pouch and S. A. Alterovitz, eds.), Materials Science Forum **52**, **53**, Trans Tech Publications, Zurich, Switzerland, 41 (1990).
11. J. Wagner and P. Lautenschlager, *J. Appl. Phys.* **56**, 2044 (1986).
12. K. Mui, D. K. Basa, F. W. Smith, and R. Corderman, Phys. Rev. **B35**, 8089 (1987).
13. R. T. Moravec and J. C. Lee, *J. Vac. Sci. Technol.* **20**, 338, (1982).
14. D. A. Anderson, *Phil. Mag.* **35**, 17 (1977).
15. K. Fujii, N. Shohata, M. Mikami, and M. Yonezawa, *Appl. Phys. Lett.* **47**, 370 (1985).
16. V. Natarajan, J. D. Lamb, J. A. Woollam, D. C. Liu, and D. Gulino, *J. Vac. Sci. Technol.* **A3**, 681 (1985).
17. J. A. Woollam, G. H. Bu-Abbud, J. Oh, P. G. Snyder, J. D. Lamb, D. C. Ingram, and A. K. Rai, "Proc. of Symp. on Dielectric Films on Compound Semiconductors," (V. K. Kapoor, D. J. Connolly and Y. H. Wong, eds.), Electrochemical Society, Pennington, N.J., 289 (1986).
18. A. A. Khan, D. Mathine, J. A. Woollam, and Y. Chung, *Phys. Rev.* **B28**, 7229 (1983).
19. S. A. Alterovitz, J. D. Warner, D. C. Liu, J. J. Pouch, *J. Electrochem. Soc.* **133**, 2339 (1986).
20. E. Staryga, A. Lipinski, S. Mitura, and Z. Has, *Thin Solid Films* **145**, 17 (1986).
21. S. Lin and S. Chen, *J. Mater. Res.* **2**, 645 (1982).
22. S. Orzeszko, B. N. De, P. G. Snyder, J. A. Woollam, J. J. Pouch, and S. A. Alterovitz, *J. Chimie Physiq.* **84**, 1469 (1987).
23. S. A. Alterovitz, J. J. Pouch, J. D. Warner, *MRS Symp. Proc.* **92**, 311 (1987).
24. S. A. Alterovitz, R. M. Sieg, W. S. Shoemaker, and J. J. Pouch, *MRS Symp. Proc.* **152**, 21 (1989).
25. R. W. Collins, *Appl. Phys. Lett.* **52**, 2025 (1988).
26. R. W. Collins, in "Properties and Characterization of Amorphous Carbon Films," (J. J. Pouch and S. A. Alterovitz, eds.), Materials Science Forum **52**, **53**, Trans Tech Publications, Zurich, Switzerland, 341 (1990).
27. H. C. Tsai and B. D. Bogy, *J. Vac. Sci. Tech.* **A5**, 3287 (1988).
28. J. A. Woollam, B. N. De, L. Y. Chen, J. J. Pouch, S. A. Alterovitz, *Mat. Res. Soc. Symp. Proc.* **152**, 27 (1989).

29. B. N. De, S. Orzeszko, J. A. Woollam, D. C. Ingram, and A. J. McCormick, *Proc SPIE* **969**, 60 (1988).
30. J. A. Woollam, H. Chang, and V. Natarajan, *Appl. Phys. Commun.* **5**, 263 (1985).
31. R. O. Dillon, J. A. Woollam, and V. Katkanant, *Phys. Rev.* **B57**, 3482 (1984).
32. A. R. Forouhi and I. Bloomer, *Phys. Rev.* **B34**, 7018 (1986).
33. N. Savvides, in "Amorphous Hydrogenated Carbon Films," (P. Koidl and P. Oelhafen, eds.), Les Editions de Physique, Paris, 275 (1987); *E-MRS Symposia Proceedings* **XVII**.
34. N. Savvides, *J. Appl. Phys.* **59**, 4133 (1986).
35. N. Savvides, *Thin Solid Films* **163**, 13 (1988).
36. E. T. Arakawa, M. W. Williams, and T. Inagaki, *J. Appl. Phys.* **48**, 3176 (1977).
37. E. T. Arakawa, S. M. Dolfini, J. C. Ashley, and M. W. Williams, *Phys. Rev.* **B31**, 8097 (1985).

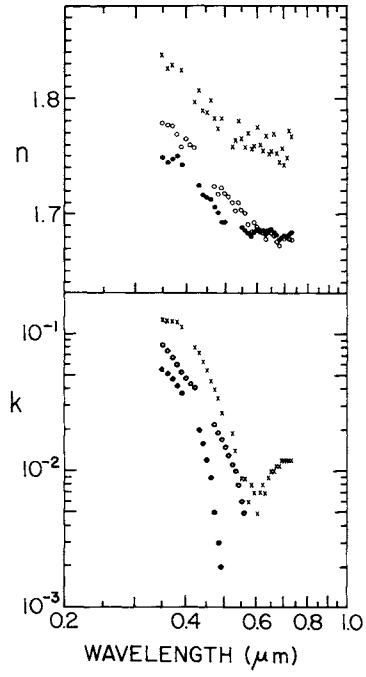


**Fig. 1.** Plot of $n$ and $k$ versus wavelength in micrometers for a-C : H. Experimental values are listed in Tables IIa (○), IIb (●), and IIc ($x$).

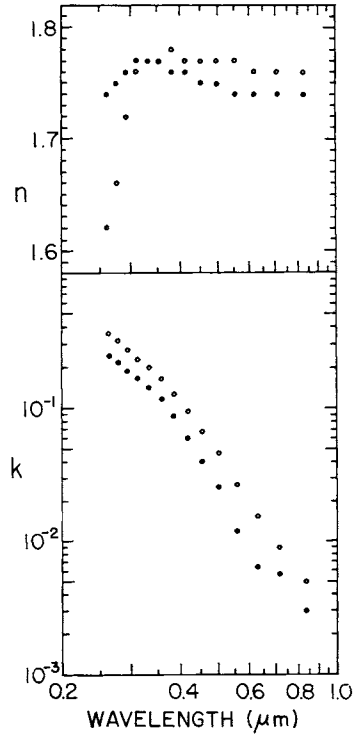


**Fig. 2.** Plot of $n$ and $k$ versus wavelength in micrometers for a-C : H. Experimental values are listed in Tables IVa (●), and IVb (○).

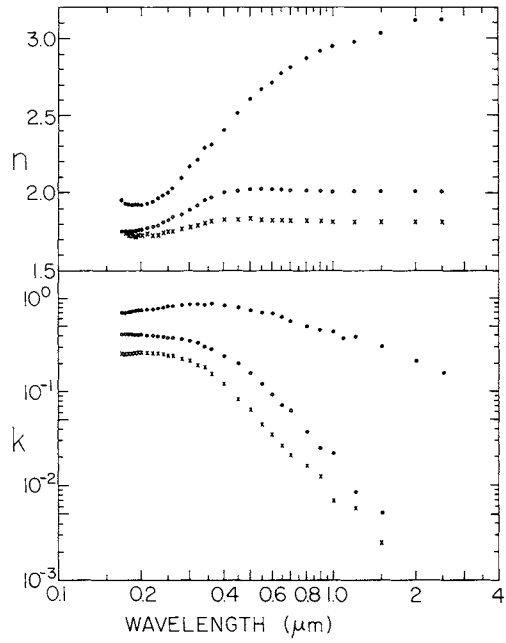


**Fig. 3.** Plot of $n$ and $k$ versus wavelength in micrometers for a-C : H. Experimental values are listed in Tables VIa (●), VIb (○), and VIc ($x$).

**TABLE I**

**Dispersion-Relation Parameters for a-C : H Films (Eqs. 1–5) Prepared by Plasma Deposition on Silicon Wafer Substrates [24, 32]. $T$ is the Annealing Temperature**

| $P$(W) | $T$(C) | $A$ | $B$ (eV) | $C$ (eV$^2$) | $E_g$ (eV) | $n(\infty)$ |
|---|---|---|---|---|---|---|
| 50 | <25 | .06 | 6.39 | 12.67 | 1.64 | 1.63 |
| 100 | <25 | .01 | 6.46 | 10.51 | 2.70 | 1.7 |
| 150 | <25 | .05 | 5.90 | 9.75 | 2.23 | 1.67 |
| 200 | <25 | .11 | 5.99 | 11.73 | 1.65 | 1.69 |
| 150 | 400 | .06 | 5.10 | 7.20 | 1.90 | 1.70 |
| 150 | 600 | .40 | 3.66 | 4.22 | 1.03 | 1.58 |
| 150 | 750 | .85 | 1.21 | 1.85 | 0.39 | 1.71 |

**TABLE IIa**

**Experimental Values of *n* and *k* for a-C:H. Deposition Conditions Are 50 W Plasma Power, Room Temperature Substrate, No Post-Deposition Anneal [24]**

| eV | $cm^{-1}$ | μm | n | k |
|---|---|---|---|---|
| 3.543 | 28,571 | 0.350 | 1.779 | 0.084 |
| 3.444 | 27,778 | 0.360 | 1.777 | 0.076 |
| 3.351 | 27,027 | 0.370 | 1.776 | 0.068 |
| 3.263 | 26,318 | 0.380 | 1.769 | 0.060 |
| 3.179 | 25,641 | 0.390 | 1.758 | 0.053 |
| 3.100 | 25,000 | 0.400 | 1.765 | 0.048 |
| 3.024 | 24,390 | 0.410 | 1.760 | 0.044 |
| 2.952 | 23,809 | 0.420 | 1.758 | 0.041 |
| 2.638 | 21,277 | 0.470 | 1.724 | 0.022 |
| 2.583 | 20,833 | 0.480 | 1.717 | 0.019 |
| 2.531 | 20,408 | 0.490 | 1.723 | 0.017 |
| 2.480 | 20,000 | 0.500 | 1.718 | 0.015 |
| 2.431 | 19,600 | 0.510 | 1.715 | 0.013 |
| 2.385 | 19,230 | 0.520 | 1.710 | 0.011 |
| 2.340 | 18,868 | 0.530 | 1.703 | 0.010 |
| 2.296 | 18,518 | 0.540 | 1.710 | 0.008 |
| 2.255 | 18,182 | 0.550 | 1.704 | 0.006 |
| 2.214 | 17,859 | 0.560 | 1.701 | 0.005 |
| 2.175 | 17,543 | 0.570 | 1.691 | |
| 2.138 | 17,244 | 0.580 | 1.685 | |
| 2.102 | 16,949 | 0.590 | 1.693 | |
| 2.067 | 16,667 | 0.600 | 1.689 | |
| 2.033 | 16,393 | 0.610 | 1.687 | |
| 2.000 | 16,129 | 0.620 | 1.684 | |
| 1.968 | 15,873 | 0.630 | 1.678 | |
| 1.938 | 15,625 | 0.640 | 1.686 | |
| 1.908 | 15,385 | 0.650 | 1.683 | |
| 1.879 | 15,151 | 0.660 | 1.681 | |
| 1.851 | 14,925 | 0.670 | 1.676 | |
| 1.824 | 14,706 | 0.680 | 1.672 | |
| 1.797 | 14,493 | 0.690 | 1.680 | |
| 1.771 | 14,285 | 0.700 | 1.678 | |
| 1.746 | 14,085 | 0.710 | 1.678 | |
| 1.722 | 13,889 | 0.720 | 1.678 | |
| 1.699 | 13,119 | 0.730 | 1.677 | |

**TABLE IIb**

**Experimental Values of *n* and *k* for a-C:H. Deposition Conditions Are 150 W Plasma Power, Room Temperature Substrate, No Post-Deposition Anneal, [24]**

| eV | cm-1 | μm | n | k |
|---|---|---|---|---|
| 3.543 | 28,571 | 0.350 | 1.749 | 0.056 |
| 3.444 | 27,778 | 0.360 | 1.745 | 0.052 |
| 3.351 | 27,027 | 0.370 | 1.748 | 0.047 |
| 3.263 | 26,318 | 0.380 | 1.750 | 0.042 |
| 3.179 | 25,641 | 0.390 | 1.743 | 0.037 |
| 2.884 | 23,256 | 0.430 | 1.725 | 0.020 |
| 2.818 | 22,729 | 0.440 | 1.717 | 0.016 |
| 2.756 | 22,228 | 0.450 | 1.715 | 0.012 |
| 2.696 | 21,738 | 0.460 | 1.713 | 0.009 |
| 2.638 | 21,270 | 0.470 | 1.706 | 0.005 |
| 2.583 | 20,833 | 0.480 | 1.701 | 0.003 |
| 2.531 | 20,408 | 0.490 | 1.693 | 0.002 |
| 2.480 | 20,000 | 0.500 | 1.693 | |
| 2.255 | 18,182 | 0.550 | 1.689 | |
| 2.214 | 17,857 | 0.560 | 1.686 | |
| 2.175 | 17,541 | 0.570 | 1.684 | |
| 2.138 | 17,241 | 0.580 | 1.681 | |
| 2.102 | 16,949 | 0.590 | 1.684 | |
| 2.067 | 16,667 | 0.600 | 1.687 | |
| 2.033 | 16,393 | 0.610 | 1.685 | |
| 2.000 | 16,129 | 0.620 | 1.686 | |
| 1.968 | 15,893 | 0.630 | 1.683 | |
| 1.938 | 15,625 | 0.640 | 1.685 | |
| 1.908 | 15,385 | 0.650 | 1.687 | |
| 1.879 | 15,158 | 0.660 | 1.684 | |
| 1.851 | 14,925 | 0.670 | 1.682 | |
| 1.824 | 14,706 | 0.680 | 1.678 | |
| 1.797 | 14,490 | 0.690 | 1.680 | |
| 1.771 | 14,285 | 0.700 | 1.682 | |
| 1.746 | 14,085 | 0.710 | 1.680 | |
| 1.722 | 13,889 | 0.720 | 1.683 | |
| 1.699 | 13,699 | 0.730 | 1.685 | |

**TABLE IIc**

**Experimental Values of *n* and *k* for a-C:H. Deposition Conditions Are 150 W Plasma Power, 400°C Post-Deposition Anneal [24]**

| eV | $cm^{-1}$ | μm | n | k |
|---|---|---|---|---|
| 3.543 | 28,571 | 0.350 | 1.838 | 0.129 |
| 3.444 | 27,778 | 0.360 | 1.826 | 0.127 |
| 3.351 | 27,027 | 0.370 | 1.829 | 0.126 |
| 3.263 | 26,316 | 0.380 | 1.845 | 0.124 |
| 3.179 | 25,641 | 0.390 | 1.825 | 0.113 |
| 2.952 | 23,810 | 0.420 | 1.797 | 0.082 |
| 2.884 | 23,256 | 0.430 | 1.807 | 0.074 |
| 2.818 | 22,727 | 0.440 | 1.789 | 0.064 |
| 2.756 | 22,222 | 0.450 | 1.788 | 0.055 |
| 2.696 | 21,739 | 0.460 | 1.798 | 0.046 |
| 2.638 | 21,277 | 0.470 | 1.782 | 0.040 |
| 2.583 | 20,833 | 0.480 | 1.774 | 0.034 |
| 2.531 | 20,108 | 0.490 | 1.783 | 0.027 |
| 2.385 | 19,231 | 0.520 | 1.758 | 0.019 |
| 2.340 | 18,868 | 0.530 | 1.764 | 0.014 |
| 2.296 | 18,519 | 0.540 | 1.780 | 0.008 |
| 2.255 | 18,182 | 0.550 | 1.765 | 0.009 |
| 2.214 | 17,857 | 0.560 | 1.758 | 0.009 |
| 2.175 | 17,543 | 0.570 | 1.770 | 0.006 |
| 2.138 | 17,244 | 0.580 | 1.756 | 0.008 |
| 2.102 | 16,949 | 0.590 | 1.759 | 0.007 |
| 2.067 | 16,667 | 0.600 | 1.775 | 0.005 |
| 2.033 | 16,393 | 0.610 | 1.760 | 0.007 |
| 2.000 | 16,129 | 0.620 | 1.755 | 0.008 |
| 1.968 | 15,873 | 0.630 | 1.768 | 0.007 |
| 1.938 | 15,625 | 0.640 | 1.752 | 0.009 |
| 1.908 | 15,385 | 0.650 | 1.754 | 0.010 |
| 1.879 | 15,152 | 0.660 | 1.769 | 0.010 |
| 1.851 | 14,925 | 0.670 | 1.752 | 0.011 |
| 1.824 | 14,906 | 0.680 | 1.745 | 0.011 |
| 1.797 | 14,492 | 0.690 | 1.757 | 0.012 |
| 1.771 | 14,286 | 0.700 | 1.743 | 0.012 |
| 1.746 | 14,085 | 0.710 | 1.749 | 0.012 |
| 1.722 | 13,889 | 0.720 | 1.771 | 0.012 |
| 1.699 | 13,699 | 0.730 | 1.767 | 0.012 |

TABLE III

**Experimental Values of *n* and *k* for a-C:H. Deposition Conditions Are 150 W Plasma Power, Room Temperature Substrate, No Post-Deposition Anneal [6, 28]**

| eV | $cm^{-1}$ | μm | n | k |
|---|---|---|---|---|
| 0.3100 | 2,500 | 4 | 1.65+0.05 | 0.01 |
| 0.1240 | 1,000 | 10 | 1.75+0.15 | 0.01 |

TABLE IVa

**Experimental Values of *n* and *k* for a-C:H. Deposition Conditions Are dc Glow Discharge, Substrate at 250°C, No Post-Deposition Anneal [3]**

| eV | $cm^{-1}$ | μm | n | k |
|---|---|---|---|---|
| 4.75 | 38,311 | 0.2611 | 1.74 | 0.246 |
| 4.50 | 36,295 | 0.2755 | 1.75 | 0.220 |
| 4.25 | 34,298 | 0.2918 | 1.76 | 0.195 |
| 4.00 | 32,262 | 0.3100 | 1.77 | 0.168 |
| 3.75 | 30,245 | 0.3307 | 1.77 | 0.144 |
| 3.50 | 28,229 | 0.3543 | 1.77 | 0.119 |
| 3.25 | 26,213 | 0.3815 | 1.76 | 0.089 |
| 3.00 | 24,196 | 0.4133 | 1.76 | 0.061 |
| 2.75 | 22,180 | 0.4509 | 1.75 | 0.041 |
| 2.50 | 20,164 | 0.4960 | 1.75 | 0.026 |
| 2.25 | 18,147 | 0.5511 | 1.74 | 0.0120 |
| 2.00 | 16,131 | 0.6200 | 1.74 | 0.0065 |
| 1.75 | 14,115 | 0.7086 | 1.74 | 0.0057 |
| 1.50 | 12,098 | 0.8267 | 1.74 | 0.0030 |

**TABLE IVb**

**Experimental Values of $n$ and $k$ for a-C:H. Deposition Conditions Are dc glow Discharge, Substrate at 250°C, 350°C Post-Deposition Anneal [3]**

| eV | $cm^{-1}$ | μm | n | k |
|---|---|---|---|---|
| 4.75 | 38,311 | 0.2611 | 1.62 | 0.360 |
| 4.50 | 36,295 | 0.2755 | 1.66 | 0.320 |
| 4.25 | 34,278 | 0.2918 | 1.72 | 0.273 |
| 4.00 | 32,262 | 0.3100 | 1.76 | 0.234 |
| 3.75 | 30,246 | 0.3307 | 1.77 | 0.203 |
| 3.50 | 28,229 | 0.3543 | 1.77 | 0.168 |
| 3.25 | 26,213 | 0.3815 | 1.78 | 0.129 |
| 3.00 | 24,196 | 0.4133 | 1.77 | 0.096 |
| 2.75 | 22,180 | 0.4509 | 1.77 | 0.068 |
| 2.50 | 20,164 | 0.4960 | 1.77 | 0.047 |
| 2.25 | 18,147 | 0.5511 | 1.77 | 0.027 |
| 2.00 | 16,131 | 0.6200 | 1.76 | 0.0155 |
| 1.75 | 14,115 | 0.7036 | 1.76 | 0.0090 |
| 1.50 | 12,098 | 0.8267 | 1.76 | 0.0050 |

**TABLE V**

**Deposition Parameters. ($P_H$ = Partial Pressure of Hydrogen Gas; $E_i$ = Ion Energy; Ar+/C = Ion to Condensing Carbon Atom Arrival Rate Ratio; $E_t$/C = Ion Energy per C Atom; the Partial Pressure of Argon Gas Was 1 Pa; $C_H$ Is the Hydrogen Concentration [33–35])**

| Specimen | Power (W) | $P_H$ (Pa) | $C_H$ (at.%) | $E_i$ (eV) | Ar/C | $E_t$/C (eV) |
|---|---|---|---|---|---|---|
| 1 | 500 | 0 | 0 | 13 | 2.2 | 29 |
| 2 | 50 | 0 | 0 | 14 | 2.9 | 41 |
| 3 | 10 | 0 | 0 | 16 | 3.7 | 59 |
| 4 | 500 | 0.1 | 4 | 13 | 2.2 | 29 |
| 5 | 50 | 0.1 | 12 | 16 | 2.9 | 46 |
| 6 | 10 | 0.1 | 18 | 18 | 3.7 | 67 |
| 7 | 500 | 0.5 | 13 | 14 | 2.2 | 31 |
| 8 | 50 | 0.5 | 20 | 18 | 2.9 | 52 |
| 9 | 10 | 0.5 | 25 | 20 | 3.7 | 74 |

**TABLE VIa**

**Experimental *n* and *k* for Ion Assisted Deposited a-C:H Specimen No. 1 [33–35]**

| eV | $cm^{-1}$ | μm | n | k |
|---|---|---|---|---|
| 7.294 | 58,824 | 0.170 | 1.957 | 0.705 |
| 7.086 | 57,143 | 0.175 | 1.938 | 0.713 |
| 6.889 | 55,555 | 0.180 | 1.930 | 0.722 |
| 6.703 | 54,054 | 0.185 | 1.924 | 0.730 |
| 6.526 | 52,638 | 0.190 | 1.929 | 0.744 |
| 6.359 | 51,282 | 0.195 | 1.928 | 0.748 |
| 6.200 | 50,000 | 0.20 | 1.918 | 0.750 |
| 5.905 | 47,619 | 0.21 | 1.932 | 0.767 |
| 5.636 | 45,455 | 0.22 | 1.948 | 0.777 |
| 5.391 | 43,478 | 0.23 | 1.969 | 0.790 |
| 5.167 | 41,666 | 0.24 | 1.986 | 0.801 |
| 4.960 | 40,000 | 0.25 | 2.004 | 0.825 |
| 4.769 | 38,462 | 0.26 | 2.032 | 0.835 |
| 4.429 | 35,714 | 0.28 | 2.100 | 0.851 |
| 4.133 | 33,333 | 0.30 | 2.171 | 0.866 |
| 3.875 | 31,250 | 0.32 | 2.217 | 0.875 |
| 3.647 | 29,412 | 0.34 | 2.292 | 0.865 |
| 3.444 | 27,778 | 0.36 | 2.312 | 0.881 |
| 3.100 | 25,000 | 0.40 | 2.408 | 0.853 |
| 2.756 | 22,222 | 0.45 | 2.518 | 0.805 |
| 2.480 | 20,000 | 0.50 | 2.610 | 0.754 |
| 2.255 | 18,182 | 0.55 | 2.672 | 0.717 |
| 2.067 | 16,667 | 0.60 | 2.715 | 0.692 |
| 1.908 | 15,385 | 0.65 | 2.773 | 0.641 |
| 1.771 | 14,286 | 0.70 | 2.815 | 0.579 |
| 1.550 | 12,500 | 0.80 | 2.875 | 0.505 |
| 1.378 | 11,111 | 0.90 | 2.926 | 0.462 |
| 1.240 | 10,000 | 1.0 | 2.951 | 0.442 |
| 1.033 | 8,333 | 1.2 | 2.982 | 0.390 |
| 0.827 | 6,666 | 1.5 | 3.037 | 0.309 |
| 0.620 | 5,000 | 2.0 | 3.123 | 0.217 |
| 0.496 | 4,000 | 2.5 | 3.125 | 0.160 |

TABLE VIb

Experimental $n$ and $k$ for Ion-Assisted Deposited a-C:H Specimen No. 5 [33–35]

| eV | $cm^{-1}$ | μm | n | k |
|---|---|---|---|---|
| 7.294 | 58,824 | 0.170 | 1.750 | 0.415 |
| 7.086 | 57,143 | 0.175 | 1.750 | 0.414 |
| 6.889 | 55,555 | 0.180 | 1.753 | 0.412 |
| 6.703 | 54,054 | 0.185 | 1.756 | 0.410 |
| 6.526 | 52,638 | 0.190 | 1.758 | 0.409 |
| 6.359 | 51,282 | 0.195 | 1.766 | 0.405 |
| 6.200 | 50,000 | 0.20 | 1.767 | 0.405 |
| 5.905 | 47,619 | 0.21 | 1.780 | 0.401 |
| 5.636 | 45,455 | 0.22 | 1.787 | 0.400 |
| 5.391 | 43,478 | 0.23 | 1.796 | 0.393 |
| 5.167 | 41,666 | 0.24 | 1.813 | 0.388 |
| 4.960 | 40,000 | 0.25 | 1.828 | 0.379 |
| 4.769 | 38,462 | 0.26 | 1.848 | 0.376 |
| 4.429 | 35,714 | 0.28 | 1.868 | 0.368 |
| 4.133 | 33,333 | 0.30 | 1.897 | 0.352 |
| 3.875 | 31,250 | 0.32 | 1.925 | 0.336 |
| 3.647 | 29,412 | 0.34 | 1.958 | 0.304 |
| 3.444 | 27,778 | 0.36 | 1.975 | 0.287 |
| 3.100 | 25,000 | 0.40 | 2.007 | 0.242 |
| 2.756 | 22,222 | 0.45 | 2.016 | 0.201 |
| 2.480 | 20,000 | 0.50 | 2.028 | 0.160 |
| 2.255 | 18,182 | 0.55 | 2.029 | 0.121 |
| 2.067 | 16,664 | 0.60 | 2.026 | 0.093 |
| 1.908 | 15,385 | 0.65 | 2.022 | 0.071 |
| 1.771 | 14,286 | 0.70 | 2.019 | 0.062 |
| 1.550 | 12,500 | 0.80 | 2.018 | 0.037 |
| 1.378 | 11,111 | 0.90 | 2.017 | 0.025 |
| 1.240 | 10,000 | 1.0 | 2.013 | 0.022 |
| 1.033 | 8,333 | 1.2 | 2.017 | 0.008 |
| 0.827 | 6,666 | 1.5 | 2.013 | 0.005 |
| 0.620 | 5,000 | 2.0 | 2.013 | <0.001 |
| 0.496 | 4,000 | 2.5 | 2.013 | |

**TABLE VIc**

**Experimental *n* and *k* for Ion-Assisted Deposited a-C:H Specimen No. 9 [33–35]**

| eV | $cm^{-1}$ | μm | n | k |
|---|---|---|---|---|
| 7.294 | 58,824 | 0.170 | 1.741 | 0.259 |
| 7.086 | 57,143 | 0.175 | 1.735 | 0.257 |
| 6.889 | 55,555 | 0.180 | 1.730 | 0.259 |
| 6.703 | 54,054 | 0.185 | 1.724 | 0.259 |
| 6.526 | 52,638 | 0.190 | 1.718 | 0.261 |
| 6.359 | 51,282 | 0.195 | 1.725 | 0.263 |
| 6.200 | 50,000 | 0.20 | 1.728 | 0.264 |
| 5.905 | 47,619 | 0.21 | 1.737 | 0.261 |
| 5.636 | 45,455 | 0.22 | 1.727 | 0.260 |
| 5.391 | 43,478 | 0.23 | 1.730 | 0.256 |
| 5.167 | 41,666 | 0.24 | 1.743 | 0.251 |
| 4.960 | 40,000 | 0.25 | 1.749 | 0.246 |
| 4.769 | 39,462 | 0.26 | 1.753 | 0.242 |
| 4.429 | 35,714 | 0.28 | 1.772 | 0.226 |
| 4.133 | 33,333 | 0.30 | 1.783 | 0.218 |
| 3.875 | 31,250 | 0.32 | 1.798 | 0.193 |
| 3.647 | 29,412 | 0.34 | 1.809 | 0.185 |
| 3.444 | 27,778 | 0.36 | 1.820 | 0.156 |
| 3.100 | 25,000 | 0.40 | 1.831 | 0.121 |
| 2.756 | 22,222 | 0.45 | 1.830 | 0.083 |
| 2.480 | 20,000 | 0.50 | 1.836 | 0.065 |
| 2.255 | 18,182 | 0.55 | 1.830 | 0.045 |
| 2.067 | 16,667 | 0.60 | 1.826 | 0.035 |
| 1.908 | 15,385 | 0.65 | 1.822 | 0.027 |
| 1.771 | 14,286 | 0.70 | 1.822 | 0.021 |
| 1.550 | 12,500 | 0.80 | 1.821 | 0.016 |
| 1.378 | 11,111 | 0.90 | 1.819 | 0.013 |
| 1.240 | 10,000 | 1.0 | 1.820 | 0.007 |
| 1.033 | 8,333 | 1.2 | 1.82 | 0.006 |
| 0.827 | 6,666 | 1.5 | 1.819 | 0.002 |
| 0.620 | 5,000 | 2.0 | 1.819 | <0.001 |
| 0.496 | 4,000 | 2.5 | 1.818 | |

TABLE VII

**Experimental Values of $n$ and $k$ for Arc-Evaporated Carbon. After Arakawa *et al.* [36, 37]**

| eV | $cm^{-1}$ | μm | n | k |
|---|---|---|---|---|
| 10.00 | 80,655 | 0.1240 | 1.66 | 0.795 |
| 9.00 | 72,589 | 0.1378 | 1.70 | 0.713 |
| 8.00 | 64,524 | 0.1550 | 1.71 | 0.656 |
| 7.00 | 56,458 | 0.1771 | 1.70 | 0.628 |
| 6.00 | 48,393 | 0.2066 | 1.70 | 0.646 |
| 5.00 | 40,327 | 0.2480 | 1.73 | 0.712 |
| 4.00 | 32,262 | 0.3100 | 1.84 | 0.808 |
| 3.8 | 30,649 | 0.3263 | 1.90 | 0.91 |
| 3.6 | 29,036 | 0.3444 | 1.94 | 0.92 |
| 3.4 | 27,423 | 0.3647 | 2.00 | 0.92 |
| 3.2 | 25,810 | 0.3884 | 2.06 | 0.91 |
| 3.0 | 24,196 | 0.4133 | 2.11 | 0.90 |
| 2.8 | 22,583 | 0.4428 | 2.17 | 0.89 |
| 2.6 | 20,970 | 0.4789 | 2.24 | 0.88 |
| 2.4 | 19,357 | 0.5166 | 2.30 | 0.87 |
| 2.2 | 17,744 | 0.5636 | 2.38 | 0.82 |
| 2.0 | 16,131 | 0.6199 | 2.43 | 0.75 |
| 1.8 | 14,518 | 0.6888 | 2.43 | 0.70 |
| 1.6 | 12,905 | 0.7749 | 2.33 | 0.71 |
| 1.4 | 11,292 | 0.8856 | 2.24 | 0.80 |
| 1.2 | 9,679 | 1.033 | 2.26 | 1.09 |
| 1.0 | 8,065 | 1.240 | 2.63 | 1.47 |
| 0.8 | 6,452 | 1.550 | 3.34 | 1.63 |
| 0.7 | 5,646 | 1.771 | 3.67 | 1.60 |
| 0.6 | 4,839 | 2.066 | 3.73 | 1.54 |

# Cesium Iodide (CsI)

JOHN E. ELDRIDGE
Department of Physics
University of British Columbia
Vancouver, British Columbia, Canada

The room-temperature values of $n$ and $k$ tabulated here (Table I, Fig. 1) were obtained from the following works and references therein: in the millimeter region, an individual measurement of $n$ at 2 mm (5 $cm^{-1}$) is from Dianov and Irisova [1]; both $n$ and $k$ at selected points in the submillimeter region, 300 $GH_z$ (10 $cm^{-1}$), 500 $GH_z$ (16.7 $cm^{-1}$) and 700 $GH_z$ (23.3 $cm^{-1}$) are from Bystrov *et al.* [2]; values of $k$ in the far-infrared region at 14–56 $cm^{-1}$ and at 94–200 $cm^{-1}$ are from Beairsto and Eldridge [3]; over the reststrahlen peak, from just below 60 $cm^{-1}$ to 94 $cm^{-1}$, $n$ and $k$ are given by Vergnat *et al.* [4], and values of $n$ are continued into the wings by the same authors [4, 5]; in the transparent region, which covers the infrared and the visible from 67 $\mu$m (149 $cm^{-1}$) to 0.25 $\mu$m (40,000 $cm^{-1}$), values of $n$ are from Li [6], who relied mainly on the data of Rodney [7]; in the vacuum ultraviolet from 5 eV (0.25 $\mu$m) to 11.4 eV (0.11 $\mu$m) $n$ and $k$ values are from Said and Green [8]; in the low-energy X-ray region from 100 eV (124 Å) to 2000 eV (6.2 Å), *calculated* values of $n$ and $k$ are from Henke *et al.* [9].

Cesium iodide has the lowest-energy reststrahlen band of all the alkali halides and common diatomic optical-window crystals, with a room-temperature peak in extinction coefficient, $k$, near 63 $cm^{-1}$ (159 $\mu$m, 7.8 meV. Apart from the structure in this strong and relatively broad resonance, there is, of course, no other intrinsic absorption until electronic transitions in the vacuum ultraviolet. For this reason it is a common window material in infrared spectroscopy, providing the largest range to low energies in the far-infrared region, (for example, a window of 3 mm thickness will transmit down to approximately 150 $cm^{-1}$). Although it is very soft, with some care it can be used with indium O-rings for low-temperature studies. Since the absorption in the wings falls off very rapidly, the intrinsic absorption in the infrared region is extremely low, offering promise for CsI, as a low-loss, light-guide material and as windows for high-intensity laser beams.


Copyright © 1991 by Academic Press.
All rights of reproduction in any form reserved.
ISBN 0-12-544422-2

The reststrahlen band is due to the only optically active vibration in the crystal, the doubly degenerate, transverse-optic (TO) mode with zero wave vector, which has a frequency inversely proportional to the reduced mass of Cs and I. The structure in the wings is due to the frequency-dependence of the damping of this TO mode. This damping, in turn, is due to the two- and higher-phonon processes by which the TO mode can relax when energy and momentum are conserved. Calculations of this damping for CsI, and the resulting absorption through the reststrahlen band, give good agreement with the experiment data [10, 3]. The most accurate method of measuring $n$ and $k$ in this region would be that of dispersive-reflection spectroscopy (also known as asymmetric Fourier-transform spectroscopy), which was used in the investigations of NaCl and KCl, as well as some of the semiconductors reported in *HOC I.* In such a method $n$ and $k$ are measured directly, without the need for a Kramers–Kronig analysis or a fit to several fictitious Lorentzian oscillators. No such experiment has, however, been performed so far for CsI. The peak values of $n$ and $k$ reported here have therefore been obtained from a Kramers–Kronig analysis of the power reflectivity [4], which necessarily misses much of the two-phonon structure in $n$, above the resonance where $n$ is small.

Starting at the lowest energy, Dianov and Irisova [1] measured $n$ at 2 mm (5 $cm^{-1}$) at 300 K and 77 K with a Michelson interferometer. The room-temperature value agrees with that measured at 300 $GH_z$ ($10^{-1}$) by Bystrov *et al.* [2] using an "Epsilon backward-wave-tube submillimeter spectrometer." They also reported $n$ and $k$ values at 500 $GH_z$ (16.7 $cm^{-1}$) and 700 $GH_z$ (23.3 $cm^{-1}$). The $k$ values agree with those obtained by Beairsto and Eldridge [3] from transmission measurements through single crystals in a Michelson interferometer. Samples ranged in thickness from 0.007 cm to 0.8 cm. They were cut with a wire saw and then polished using jeweller's rouge in ethylene glycol. After polishing, they were cleaned in acetone and then trichloroethylene. $k$ was obtained from $\alpha/4\pi\bar{\nu}$, and $\alpha$ was extracted from the expression for the transmitted intensity, $I$, given by

$$I=\frac{I_0(1-R)^2(1+k^2/n^2)e^{-\alpha d}}{1-R^2e^{-2\alpha d}}. \tag{1}$$

Measured values of $R$ were used. The term $(1+k^2/n^2)$ is negligible except when close to the resonance on the high-frequency side. These results show $k$ to be fairly smooth below the resonance, but Love *et al.*'s accurate low-temperature measurements on KI crystals up to 10 cm long [11] show that two-phonon structure can be observed in these materials.

The thinnest crystal used in Ref. [3] did not transmit between 56 $cm^{-1}$ and 94 $cm^{-1}$. The two models used in the reflectivity analysis [4, 5] give $n$

and $k$ values that can differ by up to 50%. The Kramers–Kronig values [4] are tabulated, since they are more directly obtained, but these are supplemented with Lorentz-model values [5] in the wings. The accuracy in the wings is poor and, as has been mentioned, structure is missing above the resonance. The reflectivity measurements were performed on a 15° wedged single crystal, and the authors report a 3% reproducibility.

In the wide transparent region from 67 $\mu$m (150 $cm^{-1}$) to 0.25 $\mu$m (40,000 $cm^{-1}$), Li [6] has tabulated very accurate values of $n$. Starting with the 297 K data of Rodney [7], which Li reduced to 293 K, and using the infrared absorption peak at 161.29 $\mu$m (detailed earlier [4]), together with the seven known absorption peaks in the vacuum ultraviolet, Li fitted the following dispersion equation of the Sellmeier type,

$$n^2 = 1.27587 + \frac{0.68689\lambda^2}{\lambda^2-(0.130)^2} + \frac{0.26090\lambda^2}{\lambda^2-(0.147)^2} + \frac{0.06256\lambda^2}{\lambda^2-(0.163)^2} + \frac{0.06527\lambda^2}{\lambda^2-(0.177)^2} + \frac{0.14991\lambda^2}{\lambda^2-(0.185)^2} + \frac{0.51818\lambda^2}{\lambda^2-(0.206)^2} + \frac{0.01918\lambda^2}{\lambda^2-(0.218)^2} + \frac{3.38229\lambda^2}{(\lambda^2-161.29)^2}, \quad (2)$$

where $\lambda$ is in $\mu$m. Values from Eq. 2 are tabulated, although to greater accuracy than warranted by the experiment for the purpose of smoothness and internal comparison. Rodney's measurements of minimum deviation were performed on a 25° prism sample, loaned by the Harshaw Chemical Company, in two temperature-controlled spectrometers. The precision of the index measurements was reduced by the small wedge angle, since 60° is closer to the optimum, and instrumental factors reduced the wavelength accuracy when broad reference bands were used. Only the third decimal place is meaningful between 67 $\mu$m (150 $cm^{-1}$) and 50 $\mu$m (200 $cm^{-1}$), and the fourth decimal place elsewhere. The estimated uncertainty decreases from $1 \times 10^{-3}$ at the low-energy limit to $1 \times 10^{-4}$ near the high-energy limit. As an example of this accuracy, comparison may be made with the results of Selvarajan *et al.* [12], who later performed similar measurements at 300 K and 80 K over the smaller range from 30 $\mu m^{-1}$ (333 $cm^{-1}$) to 2 $\mu$m (5000 $cm^{-1}$). After correcting for the temperature difference, these results agree to within $2–3 \times 10^{-4}$ with those of Li, the former being consistently higher.

No measurements of $k$ beyond 200 $cm^{-1}$ have been found. Measurements of the absorption in the transparent region have, however, been performed

using laser calorimetry, but these have all measured impurity absorption. Plotnichenko *et al.* [13] measured the volume absorption coefficient at several laser wavelengths, yielding $k$ values of $7.6\times10^{-10}$, $4.4\times10^{-10}$, and $7.6\times10^{-10}$ at $10.6\,\mu$m ($943\,\text{cm}^{-1}$), $5.54\,\mu$m ($1805\,\text{cm}^{-1}$), and $1.06\,\mu$m ($9433\,\text{cm}^{-1}$), respectively. Even though very small, and claimed by the authors to be the lowest value at $10\,\mu$m of any infrared material, these values are still orders of magnitude higher than the calculated intrinsic $k$ due to the combination of multiphonon absorption and Mandel'shtam–Brillouin scattering.

In the vacuum ultraviolet, $n$ and $k$ are given by Said and Green [8] at 300 K and 25 K between 5 eV ($40{,}330\,\text{cm}^{-1}$, $0.248\,\mu$) and 11.4 eV ($91950\,\text{cm}^{-1}$, $0.11\,\mu$m). These were obtained by a Kramers–Kronig analysis of the power reflectivity. In this region the principal features of the reflectivity spectrum are due to excitons and the lower interband transitions, since the direct band gap between the valence-band maximum and the conduction-band minimum is calculated to be about 6.4 eV. There are seven discernible broad features, as mentioned in Li's fit to Eq. 2, which sharpen considerably at 25 K, revealing further structure. After unsuccessful attempts to cleave the samples *in situ*, Said and Green mechanically polished them with fine alumina in mineral oil, thoroughly cleaned them in an ultrasonic bath to remove the aluminum, and kept them in high vacuum until required. Prior to insertion in the reflectometer, the samples were annealed for several hours at 400 K to remove any surface damage. Their results have been read from the graphs at 0.1 eV intervals and have been tabulated. They differ considerably from the results of Lamatsch *et al.* [14] between 2500 Å (5 eV) and 2000 Å (6.2 eV). Lamatsch *et al.*'s results were obtained by analyzing the transmission and reflection spectra of a thin film. Although the two features in this interval are similar to those in Ref. [8], $n$ and $k$ values disagree by more than a factor of two. Lamatsch *et al.* also noticed discrepancies in magnitude between the reflection spectrum obtained from a bulk sample and that calculated from their thin-film values of $n$ and $k$. They attributed these discrepancies to the different effect that localized excitons have on the absorption spectra of films and bulk samples. Only the bulk-sample data from Ref. [8] have therefore been tabulated here.

Beyond 11.4 eV, no values of $n$ and $k$ have been found. Many studies of total absorption have been performed, usually through thin films, which yield spectra of the absorption coefficient $\mu$ either in arbitrary or in absolute units. Those performed before 1977 have been summarized by Haelbich *et al.* [15]. These spectra are very similar to the $k$ spectra, as may be seen by comparing the work above in Ref. [8] at 25 K with the 10 K $\mu$ spectra of Teegarden and Baldini [16], so that the structure in $k$, if not the absolute magnitude, may be found. In particular, Saito *et al.* [17] give $\mu$ in arbitrary units at room temperature between 12 eV and 24 eV; Cardona *et*

*al.* [18] give absolute values of $\mu$ between 50 eV and 190 eV; Lukirskii and Zimkina [19] give $\mu$ in arbitrary units between 50 eV and 500 eV; and Sugiura and Kiyono [20] give $\mu$ in arbitrary units at the Cs and I X-ray $L$ edges around 5 kV.

For several materials, good agreement has been found previously in the soft X-ray region between experimental values and those calculated using the atomic-scattering factors of Henke *et al.* [9] (see, for instance, Ni, Ag, Au, and $SiO_2$ in *HOC I*). We have therefore tabulated the calculated values of $n$ and $k$ for CsI between 100 eV and 2000 eV, which includes the $M$ absorption edges. In scattering theory, the refractive index is given as

$$n = 1 - \delta - i\beta, \tag{3}$$

where

$$\delta = \frac{r_0 \lambda^2}{2\pi} N \bar{f}_1$$

$$\beta = \frac{r_0 \lambda^2}{2\pi} N \bar{f}_2. \tag{4}$$

Here, $r_0 = e^2/mc^2$, the classical electron radius, equal to $2.814 \times 10^{-13}$ cm; $N$ is the density of atoms per unit volume; and $\bar{f}_1$ and $\bar{f}_2$ are the sum of the scattering factors, which are listed in [9].

## REFERENCES


1. E. M. Dianov and N. A. Irisova, *Sov. Phys.-Solid State* **8**, 1807 (1967).
2. V. P. Bystrov, Y. G. Goncharov, G. V. Kozlov, and A. F. Kupriyanenko, *Sov. Phys.-Tech. Phys.* **31**, 1206 (1986).
3. J. A. B. Beairsto and J. E. Eldridge, *Can. J. Phys.* **51**, 2550 (1973).
4. P. P. Vergnat, J. Claudel, A. Hadni, P. Strimer, and F. Vermillard, *J. de Phys.* **30**, 723 (1969) (data obtained from a Kramers–Kronig analysis).
5. Ibid. (data obtained from a Lorentz analysis).
6. H. H. Li, *J. Phys. Chem. Refer. Data* **5**, 329 (1976).
7. W. S. Rodney, *J. Opt. Soc. Am.* **45**, 987 (1955).
8. K. I. Said and G. W. Green, *J. Phys.* **C10**, 479 (1977).
9. B. L. Henke, P. Lee, T. J. Tanaka, R. L. Shimabukuro, and B. K. Fujikawa, in "Low Energy X-Ray Diagnostics—1981," (D. T. Attwood and B. L. Henke, eds.), AIP Conf. Proc. no. 75, American Institute of Physics, New York, 340 (1981).
10. J. E. Eldridge, R. Howard, and P. R. Staal, *Can. J. Phys.* **55**, 227 (1977).
11. S. P. Love, W. P. Ambrose, and A. J. Sievers, *Phys. Rev.* **B39**, 10352 (1989).
12. A. Selvarajan, J. L. Swedberg, A. G. DeBell, and W. L. Wolfe, *Appl. Opt.* **18**, 3116 (1979).

13. V. G. Plotnichenko, V. K. Sysoev, and I. G. Firsov, *Sov. J. Opt. Technol.* **50**, 563, (1983).
14. H. Lamatsch, J. Rossel, and E. Saurer, *Phys. Stat. Solidi (b)* **49**, 311 (1972).
15. R. P. Haelbich, M. Iwan, and E. E. Koch, "Physik Daten-Physics Data," Fach-information Zentrum, Karlsruhe, 152 (1977).
16. K. Teegarden and G. Baldini, *Phys. Rev.* **155**, 896 (1967).
17. H. Saito, S. Saito, R. Onaka, and B. Ikeo, *J. Phys. Soc. Japan* **24**, 1095 (1968).
18. M. Cardona, R. Haensel, D. W. Lynch, and B. Sonntag, *Phys. Rev.* **B2**, 1117 (1970).
19. A. P. Lukirskii and T. M. Zimkina, "Röntgenspektren und chemische Bindung," Karl-Marx-Univ., Leipzig, 187 (1966).
20. C. Sugiura and S. Kiyono, Technology Reports, Tohoku Univ. **35**, 119 (1970); Ibid. **35**, 61 (1970).

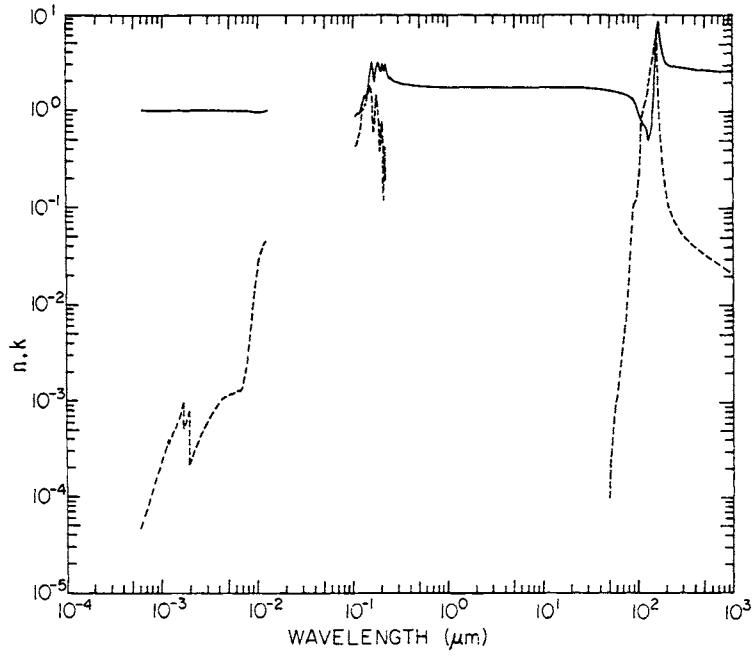


**Fig. 1.** Log–log plot of $n$ (solid line) and $k$ (dashed line) versus wavelength in micrometers for cesium iodide.

TABLE I

Values of $n$ and $k$ for Cesium Iodide from Various References[a]

| eV | $cm^{-1}$ | Å | $n$ | $k$ |
|---|---|---|---|---|
| 2000 | | 6.2 | 0.999822 [9] | $4.71 \times 10^{-5}$ [9] |
| 1952 | | 6.35 | 0.999814 | 5.11 |
| 1905 | | 6.51 | 0.999804 | 5.55 |
| 1860 | | 6.67 | 0.999795 | 6.02 |
| 1815 | | 6.83 | 0.999786 | 6.52 |
| 1772 | | 7.00 | 0.999776 | 7.07 |
| 1730 | | 7.17 | 0.999765 | 7.67 |
| 1688 | | 7.34 | 0.999755 | 8.29 |
| 1648 | | 7.52 | 0.999744 | 8.98 |
| 1609 | | 7.71 | 0.999732 | $9.74 \times 10^{-5}$ |
| 1570 | | 7.90 | 0.999720 | $1.06 \times 10^{-4}$ |
| 1533 | | 8.09 | 0.999709 | 1.14 |
| 1496 | | 8.29 | 0.999696 | 1.24 |
| 1460 | | 8.49 | 0.999683 | 1.34 |
| 1426 | | 8.69 | 0.999671 | 1.45 |
| 1392 | | 8.91 | 0.999657 | 1.57 |
| 1358 | | 9.13 | 0.999643 | 1.70 |
| 1326 | | 9.35 | 0.999630 | 1.83 |
| 1294 | | 9.58 | 0.999616 | 1.98 |
| 1263 | | 9.82 | 0.999602 | 2.15 |
| 1233 | | 10.06 | 0.999589 | 2.32 |
| 1204 | | 10.30 | 0.999576 | 2.49 |
| 1175 | | 10.55 | 0.999563 | 2.68 |
| 1147 | | 10.81 | 0.999551 | 2.89 |
| 1119 | | 11.08 | 0.999540 | 3.12 |
| 1093 | | 11.34 | 0.999530 | 3.35 |
| 1067 | | 11.62 | 0.999527 | 3.61 |
| 1041 | | 11.91 | 0.999533 | 3.90 |
| 1016 | | 12.20 | 0.999527 | 3.69 |
| 992 | | 12.50 | 0.999494 | 3.90 |
| 968 | | 12.81 | 0.999473 | 4.22 |
| 945 | | 13.12 | 0.999459 | 4.56 |
| 923 | | 13.43 | 0.999455 | 4.86 |
| 901 | | 13.76 | 0.999447 | 5.08 |
| 879 | | 14.10 | 0.999434 | 5.32 |
| 858 | | 14.45 | 0.999412 | 5.58 |
| 838 | | 14.79 | 0.999390 | 6.00 |
| 818 | | 15.16 | 0.999379 | 6.57 |
| 798 | | 15.54 | 0.999389 | 7.20 |
| 779 | | 15.92 | 0.999434 | 7.88 |
| 760 | | 16.31 | 0.999525 | 8.65 |
| 742 | | 16.71 | 0.999649 | 9.48 |
| 725 | | 17.10 | 1.000202 | 5.23 |
| 707 | | 17.54 | 0.999730 | 5.68 |
| 690 | | 17.97 | 0.999633 | 6.15 |

(continued)

TABLE I (*Continued*)

**Cesium Iodide**

| eV | $cm^{-1}$ | Å | $n$ | $k$ |
|---|---|---|---|---|
| 674 | | 18.39 | 0.999605 | 6.64 |
| 658 | | 18.84 | 0.999658 | 7.24 |
| 642 | | 19.31 | 0.999781 | 7.91 |
| 627 | | 19.77 | 1.000059 | 2.29 |
| 612 | | 20.26 | 0.999702 | 2.43 |
| 597 | | 20.77 | 0.999512 | 2.58 |
| 583 | | 21.27 | 0.999403 | 2.74 |
| 569 | | 21.79 | 0.999312 | 2.91 |
| 555 | | 22.34 | 0.999230 | 3.09 |
| 542 | | 22.87 | 0.999158 | 3.28 |
| 529 | | 23.44 | 0.999082 | 3.47 |
| 516 | | 24.03 | 0.999008 | 3.68 |
| 504 | | 24.60 | 0.99894 | 3.88 |
| 492 | | 25.20 | 0.99886 | 4.10 |
| 480 | | 25.83 | 0.99879 | 4.33 |
| 469 | | 26.4 | 0.99872 | 4.56 |
| 458 | | 27.1 | 0.99863 | 4.83 |
| 447 | | 27.7 | 0.99856 | 5.10 |
| 436 | | 28.4 | 0.99848 | 5.37 |
| 426 | | 29.1 | 0.99840 | 5.65 |
| 415 | | 29.9 | 0.99831 | 5.97 |
| 406 | | 30.5 | 0.99824 | 6.22 |
| 396 | | 31.3 | 0.99814 | 6.56 |
| 386 | | 32.1 | 0.99805 | 6.85 |
| 377 | | 32.9 | 0.99795 | 7.15 |
| 368 | | 33.7 | 0.99785 | 7.44 |
| 359 | | 34.5 | 0.99775 | 7.72 |
| 351 | | 35.3 | 0.99764 | 8.01 |
| 342 | | 36.3 | 0.99751 | 8.36 |
| 334 | | 37.1 | 0.99740 | 8.63 |
| 326 | | 38.0 | 0.99728 | 8.92 |
| 318 | | 39.0 | 0.99714 | 9.27 |
| 311 | | 39.9 | 0.99701 | 9.55 |
| 303 | | 40.9 | 0.99686 | $9.85 \times 10^{-4}$ |
| 296 | | 41.9 | 0.99671 | $1.01 \times 10^{-3}$ |
| 289 | | 42.9 | 0.99655 | 1.04 |
| 282 | | 44.0 | 0.99637 | 1.07 |
| 275 | | 45.1 | 0.99619 | 1.10 |
| 269 | | 46.1 | 0.99602 | 1.11 |
| 262 | | 47.3 | 0.99580 | 1.13 |
| 256 | | 48.4 | 0.99559 | 1.14 |
| 250 | | 49.6 | 0.99536 | 1.16 |
| 244 | | 50.8 | 0.99510 | 1.17 |
| 238 | | 52.1 | 0.99481 | 1.18 |
| 232 | | 53.4 | 0.99451 | 1.19 |

(continued)

TABLE I (*Continued*)

Cesium Iodide

| eV | $cm^{-1}$ | Å | $n$ | $k$ |
|---|---|---|---|---|
| 227 | | 54.6 | 0.99421 | 1.19 |
| 221 | | 56.1 | 0.99382 | 1.20 |
| 216 | | 57.4 | 0.99347 | 1.21 |
| 211 | | 58.8 | 0.99306 | 1.22 |
| 206 | | 60.2 | 0.99262 | 1.23 |
| 201 | | 61.7 | 0.99213 | 1.25 |
| 196 | | 63.3 | 0.99158 | 1.28 |
| 191 | | 64.9 | 0.99100 | 1.29 |
| 187 | | 66.3 | 0.99041 | 1.28 |
| 182 | | 68.1 | 0.9895 | 1.30 |
| 178 | | 69.7 | 0.9888 | 1.40 |
| 174 | | 71.3 | 0.9880 | 1.52 |
| 170 | | 72.9 | 0.9871 | 1.68 |
| 166 | | 74.7 | 0.9860 | 1.91 |
| 162 | | 76.5 | 0.9848 | 2.20 |
| 158 | | 78.5 | 0.9835 | 2.61 |
| 154 | | 80.5 | 0.9820 | 3.17 |
| 150 | | 82.7 | 0.9803 | 3.97 |
| 147 | | 84.3 | 0.9790 | 4.71 |
| 143 | | 86.7 | 0.9770 | 5.97 |
| 140 | | 88.6 | 0.9752 | 7.37 |
| 136 | | 91.2 | 0.9731 | $9.84 \times 10^{-3}$ |
| 133 | | 93.2 | 0.9716 | $1.21 \times 10^{-2}$ |
| 130 | | 95.4 | 0.9703 | 1.50 |
| 127 | | 97.6 | 0.9696 | 1.81 |
| 124 | | 100.0 | 0.9691 | 2.14 |
| 121 | | 102.5 | 0.9691 | 2.50 |
| 118 | | 105.1 | 0.9696 | 2.91 |
| 115 | | 107.8 | 0.9714 | 3.34 |
| 112 | | 110.7 | 0.9737 | 3.65 |
| 110 | | 112.7 | 0.9755 | 3.84 |
| 107 | | 115.9 | 0.9784 | 4.12 |
| 104 | | 119.2 | 0.9818 | 4.36 |
| 102 | | 121.5 | 0.9842 | 4.48 |
| 100 | | 124.0 | 0.9869 | 4.62 |

(continued)

TABLE I (*Continued*)

**Cesium Iodide**

| eV | $cm^{-1}$ | $\mu m$ | $n$ | $k$ |
|---|---|---|---|---|
| 11.4 | 91950 | 0.1088 | | 0.428 [8] |
| 11.3 | 91140 | 0.1097 | 0.86 [8] | 0.445 |
| 11.2 | 90330 | 0.1107 | 0.88 | 0.453 |
| 11.1 | 89530 | 0.1117 | 0.91 | 0.473 |
| 11.0 | 88720 | 0.1127 | 0.93 | 0.478 |
| 10.9 | 87910 | 0.1137 | 0.93 | 0.478 |
| 10.8 | 87110 | 0.1148 | 0.93 | 0.486 |
| 10.7 | 86300 | 0.1159 | 0.93 | 0.490 |
| 10.6 | 85490 | 0.1170 | 0.93 | 0.506 |
| 10.5 | 84690 | 0.1181 | 0.91 | 0.531 |
| 10.4 | 83880 | 0.1192 | 0.92 | 0.576 |
| 10.3 | 83070 | 0.1204 | 0.93 | 0.629 |
| 10.2 | 82270 | 0.1216 | 0.95 | 0.694 |
| 10.1 | 81460 | 0.1228 | 0.98 | 0.771 |
| 10.0 | 80650 | 0.1240 | 1.04 | 0.853 |
| 9.9 | 79850 | 0.1252 | 1.10 | 0.939 |
| 9.8 | 79040 | 0.1265 | 1.16 | 1.016 |
| 9.7 | 78240 | 0.1278 | 1.22 | 1.045 |
| 9.6 | 77430 | 0.1292 | 1.27 | 1.029 |
| 9.5 | 76620 | 0.1305 | 1.31 | 1.012 |
| 9.4 | 75820 | 0.1319 | 1.34 | 1.037 |
| 9.3 | 75010 | 0.1333 | 1.37 | 1.061 |
| 9.2 | 74200 | 0.1348 | 1.39 | 1.073 |
| 9.1 | 73400 | 0.1362 | 1.40 | 1.098 |
| 9.0 | 72590 | 0.1378 | 1.40 | 1.127 |
| 8.9 | 71780 | 0.1393 | 1.40 | 1.143 |
| 8.8 | 70980 | 0.1409 | 1.39 | 1.184 |
| 8.7 | 70170 | 0.1425 | 1.42 | 1.298 |
| 8.6 | 69360 | 0.1442 | 1.46 | 1.420 |
| 8.5 | 68560 | 0.1459 | 1.53 | 1.498 |
| 8.4 | 67750 | 0.1476 | 1.72 | 1.714 |
| 8.3 | 66940 | 0.1494 | 1.95 | 1.824 |
| 8.2 | 66140 | 0.1512 | 2.12 | 1.824 |
| 8.1 | 65330 | 0.1531 | 2.41 | 1.857 |
| 8.0 | 64520 | 0.1550 | 2.56 | 1.763 |
| 7.9 | 63720 | 0.1569 | 2.73 | 1.678 |
| 7.8 | 62910 | 0.1590 | 2.95 | 1.571 |
| 7.7 | 62100 | 0.1610 | 3.15 | 1.347 |
| 7.6 | 61300 | 0.1631 | 3.08 | 0.824 |
| 7.5 | 60490 | 0.1653 | 2.73 | 0.649 |
| 7.4 | 59680 | 0.1675 | 2.39 | 0.612 |
| 7.3 | 58880 | 0.1698 | 2.13 | 0.690 |
| 7.2 | 58070 | 0.1722 | 2.01 | 0.878 |
| 7.1 | 57260 | 0.1746 | 2.11 | 1.253 |
| 7.0 | 56460 | 0.1771 | 2.38 | 1.461 |

(continued)

TABLE I (*Continued*)

Cesium Iodide

| eV | $cm^{-1}$ | $\mu m$ | $n$ | $k$ |
|---|---|---|---|---|
| 6.9 | 55650 | 0.1797 | 2.81 | 1.376 |
| 6.8 | 54850 | 0.1823 | 2.84 | 1.139 |
| 6.7 | 54040 | 0.1851 | 3.05 | 1.102 |
| 6.6 | 53230 | 0.1879 | 3.18 | 0.922 |
| 6.5 | 52430 | 0.1907 | 2.96 | 0.514 |
| 6.4 | 51620 | 0.1937 | 2.79 | 0.371 |
| 6.3 | 50810 | 0.1968 | 2.66 | 0.404 |
| 6.2 | 50010 | 0.2000 | 2.55 | 0.424 |
| 6.1 | 49200 | 0.2033 | 2.53 | 0.543 |
| 6.0 | 48390 | 0.2066 | 2.86 | 0.784 |
| 5.9 | 47590 | 0.2101 | 3.05 | 0.490 |
| 5.8 | 46780 | 0.2138 | 2.81 | 0.118 |
| 5.7 | 45970 | 0.2175 | 2.59 | 0.208 |
| 5.6 | 45170 | 0.2214 | 2.99 | 0.408 |
| 5.5 | 44360 | 0.2254 | 2.97 | 0.196 |
| 5.4 | 43550 | 0.2296 | 2.76 | |
| 5.3 | 42750 | 0.2339 | 2.48 | |
| 5.2 | 41940 | 0.2384 | 2.33 | |
| 5.1 | 41130 | 0.2431 | 2.21 | |
| 5.0 | 40330 | 0.2480 | 2.14 | |
| 4.959 | 40000 | 0.250 | 2.20938 [6] | |
| 4.920 | 39680 | 0.252 | 2.19248 | |
| 4.881 | 39370 | 0.254 | 2.17676 | |
| 4.843 | 39060 | 0.256 | 2.16208 | |
| 4.806 | 38760 | 0.258 | 2.14834 | |
| 4.769 | 38460 | 0.260 | 2.13545 | |
| 4.732 | 38170 | 0.262 | 2.12333 | |
| 4.696 | 37880 | 0.264 | 2.11190 | |
| 4.661 | 37590 | 0.266 | 2.10110 | |
| 4.626 | 37310 | 0.268 | 2.09089 | |
| 4.592 | 37040 | 0.270 | 2.08121 | |
| 4.558 | 36760 | 0.272 | 2.07202 | |
| 4.525 | 36500 | 0.274 | 2.06328 | |
| 4.492 | 36230 | 0.276 | 2.05496 | |
| 4.460 | 35970 | 0.278 | 2.04703 | |
| 4.428 | 35710 | 0.280 | 2.03946 | |
| 4.397 | 35460 | 0.282 | 2.03222 | |
| 4.366 | 35210 | 0.284 | 2.02530 | |
| 4.335 | 34970 | 0.286 | 2.01867 | |
| 4.305 | 34720 | 0.288 | 2.01232 | |
| 4.275 | 34480 | 0.290 | 2.00622 | |
| 4.246 | 34250 | 0.292 | 2.00037 | |
| 4.217 | 34010 | 0.294 | 1.99474 | |
| 4.189 | 33780 | 0.296 | 1.98932 | |
| 4.161 | 33560 | 0.298 | 1.98411 | |

(continued)

TABLE I (*Continued*)

Cesium Iodide

| eV | $cm^{-1}$ | $\mu m$ | $n$ | $k$ |
|---|---|---|---|---|
| 4.133 | 33330 | 0.300 | 1.97909 | |
| 4.065 | 32790 | 0.305 | 1.96731 | |
| 4.000 | 32260 | 0.310 | 1.95651 | |
| 3.936 | 31750 | 0.315 | 1.94658 | |
| 3.875 | 31250 | 0.320 | 1.93741 | |
| 3.815 | 30770 | 0.325 | 1.92893 | |
| 3.757 | 30300 | 0.330 | 1.92106 | |
| 3.701 | 29850 | 0.335 | 1.91373 | |
| 3.647 | 29410 | 0.340 | 1.90690 | |
| 3.594 | 28990 | 0.345 | 1.90051 | |
| 3.542 | 28570 | 0.350 | 1.89453 | |
| 3.493 | 28170 | 0.355 | 1.88891 | |
| 3.444 | 27780 | 0.360 | 1.88363 | |
| 3.397 | 27400 | 0.365 | 1.87866 | |
| 3.351 | 27030 | 0.370 | 1.87397 | |
| 3.306 | 26670 | 0.375 | 1.86954 | |
| 3.263 | 26320 | 0.380 | 1.86535 | |
| 3.220 | 25970 | 0.385 | 1.86138 | |
| 3.179 | 25640 | 0.390 | 1.85762 | |
| 3.139 | 25320 | 0.395 | 1.85404 | |
| 3.100 | 25000 | 0.40 | 1.85064 | |
| 3.024 | 24390 | 0.41 | 1.84433 | |
| 2.952 | 23810 | 0.42 | 1.83859 | |
| 2.883 | 23260 | 0.43 | 1.83336 | |
| 2.818 | 22730 | 0.44 | 1.82857 | |
| 2.755 | 22220 | 0.45 | 1.82417 | |
| 2.695 | 21740 | 0.46 | 1.82012 | |
| 2.638 | 21280 | 0.47 | 1.81637 | |
| 2.583 | 20830 | 0.48 | 1.81291 | |
| 2.530 | 20410 | 0.49 | 1.80970 | |
| 2.480 | 20000 | 0.50 | 1.80672 | |
| 2.431 | 19610 | 0.51 | 1.80393 | |
| 2.384 | 19230 | 0.52 | 1.80134 | |
| 2.339 | 18870 | 0.53 | 1.79891 | |
| 2.296 | 18520 | 0.54 | 1.79664 | |
| 2.254 | 18180 | 0.55 | 1.79451 | |
| 2.214 | 17860 | 0.56 | 1.79250 | |
| 2.175 | 17540 | 0.57 | 1.79062 | |
| 2.138 | 17240 | 0.58 | 1.78884 | |
| 2.101 | 16950 | 0.59 | 1.78717 | |
| 2.066 | 16670 | 0.60 | 1.78559 | |
| 2.000 | 16130 | 0.62 | 1.78268 | |
| 1.937 | 15630 | 0.64 | 1.78006 | |
| 1.879 | 15150 | 0.66 | 1.77770 | |
| 1.823 | 14710 | 0.68 | 1.77557 | |

(continued)

TABLE I (*Continued*)

Cesium Iodide

| eV | $cm^{-1}$ | $\mu m$ | $n$ | $k$ |
|---|---|---|---|---|
| 1.771 | 14290 | 0.70 | 1.77363 | |
| 1.722 | 13890 | 0.72 | 1.77186 | |
| 1.675 | 13510 | 0.74 | 1.77025 | |
| 1.631 | 13160 | 0.76 | 1.76877 | |
| 1.590 | 12820 | 0.78 | 1.76741 | |
| 1.550 | 12500 | 0.80 | 1.76615 | |
| 1.512 | 12200 | 0.82 | 1.76500 | |
| 1.476 | 11900 | 0.84 | 1.76392 | |
| 1.442 | 11630 | 0.86 | 1.76293 | |
| 1.409 | 11360 | 0.88 | 1.76201 | |
| 1.378 | 11110 | 0.90 | 1.76115 | |
| 1.348 | 10870 | 0.92 | 1.76035 | |
| 1.319 | 10640 | 0.94 | 1.75960 | |
| 1.292 | 10420 | 0.96 | 1.75890 | |
| 1.265 | 10200 | 0.98 | 1.75824 | |
| 1.240 | 10000 | 1.00 | 1.75736 | |
| 1.181 | 9524 | 1.05 | 1.75624 | |
| 1.127 | 9091 | 1.10 | 1.75505 | |
| 1.078 | 8696 | 1.15 | 1.75401 | |
| 1.033 | 8333 | 1.20 | 1.75310 | |
| 0.9919 | 8000 | 1.25 | 1.75230 | |
| 0.9537 | 7692 | 1.30 | 1.75160 | |
| 0.9184 | 7407 | 1.35 | 1.75097 | |
| 0.8856 | 7143 | 1.40 | 1.75040 | |
| 0.8551 | 6896 | 1.45 | 1.74990 | |
| 0.8267 | 6667 | 1.50 | 1.74944 | |
| 0.7999 | 6452 | 1.55 | 1.74903 | |
| 0.7749 | 6250 | 1.60 | 1.74866 | |
| 0.7514 | 6061 | 1.65 | 1.74832 | |
| 0.7293 | 5882 | 1.70 | 1.74801 | |
| 0.7085 | 5714 | 1.75 | 1.74772 | |
| 0.6888 | 5556 | 1.80 | 1.74746 | |
| 0.6702 | 5405 | 1.85 | 1.74721 | |
| 0.6526 | 5263 | 1.90 | 1.74699 | |
| 0.6358 | 5128 | 1.95 | 1.74678 | |
| 0.6199 | 5000 | 2.00 | 1.74659 | |
| 0.6048 | 4878 | 2.05 | 1.74641 | |
| 0.5904 | 4762 | 2.10 | 1.74625 | |
| 0.5767 | 4651 | 2.15 | 1.74609 | |
| 0.5636 | 4545 | 2.20 | 1.74594 | |
| 0.5510 | 4444 | 2.25 | 1.74581 | |
| 0.5391 | 4348 | 2.30 | 1.74568 | |
| 0.5276 | 4255 | 2.35 | 1.74555 | |
| 0.5166 | 4167 | 2.40 | 1.74544 | |
| 0.5061 | 4082 | 2.45 | 1.74533 | |

(continued)

TABLE I (*Continued*)

Cesium Iodide

| eV | $cm^{-1}$ | $\mu m$ | $n$ | $k$ |
|---|---|---|---|---|
| 0.4959 | 4000 | 2.50 | 1.74523 | |
| 0.4862 | 3922 | 2.55 | 1.74513 | |
| 0.4769 | 3846 | 2.60 | 1.74504 | |
| 0.4679 | 3774 | 2.65 | 1.74495 | |
| 0.4592 | 3704 | 2.70 | 1.74487 | |
| 0.4509 | 3636 | 2.75 | 1.74479 | |
| 0.4428 | 3571 | 2.80 | 1.74471 | |
| 0.4350 | 3509 | 2.85 | 1.74464 | |
| 0.4275 | 3448 | 2.90 | 1.74457 | |
| 0.4203 | 3390 | 2.95 | 1.74450 | |
| 0.4133 | 3333 | 3.00 | 1.74443 | |
| 0.4065 | 3279 | 3.05 | 1.74437 | |
| 0.4000 | 3226 | 3.10 | 1.74431 | |
| 0.3936 | 3175 | 3.15 | 1.74425 | |
| 0.3875 | 3125 | 3.20 | 1.74420 | |
| 0.3815 | 3077 | 3.25 | 1.74414 | |
| 0.3757 | 3030 | 3.30 | 1.74409 | |
| 0.3701 | 2985 | 3.35 | 1.74404 | |
| 0.3647 | 2941 | 3.40 | 1.74399 | |
| 0.3594 | 2899 | 3.45 | 1.74394 | |
| 0.3542 | 2857 | 3.50 | 1.74390 | |
| 0.3493 | 2817 | 3.55 | 1.74385 | |
| 0.3444 | 2778 | 3.60 | 1.74381 | |
| 0.3397 | 2740 | 3.65 | 1.74376 | |
| 0.3351 | 2703 | 3.70 | 1.74372 | |
| 0.3306 | 2667 | 3.75 | 1.74368 | |
| 0.3263 | 2632 | 3.80 | 1.74364 | |
| 0.3220 | 2597 | 3.85 | 1.74360 | |
| 0.3179 | 2564 | 3.90 | 1.74356 | |
| 0.3139 | 2532 | 3.95 | 1.74352 | |
| 0.3100 | 2500 | 4.00 | 1.74349 | |
| 0.3061 | 2469 | 4.05 | 1.74345 | |
| 0.3024 | 2439 | 4.10 | 1.74341 | |
| 0.2988 | 2410 | 4.15 | 1.74338 | |
| 0.2952 | 2381 | 4.20 | 1.74334 | |
| 0.2917 | 2353 | 4.25 | 1.74331 | |
| 0.2883 | 2326 | 4.30 | 1.74327 | |
| 0.2850 | 2299 | 4.35 | 1.74324 | |
| 0.2818 | 2273 | 4.40 | 1.74321 | |
| 0.2786 | 2247 | 4.45 | 1.74317 | |
| 0.2755 | 2222 | 4.50 | 1.74314 | |
| 0.2725 | 2198 | 4.55 | 1.74311 | |
| 0.2695 | 2174 | 4.60 | 1.74308 | |
| 0.2666 | 2151 | 4.65 | 1.74305 | |
| 0.2638 | 2128 | 4.70 | 1.74302 | |

(continued)

TABLE I (*Continued*)

**Cesium Iodide**

| eV | $cm^{-1}$ | $\mu m$ | $n$ | $k$ |
|---|---|---|---|---|
| 0.2610 | 2105 | 4.75 | 1.74298 | |
| 0.2583 | 2083 | 4.80 | 1.74295 | |
| 0.2556 | 2062 | 4.85 | 1.74292 | |
| 0.2530 | 2041 | 4.90 | 1.74289 | |
| 0.2505 | 2020 | 4.95 | 1.74286 | |
| 0.2480 | 2000 | 5.0 | 1.74283 | |
| 0.2431 | 1961 | 5.1 | 1.74277 | |
| 0.2384 | 1923 | 5.2 | 1.74271 | |
| 0.2339 | 1887 | 5.3 | 1.74265 | |
| 0.2296 | 1852 | 5.4 | 1.74260 | |
| 0.2254 | 1818 | 5.5 | 1.74254 | |
| 0.2214 | 1786 | 5.6 | 1.74248 | |
| 0.2175 | 1754 | 5.7 | 1.74242 | |
| 0.2138 | 1724 | 5.8 | 1.74236 | |
| 0.2101 | 1695 | 5.9 | 1.74231 | |
| 0.2066 | 1667 | 6.0 | 1.74225 | |
| 0.2033 | 1639 | 6.1 | 1.74219 | |
| 0.2000 | 1613 | 6.2 | 1.74213 | |
| 0.1968 | 1587 | 6.3 | 1.74207 | |
| 0.1937 | 1563 | 6.4 | 1.74202 | |
| 0.1908 | 1538 | 6.5 | 1.74196 | |
| 0.1879 | 1515 | 6.6 | 1.74190 | |
| 0.1851 | 1493 | 6.7 | 1.74184 | |
| 0.1823 | 1471 | 6.8 | 1.74178 | |
| 0.1797 | 1449 | 6.9 | 1.74172 | |
| 0.1771 | 1429 | 7.0 | 1.74166 | |
| 0.1746 | 1408 | 7.1 | 1.74160 | |
| 0.1722 | 1389 | 7.2 | 1.74154 | |
| 0.1698 | 1370 | 7.3 | 1.74147 | |
| 0.1675 | 1351 | 7.4 | 1.74141 | |
| 0.1653 | 1333 | 7.5 | 1.74135 | |
| 0.1631 | 1316 | 7.6 | 1.74129 | |
| 0.1610 | 1299 | 7.7 | 1.74122 | |
| 0.1590 | 1282 | 7.8 | 1.74116 | |
| 0.1569 | 1266 | 7.9 | 1.74109 | |
| 0.1550 | 1250 | 8.0 | 1.74103 | |
| 0.1531 | 1235 | 8.1 | 1.74096 | |
| 0.1512 | 1220 | 8.2 | 1.74090 | |
| 0.1494 | 1205 | 8.3 | 1.74083 | |
| 0.1476 | 1190 | 8.4 | 1.74076 | |
| 0.1459 | 1176 | 8.5 | 1.74069 | |
| 0.1442 | 1163 | 8.6 | 1.74063 | |
| 0.1425 | 1149 | 8.7 | 1.74056 | |
| 0.1409 | 1136 | 8.8 | 1.74049 | |
| 0.1393 | 1124 | 8.9 | 1.74042 | |

(continued)

TABLE I (*Continued*)

**Cesium Iodide**

| eV | $cm^{-1}$ | $\mu m$ | $n$ | $k$ |
|---|---|---|---|---|
| 0.1378 | 1111 | 9.0 | 1.74034 | |
| 0.1362 | 1099 | 9.1 | 1.74027 | |
| 0.1348 | 1087 | 9.2 | 1.74020 | |
| 0.1333 | 1075 | 9.3 | 1.74013 | |
| 0.1319 | 1064 | 9.4 | 1.74005 | |
| 0.1305 | 1053 | 9.5 | 1.73998 | |
| 0.1292 | 1042 | 9.6 | 1.73990 | |
| 0.1278 | 1031 | 9.7 | 1.73983 | |
| 0.1265 | 1020 | 9.8 | 1.73975 | |
| 0.1252 | 1010 | 9.9 | 1.73967 | |
| 0.1240 | 1000 | 10.0 | 1.73960 | |
| 0.1216 | 980.4 | 10.2 | 1.73944 | |
| 0.1192 | 961.5 | 10.4 | 1.73928 | |
| 0.1170 | 943.4 | 10.6 | 1.73911 | |
| 0.1148 | 925.9 | 10.8 | 1.73895 | |
| 0.1127 | 909.1 | 11.0 | 1.73878 | |
| 0.1107 | 892.9 | 11.2 | 1.73861 | |
| 0.1088 | 877.2 | 11.4 | 1.73843 | |
| 0.1069 | 862.1 | 11.6 | 1.73826 | |
| 0.1051 | 847.5 | 11.8 | 1.73808 | |
| 0.1033 | 833.3 | 12.0 | 1.73789 | |
| 0.1016 | 819.7 | 12.2 | 1.73771 | |
| 0.09999 | 806.5 | 12.4 | 1.73752 | |
| 0.09840 | 793.7 | 12.6 | 1.73732 | |
| 0.09686 | 781.3 | 12.8 | 1.73713 | |
| 0.09537 | 769.2 | 13.0 | 1.73693 | |
| 0.09393 | 757.6 | 13.2 | 1.73673 | |
| 0.09253 | 746.3 | 13.4 | 1.73653 | |
| 0.09117 | 735.3 | 13.6 | 1.73632 | |
| 0.08984 | 724.6 | 13.8 | 1.73611 | |
| 0.08856 | 714.3 | 14.0 | 1.73589 | |
| 0.08731 | 704.2 | 14.2 | 1.73568 | |
| 0.08610 | 694.4 | 14.4 | 1.73546 | |
| 0.08492 | 684.9 | 14.6 | 1.73524 | |
| 0.08377 | 675.7 | 14.8 | 1.73501 | |
| 0.08266 | 666.7 | 15.0 | 1.73478 | |
| 0.08157 | 657.9 | 15.2 | 1.73455 | |
| 0.08051 | 649.4 | 15.4 | 1.73431 | |
| 0.07948 | 641.0 | 15.6 | 1.73408 | |
| 0.07847 | 632.9 | 15.8 | 1.73383 | |
| 0.07749 | 625.0 | 16.0 | 1.73359 | |
| 0.07653 | 617.3 | 16.2 | 1.73334 | |
| 0.07560 | 609.8 | 16.4 | 1.73309 | |
| 0.07469 | 602.4 | 16.6 | 1.73284 | |
| 0.07380 | 595.2 | 16.8 | 1.73258 | |

(continued)

TABLE I (*Continued*)

Cesium Iodide

| eV | $cm^{-1}$ | $\mu m$ | $n$ | $k$ |
|---|---|---|---|---|
| 0.07293 | 588.2 | 17.0 | 1.73232 | |
| 0.07208 | 581.4 | 17.2 | 1.73206 | |
| 0.07126 | 574.7 | 17.4 | 1.73179 | |
| 0.07045 | 568.2 | 17.6 | 1.73152 | |
| 0.06965 | 561.8 | 17.8 | 1.73124 | |
| 0.06888 | 555.6 | 18.0 | 1.73097 | |
| 0.06812 | 549.5 | 18.2 | 1.73069 | |
| 0.06738 | 543.5 | 18.4 | 1.73041 | |
| 0.06669 | 537.6 | 18.6 | 1.73012 | |
| 0.06596 | 531.9 | 18.8 | 1.72983 | |
| 0.06526 | 526.3 | 19.0 | 1.72954 | |
| 0.06458 | 520.8 | 19.2 | 1.72924 | |
| 0.06391 | 515.5 | 19.4 | 1.72894 | |
| 0.06326 | 510.2 | 19.6 | 1.72864 | |
| 0.06262 | 505.1 | 19.8 | 1.72833 | |
| 0.06199 | 500.0 | 20.0 | 1.72802 | |
| 0.06048 | 487.8 | 20.5 | 1.72723 | |
| 0.05904 | 476.2 | 21.0 | 1.72642 | |
| 0.05767 | 465.1 | 21.5 | 1.72559 | |
| 0.05636 | 454.5 | 22.0 | 1.72474 | |
| 0.05510 | 444.4 | 22.5 | 1.72387 | |
| 0.05391 | 434.8 | 23.0 | 1.72298 | |
| 0.05276 | 425.5 | 23.5 | 1.72206 | |
| 0.05166 | 416.7 | 24.0 | 1.72112 | |
| 0.05061 | 408.2 | 24.5 | 1.72016 | |
| 0.04959 | 400.0 | 25.0 | 1.71918 | |
| 0.04862 | 392.2 | 25.5 | 1.71817 | |
| 0.04769 | 384.6 | 26.0 | 1.71715 | |
| 0.04679 | 377.4 | 26.5 | 1.71610 | |
| 0.04592 | 370.4 | 27.0 | 1.71502 | |
| 0.04509 | 363.6 | 27.5 | 1.71392 | |
| 0.04428 | 357.1 | 28.0 | 1.71281 | |
| 0.04350 | 350.9 | 28.5 | 1.71167 | |
| 0.04275 | 344.8 | 29.0 | 1.71050 | |
| 0.04203 | 339.0 | 29.5 | 1.70931 | |
| 0.04133 | 333.3 | 30.0 | 1.70810 | |
| 0.04065 | 327.9 | 30.5 | 1.70686 | |
| 0.04000 | 322.6 | 31.0 | 1.70560 | |
| 0.03936 | 317.5 | 31.5 | 1.70431 | |
| 0.03875 | 312.5 | 32.0 | 1.70300 | |
| 0.03815 | 307.7 | 32.5 | 1.70166 | |
| 0.03757 | 303.0 | 33.0 | 1.70030 | |
| 0.03701 | 298.5 | 33.5 | 1.69891 | |
| 0.03647 | 294.1 | 34.0 | 1.69750 | |
| 0.03594 | 289.9 | 34.5 | 1.69606 | |

(continued)

TABLE I (*Continued*)

**Cesium Iodide**

| eV | $cm^{-1}$ | $\mu m$ | $n$ | $k$ |
|---|---|---|---|---|
| 0.03542 | 285.7 | 35.0 | 1.69460 | |
| 0.03493 | 281.7 | 35.5 | 1.69310 | |
| 0.03444 | 277.8 | 36.0 | 1.69158 | |
| 0.03397 | 274.0 | 36.5 | 1.69004 | |
| 0.03351 | 270.3 | 37.0 | 1.68846 | |
| 0.03306 | 266.7 | 37.5 | 1.68686 | |
| 0.03263 | 263.2 | 38.0 | 1.68523 | |
| 0.03220 | 259.7 | 38.5 | 1.68358 | |
| 0.03179 | 256.4 | 39.0 | 1.68189 | |
| 0.03139 | 253.2 | 39.5 | 1.68017 | |
| 0.03100 | 250.0 | 40.0 | 1.67843 | |
| 0.03061 | 246.9 | 40.5 | 1.67666 | |
| 0.03024 | 243.9 | 41.0 | 1.67485 | |
| 0.02988 | 241.0 | 41.5 | 1.67302 | |
| 0.02952 | 238.1 | 42.0 | 1.67115 | |
| 0.02917 | 235.3 | 42.5 | 1.66926 | |
| 0.02883 | 232.6 | 43.0 | 1.66733 | |
| 0.02850 | 229.9 | 43.5 | 1.66537 | |
| 0.02818 | 227.3 | 44.0 | 1.66338 | |
| 0.02786 | 224.7 | 44.5 | 1.66136 | |
| 0.02755 | 222.2 | 45.0 | 1.65930 | |
| 0.02725 | 219.8 | 45.5 | 1.65721 | |
| 0.02695 | 217.4 | 46.0 | 1.65509 | |
| 0.02666 | 215.1 | 46.5 | 1.65293 | |
| 0.02638 | 212.8 | 47.0 | 1.65073 | |
| 0.02610 | 210.5 | 47.5 | 1.64851 | |
| 0.02583 | 208.3 | 48.0 | 1.64624 | |
| 0.02556 | 206.2 | 48.5 | 1.64394 | |
| 0.02530 | 204.1 | 49.0 | 1.64161 | |
| 0.02505 | 202.0 | 49.5 | 1.63923 | |
| 0.02480 | 200.0 | 50.0 | 1.63682 | $9.9 \times 10^{-5}$ [3] |
| 0.02455 | 198.0 | 50.5 | 1.63437 | $1.15 \times 10^{-4}$ |
| 0.02431 | 196.1 | 51.0 | 1.63188 | |
| 0.02430 | 196.0 | 51.0 | | 1.43 |
| 0.02407 | 194.2 | 51.5 | 1.62935 | |
| 0.02405 | 194.0 | 51.5 | | 1.78 |
| 0.02384 | 192.3 | 52.0 | 1.62679 | |
| 0.02381 | 192.0 | 52.1 | | 2.22 |
| 0.02362 | 190.5 | 52.5 | 1.62418 | |
| 0.02356 | 190.0 | 52.6 | | 2.76 |
| 0.02339 | 188.7 | 53.0 | 1.62153 | |
| 0.02331 | 188.0 | 53.2 | | 3.21 |
| 0.02317 | 186.9 | 53.5 | 1.61884 | |
| 0.02306 | 186.0 | 53.8 | | 3.72 |
| 0.02296 | 185.2 | 54.0 | 1.61610 | |

(continued)

TABLE I (*Continued*)

**Cesium Iodide**

| eV | $cm^{-1}$ | $\mu m$ | $n$ | $k$ |
|---|---|---|---|---|
| 0.02281 | 184.0 | 54.35 | | 4.32 |
| 0.02275 | 183.5 | 54.5 | 1.61332 | |
| 0.02257 | 182.0 | 54.95 | | 5.02 |
| 0.02254 | 181.8 | 55.0 | 1.61050 | |
| 0.02234 | 180.2 | 55.5 | 1.60764 | |
| 0.02232 | 180.0 | 55.56 | | 5.83 |
| 0.02214 | 178.6 | 56.0 | 1.60473 | |
| 0.02207 | 178.0 | 56.18 | | 6.78 |
| 0.02194 | 177.0 | 56.5 | 1.60177 | |
| 0.02182 | 176.0 | 56.82 | | 7.35 |
| 0.02175 | 175.4 | 57.0 | 1.59877 | |
| 0.02157 | 174.0 | 57.47 | | 8.0 |
| 0.02156 | 173.9 | 57.5 | 1.59572 | |
| 0.02138 | 172.4 | 58.0 | 1.59262 | |
| 0.02133 | 172.0 | 58.14 | | 8.6 |
| 0.02119 | 170.9 | 58.5 | 1.58947 | |
| 0.02108 | 170.0 | 58.82 | | $9.4 \times 10^{-4}$ |
| 0.02101 | 169.5 | 59.0 | 1.58628 | |
| 0.02084 | 168.1 | 59.5 | 1.58303 | |
| 0.02083 | 168.0 | 59.52 | | $1.05 \times 10^{-3}$ |
| 0.02066 | 166.7 | 60.0 | 1.57973 | |
| 0.02058 | 166.0 | 60.24 | | 1.18 |
| 0.02049 | 165.3 | 60.5 | 1.57637 | |
| 0.02033 | 164.0 | 60.98 | | 1.37 |
| 0.02032 | 163.9 | 61.0 | 1.57297 | |
| 0.02016 | 162.6 | 61.5 | 1.56951 | |
| 0.02009 | 162.0 | 61.73 | | 1.49 |
| 0.02000 | 161.3 | 62.0 | 1.56599 | |
| 0.01984 | 160.0 | 62.50 | 1.56242 | 1.62 |
| 0.01968 | 158.7 | 63.0 | 1.55879 | |
| 0.01959 | 158.0 | 63.29 | | 1.76 |
| 0.01953 | 157.5 | 63.5 | 1.55510 | |
| 0.01937 | 156.2 | 64.0 | 1.55136 | |
| 0.01934 | 156.0 | 64.10 | | 1.97 |
| 0.01922 | 155.0 | 64.5 | 1.54755 | |
| 0.01909 | 154.0 | 64.94 | | 2.22 |
| 0.01907 | 153.8 | 65.0 | 1.54368 | |
| 0.01893 | 152.7 | 65.5 | 1.53974 | |
| 0.01885 | 152.0 | 65.79 | | 2.41 |
| 0.01879 | 151.5 | 66.0 | 1.53575 | |
| 0.01864 | 150.4 | 66.5 | 1.53168 | |
| 0.01860 | 150.0 | 66.67 | | 2.61 |
| 0.01851 | 149.2 | 67.0 | 1.52755 | |
| 0.01835 | 148 | 67.50 | | 3.04 |
| 0.01810 | 146 | 68.49 | | 3.30 |

(continued)

TABLE I (*Continued*)

Cesium Iodide

| eV | $cm^{-1}$ | $\mu m$ | $n$ | $k$ |
|---|---|---|---|---|
| 0.01798 | 145 | 69.0 | 1.52 [5] | |
| 0.01785 | 144 | 69.44 | | 3.72 |
| 0.01761 | 142 | 70.4 | | 4.05 |
| 0.01736 | 140 | 71.4 | 1.51 | 4.6 |
| 0.01711 | 138 | 72.46 | | 4.9 |
| 0.01686 | 136 | 73.53 | | 5.8 |
| 0.01674 | 135 | 74.1 | 1.5 | |
| 0.01661 | 134 | 74.63 | | 6.7 |
| 0.01637 | 132 | 75.76 | | 7.3 |
| 0.01612 | 130 | 76.9 | 1.48 | $8.5 \times 10^{-3}$ |
| 0.01587 | 128 | 78.13 | | $1.0 \times 10^{-2}$ |
| 0.01562 | 126 | 79.37 | | 1.2 |
| 0.01550 | 125 | 80.0 | 1.45 | |
| 0.01537 | 124 | 80.65 | | 1.6 |
| 0.01513 | 122 | 81.97 | | 2.1 |
| 0.01488 | 120 | 83.3 | 1.40 | 2.8 |
| 0.01463 | 118 | 84.75 | | 4.0 |
| 0.01438 | 116 | 86.21 | | 5.4 |
| 0.01426 | 115 | 87.0 | 1.35 | |
| 0.01413 | 114 | 87.72 | | $7.5 \times 10^{-2}$ |
| 0.01389 | 112 | 89.29 | | 0.105 |
| 0.01364 | 110 | 90.9 | 1.3 | 0.110 |
| 0.01339 | 108 | 92.59 | | 0.115 |
| 0.01314 | 106 | 94.34 | | 0.119 |
| 0.01302 | 105 | 95.2 | 1.2 | |
| 0.01289 | 104 | 96.15 | | 0.125 |
| 0.01265 | 102 | 98.04 | | 0.142 |
| 0.01240 | 100 | 100.0 | 1.0 | 0.155 |
| 0.01215 | 98 | 102.0 | | 0.188 |
| 0.01190 | 96 | 104.2 | | 0.220 |
| 0.01165 | 94 | 106.4 | 0.85 [4] | 0.287 |
| | | | | 0.7 [4] |
| 0.01134 | 91.5 | 109.2 | 0.79 | |
| 0.01121 | 90.4 | 110.6 | | 0.8 |
| 0.01095 | 88.3 | 113.3 | 0.75 | |
| 0.01076 | 86.8 | 115.2 | | 1.1 |
| 0.01055 | 85.1 | 117.5 | 0.72 | |
| 0.01033 | 83.3 | 120.0 | | 1.2 |
| 0.01015 | 81.9 | 122.1 | 0.68 | |
| $9.968 \times 10^{-3}$ | 80.4 | 124.4 | | 1.4 |
| 9.758 | 78.7 | 127.1 | 0.57 | |
| 9.621 | 77.6 | 128.9 | | 1.8 |
| 9.448 | 76.2 | 131.2 | 0.50 | |
| 9.361 | 75.5 | 132.4 | | 2.2 |
| 9.088 | 73.3 | 136.4 | 0.57 | 2.6 |

(continued)

TABLE I (*Continued*)

**Cesium Iodide**

| eV | $cm^{-1}$ | $\mu m$ | $n$ | $k$ |
|---|---|---|---|---|
| 8.828 | 71.2 | 140.4 | | 3.0 |
| 8.741 | 70.5 | 141.8 | 0.64 | |
| 8.567 | 69.1 | 144.7 | | 3.4 |
| 8.394 | 67.7 | 147.7 | 0.99 | |
| 8.344 | 67.3 | 148.6 | | 3.8 |
| 8.208 | 66.2 | 151.1 | 1.42 | 4.4 |
| 8.121 | 65.5 | 152.7 | 1.91 | 5.1 |
| 8.034 | 64.8 | 154.3 | 2.55 | 5.6 |
| 7.947 | 64.1 | 156.0 | | 6.3 |
| 7.898 | 63.7 | 157.0 | 3.26 | |
| 7.873 | 63.5 | 157.5 | 3.82 | |
| 7.861 | 63.4 | 157.7 | 4.53 | 6.7 |
| 7.836 | 63.2 | 158.2 | 5.24 | |
| 7.799 | 62.9 | 159.0 | 5.95 | |
| 7.774 | 62.7 | 159.5 | 6.66 | 6.4 |
| 7.749 | 62.5 | 160.0 | | 5.9 |
| 7.724 | 62.3 | 160.5 | 7.79 | 5.2 |
| 7.699 | 62.1 | 161.0 | | 4.7 |
| 7.687 | 62.0 | 161.3 | | 4.1 |
| 7.637 | 61.6 | 162.3 | | 3.6 |
| 7.600 | 61.3 | 163.1 | 8.36 | 2.9 |
| 7.563 | 61.0 | 163.9 | | 2.2 |
| 7.501 | 60.5 | 165.3 | 8.78 | 1.5 |
| 7.464 | 60.2 | 166.1 | 8.22 | 0.82 |
| 7.414 | 59.8 | 167.2 | 7.65 | |
| 7.328 | 59.1 | 169.2 | 7.01 | |
| 7.241 | 58.4 | 171.2 | 6.51 | |
| 7.204 | 58.1 | 172.1 | 6.02 | |
| 7.104 | 57.3 | 174.5 | 5.45 | |
| 6.980 | 56.3 | 177.6 | 4.96 | |
| 6.943 | 56.0 | 178.6 | | 0.48 [5] |
| | | | | 0.296 [3] |
| 6.894 | 55.6 | 179.9 | 4.46 | |
| 6.695 | 54.0 | 185.2 | 4.00 | 0.250 |
| 6.534 | 52.7 | 189.8 | 3.54 | |
| 6.447 | 52.0 | 192.3 | | 0.171 |
| 6.274 | 50.6 | 197.6 | 3.26 | |
| 6.199 | 50.0 | 200.0 | | 0.144 |
| | | | | 0.17 [5] |
| 5.951 | 48.0 | 208.3 | | 0.114 [3] |
| 5.703 | 46.0 | 217.4 | | 0.100 |
| 5.579 | 45.0 | 222.2 | 2.91 | |
| 5.455 | 44.0 | 227.3 | | 0.088 |
| 5.207 | 42.0 | 238.1 | | 0.077 |
| 4.959 | 40.0 | 250.0 | 2.87 | 0.071 |

(continued)

TABLE I (*Continued*)

Cesium Iodide

| eV | $cm^{-1}$ | $\mu m$ | $n$ | $k$ |
|---|---|---|---|---|
| 4.711 | 38.0 | 263.2 | | 0.067 |
| 4.463 | 36.0 | 277.8 | | 0.058 |
| 4.339 | 35.0 | 285.7 | 2.84 | |
| 4.215 | 34.0 | 294.1 | | 0.053 |
| 3.968 | 32.0 | 312.5 | | 0.049 |
| 3.720 | 30.0 | 333.3 | 2.81 | 0.046 |
| 3.472 | 28.0 | 357.1 | | 0.042 |
| 3.224 | 26.0 | 384.6 | | 0.043 |
| 2.976 | 24.0 | 416.7 | | 0.038 |
| 2.889 | 23.3 | 429.2 | 2.63 [2] | 0.039 [2] |
| 2.728 | 22.0 | 454.5 | | 0.036 [3] |
| 2.480 | 20.0 | 500 | | 0.032 |
| 2.232 | 18.0 | 556 | | 0.031 |
| 2.071 | 16.7 | 599 | 2.59 | 0.031 [2] |
| 1.984 | 16.0 | 625 | | 0.028 [3] |
| 1.736 | 14.0 | 714 | | 0.026 |
| 1.240 | 10.0 | 1000 | 2.56 | 0.021 [2] |
| $6.199 \times 10^{-4}$ | 5.0 | 2000 | 2.54 [1] | |

[a]Tabulation of $n$ and $k$ as a function of photon energy (electron volts), wave number (inverse centimeters), and wavelength (Angstroms or micrometers). References for the data are given in brackets and apply to all data below the brackets until a new reference appears; $k$ is often very small and exponents are given for numbers smaller than $10^{-2}$. The power of 10 applies for all data below the exponent until a new exponent appears or the exponent becomes $10^{-1}$, whereupon the number is given in decimal form.

# Copper Oxides ($Cu_2O$, CuO)

CARL G. RIBBING and ARNE ROOS
Institute of Technology
Uppsala University
Uppsala, Sweden

The established stoichometric copper oxides, cuprous oxide, $Cu_2O$ ("red") and cupric oxide, CuO ("black"), form cubic and monoclinic unit cells in their respective equilibrium crystalline forms [1]. Reports on the phase $CuO_{.67}$, described as a gross defect structure of $Cu_2O$, are found in the literature [2, 3], but will not be considered here. It has furthermore been claimed that $Cu_2O$ is actually not an equilibrium structure at temperatures below 375 °C and therefore decomposes very slowly at room temperature into metallic copper and cupric oxide [4]. The Cu-O phase diagram is markedly pressure dependent, such that a CuO layer transforms into $Cu_2O$ and eventually into metallic copper when placed in vacuum.

Cuprous oxide is a semiconductor with a direct band gap of 2.17 eV. It has been the object of several basic studies concerning optical-band-gap absorption, its temperature dependence, and the interpretation of the low-temperature absorption line spectrum below the gap as transitions to excitonic levels [5–7]. The partly ionic character of the bonding causes structures in the optical functions in the infrared spectral region. The strongest IR-active mode, corresponding to the residual-ray region, was located at 609 $cm^{-1}$ (16.4 $\mu$m) [8]. A secondary lattice mode at 146 $cm^{-1}$ (68 $\mu$m) is reported for polycrystalline samples [9]. Several other lattice modes have been identified in later work and attributed to defects, impurities, and nonstoichiometry, and somewhat varying positions of the major lattice mode are given in the literature, which also include several Raman studies [9–11]. The recent discovery of high-temperature superconductors in which a key role seems to be played by the copper oxide in the formation of Cooper pairs has renewed the interest in the infrared properties of the copper oxides [12].

Considerably less has been reported about the black cupric oxide CuO. It is also a semiconductor, obviously with a smaller optical band gap than the red oxide. The values reported in the literature vary within the range 1.2–1.5 eV. A wet photoelectrochemical technique was used to obtain an indirect energy gap of 1.35 eV [13]. Early measurements on a bulk,


Copyright © 1991 by Academic Press.
All rights of reproduction in any form reserved.
ISBN 0-12-544422-2

polycrystalline sample, sintered in an oxygen atmosphere, resulted in an absorption edge too shallow to define an energy gap [14]. Simultaneous measurements on reactively sputtered films were also used to derive the optical constants without specifying an energy gap [15]. Recent transmittance measurements versus thickness on thin films prepared by rf, reactive sputtering gave an energy gap value of $1.21 \pm .05$ eV [16].

Much of the work on the physical properties of the copper oxides has been motivated by various technical applications. Cuprous oxide was one of the very early model semiconductors, and the discovery of the $Cu_2O$–Cu rectifier dates back to 1920 [17]. The use of cupric oxide on copper as a photoelectric and/or photoconductive material was suggested even earlier [18]. It is still of technical interest [19] to utilize this metal–oxide system as a possible low-cost solar cell. Oxidizing copper has furthermore been one of the alternatives to prepare the selectively absorbing surface of a thermal solar collector [20]. In this application the black oxide results in higher efficiency owing to its higher absorption of solar radiation. Several methods have been used to oxidize a copper base giving optimum performance in terms of selectivity and stability [21], and the use of a warm mixture of acids has been commercialized [22]. It has been demonstrated that the wet-oxidation techniques result in a rough interface between the oxide and the metal, which significantly increases the solar absorption [23, 24].

The ease with which oxidation of copper can take place is partly a corrosion problem, but it is also one of the reasons for the technical interest in this system. Even relatively thick layers of copper can be transformed into either one of the stoichiometric oxides, merely by heating in air. The green hue of old copper roofs is often (but incorrectly) said to be due to copper oxide. Instead, this surface is formed in the presence of water together with some other substances. It consists mainly of copper hydroxysulfate or, especially in coastal areas, copper hydroxychloride. From a basic point of view, the fact that copper is an easily oxidized noble metal with the typical strong tendency for diffusion creates a strong incentive for careful studies of the oxidation mechanism, rate laws, temperature dependence, and so on. The literature on the oxidation of copper is therefore very rich [25–28]. Copper is also a suitable metal for the study of laser-oxidation techniques [29, 30].

The thermal oxidation of copper, in contrast to wet oxidation, produces a rough oxide–metal interface that is *not* absorbing, but causes strong light scattering in the visible and near-infrared regions. The amount of scattering and its conspicous spectral dependence was used to determine the RMS roughness amplitude of both the air–oxide and oxide–metal uncorrelated interfaces [31, 32]. Here the $Cu_2O$–Cu served as a model system because of the exceptional magnitude of the light scattering.

For reasons made obvious above, there is a wealth of published optical constants for the cuprous oxide in the visible and near-infrared spectral

regions and considerably less data for cupric oxide in the same spectral regions. It has not been possible to find published optical constants for either one of the copper oxides in the vacuum UV or soft X-ray regions, however. Tables I and II and Figs. 1 and 2 therefore cover only the near UV, down to 300 nm. The valence bands and the core-level positions have been determined by electron spectroscopy as part of basic investigations about satellite formation in photoelectron spectra [33, 34]. Without knowledge of the numerical values of the optical functions, we can predict that they will exhibit oscillator structures, in the case of CuO around the core levels: O(1s)-530 eV ($\lambda = 2.34$ nm), $Cu(2p_{3/2})-933$ eV (1.33 nm) and $Cu(2p_{1/2})-954$ eV (1.30 nm). In $Cu_2O$ there is a 1.2 eV chemical shift in the copper levels toward lower binding energy whereas the O(1s) is unchanged.

For the cuprous oxide in the visible region, data have been selected for thermally oxidized copper films, which have been prepared in different thicknesses to allow combined $R$ and $T$ measurements. The optical thickness $nd$ was calculated from the position of the interference fringes, and the refractive index was determined from their envelope function in the region of low absorption. The values from Ref. [35] cover the broadest region and are somewhat higher than the data from Refs. [36] (electrodeposited), [37], and [14]. The values given are also marginally higher than those obtained from the dispersion relation [36]

$$n^2(\lambda) = 1 + A\lambda^2/(\lambda^2 - B),$$

which can be used for wavelengths longer than 0.550 $\mu$m; here, $A = 4.81$ $(\mu m)^{-2}$ and $B = 0.125$ $(\mu m)^2$. At shorter wavelengths this relation gives values that are too high, however. The $k$ values are significantly lower than those obtained for sintered powder [14] and slightly higher than those of Ref. [37].

The optical constants given here for cupric oxide have also been determined for thermally oxidized copper films [35]. In the visible part of the spectrum, the $n$ and $k$ values are in good agreement with those of Ref. [3]. In contrast, both functions are significantly lower than those of Refs. [2] and [14] as well as those for *rf* reactively sputtered films in Ref. [16].

For the cuprous oxide in the infrared, optical reflectance measurements on single crystals [8, 11] or polycrystalline films [9] were performed. Kramers–Kronig analysis of these spectra [11] or additional transmittance measurements on polycrystalline films [8, 9] were used to derive the optical constants in the vicinity of the resonance frequencies. It was found that the Lyddane–Sachs–Teller relation was valid for cuprous oxide, and the dielectric constant $\varepsilon_0$ is equal to 7.4 in the low-frequency region [11]. The $\varepsilon_0$ value given by O'Keeffe [8] ($\varepsilon_0 = 6.46$) does not take the low-frequency

resonance at 146 $cm^{-1}$ into account, but is in excellent agreement with the $\varepsilon_\infty$ value ($\varepsilon_\infty = 6.5$) for this resonance.

It has not been possible to find published values of $n$ and $k$ in the infrared region for cupric oxide. Poling [38] reports absorbance spectra for CuO without giving the $n$ and $k$ values. The oxide exhibits an intense single band around 510 $cm^{-1}$. This is the only significant band in the 230–4000 $cm^{-1}$ region.

## REFERENCES


1. M. Hansen, "Constitution of Binary Alloys," 2nd ed., McGraw Hill, New York, 604 (1958).
2. H. Wieder and A. W. Czanderna, *J. Appl. Phys.* **37**, 184 (1966).
3. P. C. Ladelfe, A. W. Czanderna, and J. R. Biegen, *Thin Solid Films* **10**, 403 (1972).
4. R. Vogel and W. Pocher, *Z. Metallkunde* **21**, 333 and 368 (1929).
5. Y. F. Gross, *Izvest, Akad. Nauk. S.S.S.R. Ser.* **84**, 261 and 471 (1952). Translated in *Bull. Acad. Sc. (USSR)* **20**, 79 (1956).
6. J. H. Apfel and L. N. Hadley, *Phys. Rev.* **100**, 1689 (1955).
7. P. W. Baumeister, *Phys. Rev.* **121**, 359 (1961).
8. M. O'Keeffe, *J. Chem. Phys.* **39**, 1789 (1963).
9. E. C. Heltemes, *Phys. Rev.* **141**, 803 (1966).
10. J. Reydellet, M. Balkanski, and D. Trivich, *Phys. Stat. Solidi (b)* **52**, 175 (1972).
11. P. Dawson, M. M. Hargreave, and G. R. Wilkinson, *J. Phys. Chem. Solids* **34**, 2201 (1973).
12. G. Wendin, *Physica Scripta* **T27**, 31 (1989).
13. F. P. Koffyberg and F. A. Benko, *J. Appl. Phys.* **53**, 1173 (1982).
14. T. Tanaka, *Jap. J. Appl. Phys.* **18**, 1043 (1979).
15. V. F. Drobny and D. L. Pulfrey, *Thin Solid Films* **61**, 89 (1979).
16. A. E. Rakhshani and F. K. Barakat, *Materials Lett.* **6**, 37 (1987).
17. L. O. Grondahl, *Rev. Mod. Phys.* **5**, 141 (1933).
18. A. H. Pfund, *Phys. Rev.* **3**, 289 (1916).
19. A. E. Rakhshani, *Solid-State Electr.* **29**, 7 (1986).
20. B. O. Seraphin, in "Solar Energy Conversion—Solid State Physics Aspects," (B. O. Seraphin, ed.), Springer-Verlag, Berlin, (1979).
21. D. J. Close, "Commonwealth Scientific and Industrial Research Organization," Australia, Engineering section, Report E. D. 7, (1962).
22. "Ebonol" of Enthone, Inc., New Haven, Conn.
23. A. Roos, T. Chibuye, and B. Karlsson, *Solar Energy Mat.* **7**, 453 (1983).
24. A. Roos and B. Karlsson, *Solar Energy Mat.* **7**, 467 (1983).
25. A. Rönnquist and H. Fischmeister, *J. Inst. Metals* **89**, 65 (1960–1961).
26. J. V. Cathcart, G. F. Petersen, and C. J. Sparks, in "Surfaces and Interfaces," Vol. 1, (J. J. Burke, ed.) Syracuse University Press, New York, 333 (1967).
27. C. Tsiranovits, J. G. Antonopoulos, and J. Stoemenos, *Thin Solid Films* **71**, 133 (1980).
28. S. K. Roy and C. Sircar, *Oxidation of Metals* **15**, 9 (1981).
29. L. Baufay, F. A. Houle, and R. J. Wilson, *J. Appl. Phys.* **61**, 4640 (1987).
30. M. Wautelet and R. Andrew, *Phil. Mag. B* **55**, 261 (1987).
31. A. Roos, M. Bergkvist, and C. G. Ribbing, *Appl. Opt.* **28**, 1360 (1989).
32. M. Bergkvist, A. Roos, C. G. Ribbing, J. M. Bennett, and L. Mattsson *Appl. Opt.*, **28**, 3902 (1989).
33. A. Rosencwaig and G. K. Wertheim, *J. Electron Spectrosc. Relat. Phenom.* **1**, 493 (1972/73).

34. H. Siegbahn and L. Karlsson, in "Handbuch der Physik," (W. Mehlhorn, ed), Vol. xxxi, Springer–Verlag, Berlin, 215 (1982).
35. B. Karlsson, C. G. Ribbing, A. Roos, E. Valkonen, and T. Karlsson, *Physica Scripta* **25**, 826 (1982).
36. A. E. Rakhshani, *J. Appl. Phys.* **62**, 1528 (1987).
37. K. Bärwinkel and H. J. Schmidt, *Thin Solid Films* **59**, 373 (1979).
38. G. W. Poling, *J. Electrochem. Soc.* **116**, 958 (1969).
39. Interpolated values of *n*.

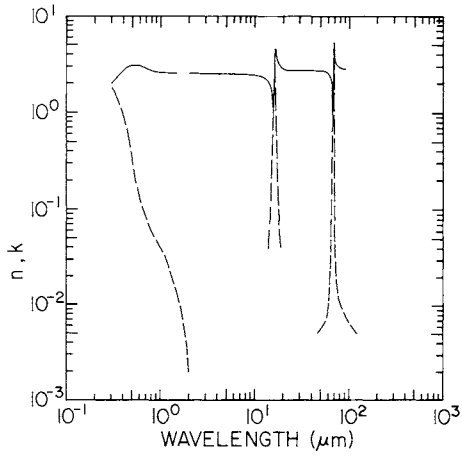


**Fig. 1.** Log–log plot of *n* (solid line) and *k* (dashed line) versus wavelength in micrometers for cuprous oxide ($Cu_2O$).

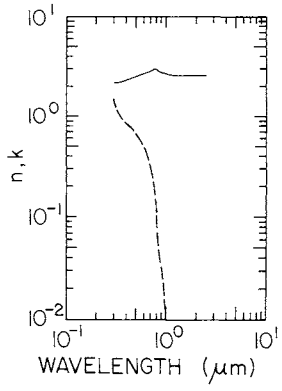


**Fig. 2.** Log–log plot of *n* (solid line) and *k* (dashed line) versus wavelength in micrometers for cupric oxide (CuO).

**TABLE I**

**Values of $n$ and $k$ for Cuprous Oxide Obtained from Various References[a]**

| eV | $cm^{-1}$ | μm | $n$ | $k$ |
|---|---|---|---|---|
| 4.133 | 33,330 | 0.3 | 2.0 [35] | 1.85 [35] |
| 3.542 | 28,570 | 0.35 | 2.40 | 1.44 |
| 3.100 | 25,000 | 0.40 | 2.80 | 0.99 |
| 2.756 | 22,220 | 0.45 | 3.06 | 0.60 |
| 2.480 | 20,000 | 0.50 | 3.12 | 0.35 |
| 2.255 | 18,180 | 0.55 | 3.10 | 0.19 |
| 2.067 | 16,670 | 0.60 | 3.02 | 0.13 |
| 1.908 | 15,380 | 0.65 | 2.90 | 0.10 |
| 1.771 | 14,290 | 0.70 | 2.83 | 0.083 |
| 1.653 | 13,330 | 0.75 | 2.77 | 0.070 |
| 1.550 | 12,500 | 0.80 | 2.70 | 0.060 |
| 1.459 | 11,770 | 0.85 | 2.66 | 0.053 |
| 1.378 | 11,110 | 0.90 | 2.63 | 0.048 |
| 1.305 | 10,530 | 0.95 | 2.61 | 0.043 |
| 1.240 | 10,000 | 1.00 | 2.60 | 0.040 |
| 1.127 | 9,090 | 1.10 | 2.59 | 0.033 |
| 1.033 | 8,330 | 1.20 | 2.58 | 0.027 |
| 0.954 | 7,690 | 1.30 | 2.57 | 0.021 |
| 0.886 | 7,110 | 1.40 | 2.57 | 0.017 |
| 0.827 | 6,670 | 1.50 | 2.57 | 0.013 |
| 0.620 | 5,000 | 2.00 | 2.56 | 0.002 |
| 0.496 | 4,000 | 2.5 | 2.56 | |
| 0.413 | 3,333 | 3.0 | 2.55 [39] | |
| 0.310 | 2,500 | 4.0 | 2.54 | |
| 0.248 | 2,000 | 5.0 | 2.53 | |
| 0.207 | 1,667 | 6.0 | 2.52 | |
| 0.177 | 1,429 | 7.0 | 2.51 | |
| 0.155 | 1,250 | 8.0 | 2.50 [8] | |
| 0.138 | 1,111 | 9.0 | 2.48 | |
| 0.124 | 1,000 | 10.0 | 2.46 | |
| 0.113 | 909.1 | 11.0 | 2.42 | |
| 0.103 | 833.3 | 12.0 | 2.37 | |
| 0.0954 | 769.2 | 13.0 | 2.29 | |
| 0.0886 | 714.3 | 14.0 | 2.15 | 0.04 [8] |
| 0.0827 | 666.7 | 15.0 | 1.79 | 0.13 |
| 0.0800 | 645.2 | 15.5 | 1.13 | 0.46 |
| 0.0785 | 632.9 | 15.8 | 0.92 | 1.68 |
| 0.0775 | 625.0 | 16.0 | 1.09 | 2.52 |
| 0.0761 | 613.5 | 16.3 | 2.94 | 3.49 |
| 0.0752 | 606.1 | 16.5 | 4.71 | 2.27 |
| 0.0729 | 588.2 | 17.0 | 3.78 | 0.42 |

[a] References are indicated in brackets

(continued)

**TABLE I (*Continued*)**

**Cuprous Oxide ($Cu_2O$)**

| eV | $cm^{-1}$ | μm | *n* | *k* |
|---|---|---|---|---|
| 0.0709 | 571.4 | 17.5 | 3.42 | 0.17 |
| 0.0689 | 555.6 | 18.0 | 3.21 | 0.08 |
| 0.0653 | 526.3 | 19.0 | 2.98 | 0.04 |
| 0.0620 | 500.0 | 20.0 | 2.89 | 0 |
| 0.0590 | 476.2 | 21.0 | 2.82 | |
| 0.0564 | 454.5 | 22.0 | 2.79 | |
| 0.0539 | 434.7 | 23.0 | 2.77 | |
| 0.0517 | 416.7 | 24.0 | 2.76 | |
| 0.0496 | 400.0 | 25.0 | 2.75 | |
| 0.0413 | 333 | 30.0 | 2.75 [39] | |
| 0.0354 | 286 | 35.0 | 2.75 | |
| 0.0310 | 250 | 40.0 | 2.75 | |
| 0.0273 | 220 | 45.5 | 2.75 | 0.005 [9] |
| 0.0248 | 200 | 50.0 | 2.74 | 0.006 |
| 0.0223 | 180 | 55.56 | 2.72 [11] | 0.006 |
| 0.0211 | 170 | 58.82 | 2.66 | 0.009 |
| 0.0198 | 160 | 62.50 | 2.42 | 0.017 |
| 0.0192 | 155 | 64.52 | 2.18 | 0.05 [11] |
| 0.0188 | 152 | 65.79 | 1.81 | 0.10 |
| 0.0186 | 150 | 66.67 | 1.19 | 0.59 |
| 0.01844 | 148.7 | 67.25 | 0.89 | 1.88 |
| 0.01823 | 147 | 68.03 | 3.37 | 3.97 |
| 0.01819 | 146.7 | 68.17 | 4.56 | 4.37 |
| 0.01810 | 146 | 68.49 | 5.56 | 2.78 |
| 0.01786 | 144 | 69.44 | 3.97 | 0.20 |
| 0.01761 | 142 | 70.42 | 3.47 | 0.08 |
| 0.01736 | 140 | 71.43 | 3.21 | 0.04 |
| 0.0161 | 130 | 76.9 | 2.98 | 0.013 [9] |
| 0.0149 | 120 | 83.3 | 2.92 | 0.010 |
| 0.0136 | 110 | 90.9 | 2.84 | 0.008 |
| 0.0124 | 100 | 100.0 | | 0.007 |
| 0.00992 | 80 | 125.0 | | 0.005 |

[a] References are indicated in brackets.

TABLE II

**Values of $n$ and $k$ for Cupric Oxide Obtained from Various References[a]**

| eV | $cm^{-1}$ | μm | $n$ | $k$ |
|---|---|---|---|---|
| 4.133 | 33,330 | 0.30 | 2.18 [35] | 1.50 [35] |
| 3.542 | 28,570 | 0.35 | 2.24 | 1.03 |
| 3.100 | 25,000 | 0.40 | 2.34 | 0.87 |
| 2.756 | 22,220 | 0.45 | 2.45 | 0.77 |
| 2.480 | 20,000 | 0.50 | 2.54 | 0.68 |
| 2.255 | 18,180 | 0.55 | 2.58 | 0.59 |
| 2.067 | 16,670 | 0.60 | 2.65 | 0.50 |
| 1.908 | 15,380 | 0.65 | 2.72 | 0.40 |
| 1.771 | 14,290 | 0.70 | 2.88 | 0.31 |
| 1.653 | 13,330 | 0.75 | 2.97 | 0.22 |
| 1.550 | 12,500 | 0.80 | 2.94 | 0.11 |
| 1.459 | 11,770 | 0.85 | 2.81 | 0.04 |
| 1.378 | 11,110 | 0.90 | 2.74 | 0.03 |
| 1.305 | 10,530 | 0.95 | 2.69 | 0.02 |
| 1.240 | 10,000 | 1.00 | 2.65 | 0.01 |
| 1.127 | 9,090 | 1.10 | 2.61 | |
| 1.033 | 8,330 | 1.20 | 2.58 | |
| 0.954 | 7,690 | 1.30 | 2.57 | |
| 0.886 | 7,110 | 1.40 | 2.56 | |
| 0.827 | 6,670 | 1.50 | 2.56 | |
| 0.620 | 5,000 | 2.00 | 2.55 | |
| 0.496 | 4,000 | 2.5 | 2.55 | |

[a] References are indicated in brackets.

# Magnesium Aluminum Spinel ($MgAl_2O_4$)

WILLIAM J. TROPF and MICHAEL E. THOMAS
Applied Physics Laboratory
The Johns Hopkins University
Laurel, Maryland

Magnesium aluminum spinel (the mineral spinel) is face-centered cubic material, the prototype for the spinel structural family, which includes binary oxides, sulfides, selenides, as well as many other materials (see ALON, this volume). The space group is $O_h^7$ or $Fd3m$, unit cell length is 0.8084 nm, and the unit cell has eight formula units (56 atoms). Theoretical density is 3.58 g/cm$^3$, and melting point is 2378 K [1] to 2408 K [2].

In the normal spinel structure, magnesium ions occupy tetrahedral sites with $T_d$ symmetry, aluminum ions occupy distorted octrahedral sites with $D_{3d}$ symmetry, and the oxygen ions are at sites with $C_{3v}$ symmetry. The positions of the ions in the unit cell have been determined by both X-ray and neutron diffraction techniques [3–6].

There is also an "inverse" spinel structure, wherein the aluminum ions occupy both $T_d$ and $D_{3d}$ sites, and the magnesium ions occupy some of the $D_{3d}$ sites. The occurrence of the normal, inverse, or in-between structure depends on ionic size, method of preparation, and composition. Natural magnesium aluminum spinel has the normal spinel structure, although there is evidence that synthetic forms of spinel prepared at high temperature have the inverse structure [5, 7]. Disordering in both natural and synthetic near-stoichiometric spinel crystals is apparently caused by heating [7, 8], the structural transition taking place at 750–800 °C. This transition is apparently irreversible.

The composition of magnesium aluminum spinel varies from near-stoichiometric to highly alumina-rich. The compositions have the general formula $MgO \times mAl_2O_3$, where $m$ varies from 0.9 up to 4. All formulations have the spinel structure (with vacancies at octrahedral sites when $m \neq 1$), with the lattice constant continuously decreasing as $m$ goes from 1 to 3.5 [3, 9]. As $m$ increases above 1, cation vacancies appear and typically occupy octrahedral sites [5].


Copyright © 1991 by Academic Press.
All rights of reproduction in any form reserved.
ISBN 0-12-544422-2

Spinel is a naturally occurring mineral, sometimes with gem quality. Optical-quality spinel can be synthetically made with a variety of techniques, including growth using the Czochralski method [10], the gradient-furnace technique [11], as well as by hot pressing of powder [2, 12], press forging [13], flame fusion (Verneuil method) [3, 14], and fusion casting [15].

Little information on optical constants in the electronic region is available. Summers *et al.* [16] report an absorption edge (onset of significant electronic absorption) 7.75 eV. Woosley *et al.* [17] report a band gap of about 9 eV, with evidence of exciton formation in the 6–8 eV range, band-to-band transitions begining at 8–9 eV, and photoemission from the top of the valence band beginning at energies above 11 eV. The valance band is estimated by Woosley to be 8–9 eV wide.

Refractive-index measurements of natural spinels were made by Schlossmacher [18], who reported real and imaginary parts of the index of refraction for red-, blue-, and violet-colored crystals. Index data from the lowest absorption ("bright red") natural crystal agrees well with recent measurements (see below). Wickersheim and LaFever [19] report that the index of refraction increases with greater alumina content. They found an index of 1.708 for stoichiometric spinel and 1.717–1.720 for alumina-rich ($m=3.5$) commercial spinel using a blue filter. Roy and Hastert [2] reported visible and IR measurements made by Kodak on artificial spinel. Visible and near-IR measurements agree well with other data, but the accuracy of IR measurements above $1\,\mu$m is doubtful. Vadem *et al.* [20] measured the refractive index of stoichiometric and nonstoichiometric ($m\approx 2.7$) spinel at $0.5893\,\mu$m and obtained values of 1.718 and 1.724, respectively. They also measured the pressure and temperature dependence of their samples, obtaining $dn/dT$ of $9.05\times 10^{-6}$ for stoichiometric and $9.34\times 10^{-6}$ for nonstoichiometric spinel.

Recent index-of-refraction measurements of Coors Optical Systems Company's stoichiometric spinel made in the UV and visible by General Dynamics [21] and the visible and near-IR by Schott Glass [22] are self-consistent and agree well with index data for low-absorption natural spinel [18].

Spinel refractive-index data for the visible and IR transparent region are summarized with a Sellmeier formula of the form

$$n^2-1=\frac{18.96\times 10^9}{(100,080)^2-\nu^2}+\frac{1.2234\times 10^6}{(527.18)^2-\nu^2}, \tag{1}$$

where $\nu$ is the frequency in wave numbers. This formula is applicable to bulk crystalline (or polycrystalline) stoichiometric spinel with low impurity and defect concentration and is accurate to $\pm 0.001$. Figure 1 compares the

index-of-refraction data from several sources to Eq 1. Evaporated thin films made with spinel material have a wide index-of-refraction variation and nonstoichiometric composition [23].

Absorption in the transparent region (0.25–5 $\mu$m) is governed by impurities and defects. The structure and visible optical absorption of spinel with various amounts of chromium, cobalt, and iron have been widely studied [24–27]. Optical effects of X-ray, $\gamma$-ray [28, 29], electron [16], and neutron [16, 30] irradiation are well-known. An $F$ center at 5.3 eV (234 nm), an $F^+$ center at 4.75 eV (261 nm), and a $V$ center at 3.2 eV (387 nm) are known [16, 31]. The most prominent IR absorption feature is the $OH^-$ absorption band that occurs at 3345 $cm^{-1}$ [9, 15, 19, 32]. Nonstoichiometric spinel has an additional $OH^-$ absorption band at 3528 $cm^{-1}$ that grows with increasing alumina content [3, 9, 15, 19, 32].

The dominant loss mechanism in the visible and near-IR transparent region of polycrystalline spinel is scatter. Bulk scatter in polycrystalline spinel is low and decreases with increasing wavelength [2].

Absorption at the IR edge of transparency is dominated by multiphonon absorption. A model of multiphonon absorption for spinel has been developed and validated with experimental data over a wide temperature range [33]. The fundamental (one-phonon) lattice vibrations occur in the 300–800 $cm^{-1}$ spectral region. Group theory predicts the following phonon modes for spinel [34–36]:

$$\Gamma = A_{1g} + E_g + F_{1g} + 3F_{2g} + 2A_{2u} + 2E_u + 4F_{1u} + 2F_{2u}. \quad (2)$$

The Raman-active modes are $A_{1g}$, $E_g$, and $F_{2g}$, and the $F_{1u}$ modes are IR-active. Table I lists locations of the IR modes (transverse optical frequency) observed by several researchers [37–39]. There is good agreement on the location of three prominent modes; the fourth mode is either weak or masked by the other three. Also, other weak modes not predicted by group theory may be present because of disorder or lack of stoichiometry [35]. In particular, an absorption peak near 818 $cm^{-1}$ becomes prominent as the alumina concentration is increased, as demonstrated by Hafner and Laves [8] and Wang and Zanzucchi [40]. Table II gives mode locations, widths, and strengths as determined by Thomas [39]. Temperature dependence of these modes has been measured over the range 290–775 K.

Table II also lists both the transverse and longitudinal optical frequencies of spinel. The transverse optical frequencies are the mode locations; the maximum longitudinal is an important parameter in the multiphonon model [33], since it designates the maximum phonon frequency.

At frequencies below the lowest fundamental optical mode, absorption decreases and the material becomes transparent. The magnitude of absorption is thought to be a combination of contributions from both the tail of

the fundamental lattice vibrations and various multiphonon difference bands. The index of refraction now also includes the effect of lattice vibrations.

The low-frequency real index of refraction (dielectric constant $\approx n^2$) of spinel was measured by Wang and Zanzucchi [40], Westphal and Iglesias [41], Stead and Simonis [42], and Ho [43]. These values lie between 2.88 and 2.90, which are slightly higher that the value of 2.86 determined from Table II. Wang [3] reported very little change in dielectric constant when $m$ ranged from 1 to 3. Temperature dependence of the low-frequency index of refraction is given by Westphal and Iglesias [41] as $2.5 \times 10^{-4}$/K (average, 25–455 °C) and by Ho [43] as $2.3 \times 10^{-4}$/K (average, 23–300 °C), $2.8 \times 10^{-4}$/K (average, 23–1000 °C), and $3.0 \times 10^{-4}$/K (average, 23–1200 °C). Stead and Simonis [42] also give values for the imaginary index of refraction ($k$) in the 5–15 $cm^{-1}$ region. Estimates of the imaginary index of refraction made from the low-frequency side (red wing) of the fundamental modes (Table II) are about 72% of the experimental value determined by Stead and Simonis [42] at 5 $cm^{-1}$, with better agreement at higher frequency.

Table III was constructed from measurements reported in the literature as well as model predictions. Real-index ($n$) data in the visible and near IR are taken from the measurements of Furutani [21] and Scheller [22].

Lattice-vibration-model results [39] are used to calculate real-index data from 0–9600 $cm^{-1}$ and imaginary index data from 5–5000 $cm^{-1}$. Laser calorimetry results for $k$ at 2.9 and 3.9 $\mu$m by Detrio and Greason [44] give extrinsic measurements of the imaginary part of the index of refraction, based on thin samples with the lowest absorption coefficients. Of particular note is the imaginary index of refraction at 2.9 $\mu$m, which lies on the $OH^-$ absorption feature of spinel.

Measurements of Stead and Simonis [42] and others [40, 41, 43] are used to represent the low-frequency characteristics of spinel. In this region, one-phonon-model contributions [39] to $k$ are 70 to 100% of measured values [42], and index predictions are 0.7 to 1.5% low compared with measured values [40–43]. Two- and three-phonon difference bands presumably account for the unaccounted portion of $k$.

The accuracy of available index data is unknown. In all data, the uncertainty in the values is probably in the least-significant digit reported in Table III. In spectral regions where several sources of data exist, there is a large disparity between references.

Figure 2 shows a composite of the complex index of refraction based on the data of Table III.

Table IV gives temperature dependence for the real part of the index of refraction. Measurements of $dn/dT$ by Vadem *et al.* [20], Westphal and Iglesias [41], and Ho [43] are included.

Temperature-dependent absorption computed from optical models of

spinel [39] has been used to estimate total hemispherical emissivity of pure, transparent spinel over the range 200–1000 K, where the models are expected to give the best results, and defect absorption is believed to be insignificant. These results were obtained by estimating the complex refractive index at a given temperature, calculating directional emittance for a specific slab thickness, integrating over angle, and convolving the resulting spectral hemispherical emittances with the Planck function.

Table V gives the resulting total hemispherical emittance for semi-infinite slabs as a function of slab thickness. Since total hemispherical emissivity is an important function for radiation-relief calculations and may be needed to correct property measurements such as thermal conductivity, we have included this calculated result.

## REFERENCES


1. A. M. Alper, R. N. McNally, P. G. Ribbe, and R. C. Doman, "The System $MgO$–$MgAl_2O_4$," *J. Am. Ceram. Soc.* **45**, 264 (1962).
2. D. W. Roy and J. L. Hastert, "Polycrystalline $MgAl_2O_4$ (Spinel) for Use as Windows and Domes from 0.3 to 6.0 Micrometers," *Proc. SPIE* **400**, 37 (1983).
3. C. C. Wang, "Growth and Characterization of Spinel Single Crystals for Substrate Use in Integrated Electronics," *J. Appl. Phys.* **40**, 3433 (1969).
4. G. E. Bacon, "A Neutron-Diffraction Study of Magnesium Aluminium Oxide," *Acta Cryst.* **5**, 684 (1952).
5. Von H. Jagodzinski and H. Saalfeld, "Cation Distribution and Structural Relations in Mg-Al-Spinel," *Z. Kristallogr.* **110**, 197 (1958).
6. P. Fischer, "Neutron Diffraction Investigation of the Structure of $MgAl_2O_4$ and $ZnAl_2O_4$ Spinel as a Function of Previous History," *Z. Kristallogr.* **124**, 275 (1967).
7. U. Schmocker, H. R. Boesch, and F. Waldner, "A Direct Determination of Cation Disorder in $MgAl_2O_4$ Spinel by ESR," *Phys. Lett.* **40A**, 237 (1972).
8. S. Hafner and F. Laves, "Order/Disorder and Infrared Absorption III. The Systems $MgAl_2O_4$-$Al_2O_3$ and $MgAl_2O_4$-$LiAl_5O_8$," *Z. Kristallogr.* **115**, 321 (1961).
9. J. S. Reed, "Optical Absorption Spectra of $Cr^{3+}$ in $MgO \cdot Al_2O_3$-$MgO \cdot 3.5Al_2O_3$ Spinels," *J. Am. Ceram. Soc.* **54**, 202 (1971).
10. B. Cockayne and M. Chesswas, "The Vertical Pulling of $MgAl_2O_4$ Single Crystals," *J. Mater. Sci.* **2**, 498 (1967).
11. D. Viechnicki, F. Schmid, and J. W. McCauley, "Growth of Nearly Stoichiometric $MgAl_2O_4$ Spinel Single Crystals by a Gradient Furnace Technique," *J. Appl. Phys.* **43**, 4508 (1972).
12. T. M. Hartnett and R. L. Gentilman, "Optical and Mechanical Properties of Highly Transparent Spinel and ALON Domes," *Proc. SPIE* **505**, 15 (1984).
13. P. F. Becher, "Press-Forged $Al_2O_3$-Rich Spinel Crystals for IR Applications," *Bull. Am. Ceram. Soc.* **56**, 1015 (1977).
14. R. A. LaFever and G. W. Clark, "Multiple-Tube Flame Fusion Burner for the Growth of Oxide Single Crystals," *Rev. Sci. Instr.* **33**, 769 (1962).
15. R. L. Gentilman, "Fusion-Casting of Transparent Spinel," *Bull. Am. Ceram. Soc.* **60**, 906 (1981).
16. G. P. Summers, G. S. White, K. H. Lee, and J. H. Crawford, 'Radiation Damage in $MgAl_2O_4$," *Phys. Rev. B* **21**, 2578 (1980).
17. J. D. Woosley, C. Wood, E. Sonder, and R. A. Weeks, "Photoelectric Effects in Magnesium Aluminium Spinel," *Phys. Rev. B* **22**, 1065 (1980).

18. K. Schlossmacher, "Absorption and Refraction of the Red, Blue, and Violet Spinels of Ceylon," *Z. Kristallogr.* **72**, 447 (1930).
19. K. A. Wickersheim and R. A. LaFever, "Optical Properties of Synthetic Spinel," *J. Opt. Soc. Am.* **50**, 831 (1960).
20. K. Vadem, J. L. Kirk, and B. N. N. Achar, "Piezo- and Thermo-Optic Behavior of Spinel ($MgAl_2O_4$)," *J. Solid State Chem.* **12**, 213 (1975).
21. N. Furutani, General Dynamics, Valley Systems Division, personal communcation (Oct. 5, 1989).
22. R. J. Scheller, Schott Glass Technologies, Inc., personal communication (June 20, 1989).
23. J. B. Hearney, G. Hass, and M. McFarland, "Spinel ($Al_2O_3$:MgO): Refractive-Index Variations and Lack of Stoichiometry in Evaporated Films," *Appl. Opt.* **14**, 2335 (1981).
24. G. A. Slack, "$FeAl_2O_4$-$MgAl_2O_4$: Growth and Some Thermal, Optical, and Magnetic Properties of Mixed Single Crystals," *Phys. Rev.* **134A**, 1268 (1964).
25. P. K. Sharpe and J. C. Vickerman, "Solid State Properties of Copper Containing Spinel Solutions ($Cu_xMg_{1-x}Al_2O_4$)," *J. Chem. Soc. Faraday Trans. I* **73**, 505 (1977).
26. C. Angeletti, F. Pele, and P. Porta, "Structure and Catalytic Activity of $Co_xMg_{1-x}Al_2O_4$ Spinel Solid Solutions," *J. Chem. Soc. Faraday Trans. I* **73**, 1972 (1977).
27. W. Strek, P. Deren, and B. Jezowska-Trzebiatoeska, "Optical Properties of $Cr^{3+}$ in $MgAl_2O_4$ Spinel," *Physica B* **152**, 379 (1988).
28. G. S. White, K. H. Lee, and J. H. Crawford, "Effects of $\lambda$-Irradiation upon the Optical Behavior of Spinel," *Phys. Stat. Solidi (a)* **42**, K137 (1977).
29. G. S. White, R. V. Jones, and J. H. Crawford, "Optical Spectra of $MgAl_2O_4$ Crystals Exposed to Ionizing Radiation," *J. Appl. Phys.* **53**, 265 (1982).
30. L. S. Cain, G. J. Pogatshnik, and Y. Chin, "Optical Transitions in Neutron-Irradiated $MgAl_2O_4$ Spinel Crystals," *Phys. Rev. B* **37**, 2645 (1988).
31. P. K. Bandyopadhyay and G. P. Summers, "Luminescence and Photoconductivity in Magnesium Aluminum Spinel," *Phys. Rev. B* **31**, 2422 (1985).
32. E. Sonder and R. A. Weeks, "Behavior of Electrical Conduction of Spinel and Other Insulating Oxides in Moderate Electric Fields at High Temperature," *J. Appl. Phys.* **56**, 2365 (1984).
33. M. E. Thomas, R. I. Joseph, and W. J. Tropf, "Infrared Transmission Properties of Sapphire, Spinel, Yttria, and ALON as a Function of Temperature and Frequency," *Appl. Opt.* **27**, 239 (1988).
34. H. D. Lutz, "Lattice Vibrational Spectra. III. Symmetry Coordinates and Vibrational Forms of Lattice Vibrations in Spinel," *Z. Naturforsch. A* **24**, 1417 (1969).
35. W. B. White and B. A. DeAngelis, "Interpretation of the Vibrational Spectra of Spinels," *Spectrochim. Acta* **23A**, 985 (1967).
36. J. Preudhomme and P. Tarte, "Infrared Studies of Spinels-III: The Normal II–III Spinels," *Spectrochim. Acta* **27A**, 1817 (1971).
37. M. P. O'Horo, A. L. Frisillo, and W. B. White, "Lattice Vibrations of $MgAl_2O_4$ Spinel, *J. Phys. Chem. Solids* **34**, 23 (1973).
38. M. E. Striefler and S. I. Boldish, "Transverse and Longitudinal Optic Frequencies of Spinel $MgAl_2O_4$," *J. Phys.* **C11**, L237 (1978).
39. M. E. Thomas, "A Computer Code for Modelling Optical Properties of Window Materials," *Proc. SPIE* **1112**, 260 (1989). Mode parameters in Tables I and II have been improved over the values given in the reference.
40. C. C. Wang and P. J. Zanzucchi, "Dielectric and Optical Properties of Stoichiometric Magnesium Aluminate Spinel Single Crystals," *J. Electrochem. Soc.* **118**, 586 (1971).
41. W. B. Westphal and J. Iglesias, Dielectric Spectroscopy of High-Temperature Materials, Air Force Materials Laboratory Report AFML-TR-71-66, April (1971). (Available from NTIS as AD 884597.)

42. M. Stead and G. Simonis, "Near Millimeter Wave Characterization of Dual Mode Maerials," *Appl. Opt.* **28**, 1874 (1989).
43. W. W. Ho, "High-Temperature Dielectric Properties of Polycrystalline Ceramics," in "MRS Symposium M," Reno (April 6, 1988).
44. J. A. Detrio and P. Greason, University of Dayton, personal communication (April 8, 1988).

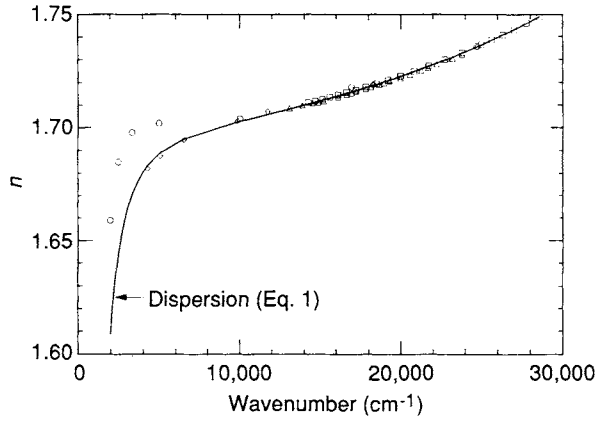


**Fig. 1.** Index of refraction ($n$) versus wave number in $cm^{-1}$ for magnesium aluminum spinel. Data from Schlossmacher [18] (triangles), Furutani [21] (squares), Scheller [22] (diamonds), and Roy and Hastert [2] (circles) are compared with the dispersion equation (solid line) given in the text.

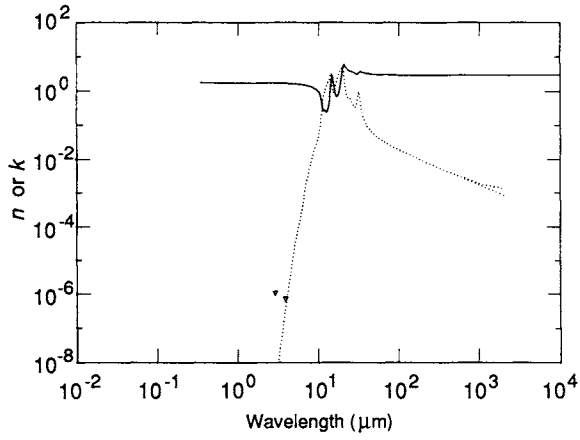


**Fig. 2.** Log–log plot of $n$ (solid line) and $k$ (dashed line) versus wavelength in micrometers for magnesium aluminum spinel. Data from various sources sometimes do not join together in overlap regions. Symbols are laser-colarimetry measurements of $k$.

**TABLE I**

**Determination of Spinel Infrared Lattice-Vibration Frequencies ($cm^{-1}$)[a]**

| O'Horo *et al.* [37] | Striefer [38] | | | | Thomas [39] |
|---|---|---|---|---|---|
| | 4-pole fits | | | | |
| 4-pole fit | #1 | #2 | #3 | 6-pole fit | 7-pole fit |
| 305 | 305 | 305 | 306 | 306 | 307 |
| 428(w) | | 416*(s) | | 363 | 400* |
| 485(s) | 490(s) | 491(s) | 490(s) | 491(s) | 482(s) |
| | | | | | 505 |
| | 580(w) | | | 581(w) | 580* |
| 670 | 670 | 676 | 674 | 674 | 675 |
| | | | 812(w) | 812(w) | 815(w) |

[a]References are indicated in brackets. Letters in parentheses indicate mode strength: s = strong, w = weak. Asterisks indicate very broad modes (probably made of many modes and caused by defects). Modes at 305–308, 482–491, and 670–675 are three of the four spinel fundamental lattice vibrations. The mode at 812–815 is likely caused by nonstoichiometry (see [40]). O'Horo *et al.* [37] give the following Raman-active mode locations: 311, 492, 611 ($F_{2g}$); 410 ($E_g$); and 772 ($A_{1g}$).

**TABLE II**

**Fundamental Infrared Lattice-Vibration Parameters of Spinel[a]**

| Mode | Transverse optical frequency ($cm^{-1}$) | Strength | Normalized width | Longitudinal optical frequency ($cm^{-1}$) | Refs. |
|---|---|---|---|---|---|
| 1* | 307 | 0.45 | 0.080 | 311 | [37-39] |
| 2 | 400 | 0.50 | 0.20 | — | [39] |
| 3* | 482 | 2.70 | 0.065 | 497 | [37-39] |
| 4 | 505 | 0.80 | 0.080 | — | [39] |
| 5 | 580 | 0.15 | 0.30 | 603 | [38,39] |
| 6* | 675 | 0.66 | 0.045 | 800 | [37-39] |
| 7 | 815 | 0.01 | 0.065 | 869 | [38,39] |
| | | Total = 5.27 | | | |

[a]The transverse optical frequency ($\nu_j$) is the location of the mode. Modes marked with an asterisk are three of the four fundamental IR modes ($F_{1u}$). Frequently, one mode of greater strength (e.g., 3.5) is substituted for our modes 3 and 4 [36-38]. Preudhomme and Tarte [36] identified mode 5 as the fourth fundamental IR vibration by analogy to other spinels. The strength ($\Delta\epsilon_j$) is the contribution of the mode to the dielectric constant. The normalized width ($\gamma_j$) is the mode width divided by the mode frequency. The complex dielectric constant ($\epsilon$) is then modeled as a function of frequency ($\nu$) by

$$\epsilon(\nu) = \epsilon_\infty + \sum_j \frac{\Delta\epsilon_j \nu_j^2}{\nu_j^2 - \nu^2 + i\gamma_j \nu_j \nu} ,$$

where the $\epsilon_\infty$ term (= 2.892) represents the electronic contributions to the dielectric constant (plus one). This model has a static dielectric constant of 8.16.

TABLE III

**Values of $n$ and $k$ Obtained from Various References for Spinel[a]**

| eV | $cm^{-1}$ | $\mu m$ | $n$ | $n$ | $n$ | $n$ |
|---|---|---|---|---|---|---|
| 3.542 | 28571 | 0.350 | | | 1.7489 [21] | |
| 3.444 | 27778 | 0.360 | | | 1.7461 | |
| 3.351 | 27027 | 0.370 | | | 1.7433 | |
| 3.263 | 26316 | 0.380 | | | 1.7409 | |
| 3.179 | 25641 | 0.390 | | | 1.7389 | |
| 3.100 | 25000 | 0.400 | | | 1.7368 | |
| 3.064 | 24710 | 0.40466 | 1.73574 [22] | 1.736 [2] | | |
| 2.952 | 23810 | 0.420 | | | 1.7332 | 1.7324 [18] |
| 2.878 | 23213 | 0.4308 | | | | 1.7306 |
| 2.845 | 22944.7 | 0.43583 | 1.73054 | | | |
| 2.818 | 22727 | 0.440 | | | 1.7302 | |
| 2.755 | 22222 | 0.450 | | | | 1.7281 |
| 2.695 | 21739 | 0.460 | | | 1.7273 | |
| 2.691 | 21701 | 0.4608 | | | | 1.7264 |
| 2.638 | 21277 | 0.470 | | | | 1.7252 |
| 2.583 | 20833 | 0.480 | | | 1.7250 | |
| 2.551 | 20572 | 0.4861 | | | | 1.7234 |
| 2.480 | 20000 | 0.500 | | | 1.7229 | 1.7219 |
| 2.397 | 19331 | 0.5173 | | | | 1.7207 |
| 2.384 | 19231 | 0.520 | | | 1.7211 | |
| 2.353 | 18975 | 0.527 | | | | 1.7197 |
| 2.317 | 18688 | 0.5351 | | | | 1.7191 |
| 2.296 | 18519 | 0.540 | | | 1.7195 | |
| 2.270 | 18312 | 0.54607 | 1.71896 | 1.719 | | |
| 2.254 | 18182 | 0.550 | | | | 1.7180 |
| 2.214 | 17857 | 0.560 | | | 1.7180 | 1.7172 |
| 2.138 | 17241 | 0.580 | | | 1.7167 | 1.7160 |
| 2.104 | 16969 | 0.5893 | | 1.718 [20] | | 1.7154 |
| 2.066 | 16667 | 0.600 | | | 1.7156 | 1.7146 |
| 2.000 | 16129 | 0.620 | | | 1.7145 | 1.7135 |
| 1.937 | 15625 | 0.640 | | | 1.7135 | |
| 1.889 | 15237 | 0.6563 | | | | 1.7118 |
| 1.879 | 15152 | 0.660 | | | 1.7126 | |
| 1.848 | 14908 | 0.6708 | | | | 1.7112 |
| 1.823 | 14706 | 0.680 | | | 1.7119 | |
| 1.803 | 14543 | 0.6876 | | | | 1.7109 |
| 1.771 | 14286 | 0.700 | | | 1.7111 | |
| 1.725 | 13912.1 | 0.7188 | | | | 1.7099 |
| 1.625 | 13109.6 | 0.7628 | | | | 1.7086 |
| 1.455 | 11735.6 | 0.85211 | 1.70728 | | | |
| 1.240 | 10000 | 1.0000 | | 1.704 [2] | | |
| 1.223 | 9862.1 | 1.01398 | 1.70300 | 1.703 | | |

(*continued*)

**TABLE III (*Continued*)**

**Spinel**

| eV | $cm^{-1}$ | $\mu m$ | $n$ | $n$ | $n$ | $k$ | |
|---|---|---|---|---|---|---|---|
| 1.190 | 9600 | 1.0417 | | | 1.702 | | [39] |
| 1.165 | 9400 | 1.0638 | | | 1.701 | | |
| 1.141 | 9200 | 1.0870 | | | 1.701 | | |
| 1.116 | 9000 | 1.1111 | | | 1.700 | | |
| 1.091 | 8800 | 1.1364 | | | 1.700 | | |
| 1.066 | 8600 | 1.1628 | | | 1.700 | | |
| 1.041 | 8400 | 1.1905 | | | 1.699 | | |
| 1.017 | 8200 | 1.2195 | | | 1.699 | | |
| 0.9919 | 8000 | 1.2500 | | | 1.698 | | |
| 0.9671 | 7800 | 1.2821 | | | 1.698 | | |
| 0.9423 | 7600 | 1.3158 | | | 1.697 | | |
| 0.9175 | 7400 | 1.3514 | | | 1.697 | | |
| 0.8927 | 7200 | 1.3889 | | | 1.696 | | |
| 0.8679 | 7000 | 1.4286 | | | 1.695 | | |
| 0.8431 | 6800 | 1.4706 | | | 1.695 | | |
| 0.8183 | 6600 | 1.5152 | | | 1.694 | | |
| 0.8106 | 6537.74 | 1.52958 | 1.69468 | | | | |
| 0.7935 | 6400 | 1.5625 | | | 1.693 | | |
| 0.7687 | 6200 | 1.6129 | | | 1.693 | | |
| 0.7439 | 6000 | 1.6667 | | | 1.692 | | |
| 0.7191 | 5800 | 1.7241 | | | 1.691 | | |
| 0.6943 | 5600 | 1.7857 | | | 1.690 | | |
| 0.6695 | 5400 | 1.8519 | | | 1.689 | | |
| 0.6447 | 5200 | 1.9231 | | | 1.688 | | |
| 0.6293 | 5075.91 | 1.97009 | 1.68763 | | | | |
| 0.6199 | 5000 | 2.0000 | | 1.702 | 1.686 | $2.2\cdot10^{-13}$ | [39] |
| 0.6075 | 4900 | 2.0408 | | | 1.686 | $4.4\cdot10^{-13}$ | |
| 0.5951 | 4800 | 2.0833 | | | 1.685 | $8.6\cdot10^{-13}$ | |
| 0.5827 | 4700 | 2.1277 | | | 1.684 | $1.6\cdot10^{-12}$ | |
| 0.5703 | 4600 | 2.1739 | | | 1.683 | $2.9\cdot10^{-12}$ | |
| 0.5579 | 4500 | 2.2222 | | | 1.682 | $5.2\cdot10^{-12}$ | |
| 0.5455 | 4400 | 2.2727 | | | 1.681 | $9.0\cdot10^{-12}$ | |
| 0.5332 | 4300.30 | 2.32542 | 1.68194 | | | | |
| 0.5331 | 4300 | 2.3256 | | | 1.680 | $1.6\cdot10^{-11}$ | |
| 0.5207 | 4200 | 2.3810 | | | 1.679 | $2.7\cdot10^{-11}$ | |
| 0.5083 | 4100 | 2.4390 | | | 1.678 | $4.6\cdot10^{-11}$ | |
| 0.4959 | 4000 | 2.5000 | | | 1.677 | $8.0\cdot10^{-11}$ | |
| 0.4835 | 3900 | 2.5641 | | | 1.675 | $1.4\cdot10^{-10}$ | |
| 0.4711 | 3800 | 2.6316 | | | 1.674 | $2.4\cdot10^{-10}$ | |
| 0.4587 | 3700 | 2.7027 | | | 1.672 | $4.2\cdot10^{-10}$ | |
| 0.4463 | 3600 | 2.7778 | | | 1.671 | $7.3\cdot10^{-10}$ | |
| 0.4339 | 3500 | 2.8571 | | | 1.669 | $1.3\cdot10^{-9}$ | |
| 0.4275 | 3448 | 2.9000 | | | | $1.0\cdot10^{-6}$ | [44] |
| 0.4215 | 3400 | 2.9412 | | | 1.667 | $2.3\cdot10^{-9}$ | [39] |

(*continued*)

**TABLE III (*Continued*)**

**Spinel**

| eV | $cm^{-1}$ | $\mu m$ | $n$ | $k$ | $n$ | $k$ |
|---|---|---|---|---|---|---|
| 0.1017 | 820 | 12.195 | | | 0.274 | 0.94 |
| 0.0992 | 800 | 12.500 | | | 0.259 | 1.1 |
| 0.0967 | 780 | 12.821 | | | 0.240 | 1.3 |
| 0.0942 | 760 | 13.158 | | | 0.255 | 1.6 |
| 0.0917 | 740 | 13.514 | | | 0.307 | 1.9 |
| 0.0893 | 720 | 13.889 | | | 0.431 | 2.2 |
| 0.0868 | 700 | 14.286 | | | 0.792 | 2.8 |
| 0.0843 | 680 | 14.706 | | | 2.150 | 3.2 |
| 0.0818 | 660 | 15.152 | | | 2.799 | 1.5 |
| 0.0794 | 640 | 15.625 | | | 1.943 | 0.87 |
| 0.0769 | 620 | 16.129 | | | 1.232 | 0.96 |
| 0.0744 | 600 | 16.667 | | | 0.805 | 1.4 |
| 0.0719 | 580 | 17.241 | | | 0.682 | 2.0 |
| 0.0694 | 560 | 17.857 | | | 0.718 | 2.6 |
| 0.0670 | 540 | 18.519 | | | 0.931 | 3.3 |
| 0.0645 | 520 | 19.231 | | | 1.576 | 4.1 |
| 0.0620 | 500 | 20.000 | | | 2.938 | 4.7 |
| 0.0608 | 490 | 20.408 | | | 4.040 | 4.9 |
| 0.0595 | 480 | 20.833 | | | 5.550 | 4.1 |
| 0.0583 | 470 | 21.277 | | | 5.904 | 2.5 |
| 0.0570 | 460 | 21.739 | | | 5.460 | 1.5 |
| 0.0558 | 450 | 22.222 | | | 4.967 | 1.1 |
| 0.0546 | 440 | 22.727 | | | 4.569 | 0.82 |
| 0.0533 | 430 | 23.256 | | | 4.264 | 0.69 |
| 0.0521 | 420 | 23.810 | | | 4.039 | 0.64 |
| 0.0508 | 410 | 24.390 | | | 3.888 | 0.62 |
| 0.0496 | 400 | 25.000 | | | 3.795 | 0.60 |
| 0.0484 | 390 | 25.641 | | | 3.730 | 0.55 |
| 0.0471 | 380 | 26.316 | | | 3.662 | 0.49 |
| 0.0459 | 370 | 27.027 | | | 3.576 | 0.42 |
| 0.0446 | 360 | 27.778 | | | 3.476 | 0.37 |
| 0.0434 | 350 | 28.571 | | | 3.363 | 0.34 |
| 0.0422 | 340 | 29.412 | | | 3.238 | 0.34 |
| 0.0409 | 330 | 30.303 | | | 3.097 | 0.40 |
| 0.0397 | 320 | 31.250 | | | 2.988 | 0.61 |
| 0.0384 | 310 | 32.258 | | | 3.242 | 0.95 |
| 0.0372 | 300 | 33.333 | | | 3.679 | 0.69 |
| 0.0360 | 290 | 34.483 | | | 3.634 | 0.37 |
| 0.0347 | 280 | 35.714 | | | 3.509 | 0.23 |
| 0.0335 | 270 | 37.037 | | | 3.408 | 0.16 |
| 0.0322 | 260 | 38.462 | | | 3.330 | 0.13 |
| 0.0310 | 250 | 40.000 | | | 3.267 | 0.10 |
| 0.0298 | 240 | 41.667 | | | 3.216 | 0.088 |
| 0.0285 | 230 | 43.478 | | | 3.172 | 0.077 |

(*continued*)

**TABLE III (*Continued*)**

**Spinel**

| eV | $cm^{-1}$ | $\mu m$ | $n$ | $k$ | $n$ | $k$ |
|---|---|---|---|---|---|---|
| 0.0273 | 220 | 45.455 | | | 3.134 | 0.067 |
| 0.0260 | 210 | 47.619 | | | 3.101 | 0.060 |
| 0.0248 | 200 | 50.000 | | | 3.071 | 0.054 |
| 0.0236 | 190 | 52.632 | | | 3.045 | 0.048 |
| 0.0223 | 180 | 55.556 | | | 3.022 | 0.044 |
| 0.0211 | 170 | 58.824 | | | 3.001 | 0.039 |
| 0.0198 | 160 | 62.500 | | | 2.982 | 0.036 |
| 0.0186 | 150 | 66.667 | | | 2.965 | 0.032 |
| 0.0174 | 140 | 71.429 | | | 2.949 | 0.029 |
| 0.0161 | 130 | 76.923 | | | 2.935 | 0.026 |
| 0.0149 | 120 | 83.333 | | | 2.923 | 0.024 |
| 0.0136 | 110 | 90.909 | | | 2.912 | 0.021 |
| 0.0124 | 100 | 100.00 | | | 2.902 | 0.019 |
| 0.0112 | 90 | 111.11 | | | 2.893 | 0.017 |
| 0.0099 | 80 | 125.00 | | | 2.885 | 0.015 |
| 0.0087 | 70 | 142.86 | | | 2.878 | 0.013 |
| 0.0074 | 60 | 166.67 | | | 2.873 | 0.011 |
| 0.0062 | 50 | 200.00 | | | 2.868 | $8.8 \cdot 10^{-3}$ |
| 0.0050 | 40 | 250.00 | | | 2.864 | $7.0 \cdot 10^{-3}$ |
| 0.0037 | 30 | 33.333 | | | 2.861 | $5.2 \cdot 10^{-3}$ |
| 0.0025 | 20 | 500.00 | | | 2.859 | $3.5 \cdot 10^{-3}$ |
| 0.0019 | 15 | 666.67 | | $2.4 \cdot 10^{-3}$ [42] | 2.858 | $2.6 \cdot 10^{-3}$ |
| 0.0012 | 10 | 1000.0 | 2.88 [42] | $1.8 \cdot 10^{-3}$ | 2.857 | $1.7 \cdot 10^{-3}$ |
| 0.0006 | 5 | 2000.0 | | $1.2 \cdot 10^{-3}$ | 2.857 | $8.6 \cdot 10^{-4}$ |
| 0.0000 | 0 | $\infty$ | 2.90 [40] | | 2.857 | |
| | | | 2.88 [41] | | | |
| | | | 2.88–2.90 [43] | | | |

[a]References are indicated in brackets.

**TABLE V**

**Values of $dn/dT$ Obtained from Various References for Spinel[a]**

| eV | $cm^{-1}$ | $\mu m$ | $dn/dT$ (1/K) | Notes |
|---|---|---|---|---|
| 2.104 | 16969 | 0.5893 | $0.90_5 \cdot 10^{-5}$ | Measurement [20] |
| 1.959 | 15803 | 0.6328 | $1.2 \cdot 10^{-5}$ | Our measurement |
| 0.310 | 2500 | 4.0000 | $3.1 \cdot 10^{-6}$ | Model [39] |
| 0.0 | 0 | $\infty$ | $2.5 \cdot 10^{-4}$ | 4 GHz, 25–455°C [41] |
| | | | $2.8 \cdot 10^{-4}$ | 35 GHz, 23–1000°C [43] |

[a]References are indicated in brackets.

**TABLE IV**

**Calculated Total Hemispherical Emissivity for Spinel**

| Temperature (K) | Thickness (cm) | | | |
|---|---|---|---|---|
| | 0.10 | 0.25 | 0.50 | 1.25 |
| 200 | 0.56 | 0.57 | 0.57 | 0.57 |
| 300 | 0.59 | 0.60 | 0.61 | 0.62 |
| 400 | 0.59 | 0.62 | 0.64 | 0.66 |
| 500 | 0.54 | 0.59 | 0.62 | 0.65 |
| 600 | 0.48 | 0.53 | 0.57 | 0.61 |
| 700 | 0.42 | 0.47 | 0.51 | 0.55 |
| 800 | 0.36 | 0.41 | 0.45 | 0.49 |
| 900 | 0.31 | 0.36 | 0.40 | 0.44 |
| 1000 | 0.27 | 0.31 | 0.35 | 0.39 |

**TABLE III *(Continued)***

**Spinel**

| eV | $cm^{-1}$ | $\mu m$ | $n$ | $k$ | $n$ | $k$ |
|---|---|---|---|---|---|---|
| 0.4133 | 3333 | 3.0000 | 1.698 [2] | | | |
| 0.4092 | 3300 | 3.0303 | | | 1.664 | $4.1\cdot10^{-9}$ |
| 0.3968 | 3200 | 3.1250 | | | 1.662 | $7.5\cdot10^{-9}$ |
| 0.3844 | 3100 | 3.2258 | | | 1.659 | $1.4\cdot10^{-8}$ |
| 0.3720 | 3000 | 3.3333 | | | 1.656 | $2.4\cdot10^{-8}$ |
| 0.3596 | 2900 | 3.4483 | | | 1.653 | $4.5\cdot10^{-8}$ |
| 0.3472 | 2800 | 3.5714 | | | 1.649 | $8.4\cdot10^{-8}$ |
| 0.3348 | 2700 | 3.7037 | | | 1.645 | $1.6\cdot10^{-7}$ |
| 0.3224 | 2600 | 3.8462 | | | 1.640 | $3.1\cdot10^{-7}$ |
| 0.3179 | 2564 | 3.9000 | | $6.8\cdot10^{-7}$ [44] | | |
| 0.3100 | 2500 | 4.0000 | 1.685 | | 1.635 | $5.9\cdot10^{-7}$ |
| 0.2976 | 2400 | 4.1667 | | | 1.629 | $1.1\cdot10^{-6}$ |
| 0.2852 | 2300 | 4.3478 | | | 1.622 | $2.1\cdot10^{-6}$ |
| 0.2728 | 2200 | 4.5455 | | | 1.614 | $4.1\cdot10^{-6}$ |
| 0.2604 | 2100 | 4.7619 | | | 1.605 | $8.6\cdot10^{-6}$ |
| 0.2480 | 2000 | 5.0000 | 1.659 | | 1.594 | $1.8\cdot10^{-5}$ |
| 0.2418 | 1950 | 5.1282 | | | 1.587 | $2.6\cdot10^{-5}$ |
| 0.2356 | 1900 | 5.2632 | | | 1.581 | $3.7\cdot10^{-5}$ |
| 0.2294 | 1850 | 5.4054 | | | 1.573 | $5.2\cdot10^{-5}$ |
| 0.2232 | 1800 | 5.5556 | | | 1.565 | $7.1\cdot10^{-5}$ |
| 0.2170 | 1750 | 5.7143 | | | 1.556 | $1.0\cdot10^{-4}$ |
| 0.2108 | 1700 | 5.8824 | | | 1.545 | $1.4\cdot10^{-4}$ |
| 0.2046 | 1650 | 6.0606 | | | 1.534 | $2.0\cdot10^{-4}$ |
| 0.1984 | 1600 | 6.2500 | | | 1.522 | $2.9\cdot10^{-4}$ |
| 0.1922 | 1550 | 6.4516 | | | 1.507 | $4.4\cdot10^{-4}$ |
| 0.1860 | 1500 | 6.6667 | | | 1.491 | $6.9\cdot10^{-4}$ |
| 0.1798 | 1450 | 6.8966 | | | 1.473 | $1.1\cdot10^{-3}$ |
| 0.1736 | 1400 | 7.1429 | | | 1.451 | $1.8\cdot10^{-3}$ |
| 0.1674 | 1350 | 7.4074 | | | 1.427 | $2.8\cdot10^{-3}$ |
| 0.1612 | 1300 | 7.6923 | | | 1.398 | $4.4\cdot10^{-3}$ |
| 0.1550 | 1250 | 8.0000 | | | 1.363 | $6.6\cdot10^{-3}$ |
| 0.1488 | 1200 | 8.3333 | | | 1.322 | $9.8\cdot10^{-3}$ |
| 0.1426 | 1150 | 8.6957 | | | 1.271 | 0.014 |
| 0.1364 | 1100 | 9.0909 | | | 1.206 | 0.020 |
| 0.1302 | 1050 | 9.5238 | | | 1.122 | 0.028 |
| 0.1240 | 1000 | 10.000 | | | 1.006 | 0.041 |
| 0.1215 | 980 | 10.204 | | | 0.946 | 0.049 |
| 0.1190 | 960 | 10.417 | | | 0.875 | 0.061 |
| 0.1165 | 940 | 10.683 | | | 0.789 | 0.079 |
| 0.1141 | 920 | 10.870 | | | 0.680 | 0.11 |
| 0.1116 | 900 | 11.111 | | | 0.539 | 0.17 |
| 0.1091 | 880 | 11.364 | | | 0.377 | 0.32 |
| 0.1066 | 860 | 11.628 | | | 0.282 | 0.54 |
| 0.1041 | 840 | 11.905 | | | 0.255 | 0.76 |

*(continued)*

# Magnesium Fluoride ($MgF_2$)

THOMAS M. COTTER, MICHAEL E. THOMAS,
and WILLIAM J. TROPF
Applied Physics Laboratory
The Johns Hopkins University
Laurel, Maryland

Magnesium fluoride is a tetragonal material with $TiO_2$ (rutile) structure. The space group is $D_{4h}^{14}$ or $P4_2/mnm$. The unit cell contains two formula units (six atoms). Dimensions of the cell (at 27 °C) are 0.4623 nm along the $a$ axis and 0.3052 nm along the $c$ axis [1, also see 2]. Theoretical density is 3.177 g/cm$^3$ and melting point is $1528 \pm 3$ K [2]. A melting point of 1543 K is also reported [3].

Magnesium ions occupy octahedral sites with $D_{2h}$ point symmetry. Six fluorine ions at sites with $C_{2v}$ symmetry surround each magnesium ion. Fluorine-ion positions in the unit cell are known from X-ray diffraction measurements [1, 2].

A wide transparency range from 0.12 to 8 μm [2], good mechanical properties, and low optical index of refraction make magnesium fluoride a desirable material for coatings and interference filters. $MgF_2$ is a positive uniaxial material, with its highest birefringence in the UV. Except for lithium fluoride, $MgF_2$ has the shortest wavelength cutoff of any common optical material.

Magnesium fluoride occurs naturally as the mineral selliate [3]. Single-crystal $MgF_2$ [3, 4] is widely used for windows, lenses, polarizers, and other optical components. Optical-quality, hot-pressed polycrystalline $MgF_2$ is also used for optical components, particularly in the infrared. IRTRAN 1 [5] is a trade name for hot-pressed $MgF_2$ made by Kodak; KO-1 is an equivalent Soviet material [6]. Olsen and McBride [7] compare properties of IRTRAN 1 and single-crystal magnesium fluoride.

$MgF_2$ has been used as a divalent-ion host material for solid-state lasers. Vanadium, nickel, and cobalt have been used as dopants to produce tunable solid-state lasers in the infrared [8, 9].

The UV and IR transparency of magnesium fluoride lends itself to many applications. $MgF_2$ has been used as a window material for UV detectors in space applications [10, 11]. The birefringence is used to polarize light in the UV [12–14]. One such polarizer, operating from the UV to the IR, has


Copyright © 1991 by Academic Press.
All rights of reproduction in any form reserved.
ISBN 0-12-544422-2

been constructed [15]. The low index of $MgF_2$ in the IR led to its use as a Soleil compensator in the IR [16]. Magnesium fluoride is also used as a thin film to coat aluminum mirrors for enhanced reflectivity in the vacuum UV [17, 18]. Because of the relatively low index, magnesium fluoride is also used as an antireflection coating for lenses and as a low-index layer in dielectric interference filters.

Magnesium fluoride has a band gap of approximately 11.8 eV. Optical constants from the UV through the XUV have been measured for single-crystal magnesium fluoride [19–22]. The lowest-energy electronic feature of the magnesium fluoride spectrum is an exciton peak centered near 11.8 eV [20, 21]. This is due to an exciton peak at 11.6 eV for the extraordinary component and at 12.2 eV for the ordinary component [22]. The exciton peak obscures the UV absorption edge in this region, measured at 10.9 eV [20]. Although an absorption band beginning at 1320 Å has been observed, the transmission does not drop significantly until 1150 Å (10.8 eV) [2], which is close to the measured absorption edge. The interband transitions begin near 12.2 eV [21], at 12.4 eV for the extraordinary and 12.6 eV for the ordinary ray [22]. The extraordinary-ray absorption curve has structure at 18.6 eV and the ordinary ray at 15 and 20.5 eV [22]. Broad absorption structure near 20.8 eV is attributed to interband transitions [20]. These transitions are believed to arise from transitions from the upper valence band of fluorine ($2p^6$) to the conduction band of magnesium ($3s + 3p$) [21]. A peak at 24.5 eV is attributed to a plasmon [20, 21]. The plasmon peak is composed of an extraordinary-ray component at 24.3 eV and an ordinary-ray component at 24.6 eV [22]. Structure seen in the absorption coefficient from 27–40 eV is attributed to interband transitions $2s^2$ level of the fluorine ion to the conduction band [19, 21]. In the 40–56 eV region, two absorption peaks exist: an absorption peak at 47.5 eV caused by a double plasmon and a peak at 54.6 eV attributed to an exciton [19]. Structure from 56–62 eV is attributed to transitions of $2p^6$ electrons of magnesium to the conduction band [19].

Refractive-index data for the $MgF_2$ transparent region from the UV through the IR are given by many sources [2, 12, 23–27]. Dodge [27] fitted index data (at 19°C) to a Sellmeier-type dispersion relationship of the form

$$n_o^2 - 1 = \frac{2.5903553 \times 10^{10}}{(230,499.30)^2 - \nu^2} + \frac{4.4543708 \times 10^9}{(105,692.13)^2 - \nu^2} + \frac{4.0838897 \times 10^5}{(420.28101)^2 - \nu^2} \tag{1a}$$

and

$$n_e^2 - 1 = \frac{3.0458725 \times 10^{10}}{(271,424.78)^2 - \nu^2} + \frac{6.1300694 \times 10^9}{(110,178.73)^2 - \nu^2} + \frac{4.4070997 \times 10^5}{(420.66305)^2 - \nu^2}, \tag{1b}$$

where $\nu$ is the frequency in wave numbers. Equation 1 represents electro-

nic resonances with the first two terms and all IR resonances with the third term. These terms fall in the middle of the measured electronic transitions and lattice vibrations, respectively. The overall accuracy of index calculated from Eq. 1 is quoted as better than $2\times10^{-5}$ over the 1400–50,000 $cm^{-1}$ range.

Change in the index of refraction with temperature, pressure, and stress is available. Thermo-optic data are given by many sources [2, 28–30] without good agreement; data from the National Bureau of Standards [28] are considered comprehensive, cover a wide temperature range, and agree well with recent measurements of the temperature dependence of optical dispersion [30]. The elastic properties of $MgF_2$ have been reported in the form of elastic constants, photoelastic constants, and piezoelectric constants [31, 32].

Optical properties of thin films of magnesium fluoride have been studied extensively. Much disparity exists between published data due to variations of the conditions and method of preparation of the sample under study [33–37]. In addition, thin-film properties usually do not match single-crystal properties [19, 20]. Consequently, this article concentrates on properties of single crystals.

Radiation damage of $MgF_2$ is described elsewhere [38]. Studies of radiation effects on the absorption of magnesium fluoride have revealed absorption bands in the UV. Three prominent absorption peaks at 117, 260, and 370 nm develop, which can be attributed to the creation of *F* centers by radiation [38]. No observations of IR absorption due to radiation have been reported [38]. The characterization of the fluorescence of $MgF_2$ has also been undertaken [38, 39].

Absorption at the IR edge of transparency is dominated by multiphonon absorption [40]. A model of multiphonon absorption [41] has been developed and confirmed with experimental data over a wide temperature range. Model constants for the ordinary ray of $MgF_2$ are given by Thomas and Joseph [42].

The fundamental (one-phonon) lattice vibrations occur in the 250–625 $cm^{-1}$ spectral region. Group theory predicts the following phonon modes for $MgF_2$ [43–46]:

$$\Gamma = A_{1g} + A_{2g} + A_{2u} + B_{1g} + B_{2g} + 2B_{1u} + E_g + 3E_u, \tag{2}$$

where the $A_{2g}$ and $B_{1u}$ modes are optically inactive, the $A_{2u}$ ($\mathbf{E}\|c$) and $E_u$ ($\mathbf{E}\perp c$) modes are IR-active, and the remaining modes are Raman-active. Table I lists the IR modes as determined by Barker [44], Thomas and Joseph [42], and Giordano and Benoit [46]. Locations of the Raman modes are given by Porto *et al.* [45] as 92 ($B_{1g}$), 295 ($E_g$), 410 ($A_{1g}$), and 515 ($B_{2g}$) $cm^{-1}$.

Table I also lists both the transverse and longitudinal optical frequen-

cies. The transverse optical frequencies are the mode locations; the maximum longitudinal-mode frequency is an important parameter in the multiphonon-absorption model [41], since it designates the maximum phonon frequency.

At frequencies below the lowest-frequency transverse optical mode, absorption decreases and the material becomes transparent. The magnitude of absorption is thought to be a combination of contributions from both the tail of the fundamental lattice vibrations and various multiphonon difference bands. The index of refraction now also includes the effect of lattice vibrations. Estimates of low-frequency absorption made from the red wing of the fundamental modes (Table I) for $MgF_2$ are about 60% of the ordinary-ray imaginary index of refraction and 95% of the extraordinary-ray values determined by Bystrov *et al.* [47] in the 10–23 $cm^{-1}$ region. Measurements of two different sintered samples of polycrystalline $MgF_2$ by Stead and Simonis [48] showed yet higher absorption.

The low-frequency index of refraction of magnesium fluoride is given by Fontanella *et al.* [49] at 1000 Hz and by Bystrov *et al.* [47] for the 300–700 GHz range. These data agree with each other and with the data in Table I except for the slightly higher extraordinary-ray value given by Fontanella *et al.* [49]. No temperature-dependent low-frequency index data were found, but pressure dependence is given by Link *et al.* [50].

Table II was constructed from measurements reported in the literature as well as model predictions [51]. Real-index data ($n$) from 10–83 eV and imaginary-index ($k$) data from 11–83 eV are taken from several sources [19–22]. The measurements by Hanson *et al.* [19], Williams *et al.* [20], and Stephan *et al.* [21] did not distinguish between ordinary- and extraordinary-ray components. These data can be considered to be an "average" for the crystal. Thomas *et al.*'s [22] measurement of ordinary- and extraordinary-ray optical constants for the 11–28 eV region are also included.

Ordinary-ray index data in the 0.115–0.200 μm region are taken from Williams and Arakawa [23], supplemented by measurements of Steinmetz *et al.* [12]. Extraordinary-ray data for this region are obtained by combining ordinary-ray data with the anomalous dispersion data of Chandrasekharan and Damany [24]. Both ordinary- and extraordinary-ray data in the 1400–50,000 $cm^{-1}$ range are calculated from the Sellmeier dispersion relationships (Eq. 1) of Dodge [27]. One value of ordinary-ray absorption coefficient is given by Steinmetz *et al.* [12].

Single [51] and multiphonon [41] lattice-vibration models are used to estimate the complex index of refraction for wavelengths of 7.41 μm and longer. Measurements of Bystrov *et al.* [47], and Fontanella *et al.* [49] are the best available low-frequency index data.

The accuracy of index measurements in the electronic region is relatively poor; estimated errors are approximately 10%. Data from Hanson *et al.*

[19] and Williams *et al.* [20] agree well in the overlap region (20–27 eV). Data from Stephan *et al.* [21] have consistently lower $n$ and higher $k$ compared with other sources [19, 20]. Data from Thomas *et al.* [22] have precision on the order of ±5%.

The real-index data from 0.115–0.200 μm have a quoted accuracy of ±0.002; the dispersion formula of Dodge [27] represents the data from 0.2–7.0 μm within ±0.00002. The accuracy of complex-index data at longer wavelength is unknown, but uncertainty in the values is probably in the least-significant digit reported in Table II (that is, $n$ accurate to ±0.01 and $k$ to about 5%). Low-frequency real-index measurements of Fontanella *et al.* [49] are given an accuracy of ±0.001. Bystrov *et al.* [47] states the accuracy of $n$ to be ±0.005 and $k$ to be within ±5%.

Figures 1 and 2 show a composite of the complex index of refraction based on the data of Table II. Figure 1 gives the ordinary-ray index and Fig. 2 shows the extraordinary-ray properties. Complex index-of-refraction data for the electronic region (wavelengths below 0.05 μm) derived from unpolarized measurements with an unknown mix of ordinary- and extraordinary-ray index are included in Fig. 1.

Tables III and IV give temperature dependence for the real part of the index of refraction. Measurements of $dn/dT$ by Feldman *et al.* [28] typically have a standard deviation to a linear temperature-dependence fit of $0.1 \times 10^{-6}$/K.

## REFERENCES


1. R. W. G. Wyckoff, "Crystal Structures," Interscience Publishers, New York, 251 (1963).
2. A. Duncanson and R. W. H. Stevenson, "Some Properties of Magnesium Fluoride Crystallized from the Melt," *Proc. Phys. Soc. (London)* **72**, 1001 (1958).
3. W. A. Hargreaves, "Magnesium Fluoride Update and Summary of Optical Properties," *Laser focus* **18**, 86 (1982).
4. "Crystal Optics," Catalog OP 101, Harshaw/Filtrol, Solon, Ohio, 26 (1985).
5. "Kodak IRTRAN Infrared Optical Materials," Publication U-72, Eastman Kodak Company, Rochester, New York, (1971).
6. I. V. Men', F. K. Volynets, and Y. P. Smirnaya, "The Emissivity of KO-1 Optical Ceramic," *Sov. J. Opt. Tech.* **41**, 95 (1974).
7. A. L. Olsen and W. R. McBride, "Transmittance of Single-Crystal Magnesium Fluroide and IRTRAN-1 in the 0.2 to 15 $\mu$ Range," *J. Opt. Soc. Am.* **53**, 1003 (1963).
8. L. F. Johnson and H. J. Guggenheim, "Phonon-Terminated Optical Masers," *Phys. Rev.* **149**, 179 (1967).
9. P. F. Moulton, "Pulse-Pumped Operation of Divalent Transition-Metal Lasers," *IEEE J. Quantum Electro.* **QE-18**, 1185 (1982).
10. D. Gormly, M. Bottema, B. Darnell, W. Fowler, and W. Medenica, "Fabrication of $MgF_2$ and LiF Windows for the Hubble Space Telescope Imaging Spectrograph," *Proc. SPIE* **992**, 139 (1988).
11. W. Vishman, A. G. Eubanks, G. F. Pieper, and J. H. Bredekamp, "Photomultiplier Window Materials under Electron Irradiation: Fluorescence and Phosphorescence," *Appl. Opt.* **14**, 2104 (1975).

12. D. L. Steinmetz, W. G. Phillips, M. Wirick, and F. F. Forbes, "Polarizer for the Vacuum Ultraviolet," *Appl. Opt.* **6**, 1001 (1967).
13. G. Hass and W. R. Hunter, "Reflection Polarizers for the Vacuum Ultraviolet Using Al + $MgF_2$ Mirrors and an $MgF_2$ Plate," *Appl. Opt.* **17**, 76 (1978).
14. W. C. Johnson, Jr., "Magnesium Fluoride Polarizing Prism for the Vacuum Ultraviolet," *Rev. Sci. Instrum.* **35**, 1375 (1964).
15. G. C. Morris and A. S. Abramson, "Single Rochon Prisms for Light Polarization Between 1400–70,000 Å," *Appl. Opt.* **8**, 1249 (1969).
16. E. D. Palik, "A $MgF_2$ Soleil Compensator for the Near Infrared," *Appl. Opt.* **7**, 978 (1968).
17. W. R. Hunter, J. F. Osantowski, and G. Hass, "Reflectance of Aluminum Overcoated with $MgF_2$ and LiF in the Wavelength Region from 1600 Å to 300 Å at Various Angles of Incidence," *Appl. Opt.* **10**, 540 (1971).
18. B. Bates and D. J. McCartney, "Optical Properties of Multilayer Overcoated Aluminum Films in the UV (2000–2500 Å)," *Appl. Opt.* **15**, 2216 (1976).
19. W. F. Hanson, E. T. Arakawa, and M. W. Williams, "Optical Properties of MgO and $MgF_2$ in the Extreme Ultraviolet Region," *J. Appl. Phys.* **43**, 1661 (1972).
20. M. W. Williams, R. A. MacRae, and E. T. Arakawa, "Optical Properties of Magnesium Fluoride in the Vacuum Ultraviolet," *J. Appl. Phys.* **38**, 1701 (1967).
21. G. Stephan, Y. Le Calvez, J. C. Lemonier, and S. Robin, "Properties Optiques et Spectre Electronique du $MgF_2$ et du $CaF_2$ de 10 à 48 eV," *J. Phys. Chem. Solids* **30**, 601 (1969).
22. J. Thomas, G. Stephan, J. C. Lemonnier, M. Nisar, and S. Robin, "Optical Anisotropy of $MgF_2$ in Its UV Absorption Region," *Phys. Stat. Solidi B* **56**, 163 (1973).
23. M. W. Williams and E. T. Arakawa, "Optical Properties of Crystalline $MgF_2$ from 115 to 400 nm," *Appl. Opt.* **18**, 1477 (1979).
24. V. Chandrasekharan and H. Damany, "Anomalous Dispersion of Birefringence of Sapphire and Magnesium Fluoride in the Vacuum Ultraviolet," *Appl. Opt.* **8**, 671 (1969).
25. W. L. Wolfe, "Properties of Optical Materials," in "Handbook of Optics" (W. G. Driscoll, ed.), McGraw-Hill, New York, 7–95 (1978).
26. H. H. Li, "Refractive Index of Alkaline Earth Halides and Its Wavelength and Temperature Derivatives," *J. Phys. Chem. Ref. Data* **9**, 161 (1980).
27. M. J. Dodge, "Refractive Properties of Magnesium Fluoride," *Appl. Opt.* **23**, 1980 (1984).
28. A. Feldman, D. Horowitz, R. M. Waxler, and M. J. Dodge, "Optical Materials Characterization Final Technical Report, February 1, 1978–September 30, 1978," National Bureau of Standards Technical Note 993, 49 (February 1979).
29. P. H. Lissberger, A. K. Roy, I. W. Salter, and J. A. Shan, "Thermal and Structural Constraints of Magnesium Fluoride and Zinc Sulphide for Optical Coating Applications," *Opt. Acta* **33**, 925 (1986).
30. D. P. Belanger, A. R. King, and V. Jaccarine, "Temperature Dependence of the Optical Birefringence of $MnF_2$, $MgF_2$, and $ZnF_2$," *Phys. Rev. B* **29**, 2636 (1984).
31. S. Chung, "Photoelastic Properties of Magnesium Fluoride," in "Basic Optical Properties of Materials, Summaries of Papers," National Bureau of Standards Special Publication 574, 213 (May 1980).
32. I. I. Afranas'ev, L. K. Andrianova, I. Y. Mamontov, and V. M. Reiterov "Photoelastic Properties and Residual Stresses in Magnesium Fluoride Crystals," *Sov. Phys. Solid State* **17**, 2006 (1975).
33. D. Smith and P. Baumeister, "Refractive Index of Some Oxide and Fluoride Coating Materials," *Appl. Opt.* **18**, 111 (1979).
34. O. R. Wood II, H. G. Craighead, J. E. Sweeney, and P. J. Maloney, "Vacuum Ultraviolet Loss in Magnesium Fluoride Films," *Appl. Opt.* **23**, 3644 (1984).

35. P. J. Martin, W. G. Sainty, R. P. Netterfield, D. R. McKenzie, D. J. H. Cockayne, S. H. Sie, O. R. Wood, and H. G. Craighead, "Influence of Ion Assistance on the Optical Properties of $MgF_2$," *Appl. Opt.* **26**, 1235 (1987).
36. A. S. Barrière and A. Lachter, "Optical Transitions in Disordered Thin Films of the Ionic Compounds $MgF_2$ and $AlF_3$ as a Function of Their Conditions of Preparation," *Appl. Opt.* **16**, 2865 (1977).
37. J. M. Siqueiros, R. Machorro, and L. E. Regalado, "Determination of the Optical Constants of $MgF_2$ and ZnS from Spectrophotometric Measurements and the Classical Oscillator Method," *Appl. Opt.* **27**, 2549 (1988).
38. M. J. Weber, ed., "CRC Handbook of Laser Science and Technology, Volume 3: Optical Materials; Part 1: Nonlinear Optical Properties/Radiation Damage," CRC Press, Boca Raton, Fla., 304 (1988).
39. W. Viehmann, A. G. Eubanks, G. F. Pieper, and J. H. Bredekamp, "Photomultiplier Window Materials under Electron Irradiation: Fluroescence and Phosphoresence," *Appl. Opt.* **14**, 2104 (1975).
40. T. F. Deutsch, "Absorption Coefficient of Infrared Laser Window Materials," *J. Phys. Chem. Solids* **34**, 2091 (1973).
41. M. E. Thomas, R. I. Joseph, and W. J. Tropf, "Infrared Transmission Properties of Sapphire, Spinel, Yttria, and ALON as a Function of Frequency and Temperature," *Appl. Opt.* **27**, 239 (1988).
42. M. E. Thomas and R. I. Joseph, "A Comprehensive Model for the Intrinsic Transmission Properties of Optical Windows," *Proc. SPIE* **929**, 87 (1988).
43. G. R. Hunt and C. H. Perry, "Far-Infrared Reflectance and Transmittance of Potassium Magnesium Fluoride and Magnesium Fluoride," *Phys. Rev.* **134**, A688 (1964).
44. A. S. Barker, "Transverse and Longitudinal Optic Mode Study in $MgF_2$ and $ZnF_2$," *Phys. Rev.* **136**, A1290 (1964).
45. S. P. S. Porto, P. A. Fleury, and T. C. Damen, "Raman Spectra of $TiO_2$, $MgF_2$, $ZnF_2$, $FeF_2$, and $MnF_2$," *Phys. Rev.* **154**, 522 (1967).
46. J. Giordano and C. Benoit, "Infrared Spectra of Iron, Zinc, and Magnesium Fluorides: I. Analysis of Results," *J. Phys. C: Solid State Phys.* **21**, 2749 (1988).
47. V. P. Bystrov, Y. G. Goncharov, G. V. Kozlov, and A. F. Kupriyanenko, "Dielectric Properties of Optical Crystals at Submillimeter Wavelengths," *Sov. Phys. Tech. Phys.* **31**, 1206 (1986).
48. M. Stead and G. Simonis, "Near Millimeter Wave Characterization of Dual Mode Materials," *Appl. Opt.* **28**, 1874 (1989).
49. J. Fontanella, C. Andeen, and D. Schuele, "Low-Frequency Dielectric Constants of $\alpha$-Quartz, Sapphire, $MgF_2$, and MgO," *J. Appl. Phys.* **45**, 2852 (1974).
50. J. Link, M. C. Wintersgill, J. J. Fontanella, V. E. Bean, and C. G. Andeen, "Pressure Variation of the Low Frequency Dielectric Constants of Some Anisotropic Crystals," *J. Appl. Phys.* **52**, 936 (1981).
51. M. E. Thomas, "A Computer Code for Modeling Optical Properties of Window Materials," *Proc. SPIE* **1112**, 260 (1989).

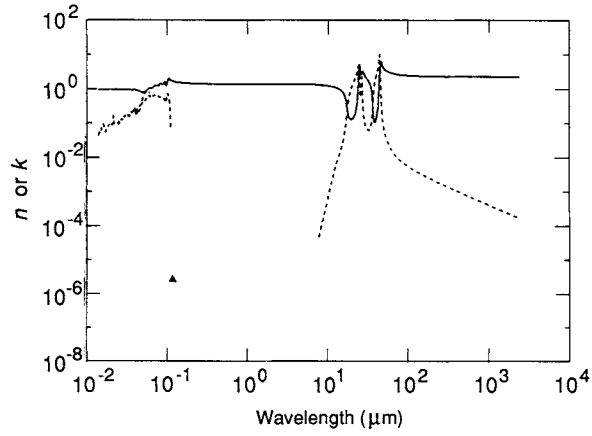


**Fig. 1.** Log–log plot of $n_o$ (solid line) and $k_o$ (dashed line) versus wavelength in micrometers for the ordinary ray of magnesium fluoride. Data below 0.05 μm (electronic region) are combined ordinary- and extraordinary-ray results.

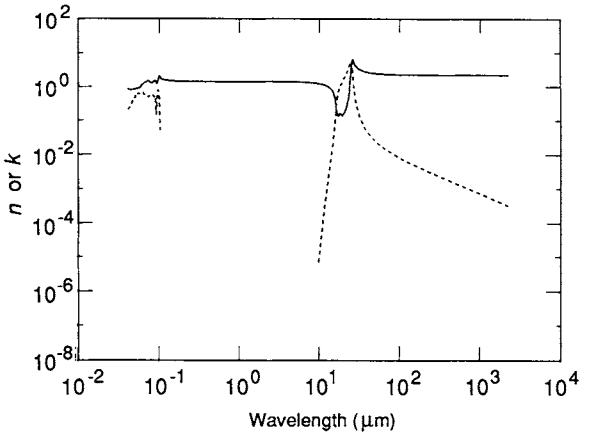


**Fig. 2.** Log–log plot of $n_e$ (solid line) and $k_e$ (dashed line) versus wavelength in micrometers for the extraordinary ray of magnesium fluoride.

**TABLE I**

**Fundamental Infrared Lattice Vibration Parameters for $MgF_2$[a]**

| Mode | Transverse optical frequency ($cm^{-1}$) | Strength | Normalized width | Longitudinal optical frequency ($cm^{-1}$) | Refs. |
|---|---|---|---|---|---|
| | | E ⊥ c axis (ordinary ray) | | | |
| 1 | 247 | 2.22 | 0.014 | 303 | [44] |
| 2 | 410 | 0.19 | 0.033 | 415 | [44] |
| 3 | 450 | 1.14 | 0.058 | 617 | [44] |
| | Total = 3.55 | | | | |
| 1 | 248 | 2.23 | 0.0115 | 302 | [51] |
| 2 | 408.5 | 0.22 | 0.0165 | 414 | [51] |
| 3 | 447 | 1.10 | 0.025 | 621 | [51] |
| 4[b] | 535 | 0.05 | 0.3 | | [51] |
| | Total = 3.60 | | | | |
| 1 | 251 | | | 304 | [46] |
| 2 | 413 | | | 422 | [46] |
| 3 | 452 | | | 610 | [46] |
| | Total = 3.38 | | | | |
| | | E ∥ c axis (extraordinary ray) | | | |
| 1 | 399 | 2.7 | 0.048 | 625 | [44] |
| 2[c] | 556 | 0.01 | 0.08 | | |
| | Total = 2.71 | | | | |
| 1 | 404 | 2.69 | | 626 | [46] |

[a]The frequency ($\nu_j$) is the location of the mode (transverse optical frequency). The strength ($\Delta\epsilon_j$) is the contribution of the mode to the dielectric constant. The normalized width ($\gamma_j$) is the mode width divided by the mode frequency. The complex dielectric constant ($\epsilon$) is then modeled as a function of frequency ($\nu$) by:

$$\epsilon(\nu) = \epsilon_\infty + \sum_j \frac{\Delta\epsilon_j \, \nu_j^2}{\nu_j^2 - \nu^2 + i\gamma_j\nu_j\nu} ,$$

where the $\epsilon_\infty$ term (= 1.886 for E ⊥ c and 1.918 for E ∥ c axis) represents the electronic contributions to the dielectric constant (plus one).

[b]Mode 4 (E ⊥ c) is probably caused by an impurity.

[c]Barker [44] identifies this as a weak forbidden mode.

**TABLE II**

**Values of $n$ and $k$ Obtained from Various References for Magnesium Fluoride[a]**

| eV | $cm^{-1}$ | $\mu m$ | $n$ | $k$ | $n$ | $k$ |
|---|---|---|---|---|---|---|
| 83.0 | 669608 | 0.0149 | 0.906 [19] | 0.046 [19] | | |
| 78.5 | 633511 | 0.0158 | 0.912 | 0.070 | | |
| 76.9 | 620336 | 0.0161 | 0.906 | 0.064 | | |
| 75.5 | 608714 | 0.0164 | 0.906 | 0.081 | | |
| 74.2 | 598809 | 0.0167 | 0.902 | 0.083 | | |
| 72.3 | 583074 | 0.0172 | 0.918 | 0.095 | | |
| 68.5 | 552191 | 0.0181 | 0.902 | 0.055 | | |
| 66.0 | 532322 | 0.0188 | 0.915 | 0.073 | | |
| 65.0 | 524256 | 0.0191 | 0.917 | 0.076 | | |
| 64.0 | 516191 | 0.0194 | 0.919 | 0.079 | | |
| 63.0 | 508125 | 0.0197 | 0.921 | 0.083 | | |
| 62.0 | 500060 | 0.0200 | 0.923 | 0.090 | | |
| 61.0 | 491994 | 0.0203 | 0.924 | 0.095 | | |
| 60.0 | 483929 | 0.0207 | 0.926 | 0.096 | | |
| 59.0 | 475863 | 0.0210 | 0.926 | 0.093 | | |
| 58.0 | 467798 | 0.0214 | 0.925 | 0.090 | | |
| 57.0 | 459732 | 0.0218 | 0.925 | 0.092 | | |
| 56.0 | 451667 | 0.0221 | 0.913 | 0.094 | | |
| 55.0 | 443601 | 0.0225 | 0.936 | 0.165 | | |
| 54.0 | 435536 | 0.0230 | 0.940 | 0.103 | | |
| 53.0 | 427470 | 0.0234 | 0.934 | 0.098 | | |
| 52.0 | 419405 | 0.0238 | 0.930 | 0.098 | | |
| 51.0 | 411339 | 0.0243 | 0.927 | 0.100 | | |
| 50.0 | 403274 | 0.0248 | 0.925 | 0.103 | | |
| 49.0 | 395209 | 0.0253 | 0.922 | 0.107 | | |
| 48.0 | 387143 | 0.0258 | 0.920 | 0.111 | | |
| 47.5 | 383110 | 0.0261 | 0.920 | 0.113 | 0.957 [21] | 0.092 [21] |
| 47.0 | 379078 | 0.0264 | 0.919 | 0.115 | 0.956 | 0.096 |
| 46.5 | 375045 | 0.0267 | 0.919 | 0.118 | 0.955 | 0.099 |
| 46.0 | 371012 | 0.0270 | 0.919 | 0.120 | 0.954 | 0.103 |
| 45.5 | 366979 | 0.0272 | 0.918 | 0.122 | 0.952 | 0.107 |
| 45.0 | 362947 | 0.0276 | 0.918 | 0.125 | 0.949 | 0.110 |
| 44.5 | 358914 | 0.0279 | 0.918 | 0.128 | 0.949 | 0.114 |
| 44.0 | 354881 | 0.0282 | 0.918 | 0.131 | 0.947 | 0.119 |
| 43.5 | 350848 | 0.0285 | 0.918 | 0.134 | 0.942 | 0.125 |
| 43.0 | 346816 | 0.0288 | 0.918 | 0.137 | 0.936 | 0.130 |
| 42.5 | 342783 | 0.0292 | 0.918 | 0.142 | 0.929 | 0.129 |
| 42.0 | 338750 | 0.0295 | 0.918 | 0.145 | 0.922 | 0.129 |
| 41.5 | 334717 | 0.0299 | 0.918 | 0.150 | 0.914 | 0.129 |
| 41.0 | 330685 | 0.0302 | 0.919 | 0.154 | 0.907 | 0.131 |
| 40.5 | 326652 | 0.0306 | 0.919 | 0.159 | 0.899 | 0.139 |
| 40.0 | 322619 | 0.0310 | 0.919 | 0.163 | 0.885 | 0.149 |
| 39.5 | 318586 | 0.0314 | 0.919 | 0.167 | 0.894 | 0.158 |
| 39.0 | 314554 | 0.0318 | 0.920 | 0.171 | 0.894 | 0.169 |

(*continued*)

**TABLE II (*Continued*)**

**Magnesium Fluoride**

| eV | $cm^{-1}$ | $\mu m$ | $n$ | $k$ | $n$ | $k$ |
|---|---|---|---|---|---|---|
| 38.5 | 310521 | 0.0322 | 0.921 | 0.172 | 0.898 | 0.170 |
| 38.0 | 306488 | 0.0326 | 0.922 | 0.173 | 0.902 | 0.168 |
| 37.5 | 302456 | 0.0331 | 0.923 | 0.174 | 0.901 | 0.165 |
| 37.0 | 298423 | 0.0335 | 0.924 | 0.175 | 0.900 | 0.162 |
| 36.5 | 294390 | 0.0340 | 0.921 | 0.175 | 0.899 | 0.160 |
| 36.0 | 290357 | 0.0344 | 0.925 | 0.175 | 0.896 | 0.159 |
| 35.5 | 286325 | 0.0349 | 0.925 | 0.175 | 0.897 | 0.159 |
| 35.0 | 282292 | 0.0354 | 0.925 | 0.175 | 0.898 | 0.162 |
| 34.5 | 278259 | 0.0359 | 0.918 | 0.177 | 0.899 | 0.166 |
| 34.0 | 274226 | 0.0365 | 0.904 | 0.179 | 0.893 | 0.176 |
| 33.5 | 270194 | 0.0370 | 0.898 | 0.183 | 0.890 | 0.188 |
| 33.0 | 266161 | 0.0376 | 0.893 | 0.190 | 0.888 | 0.206 |
| 32.5 | 262128 | 0.0381 | 0.891 | 0.200 | 0.887 | 0.224 |
| 32.0 | 258095 | 0.0387 | 0.897 | 0.210 | 0.880 | 0.221 |
| 31.5 | 254063 | 0.0394 | 0.904 | 0.219 | 0.867 | 0.199 |
| 31.0 | 250030 | 0.0400 | 0.910 | 0.228 | 0.858 | 0.200 |
| 30.5 | 245997 | 0.0407 | 0.910 | 0.232 | 0.857 | 0.235 |
| 30.0 | 241964 | 0.0413 | 0.907 | 0.228 | 0.865 | 0.283 |
| 29.5 | 237932 | 0.0420 | 0.898 | 0.224 | 0.876 | 0.273 |
| 29.0 | 233899 | 0.0428 | 0.885 | 0.221 | 0.873 | 0.184 |
| 28.5 | 229866 | 0.0435 | 0.875 | 0.234 | 0.850 | 0.164 |
| 28.0 | 225833 | 0.0443 | 0.865 | 0.254 | 0.842 | 0.200 |
| 27.5 | 221801 | 0.0451 | 0.855 | 0.264 | 0.841 | 0.232 |
| 27.0 | 217768 | 0.0459 | 0.842 | 0.272 | 0.822 | 0.227 |
| 26.5 | 213735 | 0.0468 | 0.824 | 0.282 | 0.812 | 0.246 |
| 26.0 | 209702 | 0.0477 | 0.805 | 0.308 | 0.801 | 0.267 |
| 25.5 | 205670 | 0.0486 | 0.789 | 0.336 | 0.787 | 0.294 |
| 25.0 | 201637 | 0.0496 | 0.779 | 0.384 | 0.771 | 0.324 |
| 24.5 | 197604 | 0.0506 | 0.769 | 0.443 | 0.758 | 0.361 |
| 24.0 | 193572 | 0.0517 | 0.788 | 0.524 | 0.736 | 0.410 |
| 23.5 | 189539 | 0.0528 | 0.816 | 0.610 | 0.742 | 0.445 |
| 23.0 | 185506 | 0.0539 | 0.856 | 0.666 | 0.765 | 0.475 |
| 22.5 | 181473 | 0.0551 | 0.900 | 0.729 | 0.820 | 0.546 |
| 22.0 | 177441 | 0.0564 | 0.946 | 0.771 | 0.849 | 0.564 |
| 21.5 | 173408 | 0.0577 | 1.012 | 0.807 | 0.898 | 0.624 |
| 21.0 | 169375 | 0.0590 | 1.102 | 0.819 | 0.891 | 0.616 |
| 20.5 | 165342 | 0.0605 | 1.184 | 0.805 | 0.965 | 0.643 |
| 20.0 | 161310 | 0.0620 | 1.266 | 0.767 | 0.981 | 0.646 |
| 19.8 | 159697 | 0.0626 | | | 0.995 | 0.642 |
| 19.6 | 158083 | 0.0633 | | | 1.000 | 0.645 |
| 19.4 | 156470 | 0.0639 | | | 0.996 | 0.615 |
| 19.2 | 154857 | 0.0646 | | | 1.001 | 0.605 |
| 19.0 | 153244 | 0.0653 | | | 1.012 | 0.615 |
| 18.8 | 151631 | 0.0659 | | | 1.021 | 0.618 |

(*continued*)

**TABLE II (*Continued*)**

**Magnesium Fluoride**

| eV | $cm^{-1}$ | $\mu m$ | $n$ | $k$ | $n$ | $k$ |
|---|---|---|---|---|---|---|
| 18.6 | 150018 | 0.0667 | | | 1.034 | 0.626 |
| 18.4 | 148405 | 0.0674 | | | 1.048 | 0.636 |
| 18.2 | 146792 | 0.0681 | | | 1.072 | 0.661 |
| 18.0 | 145179 | 0.0689 | 1.322 [20] | 0.671 [20] | 1.093 | 0.651 |
| 17.8 | 143566 | 0.0697 | 1.337 | 0.658 | 1.095 | 0.654 |
| 17.6 | 141952 | 0.0704 | 1.347 | 0.657 | 1.103 | 0.661 |
| 17.4 | 140339 | 0.0713 | 1.356 | 0.660 | 1.114 | 0.660 |
| 17.2 | 138726 | 0.0721 | 1.359 | 0.665 | 1.090 | 0.665 |
| 17.0 | 137113 | 0.0729 | 1.354 | 0.661 | 1.080 | 0.663 |
| 16.8 | 135500 | 0.0738 | 1.348 | 0.605 | 1.108 | 0.670 |
| 16.6 | 133887 | 0.0747 | 1.346 | 0.631 | 1.143 | 0.676 |
| 16.4 | 132274 | 0.0756 | 1.369 | 0.606 | 1.180 | 0.689 |
| 16.2 | 130661 | 0.0765 | 1.387 | 0.575 | 1.195 | 0.664 |
| 16.0 | 129048 | 0.0775 | 1.435 | 0.547 | 1.196 | 0.639 |
| 15.9 | 128241 | 0.0780 | 1.449 | 0.539 | 1.195 | 0.630 |
| 15.8 | 127435 | 0.0785 | 1.457 | 0.533 | 1.195 | 0.625 |
| 15.7 | 126628 | 0.0790 | 1.465 | 0.528 | 1.193 | 0.623 |
| 15.6 | 125821 | 0.0795 | 1.474 | 0.529 | 1.191 | 0.620 |
| 15.5 | 125015 | 0.0800 | 1.483 | 0.529 | 1.190 | 0.617 |
| 15.4 | 124208 | 0.0805 | 1.490 | 0.531 | 1.196 | 0.623 |
| 15.3 | 123402 | 0.0810 | 1.495 | 0.533 | 1.209 | 0.631 |
| 15.2 | 122595 | 0.0816 | 1.500 | 0.536 | 1.228 | 0.635 |
| 15.1 | 121789 | 0.0821 | 1.505 | 0.538 | 1.248 | 0.638 |
| 15.0 | 120982 | 0.0827 | 1.508 | 0.533 | 1.256 | 0.630 |
| 14.9 | 120176 | 0.0832 | 1.510 | 0.520 | 1.257 | 0.622 |
| 14.8 | 119369 | 0.0838 | 1.512 | 0.510 | 1.257 | 0.614 |
| 14.7 | 118563 | 0.0843 | 1.513 | 0.501 | 1.257 | 0.608 |
| 14.6 | 117756 | 0.0849 | 1.508 | 0.501 | 1.258 | 0.602 |
| 14.5 | 116949 | 0.0855 | 1.498 | 0.502 | 1.262 | 0.600 |
| 14.4 | 116143 | 0.0861 | 1.488 | 0.504 | 1.268 | 0.596 |
| 14.3 | 115336 | 0.0867 | 1.481 | 0.514 | 1.268 | 0.595 |
| 14.2 | 114530 | 0.0873 | 1.470 | 0.518 | 1.260 | 0.598 |
| 14.1 | 113723 | 0.0879 | 1.473 | 0.517 | 1.250 | 0.602 |
| 14.0 | 112917 | 0.0886 | 1.496 | 0.507 | 1.237 | 0.607 |
| 13.9 | 112110 | 0.0892 | 1.520 | 0.496 | 1.234 | 0.607 |
| 13.8 | 111304 | 0.0898 | 1.541 | 0.484 | 1.231 | 0.608 |
| 13.7 | 110497 | 0.0905 | 1.561 | 0.473 | 1.236 | 0.605 |
| 13.6 | 109691 | 0.0912 | 1.573 | 0.463 | 1.239 | 0.606 |
| 13.5 | 108884 | 0.0918 | 1.584 | 0.453 | 1.242 | 0.606 |
| 13.4 | 108077 | 0.0925 | 1.588 | 0.444 | 1.235 | 0.603 |
| 13.3 | 107271 | 0.0932 | 1.585 | 0.448 | 1.225 | 0.594 |
| 13.2 | 106464 | 0.0939 | 1.562 | 0.453 | 1.215 | 0.585 |
| 13.1 | 105658 | 0.0946 | 1.555 | 0.454 | 1.202 | 0.577 |
| 13.0 | 104851 | 0.0954 | 1.561 | 0.429 | 1.192 | 0.568 |

(*continued*)

**TABLE II (*Continued*)**

**Magnesium Fluoride**

| eV | $cm^{-1}$ | $\mu$m | $n$ | $k$ | $n$ | $k$ |
|---|---|---|---|---|---|---|
| 12.9 | 104045 | 0.0961 | 1.566 | 0.393 | 1.192 | 0.553 |
| 12.8 | 103238 | 0.0969 | 1.579 | 0.357 | 1.240 | 0.530 |
| 12.7 | 102432 | 0.0976 | 1.574 | 0.332 | 1.297 | 0.526 |
| 12.6 | 101625 | 0.0984 | 1.501 | 0.329 | 1.272 | 0.558 |
| 12.5 | 100818 | 0.0992 | 1.409 | 0.364 | 1.258 | 0.593 |
| 12.4 | 100012 | 0.1000 | 1.330 | 0.409 | 1.232 | 0.636 |
| 12.3 | 99205 | 0.1008 | 1.269 | 0.451 | 1.212 | 0.676 |
| 12.2 | 98399 | 0.1016 | 1.231 | 0.491 | 1.194 | 0.717 |
| 12.1 | 97592 | 0.1025 | 1.207 | 0.542 | 1.177 | 0.758 |
| 12.0 | 96786 | 0.1033 | 1.351 | 0.723 | 1.176 | 0.790 |
| 11.9 | 95979 | 0.1042 | 1.603 | 0.953 | 1.235 | 0.828 |
| 11.8 | 95173 | 0.1051 | 1.759 | 1.073 | 1.343 | 0.834 |
| 11.7 | 94366 | 0.1060 | 1.872 | 1.024 | 1.477 | 0.831 |
| 11.6 | 93560 | 0.1069 | 2.201 | 0.807 | 1.573 | 0.822 |
| 11.5 | 92753 | 0.1078 | 2.258 | 0.683 | 1.617 | 0.826 |
| 11.4 | 91946 | 0.1088 | 2.245 | 0.524 | 1.645 | 0.793 |
| 11.3 | 91140 | 0.1097 | 2.219 | 0.332 | 1.689 | 0.640 |
| 11.2 | 90333 | 0.1107 | 2.123 | 0.220 | 1.671 | 0.478 |
| 11.1 | 89527 | 0.1117 | 2.010 | 0.110 | 1.590 | 0.341 |
| 11.0 | 88720 | 0.1127 | 1.956 | 0.058 | 1.519 | 0.197 |
| 10.9 | 87914 | 0.1137 | 1.904 | | 1.490 | 0.028 |
| 10.8 | 87107 | 0.1148 | 1.883 | | 1.480 | |
| 10.7 | 86301 | 0.1159 | 1.812 | | 1.469 | |
| 10.6 | 85494 | 0.1170 | 1.773 | | 1.463 | |
| 10.5 | 84688 | 0.1181 | 1.734 | | 1.459 | |
| 10.4 | 83881 | 0.1192 | 1.694 | | 1.456 | |
| 10.3 | 83074 | 0.1204 | 1.660 | | 1.453 | |
| 10.2 | 82268 | 0.1216 | 1.630 | | 1.449 | |
| 10.1 | 81461 | 0.1228 | 1.615 | | 1.446 | |
| 10.0 | 80655 | 0.1240 | 1.601 | | 1.443 | |

| eV | $cm^{-1}$ | $\mu$m | $n_o$ | $k_o$ | $n_e$ | $k_e$ |
|---|---|---|---|---|---|---|
| 27.0 | 217768 | 0.0459 | 0.811 [22] | 0.214 [22] | 0.832 [22] | 0.214 [22] |
| 26.5 | 213735 | 0.0468 | 0.796 | 0.240 | 0.816 | 0.223 |
| 26.0 | 209702 | 0.0477 | 0.784 | 0.282 | 0.803 | 0.241 |
| 25.5 | 205670 | 0.0486 | 0.770 | 0.322 | 0.790 | 0.261 |
| 25.0 | 201637 | 0.0496 | 0.765 | 0.361 | 0.794 | 0.289 |
| 24.5 | 197604 | 0.0506 | 0.756 | 0.398 | 0.799 | 0.332 |
| 24.0 | 193572 | 0.0517 | 0.763 | 0.422 | 0.807 | 0.369 |
| 23.5 | 189539 | 0.0528 | 0.774 | 0.441 | 0.816 | 0.405 |
| 23.0 | 185506 | 0.0539 | 0.790 | 0.456 | 0.827 | 0.441 |
| 22.5 | 181473 | 0.0551 | 0.809 | 0.469 | 0.837 | 0.468 |
| 22.0 | 177441 | 0.0564 | 0.837 | 0.493 | 0.847 | 0.598 |

(*continued*)

**TABLE II (*Continued*)**

**Magnesium Fluoride**

| eV | $cm^{-1}$ | $\mu m$ | $n_o$ | $k_o$ | $n_e$ | $k_e$ |
|---|---|---|---|---|---|---|
| 21.5 | 173408 | 0.0577 | 0.886 | 0.545 | 0.866 | 0.588 |
| 21.0 | 169375 | 0.0590 | 0.959 | 0.600 | 0.881 | 0.614 |
| 20.5 | 165342 | 0.0605 | 1.003 | 0.607 | 0.894 | 0.612 |
| 20.0 | 161310 | 0.0620 | 1.010 | 0.610 | 0.905 | 0.607 |
| 19.5 | 157277 | 0.0636 | 1.006 | 0.541 | 0.919 | 0.607 |
| 19.0 | 153244 | 0.0653 | 1.000 | 0.540 | 0.983 | 0.623 |
| 18.5 | 149211 | 0.0670 | 1.008 | 0.572 | 1.117 | 0.652 |
| 18.0 | 145179 | 0.0689 | 1.080 | 0.604 | 1.151 | 0.652 |
| 17.5 | 141146 | 0.0708 | 1.180 | 0.627 | 1.264 | 0.620 |
| 17.0 | 137113 | 0.0729 | 1.189 | 0.632 | 1.317 | 0.575 |
| 16.5 | 133080 | 0.0751 | 1.186 | 0.626 | 1.353 | 0.561 |
| 16.0 | 129048 | 0.0775 | 1.184 | 0.608 | 1.416 | 0.556 |
| 15.5 | 125015 | 0.0800 | 1.192 | 0.581 | 1.513 | 0.496 |
| 15.0 | 120982 | 0.0827 | 1.354 | 0.555 | 1.387 | 0.508 |
| 14.5 | 116949 | 0.0855 | 1.342 | 0.548 | 1.299 | 0.550 |
| 14.0 | 112917 | 0.0886 | 1.257 | 0.529 | 1.272 | 0.520 |
| 13.5 | 108884 | 0.0918 | 1.343 | 0.514 | 1.348 | 0.538 |
| 13.0 | 104851 | 0.0954 | 1.546 | 0.467 | 1.449 | 0.504 |
| 12.8 | 103238 | 0.0969 | 1.281 | 0.386 | 1.423 | 0.463 |
| 12.6 | 101625 | 0.0984 | 1.162 | 0.405 | 1.419 | 0.485 |
| 12.4 | 100012 | 0.1000 | 1.222 | 0.545 | 1.470 | 0.224 |
| 12.2 | 98399 | 0.1016 | 1.465 | 0.709 | 1.346 | 0.151 |
| 12.0 | 96786 | 0.1033 | 1.693 | 0.714 | 1.223 | 0.462 |
| 11.8 | 95173 | 0.1051 | 1.923 | 0.620 | 1.343 | 0.752 |
| 11.6 | 93560 | 0.1069 | 1.943 | 0.515 | 1.636 | 0.777 |
| 11.4 | 91946 | 0.1088 | 1.834 | 0.380 | 1.911 | 0.612 |
| 11.2 | 90333 | 0.1107 | 1.701 | 0.241 | 1.988 | 0.401 |
| 11.0 | 88720 | 0.1127 | 1.538 | 0.063 | 1.931 | 0.054 |
| 10.9 | 87914 | 0.1137 | | | 1.892 | |
| 10.8 | 87107 | 0.1148 | | | 1.776 | |
| 10.781 | 86957 | 0.115 | 1.714 [23] | | 1.694[b] | |
| 10.7 | 86301 | 0.1159 | | | 1.657 [22] | |
| 10.332 | 83333 | 0.120 | 1.626 | | 1.626[b] | |
| 10.230 | 82508 | 0.1212 | | $3.3 \cdot 10^{-6}$ [12] | | |
| 9.919 | 80000 | 0.125 | 1.588 | | 1.597[b] | |
| 9.537 | 76923 | 0.130 | 1.555 | | 1.567[b] | |
| 8.856 | 71429 | 0.140 | 1.513 | | 1.527[b] | |
| 8.266 | 66667 | 0.150 | 1.484 | | 1.498[b] | |
| 7.749 | 62500 | 0.160 | 1.464 | | 1.478[b] | |
| 7.293 | 58824 | 0.170 | 1.451 | | 1.465[b] | |
| 6.965 | 56180 | 0.1780 | 1.43975 [12] | | 1.45365 [12] | |
| 6.888 | 55556 | 0.180 | 1.440 [23] | | | |
| 6.702 | 54054 | 0.1850 | 1.43424 [12] | | 1.44797 | |
| 6.526 | 52632 | 0.190 | 1.430 [23] | | | |

(*continued*)

**TABLE II (*Continued*)**

**Magnesium Fluoride**

| eV | $cm^{-1}$ | $\mu m$ | $n_o$ | $k_o$ | $n_e$ | $k_e$ |
|---|---|---|---|---|---|---|
| 6.199 | 50000 | 0.200 | 1.42309 [27] | | 1.43657 [27] | |
| 5.904 | 47619 | 0.210 | 1.41754 | | 1.43085 | |
| 5.636 | 45455 | 0.220 | 1.41291 | | 1.42608 | |
| 5.391 | 43478 | 0.230 | 1.40900 | | 1.42204 | |
| 5.166 | 41667 | 0.240 | 1.40567 | | 1.41859 | |
| 4.959 | 40000 | 0.250 | 1.40280 | | 1.41562 | |
| 4.769 | 38462 | 0.260 | 1.40030 | | 1.41303 | |
| 4.592 | 37037 | 0.270 | 1.39812 | | 1.41077 | |
| 4.428 | 35714 | 0.280 | 1.39620 | | 1.40877 | |
| 4.275 | 34483 | 0.290 | 1.39450 | | 1.40700 | |
| 4.133 | 33333 | 0.300 | 1.39298 | | 1.40543 | |
| 4.000 | 32258 | 0.310 | 1.39162 | | 1.40402 | |
| 3.875 | 31250 | 0.320 | 1.39040 | | 1.40275 | |
| 3.757 | 30303 | 0.330 | 1.38930 | | 1.40160 | |
| 3.647 | 29412 | 0.340 | 1.38830 | | 1.40056 | |
| 3.542 | 28571 | 0.350 | 1.38739 | | 1.39961 | |
| 3.444 | 27778 | 0.360 | 1.38656 | | 1.39875 | |
| 3.351 | 27027 | 0.370 | 1.38580 | | 1.39796 | |
| 3.263 | 26316 | 0.380 | 1.38510 | | 1.39723 | |
| 3.179 | 25641 | 0.390 | 1.38446 | | 1.39656 | |
| 3.100 | 25000 | 0.400 | 1.38387 | | 1.39594 | |
| 2.952 | 23810 | 0.420 | 1.38281 | | 1.39484 | |
| 2.818 | 22727 | 0.440 | 1.38189 | | 1.39389 | |
| 2.695 | 21739 | 0.460 | 1.38110 | | 1.39306 | |
| 2.583 | 20833 | 0.480 | 1.38040 | | 1.39233 | |
| 2.480 | 20000 | 0.500 | 1.37978 | | 1.39168 | |
| 2.384 | 19231 | 0.520 | 1.37923 | | 1.39111 | |
| 2.296 | 18519 | 0.540 | 1.37873 | | 1.39059 | |
| 2.214 | 17857 | 0.560 | 1.37829 | | 1.39013 | |
| 2.138 | 17241 | 0.580 | 1.37789 | | 1.38971 | |
| 2.066 | 16667 | 0.600 | 1.37752 | | 1.38932 | |
| 2.000 | 16129 | 0.620 | 1.37718 | | 1.38897 | |
| 1.937 | 15625 | 0.640 | 1.37688 | | 1.38865 | |
| 1.879 | 15152 | 0.660 | 1.37659 | | 1.38835 | |
| 1.823 | 14706 | 0.680 | 1.37633 | | 1.38808 | |
| 1.771 | 14286 | 0.700 | 1.37608 | | 1.38782 | |
| 1.722 | 13889 | 0.720 | 1.37585 | | 1.38758 | |
| 1.675 | 13514 | 0.740 | 1.37563 | | 1.38735 | |
| 1.631 | 13158 | 0.760 | 1.37543 | | 1.38714 | |
| 1.590 | 12821 | 0.780 | 1.37524 | | 1.38693 | |
| 1.550 | 12500 | 0.800 | 1.37506 | | 1.38674 | |
| 1.512 | 12195 | 0.820 | 1.37488 | | 1.38656 | |
| 1.476 | 11905 | 0.840 | 1.37472 | | 1.38639 | |
| 1.442 | 11628 | 0.860 | 1.37456 | | 1.38622 | |

(*continued*)

**TABLE II (*Continued*)**

**Magnesium Fluoride**

| eV | $cm^{-1}$ | $\mu m$ | $n_o$ | $k_o$ | $n_e$ | $k_e$ |
|---|---|---|---|---|---|---|
| 1.409 | 11364 | 0.880 | 1.37440 | | 1.38606 | |
| 1.378 | 11111 | 0.900 | 1.37426 | | 1.38590 | |
| 1.348 | 10870 | 0.920 | 1.37411 | | 1.38575 | |
| 1.319 | 10638 | 0.940 | 1.37398 | | 1.38561 | |
| 1.292 | 10417 | 0.960 | 1.37384 | | 1.38546 | |
| 1.265 | 10204 | 0.980 | 1.37371 | | 1.38533 | |
| 1.240 | 10000 | 1.0000 | 1.37358 | | 1.38519 | |
| 1.215 | 9800 | 1.0204 | 1.37346 | | 1.38506 | |
| 1.190 | 9600 | 1.0417 | 1.37333 | | 1.38492 | |
| 1.165 | 9400 | 1.0638 | 1.37319 | | 1.38478 | |
| 1.141 | 9200 | 1.0870 | 1.37306 | | 1.38464 | |
| 1.116 | 9000 | 1.1111 | 1.37292 | | 1.38449 | |
| 1.091 | 8800 | 1.1364 | 1.37277 | | 1.38434 | |
| 1.066 | 8600 | 1.1628 | 1.37263 | | 1.38418 | |
| 1.041 | 8400 | 1.1905 | 1.37247 | | 1.38402 | |
| 1.017 | 8200 | 1.2195 | 1.37231 | | 1.38385 | |
| 0.9919 | 8000 | 1.2500 | 1.37215 | | 1.38367 | |
| 0.9671 | 7800 | 1.2821 | 1.37197 | | 1.38349 | |
| 0.9423 | 7600 | 1.3158 | 1.37179 | | 1.38329 | |
| 0.9175 | 7400 | 1.3514 | 1.37160 | | 1.38309 | |
| 0.8927 | 7200 | 1.3889 | 1.37140 | | 1.38287 | |
| 0.8679 | 7000 | 1.4286 | 1.37118 | | 1.38265 | |
| 0.8431 | 6800 | 1.4706 | 1.37096 | | 1.38240 | |
| 0.8183 | 6600 | 1.5152 | 1.37071 | | 1.38214 | |
| 0.7935 | 6400 | 1.5625 | 1.37045 | | 1.38186 | |
| 0.7687 | 6200 | 1.6129 | 1.37017 | | 1.38156 | |
| 0.7439 | 6000 | 1.6667 | 1.36986 | | 1.38124 | |
| 0.7191 | 5800 | 1.7241 | 1.36953 | | 1.38088 | |
| 0.6943 | 5600 | 1.7857 | 1.36917 | | 1.38049 | |
| 0.6695 | 5400 | 1.8519 | 1.36877 | | 1.38007 | |
| 0.6447 | 5200 | 1.9231 | 1.36833 | | 1.37960 | |
| 0.6199 | 5000 | 2.0000 | 1.36784 | | 1.37907 | |
| 0.6075 | 4900 | 2.0408 | 1.36757 | | 1.37879 | |
| 0.5951 | 4800 | 2.0833 | 1.36729 | | 1.37849 | |
| 0.5827 | 4700 | 2.1277 | 1.36699 | | 1.37817 | |
| 0.5703 | 4600 | 2.1739 | 1.36667 | | 1.37783 | |
| 0.5579 | 4500 | 2.2222 | 1.36633 | | 1.37747 | |
| 0.5455 | 4400 | 2.2727 | 1.36597 | | 1.37708 | |
| 0.5331 | 4300 | 2.3256 | 1.36559 | | 1.37667 | |
| 0.5207 | 4200 | 2.3810 | 1.36518 | | 1.37623 | |
| 0.5083 | 4100 | 2.4390 | 1.36474 | | 1.37576 | |
| 0.4959 | 4000 | 2.5000 | 1.36426 | | 1.37525 | |
| 0.4835 | 3900 | 2.5641 | 1.36375 | | 1.37471 | |
| 0.4711 | 3800 | 2.6316 | 1.36320 | | 1.37412 | |

(*continued*)

**TABLE II (*Continued*)**

**Magnesium Fluoride**

| eV | $cm^{-1}$ | $\mu m$ | $n_o$ | $k_o$ | $n_e$ | $k_e$ |
|---|---|---|---|---|---|---|
| 0.4587 | 3700 | 2.7027 | 1.36261 | | 1.37348 | |
| 0.4463 | 3600 | 2.7778 | 1.36196 | | 1.37279 | |
| 0.4339 | 3500 | 2.8571 | 1.36126 | | 1.37204 | |
| 0.4215 | 3400 | 2.9412 | 1.36049 | | 1.37122 | |
| 0.4092 | 3300 | 3.0303 | 1.35966 | | 1.37033 | |
| 0.3968 | 3200 | 3.1250 | 1.35874 | | 1.36934 | |
| 0.3844 | 3100 | 3.2258 | 1.35773 | | 1.36827 | |
| 0.3720 | 3000 | 3.3333 | 1.35662 | | 1.36707 | |
| 0.3596 | 2900 | 3.4483 | 1.35539 | | 1.36575 | |
| 0.3472 | 2800 | 3.5714 | 1.35402 | | 1.36429 | |
| 0.3348 | 2700 | 3.7037 | 1.35249 | | 1.36265 | |
| 0.3224 | 2600 | 3.8462 | 1.35077 | | 1.36080 | |
| 0.3100 | 2500 | 4.0000 | 1.34883 | | 1.35873 | |
| 0.2976 | 2400 | 4.1667 | 1.34663 | | 1.35637 | |
| 0.2852 | 2300 | 4.3478 | 1.34412 | | 1.35369 | |
| 0.2728 | 2200 | 4.5455 | 1.34125 | | 1.35060 | |
| 0.2604 | 2100 | 4.7619 | 1.33792 | | 1.34704 | |
| 0.2480 | 2000 | 5.0000 | 1.33404 | $4.2 \cdot 10^{-7}$ [51] | 1.34288 | |
| 0.2418 | 1950 | 5.1282 | 1.33186 | $6.0 \cdot 10^{-7}$ | 1.34054 | |
| 0.2356 | 1900 | 5.2632 | 1.32948 | $8.5 \cdot 10^{-7}$ | 1.33799 | |
| 0.2294 | 1850 | 5.4054 | 1.32689 | $1.2 \cdot 10^{-6}$ | 1.33521 | |
| 0.2232 | 1800 | 5.5556 | 1.32406 | $1.7 \cdot 10^{-6}$ | 1.33217 | |
| 0.2170 | 1750 | 5.7143 | 1.32096 | $2.5 \cdot 10^{-6}$ | 1.32885 | |
| 0.2108 | 1700 | 5.8824 | 1.31754 | $3.6 \cdot 10^{-6}$ | 1.32518 | |
| 0.2046 | 1650 | 6.0606 | 1.31378 | $5.1 \cdot 10^{-6}$ | 1.32114 | |
| 0.1984 | 1600 | 6.2500 | 1.30961 | $7.4 \cdot 10^{-6}$ | 1.31666 | |
| 0.1922 | 1550 | 6.4516 | 1.30497 | $1.1 \cdot 10^{-5}$ | 1.31168 | |
| 0.1860 | 1500 | 6.6667 | 1.29978 | $1.6 \cdot 10^{-5}$ | 1.30611 | |
| 0.1798 | 1450 | 6.8966 | 1.29396 | $2.4 \cdot 10^{-5}$ | 1.29986 | |
| 0.1736 | 1400 | 7.1429 | 1.28740 | $3.7 \cdot 10^{-5}$ | 1.29280 | |
| 0.1674 | 1350 | 7.4074 | 1.281 [51] | $5.7 \cdot 10^{-5}$ | 1.288 [51] | |
| 0.1612 | 1300 | 7.6923 | 1.273 | $8.6 \cdot 10^{-5}$ | 1.279 | |
| 0.1550 | 1250 | 8.0000 | 1.264 | $1.3 \cdot 10^{-4}$ | 1.269 | |
| 0.1488 | 1200 | 8.3333 | 1.252 | $1.9 \cdot 10^{-4}$ | 1.257 | |
| 0.1426 | 1150 | 8.6957 | 1.240 | $2.8 \cdot 10^{-4}$ | 1.243 | |
| 0.1364 | 1100 | 9.0909 | 1.224 | $4.4 \cdot 10^{-4}$ | 1.227 | |
| 0.1302 | 1050 | 9.5238 | 1.206 | $7.1 \cdot 10^{-4}$ | 1.208 | |
| 0.1240 | 1000 | 10.0000 | 1.18 | $1.2 \cdot 10^{-3}$ | 1.18 | |
| 0.1215 | 980 | 10.204 | 1.17 | $1.5 \cdot 10^{-3}$ | 1.17 | |
| 0.1190 | 960 | 10.417 | 1.16 | $1.9 \cdot 10^{-3}$ | 1.16 | |
| 0.1165 | 940 | 10.638 | 1.15 | $2.4 \cdot 10^{-3}$ | 1.15 | |
| 0.1141 | 920 | 10.870 | 1.14 | $3.0 \cdot 10^{-3}$ | 1.13 | |
| 0.1116 | 900 | 11.111 | 1.12 | $3.7 \cdot 10^{-3}$ | 1.12 | |
| 0.1091 | 880 | 11.364 | 1.11 | $4.6 \cdot 10^{-3}$ | 1.10 | |

(*continued*)

**TABLE II (*Continued*)**

**Magnesium Fluoride**

| eV | $cm^{-1}$ | $\mu m$ | $n_o$ | $k_o$ | $n_e$ | $k_e$ |
|---|---|---|---|---|---|---|
| 0.1066 | 860 | 11.628 | 1.09 | $5.7 \cdot 10^{-3}$ | 1.08 | |
| 0.1041 | 840 | 11.905 | 1.07 | $6.9 \cdot 10^{-3}$ | 1.06 | |
| 0.1017 | 820 | 12.195 | 1.04 | $8.4 \cdot 10^{-3}$ | 1.04 | |
| 0.0992 | 800 | 12.500 | 1.02 | 0.010 | 1.01 | |
| 0.0967 | 780 | 12.821 | 0.99 | 0.012 | 0.98 | |
| 0.0942 | 760 | 13.158 | 0.95 | 0.015 | 0.94 | |
| 0.0917 | 740 | 13.514 | 0.91 | 0.018 | 0.89 | |
| 0.0893 | 720 | 13.889 | 0.86 | 0.022 | 0.84 | $7.2 \cdot 10^{-3}$ [51] |
| 0.0868 | 700 | 14.286 | 0.79 | 0.029 | 0.78 | 0.012 |
| 0.0843 | 680 | 14.706 | 0.71 | 0.041 | 0.69 | 0.021 |
| 0.0818 | 660 | 15.152 | 0.61 | 0.062 | 0.58 | 0.039 |
| 0.0794 | 640 | 15.625 | 0.47 | 0.11 | 0.43 | 0.084 |
| 0.0769 | 620 | 16.129 | 0.28 | 0.24 | 0.22 | 0.26 |
| 0.0744 | 600 | 16.667 | 0.17 | 0.50 | 0.14 | 0.53 |
| 0.0719 | 580 | 17.241 | 0.14 | 0.73 | 0.14 | 0.76 |
| 0.0694 | 560 | 17.857 | 0.14 | 0.96 | 0.16 | 0.95 |
| 0.0670 | 540 | 18.519 | 0.14 | 1.2 | 0.15 | 1.1 |
| 0.0645 | 520 | 19.231 | 0.15 | 1.5 | 0.14 | 1.4 |
| 0.0620 | 500 | 20.000 | 0.17 | 1.9 | 0.15 | 1.7 |
| 0.0608 | 490 | 20.408 | 0.21 | 2.2 | 0.17 | 1.8 |
| 0.0595 | 480 | 20.833 | 0.27 | 2.5 | 0.19 | 2.0 |
| 0.0583 | 470 | 21.277 | 0.42 | 3.1 | 0.23 | 2.2 |
| 0.0570 | 460 | 21.739 | 0.86 | 4.0 | 0.27 | 2.5 |
| 0.0558 | 450 | 22.222 | 3.11 | 5.3 | 0.34 | 2.8 |
| 0.0546 | 440 | 22.727 | 4.97 | 1.8 | 0.46 | 3.2 |
| 0.0533 | 430 | 23.256 | 3.58 | 0.68 | 0.66 | 3.7 |
| 0.0521 | 420 | 23.810 | 2.59 | 0.58 | 1.08 | 4.4 |
| 0.0508 | 410 | 24.390 | 2.70 | 2.2 | 2.19 | 5.5 |
| 0.0496 | 400 | 25.000 | 3.30 | 0.39 | 5.09 | 5.5 |
| 0.0484 | 390 | 25.641 | 2.74 | 0.17 | 6.07 | 2.5 |
| 0.0471 | 380 | 26.316 | 2.43 | 0.12 | 5.15 | 1.1 |
| 0.0459 | 370 | 27.027 | 2.21 | 0.091 | 4.45 | 0.62 |
| 0.0446 | 360 | 27.778 | 2.02 | 0.078 | 3.98 | 0.40 |
| 0.0434 | 350 | 28.571 | 1.84 | 0.070 | 3.65 | 0.28 |
| 0.0422 | 340 | 29.412 | 1.66 | 0.068 | 3.41 | 0.21 |
| 0.0409 | 330 | 30.303 | 1.46 | 0.071 | 3.22 | 0.16 |
| 0.0397 | 320 | 31.250 | 1.20 | 0.083 | 3.07 | 0.13 |
| 0.0384 | 310 | 32.258 | 0.81 | 0.13 | 2.95 | 0.11 |
| 0.0372 | 300 | 33.333 | 0.18 | 0.64 | 2.85 | 0.090 |
| 0.0360 | 290 | 34.483 | 0.11 | 1.3 | 2.76 | 0.076 |
| 0.0347 | 280 | 35.714 | 0.11 | 2.0 | 2.69 | 0.065 |
| 0.0335 | 270 | 37.037 | 0.15 | 2.8 | 2.63 | 0.057 |
| 0.0322 | 260 | 38.462 | 0.32 | 4.3 | 2.57 | 0.050 |
| 0.0310 | 250 | 40.000 | 3.25 | 9.9 | 2.52 | 0.044 |

(*continued*)

**TABLE II (*Continued*)**

**Magnesium Fluoride**

| eV | $cm^{-1}$ | μm | $n_o$ | $k_o$ | $n_e$ | $k_e$ |
|---|---|---|---|---|---|---|
| 0.0298 | 240 | 41.667 | 6.19 | 0.49 | 2.48 | 0.039 |
| 0.0285 | 230 | 43.478 | 4.43 | 0.14 | 2.44 | 0.034 |
| 0.0273 | 220 | 45.455 | 3.76 | 0.072 | 2.41 | 0.031 |
| 0.0260 | 210 | 47.619 | 3.40 | 0.045 | 2.38 | 0.027 |
| 0.0248 | 200 | 50.000 | 3.16 | 0.032 | 2.35 | 0.025 |
| 0.0236 | 190 | 52.632 | 2.99 | 0.024 | 2.33 | 0.022 |
| 0.0223 | 180 | 55.556 | 2.87 | 0.019 | 2.31 | 0.020 |
| 0.0211 | 170 | 58.824 | 2.78 | 0.015 | 2.29 | 0.018 |
| 0.0198 | 160 | 62.500 | 2.70 | 0.013 | 2.27 | 0.016 |
| 0.0186 | 150 | 66.667 | 2.64 | 0.011 | 2.25 | 0.015 |
| 0.0174 | 140 | 71.429 | 2.59 | $9.3 \cdot 10^{-3}$ | 2.24 | 0.013 |
| 0.0161 | 130 | 76.923 | 2.54 | $8.0 \cdot 10^{-3}$ | 2.22 | 0.012 |
| 0.0149 | 120 | 83.333 | 2.51 | $7.0 \cdot 10^{-3}$ | 2.21 | 0.011 |
| 0.0136 | 110 | 90.909 | 2.48 | $6.1 \cdot 10^{-3}$ | 2.20 | $9.5 \cdot 10^{-3}$ |
| 0.0124 | 100 | 100.00 | 2.45 | $5.2 \cdot 10^{-3}$ | 2.19 | $8.5 \cdot 10^{-3}$ |
| 0.0112 | 90 | 111.11 | 2.43 | $4.5 \cdot 10^{-3}$ | 2.18 | $7.5 \cdot 10^{-3}$ |
| 0.0099 | 80 | 125.00 | 2.41 | $3.9 \cdot 10^{-3}$ | 2.18 | $6.5 \cdot 10^{-3}$ |
| 0.0087 | 70 | 142.86 | 2.39 | $3.3 \cdot 10^{-3}$ | 2.17 | $5.6 \cdot 10^{-3}$ |
| 0.0074 | 60 | 166.67 | 2.38 | $2.8 \cdot 10^{-3}$ | 2.17 | $4.7 \cdot 10^{-3}$ |
| 0.0062 | 50 | 200.00 | 2.37 | $2.3 \cdot 10^{-3}$ | 2.16 | $3.9 \cdot 10^{-3}$ |
| 0.0050 | 40 | 250.00 | 2.36 | $1.8 \cdot 10^{-3}$ | 2.16 | $3.1 \cdot 10^{-3}$ |
| 0.0037 | 30 | 333.33 | 2.35 | $1.3 \cdot 10^{-3}$ | 2.15 | $2.3 \cdot 10^{-3}$ |
| 0.0029 | 23.3 | 428.57 | 2.354 [47] | $2.4 \cdot 10^{-3}$ [47] | 2.190 [47] | $2.8 \cdot 10^{-3}$ [47] |
| 0.0025 | 20 | 500.0 | 2.35 [51] | $8.7 \cdot 10^{-4}$ [51] | 2.15 [51] | $1.5 \cdot 10^{-3}$ [51] |
| 0.0021 | 16.7 | 600.0 | 2.345 [47] | $1.4 \cdot 10^{-3}$ [47] | 2.181 [47] | $1.7 \cdot 10^{-3}$ [47] |
| 0.0019 | 15 | 666.67 | 2.34 [51] | $6.5 \cdot 10^{-4}$ [51] | 2.15 [51] | $1.1 \cdot 10^{-3}$ [51] |
| 0.0012 | 10 | 1000.0 | 2.335 [47] | $7.0 \cdot 10^{-4}$ [47] | 2.173 [47] | $8.0 \cdot 10^{-4}$ [47] |
| | | | 2.34 [51] | $4.3 \cdot 10^{-4}$ [51] | 2.15 [51] | $7.6 \cdot 10^{-4}$ [51] |
| 0.0006 | 5 | 2000.0 | 2.34 | $2.2 \cdot 10^{-4}$ | 2.15 | $3.8 \cdot 10^{-4}$ |
| 0.0000 | ≈0 | — | 2.34 | 0 | 2.15 | 0 |
| | | | 2.345 [49] | | 2.197 [49] | |

[a]References are indicated in brackets.

[b]Ordinary data from Williams and Arakawa [23] and anomalous dispersion data from Chandrasekharan and Damany [24] are combined to estimate extraordinary-ray index.

**TABLE III**

**Values of $dn_0/dT$ Obtained from Various References for Magnesium Fluoride**

| eV | $cm^{-1}$ | $\mu$m | $dn_o/dT$ (1/K) | Notes |
|---|---|---|---|---|
| 2.708 | 21839 | 0.4579 | $1.47 \cdot 10^{-6}$ | 20°C [28] |
| 1.959 | 15803 | 0.6328 | $1.12 \cdot 10^{-6}$ | 20°C [28] |
| 1.078 | 8696 | 1.15 | $0.88 \cdot 10^{-6}$ | 20°C [28] |
| 0.366 | 2950 | 3.39 | $1.1 \cdot 10^{-6}$ | 20°C [28] |
| 0.0 | $\approx 0$ | — | $1.0 \cdot 10^{-4}$ | Our data [51] |

**TABLE IV**

**Values of $dn_e/dT$ Obtained from Various References for Magnesium Fluoride**

| eV | $cm^{-1}$ | $\mu$m | $dn_e/dT$ (1/K) | Notes |
|---|---|---|---|---|
| 2.708 | 21839 | 0.4579 | $0.86 \cdot 10^{-6}$ | 20°C [28] |
| 1.959 | 15803 | 0.6328 | $0.58 \cdot 10^{-6}$ | 20°C [28] |
| 1.078 | 8696 | 1.15 | $0.32 \cdot 10^{-6}$ | 20°C [28] |
| 0.366 | 2950 | 3.39 | $0.6 \cdot 10^{-6}$ | 20°C [28] |

# Magnesium Oxide (MgO)

DAVID M. ROESSLER
General Motors Research Laboratories
Warren, Michigan
and
DONALD R. HUFFMAN
Physics Department
University of Arizona
Tucson, Arizona

Magnesium oxide is an ionic material, crystallizing in the rock-salt structure and cleaving on (100) and (111) planes. It is found in nature as periclase or $\beta$-magnesia. MgO has a molecular weight of 40.32, a density of 3.576 kg/m$^3$ at 25°C, and a lattice parameter of 4.215 Å. It is insoluble in water but atmospheric moisture reacts with the surface to form a thin film, which can be easily polished off. High physical strength and stability, a melting point near 2852°C, and excellent optical transparency (absorption coefficient less than 1 cm$^{-1}$) throughout the range 0.25 to 6.8 μm, combine to make the material of considerable interest.

Very pure, microcrystalline powders can be prepared in several ways and exhibit high (over 90%) diffuse reflectance throughout the visible region and extending into both the ultraviolet (UV) and infrared (IR). As such, they have been of interest as reference standards in optical work and as coatings in devices such as integrating spheres. Similar optical properties are exhibited by "smoked" or "fumed" MgO, produced by burning magnesium ribbon and collecting the smoke on a substrate. However, pressed, sintered material can be made to have optical properties close to those of the single crystal. It has been used for a variety of optical purposes, particularly as window and substrate material.

In the mid-1970s, one of us [1] presented a composite picture of the dielectric parameters, $\varepsilon_1$ and $\varepsilon_2$, of MgO in the range 0.02 to 28 eV. The present review includes more recent data, extends the spectral range, and focuses on the $n$ and $k$ values (Table I and Fig. 1).

*X-Ray and Ultraviolet Range*

The only quantitative data published on the optical properties of MgO at photon energies above about 120 eV appear to be those of Maeda *et al.* [2],


Copyright © 1991 by Academic Press.
All rights of reproduction in any form reserved.
ISBN 0-12-544422-2

in the range 500 to 590 eV. Using bremsstrahlung radiation from a tungsten target, in conjunction with an X-ray spectrometer, they were able to measure the transmission of MgO films deposited onto 350 nm-thick aluminum foil. From the spectra of films with thicknesses of 50 nm and 200 nm, they derived the absorption coefficient in the region of the oxygen $K$ absorption edge. The absorption increases sharply near 535 eV, from a background level of about $5 \times 10^3$ cm$^{-1}$ to a maximum value of $7 \times 10^4$ cm$^{-1}$ at 539 eV. There are several smaller peaks to higher energies. Photoelectric-yield spectra [3] measured on powdered MgO show similar structure. The tabulated values of $k$ (Table I) in the range 500 to 590 eV have been calculated from the absorption-coefficient data of Maeda *et al.* [2]. The data scatter indicates an uncertainty of at least $\pm 10\%$.

The region 30 to 100 eV has been explored more extensively. Townsend [4] explored the Mg $L_{2,3}$ edge in MgO, which occurs near 55 eV. He oxidized magnesium foils and measured their opacity in the range 80 to 350 Å, using a concave grating spectrograph and a spark-discharge light source. He assumed that the densities of the foils were the same as that of the bulk materials, in order to estimate the thickness of the MgO film. Taking his value of 171 nm for the thickness of one sample, we can calculate $k$ from the opacity data. The resulting $k$ values increase from less than 0.015 at a wavelength of 100 Å to about 0.06 at 320 Å. Superimposed on this background is the structure associated with the Mg $L$ edges.

Fomichev *et al.* [5] used an X-ray spectrometer with a diffraction grating to examine the absorption spectra of MgO layers of unknown thickness. The material was prepared by burning magnesium in air and depositing the product onto a nitrocellulose substrate. Absorption data are shown on an arbitrary intensity scale in the range 50 to 68 eV but show the $L$ edge structure, similar to that in Townsend's work. They were also able to measure the $K$ absorption of oxygen, just above 535 eV. Their data, in arbitrary intensity units, cover the range 535 to 570 eV, and show similar features to those studied later in more detail by Maeda *et al.* [2]. The earlier work [5] is not quite as well resolved or sophisticated, and the absorption peaks are systematically displaced to higher energies by about 5 eV. A follow-up paper [6] presented more extensive data for the 35 to 100 eV region. In neither paper [5, 6] is film thickness quoted.

Although only optical density data are available in the literature for the range 80 to 120 eV, there are $k$ data at lower energies. Further, in the overlap region below 80 eV, the primary spectral structure in both Townsend's data [4] and in those of Fomichev and Zhukova [6] replicates that in the work on single crystals to be described later. There are small displacements in peak energies, but the general agreement is good enough for us to calibrate the optical-density data and derive equivalent $k$ values. We have therefore normalized both sets of optical-density data to give $k$ values in agreement with the lower energy data, and used the resultant

values above 80 eV in Table I. The uncertainty in $k$ is high, over $\pm 50\%$, because the MgO samples were prepared from burning magnesium rather than in the form of single crystals.

Hanson [7] was able to measure the optical properties of single crystals in the range 29 to 80 eV and provide quantitative data for both $n$ and $k$. He used a high-voltage capillary discharge in air to provide a line-emission source. He then measured the reflectance of single-crystal MgO and the transmittance of amorphous thin films. The single crystals were cleaved along the (100) plane immediately before they were transferred to the vacuum chamber. Data were recorded for 12 angles of incidence in the range 20 to 75° and used to determine $n$ and $k$ from a least-squares fit to the Fresnel equations. However, data scatter, particularly in $k$, was rather large. The data were therefore used in conjunction with a Kramers–Kronig (K–K) analysis of 15° incidence reflectance data to provide final values. Transmittance data on two films, about 28 nm and 78 nm thick, respectively, were also used to derive $k$ values.

As noted previously, the data published by Hanson and his coworkers [7, 8] show structural features similar to those of Townsend [4] and Fomichev *et al.* [5, 6], including the Mg $L$ edge. The $k$ values for his thin films are about a factor of two greater than those of Townsend, rising from 0.04 at 72 eV to about 0.12 at 29 eV. The single-crystal data for $k$ show considerable scatter but are generally larger than those for the thin films. Values at 72 eV are in the range 0.06 to 0.1; at 29 eV, the values are in the range 0.17 to 0.25. The $n$ values for the single crystal [8] show much less scatter. They are relatively flat, staying within the values 0.91 to 0.99 throughout the range 29 to 80 eV.

There are several sources of reflectance data on single-crystal MgO in the range 7 to 30 eV. Combining the best of these with the reflectance data of Hanson *et al.* [8] gives us a continuous spectrum for the range 6 to 72 eV. We can then use a K–K analysis to compute the corresponding values of $n$ and $k$. Some of the published data are only on a relative reflectance scale, but there is general agreement regarding the primary spectral features. However, there are substantial variations in the absolute magnitude of the reflectance, especially in the 7.6 eV exciton region. The published data on the optical constants show corresponding variations, and we must therefore consider what reflectance data to use as a primary source for $n$ and $k$.

Nelson [9] measured the relative reflectance of a cleaved, single crystal obtained from the Norton Research Corporation (Canada), Ltd., Niagara Falls, Ontario, in the wavelength range 90 to 175 nm. He observed three peaks: the one at 164 nm narrowed in measurements at 140 K, whereas the broad structure near 115 nm and the peak at 93 nm seemed to be temperature-insensitive. At room temperature, the three structures had comparable reflectance; at 140 K, the longest wavelength peak, assumed to be excitonic, was higher. Nelson believed that the absorption coefficient

for the exciton was of the order of $10^6$ cm$^{-1}$. The value of $k$ would therefore be of the order of unity.

Reiling and Hensley [10] measured the relative reflectance of freshly cleaved surfaces of several single crystals at 45° incidence, and the absorption of both thin cleaved samples and films evaporated onto LiF substrates. The main features resemble those in Nelson's data [9], the biggest difference being a sharp drop in reflectance on the high-energy side of the exciton peak. Some single crystals grown in their own University of Missouri laboratory showed both the sharpest exciton peak in reflection, and also the lowest absorption on the low-energy tail of this peak. The absorption coefficient was between 30 and 50 cm$^{-1}$ throughout the range 5.8 to 7.0 eV for this material, whereas other crystals (Norton) had absorption coefficients of about 75 cm$^{-1}$ at 5.8 eV, increasing to about 285 cm$^{-1}$ at 7.0 eV. The $k$ value for the Missouri material is about $5 \times 10^{-5}$ from 5.8 eV to nearly 7 eV, even though there was some evidence of extrinsic structure in both the reflection and absorption low-energy tails of the exciton peak. The intrinsic absorption increased very rapidly beyond about 7.4 eV, being well above 500 cm$^{-1}$ at 7.5 eV for all crystals examined (at room temperature).

Harris [11] was able to measure the absolute reflectance of MgO in the ultraviolet. He used a hydrogen discharge tube for a light source. This provides a strong continuum at energies below 7.5 eV and line emission at higher energies. A vertically mounted, rotatable, phosphor-coated light pipe coupled to a blue-sensitive photomultiplier enabled absolute measurements to be made. Roessler [12], using the same equipment, extended these data, made measurements at both 15° and 45° incidence, and also used the K–K relations to derive the dielectric parameters. The near-normal-incidence data in the range 4 to 14 eV show structure very similar to those of Reiling and Hensley [10] and Nelson [9]. The room-temperature reflectance at the exciton peak was over 22% and dropped sharply to just under 11% on the high-energy side (near 8 eV). The broad peak near 11 eV had a reflectance of about 17%, while the peak just above 13 eV had a reflectance of about 23%.

Roessler and Walker [13] made studies of the exciton reflectance at both room temperature and at 77 K. The crystal was cleaved in air but transferred to a vacuum system of the reflectometer within about two minutes. At 300 K, the exciton peak had a reflectance of about 25% at 7.60 eV, whereas crystal surfaces exposed to laboratory air for three days showed reflectances of 20–23%. Data on the best surface were reproducible to within 2% while the sample was maintained in the vacuum system. At 77 K, the exciton structure exhibits two peaks at 7.69 and 7.76 eV. Later, Whited and Walker [14] showed that additional structure can be seen at 25 K, reflectance peaks occurring at 7.689, 7.715, 7.752, and 7.768 eV.

Studies [15] over a more extended range (4 to 12 eV) confirmed earlier

findings that only the exciton structure showed strong temperature dependence, whereas the reflectance in the region 8 to 12 eV was virtually unchanged between room temperature and 77 K. It was again noted that surfaces exposed for several days to laboratory air deteriorated, as indicated by lowering of the exciton reflection peak and a slight broadening of the spectral features. The best surfaces had peak reflectances of about 27.5% at 7.6 eV, 23% at 11 eV, and 31.5% at 13.5 eV (all at room temperature).

Roessler and Walker [16] used a pulsed discharge in argon to provide line emission beyond the hydrogen-discharge limit, and were able to extend their reflectance data to 28 eV. A very broad composite structure was seen in the 16 to 23 eV region, peak reflectances being about 25%. The data were recorded at 8° incidence and repeated on several freshly cleaved, single-crystal samples (all from Semi-Elements, Inc., Saxonburg, Pennsylvania). Light-source emission lines exhibiting intensity fluctuations of more than 5% were not used in the final computation of the reflectance. A K–K inversion was used to generate $n$ and $k$ values from these reflectance data [17].

Williams and Arakawa [18] also measured the reflectance of cleaved, single crystals of MgO in the same energy range. Their samples were obtained from Muscle Shoals Minerals Company, Barton, Alabama, and from J. Burrow of Bristol University, U.K., and were cleaved in the (100) plane. They contained from 10 to 57 ppm of Fe. The data were recorded at 15° incidence and qualitatively very closely resemble the Roessler and Walker data [16] in spectral structure. However, the absolute reflectance was slightly less: their exciton-peak reflectance was only 22%, the 11 eV peak had a reflectance of 19%, the 13.5 eV peak had a reflectance of 27%, and the broad structure near 20 eV had maximum values near 20%. Thus, the peaks were about 0.04 to 0.05 lower in absolute reflectance than those of Roessler and Walker. Williams and Arakawa noted that there were variations in absolute reflectance between their own samples. They also used the K–K relation to compute $n$ and $k$ values from the reflectance.

Freehouf [19] measured the reflectance of a single-crystal sample of MgO over the range 4 to 30 eV, using synchrotron radiation. Data were recorded for sample temperatures in the range 100 to 400 K. The sample was cleaved in air just prior to being mounted in the vacuum system. Measurements were also made on a polished sample and showed considerable broadening of the exciton structure near 7.5 eV, but little difference at higher energies. He estimated the absolute values of reflectance to be correct to $\pm 0.03$. The room-temperature data have almost identical structure to that revealed by the earlier work [16, 18], and the absolute magnitudes lie between the two previous sets of data over this range. These data are of particular interest because of the use of a continuum rather than a line source. In principle, this should provide more reliable details of

optical structure, especially above 20 eV, where there are often gaps of up to 0.5 eV between emission lines. Freehouf also used a K–K inversion of the reflectance to compute the optical constants, but shows the $\varepsilon_2$ data only at 100 K.

Mikhailin *et al.* [20] measured the relative reflectance at 15° incidence of cleaved single crystals in the range 15 to 40 eV, using the DESY synchrotron light source. There were only minor differences from earlier data, mainly in the 20 eV structure. Kuusmann and Fel'dbakh [21] measured the relative reflectance in the exciton region at 10 K, and saw fine structure similar to that observed in the 25 K data of Whited and Walker [14]. French and Coble [22] made preliminary measurements of the room-temperature reflectance of MgO in the range 7.5 to 14.5 eV. Details of the measurement, including crystal quality, were not given, but the absolute values of the reflectance are low. The exciton-peak reflectance, for example, was only 18.5%.

Summarizing the reflectance data, we find that reports of the value at the 7.6 eV exciton peak vary from as low as 18.5% to as high as 27.5%. The variations are slightly smaller at the higher-energy peaks: values for the peak near 21 eV range were from 19% to 25%. In general, we believe that the data corresponding most closely to intrinsic bulk MgO are those with the highest reflectance values and the sharpest spectral features. The exciton peak near 21 eV range from 19% to 25%. In general, we believe that the higher-energy features seem to be remarkably durable in terms of qualitative structure.

In this connection we note the results of Carden *et al.* [23] on the ion bombardment of an electropolished single crystal of magnesium. This process promotes rapid growth of an oxide layer, which can be monitored by optical reflectance measurements. They measured the reflectance in the range 8.3 to 41.3 eV, using the synchrotron radiation from the University of Wisconsin storage ring. The optical reflectance after bombardment was much lower than before in the range below 12 eV, but virtually unchanged at higher energies. The film was sufficiently like MgO to exhibit weak reflectance structure near 11 eV, 13 eV , and 20 eV, although the reflectance throughout this region was less than 4%.

The preferred reflectance data in the range 5 to 17 eV are those of Roessler and Walker [16]. They exhibit the highest and sharpest reflectance values; the low-energy tail of the exciton peak extrapolates smoothly onto values of the reflectance computed from reliable refractive-index data; and there is close agreement with the synchrotron data of Freehouf [19] in the 11 to 17 eV range. In the range 17 to 23 eV, we believe the reflectivity of single-crystal MgO is slightly lower than the Roessler and Walker data and closer to the values measured by Freehouf. The line emission from the spark discharge in argon [16] is not as stable in intensity as the light from the synchrotron source [19], and the data scatter is

significantly larger than in the hydrogen-discharge light-source range. Both sets of data [16, 19] differ by only about ±0.02 in absolute reflectance in this region, well within the estimated uncertainty. Above 23 eV, we extrapolated the reflectance to join the data of Hanson *et al.* [7, 8].

The final values of $n$ and $k$ used for Table I for the range 6 to 75 eV were obtained from a K–K inversion of the reflectance data selected as above. We took precautions to minimize computational errors introduced by integration of the reflectance data over a limited energy range. The low-energy tail was extrapolated smoothly to below 1 eV, using known values of the refractive index (discussed later), whereas the upper end of the spectrum was extrapolated to 800 eV on the assumption that the reflectance varied inversely with the fourth power of the energy. Further, we employed the correction technique described by Roessler [24] for dealing with K–K analysis in limited spectral regions. By varying the width of the spectral range, we estimate that our use of the K–K analysis contributes an uncertainty of less than ±0.003 to the tabulated values of $n$ and $k$. However, the total uncertainty in the final values of $n$ and $k$ in the range 7 to 75 eV is at least ±0.05. This is primarily because the relative uncertainty in the original reflectance measurements is at least 3%. Three decimal places are used in Table I to emphasize the spectral structure in $n$ and $k$ rather than to denote true precision. Our present values of $n$ and $k$ in the range 20 to 30 eV are systematically lower than those reported by previous groups [8, 18, 19].

Several workers have measured the electron-energy-loss spectra (EELS) of MgO and compared the spectral features with those obtained optically. Venghaus [25] analyzed his 60 kV EELS spectrum with a K–K transformation and obtained the dielectric parameters, $\varepsilon_1$ and $\varepsilon_2$, in the range 0 to 80 eV. There is remarkable agreement with the optical data of Roessler and Walker [16] in the region of spectral range overlap, 5 to 28 eV. Every feature, with the obvious exception of the 7.6 eV exciton, is reproduced.

Reflection-electron-energy-loss spectra from excellent, cleaved surfaces of single-crystal MgO [26] also reproduce the optical structure in the range 5 to 28 eV. Kambe *et al.* [27] explored several spectral energy regions via EELS from MgO crystallites. Their data, in arbitrary intensity units, cover several ranges: 0 to 60 eV, showing the plasmon loss just above 20 eV; 40 to 120 eV, showing the Mg $L$ edges; 500 to 750 eV, showing the oxygen $K$ edge; and 1250 to 1500 eV, showing the Mg $K$ edge. Where corresponding optical data exist, there is good agreement for the spectral structure. The EEL spectra in the region of the Mg $L$ edges show peaks close to those seen in the optical data [4, 5, 6]; similarly, there is good agreement for the oxygen $K$ edge [2, 5]. We do not know of any optical data in the region of the Mg $K$ edge, but on the basis of the EEL spectra, the value of $k$ should show a small increase above 1310 eV.

A derivation of both $n$ and $k$ from EELS in the range 15 to 40 eV has

been made for evaporated films of MgO [28]. The exciton structure is missing, as anticipated, and the spectra lack the fine detail of the optical data. However, there are some interesting similarities to the present values of $n$ and $k$ in terms of general spectral dependence, despite the differences in both material (thin film rather than bulk single crystal) and experimental probe (EELS rather than optical reflectance).

*Absorption in the Near-UV through Near-IR Region*

MgO has excellent transparency throughout the near UV, visible, and near IR. In good material the value of $k$ is less than $10^{-4}$ throughout the wavelength region 0.17 to 7.3 μm, and less than $10^{-7}$ in part of this range. Impurities and other defects can significantly increase this absorption. For example, Hibben [29] did some early work on the absorption induced by UV irradiation. The present review will generally exclude discussion of extrinsic features, except insofar as the associated absorption is presumed to be greater than that of any intrinsic absorption.

Molnar and Hartman [30] reported the effect of 40 kV X-irradiation on the absorption in the 0.2 to 0.9 μm region. They induced at least three bands, with peaks at 0.22 μm, 0.285 μm, and 0.525 μm. Although they did not show the absorption of preirradiated crystals, their data can be regarded as upper bounds to the intrinsic absorption. The value of $k$ is then less than $3 \times 10^{-5}$ at 0.2 μm, less than $4 \times 10^{-6}$ near 0.35 μm, and less than $10^{-6}$ beyond 0.85 μm. The crystals were obtained from the Norton Research Corporation (Canada) Ltd.; some were very clear, and others had a slight yellow or greenish tint. The absorption data reported were from clear samples, which, from spectrographic analysis, revealed no impurities other than about 0.1% of calcium.

Tyler and Sproull [31] measured the transmittance of three unpolished MgO crystals (Norton), in the wavelength range 0.2 to 0.4 μm. They showed comparable absorption: at 0.21 μm, the absorption coefficient was estimated to be about 15 $cm^{-1}$ ($k = 2.5 \times 10^{-5}$), and to result partly from impurities.

Weber [32] measured the transmission of plates of MgO with thicknesses of 0.42 and 0.92 mm, which had been heated in various atmospheres of excess oxygen and excess metal. He derived the absorption coefficient in the range 1.5 to 8 eV and noted the treatment-senstive structure. For the least-absorbing samples, $k$ was about $6.5 \times 10^{-5}$ at 6.075 eV (0.204 μm), decreasing monotonically to $3.1 \times 10^{-6}$ at 5.0 eV, and being too small to measure at 4.5 eV.

Johnson [33] obtained some very clear, synthetic single crystals from several sources and cleaved them to obtain plates with thicknesses of 0.27 to 0.75 mm. The purest samples, grown at the University of Missouri, contained only a few parts per million of Ca, Fe, Na, and Ni, as principal impurities. They had a blue-ultraviolet fluorescence under UV excitation,

whereas less pure samples (from Norton and from the Lamp Division of thue General Electric Company, Cleveland, Ohio (GE)) were nonluminescent. The absorption coefficient, uncorrected for surface reflection losses, was derived from transmission measurements in the range 0.16 to 0.35 μm. The GE and Missouri samples had very similar absorption; the Norton material had about twice as much absorption at wavelengths longer than 0.175 μm. All samples had absorption coefficients greater than 400 $cm^{-1}$ at 0.16 μm. The absorption dropped to 20 $cm^{-1}$ at 0.18 μm in the Missouri samples and to 6 $cm^{-1}$ at 0.22 μm.

Johnson's data [33] provide the lowest values of $k$ reported for the range 7.3 to 6.7 eV, and extrapolate smoothly to the values determined by K–K analysis at higher energies. We therefore use these in Table I.

Peria [34] examined the 3 to 6 eV UV absorption of MgO crystals from a wide variety of sources. The transmittance was measured on cleaved samples from 0.2 to 1 mm thick. Most showed extrinsic absorption features consisting of various admixtures of bands at 4.3, 4.8, and 5.7 eV. These could often be reduced if the samples were heated in vacuum. The $k$ values in the least absorbing material decrease from about $2.5 \times 10^{-5}$ at 5.8 eV to $3.3 \times 10^{-6}$ at 5.1 eV, and are lower than found in any other work in the 5 to 5.5 eV range.

Ballesteros *et al.* [35, 36] recently made an extensive study of optical absorption in a variety of MgO crystals, with controlled metal impurities and subjected to various heat treatments. Absorption coefficients are given for the range 2 to 6.5 eV. The most transparent material is slightly more absorbing than that of Peria [34] below 5.5 eV but provides lower values of $k$ at higher energies, joining smoothly onto Johnson's data [33] above 6.5 eV.

The few data that exist for $k$ in the 2 to 5 eV range all exhibit structure indicating that extrinsic absorption is present. The most precise measurements are probably those of Harrington *et al.* [37], who used combined wavlength-modulation and laser-calorimetric techniques to measure the low absorption in the 2.4 to 3.6 eV range. The wavelength-modulation spectra give the derivative of the absorption coefficient. This is then integrated, the constant of integration being given via Ar-ion-laser calorimetric measurements at the discrete laser-line wavelengths. No details of the samples were given. The absorption coefficient decreased from about 0.3 $cm^{-1}$ at 0.355 μm to about 0.02 $cm^{-1}$ at 0.502 μm, the latter giving a $k$ value of $8 \times 10^{-8}$.

A completely different technique was used by Sakhnovskii [38], who determined absorption coefficients from a detailed analysis of the diffuse reflection of powdered MgO in the range 0.24 to 1 μm. The powder was obtained by burning magnesium shavings on a steel plate, and the measurements were performed with an integrating photometer. The values of $k$ derived from his data are within a factor of three of those derived from the

single-crystal data [32–37]. The earlier data of Molnar and Hartman [30] give values of $k$ between five and ten times those of Sakhnovskii over the range 2 to 5 eV, but both show the same general spectral features, including a broad absorption minimum near 3 eV.

Most of the data for $k$ that exist in the range 0.3 to 2 eV (4 to 0.6 μm) were made at discrete laser wavelengths: 1.319 μm (modified Nd:YAG), 2.7 μm (HF), and 3.8 μm (DF). There are strong impurity bands in this region, probably associated with oxygen or $OH^-$. Values of $k$ derived from different sources range from about $2\times10^{-8}$ to a few times $10^{-6}$.

Harrington *et al.* [39] used standard laser-calorimetric methods and analysed their data from a single-crystal sample (Norton Company) to derive the absorption coefficients at 2.7 and 3.8 μm. They showed that the respective values of $4.0\times10^{-2}\,\mathrm{cm}^{-1}$ ($k=8.6\times10^{-7}$) and $5.4\times10^{-3}\,\mathrm{cm}^{-1}$ ($k=1.6\times10^{-7}$) indicate extrinsic absorption contributions.

Laser calorimetry was also used by Fernelius *et al.* [40] to measure the absorption of some polished Norton crystals at 1.319, 2.7, and 3.8 μm. Spectral traces indicated extrinsic absorption features in this wavelength range, and absorption measurements varied significantly with the sample at 2.7 μm. However, a sample that appeared slightly yellow-green in color was less absorbing at 2.7 μm than a very clear sample. The average value of $k$ was $3\times10^{-6}$. At $\lambda=3.8$ μm, $k$ varied from $2.8\times10^{-7}$ to $3.2\times10^{-7}$. The absorption values originally reported for the 1.319 μm wavelength were revised later [41]. The $k$ values for two samples were $7.1\times10^{-8}$ and $9.2\times10^{-8}$, the tinted sample having lower absorption than the clear crystal, possibly because of its superior surface polish.

The lowest values of absorption at 2.7 and 3.8 μm were obtained by Hordvik and Skolnik [42], using a photoacoustic technique. They examined a mechanically polished MgO crystal supplied by Norton. The photoacoustic technique allows separation of the bulk and surface contributions. At 2.7 μm, the bulk absorption coefficient was $5.2\times10^{-3}\,\mathrm{cm}^{-1}$ ($k=1.1\times10^{-7}$), and the loss per surface was $9\times10^{-4}\,\mathrm{cm}^{-1}$. At 3.8 μm, the bulk value was $6.7\times10^{-4}\,\mathrm{cm}^{-1}$ ($k=2.0\times10^{-8}$), and the loss per surface was $1\times10^{-4}\,\mathrm{cm}^{-1}$. Hordvik and Skolnik also show bulk-absorption-coefficient data extending from 3.8 μm to 8.4 μm. The $k$ values derived from these data are among those we consider most representative of intrinsic bulk material.

Infrared wavelength-modulation spectroscopy [43] of a Linde A polished single crystal of MgO from Optovac, North Brookfield, Massachusetts, shows extrinsic structure in the absorption coefficient throughout the region 2.5–5 μm. Although this changed slightly, depending on whether the sample was measured in normal laboratory air or in a dry-nitrogen atmosphere, the total absorption remained small. The data were normalized to a value of $7.6\times10^{-3}\,\mathrm{cm}^{-1}$ ($k=2.3\times10^{-7}$) at $\lambda=3.8$ μm. This results in $k$ values of less than $3\times10^{-7}$ throughout the range. These values

are lower than those of Hordvik and Skolnik near 5 μm and do not extrapolate as smoothly onto the available longer-wavelength data.

*Refractive Index in and near the Visible Region*

Early measurements of the refractive index of MgO in the visible region generally employed prisms, and were reported to three or four decimal places. References [44–49] describe some of this work, which was subsequently compiled and analyzed by Haase [50].

An extensive study was made by Strong and Brice [51], who cut two prisms from one of several very pure Norton MgO crystals and used a minimum-deviation method to measure the refractive index at 23°C in the range $\lambda = 0.2536$ μm to $\lambda = 0.7065$ μm. The corresponding values for $n$ were quoted to four decimal places in the ultraviolet and to five decimal places in the visible region, and decreased from 1.8450 to 1.73126. Measurements were also made at 2°C and $dn/dT$ was determined to be $1.47 \times 10^{-5}$/°C at $\lambda = 0.4861$ μm ($n = 1.74711$) and to be $1.14 \times 10^{-5}$/°C at $\lambda = 0.6563$ μm ($n = 1.73340$).

Radhakrishnan [52] found that the 23°C data of Strong and Brice could be fit to within ±0.003 over the range 0.2967 to 0.7065 μm by the formula

$$n^2 = 1.3224 + \frac{1.6294\lambda^2}{(\lambda^2 - 0.01387)}. \tag{1}$$

Peria [34] has a slightly different equation, which fits the whole spectral range with the same degree of fit.

Radhakrishnan also measured the temperature coefficient of the refractive index of a polished, strain-free crystal at the wavelengths 0.4358, 0.5461, and 0.5893 μm. He used an interferometric method from room temperature up to 400°C, and found that $dn/dT$ decreased slightly with wavelength but did not vary with temperature. Later [53], he extended the wavelength coverage to 0.4047 μm and 0.3650 μm, confirming the trends seen earlier. His values for $dn/dT$ decrease from $1.95 \times 10^{-5}$/°C at 0.3650 μm to $1.60 \times 10^{-5}$/°C at 0.5893 μm.

The most detailed refractive-index data for MgO are those of Stephens and Malitson at NBS [54]. Measurements were made on two prisms of magnesium oxide crystals of "excellent optical quality" by the minimum-deviation method in the wavelength range $\lambda = 0.36117$ μm to $\lambda = 5.35$ μm. In the visible region, measurements were made at temperatures near 20°C, 30°C, and 40°C, at each of nine wavelengths. These data were then averaged for the two prisms. The final values of the refractive index at 30°C were found to fit a four-constant dispersion equation:

$$n^2 = 2.957019 - 0.0101373\lambda^2 + \frac{0.0216485}{(\lambda^2 - 0.0158650)} \tag{2}$$

The computed values are within $\pm 6 \times 10^{-6}$ of the averaged, corrected values, throughout the visible region.

Stephens and Malitson fitted the 23.3°C refractive-index data for the whole wavelength range from 0.36117 to 5.35 μm to a five-constant dispersion equation:

$$n^2 = 2.956362 - 0.01062387\lambda^2 - 0.0000204968\lambda^4 + \frac{0.02195770}{(\lambda^2 - 0.01428322)}. \tag{3}$$

The values computed from this formula are systematically lower than those of Strong and Brice at the same temperature by about $3.7 \times 10^{-4}$.

Saksena and Viswanathan [55] have given a slightly different dispersion equation for the 23°C NBS data, but without improving the fit. Dodge [56] has fitted the 20 °C NBS data to the following equation:

$$n^2 = 1 + \frac{1.111033\lambda^2}{\lambda^2 - 0.005076} + \frac{0.8460085\lambda^2}{\lambda^2 - 0.018912} + \frac{7.808527\lambda^2}{\lambda^2 - 723.2345}. \tag{4}$$

More recent measurements confirm the results of Stephens and Malitson. For example, the compilation by Moses [57] includes data on a 99.7% pure single crystal (Norton) [58]. Values of $n$ were measured at about 25 °C in the range 0.6907 to 5.35 μm and agree to five decimal places with the Stephens and Malitson values. Herzberger and Salzberg [59] measured several samples of MgO, found no significant differences from the NBS data, but provided a different dispersion equation:

$$n = 1.71960 + 0.006305L - 0.000090L^2 - 0.0031356\lambda^2 - 0.00000770\lambda^4, \tag{5}$$

where $L = 1/(\lambda^2 - 0.028)$.

They did not state the temperature: we assume it to be 20 ± 5°C. Stephens and Malitson [54] estimated $dn/dT$ at 20°C to be $1.36 \times 10^{-5}$/°C at $\lambda = 0.7679$ μm, increasing to $1.89 \times 10^{-5}$/°C at $\lambda = 0.4047$ μm. An uncertainty of ±5°C therefore gives an uncertainty of about ±0.0001 in $n$.

The values of $n$ tabulated over the range 5 to 0.21 eV (0.25 to 5.9 μm) are based primarily on the work of Stephens and Malitson [54]. We quote their experimental values to five decimal places, and use Eq. 3 to give

values of $n$ to four decimal places at other wavelengths. The high-energy tail of their data was extrapolated smoothly onto the $n$ values computed from the K–K analysis of the UV reflectance. Supplemental data are included from various references [56, 58, 59]. Although we quote the NBS data [54] to five decimal places, we believe the uncertainty in the tabulated values of $n$ in the range 0.5 to 3.5 eV is $\pm 0.0001$. It is about $\pm 0.002$ in the range 3.5 to 7.3 eV, and about $\pm 0.0005$ at energies below 0.5 eV.

Irtran 5 is a hot-pressed, polycrystalline compact of MgO and has been used extensively in much infrared work. The Eastman Kodak Company no longer manufacturers it. However, the company published index-of-refraction values for this material in the range 1 to 9 μm, and a convenient list appears in the *Handbook of Optics* [60]. These data were determined experimentally and fitted to an interpolation formula by a least-squares method. Despite the different form of MgO, the values of $n$ differ by less than $\pm 0.001$ from the single-crystal data of Stephens and Malitson in the overlapping range (1 to 5.35 μm).

Derivations of $n$ from reflection methods are usually less precise than those obtained via transmission. An early example is the work of Barnes *et al.* [61], who measured the reflectance of a single crystal of MgO (Norton) in the wavelength range 1 to 15.5 μm. They assumed negligible absorption in the range 1 to 8 μm and derived $n$ in this region from the Fresnel equation for normal incidence:

$$n = \frac{(1 - \sqrt{R})}{(1 + \sqrt{R})}. \tag{6}$$

Hanna [62] found little difference between the reflectance spectra of single-crystal and polycrystalline MgO in the range 4000 to 300 $cm^{-1}$. Using the Fresnel equation, he derived values of $n$ that are systematically lower than those of Stephens and Malitson by at least 0.03.

A novel approach was adopted by Welber [63], who used an index-matching technique and measured the transmission of an alkali–halide matrix containing MgO powder. This enabled him to determine $n$ in the wavelength range 5 to 8 μm. The data near 5 μm accord well with the NBS results [54] despite the difference in the nature of the samples.

*Thin Films, UV–VIS*

As noted previously, the optical properties of thin films often differ significantly from those of the bulk material. In spectral regions of nominal transparency, impurities and surface defects in the film may contribute additional absorption. However, if the films contain many voids, there may be spectral regions in which values of $k$ are less than those of bulk material.

The following section discusses thin-film data in the near-UV through near-IR regions.

Reiling and Hensley [10] prepared thin (65 nm) films of MgO by evaporating magnesium metal onto polished, cleaved LiF substrates and baking them at 650°C in air. The transmission spectra showed only a weak exciton feature superimposed on the main absorption. However, this peak moved slightly to higher energy as the temperature decreased from 25 to −170°C. Absorption coefficients, uncorrected for reflection losses, were about $2\times10^5\,\mathrm{cm}^{-1}$ near the exciton structure at 7.8 eV, and reached a maximum value of about $3\times10^5\,\mathrm{cm}^{-1}$ near 10.5 eV. The corresponding values of $k$ are about 0.25 and 0.28, respectively, or about a quarter of the value in single-crystal material.

Malherbe [64] used an electron beam to evaporate thin films of MgO in high vacuum. He baked the films at 450°C to decrease extrinsic absorption and tried to protect them from water-vapor contamination. However, his values of $n$ decrease from 1.99 at 0.186 μm to 1.73 at 0.248 μm, considerably lower than the single-crystal values of about 2.10 and 1.86, respectively. His $k$ values decrease from about 0.022 at 0.198 μm to $3\times10^{-4}$ at 0.251 μm. By contrast, Johnson's single-crystal data [33] show $k$ values of about $1.5\times10^{-5}$ at 0.198 μm, and Weber's single-crystal data [32] show $k$ to be below $3\times10^{-6}$ at 0.251 μm. Thus, the thin-film absorption in this region is two to three orders of magnitude greater than that found in single crystals.

Bradford *et al.* [65] examined the optical properties of evaporated films, using both Irtran 5 and 99.9% pure MgO as starting material. The absorption was negligible throughout the 0.22 to 8.0 μm region, and values of the refractive index derived by three different techniques (interferometric and polarimetric) agreed within 1%. The films were crystalline, with the same cubic structure and lattice constant as the bulk material, whether deposited at 50°C or 300°C onto various substrates. The crystallites were larger at the higher deposition temperature and had refractive indices identical to those of single-crystal MgO in the visible region and identical to those of Irtran 5 in the infrared. However, the refractive index of the films deposited at 50°C was about 2.3% lower, a difference attributed to the presence of more boundary-layer material between the crystallites. For the 50°C films, $n=1.70$ at $\lambda=0.55$ μm, and $n=1.62$ at $\lambda=4$ μm. The corresponding values for the 300°C films were 1.74 and 1.66.

It was noted that a hazy, bluish, scattering coating formed on films exposed to normal air [65]. Deitch *et al.* [66] used RF sputtering to prepare MgO films and observed formation of a white haze on the films after exposure to air. They measured $n$ at only one wavelength (0.6328 μm), and found that it varied from 1.72 to 1.75 as the sputtering atmosphere was varied from part oxygen/part argon to pure argon. These values are close

to the single-crystal value of 1.7346, whereas films that were electron-beam evaporated by Kersten *et al.* [67] had $n$ values in the range 1.684 to 1.702, depending on the substrate. These authors deposited films at 50°C as dielectric planar waveguides and derived $n$ from knowledge of the film thickness and the angle of coupling between the waveguide and a prism for He–Ne light at 0.6328 μm. Measurements of the absorption losses indicate a value of $k$ of about $3 \times 10^{-5}$, at least two orders of magnitude greater than that assumed for single-crystal material.

Reale [68] studied the refractive index of electron-beam evaporated MgO films as a function of the temperature of deposition onto clean, flat, soda-lime glass substrates. Impurities were removed by heating the films at 400°C in vacuum for two hours. The refractive index was determined from interference structure in the reflectance and transmittance spectra obtained with a normal-incidence, double-beam spectrophotometer. No wavelength is given, but the data are claimed to be consistent with those of Bradford *et al.* [65]. The value of $n$ increased from 1.70 for films deposited at 50°C, to about 1.74 for films deposited at 200°C. Increasing the deposition temperature to 300°C produced a further but negligible increase in $n$. The films were described as being polycrystalline and the change in $n$ ascribed to a reduction in intergranular boundaries as deposition temperatures increased.

Harrington *et al.* [69] used a laser calorimeter to measure the aborption in electron-beam evaporated MgO films. They tried to minimize extrinsic absorption by using high-purity starting material. The films were deposited onto carefully cleaned, polished CaF substrates, at temperatures in the range 50 to 200°C. Thicknesses were from $\lambda/2$ to $\lambda$ at 3.8 μm, in order to simplify the subsequent optical analysis. The values of $k$ were $2.2 \times 10^{-3}$ at $\lambda = 3.8$ μm, and $6.2 \times 10^{-3}$ at 2.8 μm; these values are from three to four orders of magnitude higher than found in bulk crystals.

Blanc [70] presents both $n$ and $k$ values for evaporated films of thicknesses 50 to 250 nm in the range 0.170 to 0.250 μm. The refractive index of these films, evaporated onto silica substrates at 250°C, is about 7% lower than that of single-crystal bulk material. However, the absortion in these films is at least two orders of magnitude greater than that of bulk material: $k$ is about 0.001 at $\lambda = 0.2026$ μm and increases to 0.01 at $\lambda = 0.1779$ μm.

Aboelfotoh and Ramsey [71] also examined the UV absorption of electron-beam evaporated films. Their films, about 300 nm thick, were deposited onto fused-silica substrates. Spectra were recorded in the range 3 to 7 eV with a Beckmann DK-2A spectrophotometer. A variety of extrinsic absorption features were seen, which varied with deposition temperature and subsequent heating of the films in air or under vacuum. Some of this structure closely resembles that seen by other workers in MgO, which has been subjected to treatments such as X-irradiation, UV-irradiation, additive coloration, or mechanical deformation, and variously ascribed to

Fe impurities, interstitial oxygen, and so on. All the films exhibited absorption coefficients greater than $6 \times 10^4\,\mathrm{cm}^{-1}$ at 7 eV, corresponding to $k$ values above 0.08, almost an order of magnitude greater than those in single crystals.

Maclean and Duley [72, 73] measured the transmission of MgO films prepared by the laser evaporation of high-purity Norton MgO crystals. Data were recorded in the range 0.135 to 0.240 μm for films of thicknesses between 21 and 93 nm. These films were amorphous and showed no evidence of the strong exciton structure near 0.163 μm seen in single-crystal material. The absorption coefficient did not vary strongly with film thickness but was very much larger than that of single crystals for wavelengths longer than 0.17 μm. (At shorter wavelengths, that is, to the high-energy side of the exciton feature, the films were slightly *less* absorbing than single crystals.) Annealing films in air at temperatures up to 800°C did not decrease the absorption but did produce a weak exciton structure at 0.16 μm. Other structure seen on the absorption tail of both amorphous and partially recrystallized films was attributed to absorption by surface defects, and associated with $O^{2-}$ ions in particular.

*Infrared Region*

In addition to the earlier compilation of the dielectric functions [1], there are three other surveys of the infrared properties of MgO that contain optical constants: one by DeWitt of the Thermophysical Properties Research Center at Purdue [74], that by Moses from Hughes Aircraft Company [57], and the other by Whitson of the Aerospace Corporation [75]. The last contains extensive tabulations of infrared data in digital form taken from the original papers, including tables of "representative" or "best" values of $n$ and $k$. This part of Whitson's work thus has much in common with the present section of this work. However, we have done a completely independent evaluation of the published infrared results, supplemented by original measurements in the regions where adequate data were missing or were questionable. Only after the infrared part of Table I was assembled was a comparison made with the Aerospace handbook values, which overall showed rather good agreement at the higher infrared frequencies.

Many measurements of optical properties have been made on MgO particulate samples, especially MgO smoke, which is easily prepared by burning magnesium ribbon in air. Extensive infrared measurements have been performed to study small-particle optical properties, such as surface modes in these samples. For an introduction to this field, Section 12.3.5 of the monograph by Bohren and Huffman [76] is suggested reading. For the purpose of arriving at the most reliable optical constants of MgO, however, we have deliberately omitted work on powders and smoke because of the complex behavior they show, and have relied exclusively on measurements

taken from bulk single crystals. Similarly, measurements on Irtran 5 have been excluded, although some comments on comparisons are included. Emphasis is exclusively on the room-temperature region.

In the infrared region the absorption of MgO begins to rise toward a reststrahlen peak in absorption near 400 $cm^{-1}$ (25 μm). In this spectral region the absorption is so high that reflectance techniques must be employed to derive optical constants, whether by a K–K analysis of the reflectance at one angle, multiangle reflectance analysis, or by means of an oscillator fit to specular reflectance spectra. On both the low- and high-frequency sides of the restsrahlen region, there occur spectral ranges where absorption is weak enough for transmission to be carried out on cut or cleaved and polished single-crystal samples.

In this review we proceed to discuss the infrared in three regions. The first ranges from about 2000 $cm^{-1}$ to about 750 $cm^{-1}$ (5 to 13 μm), where multiphonon processes apparently dominate the absorption and where transmission measurements can be made. The second is the reststrahlen region, stretching from about 750 $cm^{-1}$ down to about 300 $cm^{-1}$: here, $k$ is greater than 0.1 and reflectance measurements are employed. Below 300 $cm^{-1}$ in the far infrared, $k$ values again fall below 0.1, low enough for transmission measurements.

Workers reporting infrared transmission measurements on solids are not always interested in extracting optical constants from their measurements, so we have had to undertake this task. When only transmission or absorptance measurements are given, it is necessary to apply a correction for surface reflection. This can be based either on measured reflectance values or on values calculated from $n$ via the Fresnel equations. Among several possible choices for this task we have chosen the work of Piriou and Cabannes [77], who fitted reflectance data with a classical oscillator model. These authors made a special effort to achieve agreement with the accurate $n$ values of Stephens and Malitson in the near infrared [54]. The same calculations also agree quite well with results in Duesler's thesis of K–K analysis for $n$ tabulated from 20 to 300 $cm^{-1}$ [78]. In addition to providing the reflection coefficients, the $n$ values provided by Piriou and Cabannes have been used in the tabulation. It was also found that their oscillator fit [77] produced excellent agreement, both with K–K results in the far infrared at wavelengths longer than 100 μm (100 $cm^{-1}$) and with analysis of interference fringes in our own transmission measurements. Because of these facts, we used the same classical oscillator fit to determine the reflection corrections in the far infrared.

There have been numerous transmission measurements on single-crystal samples of MgO in the multiphonon absorption region between about 2000 and 1050 $cm^{-1}$ (5 to 9.5 μm). The earliest work was by Barnes and coworkers [61, 79]. Burstein *et al.* [80] were concerned about some anomalies in these early data and made both reflection and transmission measure-

ments on cleaved single crystals. They present a plot of the absorption coefficient, $\alpha$, rising from a value of about $1\,cm^{-1}$ near $6\,\mu m$ to over $500\,cm^{-1}$ near $14\,\mu m$. Willmott [81] measured transmission for four thicknesses of cleaved MgO ranging from 0.076 to 0.468 mm, gave tabulated values of $k$ for 10 wavelengths, and showed a curve of both $n$ and $k$ from about 7 to 25 μm, parts of which were based on smoked MgO. Despite the use of a single monochromator with a natural-rock-salt prism, these measurements agree quite well with more recent work with a later generation of commercial infrared monochromators. Other such measurements are reported in the papers by Oppenheim and Goldman [82], Billard *et al.* [83], Cabannes and Billard [84], and Hanna [62].

The values of $k$ tabulated in the range 6 to 14 μm rely primarily on two papers, one by Gourley and Runciman [85] and the other by Piriou and Cabannes [86]. Gourley and Runciman measured the transmission of 0.037 to 5 mm-thick cleaved and ground platelets and presented their data in the form of absorption coefficient spectra at 35 and 305 K. Piriou and Cabannes [86] cleaved and polished samples to thicknesses ranging from 0.064 to 20 mm, and reported measurements at 77 and 273 K. They present transmission curves as far as $1700\,cm^{-1}$ and the corresponding absorption coefficient data over the spectral range 700 to $1500\,cm^{-1}$ (14.3 to 6.7 μm).

In the region from 2000 to about $1000\,cm^{-1}$, there are systematic differences between the two sets of data [85, 86]. The Piriou and Cabannes values become increasingly lower than those of Gourley and Runciman toward higher frequencies, but in agreement with Ref. [83]. The difference approaches a factor of two at $1700\,cm^{-1}$. We made an attempt to resolve this discrepancy by making our own measurements on cleaved MgO, with results intermediate between the two. The absorption in this spectral region is dominated by contributions from nonintrinsic proceses, and we believe that the differences in the data reflect differences between individual samples and between sample-preparation techniques. The values of $k$ selected for Table I in the range 1700 to $1050\,cm^{-1}$ are based on the Piriou and Cabannes data [86], because of their lower values.

From 1050 to $750\,cm^{-1}$ there is excellent agreement between values of $k$ derived from the absorption coefficients of Piriou and Cabannes and from the optical density curves (absorptance) of Gourley and Runciman [85]. Values in the table are taken from the smoothed curve of these data plots and therefore represent the average of these two sources.

The absorption rapidly rises in the region below $800\,cm^{-1}$, and it becomes impractical to produce samples from bulk single crystals that are sufficiently thin to make transmission techniques useful. Although some of the older works resorted to smoke or powder samples, it seems preferable to use reflectance techniques on single-crystal material, if one is interested in the intrinsic optical properties. One of the earliest analyses by reflectance techniques was by Häfele [87], who used reflectance at two different

angles to derive optical constants. Jasperse *et al.* [88] measured near-normal-incidence (11°) reflectance on single-crystal samples that had been cut, polished, and annealed. Measurements were made from 200 to 800 $cm^{-1}$ at several temperatures in the range 8.5 to 1950 K. The data were analyzed by fitting the reflectance with a two-oscillator classical dispersion model, using the equations

$$\varepsilon_1 = n^2 - k^2 = \varepsilon_\infty + \sum_j \frac{4\pi\rho_j \nu_j^2(\nu_j^2 - \nu^2)}{(\nu_j^2 - \nu^2)^2 + (\gamma_j \nu)^2} \tag{7}$$

$$\varepsilon_2 = 2nk = \sum_j \frac{4\pi\rho_j \nu_j^2(\gamma_j \nu)}{(\nu_j^2 - \nu^2)^2 + (\gamma_j \nu)^2}. \tag{8}$$

Kachare *et al.* [89] reanalyzed these results and emphasized the superiority of using a K–K analysis of the reflectance data. Piriou and Cabannes [77] made similar specular-reflectance measurements between about 300 and 1000 $cm^{-1}$ and analyzed the measurements with both a two-oscillator fit and a K–K analysis. These authors had previously made extensive studies of absorption in MgO outside of the reststrahlen region [86] and used the results in adjusting the oscillator parameters for proper fits to these accurate $k$ values. It was for this reason that we adopted their model to calculate reflection corrections at both lower and higher frequencies than the reststrahlen region, as mentioned earlier. The oscillator parameters used by Piriou and Cabannes are

$$\varepsilon_\infty = 2.964,\ \nu_1 = 396\ cm^{-1},\ 4\pi\rho_1 = 6.80,\ \gamma_1/\nu_1 = 0.0192,$$

$$\nu_2 = 643\ cm^{-1},\ 4\pi\rho = 0.043,\ \text{and}\ \gamma_2/\nu_2 = 0.140.$$

Andermann and Duesler [90] paid considerable attention to factors affecting the K–K results for MgO, especially in the very low reflectance region near 840 $cm^{-1}$ and in the shoulder region at about 720 $cm^{-1}$, where the reflectance is rapidly rising. These authors showed that even the position of the maximum absorption peak near 400 $cm^{-1}$ can be affected by slight errors in these regions away from the peak. By taking special care in these regions they have analyzed a composite of their own reflectance data and those of Piriou and Cabannes [77] to obtain a revised set of optical constants derived from the K–K technique. The values are available in tabular form in the thesis of Duesler [78] and are those presented in Table I

for the range 740 to 320 $cm^{-1}$. There is, in fact, very little difference (averaging a few percent relative difference) in the range 740 to 400 $cm^{-1}$ between the various $k$ values taken from the oscillator fits of Piriou and Cabannes [77] and Jasperse *et al.* [88], and the K–K technique of Andermann and Duesler [90]. In the 400 to 300 $cm^{-1}$ region, where $k$ rapidly decreases, there are much greater differences (approaching a factor of two).

In the far infrared beyond the strong reststrahlen peak, there are some distinct gaps in the reported optical constants of single-crystal MgO. This situation is worse for the 100 to 300 $cm^{-1}$ region than below 100 $cm^{-1}$. In the latter region, Rowntree [91] determined $k$ values from measurements of transmission. Billard *et al.* [92] measured absorption in monocrystalline samples of several thicknesses in the 20 to 350 $cm^{-1}$ spectral range, and at temperatures of 300 to 1350 K. Unfortunately, they plot absorption coefficient versus temperature at only three frequencies: 50, 70, and 90 $cm^{-1}$. At higher frequencies up to about 300 $cm^{-1}$, where we feel the K–K results become suitably accurate, we could find no pertinent measurements except for those of Hanna [62], used in Whitson's compilation [75]. However, these data were for hot-pressed powders of MgO, and not necessarily characteristic of bulk-single-crystal values.

Because of the inadequate information about the absorption in the spectral region between 100 and 300 $cm^{-1}$, one of us (DRH) collaborated with W. Kratschmer to fill this gap. A Fourier-transform infrared spectrophotometer was used to make transmission measurements at room temperature on cleaved slabs of MgO. The thicknesses were 0.0405, 2.55, and 6.12 mm. Further details of these measurements and a discussion of their physical implications will be published elsewhere [93], but we believe the $k$ values themselves are useful enough to include in the present compilation. Our own recent measurements agree rather well with those of Rowntree [91] within the region of overlap up to 85 $cm^{-1}$, so we have used his values at lower wave numbers in Table I. Rowntree estimates the experimental uncertainty in his room-temperature measurements to be $\pm 20\%$. This may be on the conservative side; our independent determinations of $k$ in the 50 to 85 $cm^{-1}$ region agree with his to better than 10%. Above 85 $cm^{-1}$, however, measurements on our 0.0405 mm sample depart seriously from the high-frequency tail of the Rowntree curve. Our data rise to a peak at about 105 $cm^{-1}$, followed by a gentle decline toward higher frequencies. Billard *et al.* [92] qualitatively described a somewhat similar behavior as "absorption abruptly rises to a considerable level at 100 $cm^{-1}$ and then stays at this level over about 100 $cm^{-1}$ before increasing again." These authors did not give the spectral absorption curve. Our values for $k$ quoted in Table I are probably accurate to within about 10% except toward the high-frequency end, where increasingly small transmission may limit the accuracy to about 30% at the last point. There remains the region 275 to

300 $cm^{-1}$, where there appears to be no good data, but a reasonable extrapolation now appears to be possible in this gap.

As noted earlier, the values of $n$ in Table I in the region below 270 $cm^{-1}$ are based on a classical oscillator fit to reflectance data [77]. However, Rowntree [91] made a more direct experimental determination of $n$ from interference spectra in the range 100 to 10 $cm^{-1}$. His values agree to within about $\pm 0.01$ with those in Table I.

For completeness, we note that the commonly accepted value of the static dielectric constant, $\varepsilon_0$, is 9.8. This was obtained experimentally by a capacitance technique by Højendahl [94] and later by analysis of optical data [91, 95].

## ACKNOWLEDGMENTS

We thank Drs. N. C. Fernelius (Wright–Patterson Air Force Base, Dayton), J. L. Freehouf (IBM, Yorktown Heights), W. F. Hanson (University of Texas, Radiological Physics Center), D. R. McKenzie (University of Sydney, Australia), and E. T. Arakawa and Y. Chen (both of Oak Ridge National Laboratory, Tennessee), for providing us with further information, including digitized data, from their original research.

## REFERENCES

1. D. R. Huffman, *Advances in Physics* **26**, 129 (1977).
2. K. Maeda, M. Uda, and Y. Hayasi, *Phys. Letters* **112A**, 431 (1985).
3. S. Nakai, T. Mitsuishi, H. Sugawara, H. Maezawa, T. Matsukawa, S. Mitani, K. Yamasaki, and T. Fujikawa, *Phys. Rev.* **B36**, 9241 (1987).
4. J. R. Townsend, *Phys. Rev.* **92**, 556 (1953).
5. V. A. Fomichev, T. M. Zimkina, and I. I. Zhukova, *Sov. Phys. Solid State* **10**, 2421 (1969).
6. V. A. Fomichev and I. I. Zhukova, *Sov. Phys. Solid State* **10**, 2992 (1969).
7. W. F. Hanson, Ph.D. Thesis, University of Tennessee, 1971.
8. W. F. Hanson, E. T. Arakawa, and M. W. Williams, *J. Appl. Phys.* **43**, 1661 (1972).
9. J. R. Nelson, *Phys. Rev.* **99**, 1902 (1955).
10. G. H. Reiling and E. B. Hensley, *Phys. Rev.* **112**, 1106 (1958).
11. P. V. Harris, Ph.D. Thesis, University of London, unpublished (1963).
12. D. M. Roessler, *Brit. J. Applied Phys.* **16**, 1359 (1965).
13. D. M. Roessler and W. C. Walker, *Phys. Rev. Letters* **17**, 319 (1966).
14. R. C. Whited and W. C. Walker, *Phys. Rev. Letters* **22**, 1428 (1969).
15. M. L. Cohen, P. J. Lin, D. M. Roessler, and W. C. Walker, *Phys. Rev.* **155**, 992 (1967).
16. D. M. Roessler and W. C. Walker, *Phys. Rev.* **159**, 733 (1967).
17. D. M. Roessler and W. C. Walker, *J. Opt. Soc. Am.* **57**, 835 (1967).
18. M. W. Williams and E. T. Arakawa, *J. Appl. Phys.* **38**, 5272 (1967).
19. J. L. Freehouf, *Phys. Rev.* **B7**, 3810 (1973).

20. V. Mikhailin, E. E. Koch, and M. Skibowski, in "Proc, 4th Int. Conf. Vac. Ultraviolet Radiation Phys.," (E. E. Koch, R. Haensel, and C. Kunz, eds.), Pergamon Press, Oxford, England, 401 (1974).
21. I. L. Kuusmann and E. K. Fel'dbakh, *Sov. Phys. Solid State* **23**, 259 (1981).
22. R. H. French and R. L. Coble, *Ann. Isr. Phys. Soc.* **6**, 261 (1984).
23. J. Carden, F. Ferrandino, J. Larsen, W. Wall, and J. R. Stevenson, in "Proc. 4th Int. Conf. Vac. Ultraviolet Radiation Phys.," (E. E. Koch, R. Haensel, and C. Kunz, eds.), Pergamon Press, Oxford, England, 572 (1974).
24. D. M. Roessler, *Brit. J. Appl. Phys.* **16**, 1119 (1965).
25. H. Venghaus, *Optics Comm.* **2**, 447 (1971).
26. V. E. Henrich, G. Dresselhaus, and H. J. Zeiger, *Phys. Rev.* **B22**, 4764 (1980).
27. K. Kambe, D. Krahl, and K.-H. Herrmann, *Ultramicroscopy* **6**, 157 (1981).
28. P. J. Martin, W. G. Sainty, R. P. Netterfield, D. R. McKenzie, D. J. H. Cockayne, S. H. Sie, O. R. Wood, and H. G. Craighead, *App. Opt.* **26**, 1235 (1987).
29. J. H. Hibben, *Phys. Rev.* **51**, 530 (1937).
30. J. P. Molnar and C. D. Hartman, *Phys. Rev.* **79**, 1015 (1950).
31. W. W. Tyler and R. L. Sproull, *Phys. Rev.* **83**, 548 (1951).
32. H. Weber, *Zeitschr. Physik* **130**, 392 (1951).
33. P. D. Johnson, *Phys. Rev.* **94**, 845 (1954).
34. W. T. Peria, *Phys. Rev.* **112**, 423 (1958).
35. C. Ballesteros, R. Gonzalez, and Y. Chen, *Phys. Rev.* **B37**, 8008 (1988).
36. C. Ballesteros, R. Gonzalez, S. J. Pennycook, and Y. Chen, *Phys. Rev.* **B38**, 4231 (1988).
37. J. A. Harrington, B. L. Bobbs, M. Braunstein, R. K. Kim, R. Stearns, and R. Braunstein, *Appl. Opt.* **17**, 1541 (1978).
38. M. Y. Sakhnovskii, *Opt. & Spectros.* **18**, 100 (1965).
39. J. A. Harrington, D. A. Gregory, and W. F. Otto, Jr., *Appl. Opt.* **15**, 1953 (1976).
40. N. C. Fernelius, G. S. Coble, D. V. Dempsey, J. A. Detrio, J. A. Fox, P. R. Greason, G. T. Johnston, and D. B. O'Quinn, *SPIE* **297**, 137 (1981).
41. N. C. Fernelius, R. J. Harris, D. B. O'Quinn, M. E. Gangl, D. V. Dempsey, and W. L. Knecht, *Opt. Eng.* **22**, 411 (1983).
42. A. Hordvik and L. Skolnik, *Appl. Opt.* **16**, 2919 (1977).
43. R. Braunstein, R. K. Kim, and M. Braunstein, NBS Special Publication 620, U.S. Government Printing Office, Washington, D.C., (1980).
44. E. S. Larsen, *Bull. Soc. Franc. Mineral.* **16**, 177 (1893).
45. E. Mallard, *Bull. Soc. Franc. Mineral.* **16**, 16 (1893).
46. E. Sommerfeldt, *Centralbl. Min. Geol. Pal.* 212 (1907).
47. F. E. Wright, *Anorg. Chemie* **68**, 410 (1910).
48. O. Westphal, *Centralbl. Min. Geol. Pal.* 516 (1913).
49. J. B. Ferguson and H. E. Merwin, *Amer. J. Science (Fourth Series)* **48**, no. 284, 81 (1919).
50. M. Haase, *Z. Kristallograph.* **65**, 509 (1927).
51. J. Strong and R. T. Brice, *J. Opt. Soc. Amer.* **25**, 207 (1935).
52. T. Radhakrishnan, *Proc. Indian Acad. Sci.* **31A**, 229 (1950).
53. T. Radhakrishnan, *Proc. Indian Acad. Sci.* **33A**, 22 (1951).
54. R. E. Stephens and I. H. Malitson, *J. Research Nat. Bur. Stand.* **49**, no. 4, 249 (1952).
55. B. D. Saksena and S. Viswanathan, *Proc. Phys. Soc.* **B69**, 129 (1956).
56. M. J. Dodge, in "CRC Handbook of Laser Science and Technology," (M. J. Weber, ed.), Vol. IV, CRC Press, Inc., Boca Raton, Florida, 31 (1986).
57. A. J. Moses, "Refractive Index of Optical Materials in the Infrared Region", EPIC Report DS-1966 (January 1970), Hughes Aircraft Company, Culver City, California; Government Report AD 704555 (1970).

58. Norton Company Refractories Division, Report #P-1.5-1, March 1, 1962.
59. M. Herzberger and C. D. Salzberg, *J. Opt. Soc. Amer.* **52**, 420 (1962).
60. "Handbook of Optics," (W. G. Driscoll and W. Vaughan, eds.), McGraw-Hill, New York, 7–93 (1978).
61. R. B. Barnes, R. R. Brattain, and F. Seitz, *Phys. Rev.* **48**, 582 (1935).
62. R. Hanna, *J. Amer. Ceram. Soc.* **48**, 376 (1965).
63. B. Welber, *Appl. Opt.* **6**, 925 (1967).
64. A. Malherbe, *Nouv. Rev. Opt. Appl.* **2**, 337 (1971).
65. A. P. Bradford, G. Hass, and M. McFarland, *Appl. Opt.* **11**, 2242 (1972).
66. R. H. Deitch, E. J. West, T. G. Giallorenzi, and J. F. Weller, *Appl. Opt.* **13**, 712 (1974).
67. R. T. Kersten, H. F. Mahlein, and W. Rauscher, *Thin Solid Films* **28**, 369 (1974).
68. C. Reale, *Comptes Rendus Acad. Bulgar. Sci. (Bulgaria)* **31**, 281 (1978).
69. J. A. Harrington, J. E. Rudisill, and M. Braunstein, *Appl. Opt.* **17**, 2798 (1978).
70. M. Blanc, *J. Optics (Paris)* **11**, 127 (1980).
71. M. O. Aboelfotoh and J. N. Ramsey, *Thin Solid Films* **91**, 191 (1982).
72. S. G. MacLean and W. W. Duley, *Astrophys. J.* **252**, L25 (1982).
73. S. G. MacLean and W. W. Duley, *J. Phys. Chem. Solids* **45**, 223 (1984).
74. D. P. DeWitt, "Handbook of the Optical, Thermal, and Mechanical Properties of Six Polycrystalline Dielectric Materials," Purdue Univ. Thermophysical Properties Research Center rept. #TPRC-19, Dec. 1972.
75. M. E. Whitson, Jr., "Handbook of the Infrared Optical Properties of $Al_2O_3$, Carbon, MgO, and $ZrO_2$," Vol. I & II, Govt. Doc. AD-A013 722/4G, June 4, 1975, Rept. TR-0075(5548)-2-Vol 1&2 SAMSO-TR-75-131-Vol-1&2.
76. C. F. Bohren and D. R. Huffman, "Absorption and Scattering of Light by Small Particles," Wiley, New York, (1983).
77. B. Piriou and F. Cabannes, *Optica Acta* **15**, 271, (1968).
78. E. Duesler, "The Kramers–Kronig Dispersion Analysis of MgO Infrared Reflectance Data," M. S. Thesis, University of Hawaii (1968).
79. R. B. Barnes and R. R. Brattain, *Phys. Rev.* **47**, 416 (1935).
80. E. Burstein, J. J. Oberly, and E. K. Plyler, *Proc. Indian Acad. Sci.* **28A**, 388 (1948).
81. J. C. Willmott, *Phys. Soc. Proc. (London)* **63A**, 389 (1950).
82. U. P. Oppenheim and A. Goldman, *J. Opt. Soc. Am.* **54**, 127 (1964).
83. D. Billard, J.-L. Servoin, F. Gervais, and B. Piriou, *High Temp. High Pressures* **11**, 415 (1979).
84. F. Cabannes and D. Billard, *Int. J. Thermophysics* **8**, 97 (1987).
85. J. T. Gourley and W. A. Runciman, *J. Phys. C: Solid State Phys.* **6**, 583 (1973).
86. B. Piriou and F. Cabannes, *C. R. Acad. Sci. Paris* **264B**, 630 (1967).
87. H. G. Häfele, *Ann. Phys.* **10**, 321 (1963).
88. J. R. Jasperse, A. Kahan, J. N. Plendl, and S. S. Mitra, *Phys. Rev.* **146**, 526 (1966).
89. A. Kachare, G. Andermann, and L. R. Brantley, *J. Phys. Chem, Solids* **33**, 467 (1972).
90. G. Andermann and E. Duesler, *J. Opt. Soc. Am.* **60**, 53 (1970).
91. R. F. Rowntree, "Measurements of the Optical Constants of Magnesium Oxide and Calcium Tungstate (spectral region between 10 $cm^{-1}$ and 100 $cm^{-1}$ at 300 K and 90 K)," Ph.D. Thesis, Ohio State University (1963); also Ohio State Univ. Sci. Report 4 (1963) and AFCRL-63-454.
92. D. Billard, F. Gervais, and B. Piriou, *Int. J. Infrared and Millimeter Waves* **1**, 641 (1980).
93. D. R. Huffman and W. Kratschmer, private communication (1989).
94. K. Højendahl, Det Kgl. Danske Videnskabernes Selskab., *Mathematisk-fysiske Meddelelser.* **16**, 3 (1938).
95. O. L. Anderson and P. Glyn, *J. Phys. Chem. Solids* **26**, 1961 (1965).
96. Based on present analysis of optical density data above 80 eV and a Kramers–Kronig analysis of composite reflectance spectra at lower energies (see text).

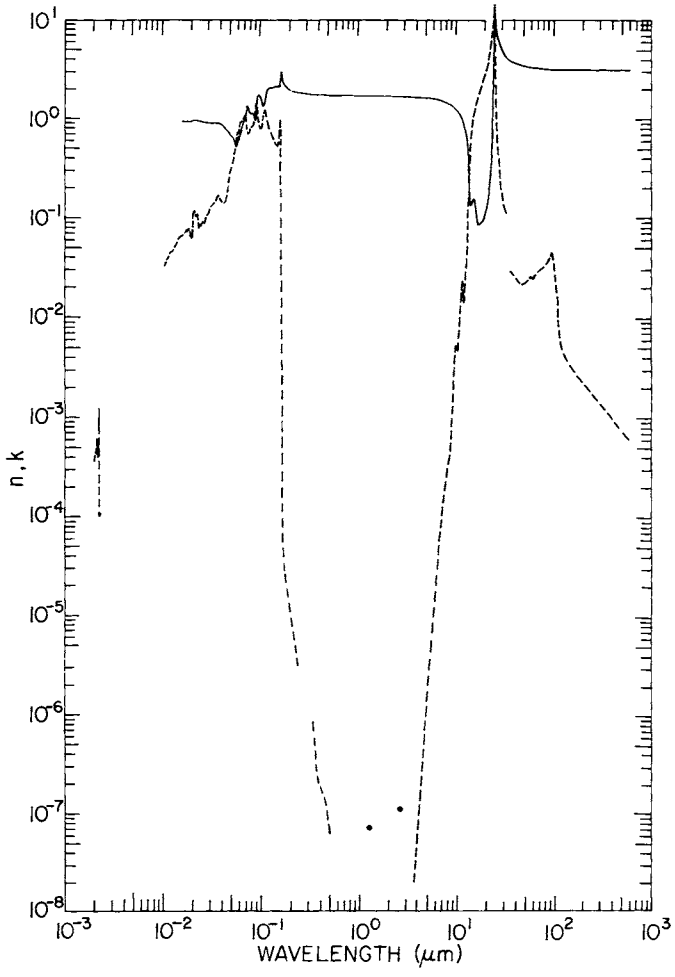


**Fig. 1.** Log–log plot of $n$ (solid line) and $k$ (dashed line) versus wavelength in micrometers for magnesium oxide.

TABLE I

Values of $n$ and $k$ for Magnesium Oxide Obtained from Various References[a]

| eV | $cm^{-1}$ | nm | n | k |
|---|---|---|---|---|
| 586 | | 2.116 | | $3.69 \times 10^{-4}$ [2] |
| 584 | | 2.123 | | 3.86 |
| 582 | | 2.130 | | 4.06 |
| 580 | | 2.138 | | 4.25 |
| 579 | | 2.141 | | 4.35 |
| 578 | | 2.145 | | 4.42 |
| 576 | | 2.153 | | 4.48 |
| 575 | | 2.156 | | 4.47 |
| 574 | | 2.160 | | 4.41 |
| 573 | | 2.164 | | 4.31 |
| 572 | | 2.168 | | 4.23 |
| 571 | | 2.171 | | 4.29 |
| 570 | | 2.175 | | 4.40 |
| 569 | | 2.179 | | 4.44 |
| 568 | | 2.183 | | 4.39 |
| 567.5 | | 2.185 | | 4.37 |
| 567 | | 2.187 | | 4.40 |
| 565 | | 2.194 | | 4.50 |
| 563 | | 2.202 | | 4.66 |
| 562 | | 2.206 | | 4.85 |
| 561 | | 2.210 | | 5.27 |
| 560 | | 2.214 | | 5.89 |
| 559 | | 2.218 | | 6.29 |
| 558.2 | | 2.221 | | 6.35 |
| 558 | | 2.222 | | 6.35 |
| 557 | | 2.226 | | 6.13 |
| 556 | | 2.230 | | 5.53 |
| 555 | | 2.234 | | 4.99 |
| 554 | | 2.238 | | 4.63 |
| 553 | | 2.242 | | 4.27 |
| 552.5 | | 2.244 | | 4.20 |
| 552.4 | | 2.245 | | 4.19 |
| 552 | | 2.246 | | 4.20 |
| 551 | | 2.250 | | 4.35 |
| 550 | | 2.254 | | 4.57 |
| 549 | | 2.258 | | 4.97 |
| 548.5 | | 2.260 | | 5.75 |
| 548 | | 2.262 | | 6.18 |
| 547.5 | | 2.265 | | 6.51 |
| 547 | | 2.267 | | 6.36 |
| 546 | | 2.271 | | 5.26 |
| 545 | | 2.275 | | 4.32 |
| 544.5 | | 2.277 | | 4.10 |
| 544 | | 2.279 | | 4.00 |
| 543 | | 2.283 | | 4.62 |

TABLE I (*Continued*)

Magnesium Oxide

| eV | $cm^{-1}$ | nm | n | k |
|---|---|---|---|---|
| 542 | | 2.288 | | $6.15 \times 10^{-4}$ |
| 541 | | 2.292 | | 8.19 |
| 540.5 | | 2.294 | | $9.50 \times 10^{-4}$ |
| 540 | | 2.296 | | $1.08 \times 10^{-3}$ |
| 539.5 | | 2.298 | | 1.20 |
| 539.3 | | 2.299 | | 1.24 |
| 539.2 | | 2.300 | | 1.26 |
| 539 | | 2.300 | | 1.25 |
| 538.5 | | 2.302 | | $1.18 \times 10^{-3}$ |
| 538 | | 2.305 | | $9.81 \times 10^{-4}$ |
| 537.5 | | 2.307 | | 8.48 |
| 537 | | 2.309 | | 7.41 |
| 536.5 | | 2.311 | | 6.37 |
| 536 | | 2.313 | | 5.32 |
| 535.5 | | 2.315 | | 4.28 |
| 535 | | 2.317 | | 3.23 |
| 534.5 | | 2.320 | | 2.30 |
| 534 | | 2.322 | | 1.75 |
| 533 | | 2.326 | | 1.40 |
| 530 | | 2.339 | | 1.18 |
| 527 | | 2.353 | | 1.08 |
| 524 | | 2.366 | | 1.04 |
| 517 | | 2.398 | | 1.03 |
| 513 | | 2.417 | | 1.02 |
| 507 | | 2.445 | | 1.06 |
| 503 | | 2.465 | | $1.09 \times 10^{-4}$ |

| eV | $cm^{-1}$ | μm | n | k |
|---|---|---|---|---|
| 121 | | 0.01025 | | 0.033 [96] |
| 118.5 | | 0.01046 | | 0.034 |
| 116 | | 0.01069 | | 0.035 |
| 114 | | 0.01088 | | 0.036 |
| 112 | | 0.01107 | | 0.037 |
| 110 | | 0.01127 | | 0.038 |
| 108 | | 0.01148 | | 0.040 |
| 106.5 | | 0.01164 | | 0.041 |
| 105 | | 0.01181 | | 0.043 |
| 104 | | 0.01192 | | 0.045 |
| 103.5 | | 0.01198 | | 0.045 |
| 101.5 | | 0.01222 | | 0.043 |
| 99.5 | | 0.01246 | | 0.045 |
| 98 | | 0.01265 | | 0.046 |
| 96.5 | | 0.01285 | | 0.045 |

TABLE I (*Continued*)

Magnesium Oxide

| eV | $cm^{-1}$ | μm | n | k |
|---|---|---|---|---|
| 95 | | 0.01305 | | 0.045 |
| 93.5 | | 0.01326 | | 0.046 |
| 92 | | 0.01348 | | 0.048 |
| 90 | | 0.01378 | | 0.051 |
| 88.5 | | 0.01401 | | 0.052 |
| 86 | | 0.01442 | | 0.053 |
| 84.5 | | 0.01467 | | 0.054 |
| 82.5 | | 0.01503 | | 0.056 |
| 80.5 | | 0.01540 | | 0.060 |
| 80 | | 0.01550 | | 0.061 |
| 78.5 | | 0.01579 | | 0.065 |
| 76.5 | | 0.01621 | | 0.069 |
| 75 | | 0.01653 | 0.951 [96] | 0.070 |
| 74 | | 0.01675 | 0.952 | 0.070 |
| 73 | | 0.01698 | 0.954 | 0.069 |
| 72 | | 0.01722 | 0.954 | 0.069 |
| 70 | | 0.01771 | 0.952 | 0.074 |
| 68 | | 0.01823 | 0.952 | 0.077 |
| 66 | | 0.01879 | 0.958 | 0.076 |
| 65 | | 0.01907 | 0.962 | 0.073 |
| 64 | | 0.01937 | 0.964 | 0.064 |
| 63 | | 0.01968 | 0.965 | 0.063 |
| 62 | | 0.02000 | 0.960 | 0.064 |
| 61 | | 0.02033 | 0.950 | 0.067 |
| 60 | | 0.02066 | 0.938 | 0.071 |
| 59 | | 0.02101 | 0.925 | 0.081 |
| 58 | | 0.02138 | 0.926 | 0.113 |
| 57 | | 0.02175 | 0.954 | 0.117 |
| 56 | | 0.02214 | 0.964 | 0.105 |
| 55 | | 0.02254 | 0.964 | 0.105 |
| 54.5 | | 0.02275 | 0.965 | 0.104 |
| 54 | | 0.02296 | 0.966 | 0.106 |
| 53 | | 0.02339 | 0.975 | 0.109 |
| 52 | | 0.02384 | 0.985 | 0.094 |
| 51.5 | | 0.02407 | 0.981 | 0.082 |
| 51 | | 0.02431 | 0.972 | 0.079 |
| 50 | | 0.02480 | 0.963 | 0.084 |
| 49 | | 0.02530 | 0.960 | 0.083 |
| 48 | | 0.02583 | 0.955 | 0.085 |
| 47 | | 0.02638 | 0.950 | 0.084 |
| 46 | | 0.02695 | 0.943 | 0.090 |
| 45 | | 0.02755 | 0.940 | 0.088 |
| 44 | | 0.02818 | 0.930 | 0.094 |
| 43 | | 0.02883 | 0.926 | 0.103 |
| 42 | | 0.02952 | 0.924 | 0.106 |

TABLE I (*Continued*)

Magnesium Oxide

| eV | $cm^{-1}$ | $\mu m$ | n | k |
|---|---|---|---|---|
| 41 | | 0.03024 | 0.918 | 0.113 |
| 40 | | 0.03100 | 0.915 | 0.123 |
| 39 | | 0.03179 | 0.916 | 0.129 |
| 38 | | 0.03263 | 0.915 | 0.133 |
| 37 | | 0.03351 | 0.912 | 0.138 |
| 36 | | 0.03444 | 0.909 | 0.140 |
| 35.5 | | 0.03493 | 0.903 | 0.143 |
| 35 | | 0.03542 | 0.898 | 0.153 |
| 34 | | 0.03647 | 0.902 | 0.165 |
| 33 | | 0.03757 | 0.908 | 0.169 |
| 32 | | 0.03875 | 0.913 | 0.166 |
| 31.5 | | 0.03936 | 0.913 | 0.160 |
| 31 | | 0.03999 | 0.909 | 0.153 |
| 30.5 | | 0.04065 | 0.901 | 0.145 |
| 30 | | 0.04133 | 0.887 | 0.142 |
| 29 | | 0.04275 | 0.862 | 0.142 |
| 28 | | 0.04428 | 0.830 | 0.142 |
| 27.5 | | 0.04509 | 0.806 | 0.146 |
| 27 | | 0.04592 | 0.781 | 0.155 |
| 26.5 | | 0.04679 | 0.754 | 0.168 |
| 26 | | 0.04769 | 0.724 | 0.188 |
| 25.5 | | 0.04862 | 0.694 | 0.221 |
| 25.0 | | 0.04959 | 0.677 | 0.264 |
| 24.9 | | 0.04979 | 0.675 | 0.275 |
| 24.8 | | 0.04999 | 0.675 | 0.287 |
| 24.5 | | 0.05061 | 0.689 | 0.303 |
| 24.3 | | 0.05102 | 0.692 | 0.304 |
| 24.1 | | 0.05145 | 0.684 | 0.309 |
| 24.0 | | 0.05166 | 0.680 | 0.313 |
| 23.9 | | 0.05188 | 0.678 | 0.319 |
| 23.7 | | 0.05231 | 0.677 | 0.325 |
| 23.5 | | 0.05276 | 0.669 | 0.328 |
| 23.3 | | 0.05321 | 0.658 | 0.334 |
| 23.0 | | 0.05391 | 0.636 | 0.348 |
| 22.7 | | 0.05462 | 0.612 | 0.365 |
| 22.5 | | 0.05510 | 0.589 | 0.382 |
| 22.2 | | 0.05585 | 0.553 | 0.423 |
| 22.0 | | 0.05636 | 0.531 | 0.464 |
| 21.8 | | 0.05687 | 0.522 | 0.511 |
| 21.6 | | 0.05740 | 0.519 | 0.507 |
| 21.5 | | 0.05767 | 0.522 | 0.586 |
| 21.4 | | 0.05794 | 0.526 | 0.614 |
| 21.3 | | 0.05821 | 0.535 | 0.642 |
| 21.2 | | 0.05848 | 0.550 | 0.669 |

TABLE I (*Continued*)

Magnesium Oxide

| eV | $cm^{-1}$ | μm | n | k |
|---|---|---|---|---|
| 21.1 | | 0.05876 | 0.568 | 0.693 |
| 21.0 | | 0.05904 | 0.592 | 0.716 |
| 20.9 | | 0.05932 | 0.624 | 0.723 |
| 20.8 | | 0.05961 | 0.645 | 0.720 |
| 20.7 | | 0.05990 | 0.659 | 0.723 |
| 20.6 | | 0.06019 | 0.676 | 0.710 |
| 20.5 | | 0.06048 | 0.673 | 0.704 |
| 20.4 | | 0.06078 | 0.669 | 0.704 |
| 20.3 | | 0.06108 | 0.661 | 0.707 |
| 20.2 | | 0.06138 | 0.651 | 0.716 |
| 20.0 | | 0.06199 | 0.632 | 0.752 |
| 19.9 | | 0.06230 | 0.625 | 0.786 |
| 19.8 | | 0.06262 | 0.635 | 0.820 |
| 19.7 | | 0.06294 | 0.652 | 0.847 |
| 19.6 | | 0.06326 | 0.670 | 0.871 |
| 19.5 | | 0.06358 | 0.691 | 0.892 |
| 19.4 | | 0.06391 | 0.714 | 0.911 |
| 19.3 | | 0.06424 | 0.743 | 0.930 |
| 19.2 | | 0.06458 | 0.776 | 0.918 |
| 19.1 | | 0.06491 | 0.780 | 0.929 |
| 19.05 | | 0.06508 | 0.792 | 0.929 |
| 19.0 | | 0.06525 | 0.798 | 0.929 |
| 18.9 | | 0.06560 | 0.807 | 0.935 |
| 18.8 | | 0.06595 | 0.817 | 0.944 |
| 18.7 | | 0.06630 | 0.828 | 0.955 |
| 18.6 | | 0.06666 | 0.842 | 0.969 |
| 18.5 | | 0.06702 | 0.859 | 0.982 |
| 18.35 | | 0.06757 | 0.887 | 0.996 |
| 18.2 | | 0.06812 | 0.915 | 1.007 |
| 18.1 | | 0.06850 | 0.931 | 1.014 |
| 18.0 | | 0.06888 | 0.947 | 1.023 |
| 17.9 | | 0.06926 | 0.964 | 1.034 |
| 17.8 | | 0.06965 | 0.984 | 1.049 |
| 17.7 | | 0.07005 | 1.009 | 1.064 |
| 17.65 | | 0.07025 | 1.025 | 1.074 |
| 17.6 | | 0.07045 | 1.046 | 1.082 |
| 17.5 | | 0.07085 | 1.087 | 1.074 |
| 17.4 | | 0.07126 | 1.119 | 1.081 |
| 17.3 | | 0.07167 | 1.166 | 1.074 |
| 17.2 | | 0.07208 | 1.203 | 1.043 |
| 17.1 | | 0.07251 | 1.224 | 1.023 |
| 17.0 | | 0.07293 | 1.241 | 1.001 |
| 16.95 | | 0.07315 | 1.248 | 1.001 |
| 16.9 | | 0.07336 | 1.265 | 1.000 |
| 16.8 | | 0.07380 | 1.301 | 0.976 |

TABLE I (*Continued*)

Magnesium Oxide

| eV | $cm^{-1}$ | $\mu m$ | n | k |
|---|---|---|---|---|
| 16.7 | | 0.07424 | 1.333 | 0.941 |
| 16.6 | | 0.07469 | 1.341 | 0.883 |
| 16.5 | | 0.07514 | 1.344 | 0.862 |
| 16.4 | | 0.07560 | 1.346 | 0.810 |
| 16.3 | | 0.07606 | 1.337 | 0.774 |
| 16.2 | | 0.07653 | 1.301 | 0.714 |
| 16.1 | | 0.07701 | 1.247 | 0.705 |
| 16.0 | | 0.07749 | 1.214 | 0.724 |
| 15.9 | | 0.07798 | 1.195 | 0.727 |
| 15.8 | | 0.07847 | 1.173 | 0.736 |
| 15.7 | | 0.07897 | 1.160 | 0.760 |
| 15.5 | | 0.07999 | 1.149 | 0.773 |
| 15.4 | | 0.08051 | 1.141 | 0.788 |
| 15.3 | | 0.08104 | 1.135 | 0.798 |
| 15.2 | | 0.08157 | 1.131 | 0.819 |
| 15.1 | | 0.08211 | 1.139 | 0.835 |
| 15.0 | | 0.08266 | 1.147 | 0.841 |
| 14.9 | | 0.08321 | 1.149 | 0.843 |
| 14.8 | | 0.08377 | 1.150 | 0.852 |
| 14.7 | | 0.08434 | 1.149 | 0.847 |
| 14.6 | | 0.08492 | 1.137 | 0.851 |
| 14.5 | | 0.08551 | 1.120 | 0.864 |
| 14.4 | | 0.08610 | 1.115 | 0.883 |
| 14.3 | | 0.08670 | 1.110 | 0.903 |
| 14.2 | | 0.08731 | 1.106 | 0.919 |
| 14.1 | | 0.08793 | 1.094 | 0.929 |
| 14.0 | | 0.08856 | 1.065 | 0.947 |
| 13.9 | | 0.08920 | 1.023 | 0.994 |
| 13.8 | | 0.08984 | 0.990 | 1.087 |
| 13.75 | | 0.09017 | 0.984 | 1.133 |
| 13.7 | | 0.09050 | 0.980 | 1.218 |
| 13.6 | | 0.09116 | 1.054 | 1.350 |
| 13.55 | | 0.09150 | 1.111 | 1.418 |
| 13.5 | | 0.09184 | 1.191 | 1.471 |
| 13.45 | | 0.09218 | 1.283 | 1.499 |
| 13.4 | | 0.09253 | 1.374 | 1.507 |
| 13.35 | | 0.09287 | 1.463 | 1.503 |
| 13.3 | | 0.09322 | 1.549 | 1.479 |
| 13.25 | | 0.09357 | 1.632 | 1.446 |
| 13.2 | | 0.09393 | 1.702 | 1.380 |
| 13.15 | | 0.09428 | 1.744 | 1.312 |
| 13.1 | | 0.09464 | 1.768 | 1.248 |
| 13.05 | | 0.09501 | 1.779 | 1.193 |
| 13.0 | | 0.09537 | 1.786 | 1.147 |
| 12.95 | | 0.09574 | 1.789 | 1.103 |

TABLE I (*Continued*)

Magnesium Oxide

| eV | $cm^{-1}$ | μm | n | k |
|---|---|---|---|---|
| 12.9 | | 0.09611 | 1.788 | 1.065 |
| 12.8 | | 0.09686 | 1.779 | 0.997 |
| 12.6 | | 0.09840 | 1.745 | 0.894 |
| 12.5 | | 0.09919 | 1.723 | 0.858 |
| 12.4 | | 0.1000 | 1.694 | 0.824 |
| 12.1 | | 0.1025 | 1.603 | 0.770 |
| 12.0 | | 0.1033 | 1.565 | 0.765 |
| 11.9 | | 0.1042 | 1.520 | 0.767 |
| 11.8 | | 0.1051 | 1.473 | 0.787 |
| 11.65 | | 0.1064 | 1.397 | 0.839 |
| 11.6 | | 0.1069 | 1.370 | 0.890 |
| 11.5 | | 0.1078 | 1.371 | 1.000 |
| 11.4 | | 0.1088 | 1.409 | 1.081 |
| 11.3 | | 0.1097 | 1.468 | 1.161 |
| 11.2 | | 0.1107 | 1.555 | 1.210 |
| 11.15 | | 0.1112 | 1.601 | 1.220 |
| 11.1 | | 0.1117 | 1.646 | 1.230 |
| 11.0 | | 0.1127 | 1.735 | 1.228 |
| 10.9 | | 0.1137 | 1.814 | 1.202 |
| 10.8 | | 0.1148 | 1.877 | 1.166 |
| 10.5 | | 0.1181 | 1.999 | 1.041 |
| 10.2 | | 0.1216 | 2.045 | 0.921 |
| 10.0 | | 0.1240 | 2.061 | 0.867 |
| 9.8 | | 0.1265 | 2.074 | 0.819 |
| 9.7 | | 0.1278 | 2.079 | 0.798 |
| 9.5 | | 0.1305 | 2.091 | 0.761 |
| 9.3 | | 0.1333 | 2.103 | 0.728 |
| 9.0 | | 0.1378 | 2.130 | 0.679 |
| 8.8 | | 0.1409 | 2.147 | 0.642 |
| 8.5 | | 0.1459 | 2.160 | 0.587 |
| 8.2 | | 0.1512 | 2.171 | 0.545 |
| 8.1 | | 0.1531 | 2.168 | 0.532 |
| 8.0 | | 0.1550 | 2.154 | 0.530 |
| 7.95 | | 0.1560 | 2.145 | 0.539 |
| 7.90 | | 0.1569 | 2.137 | 0.558 |
| 7.85 | | 0.1579 | 2.127 | 0.589 |
| 7.83 | | 0.1583 | 2.126 | 0.611 |
| 7.80 | | 0.1590 | 2.132 | 0.651 |
| 7.75 | | 0.1600 | 2.180 | 0.731 |
| 7.70 | | 0.1610 | 2.270 | 0.813 |
| 7.68 | | 0.1614 | 2.327 | 0.851 |
| 7.66 | | 0.1619 | 2.389 | 0.885 |
| 7.64 | | 0.1623 | 2.498 | 0.936 |
| 7.63 | | 0.1625 | 2.574 | 0.949 |
| 7.62 | | 0.1627 | 2.665 | 0.944 |
| 7.61 | | 0.1629 | 2.753 | 0.912 |

TABLE I (*Continued*)

**Magnesium Oxide**

| eV | $cm^{-1}$ | $\mu m$ | n | k |
|---|---|---|---|---|
| 7.60 | | 0.1631 | 2.839 | 0.866 |
| 7.59 | | 0.1634 | 2.922 | 0.800 |
| 7.58 | | 0.1636 | 2.994 | 0.711 |
| 7.57 | | 0.1638 | 3.048 | 0.600 |
| 7.56 | | 0.1640 | 3.061 | 0.474 |
| 7.55 | | 0.1642 | 3.035 | 0.360 |
| 7.54 | | 0.1644 | 2.999 | 0.272 |
| 7.53 | | 0.1647 | 2.944 | 0.204 |
| 7.52 | | 0.1649 | 2.892 | 0.149 |
| 7.50 | | 0.1653 | 2.793 | 0.076 |
| 7.48 | | 0.1658 | 2.701 | 0.039 |
| 7.45 | | 0.1664 | 2.603 | 0.018 |
| 7.40 | | 0.1675 | 2.494 | 0.002 |
| 7.35 | | 0.1687 | 2.419 | |
| 7.30 | | 0.1698 | 2.363 | |
| 7.28 | | 0.1703 | 2.346 | $1.36 \times 10^{-4}$ [33] |
| 7.25 | | 0.1710 | 2.319 | |
| 7.20 | | 0.1722 | 2.281 | $7.6 \times 10^{-5}$ |
| 7.185 | | 0.1726 | 2.269 | 6.87 |
| 7.15 | | 0.1734 | 2.248 | |
| 7.14 | | 0.1737 | 2.241 | 5.53 |
| 7.10 | | 0.1746 | 2.220 | |
| 7.06 | | 0.1757 | 2.198 | 4.19 |
| 7.05 | | 0.1759 | 2.196 | |
| 7.00 | | 0.1771 | 2.176 | 3.7 |
| 6.90 | | 0.1797 | 2.141 | |
| 6.89 | | 0.1800 | 2.138 | 2.86 |
| 6.80 | | 0.1823 | 2.110 | |
| 6.70 | | 0.1851 | 2.084 | 2.00 |
| 6.60 | | 0.1879 | 2.060 | |
| 6.50 | | 0.1907 | 2.039 | 1.39 [36] |
| 6.40 | | 0.1937 | 2.020 | |
| 6.20 | 50,000 | 0.2000 | 1.986 | 1.11 |
| 6.00 | 48,393 | 0.2066 | 1.958 | $1.0 \times 10^{-5}$ |
| 5.80 | 46,780 | 0.2138 | 1.933 | $8.5 \times 10^{-6}$ |
| 5.60 | 45,167 | 0.2214 | 1.911 | 7.0 [34] |
| 5.50 | 44,360 | 0.2254 | 1.901 | 6.0 |
| 5.40 | 43,554 | 0.2296 | 1.892 | 5.0 |
| 5.20 | 41,941 | 0.2384 | 1.874 | 3.7 |
| 5.09 | 41,054 | 0.2436 | 1.865 | 3.2 |
| 5.00 | 40,328 | 0.2480 | 1.858 | $3.1 \times 10^{-6}$ [32] |
| 4.75 | 38,311 | 0.2610 | 1.840 | |
| 4.50 | 36,295 | 0.2755 | 1.824 | |
| 4.25 | 34,279 | 0.2917 | 1.810 | |
| 4.00 | 32,262 | 0.3100 | 1.798 | |
| 3.75 | 30,246 | 0.3306 | 1.785 | |

TABLE I (*Continued*)

**Magnesium Oxide**

| eV | $cm^{-1}$ | μm | n | k |
|---|---|---|---|---|
| 3.531 | 28,482 | 0.3511 | 1.7768 [56] | |
| 3.487 | 28,125 | 0.3556 | 1.7755 [54] | $8.5 \times 10^{-7}$ [37] |
| 3.435 | 27,705 | 0.3609 | 1.7732 | 5.75 |
| 3.433 | 27,688 | 0.36117 | 1.77318 | 5.65 |
| 3.397 | 27,396 | 0.36502 | 1.77186 | 4.9 |
| 3.245 | 26,173 | 0.3821 | 1.7668 | 2.75 |
| 3.206 | 25,859 | 0.3867 | 1.7655 | 2.45 |
| 3.152 | 25,423 | 0.3934 | 1.7638 | 2.2 |
| 3.064 | 24,710 | 0.4047 | 1.76104 | 1.95 |
| 2.877 | 23,205 | 0.4310 | 1.7557 | 1.7 |
| 2.845 | 22,946 | 0.4358 | 1.75471 | 1.65 |
| 2.708 | 21,839 | 0.4579 | 1.7512 | 1.45 |
| 2.594 | 20,922 | 0.4780 | 1.7483 | 1.15 |
| 2.551 | 20,572 | 0.4861 | 1.74711 | $1.0 \times 10^{-7}$ |
| 2.541 | 20,492 | 0.4880 | 1.7469 [56] | $9.75 \times 10^{-8}$ |
| 2.480 | 20,000 | 0.5 | 1.7454 [59] | 8.25 |
| 2.468 | 19,906 | 0.5024 | 1.7453 [54] | 8.0 |
| 2.438 | 19,666 | 0.5085 | 1.74446 | 7.0 |
| 2.410 | 19,436 | 0.5145 | 1.7439 | 6.55 |
| 2.270 | 18,312 | 0.5461 | 1.74077 | |
| 2.104 | 16,969 | 0.5893 | 1.73737 | |
| 1.959 | 15,803 | 0.6328 | 1.7346 [56] | |
| 1.926 | 15,533 | 0.6438 | 1.73400 [54] | |
| 1.889 | 15,237 | 0.6563 | 1.73335 | |
| 1.857 | 14,975 | 0.6678 | 1.73277 | |
| 1.795 | 14,478 | 0.6907 | 1.73191 [58] | |
| 1.755 | 14,154 | 0.7065 | 1.73101 [54] | |
| 1.615 | 13,023 | 0.7679 | 1.72872 | |
| 1.240 | 10,000 | 1.0 | 1.7229 [59] | |
| 1.223 | 9,862 | 1.01398 | 1.72259 [58] | |
| 1.170 | 9,434 | 1.06 | 1.7217 [56] | |
| 1.099 | 8,860 | 1.12866 | 1.72059 [54] | |
| 0.9400 | 7,582 | 1.319 | 1.7177 | $7.1 \times 10^{-8}$ [41] |
| 0.9068 | 7,314 | 1.36728 | 1.71715 | |
| 0.8266 | 6,667 | 1.5 | 1.7153 [59] | |
| 0.8106 | 6,538 | 1.52952 | 1.71496 [54] | |
| 0.7999 | 6,452 | 1.55 | 1.7147 [56] | |
| 0.7322 | 5,906 | 1.6932 | 1.71281 [54] | |
| 0.7254 | 5,851 | 1.7092 | 1.71258 | |
| 0.6838 | 5,516 | 1.81307 | 1.71108 | |
| 0.6293 | 5,076 | 1.97009 | 1.70885 [58] | |
| 0.6199 | 5,000 | 2.0 | 1.7085 [59] | |
| 0.5512 | 4,446 | 2.24929 | 1.70470 [54] | |
| 0.5332 | 4,300 | 2.32542 | 1.70350 | |
| 0.4959 | 4,000 | 2.5 | 1.7007 [59] | |
| 0.4592 | 3,704 | 2.7 | 1.6973 [54] | $1.1 \times 10^{-7}$ [42] |

TABLE I (*Continued*)

Magnesium Oxide

| eV | $cm^{-1}$ | $\mu m$ | n | k |
|---|---|---|---|---|
| 0.4428 | 3,571 | 2.8 | 1.6954 [56] | |
| 0.4133 | 3,333 | 3.0 | 1.6915 [59] | |
| 0.3753 | 3,027 | 3.3033 | 1.68526 [58] | |
| 0.3720 | 3,000 | 3.333 | 1.6846 [54] | |
| 0.3596 | 2,900 | 3.448 | 1.6820 | |
| 0.3542 | 2,857 | 3.5 | 1.6806 [59] | |
| 0.3535 | 2,851 | 3.5078 | 1.68055 [54] | |
| 0.3472 | 2,800 | 3.571 | 1.6791 | |
| 0.3348 | 2,700 | 3.704 | 1.6758 | |
| 0.3263 | 2,632 | 3.8 | 1.6734 | $2.0 \times 10^{-8}$ [42] |
| 0.3224 | 2,600 | 3.846 | 1.6722 | |
| 0.3100 | 2,500 | 4.0 | 1.6679 [59] | 3.7 |
| 0.2976 | 2,400 | 4.167 | 1.6634 [54] | $7.4 \times 10^{-8}$ |
| 0.2912 | 2,349 | 4.258 | 1.66039 [58] | $1.0 \times 10^{-7}$ |
| 0.2852 | 2,300 | 4.348 | 1.6581 [54] | 1.5 |
| 0.2755 | 2,222 | 4.5 | 1.6533 [59] | 2.5 |
| 0.2728 | 2,200 | 4.545 | 1.6520 [54] | 2.9 |
| 0.2604 | 2,100 | 4.762 | 1.6450 | $5.8 \times 10^{-7}$ |
| 0.2480 | 2,000 | 5.0 | 1.6373 | $1.2 \times 10^{-6}$ |
| 0.2418 | 1,950 | 5.128 | 1.6328 [77] | 1.63 [83] |
| 0.2380 | 1,920 | 5.208 | 1.6299 | 2.0 [42] |
| 0.2356 | 1,900 | 5.263 | 1.6278 | 2.3 |
| 0.2331 | 1,880 | 5.319 | 1.6256 | 2.7 |
| 0.2306 | 1,860 | 5.376 | 1.6233 | 3.1 |
| 0.2281 | 1,840 | 5.435 | 1.6210 | 3.5 |
| 0.2257 | 1,820 | 5.495 | 1.6186 | 4.0 |
| 0.2231 | 1,800 | 5.555 | 1.6161 | 4.6 |
| 0.2207 | 1,780 | 5.618 | 1.6135 | 5.3 |
| 0.2182 | 1,760 | 5.682 | 1.6108 | 6.1 |
| 0.2157 | 1,740 | 5.747 | 1.6080 | 7.1 |
| 0.2132 | 1,720 | 5.814 | 1.6051 | 8.1 |
| 0.2108 | 1,700 | 5.882 | 1.6021 | $9.0 \times 10^{-6}$ [86] |
| 0.2083 | 1,680 | 5.952 | 1.5989 | $1.1 \times 10^{-5}$ [42] |
| 0.2058 | 1,660 | 6.024 | 1.5957 | 1.2 |
| 0.2033 | 1,640 | 6.098 | 1.5922 | 1.4 |
| 0.2008 | 1,620 | 6.172 | 1.5887 | 1.6 |
| 0.1984 | 1,600 | 6.250 | 1.5849 | 1.83 [86] |
| 0.1959 | 1,580 | 6.329 | 1.5811 | 2.2 [42] |
| 0.1934 | 1,560 | 6.410 | 1.5770 | 2.5 |
| 0.1909 | 1,540 | 6.494 | 1.5727 | 2.9 |
| 0.1884 | 1,520 | 6.579 | 1.5683 | 3.3 |
| 0.1860 | 1,500 | 6.667 | 1.5636 | 4.60 [86] |
| 0.1835 | 1,480 | 6.757 | 1.5510 | 5.38 |
| 0.1810 | 1,460 | 6.849 | 1.5536 | 5.98 |
| 0.1785 | 1,440 | 6.944 | 1.548 | 7.00 |

TABLE I (*Continued*)

Magnesium Oxide

| eV | $cm^{-1}$ | $\mu m$ | n | k |
|---|---|---|---|---|
| 0.1760 | 1,420 | 7.042 | 1.543 | $7.89 \times 10^{-5}$ |
| 0.1736 | 1,400 | 7.143 | 1.537 | 8.59 |
| 0.1711 | 1,380 | 7.246 | 1.530 | $9.30 \times 10^{-5}$ |
| 0.1686 | 1,360 | 7.352 | 1.524 | $1.03 \times 10^{-4}$ |
| 0.1661 | 1,340 | 7.463 | 1.517 | 1.15 |
| 0.1637 | 1,320 | 7.576 | 1.509 | 1.31 |
| 0.1612 | 1,300 | 7.692 | 1.502 | 1.54 |
| 0.1587 | 1,280 | 7.812 | 1.493 | 1.84 |
| 0.1562 | 1,260 | 7.936 | 1.485 | 2.11 |
| 0.1537 | 1,240 | 8.065 | 1.475 | 2.47 |
| 0.1513 | 1,220 | 8.197 | 1.465 | 2.73 |
| 0.1488 | 1,200 | 8.333 | 1.455 | 3.09 |
| 0.1463 | 1,180 | 8.475 | 1.443 | 3.26 |
| 0.1438 | 1,160 | 8.621 | 1.431 | 3.52 |
| 0.1413 | 1,140 | 8.772 | 1.418 | 4.14 |
| 0.1389 | 1,120 | 8.929 | 1.404 | 5.76 |
| 0.1364 | 1,100 | 9.091 | 1.389 | 6.27 |
| 0.1339 | 1,080 | 9.259 | 1.373 | $8.47 \times 10^{-4}$ |
| 0.1314 | 1,060 | 9.434 | 1.355 | $1.07 \times 10^{-3}$ |
| 0.1302 | 1,050 | 9.524 | 1.346 | 1.33 |
| 0.1289 | 1,040 | 9.615 | 1.336 | 1.58 [85,86] |
| 0.1277 | 1,030 | 9.709 | 1.326 | 1.92 |
| 0.1265 | 1,020 | 9.804 | 1.315 | 2.44 |
| 0.1252 | 1,010 | 9.901 | 1.304 | 3.02 |
| 0.1240 | 1,000 | 10.00 | 1.292 | 3.90 |
| 0.1227 | 990 | 10.10 | 1.280 | 4.70 |
| 0.1215 | 980 | 10.20 | 1.267 | 5.13 |
| 0.1202 | 970 | 10.31 | 1.253 | 4.29 |
| 0.1190 | 960 | 10.42 | 1.239 | 3.55 |
| 0.1178 | 950 | 10.53 | 1.224 | 3.40 |
| 0.1165 | 940 | 10.64 | 1.209 | 3.70 |
| 0.1153 | 930 | 10.75 | 1.191 | 4.58 |
| 0.1141 | 920 | 10.87 | 1.174 | 5.91 |
| 0.1128 | 910 | 10.99 | 1.155 | $7.80 \times 10^{-3}$ |
| 0.1116 | 900 | 11.11 | 1.135 | 0.0102 |
| 0.1103 | 890 | 11.24 | 1.114 | 0.0137 |
| 0.1091 | 880 | 11.36 | 1.091 | 0.0162 |
| 0.1079 | 870 | 11.49 | 1.067 | 0.0196 |
| 0.1066 | 860 | 11.63 | 1.041 | 0.0223 |
| 0.1060 | 855 | 11.70 | 1.027 | 0.0229 |
| 0.1054 | 850 | 11.76 | 1.013 | 0.0227 |
| 0.1041 | 840 | 11.90 | 0.982 | 0.0205 |
| 0.1029 | 830 | 12.05 | 0.949 | 0.0171 |
| 0.1017 | 820 | 12.20 | 0.913 | 0.0147 |
| 0.1010 | 815 | 12.27 | 0.893 | 0.0143 |

TABLE I (*Continued*)

Magnesium Oxide

| eV | $cm^{-1}$ | μm | n | k |
|---|---|---|---|---|
| 0.1004 | 810 | 12.35 | 0.873 | 0.0146 |
| 0.0992 | 800 | 12.50 | 0.829 | 0.0167 |
| 0.0979 | 790 | 12.66 | 0.780 | 0.0236 |
| 0.0967 | 780 | 12.82 | 0.724 | 0.0295 |
| 0.0955 | 770 | 12.99 | 0.660 | 0.0346 |
| 0.0930 | 750 | 13.33 | 0.503 | 0.0475 |
| 0.0918 | 740 | 13.51 | 0.393 | 0.0913 [78] |
| 0.0905 | 730 | 13.70 | 0.267 | 0.172 |
| 0.0893 | 720 | 13.89 | 0.156 | 0.317 |
| 0.0880 | 710 | 14.08 | 0.139 | 0.478 |
| 0.0868 | 700 | 14.29 | 0.132 | 0.595 |
| 0.0856 | 690 | 14.49 | 0.134 | 0.692 |
| 0.0843 | 680 | 14.71 | 0.136 [78] | 0.787 |
| 0.0831 | 670 | 14.93 | 0.143 | 0.877 |
| 0.0818 | 660 | 15.15 | 0.154 | 0.955 |
| 0.0806 | 650 | 15.38 | 0.155 | 1.03 |
| 0.0794 | 640 | 15.63 | 0.151 | 1.09 |
| 0.0781 | 630 | 15.87 | 0.135 | 1.17 |
| 0.0769 | 620 | 16.13 | 0.116 | 1.26 |
| 0.0756 | 610 | 16.39 | 0.108 | 1.35 |
| 0.0744 | 600 | 16.67 | 0.098 | 1.45 |
| 0.0732 | 590 | 16.95 | 0.086 | 1.56 |
| 0.0719 | 580 | 17.24 | 0.087 | 1.67 |
| 0.0707 | 570 | 17.54 | 0.086 | 1.78 |
| 0.0694 | 560 | 17.86 | 0.088 | 1.90 |
| 0.0682 | 550 | 18.18 | 0.089 | 2.03 |
| 0.0670 | 540 | 18.52 | 0.091 | 2.16 |
| 0.0657 | 530 | 18.87 | 0.093 | 2.31 |
| 0.0645 | 520 | 19.23 | 0.097 | 2.47 |
| 0.0632 | 510 | 19.61 | 0.102 | 2.64 |
| 0.0620 | 500 | 20.00 | 0.109 | 2.84 |
| 0.0608 | 490 | 20.41 | 0.119 | 3.06 |
| 0.0595 | 480 | 20.83 | 0.131 | 3.31 |
| 0.0583 | 470 | 21.28 | 0.148 | 3.60 |
| 0.0570 | 460 | 21.74 | 0.170 | 3.95 |
| 0.0558 | 450 | 22.22 | 0.207 | 4.39 |
| 0.0546 | 440 | 22.73 | 0.261 | 4.95 |
| 0.0533 | 430 | 23.26 | 0.362 | 5.71 |
| 0.0521 | 420 | 23.81 | 0.543 | 6.86 |
| 0.0508 | 410 | 24.39 | 1.01 | 8.97 |
| 0.0496 | 400 | 25.00 | 5.05 | 15.20 |
| 0.0484 | 390 | 25.64 | 13.50 | 4.06 |
| 0.0471 | 380 | 26.32 | 9.28 | 1.02 |
| 0.0459 | 370 | 27.03 | 7.44 | 0.56 |
| 0.0446 | 360 | 27.78 | 6.46 | 0.379 |
| 0.0434 | 350 | 28.57 | 5.83 | 0.266 |

TABLE I (*Continued*)

Magnesium Oxide

| eV | $cm^{-1}$ | $\mu m$ | n | k |
|---|---|---|---|---|
| 0.0425 | 340 | 29.41 | 5.35 | 0.208 |
| 0.0409 | 330 | 30.30 | 5.03 | 0.168 |
| 0.0397 | 320 | 31.25 | 4.74 | 0.129 |
| 0.0384 | 310 | 32.26 | 4.51 | 0.126 |
| 0.0372 | 300 | 33.33 | 4.36 | 0.113 |
| 0.0335 | 270 | 37.04 | 3.97 [77] | 0.029 [93] |
| 0.0322 | 260 | 38.46 | 3.87 | 0.0276 |
| 0.0310 | 250 | 40.00 | 3.78 | 0.0265 |
| 0.0298 | 240 | 41.67 | 3.71 | 0.0254 |
| 0.0285 | 230 | 43.47 | 3.64 | 0.0233 |
| 0.0273 | 220 | 45.46 | 3.58 | 0.0215 |
| 0.0260 | 210 | 47.62 | 3.53 | 0.0214 |
| 0.0248 | 200 | 50.00 | 3.48 | 0.0218 |
| 0.0236 | 190 | 52.63 | 3.44 | 0.0220 |
| 0.0223 | 180 | 55.56 | 3.40 | 0.0236 |
| 0.0211 | 170 | 58.82 | 3.37 | 0.0255 |
| 0.0198 | 160 | 62.50 | 3.34 | 0.0246 |
| 0.0186 | 150 | 66.67 | 3.31 | 0.0280 |
| 0.0174 | 140 | 71.43 | 3.28 | 0.0299 |
| 0.0161 | 130 | 76.92 | 3.26 | 0.0313 |
| 0.0149 | 120 | 83.33 | 3.24 | 0.0338 |
| 0.0136 | 110 | 90.91 | 3.22 | 0.0387 |
| 0.0130 | 105 | 95.24 | 3.21 | 0.0455 |
| 0.0124 | 100 | 100.00 | 3.20 | 0.0356 |
| 0.0118 | 95 | 105.2 | 3.20 | 0.0236 |
| 0.0112 | 90 | 111.1 | 3.19 | 0.0146 |
| 0.0105 | 85 | 117.6 | 3.18 | $6.2 \times 10^{-3}$ [91] |
| 0.0099 | 80 | 125.0 | 3.178 | 4.8 |
| 0.0093 | 75 | 133.3 | 3.172 | 3.9 |
| 0.0087 | 70 | 142.9 | 3.167 | 3.42 |
| 0.0081 | 65 | 153.8 | 3.162 | 3.15 |
| 0.0074 | 60 | 166.7 | 3.157 | 2.80 |
| 0.0068 | 55 | 181.8 | 3.153 | 2.53 |
| 0.0062 | 50 | 200.0 | 3.149 | 2.28 |
| 0.0056 | 45 | 222.2 | 3.146 | 2.00 |
| 0.0049 | 40 | 250.0 | 3.143 | 1.79 |
| 0.0043 | 35 | 285.7 | 3.140 | 1.51 |
| 0.0037 | 30 | 333.3 | 3.138 | $1.21 \times 10^{-3}$ |
| 0.0031 | 25 | 400.0 | 3.136 | $9.8 \times 10^{-4}$ |
| 0.0025 | 20 | 500.0 | 3.134 | 7.3 |
| 0.0020 | 16 | 625.0 | 3.133 | $5.8 \times 10^{-4}$ |

[a]References are given in brackets.

# Polyethylene $(C_2H_4)_n$

J. ASHOK and P. L. H. VARAPRASAD
Applied Physics Department
Andhra University
Visakhapatnam, India
and
J. R. BIRCH
Division of Electrical Science
National Physical Laboratory
Teddington, Middlesex TW11 0LW, United Kingdom

In the papers to be discussed, a variety of polyethylenes have been studied, so one cannot hope to collect $n$ and $k$ over a wide spectral range for a given type of material. Luckily, the variations among materials are usually less than a factor of two where spectra overlap.

Ideal polyethylene forms a planar (zigzag) carbon chain constructed with C═C and C═H $\sigma$ bonds only (see inset in Fig. 1). The unit cell contains two $C_2H_4$ molecules. Normal commercial low-density polyethylene is usually around 80% crystalline [1]. Partridge [2], however, reports a crystallinity of only 55%. The values of bond length and bond angle are 1.53 Å and 112°, respectively. The refractive index for amorphous specimens is given as 1.49 and for crystalline material as $\alpha \approx \beta = 1.52$ and $\gamma = 1.582$ at $\lambda = 5461$ Å (where $\alpha$, $\beta$, and $\gamma$ are the refractive indices along the $a$, $b$, and $c$ crystallographic directions) [3–5].

Light-scattering experiments made by Partridge [6] have shown considerable scattering by thick polyethylene samples. A method of correcting for light scattering has been discussed in this paper.

Optical properties of polyethylene in the photon energy range 76–0.5 eV have been measured by Painter *et al.* [7]. Various transmission techniques were used over nearly the entire range; free-standing Glad Wrap (Union Carbide registered trade name); Dow Corning polyethylene pellets evaporated onto one half of a $MgF_2$ disk; polyethylene evaporated onto one half of a thick layer of *p*-terphenyl covering a glass slide. The *p*-terphenyl is fluorescent, so light passing through the polyethylene produces light emission in the *p*-terphenyl, which is measured through the glass slide. It is probable that the polyethylene was not highly crystalline (and perhaps it was even amorphous). The UV structure is primarily due to the chain carbon atoms and is probably similar for crystalline or amorphous polyethylene. We assume unpolarized light was used and that normal incidence


Copyright © 1991 by Academic Press.
All rights of reproduction in any form reserved.
ISBN 0-12-544422-2

was maintained with the Cary and Seya–Namioka monochromators used. The index of refraction was measured using a critical-angle measurement. A polyethylene film was deposited onto the flat side of sapphire hemicylinder. The angle of incidence was varied to detect the critical angle. Painter *et al.* extrapolated their $k$ values to high energy and calculated the contribution of the C atomic scattering cross-section at 282 eV. Although there is concern about light scattering in polyethylene (samples are often not clear to the eye), this does not appear to have been a problem into the short-wavelength UV. The results for $n$ and $k$ obtained from tables and graphs in Ref. [7] are listed in Table I and plotted in Fig. 1.

Ritsko [1] reported measurements on films of polyethylene prepared from solvent evaporation. The thickness of the films was about 1000–2000 Å. They obtained values of the real and imaginary parts of the dielectric constants from measurements of energy-loss spectra and application of Kramers–Kronig analysis. The energy-loss spectra of an electron beam were recorded as a function of scattering angles $\theta$ or momentum transfer $\Phi$. The samples were exposed to the incident beam for five minutes at $\theta = 0$. The energy-loss probability or differential scattering cross-section per unit energy loss $E$ per unit solid angle $\Omega$ is a function of $\varepsilon$, the complex dielectric response function with real and imaginary parts $\varepsilon_1$ and $\varepsilon_2$, respectively [8].

Since the energy-loss spectrum is proportional to the energy-loss function $\mathrm{Im}(-1/\varepsilon)$, the constant of proportionality can be determined by normalizing the spectrum to the known value of the refractive index 1.4907 at 2.22 eV [9]. In addition, a correction for multiple inelastic scattering was made for the spectrum. Once the energy-loss function was normalized and multiple scattering eliminated, the function $\mathrm{Re}(-1/\varepsilon)$ was computed from the Kramers–Kronig relation, and hence, $\varepsilon_1$ and $\varepsilon_2$ could be calculated [10]. The complex refractive index $(n+ik) = \sqrt{\varepsilon}$ is listed in Table I. Where overlap occurs, these values agree well with those of Painter *et al.*

The $n$ curve shows a peak near 7.2 eV. The peak was also reported by Tanaka [11]. This peak in $n$ gives an approximate value for the optical band gap.

The values of the absorption edge show considerable variation as reported by different authors [12]. This is likely to have been caused by the choice of polyethylenes used (high density or low density) and the difference in the preparation of specimens. The drawn-film samples exhibit anisotropy.

The values of refractive index obtained for polyethylene depend critically on the method of film preparation. The density of the film depends on the method of preparation. It is possible to introduce methyl groups ($CH_3$) and vinyl groups ($C_2H_3$) into the regular $=CH_2=CH_2=CH_2=$ sequence. If the number of $CH_3$ groups per 1000 C atoms is 83, the refractive index

for the Na $D$ line (5890 Å) is 1.5060; it increases to 1.5260 when 16 $CH_3$ groups are present per 1000 C atoms (see inset in Fig. 1).

The variation of refractive index with temperature for low-density polyethylene seems to be greater than that for high-density polyethylene. The variation for a temperature change from 70° to 124 °C is about 0.05 for low-density polyethylene, and from 130° to 154 °C it is about 0.07 for high-density polyethylene.

The properties of polyethylene films prepared by the solvent-evaporation technique are dependent on a number of parameters, such as the solvent used, the starting concentration, the temperatures, and speed in cases when the evaporation was effected by centrifugal rotation.

At a spin speed of 3000 RPM, a solution of 0.05% by weight of polyethylene in $CCl_4$ yields films of density 0.914 gm/cm$^3$ and refractive index $1.459 + i0.023$ at 2.254 eV; when the concentration is increased to 0.4% by weight, the refractive index changes to about 1.502. When the spin speed increases to 4000 RPM, the 0.4% concentration solution gives films of refractive index 1.457 [13].

A change in solvent also makes a difference. A starting solution of low-density polyethylene in xylene with 0.05% by weight at a spin speed of 1000 RPM yields films of density 0.923 gm/cm$^3$ and refractive index $1.464 + i0.021$ at 2.254 eV. When the concentration is increased to 0.4% by weight, the refractive index changes to $1.501 + i0.004$. When the specimen speed increases to 4000 RPM, the 0.4% by weight solution yields films of refractive index $1.495 + i0.011$ [13].

Although the vibrational absorption bands of polyethylene are well-known, we could not find a determination of the optical constants in the 2–20 μm region. The structure of crystalline polyethylene was determined long ago, and most spectroscopic efforts were directed towards assigning the many vibration modes of the various kinds of polyethylene (14–17). These include the orthorhombic crystal with two $CH_2$ groups repeating themselves in zigzag carbon skeleton chains throughout the crystal: $(C_2H_4)n$. However, various types of branching can occur, which lead to subtle additional features in the spectrum, and methyl and vinyl groups can occur along the chains. Although Krimm *et al.* [14] measured spectra of oriented crystal samples with polarized light, we have elected to use unpolarized spectra of Nielsen and Woollett [15] to determine approximate $k$ values. They present transmittance spectra of a specific kind of polyethylene (Marlex 50) for three thicknesses. Marlex 50 is 95% crystalline with less than two methyl groups per 1000 carbon atoms and one vinyl group per molecule (for each $C_2H_4$ molecule, one H is missing). Nearly all the absorption lines (designated $s$ (strong), $m$ (medium) and $w$ (weak)) are the same in a number of different polyethylenes [17].

We assumed $n = 1.5$ throughout the near IR and calculated $k$ using the equation $T/T_o = (1 - R)^2 \exp(-\alpha x)$, where $R$ is the single-surface reflecti-

vity $R=(n-1)^2/(n+1)^2$, since $k \ll n$ in the near IR; $\alpha=4\pi k/\lambda$ is the absorption coefficient, and $x$ is the film thickness. This formula assumes that interference effects are averaged out, which is suggested by most of the spectra. Because $k$ is small even at vibrational resonances, the dispersion should be small, and assuming that $n$ is a constant is reasonable. The $k$ values outside of resonances varied by as much as a factor of two among the three thicknesses, suggesting some scattering effects especially at shorter wavelengths. We suggest that the $k$ values at resonances are probably good to $\pm 30\%$. In Fig. 1 the density of absorption lines is so great that it is not possible to resolve every line, although in Table I every line is defined by several data points. We have rounded off the $k$ values to two significant figures; this loses only a few weak structures in the spectrum.

In the far-infrared region of the electromagnetic spectrum ($\lambda > 20$ μm), polyethylene is one of the most widely used materials for the fabrication of optical elements such as windows and lenses. This is due not only to its transparency, but also to its availability, low cost, machinability, and relative stability. As a consequence, its power transmission properties in this spectral region have been studied by many authors (see, for example, some reviews [18–20]). However, the optical properties of polyethylene, and indeed of many other polymers in the far infrared, are known to be specimen dependent, and can vary significantly depending on the past history of the specimen. In this spectral region, for example, it is not unusual to find differences of up to a factor of two between the absorption spectra of specimens with different histories. Some of the factors that affect this will include the particular manufacturing process used (extrusion, or vacuum- or injection-molding) and the density and degree of crystallinity achieved in the final material. The optical properties will also be varied by the presence in the material of impurities such as antioxidants, agents to improve flow during the manufacturing process, heavy-metal salts or oxides as residues of the catalysts used in polymerization, and microdroplets of water. Similarly, exposure of the material to environmental factors such as high temperatures, ultraviolet radiation, mechanical stress, and high-energy irradiation can significantly change the far-infrared optical constants of this material. It is therefore difficult to arrive at a unique set of intrinsic optical constants for polyethylene in the far-infrared. This problem is further aggravated by the fact that although there have been many measurements of the transmission properties of this material, there is little detailed quantitative information available on the spectral variation of both optical constants over this region. This critique will discuss, therefore, such data as are available with a view to providing typical values of the optical constants and their spectral variation across the far infrared. These values can be used to give reasonable calculations of the consequences of using a polyethylene-based optical element in an optical system. However, in applications where such calculations are critical to an evaluation of

system performance, it might well be best to measure the optical constants of the particular piece of polyethylene that is to be used. In most of the original publications the measurements have been made by Fourier-transform spectroscopy, so the independent spectral variable is given as wave number in reciprocal centimeters. Similarly, in most far-infrared measurements the dissipative part of the complex refractive index is usually described by the power absorption coefficient, $\alpha$, rather than the extinction coefficient, $k$. The two parameters are related by

$$\alpha = 4\pi\nu k, \tag{1}$$

in which $\nu$ is the wave number.

The best optical-constant data for polyethylene in the far infrared are presently provided by the technique of dispersive Fourier-transform spectroscopy (DFTS) [21–23]. This is because of the measurement precision and accuracy that can be achieved, together with the wide broad-band spectral coverage available with the technique. Under the ideal conditions of a perfectly homogeneous, plane-parallel-sided specimen, measurements that are limited by random uncertainties of better than parts in $10^5$ in the refractive index and better than a few percent in the extinction coefficient can readily be achieved for a low-loss material such as polyethylene. Ideal conditions, however, are rarely found for a mechanically soft material such as polyethylene. Nonetheless, some of the DFTS measurements on this material will be seen to provide the most representative optical-constant data set. In this technique both the attenuation and the phase shift imposed on an electromagnetic wave that propagates through a specimen are directly measured, and the optical constants calculated from these measured parameters via Fresnel's relations for the complex transmission and reflection coefficients of an interface between dissimilar media.

Most of the DFTS studies on polyethylene have been at near-millimeter wavelengths. The first of these [24, 25] covered the spectral region between 4 and 40 $cm^{-1}$ (wavelengths from 2.5 mm to 250 μm) and reported the results of measurements at a temperature of 290 K on specimens of low- and high-density polyethylene, although density values were not given. These optical-constant spectra reveal the general behavior found in such measurements on polyethylene. The refractive index spectra (refraction spectra) are virtually wave number independent at the parts-in-$10^3$ level, taking mean values of 1.5138 for low-density polyethylene (LDPE) and 1.5246 for high-density polyethylene (HDPE). The power absorption coefficient spectra for the two densities both increase monotonically with increasing wave number, with that of LDPE being systematically some 0.002–0.006 $cm^{-1}$ below that of HDPE. Typically, the random uncertainties in these measurements were estimated to be between ±0.002 and

$\pm 0.005\ cm^{-1}$ in the absorption coefficient, corresponding to random uncertainties of a few times $10^{-5}$ in the extinction coefficient. In the refraction spectra the random variation was about $10^{-5}$, increasing to a few times that at either end of the measured spectral range.

Other subsequent near-millimeter-wavelength DFTS measurements on HDPE [26, 27] at a temperature of 299 K with, again, an unspecified density, gave absorption spectra in broad agreement with the earlier studies, although the mean level of the refraction spectrum (~1.5184) fell between those of the earlier LDPE and HDPE measurements. DFTS measurements of the temperature variation of the refraction spectra of the same LDPE and HDPE specimens measured in the 290 K measurements of Birch *et al.* [24, 25] have been made between 4.2 and 300 K in the spectral region 10 to $30\ cm^{-1}$ [28]. These showed the overall level of the refraction spectrum to increase with decreasing temperature between 300 and 40 K, as one would qualitatively expect on thermal-contraction grounds, and then to decrease slightly down to 4.2 K. At temperatures near 300 K the slope of both refraction temperature data sets varied at a rate of approximately $-2.5 \times 10^{-4}\ K^{-1}$. In both LDPE and HDPE these measurements showed the overall level of the refraction spectra to increase by about 2.5% and 2.8%, respectively, between 300 and 40 K.

Moving away from the near millimeter into the far infrared, one finds DFTS measurements on polyethylene at a temperature of 298 K in the spectral range from ~30 to $200\ cm^{-1}$ [29, 30]. Although the overall level of the refraction spectra in these works is consistent with that of the near-millimeter-wave studies, both the refraction spectrum and the corresponding absorption spectrum appear with quite large discrete features. One of these, the $73\ cm^{-1}$ $B_{1u}$ lattice mode [31, 32] is a well-known feature of the infrared spectrum of polyethylene, but the other features near 105 and $142\ cm^{-1}$ are reported for the first time. It may be best to treat these as either measurement artifacts of some kind or as representing some extrinsic contribution to the optical constants from some unexpected impurity. There are two reasons for this, in addition to that of these measurements being the only observation of such structure in polyethylene spectra. First, in one case [29], the absorption spectrum is shown accompanied by that for a specimen of the polymer TPX, another widely studied far-infrared material. This also contains discrete features at similar wave numbers. One at $105\ cm^{-1}$ has not been reported in other studies on TPX; one at $141.7\ cm^{-1}$ has been seen in other measurements [33, 34], but only as a weak, rather narrow band, and not as prominent and as broad as shown in Afsar *et al.* [29]. The second reason for discounting these features as intrinsic features of the polyethylene spectrum cómes from the lack of consistent corresponding dispersion in the refraction spectra. The two features in the absorption spectrum are very similar in width and intensity, and one would therefore expect to observe similar dispersions in the

refraction spectrum, whereas one finds a region of dispersion across the 142 $cm^{-1}$ position but none in the region of 105 $cm^{-1}$.

There have also been other, more recent, DFTS measurements on polyethylene in the far infrared [35] that do not show the discrete features found in Afsar *et al.* [29, 30]. These were on both LDPE and HDPE in the spectral region from 50 to 450 $cm^{-1}$ at a temperature of 293 K. The densities of the two specimens were not given. The corresponding spectra for the two specimens are qualitatively similar in their larger-scale features. The random uncertainties in these spectra were estimated as about $10^{-5}$ in the refraction spectra and about 0.05 $cm^{-1}$ in the absorption spectra, over most of the measured spectral range. Both absorption spectra clearly show the $B_{1u}$ lattice mode in the region of 73 $cm^{-1}$, although it is nearly three times more intense in the HDPE spectrum, reflecting the higher degree of crystallinity in that specimen. The two refraction spectra similarly show the corresponding dispersion associated with the band. At higher wave numbers the HDPE absorption spectrum increases with increasing wave number to reach a broad maximum in the region of 200 $cm^{-1}$, before falling to a shallow minimum around 300 $cm^{-1}$, and then rising again. The HDPE refraction spectra falls to a shallow minimum between 200 and 250 $cm^{-1}$, and then rises with increasing wave number to be consistent with the increasing absorption. The LDPE spectra show similar overall behavior, although the broad band is present only as a shoulder in the absorption spectrum. Both refraction spectra show a clear but small localized region of dispersion in the region of 94 $cm^{-1}$ with corresponding weak shoulders in the absorption spectra. Fleming *et al.* [36], in a study of temperature effects in the far-infrared absorption of polyethylene, assign a weak band at 94 $cm^{-1}$ to the $B_{2u}$ lattice band, which was first observed at 110 $cm^{-1}$ at a temperature of 2 K [37].

There have been a considerable number of measurements of the power transmission spectrum of polyethylene in the far infrared using conventional Fourier-transform spectroscopy (FTS). Such measurements can be converted into optical-constant data in a number of ways. First, if the measurements are such that a channel spectrum due to multiple-beam interference between internally reflected rays is resolved, then various methods exist for deriving a refractive-index spectrum from the period of the channel spectrum. The measurements can then be repeated or the results reprocessed to give a spectrum with reduced spectral resolution and no channel spectrum. The refraction spectrum can then be used to derive the absorption spectrum from the transmission spectrum. If channel-spectra methods are not used, then a value for the refractive index could be taken from the literature, for example, and used to calculate the absorption spectrum from the transmission spectrum. Alternatively, measurements can be made on two specimens of different thicknesses of the material under investigation. The absorption spectrum is then calculated

from the ratio of the transmission spectra of the two specimens using an expression that assumes single-pass transmission through the specimens, with no contributions from internally reflected rays. In many of the FTS measurements on polyethylene the manner in which the absorption spectrum has been obtained is often not explicitly stated. It can be difficult, therefore, to assess such data, especially if they differ in a significant way from other results.

Loewenstein and Smith [38] developed a channel-spectrum method and published a number of papers on the far-infrared optical constants of a range of materials, including high-density polyethylene [39]. Over their measured wave number range of 50 to 250 $cm^{-1}$ the derived refraction spectrum was virtually constant at a level of about 1.520 with an experimental uncertainty of 0.1% (~0.001), which is consistent with the DFTS results of Birch [35] on HDPE, given the absence of quoted density values. The measured absorption spectrum of the specimen of Smith and Loewenstein [39], however, is up to a factor of two greater than those of both the DFTS studies already discussed and of non-DFTS studies to be discussed subsequently. Their spectrum is presented with estimated uncertainties, presumably random, of about 10%. Again, given the uncertainties imposed by the lack of knowledge of specimen history, it is not possible to discuss such differences in the context of specimen-to-specimen variations or systematic measurement errors. However, the absorption measurements of Smith and Loewenstein [39] are certainly unusual in that they show no $B_{1u}$ lattice mode in the vicinity of 73 $cm^{-1}$. Coleman *et al.* [40] have also used a channel spectrum approach to determine the optical constants of both LDPE and HDPE between 25 and 500 $cm^{-1}$. Although their absorption spectra are not dissimilar from those of the other measurements considered in this critique, their refraction spectra show overall dispersions across this spectral range (~0.03 for LDPE and ~0.08 for HDPE) that are more than an order of magnitude greater than those found by the various DFTS studies.

Measurements by Chantry *et al.* [41] are representative of what can be achieved by two-thickness FTS methods. They derived the absorption spectrum of both LDPE and HDPE in the region from 20 to 220 $cm^{-1}$. In addition to the broad-band FTS measurements, the coefficient at 29.7 $cm^{-1}$ was also derived from transmission measurements made using a hydrogen-cyanide laser as a radiation source. The measurement temperature was not specified, but was clearly that of the ambient laboratory environment from the description of their apparatus. Specimen densities were not given. In the spectral region above 50 $cm^{-1}$ their absorption spectra are in general agreement with other FTS and DFTS studies, with a clearly resolved $B_{1u}$ band at 73 $cm^{-1}$ superimposed on the increasing background absorption to higher wave numbers. In the region below 50 $cm^{-1}$ Chantry *et al.* found little difference between the absorption spectra of LDPE and HDPE,

which is consistent with the DFTS data of Birch *et al.* [24, 25], which found differences of less than 0.006 $cm^{-1}$ between the spectra of the two forms of the material in the region below 40 $cm^{-1}$. Chantry *et al.* were able to fit their absorption data to the following quadratic:

$$\alpha(\nu) = 8 \times 10^{-4}\nu + 1.4 \times 10^{-4}\nu^2 \tag{2}$$

in the wave number region between 2 and 50 $cm^{-1}$. Their HCN-laser determination of the absorption coefficient at 29.7 $cm^{-1}$ was in good agreement with the value predicted by Eq. 2.

The spectrum calculated from Eq. 2 gives a reasonable fit to most of the published data on polyethylene in this spectral region, although it predicts values that are somewhat below the trend of some of the DFTS near-millimeter-wave measurements. It would not be unreasonable, therefore, to use it to provide a guide to expected absorption levels, although as discussed previously, for some applications it might be prudent to determine the absorption spectrum of the particular material to be used. Chantry *et al.* [41] proceeded to derive an equation for the spectral variation of the loss tangent of polyethylene from Eq. 2. One should note two things about this: first, that it was stated to have been derived using a value for the refractive index (1.461) that is lower than those generally associated with either LDPE or HDPE, and which may have been taken from earlier hydrogen-cyanide laser measurements at 891 GHz [42]); second, that the numerical constants of that equation are not consistent with that value of the refractive index. The correct values would be slightly different.

There have been a number of monochromatic determinations of the optical constants of polyethylene using coherent sources. Bicanic and Dymanus [43], for example, have determined the absorption coefficient at 29.7 $cm^{-1}$ of a unspecified specimen 0.21 mm thick, at room temperature using an HCN laser to measure its power-transmission coefficient. They used a literature value of the refractive index to correct for reflection effects and found a value of 0.27 $cm^{-1}$, which is about twice the values given by DFTS studies and predicted by Eq. 2. If one were to assume the Eq. 2 value, the absorption loss for this specimen would be about 3% in the presence of a 7% reflection loss. Such a small loss could easily be obscured by systematic effects in a measurement with coherent radiation. This could well account for their relatively high value.

Llewellyn-Jones *et al.* [44] have determined the absorption coefficients of LDPE and HDPE specimens with densities of 0.89 and 0.93 $g\,cm^{-3}$, respectively, using an untuned cavity technique at 156 GHz (5.2 $cm^{-1}$). Their results of 0.013 and 0.012 $cm^{-1}$) (LDPE and HDPE) are somewhat higher than the prediction of Eq. 2 (0.008 $cm^{-1}$), but in good agreement

with DFTS results [24–27].

Monochromatic measurements can also be used to determine the refractive index. Early measurements by Chamberlain and Gebbie [42], for example, demonstrated how a Michelson interferometer and a laser source could be used to give such information, by placing the specimen within one arm of the interferometer and rotating it slightly to vary the optical path through the specimen. Such a measurement on polyethylene led to a value of $1.461 \pm 0.023$ at 337 μm wavelength, which is low in comparison with more recent values.

Stützel *et al.* [45], in a noninterferometric approach, used the Abbe method in which the refractive index is found from the angle of incidence that causes a right triangular prism to retro-reflect incident radiation. With this method Stützel *et al.* determined the refractive indices of polyethylene specimens of different, quoted, crystallinities at 296 K for wavelengths of 118 and 570 μm using an optically pumped gas laser. In addition, they determined the temperature variation of the refractive index of a 27% crystalline specimen between 5 and 290 K at an unspecified wavelength, but presumably either 118 or 570 μm. Their result showed the refractive index generally increasing with decreasing temperature in good agreement with previous DFTS results [28], although their finer temperature resolution revealed abrupt changes of slope at 50 and 110 K, whereas only the former had been seen in the DFTS study. Near to room temperature, Stützel *et al.* found the slope of their data to be approximately $-13 \times 10^{-4}\,K^{-1}$, which is larger than the $-2.5 \times 10^{-4}\,K^{-1}$ of the DFTS measurements [28], but this difference may again only reflect the finer temperature resolution of the former study. Alvarez *et al.* [46] have also measured the refraction spectrum of a Rigidex polyethylene between 50 and 200 $cm^{-1}$ at 1.6 and 300 K. They found a 6% increase in the overall level of the refraction spectrum in going to 1.6 K, which is about twice that found in the other temperature-variation studies [28, 45].

In this next section the results of a number of papers are discussed to illustrate the extent to which the optical constants of polyethylene will depend on extrinsic factors, which prevent one from talking in terms of unique intrinsic data for this material. Davies and Haigh [47] and Ayers *et al.* [48], for example, describe the results of FTS absorption studies on both LDPE and HDPE specimens manufactured by a vacuum-melt extraction and casting technique, which produces bulk material from polymer powder free of additives. The processing avoids oxidation effects and removes volatile impurities and microscopic gas bubbles. Materials produced by this process were shown to have absorption spectra reduced by factors of up to two from those generally associated with this material in the far infrared. In addition, microwave bridge measurements [48] showed loss-angle reductions by a factor of three at 27.8 GHz. To the extent that this vacuum-melt extraction process yields purer material than that generally available

for far-infrared applications, these measurements of its absorption spectra [47, 48] may be taken as providing a close approach to the intrinsic-polyethylene absorption spectra.

There have been a number of studies of the variation in line position of the $B_{1u}$ and $B_{2u}$ lattice modes with various macroscopic parameters. Bank and Krimm [32], for example, used a grating spectrophotometer to make transmission measurements at temperatures of 103 and 303 K, which demonstrated the sensitivity of the line shape, line intensity, and line position of the $B_{1u}$ mode to both temperature and degree of crystallinity. Similar FTS-based measurements have been reported by Zirke and Meissner [49]. These are the effects that cause significant changes to the optical constants only in the region within about 5 $cm^{-1}$ of line center, and will not be relevant to many applications. Nonetheless, it is important to be aware of them. Other similar temperature-dependent studies have been reported by Fleming *et al.* [36], Stone and Williams [50], Frank *et al.* [51], and Goldstein *et al.* [52]. Frank *et al.* [53] report the appearance of an absorption band at 39 $cm^{-1}$ in the absorption spectrum of high-pressure annealed specimens when the specimen temperature was below 170 K. The band intensified with decreasing temperature but did not shift its position.

There have also been some far-infrared studies of the effects of neutron and gamma-ray irradiation on the optical constants of polyethylene. Frank [54], for example, has demonstrated the effect that high-energy irradiation has on the absorption spectra of LDPE and HDPE in the region between 50 and 90 $cm^{-1}$. The intensity of the $B_{1u}$ mode was not affected, whereas the overall level of the broad background absorption was almost doubled for radiation doses of 50 Mrad. Eberhagen and Fahrbach [55], working at much higher radiation doses, demonstrated an onset of radiation-induced transmission loss at doses above $10^9$ rad, which led to a fourfold reduction in the transmission coefficient of a specimen 5 mm thick at 0.2 mm wavelength (50 $cm^{-1}$) by a dose of $10^{10}$ rad.

Finally, it is well-known that the application of stress to a polymer, either during its manufacture or subsequently, will yield material in which the molecular chain axes are preferentially aligned in certain directions. This will result in the optical constants exhibiting both birefringence and dichroism. Jacobsson and Hård [56], for example, using what was essentially a monochromatic version of DFTS, found birefringence, which varied with spatial position by between 0.01 and 0.025 at a wavelength of 70.5 μm in an injection-molded specimen of HDPE. Similarly, Read *et al.* [57] report the results of birefringence measurements on a LDPE sheet 0.33 mm thick, which had been stretched to a draw ratio of one to four; it was found to have a virtually constant in-plane birefringence of 0.016 from 0.546 μm wavelength in the visible, though the far infrared, and out to 8.6 mm wavelength in the microwave.

In conclusion, then, concerning the optical constants of polyethylene in

the far-infrared spectral region, one can see the difficulties of arriving at a definitive set of data that represents the intrinsic properties of this material. It is much easier instead to define a reasonably representative set of spectra for the real and imaginary parts of the complex refractive index, which one can use as a guide to expected, typical values. Thus, some of the DFTS results that have been discussed [24, 25, 35] have been used to supply such data, and these are presented in Fig. 1 and Table II. These references were chosen in part because they offer the widest spectral coverage combined with precise and accurate data, data with sufficiently low random uncertainties that the weak refractive-index dispersion associated with the intrinsic lattice modes is clearly resolved. They were chosen also because they were readily available to the author in a tabulated form and did not need to be read from a graph with the consequential loss of accuracy. This should not be taken as a claim for any special status for this data. Given the problem of specimen-to-specimen variation that this critique has discussed, these data should be taken only as typical of what might be found in a particular specimen. The far-infrared spectrum of Fig. 1 is not a definitive polyethylene spectrum. In Fig. 1 the featureless line labeled $n$ represents the refractive index of both LDPE and HDPE material. The small differences between these spectra, and their dispersions, cannot be seen on the scale of the figure. The two curves labeled LDPE and HDPE represent the far-infrared $k$ spectra [35]. The curve labeled $a$ is a composite from the near-millimeter-wave $k$ spectra of both LDPE and HDPE of Birch *et al.* [24, 25]; the curve labelled $b$ is the $k$ spectrum calculated from Eq. 2. Since the details of the refraction spectra are not resolved in Fig. 1, they are shown replotted on expanded scales in the linear–linear representation of Fig. 2. Now the dispersion due to the 73 $cm^{-1}$ mode is seen clearly.

## REFERENCES

1. J. J. Ritsko, *J. Chem. Phys.* **70**, 5343 (1979).
2. R. H. Partridge, *J. Chem. Phys.* **45**, 1685 (1966).
3. C. W. Bunn, *Trans. Faraday Soc.* **35**, 482 (1939).
4. A. Charlesby, *Proc. Phys. Soc. (London)* **57**, 496 (1945).
5. J. J. Trillat, *Compt. Rend. Acad. Sci.* **230**, 1522 (1950).
6. R. H. Partridge, *J. Chem. Phys.* **45**, 1679 (1966).
7. L. R. Painter, E. T. Arakawa, M. W. Williams, and J. C. Ashley, *Rad. Res.* **83**, 1 (1980).
8. J. Pflüger and J. Fink, "Determination of Optical Constants by High-Energy, Electron-Energy-Loss Spectroscopy (EELS)," this volume.
9. S. L. Aggarwal, "Polymer Handbook," Interscience, New York, PVI-41 (1967).
10. J. J. Ritsko, L. J. Brillson, R. W. Bigelow, and T. J. Fabish, *J. Chem. Phys.* **69**, 3931 (1978).
11. T. Tanaka, *J. Appl. Phys.* **44**, 2430 (1973).
12. S. Hashimoto, K. Seki, N. Sato, and H. Inokuchi, *J. Chem. Phys.* **76**, 163 (1982).
13. J. Ashok, P. Varaprasad, and S. Avadhani, unpublished data.

14. S. Krimm, C. Y. Liang, and G. B. B. M. Sutherland, *J. Chem. Phys.* **25**, 549 (1956).
15. J. R. Nielsen and A. H. Woollett, *J. Chem. Phys.* **26**, 1391 (1957).
16. R. Zbinden, "Infrared Spectroscopy of High Polymers," Academic Press, New York, Chap. II (1964).
17. P. C. Painter, M. M. Coleman, and J. L. Koenig, "The Theory of Vibrational Spectroscopy and its Application to Polymeric Materials," Wiley, New York, (1982).
18. G. W. Chantry and J. E. Chamberlain, in "Polymer Science," (A. D. Jenkins, ed.), North-Holland, Amsterdam, Ch. 20 (1972).
19. W. F. X. Frank and U. Leute, in "Infrared and Millimeter Waves," (K. J. Button, ed.), Vol. 8, Academic Press, New York, Ch. 2 (1983).
20. J. F. Rabolt, in "Infrared and Millimeter Waves," (K. J. Button, ed.), Vol. 12, Academic Press, New York, Ch. 2 (1984).
21. J. R. Birch and T. J. Parker, in "Infrared and Millimeter Waves," (K. J. Button, ed.), Vol. 2, Academic Press, New York, Ch. 3 (1979).
22. J.R. Birch, *Mikrochimica Acta [Wien]* **III**, 105 (1987).
23. G. J. Simonis, in "Handbook of Optical Constants of Solids," (E. D. Palik, ed.), Academic Press, Orlando, Ch. 8 (1985).
24. J. R. Birch, J. D. Dromey, and J. Lesurf, *NPL Report DES* **69**, (1981).
25. J. R. Birch, J. D. Dromey, and J. Lesurf, *Infrared Physics* **21**, 225 (1981).
26. M. N. Afsar, *IEEE Trans. Microwave Theory Tech.* **MTT-33**, 1410 (1985).
27. M. N. Afsar, *IEEE Trans. Instrumentation Meas.* **IM-33**, 530 (1987).
28. J. R. Birch and K. F. Ping, *Infrared Physics* **24**, 309 (1984).
29. M. N. Afsar, J. Chamberlain, and G. W. Chantry, *IEEE Trans. Instrumentation Meas.* **IM-25**, 290 (1976).
30. M. N. Afsar, *NPL Report DES* **42**, (1977).
31. S. Krimm and M. I. Bank, *J. Chem. Phys.* **42**, 4059 (1965).
32. M. I. Bank and S. Krimm, *J. App. Phys.* **39**, 4951 (1968).
33. G. W. Chantry, H. M. Evans, J. W. Fleming, and H. A. Gebbie, *Infrared Physics* **9**, 31 (1969).
34. J. R. Birch and E. A. Nicol, *Infrared Physics* **24**, 573 (1984).
35. J. R. Birch, *Infrared Physics* **30**, 195 (1990).
36. J. W. Fleming, G. W. Chantry, P. A. Turner, E. A. Nicol, H. A. Willis, and M. E. A. Cudby, *Chem. Phys. Lett.* **17**, 84 (1972).
37. G. D. Dean and D. H. Martin, *Chem. Phys. Lett.* **1**, 415 (1967).
38. E. V. Loewenstein and D. R. Smith, *Appl. Opt.* **10**, 577 (1971).
39. D. R. Smith and E. V. Loewenstein, *Appl. Opt.* **14**, 1335 (1975).
40. P. D. Coleman, G. Sherman, D. Parsons, and D. Akitt, in "Proc. Symposium on Submillimeter Waves," Polytechnic Press, New York, (1971).
41. G. W. Chantry, J. W. Fleming, P. M. Smith, M. Cudby and H. A. Willis, *Chem. Phys. Lett.* **10**, 473 (1971).
42. J. E. Chamberlain and H. A. Gebbie, *Nature* **206**, 602 (1965).
43. D. D. Bicanic and A. Dymanus, *Infrared Physics* **14**, 153 (1974).
44. D. T. Llewellyn-Jones, R. J. Knight, P. H. Moffat, and H. A. Gebbie, *IEE Proc.* **127**, 535 (1980).
45. P. Stützel, H. D. Tegtmeier, and M. Tacke, *Infrared Physics* **28**, 67 (1988).
46. J. A. Alvarez, R. E. Jennings, and A. F. M. Moorwood, *Infrared Physics* **15**, 45 (1975).
47. G. J. Davies and J. Haigh, *Infrared Physics* **14**, 183 (1974).
48. S. Ayers, G. J. Davies, J. Haigh, D. Marr and A. E. Parker, *Proc. IEE* **121**, 1447 (1974).
49. J. Zirke and M. Meissner, *Infrared Physics* **18**, 871 (1978).
50. N. W. B. Stone and D. Williams, *Appl. Opt.* **5**, 353 (1966).
51. W. Frank, H. Schmidt, and W. Wulff, *J. Polymer Sci.* **61**, 317 (1977).
52. M. Goldstein, D. Stephenson, and W. F. Maddams, *Polymer Comm.* **24**, 2459 (1983).

53. W. F. X. Frank, H. Schmidt, B. Heise, G. W. Chantry, E. A. Nicol, H. A. Willis and M. E. A. Cudby, *Polymer* **22**, 17 (1981).
54. W. Frank, *Polymer Letters* **15**, 679 (1977).
55. A. Eberhagen and H.-U. Fahrbach, *Intl. J. Infrared and Millimeter Waves* **3**, 297 (1982).
56. S. Jacobsson and S. Hård, *Rev. Sci. Instr.* **53**, 1012 (1982).
57. B. E. Read, J. C. Duncan, and D. E. Meyer, *Polymer Testing* **4**, 143 (1984).

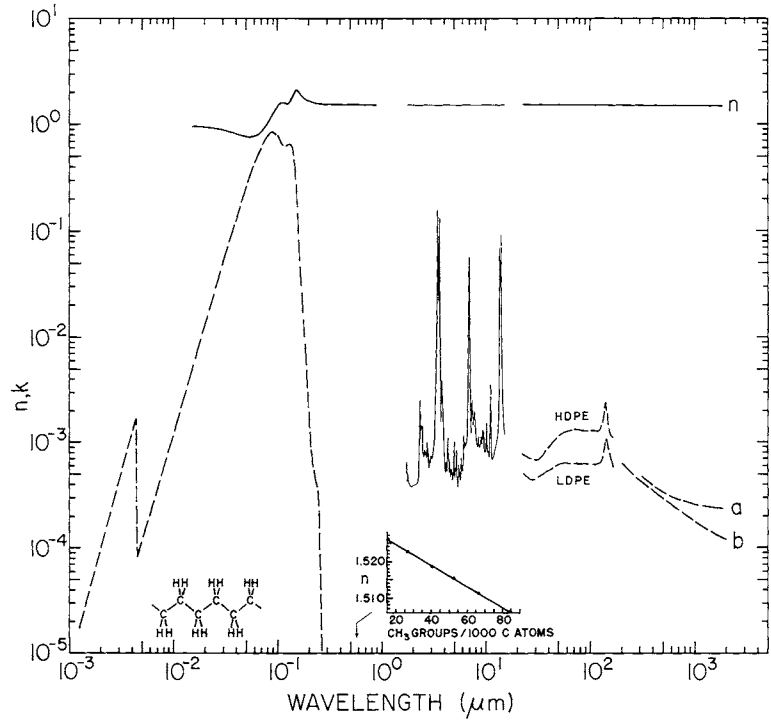


**Fig. 1.** Log–log plot of $n$ (solid line) and $k$ (dashed line) versus wavelength in micrometers for polyethylene. For the near IR, $k$ is given by the thin solid line in order to show some of the detailed structure. The insets represent (1) the C-chain structure and (2) the variation of $n$ with $CH_3$ groups at 0.589 μm.

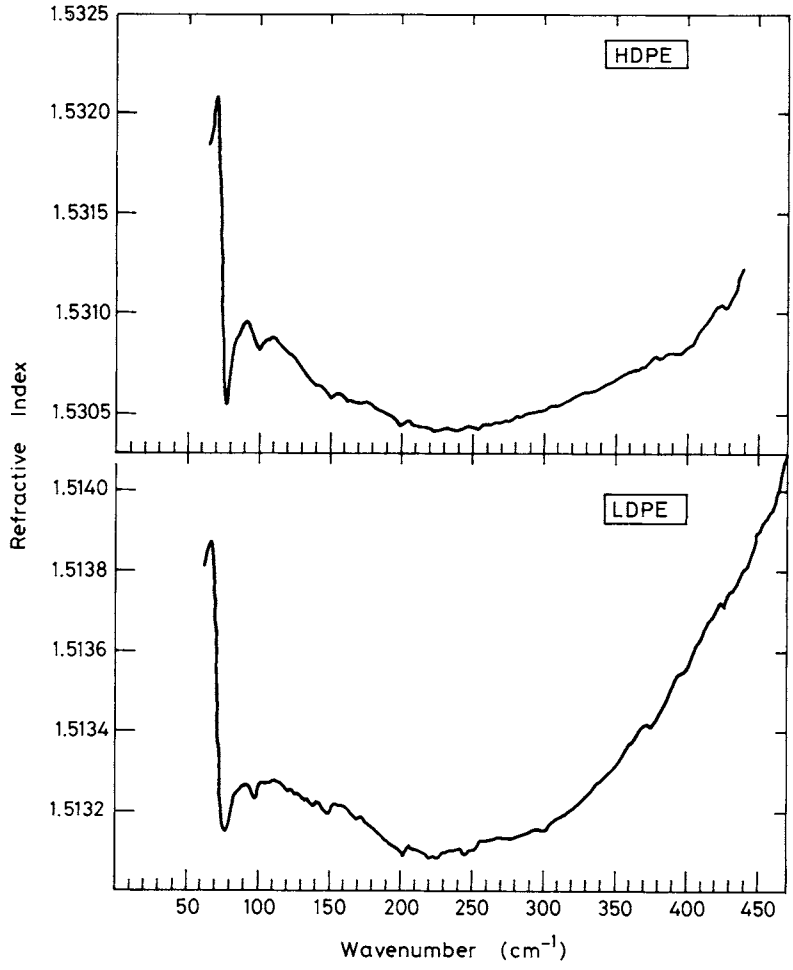


**Fig. 2.** Linear–linear plot of $n$ versus wave number for high-density and low-density polyethylene showing dispersion of the low-frequency vibration mode.

TABLE I

Values of $n$ and $k$ for Polyethylene from Various References[a]

| eV | $cm^{-1}$ | μm | n | k | n | k |
|---|---|---|---|---|---|---|
| 1000 | | 0.001240 | | $1.8 \times 10^{-5}$ [7] | | |
| 900 | | 0.001378 | | 2.3 | | |
| 800 | | 0.001550 | | 4.0 | | |
| 700 | | 0.001771 | | $7.0 \times 10^{-5}$ | | |
| 600 | | 0.002066 | | $1.1 \times 10^{-4}$ | | |
| 500 | | 0.002480 | | 2.1 | | |
| 400 | | 0.003100 | | $5.0 \times 10^{-4}$ | | |
| 300 | | 0.004133 | | $1.4 \times 10^{-3}$ | | |
| 282 | | 0.004379 | | $1.7 \times 10^{-3}$ | | |
| 280 | | 0.004428 | | $8.6 \times 10^{-5}$ | | |
| 200 | | 0.006199 | | $2.3 \times 10^{-4}$ | | |
| 150 | | 0.008266 | | $6.0 \times 10^{-4}$ | | |
| 100 | | 0.01240 | | $2.5 \times 10^{-3}$ | | |
| 80 | | 0.01550 | 0.97[7] | | | |
| 70 | | 0.01771 | 0.96 | | | |
| 60 | | 0.02066 | 0.94 | $1.38 \times 10^{-2}$ | | |
| 50 | | 0.02480 | 0.92 | 2.5 | | |
| 40 | | 0.03100 | 0.89 | $5.5 \times 10^{-2}$ | | |
| 35 | | 0.03542 | 0.86 | | | |
| 33 | | 0.03757 | | | 0.844[1] | 0.113[1] |
| 32 | | 0.03875 | | | 0.839 | 0.119 |
| 31 | | 0.04000 | | | 0.835 | 0.132 |
| 30 | | 0.04133 | 0.805 | 0.130 | 0.825 | 0.145 |
| 29 | | 0.04275 | 0.80 | | 0.818 | 0.171 |
| 28 | | 0.04428 | 0.79 | | 0.809 | 0.185 |
| 27 | | 0.04592 | 0.785 | | 0.809 | 0.210 |
| 26 | | 0.04769 | 0.78 | | 0.804 | 0.236 |
| 25 | | 0.04959 | 0.775 | 0.245 | 0.803 | 0.274 |
| 24 | | 0.05166 | 0.77 | | 0.788 | 0.317 |
| 23 | | 0.05391 | 0.77 | | 0.796 | 0.365 |
| 22 | | 0.05636 | 0.77 | | 0.795 | 0.403 |
| 21 | | 0.05904 | 0.775 | | 0.808 | 0.439 |
| 20 | | 0.06199 | 0.78 | 0.440 | 0.818 | 0.489 |
| 19 | | 0.06526 | 0.81 | 0.500 | 0.836 | 0.538 |
| 18 | | 0.06888 | 0.83 | 0.565 | 0.868 | 0.594 |
| 17 | | 0.07293 | 0.88 | 0.64 | 0.916 | 0.655 |
| 16 | | 0.07749 | 0.96 | 0.720 | 0.981 | 0.723 |
| 15 | | 0.08266 | 1.03 | 0.805 | 1.05 | 0.798 |
| 14 | | 0.08856 | 1.18 | 0.860 | 1.24 | 0.887 |
| 13 | | 0.09537 | 1.35 | 0.807 | 1.40 | 0.849 |
| 12 | 96786 | 0.1033 | 1.52 | 0.680 | 1.55 | 0.746 |
| 11 | 88720 | 0.1127 | 1.55 | 0.550 | 1.61 | 0.622 |
| 10 | 80655 | 0.1240 | 1.53 | 0.580 | 1.64 | 0.610 |
| 9.8 | 79042 | 0.1265 | | 0.600 | | |
| 9.6 | 77429 | 0.1292 | | 0.615 | | |
| 9.4 | 75816 | 0.1319 | | 0.635 | | |
| 9.2 | 74202 | 0.1348 | | 0.650 | | |
| 9.0 | 72589 | 0.1378 | 1.66 | 0.655 | 1.758 | 0.626 |
| 8.85 | 71379 | 0.1401 | | | 1.810 | 0.604 |

TABLE I (*Continued*)

Polyethylene

| eV | $cm^{-1}$ | μm | n | k | n | k |
|---|---|---|---|---|---|---|
| 8.8 | 70976 | 0.1409 | | 0.640 | | |
| 8.7 | 70170 | 0.1425 | | | 1.934 | 0.565 |
| 8.6 | 69363 | 0.1442 | | 0.620 | | |
| 8.55 | 68960 | 0.1450 | | | 1.981 | 0.472 |
| 8.4 | 67750 | 0.1476 | | 0.530 | 2.065 | 0.380 |
| 8.25 | 66540 | 0.1503 | | | 2.076 | 0.318 |
| 8.2 | 66137 | 0.1512 | | 0.385 | | |
| 8.10 | 65330 | 0.1531 | | | 2.067 | 0.252 |
| 8.0 | 64524 | 0.1550 | 2.08 | 0.240 | | |
| 7.95 | 64121 | 0.1560 | | | 2.634 | 0.128 |
| 7.8 | 62911 | 0.1590 | | 0.145 | 1.964 | $8.15 \times 10^{-2}$ |
| 7.65 | 61701 | 0.1621 | | | 1.924 | 4.67 |
| 7.6 | 61298 | 0.1631 | | $8.4 \times 10^{-2}$ | | |
| 7.5 | 60491 | 0.1653 | | | 1.877 | 3.73 |
| 7.4 | 59685 | 0.1675 | | 4.5 | | |
| 7.35 | 59281 | 0.1687 | | | 1.809 | 3.04 |
| 7.2 | 58071 | 0.1722 | | 2.5 | 1.732 | 2.30 |
| 7.05 | 56862 | 0.1759 | | | 1.715 | $1.74 \times 10^{-2}$ |
| 7.0 | 56458 | 0.1771 | 1.76 | $1.35 \times 10^{-2}$ | | |
| 6.9 | 55652 | 0.1797 | | | 1.694 | $8.8 \times 10^{-3}$ |
| 6.8 | 54845 | 0.1823 | | $7.70 \times 10^{-3}$ | | |
| 6.75 | 54442 | 0.1837 | | | 1.661 | |
| 6.6 | 53232 | 0.1879 | | 4.20 | 1.643 | |
| 6.45 | 52022 | 0.1922 | | | 1.634 | |
| 6.4 | 51619 | 0.1937 | | 2.35 | | |
| 6.3 | 50813 | 0.1968 | | | 1.619 | |
| 6.2 | 50000 | 0.2000 | | $1.40 \times 10^{-3}$ | | |
| 6.15 | 49603 | 0.2016 | | | 1.608 | |
| 6.0 | 48393 | 0.2066 | 1.65 | $8.6 \times 10^{-4}$ | 1.597 | |
| 5.85 | 47183 | 0.2119 | | | 1.578 | |
| 5.8 | 46780 | 0.2138 | | 6.3 | | |
| 5.75 | 46377 | 0.2156 | | | 1.568 | |
| 5.6 | 45167 | 0.2214 | | 5.1 | | |
| 5.55 | 44763 | 0.2234 | | | 1.559 | |
| 5.4 | 43554 | 0.2296 | | 4.4 | 1.549 | |
| 5.25 | 42344 | 0.2361 | | | 1.543 | |
| 5.2 | 41940 | 0.2384 | | 3.8 | | |
| 5.1 | 41134 | 0.2431 | | | 1.533 | |
| 5.0 | 40327 | 0.2480 | 1.6 | 2.5 | | |
| 4.95 | 39924 | 0.2505 | | | 1.523 | |
| 4.9 | 39521 | 0.2530 | | $1 \times 10^{-4}$ | | |
| 4.8 | 38714 | 0.2583 | | | 1.517 | |
| 4.7 | 37908 | 0.2638 | | $1 \times 10^{-5}$ | | |
| 4.65 | 37504 | 0.2666 | | | 1.513 | |
| 4.5 | 36295 | 0.2755 | | | 1.510 | |
| 4.35 | 35085 | 0.2850 | | | 1.507 | |
| 4.20 | 33875 | 0.2952 | | | 1.505 | |
| 4.05 | 32665 | 0.3061 | | | 1.502 | |
| 3.90 | 31455 | 0.3179 | | | 1.500 | |

TABLE I (*Continued*)

Polyethylene

| eV | $cm^{-1}$ | μm | n | k | n | k |
|---|---|---|---|---|---|---|
| 3.75 | 30245 | 0.3306 | | | 1.498 | |
| 3.60 | 29036 | 0.3444 | | | 1.498 | |
| 3.45 | 27826 | 0.3594 | | | 1.498 | |
| 3.30 | 26616 | 0.3757 | | | 1.498 | |
| 3.15 | 25406 | 0.3936 | | | 1.497 | |
| 3.00 | 24196 | 0.4133 | | | 1.495 | |
| 2.85 | 22987 | 0.4350 | | | 1.495 | |
| 2.70 | 21777 | 0.4592 | | | 1.493 | |
| 2.55 | 20567 | 0.4862 | | | 1.492 | |
| 2.40 | 19357 | 0.5166 | | | 1.490 | |
| 2.25 | 18147 | 0.5511 | | | 1.490 | |
| | | | 1.5260[9] | | 1.4590[13] | $2.3 \times 10^{-2}$[13] |
| 2.10 | 16935 | 0.5904 | | | 1.482[1] | |
| 1.95 | 15728 | 0.6358 | | | 1.480 | |
| 1.80 | 14518 | 0.6888 | | | 1.478 | |
| 1.65 | 13308 | 0.7514 | | | 1.476 | |
| 1.50 | 12098 | 0.8266 | | | 1.471 | |
| 1.35 | 10888 | 0.9184 | | | 1.466 | |
| 0.7191 | 5800 | 1.724 | 1.5[15][b] | $5.0 \times 10^{-4}$[15] | | |
| 0.7179 | 5790 | 1.727 | | 5.3 | | |
| 0.7166 | 5780 | 1.730 | | 5.7 | | |
| 0.7154 | 5770 | 1.733 | | 6.2 | | |
| 0.7142 | 5760 | 1.736 | | 5.7 | | |
| 0.7129 | 5750 | 1.739 | | 4.8 | | |
| 0.7117 | 5740 | 1.742 | | 4.5 | | |
| 0.7092 | 5720 | 1.748 | | 4.1 | | |
| 0.7067 | 5700 | 1.754 | | 4.1 | | |
| 0.7042 | 5680 | 1.761 | | 4.3 | | |
| 0.7030 | 5670 | 1.764 | | 4.7 | | |
| 0.7018 | 5660 | 1.767 | | 4.8 | | |
| 0.7005 | 5650 | 1.770 | | 4.6 | | |
| 0.6993 | 5640 | 1.773 | | 4.4 | | |
| 0.6968 | 5620 | 1.779 | | 4.1 | | |
| 0.6943 | 5600 | 1.786 | | 4.1 | | |
| 0.6819 | 5500 | 1.818 | | 4.0 | | |
| 0.6695 | 5400 | 1.852 | | 3.8 | | |
| 0.6571 | 5300 | 1.887 | | 3.7 | | |
| 0.6447 | 5200 | 1.923 | | 3.7 | | |
| 0.6323 | 5100 | 1.961 | | 3.8 | | |
| 0.6199 | 5000 | 2.000 | | 3.8 | | |
| 0.6075 | 4900 | 2.041 | | 3.8 | | |
| 0.5951 | 4800 | 2.083 | | 3.8 | | |
| 0.5827 | 4700 | 2.128 | | 3.8 | | |
| 0.5703 | 4600 | 2.174 | | 3.9 | | |
| 0.5579 | 4500 | 2.222 | | 4.0 | | |
| 0.5555 | 4480 | 2.232 | | 4.2 | | |
| 0.5530 | 4460 | 2.242 | | 4.4 | | |
| 0.5505 | 4440 | 2.252 | | 4.6 | | |

TABLE I (*Continued*)

Polyethylene

| eV | $cm^{-1}$ | μm | n | k |
|---|---|---|---|---|
| 0.5480 | 4420 | 2.262 | | 5.0 |
| 0.5455 | 4400 | 2.273 | | 5.7 |
| 0.5431 | 4380 | 2.283 | | 7.1 |
| 0.5406 | 4360 | 2.294 | | $9.4 \times 10^{-4}$ |
| 0.5393 | 4350 | 2.299 | | $1.2 \times 10^{-3}$ |
| 0.5381 | 4340 | 2.304 | | 1.9 |
| 0.5369 | 4330 | 2.309 | | 2.5 |
| 0.5356 | 4320 | 2.315 | | 1.7 |
| 0.5344 | 4310 | 2.320 | | 1.0 |
| 0.5331 | 4300 | 2.326 | | 1.2 |
| 0.5307 | 4280 | 2.336 | | 1.2 |
| 0.5294 | 4270 | 2.342 | | 1.3 |
| 0.5282 | 4260 | 2.347 | | 1.5 |
| 0.5269 | 4250 | 2.353 | | 1.8 |
| 0.5257 | 4240 | 2.358 | | 1.2 |
| 0.5232 | 4220 | 2.370 | | 1.2 |
| 0.5207 | 4200 | 2.381 | | 1.4 |
| 0.5183 | 4180 | 2.392 | | 1.4 |
| 0.5170 | 4170 | 2.398 | | 1.4 |
| 0.5158 | 4160 | 2.404 | | 1.4 |
| 0.5145 | 4150 | 2.410 | | 1.4 |
| 0.5133 | 4140 | 2.415 | | 1.4 |
| 0.5121 | 4130 | 2.421 | | 1.3 |
| 0.5108 | 4120 | 2.427 | | 1.4 |
| 0.5096 | 4110 | 2.433 | | 1.4 |
| 0.5083 | 4100 | 2.439 | | 1.4 |
| 0.5071 | 4090 | 2.445 | | 1.1 |
| 0.5059 | 4080 | 2.451 | | $1.0 \times 10^{-3}$ |
| 0.5034 | 4060 | 2.463 | | $9.4 \times 10^{-4}$ |
| 0.5009 | 4040 | 2.475 | | 8.6 |
| 0.4984 | 4020 | 2.488 | | 8.4 |
| 0.4959 | 4000 | 2.500 | | 7.1 |
| 0.4947 | 3990 | 2.506 | | 7.3 |
| 0.4935 | 3980 | 2.513 | | 7.4 |
| 0.4922 | 3970 | 2.519 | | 7.0 |
| 0.4910 | 3960 | 2.525 | | 7.2 |
| 0.4885 | 3940 | 2.538 | | 7.2 |
| 0.4860 | 3920 | 2.551 | | 7.9 |
| 0.4835 | 3900 | 2.564 | | 8.1 |
| 0.4811 | 3880 | 2.577 | | 8.0 |
| 0.4786 | 3860 | 2.591 | | 7.7 |
| 0.4761 | 3840 | 2.604 | | 7.4 |
| 0.4736 | 3820 | 2.618 | | 7.8 |
| 0.4711 | 3800 | 2.632 | | 7.7 |
| 0.4687 | 3780 | 2.646 | | 7.3 |
| 0.4662 | 3760 | 2.660 | | 7.0 |
| 0.4637 | 3740 | 2.674 | | 6.8 |
| 0.4612 | 3720 | 2.688 | | 6.9 |
| 0.4587 | 3700 | 2.703 | | 7.0 |

TABLE I (*Continued*)

Polyethylene

| eV | $cm^{-1}$ | μm | n | k |
|---|---|---|---|---|
| 0.4563 | 3680 | 2.717 | | 9.8 |
| 0.4538 | 3660 | 2.732 | | 8.0 |
| 0.4525 | 3650 | 2.740 | | 8.6 |
| 0.4513 | 3640 | 2.747 | | 8.1 |
| 0.4501 | 3630 | 2.755 | | 8.0 |
| 0.4488 | 3620 | 2.762 | | $7.6 \times 10^{-4}$ |
| 0.4476 | 3610 | 2.770 | | $1.0 \times 10^{-3}$ |
| 0.4463 | 3600 | 2.778 | | $8.6 \times 10^{-4}$ |
| 0.4439 | 3580 | 2.793 | | 6.4 |
| 0.4414 | 3560 | 2.809 | | 5.8 |
| 0.4389 | 3540 | 2.825 | | 5.5 |
| 0.4364 | 3520 | 2.841 | | 5.5 |
| 0.4339 | 3500 | 2.857 | | 5.5 |
| 0.4315 | 3480 | 2.874 | | 5.9 |
| 0.4290 | 3460 | 2.890 | | 6.2 |
| 0.4265 | 3440 | 2.907 | | 6.6 |
| 0.4240 | 3420 | 2.924 | | 6.4 |
| 0.4215 | 3400 | 2.941 | | 6.4 |
| 0.4203 | 3390 | 2.950 | | 6.8 |
| 0.4191 | 3380 | 2.959 | | 7.2 |
| 0.4178 | 3370 | 2.967 | | 7.3 |
| 0.4166 | 3360 | 2.976 | | 7.1 |
| 0.4141 | 3340 | 2.994 | | 6.8 |
| 0.4116 | 3320 | 3.012 | | 6.8 |
| 0.4092 | 3300 | 3.030 | | 6.8 |
| 0.4067 | 3280 | 3.049 | | 6.8 |
| 0.4042 | 3260 | 3.067 | | 7.1 |
| 0.4017 | 3240 | 3.086 | | 7.3 |
| 0.3992 | 3220 | 3.106 | | 7.6 |
| 0.3968 | 3200 | 3.125 | | 7.7 |
| 0.3943 | 3180 | 3.145 | | 7.9 |
| 0.3918 | 3160 | 3.165 | | 8.6 |
| 0.3893 | 3140 | 3.185 | | $9.5 \times 10^{-4}$ |
| 0.3868 | 3120 | 3.205 | | $1.8 \times 10^{-3}$ |
| 0.3844 | 3100 | 3.226 | | 1.5 |
| 0.3819 | 3080 | 3.247 | | 2.3 |
| 0.3794 | 3060 | 3.268 | | 2.7 |
| 0.3769 | 3040 | 3.289 | | 3.1 |
| 0.3744 | 3020 | 3.311 | | 3.8 |
| 0.3720 | 3000 | 3.333 | | 4.5 |
| 0.3695 | 2980 | 3.356 | | 6.1 |
| 0.3670 | 2960 | 3.378 | | $9.5 \times 10^{-3}$ |
| 0.3645 | 2940 | 3.401 | | $2.8 \times 10^{-2}$ |
| 0.3633 | 2930 | 3.413 | | $7.3 \times 10^{-2}$ |
| 0.3620 | 2920 | 3.425 | | $1.9 \times 10^{-1}$ |
| 0.3608 | 2910 | 3.436 | | $8.8 \times 10^{-2}$ |
| 0.3596 | 2900 | 3.448 | | 5.2 |
| 0.3583 | 2890 | 3.460 | | 4.6 |
| 0.3571 | 2880 | 3.472 | | 2.5 |

TABLE I (*Continued*)

Polyethylene

| eV | $cm^{-1}$ | μm | n | k |
|---|---|---|---|---|
| 0.3558 | 2870 | 3.484 | | 2.2 |
| 0.3546 | 2860 | 3.497 | | $3.3 \times 10^{-2}$ |
| 0.3534 | 2850 | 3.509 | | $1.5 \times 10^{-1}$ |
| 0.3521 | 2840 | 3.521 | | $3.6 \times 10^{-2}$ |
| 0.3509 | 2830 | 3.534 | | 1.5 |
| 0.3496 | 2820 | 3.546 | | $1.1 \times 10^{-2}$ |
| 0.3472 | 2800 | 3.571 | | $7.8 \times 10^{-3}$ |
| 0.3447 | 2780 | 3.597 | | 3.6 |
| 0.3422 | 2760 | 3.623 | | 2.9 |
| 0.3397 | 2740 | 3.650 | | 2.6 |
| 0.3372 | 2720 | 3.676 | | 2.4 |
| 0.3348 | 2700 | 3.703 | | 2.1 |
| 0.3323 | 2680 | 3.731 | | 1.8 |
| 0.3310 | 2670 | 3.745 | | 2.3 |
| 0.3298 | 2660 | 3.759 | | 3.8 |
| 0.3286 | 2650 | 3.774 | | 2.4 |
| 0.3273 | 2640 | 3.788 | | 2.8 |
| 0.3261 | 2630 | 3.802 | | 2.5 |
| 0.3248 | 2620 | 3.817 | | 2.5 |
| 0.3224 | 2600 | 3.846 | | 1.8 |
| 0.3199 | 2580 | 3.876 | | 1.5 |
| 0.3174 | 2560 | 3.906 | | 1.4 |
| 0.3162 | 2550 | 3.922 | | 1.0 |
| 0.3149 | 2540 | 3.937 | | $1.1 \times 10^{-3}$ |
| 0.3137 | 2530 | 3.953 | | $8.5 \times 10^{-4}$ |
| 0.3124 | 2520 | 3.968 | | $1.1 \times 10^{-3}$ |
| 0.3100 | 2500 | 4.000 | | $6.3 \times 10^{-4}$ |
| 0.3087 | 2490 | 4.016 | | 6.1 |
| 0.3075 | 2480 | 4.032 | | 6.4 |
| 0.3062 | 2470 | 4.049 | | 5.8 |
| 0.3050 | 2460 | 4.065 | | 5.1 |
| 0.3025 | 2440 | 4.098 | | 5.0 |
| 0.3000 | 2420 | 4.132 | | 6.3 |
| 0.2988 | 2410 | 4.149 | | 6.3 |
| 0.2976 | 2400 | 4.167 | | 5.7 |
| 0.2951 | 2380 | 4.202 | | 5.2 |
| 0.2926 | 2360 | 4.237 | | $6.7 \times 10^{-4}$ |
| 0.2914 | 2350 | 4.255 | | $1.1 \times 10^{-3}$ |
| 0.2901 | 2340 | 4.274 | | 1.1 |
| 0.2889 | 2330 | 4.292 | | $1.1 \times 10^{-3}$ |
| 0.2876 | 2320 | 4.310 | | $9.6 \times 10^{-4}$ |
| 0.2852 | 2300 | 4.348 | | 6.8 |
| 0.2839 | 2290 | 4.367 | | 6.6 |
| 0.2827 | 2280 | 4.386 | | 7.0 |
| 0.2814 | 2270 | 4.405 | | 6.3 |
| 0.2802 | 2260 | 4.425 | | 5.1 |
| 0.2790 | 2250 | 4.444 | | 5.0 |
| 0.2777 | 2240 | 4.464 | | 6.2 |
| 0.2765 | 2230 | 4.484 | | 4.5 |

TABLE I (*Continued*)

Polyethylene

| eV | $cm^{-1}$ | μm | n | k |
|---|---|---|---|---|
| 0.2752 | 2220 | 4.505 | | 5.2 |
| 0.2740 | 2210 | 4.525 | | 4.6 |
| 0.2728 | 2200 | 4.545 | | 4.6 |
| 0.2715 | 2190 | 4.566 | | 4.9 |
| 0.2703 | 2180 | 4.587 | | 4.9 |
| 0.2690 | 2170 | 4.608 | | 4.9 |
| 0.2678 | 2160 | 4.630 | | 5.4 |
| 0.2666 | 2150 | 4.651 | | 5.7 |
| 0.2653 | 2140 | 4.673 | | 5.3 |
| 0.2641 | 2130 | 4.695 | | 4.5 |
| 0.2628 | 2120 | 4.717 | | 4.2 |
| 0.2604 | 2100 | 4.762 | | 4.3 |
| 0.2579 | 2080 | 4.808 | | 4.4 |
| 0.2554 | 2060 | 4.854 | | 5.0 |
| 0.2529 | 2040 | 4.902 | | 6.9 |
| 0.2517 | 2030 | 4.926 | | $8.3 \times 10^{-4}$ |
| 0.2505 | 2020 | 4.950 | | $1.0 \times 10^{-3}$ |
| 0.2492 | 2010 | 4.975 | | $6.2 \times 10^{-4}$ |
| 0.2480 | 2000 | 5.000 | | 5.0 |
| 0.2455 | 1980 | 5.051 | | 4.5 |
| 0.2430 | 1960 | 5.102 | | 5.3 |
| 0.2418 | 1950 | 5.128 | | 5.3 |
| 0.2405 | 1940 | 5.155 | | 5.1 |
| 0.2381 | 1920 | 5.208 | | 5.5 |
| 0.2368 | 1910 | 5.236 | | 6.4 |
| 0.2356 | 1900 | 5.263 | | 8.1 |
| 0.2343 | 1890 | 5.291 | | 7.3 |
| 0.2331 | 1880 | 5.319 | | 4.5 |
| 0.2306 | 1860 | 5.376 | | 3.6 |
| 0.2281 | 1840 | 5.435 | | 3.9 |
| 0.2269 | 1830 | 5.464 | | 4.7 |
| 0.2257 | 1820 | 5.495 | | 5.9 |
| 0.2244 | 1810 | 5.525 | | 4.9 |
| 0.2232 | 1800 | 5.556 | | 4.6 |
| 0.2219 | 1790 | 5.587 | | 4.4 |
| 0.2207 | 1780 | 5.618 | | 4.3 |
| 0.2195 | 1770 | 5.650 | | 4.3 |
| 0.2182 | 1760 | 5.682 | | 4.6 |
| 0.2170 | 1750 | 5.714 | | 5.4 |
| 0.2157 | 1740 | 5.747 | | 6.9 |
| 0.2145 | 1730 | 5.780 | | 7.0 |
| 0.2133 | 1720 | 5.814 | | 6.2 |
| 0.2120 | 1710 | 5.848 | | 5.5 |
| 0.2108 | 1700 | 5.882 | | 5.2 |
| 0.2095 | 1690 | 5.917 | | 5.2 |
| 0.2083 | 1680 | 5.952 | | 5.2 |
| 0.2071 | 1670 | 5.988 | | 5.2 |
| 0.2058 | 1660 | 6.024 | | 5.4 |
| 0.2046 | 1650 | 6.061 | | $6.7 \times 10^{-4}$ |

TABLE I (*Continued*)

Polyethylene

| eV | $cm^{-1}$ | μm | n | k |
|---|---|---|---|---|
| 0.2033 | 1640 | 6.098 | | $1.2 \times 10^{-3}$ |
| 0.2021 | 1630 | 6.135 | | $8.8 \times 10^{-4}$ |
| 0.2009 | 1620 | 6.173 | | 8.3 |
| 0.1996 | 1610 | 6.211 | | 8.7 |
| 0.1984 | 1600 | 6.250 | | 9.2 |
| 0.1971 | 1590 | 6.289 | | 9.9 |
| 0.1959 | 1580 | 6.329 | | 9.7 |
| 0.1947 | 1570 | 6.369 | | 9.0 |
| 0.1934 | 1560 | 6.410 | | 9.0 |
| 0.1922 | 1550 | 6.452 | | $9.7 \times 10^{-4}$ |
| 0.1909 | 1540 | 6.494 | | $1.1 \times 10^{-3}$ |
| 0.1897 | 1530 | 6.536 | | 1.2 |
| 0.1885 | 1520 | 6.579 | | 1.3 |
| 0.1872 | 1510 | 6.623 | | 1.6 |
| 0.1860 | 1500 | 6.667 | | 2.9 |
| 0.1847 | 1490 | 6.711 | | $5.4 \times 10^{-3}$ |
| 0.1841 | 1485 | 6.734 | | $1.7 \times 10^{-2}$ |
| 0.1835 | 1480 | 6.757 | | 4.5 |
| 0.1829 | 1475 | 6.780 | | 3.5 |
| 0.1823 | 1470 | 6.803 | | 3.0 |
| 0.1816 | 1465 | 6.826 | | 5.5 |
| 0.1810 | 1460 | 6.849 | | $2.8 \times 10^{-2}$ |
| 0.1798 | 1450 | 6.897 | | $8.5 \times 10^{-3}$ |
| 0.1785 | 1440 | 6.944 | | 5.9 |
| 0.1773 | 1430 | 6.993 | | 4.1 |
| 0.1761 | 1420 | 7.042 | | 3.0 |
| 0.1748 | 1410 | 7.092 | | 2.4 |
| 0.1736 | 1400 | 7.143 | | 2.1 |
| 0.1723 | 1390 | 7.194 | | 1.2 |
| 0.1711 | 1380 | 7.246 | | 1.6 |
| 0.1705 | 1375 | 7.273 | | 2.2 |
| 0.1699 | 1370 | 7.299 | | 2.9 |
| 0.1692 | 1365 | 7.326 | | 2.8 |
| 0.1686 | 1360 | 7.353 | | 2.5 |
| 0.1680 | 1355 | 7.380 | | 2.4 |
| 0.1674 | 1350 | 7.407 | | 2.4 |
| 0.1661 | 1340 | 7.463 | | 2.1 |
| 0.1649 | 1330 | 7.519 | | 1.5 |
| 0.1637 | 1320 | 7.576 | | 1.5 |
| 0.1624 | 1310 | 7.634 | | 1.9 |
| 0.1612 | 1300 | 7.692 | | 2.0 |
| 0.1599 | 1290 | 7.752 | | 1.8 |
| 0.1587 | 1280 | 7.813 | | 1.6 |
| 0.1575 | 1270 | 7.874 | | 1.3 |
| 0.1562 | 1260 | 7.937 | | 1.2 |
| 0.1550 | 1250 | 8.000 | | 1.1 |
| 0.1537 | 1240 | 8.065 | | 1.0 |
| 0.1525 | 1230 | 8.130 | | $1.0 \times 10^{-3}$ |
| 0.1513 | 1220 | 8.197 | | $9.6 \times 10^{-4}$ |

TABLE I (*Continued*)

Polyethylene

| eV | $cm^{-1}$ | μm | n | k |
|---|---|---|---|---|
| 0.1500 | 1210 | 8.264 | | 9.2 |
| 0.1488 | 1200 | 8.333 | | 8.9 |
| 0.1475 | 1190 | 8.403 | | 9.3 |
| 0.1469 | 1185 | 8.439 | | 9.1 |
| 0.1463 | 1180 | 8.475 | | $9.4 \times 10^{-4}$ |
| 0.1457 | 1175 | 8.511 | | $1.2 \times 10^{-3}$ |
| 0.1451 | 1170 | 8.547 | | $9.9 \times 10^{-4}$ |
| 0.1444 | 1165 | 8.584 | | 9.7 |
| 0.1438 | 1160 | 8.621 | | 9.9 |
| 0.1426 | 1150 | 8.696 | | 9.5 |
| 0.1413 | 1140 | 8.772 | | 9.6 |
| 0.1401 | 1130 | 8.850 | | $9.9 \times 10^{-4}$ |
| 0.1389 | 1120 | 8.929 | | $1.1 \times 10^{-3}$ |
| 0.1376 | 1110 | 9.009 | | $1.1 \times 10^{-3}$ |
| 0.1364 | 1100 | 9.091 | | $9.4 \times 10^{-4}$ |
| 0.1351 | 1090 | 9.174 | | $1.1 \times 10^{-3}$ |
| 0.1339 | 1080 | 9.259 | | 1.3 |
| 0.1333 | 1075 | 9.302 | | 1.3 |
| 0.1327 | 1070 | 9.346 | | 1.2 |
| 0.1320 | 1065 | 9.390 | | 1.2 |
| 0.1314 | 1060 | 9.434 | | 1.1 |
| 0.1308 | 1055 | 9.479 | | 1.1 |
| 0.1302 | 1050 | 9.524 | | $1.1 \times 10^{-3}$ |
| 0.1296 | 1045 | 9.569 | | $9.3 \times 10^{-4}$ |
| 0.1289 | 1040 | 9.615 | | 9.2 |
| 0.1277 | 1030 | 9.709 | | 8.2 |
| 0.1265 | 1020 | 9.804 | | 8.1 |
| 0.1252 | 1010 | 9.901 | | $8.3 \times 10^{-4}$ |
| 0.1240 | 1000 | 10.00 | | $1.0 \times 10^{-3}$ |
| 0.1234 | 995 | 10.05 | | 1.3 |
| 0.1227 | 990 | 10.10 | | 1.5 |
| 0.1221 | 985 | 10.15 | | 1.3 |
| 0.1215 | 980 | 10.20 | | $1.1 \times 10^{-3}$ |
| 0.1209 | 975 | 10.26 | | $8.0 \times 10^{-4}$ |
| 0.1203 | 970 | 10.31 | | 8.4 |
| 0.1196 | 965 | 10.36 | | 9.1 |
| 0.1190 | 960 | 10.42 | | 8.5 |
| 0.1184 | 955 | 10.47 | | 8.3 |
| 0.1178 | 950 | 10.53 | | 8.2 |
| 0.1165 | 940 | 10.64 | | 8.3 |
| 0.1153 | 930 | 10.75 | | $8.7 \times 10^{-4}$ |
| 0.1141 | 920 | 10.87 | | $1.0 \times 10^{-3}$ |
| 0.1134 | 915 | 10.93 | | 1.6 |
| 0.1131 | 912.5 | 10.96 | | 2.3 |
| 0.1128 | 910 | 10.99 | | 3.5 |
| 0.1125 | 907.5 | 11.02 | | 3.6 |
| 0.1122 | 905 | 11.05 | | 2.7 |
| 0.1116 | 900 | 11.11 | | $1.7 \times 10^{-3}$ |
| 0.1103 | 890 | 11.24 | | $9.0 \times 10^{-4}$ |

TABLE I (*Continued*)

Polyethylene

| eV | $cm^{-1}$ | μm | n | k |
|---|---|---|---|---|
| 0.1091 | 880 | 11.36 | | 8.1 |
| 0.1079 | 870 | 11.49 | | 6.7 |
| 0.1066 | 860 | 11.63 | | 7.2 |
| 0.1054 | 850 | 11.76 | | 7.6 |
| 0.1041 | 840 | 11.90 | | 7.8 |
| 0.1029 | 830 | 12.05 | | 8.2 |
| 0.1017 | 820 | 12.20 | | 8.7 |
| 0.1004 | 810 | 12.35 | | $9.5 \times 10^{-4}$ |
| 0.09919 | 800 | 12.50 | | $1.0 \times 10^{-3}$ |
| 0.09795 | 790 | 12.66 | | 1.1 |
| 0.09671 | 780 | 12.82 | | 1.1 |
| 0.09547 | 770 | 12.99 | | 1.3 |
| 0.09423 | 760 | 13.16 | | 1.6 |
| 0.09299 | 750 | 13.33 | | 2.3 |
| 0.09175 | 740 | 13.51 | | $6.4 \times 10^{-3}$ |
| 0.09113 | 735 | 13.61 | | $1.9 \times 10^{-2}$ |
| 0.09051 | 730 | 13.70 | | 8.1 |
| 0.08989 | 725 | 13.79 | | 2.9 |
| 0.08927 | 720 | 13.89 | | 7.0 |
| 0.08865 | 715 | 13.99 | | 1.9 |
| 0.08803 | 710 | 14.08 | | $1.2 \times 10^{-2}$ |
| 0.08679 | 700 | 14.29 | | $3.5 \times 10^{-3}$ |
| 0.08555 | 690 | 14.49 | | 1.9 |
| 0.08431 | 680 | 14.71 | | 1.5 |
| 0.08307 | 670 | 14.93 | | 1.2 |

[a] References are given in square brackets.
[b] n = 1.5 was assumed constant down to 670 $cm^{-1}$ for the calculation of k.

**TABLE II**

**Values of *n* and *k* for Polyethylene Obtained from Various References[a]**

| eV | $cm^{-1}$ | μm | n[b] | k[b] | n[c] | k[c] |
|---|---|---|---|---|---|---|
| 0.05567 | 449.2 | 22.26 | 1.51390[35] | 0.00050[35] | 1.53119[35] | 0.00077[35] |
| 0.05542 | 447.3 | 22.36 | 1.51388 | 0.00050 | 1.53122 | 0.00079 |
| 0.05518 | 445.3 | 22.46 | 1.51384 | 0.00050 | 1.53123 | 0.00073 |
| 0.05494 | 443.4 | 22.56 | 1.51381 | 0.00050 | 1.53117 | 0.00075 |
| 0.05470 | 441.4 | 22.65 | 1.51380 | 0.00049 | 1.53104 | 0.00090 |
| 0.05446 | 439.4 | 22.76 | 1.51380 | 0.00049 | 1.53121 | 0.00075 |
| 0.05421 | 437.5 | 22.86 | 1.51378 | 0.00051 | 1.53119 | 0.00068 |
| 0.05397 | 435.6 | 22.96 | 1.51376 | 0.00051 | 1.53115 | 0.00070 |
| 0.05373 | 433.6 | 23.06 | 1.51375 | 0.00051 | 1.53110 | 0.00071 |
| 0.05349 | 431.6 | 23.17 | 1.51375 | 0.00053 | 1.53108 | 0.00071 |
| 0.05325 | 429.7 | 23.27 | 1.51374 | 0.00053 | 1.53104 | 0.00070 |
| 0.05300 | 427.7 | 23.38 | 1.51373 | 0.00051 | 1.53102 | 0.00069 |
| 0.05276 | 425.8 | 23.49 | 1.51371 | 0.00050 | 1.53104 | 0.00070 |
| 0.05252 | 423.8 | 23.59 | 1.51372 | 0.00049 | 1.53104 | 0.00071 |
| 0.05228 | 421.9 | 23.70 | 1.51371 | 0.00049 | 1.53103 | 0.00070 |
| 0.05203 | 419.9 | 23.81 | 1.51370 | 0.00050 | 1.53102 | 0.00067 |
| 0.05179 | 418.0 | 23.93 | 1.51369 | 0.00049 | 1.53100 | 0.00067 |
| 0.05155 | 416.0 | 24.04 | 1.51368 | 0.00047 | 1.53098 | 0.00069 |
| 0.05131 | 414.1 | 24.15 | 1.51367 | 0.00047 | 1.53095 | 0.00070 |
| 0.05107 | 412.1 | 24.27 | 1.51365 | 0.00046 | 1.53094 | 0.00069 |
| 0.05082 | 410.2 | 24.38 | 1.51364 | 0.00045 | 1.53093 | 0.00067 |
| 0.05058 | 408.2 | 24.50 | 1.51362 | 0.00045 | 1.53091 | 0.00067 |
| 0.05034 | 406.2 | 24.62 | 1.51361 | 0.00045 | 1.53089 | 0.00068 |
| 0.05010 | 404.3 | 24.73 | 1.51360 | 0.00045 | 1.53086 | 0.00068 |
| 0.04986 | 402.3 | 24.85 | 1.51358 | 0.00045 | 1.53083 | 0.00067 |
| 0.04961 | 400.4 | 24.98 | 1.51357 | 0.00045 | 1.53083 | 0.00065 |
| 0.04937 | 398.4 | 25.10 | 1.51355 | 0.00046 | 1.53083 | 0.00065 |
| 0.04913 | 396.5 | 25.22 | 1.51355 | 0.00046 | 1.53081 | 0.00066 |
| 0.04889 | 394.5 | 25.35 | 1.51354 | 0.00044 | 1.53080 | 0.00066 |
| 0.04865 | 392.6 | 25.47 | 1.51354 | 0.00044 | 1.53080 | 0.00067 |
| 0.04840 | 390.6 | 25.60 | 1.51352 | 0.00044 | 1.53080 | 0.00068 |
| 0.04816 | 388.7 | 25.73 | 1.51350 | 0.00044 | 1.53079 | 0.00068 |
| 0.04792 | 386.7 | 25.86 | 1.51349 | 0.00044 | 1.53079 | 0.00069 |
| 0.04768 | 384.8 | 25.99 | 1.51348 | 0.00044 | 1.53079 | 0.00071 |
| 0.04744 | 382.8 | 26.12 | 1.51346 | 0.00044 | 1.53078 | 0.00071 |
| 0.04719 | 380.9 | 26.26 | 1.51344 | 0.00044 | 1.53077 | 0.00069 |
| 0.04695 | 378.9 | 26.39 | 1.51343 | 0.00044 | 1.53078 | 0.00070 |
| 0.04671 | 376.9 | 26.53 | 1.51342 | 0.00044 | 1.53078 | 0.00071 |
| 0.04647 | 375.0 | 26.67 | 1.51341 | 0.00045 | 1.53077 | 0.00071 |
| 0.04623 | 373.0 | 26.81 | 1.51342 | 0.00045 | 1.53077 | 0.00070 |
| 0.04598 | 371.1 | 26.95 | 1.51342 | 0.00045 | 1.53074 | 0.00071 |
| 0.04574 | 369.1 | 27.09 | 1.51341 | 0.00044 | 1.53073 | 0.00071 |
| 0.04550 | 367.2 | 27.23 | 1.51341 | 0.00043 | 1.53073 | 0.00070 |
| 0.04526 | 365.2 | 27.38 | 1.51340 | 0.00043 | 1.53072 | 0.00069 |
| 0.04502 | 363.3 | 27.53 | 1.51339 | 0.00043 | 1.53071 | 0.00069 |
| 0.04477 | 361.3 | 27.68 | 1.51338 | 0.00042 | 1.53072 | 0.00069 |
| 0.04453 | 359.4 | 27.83 | 1.51337 | 0.00042 | 1.53072 | 0.00068 |
| 0.04429 | 357.4 | 27.98 | 1.51336 | 0.00042 | 1.53071 | 0.00067 |
| 0.04405 | 355.5 | 28.13 | 1.51334 | 0.00042 | 1.53070 | 0.00067 |
| 0.04381 | 353.5 | 28.29 | 1.51333 | 0.00042 | 1.53069 | 0.00067 |
| 0.04356 | 351.6 | 28.44 | 1.51332 | 0.00042 | 1.53068 | 0.00067 |

**TABLE II (*Continued*)**

**Polyethylene**

| eV | $cm^{-1}$ | μm | $n^b$ | $k^b$ | $n^c$ | $k^c$ |
|---|---|---|---|---|---|---|
| 0.04332 | 349.6 | 28.60 | 1.51332 | 0.00042 | 1.53067 | 0.00066 |
| 0.04308 | 347.7 | 28.76 | 1.51331 | 0.00042 | 1.53067 | 0.00066 |
| 0.04284 | 345.7 | 28.93 | 1.51330 | 0.00042 | 1.53065 | 0.00066 |
| 0.04260 | 343.7 | 29.09 | 1.51329 | 0.00042 | 1.53065 | 0.00066 |
| 0.04235 | 341.8 | 29.26 | 1.51328 | 0.00042 | 1.53064 | 0.00066 |
| 0.04211 | 339.8 | 29.43 | 1.51328 | 0.00042 | 1.53064 | 0.00066 |
| 0.04187 | 337.9 | 29.60 | 1.51327 | 0.00043 | 1.53063 | 0.00066 |
| 0.04163 | 335.9 | 29.77 | 1.51327 | 0.00043 | 1.53062 | 0.00066 |
| 0.04139 | 334.0 | 29.94 | 1.51326 | 0.00043 | 1.53061 | 0.00066 |
| 0.04114 | 332.0 | 30.12 | 1.51325 | 0.00043 | 1.53061 | 0.00066 |
| 0.04090 | 330.1 | 30.30 | 1.51324 | 0.00043 | 1.53060 | 0.00065 |
| 0.04066 | 328.1 | 30.48 | 1.51323 | 0.00044 | 1.53060 | 0.00066 |
| 0.04042 | 326.2 | 30.66 | 1.51322 | 0.00044 | 1.53060 | 0.00066 |
| 0.04018 | 324.2 | 30.84 | 1.51322 | 0.00044 | 1.53060 | 0.00066 |
| 0.03993 | 322.3 | 31.03 | 1.51321 | 0.00044 | 1.53059 | 0.00066 |
| 0.03969 | 320.3 | 31.22 | 1.51321 | 0.00044 | 1.53058 | 0.00066 |
| 0.03945 | 318.4 | 31.41 | 1.51320 | 0.00044 | 1.53057 | 0.00066 |
| 0.03921 | 316.4 | 31.60 | 1.51320 | 0.00045 | 1.53057 | 0.00067 |
| 0.03897 | 314.4 | 31.80 | 1.51319 | 0.00045 | 1.53056 | 0.00067 |
| 0.03872 | 312.5 | 32.00 | 1.51319 | 0.00046 | 1.53055 | 0.00066 |
| 0.03848 | 310.6 | 32.20 | 1.51319 | 0.00046 | 1.53054 | 0.00066 |
| 0.03824 | 308.6 | 32.41 | 1.51318 | 0.00046 | 1.53054 | 0.00067 |
| 0.03800 | 306.6 | 32.61 | 1.51318 | 0.00046 | 1.53053 | 0.00068 |
| 0.03776 | 304.7 | 32.82 | 1.51317 | 0.00046 | 1.53054 | 0.00068 |
| 0.03751 | 302.7 | 33.03 | 1.51316 | 0.00046 | 1.53054 | 0.00068 |
| 0.03727 | 300.8 | 33.25 | 1.51315 | 0.00047 | 1.53053 | 0.00068 |
| 0.03703 | 298.8 | 33.46 | 1.51315 | 0.00047 | 1.53052 | 0.00069 |
| 0.03679 | 296.9 | 33.68 | 1.51315 | 0.00048 | 1.53051 | 0.00070 |
| 0.03655 | 294.9 | 33.91 | 1.51316 | 0.00048 | 1.53051 | 0.00070 |
| 0.03630 | 293.0 | 34.13 | 1.51316 | 0.00048 | 1.53051 | 0.00070 |
| 0.03606 | 291.0 | 34.36 | 1.51315 | 0.00048 | 1.53051 | 0.00071 |
| 0.03582 | 289.1 | 34.59 | 1.51315 | 0.00049 | 1.53050 | 0.00072 |
| 0.03558 | 287.1 | 34.83 | 1.51315 | 0.00049 | 1.53050 | 0.00072 |
| 0.03534 | 285.2 | 35.07 | 1.51314 | 0.00049 | 1.53050 | 0.00072 |
| 0.03509 | 283.2 | 35.31 | 1.51314 | 0.00050 | 1.53048 | 0.00073 |
| 0.03485 | 281.2 | 35.56 | 1.51314 | 0.00050 | 1.53048 | 0.00073 |
| 0.03461 | 279.3 | 35.80 | 1.51314 | 0.00050 | 1.53048 | 0.00074 |
| 0.03437 | 277.3 | 36.06 | 1.51313 | 0.00050 | 1.53047 | 0.00076 |
| 0.03413 | 275.4 | 36.31 | 1.51314 | 0.00050 | 1.53047 | 0.00077 |
| 0.03388 | 273.4 | 36.57 | 1.51314 | 0.00050 | 1.53046 | 0.00077 |
| 0.03364 | 271.5 | 36.83 | 1.51314 | 0.00050 | 1.53047 | 0.00078 |
| 0.03340 | 269.5 | 37.10 | 1.51314 | 0.00050 | 1.53046 | 0.00078 |
| 0.03316 | 267.6 | 37.37 | 1.51314 | 0.00050 | 1.53046 | 0.00079 |
| 0.03292 | 265.6 | 37.65 | 1.51314 | 0.00050 | 1.53046 | 0.00079 |
| 0.03267 | 263.7 | 37.93 | 1.51313 | 0.00050 | 1.53046 | 0.00080 |
| 0.03243 | 261.7 | 38.21 | 1.51313 | 0.00050 | 1.53045 | 0.00080 |
| 0.03219 | 259.8 | 38.50 | 1.51313 | 0.00050 | 1.53044 | 0.00081 |
| 0.03195 | 257.8 | 38.79 | 1.51313 | 0.00050 | 1.53044 | 0.00082 |
| 0.03171 | 255.9 | 39.08 | 1.51313 | 0.00051 | 1.53045 | 0.00083 |
| 0.03146 | 253.9 | 39.38 | 1.51312 | 0.00051 | 1.53044 | 0.00085 |
| 0.03122 | 251.9 | 39.69 | 1.51311 | 0.00051 | 1.53043 | 0.00086 |

**TABLE II (*Continued*)**

**Polyethylene**

| eV | $cm^{-1}$ | μm | $n^b$ | $k^b$ | $n^c$ | $k^c$ |
|---|---|---|---|---|---|---|
| 0.03098 | 250.0 | 40.00 | 1.51311 | 0.00051 | 1.53043 | 0.00087 |
| 0.03074 | 248.0 | 40.31 | 1.51310 | 0.00051 | 1.53044 | 0.00088 |
| 0.03049 | 246.1 | 40.63 | 1.51310 | 0.00052 | 1.53044 | 0.00088 |
| 0.03025 | 244.1 | 40.96 | 1.51310 | 0.00052 | 1.53044 | 0.00089 |
| 0.03001 | 242.2 | 41.29 | 1.51310 | 0.00052 | 1.53043 | 0.00091 |
| 0.02977 | 240.2 | 41.63 | 1.51310 | 0.00052 | 1.53042 | 0.00092 |
| 0.02953 | 238.3 | 41.97 | 1.51310 | 0.00053 | 1.53041 | 0.00094 |
| 0.02928 | 236.3 | 42.31 | 1.51310 | 0.00053 | 1.53042 | 0.00095 |
| 0.02904 | 234.4 | 42.67 | 1.51310 | 0.00054 | 1.53043 | 0.00096 |
| 0.02880 | 232.4 | 43.03 | 1.51310 | 0.00054 | 1.53043 | 0.00096 |
| 0.02856 | 230.5 | 43.39 | 1.51310 | 0.00054 | 1.53043 | 0.00097 |
| 0.02832 | 228.5 | 43.76 | 1.51310 | 0.00054 | 1.53043 | 0.00098 |
| 0.02807 | 226.6 | 44.14 | 1.51309 | 0.00055 | 1.53042 | 0.00099 |
| 0.02783 | 224.6 | 44.52 | 1.51308 | 0.00055 | 1.53042 | 0.00099 |
| 0.02759 | 222.7 | 44.91 | 1.51309 | 0.00056 | 1.53041 | 0.00101 |
| 0.02735 | 220.7 | 45.31 | 1.51309 | 0.00056 | 1.53041 | 0.00102 |
| 0.02711 | 218.7 | 45.71 | 1.51309 | 0.00057 | 1.53042 | 0.00104 |
| 0.02686 | 216.8 | 46.13 | 1.51309 | 0.00058 | 1.53044 | 0.00107 |
| 0.02662 | 214.8 | 46.55 | 1.51310 | 0.00059 | 1.53044 | 0.00107 |
| 0.02638 | 212.9 | 46.97 | 1.51310 | 0.00059 | 1.53043 | 0.00106 |
| 0.02614 | 210.9 | 47.41 | 1.51310 | 0.00059 | 1.53044 | 0.00106 |
| 0.02590 | 209.0 | 47.85 | 1.51310 | 0.00060 | 1.53045 | 0.00106 |
| 0.02565 | 207.0 | 48.30 | 1.51311 | 0.00060 | 1.53044 | 0.00108 |
| 0.02541 | 205.1 | 48.76 | 1.51311 | 0.00060 | 1.53045 | 0.00111 |
| 0.02517 | 203.1 | 49.23 | 1.51310 | 0.00060 | 1.53047 | 0.00112 |
| 0.02493 | 201.2 | 49.71 | 1.51309 | 0.00060 | 1.53046 | 0.00114 |
| 0.02469 | 199.2 | 50.20 | 1.51310 | 0.00061 | 1.53045 | 0.00115 |
| 0.02444 | 197.3 | 50.69 | 1.51311 | 0.00061 | 1.53044 | 0.00115 |
| 0.02420 | 195.3 | 51.20 | 1.51311 | 0.00062 | 1.53045 | 0.00117 |
| 0.02396 | 193.4 | 51.72 | 1.51312 | 0.00062 | 1.53046 | 0.00119 |
| 0.02372 | 191.4 | 52.24 | 1.51313 | 0.00062 | 1.53048 | 0.00118 |
| 0.02348 | 189.4 | 52.78 | 1.51313 | 0.00062 | 1.53050 | 0.00116 |
| 0.02323 | 187.5 | 53.33 | 1.51313 | 0.00062 | 1.53051 | 0.00118 |
| 0.02299 | 185.5 | 53.89 | 1.51314 | 0.00062 | 1.53051 | 0.00120 |
| 0.02275 | 183.6 | 54.47 | 1.51315 | 0.00063 | 1.53052 | 0.00120 |
| 0.02251 | 181.6 | 55.05 | 1.51316 | 0.00063 | 1.53052 | 0.00119 |
| 0.02227 | 179.7 | 55.65 | 1.51316 | 0.00063 | 1.53053 | 0.00119 |
| 0.02202 | 177.7 | 56.26 | 1.51316 | 0.00063 | 1.53055 | 0.00120 |
| 0.02178 | 175.8 | 56.89 | 1.51317 | 0.00063 | 1.53056 | 0.00122 |
| 0.02154 | 173.8 | 57.53 | 1.51318 | 0.00062 | 1.53056 | 0.00124 |
| 0.02130 | 171.9 | 58.18 | 1.51319 | 0.00062 | 1.53057 | 0.00122 |
| 0.02106 | 169.9 | 58.85 | 1.51318 | 0.00062 | 1.53056 | 0.00122 |
| 0.02081 | 168.0 | 59.53 | 1.51318 | 0.00062 | 1.53056 | 0.00124 |
| 0.02057 | 166.0 | 60.24 | 1.51319 | 0.00062 | 1.53056 | 0.00125 |
| 0.02033 | 164.1 | 60.95 | 1.51320 | 0.00062 | 1.53057 | 0.00126 |
| 0.02009 | 162.1 | 61.69 | 1.51321 | 0.00062 | 1.53057 | 0.00126 |
| 0.01985 | 160.2 | 62.44 | 1.51321 | 0.00061 | 1.53056 | 0.00125 |
| 0.01960 | 158.2 | 63.21 | 1.51321 | 0.00061 | 1.53058 | 0.00125 |
| 0.01936 | 156.2 | 64.00 | 1.51321 | 0.00060 | 1.53060 | 0.00125 |
| 0.01912 | 154.3 | 64.81 | 1.51322 | 0.00060 | 1.53060 | 0.00126 |
| 0.01888 | 152.3 | 65.64 | 1.51322 | 0.00060 | 1.53060 | 0.00127 |

TABLE II (*Continued*)

**Polyethylene**

| eV | $cm^{-1}$ | μm | $n^b$ | $k^b$ | $n^c$ | $k^c$ |
|---|---|---|---|---|---|---|
| 0.01864 | 150.4 | 66.49 | 1.51320 | 0.00060 | 1.53059 | 0.00128 |
| 0.01839 | 148.4 | 67.37 | 1.51319 | 0.00060 | 1.53058 | 0.00127 |
| 0.01815 | 146.5 | 68.27 | 1.51320 | 0.00060 | 1.53060 | 0.00129 |
| 0.01791 | 144.5 | 69.19 | 1.51321 | 0.00059 | 1.53063 | 0.00131 |
| 0.01767 | 142.6 | 70.14 | 1.51322 | 0.00059 | 1.53064 | 0.00131 |
| 0.01743 | 140.6 | 71.11 | 1.51322 | 0.00059 | 1.53064 | 0.00130 |
| 0.01718 | 138.7 | 72.11 | 1.51321 | 0.00059 | 1.53064 | 0.00130 |
| 0.01694 | 136.7 | 73.14 | 1.51322 | 0.00060 | 1.53065 | 0.00131 |
| 0.01670 | 134.8 | 74.20 | 1.51323 | 0.00060 | 1.53067 | 0.00132 |
| 0.01646 | 132.8 | 75.29 | 1.51323 | 0.00061 | 1.53067 | 0.00132 |
| 0.01622 | 130.9 | 76.42 | 1.51323 | 0.00061 | 1.53069 | 0.00134 |
| 0.01597 | 128.9 | 77.58 | 1.51324 | 0.00061 | 1.53072 | 0.00134 |
| 0.01573 | 126.9 | 78.77 | 1.51324 | 0.00061 | 1.53074 | 0.00133 |
| 0.01549 | 125.0 | 80.00 | 1.51324 | 0.00061 | 1.53076 | 0.00132 |
| 0.01525 | 123.0 | 81.27 | 1.51325 | 0.00061 | 1.53078 | 0.00130 |
| 0.01501 | 121.1 | 82.58 | 1.51325 | 0.00060 | 1.53079 | 0.00128 |
| 0.01476 | 119.1 | 83.93 | 1.51325 | 0.00060 | 1.53079 | 0.00127 |
| 0.01452 | 117.2 | 85.33 | 1.51326 | 0.00061 | 1.53081 | 0.00127 |
| 0.01428 | 115.2 | 86.78 | 1.51327 | 0.00061 | 1.53083 | 0.00126 |
| 0.01404 | 113.3 | 88.28 | 1.51328 | 0.00061 | 1.53084 | 0.00128 |
| 0.01380 | 111.3 | 89.82 | 1.51328 | 0.00061 | 1.53086 | 0.00127 |
| 0.01355 | 109.4 | 91.43 | 1.51327 | 0.00061 | 1.53088 | 0.00125 |
| 0.01331 | 107.4 | 93.09 | 1.51327 | 0.00061 | 1.53088 | 0.00124 |
| 0.01307 | 105.5 | 94.81 | 1.51327 | 0.00060 | 1.53087 | 0.00123 |
| 0.01283 | 103.5 | 96.60 | 1.51327 | 0.00060 | 1.53086 | 0.00123 |
| 0.01259 | 101.6 | 98.46 | 1.51327 | 0.00061 | 1.53085 | 0.00126 |
| 0.01234 | 99.6 | 100.4 | 1.51325 | 0.00060 | 1.53082 | 0.00129 |
| 0.01210 | 97.7 | 102.4 | 1.51323 | 0.00061 | 1.53083 | 0.00128 |
| 0.01186 | 95.7 | 104.5 | 1.51325 | 0.00061 | 1.53087 | 0.00127 |
| 0.01162 | 93.7 | 106.7 | 1.51326 | 0.00060 | 1.53091 | 0.00128 |
| 0.01138 | 91.8 | 108.9 | 1.51327 | 0.00059 | 1.53094 | 0.00128 |
| 0.01113 | 89.8 | 111.3 | 1.51327 | 0.00059 | 1.53096 | 0.00125 |
| 0.01089 | 87.9 | 113.8 | 1.51326 | 0.00060 | 1.53094 | 0.00123 |
| 0.01065 | 85.9 | 116.4 | 1.51325 | 0.00061 | 1.53091 | 0.00123 |
| 0.01041 | 84.0 | 119.1 | 1.51324 | 0.00062 | 1.53088 | 0.00123 |
| 0.01016 | 82.0 | 121.9 | 1.51322 | 0.00062 | 1.53083 | 0.00124 |
| 0.00992 | 80.1 | 124.9 | 1.51319 | 0.00062 | 1.53075 | 0.00130 |
| 0.00968 | 78.1 | 128.0 | 1.51315 | 0.00066 | 1.53063 | 0.00142 |
| 0.00944 | 76.2 | 131.3 | 1.51314 | 0.00072 | 1.53053 | 0.00159 |
| 0.00920 | 74.2 | 134.7 | 1.51315 | 0.00082 | 1.53073 | 0.00201 |
| 0.00895 | 72.3 | 138.4 | 1.51327 | 0.00098 | 1.53163 | 0.00232 |
| 0.00871 | 70.3 | 142.2 | 1.51358 | 0.00103 | 1.53207 | 0.00188 |
| 0.00847 | 68.4 | 146.3 | 1.51381 | 0.00088 | 1.53200 | 0.00150 |
| 0.00823 | 66.4 | 150.6 | 1.51387 | 0.00074 | 1.53188 | 0.00129 |
| 0.00799 | 64.4 | 155.1 | 1.51385 | 0.00065 | 1.53182 | 0.00115 |
| 0.00774 | 62.5 | 160.0 | 1.51381 | 0.00060 | 1.53186 | 0.00109 |
| 0.00750 | 60.5 | 165.2 | 1.51381 | 0.00057 | 1.53188 | 0.00109 |
| 0.00620 | 50.0 | 200.0 | | 0.00062[41] | | |
| 0.00558 | 45.0 | 222.2 | | 0.00056 | | |
| 0.00496 | 40.0 | 250.0 | | 0.00051 | | |
| 0.00434 | 35.0 | 285.7 | | 0.00045 | | |

**TABLE II (*Continued*)**

**Polyethylene**

| eV | $cm^{-1}$ | μm | $n^b$ | $k^b$ | $n^c$ | $k^c$ |
|---|---|---|---|---|---|---|
| 0.00372 | 30.0 | 333.3 | | 0.00040 | | |
| 0.00310 | 25.0 | 400.0 | | 0.00034 | | |
| 0.00248 | 20.0 | 500.0 | | 0.00029 | | |
| 0.00186 | 15.0 | 666.7 | | 0.00023 | | |
| 0.00124 | 10.0 | 1000 | | 0.00017 | | |
| 0.000620 | 5.0 | 2000 | | 0.00012 | | |
| 0.00399 | 32.2 | 310.3 | 1.51362[25] | 0.00047[25] | 1.52454[25] | 0.00048[25] |
| 0.00393 | 31.7 | 315.1 | 1.51363 | 0.00046 | 1.52458 | 0.00046 |
| 0.00387 | 31.2 | 320.0 | 1.51363 | 0.00045 | 1.52458 | 0.00045 |
| 0.00381 | 30.8 | 325.1 | 1.51363 | 0.00043 | 1.52460 | 0.00045 |
| 0.00375 | 30.3 | 330.4 | 1.51362 | 0.00044 | 1.52460 | 0.00043 |
| 0.00369 | 29.8 | 335.7 | 1.51362 | 0.00044 | 1.52462 | 0.00044 |
| 0.00363 | 29.3 | 341.3 | 1.51362 | 0.00043 | 1.52462 | 0.00042 |
| 0.00357 | 28.8 | 347.1 | 1.51363 | 0.00042 | 1.52465 | 0.00041 |
| 0.00351 | 28.3 | 353.1 | 1.51363 | 0.00041 | 1.52466 | 0.00040 |
| 0.00345 | 27.8 | 359.3 | 1.51361 | 0.00041 | 1.52465 | 0.00040 |
| 0.00339 | 27.3 | 365.8 | 1.51362 | 0.00041 | 1.52465 | 0.00041 |
| 0.00333 | 26.9 | 372.3 | 1.51362 | 0.00041 | 1.52466 | 0.00039 |
| 0.00327 | 26.4 | 379.2 | 1.51362 | 0.00040 | 1.52467 | 0.00040 |
| 0.00321 | 25.9 | 386.4 | 1.51362 | 0.00039 | 1.52467 | 0.00038 |
| 0.00315 | 25.4 | 393.9 | 1.51363 | 0.00039 | 1.52471 | 0.00038 |
| 0.00309 | 24.9 | 401.6 | 1.51364 | 0.00038 | 1.52458 | 0.00037 |
| 0.00302 | 24.4 | 409.7 | 1.51364 | 0.00037 | 1.52464 | 0.00036 |
| 0.00297 | 23.9 | 417.9 | 1.51364 | 0.00037 | 1.52467 | 0.00035 |
| 0.00290 | 23.4 | 426.6 | 1.51365 | 0.00037 | 1.52467 | 0.00034 |
| 0.00284 | 22.9 | 435.7 | 1.51365 | 0.00036 | 1.52468 | 0.00034 |
| 0.00278 | 22.5 | 445.2 | 1.51368 | 0.00036 | 1.52467 | 0.00033 |
| 0.00272 | 22.0 | 455.2 | 1.51371 | 0.00034 | 1.52467 | 0.00033 |
| 0.00266 | 21.5 | 465.6 | 1.51371 | 0.00034 | 1.52467 | 0.00032 |
| 0.00260 | 21.0 | 476.2 | 1.51370 | 0.00034 | 1.52467 | 0.00031 |
| 0.00254 | 20.5 | 487.6 | 1.51369 | 0.00035 | 1.52468 | 0.00029 |
| 0.00248 | 20.0 | 499.5 | 1.51371 | 0.00034 | 1.52469 | 0.00031 |
| 0.00242 | 19.5 | 512.0 | 1.51372 | 0.00032 | 1.52468 | 0.00030 |
| 0.00236 | 19.0 | 525.2 | 1.51373 | 0.00031 | 1.52473 | 0.00028 |
| 0.00230 | 18.5 | 539.1 | 1.51373 | 0.00029 | 1.52454 | 0.00030 |
| 0.00224 | 18.1 | 553.4 | 1.51373 | 0.00030 | 1.52461 | 0.00030 |
| 0.00218 | 17.6 | 568.8 | 1.51377 | 0.00031 | 1.52463 | 0.00030 |
| 0.00212 | 17.1 | 585.1 | 1.51380 | 0.00029 | 1.52465 | 0.00031 |
| 0.00206 | 16.6 | 602.4 | 1.51380 | 0.00028 | 1.52464 | 0.00030 |
| 0.00200 | 16.1 | 620.7 | 1.51382 | 0.00029 | 1.52462 | 0.00030 |
| 0.00194 | 15.6 | 640.2 | 1.51383 | 0.00029 | 1.52462 | 0.00031 |
| 0.00188 | 15.1 | 660.5 | 1.51386 | 0.00029 | 1.52464 | 0.00031 |
| 0.00182 | 14.6 | 682.6 | 1.51391 | 0.00029 | 1.52458 | 0.00032 |
| 0.00175 | 14.2 | 706.2 | 1.51395 | 0.00022 | 1.52459 | 0.00030 |
| 0.00169 | 13.7 | 731.5 | 1.51395 | 0.00029 | 1.52457 | 0.00030 |
| 0.00163 | 13.2 | 758.7 | 1.51391 | 0.00028 | 1.52462 | 0.00029 |
| 0.00157 | 12.7 | 787.4 | 1.51390 | 0.00027 | 1.52464 | 0.00029 |
| 0.00151 | 12.2 | 819.0 | 1.51397 | 0.00027 | 1.52471 | 0.00029 |
| 0.00145 | 11.7 | 853.2 | 1.51404 | 0.00023 | 1.52476 | 0.00029 |
| 0.00139 | 11.2 | 890.5 | 1.51406 | 0.00020 | 1.52476 | 0.00028 |

TABLE II (*Continued*)

Polyethylene

| eV | $cm^{-1}$ | μm | n[b] | k[b] | n[c] | k[c] |
|---|---|---|---|---|---|---|
| 0.00133 | 10.7 | 931.1 | 1.51406 | 0.00021 | 1.52470 | 0.00028 |
| 0.00127 | 10.2 | 975.6 | 1.51407 | 0.00022 | 1.52468 | 0.00030 |
| 0.00121 | 9.8 | 1024 | 1.51407 | 0.00022 | 1.52472 | 0.00028 |
| 0.00115 | 9.3 | 1078 | 1.51404 | 0.00022 | 1.52472 | 0.00025 |
| 0.00109 | 8.8 | 1138 | 1.51399 | 0.00023 | 1.52473 | 0.00026 |
| 0.00103 | 8.3 | 1205 | 1.51395 | 0.00023 | 1.52473 | 0.00028 |
| 0.00097 | 7.8 | 1280 | 1.51402 | 0.00023 | 1.52475 | 0.00025 |
| 0.00091 | 7.3 | 1366 | 1.51409 | 0.00024 | 1.52479 | 0.00022 |
| 0.00085 | 6.8 | 1462 | 1.51407 | 0.00023 | 1.52476 | 0.00022 |
| 0.00079 | 6.3 | 1575 | 1.51408 | 0.00024 | 1.52468 | 0.00025 |
| 0.00073 | 5.9 | 1706 | 1.51410 | 0.00022 | 1.52463 | 0.00024 |
| 0.00067 | 5.4 | 1862 | 1.51405 | 0.00024 | 1.52461 | 0.00024 |

[a]References are given in square brackets.
[b]Low-density polyethylene data (LDPE).
[c]High-density polyethylene data (HDPE).

# Potassium Bromide (KBr)

EDWARD D. PALIK
Institute for Physical Science and Technology
University of Maryland
College Park, Maryland

The selected optical constants $n$ and $k$ are collected in Table I and plotted in Fig. 1. There is some overlap of data to indicate the typical variations that occur from lab to lab. The eV, $cm^{-1}$, or μm units of the original data are usually listed with three or fewer significant figures (eV, for example, as read off a graph), and the other two units ($cm^{-1}$ and μm) are listed with four figures. Although $n$ and $k$ are often listed with two decimal places (and at least three significant figures) in the IR and UV, the accuracy (absolute value) is probably poorer, but the precision is good enough to show structure in the original measurements (multiphonon peaks in the IR and peaks in interband absorption in the UV). In the transparent visible and near-IR regions, $n$ is known to four or five figures.

Starting at low frequency, we note that a simple capacity measurement of the loss tangent, $\tan\delta = \varepsilon_2/\varepsilon_1$, and the real part of the dielectric function, $\varepsilon_1$, have been nearly forgotten. Breckenridge [1] measured these parameters from $10^2$ to $10^8$ Hz for KBr at 85 °C. However, to see an effect in $\varepsilon_2$, it was necessary to heat-treat the sample to produce defects; this gave rise to extrinsic absorption, which is not of particular interest here, and these numbers are not tabulated. The low-frequency (nearly dc) dielectric constant at 85 °C was found to be 4.90, which yields $n = 2.21$, in agreement with higher frequency, room-temperature values cited in Table I.

For somewhat higher frequencies, at 9.8, 35.4 and 116 GHz, Owens [2] has measured the capacity at 25 °C and cited several other values by other workers. These values of $\varepsilon_1$ and $\varepsilon_2$ along with far-IR values of Genzel *et al.* [3] and Stolen and Dransfeld [4] have been used by Sparks *et al.* [5] in a model invoking two-phonon difference processes in the range 0.5 to 33 $cm^{-1}$. We emphasize the calculated results for 293 K, since these fit the measured values over most of the range to better than ±50% (the largest deviation between theory and experiment); we list some other values also. Genzel *et al.* did not specify room temperature for their grating-spectrometer transmission measurements; Stolen and Dransfeld made


Copyright © 1991 by Academic Press.
All rights of reproduction in any form reserved.
ISBN 0-12-544422-2

transmission measurements with a grating spectrometer at three wavelengths (320, 500, and 900 μm) as a function of temperature from 15 to 420 K. Samples were presumably mechanically polished with conventional grits. Quality of surface is usually not an issue at these long wavelengths.

The spectral region 20 to 240 $cm^{-1}$ has been covered by Johnson and Bell [6] using asymmetric Fourier-transform spectroscopy. This technique yielded the phase and amplitude of the reflectivity directly with no need for Kramers–Kronig analysis or a Lorentz-oscillator-model fit. The reststrahlen minimum was measured to be 0.0008, indicating little or no polishing damage. Resolution was 2 $cm^{-1}$. Sample temperature was 300 K. Shoulders on the low- and high-frequency sides of the transverse optical phonon frequency are due to difference and sum phonon absorption bands, respectively. We have read graphs to obtain $n$ and $k$.

For the region 250 to 700 $cm^{-1}$ Deutsch [7] has collected the absorption coefficient $\alpha$ from several sources all more or less at room temperature. Transmission measurements of slab samples were used in all cases. We have read an experimental curve to obtain $\alpha$ and converted to $k$ with the equation $k = \alpha\lambda/4\pi$. McGill *et al.* [8] have developed a model for multiphonon absorption and used it to fit these experimental data.

Laser calorimetry has been performed in the $CO_2$-laser region by at least two groups [9, 10]. The temperature rise is measured with thermocouples upon irradiation of the sample with a specific laser wavelength. The technique is very sensitive and can be used to distinguish between surface absorption and bulk absorption. Surface absorption can occur due to surface properties such as roughness and adsorption of gaseous species from the air, such as water, hydrocarbons, and so on. Bulk absorption can occur due to intrinsic processes for the purest materials or extrinsic processes due to impurity molecules ($SO_4$, $NO_2$, $HCCO_3$, and so forth) "grown" into the materials. We chose the data of Ref. [9] because they showed the smallest absorption (indicating the purest material).

In the transparent region 42 to 0.2 μm, Li [11] has collected and analyzed a great deal of $n$ data from many references. Prism minimum deviation was the experimental method in most cases. He has fitted a Sellmeier-type equation with eleven adjustable parameters to represent the data to the fifth decimal place. The dispersion formula for 293 K is

$$n^2 = 1.39408 + \frac{0.79221\lambda^4}{\lambda^2 - (0.146)^2} + \frac{0.01981\lambda^2}{\lambda^2 - (0.173)^2}$$

$$+ \frac{0.15587\lambda^2}{\lambda^2 - (0.187)^2} + \frac{0.17673\lambda^2}{\lambda^2 - (60.61)^2} + \frac{2.06217\lambda^2}{\lambda^2 - (87.72)^2}.$$

This indicates that $\lambda_T = 87.72$ μm (114.0 $cm^{-1}$). For the spectral range

0.25 to 26 μm, Li states that the fourth decimal place is meaningful, with estimated uncertainties in the range 0.0001 to 0.0005. To either side the uncertainty moves to the third decimal place.

Li has also provided a temperature-dependence formula of the form

$$2n\frac{dn}{dT} = -11.61(n^2-1) + 0.39 + \frac{3.944\lambda^4}{(\lambda^2-0.03497)^2} + \frac{182.88\lambda^2}{(\lambda^2-7694.80)^2},$$

where $dn/dT$ is in units of $10^{-5}$/K and $\lambda$ is in μm. Note that a 3 K difference in room temperature between labs begins to affect the fourth decimal place.

The fundamental band gap of KBr is at ~6.6 eV, and there exists much data for the region 6 to 30 eV as discussed in Refs. [12–14]. We have usually selected the more recent measurements and/or those showing more structure in the reflectivity. Although much of the data involved electron-energy-loss measurements on thin films, we have ignored this nonoptical way of determining the imaginary part of the dielectric function, because thin films are deposited and usually represent defected, polycrystalline material with voids, not bulk material. Bulk crystals cleaved in UHV are presumably the best samples for reflectivity, so synchrotron data are to be preferred.

Tomiki *et al.* measured the optical constants in the range 5.5 to 12 eV using thin plates at the band edge [13] and reflectivity and Kramers–Kronig (K–K) analysis in the opaque region at 301 K [14]. Verification of Erbach's rule at the band edge was discussed in detail [13]. Small variations between eV and $cm^{-1}$ occur between data of Refs. [13] and [14] because we read eV from a graph in [13] and converted to $cm^{-1}$ using 8065.48 $cm^{-1}$/eV, whereas Tomiki supplied original data using 8066.0 $cm^{-1}$/eV.

Antinori *et al.* [15] used a continuum He discharge lamp as a source of radiation in the range 13.5 to 20.5 eV. A 1-m grating spectrometer gave a resolution of better than 1.8 Å at 990 Å. Samples were cleaved in air and then put into the sample chamber, which was pumped to $10^{-5}$ torr. The reflectivity was K–K analyzed using the data of Rubloff [12] and Blechschmidt *et al.* [16] to cover the lower and higher energy ranges, respectively, as is required by K–K analysis. We have read the values of $\varepsilon_1$, $\varepsilon_2$ from a graph and obtained the numbers listed from the equations

$$2n^2 = \varepsilon_1 + \sqrt{\varepsilon_1^2 + \varepsilon_2^2}$$

$$2k^2 = -\varepsilon_1 + \sqrt{\varepsilon_1^2 + \varepsilon_2^2}.$$

From 13 to 31 eV we have used data of Blechschmidt *et al.* [16]. The experiments were performed at the Deutsche Elektronen-Synchrotron with a normal-incidence monochromator in a modified Wadsworth mount. Single crystals were freshly cleaved and put into the vacuum of $5 \times 10^{-8}$ torr. Angle of incidence was varied from 15 to 75° for both $\|(p)$ and $\perp(s)$ polarizations using angles on both sides of the normal for increased accuracy. $R$ was then used to calculate $\varepsilon_1$ and $\varepsilon_2$. We then calculated $n$ and $k$ from graph values of $\varepsilon_1$ and $\varepsilon_2$.

From 25 to 40 eV we have chosen the $\varepsilon_1$, $\varepsilon_2$ data of Stephan *et al.* [17]; it shows a little more detail than the data of Blechschmidt *et al.* [16] and covers a wider spectral region. The data were obtained with a grating spectrometer with an 82° angle of incidence. The source was a spark discharge with a 15 Hz rate. Sample reflectivity was measured at three angles of incidence using polarized light. We have overlapped the above UV data to give an indication of the accuracy from lab to lab.

Above 40 eV absorption decreases steadily with little structure. The data of Brown *et al.* [18] cover the range 70 to 200 eV. A grating monochromator was used at an 86° angle of incidence. The source was the Stoughton, Wisconsin, synchrotron. The films were evaporated *in situ* onto Formvar, carbon, or gold substrates whose transmission had been previously measured. Thicknesses were determined by a crystal-quartz thickness monitor.

Far above these energies the $L$ and $K$ absorption edges of K and Br are reached. These features occur at $K$(K), 3608 eV; $K$(Br), 13470 eV; $L_{2,3}$ (K), 295 eV; $L_1$ (Br), 1781 eV; $L_2$ (Br), 1599 eV; $L_3$ (Br), 1553 eV; $N_1$(Br), 31.3 eV. The $M$ absorption edges for atomic K and Br are not defined in Ref. [19]. Other atomic energy states are presumably mixed into the conduction-band structure seen in $k$ in the lower-energy region [12].

## REFERENCES


1. R. G. Breckenridge, *J. Chem. Phys.* **16**, 959 (1948).
2. J. C. Owens, *Phys. Rev.* **181**, 1228 (1969).
3. L. Genzel, H. Happ, and R. Weber, *Z. Physik* **154**, 13 (1959).
4. R. Stolen and K. Dransfeld, *Phys. Rev.* **139A**, 1295 (1965).
5. M. Sparks, D. F. King, and D. L. Mills, *Phys. Rev.* **B26**, 6987 (1982).
6. K. W. Johnson and E. E. Bell, *Phys. Rev.* **187**, 1044 (1969).
7. T. F. Deutsch, *J. Phys. Chem. Solids* **34**, 2091 (1973).
8. T. C. McGill, R. W. Hellwarth, M. Mangir, and H. V. Winston, *J. Phys. Chem. Solids* **34**, 2105 (1973).
9. J. M. Rowe and J. A. Harrington, *Proc. 5th IR Laser Window Conf.* (1976); and private communication.
10. T. Hidaka, T. Morikawa, and J. Shimada, *Appl. Opt.* **19**, 3763 (1980).
11. H. H. Li, *J. Phys. Chem. Ref. Data* **5**, 345 (1976).
12. G. W. Rubloff, *Phys. Rev.* **B5**, 662 (1972).
13. T. Tomiki, T. Miyata, and H. Tsukamoto, *Z. Naturforsch.* **29a**, 145 (1974).

14. T. Tomiki, T. Miyata, and H. Tsukamoto, *J. Phys. Soc. Japan* **35**, 495 (1973); and private communication.
15. M. Antinori, A. Balzarotti, and M. Piacentini, *Phys. Rev.* **B7**, 1541 (1973).
16. D. Blechschmidt, *Phys. Stat. Sol.* **B36**, 625 (1969).
17. G. Stephan, E. Garignon, and S. Robin, *Comp. Rend. Sci. Paris* **268C**, 408 (1969).
18. F. C. Brown, C. Gahwiller, H. Fujita, A. B. Kung, W. Scheifley, and N. Carrera, *Phys. Rev.* **B2**, 2126 (1970).
19. American Institute of Physics Handbook, (D. E. Gray, ed.), Third Edition, McGraw-Hill, New York, 7 (1982).

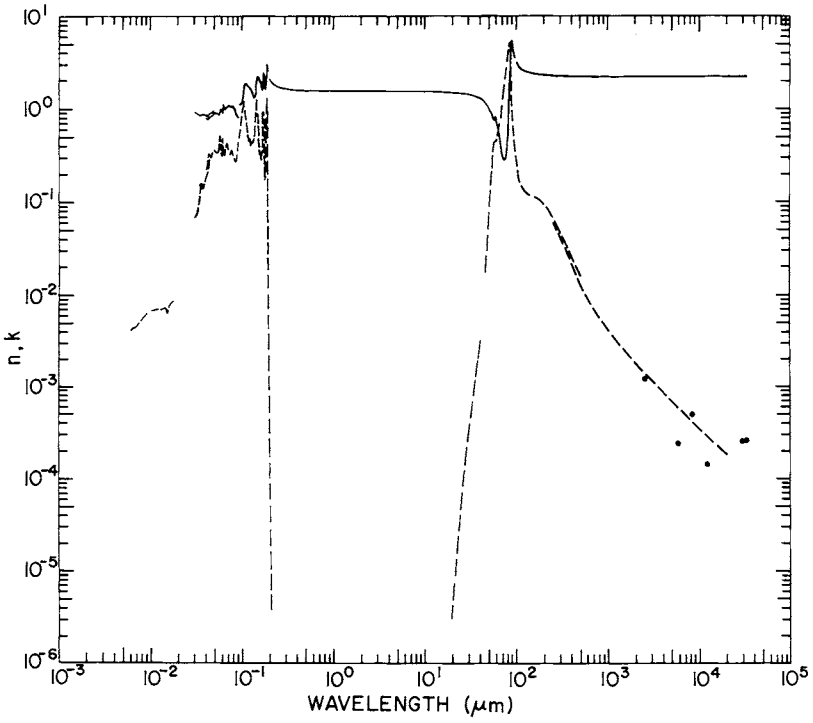


**Fig. 1.** Log–log plot of $n$ (solid line) and $k$ (dashed line) versus wavelength in micrometers for potassium bromide.

**TABLE I**

**Values of *n* and *k* for Potassium Bromide from Various References[a]**

| eV | $cm^{-1}$ | Å | n | k |
|---|---|---|---|---|
| 200 | | 61.99 | | $4.17 \times 10^{-3}$ [18] |
| 195 | | 63.58 | | $4.40 \times 10^{-3}$ |
| 192.5 | | 64.40 | | $4.43 \times 10^{-3}$ |
| 190 | | 65.26 | | $4.52 \times 10^{-3}$ |
| 187.5 | | 66.12 | | $4.68 \times 10^{-3}$ |
| 185 | | 67.02 | | $4.47 \times 10^{-3}$ |
| 180 | | 68.88 | | $4.63 \times 10^{-3}$ |
| 175 | | 70.85 | | $4.79 \times 10^{-3}$ |
| 170 | | 72.93 | | $4.97 \times 10^{-3}$ |
| 165 | | 75.14 | | $5.14 \times 10^{-3}$ |
| 160 | | 77.49 | | $5.30 \times 10^{-3}$ |
| 155 | | 79.99 | | $5.51 \times 10^{-3}$ |
| 150 | | 82.65 | | $5.75 \times 10^{-3}$ |
| 145 | | 85.51 | | $6.00 \times 10^{-3}$ |
| 140 | | 88.56 | | $6.20 \times 10^{-3}$ |
| 135 | | 91.84 | | $6.35 \times 10^{-3}$ |
| 130 | | 95.37 | | $6.49 \times 10^{-3}$ |
| 125 | | 99.19 | | $6.59 \times 10^{-3}$ |
| 120 | | 103.3 | | $6.74 \times 10^{-3}$ |
| 115 | | 107.8 | | $6.82 \times 10^{-3}$ |
| 110 | | 112.7 | | $6.91 \times 10^{-3}$ |
| 105 | | 118.1 | | $6.95 \times 10^{-3}$ |
| 100 | | 124.0 | | $6.91 \times 10^{-3}$ |
| 95 | | 130.5 | | $6.91 \times 10^{-3}$ |
| 90 | | 137.8 | | $7.04 \times 10^{-3}$ |
| 89 | | 139.3 | | $7.12 \times 10^{-3}$ |
| 88 | | 140.8 | | $7.19 \times 10^{-3}$ |
| 87 | | 142.5 | | $7.26 \times 10^{-3}$ |
| 86 | | 144.1 | | $7.28 \times 10^{-3}$ |
| 85 | | 145.9 | | $7.20 \times 10^{-3}$ |
| 84 | | 147.6 | | $6.93 \times 10^{-3}$ |
| 83 | | 149.3 | | $6.66 \times 10^{-3}$ |
| 82 | | 151.2 | | $6.38 \times 10^{-3}$ |
| 81 | | 153.0 | | $6.33 \times 10^{-3}$ |
| 80.5 | | 154.0 | | $6.40 \times 10^{-3}$ |
| 80 | | 155.0 | | $7.03 \times 10^{-3}$ |
| 79.5 | | 155.9 | | $7.38 \times 10^{-3}$ |
| 79 | | 156.9 | | $7.80 \times 10^{-3}$ |
| 78.5 | | 157.9 | | $8.42 \times 10^{-3}$ |
| 78 | | 158.9 | | $8.22 \times 10^{-3}$ |
| 77.5 | | 159.9 | | $8.15 \times 10^{-3}$ |
| 77 | | 161.0 | | $8.04 \times 10^{-3}$ |
| 76.5 | | 162.0 | | $8.06 \times 10^{-3}$ |
| 76 | | 163.1 | | $7.98 \times 10^{-3}$ |
| 75.5 | | 164.2 | | $8.04 \times 10^{-3}$ |
| 75 | | 165.3 | | $8.09 \times 10^{-3}$ |
| 74.5 | | 166.4 | | $8.87 \times 10^{-3}$ |
| 74 | | 167.5 | | $9.60 \times 10^{-3}$ |

TABLE I (*Continued*)

**Potassium Bromide**

| eV | $cm^{-1}$ | Å | n | k |
|---|---|---|---|---|
| 73.5 | | 168.6 | | $9.46 \times 10^{-3}$ |
| 73 | | 169.8 | | $9.87 \times 10^{-3}$ |
| 72.5 | | 171.0 | | $8.44 \times 10^{-3}$ |
| 72 | | 172.2 | | $7.54 \times 10^{-3}$ |
| 71.5 | | 173.4 | | $6.76 \times 10^{-3}$ |
| 71 | | 174.6 | | $6.67 \times 10^{-3}$ |
| 70.5 | | 175.8 | | $6.71 \times 10^{-3}$ |
| 70 | | 177.1 | | $6.76 \times 10^{-3}$ |

| eV | $cm^{-1}$ | μm | n | k |
|---|---|---|---|---|
| 40 | | 0.03099 | 0.91[17] | $6.9 \times 10^{-2}$[17] |
| 39.5 | | 0.03138 | 0.90 | $7.1 \times 10^{-2}$ |
| 39 | | 0.03179 | 0.90 | $7.2 \times 10^{-2}$ |
| 38.5 | | 0.03220 | 0.89 | $7.6 \times 10^{-2}$ |
| 38 | | 0.03262 | 0.88 | $8.0 \times 10^{-2}$ |
| 37.5 | | 0.03306 | 0.87 | $8.6 \times 10^{-2}$ |
| 37 | | 0.03350 | 0.86 | $9.3 \times 10^{-2}$ |
| 36.5 | | 0.03396 | 0.84 | 0.11 |
| 36 | | 0.03444 | 0.84 | 0.13 |
| 35.5 | | 0.03492 | 0.85 | 0.14 |
| 35 | | 0.03542 | 0.85 | 0.15 |
| 34.5 | | 0.03593 | 0.86 | 0.15 |
| 34 | | 0.03646 | 0.87 | 0.15 |
| 33.5 | | 0.03701 | 0.88 | 0.15 |
| 33 | | 0.03757 | 0.88 | 0.14 |
| 32.5 | | 0.03814 | 0.86 | 0.14 |
| 32 | | 0.03874 | 0.85 | 0.15 |
| 31.5 | | 0.03936 | 0.85 | 0.16 |
| 31 | | 0.03999 | 0.84 | 0.18 |
| | | | 0.80[16] | |
| 30.5 | | 0.04065 | 0.84[17] | 0.18[17] |
| | | | 0.80[16] | |
| 30 | | 0.04132 | 0.84[17] | 0.19[17] |
| | | | 0.78[16] | 0.22[16] |
| 29.5 | | 0.04202 | 0.83[17] | 0.20[17] |
| | | | 0.77[16] | 0.23[16] |
| 29 | | 0.04275 | 0.81[17] | 0.22[17] |
| | | | 0.76[16] | 0.26[16] |
| 28.5 | | 0.04350 | 0.82[17] | 0.29[17] |
| | | | 0.76[16] | 0.31[16] |
| 28 | | 0.04428 | 0.88[17] | 0.32[17] |
| | | | 0.79[16] | 0.33[16] |
| 27.5 | | 0.04508 | 0.92[17] | 0.29[17] |
| | | | 0.84[16] | 0.31[16] |
| 27 | | 0.04592 | 0.91[17] | 0.26[17] |
| | | | 0.84[16] | 0.30[16] |

**TABLE I (*Continued*)**

**Potassium Bromide**

| eV | $cm^{-1}$ | μm | n | k |
|---|---|---|---|---|
| 26.5 | | 0.04678 | 0.89[17] | 0.27[17] |
| | | | 0.83[16] | 0.31[16] |
| 26 | | 0.04769 | 0.89[17] | 0.30[17] |
| | | | 0.82[16] | 0.34[16] |
| 25.5 | | 0.04959 | 0.92[17] | 0.33[17] |
| | | | 0.85[16] | 0.34[16] |
| 25 | | 0.04959 | 0.95[17] | 0.33[17] |
| | | | 0.88[16] | 0.35[16] |
| 24.5 | | 0.05060 | 0.90 | 0.35 |
| 24 | | 0.05166 | 0.90 | 0.34 |
| 23.5 | | 0.05275 | 0.90 | 0.33 |
| 23 | | 0.05391 | 0.89 | 0.33 |
| 22.5 | | 0.05510 | 0.88 | 0.34 |
| 22 | | 0.05636 | 0.87 | 0.35 |
| 21.75 | | 0.05700 | 0.86 | 0.38 |
| 21.5 | | 0.05766 | 0.85 | 0.40 |
| 21.25 | | 0.05834 | 0.85 | 0.52 |
| 21 | | 0.05904 | 0.98 | 0.47 |
| 20.75 | | 0.05975 | 0.98 | 0.41 |
| 20.5 | | 0.06048 | 0.97 | 0.34 |
| 20.4 | | 0.06077 | 1.01[15] | 0.31[15] |
| 20.25 | | 0.06122 | 0.95[16] | 0.34[16] |
| 20.2 | | 0.06137 | 0.96[15] | 0.34[15] |
| 20.1 | | 0.06168 | 0.92 | 0.36 |
| 20 | | 0.06199 | 0.91[16] | 0.38[16] |
| | | | 0.94[15] | 0.42[15] |
| 19.95 | | 0.06214 | 0.97 | 0.46 |
| 19.9 | | 0.06230 | 1.01 | 0.49 |
| 19.85 | | 0.06246 | 1.02 | 0.48 |
| 19.8 | | 0.06261 | 1.04 | 0.46 |
| 19.75 | | 0.06277 | 1.07 | 0.46 |
| 19.7 | | 0.06293 | 1.09 | 0.44 |
| 19.6 | | 0.06325 | 1.12 | 0.39 |
| 19.5 | | 0.06358 | 1.10 | 0.34 |
| 19.4 | | 0.06390 | 1.07 | 0.32 |
| 19.2 | | 0.06457 | 1.03 | 0.32 |
| 19.0 | | 0.06525 | 1.00 | 0.33 |
| 18.8 | | 0.06594 | 0.98 | 0.36 |
| 18.6 | | 0.06665 | 0.98 | 0.37 |
| 18.4 | | 0.06737 | 0.99 | 0.41 |
| 18.2 | | 0.06811 | 1.03 | 0.43 |
| 18.0 | | 0.06888 | 1.05 | 0.43 |
| 17.8 | | 0.06965 | 1.07 | 0.42 |
| 17.6 | | 0.07044 | 1.09 | 0.41 |
| 17.4 | | 0.07125 | 1.10 | 0.39 |
| 17.2 | | 0.07208 | 1.10 | 0.37 |
| 17.0 | | 0.07293 | 1.10 | 0.36 |
| 16.8 | | 0.07380 | 1.09 | 0.32 |

**TABLE I (*Continued*)**

**Potassium Bromide**

| eV | $cm^{-1}$ | μm | n | k |
|---|---|---|---|---|
| 16.6 | | 0.07380 | 1.09 | 0.32 |
| 16.4 | | 0.07560 | 1.09 | 0.32 |
| 16.2 | | 0.07653 | 1.05 | 0.32 |
| 16.0 | | 0.07749 | 1.03 | 0.36 |
| 15.8 | | 0.07847 | 1.07 | 0.35 |
| 15.6 | | 0.07947 | 1.07 | 0.34 |
| 15.4 | | 0.08050 | 1.07 | 0.33 |
| 15.2 | | 0.08156 | 1.06 | 0.30 |
| 15.0 | | 0.08265 | 1.04 | 0.29 |
| 14.8 | | 0.08377 | 1.01 | 0.28 |
| 14.6 | | 0.08492 | 0.98 | 0.27 |
| 14.4 | | 0.08610 | 0.95 | 0.27 |
| 14.2 | | 0.08731 | 0.90 | 0.29 |
| 14.0 | | 0.08856 | 0.86 | 0.33 |
| 13.8 | | 0.08984 | 0.84 | 0.37 |
| 13.6 | | 0.09116 | 0.82 | 0.40 |
| 13.4 | | 0.09253 | 0.79 | 0.45 |
| 13.2 | | 0.09393 | | 0.50[15] |
| 13.05 | | 0.09500 | 1.133[14] | 0.645[14] |
| 13.0 | | 0.09537 | | 0.61[15] |
| 12.83 | | 0.09666 | 1.107 | 0.656[14] |
| 12.60 | | 0.09840 | 1.086 | 0.758 |
| 12.37 | | 0.1002 | 1.113 | 0.854 |
| 12.20 | | 0.1016 | 1.132 | 0.938 |
| 11.99 | | 0.1034 | 1.207 | 1.058 |
| 11.84 | | 0.1047 | 1.341 | 1.166 |
| 11.64 | | 0.1065 | 1.621 | 1.192 |
| 11.43 | | 0.1085 | 1.851 | 0.986 |
| 11.23 | | 0.1104 | 1.859 | 0.838 |
| 11.00 | | 0.1128 | 1.838 | 0.655 |
| 10.94 | | 0.1133 | 1.824 | 0.634 |
| 10.82 | | 0.1146 | 1.824 | 0.571 |
| 10.69 | | 0.1160 | 1.760 | 0.532 |
| 10.63 | | 0.1166 | 1.752 | 0.520 |
| 10.52 | | 0.1178 | 1.719 | 0.494 |
| 10.42 | | 0.1189 | 1.704 | 0.501 |
| 10.33 | | 0.1200 | 1.687 | 0.504 |
| 10.20 | | 0.1216 | 1.684 | 0.458 |
| 10.13 | | 0.1223 | 1.635 | 0.473 |
| 9.890 | | 0.1254 | 1.670 | 0.424 |
| 9.807 | | 0.1264 | 1.606 | 0.413 |
| 9.712 | | 0.1277 | 1.588 | 0.433 |
| 9.611 | | 0.1290 | 1.569 | 0.432 |
| 9.520 | | 0.1302 | 1.539 | 0.414 |
| 9.356 | | 0.1325 | 1.488 | 0.434 |
| 9.294 | | 0.1334 | 1.452 | 0.413 |
| 9.203 | | 0.1347 | 1.369 | 0.449 |
| 9.093 | | 0.1363 | 1.303 | 0.553 |

TABLE I (*Continued*)

**Potassium Bromide**

| eV | $cm^{-1}$ | μm | n | k |
|---|---|---|---|---|
| 9.002 | | 0.1377 | 1.282 | 0.698 |
| 8.894 | | 0.1394 | 1.335 | 0.797 |
| 8.801 | | 0.1409 | 1.341 | 0.879 |
| 8.712 | | 0.1423 | 1.390 | 1.073 |
| 8.604 | | 0.1441 | 1.702 | 1.267 |
| 8.504 | | 0.1458 | 2.042 | 1.125 |
| 8.409 | | 0.1474 | 2.150 | 0.929 |
| 8.291 | | 0.1495 | 2.153 | 0.774 |
| 8.203 | | 0.1511 | 2.195 | 0.650 |
| 8.091 | | 0.1532 | 2.192 | 0.551 |
| 8.011 | | 0.1548 | 2.158 | 0.437 |
| 7.899 | | 0.1570 | 2.056 | 0.330 |
| 7.840 | | 0.1581 | 1.990 | 0.297 |
| 7.790 | | 0.1592 | 1.950 | 0.333 |
| 7.752 | | 0.1599 | 1.953 | 0.334 |
| 7.710 | | 0.1608 | 1.910 | 0.348 |
| 7.648 | | 0.1621 | 1.946 | 0.312 |
| 7.613 | | 0.1629 | 1.875 | 0.278 |
| 7.557 | | 0.1640 | 1.808 | 0.303 |
| 7.506 | | 0.1652 | 1.802 | 0.307 |
| 7.446 | | 0.1665 | 1.713 | 0.347 |
| 7.402 | | 0.1675 | 1.649 | 0.397 |
| 7.358 | | 0.1685 | 1.613 | 0.480 |
| 7.293 | | 0.1700 | 1.593 | 0.662 |
| 7.250 | | 0.1710 | 1.650 | 0.809 |
| 7.208 | | 0.1720 | 1.799 | 0.925 |
| 7.146 | | 0.1735 | 2.142 | 0.983 |
| 7.105 | | 0.1745 | 2.349 | 0.826 |
| 7.044 | | 0.1760 | 2.433 | 0.486 |
| 7.004 | | 0.1770 | 2.348 | 0.322 |
| 6.945 | | 0.1785 | 2.174 | 0.179 |
| 6.907 | | 0.1795 | 2.029 | 0.172 |
| 6.850 | | 0.1810 | 1.863 | 0.229 |
| 6.793 | 54,790 | 0.1825 | 1.732 | 0.345 |
| 6.756 | 54,500 | 0.1835 | 1.669 | 0.473 |
| 6.701 | 54,050 | 0.1850 | 1.679 | 0.774 |
| 6.7 | 54,080 | 0.1850 | | 0.780[13] |
| 6.65 | 53,680 | 0.1864 | | 0.564 |
| 6.648 | 53,620 | 0.1865 | 1.876 | 1.070[14] |
| 6.6 | 53,280 | 0.1879 | | 1.26[13] |
| 6.595 | 53,190 | 0.1880 | 2.348 | 1.279[14] |
| 6.55 | 52,870 | 0.1893 | | 0.678[13] |
| 6.542 | 52,770 | 0.1895 | 2.977 | 0.846[14] |
| 6.508 | 52,490 | 0.1905 | 2.957 | 0.444 |
| 6.5 | 52,470 | 0.1907 | | 0.334[13] |
| 6.457 | 52,080 | 0.1920 | 2.761 | 0.131[14] |
| 6.45 | 52,020 | 0.1922 | | $6.12 \times 10^{-2}$[13] |
| 6.407 | 51,680 | 0.1935 | 2.549 | $2.31 \times 10^{-2}$[14] |

**TABLE I (*Continued*)**

**Potassium Bromide**

| eV | $cm^{-1}$ | μm | n | k |
|---|---|---|---|---|
| 6.4 | 51,620 | 0.1937 | | $1.70 \times 10^{-2}$ [13] |
| 6.35 | 51,220 | 0.1953 | | $3.89 \times 10^{-3}$ |
| 6.3 | 50,810 | 0.1968 | | $9.71 \times 10^{-4}$ |
| 6.25 | 50,410 | 0.1984 | | $2.53 \times 10^{-4}$ |
| 6.2 | 50,010 | 0.2000 | | $6.37 \times 10^{-5}$ |
| 6.199 | 50,000 | 0.20 | 2.09953[11] | |
| 6.15 | 49,600 | 0.2016 | | $3.05 \times 10^{-5}$ [13] |
| 6.1 | 49,200 | 0.2033 | | $1.62 \times 10^{-5}$ |
| 6.05 | 48,800 | 0.2049 | | $9.78 \times 10^{-6}$ |
| 6.0 | 48,390 | 0.2066 | | $5.75 \times 10^{-6}$ |
| 5.95 | 47,990 | 0.2048 | | $4.24 \times 10^{-6}$ |
| 5.904 | 47,620 | 0.21 | 1.93440[11] | |
| 5.9 | 47,590 | 0.2101 | | $3.68 \times 10^{-6}$ [13] |
| 5.636 | 45,450 | 0.22 | 1.85023[11] | |
| 5.391 | 43,480 | 0.23 | 1.79622 | |
| 5.166 | 41,670 | 0.24 | 1.75773 | |
| 4.959 | 40,000 | 0.25 | 1.72863 | |
| 4.769 | 38,460 | 0.26 | 1.70575 | |
| 4.592 | 37,040 | 0.27 | 1.68725 | |
| 4.428 | 35,710 | 0.28 | 1.67197 | |
| 4.275 | 34,480 | 0.29 | 1.65915 | |
| 4.133 | 33,330 | 0.30 | 1.64825 | |
| 3.999 | 32,260 | 0.31 | 1.63886 | |
| 3.874 | 31,250 | 0.32 | 1.63071 | |
| 3.757 | 30,300 | 0.33 | 1.62357 | |
| 3.647 | 29,410 | 0.34 | 1.61727 | |
| 3.542 | 28,570 | 0.35 | 1.61167 | |
| 3.444 | 27,780 | 0.36 | 1.60668 | |
| 3.351 | 27,030 | 0.37 | 1.60220 | |
| 3.263 | 26,320 | 0.38 | 1.59816 | |
| 3.179 | 25,640 | 0.39 | 1.59450 | |
| 3.100 | 25,000 | 0.40 | 1.59117 | |
| 2.952 | 23,810 | 0.42 | 1.58537 | |
| 2.818 | 22,730 | 0.44 | 1.58048 | |
| 2.695 | 21,740 | 0.46 | 1.57632 | |
| 2.583 | 20,830 | 0.48 | 1.57274 | |
| 2.480 | 20,000 | 0.50 | 1.56964 | |
| 2.384 | 19,230 | 0.52 | 1.56694 | |
| 2.296 | 18,520 | 0.54 | 1.56456 | |
| 2.214 | 17,860 | 0.56 | 1.56247 | |
| 2.138 | 17,240 | 0.58 | 1.56060 | |
| 2.066 | 16,670 | 0.60 | 1.55894 | |
| 2.000 | 16,130 | 0.62 | 1.55744 | |
| 1.937 | 15,630 | 0.64 | 1.55610 | |
| 1.879 | 15,150 | 0.66 | 1.55488 | |
| 1.823 | 14,710 | 0.68 | 1.55378 | |
| 1.771 | 14,290 | 0.70 | 1.55278 | |
| 1.722 | 13,890 | 0.72 | 1.55186 | |

TABLE I (*Continued*)

**Potassium Bromide**

| eV | $cm^{-1}$ | μm | n | k |
|---|---|---|---|---|
| 1.675 | 13,510 | 0.74 | 1.55102 | |
| 1.631 | 13,160 | 0.76 | 1.55025 | |
| 1.590 | 12,820 | 0.78 | 1.54954 | |
| 1.550 | 12,500 | 0.80 | 1.54888 | |
| 1.512 | 12,200 | 0.82 | 1.54828 | |
| 1.476 | 11,900 | 0.84 | 1.54772 | |
| 1.442 | 11,630 | 0.86 | 1.54720 | |
| 1.409 | 11,360 | 0.88 | 1.54671 | |
| 1.378 | 11,110 | 0.90 | 1.54626 | |
| 1.348 | 10,870 | 0.92 | 1.54584 | |
| 1.319 | 10,640 | 0.94 | 1.54544 | |
| 1.291 | 10,420 | 0.96 | 1.54507 | |
| 1.265 | 10,200 | 0.98 | 1.54472 | |
| 1.240 | 10,000 | 1.00 | 1.54440 | |
| 1.033 | 8,333 | 1.2 | 1.54198 | |
| 0.8856 | 7,143 | 1.4 | 1.54052 | |
| 0.7749 | 6,250 | 1.6 | 1.53955 | |
| 0.6888 | 5,556 | 1.8 | 1.53901 | |
| 0.6199 | 5,000 | 2.0 | 1.53833 | |
| 0.5636 | 4,545 | 2.2 | 1.53792 | |
| 0.5166 | 4,167 | 2.4 | 1.53758 | |
| 0.4769 | 3,046 | 2.6 | 1.53728 | |
| 0.4428 | 3,571 | 2.8 | 1.53702 | |
| 0.4133 | 3,333 | 3.0 | 1.53677 | |
| 0.3874 | 3,125 | 3.2 | 1.53655 | |
| 0.3647 | 2,941 | 3.4 | 1.53633 | |
| 0.3444 | 2,778 | 3.6 | 1.53611 | |
| 0.3263 | 2,632 | 3.8 | 1.53590 | |
| 0.3100 | 2,500 | 4.0 | 1.53569 | |
| 0.2952 | 2,381 | 4.2 | 1.53547 | |
| 0.2818 | 2,273 | 4.4 | 1.53526 | |
| 0.2695 | 2,174 | 4.6 | 1.53504 | |
| 0.2583 | 2,083 | 4.8 | 1.53482 | |
| 0.2480 | 2,000 | 5.0 | 1.53459 | |
| 0.2384 | 1,923 | 5.2 | 1.53435 | |
| 0.2296 | 1,852 | 5.4 | 1.53411 | |
| 0.2214 | 1,786 | 5.6 | 1.53386 | |
| 0.2138 | 1,724 | 5.8 | 1.53361 | |
| 0.2066 | 1,667 | 6.0 | 1.53335 | |
| 0.2000 | 1,613 | 6.2 | 1.53308 | |
| 0.1937 | 1,563 | 6.4 | 1.53281 | |
| 0.1879 | 1,515 | 6.6 | 1.53253 | |
| 0.1823 | 1,471 | 6.8 | 1.53224 | |
| 0.1771 | 1,429 | 7.0 | 1.53194 | |
| 0.1722 | 1,389 | 7.2 | 1.53163 | |
| 0.1675 | 1,351 | 7.4 | 1.53132 | |
| 0.1631 | 1,316 | 7.6 | 1.53100 | |
| 0.1590 | 1,282 | 7.8 | 1.53067 | |

**TABLE I (*Continued*)**

**Potassium Bromide**

| eV | $cm^{-1}$ | μm | n | k |
|---|---|---|---|---|
| 0.1550 | 1,250 | 8.0 | 1.53033 | |
| 0.1512 | 1,220 | 8.2 | 1.52998 | |
| 0.1476 | 1,190 | 8.4 | 1.52962 | |
| 0.1441 | 1,163 | 8.6 | 1.52926 | |
| 0.1409 | 1,136 | 8.8 | 1.52889 | |
| 0.1378 | 1,111 | 9.0 | 1.52851 | |
| 0.1348 | 1,087 | 9.2 | 1.52812 | |
| 0.1319 | 1,064 | 9.4 | 1.52772 | |
| 0.1300 | 1,049 | 9.536 | | $2.5 \times 10^{-9}$ [9] |
| 0.1291 | 1,042 | 9.6 | 1.52731 | |
| 0.1284 | 1,035 | 9.657 | | $2.0 \times 10^{-9}$ |
| 0.1265 | 1,020 | 9.8 | 1.52689 | |
| 0.1240 | 1,000 | 10.0 | 1.52647 | |
| 0.1221 | 984.4 | 10.159 | | $1.8 \times 10^{-9}$ |
| 0.1216 | 980.4 | 10.2 | 1.52603 | |
| 0.1203 | 970.5 | 10.303 | | $1.2 \times 10^{-9}$ |
| 0.1192 | 961.5 | 10.4 | 1.52559 | |
| 0.1179 | 951.2 | 10.513 | | $2.3 \times 10^{-9}$ |
| 0.1171 | 944.2 | 10.591 | | $1.0 \times 10^{-9}$ |
| 0.1170 | 943.4 | 10.6 | 1.52514 | |
| 0.1148 | 925.9 | 10.8 | 1.52467 | |
| 0.1127 | 909.1 | 11.0 | 1.52420 | |
| 0.1107 | 892.9 | 11.2 | 1.52372 | |
| 0.1088 | 877.2 | 11.4 | 1.52323 | |
| 0.1069 | 862.1 | 11.6 | 1.52273 | |
| 0.1051 | 847.5 | 11.8 | 1.52222 | |
| 0.1033 | 833.3 | 12.0 | 1.52171 | |
| 0.1016 | 819.7 | 12.2 | 1.52118 | |
| 0.09999 | 806.5 | 12.4 | 1.52064 | |
| 0.09840 | 793.7 | 12.6 | 1.52009 | |
| 0.09686 | 781.3 | 12.8 | 1.51954 | |
| 0.09537 | 769.2 | 13.0 | 1.51897 | |
| 0.09393 | 757.6 | 13.2 | 1.51840 | |
| 0.09252 | 746.3 | 13.4 | 1.51781 | |
| 0.09116 | 735.3 | 13.6 | 1.51721 | |
| 0.08984 | 724.6 | 13.8 | 1.51661 | |
| 0.08856 | 714.3 | 14.0 | 1.51599 | |
| 0.08731 | 704.2 | 14.2 | 1.51536 | |
| 0.08610 | 694.4 | 14.4 | 1.51473 | |
| 0.08492 | 684.9 | 14.6 | 1.51408 | |
| 0.08377 | 675.7 | 14.8 | 1.51342 | |
| 0.08265 | 666.7 | 15.0 | 1.51275 | |
| 0.08157 | 657.9 | 15.2 | 1.51208 | |
| 0.08059 | 650 | 15.38 | | $5.5 \times 10^{-8}$ [7] |
| 0.08051 | 649.4 | 15.4 | 1.51139 | |
| 0.07948 | 641.0 | 15.6 | 1.51069 | |
| 0.07847 | 632.9 | 15.8 | 1.50998 | |
| 0.07749 | 625.0 | 16.0 | 1.50926 | |

**TABLE I (*Continued*)**

**Potassium Bromide**

| eV | $cm^{-1}$ | μm | n | k |
|---|---|---|---|---|
| 0.07653 | 617.3 | 16.2 | 1.50852 | |
| 0.07560 | 609.8 | 16.4 | 1.50778 | |
| 0.07469 | 602.4 | 16.6 | 1.50703 | |
| 0.07439 | 600 | 16.67 | | $2.1 \times 10^{-7}$ |
| 0.07380 | 595.2 | 16.8 | 1.50626 | |
| 0.07293 | 588.2 | 17.0 | 1.50548 | |
| 0.07208 | 581.4 | 17.2 | 1.50470 | |
| 0.07125 | 574.7 | 17.4 | 1.50390 | |
| 0.07044 | 568.2 | 17.6 | 1.50309 | |
| 0.06965 | 561.8 | 17.8 | 1.50227 | |
| 0.06888 | 555.6 | 18.0 | 1.50143 | |
| 0.06819 | 550 | 18.18 | | $7.8 \times 10^{-7}$ |
| 0.06812 | 549.4 | 18.2 | 1.50059 | |
| 0.06738 | 543.5 | 18.4 | 1.49973 | |
| 0.06666 | 537.6 | 18.6 | 1.49886 | |
| 0.06595 | 531.9 | 18.8 | 1.49798 | |
| 0.06525 | 526.3 | 19.0 | 1.49709 | |
| 0.06457 | 520.8 | 19.2 | 1.49618 | |
| 0.06391 | 515.5 | 19.4 | 1.49526 | |
| 0.06326 | 510.2 | 19.6 | 1.49433 | |
| 0.06262 | 505.1 | 19.8 | 1.49339 | |
| 0.06199 | 500.0 | 20.0 | 1.49243 | |
| | | | | $3.0 \times 10^{-6}$ |
| 0.06048 | 487.8 | 20.5 | 1.48999 | |
| 0.05904 | 476.2 | 21.0 | 1.48746 | |
| 0.05767 | 465.1 | 21.5 | 1.48485 | |
| 0.05636 | 454.5 | 22.0 | 1.48215 | |
| 0.05579 | 450 | 22.22 | | $1.2 \times 10^{-5}$ |
| 0.05510 | 444.4 | 22.5 | 1.47937 | |
| 0.05391 | 434.8 | 23.0 | 1.47650 | |
| 0.05276 | 425.5 | 23.5 | 1.47353 | |
| 0.05166 | 416.7 | 24.0 | 1.47047 | |
| 0.05060 | 408.2 | 24.5 | 1.46732 | |
| 0.04959 | 400.0 | 25.0 | 1.46406 | |
| | | | | $4.8 \times 10^{-5}$ |
| 0.04862 | 392.2 | 25.5 | 1.46070 | |
| 0.04769 | 384.6 | 26.0 | 1.45723 | |
| 0.04679 | 377.4 | 26.5 | 1.45366 | |
| 0.04592 | 370.4 | 27.0 | 1.44998 | |
| 0.04508 | 363.6 | 27.5 | 1.44618 | |
| 0.04428 | 357.1 | 28.0 | 1.44226 | |
| 0.04350 | 350.9 | 28.5 | 1.43821 | |
| 0.04339 | 350 | 28.57 | | $2.0 \times 10^{-4}$ |
| 0.04275 | 344.8 | 29.0 | 1.43404 | |
| 0.04203 | 339.0 | 29.5 | 1.42974 | |
| 0.04133 | 333.3 | 30.0 | 1.42531 | |
| 0.04065 | 327.9 | 30.5 | 1.42073 | |
| 0.03999 | 322.6 | 31.0 | 1.41601 | |

**TABLE I (*Continued*)**

**Potassium Bromide**

| eV | $cm^{-1}$ | μm | n | k |
|---|---|---|---|---|
| 0.03936 | 317.5 | 31.5 | 1.41114 | |
| 0.03874 | 312.5 | 32.0 | 1.40611 | |
| 0.03815 | 307.7 | 32.5 | 1.40091 | |
| 0.03757 | 303.0 | 33.0 | 1.39555 | |
| 0.03720 | 300 | 33.33 | | $8.5 \times 10^{-4}$ |
| 0.03701 | 298.5 | 33.5 | 1.39001 | |
| 0.03647 | 294.1 | 34.0 | 1.38429 | |
| 0.03594 | 289.9 | 34.5 | 1.37838 | |
| 0.03542 | 285.7 | 35.0 | 1.37227 | |
| 0.03493 | 281.7 | 35.5 | 1.36595 | |
| 0.03444 | 277.8 | 36.0 | 1.35941 | |
| 0.03397 | 274.0 | 36.5 | 1.35264 | |
| 0.03351 | 270.3 | 37.0 | 1.34563 | |
| 0.03306 | 266.7 | 37.5 | 1.33837 | |
| 0.03263 | 263.2 | 38.0 | 1.33084 | |
| 0.03220 | 259.7 | 38.5 | 1.32304 | |
| 0.03179 | 256.4 | 39.0 | 1.31494 | |
| 0.03139 | 253.2 | 39.5 | 1.30653 | |
| 0.03100 | 250.0 | 40.0 | 1.29779 | |
| | | | 1.35[6] | $3.2 \times 10^{-3}$ |
| 0.03061 | 246.9 | 40.5 | 1.28870[11] | |
| 0.03024 | 243.9 | 41.0 | 1.27924 | |
| 0.02988 | 241.0 | 41.5 | 1.26939 | |
| 0.02976 | 240 | 41.67 | 1.33[6] | |
| 0.02952 | 238.1 | 42.0 | 1.25911[11] | |
| 0.02852 | 230 | 43.48 | 1.30[6] | |
| 0.02728 | 220 | 45.45 | 1.20 | $1.7 \times 10^{-2}$[6] |
| 0.02604 | 210 | 47.62 | 1.10 | $2.9 \times 10^{-2}$ |
| 0.02480 | 200 | 50.00 | 1.00 | $6.0 \times 10^{-2}$ |
| 0.02418 | 195 | 51.28 | 0.93 | 0.11 |
| 0.02356 | 190 | 52.63 | 0.90 | 0.18 |
| 0.02294 | 185 | 54.05 | 0.89 | 0.20 |
| 0.02232 | 180 | 55.55 | 0.83 | 0.22 |
| 0.02170 | 175 | 57.14 | 0.76 | 0.39 |
| 0.02108 | 170 | 58.82 | 0.76 | 0.44 |
| 0.02046 | 165 | 60.61 | 0.80 | 0.44 |
| 0.01984 | 160 | 62.50 | 0.76 | 0.47 |
| 0.01922 | 155 | 64.52 | 0.60 | 0.58 |
| 0.01860 | 150 | 66.67 | 0.48 | 0.72 |
| 0.01798 | 145 | 68.97 | 0.39 | 0.90 |
| 0.01736 | 140 | 71.43 | 0.32 | 1.2 |
| 0.01674 | 135 | 74.07 | 0.29 | 2.0 |
| 0.01612 | 130 | 76.92 | 0.30 | 2.0 |
| 0.01550 | 125 | 80.00 | 0.33 | 2.9 |
| 0.01488 | 120 | 83.33 | 0.65 | 4.3 |
| 0.01426 | 115 | 86.96 | 3.00 | 5.3 |
| 0.01364 | 110 | 90.91 | 5.50 | 1.0 |
| 0.01302 | 105 | 95.24 | 3.90 | 0.54 |
| 0.01116 | 100 | 100.0 | 3.40 | 0.33 |

TABLE I (*Continued*)

**Potassium Bromide**

| eV | $cm^{-1}$ | μm | n | k |
|---|---|---|---|---|
| 0.01177 | 95 | 105.3 | 3.10 | 0.20 |
| 0.01116 | 90 | 111.1 | 2.80 | 0.15 |
| 0.01054 | 85 | 117.6 | 2.60 | 0.13 |
| 0.00991 | 80 | 125.0 | 2.52 | 0.125 |
| 0.00867 | 70 | 142.8 | 2.40 | 0.12 |
| 0.00743 | 60 | 166.7 | 2.35 | 0.11 |
| 0.00619 | 50 | 200.0 | 2.30 | $9.3\times10^{-2}$ |
| | | | | $9.5\times10^{-2}$ [5] |
| 0.00495 | 40 | 250.0 | 2.28 | $6.8\times10^{-2}$ [6] |
| | | | | $6.2\times10^{-2}$ [5] |
| 0.00372 | 30 | 333.3 | 2.24 | $3.7\times10^{-2}$ [6] |
| | | | | $3.4\times10^{-2}$ [5] |
| 0.00248 | 20 | 500.0 | 2.20 | $1.6\times10^{-2}$ [6] |
| | | | | $1.2\times10^{-2}$ [5] |
| 0.001240 | 10 | 1000 | | $4.2\times10^{-3}$ |
| 0.001116 | 9.0 | 1111 | | $3.7\times10^{-3}$ |
| 0.000991 | 8.0 | 1250 | | $3.1\times10^{-3}$ |
| 0.000867 | 7.0 | 1429 | | $2.6\times10^{-3}$ |
| 0.000743 | 6.0 | 1667 | | $2.3\times10^{-3}$ |
| 0.000619 | 5.0 | 2000 | | $1.8\times10^{-3}$ |
| 0.000495 | 4.0 | 2500 | | $1.4\times10^{-3}$ |
| 0.000479 | 3.87 | 2584 | 2.21[2] | $1.18\times10^{-3}$ [2] |
| 0.000372 | 3.0 | 3333 | | $1.1\times10^{-3}$ [5] |
| 0.000248 | 2.0 | 5000 | | $6.8\times10^{-4}$ |
| 0.000207 | 1.67 | 6000 | 2.19 | $2.40\times10^{-4}$ [2] |
| 0.0001463 | 1.18 | 8500 | 2.21 | $4.99\times10^{-4}$ |
| 0.0001240 | 1.0 | 10000 | | $3.4\times10^{-4}$ [5] |
| 0.0001116 | 0.9 | 11110 | | $3.1\times10^{-4}$ |
| 0.00009919 | 0.8 | 12500 | | $2.8\times10^{-4}$ |
| | | | 2.20 | $1.43\times10^{-4}$ [2] |
| 0.00008679 | 0.7 | 14290 | | $2.4\times10^{-4}$ [5] |
| 0.00007439 | 0.6 | 16670 | | $2.3\times10^{-4}$ |
| 0.00006199 | 0.5 | 20000 | | $1.8\times10^{-4}$ |
| 0.00004141 | 0.334 | 30000 | 2.21 | $2.54\times10^{-4}$ [2] |
| 0.00003682 | 0.297 | 33200 | 2.22 | $2.61\times10^{-4}$ |

[a] References are indicated in brackets.

# Potassium Dihydrogen Phosphate ($KH_2PO_4$, KDP) and Three of Its Isomorphs

DAVID F. EDWARDS and RICHARD H. WHITE
University of California
Lawrence Livermore National Laboratory
Livermore, California

Potassium dihydrogen phosphate (KDP) is perhaps the best known, most extensively studied, and most widely used crystal in laser technology. Crystals of KDP are used for frequency-upconversion operation in high-power laser systems. At the present time the NOVA laser at Lawrence Livermore National Laboratory uses KDP crystals for upconversion from the fundamental wavelength, 1.053 μm, to the second, third, and fourth harmonics, 0.527 μm, 0.351 μm, and 0.263 μm, respectively. KDP is also the primary nonlinear optical material being used at the major laser facilities in France, Great Britain, Japan, China, and the Soviet Union. Ammonium dihydrogen phosphate (ADP) and the deuterated crystals (labeled D*) AD*P and KD*P have also found use in state-of-the-art nonlinear optical devices.

For each application of these nonlinear crystals, a precise knowledge is required of the crystal's refractive index as a function of wavelength. In addition, crystal temperature has a sensitive effect on the indices within the precision range of interest. The first precise measurement of the indices of refraction of KDP and ADP for a broad wavelength range was that of Zernike [1]. He measured the indices at 25 wavelengths between 2138 Å and 1.529 μm and at 24.8°±0.2 °C. He reports his indices to be accurate to at least $\pm 3 \times 10^{-5}$. Zernike used the method of known incidence used by Rydberg [2] and Tilton *et al.* [3]. For this method a prism of the material to be measured is inserted into a Littrow-type mount monochromator. The deviation is measured for different wavelengths by measuring the angle over which the Littrow mirror had to be rotated to pass a particular wavelength to the exit slit. More recently, Kirby and DeShazer [4] reported the index measurements for KDP, KD*P, ADP, AD*P and


Copyright © 1991 by Academic Press.
All rights of reproduction in any form reserved.
ISBN 0-12-544422-2

several other nonlinear crystals isomorphic to KDP. Their measurements were at 16 wavelengths from 4046 Å to 1.06 μm and a sample temperature of 33.0°±0.4 °C. This slightly elevated temperature was used to remove any absorbed water vapor on the crystal faces owing to the hygroscopic nature of these crystals. The method of minimum deviation [5] was used to measure the indices. For the deuterated crystals the index values depend on the deuterium concentration. The KD*P and AD*P crystals of Kirby and DeShazer had 96% deuterium replacement for hydrogen. Phillips [6] and Yamazaki and Ogawa [7] report indices for partially deuterated (about 90%) KD*P.

Kirby and DeShazer show that the index values vary from about $6\times10^{-5}$ to $60\times10^{-5}$ in the visible region for KDP crystals from different crystal growers. They correlated these differences with deviations in the crystal-lattice parameters and speculate that crystalline defects incorporated during the crystal-growth process are the cause of the lattice-parameter variations.

The measured values of Zernike [1] and Kirby and DeShazer [4] were fit separately to both a Herzberger-type and a modified Sellmeier-type dispersion formula. These two measurements ([1] and [4]) were made at slightly different temperatures. The importance of the index sensitivity to temperature is the reason for reporting both fits. Given in Tables I–IV and plotted in Figs. 1–4 are the calculated indices of refraction for KDP, ADP, KD*P, and AD*P, respectively. The reported indices of other authors were not used in these fits for several reasons, including poorly defined sample temperatures, lack of precision, or untabulated data that could not be accurately read from their curves [6–9].

The Herzberger-type dispersion formula is [10]

$$n = A + BL + CL^2 + D\lambda^2 + E\lambda^4,$$

where $L = 1/(\lambda^2 - 2.80\times10^6)$ with $\lambda$ in angstroms. As explained by Herzberger, the $2.80\times10^6$ is the square of the mean asymptote for the short-wavelength abrupt increase in the index for 15 materials (KDP, KD*P, ADP, and AD*P not included). The coefficients, evaluated by least squares, are given in Table V. Zernike did not measure deuterated samples so no coefficients are listed for KD*P or AD*P at 24.8 °C. The RMS errors between the measured values and the dispersion-formula calculated indices are given in the fourth column. These errors (%) range from about $2\times10^{-5}$ to $4\times10^{-4}$.

The data of Zernike and of Kirby and DeShazer were also independently fit to a modified Sellmeier-type dispersion formula for the convenience of the reader. These Sellmeier values are not tabulated here. The modified Sellmeier-type formula used here is not the same as introduced by Zernike

[1] and used by Kirby and DeShazer [4]. Our dispersion formula is

$$n^2 = 1 + A/(\lambda^2 - B) + C\lambda^2/(\lambda^2 - D),$$

where the wavelength $\lambda$ is in angstroms. This form is preferred to that of Zernike because of the rate and uniqueness of convergence of the regressive fit. The Zernike modified formula will converge to a local minimum depending on the initial guesses for the coefficients, and does not result in a unique coefficient set. This nonuniqueness of the Zernike modified formula can also be demonstrated by straightforward algebra. Zernike's modified formula is of the form

$$n^2 = A + B/(\lambda^2 - C) + D\lambda^2/(\lambda^2 - E).$$

Adding and subtracting $(-B/C + D)$ results in a formula of identical form but with the new coefficients in terms of the original coefficients.

The coefficient sets for our modified Sellmeier-type dispersion formula are given in Table VI. As before, coefficients are given for both 33.0° and 24.8 °C to demonstrate the temperature sensitivity of the indices. No data are given for the deuterated crystals at 24.8 °C because Zernike did not include these crystals in his measurements. The RMS error between the measured indices and the calculated values is given in Column 4, Table V. Overall, the fits for the two temperatures are within a few places in the fourth decimal with the one exception.

A comparison of the Zernike data at 24.8 °C with those of Kirby and DeShazer at 33.0 °C shows that the indices are sensitively dependent on sample temperature. The temperature dependence of the indices for KDP, KD*P, and ADP have been measured by several groups. Phillips [6] measured the indices of KDP, KD*P, and ADP at about nine wavelengths and three or four temperatures between the Curie point and room temperature. He estimates the data accuracy to be $\pm 10^{-4}$. Yamazaki and Ogawa [7] measured the temperature dependence for three wavelengths for these same materials and over the same temperature range as Phillips, and their results are similar. Likewise, similar results are reported by Onaka and Kawamura [8] for KDP, Onaka and Takeda [8] for ADP, and Barnes *et al.* [9] for KDP, KD*P, and ADP. An intercomparison of the predicted indices of Refs. [6–9] with the measured values of Refs. [1, 4] for small temperature intervals shows an internal consistency of $10^{-4}$ or smaller with the data of Onaka and Kawamura [8] having the greatest discrepancy. Phillips [6] has given the following empirical equation for the temperature change of index:

$$\Delta n = (n^2 + an + b)c(298 - T),$$

where $T$ is the temperature in K. The values of the coefficients are given in Table VII.

Davis and Vedam [11] have measured the pressure dependence of the refractive indices at 5893 Å for KDP and ADP under hydrostatic conditions to 7 kbars. Both the ordinary and extraordinary indices were found to vary linearly with pressure for both materials. From their data the slopes of the index change with pressure curves are $+1.55 \times 10^3$/kbar and $+1.31 \times 10^3$/kbar for the KDP ordinary and extraordinary values, respectively. For ADP the values are $1.43 \times 10^3$/kbar and $1.12 \times 10^3$/kbar. They measured no deuterated crystals.

The reststrahlen spectrum of KDP and some of its isomorphs have been studied by several groups with emphasis on the low-frequency vibrational modes, one of which goes soft as the temperature is lowered below room temperature to the Curie temperature [12–22]. The coupling of these modes produces broad reflection peaks, which have been fitted with various models. Many of these references do not give information on all four parameters, $\varepsilon'$ and $\varepsilon''$ for $(\mathbf{E} \perp c)$ and $(\mathbf{E} \| c)$, and the notation varies ($\| c \equiv c$, $\perp c \equiv a$). Often the graphs are too small to read. Raman-scattering studies of the phonon modes also abound [23–27].

In lieu of an extended study of this complicated IR spectral region to sort out the $n$ and $k$ values, we have listed in Table VIII various references with some pertinent information and leave it to the reader to examine the data directly. Much information about KDP and some of its isomorphs is given in Ref. [28].

## REFERENCES


1. F. Zernike, "Refractive Indices of Ammonium Dihydrogen Phosphate and Potassium Dihydrogen Phosphate between 2000 Å and 1.5 μ," *J. Opt. Soc. Am.* **54**, 1215 (1964).
2. F. Rydberg, *Poggendorfs Ann.* **14**, 45 (1828).
3. L. W. Tilton, E. K. Plyler, and R. E. Stephens, *J. Res. Natl. Bur. Std. (U.S.)* **43**, 81 (1949).
4. K. W. Kirby and L. G. DeShazer, "Refractive Indices of 14 Nonlinear Crystals Isomorphic to $KH_2PO_4$," *J. Opt. Soc. Am.* **B4**, 1072 (1987).
5. L. W. Taylor, "College Manual of Optics," Ginn, Boston, (1924).
6. R. A. Phillips, "Temperature Variation of the Index of Refraction of ADP, KDP, and Deuterated KDP," *J. Opt. Soc. Am.* **56**, 629 (1966).
7. M. Yamazaki and T. Ogawa, "Temperature Dependence of the Refractive Indices of $NH_4H_2PO_4$, $KH_2PO_4$ and Partially Deuterated $KH_2PO_4$," *Appl. Opt.* **5**, 1407 (1966).
8. R. Onaka and T. Takeda, "Temperature Dependence of the Refractive Indices of KDP," *J. Phys. Soc. Jap.* **50**, 3695 (1981); R. Onaka and T. Takeda "Temperature Dependence of the Refractive Indices of ADP," *J. Phys. Soc. Jap.* **51**, 3258 (1982).
9. N. P. Barnes, D. J. Gettemy, and R. S. Adhav, "Variation of the Refractive Index with Temperature and the Tuning Rate for KDP Isomorphs," *J. Opt. Soc. Am.* **72**, 895 (1982).
10. M. Herzberger and C. D. Salzberg, "Refractive Indices of Infrared Optical Materials and Color Correction of Infrared Lenses," *J. Opt. Soc. Am.* **52**, 420 (1962); M. Herzberger,

"Color Correction in Optical Systems and a New Dispersion Formula," *Opt. Acta* **6**, 197 (1959).
11. T. A. Davis and K. Vedam, "Pressure Dependence of the Refractive Indices of the Tetragonal Crystals: ADP, KDP, $CaMoO_4$, $CaWO_4$, and Rutile," *J. Opt. Soc. Am.* **58**, 1446 (1968).
12. G. M. Murphy, G. Weiner, and J. J. Oberly, "Infrared Reflection Spectra of Phosphate and Arsenate Crystals," *J. Chem. Phys.* **22**, 1321 (1954).
13. A. S. Barker, Jr., and M. Tinkham, "Far-Infrared Dielectric Measurements on Potassium Dihydrogen Phosphate, Triglycerine Sulfate, and Rutile," *J. Chem. Phys.* **38**, 2257 (1963).
14. F. Sugawara and T. Nakamura, "Far-Infrared Reflectivity Spectra of $KH_2PO_4$ Crystal," *J. Phys. Soc. Jpn.* **28**, 158 (1970).
15. F. Bréhat and A. Hadni, "Transmission du phosphate diacide de potassium dans l'infrarouge lointain dans les phases para et ferroélectriques," *C.R. Acad. Sci. Paris* **271**, B1137 (1970).
16. E. Wiener-Arnear, S. Levin, and I. Pelah, "Proton Dynamics in $KH_2PO_4$ Type Ferroelectrics Studied by Infrared Absorption," *J. Chem. Phys.* **52**, 2881 (1970); "Antiferroelectric Transitions in $NH_4H_2PO_4$ and $NH_4H_2AsO_4$ Studied in Infrared Absorption," *J. Chem. Phys.* **52**, 2891 (1970).
17. T. Kawamura and A. Mitsuishi, "Raman and Far-Infrared Spectra of $KH_2PO_4$ and $NH_4H_2PO_4$," *Technology Reports Osaka University* **23**, 365 (1973); T. Kawamura, A. Mitsuishi, and H. Yoshinaga, Proc. 2nd Inter. Meeting on Ferroelectrics, *J. Phys. Soc. Jpn.* **28** Suppl., 227 (1970).
18. T. Kawamura, A. Mitsuishi, N. Furuya, and O. Shimomura, "Far-Infrared and Raman Spectra of $KD_2PO_4$," *Opt. Commum.* **10**, 337 (1974); T. Kawamura, A. Mitsuishi, N. Furuya, and O. Shimomura, "Optical Properties of $KD_2PO_4$ Crystal in the Low-Wavenumber Region," Technology Reports Osaka University **24**, 429 (1974).
19. F. Onyango, W. Smith, and J. F. Angress, "I. R. Reflection and Transmission Properties of $KH_2PO_4$," *J. Phys. Chem. Solids* **36**, 309 (1975).
20. K. E. Gauss, H. Happ, and G. Rother, "Millimeter Wave and Far-Infrared Investigation on KDP with Asymmetric Interferometers," *Phys. Stat. Solidi (b)* **72**, 623 (1975).
21. D. A. Ledsham, W. G. Chambers, and T. J. Parker, "Dispersive Reflection Spectroscopy in the Far Infrared Using a Polarising Interferometer," *Infrared Physics* **16**, 515 (1976).
22. D. A. Ledsham, W. G. Chambers, and T. J. Parker, "Far Infrared Measurements on $KH_2PO_4$ Using Dispersive Reflection Spectroscopy," *Infrared Physics* **17**, 165 (1977).
23. R. L. Reese, I. J. Fritz, and H. Z. Cummins, "Simultaneous Observation of the Soft Ferroelectric and Acoustic Modes of $KD_2PO_4$, *Solid State Commum.* **9**, 327 (1971).
24. D. K. Agrawal and C. H. Perry, "The Temperature Dependent Raman Spectra of KDP, KD*P, KDA and ADP," Proc. 2nd International Conference on Light Scattering in Solids, (M. Balkanski, ed.), Flammarion, Paris, 429 (1971).
25. H. Hammer, "Raman Spectra of Crystals of the $KH_2PO_4$-Type in Their Paraelectric and Low Temperature Phases," Proc. 2nd International Conference on Light Scattering in Solids," (M. Balkanski, ed.), Flammarion, Paris, 425 (1971).
26. C. Y. She, T. W. Broberg, L. S. Wall, and D. F. Edwards, "Effect of Proton-Photon Coupling on the Ferroelectric Mode in $KH_2PO_4$," *Phys. Rev.* **B6**, 1847 (1972).
27. N. Lagakos and H. Z. Cummins, "Preliminary Observation of a Central Peak in the Light-Scattering Spectrum of $KH_2PO_4$," *Phys. Rev.* **B10**, 1063 (1974).
28. K.-H. Hellwege, ed., "Landolt-Börnstein Numerical Data and Functional Relationships in Science and Technology," Vol. III/16b, Springer-Verlag, Berlin, (1983).

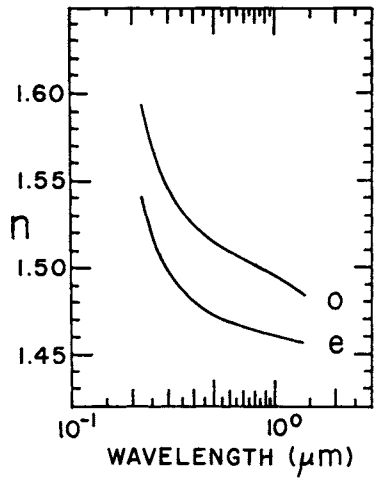


**Fig. 1.** Plot of $n_o$, $n_e$ versus wavelength in micrometers for KDP.

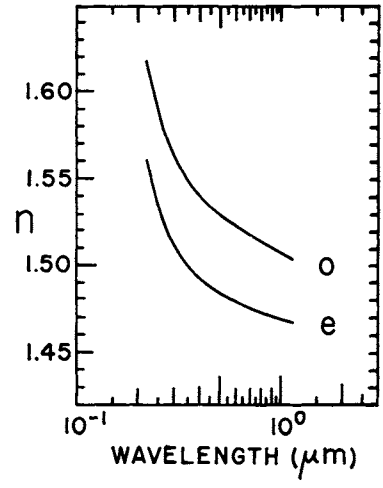


**Fig. 2.** Plot of $n_o$, $n_e$ versus wavelength in micrometers for ADP.

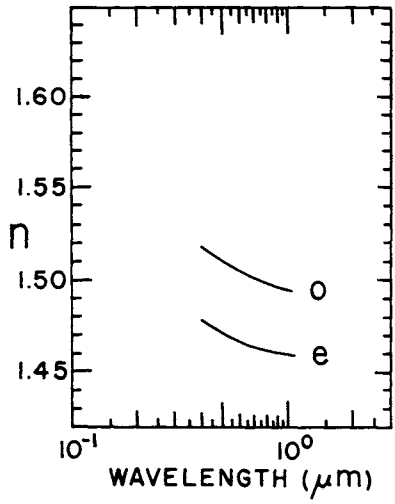


**Fig. 3.** Plot of $n_o$, $n_e$ versus wavelength in micrometers for KD*P.

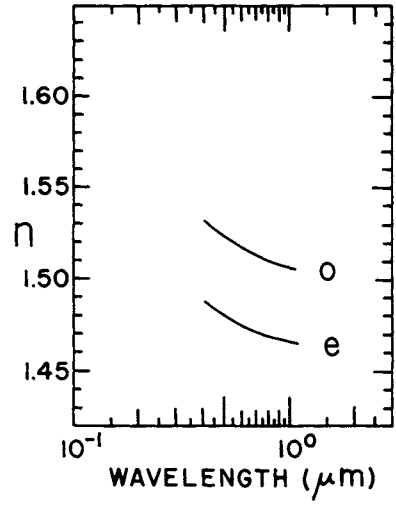


**Fig. 4.** Plot of $n_o$, $n_e$ versus wavelength in micrometers for AD*P.

TABLE I

Values of $n$ for KDP at 24.8°C and 33.0°C[a]

| | | | 24.8 ± 0.2 C | | 33.0 ± 0.4 C | |
|---|---|---|---|---|---|---|
| eV | $cm^{-1}$ | μm | $n_o$ | $n_e$ | $n_o$ | $n_e$ |
| 5.636 | 45,455 | 0.220 | 1.5951[1] | 1.5413[1] | | |
| 5.167 | 41,667 | 0.240 | 1.5767 | 1.5257 | | |
| 4.769 | 38,462 | 0.260 | 1.5626 | 1.5134 | | |
| 4.429 | 35,714 | 0.280 | 1.5523 | 1.5044 | | |
| 4.133 | 33,333 | 0.300 | 1.5444 | 1.4975 | | |
| 3.875 | 31,250 | 0.320 | 1.5385 | 1.4923 | | |
| 3.647 | 29,412 | 0.340 | 1.5337 | 1.4881 | | |
| 3.444 | 27,778 | 0.360 | 1.5299 | 1.4848 | | |
| 3.263 | 26,316 | 0.380 | 1.5267 | 1.4820 | | |
| 3.100 | 25,000 | 0.400 | 1.5240 | 1.4797 | 1.5238[4] | 1.4798[4] |
| 2.952 | 23,810 | 0.420 | 1.5217 | 1.4778 | 1.5214 | 1.4777 |
| 2.818 | 22,727 | 0.440 | 1.5197 | 1.4761 | 1.5192 | 1.4760 |
| 2.696 | 21,739 | 0.460 | 1.5179 | 1.4747 | 1.5174 | 1.4745 |
| 2.583 | 20,833 | 0.480 | 1.5164 | 1.4735 | 1.5157 | 1.4731 |
| 2.480 | 20,000 | 0.500 | 1.5150 | 1.4724 | 1.5142 | 1.4720 |
| 2.385 | 19,231 | 0.520 | 1.5137 | 1.4714 | 1.5129 | 1.4710 |
| 2.296 | 18,519 | 0.540 | 1.5125 | 1.4705 | 1.5117 | 1.4700 |
| 2.214 | 17,857 | 0.560 | 1.5114 | 1.4697 | 1.5106 | 1.4692 |
| 2.138 | 17,241 | 0.580 | 1.5104 | 1.4690 | 1.5096 | 1.4685 |
| 2.067 | 16,667 | 0.600 | 1.5095 | 1.4683 | 1.5086 | 1.4678 |
| 2.000 | 16,129 | 0.620 | 1.5086 | 1.4677 | 1.5077 | 1.4672 |
| 1.938 | 15,625 | 0.640 | 1.5077 | 1.4671 | 1.5069 | 1.4666 |
| 1.879 | 15,152 | 0.660 | 1.5069 | 1.4666 | 1.5061 | 1.4661 |
| 1.824 | 14,706 | 0.680 | 1.5061 | 1.4661 | 1.5053 | 1.4656 |
| 1.771 | 14,286 | 0.700 | 1.5053 | 1.4656 | 1.5046 | 1.4651 |
| 1.722 | 13,889 | 0.720 | 1.5046 | 1.4652 | 1.5039 | 1.4647 |
| 1.676 | 13,514 | 0.740 | 1.5039 | 1.4648 | 1.5032 | 1.4643 |
| 1.632 | 13,158 | 0.760 | 1.5032 | 1.4644 | 1.5026 | 1.4639 |
| 1.590 | 12,821 | 0.780 | 1.5025 | 1.4640 | 1.5020 | 1.4635 |
| 1.550 | 12,500 | 0.800 | 1.5018 | 1.4636 | 1.5013 | 1.4632 |
| 1,512 | 12,195 | 0.820 | 1.5011 | 1.4633 | 1.5007 | 1.4628 |
| 1.476 | 11,905 | 0.840 | 1.5005 | 1.4629 | 1.5001 | 1.4625 |
| 1.442 | 11,628 | 0.860 | 1.4998 | 1.4626 | 1.4996 | 1.4622 |
| 1.409 | 11,364 | 0.880 | 1.4992 | 1.4623 | 1.4990 | 1.4619 |
| 1.378 | 11,111 | 0.900 | 1.4986 | 1.4620 | 1.4984 | 1.4617 |
| 1.348 | 10,870 | 0.920 | 1.4979 | 1.4617 | 1.4978 | 1.4614 |
| 1.319 | 10,638 | 0.940 | 1.4973 | 1.4614 | 1.4973 | 1.4612 |
| 1.292 | 10,417 | 0.960 | 1.4967 | 1.4611 | 1.4967 | 1.4609 |
| 1.265 | 10,204 | 0.980 | 1.4961 | 1.4608 | 1.4962 | 1.4607 |
| 1.240 | 10,000 | 1.000 | 1.4954 | 1.4606 | 1.4956 | 1.4605 |
| 1.216 | 9,804 | 1.020 | 1.4948 | 1.4603 | 1.4950 | 1.4603 |
| 1.192 | 9,615 | 1.040 | 1.4942 | 1.4600 | 1.4945 | 1.4601 |
| 1.170 | 9,434 | 1.060 | 1.4936 | 1.4598 | 1.4936 | 1.4599 |
| 1.148 | 9,259 | 1.080 | 1.4930 | 1.4595 | | |
| 1.127 | 9,091 | 1.10 | 1.4924 | 1.4593 | | |

TABLE I (*Continued*)

KDP

| eV | $cm^{-1}$ | μm | $n_o$ | $n_e$ | $n_o$ | $n_e$ |
|---|---|---|---|---|---|---|
| 1.107 | 8,929 | 1.12 | 1.4918 | 1.4591 | | |
| 1.088 | 8,772 | 1.14 | 1.4912 | 1.4588 | | |
| 1.069 | 8,621 | 1.16 | 1.4906 | 1.4586 | | |
| 1.051 | 8,475 | 1.18 | 1.4900 | 1.4584 | | |
| 1.033 | 8,333 | 1.20 | 1.4895 | 1.4581 | | |
| 1.016 | 8,197 | 1.22 | 1.4889 | 1.4579 | | |
| 1.000 | 8,065 | 1.24 | 1.4883 | 1.4577 | | |
| 0.9840 | 7,937 | 1.26 | 1.4877 | 1.4575 | | |
| 0.9686 | 7,813 | 1.28 | 1.4872 | 1.4573 | | |
| 0.9537 | 7,692 | 1.30 | 1.4866 | 1.4571 | | |
| 0.9393 | 7,576 | 1.32 | 1.4861 | 1.4569 | | |
| 0.9253 | 7,463 | 1.34 | 1.4855 | 1.4567 | | |
| 0.9117 | 7,353 | 1.36 | 1.4850 | 1.4565 | | |

[a] The indices were calculated with the Herzberger-type formula. The number in brackets indicates the data reference.

**TABLE II**

**Values of $n$ for ADP at 24.8°C and 33.0°C[a]**

| | | | 24.8 ± 0.2 C | | 33.0 ± 0.4 C | |
|---|---|---|---|---|---|---|
| eV | $cm^{-1}$ | μm | $n_o$ | $n_e$ | $n_o$ | $n_e$ |
| 5.636 | 45,455 | 0.220 | 1.6186[1] | 1.5609[1] | | |
| 5.167 | 41,667 | 0.240 | 1.5981 | 1.5429 | | |
| 4.769 | 38,462 | 0.260 | 1.5827 | 1.5293 | | |
| 4.429 | 35,714 | 0.280 | 1.5715 | 1.5193 | | |
| 4.133 | 33,333 | 0.300 | 1.5630 | 1.5119 | | |
| 3.875 | 31,250 | 0.320 | 1.5565 | 1.5062 | | |
| 3.647 | 29,412 | 0.340 | 1.5513 | 1.5016 | | |
| 3.444 | 27,778 | 0.360 | 1.5470 | 1.4979 | | |
| 3.263 | 26,316 | 0.380 | 1.5435 | 1.4949 | | |
| 3.100 | 25,000 | 0.400 | 1.5405 | 1.4923 | 1.5396[4] | 1.4920[4] |
| 2,952 | 23,810 | 0.420 | 1.5379 | 1.4901 | 1.5368 | 1.4897 |
| 2.818 | 22,727 | 0.440 | 1.5357 | 1.4882 | 1.5344 | 1.4877 |
| 2.696 | 21,739 | 0.460 | 1.5337 | 1.4865 | 1.5324 | 1.4860 |
| 2.583 | 20,833 | 0.480 | 1.5319 | 1.4851 | 1.5306 | 1.4845 |
| 2.480 | 20,000 | 0.500 | 1.5303 | 1.4837 | 1.5290 | 1.4832 |
| 2.385 | 19,231 | 0.520 | 1.5288 | 1.4825 | 1.5276 | 1.4820 |
| 2.296 | 18,519 | 0.540 | 1.5274 | 1.4814 | 1.5263 | 1.4810 |
| 2.214 | 17,857 | 0.560 | 1.5261 | 1.4804 | 1.5251 | 1.4800 |
| 2.138 | 17,241 | 0.580 | 1.5249 | 1.4795 | 1.5240 | 1.4791 |
| 2.067 | 16,667 | 0.600 | 1.5238 | 1.4786 | 1.5229 | 1.4783 |
| 2.000 | 16,129 | 0.620 | 1.5227 | 1.4778 | 1.5219 | 1.4776 |
| 1.938 | 15,625 | 0.640 | 1.5217 | 1.4770 | 1.5209 | 1.4769 |
| 1.879 | 15,152 | 0.660 | 1.5207 | 1.4763 | 1.5200 | 1.4763 |
| 1.824 | 14,706 | 0.680 | 1.5197 | 1.4756 | 1.5191 | 1.4757 |
| 1.771 | 14,286 | 0.700 | 1.5188 | 1.4749 | 1.5183 | 1.4751 |
| 1.722 | 13,889 | 0.720 | 1.5179 | 1.4743 | 1.5175 | 1.4746 |
| 1.676 | 13,514 | 0.740 | 1.5170 | 1.4737 | 1.5167 | 1.4741 |
| 1.632 | 13,158 | 0.760 | 1.5162 | 1.4732 | 1.5159 | 1.4736 |
| 1.590 | 12,821 | 0.780 | 1.5154 | 1.4726 | 1.5152 | 1.4731 |
| 1.550 | 12,500 | 0.800 | 1.5146 | 1.4721 | 1.5145 | 1.4727 |
| 1.512 | 12,195 | 0.820 | 1.5138 | 1.4716 | 1.5139 | 1.4722 |
| 1.476 | 11,905 | 0.840 | 1.5131 | 1.4712 | 1.5132 | 1.4718 |
| 1.442 | 11,628 | 0.860 | 1.5123 | 1.4707 | 1.5126 | 1.4714 |
| 1.409 | 11,364 | 0.880 | 1.5116 | 1.4703 | 1.5121 | 1.4710 |
| 1.378 | 11,111 | 0.900 | 1.5109 | 1.4699 | 1.5115 | 1.4707 |
| 1.348 | 10,870 | 0.920 | 1.5103 | 1.4695 | 1.5110 | 1.4703 |
| 1.319 | 10,638 | 0.940 | 1.5096 | 1.4692 | 1.5106 | 1.4700 |
| 1.292 | 10,417 | 0.960 | 1.5090 | 1.4688 | 1.5101 | 1.4696 |
| 1.265 | 10,204 | 0.980 | 1.5084 | 1.4685 | 1.5100 | 1.4693 |
| 1.240 | 10,000 | 1.000 | 1.5078 | 1.4683 | 1.5094 | 1.4689 |
| 1.216 | 9,804 | 1.020 | 1.5072 | 1.4680 | 1.5091 | 1.4686 |
| 1.192 | 9,615 | 1.040 | 1.5067 | 1.4678 | 1.5089 | 1.4683 |
| 1.170 | 9,434 | 1.060 | 1.5061 | 1.4676 | 1.5087 | 1.4680 |
| 1.148 | 9,259 | 1.080 | 1.5056 | 1.4674 | | |
| 1.127 | 9,091 | 1.100 | 1.5052 | 1.4673 | | |
| 1.107 | 8,929 | 1.120 | 1.5047 | 1.4672 | | |

**TABLE II** (*continued*)

**ADP**

| eV | $cm^{-1}$ | μm | $n_o$ | $n_e$ | $n_o$ | $n_e$ |
|---|---|---|---|---|---|---|
| 1.088 | 8,772 | 1.140 | 1.5043 | 1.4671 | | |
| 1.069 | 8,621 | 1.160 | 1.5039 | 1.4670 | | |

[a] The indices were calculated with the Herzberger-type formula. The numbers in brackets indicate the data reference.

TABLE III

Value of *n* for KD*P at 33.0°C[a]

| eV | $cm^{-1}$ | μm | $n_o$ | $n_e$ |
|---|---|---|---|---|
| 3.100 | 25,000 | 0.400 | 1.5183[4] | 1.4774[4] |
| 2.952 | 23,810 | 0.420 | 1.5159 | 1.4755 |
| 2.818 | 22,727 | 0.440 | 1.5139 | 1.4738 |
| 2.696 | 21,739 | 0.460 | 1.5121 | 1.4723 |
| 2.583 | 20,833 | 0.480 | 1.5106 | 1.4710 |
| 2.480 | 20,000 | 0.500 | 1.5092 | 1.4699 |
| 2.385 | 19,231 | 0.520 | 1.5080 | 1.4689 |
| 2.296 | 18,519 | 0.540 | 1.5069 | 1.4680 |
| 2.214 | 17,857 | 0.560 | 1.5060 | 1.4672 |
| 2.138 | 17,241 | 0.580 | 1.5051 | 1.4664 |
| 2.067 | 16,667 | 0.600 | 1.5042 | 1.4658 |
| 2.000 | 16,127 | 0.620 | 1.5035 | 1.4652 |
| 1.938 | 15,625 | 0.640 | 1.5028 | 1.4646 |
| 1.879 | 15,152 | 0.660 | 1.5021 | 1.4641 |
| 1.824 | 14,706 | 0.680 | 1.5015 | 1.4636 |
| 1.771 | 14,286 | 0.700 | 1.5009 | 1.4632 |
| 1.722 | 13,889 | 0.720 | 1.5003 | 1.4628 |
| 1.676 | 13,514 | 0.740 | 1.4998 | 1.4624 |
| 1.632 | 13,158 | 0.760 | 1.4993 | 1.4620 |
| 1.590 | 12,821 | 0.780 | 1.4988 | 1.4617 |
| 1.550 | 12,500 | 0.800 | 1.4983 | 1.4614 |
| 1.512 | 12,195 | 0.820 | 1.4979 | 1.4611 |
| 1.476 | 11,905 | 0.840 | 1.4974 | 1.4608 |
| 1.442 | 11,628 | 0.860 | 1.4970 | 1.4605 |
| 1.409 | 11,364 | 0.880 | 1.4966 | 1.4602 |
| 1.378 | 11,111 | 0.900 | 1.4962 | 1.4600 |
| 1.348 | 10,870 | 0.920 | 1.4958 | 1.4597 |
| 1.319 | 10,638 | 0.940 | 1.4954 | 1.4595 |
| 1.292 | 10,417 | 0.960 | 1.4950 | 1.4593 |
| 1.265 | 10,204 | 0.980 | 1.4946 | 1.4591 |
| 1.240 | 10,000 | 1.000 | 1.4943 | 1.4589 |
| 1.216 | 9,804 | 1.020 | 1.4939 | 1.4587 |
| 1.192 | 9,615 | 1.040 | 1.4936 | 1.4585 |
| 1.170 | 9,434 | 1.060 | 1.4932 | 1.4583 |

[a] The indices were calculated with the Herzberger-type formula. The number in brackets indicates the data reference.

TABLE IV

Value of $n$ for AD*P at 33.0°C[a]

| eV | $cm^{-1}$ | μm | $n_o$ | $n_e$ |
|---|---|---|---|---|
| 3.100 | 25,000 | 0.400 | 1.5328[4] | 1.4879[4] |
| 2.952 | 23,810 | 0.420 | 1.5303 | 1.4857 |
| 2.818 | 22,727 | 0.440 | 1.5281 | 1.4839 |
| 2.696 | 21,739 | 0.460 | 1.5262 | 1.4822 |
| 2.583 | 20,833 | 0.480 | 1.5245 | 1.4808 |
| 2,480 | 20,000 | 0.500 | 1.5230 | 1.4795 |
| 2.385 | 19,231 | 0.520 | 1.5217 | 1.4784 |
| 2.296 | 18,519 | 0.540 | 1.5205 | 1.4774 |
| 2.214 | 17,857 | 0.560 | 1.5194 | 1.4765 |
| 2.138 | 17,241 | 0.580 | 1.5185 | 1.4756 |
| 2.067 | 16,667 | 0.600 | 1.5175 | 1.4749 |
| 2.000 | 16,127 | 0.620 | 1.5167 | 1.4742 |
| 1.938 | 15,625 | 0.640 | 1.5159 | 1.4736 |
| 1.879 | 15,152 | 0.660 | 1.5152 | 1.4730 |
| 1.824 | 14,706 | 0.680 | 1.5145 | 1.4724 |
| 1.771 | 14,286 | 0.700 | 1.5138 | 1.4719 |
| 1.722 | 13,889 | 0.720 | 1.5132 | 1.4715 |
| 1.676 | 13,514 | 0.740 | 1.5126 | 1.4710 |
| 1.632 | 13,158 | 0.760 | 1.5121 | 1.4706 |
| 1.590 | 12,821 | 0.780 | 1.5115 | 1.4702 |
| 1.550 | 12,500 | 0.800 | 1.5110 | 1.4698 |
| 1.512 | 12,195 | 0.820 | 1.5105 | 1.4695 |
| 1.476 | 11,905 | 0.840 | 1.5100 | 1.4691 |
| 1.442 | 11,628 | 0.860 | 1.5095 | 1.4688 |
| 1.409 | 11,364 | 0.880 | 1.5090 | 1.4685 |
| 1.378 | 11,111 | 0.900 | 1.5085 | 1.4682 |
| 1.348 | 10,870 | 0.920 | 1.5081 | 1.4679 |
| 1.319 | 10,638 | 0.940 | 1.5076 | 1.4676 |
| 1.292 | 10,417 | 0.960 | 1.5072 | 1.4673 |
| 1.265 | 10,204 | 0.980 | 1.5068 | 1.4670 |
| 1.240 | 10,000 | 1.000 | 1.5063 | 1.4668 |
| 1.216 | 9,804 | 1.020 | 1.5059 | 1.4665 |
| 1.192 | 9,615 | 1.040 | 1.5055 | 1.4662 |
| 1.170 | 9,434 | 1.060 | 1.5051 | 1.4660 |

[a] The indices were calculated with the Herzberger-type formula. The number in brackets indicates the data reference.

TABLE V

Herzberger-type Dispersion Formula Coefficients $n = A + BL + CL^2 + D\lambda^2 + E\lambda^4$

| Material | Temp (C) | | RMS error % | A | B | C | D | E |
|---|---|---|---|---|---|---|---|---|
| KDP | 33.0 | $n_o$ | 0.00326 | 1.503444 | $3.162307 \times 10^5$ | $-3.029850 \times 10^{11}$ | $-1.152066 \times 10^{-10}$ | $4.545059 \times 10^{-20}$ |
| | | $n_e$ | 0.00376 | 1.462149 | $2.554564 \times 10^5$ | $-1.406152 \times 10^{11}$ | $-5.962811 \times 10^{-11}$ | $1.701670 \times 10^{-19}$ |
| | 24.8 | $n_o$ | 0.0375 | 1.507233 | $2.691571 \times 10^5$ | $-1.800594 \times 10^{11}$ | $-1.655975 \times 10^{-10}$ | $2.017312 \times 10^{-19}$ |
| | | $n_e$ | 0.0218 | 1.463170 | $2.439193 \times 10^5$ | $-1.712637 \times 10^{11}$ | $-6.011992 \times 10^{-11}$ | $9.221139 \times 10^{-20}$ |
| KD*P | 33.0 | $n_o$ | 0.00166 | 1.499050 | $2.763783 \times 10^5$ | $-4.759414 \times 10^{10}$ | $-9.103436 \times 10^{-11}$ | $1.482297 \times 10^{-19}$ |
| | | $n_e$ | 0.00167 | 1.458701 | $2.815843 \times 10^5$ | $-3.633300 \times 10^{11}$ | $-3.235631 \times 10^{-11}$ | $5.360066 \times 10^{-20}$ |
| ADP | 33.0 | $n_o$ | 0.00715 | 1.527573 | $1.635962 \times 10^5$ | $8.176341 \times 10^{11}$ | $-3.372908 \times 10^{-10}$ | $1.379342 \times 10^{-18}$ |
| | | $n_e$ | 0.00137 | 1.472389 | $2.900877 \times 10^5$ | $-2.052917 \times 10^{11}$ | $-7.730910 \times 10^{-11}$ | $1.326179 \times 10^{-19}$ |
| | 24.8 | $n_o$ | 0.0285 | 1.523897 | $2.869378 \times 10^5$ | $-1.857597 \times 10^{11}$ | $-2.660808 \times 10^{-10}$ | $7.551831 \times 10^{-19}$ |
| | | $n_e$ | 0.0269 | 1.476613 | $2.552032 \times 10^5$ | $-1.661894 \times 10^{11}$ | $-1.792370 \times 10^{-10}$ | $6.965756 \times 10^{-19}$ |
| AD*P | 33.0 | $n_o$ | 0.00404 | 1.510421 | $3.407679 \times 10^5$ | $-3.825237 \times 10^{11}$ | $-7.869752 \times 10^{-11}$ | $3.167592 \times 10^{-20}$ |
| | | $n_e$ | 0.00251 | 1.467063 | $3.173115 \times 10^5$ | $-4.549975 \times 10^{11}$ | $-3.729681 \times 10^{-11}$ | $2.002751 \times 10^{-20}$ |

**TABLE VI**

**Modified Sellmeier-type Dispersion Formula Coefficients $n^2 = 1 + A/(\lambda^2 - B) + C\lambda^2/(\lambda^2 - D)$**

| Material | Temp (C) | Index | RMS error% | A | B | C | D |
|---|---|---|---|---|---|---|---|
| KDP | 33.0 | $n_o$ | 0.0356 | $2.140260 \times 10^{-9}$ | $-1.489486 \times 10^{9}$ | 1.209065 | $-1.489604 \times 10^{-9}$ |
| | | $n_e$ | 0.0107 | $4.503887 \times 10^{-10}$ | $-2.879423 \times 10^{-10}$ | 1.121333 | $-2.879296 \times 10^{-10}$ |
| | 24.8 | $n_o$ | 0.190 | $1.724871 \times 10^{-10}$ | $-1.288031 \times 10^{-11}$ | 1.221148 | $-1.319929 \times 10^{-11}$ |
| | | $n_e$ | 0.0735 | $6.406553 \times 10^{-11}$ | $9.395038 \times 10^{-11}$ | 1.121184 | $3.414367 \times 10^{-11}$ |
| KD*P | 33.0 | $n_o$ | 0.0248 | $1.087078 \times 10^{-9}$ | $-7.256670 \times 10^{-10}$ | 1.215009 | $-7.257061 \times 10^{-10}$ |
| | | $n_e$ | 0.00945 | $3.849747 \times 10^{-10}$ | $-2.374996 \times 10^{-10}$ | 1.117103 | $-2.374739 \times 10^{-10}$ |
| ADP | 33.0 | $n_o$ | 0.0212 | $1.671714 \times 10^{-9}$ | $-1.085260 \times 10^{-9}$ | 1.251347 | $-1.085304 \times 10^{-9}$ |
| | | $n_e$ | 0.0208 | $8.937086 \times 10^{-10}$ | $-6.214465 \times 10^{-10}$ | 1.141555 | $-6.214699 \times 10^{-10}$ |
| | 24.8 | $n_o$ | 0.164 | $1.572664 \times 10^{-10}$ | $1.510526 \times 10^{-11}$ | 1.265293 | $5.181578 \times 10^{-12}$ |
| | | $n_e$ | 0.0714 | $7.093846 \times 10^{-11}$ | $1.029798 \times 10^{-10}$ | 1.149624 | $3.790226 \times 10^{-11}$ |
| AD*P | 33.0 | $n_o$ | 0.0288 | $1.312696 \times 10^{-9}$ | $-8.562983 \times 10^{-10}$ | 1.248006 | $-8.563000 \times 10^{-10}$ |
| | | $n_e$ | 0.0144 | $5.720224 \times 10^{-10}$ | $-3.725013 \times 10^{-10}$ | 1.137827 | $-3.725002 \times 10^{-10}$ |

**TABLE VII**

**Values of the Coefficients for Determining the Temperature Change in Index of Refraction [6]**

$\Delta n = (n^2 + an + b)c(298\text{-}T)$

| | | $a$ | $b$ | $c(K^{-1})$ |
|---|---|---|---|---|
| KDP | $n_o$ | 0 | −1.432 | $0.402 \times 10^{-4}$ |
| | $n_e$ | 0 | −1.105 | $0.221 \times 10^{-4}$ |
| KD*P | $n_o$ | 0 | −1.047 | $0.228 \times 10^{-4}$ |
| | $n_e$ | 0 | 0 | $0.955 \times 10^{-5}$ |
| ADP | $n_o$ | −3.0297 | 2.3004 | $0.713 \times 10^{-2}$ |
| | $n_e$ | 0 | 0 | $0.675 \times 10^{-6}$ |

**TABLE VIII**

**Information about the Infrared Lattice Vibration Modes of KDP and Some of Its Isomorphs**

| Ref. | Technique | Temperature | Data | Spectrum | Material |
|---|---|---|---|---|---|
| [12] | IR refl. | 25 °C & lower | reflection | 400–10000 $cm^{-1}$ | KDP |
| [13] | IR refl. | 300 K | $\varepsilon''(a)$, $\varepsilon''(c)$ | 0–600 | KDP |
| | | | $\varepsilon''(a)$, $\varepsilon''(c)$ | 70–330 | KD*P |
| [14] | IR refl. | 300 K & lower | $\varepsilon''(c)$ | 0–400 | KDP |
| [15] | IR trans. | 300 K & lower | $k(\|c)$ | 10–200 | KDP |
| [16] | IR trans. | 300 K & lower | absorption | 250–4000 | KDP, ADP |
| [17] | IR refl. | 295 K & lower | $\varepsilon''(\|c)$, $\varepsilon''(\perp c)$ | 10–600 | KDP, ADP |
| [18] | IR refl. | 295 K & lower | $\varepsilon''(\|c)$ | 20–550 | KD*P |
| [19] | IR refl. | 290 K & lower | $\varepsilon'(a)$, $\varepsilon'(c)$ | 0–700 | KDP |
| | | | $\varepsilon''(a)$ | 0–350 | KDP |
| [20] | IR refl. | 295 K & lower | $\varepsilon'(\|c)$, $\varepsilon''(\|c)$ | 0–350 | KDP |
| | | | $\varepsilon'(\perp c)$, $\varepsilon''(\perp c)$ | 0–80 | KDP |
| [21] | IR refl. | 300 K & lower | $\varepsilon'(\|c)$, $\varepsilon''(\|c)$ | 10–210 | KDP, ADP |
| | | | $\varepsilon'(\|a)$, $\varepsilon''(\|a)$ | | |
| [22] | IR refl. | 300 K & lower | $\varepsilon'(\|c)$, $\varepsilon''(\|c)$ | 20–250 | KDP |

# Sodium Fluoride (NaF)

I. OHLÍDAL and K. NAVRÁTIL
Department of Solid State Physics
Faculty of Science
Masaryk University Brno
Kotlářská 2
611 37 Brno, Czechoslovakia

The room-temperature values of the refractive index $n$ and the extinction coefficient $k$ tabulated here (see Table I and Fig. 1) were obtained from the following works: the 0.166 μm (7.56 eV) to 0.101 μm (12.4 eV) results are from the paper of Fabre *et al.* [1]; the 0.225 μm (5.5 eV) to 0.124 μm (10.0 eV) results are from the paper of Tomiki and Miyata [2]; the 2 μm (0.62 eV) to 0.25 μm (4.96 eV) values are from Navrátil and Ohlídal's measurements [3]; the 0.578 μm (2.15 eV) to 0.186 μm (6.7 eV) results are from the paper of Kublitzky [4]; the 1.1 μm (1.13 eV) to 0.238 μm (5.2 eV) values are presented by Harting [5]; the 24 μm (0.05 eV) to 0.546 μm (2.3 eV) data are from Hohls's measurements [6] and the 111.1 μm (90 $cm^{-1}$) to 21.1 μm (475 $cm^{-1}$) values were published by Pai *et al.* [7].

The values of $n$ and $k$ presented by Fabre *et al.* [1] were obtained by interpreting spectral dependences of the reflectance of NaF films corresponding to different thicknesses. These films were produced by vacuum evaporation using resistively heated sources. The substrates of the NaF films studied were formed by glass plates. In the formula for the reflectance, a roughness of the upper boundaries of the NaF films analyzed was handled in a certain way [1, 8], such that, in the spectral region mentioned, the influence of this roughness was eliminated in determining $n$ and $k$ for these films, at least in a first approximation. Absorption is caused by excitons in this region.

Tomiki and Miyata [2] determined the values of $n$ and $k$ characterizing sodium-fluoride plates by means of the values of the transmittance and the reflectance of these plates measured in the region $0.225\ \mu m \geq \lambda \geq 0.124\ \mu m$. In this region Tomiki and Miyata's values of $n$ agree in a satisfactory way with those presented by Fabre *et al.* [1] for the NaF thin films (see Table I).


Copyright © 1991 by Academic Press.
All rights of reproduction in any form reserved.
ISBN 0-12-544422-2

However, in this region there are substantial differences between the values of $k$ presented by Tomiki and Miyata and by Fabre *et al.* One can expect that the values of $k$ determined by Tomiki and Miyata are more accurate than those determined by Fabre *et al.* The values of $k$ characterizing the NaF film studied by Fabre *et al.* are apparently too great. These values are probably influenced by the light scattering caused by volume inhomogeneities not included in the formula for the reflectance of these films (for example, this scattering can be caused by microcrystals [1]). Moreover, the other structure defects can strongly affect the correctness of the data presented by Fabre *et al.* [1] (for example, some impurities occurring in the NaF films). These effects can evidently increase the values of $k$ characterizing thin films.

In the region $2\,\mu m \geq \lambda \geq 0.25\,\mu m$, the values of the refractive index $n$ were determined using the spectral dependences of the reflectance of the NaF films evaporated onto glass and single-crystal silicon substrates. In this region the NaF films are transparent, and therefore the thickness of these films was found by the Fizeau method, and the values of $n$ were evaluated from the reflectance measured at the wavelengths of interest (the thickness of the NaF films was about 100 nm). The errors in $n$ are $\pm 0.008$ over the entire region mentioned. There is relatively good coincidence between the refractive index data of Fabre *et al.* [1] and Navrátil and Ohlídal [3]. (One can expect reasonable agreement of both sets of data after an extrapolation of the data of Fabre *et al.* [1] to longer wavelengths using a suitable dispersion formula; see Table I.) In Table I the value of $n$ given by Pulker [9] for NaF films at the wavelength of 0.55 μm is also listed. Taking into account the errors, we find that the values of $n$ published by Pulker [9] agree very well with those determined by Navrátil and Ohlídal [3].

Kublitzky [4] measured the values of $n$ characterizing sodium-fluoride prisms by the method of minimum deviation at selected wavelengths in the spectral region $0.578\,\mu m \geq \lambda \geq 0.186\,\mu m$. Harting [5] and Hohls [6] determined $n$ by the same method in the regions $41\,\mu m \geq \lambda \geq 0.238\,\mu m$ and $10.9\,\mu m \geq \lambda \geq 0.8\,\mu m$, respectively. Moreover, in the region $19.7\,\mu m \geq \lambda \geq 8.8\,\mu m$, Hohls [6] evaluated the refractive-index data of NaF using interferometric methods based on determining positions of fringes of equal chromatic order for light reflected or transmitted by sodium-fluoride slabs. Furthermore, in the region $24\,\mu m \geq \lambda \geq 0.546\,\mu m$, Hohls determined the values of $n$ and $k$ for thinned plates of sodium fluoride by means of the values of the reflectance and the transmittance of these plates measured at selected wavelengths (the thickness of the thinnest plate was 0.024 mm). The thicknesses of the sodium-fluoride plates were determined independently [6].

Pai *et al.* [7] determined the spectral dependences of both $n$ and $k$ characterizing sodium-fluoride bulk samples using amplitude and phase-reflection measurements made by dispersive Fourier transform spectros-

copy in the region 111 μm $\geq \lambda \geq$ 21.2 μm. The errors of $n$ and $k$ determined in this way are dependent on wavelength. (The greatest and/or smallest errors in both $n$ and $k$ are equal to $\pm 0.56$ and/or $\pm 0.005$ at the wavelength of about 41 μm and/or 24 μm [7]). Spectral dependences of $n$ and $k$ in the vicinity of the maximum value of $k$ at the wavelength $\lambda = 40.3$ μm are related to one-phonon absorption, corresponding to the TO phonon mode. The fine structure of the curve expressing the spectral dependence of $n$ in the region 24–34 μm may be caused by multiple-phonon processes of absorption. However, a corresponding structure in $k$ in this region is not observed (see Table I and Fig. 1). This discrepancy is probably caused by the fact that reflection techniques are not too sensitive to small changes of absorption. The structure in both the $n$ and $k$ curves in this region can be seen only when precision transmittance measurements of sufficiently thin NaF slabs are performed.

One can see that the values of $n$ and $k$ characterizing bulk NaF evaluated by the different authors at the same wavelengths agree very well (see Table I). This fact gives significant support for the correctness and reliability of the $n$ and $k$ values of bulk NaF presented here.

It should be also noted that the values of $n$ describing the NaF thin films [3] in the region 2 μm $\geq \lambda \geq$ 0.25 μm are nearly identical with those characterizing bulk NaF [4–6]. This fact implies that the packing density $p$ defined by $p = V_s/V$ (where $V_s$ and $V$ are the volume of the solid part of the film and the total volume of the film, respectively) is nearly equal to unity. This can be demonstrated if the value of $p$ characterizing the NaF thin films studied [3] is calculated by means of the following formula for the mean refractive index of films with columnar structure [10–12]:

$$n = n_s p + n_o(1 - p), \tag{1}$$

where $n$, $n_s$, and $n_o$ denote the mean refractive index, the columnar (bulk) refractive index of the film, and the refractive index of a substance filling the pores between columns. Assuming that $n_o = 1$, one obtains (using Eq. 1 and the values of $n$ and $n_s$ presented here) the value of $p = 0.98$. This means that the NaF films analyzed by Navrátil and Ohlídal [3] are formed by very close-packed columns [11, 13].

In conclusion, one can state that the refractive-index data summarized in this work represent the true values of $n$ characterizing bulk NaF in the spectral regions under consideration (see Table I and Fig. 1). (In the region 0.124 μm $\geq \lambda \geq$ 0.101 μm, this conclusion is valid for the values of $n$ determined by Fabre *et al.* [1], at least in a first approximation.) The same statement can be said for the extinction-index data, except for the region 0.124 μm $\geq \lambda \geq$ 0.101 μm. Namely, the values of $k$ determined by Fabre *et al.* [1] in the region 0.166 μm $\geq \lambda \geq$ 0.101 μm can serve only as rough

information concerning the form of the spectral dependence of $k$ of bulk NaF.

It should be noted that the refractive-index data corresponding to the region of transparency of NaF were also presented by Li [14].

## REFERENCES

1. D. Fabre, J. Romand, and B. Vodar, *J. Phys. (Paris)* **25**, 55 (1964).
2. T. Tomiki and T. Miyata, *J. Phys. Soc. Japan* **27**, 658 (1969).
3. K. Navrátil and I. Ohlídal, unpublished results.
4. A. Kublitzky, *Ann. Phys.* **20**, 793 (1934).
5. H. Harting, *Sitzungsber. Deutsch. Akad. Wiss. Ber.* **4**, 1 (1948).
6. H. W. Hohls, *Ann. Phys.* **29**, 433 (1937).
7. K. F. Pai, T. J. Parker, N. E. Tornberg, R. P. Lowndes, and W. G. Chambers, *Infrared Physics* **18**, 199 (1978).
8. P. Bousquet, *J. Phys. (Paris)* **25**, 50 (1964).
9. H. K. Pulker, *Appl. Opt.* **18**, 1969 (1979).
10. K. Kinosita and M. Nishibori, *J. Vac. Sci. Technol.* **6**, 730 (1969).
11. M. Harris, H. A. Macleod, S. Ogura, E. Pelletier, and B. Vidal, *Thin Solid Films* **57**, 173 (1979).
12. S. Ogura, N. Sugawara, and R. Hiraga, *Thin Solid Films* **30**, 3 (1975).
13. I. Ohlídal and K. Navrátil, *Thin Solid Films* **74**, 51 (1980).
14. H. H. Li, *J. Phys. Chem. Ref. Data* **5**, 345 (1976).

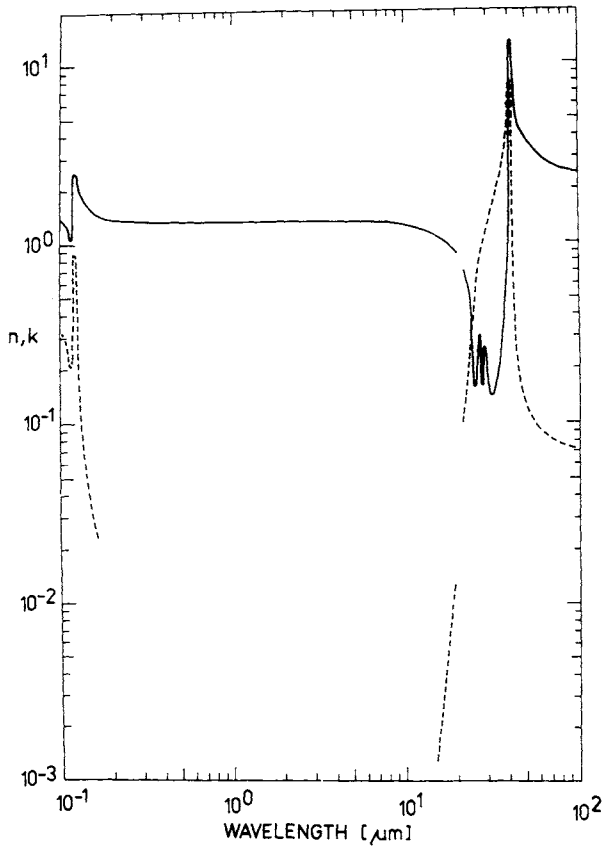


**Fig. 1.** Log–log plot of $n$ (solid line) and $k$ (dashed line) versus wavelength in micrometers for sodium fluoride.

TABLE I

Values of $n$ and $k$ for Sodium Fluoride from Various References[a]

| eV | $cm^{-1}$ | μm | n | k |
|---|---|---|---|---|
| 12.28 | 99,010 | 0.101 | 1.360[1] | 0.322[1] |
| 12.16 | 98,039 | 0.102 | 1.359 | 0.321 |
| 12.04 | 97,087 | 0.103 | 1.358 | 0.316 |
| 11.92 | 96,154 | 0.104 | 1.358 | 0.307 |
| 11.81 | 95,238 | 0.105 | 1.351 | 0.297 |
| 11.70 | 94,340 | 0.106 | 1.333 | 0.280 |
| 11.59 | 93,458 | 0.107 | 1.320 | 0.254 |
| 11.48 | 92,593 | 0.108 | 1.289 | 0.227 |
| 11.38 | 91,743 | 0.109 | 1.247 | 0.213 |
| 11.27 | 90,909 | 0.110 | 1.204 | 0.205 |
| 11.17 | 90,090 | 0.111 | 1.128 | 0.204 |
| 11.07 | 89,286 | 0.112 | 1.093 | 0.209 |
| 10.97 | 88,496 | 0.113 | 1.138 | 0.272 |
| 10.88 | 87,719 | 0.114 | 1.269 | 0.342 |
| 10.78 | 86,957 | 0.115 | 1.567 | 0.578 |
| 10.69 | 86,207 | 0.116 | 1.822 | 0.784 |
| 10.60 | 85,470 | 0.117 | 2.167 | 0.900 |
| 10.51 | 84,746 | 0.118 | 2.404 | 0.833 |
| 10.42 | 84,034 | 0.119 | 2.511 | 0.629 |
| 10.33 | 83,333 | 0.120 | 2.493 | 0.491 |
| 10.25 | 82,645 | 0.121 | 2.360 | 0.382 |
| 10.16 | 81,967 | 0.122 | 2.230 | 0.308 |
| 10.08 | 81,300 | 0.123 | 2.122 | 0.236 |
| 10.0 | 80,653 | 0.1240 | 2.00[2] | |
| | | | 2.044[1] | 0.171[1] |
| 9.919 | 80,000 | 0.125 | 1.958 | 0.140 |
| 9.9 | 79,846 | 0.1252 | 1.84[2] | $9.9\times10^{-4}$[2] |
| 9.84 | 79,365 | 0.126 | 1.911[1] | 0.120[1] |
| 9.8 | 79,040 | 0.1265 | 1.77[2] | $1.0\times10^{-4}$[2] |
| 9.763 | 78,740 | 0.127 | 1.866[1] | 0.107[1] |
| 9.687 | 78,125 | 0.128 | 1.822 | 0.096 |
| 9.611 | 77,519 | 0.129 | 1.800 | 0.087 |
| 9.6 | 77,427 | 0.1292 | 1.68[2] | $2.9\times10^{-5}$[2] |
| 9.538 | 76,923 | 0.130 | 1.756[1] | 0.080[1] |
| 9.465 | 76,336 | 0.131 | 1.736 | 0.076 |
| 9.4 | 75,814 | 0.1319 | 1.62[2] | $2.6\times10^{-5}$[2] |
| 9.393 | 75,758 | 0.132 | 1.717[1] | 0.072[1] |
| 9.322 | 75,188 | 0.133 | 1.700 | 0.069 |
| 9.253 | 74,627 | 0.134 | 1.683 | 0.064 |
| 9.2 | 74,201 | 0.1348 | 1.56[2] | $2.4\times10^{-5}$[2] |
| 9.184 | 74,074 | 0.135 | 1.667[1] | 0.061[1] |
| 9.117 | 73,529 | 0.136 | 1.652 | 0.058 |
| 9.050 | 72,993 | 0.137 | 1.638 | 0.056 |
| 9.0 | 72,588 | 0.1378 | 1.55[2] | $2.2\times10^{-5}$[2] |
| 8.985 | 72,464 | 0.138 | 1.625[1] | 0.054[1] |
| 8.920 | 71,942 | 0.139 | 1.613 | 0.052 |

(continued)

TABLE I (*Continued*)

Sodium Fluoride

| eV | $cm^{-1}$ | μm | n | k |
|---|---|---|---|---|
| 8.856 | 71,429 | 0.140 | 1.601 | 0.049 |
| 8.793 | 70,922 | 0.141 | 1.591 | 0.048 |
| 8.732 | 70,423 | 0.142 | 1.580 | 0.047 |
| 8.670 | 69,930 | 0.143 | 1.571 | 0.045 |
| 8.610 | 69,444 | 0.144 | 1.562 | 0.044 |
| 8.551 | 68,966 | 0.145 | 1.554 | 0.042 |
| 8.5 | 68,555 | 0.1459 | 1.48[2] | $1.2 \times 10^{-5}$[2] |
| 8.492 | 68,493 | 0.146 | 1.546[1] | 0.039[1] |
| 8.435 | 68,027 | 0.147 | 1.539 | 0.038 |
| 8.378 | 67,568 | 0.148 | 1.532 | 0.036 |
| 8.321 | 67,114 | 0.149 | 1.526 | 0.035 |
| 8.266 | 66,667 | 0.150 | 1.520 | 0.033 |
| 8.211 | 66,225 | 0.151 | 1.514 | 0.032 |
| 8.157 | 65,790 | 0.152 | 1.509 | 0.031 |
| 8.104 | 65,360 | 0.153 | 1.505 | 0.030 |
| 8.051 | 64,935 | 0.154 | 1.500 | 0.028 |
| 8.0 | 64,516 | 0.155 | 1.497 | 0.027 |
| | | | 1.42[2] | $2.7 \times 10^{-6}$[2] |
| 7.948 | 64,103 | 0.156 | 1.493[1] | 0.027[1] |
| 7.897 | 63,694 | 0.157 | 1.490 | 0.027 |
| 7.847 | 63,291 | 0.158 | 1.487 | 0.026 |
| 7.798 | 62,893 | 0.159 | 1.848 | 0.026 |
| 7.749 | 62,500 | 0.160 | 1.482 | 0.023 |
| 7.701 | 62,112 | 0.161 | 1.479 | 0.023 |
| 7.654 | 61,728 | 0.162 | 1.477 | 0.023 |
| 7.607 | 61,350 | 0.163 | 1.476 | 0.023 |
| 7.560 | 60,976 | 0.164 | 1.474 | 0.023 |
| 7.5 | 60,490 | 0.1653 | 1.41[2] | |
| 7.0 | 56,457 | 0.1771 | 1.40 | |
| 6.666 | 53,763 | 0.186 | 1.3930[4] | |
| 6.5 | 52,424 | 0.1908 | 1.37[2] | |
| 6.424 | 51,814 | 0.193 | 1.3850[4] | |
| 6.231 | 50,251 | 0.199 | 1.3805 | |
| 6.108 | 49,261 | 0.203 | 1.3772 | |
| 6.019 | 48,544 | 0.206 | 1.3745 | |
| 6.0 | 48,392 | 0.2067 | 1.36[2] | |
| 5.904 | 47,619 | 0.210 | 1.3718[4] | |
| 5.794 | 46,729 | 0.214 | 1.3691 | |
| 5.662 | 45,662 | 0.219 | 1.3665 | |
| 5.5 | 44,359 | 0.2254 | 1.36[2] | |
| 5.462 | 44,053 | 0.227 | 1.3630[4] | |
| 5.367 | 43,290 | 0.231 | 1.3606 | |
| 5.232 | 42,194 | 0.237 | 1.3586 | |
| 5.209 | 42,017 | 0.238 | 1.35850[5] | |
| 5.166 | 41,667 | 0.240 | 1.35792 | |
| 5.123 | 41,322 | 0.242 | 1.35717 | |

(continued)

TABLE I (*Continued*)

**Sodium Fluoride**

| eV | $cm^{-1}$ | μm | n | k |
|---|---|---|---|---|
| 5.081 | 40,984 | 0.244 | 1.35644 | |
| 5.040 | 40,650 | 0.246 | 1.35574 | |
| 5.000 | 40,323 | 0.248 | 1.35506 | |
| 4.959 | 40,000 | 0.250 | 1.35440 | |
| | | | 1.342[3] | |
| 4.920 | 39,683 | 0.252 | 1.35376[5] | |
| 4.881 | 39,370 | 0.254 | 1.35314 | |
| | | | 1.3525[4] | |
| 4.843 | 39,063 | 0.256 | 1.35254[5] | |
| 4.824 | 38,929 | 0.257 | 1.3512[4] | |
| 4.806 | 38,760 | 0.258 | 1.35197[5] | |
| 4.769 | 38,462 | 0.260 | 1.35140 | |
| | | | 1.342[3] | |
| 4.732 | 38,168 | 0.262 | 1.35084[5] | |
| 4.697 | 37,879 | 0.264 | 1.35030 | |
| 4.688 | 37,736 | 0.265 | 1.3491[4] | |
| 4.661 | 37,594 | 0.266 | 1.34987[5] | |
| 4.626 | 37,313 | 0.268 | 1.34927 | |
| 4.592 | 37,037 | 0.270 | 1.34878 | |
| | | | 1.341[3] | |
| 4.558 | 36,765 | 0.272 | 1.34830[5] | |
| 4.525 | 36,496 | 0.274 | 1.34784 | |
| 4.509 | 36,363 | 0.275 | 1.3469[4] | |
| 4.492 | 36,232 | 0.276 | 1.34738[5] | |
| 4.460 | 35,971 | 0.278 | 1.34694 | |
| 4.428 | 35,714 | 0.280 | 1.34650 | |
| | | | 1.341[3] | |
| 4.366 | 35,461 | 0.284 | 1.34567[5] | |
| 4.335 | 34,965 | 0.286 | 1.34527 | |
| 4.305 | 34,722 | 0.288 | 1.34488 | |
| 4.275 | 34,483 | 0.290 | 1.34450 | |
| | | | 1.340[3] | |
| 4.246 | 34,247 | 0.292 | 1.34413[5] | |
| 4.218 | 34,014 | 0.294 | 1.34377 | |
| 4.189 | 33,784 | 0.296 | 1.34341 | |
| 4.161 | 33,357 | 0.298 | 1.34306 | |
| 4.133 | 33,333 | 0.300 | 1.34272 | |
| | | | 1.339[3] | |
| 4.106 | 33,113 | 0.302 | 1.34293[5] | |
| | | | 1.3417[4] | |
| 4.079 | 32,895 | 0.304 | 1.34207[5] | |
| 4.052 | 32,680 | 0.306 | 1.34175 | |
| 4.026 | 32,468 | 0.308 | 1.34144 | |
| 4.000 | 32,258 | 0.310 | 1.34114 | |
| 3.974 | 32,051 | 0.312 | 1.34084 | |
| 3.961 | 31,949 | 0.313 | 1.3401[4] | |

(continued)

TABLE I (*Continued*)

Sodium Fluoride

| eV | $cm^{-1}$ | μm | n | k |
|---|---|---|---|---|
| 3.949 | 31,847 | 0.314 | 1.34055[5] | |
| 3.924 | 31,646 | 0.316 | 1.34027 | |
| 3.899 | 31,447 | 0.318 | 1.33999 | |
| 3.875 | 31,250 | 0.320 | 1.33972 | |
| | | | 1.337[3] | |
| 3.851 | 31,056 | 0.322 | 1.33945[5] | |
| 3.827 | 30,864 | 0.324 | 1.33919 | |
| 3.803 | 30,675 | 0.326 | 1.33894 | |
| 3.780 | 30,488 | 0.328 | 1.33869 | |
| 3.757 | 30,303 | 0.330 | 1.33844 | |
| | | | 1.336[3] | |
| 3.735 | 30,121 | 0.332 | 1.33820[5] | |
| 3.712 | 29,940 | 0.334 | 1.33779 | |
| 3.690 | 29,762 | 0.336 | 1.33774 | |
| 3.668 | 29,586 | 0.338 | 1.33751 | |
| 3.647 | 29,412 | 0.340 | 1.33729 | |
| | | | 1.335[3] | |
| 3.625 | 29,240 | 0.342 | 1.33707[5] | |
| 3.604 | 29,070 | 0.344 | 1.33686 | |
| 3.583 | 28,902 | 0.346 | 1.33665 | |
| 3.563 | 28,736 | 0.348 | 1.33644 | |
| 3.543 | 28,571 | 0.350 | 1.33624 | |
| | | | 1.334[3] | |
| 3.522 | 28,409 | 0.352 | 1.33604[5] | |
| 3.502 | 28,249 | 0.354 | 1.33585 | |
| 3.483 | 28,090 | 0.356 | 1.33566 | |
| 3.463 | 27,933 | 0.358 | 1.33547 | |
| 3.444 | 27,778 | 0.360 | 1.33529 | |
| | | | 1.334[3] | |
| 3.425 | 27,624 | 0.362 | 1.33511[5] | |
| 3.406 | 27,473 | 0.364 | 1.33493 | |
| 3.383 | 27,322 | 0.366 | 1.33476 | |
| | | | 1.3342[4] | |
| 3.369 | 27,174 | 0.368 | 1.33459[5] | |
| 3.351 | 27,028 | 0.370 | 1.33442 | |
| | | | 1.333[3] | |
| 3.333 | 26,882 | 0.372 | 1.33426[5] | |
| 3.315 | 26,738 | 0.374 | 1.33410 | |
| 3.298 | 26,596 | 0.376 | 1.33394 | |
| 3.280 | 26,455 | 0.378 | 1.33378 | |
| 3.263 | 26,316 | 0.380 | 1.33363 | |
| | | | 1.332[3] | |
| 3.246 | 26,178 | 0.382 | 1.33348[5] | |
| 3.229 | 26,042 | 0.384 | 1.33333 | |
| 3.212 | 25,907 | 0.386 | 1.33318 | |
| 3.196 | 25,773 | 0.388 | 1.33304 | |

(continued)

TABLE I (*Continued*)

**Sodium Fluoride**

| eV | $cm^{-1}$ | μm | n | k |
|---|---|---|---|---|
| 3.179 | 25,641 | 0.390 | 1.33290 | |
| | | | 1.331[3] | |
| 3.163 | 25,510 | 0.392 | 1.33276[5] | |
| 3.147 | 25,381 | 0.394 | 1.33262 | |
| 3.131 | 25,253 | 0.396 | 1.33249 | |
| 3.115 | 25,126 | 0.398 | 1.33236 | |
| 3.100 | 25,000 | 0.400 | 1.33224 | |
| | | | 1.331[3] | |
| 3.061 | 24,691 | 0.405 | 1.3314[4] | |
| 3.024 | 24,390 | 0.41 | 1.33162[5] | |
| 2.952 | 23,810 | 0.42 | 1.33105 | |
| 2.883 | 23,256 | 0.43 | 1.33053 | |
| 2.850 | 22,988 | 0.435 | 1.3300[4] | |
| 2.818 | 22,727 | 0.44 | 1.33004[5] | |
| 2.755 | 22,222 | 0.45 | 1.32959 | |
| | | | 1.327[3] | |
| 2.695 | 21,739 | 0.46 | 1.32916[5] | |
| 2.638 | 21,277 | 0.47 | 1.32876 | |
| 2.583 | 20,833 | 0.48 | 1.32839 | |
| 2.530 | 20,408 | 0.49 | 1.32805 | |
| 2.480 | 20,000 | 0.50 | 1.32772 | |
| | | | 1.325[3] | |
| 2.431 | 19,608 | 0.51 | 1.32741[5] | |
| 2.384 | 19,231 | 0.52 | 1.32712 | |
| 2.339 | 18,868 | 0.53 | 1.32684 | |
| 2.296 | 18,519 | 0.54 | 1.32658 | |
| 2.271 | 18,315 | 0.546 | 1.3260[4] | |
| | | | 1.3258[6] | |
| 2.254 | 18,182 | 0.55 | 1.32634[5] | |
| | | | 1.321[3] | |
| | | | 1.30[9] | |
| 2.214 | 17,857 | 0.56 | 1.32611[5] | |
| 2.175 | 17,544 | 0.57 | 1.32589 | |
| 2.145 | 17,301 | 0.578 | 1.3251[4] | |
| 2.138 | 17,241 | 0.58 | 1.32567[5] | |
| 2.101 | 16,949 | 0.59 | 1.32547 | |
| 2.067 | 16,667 | 0.60 | 1.32528 | |
| | | | 1.321[3] | |
| 2.033 | 16,393 | 0.61 | 1.32510[5] | |
| 2.000 | 16,129 | 0.62 | 1.32492 | |
| 1.968 | 15,873 | 0.63 | 1.32476 | |
| 1.937 | 15,625 | 0.64 | 1.32460 | |
| 1.908 | 15,385 | 0.65 | 1.32445 | |
| 1.879 | 15,152 | 0.66 | 1.32431 | |
| 1.851 | 14,925 | 0.67 | 1.32417 | |
| 1.823 | 14,706 | 0.68 | 1.32404 | |

(continued)

TABLE I (*Continued*)

Sodium Fluoride

| eV | $cm^{-1}$ | μm | n | k |
|---|---|---|---|---|
| 1.797 | 14,493 | 0.69 | 1.32391 | |
| 1.771 | 14,286 | 0.70 | 1.32379 | |
| | | | 1.319[3] | |
| 1.746 | 14,085 | 0.71 | 1.32367[5] | |
| 1.722 | 13,889 | 0.72 | 1.32356 | |
| 1.698 | 13,699 | 0.73 | 1.32345 | |
| 1.676 | 13,514 | 0.74 | 1.32335 | |
| 1.653 | 13,333 | 0.75 | 1.32325 | |
| 1.631 | 13,158 | 0.76 | 1.32315 | |
| 1.610 | 12,987 | 0.77 | 1.32306 | |
| 1.590 | 12,821 | 0.78 | 1.32297 | |
| 1.569 | 12,658 | 0.79 | 1.32288 | |
| 1.550 | 12,500 | 0.80 | 1.32280 | |
| | | | 1.317[3] | |
| | | | 1.3227[6] | |
| 1.531 | 12,346 | 0.81 | 1.32272[5] | |
| 1.512 | 12,195 | 0.82 | 1.32264 | |
| 1.494 | 12,048 | 0.83 | 1.32256 | |
| 1.476 | 11,905 | 0.84 | 1.32249 | |
| 1.459 | 11,765 | 0.85 | 1.32242 | |
| 1.442 | 11,628 | 0.86 | 1.32235 | |
| 1.425 | 11,494 | 0.87 | 1.32228 | |
| 1.409 | 11,364 | 0.88 | 1.32222 | |
| 1.393 | 11,236 | 0.89 | 1.32216 | |
| 1.378 | 11,111 | 0.90 | 1.32210 | |
| | | | 1.316[3] | |
| 1.363 | 10,989 | 0.91 | 1.32204[5] | |
| 1.348 | 10,870 | 0.92 | 1.32198 | |
| 1.333 | 10,753 | 0.93 | 1.32192 | |
| 1.319 | 10,638 | 0.94 | 1.32187 | |
| 1.305 | 10,526 | 0.95 | 1.32182 | |
| 1.292 | 10,417 | 0.96 | 1.32177 | |
| 1.278 | 10,309 | 0.97 | 1.32172 | |
| 1.265 | 10,204 | 0.98 | 1.32167 | |
| 1.252 | 10,101 | 0.99 | 1.32162 | |
| 1.240 | 10,000 | 1.00 | 1.32158 | |
| | | | 1.316[3] | |
| 1.228 | 9,901 | 1.01 | 1.32154[5] | |
| 1.216 | 9,804 | 1.02 | 1.32150 | |
| 1.204 | 9,709 | 1.03 | 1.32146 | |
| 1.192 | 9,615 | 1.04 | 1.32142 | |
| 1.181 | 9,524 | 1.05 | 1.32138 | |
| 1.170 | 9,434 | 1.06 | 1.32134 | |
| 1.159 | 9,346 | 1.07 | 1.32130 | |
| 1.148 | 9,259 | 1.08 | 1.32126 | |
| 1.138 | 9,174 | 1.09 | 1.32122 | |

(continued)

TABLE I (*Continued*)

**Sodium Fluoride**

| eV | $cm^{-1}$ | μm | n | k |
|---|---|---|---|---|
| 1.127 | 9,091 | 1.10 | 1.32118 | |
| 0.9763 | 7,874 | 1.27 | 1.3202[6] | |
| 0.8378 | 6,757 | 1.48 | 1.320 | |
| 0.8266 | 6,667 | 1.5 | 1.314[3] | |
| 0.7424 | 5,988 | 1.67 | 1.318[6] | |
| 0.6775 | 5,464 | 1.83 | 1.318 | |
| 0.6199 | 5,000 | 2.0 | 1.318 | |
| | | | 1.313[3] | |
| 0.4769 | 3,846 | 2.6 | 1.316[6] | |
| 0.4000 | 3,226 | 3.1 | 1.313 | |
| 0.3543 | 2,857 | 3.5 | 1.313 | |
| 0.3024 | 2,499 | 4.1 | 1.308 | |
| 0.2755 | 2,222 | 4.5 | 1.306 | |
| 0.2431 | 1,961 | 5.1 | 1.301 | |
| 0.2254 | 1,818 | 5.5 | 1.298 | |
| 0.2033 | 1,639 | 6.1 | 1.292 | |
| 0.1908 | 1,539 | 6.5 | 1.288 | |
| 0.1746 | 1,409 | 7.1 | 1.282 | |
| 0.1653 | 1,333 | 7.5 | 1.277 | $5x10^{-6}$[6] |
| 0.1550 | 1,250 | 8.0 | 1.271 | $1x10^{-5}$ |
| 0.1459 | 1,177 | 8.5 | 1.264 | 1.7 |
| 0.1378 | 1,111 | 9.0 | 1.262 | 2.3 |
| 0.1305 | 1,053 | 9.5 | 1.249 | 3.3 |
| 0.1240 | 1,000 | 10.0 | 1.241 | 4.3 |
| 0.1181 | 952.4 | 10.5 | 1.231 | 6.4 |
| 0.1127 | 909.1 | 11.0 | 1.214 | $9.6x10^{-5}$ |
| 0.1078 | 869.6 | 11.5 | 1.20 | $1.5x10^{-4}$ |
| 0.1033 | 833.3 | 12.0 | 1.19 | 2.1 |
| 0.09919 | 800.0 | 12.5 | 1.18 | 3.2 |
| 0.09538 | 769.2 | 13.0 | 1.17 | 4.7 |
| 0.09184 | 740.7 | 13.5 | 1.15 | 6.0 |
| 0.08856 | 714.3 | 14.0 | 1.14 | 7.9 |
| 0.08551 | 689.7 | 14.5 | 1.12 | $9.9x10^{-4}$ |
| 0.08266 | 666.7 | 15.0 | 1.10 | $1.3x10^{-3}$ |
| 0.08000 | 645.2 | 15.5 | 1.09 | 1.6 |
| 0.07749 | 625.0 | 16.0 | 1.07 | 2.2 |
| 0.07514 | 606.1 | 16.5 | 1.04 | 3.2 |
| 0.07293 | 588.2 | 17.0 | 1.02 | 4.7 |
| 0.07085 | 571.4 | 17.5 | 0.99 | 6.5 |
| 0.06888 | 555.6 | 18.0 | 0.97 | 8.7 |
| 0.06702 | 540.5 | 18.5 | 0.94 | $8.7x10^{-3}$ |
| 0.06526 | 526.3 | 19.0 | 0.91 | 0.013 |
| 0.06358 | 512.8 | 19.5 | 0.87 | 0.019 |
| 0.06199 | 500.0 | 20.0 | 0.80 | 0.028 |
| 0.06048 | 487.8 | 20.5 | 0.80 | 0.036 |
| 0.05904 | 476.2 | 21.0 | 0.70 | 0.047 |

(continued)

TABLE I (*Continued*)

**Sodium Fluoride**

| eV | $cm^{-1}$ | μm | n | k |
|---|---|---|---|---|
| 0.05889 | 475 | 21.05 | 0.691[7] | 0.102[7] |
| 0.05827 | 470 | 21.28 | 0.678 | 0.122 |
| 0.05765 | 465 | 21.51 | 0.646 | 0.116 |
| | | | 0.70[6] | 0.06[6] |
| 0.05703 | 460 | 21.74 | 0.616[7] | 0.136[7] |
| 0.05641 | 455 | 21.98 | 0.577 | 0.153 |
| | | | 0.60[6] | 0.075[6] |
| 0.05517 | 445 | 22.47 | 0.491[7] | 0.139[7] |
| | | | 0.50[6] | 0.115[6] |
| 0.05455 | 440 | 22.73 | 0.446[7] | 0.147[7] |
| 0.05393 | 435 | 22.99 | 0.43 | 0.201 |
| | | | 0.30[6] | 0.140[6] |
| 0.05331 | 430 | 23.26 | 0.405[7] | 0.227[7] |
| 0.05269 | 425 | 23.53 | 0.347 | 0.254 |
| | | | 0.30[6] | 0.196[6] |
| 0.05208 | 420 | 23.81 | 0.301[7] | 0.296[7] |
| 0.05166 | 416.7 | 24.0 | 0.20[6] | 0.258[6] |
| 0.05146 | 415 | 24.10 | 0.248[7] | 0.339[7] |
| 0.05084 | 410 | 24.39 | 0.215 | 0.400 |
| 0.05022 | 405 | 24.69 | 0.185 | 0.472 |
| 0.04960 | 400 | 25.00 | 0.158 | 0.545 |
| 0.04898 | 395 | 25.32 | 0.174 | 0.622 |
| 0.04836 | 390 | 25.64 | 0.198 | 0.679 |
| 0.04774 | 385 | 25.97 | 0.228 | 0.762 |
| 0.04712 | 380 | 26.32 | 0.266 | 0.825 |
| 0.04650 | 375 | 26.67 | 0.303 | 0.855 |
| 0.04588 | 370 | 27.03 | 0.282 | 0.864 |
| 0.04526 | 365 | 27.40 | 0.159 | 0.968 |
| 0.04464 | 360 | 27.78 | 0.26 | 1.00 |
| 0.04402 | 355 | 28.17 | 0.25 | 1.04 |
| 0.04340 | 350 | 28.57 | 0.24 | 1.05 |
| 0.04278 | 345 | 28.99 | 0.21 | 1.12 |
| 0.04216 | 340 | 29.41 | 0.18 | 1.20 |
| 0.04154 | 335 | 29.85 | 0.16 | 1.29 |
| 0.04092 | 330 | 30.30 | 0.16 | 1.39 |
| 0.04030 | 325 | 30.77 | 0.15 | 1.49 |
| 0.03968 | 320 | 31.25 | 0.14 | 1.57 |
| 0.03906 | 315 | 31.75 | 0.14 | 1.65 |
| 0.03844 | 310 | 32.26 | 0.14 | 1.77 |
| 0.00782 | 305 | 32.79 | 0.16 | 1.92 |
| 0.03720 | 300 | 33.33 | 0.17 | 2.04 |
| 0.03658 | 295 | 33.90 | 0.19 | 2.17 |
| 0.03596 | 290 | 34.48 | 0.21 | 2.33 |
| 0.03534 | 285 | 35.10 | 0.24 | 2.52 |
| 0.03472 | 280 | 35.71 | 0.27 | 2.71 |
| 0.03447 | 278 | 35.97 | 0.29 | 2.81 |

(continued)

TABLE I (*Continued*)

Sodium Fluoride

| eV | $cm^{-1}$ | μm | n | k |
|---|---|---|---|---|
| 0.03422 | 276 | 36.23 | 0.31 | 2.93 |
| 0.03397 | 274 | 36.50 | 0.32 | 2.96 |
| 0.03372 | 272 | 36.77 | 0.36 | 3.02 |
| 0.03348 | 270 | 37.04 | 0.40 | 3.12 |
| 0.03323 | 268 | 37.31 | 0.43 | 3.29 |
| 0.03298 | 266 | 37.59 | 0.50 | 3.51 |
| 0.03273 | 264 | 37.88 | 0.56 | 3.69 |
| 0.03248 | 262 | 38.17 | 0.62 | 3.88 |
| 0.03224 | 260 | 38.46 | 0.64 | 3.99 |
| 0.03199 | 258 | 38.76 | 0.72 | 4.24 |
| 0.03174 | 256 | 39.06 | 0.81 | 4.52 |
| 0.03149 | 254 | 39.37 | 0.97 | 4.71 |
| 0.03125 | 252 | 39.68 | 1.50 | 5.26 |
| 0.03100 | 250 | 40.00 | 3.39 | 6.95 |
| 0.03075 | 248 | 40.32 | 8.69 | 7.90 |
| 0.03050 | 246 | 40.65 | 13.23 | 4.74 |
| 0.03025 | 244 | 40.98 | 13.22 | 1.31 |
| 0.03001 | 242 | 41.32 | 11.33 | 1.00 |
| 0.02976 | 240 | 41.68 | 9.91 | 0.69 |
| 0.02951 | 238 | 42.02 | 8.60 | 0.59 |
| 0.02926 | 236 | 42.37 | 7.26 | 0.45 |
| 0.02901 | 234 | 42.74 | 6.36 | 0.31 |
| 0.02877 | 232 | 43.10 | 5.63 | 0.25 |
| 0.02852 | 230 | 43.48 | 5.02 | 0.22 |
| 0.02827 | 228 | 43.86 | 4.78 | 0.21 |
| 0.02790 | 225 | 44.44 | 4.62 | 0.19 |
| 0.02728 | 220 | 45.46 | 4.22 | 0.16 |
| 0.02666 | 215 | 46.51 | 3.95 | 0.14 |
| 0.02604 | 210 | 47.62 | 3.86 | 0.13 |
| 0.02542 | 205 | 48.78 | 3.79 | 0.12 |
| 0.02480 | 200 | 50.00 | 3.67 | 0.12 |
| 0.02418 | 195 | 51.28 | 3.53 | 0.11 |
| 0.02356 | 190 | 52.63 | 3.39 | 0.11 |
| 0.02294 | 185 | 54.05 | 3.26 | 0.11 |
| 0.02232 | 180 | 55.56 | 3.13 | 0.09 |
| 0.02170 | 175 | 57.14 | 3.02 | 0.09 |
| 0.02108 | 170 | 58.82 | 2.95 | 0.09 |
| 0.02046 | 165 | 60.61 | 2.89 | 0.09 |
| 0.01984 | 160 | 62.50 | 2.84 | 0.09 |
| 0.01860 | 150 | 66.67 | 2.75 | 0.09 |
| 0.01736 | 140 | 71.43 | 2.68 | 0.09 |
| 0.01612 | 130 | 76.92 | 2.61 | 0.11 |
| 0.01488 | 120 | 83.33 | 2.56 | 0.10 |
| 0.01364 | 110 | 90.91 | 2.53 | 0.09 |
| 0.01240 | 100 | 100.0 | 2.50 | 0.07 |
| 0.01116 | 90 | 111.1 | 2.46 | 0.06 |

[a]The references from which the values were extracted are given in brackets.

# Strontium Titanate ($SrTiO_3$)

FRANÇOIS GERVAIS
Centre de Recherches sur la Physique des Hautes Températures
Centre National de la Recherche Scientifique
45071 Orléans, France

Strontium titanate crystallizes in the cubic perovskite structure. Optical properties are therefore isotropic. Strontium titanate behaves like a ferroelectric material in the paraelectric phase. This property is referred to as *incipient ferroelectric*. The hypothetical Curie temperature would take place just below the absolute-zero temperature. As a result, the dielectric constant is strongly dependent on temperature and increases by a factor as large as 10 when the sample is cooled from room temperature to liquid-helium temperature [1]. Since the dielectric constant is the extrapolation down to zero frequency of the dielectric response, which itself is the square of the complex refractive index, optical constants also vary with temperature, but mainly in the far infrared. In addition, a phase transition related to alternate tilt of oxygen octahedra, which results in the formation of a tetragonal structure, takes place upon cooling below 105 K. The temperature dependence of data related to optical constants has been studied in various references; see Refs. [2, 3] for the UV range, Refs. [4, 5] in the visible and Refs. [6, 7] in the infrared.

Doping with $Nb^{5+}$ or reduction of strontium titanate confers semiconducting properties to the material. Then the absorption related to free carriers may drastically modify the optical constants in the infrared depending on doping level [8]. Note also that heavily doped *n*-type strontium titanate has been reported to become a superconductor below 0.7 K [9].

All data compiled in Table I and Fig. 1 were obtained by measurements on undoped single crystals at room temperature. It should also be noted that in the infrared range, the reflectivity measurements performed on a sintered and polished strontium-titanate ceramic sample are practically indistinguishable from those performed on a single crystal [10], so that data compiled here, all obtained from studies on single crystals, are valid for ceramics also.

Reflectivity measurements in the ultraviolet energy range have been performed by various authors [11–14]. Among those studies, the one that


Copyright © 1991 by Academic Press.
All rights of reproduction in any form reserved.
ISBN 0-12-544422-2

extends over the widest energy range is the one by Baüerle *et al.* [13], thus allowing a Kramers–Kronig analysis of reflectivity data. Results of such an analysis are reported in Ref. [13] and reproduced in Table I. No $n$, $k$ data were deduced from the experiments in other papers, but reflectance spectra shown in the three papers are in good agreement. Measurements of Ref. [13] were performed with the polarized synchrotron light from the storage ring DORIS at Hamburg coupled with a high-resolution monochromator.

The index of refraction in the transparent region is reported in Ref. [11] for wavelengths between 0.4 and 1.1 μm. They are in agreement with earlier measurements of Ref. [15], which were limited to a narrower wavelength range. Results of Ref. [11] determined by the angle-of-minimum-deviation method are given in Table I.

Early infrared reflectivity measurements of strontium titanate were reported by Barker and Tinkham [6]. The resolution of their measurement was not sufficient to detect a narrow infrared band observed three months later by Spitzer *et al.* [16] near 175 $cm^{-1}$, also with a prism monochromator. Spitzer *et al.* showed the failure of the usual dielectric function model,

$$\varepsilon = \varepsilon_\infty + \sum_j \Delta\varepsilon_j \frac{\Omega_{j\mathrm{TO}}^2}{\Omega_{j\mathrm{TO}}^2 - \omega^2 + i\gamma_{j\mathrm{TO}}\omega}, \tag{1}$$

expressed in terms of a sum over all the polar modes of the contributions of individual transverse optic modes, to fit the spectrum of strontium titanate. Later, Barker and Hopfield [17] introduced a mode-coupling formalism to fit the spectra of such highly polar incipient ferroelectric or ferroelectric crystals. An alternative model based on the factorized form of the dielectric response,

$$\varepsilon = \varepsilon_\infty \prod_j \frac{\Omega_{j\mathrm{LO}}^2 - \omega^2 + i\gamma_{j\mathrm{LO}}\omega}{\Omega_{j\mathrm{TO}}^2 - \omega^2 + i\gamma_{j\mathrm{TO}}\omega}, \tag{2}$$

was proposed subsequently [7] to palliate the weakness of the classical dielectric constant formula (Eq. 1) in such cases. The authors of this analysis also remeasured the infrared reflectivity spectrum with a modern Fourier-transform wide-band infrared spectrometer. Results for $n$ and $k$ obtained from a Kramers–Kronig analysis of data of Ref. [16] and from Ref. [7] by best fit of Eq. 2 to reflectivity data are compared in Table I. Both sets of data agree reasonably well.

## REFERENCES


1. T. Mitsui and W. B. Westphal, *Phys. Rev.* **124**, 1354 (1961).
2. M. Capizzi and A. Frova, *Phys. Rev. Lett.* **25**, 1298 (1970).
3. K. W. Blazey, *Phys. Rev. Lett.* **27**, 146 (1971).
4. E. Schneider, P. J. Cressman, and R. L. Holman, *J. Appl. Phys.* **53**, 4054 (1982).
5. T. Toyoda and M. Yabe, *J. Phys. D: Appl. Phys.* **16**, L251 (1983).
6. A. S. Barker and M. Tinkham, *Phys. Rev.* **125**, 1527 (1962).
7. J. L. Servoin, Y. Luspin, and F. Gervais, *Phys. Rev. B* **22**, 5501 (1980).
8. W. S. Baer, *Phys. Rev.* **144**, 734 (1966).
9. F. F. Schooley, W. R. Hosler, and M. L. Cohen, *Phys. Rev. Letters* **12**, 474 (1964).
10. F. Gervais, B. Calès, and P. Odier, *Mat. Res. Bull.* **22**, 1629 (1987).
11. M. Cardona, *Phys. Rev.* **140**, A651 (1965).
12. M. I. Cohen and R. F. Blunt, *Phys. Rev.* **168**, 929 (1968).
13. D. Baüerle, W. Braun, V. Saile, G. Sprüssel, and E. E. Koch, *Z. Physik B* **29**, 179 (1978).
14. A. M. Mamedov, *Ferroelectrics* **45**, 55 (1982).
15. S. B. Levin, N. J. Field, F. M. Plock, and L. Merker, *J. Opt. Soc. Am.* **45**, 737 (1955).
16. W. G. Spitzer, R. C. Miller, D. A. Kleinman and L. E. Howarth, *Phys. Rev.* **126**, 1710 (1962).
17. A. S. Barker and J. J. Hopfield, *Phys. Rev.* **135**, A1732 (1964).


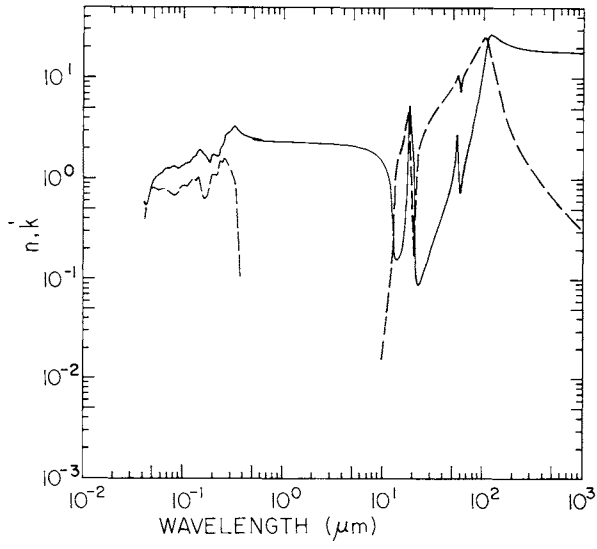


**Fig. 1.** Log–log plot of $n$ (solid line) and $k$ (dashed line) versus wavelength in micrometers for strontium titanate.

**TABLE I**

**Values of $n$ and $k$ for Strontium Titanate Obtained from Various References[a]**

| eV | $cm^{-1}$ | μm | n | k | n | k |
|---|---|---|---|---|---|---|
| 30.0 | 241,935 | 0.04133 | 0.574[13] | 0.383[13] | | |
| 29.9 | 241,129 | 0.04147 | 0.568 | 0.392 | | |
| 29.8 | 240,323 | 0.04161 | 0.563 | 0.404 | | |
| 29.7 | 239,516 | 0.04175 | 0.558 | 0.416 | | |
| 29.6 | 238,710 | 0.04189 | 0.553 | 0.427 | | |
| 29.5 | 237,903 | 0.04203 | 0.549 | 0.442 | | |
| 29.4 | 237,097 | 0.04218 | 0.547 | 0.460 | | |
| 29.3 | 236,290 | 0.04232 | 0.548 | 0.477 | | |
| 29.2 | 235,484 | 0.04247 | 0.548 | 0.494 | | |
| 29.1 | 234,677 | 0.04261 | 0.550 | 0.510 | | |
| 29.0 | 233,871 | 0.04276 | 0.552 | 0.525 | | |
| 28.9 | 233,065 | 0.04291 | 0.554 | 0.541 | | |
| 28.8 | 232,258 | 0.04305 | 0.557 | 0.557 | | |
| 28.7 | 231,452 | 0.04321 | 0.565 | 0.572 | | |
| 28.6 | 230,645 | 0.04336 | 0.572 | 0.584 | | |
| 28.5 | 229,839 | 0.04351 | 0.580 | 0.597 | | |
| 28.4 | 229,032 | 0.04365 | 0.587 | 0.609 | | |
| 28.3 | 228,226 | 0.04382 | 0.595 | 0.621 | | |
| 28.2 | 227,419 | 0.04397 | 0.603 | 0.634 | | |
| 28.1 | 226,613 | 0.04413 | 0.612 | 0.645 | | |
| 28.0 | 225,806 | 0.04429 | 0.620 | 0.655 | | |
| 27.9 | 225,000 | 0.04444 | 0.629 | 0.665 | | |
| 27.8 | 224,194 | 0.04460 | 0.638 | 0.674 | | |
| 27.7 | 223,387 | 0.04477 | 0.646 | 0.684 | | |
| 27.6 | 222,581 | 0.04493 | 0.656 | 0.694 | | |
| 27.5 | 221,774 | 0.04509 | 0.670 | 0.703 | | |
| 27.4 | 220,968 | 0.04526 | 0.683 | 0.712 | | |
| 27.3 | 220,161 | 0.04542 | 0.697 | 0.720 | | |
| 27.2 | 219,355 | 0.04559 | 0.710 | 0.728 | | |
| 27.1 | 218,548 | 0.04576 | 0.723 | 0.736 | | |
| 27.0 | 217,742 | 0.04593 | 0.736 | 0.744 | | |
| 26.9 | 216,935 | 0.04610 | 0.747 | 0.752 | | |
| 26.8 | 216,129 | 0.04627 | 0.759 | 0.760 | | |
| 26.7 | 215,323 | 0.04644 | 0.770 | 0.768 | | |
| 26.6 | 214,516 | 0.04662 | 0.782 | 0.774 | | |
| 26.5 | 213,710 | 0.04679 | 0.793 | 0.779 | | |
| 26.4 | 212,903 | 0.04697 | 0.805 | 0.784 | | |
| 26.3 | 212,097 | 0.04715 | 0.817 | 0.789 | | |
| 26.2 | 211,290 | 0.04733 | 0.828 | 0.794 | | |
| 26.1 | 210,484 | 0.04751 | 0.838 | 0.799 | | |
| 26.0 | 209,677 | 0.04769 | 0.845 | 0.802 | | |
| 25.9 | 208,871 | 0.04788 | 0.853 | 0.804 | | |
| 25.8 | 208,065 | 0.04806 | 0.860 | 0.805 | | |
| 25.7 | 207,258 | 0.04825 | 0.868 | 0.807 | | |
| 25.6 | 206,452 | 0.04844 | 0.875 | 0.809 | | |
| 25.5 | 205,645 | 0.04863 | 0.883 | 0.811 | | |
| 25.4 | 204,839 | 0.04882 | 0.890 | 0.809 | | |
| 25.3 | 204,032 | 0.04901 | 0.900 | 0.806 | | |
| 25.2 | 203,226 | 0.04921 | 0.911 | 0.803 | | |
| 25.1 | 202,419 | 0.04940 | 0.921 | 0.800 | | |

**TABLE I (*Continued*)**

**Strontium Titanate**

| eV | $cm^{-1}$ | μm | n | k | n | k |
|---|---|---|---|---|---|---|
| 25.0 | 201,613 | 0.04960 | 0.932 | 0.797 | | |
| 24.9 | 200,806 | 0.04980 | 0.942 | 0.794 | | |
| 24.8 | 200,000 | 0.05000 | 0.944 | 0.792 | | |
| 24.7 | 199,194 | 0.05020 | 0.944 | 0.791 | | |
| 24.6 | 198,387 | 0.05041 | 0.943 | 0.789 | | |
| 24.5 | 197,581 | 0.05061 | 0.943 | 0.788 | | |
| 24.4 | 196,774 | 0.05082 | 0.949 | 0.789 | | |
| 24.3 | 195,968 | 0.05103 | 0.956 | 0.794 | | |
| 24.2 | 195,161 | 0.05124 | 0.963 | 0.800 | | |
| 24.1 | 194,355 | 0.05145 | 0.969 | 0.806 | | |
| 24.0 | 193,548 | 0.05167 | 0.984 | 0.810 | | |
| 23.9 | 192,742 | 0.05188 | 0.998 | 0.808 | | |
| 23.8 | 191,935 | 0.05210 | 1.013 | 0.806 | | |
| 23.7 | 191,129 | 0.05232 | 1.022 | 0.803 | | |
| 23.6 | 190,323 | 0.05254 | 1.026 | 0.801 | | |
| 23.5 | 189,516 | 0.05277 | 1.029 | 0.798 | | |
| 23.4 | 188,710 | 0.05299 | 1.033 | 0.796 | | |
| 23.3 | 187,903 | 0.05322 | 1.037 | 0.793 | | |
| 23.2 | 187,097 | 0.05345 | 1.041 | 0.791 | | |
| 23.1 | 186,290 | 0.05368 | 1.046 | 0.788 | | |
| 23.0 | 185,484 | 0.05391 | 1.051 | 0.786 | | |
| 22.9 | 184,677 | 0.05415 | 1.056 | 0.783 | | |
| 22.8 | 183,871 | 0.05439 | 1.061 | 0.781 | | |
| 22.7 | 183,065 | 0.05463 | 1.064 | 0.779 | | |
| 22.6 | 182,258 | 0.05487 | 1.067 | 0.777 | | |
| 22.5 | 181,452 | 0.05511 | 1.070 | 0.775 | | |
| 22.4 | 180,645 | 0.05536 | 1.073 | 0.774 | | |
| 22.3 | 179,839 | 0.05561 | 1.076 | 0.773 | | |
| 22.2 | 179,032 | 0.05586 | 1.079 | 0.771 | | |
| 22.1 | 178,226 | 0.05611 | 1.082 | 0.770 | | |
| 22.0 | 177,419 | 0.05636 | 1.085 | 0.769 | | |
| 21.9 | 176,613 | 0.05662 | 1.088 | 0.767 | | |
| 21.8 | 175,806 | 0.05688 | 1.091 | 0.766 | | |
| 21.7 | 175,000 | 0.05714 | 1.095 | 0.766 | | |
| 21.6 | 174,194 | 0.05741 | 1.098 | 0.767 | | |
| 21.5 | 173,387 | 0.05767 | 1.101 | 0.768 | | |
| 21.4 | 172,581 | 0.05794 | 1.104 | 0.769 | | |
| 21.3 | 171,774 | 0.05822 | 1.107 | 0.770 | | |
| 21.2 | 170,968 | 0.05849 | 1.111 | 0.772 | | |
| 21.1 | 170,161 | 0.05877 | 1.114 | 0.773 | | |
| 21.0 | 169,355 | 0.05905 | 1.117 | 0.773 | | |
| 20.9 | 168,548 | 0.05933 | 1.122 | 0.774 | | |
| 20.8 | 167,742 | 0.05962 | 1.127 | 0.774 | | |
| 20.7 | 166,935 | 0.05990 | 1.132 | 0.775 | | |
| 20.6 | 166,129 | 0.06019 | 1.137 | 0.775 | | |
| 20.5 | 165,323 | 0.06049 | 1.142 | 0.776 | | |
| 20.4 | 164,516 | 0.06078 | 1.148 | 0.776 | | |
| 20.3 | 163,710 | 0.06108 | 1.153 | 0.777 | | |
| 20.2 | 162,903 | 0.06139 | 1.158 | 0.777 | | |
| 20.1 | 162,097 | 0.06169 | 1.163 | 0.778 | | |

**TABLE I (*Continued*)**

**Strontium Titanate**

| eV | $cm^{-1}$ | μm | n | k | n | k |
|---|---|---|---|---|---|---|
| 20.0 | 161,290 | 0.06200 | 1.169 | 0.778 | | |
| 19.9 | 160,484 | 0.06231 | 1.175 | 0.779 | | |
| 19.8 | 159,677 | 0.06263 | 1.180 | 0.779 | | |
| 19.7 | 158,871 | 0.06294 | 1.186 | 0.781 | | |
| 19.6 | 158,065 | 0.06327 | 1.192 | 0.784 | | |
| 19.5 | 157,258 | 0.06359 | 1.198 | 0.787 | | |
| 19.4 | 156,452 | 0.06392 | 1.203 | 0.790 | | |
| 19.3 | 155,645 | 0.06425 | 1.209 | 0.793 | | |
| 19.2 | 154,839 | 0.06458 | 1.215 | 0.793 | | |
| 19.1 | 154,032 | 0.06492 | 1.220 | 0.792 | | |
| 19.0 | 153,226 | 0.06526 | 1.226 | 0.790 | | |
| 18.9 | 152,419 | 0.06561 | 1.231 | 0.787 | | |
| 18.8 | 151,613 | 0.06596 | 1.237 | 0.783 | | |
| 18.7 | 150,806 | 0.06631 | 1.243 | 0.780 | | |
| 18.6 | 150,000 | 0.06667 | 1.248 | 0.776 | | |
| 18.5 | 149,194 | 0.06703 | 1.250 | 0.769 | | |
| 18.4 | 148,387 | 0.06739 | 1.252 | 0.763 | | |
| 18.3 | 147,581 | 0.06776 | 1.254 | 0.756 | | |
| 18.2 | 146,774 | 0.06813 | 1.256 | 0.750 | | |
| 18.1 | 145,968 | 0.06851 | 1.258 | 0.746 | | |
| 18.0 | 145,161 | 0.06889 | 1.260 | 0.742 | | |
| 17.9 | 144,355 | 0.06927 | 1.262 | 0.737 | | |
| 17.8 | 143,548 | 0.06966 | 1.264 | 0.733 | | |
| 17.7 | 142,742 | 0.07006 | 1.266 | 0.729 | | |
| 17.6 | 141,935 | 0.07045 | 1.268 | 0.724 | | |
| 17.5 | 141,129 | 0.07086 | 1.270 | 0.720 | | |
| 17.4 | 140,323 | 0.07126 | 1.272 | 0.718 | | |
| 17.3 | 139,516 | 0.07168 | 1.274 | 0.715 | | |
| 17.2 | 138,710 | 0.07209 | 1.275 | 0.712 | | |
| 17.1 | 137,903 | 0.07251 | 1.277 | 0.709 | | |
| 17.0 | 137,097 | 0.07294 | 1.279 | 0.707 | | |
| 16.9 | 136,290 | 0.07337 | 1.280 | 0.706 | | |
| 16.8 | 135,484 | 0.07381 | 1.280 | 0.705 | | |
| 16.7 | 134,677 | 0.07425 | 1.281 | 0.704 | | |
| 16.6 | 133,871 | 0.07470 | 1.281 | 0.704 | | |
| 16.5 | 133,065 | 0.07515 | 1.282 | 0.704 | | |
| 16.4 | 132,258 | 0.07561 | 1.288 | 0.705 | | |
| 16.3 | 131,452 | 0.07607 | 1.297 | 0.707 | | |
| 16.2 | 130,645 | 0.07654 | 1.306 | 0.709 | | |
| 16.1 | 129,839 | 0.07702 | 1.316 | 0.710 | | |
| 16.0 | 129,032 | 0.07750 | 1.320 | 0.705 | | |
| 15.9 | 128,226 | 0.07799 | 1.321 | 0.699 | | |
| 15.8 | 127,419 | 0.07848 | 1.322 | 0.692 | | |
| 15.7 | 126,613 | 0.07898 | 1.324 | 0.686 | | |
| 15.6 | 125,806 | 0.07949 | 1.322 | 0.679 | | |
| 15.5 | 125,000 | 0.08000 | 1.317 | 0.672 | | |
| 15.4 | 124,194 | 0.08052 | 1.312 | 0.665 | | |
| 15.3 | 123,387 | 0.08105 | 1.306 | 0.657 | | |
| 15.2 | 122,581 | 0.08158 | 1.297 | 0.652 | | |
| 15.1 | 121,774 | 0.08212 | 1.288 | 0.651 | | |

**TABLE I (*Continued*)**

**Strontium Titanate**

| eV | $cm^{-1}$ | μm | n | k | n | k |
|---|---|---|---|---|---|---|
| 15.0 | 120,968 | 0.08267 | 1.279 | 0.652 | | |
| 14.9 | 120,161 | 0.08322 | 1.270 | 0.658 | | |
| 14.8 | 119,355 | 0.08378 | 1.261 | 0.663 | | |
| 14.7 | 118,548 | 0.08434 | 1.254 | 0.669 | | |
| 14.6 | 117,742 | 0.08493 | 1.246 | 0.674 | | |
| 14.5 | 116,935 | 0.08552 | 1.238 | 0.680 | | |
| 14.4 | 116,129 | 0.08611 | 1.230 | 0.689 | | |
| 14.3 | 115,323 | 0.08671 | 1.228 | 0.702 | | |
| 14.2 | 114,516 | 0.08732 | 1.227 | 0.716 | | |
| 14.1 | 113,710 | 0.08794 | 1.226 | 0.729 | | |
| 14.0 | 112,903 | 0.08857 | 1.229 | 0.741 | | |
| 13.9 | 112,097 | 0.08921 | 1.234 | 0.751 | | |
| 13.8 | 111,290 | 0.08986 | 1.241 | 0.762 | | |
| 13.7 | 110,484 | 0.09051 | 1.250 | 0.773 | | |
| 13.6 | 109,677 | 0.09118 | 1.259 | 0.783 | | |
| 13.5 | 108,871 | 0.09185 | 1.268 | 0.792 | | |
| 13.4 | 108,065 | 0.09254 | 1.276 | 0.801 | | |
| 13.3 | 107,258 | 0.09323 | 1.287 | 0.810 | | |
| 13.2 | 106,452 | 0.09394 | 1.300 | 0.816 | | |
| 13.1 | 105,645 | 0.09466 | 1.312 | 0.820 | | |
| 13.0 | 104,839 | 0.09538 | 1.325 | 0.825 | | |
| 12.9 | 104,032 | 0.09612 | 1.333 | 0.829 | | |
| 12.8 | 103,226 | 0.09687 | 1.341 | 0.833 | | |
| 12.7 | 102,419 | 0.09764 | 1.349 | 0.835 | | |
| 12.6 | 101,613 | 0.09841 | 1.352 | 0.836 | | |
| 12.5 | 100,806 | 0.09920 | 1.354 | 0.838 | | |
| 12.4 | 100,000 | 0.1000 | 1.356 | 0.840 | | |
| 12.3 | 99,194 | 0.1008 | 1.362 | 0.843 | | |
| 12.2 | 98,387 | 0.1016 | 1.368 | 0.846 | | |
| 12.1 | 97,581 | 0.1025 | 1.374 | 0.850 | | |
| 12.0 | 96,774 | 0.1033 | 1.380 | 0.853 | | |
| 11.9 | 95,968 | 0.1042 | 1.386 | 0.855 | | |
| 11.8 | 95,161 | 0.1051 | 1.402 | 0.858 | | |
| 11.7 | 94,355 | 0.1060 | 1.418 | 0.860 | | |
| 11.6 | 93,548 | 0.1069 | 1.432 | 0.859 | | |
| 11.5 | 92,742 | 0.1078 | 1.445 | 0.854 | | |
| 11.4 | 91,935 | 0.1088 | 1.447 | 0.849 | | |
| 11.3 | 91,129 | 0.1097 | 1.428 | 0.845 | | |
| 11.2 | 90,323 | 0.1107 | 1.422 | 0.842 | | |
| 11.1 | 89,516 | 0.1117 | 1.425 | 0.849 | | |
| 11.0 | 88,710 | 0.1127 | 1.428 | 0.858 | | |
| 10.9 | 87,903 | 0.1138 | 1.430 | 0.867 | | |
| 10.8 | 87,097 | 0.1148 | 1.431 | 0.875 | | |
| 10.7 | 86,290 | 0.1159 | 1.426 | 0.885 | | |
| 10.6 | 85,484 | 0.1170 | 1.417 | 0.899 | | |
| 10.5 | 84,677 | 0.1181 | 1.428 | 0.916 | | |
| 10.4 | 83,871 | 0.1192 | 1.458 | 0.933 | | |
| 10.3 | 83,065 | 0.1204 | 1.480 | 0.948 | | |
| 10.2 | 82,258 | 0.1216 | 1.502 | 0.961 | | |
| 10.1 | 81,452 | 0.1228 | 1.531 | 0.974 | | |

**TABLE I (*Continued*)**

**Strontium Titanate**

| eV | $cm^{-1}$ | μm | n | k | n | k |
|---|---|---|---|---|---|---|
| 10.0 | 80,645 | 0.1240 | 1.563 | 0.989 | | |
| 9.9 | 79,839 | 0.1253 | 1.594 | 1.004 | | |
| 9.8 | 79,032 | 0.1265 | 1.623 | 1.009 | | |
| 9.7 | 78,226 | 0.1278 | 1.653 | 1.008 | | |
| 9.6 | 77,419 | 0.1292 | 1.667 | 1.003 | | |
| 9.5 | 76,613 | 0.1305 | 1.659 | 0.997 | | |
| 9.4 | 75,806 | 0.1319 | 1.643 | 0.984 | | |
| 9.3 | 75,000 | 0.1333 | 1.659 | 0.968 | | |
| 9.2 | 74,194 | 0.1348 | 1.680 | 0.963 | | |
| 9.1 | 73,387 | 0.1363 | 1.700 | 0.977 | | |
| 9.0 | 72,581 | 0.1378 | 1.734 | 1.000 | | |
| 8.9 | 71,774 | 0.1393 | 1.779 | 1.024 | | |
| 8.8 | 70,968 | 0.1409 | 1.828 | 1.015 | | |
| 8.7 | 70,161 | 0.1425 | 1.877 | 1.000 | | |
| 8.6 | 69,355 | 0.1442 | 1.926 | 0.977 | | |
| 8.5 | 68,548 | 0.1459 | 1.951 | 0.928 | | |
| 8.4 | 67,742 | 0.1476 | 1.942 | 0.857 | | |
| 8.3 | 66,935 | 0.1494 | 1.920 | 0.788 | | |
| 8.2 | 66,129 | 0.1512 | 1.893 | 0.727 | | |
| 8.1 | 65,323 | 0.1531 | 1.865 | 0.679 | | |
| 8.0 | 64,516 | 0.1550 | 1.838 | 0.672 | | |
| 7.9 | 63,710 | 0.1570 | 1.808 | 0.666 | | |
| 7.8 | 62,903 | 0.1590 | 1.777 | 0.659 | | |
| 7.7 | 62,097 | 0.1610 | 1.746 | 0.645 | | |
| 7.6 | 61,290 | 0.1632 | 1.715 | 0.631 | | |
| 7.5 | 60,484 | 0.1653 | 1.689 | 0.627 | | |
| 7.4 | 59,677 | 0.1676 | 1.663 | 0.643 | | |
| 7.3 | 58,871 | 0.1699 | 1.637 | 0.660 | | |
| 7.2 | 58,065 | 0.1722 | 1.612 | 0.674 | | |
| 7.1 | 57,258 | 0.1746 | 1.587 | 0.688 | | |
| 7.0 | 56,452 | 0.1771 | 1.563 | 0.703 | | |
| 6.9 | 55,645 | 0.1797 | 1.495 | 0.724 | | |
| 6.8 | 54,839 | 0.1824 | 1.452 | 0.838 | | |
| 6.7 | 54,032 | 0.1851 | 1.438 | 0.878 | | |
| 6.6 | 53,226 | 0.1879 | 1.558 | 0.940 | | |
| 6.5 | 52,419 | 0.1908 | 1.624 | 1.099 | | |
| 6.4 | 51,613 | 0.1937 | 1.688 | 1.106 | | |
| 6.3 | 50,806 | 0.1968 | 1.721 | 1.105 | | |
| 6.2 | 50,000 | 0.2000 | 1.753 | 1.101 | | |
| 6.1 | 49,194 | 0.2033 | 1.768 | 1.095 | | |
| 6.0 | 48,387 | 0.2067 | 1.770 | 1.089 | | |
| 5.9 | 47,581 | 0.2102 | 1.760 | 1.086 | | |
| 5.8 | 46,774 | 0.2138 | 1.745 | 1.086 | | |
| 5.7 | 45,968 | 0.2175 | 1.722 | 1.089 | | |
| 5.6 | 45,161 | 0.2214 | 1.696 | 1.130 | | |
| 5.5 | 44,355 | 0.2255 | 1.664 | 1.269 | | |
| 5.4 | 43,548 | 0.2296 | 1.719 | 1.438 | | |
| 5.3 | 42,742 | 0.2340 | 1.905 | 1.482 | | |
| 5.2 | 41,935 | 0.2385 | 2.025 | 1.484 | | |
| 5.1 | 41,129 | 0.2431 | 2.085 | 1.474 | | |

**TABLE I (*Continued*)**

**Strontium Titanate**

| eV | $cm^{-1}$ | μm | n | k | n | k |
|---|---|---|---|---|---|---|
| 5.0 | 40,323 | 0.2480 | 2.139 | 1.474 | | |
| 4.9 | 39,516 | 0.2531 | 2.218 | 1.552 | | |
| 4.8 | 38,710 | 0.2583 | 2.329 | 1.582 | | |
| 4.7 | 37,903 | 0.2638 | 2.482 | 1.570 | | |
| 4.6 | 37,097 | 0.2696 | 2.731 | 1.517 | | |
| 4.5 | 36,290 | 0.2756 | 2.785 | 1.436 | | |
| 4.4 | 35,484 | 0.2818 | 2.840 | 1.361 | | |
| 4.3 | 34,677 | 0.2884 | 2.909 | 1.277 | | |
| 4.2 | 33,871 | 0.2952 | 2.962 | 1.190 | | |
| 4.1 | 33,065 | 0.3024 | 3.026 | 1.145 | | |
| 4.0 | 32,258 | 0.3100 | 3.158 | 1.100 | | |
| 3.9 | 31,452 | 0.3179 | 3.250 | 1.045 | | |
| 3.8 | 30,645 | 0.3263 | 3.297 | 0.980 | | |
| 3.7 | 29,839 | 0.3351 | 3.320 | 0.854 | | |
| 3.6 | 29,032 | 0.3444 | 3.275 | 0.463 | | |
| 3.5 | 28,226 | 0.3543 | 3.180 | 0.245 | | |
| 3.4 | 27,419 | 0.3647 | 2.974 | 0.164 | | |
| 3.3 | 26,613 | 0.3758 | 2.812 | 0.112 | | |
| 3.2 | 25,806 | 0.3875 | 2.773 | 0.083 | | |
| 3.1 | 25,000 | 0.4000 | 2.745 | 0.058 | | |
| 3.0 | 24,194 | 0.4133 | 2.727 | 0.048 | 2.630[11] | |
| 2.9 | 23,387 | 0.4276 | 2.712 | 0.038 | 2.587 | |
| 2.8 | 22,581 | 0.4429 | 2.669 | 0.028 | 2.558 | |
| 2.7 | 21,774 | 0.4593 | 2.610 | 0.019 | 2.528 | |
| 2.6 | 20,968 | 0.4769 | 2.581 | 0.015 | 2.504 | |
| 2.5 | 20,161 | 0.4960 | 2.552 | 0.011 | 2.481 | |
| 2.4 | 19,355 | 0.5167 | 2.524 | | 2.462 | |
| 2.3 | 18,548 | 0.5391 | 2.495 | | 2.443 | |
| 2.2 | 17,742 | 0.5636 | 2.475 | | 2.426 | |
| 2.1 | 16,935 | 0.5905 | 2.456 | | 2.410 | |
| 2.0 | 16,129 | 0.6200 | 2.437 | | 2.394 | |
| 1.9 | 15,323 | 0.6526 | | | 2.382 | |
| 1.8 | 14,516 | 0.6889 | | | 2.369 | |
| 1.7 | 13,710 | 0.7294 | | | 2.358 | |
| 1.6 | 12,903 | 0.7750 | | | 2.348 | |
| 1.5 | 12,097 | 0.8267 | | | 2.339 | |
| 1.4 | 11,290 | 0.8857 | | | 2.330 | |
| 1.3 | 10,484 | 0.9538 | | | 2.321 | |
| 1.2 | 9,677 | 1.033 | | | 2.312 | |
| 1.1 | 8,871 | 1.127 | | | 2.305 | |
| 1.0 | 8,065 | 1.240 | | | 2.300 | |
| 0.9 | 7,258 | 1.378 | | | 2.291 | |
| 0.8928 | 7,200 | 1.389 | 2.268[7] | | | |
| 0.8804 | 7,100 | 1.408 | 2.268 | | | |
| 0.8680 | 7,000 | 1.429 | 2.267 | | | |
| 0.8556 | 6,900 | 1.449 | 2.267 | | | |
| 0.8432 | 6,800 | 1.471 | 2.267 | | | |
| 0.8308 | 6,700 | 1.493 | 2.266 | | | |
| 0.8184 | 6,600 | 1.515 | 2.266 | | | |
| 0.8060 | 6,500 | 1.538 | 2.265 | | | |

**TABLE I (*Continued*)**

**Strontium Titanate**

| eV | $cm^{-1}$ | μm | n | k | n | k |
|---|---|---|---|---|---|---|
| 0.7936 | 6,400 | 1.563 | 2.265 | | | |
| 0.7812 | 6,300 | 1.587 | 2.264 | | | |
| 0.7688 | 6,200 | 1.613 | 2.264 | | | |
| 0.7564 | 6,100 | 1.639 | 2.263 | | | |
| 0.7440 | 6,000 | 1.667 | 2.263 | | | |
| 0.7316 | 5,900 | 1.695 | 2.262 | | | |
| 0.7192 | 5,800 | 1.724 | 2.261 | | | |
| 0.7068 | 5,700 | 1.754 | 2.261 | | | |
| 0.6944 | 5,600 | 1.786 | 2.260 | | | |
| 0.6820 | 5,500 | 1.818 | 2.259 | | | |
| 0.6696 | 5,400 | 1.852 | 2.259 | | | |
| 0.6572 | 5,300 | 1.887 | 2.258 | | | |
| 0.6448 | 5,200 | 1.923 | 2.257 | | | |
| 0.6324 | 5,100 | 1.961 | 2.256 | | | |
| 0.6200 | 5,000 | 2.000 | 2.255 | | | |
| 0.6076 | 4,900 | 2.041 | 2.254 | | | |
| 0.5952 | 4,800 | 2.083 | 2.253 | | | |
| 0.5828 | 4,700 | 2.128 | 2.251 | | | |
| 0.5704 | 4,600 | 2.174 | 2.250 | | | |
| 0.5580 | 4,500 | 2.222 | 2.249 | | | |
| 0.5456 | 4,400 | 2.273 | 2.247 | | | |
| 0.5332 | 4,300 | 2.326 | 2.246 | | | |
| 0.5208 | 4,200 | 2.381 | 2.244 | | | |
| 0.5084 | 4,100 | 2.439 | 2.242 | | | |
| 0.4960 | 4,000 | 2.500 | 2.240 | | | |
| 0.4836 | 3,900 | 2.564 | 2.238 | | | |
| 0.4712 | 3,800 | 2.632 | 2.236 | | | |
| 0.4588 | 3,700 | 2.703 | 2.233 | | | |
| 0.4464 | 3,600 | 2.778 | 2.231 | | | |
| 0.4340 | 3,500 | 2.857 | 2.228 | | | |
| 0.4216 | 3,400 | 2.941 | 2.225 | | | |
| 0.4092 | 3,300 | 3.030 | 2.221 | | | |
| 0.3968 | 3,200 | 3.125 | 2.217 | | | |
| 0.3844 | 3,100 | 3.226 | 2.213 | | | |
| 0.3720 | 3,000 | 3.333 | 2.209 | | | |
| 0.3596 | 2,900 | 3.448 | 2.203 | | | |
| 0.3472 | 2,800 | 3.571 | 2.198 | | | |
| 0.3348 | 2,700 | 3.704 | 2.191 | | | |
| 0.3224 | 2,600 | 3.846 | 2.184 | | | |
| 0.3100 | 2,500 | 4.000 | 2.176 | | | |
| 0.2976 | 2,400 | 4.167 | 2.167 | | | |
| 0.2852 | 2,300 | 4.348 | 2.156 | | | |
| 0.2728 | 2,200 | 4.545 | 2.144 | | | |
| 0.2604 | 2,100 | 4.762 | 2.130 | | | |
| 0.2480 | 2,000 | 5.000 | 2.114 | | | |
| 0.2356 | 1,900 | 5.263 | 2.095 | | | |
| 0.2232 | 1,800 | 5.556 | 2.072 | | | |
| 0.2108 | 1,700 | 5.882 | 2.045 | | | |
| 0.1984 | 1,600 | 6.250 | 2.012 | | | |
| 0.1860 | 1,500 | 6.667 | 1.971 | | | |

**TABLE I (*Continued*)**

**Strontium Titanate**

| eV | $cm^{-1}$ | μm | n | k | n | k |
|---|---|---|---|---|---|---|
| 0.1736 | 1,400 | 7.143 | 1.919 | | | |
| 0.1612 | 1,300 | 7.692 | 1.853 | | | |
| 0.1488 | 1,200 | 8.333 | 1.764 | | | |
| 0.1364 | 1,100 | 9.091 | 1.640 | | | |
| 0.1240 | 1,000 | 10.00 | 1.455 | 0.016[7] | 1.419[17] | |
| 0.1227 | 990 | 10.10 | 1.432 | 0.018 | 1.395 | |
| 0.1215 | 980 | 10.20 | 1.407 | 0.019 | 1.371 | 0.016[17] |
| 0.1202 | 970 | 10.31 | 1.380 | 0.021 | 1.346 | 0.025 |
| 0.1190 | 960 | 10.42 | 1.353 | 0.023 | 1.327 | 0.033 |
| 0.1178 | 950 | 10.53 | 1.323 | 0.026 | 1.308 | 0.040 |
| 0.1166 | 940 | 10.64 | 1.292 | 0.028 | 1.289 | 0.044 |
| 0.1153 | 930 | 10.75 | 1.259 | 0.031 | 1.268 | 0.039 |
| 0.1141 | 920 | 10.97 | 1.223 | 0.035 | 1.241 | 0.043 |
| 0.1128 | 910 | 10.99 | 1.185 | 0.039 | 1.212 | 0.046 |
| 0.1116 | 900 | 11.11 | 1.144 | 0.043 | 1.183 | 0.030 |
| 0.1104 | 890 | 11.24 | 1.100 | 0.048 | 1.142 | 0.036 |
| 0.1091 | 880 | 11.36 | 1.052 | 0.054 | 1.080 | 0.050 |
| 0.1079 | 870 | 11.49 | 1.000 | 0.061 | 1.031 | 0.060 |
| 0.1066 | 860 | 11.63 | 0.942 | 0.069 | 0.982 | 0.068 |
| 0.1054 | 850 | 11.76 | 0.878 | 0.080 | 0.929 | 0.080 |
| 0.1042 | 840 | 11.90 | 0.805 | 0.093 | 0.880 | 0.089 |
| 0.1029 | 830 | 12.05 | 0.722 | 0.112 | 0.830 | 0.071 |
| 0.1017 | 820 | 12.20 | 0.626 | 0.139 | 0.681 | 0.053 |
| 0.1004 | 810 | 12.35 | 0.512 | 0.182 | 0.594 | 0.117 |
| 0.09920 | 800 | 12.50 | 0.383 | 0.263 | 0.522 | 0.105 |
| 0.09796 | 790 | 12.66 | 0.274 | 0.396 | 0.299 | 0.239 |
| 0.09672 | 780 | 12.82 | 0.215 | 0.545 | 0.217 | 0.397 |
| 0.09548 | 770 | 12.99 | 0.186 | 0.681 | 0.175 | 0.538 |
| 0.09424 | 760 | 13.16 | 0.170 | 0.805 | 0.139 | 0.689 |
| 0.09300 | 750 | 13.33 | 0.161 | 0.921 | 0.134 | 0.821 |
| 0.09176 | 740 | 13.51 | 0.157 | 1.030 | 0.134 | 0.941 |
| 0.09052 | 730 | 13.70 | 0.155 | 1.137 | 0.140 | 1.051 |
| 0.08928 | 720 | 13.89 | 0.155 | 1.241 | 0.146 | 1.155 |
| 0.08804 | 710 | 14.08 | 0.157 | 1.345 | 0.148 | 1.254 |
| 0.08680 | 700 | 14.29 | 0.161 | 1.449 | 0.146 | 1.357 |
| 0.08556 | 690 | 14.49 | 0.166 | 1.555 | 0.146 | 1.468 |
| 0.08432 | 680 | 14.71 | 0.172 | 1.664 | 0.150 | 1.580 |
| 0.08308 | 670 | 14.93 | 0.181 | 1.776 | 0.154 | 1.704 |
| 0.08184 | 660 | 15.15 | 0.191 | 1.894 | 0.172 | 1.833 |
| 0.08060 | 650 | 15.38 | 0.205 | 2.020 | 0.193 | 1.967 |
| 0.07936 | 640 | 15.63 | 0.222 | 2.154 | 0.221 | 2.106 |
| 0.07812 | 630 | 15.87 | 0.243 | 2.301 | 0.253 | 2.255 |
| 0.07688 | 620 | 16.13 | 0.272 | 2.465 | 0.291 | 2.422 |
| 0.07564 | 610 | 16.39 | 0.310 | 2.653 | 0.338 | 2.615 |
| 0.07440 | 600 | 16.67 | 0.364 | 2.873 | 0.405 | 2.849 |
| 0.07316 | 590 | 16.95 | 0.446 | 3.143 | 0.524 | 3.153 |
| 0.07192 | 580 | 17.24 | 0.580 | 3.490 | 0.758 | 3.528 |
| 0.07068 | 570 | 17.54 | 0.831 | 3.966 | 1.200 | 3.943 |
| 0.06944 | 560 | 17.86 | 1.405 | 4.653 | 1.938 | 4.328 |
| 0.06820 | 550 | 18.18 | 3.083 | 5.334 | 3.254 | 4.236 |

**TABLE I (*Continued*)**

**Strontium Titanate**

| eV | $cm^{-1}$ | μm | n | k | n | k |
|---|---|---|---|---|---|---|
| 0.06696 | 540 | 18.52 | 5.333 | 3.250 | 4.663 | 2.963 |
| 0.06572 | 530 | 18.87 | 4.424 | 1.169 | 4.202 | 1.288 |
| 0.06448 | 520 | 19.23 | 3.407 | 0.538 | 3.427 | 0.552 |
| 0.06324 | 510 | 19.61 | 2.669 | 0.307 | 2.724 | 0.427 |
| 0.06200 | 500 | 20.00 | 2.069 | 0.208 | 2.110 | 0.342 |
| 0.06076 | 490 | 20.41 | 1.505 | 0.173 | 1.630 | 0.207 |
| 0.05952 | 480 | 20.83 | 0.847 | 0.217 | 1.079 | 0.224 |
| 0.05828 | 470 | 21.28 | 0.185 | 0.820 | 0.267 | 0.444 |
| 0.05704 | 460 | 21.74 | 0.108 | 1.342 | 0.094 | 1.127 |
| 0.05580 | 450 | 22.22 | 0.090 | 1.690 | 0.087 | 1.510 |
| 0.05456 | 440 | 22.73 | 0.087 | 1.965 | 0.086 | 1.781 |
| 0.05332 | 430 | 23.26 | 0.089 | 2.200 | 0.085 | 2.020 |
| 0.05208 | 420 | 23.81 | 0.094 | 2.412 | 0.089 | 2.231 |
| 0.05084 | 410 | 24.39 | 0.101 | 2.610 | 0.099 | 2.431 |
| 0.04960 | 400 | 25.00 | 0.109 | 2.799 | 0.113 | 2.615 |
| 0.04836 | 390 | 25.64 | 0.119 | 2.983 | 0.126 | 2.791 |
| 0.04712 | 380 | 26.32 | 0.130 | 3.165 | 0.136 | 2.961 |
| 0.04588 | 370 | 27.03 | 0.141 | 3.347 | 0.143 | 3.134 |
| 0.04464 | 360 | 27.78 | 0.154 | 3.532 | 0.150 | 3.314 |
| 0.04340 | 350 | 28.57 | 0.168 | 3.720 | 0.166 | 3.501 |
| 0.04216 | 340 | 29.41 | 0.184 | 3.914 | 0.186 | 3.686 |
| 0.04092 | 330 | 30.30 | 0.201 | 4.115 | 0.202 | 3.870 |
| 0.03968 | 320 | 31.25 | 0.219 | 4.325 | 0.214 | 4.067 |
| 0.03844 | 310 | 32.26 | 0.240 | 4.545 | 0.226 | 4.278 |
| 0.03720 | 300 | 33.33 | 0.264 | 4.777 | 0.247 | 4.503 |
| 0.03596 | 290 | 34.48 | 0.291 | 5.024 | 0.270 | 4.738 |
| 0.03472 | 280 | 35.71 | 0.321 | 5.287 | 0.297 | 4.988 |
| 0.03348 | 270 | 37.04 | 0.356 | 5.569 | 0.326 | 5.256 |
| 0.03224 | 260 | 38.46 | 0.397 | 5.875 | 0.359 | 5.545 |
| 0.03100 | 250 | 40.00 | 0.445 | 6.208 | 0.397 | 5.859 |
| 0.02976 | 240 | 41.67 | 0.503 | 6.574 | 0.440 | 6.204 |
| 0.02852 | 230 | 43.48 | 0.574 | 6.980 | 0.486 | 6.585 |
| 0.02728 | 220 | 45.45 | 0.665 | 7.438 | 0.534 | 7.028 |
| 0.02604 | 210 | 47.62 | 0.787 | 7.964 | 0.597 | 7.565 |
| 0.02480 | 200 | 50.00 | 0.972 | 8.595 | 0.728 | 8.248 |
| 0.02356 | 190 | 52.63 | 1.323 | 9.416 | 1.071 | 9.210 |
| 0.02232 | 180 | 55.56 | 2.750 | 10.69 | 3.220 | 10.99 |
| 0.02108 | 170 | 58.82 | 0.945 | 7.341 | 1.557 | 6.799 |
| 0.01984 | 160 | 62.50 | 0.930 | 10.22 | 0.985 | 9.612 |
| 0.01860 | 150 | 66.67 | 1.363 | 11.71 | 1.265 | 11.08 |
| 0.01736 | 140 | 71.43 | 1.896 | 13.22 | 1.941 | 12.81 |
| 0.01612 | 130 | 76.92 | 2.665 | 15.02 | 2.908 | 14.10 |
| 0.01488 | 120 | 83.33 | 3.934 | 17.32 | 4.429 | 16.25 |
| 0.01364 | 110 | 90.91 | 6.323 | 20.29 | 5.706 | 18.14 |
| 0.01240 | 100 | 100.0 | 11.44 | 23.59 | 10.51 | 21.94 |
| 0.01116 | 90 | 111.1 | 21.09 | 22.91 | 18.89 | 18.57 |
| 0.009920 | 80 | 125.0 | 26.59 | 13.93 | 20.28 | 13.67 |
| 0.008680 | 70 | 142.9 | 24.90 | 7.233 | 21.34 | 9.699 |
| 0.007440 | 60 | 166.7 | 22.47 | 4.133 | 20.44 | 7.169 |
| 0.006200 | 50 | 200.0 | 20.65 | 2.576 | 20.38 | 5.650 |

**TABLE I (*Continued*)**

**Strontium Titanate**

| eV | $cm^{-1}$ | μm | n | k | n | k |
|---|---|---|---|---|---|---|
| 0.004960 | 40 | 250.0 | 19.38 | 1.675 | 20.26 | 3.933 |
| 0.003720 | 30 | 333.3 | 18.52 | 1.087 | 19.90 | 2.320 |
| 0.002480 | 20 | 500.0 | 17.97 | 0.658 | 19.23 | 0.998 |
| 0.001240 | 10 | 1000 | 17.65 | 0.311 | 18.46 | 0.185 |

a References are indicated in brackets.

# Thorium Fluoride ($ThF_4$)

I. OHLÍDAL and K. NAVRÁTIL
Department of Solid State Physics
Faculty of Science
Masaryk University
Kotlářská 2
611 37 Brno, Czechoslovakia

Thorium fluoride possesses desirable optical properties including a broad range of transparency from the UV (0.2 μm) to the mid-IR (12 μm) regions, and low dispersion and low refractive index in the visible. Therefore, this material is widely used to form low-refractive-index thin films in non-absorbing multilayer systems employed for interference devices. For example, $ThF_4$ thin films together with ZnS thin films are utilized for producing interference coatings which can be used as broad-band laser mirrors in the visible [1].

$ThF_4$ is usually evaporated using resistively heated sources. Such $ThF_4$ thin films are soft, chemically very stable, and exhibit medium tensile stress [2]. The structure of the $ThF_4$ films was examined only by Heitmann and Ritter [3] using X-ray analysis. They found that these films were amorphous. However, X-ray analysis is less sensitive for the structure analysis of polycrystalline solids and thin films than methods of the electron analysis [4]. By means of X-ray analysis it is difficult, if not impossible, to reveal microcrystals whose linear dimensions are smaller than about 5 nm [4]. Thus, the results of X-ray analysis obtained by Heitmann and Ritter [3] show that the studied $ThF_4$ films can be amorphous or polycrystalline with very small microcrystals (smaller than about 5 nm in the linear dimensions). These films have optical properties, which are dependent on a number of effects:

(1) the columnar structure, and hence, the distribution of voids or low-density regions in the film

(2) the orientation of these columns with respect to the substrate normal and their dimensions

(3) environmental stability connected with capillary condensation taking place into the open voids (sometimes called pores)


Copyright © 1991 by Academic Press.
All rights of reproduction in any form reserved.
ISBN 0-12-544422-2

(4) the form of the columns and their variation with thickness, implying inhomogeneity of the film
(5) stress in the film, and hence, birefrigence and inhomogeneity
(6) surface roughness of the upper boundary of the film.

The most important of these effects is the columnar structure. The other effects are implied in principle by this structure (except the existence of the stress in the film). Thus, to describe in a true way, the optical properties of the $ThF_4$ and similar films, one has to express the optical constants of these films with formulas representing their columnar structure in a satisfactory manner. So far, this task has been solved primarily by using suitable formulas for the optical constants of the columnar films based on effective-medium theory [5–8]. For example, within this theory the following formula is often employed for evaluating the mean refractive index $\bar{n}$ of the film considered:

$$p\frac{n_s^2-\bar{n}^2}{n_s^2+2\bar{n}^2}+(1-p)\frac{n_v^2-\bar{n}^2}{n_v^2+2\bar{n}^2}=0, \tag{1}$$

where $n_s$ and $n_v$ denote the refractive indices of the columns and voids, respectively. $p$ is the packing density defined by $p=V_s/V$, where $V_s$ and $V$ are the volume of the solid part of the film (columns) and the total volume of the film (including the voids), respectively. Equation 1, known as the Bruggeman [9] formula, is valid if the voids are filled with one nonabsorbing substance and the columns are formed by another nonabsorbing material. Of course, this equation can be generalized for an arbitrary number of materials forming the columns and the voids in the film [10] (for example, when the voids are partially filled with water and air).

So far, the values of the refractive index and the extinction coefficient of the $ThF_4$ thin films have been measured in the region $11\ \mu m \geq \lambda \geq 0.22\ \mu m$, that is, in the region of transparency of these films. The values of both optical constants of the $ThF_4$ films were primarily determined using an interpretation of experimental data (ellipsometric parameters, reflectance, and transmittance) based on single layers. The interpretation was performed within the framework of a model consisting of the single layer with ideally smooth and flat boundaries placed on a substrate. Furthermore, it was assumed that both the film and the substrate were formed by homogeneous and isotropic materials from the optical point of view. In this way either the mean optical constants of the films or the optical constants close to them were determined. These optical constants denoted by the symbols $n$ (refractive index) and $k$ (extinction coefficient) evaluated by Heitmann and Ritter [3] for the region 0.8–0.22 μm are collected in Table I and plotted in Fig. 1. Heitmann and Ritter analyzed the $ThF_4$ single layers

deposited by vacuum evaporation (molybdenum or platinum boat) onto quartz-glass substrates by using the values of reflectance of this system corresponding to the wavelengths $\lambda$ at which the optical thicknesses of these films were equal to $m\lambda/4$ ($m = 1,3,5, \ldots$).

Table I shows that, in the visible, the refractive index of the $ThF_4$ thin films is roughly constant and lies in the range 1.52–1.53 (the error in the refractive indices was less than $\pm 1\%$). The values of $n$ characterizing vacuum-evaporated $ThF_4$ single layers determined by Heisen [11] are outlined in Table I as well (Heisen evaluated the values of $n$ for wedge-shaped $ThF_4$ films using an interferometric method for $\lambda = 0.546$ and 0.4358 μm). There is relatively good agreement between the values of $n$ presented by Heitmann and Ritter [3] and Heisen [11] even when there were certain differences in preparation of the $ThF_4$ films. The values of $k$ corresponding to the near-UV, the visible, and the near-IR regions can be considered to be zero for the majority of applications of $ThF_4$ films in optics. However, if multilayer systems with a great number of films are produced (for example, the mirrors for lasers with more than 30 films), the optical losses resulting from absorption and scattering must be considered inside of every film of this system [12]. Very small absorption losses in $ThF_4$ films can be measured. The method of Ahrens *et al.* [13] (based on measuring the temperature change caused by absorption of light by the film using a thin, gold-film resistance thermometer) was used to determine the values of the absorption coefficient for the wavelengths of 0.515 and 1.06 μm [12]. The values of the absorption coefficient determined by Pulker yield the following values of the extinction coefficient: $k = 3.3 \times 10^{-5}$ and $1.3 \times 10^{-6}$ for $\lambda = 0.515$ and 1.06 μm, respectively [12].

Mouchart *et al.* [14] determined the values of both the refractive index and the extinction coefficient characterizing $ThF_4$ films in the mid-IR region $11\ \mu m \geq \lambda \geq 4\ \mu m$ by means of the spectral dependences of the transmittance (the $ThF_4$ films were deposited onto germanium substrates using electron bombardment in vacuum). They employed the method of Manifacier *et al.* [15] based on the use of the envelopes of the interference maxima and minima in the spectral dependences of the transmittance, since the $ThF_4$ films under investigation were relatively thick (2.2–4.9 μm). These authors also determined the coefficients of the following dispersion relations expressing the spectral dependences of $n$ and $k$ in the region considered:

$$n(\lambda) = A_0 + \frac{A_1}{\lambda} + \frac{A_2}{\lambda^2}, \tag{2}$$

$$k(\lambda) = B_0 + B_1\lambda + B_2\lambda^2, \tag{3}$$

The coefficients are as follows [14]: $A_0 = 1.118$, $A_1 = 2.46\ \mu m$, $A_2 = -$

2.98 μm$^2$, $B_0 = 0.00189$, $B_1 = -0.00015$ μm$^{-1}$, and $B_2 = 0.00001$ μm$^{-2}$. For the region 12 μm$\geq\lambda\geq$4 μm, the values of $n$ and $k$ calculated by Eqs. 2 and 3 are summarized in Table I and Fig. 1. It is interesting to note that the values of $n$ for $ThF_4$ films placed on ZnS substrates as determined ellipsometrically at $\lambda = 10.6$ μm by Pedinoff *et al.* [16] agree very well with those found by Mouchart *et al.* [14] at the same wavelength, if the errors of $n$ are taken into account (Pedinoff *et al.* determined the values of $n$ with the accuracy of ±1.5%).

Kim and Vedam [17] determined the spectral dependence of the refractive index of $ThF_4$ films deposited on vitreous silica substrates using spectroscopic ellipsometry in the region 0.9–0.25 μm. These authors expressed the dispersion of the refractive index $n$ by the formula

$$n^2(\lambda) = A + \frac{B\lambda^2}{\lambda^2 - \lambda_0^2}, \tag{4}$$

which represents a first approximation of the well-known Sellmeier dispersion equation,

$$n^2(\lambda) - 1 = a + \sum_{j=1} \frac{b_j\lambda^2}{\lambda^2 - \lambda_j^2}. \tag{5}$$

$a$, $b_j$, $\lambda_j$, $A$, $B$, and $\lambda_o$ are constants ($\lambda_o$ is the wavelength of the Sellmeier oscillator).

They used a three-layer model for interpreting the spectral dependences of the ellipsometric parameters [17]. Within the framework of this model, the columnar structure was assumed for both the upper and the lower layers (see Eq. 1), and therefore, eight parameters were needed. (That is, the values of $A$, $B$, and $\lambda_o$, the thicknesses characterizing all three layers, and the packing density of the upper and the lower layers must be evaluated.) From the values of $A$, $B$, and $\lambda_o$ found, that is, $A = 1.665 \pm 0.005$, $B = 0.715 \pm 0.004$, and $\lambda_o = (0.149 \pm 0.001)$ μm [17], the values of $n$ characterizing the $ThF_4$ films were calculated using Eq. 4 in the region 2 μm$\geq\lambda\geq$0.22 μm (see Table I and Fig. 1). The errors of these values are about ±0.005. The refractive index $n$ determined in this way represents the columnar refractive index $n_s$ of $ThF_4$ films.

Thus, the values of $n$ found by Kim and Vedam [17] can be considered as those for the bulk refractive index of thorium fluoride. This statement is supported by the fact that the values of $n$ determined using the results of Kim and Vedam are greater than those presented by Heitmann and Ritter at all wavelengths (see Table I). It should be noted that a spectral

dependence of the refractive index of a bulk sample of this material has not been measured yet. This means that the values of $n$ presented by Kim and Vedam represent the best ones characterizing thorium fluoride in the region $2\ \mu m \geq \lambda \geq 0.22\ \mu m$ at present. However, the three-layer model of the $ThF_4$ films used by Kim and Vedam can be improved, so that even better values of $n$ for $ThF_4$ can be obtained by reanalyzing the ellipsometric data of the $ThF_4$ films.

Dielectric [18] and metallic [19] thin films prepared by the ion-assisted deposition (IAD) process exhibit improved optical and mechanical properties; the environmental stability of these coatings is also improved. These improvements are caused by increasing the packing density of the films. The effect of IAD on the optical properties of the $ThF_4$ films deposited using a resistively heated source on unheated fused silica and sapphire substrates was examined also [20]. Bombardment of the growing $ThF_4$ films with 300 eV Ar ions was carried out during deposition. When the growing $ThF_4$ films were bombarded with an ion current density of $70\ \mu A/cm^2$, the value of $n$ (the mean refractive index) was 1.56, compared with 1.53 for the unbombarded samples at the wavelength of 0.6 μm [20]. The bombarded $ThF_4$ films exhibited high resistivity against the influence of moisture, which was demonstrated by very low absorption of these films in the water band near 3 μm. This fact implies that the packing density is close to unity. The refractive index value of 1.56 at $\lambda = 0.6\ \mu m$ agrees very well with that determined by Kim and Vedam [17], which also supports the conclusion concerning the good quality of Kim and Vedam's data.

Table I shows that the refractive-index values presented by Mouchart *et al.* [14] for the region $11\ \mu m \geq \lambda \geq 4\ \mu m$ do not correspond to those of Heitmann and Ritter [3] and Kim and Vedam [17]. Namely, the values of $n$ found by Mouchart *et al.* at $\lambda = 4\ \mu m$ and the wavelengths close to that are relatively high compared with the refractive-index values published for the wavelengths of the visible in Refs. [3] and [17]. Moreover, dispersion of $n$ presented by Mouchart *et al.* is rather pronounced. (An extrapolation of the data of Mouchart *et al.* to the visible and near-UV region gives values of $n$ substantially higher than those presented in Refs. [3] and [17]). These discrepancies may be explained by the fact that the films analyzed by Mouchart *et al.* [14] were probably formed with a mixture of thorium fluoride and thorium oxide. For example, $ThO_2$ films are characterized by considerably higher values of the refractive index than the $ThF_4$ films in the visible and near-UV region: the values of $n$ characterizing the $ThO_2$ films lie in the interval 1.75–1.9 from the visible to the near UV region [21]. Other, more reliable data of $ThF_4$ films are not available in the mid-IR region at present. Values of $n$ and $k$ of $ThF_4$ films for the far-IR region have not been presented yet, since spectrophotometric or Raman measurements have not been performed in this region (that is, optical-phonon frequencies of $ThF_4$ are not known).

In conclusion, it should be noted that thorium and its compounds are radioactive. In general, no risk of external radiation damage is present. However, incorporation of thorium compounds into the human organism does present danger. Recommended maximum permissible limits for thorium compounds in the body are outlined in Ref. [3].

## REFERENCES

1. J. Ebert, H. Panhorst, H. Küster and H. Welling, *Appl. Opt.* **18**, 818 (1979).
2. H. K. Pulker, *Appl. Opt.* **18**, 1969 (1979).
3. W. Heitmann and E. Ritter, *Appl. Opt.* **7**, 307 (1968).
4. C. S. Barrett, "Structure of Metals," McGraw-Hill, New York, (1952).
5. D. E. Aspens, *Thin Solid Films* **89**, 249 (1982).
6. K. L. Chopra, S. K. Sharma, and V. N. Yadava, *Thin Solid Films* **20**, 209 (1974).
7. M. Harris, H. A. Macleod, S. Ogura, E. Pelletier, and B. Vidal, *Thin Solid Films* **57**, 173 (1979).
8. I. Ohlídal and K. Navrátil, *Thin Solid Films* **74**, 51 (1980).
9. D. A. G. Bruggeman, *Ann. Phys. (Leipzig)* **24**, 636 (1935).
10. D. E. Aspnes, J. B. Theeten, and F. Hottier, *Phys. Rev. B* **20**, 3292 (1979).
11. A. Heisen, *Optik* **18**, 59 (1961).
12. H. K. Pulker, *Thin Solid Films* **34**, 343 (1976).
13. H. Ahrens, H. Welling, and W. Scheel, *Appl. Phys.* **1**, 69 (1973).
14. J. Mouchart, G. Lagier, and B. Pointu, *Appl. Opt.* **24**, 1808 (1985).
15. J. C. Manifacier, J. Gasiot, and J. P. Fillard, *J. Phys. E* **9**, 1002 (1976).
16. M. E. Pedinoff, M. Braunstein, and O. M. Stafsudd, *Appl. Opt.* **16**, 1849 (1977).
17. S. Y. Kim and K. Vedam, *Thin Solid Films* **166**, 325 (1988).
18. P. J. Martin, H. A. Macleod, R. P. Netherfield, C. G. Pacey, and W. G. Sainty, *Appl. Opt.* **22**, 178 (1983).
19. G. A. Al-Jumaily, J. J. McNally, J. R. McNeil, and W. C. Herrmann, Jr., *J. Vac. Sci. Technol. A* **3**, 651 (1985).
20. G. A. Al-Jumaily, L. A. Yazlovitsky, T. A. Monney, and A. Smajikiewicz, *Appl. Opt.* **26**, 3752 (1987).
21. P. H. Lissberger, *Rep. Prog. Phys.* **39**, 197 (1970).

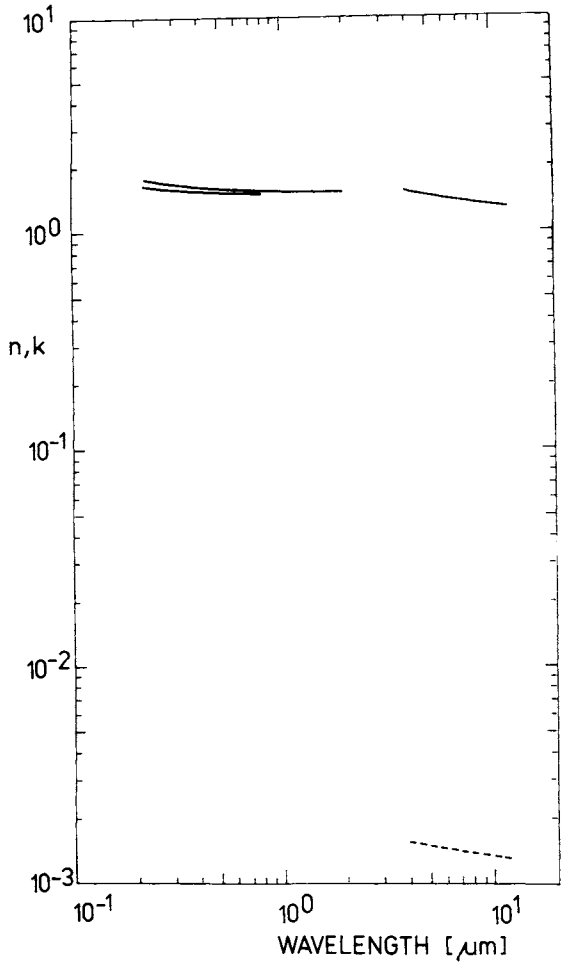


**Fig. 1.** Log–log plot of $n$ (solid line) and $k$ (dashed line) versus wavelength in micrometers for thorium fluoride.

**TABLE I**

**Values of $n$ and $k$ for deposited Thorium Fluoride from Various References[a]**

| eV | $cm^{-1}$ | μm | n | k | n | k |
|---|---|---|---|---|---|---|
| 5.635 | 45,455 | 0.22 | 1.613[3] | | 1.728[17] | |
| 5.391 | 43,478 | 0.23 | 1.599 | | 1.702 | |
| 5.166 | 41,667 | 0.24 | 1.587 | | 1.682 | |
| 4.959 | 40,000 | 0.25 | 1.577 | | 1.664 | |
| 4.769 | 38,462 | 0.26 | 1.569 | | 1.652 | |
| 4.592 | 37,037 | 0.27 | 1.563 | | 1.642 | |
| 4.428 | 35,714 | 0.28 | 1.557 | | 1.632 | |
| 4.275 | 34,483 | 0.29 | 1.553 | | 1.624 | |
| 4.133 | 33,333 | 0.30 | 1.549 | | 1.617 | |
| 4.000 | 32,258 | 0.31 | 1.545 | | 1.611 | |
| 3.875 | 31,250 | 0.32 | 1.542 | | 1.606 | |
| 3.757 | 30,303 | 0.33 | 1.540 | | 1.601 | |
| 3.646 | 29,412 | 0.34 | 1.538 | | 1.597 | |
| 3.543 | 28,571 | 0.35 | 1.536 | | 1.593 | |
| 3.444 | 27,778 | 0.36 | 1.534 | | 1.590 | |
| 3.351 | 27,027 | 0.37 | 1.532 | | 1.587 | |
| 3.263 | 26,316 | 0.38 | 1.531 | | 1.584 | |
| 3.179 | 25,641 | 0.39 | 1.530 | | 1.582 | |
| 3.100 | 25,000 | 0.40 | 1.529 | | 1.579 | |
| 3.024 | 24,390 | 0.41 | 1.528 | | 1.577 | |
| 2.952 | 23,809 | 0.42 | 1.527 | | 1.575 | |
| 2.883 | 23,256 | 0.43 | 1.526 | | 1.574 | |
| 2.845 | 22,946 | 0.4358 | 1.533[11] | | | |
| 2.818 | 22,727 | 0.44 | 1.526[3] | | 1.572 | |
| 2.755 | 22,222 | 0.45 | 1.525 | | 1.571 | |

(continued)

TABLE I (*Continued*)

**Thorium Fluoride**

| eV | $cm^{-1}$ | μm | n | k | n | k |
|---|---|---|---|---|---|---|
| 2.695 | 21,739 | 0.46 | 1.524 | | 1.569 | |
| 2.638 | 21,277 | 0.47 | 1.524 | | 1.568 | |
| 2.583 | 20,833 | 0.48 | 1.523 | | 1.567 | |
| 2.530 | 20,408 | 0.49 | 1.523 | | 1.566 | |
| 2.480 | 20,000 | 0.50 | 1.523 | | 1.565 | |
| 2.431 | 19,608 | 0.51 | 1.522 | | 1.564 | |
| 2.407 | 19,418 | 0.515 | | $3.3 \times 10^{-6}$[12] | | |
| 2.384 | 19,231 | 0.52 | 1.522[3] | | 1.563 | |
| 2.296 | 18,519 | 0.54 | 1.521 | | 1.561 | |
| 2.271 | 18,312 | 0.546 | 1.521[11] | | | |
| 2.214 | 17,857 | 0.56 | 1.521[3] | | 1.560 | |
| 2.138 | 17,241 | 0.58 | 1.520 | | 1.559 | |
| 2.066 | 16,667 | 0.60 | 1.520 | | 1.558 | |
| | | | | | 1.560[21] | |
| 2.000 | 16,129 | 0.62 | 1.520 | | 1.557[17] | |
| 1.937 | 15,625 | 0.64 | 1.519 | | 1.556 | |
| 1.879 | 15,152 | 0.66 | 1.519 | | 1.555 | |
| 1.771 | 14,286 | 0.70 | 1.519 | | 1.554 | |
| 1.676 | 13,513 | 0.74 | 1.518 | | 1.553 | |
| 1.590 | 12,821 | 0.78 | 1.518 | | 1.552 | |
| 1.550 | 12,500 | 0.80 | 1.518 | | 1.551 | |
| 1.378 | 11,111 | 0.90 | | | 1.550 | |
| 1.240 | 10,000 | 1.00 | | | 1.548 | |
| 1.170 | 9,434 | 1.06 | | $1.3 \times 10^{-6}$[12] | 1.548 | |
| 1.033 | 8,333 | 1.2 | | | 1.547 | |
| 0.8266 | 6,667 | 1.5 | | | 1.546 | |
| 0.6199 | 5,000 | 2.0 | | | 1.544 | |

(continued)

**TABLE I (*Continued*)**

**Thorium Fluoride**

| eV | $cm^{-1}$ | μm | n | k | n | k |
|---|---|---|---|---|---|---|
| 0.3100 | 2,500 | 4.0 | 1.55[14] | $1.5x10^{-3}$[14] | | |
| 0.3024 | 2,439 | 4.1 | 1.54 | 1.4 | | |
| 0.2883 | 2,326 | 4.3 | 1.53 | 1.4 | | |
| 0.2755 | 2,222 | 4.5 | 1.52 | 1.4 | | |
| 0.2638 | 2,128 | 4.7 | 1.51 | 1.4 | | |
| 0.2480 | 2,000 | 5.0 | 1.49 | 1.4 | | |
| 0.2384 | 1,923 | 5.2 | 1.48 | 1.4 | | |
| 0.2296 | 1,852 | 5.4 | 1.47 | 1.4 | | |
| 0.2214 | 1,786 | 5.6 | 1.46 | 1.4 | | |
| 0.2138 | 1,724 | 5.8 | 1.45 | 1.4 | | |
| 0.2067 | 1,667 | 6.0 | 1.45 | 1.4 | | |
| 0.2001 | 1,613 | 6.2 | 1.44 | 1.3 | | |
| 0.1937 | 1,563 | 6.4 | 1.43 | 1.3 | | |
| 0.1879 | 1,515 | 6.6 | 1.42 | 1.3 | | |
| 0.1771 | 1,429 | 7.0 | 1.41 | 1.3 | | |
| 0.1653 | 1,333 | 7.5 | 1.39 | 1.3 | | |
| 0.1550 | 1,250 | 8.0 | 1.38 | 1.3 | | |
| 0.1459 | 1,177 | 8.5 | 1.37 | 1.3 | | |
| 0.1378 | 1,111 | 9.0 | 1.35 | 1.4 | | |
| 0.1292 | 1,042 | 9.6 | 1.34 | 1.4 | | |
| 0.1240 | 1,000 | 10.0 | 1.33 | 1.4 | | |
| 0.1170 | 943.4 | 10.6 | 1.32<br>1.35[16] | $1.4x10^{-3}$ | | |
| 0.1127 | 909.1 | 11.0 | 1.32[14] | $1.4x10^{-3}$ | | |
| 0.1078 | 869.6 | 11.5 | 1.31 | 1.4 | | |
| 0.1033 | 833.3 | 12.0 | 1.30 | $1.4x10^{-3}$ | | |

[a]The references from which the values were extracted are given in brackets.

# Water ($H_2O$)

MARVIN R. QUERRY and DAVID M. WIELICZKA
Department of Physics
University of Missouri-Kansas City
Kansas City, Missouri
and
DAVID J. SEGELSTEIN
Bell Communications Research
Red Bank, New Jersey

One could easily prepare a list of several hundred primary references to the scientific literature on spectral measurements of the optical properties of water and compilations of water's refractive index and absorption coefficient. In this critique, however, we only highlight such activities during the past century. Readers interested in more detail should consult bibliographies in the references cited here. To those who contributed to the scientific literature on the optical properties of water and are not explicitly acknowledged here, we apologize. We conclude the critique with two of our previously unpublished compilations of $n$ and $k$ for water.

In 1892, Rubens [1] presented refractometer measurements of the refractive index $n(\lambda)$ of water to a long-wavelength limit of 1.256 μm. These measurements of $n(\lambda)$ were extended to a new long-wavelength limit of 2.327 μm by Seegert's [2] doctoral work in 1908. In 1908 and 1909, Rubens and Ladenberg [3] published their measurements of the reflectance and absorption spectra, and determined what was later discovered to be incorrect dispersion $n(\lambda)$ of water out to a wavelength of 18 μm. Others who measured the infrared reflectance spectrum of water in 1906, 1915, 1918, and 1931, respectively, were Pfund [4], Gehrts [5], Brieger [6], and Weingeroff [7]. General reviews of the infrared absorption spectrum of water were published in 1917, 1929, 1930, and 1934 by Fowle [8], Lecompte [9], Schaefer and Matossi [10], and Dawson and Hulburt [11], respectively. Compilations of the optical properties of water were published in 1929 by Becquerel and Rossignol [12], and in 1940 by Dorsey [13].

One can gain a historical and technical perspective from Dorsey's thorough compilation of water's optical properties. He presented data, gleaned from about 320 references, that spanned the spectral range from low frequency (dielectric constants) to the X-ray region (absorption coefficients). For example, Dorsey's Table 137 provides values for $n(\lambda)$ in the


Copyright © 1991 by Academic Press.
All rights of reproduction in any form reserved.
ISBN 0-12-544422-2

wavelength range 0.154 nm–11 mm. For the visible and ultraviolet regions, Dorsey reviewed several dispersion relations for the refractive index of water at temperatures in the range of 0–80 °C. Of particular interest to Dorsey were the data of Martens [14], Duclaux and Jeantet [15], Chéneveau [16], and Tilton and Taylor [17].

Among those who also published works prior to 1941 on the optical properties of water were Paschen [18], 1894; Coblentz [19], 1905, 1906, and 1911; Goldhammer [20], 1913; Collins [21], 1922 and 1939; Plyler [22], 1924; Dreisch [23], 1924; Hulburt [24], 1928; Cartwright [25], 1935; Williams *et al.* [26], 1936; and Fox and Martin [27], 1940.

Centeno's [28] tabulation in 1941 of $n$ and $k$ for water, and the compilation previously published by Dorsey in 1940, were benchmarks for the future of such activity and were the standard of such compilations for nearly three decades. Centeno gleaned data from 59 articles, including all those previously noted here, to determine $n$ and $k$ for water in the 0.1151–18 μm and 1–18 μm wavelength regions, respectively. Centeno's values of $n(\lambda)$ in the ultraviolet, visible, and near infrared were from Refs. [13], [16], and [17]. Centeno corrected the infrared absorption spectrum of a 90% water and 10% glycerin mixture previously measured in 1909 by Rubens and Ladenburg [3], to obtain the absorption and extinction coefficients $\alpha(\lambda) = 4\pi k(\lambda)/\lambda$ and $k(\lambda)$ of water. Possessing corrected values for $k(\lambda)$ and the normal-incidence infrared reflectance spectrum $R(\lambda)$ [3] of water, he determined $n(\lambda)$ by use of

$$R = \frac{[(n-1)^2 + k^2]}{[(n+1)^2 + k^2]}.$$

The scientific literature on the optical properties of water fell silent through the 1940s. During the 1950s the following articles on the absorption and reflectance of water appeared in the literature: studying absorption were Curcio and Petty [29], 1951; Blout and Lenormant [30], 1953; Plyler and Aquista [31], 1954; Adams and Katz [32], Ceccaldi *et al.* [33], and Potts and Wright [34], 1956; Hyman *et al.* [35], 1957; Bocharov and Krutikov [36], and Waggener [37], 1958; and Goulden [38], 1959; Kislovskii [39], 1959, studied reflectance.

Kislovskii [39], who concluded his paper with a dateline of Christmas Day, 1958, measured the reflectance spectrum and determined the first fairly reliable values of $n$ and $k$ of water in the 2.1–3.4 μm wavelength range. He used semiempirical conceptual models to compute $n$ in the 182.9 nm–1000 Km wavelength region. He also used the conceptual models to calculate $k$ in the 2.0 μm–1000 Km wavelength region. Kislovskii's determinations of $k$, the measurements of $\alpha(\lambda)$ by Curcio and Petty [29] in the 0.7–2.5 μm wavelength region, and similar measurements of $\alpha(\lambda)$ by

Plyler and Aquista [31] in the 2–42 μm wavelength region, provided the standard values of $k$ for the next six to nine years. A systematic error, however, was later discovered in the work of Plyler and Aquista. The error was corrected in part by measurement and publication of "Absolute Absorption Coefficients of Liquid Water at 2.95 μm, 4.7 μm, and 6.1 μm" by Plyler and Griff [40] in 1965.

The advent of the space age in 1957, the development of space technology in the 1960s and 1970s, and the consequent new opportunities for remote sensing of planetary atmospheres and surfaces created renewed interest in the optical properties of natural mineral materials. On Earth, water is a ubiquitous substance, and it was thus essential that some members of the scientific community again devote their interest to the optical properties of water. For the past three decades, an accurate compilation of $N = n + ik$ of liquid water and ice over the broadest possible range of frequency $\nu$ or wavelength $\lambda$ has thus been a topic of considerable interest, particularly to those engaged in the endeavor and to those who used and continue to use the data in a host of varying theoretical constructs.

During the 1960s the following articles on the optical properties of water appeared in the literature: McDonald [41], 1960; Ackermann [42], 1961; Stanevich and Yaroslavskii [43], 1961; Bayly *et al.* [44], 1963; Kondratyev *et al.* [45], 1964; Plyler and Griff [40], 1965; Thompson [46], 1965; Bagdade and Tinkham [47], 1965; Draegert *et al.* [48], 1966; and Kondratyev [49], 1969, all studied absorption. Studying reflectance were McAlister [50], 1964; Pontier and Dechambenoy [51], 1965–1966; Painter *et al.* [52], 1968–1969; Querry *et al.* [53], 1969; and Zolotarev *et al.* [54], 1969.

Pontier and Dechambenoy [51] measured reflectance spectra of water for angles of incidence of 0 degrees (1965), and 50 and 60 degrees (1966), in the 1–38 μm and 1–28 μm regions, respectively. They also measured the absorption spectrum $\alpha(\lambda)$ in the 1–40 μm wavelength region (1966). The reflectance and absorption spectra, and the appropriate Fresnel equations, were used to determine $n$ and $k$ throughout the 1–40 μm wavelength region.

In 1968, Irvine and Pollack [55] published a more extensive tabulation of $n$ and $k$ for water and ice in the 0.2–200 μm wavelength region. Although they seemed to have overlooked the work by Pontier and Dechambenoy [51], Irvine and Pollack considered data from references [21, 23, 25, 27–48] to prepare their tabulation of the optical constants of water.

In 1969 and 1970, Zolotarev *et al.* [54, 56] presented a tabulation of $N(\lambda)$ for the $1\text{–}1 \times 10^6$ μm wavelength region. In the 1970 paper [56], they used four methods to determine $n$ and $k$: measurements of absorption, reflectance, internal reflectance spectra, and Kramers–Kronig (K–K) analysis. Sources of spectral values of $k$ used in the K–K analysis to determine $n$ were the following:

| Wavelength Region | Reference |
|---|---|
| $0.2 \leq \lambda \leq 1.0\ \mu m$ | Lane and Saxton [57], 1952; Collie *et al.* [58], 1948; Gelebart and Johannin-Gillen [59], 1948; |
| $1.0 \leq \lambda \leq 2.0\ \mu m$ | Kontratyev *et al.* [45], 1964; |
| $2.0 \leq \lambda \leq 40\ \mu m$ | Zolotarev *et al.* [54, 56], 1969–70; |
| $40 \leq \lambda \leq 250\ \mu m$ | Draegert *et al.* [48], 1966; |
| $250 \leq \lambda \leq 1000\ \mu m$ | Stanevich and Yaroslavskii [43], 1961; |
| $l \geqslant 1000$ mm | Chamberlain *et al.* [60], 1966. |

In the early 1970s several measurements were made of the optical properties of water [61–69]. In 1973, Hale and Querry [70] published a tabulation of $N(l)$ for water in the 200 nm–200 mm wavelength region based on a compilation and K–K analysis of $k(\lambda)$ to obtain $n(\lambda)$. Their compilation of $k(\lambda)$ was based on data selected from 58 references spanning 81 years of the scientific literature. Then, in 1975, Downing and Williams [71] presented a tabulation of $N(\nu)$ for the 10–5,000 $cm^{-1}$ wave-number region, which also was based on a compilation and K–K analysis of $k(\nu)$ to determine $n(\nu)$.

In 1981, Segelstein [72] completed an extensive compilation of $k(\nu)$ for water throughout the $10^{-6}$ to $10^{8}\,cm^{-1}$ wave-number region. Beginning with the composite $k(\lambda)$ spectrum previously published by Hale and Querry, Segelstein incorporated data for $k(\nu)$ into the compilation for the frequency ranges and corresponding references listed below:

| Wave Number Range | Reference |
|---|---|
| $0 \leq \nu \leq 5\ cm^{-1}$ | Cole and Cole [73] |
| $5 \leq \nu \leq 500\ cm^{-1}$ | Afsar and Hasted [74] |
| $500 \leq \nu \leq 1000\ cm^{-1}$ | Robertson and Williams [62] |
| $3{,}300 \leq \nu \leq 4000\ cm^{-1}$ | Robertson and Williams [62] |
| $14{,}400 \leq \nu \leq 24{,}400\ cm^{-1}$ | Tam and Patel [75] |
| $24{,}400 \leq \nu \leq 50{,}000\ cm^{-1}$ | Lenoble and Saint-Guilly [76], and Kopelevich [77] |
| $50{,}000 \leq \nu \leq 65{,}000\ cm^{-1}$ | Painter *et al.* [78] |
| $65{,}000 \leq \nu \leq 200{,}000\ cm^{-1}$ | Heller *et al.* [68] |
| $2 \times 10^{5} \leq n \leq 4.3 \times 10^{6}\ cm^{-1}$ | $k(n) = An^{1.23}$ [72] |
| $n > 4.3 \times 10^{6}\ cm^{-1}$ | $k(n) = An^{1.63}$ [72]. |

Segelstein used an electron sum rule to test the validity of the $k(\nu)$ spectrum. Kramers–Kronig analysis of $k(\nu)$ then provided $n(\nu)$ throughout the $10^{-3}$ to $10^{6}\,cm^{-1}$ wave-number region. More specific details of Segelstein's investigation of $N(\nu)$ for water will be presented elsewhere [79], but his tabulation of $n$ and $k$ for water is presented in Table I.

Graphical presentations of the $n$ and $k$ data in Table I appear in Fig. 1. The values of $k$ in Table I are from work by several investigators, but are believed to represent $n$ and $k$ for water in a temperature range of 25°–35 °C.

The relatively large static dielectric constant $\varepsilon = n^2$ is due to the strong polar nature and polarizability of water. Also, the famous rotational absorption line at 1.26 cm wavelength, which hampered the development of radar in the early 1940s, occurs in water vapor and not in liquid water and is therefore not present in the data in Table I.

More recently Wieliczka *et al.* [80] used a wedge-shaped cell, which was an improved functional design of similar cells previously described by Robertson and Williams [62] and Tyler *et al.* [81], to determine accurate values of the Lambert absorption coefficient $\alpha(\nu)$ of water in the 500–8000 $cm^{-1}$ region. Kramers–Kronig analysis of the $k(\nu)$ spectrum determined values for $n(\nu)$. Their values of $n$ and $k$ for water are presented in Table II. The sample was purified, deionized water. The temperature of the water was approximately 30 °C.

## REFERENCES


1. H. Rubens, *Ann. Physik* **45**, 253 (1892).
2. B. Seegert, Dissertation, Berlin Universität (1908).
3. H. Rubens and E. Ladenberg, *Verh. Deut. Phys. Ges.* **10**, 227 (1908); *Verh. Deut. Phys. Ges.* **11**, 16 (1909).
4. A. H. Pfund, *Astrophys. J.* **24**, 19 (1906).
5. F. Gehrts, *Ann. Physik* **47**, 1059 (1915).
6. K. Brieger, *Ann. Physik* **57**, 287 (1918).
7. M. Weingeroff, *Z. Physik* **70**, 104 (1931).
8. F. E. Fowle, *Smith. Misc. Coll.* **68**, No. 8 (Publ. 2484) (1917).
9. J. Lecompte, *Trans. Faraday Soc.* **25**, 864 (1929).
10. C. Shaefer and F. Matossi, "Das Ultrarote Spectrum," Springer, Berlin, (1930).
11. L. H. Dawson and E. O. Hulburt, *J. Opt. Soc. Am.* **24**, 175 (1934).
12. J. Becquerel and J. Rossignol, *Int. Crit. Tab.* **5**, 268 (1929).
13. N. E. Dorsey, "Properties of the Ordinary Water Substance in all Its Phases," Reinhold, New York, 279 (1940).
14. F. F. Martens, *Ann. Physik (4)* **6**, 603 (1901).
15. J. Duclaux and P. Jeantet, *J. de Phys. (6)* **5**, 92 (1924).
16. C. Chéneveau, *Int. Nat. Crit. Tab.* **7**, 13 (1930).
17. L. W. Tilton and J. K. Taylor, *J. Res. Nat. Bur. Stand.* **20**, 419 (RP1085) (1938).
18. F. Paschen, *Wied. Ann.* **51**, 21; **52**, 216; **53**, 334 (1894).
19. W. W. Coblentz, *Bull. Bur. Stand.* **2**, No. 3, 457 (1906); **7**, No. 4, 619 (1911); *Phys. Rev.* [1] **20**, 252 (1905); [1] **23**, 125 (1906).
20. D. A. Goldhammer, "Dispersion und Absorption des Lichtes," Teubner, Leipzig, (1913).
21. J. R. Collins, *Phys. Rev.* **20**, 486 (1922); *Phys. Rev.* **55**, 470 (1939).
22. E. K. Plyler, *J. Opt. Soc. Am.* **9**, 545 (1924).
23. T. Dreisch, *Z. Physik* **30**, 200 (1924).
24. E. O. Hulburt, *J. Opt. Soc. Am.* **17**, 15 (1928).
25. C. H. Cartwright, *Nature* **135**, 872 (1935).

26. D. Williams, R. D. Weatherford, and E. K. Plyler, *J. Opt. Soc. Am.* **26**, 149 (1936).
27. J. J. Fox and A. E. Martin, *Proc. Roy. Soc. London* **174**, 234 (1940).
28. M. Centeno, V, *J. Opt. Soc. Am.* **31**, 244 (1941).
29. J. A. Curcio and C. C. Petty, *J. Opt. Soc. Am.* **41**, 302 (1951).
30. E. R. Blout and H. Lenormant, *J. Opt. Soc. Am.* **43**, 1093 (1953).
31. E. K. Plyler and N. Aquista, *J. Opt. Soc. Am.* **44**, 505 (1954).
32. R. M. Adams and J. J. Katz, *J. Opt. Soc. Am.* **46**, 895 (1956).
33. M. Ceccaldi, M. Goldman, and E. Roth, "Proceedings of the Sixth International Spectroscopy Colloquium," Pergamon, London, (1956).
34. W. J. Potts, Jr., and N. Wright, *Anal. Chem.* **28**, 1255 (1956).
35. H. H. Hyman, M. Kilpatrick, and J. J. Katz, *J. Am. Chem. Soc.* **79**, 3668 (1957).
36. Y. I. Bocharov and A. S. Krutikov, *Bull. Izv. Akad. Sci. USSR, Geophys. Ser., No. 7*, 528 (1958).
37. W. C. Waggener, *Anal. Chem.* **30**, 1569 (1958).
38. J. D. S. Goulden, *Spectrochem. Acta.* **15**, 657 (1959).
39. L. D. Kislovskii, *Opt. Spektrosk.* **7**, 201 (1959).
40. E. K. Plyler and N. Griff, *Appl. Opt.* **4**, 1663 (1965).
41. J. E. McDonald, *J. Meteorol.* **17**, 232 (1960).
42. T. Ackermann, *Z. Phys. Chem.* **27**, 253 (1961).
43. A. E. Stanevich and N. G. Yaroslavskii, *Opt. Spektrosk.* **10**, 278 (1961).
44. J. G. Bayly, V. B. Kartha, and W. H. Stevens, *Infrared Phys.* **3**, 211 (1963).
45. K. Kondratyev, M. P. Burgova, I. F. Gainulin, and G. F. Tomunova, "Problemy Fiziki Atmosfery," Sb. 2, Izd. Leningrad Univ., Leningrad, (1964).
46. W. K. Thompson, *Trans. Faraday Soc.* **61**, 2635 (1965).
47. W. Bagdade and M. Tinkham, *Bull. Am. Phys. Soc.* **10**, 1209 (1965).
48. D. A. Draegert, N. W. B. Stone, B. Curnutte, and D. Williams, *J. Opt. Soc. Am.* **56**, 64 (1966).
49. K. Kondratyev, "Radiation in the Atmosphere," Vol. 12, International Geophysical Series, Academic Press, New York, (1969).
50. E. D. McAlister, *Appl. Opt.* **3**, 609 (1964).
51. L. Pontier and C. Dechambenoy, *Ann. Geophys.* **21**, 462 (1965); **22**, 633 (1966).
52. L. R. Painter, R. N. Hamm, E. T. Arakawa, and R. D. Birkhoff, *Phys. Rev. Lett.* **21**, 282 (1968); *J. Chem. Phys.* **51**, 243 (1969).
53. M. R. Querry, B. Curnutte, and D. Williams, *J. Opt. Soc. Am.* **59**, 1299 (1969).
54. V. M. Zolotarev, B. A. Mikhailov, L. I. Alperovich, and S. I. Popov, *Opt. Spectrosc.* **27**, 430 (1969).
55. W. M. Irvine and J. B. Pollack, *Icarus* **8**, 324 (1968).
56. V. M. Zolotarev, B. A. Mikhailov, L. I. Alperovich, and S. I. Popov, *Opt. Commun.* **1**, 301 (1970).
57. J. Lane and J. A. Saxton, *Proc. Roy. Soc. (London)* **213A**, 400 (1952); Ibid. 473.
58. C. H. Collie, J. B. Hasted, D. M. Riston, *Proc. Phys. Soc.* **60**, 71 (1948); Ibid. 145.
59. F. Gelebart and A. Johannin-Gillen, *Compt. Rend. Acad. Sci. (Paris)* **262B**, 1509 (1966).
60. J. E. Chamberlain, G. W. Chantry, H. A. Gebbie, N. W. B. Stone, T. B. Taylor, and G. Wyllie, *Nature* **210**, 790 (1966).
61. A. N. Rusk, D. Williams, and M. R. Querry, *J. Opt. Soc. Am.* **61**, 895 (1971).
62. C. W. Robertson and D. Williams, *J. Opt. Soc. Am.* **61**, 1316 (1971).
63. G. M. Hale, M. R. Querry, A. N. Rusk, and D. Williams, *J. Opt. Soc. Am.* **62**, 1103 (1972).
64. G. D. Kerr, R. N. Hamm, M. W. Williams, R. D. Birkhoff, and L. R. Painter, *Phys. Rev.* **A5**, 2523 (1972).
65. B. L. Sowers, R. D. Birkhoff, and E. T. Arakawa, *J. Chem. Phys.* **57**, 583 (1972).
66. C. W. Robertson, B. Curnutte, and D. Williams, *Mol. Phys.* **26**, 183 (1973).

67. M. S. Zafar, J. B. Hasted, and J. Chamberlain, *Nature* **243**, 106 (1973).
68. J. M. Heller, Jr., R. N. Hamm, R. D. Birkhoff, and L. R. Painter, *J. Chem. Phys.* **60**, 3483 (1974).
69. K. F. Palmer and D. Williams, *J. Opt. Soc. Am.* **64**, 1107 (1974).
70. G. M. Hale and M. R. Querry, *Appl. Opt.* **12**, 555 (1973).
71. H. D. Downing and D. Williams, *J. Geophys. Res.* **80**, 1656 (1975).
72. D. J. Segelstein, "The Complex Refractive Index of Water," M. S. Thesis, University of Missouri-Kansas City (1981).
73. K. S. Cole and R. H. Cole, *J. Chem. Phys.* **9**, 341 (1941).
74. M. N. Afsar and J. B. Hasted, *J. Opt. Soc. Am.* **67**, 902 (1977).
75. A. C. Tam and C. K. N. Patel, *Appl. Opt.* **18**, 3348 (1979).
76. J. Lenoble and B. Saint-Guilly, *Compt. Rend.* **240**, 954 (1955).
77. O. V. Kopelevich, *Opt. Spektrosk.* **41**, 666 (1976); *Opt. Spectrosc.* **49**, 391 (1976).
78. L. R. Painter, R. D. Birkhoff, and E. T. Arakawa, *J. Chem. Phys.* **51**, 243 (1969).
79. D. J. Segelstein and M. R. Querry, *Appl. Opt.* (submitted).
80. D. M. Wieliczka, S. Weng, and M. R. Querry, *Appl. Opt.* **28**, 1714 (1989).
81. I. L. Tyler, G. Taylor, and M. R. Querry, *Appl. Opt.* **17**, 960 (1978).

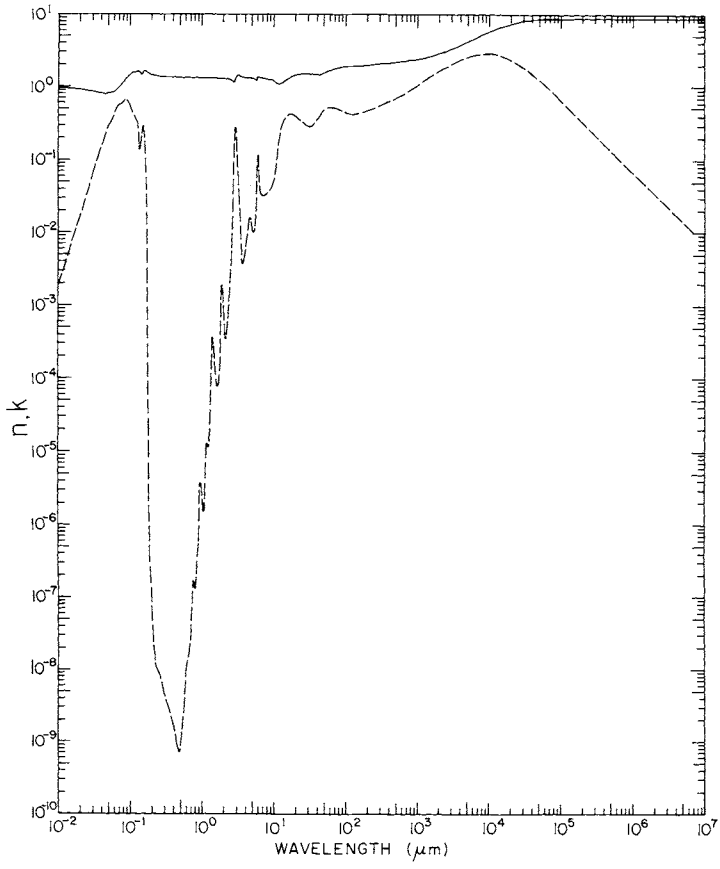


**Fig. 1.** Log–log plot of $n$ (solid line) and $k$ (dashed line) versus wavelength in micrometers for water.

**TABLE I**

**Values of *n* and *k* for Water Obtained from Ref. [72]**[a]

| eV | $cm^{-1}$ | μm | n | k |
|---|---|---|---|---|
| $1.2398 \times 10^{-7}$ | $1.000 \times 10^{-3}$ | $1.0000 \times 10^{7}$ | 8.849 [72] | $6.931 \times 10^{-3}$ [73] |
| 1.3043 | 1.052 | $9.5057 \times 10^{6}$ | 8.849 | 7.291 |
| 1.3787 | 1.112 | 8.9928 | 8.849 | 7.688 |
| 1.4605 | 1.178 | 8.4890 | 8.849 | 8.124 |
| 1.5498 | 1.250 | 8.0000 | 8.849 | 8.626 |
| 1.6540 | 1.334 | 7.4963 | 8.849 | 9.200 |
| 1.7717 | 1.429 | 6.9979 | 8.849 | $9.858 \times 10^{-3}$ |
| 1.9069 | 1.538 | 6.5020 | 8.849 | $1.061 \times 10^{-2}$ |
| 2.0668 | 1.667 | 5.9988 | 8.849 | 1.148 |
| 2.2565 | 1.820 | 5.4945 | 8.849 | 1.250 |
| 2.4797 | 2.000 | 5.0000 | 8.849 | 1.373 |
| 2.7562 | 2.223 | 4.4984 | 8.849 | 1.523 |
| 3.0996 | 2.500 | 4.0000 | 8.849 | 1.713 |
| 3.5435 | 2.858 | 3.4990 | 8.849 | 1.953 |
| 4.1337 | 3.334 | 2.9994 | 8.849 | 2.274 |
| 4.9582 | 3.999 | 2.5006 | 8.849 | 2.721 |
| 6.1992 | 5.000 | 2.0000 | 8.848 | 3.395 |
| $8.2673 \times 10^{-7}$ | $6.668 \times 10^{-3}$ | 1.4997 | 8.848 | 4.506 |
| $1.2398 \times 10^{-6}$ | $1.000 \times 10^{-2}$ | $1.0000 \times 10^{6}$ | 8.848 | 6.727 |
| 1.3043 | 1.052 | $9.5057 \times 10^{5}$ | 8.848 | 7.076 |
| 1.3787 | 1.112 | 8.9928 | 8.847 | 7.461 |
| 1.4605 | 1.178 | 8.4890 | 8.847 | 7.885 |
| 1.5498 | 1.250 | 8.0000 | 8.847 | 8.391 |
| 1.6540 | 1.334 | 7.4963 | 8.847 | 8.929 |
| 1.7717 | 1.429 | 6.9979 | 8.847 | $9.567 \times 10^{-2}$ |
| 1.9069 | 1.538 | 6.5020 | 8.847 | $1.030 \times 10^{-1}$ |
| 2.0668 | 1.667 | 5.9988 | 8.846 | 1.114 |
| 2.2565 | 1.820 | 5.4945 | 8.846 | 1.213 |
| 2.4797 | 2.000 | 5.0000 | 8.845 | 1.333 |
| 2.7562 | 2.223 | 4.4984 | 8.844 | 1.478 |
| 3.0996 | 2.500 | 4.0000 | 8.843 | 1.659 |
| 3.5435 | 2.858 | 3.4990 | 8.841 | 1.891 |
| 4.1337 | 3.334 | 2.9994 | 8.838 | 2.202 |
| 4.9582 | 3.999 | 2.5006 | 8.833 | 2.634 |
| 6.1992 | 5.000 | 2.0000 | 8.824 | 3.277 |
| $8.2673 \times 10^{-6}$ | $6.668 \times 10^{-2}$ | 1.4997 | 8.804 | 4.337 |
| $1.2398 \times 10^{-5}$ | $1.000 \times 10^{-1}$ | $1.0000 \times 10^{5}$ | 8.743 | 6.409 |
| 1.3056 | 1.053 | $9.4967 \times 10^{4}$ | 8.732 | 6.730 |
| 1.3775 | 1.111 | 9.0009 | 8.720 | 7.083 |
| 1.4593 | 1.177 | 8.4962 | 8.705 | 7.476 |
| 1.5498 | 1.250 | 8.0000 | 8.689 | 7.914 |
| 1.6527 | 1.333 | 7.5019 | 8.670 | 8.406 |
| 1.7717 | 1.429 | 6.9979 | 8.648 | 8.960 |
| 1.9081 | 1.539 | 6.4977 | 8.620 | $9.589 \times 10^{-1}$ |
| 2.0656 | 1.666 | 6.0024 | 8.587 | $1.031 \times 10^{0}$ |
| 2.2540 | 1.818 | 5.5006 | 8.546 | 1.115 |
| 2.4797 | 2.000 | 5.0000 | 8.497 | 1.212 |
| 2.7549 | 2.222 | 4.5005 | 8.436 | 1.327 |
| 3.0996 | 2.500 | 4.0000 | 8.353 | 1.463 |

[a] References used in compilation of Ref. [72] given in brackets.

**TABLE I (*Continued*)**

**Water**

| eV | $cm^{-1}$ | μm | n | k | |
|---|---|---|---|---|---|
| 3.5422 | 2.857 | 3.5002 | 8.238 | 1.627 | |
| 4.1324 | 3.333 | 3.0003 | 8.075 | 1.824 | |
| 4.9594 | 4.000 | 2.5000 | 7.831 | 2.064 | |
| 6.1992 | 5.000 | 2.0000 | 7.456 | 2.338 | |
| $8.2661 \times 10^{-5}$ | $6.667 \times 10^{-1}$ | 1.4999 | 6.867 | 2.630 | |
| $1.2398 \times 10^{-4}$ | $1.000 \times 10^{0}$ | $1.0000 \times 10^{4}$ | 5.879 | 2.830 | |
| 1.3056 | 1.053 | $9.4967 \times 10^{3}$ | 5.747 | 2.835 | |
| 1.3775 | 1.111 | 9.0009 | 5.607 | 2.832 | |
| 1.4581 | 1.176 | 8.5034 | 5.459 | 2.826 | |
| 1.5498 | 1.250 | 8.0000 | 5.305 | 2.811 | |
| 1.6527 | 1.333 | 7.5019 | 5.146 | 2.792 | |
| 1.7717 | 1.429 | 6.9979 | 4.980 | 2.766 | |
| 1.9081 | 1.539 | 6.4977 | 4.811 | 2.727 | |
| 2.0656 | 1.666 | 6.0024 | 4.631 | 2.685 | |
| 2.2540 | 1.818 | 5.5006 | 4.442 | 2.625 | |
| 2.4797 | 2.000 | 5.0000 | 4.248 | 2.551 | |
| 2.7549 | 2.222 | 4.5005 | 4.045 | 2.460 | |
| 3.0996 | 2.500 | 4.0000 | 3.829 | 2.360 | |
| 3.5422 | 2.857 | 3.5002 | 3.607 | 2.228 | |
| 4.1324 | 3.333 | 3.0003 | 3.375 | 2.079 | |
| 4.9594 | 4.000 | 2.5000 | 3.134 | 1.891 | |
| 6.1992 | 5.000 | 2.0000 | 2.882 | 1.670 | [74] |
| $8.2661 \times 10^{-4}$ | $6.667 \times 10^{0}$ | 1.4999 | 2.629 | 1.393 | |
| $1.2398 \times 10^{-3}$ | $1.000 \times 10^{1}$ | $1.0000 \times 10^{3}$ | 2.399 | $1.042 \times 10^{0}$ | |
| 1.6540 | 1.334 | $7.4963 \times 10^{2}$ | 2.290 | $8.725 \times 10^{-1}$ | |
| 2.2144 | 1.786 | 5.5991 | 2.220 | 7.359 | |
| 2.6942 | 2.173 | 4.6019 | 2.166 | 6.727 | |
| 3.4468 | 2.780 | 3.5971 | 2.099 | 5.967 | |
| 4.4300 | 3.573 | 2.7988 | 2.045 | 5.355 | |
| 5.3871 | 4.345 | 2.3015 | 2.001 | 4.964 | |
| 6.8923 | 5.559 | 1.7989 | 1.956 | 4.506 | |
| $9.5357 \times 10^{-3}$ | $7.691 \times 10^{1}$ | $1.3002 \times 10^{2}$ | 1.920 | 4.186 | |
| $1.2919 \times 10^{-2}$ | $1.042 \times 10^{2}$ | $9.5969 \times 10^{1}$ | 1.891 | 4.485 | |
| 1.4432 | 1.164 | 8.5911 | 1.860 | 4.773 | |
| 1.6304 | 1.315 | 7.6046 | 1.806 | 5.079 | |
| 1.8771 | 1.514 | 6.6050 | 1.729 | 5.233 | |
| 2.2144 | 1.786 | 5.5991 | 1.619 | 5.162 | |
| 2.5838 | 2.084 | 4.7985 | 1.520 | 4.579 | |
| 2.8864 | 2.328 | 4.2955 | 1.481 | 3.880 | |
| 3.2608 | 2.630 | 3.8023 | 1.481 | 3.190 | |
| 3.7530 | 3.027 | 3.3036 | 1.512 | 2.830 | |
| 4.4300 | 3.573 | 2.7988 | 1.546 | 2.991 | |
| 5.3871 | 4.345 | 2.3015 | 1.516 | 3.629 | |
| 6.2278 | 5.023 | 1.9908 | 1.467 | 3.952 | [62] |
| 6.3145 | 5.093 | 1.9635 | 1.460 | 4.016 | |
| 6.3877 | 5.152 | 1.9410 | 1.454 | 4.072 | |
| 6.4770 | 5.224 | 1.9142 | 1.446 | 4.110 | |
| 6.5675 | 5.297 | 1.8879 | 1.436 | 4.157 | |
| 6.6431 | 5.358 | 1.8664 | 1.428 | 4.196 | |

(*continued*)

**TABLE I (*Continued*)**

**Water**

| eV | $cm^{-1}$ | μm | n | k | |
|---|---|---|---|---|---|
| 6.7361 | 5.433 | 1.8406 | 1.418 | 4.234 | |
| 6.8291 | 5.508 | 1.8155 | 1.407 | 4.254 | |
| 6.9246 | 5.585 | 1.7905 | 1.396 | 4.264 | |
| 7.0200 | 5.662 | 1.7662 | 1.386 | 4.283 | |
| 7.1180 | 5.741 | 1.7419 | 1.375 | 4.293 | |
| 7.2333 | 5.834 | 1.7141 | 1.361 | 4.293 | |
| 7.3349 | 5.916 | 1.6903 | 1.350 | 4.293 | |
| 7.4540 | 6.012 | 1.6633 | 1.335 | 4.283 | |
| 7.5569 | 6.095 | 1.6407 | 1.323 | 4.264 | |
| 7.6796 | 6.194 | 1.6145 | 1.309 | 4.244 | |
| 7.8048 | 6.295 | 1.5886 | 1.295 | 4.205 | |
| 7.9140 | 6.383 | 1.5667 | 1.283 | 4.176 | |
| 8.0417 | 6.486 | 1.5418 | 1.268 | 4.119 | |
| 8.1917 | 6.607 | 1.5135 | 1.254 | 4.053 | |
| 8.3243 | 6.714 | 1.4894 | 1.239 | 3.998 | |
| 8.4595 | 6.823 | 1.4656 | 1.226 | 3.934 | |
| 8.6169 | 6.950 | 1.4388 | 1.209 | 3.844 | |
| 8.7571 | 7.063 | 1.4158 | 1.196 | 3.757 | |
| 8.9195 | 7.194 | 1.3900 | 1.179 | 3.646 | |
| 9.0856 | 7.328 | 1.3646 | 1.162 | 3.514 | |
| 9.2542 | 7.464 | 1.3398 | 1.146 | 3.363 | |
| 9.4266 | 7.603 | 1.3153 | 1.131 | 3.183 | |
| 9.6026 | 7.745 | 1.2912 | 1.117 | 2.977 | |
| $9.8035 \times 10^{-2}$ | 7.907 | 1.2647 | 1.105 | 2.740 | |
| $1.0008 \times 10^{-1}$ | 8.072 | 1.2389 | 1.092 | 2.476 | |
| 1.0194 | 8.222 | 1.2162 | 1.087 | 2.177 | |
| 1.0409 | 8.395 | 1.1912 | 1.087 | 1.865 | |
| 1.0650 | 8.590 | 1.1641 | 1.096 | 1.570 | |
| 1.0873 | 8.770 | 1.1403 | 1.105 | 1.321 | |
| 1.1126 | 8.974 | 1.1143 | 1.119 | $1.083 \times 10^{-1}$ | |
| 1.1386 | 9.183 | 1.0890 | 1.134 | $8.970 \times 10^{-2}$ | |
| 1.1651 | 9.397 | 1.0642 | 1.150 | 7.359 | |
| 1.1922 | 9.616 | 1.0399 | 1.167 | 6.191 | |
| 1.2229 | $9.863 \times 10^{2}$ | $1.0139 \times 10^{1}$ | 1.184 | 5.380 | |
| 1.2510 | $1.009 \times 10^{3}$ | $9.9108 \times 10^{0}$ | 1.199 | 4.929 | [70] |
| 1.2832 | 1.035 | 9.6618 | 1.211 | 4.600 | |
| 1.3192 | 1.064 | 9.3985 | 1.223 | 4.333 | |
| 1.3564 | 1.094 | 9.1408 | 1.233 | 4.110 | |
| 1.3948 | 1.125 | 8.8889 | 1.241 | 3.916 | |
| 1.4333 | 1.156 | 8.6505 | 1.249 | 3.748 | |
| 1.4767 | 1.191 | 8.3963 | 1.257 | 3.604 | |
| 1.5213 | 1.227 | 8.1500 | 1.264 | 3.490 | |
| 1.5684 | 1.265 | 7.9051 | 1.270 | 3.395 | |
| 1.6192 | 1.306 | 7.6570 | 1.277 | 3.302 | |
| 1.6763 | 1.352 | 7.3964 | 1.284 | 3.242 | |
| 1.7358 | 1.400 | 7.1429 | 1.291 | 3.205 | |
| 1.7965 | 1.449 | 6.9013 | 1.298 | 3.220 | |
| 1.8635 | 1.503 | 6.6534 | 1.309 | 3.450 | |
| 1.9379 | 1.563 | 6.3980 | 1.325 | 4.485 | |

(*continued*)

TABLE I (*Continued*)

Water

| eV | $cm^{-1}$ | μm | n | k | |
|---|---|---|---|---|---|
| 2.0011 | 1.614 | 6.1958 | 1.342 | 8.786 | |
| 2.0817 | 1.679 | 5.9559 | 1.232 | 8.646 | |
| 2.1747 | 1.754 | 5.7013 | 1.257 | 2.031 | |
| 2.2776 | 1.837 | 5.4437 | 1.282 | 1.078 | |
| 2.3842 | 1.923 | 5.2002 | 1.298 | 1.011 | |
| 2.5020 | 2.018 | 4.9554 | 1.307 | 1.312 | |
| 2.6384 | 2.128 | 4.6992 | 1.311 | 1.570 | |
| 2.7884 | 2.249 | 4.4464 | 1.315 | $1.140 \times 10^{-2}$ | |
| 2.9533 | 2.382 | 4.1982 | 1.324 | $6.883 \times 10^{-3}$ | |
| 3.1356 | 2.529 | 3.9541 | 1.337 | 4.157 | |
| 3.3526 | 2.704 | 3.6982 | 1.357 | $3.596 \times 10^{-3}$ | |
| 3.5918 | 2.897 | 3.4518 | 1.393 | $1.321 \times 10^{-2}$ | |
| 3.8758 | 3.126 | 3.1990 | 1.462 | $9.243 \times 10^{-2}$ | |
| 4.1535 | 3.350 | 2.9851 | 1.334 | $2.721 \times 10^{-1}$ | |
| 4.2204 | 3.404 | 2.9377 | 1.264 | 2.804 | [62] |
| 4.2787 | 3.451 | 2.8977 | 1.196 | 2.581 | |
| 4.3382 | 3.499 | 2.8580 | 1.145 | 2.060 | |
| 4.3990 | 3.548 | 2.8185 | 1.125 | $1.422 \times 10^{-1}$ | |
| 4.4597 | 3.597 | 2.7801 | 1.131 | $9.285 \times 10^{-2}$ | |
| 4.5230 | 3.648 | 2.7412 | 1.142 | 4.622 | |
| 4.5850 | 3.698 | 2.7042 | 1.175 | $1.640 \times 10^{-2}$ | |
| 4.6494 | 3.750 | 2.6667 | 1.199 | $7.325 \times 10^{-3}$ | |
| 4.7139 | 3.802 | 2.6302 | 1.218 | 4.016 | |
| 4.7796 | 3.855 | 2.5940 | 1.232 | 2.476 | |
| 4.8342 | 3.899 | 2.5648 | 1.240 | 2.266 | |
| 4.8565 | 3.917 | 2.5530 | 1.243 | 2.142 | |
| 4.9582 | 3.999 | 2.5006 | 1.253 | 1.900 | [70] |
| 5.0623 | 4.083 | 2.4492 | 1.261 | $1.348 \times 10^{-3}$ | |
| 5.1689 | 4.169 | 2.3987 | 1.268 | $9.095 \times 10^{-4}$ | |
| 5.2768 | 4.256 | 2.3496 | 1.273 | 6.365 | |
| 5.3871 | 4.345 | 2.3015 | 1.278 | 4.686 | |
| 5.5124 | 4.446 | 2.2492 | 1.282 | 3.739 | |
| 5.6413 | 4.550 | 2.1978 | 1.286 | 3.379 | |
| 5.7727 | 4.656 | 2.1478 | 1.289 | 3.705 | |
| 5.9066 | 4.764 | 2.0991 | 1.292 | 4.643 | |
| 6.0443 | 4.875 | 2.0513 | 1.294 | $6.742 \times 10^{-4}$ | |
| 6.1992 | 5.000 | 2.0000 | 1.297 | $1.101 \times 10^{-3}$ | |
| 6.3592 | 5.129 | 1.9497 | 1.298 | 1.848 | |
| 6.5216 | 5.260 | 1.9011 | 1.299 | $1.161 \times 10^{-3}$ | |
| 6.7051 | 5.408 | 1.8491 | 1.301 | $1.861 \times 10^{-4}$ | |
| 6.8923 | 5.559 | 1.7989 | 1.303 | 1.359 | |
| 7.0857 | 5.715 | 1.7498 | 1.305 | $1.000 \times 10^{-4}$ | |
| 7.3002 | 5.888 | 1.6984 | 1.307 | $7.743 \times 10^{-5}$ | |
| 7.5222 | 6.067 | 1.6483 | 1.308 | 7.591 | |
| 7.7515 | 6.252 | 1.5995 | 1.310 | $9.347 \times 10^{-5}$ | |
| 8.0057 | 6.457 | 1.5487 | 1.311 | $1.348 \times 10^{-4}$ | |
| 8.2673 | 6.668 | 1.4997 | 1.312 | 2.248 | |
| 8.5574 | 6.902 | 1.4489 | 1.313 | 3.637 | |
| 8.8587 | 7.145 | 1.3996 | 1.314 | $1.530 \times 10^{-4}$ | |

(*continued*)

**TABLE I (*Continued*)**

**Water**

| eV | $cm^{-1}$ | μm | n | k | |
|---|---|---|---|---|---|
| 9.1910 | 7.413 | 1.3490 | 1.315 | $4.047 \times 10^{-5}$ | |
| 9.5357 | 7.691 | 1.3002 | 1.316 | 1.400 | |
| $9.9163 \times 10^{-1}$ | 7.998 | 1.2503 | 1.317 | 1.100 | |
| $1.0337 \times 10^{0}$ | 8.337 | 1.1995 | 1.318 | $1.199 \times 10^{-5}$ | |
| 1.0774 | 8.690 | 1.1507 | 1.319 | $9.306 \times 10^{-6}$ | |
| 1.1281 | 9.099 | 1.0990 | 1.320 | 1.708 | |
| 1.1813 | $9.528 \times 10^{3}$ | 1.0495 | 1.321 | 1.419 | |
| 1.2398 | $1.000 \times 10^{4}$ | $1.0000 \times 10^{0}$ | 1.322 | 3.000 | |
| 1.2721 | 1.026 | $9.7466 \times 10^{-1}$ | 1.322 | 3.480 | |
| 1.3043 | 1.052 | 9.5057 | 1.323 | 2.932 | |
| 1.3403 | 1.081 | 9.2507 | 1.323 | $1.060 \times 10^{-6}$ | |
| 1.3787 | 1.112 | 8.9928 | 1.324 | $4.862 \times 10^{-7}$ | |
| 1.4171 | 1.143 | 8.7489 | 1.324 | 3.907 | |
| 1.4605 | 1.178 | 8.4890 | 1.325 | 2.929 | |
| 1.5039 | 1.213 | 8.2440 | 1.325 | 1.819 | |
| 1.5498 | 1.250 | 8.0000 | 1.326 | 1.250 | |
| 1.6006 | 1.291 | 7.7459 | 1.327 | 1.478 | |
| 1.6540 | 1.334 | 7.4963 | 1.327 | $1.559 \times 10^{-7}$ | |
| 1.7110 | 1.380 | 7.2464 | 1.328 | $9.137 \times 10^{-8}$ | |
| 1.7717 | 1.429 | 6.9979 | 1.329 | 3.348 | [75] |
| 1.8387 | 1.483 | 6.7431 | 1.330 | 2.177 | |
| 1.9069 | 1.538 | 6.5020 | 1.331 | 1.674 | |
| 1.9838 | 1.600 | 6.2500 | 1.332 | $1.472 \times 10^{-8}$ | |
| 2.0668 | 1.667 | 5.9988 | 1.333 | $9.634 \times 10^{-9}$ | |
| 2.1549 | 1.738 | 5.7537 | 1.334 | 3.844 | |
| 2.2565 | 1.820 | 5.4945 | 1.336 | 2.442 | |
| 2.3619 | 1.905 | 5.2493 | 1.338 | $1.640 \times 10^{-9}$ | |
| 2.4797 | 2.000 | 5.0000 | 1.339 | $9.243 \times 10^{-10}$ | |
| 2.6086 | 2.104 | 4.7529 | 1.342 | 7.011 | |
| 2.7562 | 2.223 | 4.4984 | 1.344 | $8.087 \times 10^{-10}$ | |
| 2.9198 | 2.355 | 4.2463 | 1.347 | $1.169 \times 10^{-9}$ | |
| 3.0996 | 2.500 | 4.0000 | 1.350 | 1.580 | [76], [77] |
| 3.3067 | 2.667 | 3.7495 | 1.354 | 2.031 | |
| 3.5435 | 2.858 | 3.4990 | 1.358 | 2.528 | |
| 3.8138 | 3.076 | 3.2510 | 1.364 | 3.082 | |
| 4.1337 | 3.334 | 2.9994 | 1.371 | 4.148 | |
| 4.5118 | 3.639 | 2.7480 | 1.381 | 6.292 | |
| 4.9582 | 3.999 | 2.5006 | 1.395 | $9.307 \times 10^{-9}$ | |
| 5.5124 | 4.446 | 2.2492 | 1.416 | $1.158 \times 10^{-8}$ | |
| 5.9066 | 4.764 | 2.0991 | 1.435 | $3.844 \times 10^{-8}$ | |
| 6.1992 | 5.000 | 2.0000 | 1.452 | $1.101 \times 10^{-7}$ | |
| 6.5216 | 5.260 | 1.9011 | 1.475 | $3.622 \times 10^{-7}$ | [78] |
| 6.8923 | 5.559 | 1.7989 | 1.513 | $5.995 \times 10^{-5}$ | |
| 7.1180 | 5.741 | 1.7419 | 1.549 | $1.182 \times 10^{-3}$ | |
| 7.3002 | 5.888 | 1.6984 | 1.606 | $3.998 \times 10^{-3}$ | |
| 7.4713 | 6.026 | 1.6595 | 1.647 | $7.241 \times 10^{-2}$ | |
| 7.6449 | 6.166 | 1.6218 | 1.653 | $1.351 \times 10^{-1}$ | |
| 7.8408 | 6.324 | 1.5813 | 1.641 | 2.022 | |
| 8.0417 | 6.486 | 1.5418 | 1.597 | 2.581 | |

(*continued*)

TABLE I (*Continued*)

Water

| eV | $cm^{-1}$ | μm | n | k | |
|---|---|---|---|---|---|
| 8.2673 | 6.668 | 1.4997 | 1.521 | 2.772 | [68] |
| 8.4992 | 6.855 | 1.4588 | 1.469 | 2.409 | |
| 8.7372 | 7.047 | 1.4190 | 1.462 | 1.927 | |
| 8.9815 | 7.244 | 1.3805 | 1.496 | 1.422 | |
| 9.2542 | 7.464 | 1.3398 | 1.586 | 1.489 | |
| 9.5357 | 7.691 | 1.3002 | 1.634 | 2.392 | |
| $9.8481 \times 10^{0}$ | 7.943 | 1.2590 | 1.606 | 3.220 | |
| $1.0172 \times 10^{1}$ | 8.204 | 1.2189 | 1.570 | 3.490 | |
| 1.0504 | 8.472 | 1.1804 | 1.553 | 3.705 | |
| 1.0873 | 8.770 | 1.1403 | 1.543 | 3.988 | |
| 1.1281 | 9.099 | 1.0990 | 1.529 | 4.303 | |
| 1.1705 | 9.441 | 1.0592 | 1.516 | 4.707 | |
| 1.2144 | $9.795 \times 10^{4}$ | $1.0209 \times 10^{-1}$ | 1.493 | 5.185 | |
| 1.2659 | $1.021 \times 10^{5}$ | $9.7943 \times 10^{-2}$ | 1.456 | 5.752 | |
| 1.3192 | 1.064 | 9.3985 | 1.388 | 6.292 | |
| 1.3787 | 1.112 | 8.9928 | 1.303 | 6.528 | |
| 1.4432 | 1.164 | 8.5911 | 1.215 | 6.573 | |
| 1.5114 | 1.219 | 8.2034 | 1.141 | 6.292 | |
| 1.5895 | 1.282 | 7.8003 | 1.088 | 5.981 | |
| 1.6763 | 1.352 | 7.3964 | 1.050 | 5.805 | |
| 1.7717 | 1.429 | 6.9979 | 0.982 | 5.791 | |
| 1.8771 | 1.514 | 6.6050 | 0.904 | 5.355 | |
| 2.0011 | 1.614 | 6.1958 | 0.841 | 4.558 | |
| 2.1400 | 1.726 | 5.7937 | 0.832 | 3.739 | |
| 2.2987 | 1.854 | 5.3937 | 0.835 | 3.310 | |
| 2.4797 | 2.000 | 5.0000 | 0.821 | 2.998 | |
| 2.6942 | 2.173 | 4.6019 | 0.797 | 2.414 | |
| 2.9533 | 2.382 | 4.1982 | 0.802 | 1.798 | |
| 3.2608 | 2.630 | 3.8023 | 0.820 | $1.303 \times 10^{-1}$ | |
| 3.6501 | 2.944 | 3.3967 | 0.842 | $9.074 \times 10^{-2}$ | |
| 4.1337 | 3.334 | 2.9994 | 0.867 | 6.064 | |
| 4.7685 | 3.846 | 2.6001 | 0.891 | 3.818 | |
| 5.6413 | 4.550 | 2.1978 | 0.914 | 2.227 | |
| 6.8923 | 5.559 | 1.7989 | 0.935 | $1.164 \times 10^{-2}$ | |
| $8.8587 \times 10^{1}$ | 7.145 | 1.3996 | 0.953 | $5.174 \times 10^{-3}$ | |
| $1.0337 \times 10^{2}$ | $8.337 \times 10^{5}$ | 1.1995 | 0.961 | 3.146 | |
| 1.2398 | $1.000 \times 10^{6}$ | 1.0000 | 0.968 | 1.745 | |

TABLE II

Values of $n$ and $k$ for Water Obtained from Ref. [80]

| eV | $cm^{-1}$ | μm | n | k |
|---|---|---|---|---|
| $6.3009 \times 10^{-2}$ | $5.082 \times 10^{2}$ | $1.9677 \times 10^{1}$ | 1.521 | $4.007 \times 10^{-1}$ |
| 6.6282 | 5.346 | 1.8706 | 1.484 | 4.186 |
| 7.0039 | 5.649 | 1.7702 | 1.435 | 4.274 |
| 7.4193 | 5.984 | 1.6711 | 1.381 | 4.293 |
| 7.8954 | 6.368 | 1.5704 | 1.321 | 4.176 |
| 8.4409 | 6.808 | 1.4689 | 1.260 | 3.943 |
| 9.0447 | 7.295 | 1.3708 | 1.194 | 3.546 |
| $9.7576 \times 10^{-2}$ | 7.870 | 1.2706 | 1.131 | 2.791 |
| $1.0602 \times 10^{-1}$ | 8.551 | 1.1695 | 1.113 | 1.621 |
| 1.1159 | 9.000 | 1.1111 | 1.143 | $1.006 \times 10^{-1}$ |
| 1.1407 | 9.200 | 1.0870 | 1.154 | $8.515 \times 10^{-2}$ |
| 1.1655 | 9.400 | 1.0638 | 1.168 | 7.150 |
| 1.1903 | 9.600 | 1.0417 | 1.183 | 6.130 |
| 1.2151 | $9.800 \times 10^{2}$ | 1.0204 | 1.196 | 5.370 |
| 1.2398 | $1.000 \times 10^{3}$ | $1.0000 \times 10^{1}$ | 1.208 | 4.790 |
| 1.2646 | 1.020 | $9.8039 \times 10^{0}$ | 1.219 | 4.418 |
| 1.2894 | 1.040 | 9.6154 | 1.229 | 4.142 |
| 1.3142 | 1.060 | 9.4340 | 1.237 | 3.943 |
| 1.3390 | 1.080 | 9.2593 | 1.245 | 3.788 |
| 1.3638 | 1.100 | 9.0909 | 1.251 | 3.669 |
| 1.3886 | 1.120 | 8.9286 | 1.257 | 3.591 |
| 1.4134 | 1.140 | 8.7719 | 1.262 | 3.518 |
| 1.4382 | 1.160 | 8.6207 | 1.268 | 3.476 |
| 1.4630 | 1.180 | 8.4746 | 1.272 | 3.426 |
| 1.4878 | 1.200 | 8.3333 | 1.276 | 3.401 |
| 1.5126 | 1.220 | 8.1967 | 1.279 | 3.381 |
| 1.5374 | 1.240 | 8.0645 | 1.282 | 3.343 |
| 1.5622 | 1.260 | 7.9365 | 1.285 | 3.289 |
| 1.5870 | 1.280 | 7.8125 | 1.288 | 3.295 |
| 1.6118 | 1.300 | 7.6923 | 1.291 | 3.289 |
| 1.6366 | 1.320 | 7.5758 | 1.294 | 3.263 |
| 1.6614 | 1.340 | 7.4627 | 1.296 | 3.227 |
| 1.6862 | 1.360 | 7.3529 | 1.298 | 3.202 |
| 1.7110 | 1.380 | 7.2464 | 1.301 | 3.183 |
| 1.7358 | 1.400 | 7.1429 | 1.302 | 3.170 |
| 1.7606 | 1.420 | 7.0423 | 1.304 | 3.164 |
| 1.7854 | 1.440 | 6.9444 | 1.306 | 3.168 |
| 1.8102 | 1.460 | 6.8493 | 1.309 | 3.232 |
| 1.8350 | 1.480 | 6.7568 | 1.311 | 3.287 |
| 1.8598 | 1.500 | 6.6667 | 1.314 | 3.371 |
| 1.8846 | 1.520 | 6.5789 | 1.317 | 3.520 |
| 1.9094 | 1.540 | 6.4935 | 1.322 | 3.945 |
| 1.9342 | 1.560 | 6.4103 | 1.329 | 4.543 |
| 1.9590 | 1.580 | 6.3291 | 1.343 | 5.378 |
| 1.9838 | 1.600 | 6.2500 | 1.347 | $7.112 \times 10^{-2}$ |
| 2.0086 | 1.620 | 6.1728 | 1.337 | $1.110 \times 10^{-1}$ |
| 2.0334 | 1.640 | 6.0976 | 1.302 | 1.309 |
| 2.0581 | 1.660 | 6.0241 | 1.257 | $1.214 \times 10^{-1}$ |
| 2.0829 | 1.680 | 5.9524 | 1.240 | $9.140 \times 10^{-2}$ |

(continued)

TABLE II (*Continued*)

Water

| eV | $cm^{-1}$ | μm | n | k |
|---|---|---|---|---|
| 2.1077 | 1.700 | 5.8824 | 1.235 | 5.394 |
| 2.1325 | 1.720 | 5.8140 | 1.248 | 3.635 |
| 2.1573 | 1.740 | 5.7471 | 1.261 | 2.636 |
| 2.1821 | 1.760 | 5.6818 | 1.270 | 1.770 |
| 2.2069 | 1.780 | 5.6180 | 1.275 | 1.448 |
| 2.2317 | 1.800 | 5.5556 | 1.284 | 1.274 |
| 2.2565 | 1.820 | 5.4945 | 1.289 | 1.166 |
| 2.2813 | 1.840 | 5.4348 | 1.294 | 1.083 |
| 2.3061 | 1.860 | 5.3763 | 1.298 | 1.037 |
| 2.3309 | 1.880 | 5.3191 | 1.301 | 1.032 |
| 2.3557 | 1.900 | 5.2632 | 1.304 | 1.042 |
| 2.3805 | 1.920 | 5.2083 | 1.307 | 1.049 |
| 2.4053 | 1.940 | 5.1546 | 1.310 | 1.076 |
| 2.4301 | 1.960 | 5.1020 | 1.312 | 1.136 |
| 2.4549 | 1.980 | 5.0505 | 1.314 | 1.219 |
| 2.4797 | 2.000 | 5.0000 | 1.315 | 1.291 |
| 2.5045 | 2.020 | 4.9505 | 1.316 | 1.353 |
| 2.5293 | 2.040 | 4.9020 | 1.318 | 1.434 |
| 2.5541 | 2.060 | 4.8544 | 1.318 | 1.500 |
| 2.5789 | 2.080 | 4.8077 | 1.319 | 1.549 |
| 2.6037 | 2.100 | 4.7619 | 1.320 | 1.558 |
| 2.6285 | 2.120 | 4.7170 | 1.319 | 1.551 |
| 2.6533 | 2.140 | 4.6729 | 1.319 | 1.524 |
| 2.6781 | 2.160 | 4.6296 | 1.319 | 1.481 |
| 2.7029 | 2.180 | 4.5872 | 1.319 | 1.398 |
| 2.7277 | 2.200 | 4.5455 | 1.319 | 1.315 |
| 2.7525 | 2.220 | 4.5045 | 1.320 | 1.232 |
| 2.7773 | 2.240 | 4.4643 | 1.321 | 1.151 |
| 2.8021 | 2.260 | 4.4248 | 1.322 | $1.065 \times 10^{-2}$ |
| 2.8269 | 2.280 | 4.3860 | 1.322 | $9.781 \times 10^{-3}$ |
| 2.8517 | 2.300 | 4.3478 | 1.323 | 9.127 |
| 2.8764 | 2.320 | 4.3103 | 1.324 | 8.544 |
| 2.9012 | 2.340 | 4.2735 | 1.325 | 7.862 |
| 2.9260 | 2.360 | 4.2373 | 1.327 | 7.274 |
| 2.9508 | 2.380 | 4.2017 | 1.329 | 6.813 |
| 2.9756 | 2.400 | 4.1667 | 1.330 | 6.389 |
| 3.0004 | 2.420 | 4.1322 | 1.332 | 5.984 |
| 3.0252 | 2.440 | 4.0984 | 1.334 | 5.557 |
| 3.0500 | 2.460 | 4.0650 | 1.335 | 5.155 |
| 3.0748 | 2.480 | 4.0323 | 1.337 | 4.912 |
| 3.0996 | 2.500 | 4.0000 | 1.339 | 4.636 |
| 3.1244 | 2.520 | 3.9683 | 1.342 | 4.334 |
| 3.1492 | 2.540 | 3.9370 | 1.344 | 4.076 |
| 3.1740 | 2.560 | 3.9063 | 1.346 | 3.911 |
| 3.1988 | 2.580 | 3.8760 | 1.349 | 3.781 |
| 3.2236 | 2.600 | 3.8462 | 1.352 | 3.669 |
| 3.2484 | 2.620 | 3.8168 | 1.354 | 3.588 |
| 3.2732 | 2.640 | 3.7879 | 1.355 | 3.624 |
| 3.2980 | 2.660 | 3.7594 | 1.358 | 3.712 |

(*continued*)

TABLE II (*Continued*)

Water

| eV | $cm^{-1}$ | μm | n | k |
|---|---|---|---|---|
| 3.3228 | 2.680 | 3.7313 | 1.360 | 3.803 |
| 3.3476 | 2.700 | 3.7037 | 1.362 | 3.952 |
| 3.3724 | 2.720 | 3.6765 | 1.365 | 4.220 |
| 3.3972 | 2.740 | 3.6496 | 1.368 | 4.569 |
| 3.4220 | 2.760 | 3.6232 | 1.371 | 5.002 |
| 3.4468 | 2.780 | 3.5971 | 1.375 | 5.494 |
| 3.4716 | 2.800 | 3.5714 | 1.379 | 6.121 |
| 3.4964 | 2.820 | 3.5461 | 1.383 | 6.969 |
| 3.5212 | 2.840 | 3.5211 | 1.388 | 7.954 |
| 3.5460 | 2.860 | 3.4965 | 1.392 | $9.170 \times 10^{-3}$ |
| 3.5708 | 2.880 | 3.4722 | 1.396 | $1.064 \times 10^{-2}$ |
| 3.5956 | 2.900 | 3.4483 | 1.401 | 1.243 |
| 3.6204 | 2.920 | 3.4247 | 1.406 | 1.462 |
| 3.6452 | 2.940 | 3.4014 | 1.412 | 1.736 |
| 3.6700 | 2.960 | 3.3784 | 1.418 | 1.968 |
| 3.6947 | 2.980 | 3.3557 | 1.425 | 2.588 |
| 3.7195 | 3.000 | 3.3333 | 1.431 | 3.505 |
| 3.7443 | 3.020 | 3.3113 | 1.438 | 4.289 |
| 3.7691 | 3.040 | 3.2895 | 1.445 | 4.764 |
| 3.7939 | 3.060 | 3.2680 | 1.453 | 5.405 |
| 3.8187 | 3.080 | 3.2468 | 1.460 | 6.553 |
| 3.8435 | 3.100 | 3.2258 | 1.466 | 7.932 |
| 3.8683 | 3.120 | 3.2051 | 1.472 | $9.208 \times 10^{-2}$ |
| 3.8931 | 3.140 | 3.1847 | 1.478 | $1.058 \times 10^{-1}$ |
| 3.9179 | 3.160 | 3.1646 | 1.477 | 1.232 |
| 3.9427 | 3.180 | 3.1447 | 1.476 | 1.450 |
| 3.9675 | 3.200 | 3.1250 | 1.469 | 1.656 |
| 3.9923 | 3.220 | 3.1056 | 1.463 | 1.833 |
| 4.0171 | 3.240 | 3.0864 | 1.452 | 1.990 |
| 4.0419 | 3.260 | 3.0675 | 1.433 | 2.161 |
| 4.0667 | 3.280 | 3.0488 | 1.417 | 2.267 |
| 4.0915 | 3.300 | 3.0303 | 1.407 | 2.369 |
| 4.1163 | 3.320 | 3.0120 | 1.390 | 2.487 |
| 4.1411 | 3.340 | 2.9940 | 1.375 | 2.606 |
| 4.1659 | 3.360 | 2.9762 | 1.350 | 2.740 |
| 4.1907 | 3.380 | 2.9586 | 1.323 | 2.819 |
| 4.2155 | 3.400 | 2.9412 | 1.291 | 2.854 |
| 4.2403 | 3.420 | 2.9240 | 1.254 | 2.826 |
| 4.2651 | 3.440 | 2.9070 | 1.211 | 2.765 |
| 4.2899 | 3.460 | 2.8902 | 1.180 | 2.637 |
| 4.3147 | 3.480 | 2.8736 | 1.153 | 2.451 |
| 4.3395 | 3.500 | 2.8571 | 1.135 | 2.230 |
| 4.3643 | 3.520 | 2.8409 | 1.110 | 2.032 |
| 4.3891 | 3.540 | 2.8249 | 1.083 | 1.854 |
| 4.4139 | 3.560 | 2.8090 | 1.090 | 1.613 |
| 4.4387 | 3.580 | 2.7933 | 1.091 | 1.356 |
| 4.4635 | 3.600 | 2.7778 | 1.109 | $1.129 \times 10^{-1}$ |
| 4.4883 | 3.620 | 2.7624 | 1.115 | $9.598 \times 10^{-2}$ |
| 4.5130 | 3.640 | 2.7473 | 1.112 | 7.725 |

(*continued*)

**TABLE II (*Continued*)**

**Water**

| eV | $cm^{-1}$ | μm | n | k |
|---|---|---|---|---|
| 4.5378 | 3.660 | 2.7322 | 1.131 | 4.909 |
| 4.5626 | 3.680 | 2.7174 | 1.150 | 2.388 |
| 4.5874 | 3.700 | 2.7027 | 1.164 | $1.248 \times 10^{-2}$ |
| 4.6122 | 3.720 | 2.6882 | 1.178 | $8.105 \times 10^{-3}$ |
| 4.6408 | 3.743 | 2.6717 | 1.190 | 5.456 |
| 4.6755 | 3.771 | 2.6518 | 1.204 | 3.943 |
| 4.7102 | 3.799 | 2.6323 | 1.214 | 3.163 |
| 4.7461 | 3.828 | 2.6123 | 1.222 | 2.647 |
| 4.7833 | 3.858 | 2.5920 | 1.229 | 2.316 |
| 4.8205 | 3.888 | 2.5720 | 1.236 | 2.158 |
| 4.8577 | 3.918 | 2.5523 | 1.241 | 2.099 |
| 4.8962 | 3.949 | 2.5323 | 1.245 | 2.065 |
| 4.9358 | 3.981 | 2.5119 | 1.249 | 1.984 |
| 4.9755 | 4.013 | 2.4919 | 1.253 | 1.824 |
| 5.0152 | 4.045 | 2.4722 | 1.256 | 1.586 |
| 5.0561 | 4.078 | 2.4522 | 1.259 | 1.353 |
| 5.0983 | 4.112 | 2.4319 | 1.262 | $1.156 \times 10^{-3}$ |
| 5.1404 | 4.146 | 2.4120 | 1.265 | $9.902 \times 10^{-4}$ |
| 5.1838 | 4.181 | 2.3918 | 1.267 | 8.574 |
| 5.2272 | 4.216 | 2.3719 | 1.270 | 7.381 |
| 5.2718 | 4.252 | 2.3518 | 1.272 | 6.365 |
| 5.3165 | 4.288 | 2.3321 | 1.274 | 5.513 |
| 5.3623 | 4.325 | 2.3121 | 1.276 | 4.806 |
| 5.4095 | 4.363 | 2.2920 | 1.278 | 4.244 |
| 5.4566 | 4.401 | 2.2722 | 1.279 | 3.805 |
| 5.5049 | 4.440 | 2.2523 | 1.281 | 3.501 |
| 5.5545 | 4.480 | 2.2321 | 1.283 | 3.304 |
| 5.6054 | 4.521 | 2.2119 | 1.284 | 3.217 |
| 5.6562 | 4.562 | 2.1920 | 1.286 | 3.205 |
| 5.7083 | 4.604 | 2.1720 | 1.287 | 3.324 |
| 5.7616 | 4.647 | 2.1519 | 1.288 | 3.510 |
| 5.8149 | 4.690 | 2.1322 | 1.289 | 3.817 |
| 5.8707 | 4.735 | 2.1119 | 1.291 | 4.283 |
| 5.9265 | 4.780 | 2.0921 | 1.292 | 4.919 |
| 5.9835 | 4.826 | 2.0721 | 1.293 | 5.732 |
| 6.0418 | 4.873 | 2.0521 | 1.294 | 6.780 |
| 6.1013 | 4.921 | 2.0321 | 1.295 | 8.087 |
| 6.1620 | 4.970 | 2.0121 | 1.296 | $9.765 \times 10^{-4}$ |
| 6.2240 | 5.020 | 1.9920 | 1.297 | $1.198 \times 10^{-3}$ |
| 6.2873 | 5.071 | 1.9720 | 1.297 | 1.477 |
| 6.3517 | 5.123 | 1.9520 | 1.298 | 1.785 |
| 6.4175 | 5.176 | 1.9320 | 1.298 | 1.997 |
| 6.4844 | 5.230 | 1.9120 | 1.298 | 1.849 |
| 6.5526 | 5.285 | 1.8921 | 1.298 | $1.069 \times 10^{-3}$ |
| 6.6233 | 5.342 | 1.8720 | 1.299 | $3.351 \times 10^{-4}$ |
| 6.6952 | 5.400 | 1.8519 | 1.301 | 1.674 |
| 6.7683 | 5.459 | 1.8318 | 1.301 | 1.326 |
| 6.8427 | 5.519 | 1.8119 | 1.302 | 1.267 |
| 6.9184 | 5.580 | 1.7921 | 1.303 | 1.252 |

(*continued*)

**TABLE II (*Continued*)**

**Water**

| eV | $cm^{-1}$ | μm | n | k |
|---|---|---|---|---|
| 6.9965 | 5.643 | 1.7721 | 1.304 | $1.166 \times 10^{-4}$ |
| 7.0771 | 5.708 | 1.7519 | 1.304 | $9.999 \times 10^{-5}$ |
| 7.1589 | 5.774 | 1.7319 | 1.305 | 8.617 |
| 7.2420 | 5.841 | 1.7120 | 1.306 | 7.855 |
| 7.3275 | 5.910 | 1.6920 | 1.306 | 7.432 |
| 7.4155 | 5.981 | 1.6720 | 1.307 | 7.374 |
| 7.5048 | 6.053 | 1.6521 | 1.308 | 7.470 |
| 7.5966 | 6.127 | 1.6321 | 1.308 | 7.852 |
| 7.6908 | 6.203 | 1.6121 | 1.309 | 8.420 |
| 7.7875 | 6.281 | 1.5921 | 1.309 | $9.336 \times 10^{-5}$ |
| 7.8867 | 6.361 | 1.5721 | 1.310 | $1.083 \times 10^{-4}$ |
| 7.9883 | 6.443 | 1.5521 | 1.310 | 1.288 |
| 8.0925 | 6.527 | 1.5321 | 1.311 | 1.603 |
| 8.2004 | 6.614 | 1.5119 | 1.311 | 2.034 |
| 8.3095 | 6.702 | 1.4921 | 1.312 | 2.601 |
| 8.4223 | 6.793 | 1.4721 | 1.312 | 3.223 |
| 8.5388 | 6.887 | 1.4520 | 1.313 | 3.523 |
| 8.6579 | 6.983 | 1.4320 | 1.313 | 3.368 |
| 8.7806 | 7.082 | 1.4120 | 1.313 | 2.705 |
| 8.9071 | 7.184 | 1.3920 | 1.314 | $1.311 \times 10^{-4}$ |
| 9.0373 | 7.289 | 1.3719 | 1.314 | $5.043 \times 10^{-5}$ |
| 9.1699 | 7.396 | 1.3521 | 1.315 | 3.576 |
| 9.3088 | 7.508 | 1.3319 | 1.315 | 2.588 |
| 9.4501 | 7.622 | 1.3120 | 1.316 | 1.706 |
| 9.5964 | 7.740 | 1.2920 | 1.316 | 1.327 |
| 9.7477 | 7.862 | 1.2719 | 1.316 | 1.133 |
| $9.9027 \times 10^{-1}$ | 7.987 | 1.2520 | 1.317 | 1.170 |
| $1.0064 \times 10^{0}$ | 8.117 | 1.2320 | 1.317 | 1.263 |

# Yttrium Oxide ($Y_2O_3$)

WILLIAM J. TROPF and MICHAEL E. THOMAS
Applied Physics Laboratory
The Johns Hopkins University
Laurel, Maryland

Yttrium sesquioxide (yttria) is a body-centered cubic material with bixbyite or cubic-C structure. The space group is $T_h^7$ or Ia3, unit cell length is 1.0604 nm, and the unit cell has 16 formula units (80 atoms). Theoretical density is 5.033 g/cm$^3$, melting point is 2710 K [1], and a phase change to a hexagonal form occurs at 2640 K [1].

Yttrium ions occupy two different sites, eight octahedral sites with $C_{3i}$ point symmetry and 24 prismatic sites with $C_2$ symmetry. Six oxygen ions surround each yttrium ion. Ion positions in the unit cell are known from both X-ray and neutron-diffraction measurements [2, 3].

Optical-quality, single-crystal yttria is available, typically made by the flame-fusion technique [4], and optical-quality sintered polycrystalline yttria is available in a variety of window shapes [5]. Optical-grade cubic yttria stabilized with up to 10 mole-percent thoria ("Yttralox") was previously made [6], and cubic yttria with lanthanum oxide ("lanthana-strengthened yttria") is commercially available [7, 8]. Comprehensive properties of commercial, polycrystalline yttria and lanthana-doped yttria are given in the literature [9].

Yttria is an excellent trivalent-ion host material for solid-state lasers. A variety of candidate metal-ion dopants, particularly neodymium [10], as well as many other rare-earth metals [11, 12] have been investigated.

Yttria has a band gap of approximately 6.0 eV. Several investigators have measured the optical constants from the UV through the XUV [13–16]. Earlier measurements [13, 14] used poor-quality samples and obtained results that qualitatively match recent measurements of Abramov *et al.* [15] and Tomiki *et al.* [16]. The latter measurements are considered definitive because they show the most detail, give results over the widest spectral range (3–42 eV), and agree well with the best available value of refractive index at the UV edge of the transparent region [17].

The lowest-frequency electronic feature of the yttria spectrum is an exciton peak at 6.0 eV. The peak sits on the edge of a broad resonance


Copyright © 1991 by Academic Press.
All rights of reproduction in any form reserved.
ISBN 0-12-544422-2

structure extending from 6.5–15 eV at room temperature. This broad feature arises from interband transitions between the upper valence band of oxygen ($2p^6$) to the conduction band of yttrium (4d + 5s) [15, 16]. Weaker absorption in the 15–27 eV region may be caused by transitions from the upper valence band of oxygen to higher excited conduction bands of doubly ionized yttrium [16]. At energies between 27 and 35 eV, absorption is attributed to electronic transitions from the ground state ($4p^6$) of triply ionized yttrium and the $4p^54d$ and $4p^55s$ excited states, with additional transitions to the 60.6 eV ionization level of $Y^{3+}$ postulated [16].

Tomiki *et al.* also give the temperature dependence of absorption at the UV edge of the transparent region (5.2–6.0 eV) for temperatures between 10 and 297 K and fit their measurements to an Urbach rule formulation

$$\alpha(E, T) = \alpha_0 \times \exp(-\sigma_s(T)(E_0 - E)/kT), \tag{1a}$$

where

$$\sigma_s(T) = \sigma_{s0} \times (2kT/E_{s0}) \tanh(E_{s0}/2kT). \tag{1b}$$

The constants of Eq. 1 are $\alpha_0 = 8.222 \times 10^6\ \text{cm}^{-1}$, $E_0 = 6.080$ eV, $\sigma_{s0} = 0.688$, and $E_{s0} = 0.0186$ eV. DeShazer *et al.* [18] report higher absorption values, and Nigara [17] gives even higher values.

Refractive-index data for the visible and IR transparent region of yttria are given in several sources. Wickersheim and LaFever [4] reported an index of refraction between 1.91 and 1.95 for yttria and mixed yttria–lanthana crystals. The most comprehensive data are provided by Nigara [17], who measured the index of crystals from 0.22–12 μm using different methods. His data were fitted to a Sellmeier-type dispersion relationship of the form

$$n^2 - 1 = \frac{13.4 \times 10^9}{(72{,}100)^2 - \nu^2} + \frac{7.48 \times 10^5}{(436)^2 - \nu^2}, \tag{2}$$

where $\nu$ is the frequency in wave numbers. This is the only available dispersion information for bulk yttria. Equation 2 represents electronic resonances at 72,100 $\text{cm}^{-1}$ (8.9 eV) with the first term, and IR resonances at 436 $\text{cm}^{-1}$ with the second term. These terms fall in the middle of the measured electronic transitions and lattice vibrations, respectively.

Tsukuda [19] also measured the refractive index of bulk transparent

yttria in the visible using an ellipsometry technique. His results are typically 0.5–1% below those of Nigara [17].

Smith and Baumeister [20] measured the refractive index of thin films of yttria over the 0.25–2 μm spectral range and found that the index was highly dependent on film preparation. Their measurements are significantly below those of Nigara (Eq. 2), typically by 10%, and the imaginary part of the refractive index (extinction coefficient) is much larger than is reported for bulk samples [16–18]. Thin-film refractive indices reported by Heitmann [21] are 2–3% below bulk index data [17], although more recent data by Arnon and Chou [22] also give index values 10% below that of bulk yttria.

Refractive indices of 1.92 at 0.589 μm for thoria-doped yttria (Yttralox, GE [23]) and 1.9699 at 0.546 μm for lanthana-doped yttria (an ellipsometer measurement [24]) have been reported. Equation 2 gives 1.930 and 1.937, respectively, at those two wavelengths.

Absorption in the transparent region (0.25–7 μm) is governed by impurities and defects. The most prominent absorption feature is the $OH^-$ absorption, which occurs in a broad region between 2500 and 3500 $cm^{-1}$ [4, 25, 26]. Various heat treatments can reduce the amount of $OH^-$ impurity. Defect absorption in the transparent region is highly dependent on preparation environment. Several investigators show that partial pressure of oxygen is a critical factor in producing a low level of defect absorption [10, 24, 27]. The primary defect is believed to be oxygen vacancies or interstitials. When yttria is exposed to a reducing atmosphere (for example, hydrogen) at very high temperature (>2000 K), a black form of yttria is produced [28] with very high absorption in the visible. At high temperatures (>1200 K), absorption increases, likely caused by a greater concentration of oxygen vacancies and interstitials in equilibrium [24, 29].

The dominant loss mechanism in the visible and near-IR transparent region of polycrystalline yttria is scatter. Bulk scatter in polycrystalline yttria is low and decreases with increasing wavelength [8, 9, 29].

Absorption at the IR edge of transparency is dominated by multiphonon absorption. A model of yttria multiphonon absorption has been developed and confirmed with experimental data over a wide temperature range [30]. The fundamental (one-phonon) lattice vibrations occur in the 120–555 $cm^{-1}$ spectral region. Group theory predicts the following phonon modes for yttria [31–33]:

$$\Gamma = 4E_g + 4A_g + 14F_g + 5E_u + 5A_u + 16F_u, \tag{3}$$

where all gerade modes are Raman-active, the $E_u$ and $A_u$ modes are inactive, and the 16 $F_u$ modes are IR-active. Table I lists the 11 strongest modes as determined from McDevitt and Davidson [34] (modes 1–3, location only) and Thomas [35] (modes 4–11, as well as estimated widths

and strengths for modes 1–3). Thomas also gives the temperature dependence of modes 4–11 over the 290–775 K temperature range. Nigara *et al.* [32] also give parameters for modes 5–11. Bloor and Dean [33] observe an additional IR mode at 197 $cm^{-1}$ in measurements made at 1.5 K.

Table I also lists both the transverse and longitudinal optical frequencies. The transverse optical frequencies are the mode locations; the maximum longitudinal mode frequency is an important parameter in the multiphonon absorption model [30], since it designates the maximum phonon frequency.

Characterization of the fundamental optical modes of yttria doped with 9 mole-percent lanthana [7, 8] shows similar lattice vibrational structures that are broader and red-shifted to lower frequency by 5–12 wave numbers. The multiphonon absorption edge is also red-shifted by a similar amount [30].

At frequencies below the last fundamental optical mode, absorption decreases and the material becomes transparent. The magnitude of absorption is thought to be a combination of contributions from both the tail of the fundamental lattice vibrations and various multiphonon difference bands. The index of refraction now also includes the effect of lattice vibrations. Estimates of low-frequency absorption made from the red wing of the fundamental modes (Table I) are about 40% of the imaginary index-of-refraction values determined by Stead and Simonis [36] in the 4–16 $cm^{-1}$ region. Smith and Loewenstein [37] measured the absorption coefficient of Yttralox (yttria with 10 mole-percent thoria) in the 50–200 $cm^{-1}$ region and found absorption similar to pure yttria.

The low-frequency index of refraction of yttria was measured by Stead and Simonis [36] at 3.43 (dielectric constant of 11.76), which agrees well with the measurements of Hyde [38] when corrected to full density and room temperature. The same value was obtained for Yttralox by Smith and Loewenstein [37], and a higher value of 3.49 (dielectric constant of 12.2) is given by Wei *et al.* [29] for yttria with 9 mole-percent lanthana. Westphal and Sils [39] report a room-temperature dielectric constant of 11.3 for 97% dense, 99.8% pure yttria.

Temperature dependence of the low-frequency index of refraction was measured by Hyde [38], who also found a resonance at very low frequencies (below $10^5$ Hz). His $dn/dT$ value of $1.05 \times 10^{-4}$/K ($d\varepsilon/dT = 7.2 \times 10^{-4}$/K) agrees well with the value predicted from the fundamental lattice-vibration model [35]. This model underpredicts the low-frequency index by 1.5%, probably because several weak vibrational modes have not been modelled (only 11 of the 16 modes predicted by group theory are observed and modeled).

Low-frequency dielectric constant data reported by Hyde [38] and Westphal and Sils [39] show a free-carrier effect that grows rapidly with temperature. Conductivity measurements by Tallan and Vest [27] also

indicate a growth in free carriers with temperature.

Table II was constructed from measurements reported in the literature as well as model predictions [30, 35]. Real-index ($n$) data from 2–40 eV, and imaginary-index ($k$) data from 5.2–40 eV are taken from the measurements of Tomiki *et al.* [16]. Real-index data below 6 eV (0.21–12 μm) are calculated from the Sellmeier dispersion relationship (Eq. 2) of Nigara [17]. Measurements of $k$ (determined from absorption coefficients) reported by DeShazer *et al.* [18] are also shown. These data may include significant extrinsic absorption because the values are much higher than those in Tomiki *et al.* [16].

Lattice-vibration-model results [35], using Nigara's [17] representation of the electronic contribution to index, are used to calculate the index of refraction for wavelengths of 1 μm and longer. Laser-calorimetry results for $k$ at 2.9 and 3.9 μm by Detrio and Greason [40] are also given to represent typical extrinsic absorption in the transparent region. Multiphonon absorption becomes important (greater than extrinsic absorption) at wavelengths beyond 4.5 μm. Values in the table up to 10 μm are calculated using the methods of Thomas *et al.* [30], which are validated by measurements. Beyond 10 μm, the fundamental (one-phonon) contributions become dominant. In this region, $n$ and $k$ are calculated using the parameters in Table I as described by Thomas [35]. The results are validated by comparing calculated reflection spectra to measurements.

Measurements of Stead and Simonis [36] and Hyde [38] best represent the low-frequency characteristics of yttria. In this region, one-phonon-model predictions [35] of $k$ are only 40% of measurements [36], and real-index values are 1.5% low compared to measurements [36, 38].

The accuracy of available index data is unknown. In all data, the uncertainty in the values is probably in the least significant digit reported in Table II. In spectral regions where several sources of data exist, there is a large disparity between references.

Figure 1 shows a composite of the complex index of refraction based on the data of Table II.

Table III gives temperature dependence for the real part of the index of refraction. Measurements of $dn/dT$ by Wei *et al.* [29] give $5.0 \times 10^{-5}$/K and $3.2 \times 10^{-5}$/K at wavelengths of 0.357 and 3.39 μm, respectively. Measurements made by A.P.L./J.H.U. at 0.633 μm give much lower values: $8.4 \times 10^{-6}$ for pure yttria and $8.4 \times 10^{-6}$ for lanthana-doped yttria. The temperature change in index of refraction at microwave frequencies remains nearly linear for most oxides up to 1000 K. This characteristic is likely to be true for yttria also, but has not been experimentally verified.

Temperature-dependent absorption predictions from optical models of yttria [30, 35] have been used to estimate total hemispherical emissivity of pure, transparent yttria over the 200 to 1000 K temperature range, where the models are expected to give the best results and intrinsic (temperature-

produced) defect absorption is believed to be insignificant [9]. These results were obtained by estimating the complex refractive index at a given temperature, calculating directional emittance for a specific slab thickness, integrating over angle, and convolving the resulting spectral hemispherical emittances with the Planck function.

Table IV gives the resulting total hemispherical emittance for semi-infinite slabs as a function of slab thickness. Since total hemispherical emissivity is an important function for radiation-relief calculations and is needed to correct property measurements such as thermal conductivity, we have included this calculated result.

## REFERENCES


1. L. M. Lopato, B. S. Nigmanov, A. V. Shevchenko, and Z. A. Zaitseva, "Interaction between Lanthanum Oxide and Yttrium Oxide," *Inorg. Mater.* **22**, 678 (1986).
2. M. G. Paton and E. N. Maslen, "A Refinement of the Crystal Structure of Yttria," *Acta Crystallogr.* **19**, 307 (1965).
3. B. H. O'Conner and T. M. Valentine, "A Neutron Diffraction Study of the Crystal Structure of the C-form of Yttrium Sesquioxide," *Acta Crystallogr.* **B25**, 2140 (1960).
4. K. A. Wickersheim and R. A. LaFever, "Infrared Transmittance of Crystalline Yttrium Oxide and Related Compounds," *J. Opt. Soc. Am.* **51**, 1147 (1961).
5. R. L. Gentilman, "Current and Emerging Materials for 3–5 Micron IR Transmission," *Proc. SPIE* **683**, 2 (1986).
6. C. Greskovick and N. K. Woods, "Fabrication of Transparent $ThO_2$-Doped $Y_2O_3$," *Ceram. Bull.* **52**, 473 (1973).
7. W. H. Rhodes, "Controlled Transient Solid Second-Phase Sintering of Yttria," *J. Am. Ceram. Soc.* **64**, 13 (1981).
8. W. H. Rhodes, G. C. Wei, and E. A. Trickett, "Lanthana-Doped Yttria: A New Infrared Material," *Proc. SPIE* **683**, 12 (1986).
9. W. J. Tropf and D. C. Harris, "Mechanical, Thermal, and Optical Properties of Yttria and Lanthana-Doped Yttria," *Proc. SPIE* **1112**, 9 (1989).
10. H. Tsuiki, T. Masumoto, K. Kitazawa, and K. Fueki, "Effect of Point Defects on Laser Oscillation Properties of Nd-Doped $Y_2O_3$," *Jap. J. Appl. Phys.* **21**, 1017 (1982).
11. N. C. Chang, J. B. Gruber, R. P. Leavitt, and C. A. Morrison, "Optical Spectra, Energy Levels, and Crystal-Field Analysis of Positive Rare Earth Ions in $Y_2O_3$. I. Kramers Ions in $C_2$ Sites," *J. Chem. Phys.* **76**, 3877 (1982).
12. R. P. Leavitt, J. B. Gruber, N. C. Chang, and C. A. Morrison, "Optical Spectra, Energy Levels, and Crystal-Field Analysis of Positive Rare Earth Ions in $Y_2O_3$. II. Non-Kramers Ions in $C_2$ Sites," *J. Chem. Phys.* **76**, 4775 (1982).
13. V. N. Abramov and A. I. Kuznetsov, "Fundamental Absorption of $Y_2O_3$ and $YAlO_3$," *Sov. Phys. Solid State* **20**, 399 (1978).
14. K. S. Bagdasarov, V. P. Zhuze, M. G. Karin, K. K. Sidorin, and A. I. Shelykh, "Optical Properties of Rare-Earth Sesquioxides in the Fundamental Absorption Range," *Sov. Phys. Solid State* **26**, 687 (1984).
15. V. N. Abramov, A. N. Ermoshkin, and A. I. Kuznetsov, "Optical Properties and Electron Energy Structure of $Y_2O_3$ and $Sc_2O_3$," *Sov. Phys. Solid State* **25**, 981 (1983).
16. T. Tomiki, J. Tamashiro, Y. Tanahara, A. Yamada, H. Fukutani, T. Miyahara, H. Kato, S. Shin, and M. Ishigame, "Optical Spectra of $Y_2O_3$ Single Crystals in VUV," *J. Phys. Soc. Jap.* **55**, 4543 (1986).
17. Y. Nigara, "Measurement of the Optical Constants of Yttrium Oxide," *Jap. J. Appl. Phys.* **7**, 404 (1968).

18. L. G. DeShazer, S. C. Rand, and B. A. Wechsler, "Laser Crystals," in "CRC Handbook of Laser Science and Technology, Volume V: Optical Materials; Part 3: Applications, Coatings, and Fabrication," (M. J. Weber, ed.), CRC Press, Boca Raton, Florida, 288 (1988).
19. Y. Tsukuda, "Refractive and Reflective Indices of $Y_2O_3$ Sintered Bodies," *Nippon Kagaku Kaishi (8)*, 1106 (1979).
20. D. Smith and P. Baumeister, "Refractive Index of Some Oxide and Fluoride Coating Materials," *Appl. Opt.* **18**, 111 (1979).
21. W. Heitmann, "Reactively Evaporated Films of Scandia and Yttria," *Appl. Opt.* **12**, 394 (1973).
22. O. Arnon and T. J. Chou, "Wide Band Measurement of the Refractive Index of Optical Thin Films During Their Deposition," *Thin Solid Films* **91**, 23 (1982).
23. Yttralox data sheets, available from General Electric Research and Development Center, Schenectady, New York.
24. G. C. Wei, C. Brecher, and W. H. Rhodes, "Effect of Point Defects on High-Temperature Optical Properties in Transparent Polycrystalline Lanthana-Doped Yttria," *Proc. SPIE* **683**, 146 (1986).
25. G. C. Wei, "Extrinsic $OH^-$ Absorption in Transparent Pollycrystalline Lanthana-Doped Yttria," *J. Am. Ceram. Soc.* **71**, C20 (1988).
26. J. A. Harrington and C. Greskovich, "Infrared Absorption in $ThO_2$-Doped $Y_2O_3$," *J. Appl. Phys.* **48**, 1585 (1977).
27. N. M. Tallan and R. W. Vest, "Electrical Properties and Defect Structure of $Y_2O_3$," *J. Am. Ceram. Soc.* **49**, 401 (1966).
28. Y. Tsukuda, "Properties of Black $Y_2O_3$ Sintered Bodies," *Mater. Res. Bull.* **16**, 453 (1981).
29. G. C. Wei, C. Brecher, M. R. Pascucci, E. A. Trickett, and W. H. Rhodes, "Characterization of Lanthana-Strengthened Yttria Infrared Transmitting Materials," *Proc. SPIE* **929**, 50 (1988).
30. M. E. Thomas, R. I. Joseph, and W. J. Tropf, "Infrared Transmission Properties of Sapphire, Spinel, Yttria, and ALON as a Function of Frequency and Temperature," *Appl. Opt.* **27**, 239 (1988).
31. N. V. Porotnikov, O. I. Kondratov, L. L. Kochergina, and K. I. Petrov, "Calculation of the Theoretical Vibrational Spectrum of $Y_2O_3$," *Russ. J. Inorg. Chem.* **29**, 954 (1984).
32. Y. Nigara, M. Ishigame, and T. Sakurai, "Infrared Properties of Yttrium Oxide," *J. Phys. Soc. Jap.* **30**, 453 (1971).
33. D. Bloor and J. R. Dean, "Spectroscopy of Rare Earth Oxide Systems: I. Far Infrared Spectra of the Rare Earth Sesquioxides, Cerium Oxide, and Nonstoichiometric Praseodymium and Terbium Oxides," *J. Phys. C.* **5**, 1237 (1972).
34. N. T. McDevitt and A. D. Davidson, "Infrared Lattice Spectra of Cubic Rare Earth Oxides in the Region 700 to 50 $cm^{-1}$," *J. Opt. Soc. Am.* **56**, 636 (1966).
35. M. E. Thomas, "A Computer Code for Modeling Optical Properties of Window Materials," *Proc. SPIE* **1112**, 260 (1989).
36. M. Stead and G. Simonis, "Near Millimeter Wave Characterization of Dual Mode Materials," *Appl. Opt.* **28**, 1874 (1989).
37. D. R. Smith and E. V. Loewenstein, "Optical Constants of Metal Oxides in the Far Infrared Region," *Appl. Opt.* **15**, 859 (1976).
38. G. R. Hyde, "Dielectric Properties of Sintered Yttrium Oxide," *J. Am. Ceram. Soc.* **54**, 535 (1971).
39. W. B. Westphal and A. Sils, "Dielectric Constant and Loss Data," Air Force Materials Laboratory, AFML-TR-72-39, Wright-Patterson AFB, Ohio, (April 1972).
40. J. A. Detrio and Paul Greason, University of Dayton, personal communication (April 8, 1988).

**NOTES ADDED IN PROOF**

A recent theoretical study of yttria electronic structure and bonding is given in [41]. Results agreed well with experiments.

A recent measurement of the index of refraction of 9% lanthana-doped yttria made by the minimum deviation method gave a value of $1.9294 \pm 0.0001$ at 546 nm [42]. This value, believed to be accurate, is considerably below the value given in [24], and much closer to the index of pure yttria. Other measurements between 0.4 and 2.3 μm show the same trend [42].

Details of the measurement of $dn/dT$ at 0.6368 μm in Table III are given in [43]. Spectral and directional scatter measurements of commercial ALON are given in [44].

41. W. Y. Ching and Y.-N. Xu, "Electronic and Optical Properties of Yttria," *Phys. Rev. Lett.* **65**, 895–898 (1990).
42. R. J. Scheller, Schott Glass Technologies, Inc., personal communication (April 24, 1990).
43. C. H. Lange and D. D. Duncan, "Temperature Coefficient of Refractive Index for Candidate Optical Windows," *SPIE Proc.* **1326**, 71–78 (1990).
44. C. H. Lange, D. D. Duncan, and D. G. Fischer "Imaging Performance of Crystalline and Polycrystalline Oxides," *SPIE Proc.* **1326**, 59–70 (1990).

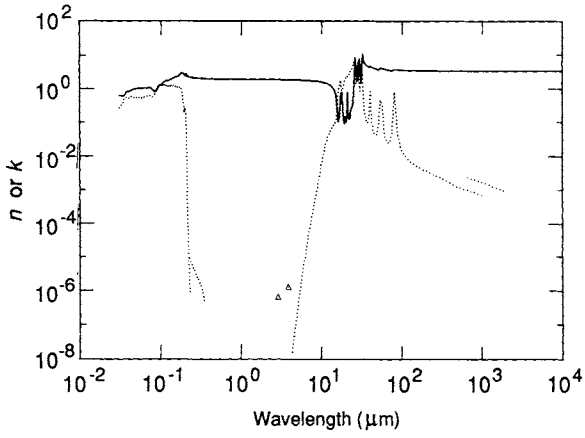


**Fig. 1.** Log–log plot of $n$ (solid line) and $k$ (dashed line) versus wavelength in micrometers for yttrium oxide. Data from various sources sometimes do not join together in overlap regions. Symbols are laser calorimetry measurements of $k$.

**TABLE I**

**Fundamental Infrared Lattice-Vibration Parameters for Yttrium Oxide[a]**

| Mode | Transverse optical frequency ($cm^{-1}$) | Strength | Normalized width | Longitudinal optical frequency ($cm^{-1}$) | Refs. |
|---|---|---|---|---|---|
| 1 | 120 | 0.20 | 0.035 | 121 | [34,35] |
| 2 | 172 | 0.10 | 0.025 | 173 | [34,35] |
| 3 | 182 | 0.15 | 0.025 | 183 | [34,35] |
| 4 | 241 | 0.20 | 0.025 | 242 | [35] |
| 5 | 303 | 2.60 | 0.0135 | 315 | [35] |
| 6 | 335 | 1.75 | 0.0115 | 359 | [35] |
| 7 | 371 | 2.65 | 0.021 | 412 | [35] |
| 8 | 415 | 0.04 | 0.011 | 456 | [35] |
| 9 | 461 | 0.05 | 0.015 | 486 | [35] |
| 10 | 490 | 0.005 | 0.018 | 535 | [35] |
| 11 | 555 | 0.095 | 0.025 | 620 | [35] |
| | | Total = 7.86 | | | |

[a]The transverse optical frequency ($\nu_j$) is the location of the mode. The strength ($\Delta\epsilon_j$) is the contribution of the mode to the dielectric constant. The normalized width ($\gamma_j$) is the mode width divided by the mode frequency. The complex dielectric constant ($\epsilon$) is then modeled as a function of frequency ($\nu$) by

$$\epsilon(\nu) = \epsilon_\infty + \sum_j \frac{\Delta\epsilon_j \nu_j^2}{\nu_j^2 - \nu^2 + i\gamma_j \nu_j \nu} ,$$

where the $\epsilon_\infty$ term (= 3.579) represents the electronic contributions to the dielectric constant (plus one). Nigara *et al.* [32] also observed modes 5-11. Bloor and Dean [33] observed a mode at 197 $cm^{-1}$ in measurements made at 1.5 K. Such a mode was not observed by McDevitt and Davidson [34].

**TABLE II**

**Values of $n$ and $k$ Obtained from Various References for Yttrium Oxide[a]**

| eV | $cm^{-1}$ | $\mu m$ | $n$ | $k$ | $n$ | $k$ |
|---|---|---|---|---|---|---|
| 40.0 | 322619 | 0.0310 | 0.624 [16] | 0.272 [16] | | |
| 39.0 | 314554 | 0.0318 | 0.624 | 0.295 | | |
| 38.0 | 306488 | 0.0326 | 0.624 | 0.314 | | |
| 37.0 | 298423 | 0.0335 | 0.623 | 0.356 | | |
| 36.0 | 290357 | 0.0344 | 0.621 | 0.388 | | |
| 35.0 | 282292 | 0.0354 | 0.621 | 0.461 | | |
| 34.0 | 274226 | 0.0365 | 0.671 | 0.535 | | |
| 33.0 | 266161 | 0.0376 | 0.775 | 0.565 | | |
| 32.0 | 258095 | 0.0387 | 0.823 | 0.535 | | |
| 31.0 | 250030 | 0.0400 | 0.832 | 0.515 | | |
| 30.0 | 241964 | 0.0413 | 0.834 | 0.543 | | |
| 29.0 | 233899 | 0.0428 | 0.876 | 0.596 | | |
| 28.0 | 225833 | 0.0443 | 0.942 | 0.567 | | |
| 27.0 | 217768 | 0.0459 | 0.965 | 0.561 | | |
| 26.0 | 209702 | 0.0477 | 0.985 | 0.551 | | |
| 25.0 | 201637 | 0.0496 | 0.997 | 0.550 | | |
| 24.5 | 197604 | 0.0506 | 1.000 | 0.554 | | |
| 24.0 | 193572 | 0.0517 | 1.016 | 0.564 | | |
| 23.5 | 189539 | 0.0528 | 1.025 | 0.563 | | |
| 23.0 | 185506 | 0.0539 | 1.039 | 0.556 | | |
| 22.5 | 181473 | 0.0551 | 1.048 | 0.547 | | |
| 22.0 | 177441 | 0.0564 | 1.045 | 0.540 | | |
| 21.5 | 173408 | 0.0577 | 1.044 | 0.545 | | |
| 21.0 | 169375 | 0.0590 | 1.041 | 0.542 | | |
| 20.5 | 165342 | 0.0605 | 1.040 | 0.543 | | |
| 20.0 | 161310 | 0.0620 | 1.041 | 0.553 | | |
| 19.5 | 157277 | 0.0636 | 1.042 | 0.560 | | |
| 19.0 | 153244 | 0.0653 | 1.042 | 0.570 | | |
| 18.5 | 149211 | 0.0670 | 1.042 | 0.584 | | |
| 18.0 | 145179 | 0.0689 | 1.039 | 0.595 | | |
| 17.5 | 141146 | 0.0708 | 1.051 | 0.618 | | |
| 17.0 | 137113 | 0.0729 | 1.072 | 0.639 | | |
| 16.5 | 133080 | 0.0751 | 1.084 | 0.631 | | |
| 16.0 | 129048 | 0.0775 | 1.062 | 0.597 | | |
| 15.5 | 125015 | 0.0800 | 0.979 | 0.578 | | |
| 15.0 | 120982 | 0.0827 | 0.892 | 0.605 | | |
| 14.5 | 116949 | 0.0855 | 0.819 | 0.702 | | |
| 14.0 | 112917 | 0.0886 | 0.829 | 0.860 | | |
| 13.9 | 112110 | 0.0892 | 0.843 | 0.900 | | |
| 13.8 | 111304 | 0.0898 | 0.857 | 0.938 | | |
| 13.7 | 110497 | 0.0905 | 0.875 | 0.971 | | |
| 13.6 | 109691 | 0.0912 | 0.894 | 1.003 | | |
| 13.5 | 108884 | 0.0918 | 0.917 | 1.035 | | |
| 13.4 | 108077 | 0.0925 | 0.940 | 1.067 | | |

(*continued*)

**TABLE II (*Continued*)**

**Yttrium Oxide**

| eV | $cm^{-1}$ | $\mu m$ | $n$ | $k$ | $n$ | $k$ |
|---|---|---|---|---|---|---|
| 13.3 | 107271 | 0.0932 | 0.973 | 1.101 | | |
| 13.2 | 106464 | 0.0939 | 1.017 | 1.137 | | |
| 13.1 | 105658 | 0.0946 | 1.043 | 1.169 | | |
| 13.0 | 104851 | 0.0954 | 1.077 | 1.196 | | |
| 12.9 | 104045 | 0.0961 | 1.143 | 1.220 | | |
| 12.8 | 103238 | 0.0969 | 1.198 | 1.243 | | |
| 12.7 | 102432 | 0.0976 | 1.247 | 1.265 | | |
| 12.6 | 101625 | 0.0984 | 1.279 | 1.281 | | |
| 12.5 | 100819 | 0.0992 | 1.287 | 1.295 | | |
| 12.4 | 100012 | 0.1000 | 1.292 | 1.290 | | |
| 12.3 | 99205 | 0.1008 | 1.296 | 1.282 | | |
| 12.2 | 98399 | 0.1016 | 1.301 | 1.267 | | |
| 12.1 | 97592 | 0.1025 | 1.305 | 1.250 | | |
| 12.0 | 96786 | 0.1033 | 1.308 | 1.238 | | |
| 11.9 | 95979 | 0.1042 | 1.323 | 1.234 | | |
| 11.8 | 95173 | 0.1051 | 1.356 | 1.235 | | |
| 11.7 | 94366 | 0.1060 | 1.390 | 1.246 | | |
| 11.6 | 93560 | 0.1069 | 1.415 | 1.259 | | |
| 11.5 | 92753 | 0.1078 | 1.440 | 1.273 | | |
| 11.4 | 91946 | 0.1088 | 1.481 | 1.285 | | |
| 11.3 | 91140 | 0.1097 | 1.520 | 1.291 | | |
| 11.2 | 90333 | 0.1107 | 1.537 | 1.297 | | |
| 11.1 | 89527 | 0.1117 | 1.543 | 1.292 | | |
| 11.0 | 88720 | 0.1127 | 1.555 | 1.286 | | |
| 10.9 | 87914 | 0.1137 | 1.575 | 1.276 | | |
| 10.8 | 87107 | 0.1148 | 1.615 | 1.264 | | |
| 10.7 | 86301 | 0.1159 | 1.643 | 1.258 | | |
| 10.6 | 85494 | 0.1170 | 1.684 | 1.264 | | |
| 10.5 | 84688 | 0.1181 | 1.704 | 1.262 | | |
| 10.4 | 83881 | 0.1192 | 1.716 | 1.252 | | |
| 10.3 | 83074 | 0.1204 | 1.721 | 1.237 | | |
| 10.2 | 82268 | 0.1216 | 1.725 | 1.221 | | |
| 10.1 | 81461 | 0.1228 | 1.730 | 1.208 | | |
| 10.0 | 80655 | 0.1240 | 1.735 | 1.196 | | |
| 9.9 | 79848 | 0.1252 | 1.741 | 1.192 | | |
| 9.8 | 79042 | 0.1265 | 1.749 | 1.170 | | |
| 9.7 | 78235 | 0.1278 | 1.757 | 1.163 | | |
| 9.6 | 77429 | 0.1292 | 1.766 | 1.165 | | |
| 9.5 | 76622 | 0.1305 | 1.782 | 1.173 | | |
| 9.4 | 75816 | 0.1319 | 1.811 | 1.180 | | |
| 9.3 | 75009 | 0.1333 | 1.857 | 1.185 | | |
| 9.2 | 74202 | 0.1348 | 1.898 | 1.197 | | |
| 9.1 | 73396 | 0.1362 | 1.908 | 1.216 | | |
| 9.0 | 72589 | 0.1378 | 1.925 | 1.235 | | |

(*continued*)

**TABLE II (*Continued*)**

**Yttrium Oxide**

| eV | $cm^{-1}$ | $\mu m$ | $n$ | $k$ | $n$ | $k$ |
|---|---|---|---|---|---|---|
| 8.9 | 71783 | 0.1393 | 1.946 | 1.266 | | |
| 8.8 | 70976 | 0.1409 | 1.975 | 1.212 | | |
| 8.7 | 70170 | 0.1425 | 2.021 | 1.211 | | |
| 8.6 | 69363 | 0.1442 | 2.051 | 1.216 | | |
| 8.5 | 68557 | 0.1459 | 2.089 | 1.221 | | |
| 8.4 | 67750 | 0.1476 | 2.139 | 1.220 | | |
| 8.3 | 66943 | 0.1494 | 2.181 | 1.217 | | |
| 8.2 | 66137 | 0.1512 | 2.196 | 1.205 | | |
| 8.1 | 65330 | 0.1531 | 2.209 | 1.188 | | |
| 8.0 | 64524 | 0.1550 | 2.222 | 1.162 | | |
| 7.9 | 63717 | 0.1569 | 2.240 | 1.136 | | |
| 7.8 | 62911 | 0.1590 | 2.265 | 1.123 | | |
| 7.7 | 62104 | 0.1610 | 2.294 | 1.124 | | |
| 7.6 | 61298 | 0.1631 | 2.314 | 1.121 | | |
| 7.5 | 60491 | 0.1653 | 2.334 | 1.110 | | |
| 7.4 | 59685 | 0.1675 | 2.418 | 1.103 | | |
| 7.3 | 58878 | 0.1698 | 2.468 | 1.110 | | |
| 7.2 | 58071 | 0.1722 | 2.523 | 1.118 | | |
| 7.1 | 57265 | 0.1746 | 2.592 | 1.118 | | |
| 7.0 | 56458 | 0.1771 | 2.682 | 1.109 | | |
| 6.9 | 55652 | 0.1797 | 2.820 | 1.093 | | |
| 6.8 | 54845 | 0.1823 | 2.916 | 1.054 | | |
| 6.7 | 54039 | 0.1851 | 2.952 | 0.926 | | |
| 6.6 | 53232 | 0.1879 | 2.947 | 0.755 | | |
| 6.5 | 52426 | 0.1907 | 2.891 | 0.590 | | |
| 6.4 | 51619 | 0.1937 | 2.801 | 0.427 | | |
| 6.3 | 50813 | 0.1968 | 2.682 | 0.276 | | |
| 6.2 | 50006 | 0.2000 | 2.628 | 0.186 | | |
| 6.1 | 49199 | 0.2033 | 2.583 | 0.249 | | |
| 6.0 | 48393 | 0.2066 | 2.652 | 0.276 | 2.386 [17] | |
| 5.9 | 47586 | 0.2101 | 2.726 | 0.129 | 2.359 | |
| 5.8 | 46780 | 0.2138 | 2.632 | 0.0113 | 2.335 | |
| 5.7 | 45973 | 0.2175 | 2.483 | $8.74 \cdot 10^{-5}$ | 2.312 | |
| 5.6 | 45167 | 0.2214 | 2.360 | $7.67 \cdot 10^{-5}$ | 2.290 | |
| 5.5 | 44360 | 0.2254 | 2.315 | $9.49 \cdot 10^{-6}$ | 2.269 | |
| 5.4 | 43554 | 0.2296 | 2.266 | $2.29 \cdot 10^{-6}$ | 2.249 | $9.0 \cdot 10^{-6}$ [18] |
| 5.3 | 42747 | 0.2339 | 2.233 | $1.05 \cdot 10^{-6}$ | 2.230 | $8.0 \cdot 10^{-6}$ |
| 5.2 | 41940 | 0.2384 | 2.199 | $7.61 \cdot 10^{-7}$ | 2.213 | $7.1 \cdot 10^{-6}$ |
| 5.1 | 41134 | 0.2431 | 2.176 | | 2.196 | $6.3 \cdot 10^{-6}$ |
| 5.0 | 40327 | 0.2480 | 2.155 | | 2.180 | $5.6 \cdot 10^{-6}$ |
| 4.9 | 39531 | 0.2530 | 2.127 | | 2.164 | $5.0 \cdot 10^{-6}$ |
| 4.8 | 38714 | 0.2583 | 2.115 | | 2.150 | $4.5 \cdot 10^{-6}$ |
| 4.7 | 37908 | 0.2638 | 2.106 | | 2.136 | $4.0 \cdot 10^{-6}$ |
| 4.6 | 37101 | 0.2695 | 2.096 | | 2.123 | $3.5 \cdot 10^{-6}$ |

(*continued*)

**TABLE II (*Continued*)**

**Yttrium Oxide**

| eV | $cm^{-1}$ | $\mu m$ | $n$ | $k$ | $n$ | $k$ |
|---|---|---|---|---|---|---|
| 4.5 | 36295 | 0.2755 | 2.085 | | 2.110 | $3.1 \cdot 10^{-6}$ |
| 4.4 | 35488 | 0.2818 | 2.073 | | 2.098 | $2.7 \cdot 10^{-6}$ |
| 4.3 | 34682 | 0.2883 | 2.062 | | 2.086 | $2.4 \cdot 10^{-6}$ |
| 4.2 | 33875 | 0.2952 | 2.052 | | 2.075 | $2.2 \cdot 10^{-6}$ |
| 4.1 | 33068 | 0.3024 | 2.042 | | 2.065 | $1.9 \cdot 10^{-6}$ |
| 4.0 | 32262 | 0.3100 | 2.034 | | 2.055 | $1.7 \cdot 10^{-6}$ |
| 3.9 | 31455 | 0.3179 | 2.025 | | 2.045 | $1.4 \cdot 10^{-6}$ |
| 3.8 | 30649 | 0.3263 | 2.017 | | 2.036 | $1.2 \cdot 10^{-6}$ |
| 3.7 | 29842 | 0.3351 | 2.010 | | 2.027 | $9 \cdot 10^{-7}$ |
| 3.6 | 29036 | 0.3444 | 2.004 | | 2.019 | $6 \cdot 10^{-7}$ |
| 3.5 | 28229 | 0.3542 | 1.998 | | 2.011 | $4 \cdot 10^{-7}$ |
| 3.4 | 27423 | 0.3647 | 1.992 | | 2.003 | |
| 3.3 | 26616 | 0.3757 | 1.985 | | 1.996 | |
| 3.2 | 25810 | 0.3875 | 1.978 | | 1.989 | |
| 3.1 | 25003 | 0.4000 | 1.971 | | 1.982 | |
| 3.0 | 24196 | 0.4133 | 1.964 | | 1.976 | |
| 2.9 | 23390 | 0.4275 | 1.959 | | 1.970 | |
| 2.8 | 22583 | 0.4428 | 1.953 | | 1.964 | |
| 2.7 | 21777 | 0.4592 | 1.948 | | 1.958 | |
| 2.6 | 20970 | 0.4769 | 1.944 | | 1.953 | |
| 2.5 | 20164 | 0.4959 | 1.940 | | 1.948 | |
| 2.48 | 20000 | 0.5000 | 1.939 | | 1.947 | |
| 2.42 | 19500 | 0.5128 | 1.938 | | 1.944 | |
| 2.4 | 19357 | 0.5166 | 1.938 | | 1.943 | |
| 2.36 | 19000 | 0.5263 | 1.937 | | 1.941 | |
| 2.3 | 18551 | 0.5391 | 1.936 | | 1.939 | |
| 2.29 | 18500 | 0.5405 | 1.936 | | 1.938 | |
| 2.23 | 18000 | 0.5556 | 1.935 | | 1.936 | |
| 2.2 | 17744 | 0.5636 | 1.934 | | 1.934 | |
| 2.17 | 17500 | 0.5714 | 1.933 | | 1.933 | |
| 2.11 | 17000 | 0.5882 | 1.932 | | 1.931 | |
| 2.1 | 16938 | 0.5904 | 1.932 | | 1.930 | |
| 2.05 | 16500 | 0.6061 | 1.931 | | 1.928 | |
| 2.0 | 16131 | 0.6199 | 1.930 | | 1.926 | |
| 1.984 | 16000 | 0.6250 | | | 1.926 | |
| 1.922 | 15500 | 0.6452 | | | 1.923 | |
| 1.860 | 15000 | 0.6667 | | | 1.921 | |
| 1.798 | 14500 | 0.6897 | | | 1.919 | |
| 1.736 | 14000 | 0.7143 | | | 1.917 | |
| 1.674 | 13500 | 0.7407 | | | 1.915 | |
| 1.612 | 13000 | 0.7692 | | | 1.913 | |
| 1.550 | 12500 | 0.8000 | | | 1.911 | |
| 1.488 | 12000 | 0.8333 | | | 1.909 | |
| 1.426 | 11500 | 0.8696 | | | 1.908 | |

(*continued*)

**TABLE II (*Continued*)**

**Yttrium Oxide**

| eV | $cm^{-1}$ | $\mu m$ | $n$ | $k$ | $n$ | $k$ |
|---|---|---|---|---|---|---|
| 1.364 | 11000 | 0.9091 | | | 1.906 | |
| 1.302 | 10500 | 0.9524 | | | 1.904 | |
| 1.240 | 10000 | 1.0000 | 1.903 [35] | | 1.903 | |
| 1.215 | 9800 | 1.0204 | 1.902 | | 1.902 | |
| 1.190 | 9600 | 1.0417 | 1.901 | | 1.902 | |
| 1.165 | 9400 | 1.0638 | 1.901 | | 1.901 | |
| 1.141 | 9200 | 1.0870 | 1.900 | | 1.900 | |
| 1.116 | 9000 | 1.1111 | 1.900 | | 1.900 | |
| 1.091 | 8800 | 1.1364 | 1.899 | | 1.899 | |
| 1.066 | 8600 | 1.1628 | 1.898 | | 1.899 | |
| 1.041 | 8400 | 1.1905 | 1.898 | | 1.898 | |
| 1.017 | 8200 | 1.2195 | 1.897 | | 1.897 | |
| 0.9919 | 8000 | 1.2500 | 1.896 | | 1.897 | |
| 0.9671 | 7800 | 1.2821 | 1.896 | | 1.896 | |
| 0.9423 | 7600 | 1.3158 | 1.895 | | 1.896 | |
| 0.9175 | 7400 | 1.3514 | 1.895 | | 1.895 | |
| 0.8927 | 7200 | 1.3889 | 1.894 | | 1.895 | |
| 0.8679 | 7000 | 1.4286 | 1.893 | | 1.894 | |
| 0.8431 | 6800 | 1.4706 | 1.893 | | 1.893 | |
| 0.8183 | 6600 | 1.5152 | 1.892 | | 1.893 | |
| 0.7935 | 6400 | 1.5625 | 1.891 | | 1.892 | |
| 0.7687 | 6200 | 1.6129 | 1.891 | | 1.891 | |
| 0.7439 | 6000 | 1.6667 | 1.890 | | 1.891 | |
| 0.7191 | 5800 | 1.7241 | 1.889 | | 1.890 | |
| 0.6943 | 5600 | 1.7857 | 1.888 | | 1.889 | |
| 0.6695 | 5400 | 1.8519 | 1.888 | | 1.889 | |
| 0.6447 | 5200 | 1.9231 | 1.887 | | 1.888 | |
| 0.6199 | 5000 | 2.0000 | 1.886 | | 1.887 | |
| 0.6075 | 4900 | 2.0408 | 1.885 | | 1.886 | |
| 0.5951 | 4800 | 2.0833 | 1.885 | | 1.886 | |
| 0.5827 | 4700 | 2.1277 | 1.884 | | 1.885 | |
| 0.5703 | 4600 | 2.1739 | 1.883 | | 1.885 | |
| 0.5579 | 4500 | 2.2222 | 1.883 | | 1.884 | |
| 0.5455 | 4400 | 2.2727 | 1.882 | | 1.884 | |
| 0.5331 | 4300 | 2.3256 | 1.881 | | 1.883 | |
| 0.5207 | 4200 | 2.3810 | 1.881 | | 1.882 | |
| 0.5083 | 4100 | 2.4390 | 1.880 | | 1.882 | |
| 0.4959 | 4000 | 2.5000 | 1.879 | | 1.881 | |
| 0.4835 | 3900 | 2.5641 | 1.878 | | 1.880 | |
| 0.4711 | 3800 | 2.6316 | 1.877 | | 1.879 | |
| 0.4587 | 3700 | 2.7027 | 1.876 | | 1.879 | |
| 0.4463 | 3600 | 2.7778 | 1.875 | | 1.878 | |
| 0.4339 | 3500 | 2.8571 | 1.874 | | 1.877 | |
| 0.4275 | 3448 | 2.9000 | 1.873 | | 1.876 | $6.5 \cdot 10^{-7}$ [40] |

(*continued*)

**TABLE II (*Continued*)**

**Yttrium Oxide**

| eV | $cm^{-1}$ | $\mu$m | $n$ | $k$ | $n$ | $k$ |
|---|---|---|---|---|---|---|
| 0.4215 | 3400 | 2.9412 | 1.873 | | 1.876 | |
| 0.4092 | 3300 | 3.0303 | 1.872 | | 1.874 | |
| 0.3968 | 3200 | 3.1250 | 1.870 | | 1.873 | |
| 0.3844 | 3100 | 3.2258 | 1.868 | | 1.872 | |
| 0.3720 | 3000 | 3.3333 | 1.867 | | 1.870 | |
| 0.3596 | 2900 | 3.4483 | 1.865 | | 1.868 | |
| 0.3472 | 2800 | 3.5714 | 1.863 | | 1.867 | |
| 0.3348 | 2700 | 3.7037 | 1.860 | | 1.864 | |
| 0.3224 | 2600 | 3.8462 | 1.858 | | 1.862 | |
| 0.3179 | 2564 | 3.9000 | 1.857 | | 1.861 | $1.3\cdot10^{-6}$ |
| 0.3100 | 2500 | 4.0000 | 1.855 | | 1.859 | |
| 0.2976 | 2400 | 4.1667 | 1.851 | | 1.856 | |
| 0.2852 | 2300 | 4.3478 | 1.847 | $1.6\cdot10^{-8}$ [35] | 1.853 | |
| 0.2728 | 2200 | 4.5455 | 1.843 | $3.7\cdot10^{-8}$ | 1.849 | |
| 0.2604 | 2100 | 4.7619 | 1.838 | $8.6\cdot10^{-8}$ | 1.845 | |
| 0.2480 | 2000 | 5.0000 | 1.832 | $2.1\cdot10^{-7}$ | 1.8394 | |
| 0.2418 | 1950 | 5.1282 | 1.83 | $3.3\cdot10^{-7}$ | 1.8364 | |
| 0.2356 | 1900 | 5.2632 | 1.82 | $5.2\cdot10^{-7}$ | 1.8332 | |
| 0.2294 | 1850 | 5.4054 | 1.82 | $8.2\cdot10^{-7}$ | 1.8298 | |
| 0.2232 | 1800 | 5.5556 | 1.82 | $1.3\cdot10^{-6}$ | 1.8259 | |
| 0.2170 | 1750 | 5.7143 | 1.81 | $2.0\cdot10^{-6}$ | 1.8218 | |
| 0.2108 | 1700 | 5.8824 | 1.81 | $3.2\cdot10^{-6}$ | 1.8172 | |
| 0.2046 | 1650 | 6.0606 | 1.80 | $5.0\cdot10^{-6}$ | 1.8121 | |
| 0.1984 | 1600 | 6.2500 | 1.80 | $8.0\cdot10^{-6}$ | 1.8065 | |
| 0.1922 | 1550 | 6.4516 | 1.79 | $1.3\cdot10^{-5}$ | 1.8002 | |
| 0.1860 | 1500 | 6.6667 | 1.78 | $2.2\cdot10^{-5}$ | 1.7932 | |
| 0.1798 | 1450 | 6.8966 | 1.77 | $3.7\cdot10^{-5}$ | 1.7854 | |
| 0.1736 | 1400 | 7.1429 | 1.76 | $6.3\cdot10^{-5}$ | 1.7765 | |
| 0.1674 | 1350 | 7.4074 | 1.75 | $1.0\cdot10^{-4}$ | 1.7665 | |
| 0.1612 | 1300 | 7.6923 | 1.74 | $1.6\cdot10^{-4}$ | 1.7550 | |
| 0.1550 | 1250 | 8.0000 | 1.72 | $2.7\cdot10^{-4}$ | 1.7417 | |
| 0.1488 | 1200 | 8.3333 | 1.71 | $4.2\cdot10^{-4}$ | 1.7263 | |
| 0.1426 | 1150 | 8.6957 | 1.69 | $7.0\cdot10^{-4}$ | 1.7082 | |
| 0.1364 | 1100 | 9.0909 | 1.67 | $1.2\cdot10^{-3}$ | 1.6867 | |
| 0.1302 | 1050 | 9.5238 | 1.64 | $2.3\cdot10^{-3}$ | 1.6609 | |
| 0.1240 | 1000 | 10.000 | 1.61 | $4.5\cdot10^{-3}$ | 1.6293 | |
| 0.1215 | 980 | 10.204 | 1.59 | $5.9\cdot10^{-3}$ | 1.6147 | |
| 0.1190 | 960 | 10.417 | 1.58 | $7.9\cdot10^{-3}$ | 1.5986 | |
| 0.1165 | 940 | 10.638 | 1.56 | $9.7\cdot10^{-3}$ | 1.5810 | |
| 0.1141 | 920 | 10.870 | 1.54 | 0.012 | 1.5615 | |
| 0.1116 | 900 | 11.111 | 1.52 | 0.015 | 1.5400 | |
| 0.1091 | 880 | 11.364 | 1.49 | 0.019 | 1.5159 | |
| 0.1066 | 860 | 11.628 | 1.47 | 0.024 | 1.4889 | |
| 0.1041 | 840 | 11.905 | 1.44 | 0.029 | 1.4584 | |

(*continued*)

**TABLE II (*Continued*)**

**Yttrium Oxide**

| eV | $cm^{-1}$ | $\mu m$ | $n$ | $k$ | $n$ | $k$ |
|---|---|---|---|---|---|---|
| 0.1017 | 820 | 12.195 | 1.41 | 0.035 | | |
| 0.0992 | 800 | 12.500 | 1.37 | 0.041 | | |
| 0.0967 | 780 | 12.821 | 1.33 | 0.048 | | |
| 0.0942 | 760 | 12.158 | 1.28 | 0.055 | | |
| 0.0917 | 740 | 13.514 | 1.22 | 0.063 | | |
| 0.0893 | 720 | 13.889 | 1.15 | 0.070 | | |
| 0.0868 | 700 | 14.286 | 1.07 | 0.078 | | |
| 0.0843 | 680 | 14.706 | 0.97 | 0.086 | | |
| 0.0818 | 660 | 15.152 | 0.83 | 0.096 | | |
| 0.0794 | 640 | 15.625 | 0.62 | 0.12 | | |
| 0.0769 | 620 | 16.129 | 0.22 | 0.26 | | |
| 0.0744 | 600 | 16.667 | 0.10 | 0.78 | | |
| 0.0719 | 580 | 17.241 | 0.15 | 1.2 | | |
| 0.0694 | 560 | 17.857 | 0.73 | 1.8 | | |
| 0.0670 | 540 | 18.519 | 0.66 | 0.65 | | |
| 0.0645 | 520 | 19.231 | 0.12 | 1.2 | | |
| 0.0620 | 500 | 20.000 | 0.09 | 1.7 | | |
| 0.0608 | 490 | 20.408 | 0.15 | 1.9 | | |
| 0.0595 | 480 | 20.833 | 0.10 | 2.1 | | |
| 0.0583 | 470 | 21.277 | 0.15 | 2.4 | | |
| 0.0570 | 460 | 21.739 | 0.77 | 2.3 | | |
| 0.0558 | 450 | 22.222 | 0.15 | 2.4 | | |
| 0.0546 | 440 | 22.727 | 0.12 | 2.7 | | |
| 0.0533 | 430 | 23.256 | 0.13 | 3.1 | | |
| 0.0521 | 420 | 23.810 | 0.22 | 3.6 | | |
| 0.0508 | 410 | 24.390 | 0.28 | 3.7 | | |
| 0.0496 | 400 | 25.000 | 0.29 | 4.4 | | |
| 0.0484 | 390 | 25.641 | 0.50 | 5.4 | | |
| 0.0471 | 380 | 26.316 | 1.38 | 7.4 | | |
| 0.0459 | 370 | 27.027 | 8.44 | 7.1 | | |
| 0.0446 | 360 | 27.778 | 5.36 | 1.4 | | |
| 0.0434 | 350 | 28.571 | 1.94 | 1.8 | | |
| 0.0422 | 340 | 29.412 | 1.68 | 6.6 | | |
| 0.0409 | 330 | 30.303 | 7.48 | 1.5 | | |
| 0.0397 | 320 | 31.250 | 3.47 | 0.86 | | |
| 0.0384 | 310 | 32.258 | 1.53 | 5.4 | | |
| 0.0372 | 300 | 33.333 | 10.88 | 2.9 | | |
| 0.0360 | 290 | 34.483 | 6.89 | 0.38 | | |
| 0.0347 | 280 | 35.714 | 5.72 | 0.17 | | |
| 0.0335 | 270 | 37.037 | 5.10 | 0.11 | | |
| 0.0322 | 260 | 38.462 | 4.67 | 0.095 | | |
| 0.0310 | 250 | 40.000 | 4.26 | 0.15 | | |
| 0.0298 | 240 | 41.667 | 4.65 | 0.82 | | |
| 0.0285 | 230 | 43.478 | 4.38 | 0.099 | | |

(*continued*)

**TABLE II (*Continued*)**

**Yttrium Oxide**

| eV | $cm^{-1}$ | $\mu m$ | $n$ | $k$ | $n$ | $k$ |
|---|---|---|---|---|---|---|
| 0.0273 | 220 | 45.455 | 4.13 | 0.052 | | |
| 0.0260 | 210 | 47.619 | 3.96 | 0.041 | | |
| 0.0248 | 200 | 50.000 | 3.80 | 0.043 | | |
| 0.0236 | 190 | 52.632 | 3.56 | 0.095 | | |
| 0.0223 | 180 | 55.556 | 4.04 | 0.47 | | |
| 0.0211 | 170 | 58.824 | 4.09 | 0.30 | | |
| 0.0198 | 160 | 62.500 | 3.79 | 0.040 | | |
| 0.0186 | 150 | 66.667 | 3.67 | 0.025 | | |
| 0.0174 | 140 | 71.429 | 3.57 | 0.024 | | |
| 0.0161 | 130 | 76.923 | 3.43 | 0.048 | | |
| 0.0149 | 120 | 83.333 | 3.63 | 0.80 | | |
| 0.0136 | 110 | 90.909 | 3.67 | 0.041 | | |
| 0.0124 | 100 | 100.00 | 3.57 | 0.016 | | |
| 0.0112 | 90 | 111.11 | 3.51 | 0.010 | | |
| 0.0099 | 80 | 125.00 | 3.48 | $7.4 \cdot 10^{-3}$ | | |
| 0.0087 | 70 | 142.86 | 3.45 | $5.8 \cdot 10^{-3}$ | | |
| 0.0074 | 60 | 166.67 | 3.43 | $4.6 \cdot 10^{-3}$ | | |
| 0.0062 | 50 | 200.00 | 3.41 | $3.7 \cdot 10^{-3}$ | | |
| 0.0050 | 40 | 250.00 | 3.40 | $2.8 \cdot 10^{-3}$ | | |
| 0.0037 | 30 | 333.33 | 3.39 | $2.0 \cdot 10^{-3}$ | | |
| 0.0025 | 20 | 500.00 | 3.38 | $1.4 \cdot 10^{-3}$ | | |
| 0.0019 | 15 | 666.67 | 3.38 | $1.0 \cdot 10^{-3}$ | | $2.3 \cdot 10^{-3}$ [36] |
| 0.0012 | 10 | 1000.0 | 3.38 | $6.7 \cdot 10^{-4}$ | | $1.7 \cdot 10^{-3}$ |
| 0.0006 | 5 | 2000.0 | 3.38 | $3.3 \cdot 10^{-4}$ | | $8.8 \cdot 10^{-4}$ |
| 0.0000 | $\approx 0$ | – | 3.38 | 0.0 | 3.43 [36,38] | |

[a]References are indicated in brackets.

**TABLE III**

**Values of *dn/dT* Obtained from Various References for Yttrium Oxide[a]**

| eV | $cm^{-1}$ | $\mu m$ | $dn/dT$ (1/K) | Notes |
|---|---|---|---|---|
| 1.959 | 15803 | 0.6328 | $8.1 \cdot 10^{-6}$ | Our measurement |
| 0.310 | 2500 | 4.0000 | $7.6 \cdot 10^{-6}$ | Model [35] |
| 0.0 | $\approx 0$ | — | $1.05 \cdot 10^{-4}$ | Measurement [38] |
| | | | $8.9 \cdot 10^{-5}$ | Model [35] |

[a]References are indicated in brackets.

**TABLE IV**

**Calculated Total Hemispherical Emissivity for Yttrium Oxide**

| Temperature (K) | Thickness (cm) | | | |
|---|---|---|---|---|
| | 0.10 | 0.25 | 0.50 | 1.25 |
| 200 | 0.49 | 0.50 | 0.50 | 0.51 |
| 300 | 0.53 | 0.56 | 0.58 | 0.60 |
| 400 | 0.48 | 0.52 | 0.56 | 0.59 |
| 500 | 0.40 | 0.45 | 0.49 | 0.53 |
| 600 | 0.33 | 0.38 | 0.41 | 0.45 |
| 700 | 0.27 | 0.31 | 0.35 | 0.39 |
| 800 | 0.22 | 0.26 | 0.29 | 0.33 |
| 900 | 0.19 | 0.22 | 0.25 | 0.28 |
| 1000 | 0.16 | 0.19 | 0.21 | 0.25 |